Geology of the West Block Area of the Late Devonian Myra Falls VHMS District, B.C., Canada

by

Brian A. McNulty

(MSc. University of British Columbia Canada, 2014)

(BSc. University of Alaska Fairbanks USA, 2007)

UNIVERSITY OF TASMANIA

A thesis submitted in fulfilment of the requirements for the degree of Doctor of Philosophy

CODES

Australia

January 2019

Table of Contents

Table of Contents

Table of Contents

Table of Contents

List of Figures

List of Figures

List of Figures

List of Figures

List of Tables

List of Appendices

Abstract

Myra Falls is a series of polymetallic, volcanic-hosted massive sulfide (VHMS) deposits located in central Vancouver Island, 90 km southwest of Campbell River, British Columbia, Canada. As of April 2013, production has exceeded 30 Mt of ore at average grades of 5.5% Zn, 1.6% Cu, 0.6% Pb, 2.0 g/t Au and 54.0 g/t Ag. There are 10 VHMS deposits at Myra Falls, which are spatially and temporally related to episodic felsic volcanism, in the Devonian Sicker Group, which define two district-scale stratigraphic members. The near surface L-M-P member is host to the Lynx, Myra, and Price orebodies. Whereas the HW, Trumpeter Zone, Battle, Extension Zone, Ridge Zone West, Ridge Zone North, and Marshall Zone orebodies are in the lower H-W member.

While previous studies have focused on the HW, Battle, and Ridge Zone West orebodies, questions regarding the lithostratigraphic architecture and the depositional age of the H-W member remain. The West Block Area provides a geological-link between the Battle and Ridge Zone West orebodies. This research presents: (1) a detailed description of the lithology and nature of VHMS mineralisation in the West Block Area; (2) a proposed geological framework linking the Battle and Ridge Zone West orebodies; (3) mineralogical and geochemical proximity indicators to ore; (4) immobile element discrimination of altered volcanic rocks from systematic pXRF analysis; (5) age constraints from U-Pb zircon geochronology of felsic volcanic rocks in the H-W and L-M-P members; and (6) develop useful criteria for exploration in the Myra Falls VHMS district and elsewhere on Vancouver Island.

Detailed and simplified district-scale cross-section interpretations of the West Block Area were generated from underground drilling, in conjunction with company data, to assess the distribution of identified lithological units, alteration, and sulfide mineralisation. Stratigraphy in the West Block Area comprises coherent, volcaniclastic and marine sedimentary rocks of the Price and lower Myra Formations. The Price Formation, at least 80 metres-thick, is characterised by a submarine, extrusive sequence of coherent, andesitic lavas and related breccias. The 150 to 175 metres-thick H-W member (lower Myra Formation) consists of syn- and post-eruptive volcanic and marine-sedimentary rocks. Polylithic siltstone, sandstone and conglomerate of the Basal Volcaniclastic Unit extends west over 500 metres to the Ridge Zone West orebody, where it marks the base of the lower Myra Formation. The Basal Volcaniclastic Unit is overlain by intercalated argillite and chert of the Caprocks Unit. The overlying HW Rhyolite comprises felsic volcaniclastic rocks, which are overlain by coherent, quartz and feldspar-phyric rhyolite, 10 to 40 metres in thickness. Coherent rhyolite domes of the West Block Area extend east over 500 metres to the Battle orebody and north over 250 metres to the Ridge Zone North orebody. A 10 to 50 metre-thick, plagioclase and pyroxene-phyric coherent andesite lava is the youngest extrusive unit of the H-W member, and overlies the HW Rhyolite, extending >500 metres to the west, above the Ridge Zone West orebody. The Hanging Wall Andesite member unconformably overlies the H-W member, and consists of polylithic, volcaniclastic sandstone and conglomerate, locally with clasts of massive sulfide and chert.

Polymetallic sulfide mineralisation in the West Block Area occurs in altered andesite of the Price Formation (footwall) and a rhyolite-dominant, volcano-sedimentary sequence of the lower Myra Formation. Styles of sulfide mineralisation are disseminated, stringer, semi-massive and massive. Disseminated sulfide is pyrite-rich, and occurs in altered, Price Formation andesite

and all rock types of the H-W member. Sphalerite-rich and pyrite-dominant stringer-style mineralisation is present in altered coherent and volcaniclastic rhyolite of the HW Rhyolite. Less common in the West Block Area are semi-massive and massive zinc-rich, polymetallic, mineralisation styles, which are hosted in altered coherent rhyolite and autobreccias of the HW Rhyolite, and polylithic conglomerate of the Basal Volcaniclastic Unit.

Volcanic-hosted massive sulfide mineralisation is located at two stratigraphic positions — upper zone and contact zone. The "upper zone" is stringer-style, semi-massive and massive sulfide mineralisation, 30 to 75 metres above the Price Formation contact. The "contact zone" comprises semi-massive and massive sulfide mineralisation at or near the Price Formation contact. Mineralisation consists of sphalerite, pyrite, chalcopyrite, and galena with accessory tennantite-tetrahedrite, stromeyerite and pearceite-polybasite. Precious metal minerals are electrum and hessite. Four paragenetic stages of mineralisation are proposed. Stage-1 includes early, inclusion-rich pyrite. Stage-2 consists of inclusion-free pyrite rimming Stage-1 pyrite accompanied by the precipitation of sphalerite, with minor galena-chalcopyrite-barite ± tennantite and tetrahedrite. Stage-3 is characterised by the modification of Stage-2 mineral phases in the form of grain coarsening, homogenisation of sphalerite(?), and local remobilisation of sulfide and sulfosalt phases. Stage-4 encompasses metamorphic remobilisation with pearceite-polybasite veinlets crosscutting Stage-2 and -3 mineral assemblages. The timing of electrum and hessite precipitation is unresolved, and could have occurred during Stage-3 and/or Stage-4.

Determining the intensity, zonation and extent of hydrothermal alteration associated with VHMS deposits can provide important implications for mineral exploration. A laterally continuous footwall alteration zone extends beneath the West Block Area and the Battle, Ridge Zone North and Ridge Zone West orebodies. Alteration of the Price Formation is mineralogically and texturally diverse. Weak alteration, defined from the Thelwood Valley locality, consists of a pervasive, texturally non-destructive, chlorite-calcite ± epidote alteration. Moderate alteration, defined from the West Block Area, consists of pervasive, texturally non-destructive, chlorite-calcite-pyrite and chlorite-sericite alteration. Intense alteration occurs in the footwall below the Ridge Zone North and Battle orebodies, and consists of feldspar-destructive, sericite-quartz-pyrite, chlorite-rich, and chlorite-sericite-pyrite alteration.

Footwall alteration associated with the West Block Area, Ridge Zone North and Battle orebodies has several mineralogical and geochemical characteristics that show systematic changes with increasing proximity to ore. The Fe/Fe+Mg of chlorite decreases from 0.49-0.27 in least to moderately altered andesite to <0.20 in intensely altered andesite immediately below ore. In general, K-mica compositions shift from phengitic in least-altered andesite to muscovitic in intensely altered andesite, proximal to ore. Least-altered footwall alteration whole-rock lithogeochemical trends, include elevated Na_2O, Rb/Sr <0.1, and moderate alteration index (AI) and Chlorite-Carbonate-Pyrite Index (CCPI) values that plot in the diagenetic field of the alteration box plot. Proximal, within 100 metres to ore, lithogeochemical trends include depleted Na_2O (≤0.75 wt. %), variably elevated S (up to 16.0 wt. %), Rb/Sr >1.0, AI values >80, and CCPI values from 35-95. Distal, up to 500 metres away from ore, lithogeochemical signatures are characterised by variable Na_2O and S values, and Rb/Sr from 0.1-1.0. Alteration

Abstract

Index and CCPI values, that plot in the hydrothermal alteration field on the alteration box plot, form an array from the least-altered andesite field to the chlorite-pyrite and white mica fields. As these mineralogical and lithogeochemical alteration trends change systematically relative to the position of ore they can be used in the exploration for other deposits in the district.

A new method for lithological discrimination of altered volcanic rocks based on systematic portable X-ray fluorescence (pXRF) analysis of drill core has been developed. A compilation of published conventional XRF lithogeochemical data from the Myra Falls VHMS district shows robust and discrete Ti/Zr trends for coherent volcanic rocks. Single-spot pXRF analysis of pressed powder dill core samples and three-spot pXRF analyses measured from the flat, cut and clean surface of drill core samples were compared with conventional XRF results from the same sample sets. Both pXRF sampling methods reproduce the laboratory XRF results for Ti and Zr, and there was no significant improvement in accuracy or precision between drill core powders and unprepared drill core samples. Calibration, estimation of total measurement uncertainty, and data reduction procedures for systematic three-spot pXRF analysis of drill core samples were developed to improve lithological logging of altered volcanic rocks. Portable-XRF analysis, combined with detailed logging of volcanic lithofacies can improve geologic and stratigraphic interpretations, which are vital for developing mineral exploration models for VHMS deposits and other economic mineral systems.

Previous attempts to date the volcanic rocks at Myra Falls have resulted in relatively imprecise crystallisation ages that do not resolve the temporal relationship between the L-M-P and H-W members. New U-Pb zircon CA-ID-TIMS results from the HW Rhyolite and LA-ICPMS results from the LMP Rhyolite, combined with published age constraints and stratigraphic relationships, confirm at least two phases of felsic volcanism at Myra Falls that were episodic over a period of ~7 million years. High precision CA-ID-TIMS results indicate that VHMS mineralisation in the Ridge Zone North orebody is hosted in 362.4 $\pm$ 0.4 Ma coherent rhyolite. For the first time, the felsic volcaniclastic stratigraphy of the L-M-P member is constrained by U-Pb zircon geochronology, with LA-ICPMS results providing a maximum deposition age of 355.5 $\pm$ 2.8 Ma for the LMP Rhyolite of the Price orebody. These age constraints at Myra Falls correlate with previously dated VHMS deposit stratigraphy in the Cowichan Lake uplift on Vancouver Island. Future VHMS mineral exploration in the Sicker Group on Vancouver Island should consider ~362 Ma felsic stratigraphy located within 200 metres of the upper contact of the Price and Nitinat Formations, as well as ~355 Ma felsic stratigraphy located in the top 100 metres of the Myra and McLaughlin Ridge Formations.

This research advances the overall understanding of the H-W member stratigraphy, the nature of hydrothermal alteration, and the temporal relationship of felsic host rocks at Myra Falls. These advancements have implications for the advancement of mineral exploration in the Myra Falls district and throughout Vancouver Island. In short, VHMS exploration targeting in the belt should focus on felsic volcanic stratigraphy (Ti/Zr ratios between 9-12) with U-Pb zircon crystallisation ages of approximately 362 Ma and 355 Ma. The siliceous Caprocks unit is a distinguishing lithological feature for the H-W member VHMS orebodies, therefore mineral exploration should also target Late Devonian marine basin depositional environments intercalated with felsic volcanic deposits and fine-grained marine sedimentation.

Statements and Declarations

Declaration of originality

This thesis contains no material which has been accepted for the award of any other degree or diploma in any tertiary institutions and, to the best of my knowledge and belief, contains no copy or paraphrase material previously published or written by another person, except where due reference is made in the text of the thesis.

Signed: **Date:** January 22, 2019

Authority of access

This thesis is not to be made available for loan or copying for a period of 12 months from the date this statement was signed; after that time limited copying is permitted in accordance with the Copyright Act 1968.

Signed: **Date:** January 22, 2019

Statement regarding published work contained in this thesis

The publisher of the paper comprising Chapter 6 hold the copyright for that content and access to the material should be sought from the *Journal of Geochemical Exploration*. The remaining non published content of the thesis may be made available for loan and limited copying and communication post a period of 12 months from the date this statement was signed in accordance with the Copyright Act 1968.

Signed: **Date:** January 22, 2019

Statements and Declarations

Statement of authorship

The following people contributed to the publication of work undertaken as part of this thesis:

Candidate: Brian McNulty, Centre of Excellence in Ore Deposits (CODES), University of Tasmania)

Author 1: Nathan Fox, Supervisor, CODES, University of Tasmania

Author 2: Ron Berry, CODES, University of Tasmania

Author 3: J. Bruce Gemmell, Supervisor, CODES, University of Tasmania

Proportion of work undertaken towards paper

Paper 1: Lithological discrimination of altered volcanic rocks based on systematic portable X-ray fluorescence analysis of drill core at the Myra Falls VHMS deposit, Canada
Located in Chapter 6 (Published).

Candidate was the primary author and with authors 1-3 contributed to the conception and design of the research. Candidate collected and interpreted new data included in the paper. Candidate compiled data from the literature included in the analysis and wrote the paper with revisions from authors 1-3.

Candidate contributed to approximately 90% to the planning, execution and preparation of the work for the paper.

We the undersigned agree with the above stated "proportion of work undertaken" for the above published peer-reviewed paper contributing to the thesis:

Signed:

J. Bruce Gemmell Supervisor, Adjunct Professor CODES, School of Natural Sciences University of Tasmania	**Sebastien Meffre** Head of Discipline, Earth Sciences School of Natural Sciences University of Tasmania
Date: January 18, 2019	January 18, 2019

Acknowledgements

Firstly I would like to thank my supervisors, Bruce Gemmell, Garry Davidson and Nathan Fox. I will never forget the day in June 2014 when Bruce offered me the opportunity to pursue a PhD in Tasmania. I will always be grateful for the endless support and encouragement from Bruce and Garry throughout the process of navigating the occasional muddy waters of research. A special thank you to Nathan, who stepped up in a big way after the unexpected loss of Garry. I have learned so much from the three of you and I cannot thank you enough for sharing your knowledge and time over the years.

This project would never have been possible if not for the support from Nyrstar Myra Falls. I would like to thank Rick Sawyer for initially setting up this project and for trusting and supporting me when I suggested different avenues of research during the life of the project. Thank you to the entire Nyrstar geology department for your support and time, including Lori, Ross and Rodger. In particular, thank you Armond for your efforts and collaboration during a stressful period of mine suspension. Thank you to the SEG Canada Foundation for a Research Grant in support of this PhD research.

I would like to acknowledge Ron Berry for his collaboration with the project and many tearoom discussions about geology and stories of Friday night pasta bake dinners with his grandkids. Thank you for sharing your knowledge and sense of humor with me over the years. The light at the end of the tunnel turned out not to be a train.

To the many brilliant minds at the University of Tasmania, specifically (in no particular order) Irina Zhukova, Sarah Gilbert, Sebastien Meffre, Jay Thompson, Sandrin Feig and Karsten Goemann. Thank you to Jane Higgins, Helen Scott, Claire Rutherford and Karen Huizing for your kindness, patience and assistance with the logistics of graduate research at UTAS. Thank you to Al Cuison and Michele Chapple-Smith, for what is a geologist without perfectly polished thin sections.

I am a firm believer that as a graduate student it is our responsibility to give back to the university community that supports us. With that in mind, I would like to thank Sebastien Meffre, Karin Orth, Martin Jutzeler, Paul Olin, Michael Roach, Rob Scott and David Cooke for opportunities to teach undergraduate students in the lab and field and participant in community outreach programs during my time at UTAS.

To my fellow PhD candidates and friends at CODES—thank you for your friendship, staff club coffees, family dinners and Tassie adventures. Thank you Sam, Tom Sr., Tristan, Jen and Tom Jr. for the best officemates a guy could ask for. Thank you to what has become my Australian Family—Ben and Georgia, Martin and Doreen, Dave and Paul, Alex and Emily, Rob and Katie, Sam and Claire, Ivan and Tamila, Isi, Chris and Indrani, and Nathan and Imogen – you made Hobart a magical place. To Volleyball Tasmania, especially Steve, Steph, Mick and Jess—thank you for welcoming me onto the court and beach. To Bee and Larriana—thank you for your friendship and providing us our first home in Tassie.

Most importantly, the completion of my PhD would not have been possible if not for the love, patience and support of my partner Cassady. I am forever grateful to you for taking this adventure with me.

To Garry Davidson

You are missed, my friend.

Chapter 1:

Introduction

Volcanic-hosted massive sulfide (VHMS) deposits are significant global resources of base and precious metals (e.g., Lydon, 1984; Barrie and Hannington, 1999; Large et al., 2001; Galley et al., 2007). VHMS deposits are unique among ore deposit classes as they are well represented in the ancient rock record (e.g., Huston et al., 2010). Since the discovery of black smokers on the seafloor in 1979 (Francheteau et al., 1979), VHMS deposits have been the subject of immense research. These investigations have examined the nature of ore-bearing hydrothermal fluids (e.g., Ohmoto and Rye, 1974; Large, 1977; Sunit and Peter, 1977; Ohmoto et al., 1983; Relvas and Barriga, 2006); mechanisms for precious metal enrichment (e.g., Hannington and Scott, 1989; Hannington et al., 1999; Vikentyev, 2006; Mercier-Langevin et al., 2010); volcanic architecture and seafloor settings (e.g., Morton et al., 1991; McPhie and Allen, 1992; Ohmoto, 1996; Hannington et al., 2005; Piercey, 2011); modes of sulfide emplacement (e.g., Eldridge et al., 1983; Doyle and Allen, 2003; Galley et al., 2006); and primary and secondary lithogeochemical signatures of volcanic host rocks (e.g., Lesher and Campbell, 1987; MacLean and Kranidiotis, 1987; Galley, 1995; Lentz, 1998; Large et al., 2001a; Hart et al., 2004; Piercey, 2010); from which a number of mineral exploration models have been proposed (e.g., Huston and Large, 1987; Franklin et al., 2005; Galley et al., 2007; Gibson et al., 2007; Barrie, 2012).

VHMS deposits can be grouped according to base metal content (Solomon, 1976; Franklin et al., 1981; Large, 1992; Franklin et al., 2005) and are divided into Cu-rich, Zn-Cu, Zn-Pb-Cu, and Pb-Zn groups according to their contained ratios of these three metals (Figure 1.1A). Due to its economic significance, VHMS deposits are also classified based on their gold content (e.g., Mercier-Langevin et al., 2010; Figure 1.1B). The Myra Falls district is comprised of Zn-Cu, polymetallic VHMS deposits with anomalous gold (Figure 1.1).

Literature on VHMS deposits emphasise a spectrum of sulfide precipitation processes from seafloor accumulation of sulfide precipitated from exhaling hydrothermal fluids to sub-seafloor replacement from circulating hydrothermal fluids (e.g., Solomon and Walshe, 1976; Eldridge et al., 1983; Lydon, 1988; Large, 1992; Doyle and Allen, 2003). Within a VHMS deposit, sulfide zones can form by a combination of both seafloor massive sulfide accumulation and sub-seafloor replacement (e.g., Doyle and Allen, 2003). The recognition of the sulfide precipitation

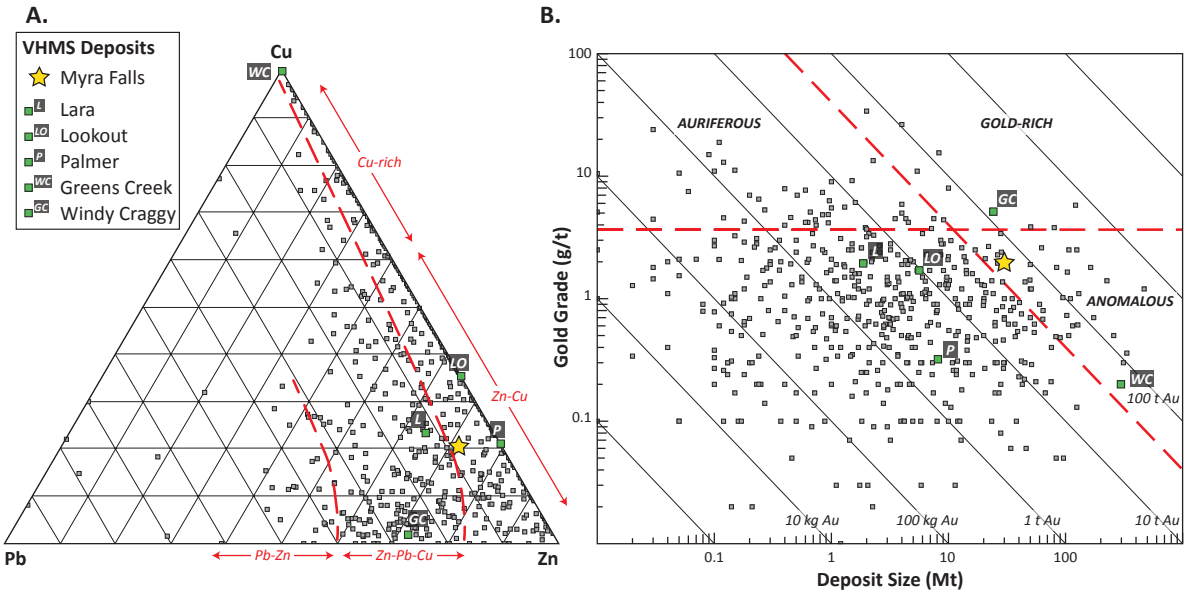

Figure 1.1 Base metal and gold classification schemes for VHMS deposits worldwide (dataset modified from Mosier et al., 2009; includes 873 deposits) A. Fields for Cu-rich, Zn-Cu, Zn-Pb-Cu, and Pb-Zn VHMS deposits, based on average ore grades in weight percent (adapted from Galley et al., 2007). B. Fields for auriferous, anomalous, gold-rich and ordinary VHMS deposits (Mercier-Langevin et al., 2010). VHMS deposits are considered auriferous if Au grade >3.46 g/t, anomalous if Au tonnage ≥31 tonnes, gold-rich if Au grade >3.46 g/t and Au tonnage ≥31 tonnes. Note that Myra Falls is classified as a Zn-Cu with anomalous gold VHMS deposit. Highlighted with green squares are selected VHMS deposits from the Wrangellia and Alexander Terranes see legend.

process is important for mineral exploration as the mineralisation mechanism is linked to the marine depositional setting. For example, exhalative, seafloor massive sulfide deposits tend to be hosted within fine-grained, slow rate of deposition, submarine volcano-sedimentary units while sub-seafloor replacement deposits occur mainly in volcaniclastic facies with rapid rates of deposition (e.g., Doyle and Allen, 2003).

The Myra Falls VHMS district is located within Strathcona Provincial Park, near Buttle Lake in central Vancouver Island, British Columbia, Canada (Figure 1.2). The underground mine is approximately 90 km southwest of Campbell River and is owned and managed by Nyrstar Myra Falls Operation. Polymetallic VHMS deposits occur in two stratigraphic members of the Devonian Sicker Group, which have a strike length of >5 km (Figure 1.3). The two members are the near surface L-M-P member and the lower H-W member.

Myra Falls is one of western Canada's most productive VHMS mines, exceeding 30 Mt of production as of April 2013 at average grades of 5.5% Zn, 1.6% Cu, 0.6% Pb, 2.0 g/t Au and 54.0 g/t Ag. The primary focus of this thesis is the West Block Area, which is located between the H-W member Battle and Ridge Zone West orebodies (Figure 1.3). Production of the Battle orebody began in 1995 with a pre-mining reserve of ~5.97 Mt at 12.5% Zn, 1.8% Cu, 0.7% Pb, 1.4 g/t Au and 53 g/t Ag. Discovered in 1990, the Ridge Zone West orebody has a pre-mining resource estimate of ~0.98 Mt at 6.8% Zn, 0.9% Cu, 0.8% Pb, 2.0 g/t Au and 72.0 g/t Ag. Current development to access the Ridge Zone West orebody traverses the West Block Area.

1.2 Mining Status and Exploration History

The Buttle Lake area has a long history of prospecting and mineral exploration activity since 1917. Mining began at Myra Falls in 1967 with commencement of the Lynx orebody open pit. Sustained mining continued through mid 2015 with mine development transitioning to an

underground operation in 1974 and the discovery of new VHMS orebodies. However, in April 2015 production was temporarily suspended. After an exhaustive asset review, Nyrstar Myra Falls Operation announced, in December of 2017, a mine restart plan that would reach full production capacity of 783,612 tonnes per year by 2021 (Davies, 2017). As of 2017, the current total proven and probable mineral reserves at Myra Falls are 4.89 Mt at average grades of 6.84% Zn, 0.91% Cu, 0.75% Pb, 1.69 g/t Au and 71.31 g/t Ag. Total measured and indicated mineral resources include 7.29 Mt at average grades of 6.59% Zn, 1.01% Cu, 0.72% Pb, 1.76 g/t Au and 69.71 g/t Ag (Nyrstar 2017 Mineral Resource and Mineral Reserve Statement, 2018).

Claims were first staked in the Myra Falls district by James Cross and Associates in 1917 and covered the surface expressions of what are now known as the Lynx, Myra and Price VHMS orebodies (Juras and Pearson, 1990). The claims received sporadic attention through 1925. In 1961, Western Mines Ltd acquired the original claims and focused mineral exploration activities on the Lynx area. Surface and underground production of the Myra orebody started in 1972 and ended in 1985. From 1978 to 1981, extensive surface and underground exploration was completed on the Price Hillside and the Price orebody was discovered, but production did not begin until 2014.

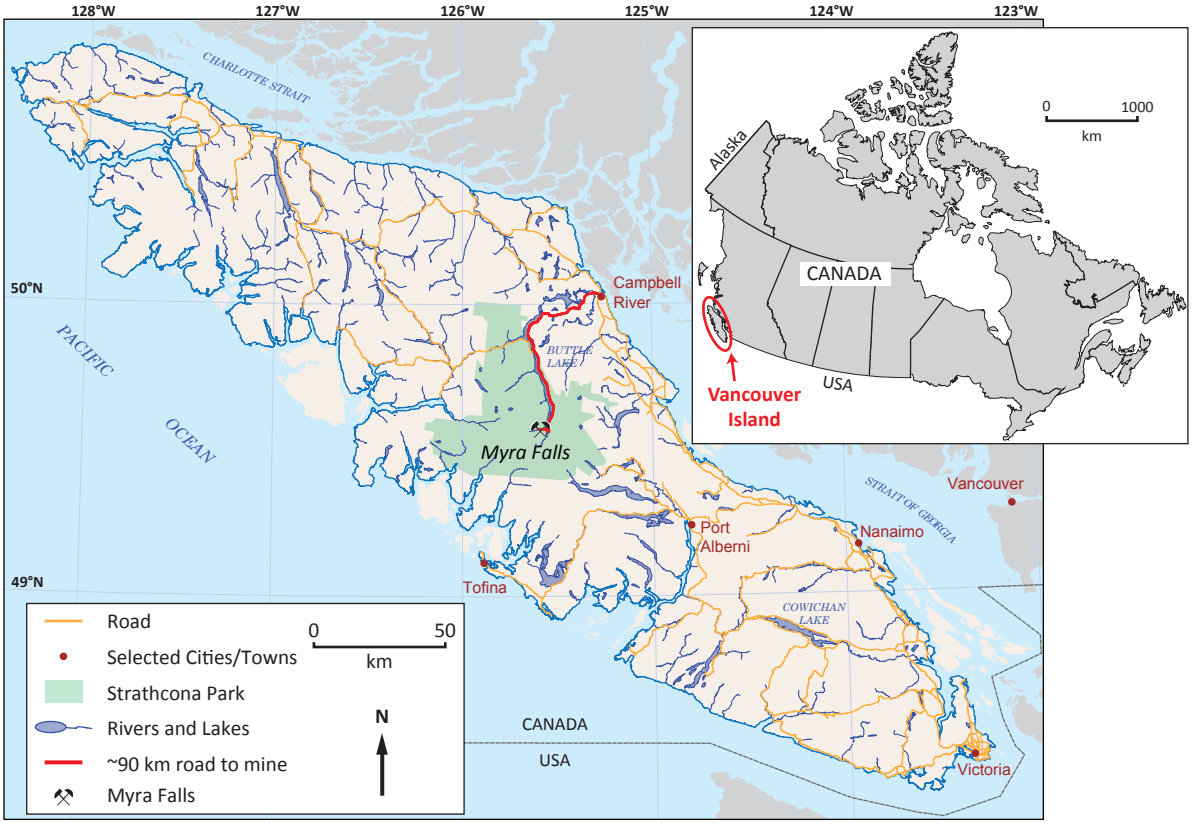

Figure 1.2 Geographic location map of the Myra Falls VHMS district. Myra Falls is located within Strathcona Provincial Park on Vancouver Island, British Columbia, Canada. Red-line highlights the ~90 km road from the mine site to the port site in Campbell River.

In 1979 the HW orebody was discovered 350 metres below the valley floor. Underground production of the HW orebody began in 1985, with the discovery of the Battle orebody in October 1991. Production of the Battle orebody began in 1995. Exploration drilling from the Lynx mine development intersected the Ridge Zone West and Marshall Zone orebodies in 1990 and 1995, respectively.

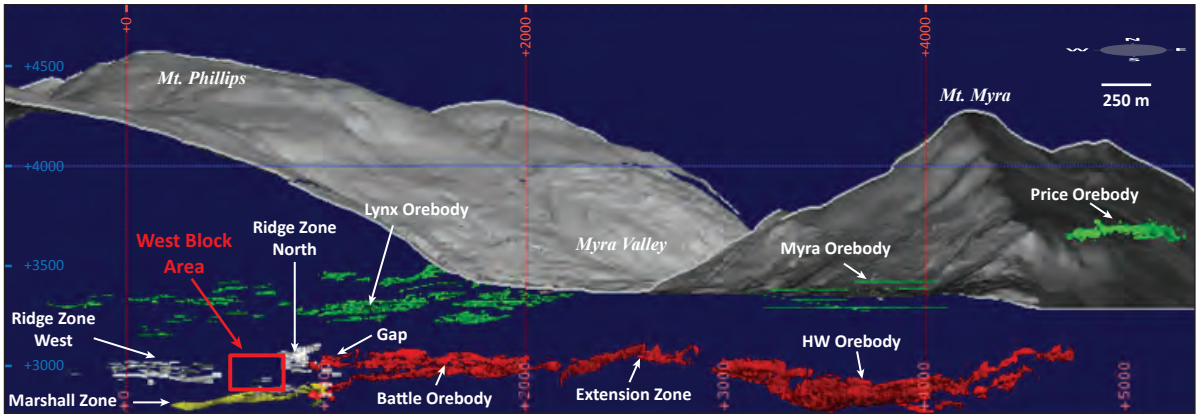

Figure 1.3 Three-dimensional view of the Myra Falls district, looking north, showing the distribution of VHMS orebodies and the West Block Area. Green polygons highlight the L-M-P member VHMS deposits whereas the red and yellow polygons highlight the H-W member VHMS deposits. Block model polygons are shown for the Price, Lynx, HW, Battle, Extension Zone, and Gap orebodies. Wireframe ore models are shown for the Marshall Zone and Ridge Zone North and Ridge Zone West orebodies. The underground workings are shown for the Myra orebody. Wireframe block models and underground development polygons and polyline data were provided by the geology department of the Nyrstar Myra Falls Operation.

Boliden Ltd acquired Western Mines Ltd in 1998 and during 2004 the Myra Falls Operation was sold to Breakwater Resources Ltd. From 2004 to 2011 Myra Falls was owned and operated by NVI Mining Ltd, a subsidiary of Breakwater Resources Ltd. Nyrstar purchased the Myra Falls Operation in 2011 and is the current owner and operator.

1.3 Previous Research

The Myra Falls VHMS district geology and the Paleozoic Sicker Group stratigraphy throughout Vancouver Island have been the subject of numerous studies by industry, government and university agencies. Clapp in 1912 completed the first geological reconnaissance of the Buttle Lake area, with subsequent mapping of the Buttle Lake and of the Paleozoic rocks elsewhere on Vancouver Island completed by Gunning (1931), Yole (1969), Jeffery (1970), Muller (1980), Brandon et al. (1986), Massey and Friday (1987), Massey et al. (1991), Massey (1992) and Yorath et al. (1999). Juras (1987) conducted the first detailed investigation of the Myra Falls VHMS district geology and established the volcanic stratigraphy, geologic setting, and general distribution of VHMS deposits, with an emphasis on the Price Hillside. Juras (1987) synthesised the Sicker Group stratigraphy of the Buttle Lake and Cowichan Lake areas on Vancouver Island, and his proposed stratigraphic nomenclature is still used.

Previous work has investigated the structural and deformation history of the Myra Falls district (Walker, 1985; Juras, 1987; Reid, 1993; Berry, 2000; and Jones, 2001) and the geology, mineralisation and alteration of the Price, HW, Battle and Marshall Zone orebodies (Seraphim, 1980; Andrew and Godwin, 1989; Robinson, 1994; Barrett and Sherlock, 1996; Godwin and Robinson, 1996; Robinson et al., 1996; Creswell, 1997; Dishaw, 1998). A collaborative research project between the Myra Falls Operation and CODES, University of Tasmania (1996-2004), provided a revised volcanic facies architecture for the Myra Falls district (Sinclair, 2000), a new district-scale structural framework (Berry, 2000; Jones et al., 2006a), the recognition of sub-seafloor replacement hydrothermal processes in the Battle and Ridge Zone West orebodies (Sinclair, 2000; Jones, 2001; Chong, 2004), and a depositional model for the Caprocks Unit above the Battle and HW orebodies (Jones et al., 2006b). Jones et al (2005) used SWIR spectrometry to identify previously unmapped hydrothermal alteration zones around the Battle and HW

orebodies. More recent research on the Myra Falls VHMS district includes the investigation of possible mechanisms for precious metal enrichment (Marshall et al., 2018) and the temporal relationship of Sicker Group volcanic host rocks and VHMS deposits across Vancouver Island (Ruks and Mortensen, 2007; Ruks et al., 2009; Ruks, 2015).

1.4 Thesis Objectives

While previous studies have focused on the HW, Battle, and Ridge Zone West orebodies, questions regarding the lithostratigraphic architecture and the depositional age of the H-W member remain. The study area provides a geological-link between the Battle and Ridge Zone West orebodies. The key objectives of this thesis are to:

1. Document the lithology and nature of VHMS mineralisation in the West Block Area
2. Propose a geological framework and ore deposit model linking the West Block Area with the Battle and Ridge Zone West orebodies
3. Identify mineralogical and geochemical proximity indicators to sulfide mineralisation
4. Assess the application of systematic portable X-ray fluorescence (pXRF) analysis of drill core to discriminate lithology of altered volcanic rocks
5. Determine the temporal relationship between the H-W and L-M-P members
6. Develop useful criteria for exploration in the Myra Falls VHMS district and elsewhere on Vancouver Island

1.5 Methodology

Fieldwork at Myra Falls was carried out from September-December 2014 and October-December 2015. Access to exploration drill core and underground development were limited post-2015 due to suspended operations. A total of 6,680 metres of drill core from 31 underground diamond drill holes were graphically logged detailing variations in lithology, alteration and sulfide mineralogy, across the West Block Area. Representative samples of lithology, mineralisation and alteration were selected for petrographic analysis and whole-rock geochemistry. Over 900 samples of drill core were selected for SWIR and pXRF analysis at CODES, University of Tasmania. Where necessary, samples were selected from previous studies on Myra Falls from the CODES rock catalogue. Detailed methodologies and sample descriptions are provided for each study in the relevant chapter with additional information documented in appendices.

1.6 Thesis framework

This introductory chapter is followed by a synthesis of the regional geological setting of the North American Cordillera with an emphasis on the VHMS metallogeny of the Insular Terranes (Chapter 2). Chapter 3, "Geology of the Myra Falls District" describes the sedimentary and volcanic lithofacies at Myra Falls, summarises the structural history, and documents the distribution and nature of the VHMS deposits within the district. Chapter 4 documents the geology, mineralisation and alteration of the West Block Area. Proximity to sulfide mineralisation indicators are evaluated in Chapter 5 using mineral and whole-rock chemistry from samples of the Price Formation footwall alteration zone. Chapter 6 presents the successful application of systematic, pXRF analysis of unprepared drill core samples to discriminate protolith of altered volcanic rocks at Myra Falls (*published in 2018 in the Journal of*

Geochemical Exploration, v. 193, p. 1-21). The episodic nature of felsic volcanism is investigated in Chapter 7 using zircon U-Pb geochronology. New, high precision CA-ID-TIMS age constraints are reported for the H-W member, and for the first time the L-M-P member is chronologically constrained using LA-ICPMS analysis. Chapter 8 provides a succinct interpretation of the lithostratigraphic architecture and genesis of the West Block Area and the surrounding H-W member VHMS deposits. Furthermore, new mineral exploration criteria are discussed for both the deposit-scale and within a regional context. In conclusion, Chapter 9 summarises the key findings of the thesis and provides suggestions for future work.

Chapter 2:

Regional Geology

Vancouver Island is located off the west coast of British Columbia, Canada (Figure 2.1). The Myra Falls VHMS deposit is located in the south-central part of Vancouver Island within the western margin of the North American Cordillera (Figure 2.1). This chapter provides an overview of the tectonostratigraphic framework of the North American Cordillera and the VHMS metallogeny of the Insular Terranes. In addition, the regional geological setting, stratigraphy, metamorphism, and structure of Vancouver Island are reviewed.

2.1 North American Cordillera

The North American Cordillera is the product of prolonged convergent margin activity since the Late Devonian. The Cordillera was constructed during five first-order tectonic events that are recorded in distinct tectonostratigraphic sequences, which are not necessarily limited to fault-bounded crustal blocks (Colpron et al., 2007). The following summary of the first order tectonic entities of the North American Cordillera is after Colpron et al. (2007):

1. Ancestral North America (Laurentia), which comprises rock units located in the Yukon-Tanana upland, Alaska Range and south-eastern British Columbia (Figure 2.1). These units are dominated by marine sedimentary sequences deposited along the Proterozoic-Triassic western Laurentian continental margin.

2. The Intermontane Terranes, which are located west of Laurentia and underlie most of British Columbia, Yukon, and Alaska (Figure 2.1). These allochthonous marginal pericratonic terranes comprise Paleozoic to Mesozoic intrusive, volcanic, sedimentary, and metamorphic rocks that represent magmatic arcs, microcontinents and oceanic basins that were accreted onto western Laurentia in the Early Mesozoic.

3. The Northern Alaska Terranes, located to the west of the Intermontane Terranes in Alaska (Figure 2.1).

4. The Insular Terranes consisting of oceanic and continental accretionary complexes that form a present-day contiguous belt of rocks that underlie portions of southwest to southeast Alaska, south-eastern corner of Yukon and western British Columbia (Figure 2.1). These

exotic terranes have diverse formation histories with variable crustal provenance links to the Appalachian, Caledonian and Baltica continental systems (Nelson and Colpron, 2007).

5. The Late Accreted Terranes in southwest British Columbia and Alaska (Figure 2.1) which comprises Mesozoic and younger arc and accretionary complexes that form the western and southern fringes to the older tectonostratigraphic elements.

2.1.1 Insular Terranes

The Insular Terranes include the Peninsular Terrane (Plafker et al., 1989), the Windy-McKinley Terrane (Jones et al., 1984), and the Alexander and Wrangellia Terranes (Monger et al., 1982). The Insular Terranes differ from the Intermontane Terranes in that their faunal records, detrital zircon age patterns, zircon Hf isotope signatures, and paleomagnetic latitudes indicate no direct pre-Carboniferous crustal provenance to the western margin of Laurentia (e.g., Colpron and Nelson, 2009; Beranek et al., 2013; Beranek et al., 2014; Israel et al., 2014).

Together the Peninsular, Windy-McKinley, Alexander and Wrangellia Terranes form a regional belt of accreted arc-related rocks from south-western Alaska to southern British Columbia (Figure 2.1). These terranes record the episodic formation of arc-related and continental platform crust from the Neoproterozoic (Alexander Terrane: Gehrels, 1990; Oliver et al., 2011) to the Jurassic (Wrangellia Terrane: e.g., Nixon and Orr, 2007).

The Peninsular Terrane extends over 1,200 km from the Alaskan Peninsula to south-central Alaska (Figure 2.1). The terrane mostly consists of Triassic and Jurassic magmatic rocks (Rioux et al., 2007), Jurassic to Cretaceous shallow-marine turbidites and minor arc-related volcanic rocks (McClelland et al., 1992). Permian arc-related volcanic, volcaniclastic, and carbonate rocks characterise the known basement of the terrane (Plafker et al., 1989; Blodgett and Stralla, 2006), which is inferred to be underlain by Late Paleozoic igneous rocks similar to those of the Alexander and Wrangellia Terranes (Blodgett and Stralla, 2006; Bacon et al., 2012).

The Windy-McKinley Terrane straddles the Alaska-Yukon border northeast of the Denali Fault (Figure 2.1; Jones et al., 1984). In Alaska the terrane comprises Mississippian-Pennsylvanian shallow-marine siliciclastic rocks, several Middle Devonian carbonate units, and rare gabbro and diorite intrusions (Richter, 1976; Gordey et al., 1991). In Yukon the terrane is characterised by argillite and mafic lavas that are intruded by ca. 229 Ma gabbro intrusions (Templeman-Kluit, 1974; Gordey et al., 1991; Mortensen and Israel, 2006). Argillite detrital zircon age populations suggest an affiliation with the Alexander Terrane (Mortensen and Israel, 2006).

The Alexander and Wrangellia Terranes comprise two of the largest terranes in the North American Cordillera (Figure 2.1). They both record multiple episodes of oceanic island arc volcanism and sedimentation (Samson et al., 1989; Samson et al., 1991), and host a number of volcanic-hosted massive sulfide (VHMS) deposits. In the Alexander Terrane, the most notable VHMS deposits are the Neoproterozoic past producing Niblack and Khayyam deposits; Ordovician-Silurian Moira Copper, Nicholas Bay, and Barrier Islands occurrences and deposits; and the Triassic Greens Creek and Windy Craggy deposits (Table 2.1; Figure 2.1). The Wrangellia Terrane contains the Late Devonian Myra Falls mine and the Lenora, Lara, and Jane deposits; and the Pennsylvanian Bedingfield and Dragon occurrences (Table 2.1; Figure 2.1).

2.1.2 Geology of the Alexander Terrane

The Alexander Terrane extends over 1,000 km from western British Columbia to south-eastern Alaska (Figure 2.1) and represents assimilation of different coeval tectonic environments to form a composite terrane (Colpron and Nelson, 2009). Neoproterozoic to early Paleozoic arc-related rocks of the Craig subterrane dominate the southern region of the Alexander Terrane in Alaska (Berg et al., 1978; Gehrels and Saleeby, 1987; Gehrels, 1990; Gehrels et al., 1996). Whereas, Proterozoic to early Paleozoic continental platform sequences of the Admiralty Subterrane are dominant in the northern part of the terrane in British Columbia (Mihalynuk et al., 1992).

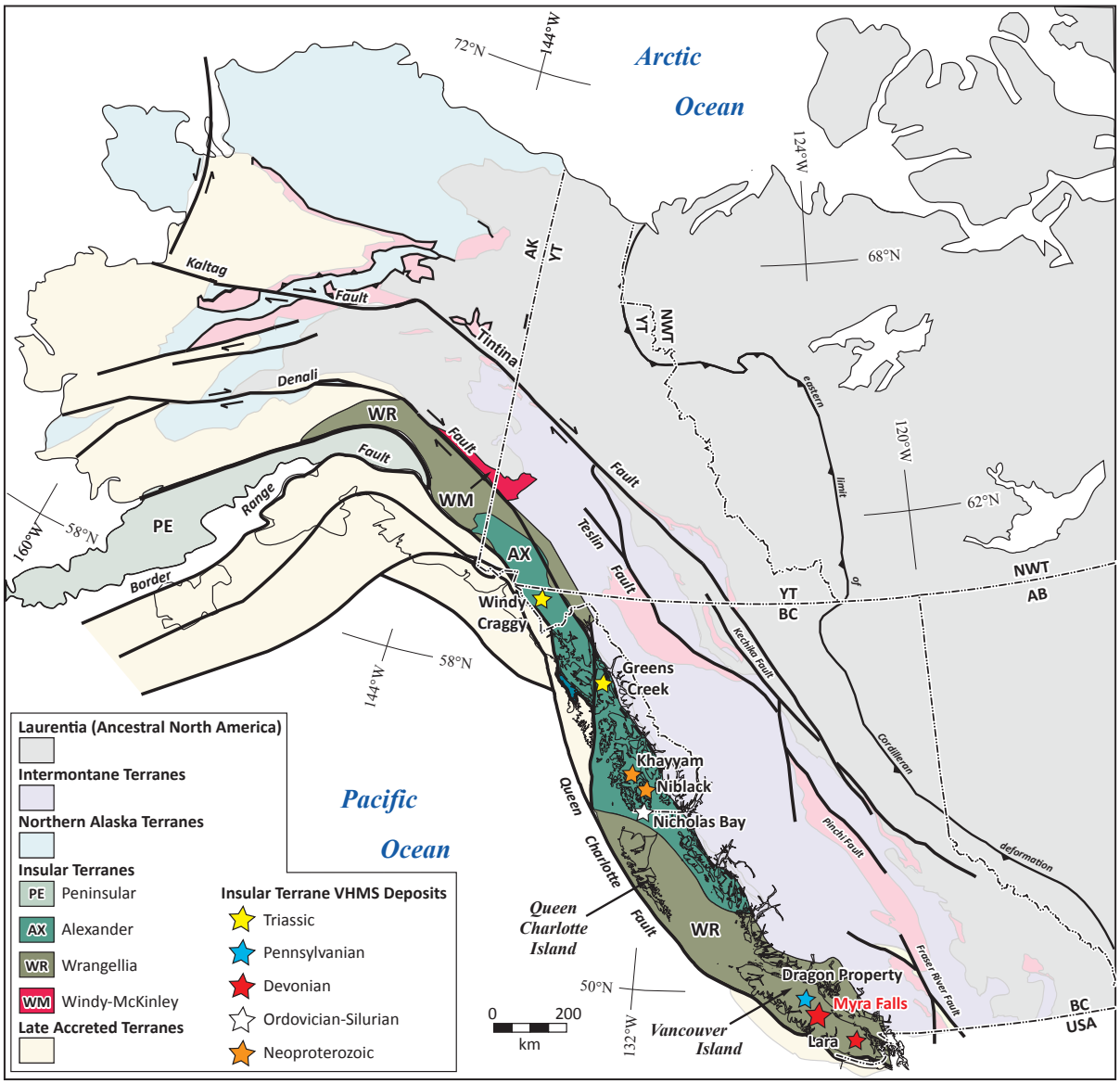

Figure 2.1 Thematic map of the first-order tectonic entities that comprise the North American Cordillera (modified from Nelson and Colpron, 2007). The Insular Terrane is subdivided into four terranes. Multiple episodes of VHMS mineralisation are present throughout the Wrangellia and Alexander Terranes, including Myra Falls on south-central Vancouver Island.

Multiple lines of evidence suggest a link to the Appalachian/Caledonian or Baltica systems for the Alexander Terrane rather than Laurentia. These include pre-Early Ordovician deformation of Late Neoproterozoic rocks (Wales Orogeny; Gehrels et al., 1996). Ordovician to Silurian arc magmatism and Silurian-Devonian deformation of the Klakas Orogeny, are

coincident with magmatism and deformation in the Canadian Appalachians and Caledonides (Bazard et al., 1995). Paleomagnetic latitudes coupled with detrital zircon U-Pb age populations and Hf isotope geochemistry from Lower Devonian sedimentary rocks indicate a crustal provenance of NE Baltica for the Alexander Terrane (Bazard et al., 1995; Soja and Antoshkina, 1997; Colpron and Nelson, 2009; Beranek et al., 2013).

2.1.3 Geology of the Wrangellia Terrane

The Wrangellia Terrane extends over 2,500 km from Vancouver Island and the north-western United States (southern Wrangellia Terrane) to eastern Alaska and Yukon (northern Wrangellia Terrane; Figure 2.1) and comprises Devonian to Early Permian arc and back-arc rocks (Jones et al., 1977; Nelson and Colpron, 2007; Ruks, 2015). The Paleozoic stratigraphy of southern Wrangellia is characterised by Late Devonian to Permian volcanic, volcaniclastic, siliciclastic, and carbonate rocks of the Sicker and Buttle Lake Groups (Massey, 1995; Yorath et al., 1999). Unconformably overlying the Paleozoic stratigraphy are Middle Triassic marine shales and Upper Triassic submarine basalt flow and carbonate rocks of the Vancouver Group (Nixon and Orr, 2007). The oldest exposed rocks of northern Wrangellia are Mississippian to Pennsylvanian arc-related volcanic and volcaniclastic rocks of the Station Creek Formation (Colpron and Nelson, 2009; Beranek et al., 2014). The Station Creek Formation is conformably overlain by Permian shallow-marine siliciclastic rocks and carbonates of the Skolai Group (Smith and MacKevett, 1970; Read and Monger, 1976; Israel et al., 2014). The Skolai Group volcanic arc is unconformably overlain by Middle Triassic marine sedimentary rocks, Upper Triassic subaerial basalt flows of the Nikolai Formation, and Late Triassic calcareous to carbonaceous turbidites (Greene, 2010).

Several lines of evidence support a tectonic and stratigraphic link between the Wrangellia and Alexander Terranes in the Paleozoic. For example, the ca. 309 Ma Barnard Glacier pluton intrudes mid-Paleozoic metamorphic rocks of the Alexander Terrane (Gardner et al., 1988), and Pennsylvanian Skolai Group strata. These relationships signify that the Alexander and Wrangellia Terranes were contiguous by the Pennsylvanian (Gardner et al., 1988; Van Staal et al., 2010) and that the late Paleozoic volcanic arc that underlies northern Wrangellia either formed upon, or at least was anchored to, older Alexander basement (Colpron and Nelson, 2009). Israel et al. (2014) argued that the Wrangellia and Alexander Terranes were linked as early as the Late Devonian based on non-arc related ca. 363 Ma gabbro intrusions present in both terranes. There is no evidence suggesting a tectonic or stratigraphic link between the post-Middle Pennsylvanian combined Alexander and Wrangellia Terranes (Insular Superterrane) with the Laurentian margin prior to the mid-Jurassic (Nelson and Colpron, 2007).

2.1.4 Insular Superterrane accretionary history

Accretion of the Insular Superterrane began along the northern Laurentian margin in the Late Jurassic and was completed by the Early Cretaceous along southern Laurentia. Late Jurassic regional structures (Saleeby, 2000) and Middle Jurassic (ca. 177-168 Ma) and Upper Jurassic-Lower Cretaceous strata of the Gravina belt overlie both terranes in south-eastern Alaska (McClelland et al., 1992; Gehrels and Berg, 1994). These structural and stratigraphic relationships record the initial accretion of the Insular Superterrane with the northern Laurentian margin (Nelson and Colpron, 2007). The collision between the Insular Superterrane and Intermontane Terranes in south-western British Columbia, is recorded by ca. 160-155 Ma intrusions, and the ductile deformation and metamorphism of the Coast Mountains (Van der Heyden, 1992). The

Table 2.1 Summary of notable VHMS deposits, prospects and showing of the Alexander and Wrangellia Terranes.

Name	Location	Terrane	Age	Type	Principal metals	Size (Mt)	Cu (%)	Zn (%)	Pb (%)	Au (g/t)	Ag (g/t)	Major reference
† Lookout	Alaska, USA	AX	Neoproterozoic	deposit	Cu, Zn, Ag, Au	5.64	0.95	1.73	-	1.7	29.5	Nowak et al. (2011)
◊ Khayyam	Alaska, USA	AX	Neoproterozoic	prospect	Cu, Zn, Ag, Au	0.07	1.7	0.93	-	2.1	10.6	Mosier et al. (2009)
Nichols Bay	Alaska, USA	AX	Ordovician-Silurian	showing	Zn, Ag							
Moira Copper	Alaska, USA	AX	Ordovician-Silurian	showing	Cu, Ag, Au	Sulfide mineralisation occurrences variably worked in the early 1900s, hosted in Ordovician-Silurian submarine volcanic rocks						Maas et al. (1995) Slack et al. (2005)
Barrier Islands	Alaska, USA	AX	Ordovician-Silurian	showing	Zn, Pb ± Ag							
† Windy Craggy	British Columbia, CA	AX	Triassic	deposit	Cu, Co, Au, Ag	297.4	1.4	-	-	0.2	3.8	Peter and Scott (1999)
◊ Greens Creek	Alaska, USA	AX	Triassic	deposit	Zn, Pb, Au, Ag	24.2	0.37	13.9	5.1	5.14	658.3	Steeves et al. (2016)
† Palmer	Alaska, USA	AX	Triassic	prospect	Cu, Zn, Au, Ag	8.13	1.41	5.25	-	0.32	31.7	www.constantinemetals.com
◊Myra Falls (LMP & HW)	British Columbia, CA	WR	Devonian	deposit	Zn, Cu, Pb, Au, Ag	30	1.6	5.5	0.6	2	54	Sawyer per. com. (2016)
◊ Lara	British Columbia, CA	WR	Devonian	prospect	Zn, Cu, Au, Ag	1.87	1	2.74	0.53	1.94	32.98	Mosier et al. (2009)
◊ Lenora	British Columbia, CA	WR	Devonian	prospect	Zn, Cu, Au, Ag	0.6	2.37	3.84	0.37	4.2	117	Mosier et al. (2009)
◊ Jane	British Columbia, CA	WR	Devonian	showing	Zn, Cu	Sulfide mineralisation occurrences variably worked in the 1900s, minor diamond-drilling in the 1980s, mineralised surface sample 16.1% Zn and 0.05% Cu						MINFILE # 092B-084
Falls and North	British Columbia, CA	WR	Pennsylvanian	showing	Zn, Pb, Au, Ag	Semi-massive sulfide occurrences with minor diamond-drilling in the 1990s, assay results up to 7.33% Zn, 1.34% Pb and 19.2 g/t Ag over 2 metre thickness						Jones (1997)
Bedingfield Area	British Columbia, CA	WR	Pennsylvanian	showing	Zn, Pb, Au, Ag	Multiple sulfide showings, geological mapping and sampling programs completed in the 1970s-1980s, mineralised surface sample 2.04% Zn, 0.16% Pb, 15.7 g/t Ag, 0.31 g/t Au						MINFILE #s 092F-227; 092F-228; 092-498; 092F-499; 092F-500

† resource estimate
◊ historic production

overlapping Early Cretaceous strata of the Gambier Assemblage provide an upper age limit on the time of accretion between the Insular Superterrane and the southern Laurentian margin (Gabrielse et al., 1991).

2.2 Geology of Vancouver Island

Vancouver Island is 406 km in length and 130 km in width and is principally characterised by Middle Paleozoic to Early Mesozoic rocks of the Wrangellia Terrane (Figure 2.2; Jones et al., 1977, Greene et al., 2008). Here the Wrangellia Terrane is locally intruded by the Cretaceous Coast Plutonic Complex in the east, and is in fault contact with the Pacific Rim Terrane and West Coast Crystalline Complex in the west (Wheeler and McFeely, 1991). Seismic surveys suggest that the crust beneath Vancouver Island consists of mafic plutonic rocks to a depth of 30 km and is underlain by an interpreted major shear zone (Welford et al., 2001). The Wrangellia Terrane on Vancouver Island consists of three volcano-sedimentary packages: (1) the Paleozoic Sicker and Buttle Lake Groups; (2) the Triassic Vancouver Group; and (3) the Jurassic Bonanza Group (Figure 2.2B; Muller, 1980; Yorath et al., 1999; Nixon and Orr, 2007). The Myra Falls VHMS deposits occur in the Late Devonian felsic volcanic stratigraphy of the Sicker Group. As such, a detailed overview of the Devonian to Carboniferous stratigraphy on Vancouver Island is provided below.

2.2.1 Paleozoic Sicker and Buttle Lake Groups

The Paleozoic Sicker Group on southern and central Vancouver Island are the oldest identified rock units in the Wrangellia Terrane (Figure 2.3). These units are exposed in the northwest trending, Buttle Lake, Cowichan Lake, Nanoose, and Bedingfield regional uplifts (Figure 2.2B; Muller, 1980; England and Calon, 1991; Yorath et al., 1999). The Sicker and Buttle Lake Groups record the development of a Late Devonian to Early Permian oceanic island arc and back arc complex. Multiple episodes of submarine felsic volcanism are present throughout the Paleozoic stratigraphy and are host to several associated VHMS deposits (Figure 2.2A). The type sections of Paleozoic stratigraphy on Vancouver Island occur in the Buttle Lake and Cowichan Lake uplifts. The stratigraphic nomenclature has been evolving since the early 1900s (Clapp, 1912; Gunning, 1931). Figure 2.4 presents a summary of the current stratigraphic nomenclature of the Sicker and Buttle Lake Groups on Vancouver Island.

2.2.1.1 Buttle Lake uplift

The Buttle Lake uplift hosts the Myra Falls VHMS district (Figure 2.2A; Table 2.1). The Paleozoic stratigraphy in the Buttle Lake uplift on central Vancouver Island was first described in detail by Juras (1987). Here the Sicker Group is subdivided into four formations: (1) Late Devonian Price; (2) Late Devonian and VHMS-hosting Myra; (3) Early Mississippian Thelwood; and (4) Middle Mississippian to Pennsylvanian Flower Ridge (Figure 2.3).

The Price Formation rocks are the oldest in the Buttle Lake uplift and comprise pyroxene and feldspar-phyric, amygdaloidal, basaltic-andesitic lavas and breccia (Juras, 1987). The Price Formation is overlain by felsic to intermediate volcanic and volcano-sedimentary rocks of the Myra Formation. The Myra Falls VHMS deposits are hosted in the felsic volcanic stratigraphy of the Myra Formation. The Thelwood Formation locally unconformably overlies the Myra Formation and is characterised by siliceous tuffaceous sediments, submarine pyroclastic and volcaniclastic deposits, and mafic sills (Juras, 1987). Conformably overlying the Thelwood Formation are basaltic volcaniclastic rocks and minor basalt flows, and associated volcano-

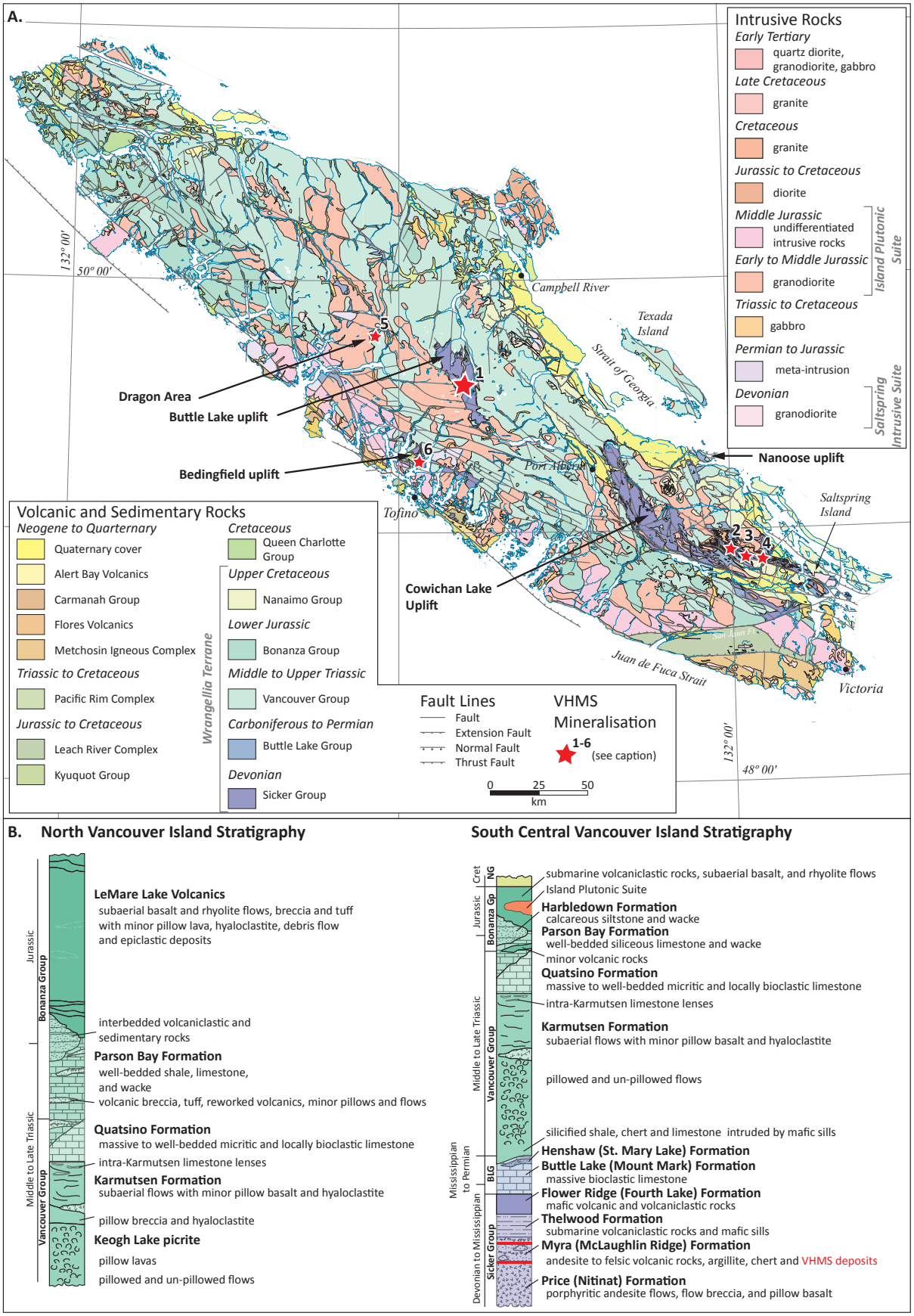

Figure 2.2 A. Geology map of Vancouver Island (Massey et al., 2005). VHMS mineralisation: 1=Myra Falls deposit, 2=Lara deposit, 3=Lenora deposit, 4=Jane deposit, 5=Dragon occurrences, and 6=Bedingfield occurrence. B. Regional stratigraphy of Vancouver Island. Column for northern Vancouver Island modified from Nixon and Orr (2007) and Greene et al. (2008). Column for south-central Vancouver Island modified from Juras (1987), Yorath et al. (1999) and Greene et al. (2008). [Cret, Cretaceous; NG, Nanaimo Group; BLG, Battle Lake Group]

sedimentary rocks of the Flower Ridge Formation (Juras, 1987). The Buttle Lake Group conformably overlies the Sicker Group (Yole, 1969) and is characterised by crinoid-bearing limestone of the Buttle Lake Formation and siliceous-calcareous epiclastic rocks of the Henshaw Formation (Figure 2.3; Yole, 1969; Jeffery, 1970; Brandon et al., 1986).

2.2.1.2 Cowichan Lake uplift

The Cowichan Lake Uplift is host to multiple VHMS deposits (Figure 2.2A; Table 2.1). Here the Sicker Group consists of four formations (Yorath et al., 1999): (1) Late Devonian Duck Lake; (2) Late Devonian Nitinat; (3) Late Devonian and VHMS-hosting McLaughlin Ridge; and (4) Early Mississippian Fourth Lake (Figure 2.3).

The oldest rocks present in the Cowichan Lake uplift are pillowed basalt, basaltic-andesite, and less abundant dacite to rhyolite flows and breccias of the Duck Lake Formation (Figure 2.3; Massey and Friday, 1987; Massey et al., 1991; Yorath et al., 1999). The overlying Nitinat Formation is in apparent conformable contact with the Duck Lake Formation, and consists of alternating intercalated lenses of agglomerate with minor-pillowed to massive mafic flows, and interbedded volcano-sedimentary beds (Yorath et al., 1999). The McLaughlin Ridge Formation conformably and gradationally overlies the Nitinat Formation and is characterised by cyclic felsic to intermediate volcaniclastic rocks with minor argillite and chert (Yorath et al., 1999). The Lenora, Lara and Jane VHMS deposits are hosted in felsic volcanic rocks of the McLaughlin Ridge Formation. The Fourth Lake Formation comprises shallow-marine rock types including siliceous argillite, shale, chert, bioclastic limestone, intermediate volcanic sandstone, and conglomerate (Yorath et al., 1999).

In the Alberni and Horne Lake areas (Figure 2.2A) the Fourth Lake Formation conformably overlies the McLaughlin Ridge Formation, however, this contact is unconformable elsewhere in the Cowichan Lake area (Massey and Friday, 1987; Massey et al., 1991; Yorath et al., 1999). Yorath et al. (1999) categorised the Fourth Lake Formation as the lowermost unit of the Buttle Lake Group, however, the lowermost Fourth Lake Formation could be a regional correlate to the Thelwood Formation of the Sicker Group (Figure 2.3; Muller, 1980; Jones, 2001; Ruks, 2015).

The Fourth Lake Formation is conformably overlain by the crinoid-bearing limestone Mount Mark Formation of the Buttle Lake Group (Figure 2.3; Yorath et al., 1999). The Mount Mark Formation is likely a regional correlate with the Buttle Lake Formation limestone (e.g., Juras, 1987). Shallow-marine epiclastic rocks of the St. Mary Lake Formation represent the uppermost stratigraphic unit of the Buttle Lake Group in the Cowichan Lake area (Yorath et al., 1999).

2.2.1.3 Nanoose uplift

The oldest exposed Paleozoic stratigraphy in the Nanoose uplift consists of Early Permian turbidites and crinoid-bearing limestones (Yorath et al., 1999; Ruks, 2015). The Early Permian marine volcano-sedimentary rocks correlate with the upper Fourth Lake Formation and limestone of the Mount Mark Formation (Figure 2.3). No VHMS deposits have been identified in the Nanoose uplift.

2.2.1.4 Bedingfield uplift

Paleozoic stratigraphy in the Bedingfield uplift occurs north of Tofino (Figure 2.2A). The stratigraphy is poorly understood in this region with geological descriptions limited to mineral

exploration assessment reports from the late 1980s (Freeze, 1986; Duncan and Ord, 1987). The oldest stratigraphy consists of submarine bimodal volcanic rocks overlain by argillite and chert, and a crinoid-bearing limestone (Freeze, 1986; Ruks et al., 2009). Massey et al. (2005) considered this volcanic rock sequence equivalent to the Late Devonian Sicker Group; however, Ruks (2015) identified a Pennsylvanian age for these rocks (312.2 ±3.7 Ma through 312.4 ±3.5 Ma and 308.3 ±3.2 Ma through 305.6 ±4.1 Ma). Polymetallic VHMS mineralisation of the Bedingfield area comprises a number of stockwork vein and disseminated sulfide occurrences associated with submarine felsic volcaniclastic rocks (Table 2.1; Freeze, 1986; Ruks, 2015).

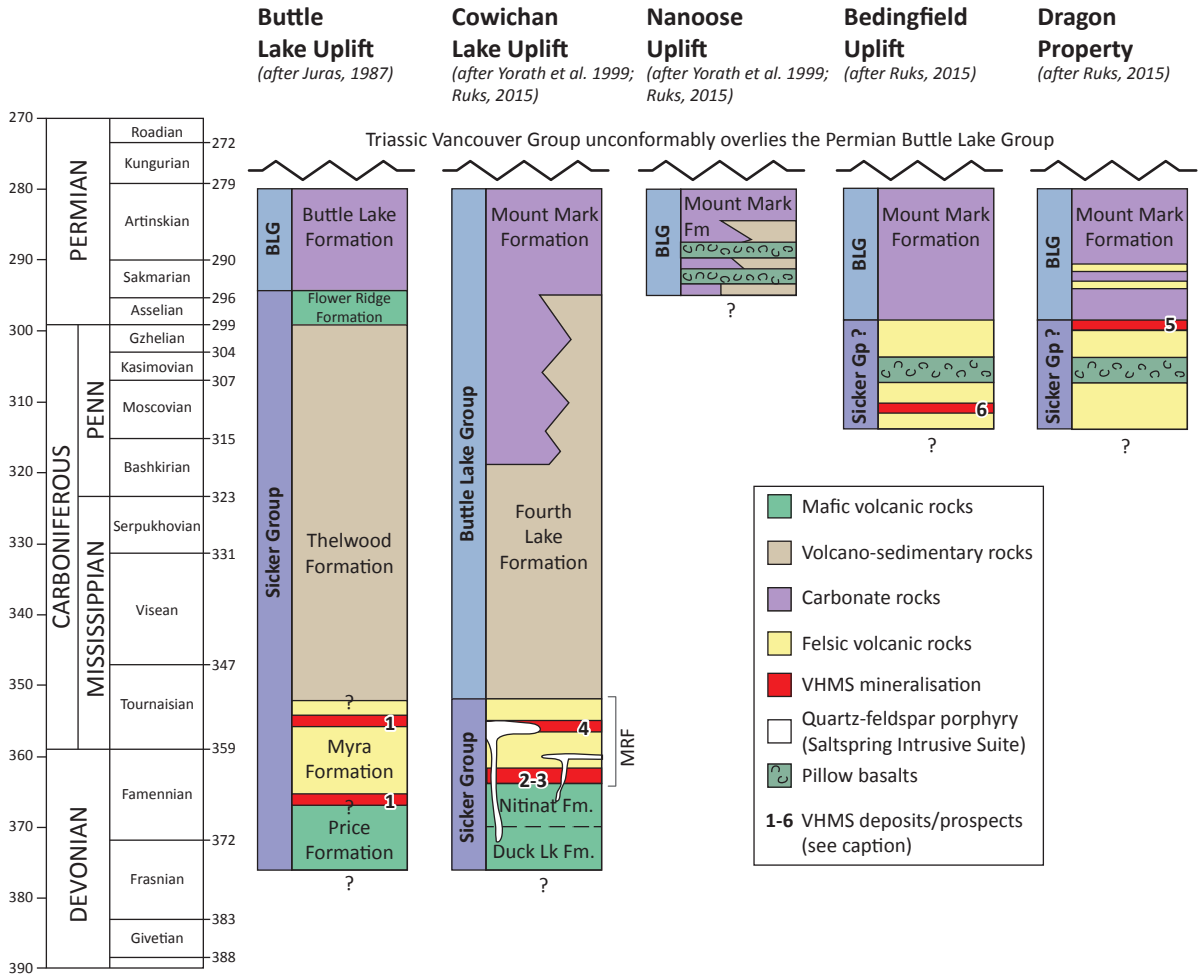

Figure 2.3 Comparative stylised time-stratigraphic columns illustrating the temporal relationships between units comprising Paleozoic Wrangellia on Vancouver Island. VHMS mineralisation: 1=Myra Falls deposit, 2=Lara deposit, 3=Lenora deposit, 4=Jane deposit, 5=Dragon occurrences, and 6=Bedingfield occurrence. Geologic time scale from Walker et al. (2012). [Fm, Formation; Gp, Group; MRF, McLaughlin Ridge Formation; BLG, Buttle Lake Group]

2.2.1.5 Dragon area

The Dragon property is located approximately 80 km west of Campbell River and 65 km northwest of Myra Falls (Figure 2.2A). Initial regional mapping by Muller (1977) documented amphibolite-facies metamorphic rocks belonging to the Sicker Group, the Buttle Lake Group, and the Karmutsen Formation. Here the stratigraphy consists of bimodal volcanic rocks conformably overlain by crinoid-bearing limestone (Kemp and Gill, 1993; Jones, 1997; Ruks et al., 2009). Zircon U-Pb geochronology by Ruks (2015) yielded a Pennsylvanian age (311.1 ±0.3 Ma through 300.0 ±3.4 Ma) for the felsic volcanic rocks, and an age of 291.6 ±2.2 Ma for

the overlying interbedded felsic tuff, chert, and argillite stratigraphy (Figure 2.3). Polymetallic sulfide mineralisation of the Falls and North VHMS occurrences are associated with rhyolite-andesite coherent and volcaniclastic rocks in the Dragon area (Table 2.1; Jones, 1997; Ruks et al., 2009).

2.2.2 Middle to Upper Triassic Vancouver Group

The base of the Vancouver Group comprises a thick succession of flood basalt that include submarine, volcaniclastic, and subaerial flows of the Karmutsen Formation (Figure 2.2B; Jones et al., 1977). The Karmutsen Formation represents a massive emergent oceanic plateau ca. 230-225 million years ago, and is overlain by shallow-marine platform carbonates of the Quatsino Formation, as well as deeper-marine siliceous, carbonaceous, and calcareous rocks with minor mafic-intermediate volcaniclastic rocks of the Parson Bay Formation (Nixon et al., 2006; Nixon and Orr, 2007).

2.2.3 Lower Jurassic Bonanza Group

The Late Triassic to Middle Jurassic Bonanza Group includes the Parson Bay Formation, an informal "volcaniclastic-sedimentary unit", and the LeMare Lake Volcanics (Figure 2.2B; Nixon and Orr, 2007). The Bonanza Group embodies a thick package of volcanic and epiclastic rocks related to the formation and erosion of the Bonanza island arc (Nixon and Orr, 2007). The Parson Bay Formation is characterised by siliciclastic-carbonate rocks intercalated with subordinate mafic to intermediate volcanic flows and volcaniclastic breccias (Nixon and Orr, 2007). The volcaniclastic-sedimentary unit is a succession of laminated to thickly bedded wacke interbedded with polylithic volcaniclastic rocks. Nixon and Orr (2007) interpreted the volcaniclastic-sedimentary unit to represent a transition between a marine succession of the Parson Bay Formation and conformable, subaerial volcanic sequence at the base of the LeMare Lake Volcanics. The LeMare Lake Volcanics are characterised by regionally extensive, subaerial basaltic to rhyolitic flows and associated volcaniclastic deposits, and is unconformably overlain by Cretaceous clastic rocks (Nixon and Orr, 2007).

2.2.4 Post accretionary stratigraphy

Cretaceous and younger, post-accretionary rocks on Vancouver Island formed after the accretion of the Insular Superterrane onto the Laurentian margin. The Lower Cretaceous Kyuquot Group is characterised by a shallow-marine clastic wedge of conglomerate, sandstone, and siltstone that unconformably overlies the Bonanza Group (Muller et al., 1981; Yorath, 1991). The mid-Cretaceous Coal Harbour Group occurs on northern Vancouver Island, and comprises a coarse arenite unit composed of sandstone, shale, minor limestone, conglomerate, and coal (Jeletzky, 1976). The Coal Harbour Group likely represents post-orogenic continental sedimentation during the uplift and erosion of the Wrangellia Terrane (Yorath, 1991). The Upper Cretaceous Nanaimo Group comprises a succession of siliciclastic rocks, which underlies the coastal plain of southeast and south-central Vancouver Island and nearby gulf islands. On its western margin, the Nanaimo Group unconformably overlies the Wrangellia Terrane (Figure 2.2A; Muller and Jeletzky, 1970). The Nanaimo Group consists of a >4 km-thick succession of marine and minor subaerial siliciclastic rocks, which were deposited in a single basin between ca. 93-66 Ma (e.g., Katnick and Mustard, 2003).

During the Tertiary, the Pacific Rim and Crescent Terranes were accreted onto Vancouver Island (Figure 2.2A; Nelson and Colpron, 2007). The Pacific Rim Terrane, located on the western

and southern regions of Vancouver Island, comprises three units. Triassic volcanic arc rocks unconformably overlain by a Jurassic-Cretaceous marine mélange of the Pacific Rim Complex (Brandon, 1989); blueschist facies metamorphosed volcanic arc rocks of the Late Jurassic to Early Cretaceous Pandora Peak unit (Rusmore and Cowan, 1985); and variably deformed meta-sedimentary and -igneous rocks of the Cretaceous Leech River Complex (Fairchild and Cowan, 1982; Rusmore and Cowan, 1985). The Eocene Crescent Terrane, located on southernmost Vancouver Island, comprises the Metchosin Igneous Complex and the Crescent Formation, which are inferred to represent an ophiolite sequence that was obducted during the Late Eocene (Massey, 1986; Yorath, 1991; Groome et al., 2003). The San Juan Fault marks the boundary between the Pacific Rim and Wrangellia Terranes (Figure 2.2A). On the western side of Vancouver Island, the San Juan Fault is overlain by undeformed sandstone and conglomerate of the latest Early Eocene to Oligocene Carmanah Group, which suggests that the Pacific Rim, Crescent, and Wrangellia Terranes were contiguous before 35 Ma (Canil et al., 2010).

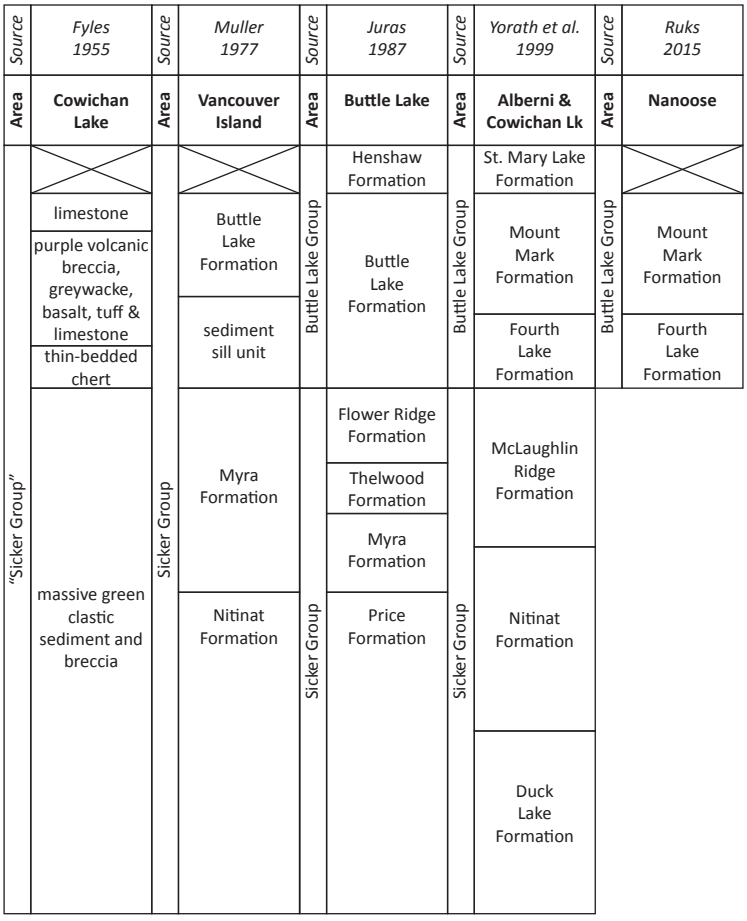

Figure 2.4 Development of stratigraphic nomenclature for the Sicker and Buttle Lake Groups, Vancouver Island, British Columbia (modified from Yorath et al., 1999). In this thesis the stratigraphic nomenclature of Juras (1987) will be used for the Myra Falls area.

2.2.5 Deformation history

The Wrangellia Terrane on Vancouver Island has experienced multiple regional deformation events from the Late Devonian to Eocene. Prior to its collision with the Laurentian margin, multiple stages of deformation in the Wrangellia Terrane produced large-scale open folds and W- to NW-trending asymmetrical folds (Muller, 1980; Massey, 1992; Yorath et al., 1999; Jones et al., 2006a). Post-Jurassic tectonism in the Wrangellia Terrane resulted in Cretaceous

transpression and Eocene extension (Muller, 1980; Nixon and Orr, 2007). These regional-scale events formed NW-SE, antiformal structures that expose Paleozoic basement of the Wrangellia Terrane (England and Calon, 1991; Massey, 1992; Nixon et al., 1994; Yorath et al., 1999; Jones et al., 2006a). These anticlinorial structures record the collision of Wrangellia Terrane with the Laurentian margin resulting in regional-scale warping. They are colloquially referred to as regional uplifts and include the Cowichan Lake, Buttle Lake, Nanoose, and Bedingfield uplifts (Figure 2.2A).

During the Middle Cretaceous, N-S compression produced strike-slip faults and minor thrust faults, followed by extension in the Late Cretaceous, which produced normal faults and the formation of the Nanaimo Basin (Muller, 1980; England and Calon, 1991; Massey, 1992; Nixon et al., 1994; Jones et al., 2006a). On the eastern side of Vancouver Island, a series of SW-verging folds and NW-trending faults affected all pre-Late Cretaceous rocks and are collectively referred to as the Cowichan Fold and Thrust Belt (Muller, 1980; England and Calon, 1991; Massey, 1992; Nixon et al., 1994; Yorath et al., 1999). These structures are the result of accretion of the outboard Pacific Rim and Crescent Terranes during the Eocene (e.g., Johnston and Acton, 2003). Post-Eocene extension resulted in the opening of the present day Queen Charlotte Basin (Figure 2.1A), located between Vancouver Island and the Queen Charlotte Islands (Massey, 1992; Nixon et al., 1994; Yorath et al., 1999; Jones et al., 2006a).

2.2.6 Regional metamorphism

Regional metamorphism on Vancouver Island is generally characterised by zeolite to lower greenschist facies conditions. Regional lower greenschist facies conditions characterise the Paleozoic Sicker Group (Juras, 1987). Whereas the Triassic Vancouver Group rocks are characterised by zeolite to prehnite-pumpellyite facies metamorphism (Brandon, 1989; Greenwood et al., 1991). The emplacement of the Jurassic Island Intrusive Suite plutons has produced isolated amphibolite facies metamorphism of the Sicker and Vancouver Groups (Juras, 1987; Greenwood et al., 1991; Massey, 1992). Post-Jurassic stratigraphy on Vancouver Island is affected by zeolite facies metamorphism related to post-deposition burial (Greenwood et al., 1991; Massey, 1992). Metamorphosed conodonts from the Permian Buttle Lake Group and Upper Triassic Parson Bay Formation, suggest a post-Permian and pre-Late Triassic age for the regional greenschist metamorphism of the Sicker Group (Brandon, 1989).

2.3 Summary

- The North American Cordillera consists of five first-order tectonic entities that are defined by their distinct tectonostratigraphic records.
- The geology of Vancouver Island principally consists of mid-Paleozoic to Early Mesozoic Wrangellia stratigraphy of the Insular Terrane.
- The Wrangellia Terrane on Vancouver Island is comprised of the Paleozoic Sicker and Buttle Lake Groups, the Upper Triassic Vancouver Group, and the Lower Jurassic Bonanza Group.
- The Paleozoic Sicker Group represents the oldest rocks identified in the Wrangellia Terrane and are exposed in a number of northwest trending uplifts on Vancouver Island.
- Regional lower greenschist facies metamorphism of Paleozoic stratigraphy is common with local amphibolite facies (e.g., the Dragon area).

- The Sicker and Buttle Lake Groups record the evolution of a Late Devonian through Early Permian island arc and arc-back arc complex.
- Devonian and Pennsylvanian submarine felsic volcanism of the Sicker Group hosts a number of polymetallic VHMS systems, including the Myra Falls deposits, on Vancouver Island.

Chapter 3:

Myra Falls Geology

Volcanic-hosted massive sulfide (VHMS) deposits encompass base metal sulfide deposits which occur in a host sequence dominated by submarine volcanic rocks (Solomon, 1976; Franklin et al., 1981; Lydon, 1984; Large, 1992). Ancient VHMS deposits are characterised by accumulations of sulfide minerals that precipitated at or near the paleo-seafloor in spatial, temporal, and genetic association with contemporaneous volcanism (Franklin et al., 2005). The volcanic strata of the Late Devonian Sicker Group host the Myra Falls polymetallic VHMS deposits (Figure 3.1). This chapter provides a geologic overview of the Myra Falls VHMS district, specifically the local stratigraphy, structure, and a summary of the VHMS orebodies.

3.1 Myra Falls Stratigraphy

The local stratigraphy at Myra Falls was first described by Juras (1987) with subsequent studies on various aspects of the host rocks to VHMS mineralisation carried out by Barrett and Sherlock (1996), Robinson et al. (1996), Sinclair (2000), Jones (2001), Chong (2004), and Jones et al. (2006b). The seminal work of Juras (1987) produced the stratigraphic framework, which is reviewed here, while the work of Sinclair (2000) was the first synthesis of the Myra Formation volcanic lithofacies across the Myra Falls VHMS district. Late Devonian through Carboniferous submarine volcanic and sedimentary rocks of the Sicker Group dominates the stratigraphy present at Myra Falls. The Sicker Group comprises four subdivisions, from oldest to youngest, the Price Formation, Myra Formation, Thelwood Formation, and the Flower Ridge Formation (Muller, 1980; Juras, 1987; Yorath et al., 1999). The following review and revision of the Myra Falls stratigraphy was produced from a literature review.

3.1.1 Price Formation

The Price Formation consists of pyroxene and feldspar-phyric and amygdaloidal basaltic-andesitic lavas and breccia (Juras, 1987) with a minimum thickness of approximately 300 metres (Jones et al., 2006). The apparent conformable transition from mafic to felsic volcano-sedimentary rocks marks the contact with the overlying Myra Formation (Figure 3.2). The Price Formation is the stratigraphic footwall to the H-W member of the Myra Formation. Because the Price Formation has only a limited surface exposure with out crops occurring at the base of the

Price Hillside (Figure 3.1), the majority of observations and descriptions of the Price Formation are from drill core and underground development.

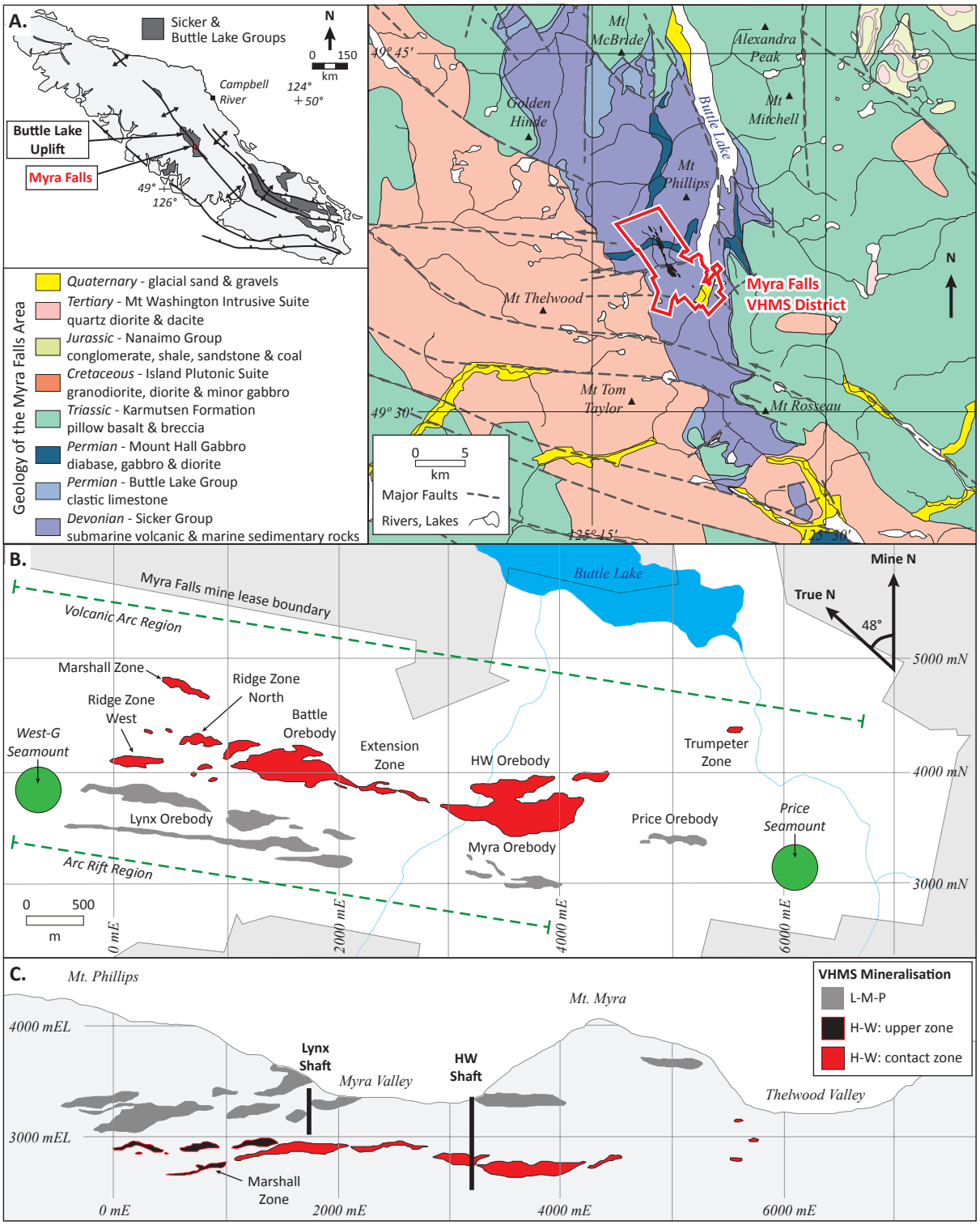

Figure 3.1 A. Geological Map of the Buttle Lake uplift (modified from Geological Survey of Canada information circular, 1995-1997). B. Simplified map showing approximate positions of volcanic source areas from Juras (1987) relative to known ore deposits. C. Schematic cross-section of the Myra Falls VHMS district.

3.1.2 Myra Formation

The Myra Formation is a complex sequence of basaltic to rhyolitic, volcaniclastic deposits and lesser coherent lavas that fill a NW-trending basin in the Myra Falls VHMS district. The Myra Formation is characterised by a ≥500-metre thick succession of relatively continuous lithological units in the NW to SE direction, but have rapid NE to SW facies variations (Figure 3.2). Juras (1987) originally divided the Myra Formation into ten informal lithostratigraphic units that were later redescribed by Sinclair (2000) and grouped into six lithofacies.

The volcanic and volcano-sedimentary stratigraphy of the Myra Formation records multiple episodes of submarine volcanism and marine sedimentation from different source regions. Juras (1987) identified four volcanic and volcano-sedimentary source regions on the periphery of a NW-trending basin (Figure 3.1B). These source regions include the NE Volcanic Arc, the Arc Rift, the Price Seamount, and the West-G Seamount. Juras (1987) also recognised that some stratigraphic units are contemporaneous across the district. The reorganisation of the layer cake stratigraphic nomenclature to volcanic lithofacies by Sinclair (2000) allowed for a simplified district scale facies interpretation. This section is a synthesis of all previous lithological observations and follows the proposed lithofacies by Sinclair (2000) to provide an updated description of the facies variations and interpreted depositional environment of the Myra Formation at Myra Falls (Figure 3.2).

Two cycles of bimodal volcanism and marine sedimentation, which occurred in the Myra Falls district are considered to be prospective for VHMS deposits (Juras, 1987; Robinson, 1994). These cycles are defined here as the lower and upper subdivisions of the Myra Formation (Table 3.1; Figure 3.2). A number of submarine coherent volcanic rock types occur in the Myra Formation and are included in the stratigraphic sequences as intercalated units (Table 3.1). The lower Myra Formation consists of the H-W member, Hanging Wall Andesite, and Lower Mixed Volcanics. The HW, Battle, Trumpeter Zone, Extension Zone, Gap, Ridge, and Marshall Zone orebodies are hosted by rhyolitic stratigraphy of the H-W member (Figure 3.1). The upper Myra Formation includes the L-M-P member, Upper Mixed Volcanics, and the Upper Mafic unit. Rhyolitic rocks of the L-M-P member host the Price, Myra, and Lynx orebodies (Figure 3.1). The upper Myra Formation crops out along the Myra Valley and on the Price Hillside (Figure 3.1), where the original sulfide showings were identified in 1917.

3.1.2.1 H-W member

The H-W member is the basal member of the Myra Formation. It consists of two lithological units: the HW Rhyolite and the HW Dacite (Table 3.1). The HW Rhyolite consists of felsic volcano-sedimentary rocks characterised by intercalated argillite, chert, and rhyolitic volcaniclastic rocks at its base with variably thick coherent rhyolite lavas and autoclastic breccia towards the top. In the northeast region of the basin, coherent rhyolite and proximal coarse volcaniclastic facies dominate the strata (Figure 3.2). Re-sedimented, syn-eruptive mass flow deposits are predominant in the south-central region of the basin.

A fine-grained sequence of variably thick argillite and chert (Caprocks) overlies the VHMS orebodies of the H-W member at Myra Falls. This facies forms a semicontinuous horizon near the base of the H-W member throughout the central region of the basin. Jones (2001) and Jones et al. (2006b) subdivided the Caprocks into three main lithofacies: (1) white chert; (2) black chert; and (3) argillite. The thickest zones of the Caprocks unit coincide with paleotogpraphic lows on the reconstructed seafloor model of Jones et al. (2006b). Siliceous caprocks (cherts)

are best developed above the Battle, Ridge, and Extension Zone orebodies, whereas argillite is present above the HW orebody and in the southern and eastern regions of the basin.

In the south-eastern region of the basin, dacitic volcanic rocks (HW Dacite) occur at the same stratigraphic level as the HW Rhyolite to the west. The HW Dacite unit is characterised by massive flows, autobreccia, and minor sills. Dacitic and rhyolitic volcanic rocks become increasing intercalated in the H-W member between the Price Seamount and HW orebody areas (Figure 3.2). The base of the H-W member in the western region of the basin is marked by graded, polylithic sandstone to volcaniclastic-conglomerate, named the Basal Volcaniclastic Unit (Table 3.1; Figure 3.2).

A number of submarine andesitic sills and flows are present in the H-W member characterised by massive, feldspar ± pyroxene phyric cores with up to 15-metre-thick jigsaw-fit, curviplanar autoclastic margins. Near the HW orebody and Ridge Zone West orebody, there are coherent andesite lavas with 5 to 20-metre-thick peperitic margins, which are interpreted to be sills that were emplaced into wet sediments (Barrett and Sherlock, 1996; Chong, 2004).

3.1.2.2 Hanging Wall Andesite member

The Hanging Wall Andesite is a discontinuous unit overlying the H-W member and locally reaches a thickness of up to 100 metres (Figure 3.2). This facies is characterised by well bedded, normal to reverse graded, feldspar crystal-rich, polylithic volcaniclastic sandstones and conglomerates. Lithic components comprise subangular to sub-rounded andesite with lesser rhyolite, argillite, chert, and rare sulfide clasts (Table 3.1).

3.1.2.3 Lower Mixed Volcanics

The Lower Mixed Volcanics unit overlies the Hanging Wall Andesite and is characterised by rhyolitic and andesitic volcaniclastic deposits that are up to 180 metres thick and have a laterally continuous extent of approximately 5 km (Table 3.1; Figure 3.2). The base of the unit comprises quartz-rich volcaniclastic sandstone and polylithic tuffaceous breccia with rhyolite and lesser andesite and basalt clasts and, locally, angular massive sulfide clasts (Juras, 1987; Sinclair, 2000). Due to the presence of massive sulfide clasts this facies was termed the "Ore Clast Breccia Unit" by Juras (1987). The "Ore Clast Breccia Unit" is overlain by an andesitic, tuffaceous volcaniclastic mudstone and breccia facies, the so-called "Lower Mixed Volcaniclastic Unit" by Juras, (1987).

3.1.2.4 L-M-P (Lynx-Myra-Price) member

The L-M-P member records a second cycle of felsic volcanism in the Myra Falls VHMS district comprising three lithological units: (1) LMP Rhyolite; (2) Upper Dacite; and (3) G-Flow (Table 3.1; Figure 3.2). The LMP Rhyolite is laterally extensive (approximately 5 km) across the basin varying in thickness from 10 to 150 metres. It is characterised by massive to thickly-bedded, quartz and feldspar crystal-rich and vitriclastic-bearing mudstones, sandstones and breccia with less abundant coherent lava (Table 3.1). The coherent lava is felsic in composition, restricted to the northeast of the basin (Figure 3.2) and was previously referred to as the "North Dacite" (Table 3.1). It is suggested here that the "North Dacite" unit terminology no longer be used given the reinterpretation of this unit here as an intercalated, coherent volcanic lithofacies of the LMP Rhyolite.

The Upper Dacite unit is a flow-dome complex of unknown thickness. Coherent, aphyric to

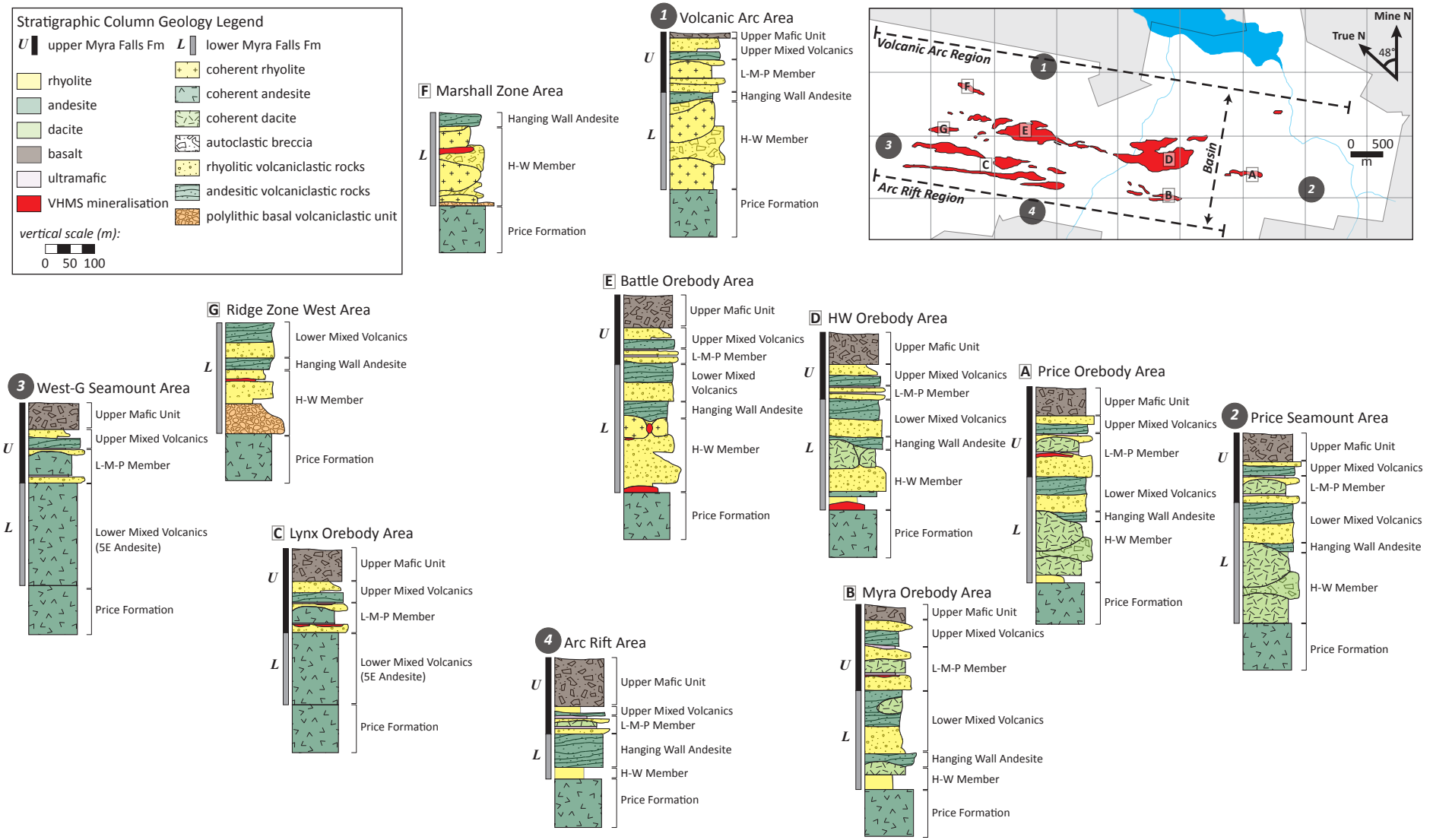

Figure 3.2 Schematic stratigraphic columns that illustrate the lateral variation of the Myra Formation stratigraphy at the Myra Falls district. Lithofacies data are from Juras (1987), Robinson (1994), Barrett and Sherlock (1996), Sinclair (2000), Jones (2001), and Chong (2004). Figure is updated and modified from Sinclair (2000) with the additions of the Price Orebody Area, Myra Orebody Area, Marshall Zone Area, and Ridge Zone West Area stratigraphic columns.

feldspar-phyric dacite is intercalated with the rhyolitic volcaniclastic rocks of the LMP Rhyolite in the Price Seamount, and Price and Myra orebody areas (Figure 3.2). The G-Flow unit consists of several thin but widespread, pillowed ultramafic flows with hyaloclastite breccias ranging from 2 to 15 metres in thickness. These flows are intercalated with rhyolitic volcaniclastic rocks of the LMP Rhyolite unit and are thickest near the West-G Seamount and Lynx orebody areas and thins towards the east (Figure 3.2). The unit is not present in the NE Volcanic Arc area and appears to thicken to the south near the Arc Rift area of the basin (Figure 3.2).

3.1.2.5 Upper Mixed Volcanics

This unit is characterised by rhyolitic, andesitic, and basaltic volcaniclastic rocks that are laterally continuous (approximately 5 km) across the basin with a total thickness of up to 100 metres. The base of the unit consists of andesitic, bedded to massive tuffaceous mudstone, sandstone, and breccia (previously referred to as the Upper Mixed Volcaniclastic unit by Juras, 1987; Table 3.1). It reaches thicknesses of up to 50 metres near the West-G Seamount and is overlain by the Upper Rhyolite unit, a succession of intercalated felsic sandstone, breccia and laminated argillite and chert. The Upper Rhyolite is up to 65-metres-thick and is laterally extensive throughout the mine property (Figure 3.2).

3.1.2.6 Upper Mafic Unit

The Upper Rhyolite is overlain by a locally thick sequence of basaltic autoclastic breccia with minor pyroxene and feldspar-phyric lavas and intercalated thin-bedded to massive argillite and chert. The unit is thickest (up to 20 m thick) in the south-central to southwest areas of the basin and thins to northeast (5 m thick; Figure 3.2). Locally the Upper Mafic unit is missing or notably thinner, and is interpreted to represent an erosional unconformity with the overlying Thelwood Formation (Juras, 1987).

3.1.3 Thelwood and Flower Ridge Formations

The Thelwood Formation is present throughout the Myra Falls district at surface. The unit locally unconformably overlies the Myra Formation and is a 270 to 500-metre-thick sequence of siliceous tuffaceous sediments, submarine volcaniclastic deposits, and mafic sills (Juras, 1987). Conformably overlying the Thelwood Formation is the uppermost Palaeozoic unit exposed at Myra Falls, the Flower Ridge Formation. The formation is characterised by basaltic volcaniclastic rocks and minor basalt flows and associated volcano-sedimentary rocks (Juras, 1987). Volcaniclastic rocks with abundant scoriaceous clasts generally mark the contact with the underlying Thelwood Formation. Only the lower 650 meters of the Flower Ridge Formation can be observed at Myra Falls; the upper contact with the overlying Buttle Lake Group occurs off the mine property (Juras, 1987).

3.2 Myra Falls Structure

Regional structural investigations by Muller (1980), Massey (1992), Nixon et al. (1994), Mackie (2002), and Nixon and Orr (2007) have documented multiple deformation events on Vancouver Island that reflect a complex tectonic history. Walker (1985), Juras and Pearson (1990), and Berry (2000) recognised multiple deformation events in the Myra Falls area, and concluded that the complexity from multiple fault reactivations could only be resolved by detailed assessment of the morphology, kinematics, mineralogy, and geometry of each generation of movement. Jones (2001) and Jones et al. (2006a) completed a comprehensive structural study at

Table 3.1 Update lithofacies table of stratigraphic units at Myra Falls.

Rhyolite facies							
Lithological unit	**Previous nomenclature**	**Member**	**Description**	**Distribution**	**Interpretation**	**Source region**	**References**
Upper Rhyolite	*Upper Rhyolite*	Upper Mixed Volcanics	1) volcaniclastic rocks: intercalated felsic sandstone to breccia	≤50 m thick, thickest in the NE and thins to SW	NE region comprises coarse volcaniclastic rocks while the SW region comprises finer-grained volcaniclastic rocks.	Volcanic Arc	Juras (1987)
			2) argillite-chert: laminated beds of grey to black argillite, white to pale green chert	1-to-15 m thick, restricted to central region	succession is restricted to the central region and likely represents a local paleo-depositional centre during quiescence of volcanic activity		
LMP Rhyolite	*Lynx-Myra-Price Horizon*	L-M-P member	1) massive to thickly bedded quartz-feldspar crystal-rich and vitriclast-bearing mudstone to breccia volcaniclastic rocks	succession is 10-to-150 m thick, extensive throughout mine property	succession consists of re-sedimented syn-eruptive mass flow deposits >> proximal coherent facies interpreted to represent a distal depositional setting compared to HW Rhyolite	Volcanic Arc	Seraphim (1980); Walker (1980); Juras (1987)
			2) coherent lavas [North Dacite]: felsic flows with associated autobreccia	restricted to the NE	only coherent facies recognized, potentially represents a NE Volcanic Arc source region		
HW Rhyolite	*HW Horizon*	H-W member	1) coherent lavas: quarts-feldspar phyric flows and domes with associated autobreccia 2) volcaniclastic rocks: normally graded rhyolitic tuffaceous sandstone and breccia; ungraded coarse volcanic breccia; laminated to thinly bedded rhyolitic siltstone 3) argillite (see caprocks) 4) basal polylithic volcaniclastic unit	succession is 15-to-250 m thick, extensive throughout mine property, thickest in the NE and thins to the SW	NE region comprises coherent flows, domes and proximal coarse volcaniclastic rocks while the SW region comprises re-sedimented syn-eruptive mass flow deposits interpreted to represent a volcanic arc	Volcanic Arc	Juras (1987); Robinson et al. (1996); Barrett & Sherlock (1996); Sinclair (2000); Chong (2004)

Lithological units have been updated, grouped, and adapted from the Sinclair (2000) lithofacies synthesis. The member nomenclature has been added to group interpreted related lithological units and facies together to aid in the district scale interpretation of units (Figure 3.2). Light grey highlight = Lower Myra Formation; Dark grey highlight = Upper Myra Formation. Previous nomenclature refers to layer cake stratigraphic terminology developed by Juras (1987).

Table 3.1 Continued

Lithological unit	Previous nomenclature	Member	Description	Distribution	Interpretation	Source region	References
			Dacite facies				
Upper Dacite	*Upper Dacite*	L-M-P member	1) coherent lavas: massive, dacite flows and domes; aphyric to porphyritic; intercalated with LMP Rhyolite	located near the Price orebody; thickness and extent unknown	source of succession unclear though Juras (1987) hypothesized the origin was the Price Seamount; however, shares same stratigraphic position as coherent felsic lavas in the LMP Rhyolite and is possibly related	Price Seamount (?)	Juras (1987); Sinclair (2000)
HW Dacite	*HW Dacite*	H-W member	1) coherent lavas: massive flows with related autobreccia and minor sills; intercalated with HW Rhyolite	≤150 m thick, restricted to east-central region	succession is thickest in the eastern region of the mine property and interpreted to represent a volcanic centre named the Price Seamount	Price Seamount	Juras (1987); Robinson (1994)
			Andesite Facies				
5E Andesite	*5E Andesite*	Lower Mixed Volcanics	1) coherent lavas: pillowed flows with autoclastic breccia; locally intercalated with LMP Rhyolite	≤250 m thick and restricted to the SW region	succession overlies Price Formation in the SE region and is interpreted to represent a second volcanic centre named the West-G Seamount	West-G seamount	Juras (1987); Sinclair (2000)
Hanging Wall Andesite	*Hanging Wall H-W Andesite*	Hanging Wall Andesite member	1) volcaniclastic rocks: bedded sandstone to conglomerate	≤100 m thick; sporadic blanket overlying HW Rhyolite north of 5E Andesite	coherent lavas of the HW Rhyolite formed paleo-barriers which restricted the depositional coverage of this unit	Arc Rift Region	Juras (1987); Robinson et al. (1996); Sinclair (2000); Jones (2001); Chong (2004)
Andesitic Sills & Flows	*Hanging Wall H-W Andesite; HW Horizon Mafic Flow Member; Mafic Sill Complex*	H-W member	1) coherent lavas: sills with associated hyaloclastite and peperite upper and lower margins; lesser flows with hyaloclastite margins	≤40 m thick sills locally intrudes HW Rhyolite; lava flows at contact between HW Rhyolite and Hanging Wall Andesite member	andesitic sills and flows represent re-activation of volcanism after the deposition of felsic volcanic material recorded by the HW Rhyolite; Hanging Wall Andesitic volcaniclastic rocks likely coeval with the emplacement of these coherent facies	Arc Rift Region	Juras (1987); Sinclair (2000); Barrett & Sherlock (1996); Chong (2004)
			Basalt Facies				
Upper Mafic Unit	*Upper Mafic Unit*	Upper Mafic Unit	1) volcaniclastic rocks: autoclastic and re-sedimented syn-eruptive deposits 2) coherent lavas: minor pyroxene-feldspar phyric flows 3) argillite-chert: subordinate facies	≤200 m thick; thickest in the SW region and thins to 5-20 m thick in the NE region	succession is interpreted to represent mafic volcanism associated with incipient arc rifting	Arc Rift Region	Juras (1987)
G-Flow	*G-Flow Unit*	L-M-P member	1) coherent lavas: flows with associated autobreccia; intercalated with LMP Rhyolite	consists of several, 2-15 m thick mafic lavas, with total thickness from 5-50 m; thickest near the Lynx orebody	the unit is thickest in near the West-G Seamount region and thins towards the Price Seamount region and represent the first major phase of ultramafic volcanism recognized at Myra Falls	Arc Rift Region	Juras (1987)

Table 3.1 Continued

Intercalated Volcano-Sedimentary Facies							
Lithological unit	**Previous nomenclature**	**Member**	**Description**	**Distribution**	**Interpretation**	**Source region**	**References**
Upper Mixed Volcanics	*Upper Mixed Volcaniclastic*	Upper Mixed Volcanics	1) volcaniclastic rocks: mafic to intermediate in composition, bedded to massive tuffaceous mudstone, sandstone, and breccia	≤50 m thick, present throughout the mine property, best developed in the central region	intermediate and felsic clasts are most abundant in the NE and mafic clasts are dominant in the SW; interpreted to represent the resumption of rift basin-filling volcano-sedimentary deposition	Arc Rift Region	Juras (1987); Sinclair (2000); Jones (2001)
Lower Mixed Volcanics	*Lower Mixed Volcanics*	Lower Mixed Volcanics	1) volcaniclastic rocks: rhyolitic matrix with variable rhyolite, andesite, and basalt volcanic clasts and angular massive sulfide clasts; ore clasts are a distinctive feature but only a minor lithological component	≤90 m thick, common above HW orebody, minor lenses above the Battle and Ridge orebodies; well developed near Price orebody below the L-M-P member	succession records multi-source input of volcanic detritus into the marine basin; combination of mass flow deposits (polylithic coarse-grained volcaniclastic rocks) a result of an active submarine volcanic edifice and turbidity currents (andesitic sandstone to mudstone)	Volcanic Arc, Price Seamount, West-G Seamount	Juras (1987); Sinclair (2000); Jones (2001)
	Lower Mixed Volcaniclastic Unit		2) volcaniclastic rocks: range from breccia to mudstone, andesitic with subordinate rhyolitic and dacitic lithic fragments	≤90 m thick, commonly overlies the rhyolitic volcaniclastic ore clast breccia unit			
Caprocks	*H-W Horizon*	H-W member	1) chert: pale grey to medium grey to white, glassy to porcellanite appearance, massive cm-m scale beds or strongly laminated	best developed above the Battle orebody, 3-5 m thick; discontinuous, thin intervals above Ridge and Extension Zone orebodies; minor chert above HW orebody	petrological features indicate that the chert above the Battle Orebody formed from the silicification of pre-existing fine-grained sediments; local chert beds near the HW Orebody formed from the silicification of argillite; parallel laminations, interbedded sandstone turbidites, presence of radiolarian fossils, and the lack of bioturbation suggest a deep, quiet depositional environment, at least below storm wave base	Volcanic Arc	Juras (1987); Robinson et al. (1996); Barrett & Sherlock (1996); Sinclair (2000); Jones (2001); Chong (2004) Jones et al. (2006b)
			2) black chert: dark grey to black, very fine-grained, glassy with conchoidal fracture, massive m-scale beds to strongly laminated	south and west of the Battle orebody; gradational transition from pale grey to black chert above Battle orebody			
			3) argillite: dark grey to black, very fine-grained, massive mm-cm scale beds to strongly laminated	≤100 m thick in southern and eastern parts of property; 35 m thick above the HW orebody; same stratigraphic position as chert facies			
			4) intercalated facies: fine rhyolitic siltstones, sandstones and minor conglomerate	variable thickness and lateral distribution across the mine property in pale grey chert, black chert and argillite facies			
Basal Polylithic Volcaniclastic	*Basal Conglomerate*	H-W member	1) volcaniclastic rocks: graded sandstone to conglomerate, intercalated with polylithic volcaniclastic beds	30-90 m thick, below Ridge Zone West, overlies Price Formation; thickens to the SW and thins to the SE	unit is located in paleo-depressions where coarse, subrounded to subangular clasts of variable provenance; deposition by mass flow processes; source direction is from the west	West-G Seamount (?)	Chong (2004)

Myra Falls and confirmed five deformation events (Figure 3.3), with early ductile deformation followed by several distinct episodes of brittle deformation. The following deformation history of Myra Falls and regional comparison is summarised from Jones et al. (2006a). References to orientations in sections 3.2.1 through 3.2.7 are true, not relative to the mine grid north.

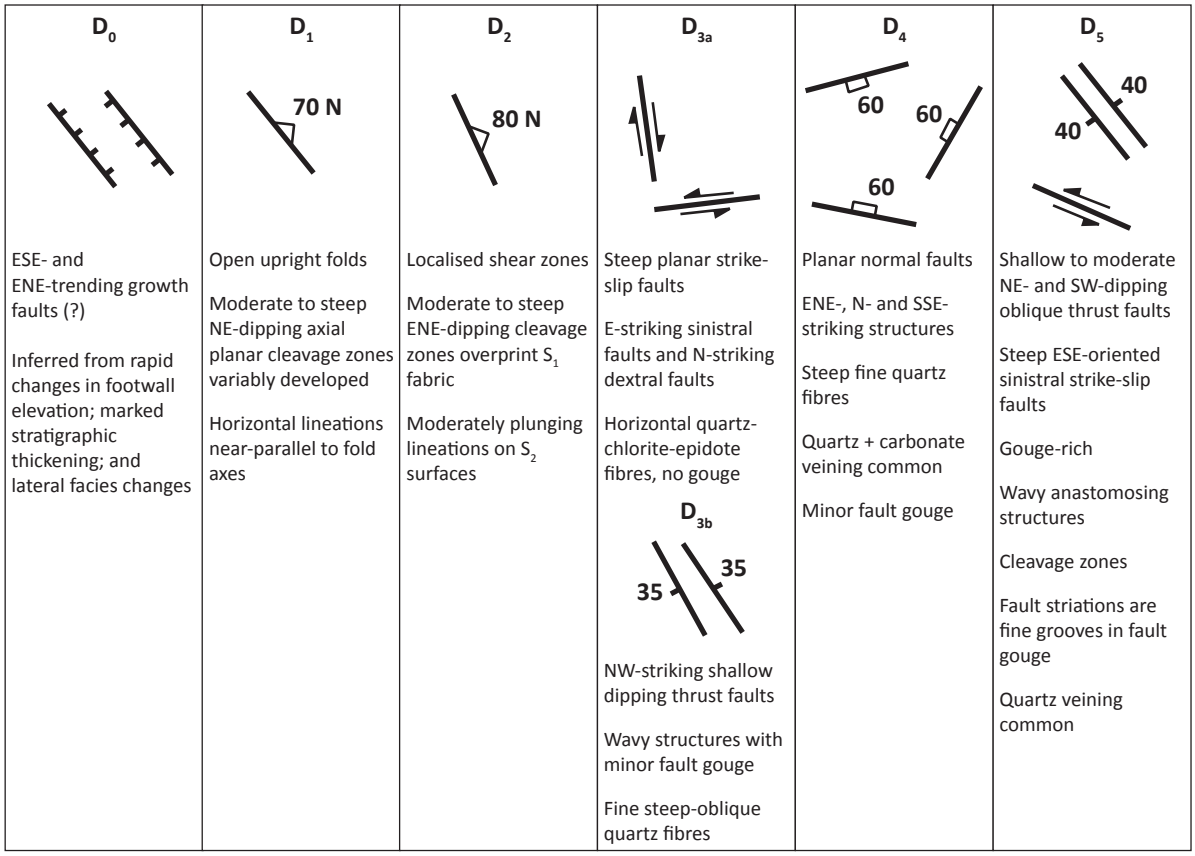

Figure 3.3 Deformation sequence at Myra Falls (Jones et al., 2006a). Structural orientations are true, not relative to mine grind north.

3.2.1 D_0 growth faults (Early to Middle Devonian)

The direct measurement of syn-depositional growth faults associated with basin formation is not possible at Myra Falls due to overprinting by subsequent deformation events. Their location and orientation, however, has been inferred from stratigraphic thickening associated with rapid changes in stratigraphic footwall elevation, lateral facies variation, and metal zonation in the VHMS deposits (Sinclair, 2000; Jones, 2001; Chong, 2004). Growth faults have an inferred east-southeast to east-northeast orientation with 10s of meters of normal displacement (e.g., Jones, 2001).

3.2.2 D_1 folding (Middle Permian to pre-Middle Triassic)

Northeast-southwest compression during D_1 produced regional northwest-trending open upright folds with a variably developed northeast-dipping axial planar S_1 cleavage (Muller, 1980; Massey, 1992b; Jones et al., 2006a). This event is responsible for the Myra Anticline, which extends through the upper Lynx, Myra, and Price orebodies (Figure 3.4). The S_1 foliation is characterised by aligned muscovite and chlorite, recrystallised quartz, and wavy carbonaceous seams that crosscut bedding at high angles.

The D_1 upright folds are observed throughout the Paleozoic rocks on Vancouver Island in the Cowichan Lake and Buttle Lake uplifts (Muller, 1980; Massey, 1992). At Myra Falls these structures also occur in the Thelwood Formation, but not in the Permian Buttle Lake Group. However, D_1 structures have been reported in the Permian Buttle Lake Group in other localities in the Buttle Lake (Jones, 2001) and Cowichan Lake uplifts (Muller, 1980). The D_1 event likely occurred prior to Wrangellia colliding with the Laurentian margin (Jones et al., 2006a).

3.2.3 D_2 shear zones (Early to Middle Jurassic)

Continued northeast-southwest shortening in the Early to Middle Jurassic during D_2 deformation produced a steep, northeast-dipping fabric (S_2), which overprints S_1 (Jones et al., 2006a). The major effect of this event was to tighten D_1 folds, as no F_2 folds have been identified at Myra Falls and the S_1 to S_2 angle is low (Jones et al., 2006a). Muller (1980), England and Calon (1991), Massey (1992), and Yorath et al. (1999) documented a second foliation in the Sicker Group rocks elsewhere in the Buttle Lake and Cowichan Lake uplifts defined by the refolding of lineations and crenulation cleavage, with no developed cleavage in the overlaying Karmutsen Formation. The D_2 event records the collision of the Wrangellia Terrane with the Laurentian margin and produced the regional northwest-trending uplifts (e.g., Buttle Lake uplift) throughout Vancouver Island by reactivation of Paleozoic folds.

3.2.4 D_3 faults (?post-Middle Cretaceous, pre-Late Cretaceous)

Northeast-southwest compression during D_3 produced two-stages of faulting at Myra Falls including early steep strike-slip faults (D_{3a} structures) which were subsequently overprinted by thrust faults and bedding parallel shears (D_{3b} structures). The majority of the D_3 faults represent minor structures at Myra Falls, with the exception of the Lynx-Phillips and Myra Price Faults (Figure 3.4). Nixon et al. (1994, 1995) and Nixon and Orr (2007) described similar strike-slip and bedding-parallel thrust faults on northern Vancouver Island. These faults postdate deposition of the Late Cretaceous Nanaimo Group.

3.2.5 D_4 normal faults (?Late Cretaceous)

Extension during D_4 produced steep, planar normal faults with variable orientations and contain minor gouge with fine, steep quartz fibres (Jones et al., 2006a). These structures overprint/reactivate steep dipping D_{3a} faults (Jones et al., 2006a). The D_4 normal faults are common at Myra Falls, most notably in the East Main Fault and North Fault zones (Figure 3.4). The offset on individual D_4 faults is typically <10 metres and faults are spaced 5 to 10 metres apart (Jones et al., 2006a). Nevertheless, the overall displacement across fault zones is substantial. For example, there is >100 metres of normal offset across the North Fault zone and 50 metres of normal displacement on the East Main Fault zone (Jones et al., 2006a). Whilst the timing of the D_4 faults is unclear, these faults consistently crosscut the D_3 faults and are most likely related to the formation of the Nanaimo Basin during the Late Cretaceous.

3.2.6 D_5 gouge-rich oblique thrust faults and strike-slip faults (Eocene)

The D_5 event produced large northwest-striking oblique thrust faults and steep, northwest- and northeast-striking strike-slip faults. These faults are distinctly different in appearance from earlier faults. They are characterised by gouge-rich fault zones with wavy to anastomosing geometries (Jones et al., 2006a) and include the reactivated Myra-Price Fault zone and the Flat Fault (Figure 3.4). The D_5 faults occur as groups of faults spaced 1 to 5 metres apart and

constitute wide, disrupted fault zones. Offsets on individual faults range from 1 to 10 metres however, the overall displacement across the 10-metre-thick Flat Fault zone is <100 metres and the Myra-Price Fault zone has at least 300 metres of displacement (Jones et al., 2006a). The Myra Falls D_5 faults correlate with the large Eocene thrust faults documented on southern Vancouver Island (England and Calon, 1991; Massey, 1992; Yorath et al., 1999). The D_5 faults are the result of deformation during the collision and accretion of the Pacific Rim and Crescent Terranes along the south-western margin of Vancouver Island (Jones et al., 2006a).

3.2.7 Displacement of the Price and Myra Formation contact

The contact between the Price and Myra Formations is a key lithostratigraphic marker in the Myra Falls VHMS district. It marks the depositional surface of the VHMS-hosting, submarine volcano-sedimentary strata of the lower Myra Formation onto the Late Devonian paleo-seafloor (Juras, 1987; Jones, 2001). No VHMS deposits are hosted in the upper Price Formation volcanic rocks on Vancouver Island. At Myra Falls, the HW and Battle orebodies occur at the base of the lower Myra Formation immediately above the Price Formation (e.g., Juras, 1987). Multiple deformation events at the Myra Falls VHMS district record the reactivation of long-lived brittle structures in the Buttle Lake uplift (Jones et al., 2006a). The reactivation of these structures has resulted in significant displacement of the Myra Falls stratigraphy, in particular across the Lynx-Phillips and Myra-Price faults (Figure 3.4).

3.3 Metamorphism and Alteration

Rocks of the Wrangellia Terrane on Vancouver Island are characterised by regional low-grade metamorphism, reaching greenschist facies grades, dominated by chlorite and biotite zones (Juras, 1987; Greenwood et al., 1991). Amphibolite grade facies may be developed locally and is related to the Jurassic emplacement of the Island Plutonic Suite (Juras, 1987; Greenwood et al., 1991). At Myra Falls, post-Permian to pre-Triassic regional burial metamorphism of the Sicker Group comprises low-grade greenschist and pumpellyite-actinolite facies rocks (Table 3.2; Brandon et al., 1986; Juras, 1987). Chlorite greenschist facies rocks are dominant in the Price and Myra Formations with ubiquitous muscovite-quartz alteration of felsic and mafic rocks near mineralised zones. Lower Myra Formation rocks of the Hanging Wall Andesite are weakly altered and are characterised by saussuritisation of feldspar, chlorite replacement

Table 3.2 Metamorphic mineral assemblages at Myra Falls (Juras, 1987).

Formation	Lithology	Mineral assemblage
Price	***basaltic andesite***	***chlorite + albite*** + actinolite + epidote
	andesite	chlorite + epidote + albite + quartz + calcite ± actinolite
Myra	basalt	chlorite + epidote + albite + actinolite ± quartz ± calcite
	basaltic andesite	epidote + albite + quartz ± chlorite ± calcite ± actinolite
	andesite	***chlorite + albite*** + quartz ± epidote ± calcite ± clinozoisite
	rhyolitic volcaniclastic rocks	***quartz + albite*** ± muscovite ± chlorite ± hematite
	quartz feldspar phyric rhyolite	***quartz + muscovite*** + albite ± chlorite
Thelwood	intermediate tuffaceous sediments	chlorite + epidote + quartz + albite + clinozoisite
	mafic sills	chlorite + albite + epidote
Flower Ridge	basalt	chlorite + epidote + albite + quartz + actinolite + calcite + pumpellyite + clinozoisite

Bold and italics text highlight the principal rock types and metamorphic mineral assemblages observed at Myra Falls

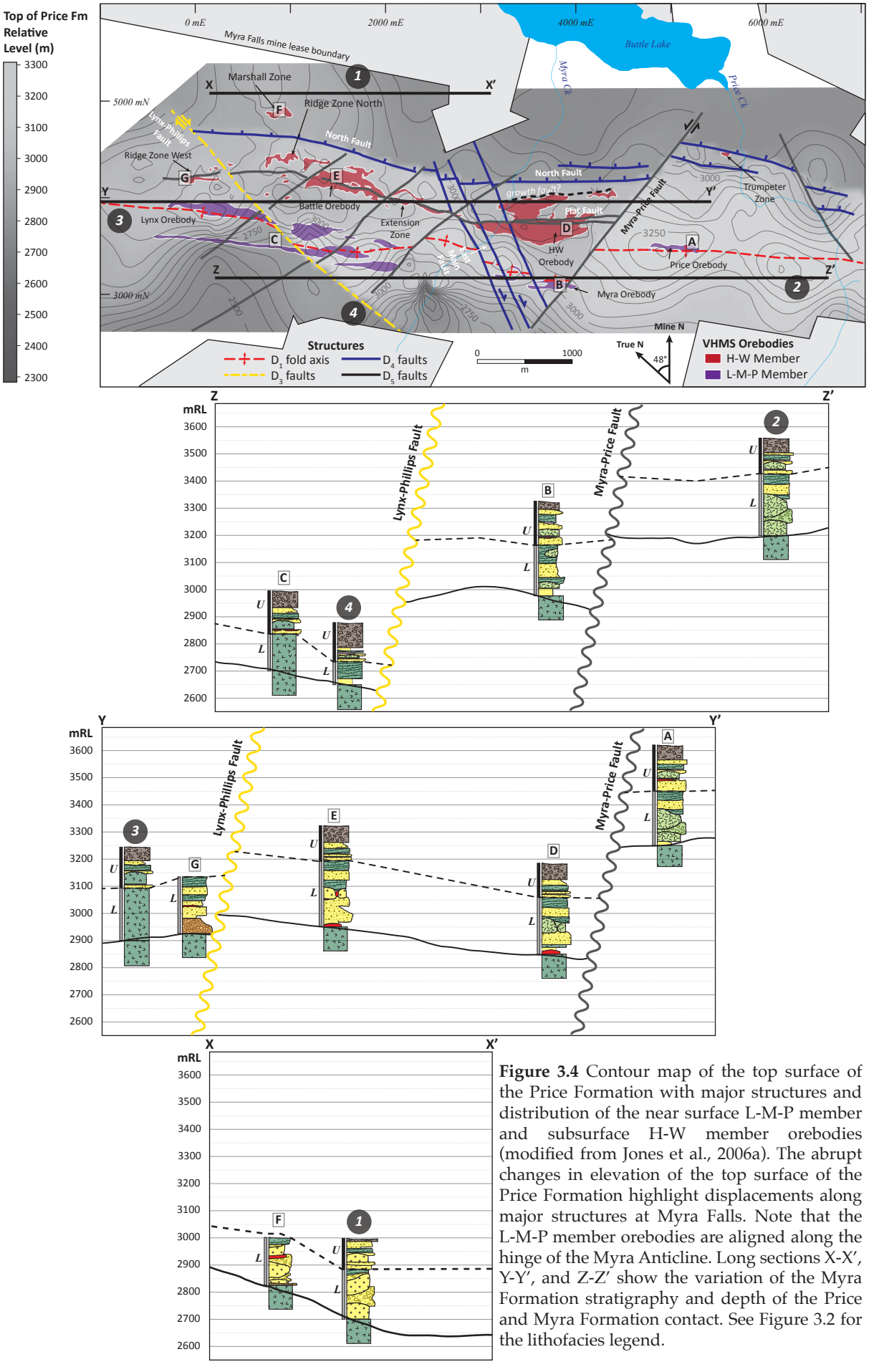

Figure 3.4 Contour map of the top surface of the Price Formation with major structures and distribution of the near surface L-M-P member and subsurface H-W member orebodies (modified from Jones et al., 2006a). The abrupt changes in elevation of the top surface of the Price Formation highlight displacements along major structures at Myra Falls. Note that the L-M-P member orebodies are aligned along the hinge of the Myra Anticline. Long sections X-X′, Y-Y′, and Z-Z′ show the variation of the Myra Formation stratigraphy and depth of the Price and Myra Formation contact. See Figure 3.2 for the lithofacies legend.

of pyroxene, and leucoxene and hematite after oxides (Juras, 1987). Pumpellyite-actinolite facies assemblages are dominant in the younger rocks of the Thelwood and Flower Ridge Formations. Conodonts from the Permian Buttle Lake Group have conodont alteration index values from 5 to 7 (Brandon et al., 1986), which suggests that metamorphic temperatures were no greater than 300°C (Epstein et al., 1977; Rejebian et al., 1987). There is no mineralogical evidence for contact metamorphism of the Sicker Group rocks at Myra Falls. However, Juras (1987) attributed the resetting of K-Ar age dates of muscovite to the emplacement of the Jurassic Island Plutonic Suite.

3.4 Myra Falls VHMS Deposits

Volcanic-hosted massive sulfide deposits at Myra Falls occur at two principal stratigraphic levels (Figure 3.5). The Myra Falls VHMS district has a minimum N-S strike length of 5 km (Figure 3.5A) and width of 2 km (Figure 3.5). As of April 2013, the operation exceeded 30 Mt of ore production at average grades of 5.5% Zn, 1.6% Cu, 0.6% Pb, 2.0 g/t Au and 54 g/t Ag (*per. comm.* Sawyer, 2015; Table 3.3). The L-M-P orebodies are located in the upper Myra Formation and oriented sub-parallel to the NW-SE trending Myra Anticline fold axis (e.g., Walker, 1985). Massive sulfide mineralisation in the Lynx orebody occurs on both limbs of the Myra Anticline. The H-W member orebodies are located in the lower Myra Formation on the northern limb of the Myra Anticline (e.g., Barrett and Sherlock, 1996). This section reviews the mineralisation styles (Table 3.4) and host rock associations of the Lynx, Myra, Price, HW, Battle and Ridge

Table 3.3 Myra Falls District pre-mining geological resources.

Orebody	Tonnes	Au (g/t)	Ag (g/t)	Cu (%)	Pb (%)	Zn (%)
Lynx	5,809,000	2.5	90.0	1.6	1.0	7.5
Myra	1,037,000	3.0	160.0	1.0	1.5	9.5
Price	381,000	2.1	73.0	1.4	1.3	9.2
HW	22,137,000	2.2	27.0	2.0	0.3	3.7
43-Block	971,000	2.6	53.0	1.7	0.5	5.8
Trumpeter	211,000	2.4	58.0	3.4	0.3	3.9
Extension	1,156,000	1.0	29.0	1.4	0.3	4.5
Battle	5,965,000	1.4	53.0	1.8	0.7	12.5
Gap	778,000	2.0	121.0	2.0	1.0	13.8
Ridge Zone North	326,000	0.8	41.0	0.7	0.8	4.7
Ridge Zone West	983,000	2.0	72.0	0.9	0.8	6.8
Marshall	1,210,000	1.6	80.0	0.5	0.6	5.3
2017 Mineral Resource◊						
Measured†	6,280,000	1.6	64.5	1.0	0.7	6.4
Indicated†	1,010,000	2.5	102.2	1.1	0.9	7.9
Inferred†	940,000	2.9	136.8	0.8	1.1	9.5

†Mineral resource includes Ridge Zone North, Ridge Zone West, Battle and Gap orebodies. ◊Cu-Pb-Zn-Ag NSR cut-off at USD 50.00 (Chong, 2004; *per. comm.* Stansell, 2018)

Zone West orebodies.

3.4.1 L-M-P member VHMS orebodies

Zinc, copper, lead, gold, and silver were extracted from semi-massive to massive sulfide ore lenses of the Lynx and Myra orebodies from the mid-1960s to earlier 1990s (Table 3.3). Ores are comprised of sulfide and sulfosalt minerals including sphalerite, chalcopyrite, galena, and tetrahedrite-tennantite with minor bornite and covellite. Native gold, native silver and electrum

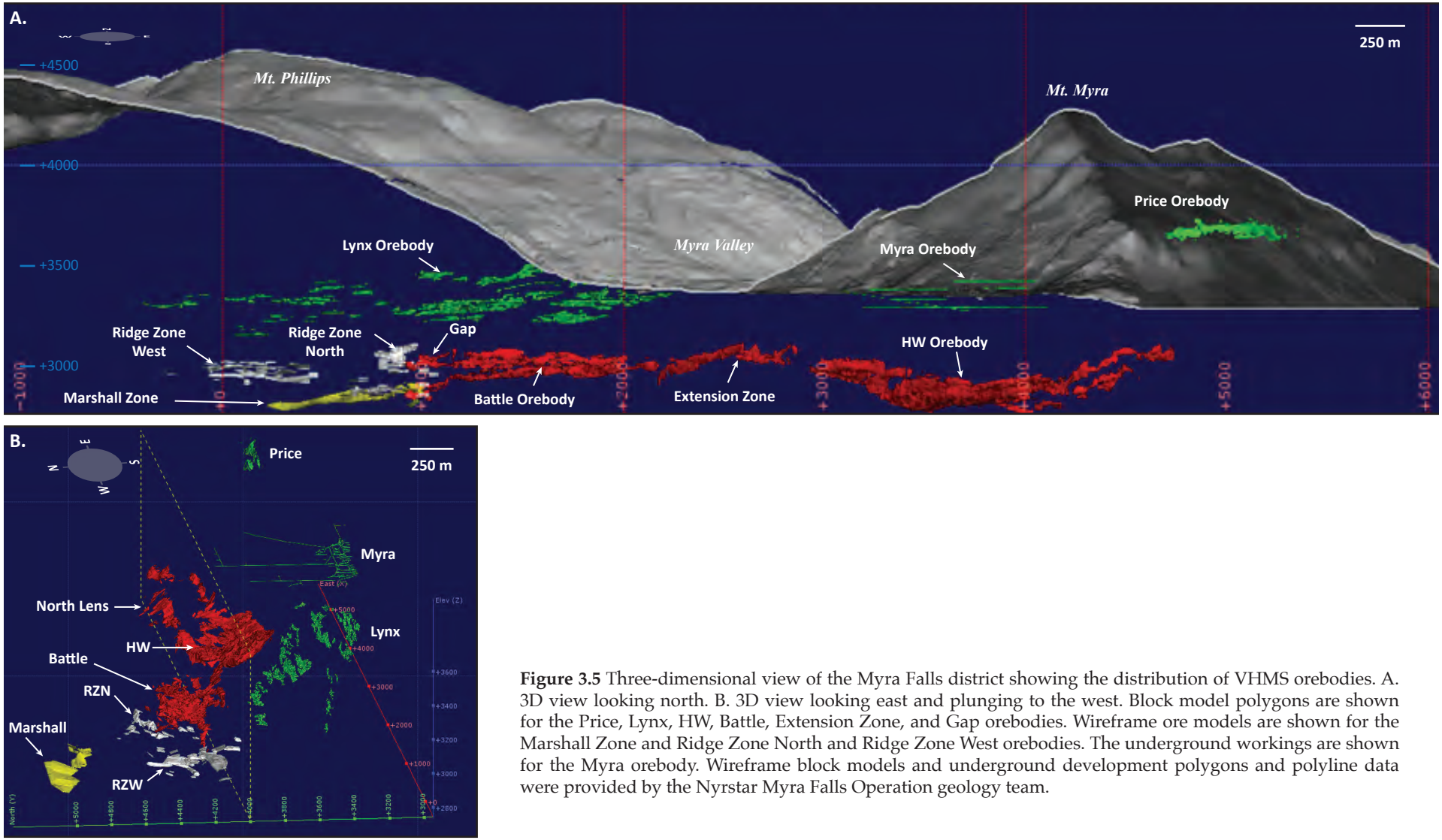

Figure 3.5 Three-dimensional view of the Myra Falls district showing the distribution of VHMS orebodies. A. 3D view looking north. B. 3D view looking east and plunging to the west. Block model polygons are shown for the Price, Lynx, HW, Battle, Extension Zone, and Gap orebodies. Wireframe ore models are shown for the Marshall Zone and Ridge Zone North and Ridge Zone West orebodies. The underground workings are shown for the Myra orebody. Wireframe block models and underground development polygons and polyline data were provided by the Nyrstar Myra Falls Operation geology team.

were also extracted from sulfide ores. Pyrite, barite, and minor pyrrhotite are locally abundant, and all ore zones are associated with variably intense quartz-sericite-pyrite alteration (e.g., Walker, 1985). The VHMS hydrothermal alteration has subsequently been metamorphosed and is now manifested by broad zones of pyrite-sericite schists (Walker, 1985). Pyrite-stringer style mineralisation is well developed beneath the Lynx and Myra orebodies (Walker, 1985). Carvalho (1979) recognised five ore mineral assemblages in the Lynx, Myra, and Price orebodies: (1) basal stringer pyrite-chalcopyrite; (2) massive pyrite; (3) massive pyrite-chalcopyrite; (4) banded to weakly banded galena-sphalerite-pyrite ± barite; and (5) massive barite. Sulfide mineralisation is hosted by variably altered and deformed rhyolitic volcaniclastic rocks of the L-M-P member, often referred to as quartz-sericite-sulfide schists (e.g., Seraphim, 1980).

3.4.2 H-W member VHMS orebodies

Polymetallic VHMS mineralisation occurs at two stratigraphic levels in the H-W member. "Upper zone" mineralisation consists of semi-massive to massive sulfide located 30 to 150 metres above the Price Formation and Myra Formation contact. Sulfide mineralisation is hosted in quartz-sericite altered rhyolitic volcaniclastic rocks, which are locally associated with quartz and feldspar-phyric coherent rhyolite flows. The "contact zone" mineralisation-style is characterised by massive sulphide lenses located at-or-near the contact between the Price and Myra Formations. Sulfide mineralisation is largely associated with tuffaceous felsic siltstones with variably thick argillite and/or chert occurring stratigraphically above the ore lenses. Sulfide lenses, which have been classified as "upper zone" mineralisation include the Marshall Zone, Gap, and Ridge orebodies along with the Upper zone of the Battle orebody and Upper lens of the HW orebody (Robinson, 1994; Barrett and Sherlock, 1996; Barrett and MacLean, 2000; Chong, 2004). Chert and argillite are located immediately above the Main Battle lens of the Battle orebody and the Main and North lenses of the HW orebody and the Trumpeter Zone orebody (Barrett and Sherlock, 1996; Jones et al., 2006b).

Jones et al. (2006b) used a paleo-reconstruction model of the Late Devonian seafloor to conclude that the argillite and chert facies were deposited in small, restricted sub-basins. The thickest deposits of chert and argillite overlie the "contact zone" massive sulfides of the HW and Battle orebodies. The relationship between massive sulfide mineralisation, fine-grained marine sedimentation, and a basinal seafloor depositional environment suggests that "contact zone" mineralisation likely precipitated at-or-on the paleo-seafloor. In contrast, the association of semi-massive sulfide mineralisation hosted in coarse volcaniclastic rocks of the "upper zone" has been interpreted to represent sub-seafloor sulfide precipitation (Robinson, 1994; Barrett and MacLean, 2000; Sinclair, 2000; Jones, 2001; Chong, 2004).

3.4.2.1 HW orebody

The HW orebody consists of the Main, Upper, and North sulfide lenses and is the largest orebody at Myra Falls (Table 3.3). The Main lens is approximately 1,200 metres in length, 500 metres wide, and up to 80 metres thick (Juras, 1987; Barrett and Sherlock, 1996). The North and Main lenses share the same stratigraphic position; whilst the Upper lens is sporadically developed with semi-massive sulfide mineralisation in altered rhyolitic volcaniclastic rocks a few 10s of metres above the Main lens. The North and Main lenses occur at the contact between the Price and Myra Formation, with stratabound massive sulfide hosted in interbedded quartz-feldspar fine to medium-grained felsic volcaniclastic rocks and black mudstones (Juras, 1987; Barrett and Sherlock, 1996). Massive sulfides in the Main and North lenses show distinct mineralogical

Table 3.4 Mineral assemblages of the Myra Falls VHMS orebodies.

Mineral Assemblage	Mineral	General mineral formula
Copper-lead-zinc-iron-rich	*sulfides*	
	pyrite	FeS_2
	sphalerite	ZnS
	galena	PbS
	chalcopyrite	$CuFeS_2$
	pyrrhotite	$Fe_{1-x}S$
	arsenopyrite	FeAsS
	sulfosalts	
	tennantite-tetrahedrite	$[(Cu,Ag)_{10}(Zn,Fe)_2]_{12}(Sb,As)_4(S,Se,Te)_{13}$
	trace minerals	
	rutile	TiO_2
	colusite	$Cu_3(As,Ge,V)S_4$
	tellurides	
	altaite	PbTe
	hessite	Ag_2Te
	pilsenite	Bi_2Te_3
Copper-rich	*sulfides*	
	bornite	Cu_5FeS_4
	covellite	CuS
	anilite	Cu_7S_4
	sulfosalts	
	renierite	$Cu_{10}(Zn_{1-x}Cu)Ge_{2-x}As_xFe_4S_{16}$
Late silver-gold-rich	*sulfides*	
	stromeyerite	CuAgS
	precious metals	
	electrum	AuAg
	native gold	Au
	native silver	Ag
gangue	sulfates, silicates, carbonate, oxides	
	barite	$BaSO_4$
	quartz	SiO_2
	muscovite (sericite)	$KAl_2(AlSi_3)O_{10}(OH)_2$
	epidote	$Ca_2(Al,Fe)_3Si_3O_{12}(OH)$
	calcite	$CaCO_3$
	gypsum	$CaSO_4 \bullet 2H_2O$
	anhydrite	$CaSO_4$
	specularite	Fe_2O_3
	smithosonite	$ZnCO_3$

Assemblages modified from Chong (2004) with mineralogical data from Chryssoullis (1989), Wilson (1993), Robinson (1994), and Sinclair (2000).

zonation (Barrett and Sherlock, 1996). The bases of the lenses comprise coarse-crystalline pyrite with rare base-metal sulfides and stratigraphically overlying this unit is an interval of massive pyrite with chalcopyrite, sphalerite, tennantite, and rare galena. The Upper lens occurs locally, stratigraphically above the Main lens, and comprises disseminated to semi-massive sphalerite with lesser bornite, galena, tennantite, and chalcopyrite, and barite mineralisation.

3.4.2.2 Battle orebody

The Battle orebody consists of the Main Battle lens and the Gap, Upper and Gopher lenses (Robinson et al., 1996; Sinclair, 2000). The Main lens has a sheet-like geometry and is approximately 1,000 metres long, up to 200 metres wide, and varies in thickness from 3 to 25 metres (e.g., Sinclair, 2000). The Main Battle and Gopher Zone lenses occur at the contact between the Price and Myra Formations and are associated with chert and fine-grained tuffaceous felsic mudstone and siltstone (Sinclair, 2000). The Upper lens and Gap Zone are associated with fine- to coarse-grained felsic volcaniclastic sandstone and breccia and coherent rhyolite (Sinclair, 2000; Jones, 2001). Production of the Battle orebody began in 1995 (Chong, 2004; Table 3.3).

Sinclair (2000) completed at detailed petrographic study of the Battle orebody and identified three ore mineral assemblages (Table 3.4). A copper-lead-zinc-iron-rich assemblage characterised by sphalerite, pyrite, chalcopyrite, galena, and tennantite-tetrahedrite with accessory rutile, tellurides, and colusite [$Cu_3(As,Ge,V)S_4$]. This assemblage has distinctive pyrite textures including framboids and delicate ring structures; chemically homogenised sphalerite; annealed galena and chalcopyrite; concentrations of chalcopyrite, galena, and pyrite along sphalerite mineral boundaries and triple junctions; and variably annealed pyrite, locally porphyroblastic. Sinclair (2000) interpreted the primary pyrite textures to represent initial sulfide precipitation followed by the copper-lead-zinc-iron-rich sulfide assemblage as the seafloor hydrothermal system developed. The coarsening and annealing of chalcopyrite, sphalerite, and galena was likely due to a combination of hydrothermal zone-refinement and metamorphic recrystallisation. Zone-refining after the model of Eldridge et al. (1983) is manifested in the Battle orebody by the mineralogical zoning of lead-zinc-rich sulfide phases at the top of the ore lenses to copper-iron-rich sulfides near the bottom, and in some localities the complete migration of copper-lead-zinc sulfides with only massive pyrite remaining at the base (Sinclair, 2000).

The second mineral assemblage is distinctly copper-rich and is characterised by bornite and anilite with accessory renierite and electrum. This assemblage is restricted to the "upper zone" position mineralisation, including the Upper lens and Gap lens of the Battle orebody (Robinson, 1994; Sinclair, 2000). This mineral assemblage overprints and replaces sulfides from the copper-lead-zinc-iron-rich assemblage. Colusite is present exclusively in the Gap and Upper lenses, constituting up to 1% of the ore in the Gap lens, where it occurs as inclusions in bornite, sphalerite, and as anhedral masses (Sinclair, 2000).

The third assemblage consists of late-stage gold-silver-rich mineralisation associated with stromeyerite [CuAgS], electrum, and minor chalcopyrite that crosscuts assemblages 1 and 2 (Sinclair, 2000). Microscopic textures of stromeyerite include vermicular-to-irregular intergrowths with anilite, irregular intergrowth in bornite, and rim and fracture fill of sphalerite grains. Sinclair (2000) interpreted these delicate and intricate intergrowths as evidence for late-remobilisation, possibly during prograde metamorphism. Stromeyerite is only observed in the Gap and Upper lenses of the Battle orebody and is commonly associated with electrum (Table 3.4).

Tellurides (altaite, hessite, and pilsenite) are present as microscopic inclusions in sulfide and sulfosalt mineral phases throughout the Battle orebody. Tellurides are anhedral, vary in size from 10 to 70 μm, and also occur as inclusions in tennantite associated with chalcopyrite

and less commonly in galena, chalcopyrite, and sphalerite (Sinclair, 2000). The relative timing of telluride precipitation is unclear.

3.4.2.3 Ridge Zone West orebody

The Ridge Zone West orebody consists of zinc-rich massive sulfide lenses, veins, and disseminations which occur over an area approximately 1,000 metres in length, 450 metres wide, and up to 70 metres thick (Chong, 2004). Economically significant individual lenses are approximately 250 metres in length and 80 metres in width, with individual thicknesses of up to 17 metres. The Ridge Zone West orebody comprises stacked sulfide zones referred to as the Upper, Main, and Lower lenses (Chong, 2004). Sulfide mineralisation is present at varying stratigraphic positions within the H-W member, 30 to 60 metres above the Price Formation and Myra Formation contact, and is classified as "upper zone" position mineralisation (Chong, 2004). The Ridge Zone West orebody has a pre-mining resource estimate of 980,000 tonnes at 6.8% Zn, 0.8% Pb, 0.9% Cu, 2.0 g/t Ag and 71.9 g/t Ag (Chong, 2004; Table 3.3).

The Lower and Upper lenses of Ridge Zone West are associated with fine-grained tuffaceous felsic mudstone (Chong, 2004). Pyrite, sphalerite, chalcopyrite, and galena mineralisation is typically disseminated-to-banded, and locally pyrite-chalcopyrite mineralisation fills brittle fractures in the siliceous mudstone. The Main lens is hosted by coarse-grained, polylithic, rhyolitic volcaniclastic rocks (Chong, 2004). Pyrite, sphalerite, chalcopyrite, and galena mineralisation is locally present as disseminations, anastomosing veins, and semi-massive to massive lenses.

The Ridge Zone West ore mineralogy is similar to the copper-lead-zinc-iron-rich sulfide assemblage described by Sinclair (2000) in the Battle orebody (Chong, 2004). Tennantite (Ag-bearing) occurs locally in the Main lens and is associated with sphalerite, chalcopyrite, galena, pyrite, and barite (Chong, 2004). Barite is ubiquitous in the Ridge Zone West orebody and is associated with sphalerite, galena, and quartz aggregates and veins with minor pyrite, chalcopyrite, and tennantite (Chong, 2004). Primary pyrite framboids are present, but are restricted to the Lower and Upper lenses. Evidence for re-crystallisation of early sulfides in the Main lens includes annealed sulfide grains, well developed triple-junctions, and migration of galena and chalcopyrite to pyrite grain boundaries (Chong, 2004). Compared to the Battle and HW orebodies, the Ridge Zone West orebody is zinc-rich, and copper-zinc sulfide zoning is poorly developed, and as such Chong (2004) attributed the re-crystallisation of ore minerals to metamorphism rather than hydrothermal zone-refining.

3.5 Summary

The local stratigraphy at Myra Falls includes rocks of the Price, Myra, Thelwood, and Flower Ridge Formations. The Myra Formation comprises two cycles of bimodal submarine volcanism and sedimentation. These two cycles are referred to as the lower and upper subdivision of the Myra Formation. Polymetallic VHMS deposits occur in the lower and upper Myra Formation and are hosted in felsic rocks of the H-W member and the L-M-P member, respectively.

- The complex submarine volcanic and sedimentary rock types at Myra Falls record the evolution of a NE-trending basin that was subsequently filled by bimodal coherent and volcaniclastic material and relatively deep marine sediments.
- In general, rhyolitic rocks are dominant in the northeast with basaltic rocks in the southeast

of the basin. In middle of the basin, the stratigraphy becomes intercalated with the addition of andesitic and dacitic volcanic material from the west (West-G Seamount) and east (Price Seamount) regions of the basin.

- Six stages of deformation have occurred at Myra Falls.
- VHMS orebodies of the H-W member have a district-scale metal zonation with copper-rich massive sulfide in the east to zinc-rich massive sulfide in the west.
- Principal base metal sulfide and sulfosalt ore minerals include sphalerite, chalcopyrite, galena with accessory tennantite-tetrahedrite, bornite, covellite, anilite, renierite, stromeyerite and colusite.
- Precious metals include native gold, native silver, electrum, hessite and stromeyerite.
- Primary gangue mineralogy consists of pyrite, barite, quartz, muscovite, chlorite and locally arsenopyrite and pyrrhotite.
- Semi-massive and massive polymetallic ores occur at two stratigraphic positions in the H-W member, which reflect changes in the sulfide deposition setting:

    1. "Contact zone" position mineralisation is located near the Price and Myra Formation contact beneath chert/argillite sedimentary rocks and is interpreted to represent seafloor sulfide accumulation.
    2. "Upper zone" position mineralisation is located 30 to 150 metres above the Price and Myra Formation contact within coarse rhyolitic volcaniclastic rocks proximal to coherent rhyolite flows, and is interpreted to represent sub-seafloor sulfide replacement.

Chapter 4:

Geology, Mineralisation and Alteration of the West Block Area

This chapter presents the first detailed description of the lithology and nature of VHMS mineralisation in the West Block Area. A lithostratigraphic framework is proposed for the West Block Area and presented on a series of detailed cross-section interpretations. The identification of faults and distribution of marine-sedimentary and volcanic rock types are further discussed using a series of district-scale, simplified cross-section interpretations that integrate the West Block Area and Ridge Zone North orebody. Sulfide mineralisation styles are described and characterised based on: (1) stratigraphic position relative to the Price Formation contact; (2) base and precious metal concentrations from drill hole assay results; and (3) sulfide and sulfosalt mineralogy determined by petrographic analysis. Alteration mineral assemblages defined from detailed drill core logging and petrographic analysis are described, and presented on detailed graphic logs and cross-section interpretations.

4.1 Methods

Thirty-one underground diamond drill holes were logged during two field seasons at Myra Falls carried out from September to December 2014 and October to December 2015. Approximately 5,850 metres of BQ and 830 metres of NQ drill core were logged detailing variations in lithology, alteration and sulfide mineralogy across the West Block Area. Samples were selected from these drill holes for detailed petrographic studies and microanalysis, which was carried out at CODES and the Central Science Laboratory (CSL) at the University of Tasmania (Appendix A). Geology and alteration cross-section interpretations were produced from integrating observations of detailed graphic logs and historic drill logs provided by the Nyrstar Myra Falls Operation. The location of the study area and distribution of detailed cross-section interpretations are summarised in Figure 4.1.

4.1.1 Discriminating lithological units

Detailed graphic logs were produced to document and interpret the geological variability in volcanic and sedimentary lithofacies identified in the West Block Area (Appendix B). Photographs of drill core boxes were examined and hand samples were collected to document and compare variations in lithology. Petrographic analysis of polished thin sections was

carried out to characterise the mineralogy and textural features of the different lithofacies discriminated in the graphic drill core logs.

4.1.2 Identifying faults from drill core

Oriented drill core was not available for this study. As a result, only the apparent angles to the core axis at the start and end of fault intervals were measured from drill core. The majority of faults observed in drill core occur as intervals of gouge and / or fragmented core. Fault intervals were documented on detailed graphic logs and larger faults were inferred from geological cross-section interpretations where possible.

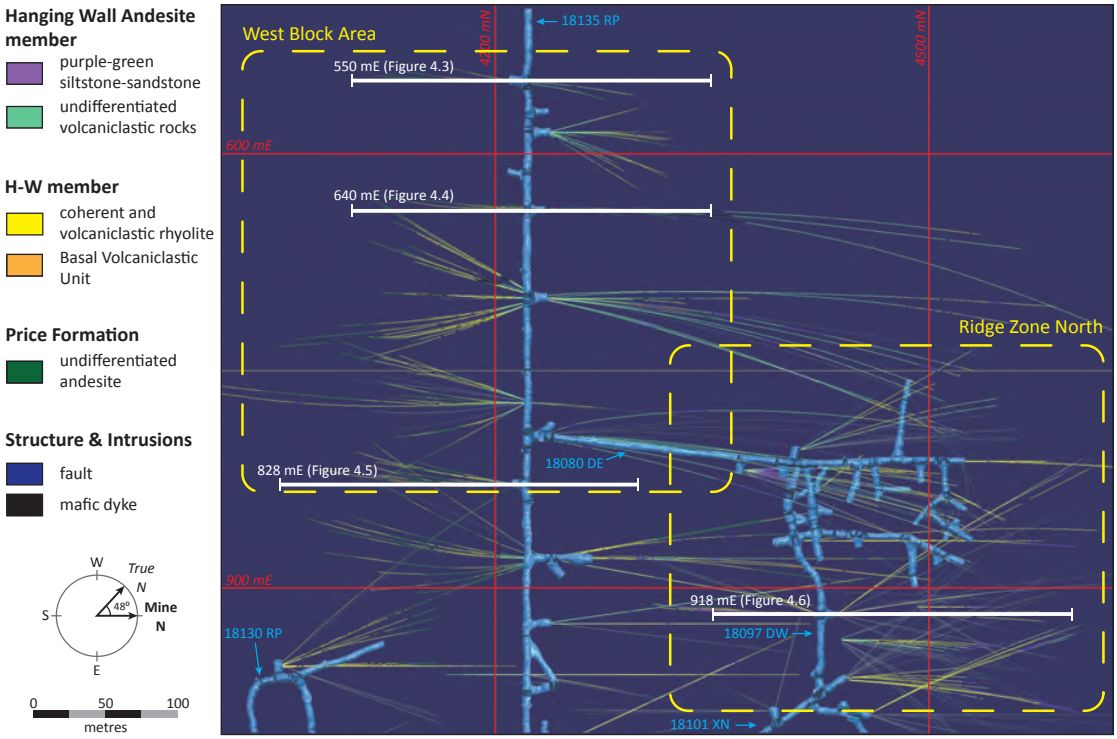

Figure 4.1 Plan view at 3,140 m relative level showing the West Block Area and Ridge Zone North localities and the locations of detailed cross-section interpretations at 550 mE, 640 mE, 828 mE and 918 mE (Figures 4.3-4.6).

4.1.3 Classification of sulfide mineralisation styles

Drill core observations and company assay results were integrated to characterise the variation in sulfide mineralisation across the West Block Area and the Ridge Zone North orebody. Sulfide textures were classified visually by detailed core logging. Drill hole assay results were used to assess base and precious metal zoning in relation to sulfide mineralisation textures. These data were combined with detailed lithology graphic logs to classify sulfide mineralisation styles based on stratigraphic position, mineralisation textures, and base and precious metal contents.

4.1.4 Sulfide, sulfosalt and telluride mineralogy

Seven polished thin sections from the West Block Area and six polished thin sections from the Ridge Zone North orebody were examined to identify sulfide, sulfosalt and precious metal-bearing minerals. Samples were selected based on drill core assay results, sulfide textures, and stratigraphic position. Reflected light and transmitted light microscopy at CODES, combined with MLA mineral mapping using a FEI MLA650 environmental scanning electron microscope

(SEM) at the CSL, UTAS was completed to preliminarily identify and locate mineral phases of interest. Initial chemical characterisation of mineral species of interest was confirmed by energy dispersive x-ray spectrometry (EDS) using a Hitachi SU-70 field emission scanning electron microscope (FE-SEM) at the CSL. Quantified mineral chemistries were measured by wavelength dispersive x-ray spectrometry (WDS) using a JEOL JXA 8530F Plus electron microprobe (EMP) at the CSL (Appendix C).

4.1.5 Characterising alteration facies

Alteration mineral facies in the West Block Area were identified from detailed drill core logging. The distribution of alteration in the West Block Area was investigated on cross-section interpretations. Alteration mineralogy and chemistry are further investigated in Chapter 5.

4.2 West Block Area Stratigraphy

The West Block Area is located between the developed Battle orebody and the resource-delineated Ridge Zone West orebody. Underground drill holes examined in this study were collared from the development of Level 18 (~3,000 metre relative level). New lithological observations from this study provide an opportunity to link the lithostratigraphic frameworks developed by Sinclair (2000) and Chong (2004) for the Battle and Ridge Zone West orebodies with the West Block Area.

Drill holes examined intersected coherent, volcaniclastic and marine sedimentary rocks of the Price and the lower Myra Formations (Figure 4.2). The Price Formation is characterised by coherent andesite with minor autoclastic breccia. The lower Myra Formation consists of coherent, volcaniclastic, and sedimentary rocks of the H-W member; andesitic volcaniclastic rocks of the Hanging Wall Andesite member; and coherent andesite lavas and autobreccias. The distribution of volcanic and sedimentary lithofacies identified from detailed graphic logging are summarised on north-south cross-section interpretations illustrated in Figures 4.3 to 4.6.

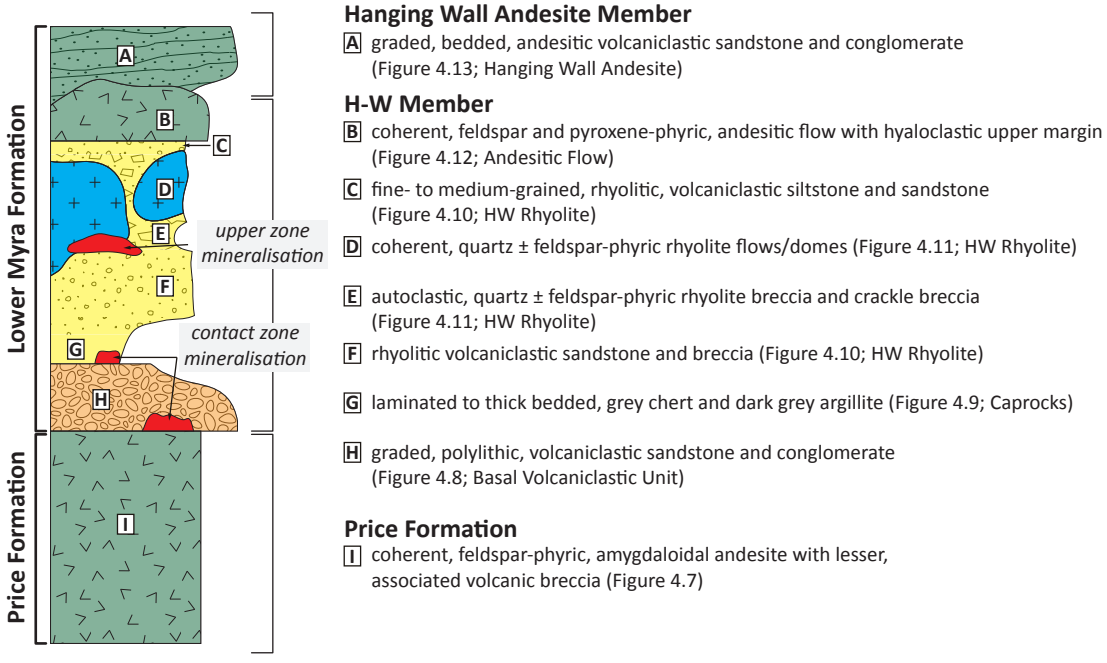

Figure 4.2 Stratigraphic column of the West Block Area lithostratigraphic units defined in this study.

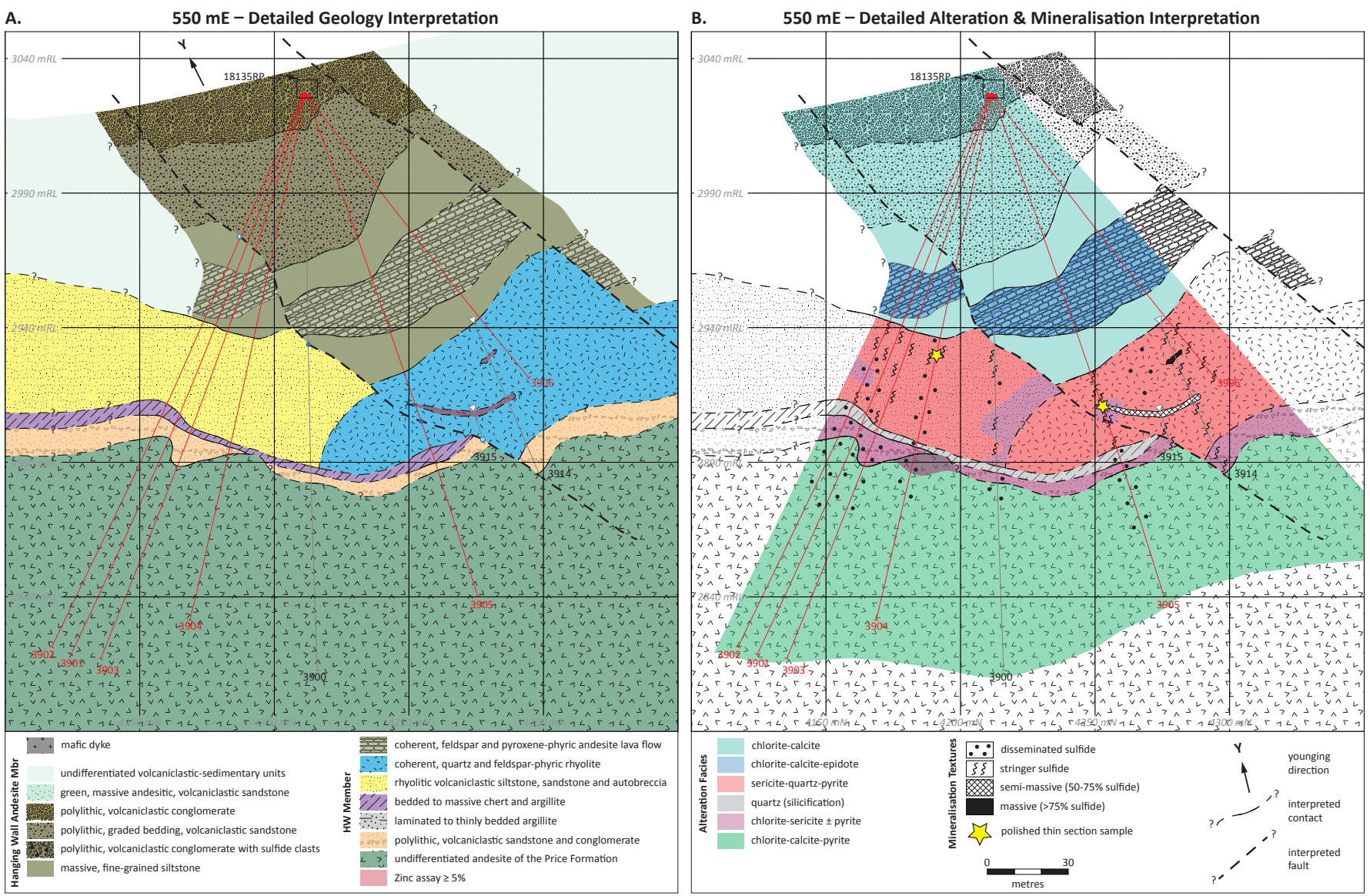

Figure 4.3 Detailed geology (A), alteration and mineralisation (B) cross-section interpretation 550 mE, looking west. Red drill-hole traces were logged by the candidate.

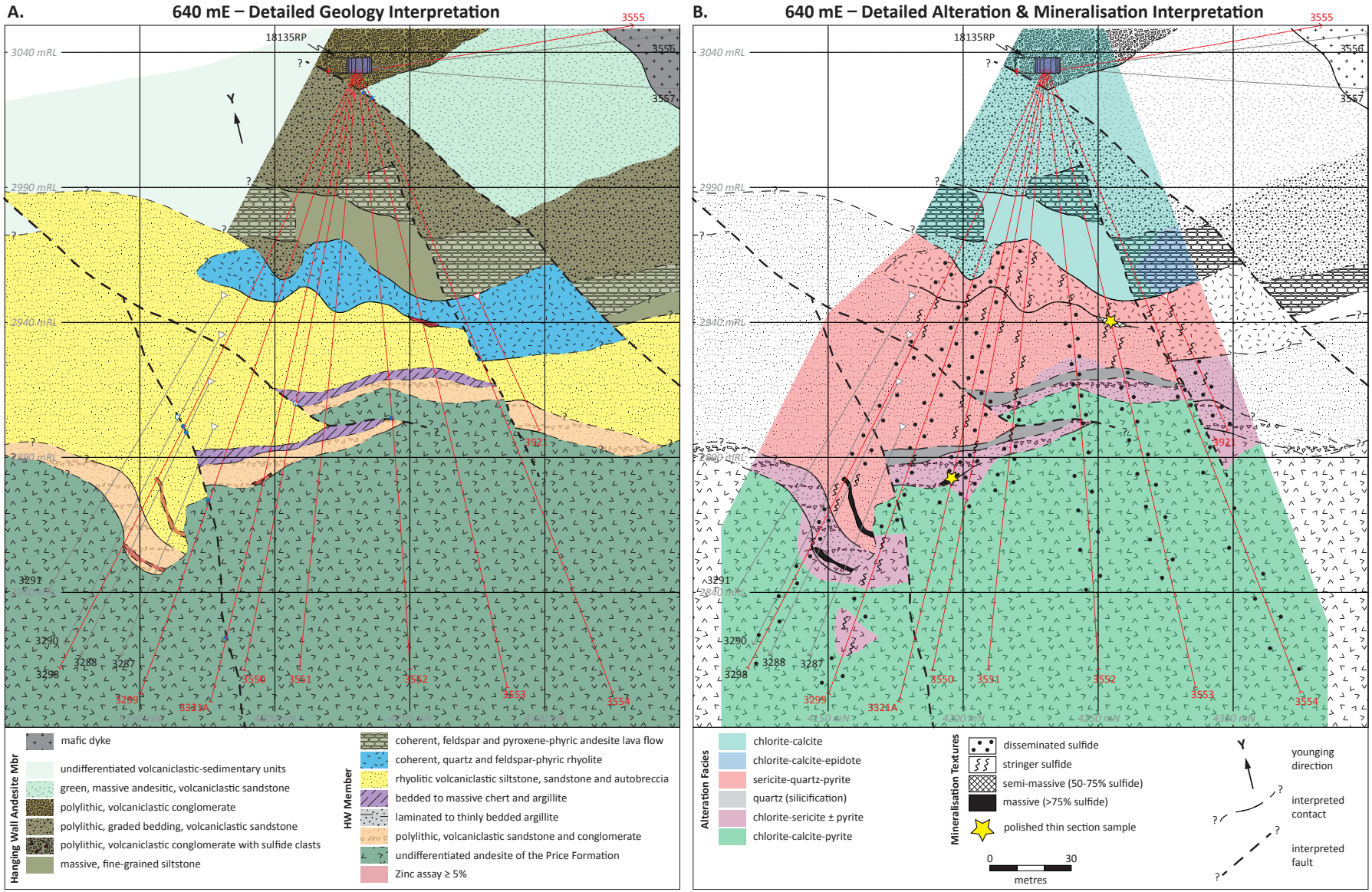

Figure 4.4 Detailed geology (A), alteration, and mineralisation (B) cross-section interpretation 640 mE, looking west. Red drill-hole traces were logged by the candidate.

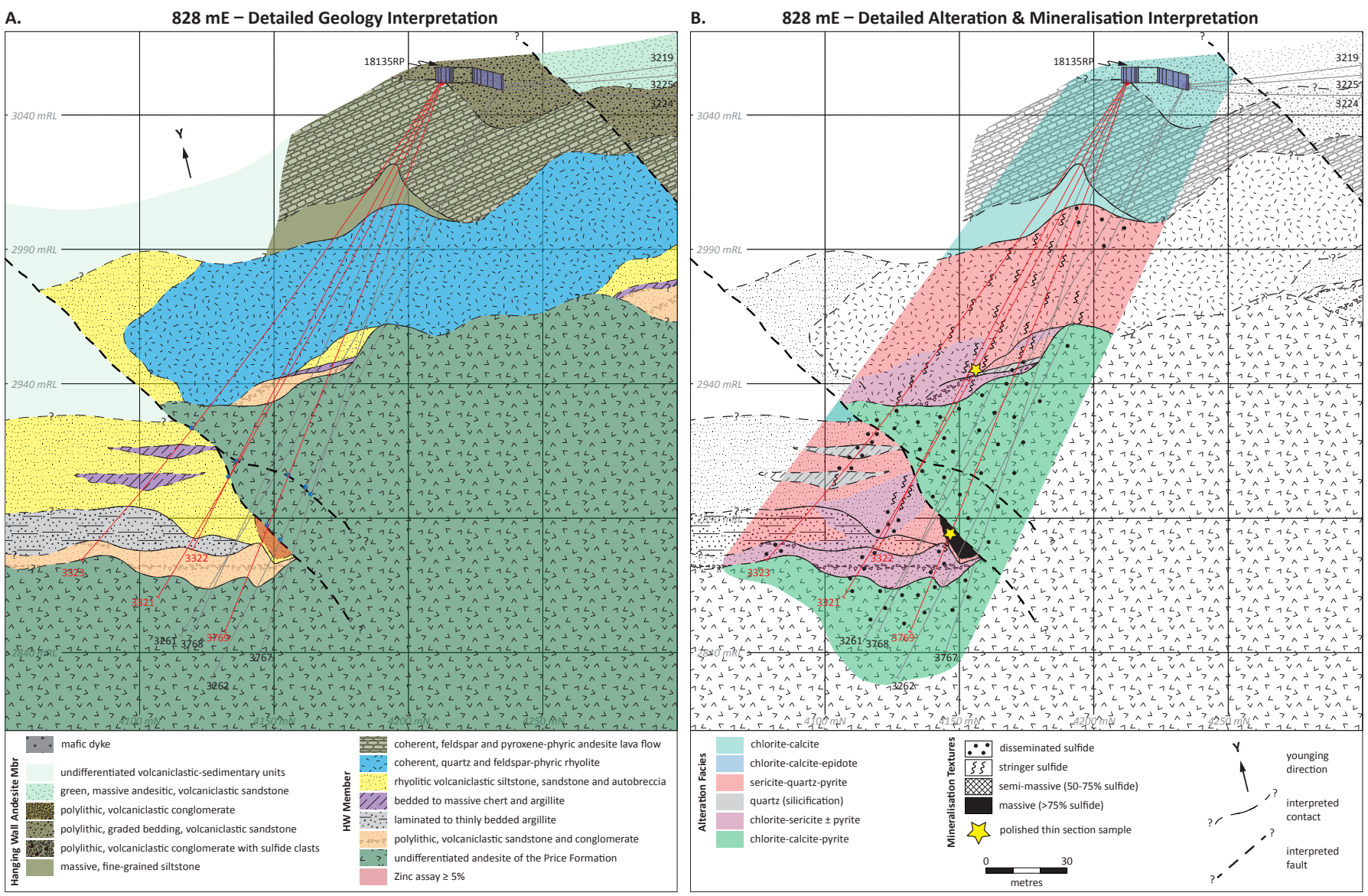

Figure 4.5 Detailed geology (A), alteration, and mineralisation (B) cross-section interpretation 828 mE, looking west. Red drill-hole traces were logged by the candidate.

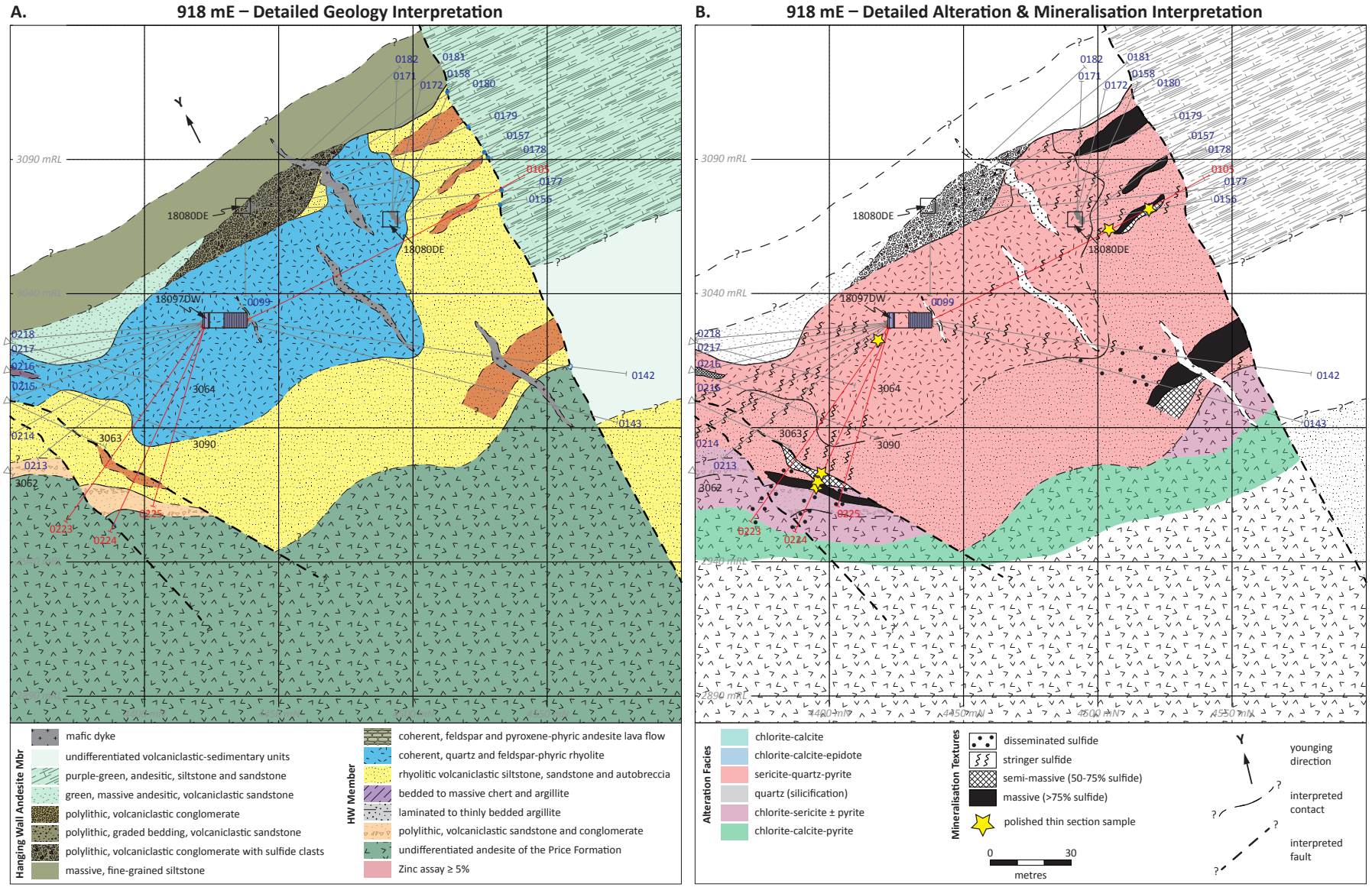

Figure 4.6 Detailed geology (A), alteration, and mineralisation (B) cross-section interpretation 918 mE, looking west. Red drill-hole traces were logged by the candidate.

4.2.1 Price Formation

Drill holes examined in the West Block Area intersected up to 80 metres of coherent andesite with subordinate volcaniclastic rocks of the Price Formation (e.g., Figure 4.4A). In drill core, coherent andesite varies from dark green to pale grey, which is interpreted to be the result of secondary chlorite-sericite-calcite ± pyrite alteration (Figure 4.7C, E). Coherent andesite lavas are feldspar-phyric with calcite-quartz amygdales and have a medium-grained, nonmagnetic groundmass (Figure 4.7). No pyroxene phenocrysts were observed.

4.2.2 Lower Myra Formation

The lower Myra Formation in the West Block Area comprises bimodal, coherent and volcaniclastic rocks with intercalated fine-grained marine sedimentary rocks (Figure 4.2). The sequence ranges from 150 to 175 metres in thickness, and consists of four lithostratigraphic units of the H-W member and one lithostratigraphic unit of the Hanging Wall Andesite member (Figures 4.3A-4.5A).

4.2.2.1 H-W member

The Basal Volcaniclastic Unit consists of normally-graded siltstone, sandstone and conglomerate, and is approximately 10 to 30 metres in thickness (e.g., Figure 4.5A). The Basal Volcaniclastic Unit of the lower Myra Formation in the West Block Area has a sharp contact with the top of the Price Formation (Figure 4.7A). This unit is matrix supported and is variably chlorite-sericite-pyrite altered, with minor disseminated chalcopyrite and sphalerite (Figure 4.8). The key lithological features of this unit are graded bedding, which indicates an upright younging direction (Figure 4.8B), and subrounded to subangular rhyolite and andesite clasts (Figure 4.8C-F).

The Caprocks are characterised by intercalated argillite and chert (Figure 4.9A). The argillite facies is brown to dark grey to black, laminated and thinly-bedded with disseminated pyrite (Figure 4.9C, E, G). Soft-sediment features such as flame structures are locally preserved (Figure 4.9E). The argillite facies is typically intercalated with chert (<1 to 10 cm thick beds; Figure 4.9A). The chert facies consists of pale grey-white, very fine-grained, silicified mudstone with diffuse bedding and laminations (Figure 4.9B, D, F). Disseminated pyrite (Figure 4.9B) is common, along with chalcopyrite-pyrite veins (Figure 4.9F). In the West Block Area the argillite-chert facies directly overlies the Basal Volcaniclastic Unit (e.g., Figure 4.3A; 4.6A) and typically ranges between 1 and 5 metres in thickness, but may be up to 15-metres-thick. Locally, ≥5-metre-thick units of interbedded argillite and chert is intercalated with rhyolitic volcaniclastic sandstones and breccia in the HW Rhyolite (Figure 4.5A).

The HW Rhyolite consists of rhyolitic volcaniclastic siltstone, sandstone and breccia, and coherent rhyolite and autobreccia. The rocks are moderately to intensely sericite-chlorite-quartz-pyrite altered. Pervasive hydrothermal alteration obscures and largely destroys primary volcanic textures in all but the least-altered HW Rhyolite rock types. Primary volcanic textures observed in hand samples include quartz, and sericite altered feldspar phenocrysts. The HW Rhyolite in the West Block Area is between 30 and 90 metres thick (Figures 4.3A-4.6A).

The rhyolitic volcaniclastic facies comprises sandstone-siltstone and less abundant breccia (Figure 4.10). Internal bed contacts appear gradational, however, they are largely indistinguishable due to alteration. Rhyolitic volcaniclastic breccia has cm-scale, subrounded to subangular quartz-phyric rhyolite clasts in a fine-grained, crystal-rich matrix (Figure 4.10B).

Rhyolitic volcaniclastic sandstones have a variably sericite altered, fine- to medium-grained crystal-rich matrix (Figure 4.10C-G).

In the West Block Area, coherent rhyolite and autobreccia facies consist of massive to clastic quartz and feldspar-phyric rhyolite. Evenly distributed, 1 to 3 mm quartz phenocrysts are the diagnostic feature of this unit (Figure 4.11E, G). Feldspar phenocrysts (2-5%) are often obscured by intense sericite alteration, but where visible comprise 1 to 2 mm tabular, white phenocrysts (Figure 4.11C, G). The groundmass consists of a mosaic of quartz, feldspar and sericite (Figure 4.11H-J). Primary volcanic quartz phenocrysts are typically embayed and can have quartz altered rims, whereas feldspar phenocrysts are variably sericite altered (Figure 4.11H-J). Margins of coherent rhyolite are marked by massive rhyolite crackle breccia and rhyolite autobreccia (Figure 4.11B, D, F). Locally, the matrix of quartz and feldspar-phyric rhyolite breccia has been replaced by sulfides (Figure 4.11F).

Quartz and feldspar-phyric rhyolite in the West Block Area varies in thickness from 10 to 40 metres and overlies the rhyolitic volcaniclastic sandstone facies (Figures 4.3A-4.5A). The lower contact is characterised by quartz and feldspar-phyric rhyolite autobreccia, ranging from 5 to 15 metres in thickness and grades upwards into massive, coherent quartz and feldspar-phyric rhyolite. Intense sericite, and locally sulfide mineralisation, obscures the nature of the lower contact.

Andesite Lava Flow is characterised by a dark green, medium-grained, and nonmagnetic groundmass with 10-20% plagioclase (0.1-1 mm) and 5% pyroxene phenocrysts (<1 mm; Figure 4.12). In the West Block Area this unit is 10 to 50 metres in thickness (Figures 4.3A-4.5A) with a 5 to 10-metre-thick carapace of jig-saw-fit, autoclastic breccia (Figure 4.12B, D). This unit is relatively unaltered, with only a minor chlorite-calcite-epidote altered groundmass.

4.2.2.2 Hanging Wall Andesite member

This member comprises andesitic, polylithic volcaniclastic sandstone and conglomerate (Figure 4.13). The base of the unit is characterised by polylithic, normal to reverse graded, volcaniclastic conglomerate and sandstone (Figure 4.13B-C) with less abundant massive siltstone. Subangular volcanic clasts are primarily andesitic with subordinate, quartz and feldspar-phyric rhyolite (Figure 4.13A, C), and rare massive sulfide and chert clasts (Figure 4.13D-E). In thin section the fine-grained matrix is calcite-chlorite altered and supports quartz crystals (<500 μm in size), fine-grained andesitic lithic fragments, and feldspar-phyric andesite clasts (Figure 4.13G-H). The upper Hanging Wall Andesite member observed in the West Block Area consists of interbedded, fining upwards, andesitic bedded sandstone and siltstone (Figure 4.13F).

4.2.3 Mafic dykes

Mafic dykes intrude rocks of the Price Formation and lower Myra Formation. Dykes are equigranular (Figure 4.14A-D) and porphyritic (Figure 4.14E-H) in texture; have a nonmagnetic groundmass and chilled margins. Dykes are generally 10 to 30-centimetres-wide and locally up to 10-metres-wide. Mafic dykes that intrude HW Rhyolite lithofacies can be variably altered to chlorite-calcite-pyrite (Figure 4.14A-B) or appear relatively less altered (Figure 4.14C-D). The intrusive relationships suggest that mafic dykes post-date deposition of the HW Rhyolite and in some cases post-date VHMS mineralisation. However, the age and magmatic affinity of these dykes were not investigated in this study.

Figure 4.7 Examples of Price Formation andesite in the West Block Area.

A. BQ drill core interval from BG18-3904 showing massive andesite of the Price Formation and contact with the Basal Volcaniclastic Unit at 137.3 metres.

B. Andesite breccia from BG18-3903 at 189.0 metres. White lines outlining clasts of andesite.

C. Sericite-calcite-pyrite altered feldspar-phyric andesite from RN18-0224 at 78.3 metres.

D. Pseudo-breccia texture in patchy, chlorite-sericite altered, amygdaloidal andesite from RN18-0223 at 88.0 metres.

E. Feldspar-phyric, massive andesite from BG18-3553 at 133.1 metres.

F. Amygdaloidal, feldspar-phyric massive andesite from BG18-3901 at 202.0 metres.

G. Medium-grained, feldspar-phyric massive andesite from BG18-3901 at 149.1 metres.

H-I. Plane polarised light and cross polarised light photomicrographs showing concentrically zoned chlorite-quartz amygdales and epidote-sericite altered feldspar phenocrysts from sample BM14-043. Red lines outlining amygdales (A) and altered feldspar phenocrysts (F).

[A, amygdale; Bvc, basal polylithic volcaniclastic unit; F, feldspar phenocryst; PA, Price Formation andesite; PPL, plane polarised light; py, pyrite; XPL, cross polarised light]

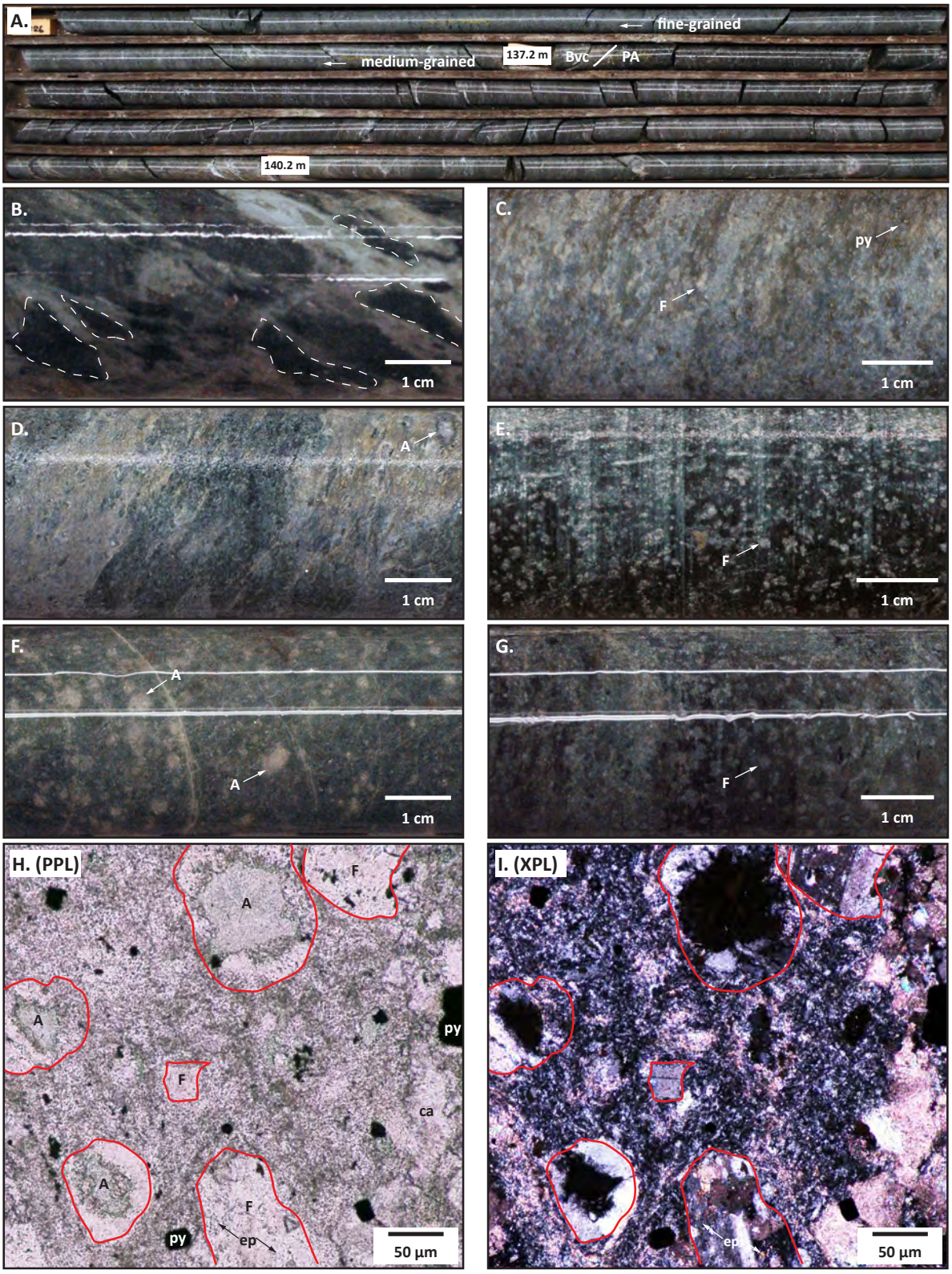
A.
fine-grained
medium-grained
137.2 m
Byc
PA
140.2 m
B.
1 cm
C.
py
F
1 cm
D.
A
1 cm
E.
F
1 cm
F.
A
A
1 cm
G.
F
1 cm
H. (PPL)
A
F
A
py
F
ca
A
F
py
ep
50 µm
I. (XPL)
ep
50 µm

Figure 4.8 Examples of Basal Volcaniclastic Unit of the lower Myra Formation in the West Block Area

A. BQ drill core interval from BG18-3903 showing coarse-grained, polylithic, volcaniclastic conglomerate intruded by ~20 cm wide mafic dykes.

B. Fining-upward, graded contact between medium-grained, polylithic, volcaniclastic sandstone and fine-grained, polylithic, volcaniclastic sandstone from BG18-3550 at 144.9 metres.

C. Chlorite-sericite-pyrite altered polylithic, volcaniclastic conglomerate with subrounded-subangular felsic and andesitic clasts from BG18-3321a at 147.5 metres. White dashed lines outlining lithic clasts.

D. Chlorite-sericite altered polylithic, volcaniclastic conglomerate with subangular lithics and disseminated pyrite-sphalerite-chalcopyrite mineralisation from BG18-3321a at 150.9 metres. White dashed lines outlining lithics.

E. Plane and cross polarised light photomicrographs of polylithic, volcaniclastic conglomerate showing quartz crystal fragments and mafic lithic clasts from sample BM14-023. Red dashed lines outlining quartz crystals and lithic clast.

F. Cross polarised light thin section scan showing clastic nature of the Basal Volcaniclastic Unit from sample BM14-023.

[cpy, chalcopyrite; L, lithic; Md, mafic dyke; PPL, plane polarised light; py, pyrite; sp, sphalerite; XPL, cross polarised light]

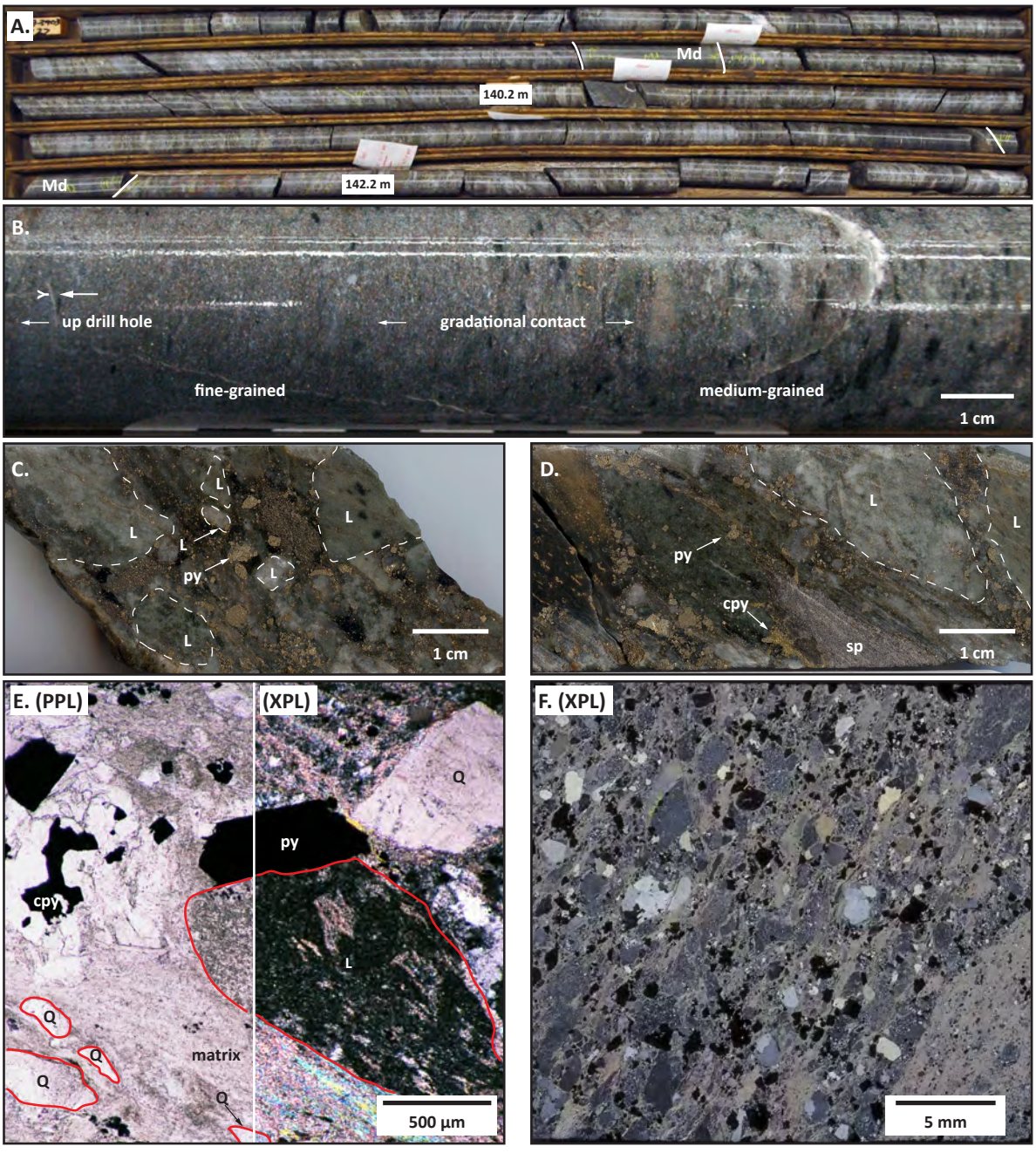
A.
Md
140.2 m
Md
142.2 m
B.
up drill hole
gradational contact
fine-grained
medium-grained
1 cm
C.
L
L
L
L
L
L
py
1 cm
D.
L
L
py
cpy
sp
1 cm
E. (PPL)
(XPL)
Q
py
cpy
L
Q
matrix
Q
Q
Q
500 µm
F. (XPL)
5 mm

Figure 4.9 Examples of argillite and chert of the Caprocks in the West Block Area.

A. BQ drill core interval from BG18-3552 showing bedded argillite (dark and light grey) and chert (white). Note the planar contact between the bedded argillite-chert with an interval of normally-graded, Basal Volcaniclastic Unit at 115.1 metres. Normally-graded bedding indicates a up-hole younging direction.

B. Example of mm-cm scale, bedded chert and argillite with pyritic layers in chert from BG18-3321a at 141.5 metres. White dashed line denotes bedding.

C. Finely-bedded argillite and chert from BG18-3551 at 111.2 metres.

D. White-grey chert from BG18-3769 at 112.3 metres.

E. Laminated, pyritic argillite with flame bedding structure suggesting an up-hole younging direction from BG18-3769 at 113.8 metres.

F. White to light grey chert with crosscutting chalcopyrite-pyrite filled fracture from BG18-3952 at 110.1 metres.

G. Thin bedded argillite with pyrite from BG18-3550 at 108.2 metres.

[A/C, argillite and chert; Bvc, basal polylithic volcaniclastic unit; cpy, chalcopyrite; py, pyrite]

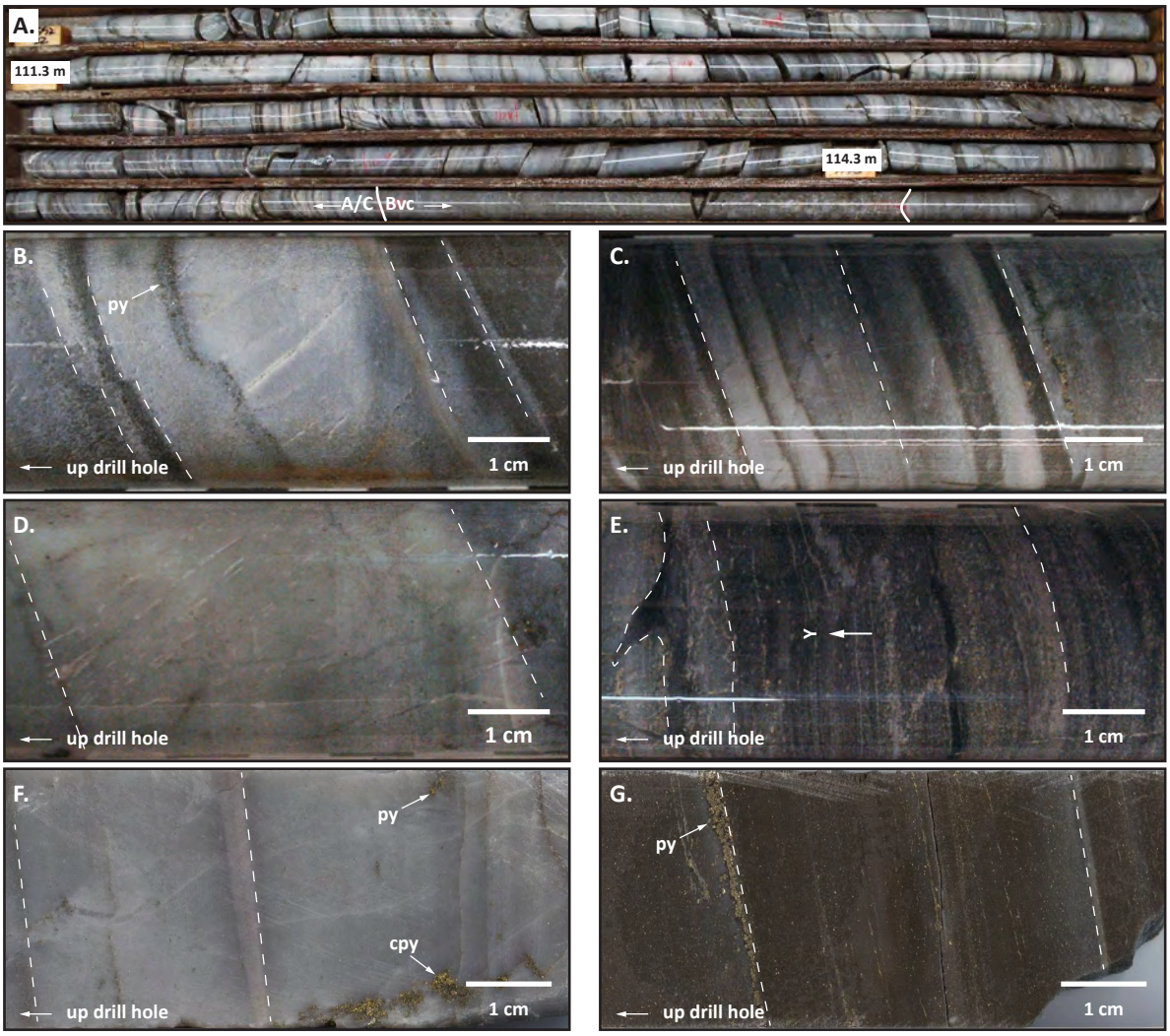
A.
111.3 m
114.3 m
A/C
Bvc
B.
py
up drill hole
1 cm
C.
up drill hole
1 cm
D.
up drill hole
1 cm
E.
y
up drill hole
1 cm
F.
py
cpy
up drill hole
1 cm
G.
py
up drill hole
1 cm

Figure 4.10 Examples of rhyolitic volcaniclastic rocks of the HW Rhyolite in the West Block Area.

A. BQ drill core interval from BG18-3321a showing sericite-pyrite altered, medium-grained, rhyolitic volcaniclastic sandstone.

B. Sericite altered, coarse-grained, rhyolitic volcaniclastic breccia with altered quartz-phyric rhyolite clasts from BG18-3298 at 185.9 metres. White dashed lines outline clast of rhyolite.

C. Sericite-pyrite altered, fine-grained, quartz crystal-rich, rhyolitic volcaniclastic sandstone from BG18-3550 at 105.1 metres.

D. Sericite-pyrite altered, rhyolitic volcaniclastic sandstone with mm-scale quartz crystals from BG18-3952 at 98.2 metres.

E. Sericite-quartz and fine-grained, sulfide altered, rhyolitic volcaniclastic sandstone with mm-scale quartz crystals from BG18-3952 at 105.2 metres.

F-G. Cross polarised light photomicrograph examples of quartz-sericite-sulfide altered, fine- to medium-grained, rhyolitic volcaniclastic sandstones from samples BM14-035 (F) and RN1504 (G).

[py, pyrite; Q, quartz; XPL, cross polarised light]

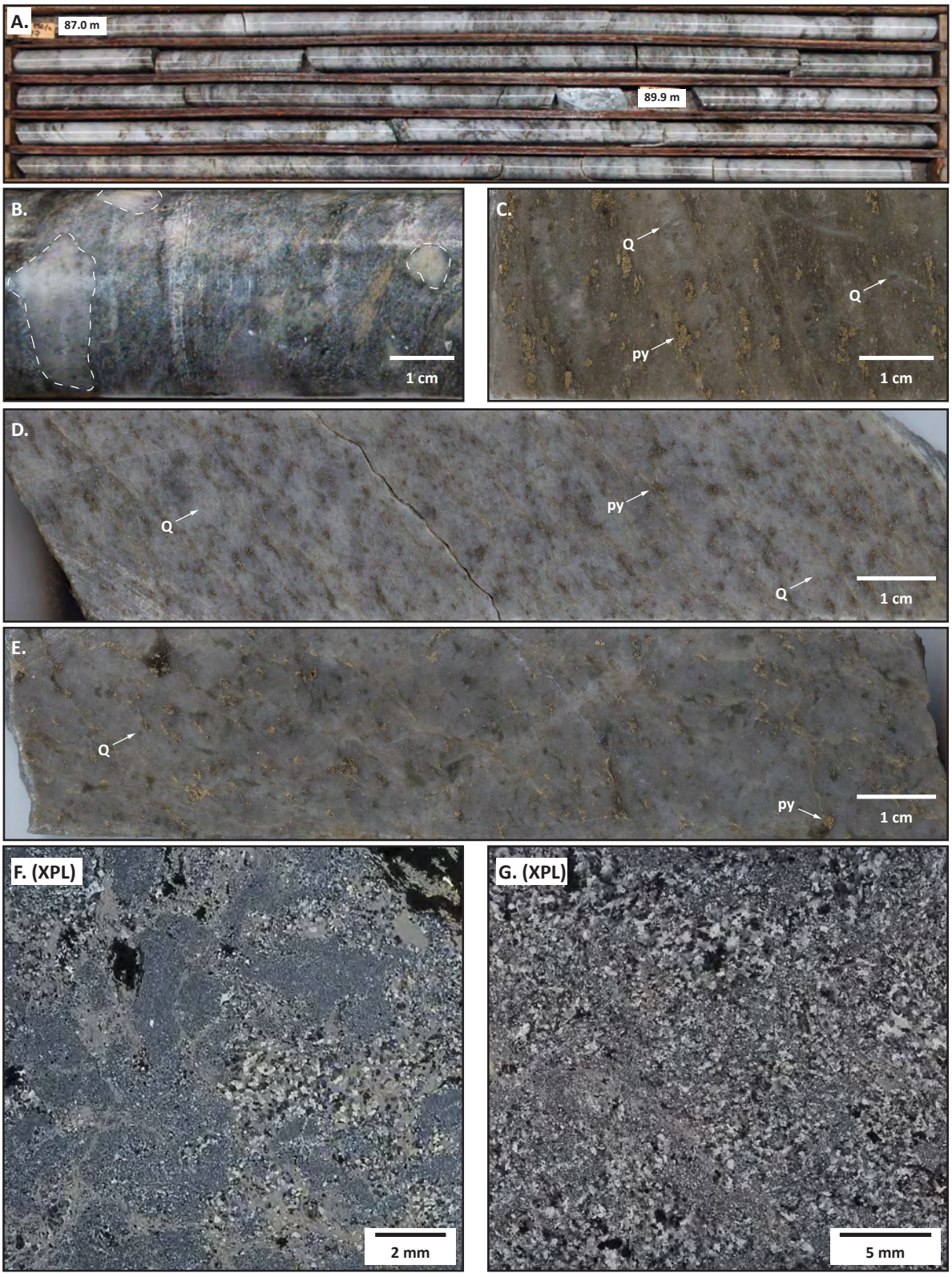
A.
87.0 m
89.9 m
B.
1 cm
C.
Q
Q
py
1 cm
D.
Q
py
Q
1 cm
E.
Q
py
1 cm
F. (XPL)
2 mm
G. (XPL)
5 mm

Figure 4.11 Examples of coherent rhyolite and rhyolite autobreccia of the HW Rhyolite in the West Block Area.

A. BQ drill core interval from BG18-3952 showing massive, sericite-pyrite altered, quartz and feldspar-phyric rhyolite.

B. Sericite-quartz altered, rhyolite crackle breccia from RN18-0225 at 48.9 metres.

C. Sericite-quartz altered, feldspar-phyric coherent rhyolite from BG18-3952 at 73.8 metres.

D. Sericite-quartz altered, coherent rhyolite autobreccia from BG18-3952 at 64.5 metres. White dashed lines outline interpreted autobreccia rhyolite clasts.

E. Sericite-quartz altered, quartz-phyric rhyolite from RN18-0224 at 43.4 metres.

F. Sericite-pyrite altered, quartz-phyric rhyolite autobreccia from BG18-3321 at 51.8 metres.

G. Sericite-quartz-pyrite altered, quartz and feldspar-phyric coherent rhyolite from BG18-3322 at 78.5 metres.

H. Cross polarised light photomicrograph of quartz phenocrysts rimmed by secondary quartz in sericite altered mosaic groundmass from sample BM14-060.

I. Cross polarised light photomicrograph of embayed primary quartz phenocryst from sample UPB08.

J. Plane polarised and cross polarised light photomicrographs of embayed primary quartz and altered feldspar phenocrysts from sample BM14-021. Red lines outline altered feldspar phenocrysts.

[F, feldspar phenocryst; PPL, plane polarised light; py, pyrite; Q, quartz phenocryst; XPL, cross polarised light]

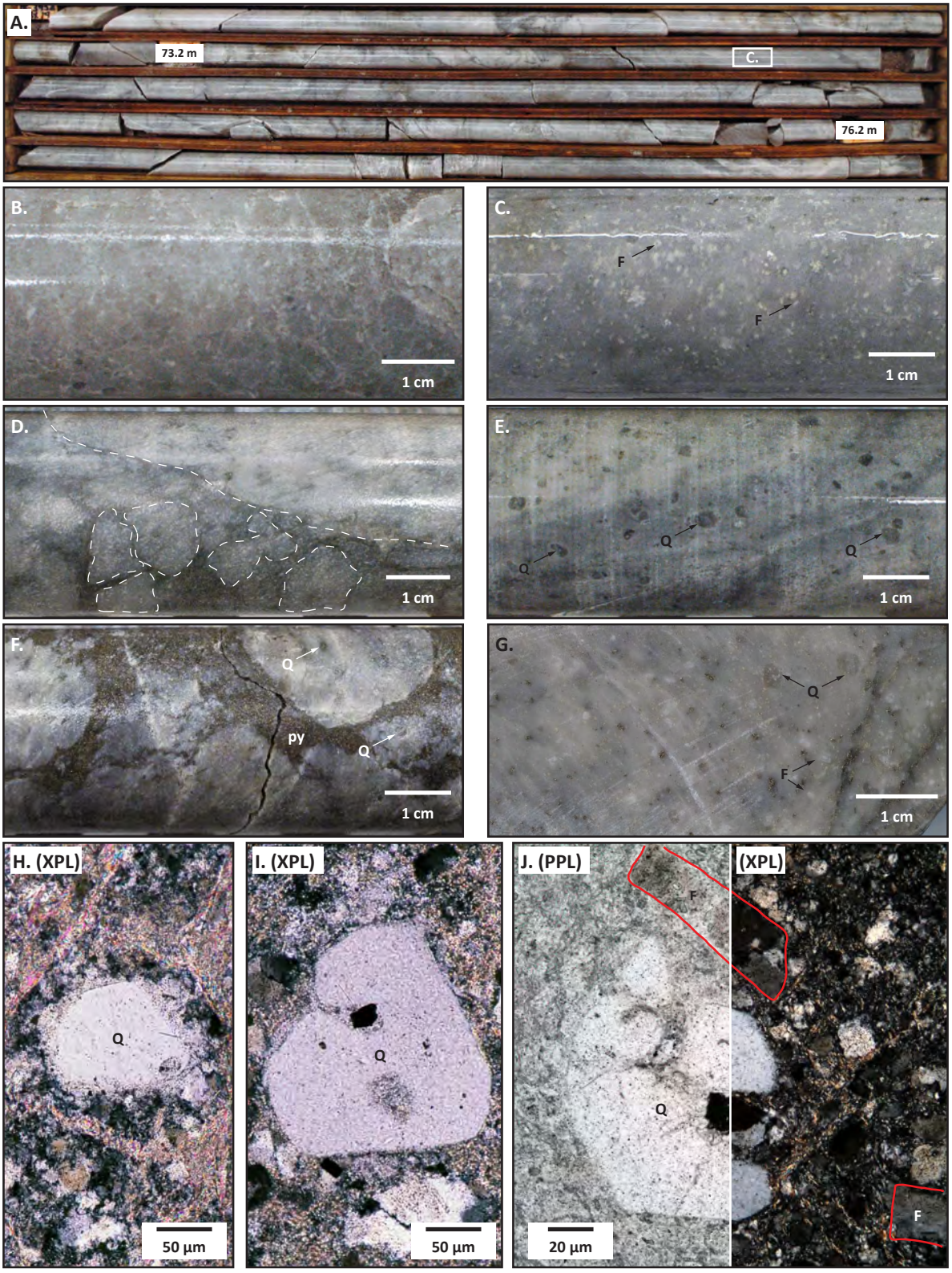
A.
73.2 m
C.
76.2 m
B.
1 cm
C.
F
F
1 cm
D.
1 cm
E.
Q
Q
Q
1 cm
F.
Q
py
Q
1 cm
G.
Q
F
1 cm
H. (XPL)
Q
50 µm
I. (XPL)
Q
50 µm
J. (PPL)
F
Q
20 µm
(XPL)
F

Figure 4.12 Examples of coherent andesite and andesite autobreccia of andesite flow unit in the West Block Area.

A. BQ drill core interval from BG18-3921 showing feldspar-phyric massive andesite.

B. Example of hyaloclastite, jig-saw-fit, andesite autobreccia from BG18-3322 at 10.0 metres.

C. Fine-grained, feldspar-phyric massive andesite from BG18-3321 at 25.7 metres.

D. Example of hyaloclastite, jig-saw-fit, feldspar and pyroxene-phyric, andesite autobreccia from BG18-3908 at 56.9 metres.

E. Feldspar and pyroxene-phyric andesite from BG18-3921 at 57.9 metres.

F. Plane polarised and cross polarised light photomicrographs of primary feldspar phenocrysts from sample BM14-012. Red lines outline feldspar phenocrysts.

G. Plane polarised and cross polarised light photomicrographs of primary pyroxene phenocrysts from sample BM14-012. Red lines outline pyroxene phenocrysts.

[F, feldspar; P, pyroxene; PPL, plane polarised light; XPL, cross polarised light]

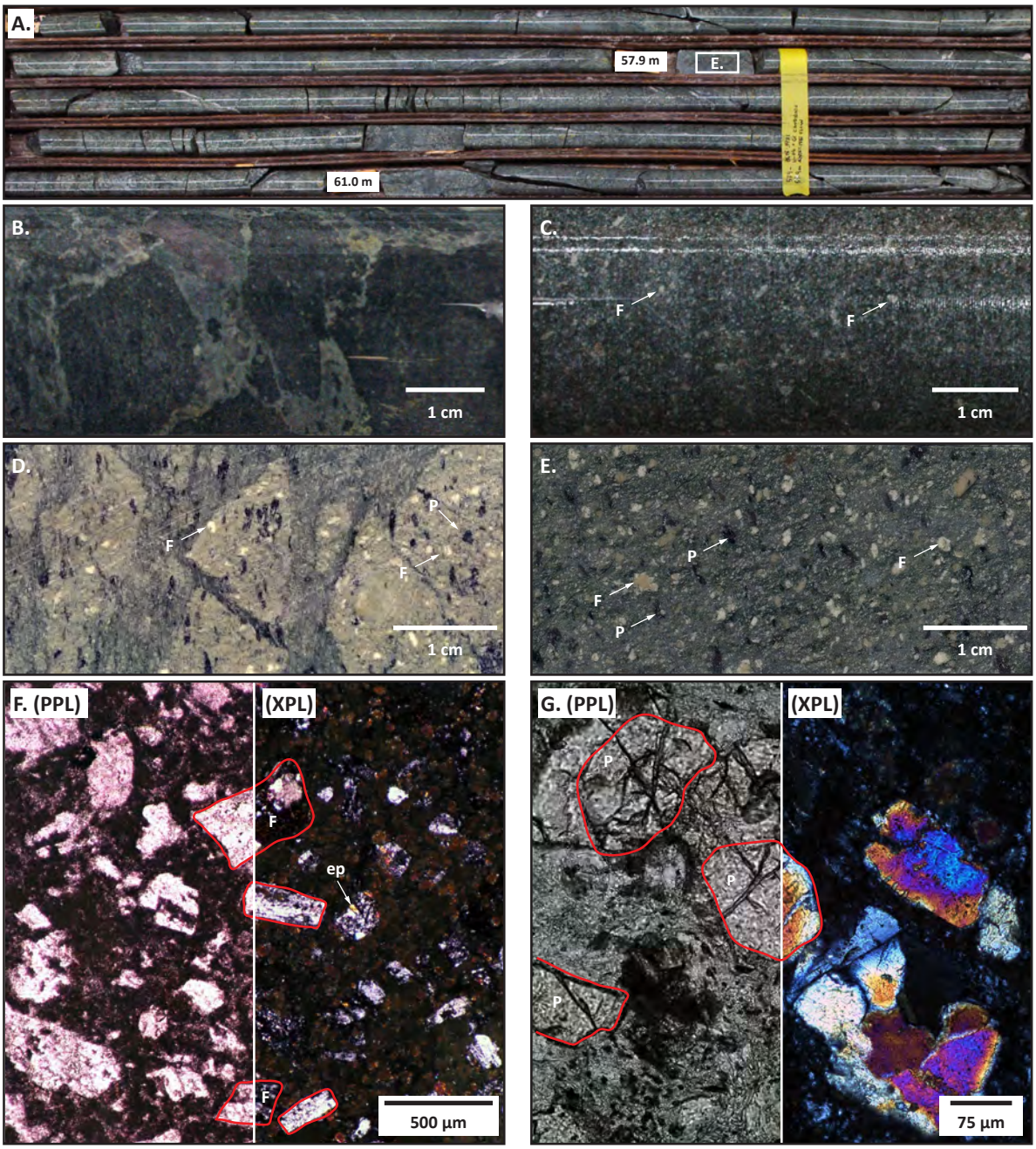
A.
57.9 m
E.
61.0 m
B.
1 cm
C.
F
F
1 cm
D.
F
P
F
1 cm
E.
P
F
F
P
1 cm
F. (PPL)
(XPL)
F
ep
F
500 µm
G. (PPL)
P
P
P
(XPL)
75 µm

Figure 4.13 Examples of the Hanging Wall Andesite member lithofacies in the West Block Area.

A. BQ drill core interval from BG18-3901 showing polylithic, andesitic, volcaniclastic sandstone and breccia.

B. Medium-grained, andesitic, volcaniclastic sandstone from BG18-3555 at 54.1 metres.

C. Polylithic, andesitic, volcaniclastic breccia with felsic and andesitic lithics from BG18-3555 at 49.7 metres. White dashed lines outline lithic clasts.

D. Example of rare massive pyrite clast in volcaniclastic andesite from BG18-3552 at 54.3 metres.

E. Example of rare chert clast in volcaniclastic andesite from BG18-3952 at 20.9 metres. Yellow line outlines clast of chert.

F. Bedded, andesitic, volcaniclastic siltstone and sandstone from BG18-3921 at 2.5 metres. Yellow lines denote bedding.

G-H. Plane polarised light photomicrographs of polylithic, andesitic, volcaniclastic breccia showing lithic clasts from sample BM14-001. Red lines outline lithic clasts and quartz crystal-fragments.

[L, lithic; PPL, plane polarised light; Q, quartz]

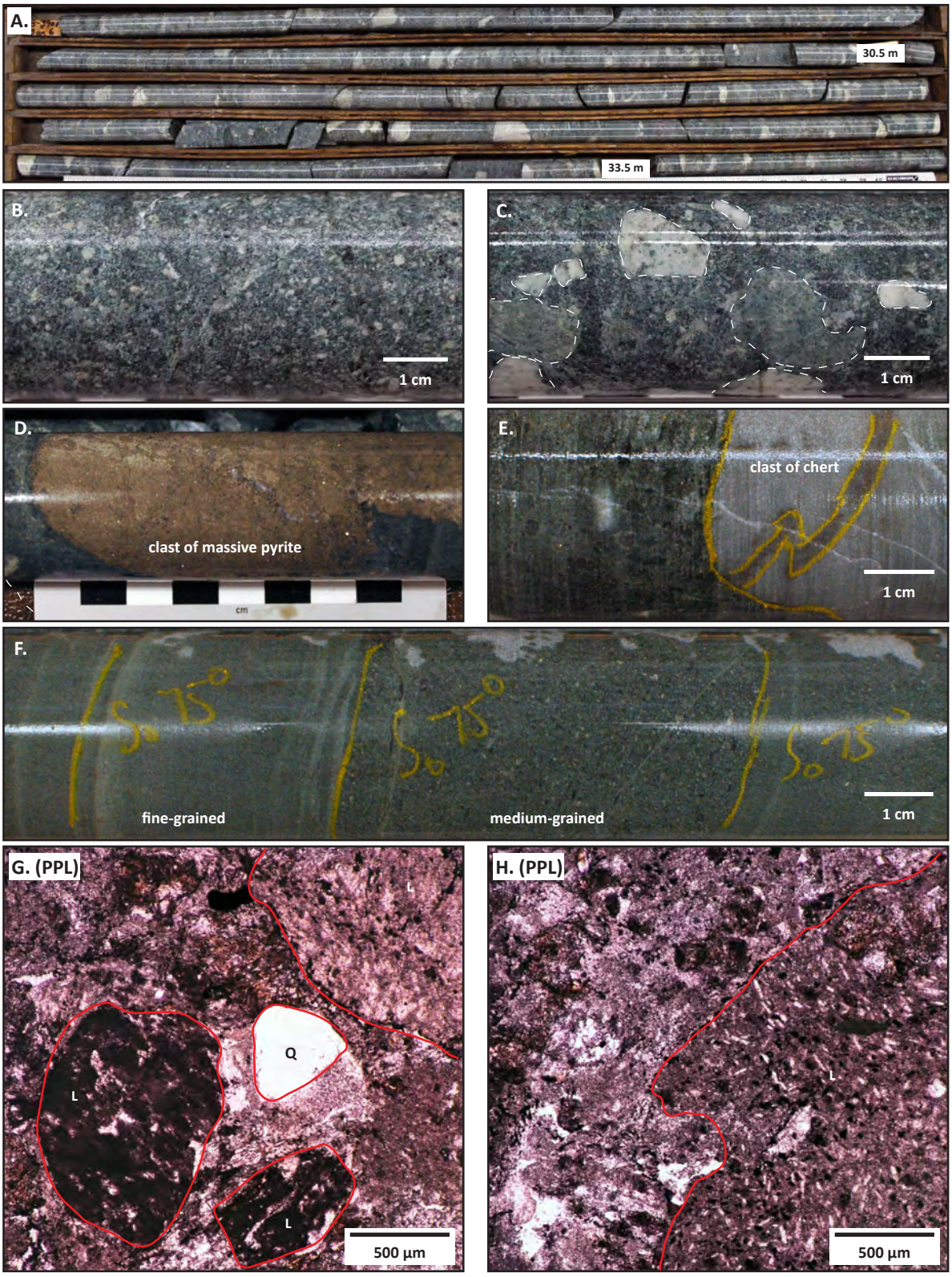
A.
30.5 m
33.5 m
B.
1 cm
C.
1 cm
D.
clast of massive pyrite
E.
clast of chert
1 cm
F.
fine-grained
medium-grained
1 cm
G. (PPL)
L
Q
L
L
500 µm
H. (PPL)
L
500 µm

Figure 4.14 BQ drill core photographs of mafic dyke intrusions in the West Block Area.

A-B. Pyrite-chlorite-calcite altered, fine-grained, mafic dykes crosscutting altered HW Rhyolite (A) from BG18-3836 at 40.4 metres and (B) from RN18-0224 at 21.5 metres.

C-D. Relatively unaltered, fine-grained, mafic dykes crosscutting HW Rhyolite (C) from BG18-3322 at 118.9 metres and (D) from BG18-3901 at 120.5 metres.

E. Relatively unaltered, amphibole and feldspar-phyric, mafic dyke crosscutting Hanging Wall Andesite polylithic, volcaniclastic sandstone from BG18-3555 at 176.0 metres.

F. Calcite altered groundmass, amphibole and feldspar-phyric, mafic dyke crosscutting HW Rhyolite from BG18-3321 at 112.1 metres.

G-H. Photomicrographs of sample BM14-037 of rock photograph F. Cross polarised and plane polarised light photomicrographs of altered amphibole phenocryst (G) and calcite-albite altered primary mafic phenocrysts and altered amphibole phenocrysts (H). Red lines outline amphibole phenocrysts.

[Am, amphibole; ca, calcite; F, feldspar; PPL, plane polarised light; py, pyrite; q, quartz; XPL, cross polarised light]

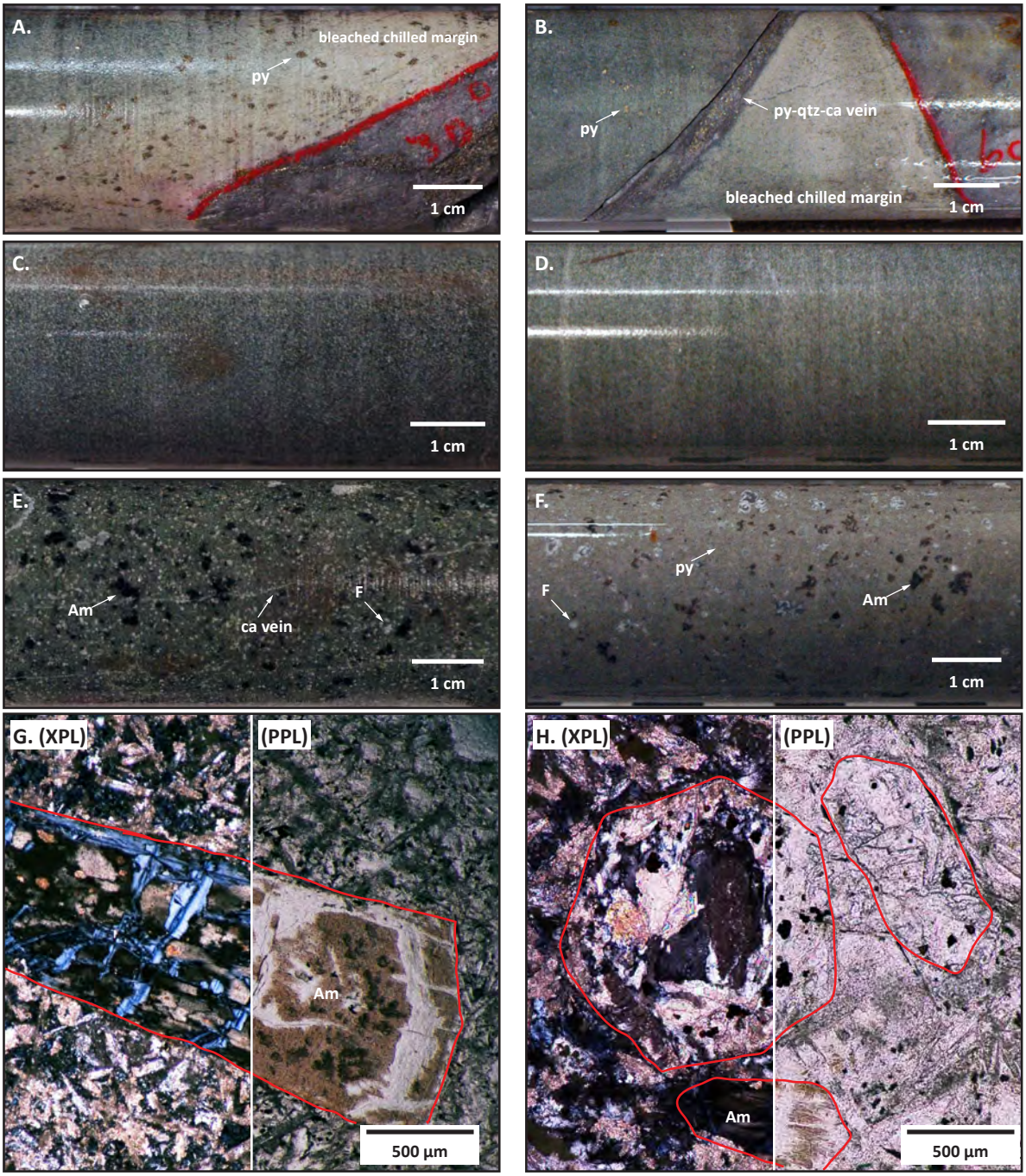
A.
bleached chilled margin
py
1 cm
B.
py
py-qtz-ca vein
bleached chilled margin
1 cm
C.
1 cm
D.
1 cm
E.
Am
ca vein
F
1 cm
F.
py
F
Am
1 cm
G. (XPL)
(PPL)
Am
500 µm
H. (XPL)
Am
(PPL)
500 µm

4.2.4 Discussion of stratigraphic relationships

Stratigraphic columns in Figure 4.15 illustrate the stratigraphic relationships of the lower Myra Formation in the West Block Area with the Ridge Zone West (Chong, 2004) and Battle orebodies (Robinson et al., 1996; Sinclair, 2000). In the Battle orebody and West Block Area localities (Figures 4.3A-4.5A), coherent rhyolite flows are a major stratigraphic component at the top of the H-W member. Rhyolitic volcaniclastic breccia and sandstone dominate the sequence below the coherent facies, and becomes interlayered with argillite, chert and rhyolitic siltstone and sandstone down section, in the West Block Area (e.g., Figure 4.5A) and near the Battle orebody. To the west of the West Block Area, the lower Myra Formation transitions to interlayered argillite, chert and felsic volcaniclastic breccia and sandstone, with no coherent rhyolite facies observed in the Ridge Zone West section (Figure 4.15A).

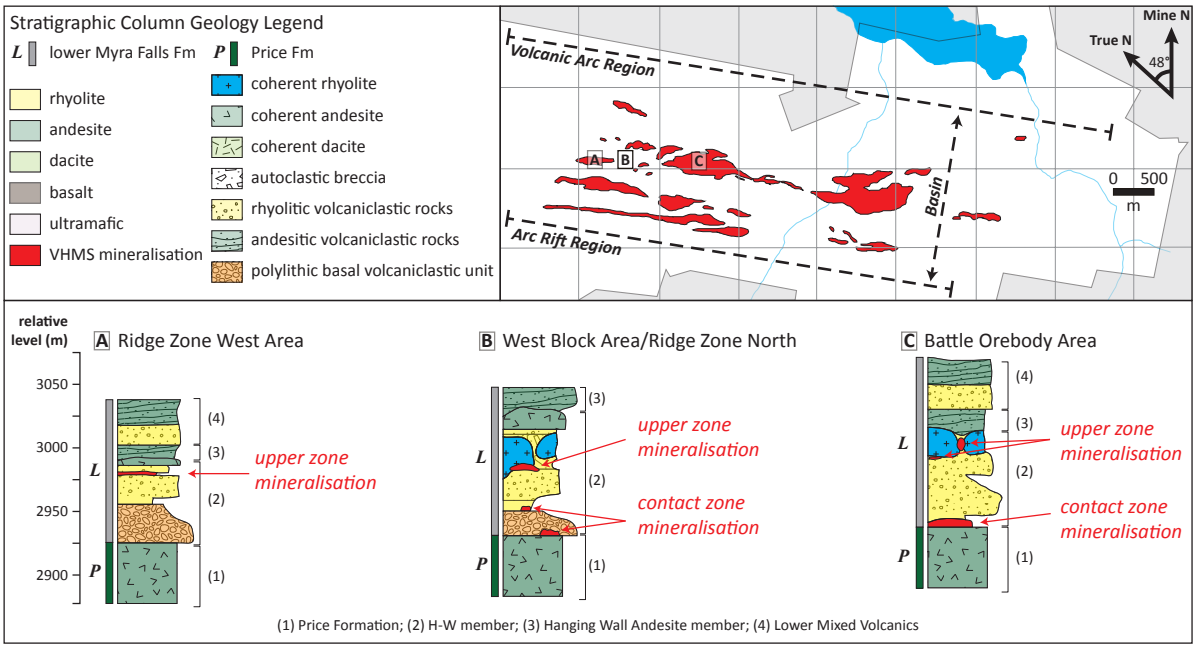

Figure 4.15 Stratigraphic columns of the lower Myra Formation in the Ridge Zone West (Chong, 2004), West Block Area / Ridge Zone North (this study), and Battle orebody (Robinson et al., 1996; Sinclair, 2000) localities.

Near the Battle orebody, the base of the lower Myra Formation is marked by either massive sulfide or rhyolitic volcaniclastic siltstone and sandstone on top of variably altered andesite of the Price Formation (Figure 4.15). In the West Block Area, a graded polylithic volcaniclastic sandstone and conglomerate unit marks the base of the lower Myra Formation (Figures 4.3A-4.5A). This unit is 10 to 30-metres-thick in the West Block Area and is up to 90-metres-thick in the Ridge Zone West locality (Chong, 2004). The Basal Volcaniclastic Unit comprises subrounded to subangular clasts of variable felsic to intermediate provenance, likely deposited by a mass flow process and highlights paleo-depressions along the paleo-seafloor (Chong, 2004). The west to east thinning of the unit suggests a source direction from the west, while graded bedding indicates that the stratigraphy is upright in the West Block Area. The Basal Volcaniclastic Unit is significant because it marks the base of the lower Myra Formation and preserves evidence of paleo-seafloor topography in the West Block Area.

Submarine, andesitic sills and lava flows are present in the lower Myra Formation in the West Block Area and Ridge Zone West orebody localities (Figure 4.15). Near the Ridge Zone

West orebody, an andesitic unit intrudes at the contact between the H-W member and the Hanging Wall Andesite member (Figure 4.15). The top and bottom contacts comprise 5 to 10-metre-thick peperitic margins, which suggest the unit is a sill (Chong, 2004). In the West Block Area, a 10 to 50-metre-thick coherent andesite with a 5 to 10-metre-thick carapace of autoclastic breccia is observed near the contact between the H-W member and the Hanging Wall Andesite member (Figures 4.3A-4.5A). In the West Block Area this coherent andesite is interpreted to be a submarine lava flow.

4.3 West Block Area and Ridge Zone North Geology

Eight cross-section interpretations were generated by integrating the lithofacies framework identified in this study with descriptions from historic logs from drill holes in the West Block Area and Ridge Zone North orebody. The cross-sections are oriented south-to-north looking west in the mine grid co-ordinate system (Figure 4.16). The vertical (2,790-3,140 metre relative level) and horizontal (4,000-4,650 metre north) extents are uniform for the set of sections. To simplify the lithological interpretations, individual rock types were grouped into one of five stratigraphic units: (1) Price Formation; (2) Basal Volcaniclastic Unit; (3) undifferentiated HW Rhyolite; (4) undifferentiated Hanging Wall Andesite member; and (5) mafic dykes. In addition to the 31 logged drill holes, 124 underground drill holes from Level 18 were re-coded using the above stratigraphic classification. Re-coding of drill core intervals was completed based on the assessment of historic drill core logs. Cross-sections 550 mE, 640 mE, 828 mE and 918 mE are discussed in further detail, whereas cross-sections 585 mE, 700 mE, 880 mE and 957 mE are provided in Appendix D.

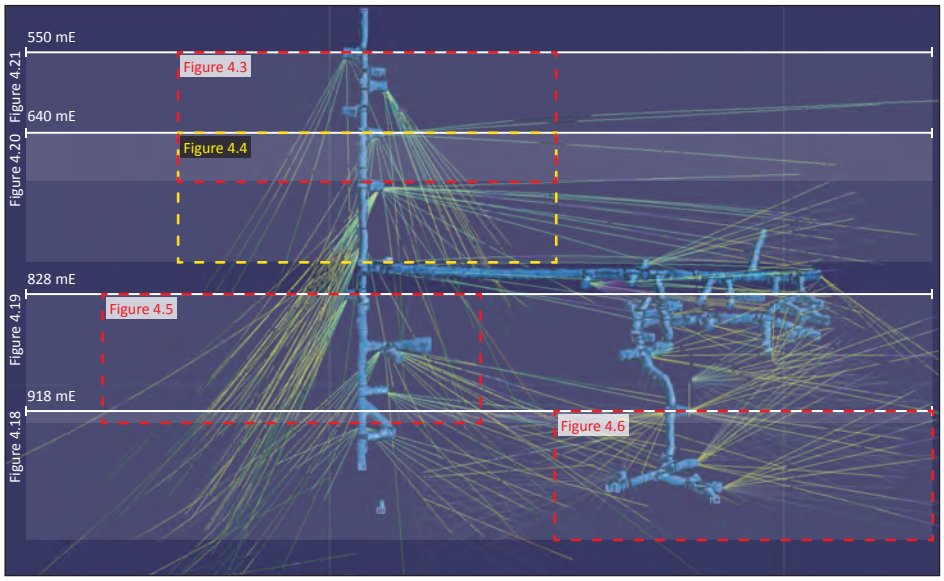

Figure 4.16 3D view looking west at +40° plunge of the West Block Area and Ridge Zone North localities. White boxes are geology cross-section interpretations across both localities (Figures 4.18-4.21). Red and yellow boxes are the locations of the detailed cross-section interpretations.

4.3.1 Identification of faults from drill core

In most cases, faults in drill core manifest as intervals of gouge and/or broken core. In some cases, a clear repetition of lithological units was observed across a fault zone (e.g., Figure 4.4). Observed fault gouge intervals in drill core vary in length from 1 to 10's of centimetres, up to 2 metres. Intervals of fault gouge were documented on detailed graphic logs, and where possible, the angle to the core axis of the upper and lower contacts was measured.

Figure 4.17 BQ drill core photograph examples of identified faults in drill core in the West Block Area. Red boxes outline the logged fault intervals.

A. Example of approximately 2.5 metre-wide interval of broken, calcite-quartz-chlorite altered, fault zone with minor fault gouge dissecting volcaniclastic andesite of the Hanging Wall Andesite member. Photograph of underground drill hole BG18-3553.

B. Example of 25 centimetre-wide fault zone that juxtaposes coherent andesite of the Price Formation adjacent to chert of the lower Myra Formation. Photograph of underground drill hole BG18-3551.

C. Example of multiple, 5 to 20 centimetre-wide, seams of fault gouge that dissect rocks of the Basal Volcaniclastic Unit and HW Rhyolite of the lower Myra Formation. Photograph of underground drill hole BG18-3321.

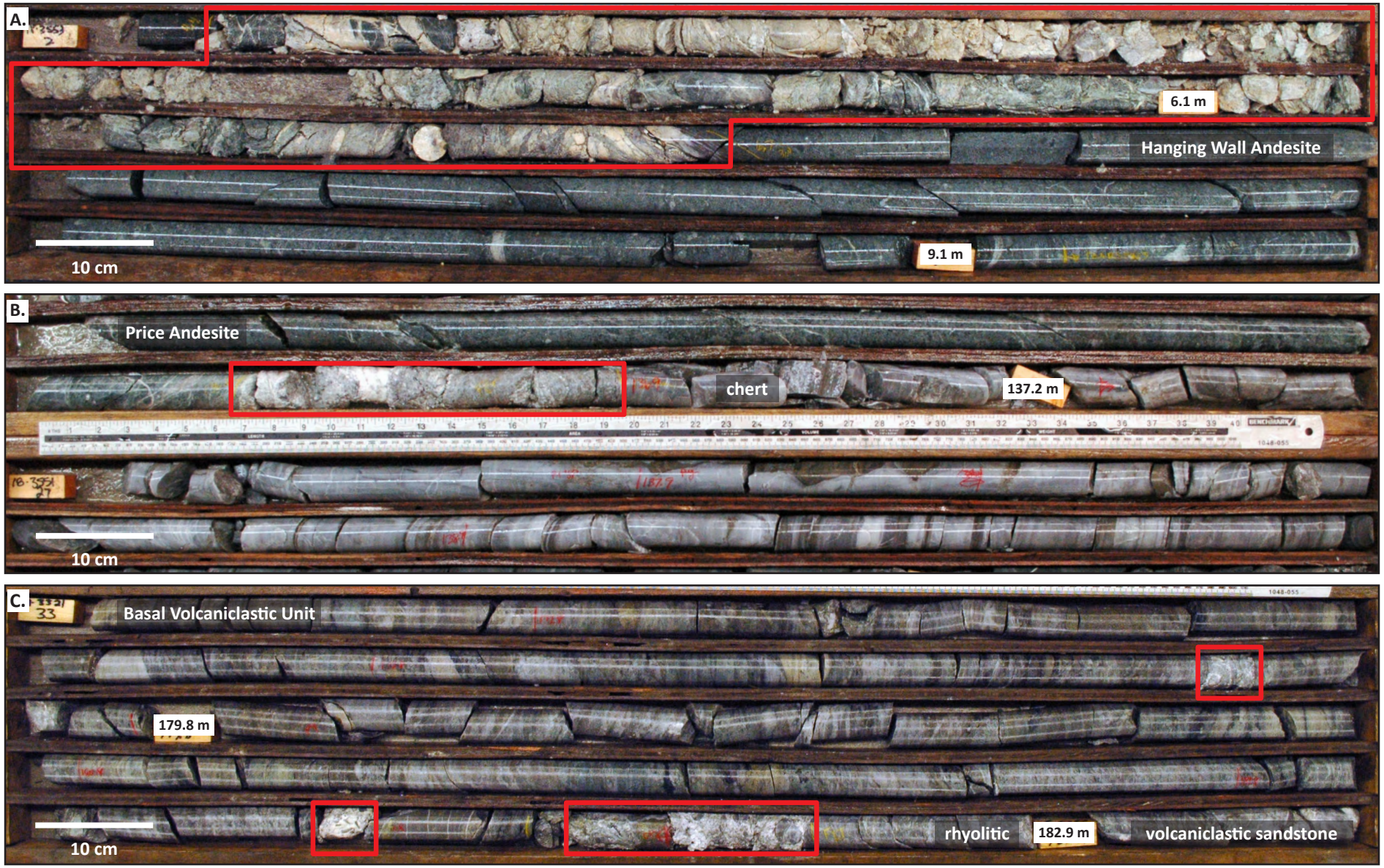
A.
6.1 m
Hanging Wall Andesite
9.1 m
10 cm
B.
Price Andesite
chert
137.2 m
10 cm
C.
Basal Volcaniclastic Unit
179.8 m
10 cm
rhyolitic
182.9 m
volcaniclastic sandstone

Two groups of faults were identified in drill core from the West Block Area based on drill core observations. Group one is characterised by zones of calcite-quartz-chlorite alteration with minor fault gouge (Figure 4.17A). Where fault gouge is present, 1 to 10-centimetre-wide seams occur throughout the chlorite-calcite-quartz altered fault zone. Group two faults are characterised by tens of centimetre-thick intervals of abundant fault gouge (Figure 4.17B). These intervals consist of fault gouge with rock fragments or intervals of fault gouge surrounded by intact drill core. In some instances, 10 to 20-centimetre-wide seams of fault gouge occur over 2-3 metre-long drill core intervals (Figure 4.17C). Gouge-rich faults are observed crosscutting all rock types in the West Block Area, whereas carbonate-quartz-chlorite faults are primarily observed within the Hanging Wall Andesite member.

The location and sense of displacement of faults were interpreted from logged fault intervals in drill core and mapped fault zones from underground development by the Nyrstar Myra Falls Operation geology team. In cases where there was limited or no drill hole data, the geometry of fault planes and lithological contacts were projected from the bounding cross-section interpretations. The sense of displacement of interpreted faults is apparent.

4.3.2 Geology cross-section interpretations

Cross-sections 918 mE and 828 mE illustrate the distribution of the HW Rhyolite stratigraphy dissected by a number of wavy, moderate to high angle, gouge-rich faults (Figures 4.18-4.19). A fault with apparent normal movement is located in the northern extent of the sections. This fault down-drops the HW Rhyolite stratigraphy by approximately 50 metres and juxtaposes HW Rhyolite against the Hanging Wall Andesite member. This fault is significant as it truncates the Ridge Zone North orebody to the north. In the southern extent of the sections, an apparent thrust fault dissects the stratigraphy (Figures 4.18-4.19). Displacement across this fault is on the order of tens of metres. There is likely some amount of oblique or strike-slip movement along these faults, however, based on current data, the exact amount of displacement is unquantifiable.

Cross-sections 640 mE and 550 mE illustrate the distribution of the HW Rhyolite in the West Block Area (Figures 4.20-4.21). North of 4,350 mN the lithological interpretation is projected from the previous cross-section interpretations (Figures 4.20-4.21). Drilling data is limited here, and restricted to long, sub-horizontal drill holes collared from the 135 Ramp of the 18 Level (18135RP). As evident in the detailed cross-section interpretations, the orientation of these drill holes results in the intersection of lithological contacts at low angles (Figures 4.3A-4.6A). The identification of moderate dipping, apparent thrust faults in the southern extent of the cross-section interpretations, explains the apparent thickening of the HW Rhyolite stratigraphy and the repetition of lithofacies in a single drill hole (Figure 4.20). While cross-section 550 mE has limited drill hole information, apparent normal faults with 30 to 50 metres of displacement dissect the stratigraphy (Figure 4.21).

From the detailed examination of drill holes in the West Block Area, a distinctive stratigraphic unit was recognised: the Basal Volcaniclastic Unit. The distribution of this unit is well constrained on cross-sections 828 mE through 550 mE (Figures 4.3A-4.5A). The distribution of the Basal Volcaniclastic Unit is less constrained north of the West Block Area. In some cases, the Basal Volcaniclastic Unit was documented in historic drill logs and the intervals of the unit were captured by the lithofacies re-coding exercise. However, in other cases, the rock unit was not documented. Without drill core photographs, the presence of this

unit could not be confirmed or denied in many of the re-coded historic logs. The identification of the Basal Volcaniclastic Unit in the West Block Area is significant, as it can be used to identify and constrain apparent fault offsets, which will improve the development of future geological models.

The nature of the contact between the HW Rhyolite and the Hanging Wall Andesite member is interpreted to be erosional. The Hanging Wall Andesite member is a polylithic volcaniclastic, sandstone and conglomerate with angular to sub-angular clasts of andesite, rhyolite, chert and massive sulfide. In the Ridge Zone North orebody, massive sulfide ore lenses are truncated at the Hanging Wall Andesite member contact (e.g., cross-section 828 mE; Figure 4.19). Historic drill logs from sections 918 mE through 828 mE between 4,300 and 4,400 mN document intervals of the Hanging Wall Andesite member near the HW Rhyolite member contact with an increased population of angular chert and massive sulfide clasts (e.g., Figure 4.6A).

The inferred wavy nature of the Price Formation and lower Myra Formation contact is, likely, due to a combination of paleo-seafloor topography and D_1 folding. The Basal Volcaniclastic Unit is interpreted to represent paleo-seafloor depocentres prior to folding (Figures 4.3A-4.6A). The geometry of the H-W member and Hanging Wall Andesite member is also inferred to represent a combination of paleo-seafloor topography and D_1 folding. Near the Ridge Zone North orebody polylithic volcaniclastic breccias overlying the H-W member contain abundant clasts of massive sulfide (e.g., Figure 4.6A). In the West Block Area, polylithic, volcaniclastic breccia overlying the H-W member contains quartz-phyric rhyolite, and rare clasts of massive sulfide and chert (Figure 4.13C-E). The clasts of quartz-phyric rhyolite, chert, and massive sulfide are interpreted to be the result of erosion of H-W member rocks followed by deposition by mass flow processes on the paleo-seafloor surface to form the Hanging Wall Andesite member.

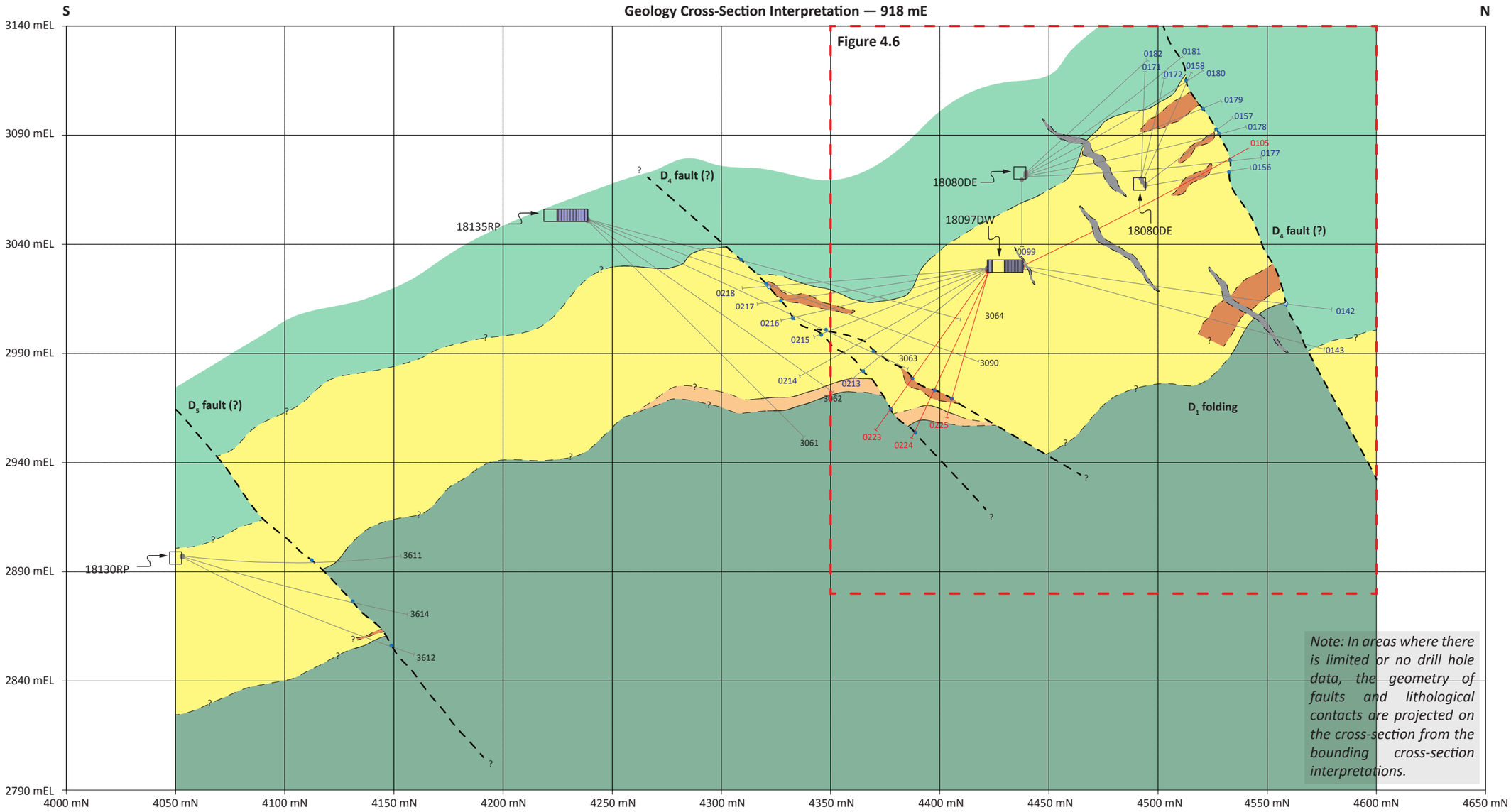

Underground Drill Holes

- Re-coded drill holes
- Logged drill holes
- Fault interval
- Projected fault interval

Underground Workings

- 18135RP

Geology Legend

- Hanging Wall Andesite Member - undifferentiated
- HW Rhyolite Member - undifferentiated
- HW Rhyolite Member - Basal Volcaniclastic Unit
- Price Formation - undifferentiated
- Mafic dyke
- Zinc assay ≥ 5%
- Lithology contact
- Inferred lithology contact
- Interpreted fault

Section Layout

Scale: 1:2,000

0 25 50 m

Section Orientation (±25 mE)

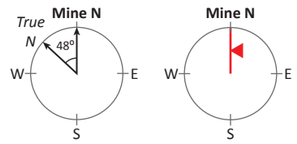

Underground Drill Holes (29 holes total)

BG18-3061 (7 m)	RN18-0099 (17 m)	RN18-0215
BG18-3062 (7 m)	RN18-0105	RN18-0216
BG18-3063 (7 m)	RN18-0142	RN18-0217
BG18-3064 (7 m)	RN18-0143	RN18-0218
BG18-3090 (7 m)	RN18-0156 (4 m)	RN18-0223
BG18-3611	RN18-0157 (4 m)	RN18-0224
BG18-3612	RN18-0158 (4 m)	RN18-0225
BG18-3614	RN18-0171 (4 m)	
	RN18-0172 (4 m)	
	RN18-0177 (4 m)	
	RN18-0178 (4 m)	
	RN18-0179 (4 m)	
	RN18-0213	
	RN18-0214	

red = logged drill holes

Figure 4.18 918 mE cross-section interpretation. Detailed cross-section interpretations are shown on Figure 4.6.

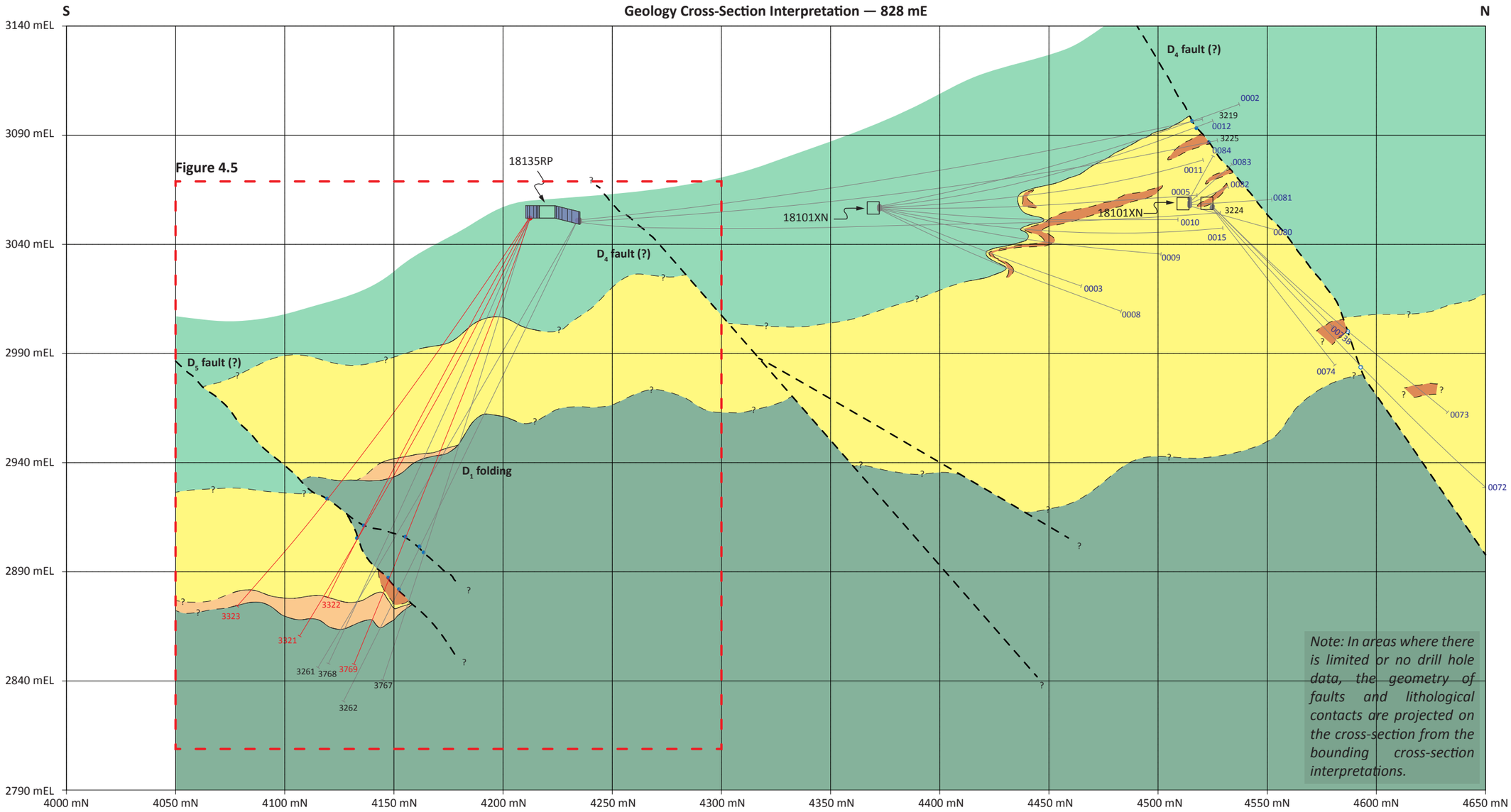

Underground Drill Holes

- Re-coded drill holes
- Logged drill holes
- Fault interval
- Projected fault interval

Underground Workings

18135RP

Geology Legend

- Hanging Wall Andesite Member - undifferentiated
- HW Rhyolite Member - undifferentiated
- HW Rhyolite Member - Basal Volcaniclastic Unit
- Price Formation - undifferentiated
- Mafic dyke
- Zinc assay ≥ 5%
- Lithology contact
- Inferred lithology contact
- Interpreted fault

Section Layout

Scale: 1:2,000

0 25 50 m

Section Orientation (±15 mE)

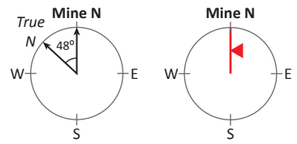

Underground Drill Holes (29 holes total)

BG18-3219	RN18-0002	RN18-0081 (6 m)
BG18-3224	RN18-0003	RN18-0082 (6 m)
BG18-3225	RN18-0005	RN18-0083 (6 m)
BG18-3261	RN18-0008 (7 m)	RN18-0084 (6 m)
BG18-3262 (3 m)	RN18-0009 (5 m)	
BG18-3321	RN18-0010 (6 m)	
BG18-3322	RN18-0011	
BG18-3323	RN18-0012	
BG18-3767	RN18-0015	
BG18-3768	RN18-0072 (9 m)	
BG18-3769	RN18-0073 (10 m)	
	RN18-0073B (15 m)	
	RN18-0074 (15 m)	
	RN18-0080 (6 m)	

red = logged drill holes

Figure 4.19 828 mE cross-section interpretation. Detailed cross-section interpretations are shown on Figure 4.5.

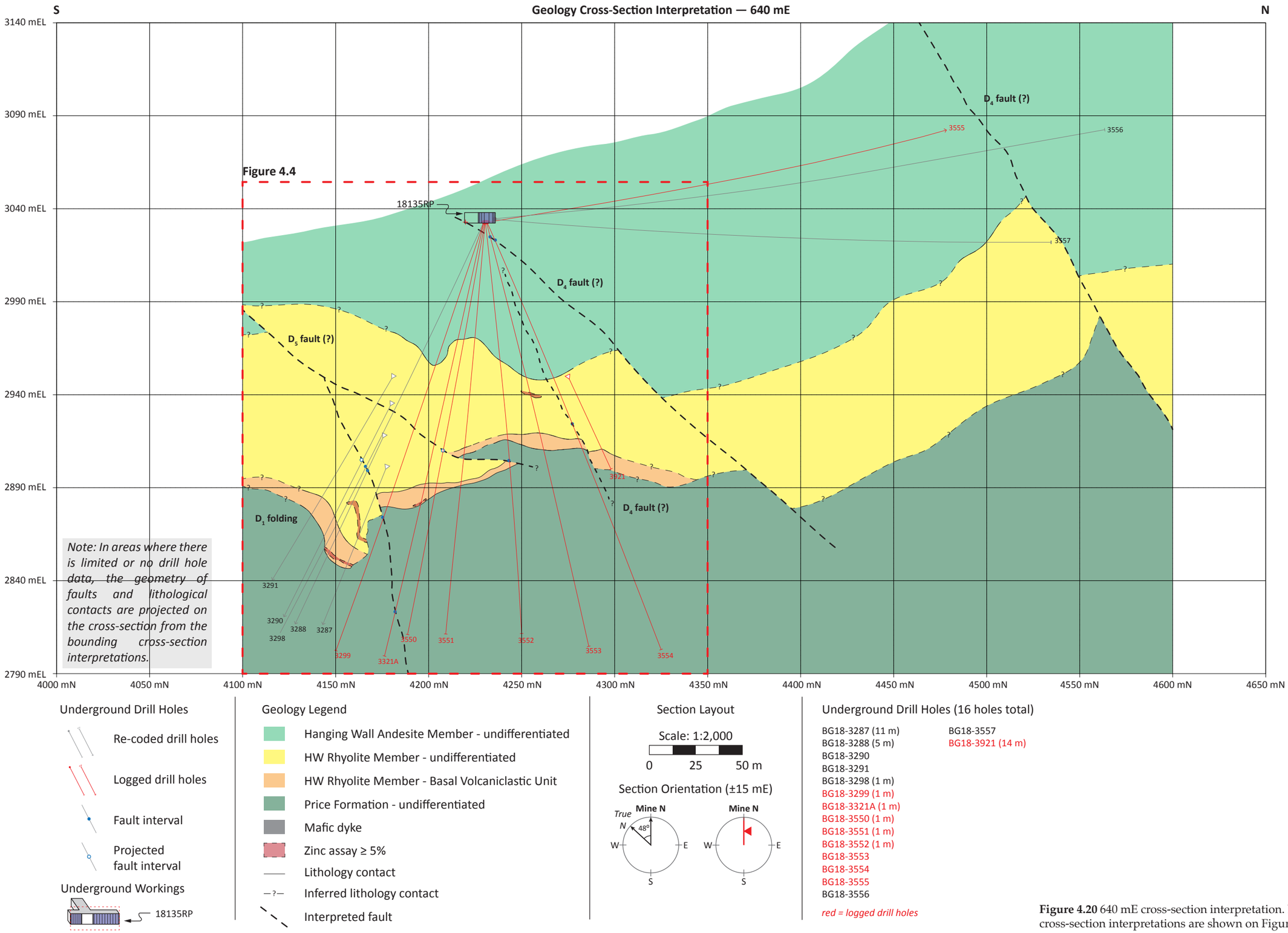

Figure 4.20 640 mE cross-section interpretation. Detailed cross-section interpretations are shown on Figure 4.4.

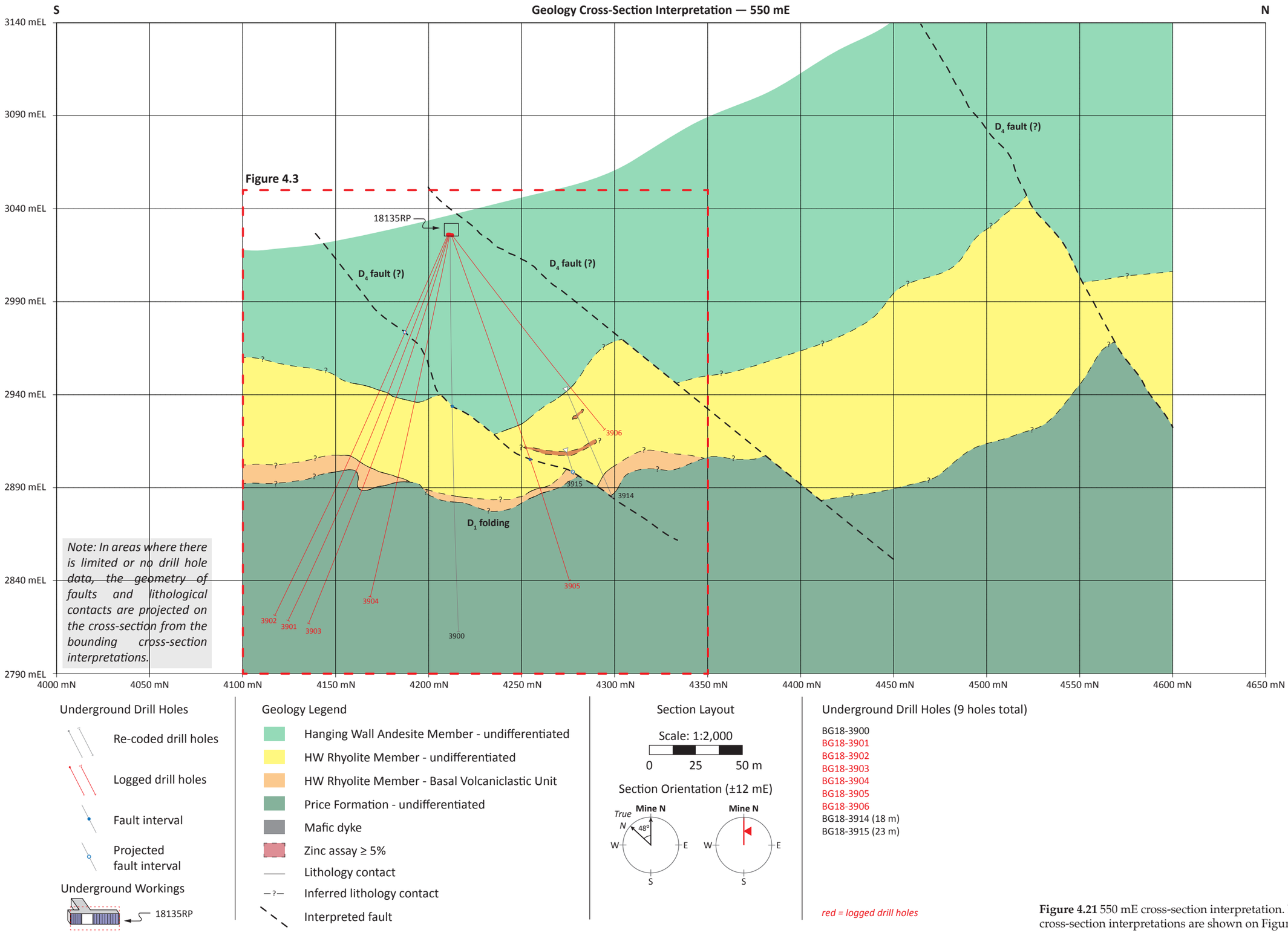

Figure 4.21 550 mE cross-section interpretation. Detailed cross-section interpretations are shown on Figure 4.3.

4.3.3 Discussion of cross-section interpretations

The deformation history of Myra Falls is complex (Walker, 1985; Juras and Pearson 1990; Berry 2000). Jones et al. (2006a) identified a range of fault styles with variable structural features and used a combination of fault geometry, morphology and kinematics to define groups of brittle faults. These fault groups comprise a range of styles from planar, gouge-free faults to anastomosing faults with abundant gouge (Jones et al., 2006a).

Faults in the West Block Area were identified in drill core from the displacement of lithological units and presence of gouge. Based on apparent angles in drill core and inferred fault plane geometries from cross-section interpretations (Figures 4.18-4.21), faults are moderate dipping planar structures with minor gouge and shallow-to-moderate dipping, gouge-rich, wavy structures. These two fault groups in the West Block Area, likely, correspond to D_4 and D_5 brittle faults as described by Jones et al. (2006a).

Northeast-southwest compression during the Middle Permian to pre-Middle Triassic produced northwest-trending folds with a major northwest-trending anticline that extends through the upper Myra Formation Lynx-Myra-Price orebodies (Muller, 1980; Massey, 1992b; Jones et al., 2006a). Jones et al. (2006a) reported open upright folds in chert and argillite of the lower Myra Formation immediately above the Battle and HW orebodies. Similar, open upright fold patterns are inferred from drill core observations and illustrated on cross-section interpretations (Figures 4.18-4.21). The inferred fold structures are consistent with the observations of Jones et al. (2006a) and correspond to parasitic folds developed subparallel to the northwest-trending Myra Anticline.

4.4 Mineralisation Styles

Zinc-rich, polymetallic sulfide mineralisation occurs in the West Block Area and Ridge Zone North orebody. Sphalerite, pyrite, chalcopyrite, galena and tennantite-tetrahedrite are the principal sulfide and sulfosalt minerals observed in drill core (Figure 4.22; Table 4.1). Styles of mineralisation include disseminated, stringer, semi-massive and massive sulfide occurrences.

Disseminated sulfide occurs in andesite of the Price Formation and all rock types of the H-W member. This sulfide mineralisation style is pyrite-rich, with abundances ranging between 5 and 15% pyrite. Discordant sulfide stringers occur in coherent and volcaniclastic rhyolite and marine-sedimentary rocks of the H-W member (Figure 4.23). Sulfide stringers in coherent and volcaniclastic rhyolite are sphalerite-pyrite ± galena, chalcopyrite, and tennantite-tetrahedrite rich or are pyrite-dominant. Stringers are wispy in geometry, millimetres to centimetres in thickness, and are associated with sericite-quartz and chlorite-sericite altered, felsic rocks (Figure 4.22A-B, H-I). Centimetre-thick pyrite-chalcopyrite stringers locally crosscut chert. Discordant, sphalerite-rich stringers are the most commonly observed style of sulfide mineralisation in the West Block Area.

Less common, in the examined drill holes in the West Block Area are semi-massive and massive zinc-rich, polymetallic sulfide mineralisation styles (Figures 4.23C; 4-24-4.25). Semi-massive sulfide is defined here as intervals of drill core comprising between 50 and 75% sulfide (e.g., Figure 4.22C), whereas massive sulfide intervals consists of >75% sulfide minerals (e.g., Figure 4.22G). In the West Block Area, laterally discordant, up to tens of centimetres-thick, semi-massive and massive sphalerite-rich mineralisation occurs in sericite-quartz altered, coherent rhyolite and rhyolite autobreccia (Figures 4.3B-4.4B; 4.23C-D). Locally, at the base

Figure 4.22 Drill core scans of honey brown, sphalerite-rich, sulfide mineralisation styles observed in the West Block Area (A-G) and Ridge Zone North orebody (H-L).

A. "Upper zone" mineralisation. Stringer-style sphalerite with minor pyrite, galena and tennantite-tetrahedrite (BM14-038). Host rock is sericite-quartz altered, rhyolite autobreccia (Figure 4.23).

B. "Upper zone" mineralisation. Stringer-style sphalerite with galena and minor tennantite-tetrahedrite (BM14-035). Host rock is sericite-quartz altered, quartz-phyric, coherent rhyolite (Figure 4.26).

C. "Upper zone" mineralisation. Semi-massive sphalerite-pyrite with minor tennantite-tetrahedrite and barite (BM14-050). Note the clast of rhyolite in the left centre field of view. Interval of mineralisation is located at the contact between sericite-quartz altered, coherent rhyolite and rhyolite autobreccia (Figure 4.24).

D. "Upper zone" mineralisation. Semi-massive sphalerite-pyrite-barite with minor galena and tennantite-tetrahedrite (BM14-041). Interval of mineralisation is located at the contact between sericite-quartz altered, coherent rhyolite and rhyolite autobreccia (Figure 4.23).

E. "Upper zone" mineralisation. Massive sphalerite with minor pyrite, chalcopyrite and galena (BM14-033). Note the irregular shaped clots of very fine-grained chlorite and sericite. Associated host rock is chlorite-sericite altered, Basal Volcaniclastic Unit (Figure 4.24).

F. "Contact zone" mineralisation. Semi-massive sphalerite-chalcopyrite with minor pyrite and galena (BM14-027). Associated host rock is chlorite-sericite altered, Basal Volcaniclastic Unit (Figure 4.25).

G. "Contact zone" mineralisation. Massive sphalerite with minor pyrite and chalcopyrite (BM14-026). Associated host rock is chlorite-sericite altered, Basal Volcaniclastic Unit (Figure 4.25).

H. "Upper zone" mineralisation. Stringer-style sphalerite-pyrite with minor tennantite-tetrahedrite and galena (BM15-099). Host rock is sericite-quartz altered, quartz-phyric, coherent rhyolite (Figure 4.27).

I. "Upper zone" mineralisation. Stringer-style sphalerite with minor pyrite-galena-chalcopyrite (BM14-053). Host rock is chlorite-sericite altered, rhyolite autobreccia (Figure 4.28).

J. "Contact zone" mineralisation. Semi-massive sphalerite-chalcopyrite-pyrite with minor tennantite-tetrahedrite (BM15-096). Associated host rock is sericite-quartz altered, rhyolitic, volcaniclastic sandstone (Figure 4.27).

K. "Contact zone" mineralisation. Massive pyrite-sphalerite-chalcopyrite mineralisation (BM15-092). Associated host rock is sericite-quartz altered, rhyolitic, volcaniclastic sandstone (Figure 4.27).

L. "Upper zone" mineralisation. Massive sphalerite with bands of pyrite-chalcopyrite and interstitial barite and minor tennantite-tetrahedrite (BM14-057). Associated host rocks are chlorite-sericite altered, argillite and rhyolitic, volcaniclastic sandstone (Figure 4.28).

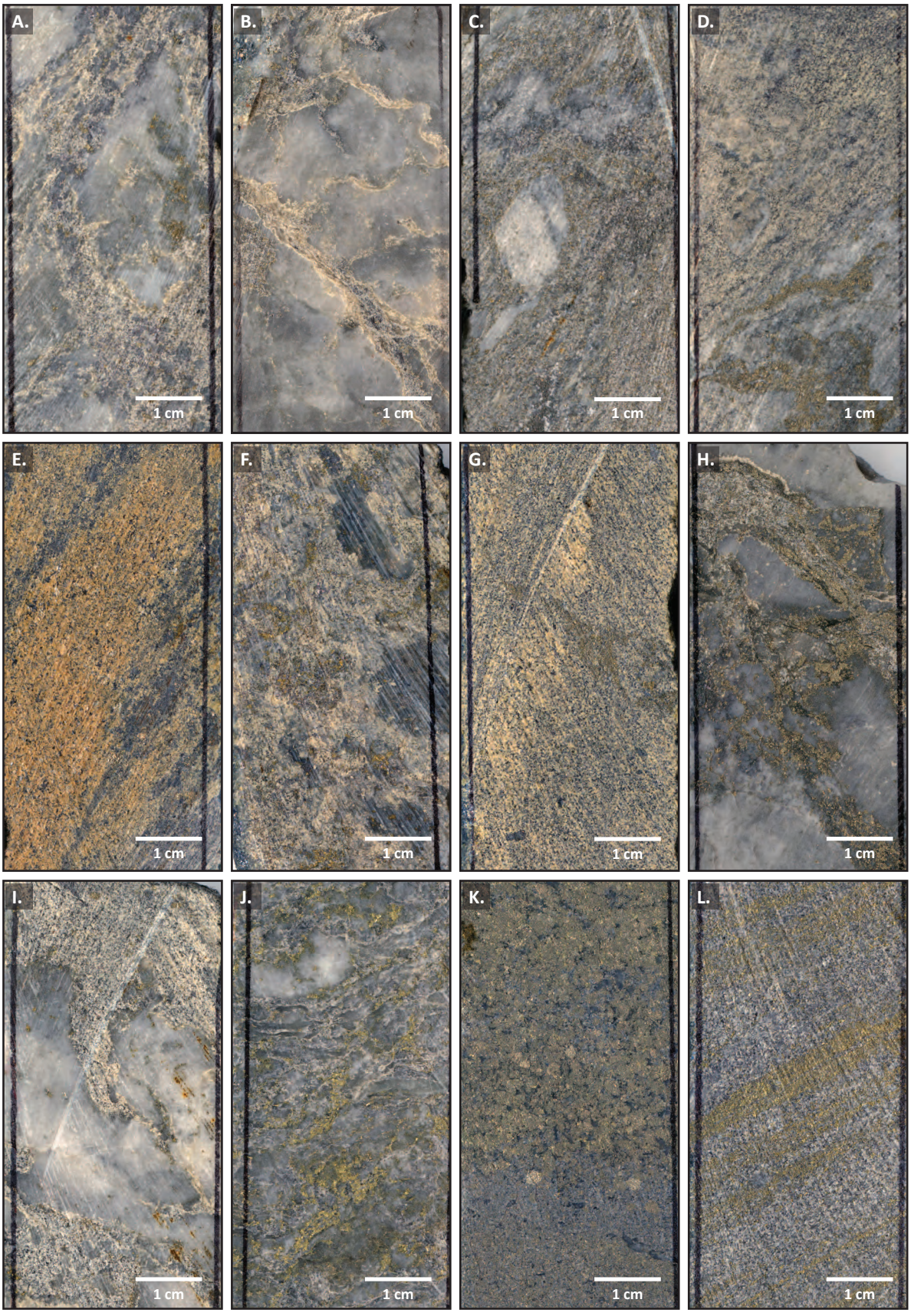
A.
1 cm
B.
1 cm
C.
1 cm
D.
1 cm
E.
1 cm
F.
1 cm
G.
1 cm
H.
1 cm
I.
1 cm
J.
1 cm
K.
1 cm
L.
1 cm

of the H-W member, semi-massive and massive sphalerite mineralisation is associated with chlorite-sericite altered, polylithic conglomerate of the Basal Volcaniclastic Unit and sericite-quartz altered rhyolitic volcaniclastic sandstone of the HW rhyolite (Figures 4.24C-D, 4.25).

Four drill holes from the Ridge Zone North orebody were also investigated. Similar to the West Block Area, discordant, wispy stringers of sphalerite ± galena, pyrite, chalcopyrite and tennantite-tetrahedrite occur in sericite-quartz altered, coherent rhyolite and chlorite-sericite altered, rhyolitic sandstone (Figures 4.22H-I; 4.27A-B; 4.28A-B). Stringers are similar in thickness, but are present in greater abundance in the Ridge Zone North orebody. Intervals of semi-massive to massive sulfide mineralisation range from 1 to 10's of meters in thickness (Figure 4.6B). In some cases, massive pyrite forms the base of the mineralised interval and transitions up stratigraphy into sphalerite-rich semi-massive to massive sulfide (Figure 4.27A, C). Alternatively, semi-massive sphalerite (Figure 4.22J) and massive, banded sphalerite-chalcopyrite-pyrite mineralisation (Figure 4.22L) form sulfide-lenses (Figure 4.28). Disseminated pyrite-chalcopyrite occurs in chlorite-sericite altered Price Formation and in the Basal Volcaniclastic Unit.

4.4.1 Stratigraphic position

Zinc-rich, polymetallic sulfide mineralisation occurs at two stratigraphic positions in the study area. To maintain the previous nomenclature of Sinclair (2000) the stratigraphic positions are referred to as "upper zone" and "contact zone" mineralisation (Figure 4.2). "Upper zone" mineralisation occurs 30 to 75 metres above the Price Formation contact (Figure 4.24A). Whereas, "contact zone" mineralisation occurs at the Price Formation contact (Figure 4.24C).

In the West Block Area, "upper zone" mineralisation is the dominant style and manifests as sphalerite-rich stringers in quartz and feldspar-phyric coherent rhyolite and coarse-grained, rhyolitic volcaniclastic sandstones and breccias (Figure 4.23C-D). Semi-massive, sulfide mineralisation appears to be spatially associated with the lithological contact between coherent and volcaniclastic rhyolite units (Figure 4.24A). Base and precious metal drill hole assays vary between stringer and semi-massive, sulfide mineralisation styles. Stringer sulfide mineralisation is characterised by 1-5% Zn, <0.5% Cu, <0.5% Pb, 0.25-0.50 g/t Au (locally >1 g/t), and 5-20 g/t Ag (Figures 4.23-4.26). Semi-massive and massive sulfide mineralisation styles have elevated base and precious metals, typically >10% Zn, variable Cu and Pb concentrations, with 1-2 g/t Au and 100-250 g/t Ag (Figures 4.23C-4.24A). "Contact zone" mineralisation style occurs as sphalerite-rich, chalcopyrite-galena-pyrite massive sulfide associated with felsic volcaniclastic and polylithic volcaniclastic strata near the Price Formation contact (Figures 4.4B-4.5B). Metal concentrations are characterised by >25% Zn, >1% Cu, variable Pb, 1-5 g/t Au (locally >10 g/t) and 50-100 g/t Ag (Figures 4.24C-4.25).

In the Ridge Zone North orebody, multiple lenses (5-15-metres-thick) of sphalerite-rich, "upper zone" semi-massive to massive, sulfide mineralisation are present 50 to 75 metres above the Price Formation contact (Figure 4.6B). Base and precious metal concentrations are characterised by >25% Zn (locally >40%), >2% Cu, >2% Pb, >1 g/t Au (locally >5 g/t) and >100 g/t Ag (Figure 4.28A). Stringer-style sphalerite mineralisation is characterised by 3-5% Zn, <0.5% Cu, variable Pb (0.5-2%) and <30 g/t Ag (Figure 4.28A). Semi-massive to massive, sphalerite-rich "contact zone" mineralisation comprises variable Zn grades (10-20%) and up to 0.5 g/t Au and 75 g/t Ag (Figure 4.27A, C).

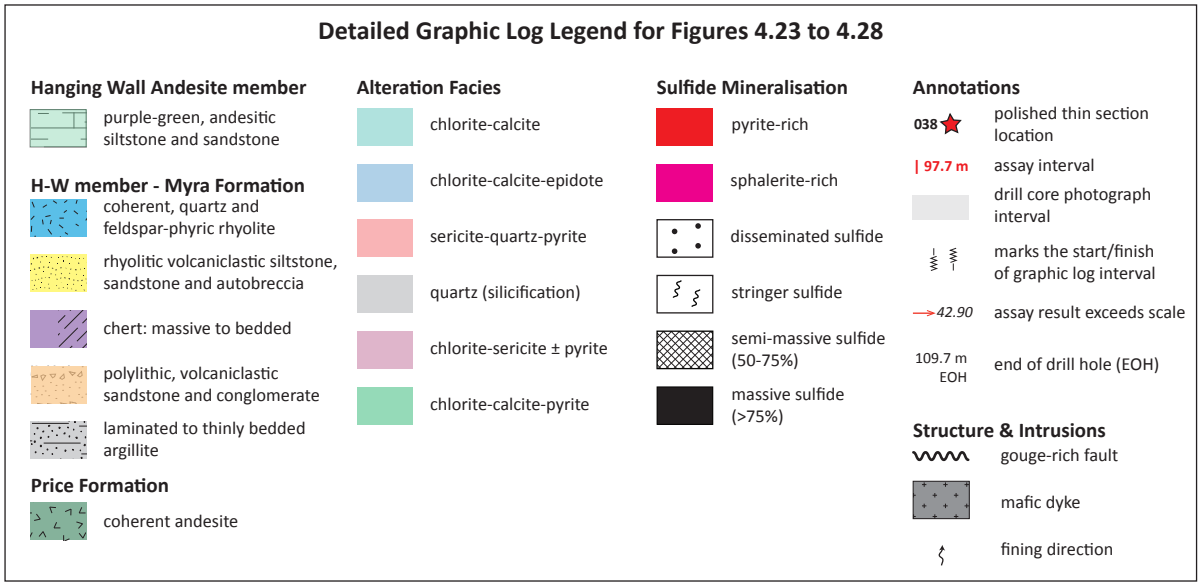
Detailed Graphic Log Legend for Figures 4.23 to 4.28
Hanging Wall Andesite member
purple-green, andesitic siltstone and sandstone
H-W member - Myra Formation
coherent, quartz and feldspar-phyric rhyolite
rhyolitic volcaniclastic siltstone, sandstone and autobreccia
chert: massive to bedded
polylithic, volcaniclastic sandstone and conglomerate
laminated to thinly bedded argillite
Price Formation
coherent andesite
Alteration Facies
chlorite-calcite
chlorite-calcite-epidote
sericite-quartz-pyrite
quartz (silicification)
chlorite-sericite ± pyrite
chlorite-calcite-pyrite
Sulfide Mineralisation
pyrite-rich
sphalerite-rich
disseminated sulfide
stringer sulfide
semi-massive sulfide (50-75%)
massive sulfide (>75%)
Annotations
038
polished thin section location
| 97.7 m
assay interval
drill core photograph interval
marks the start/finish of graphic log interval
42.90
assay result exceeds scale
109.7 m EOH
end of drill hole (EOH)
Structure & Intrusions
gouge-rich fault
mafic dyke
fining direction

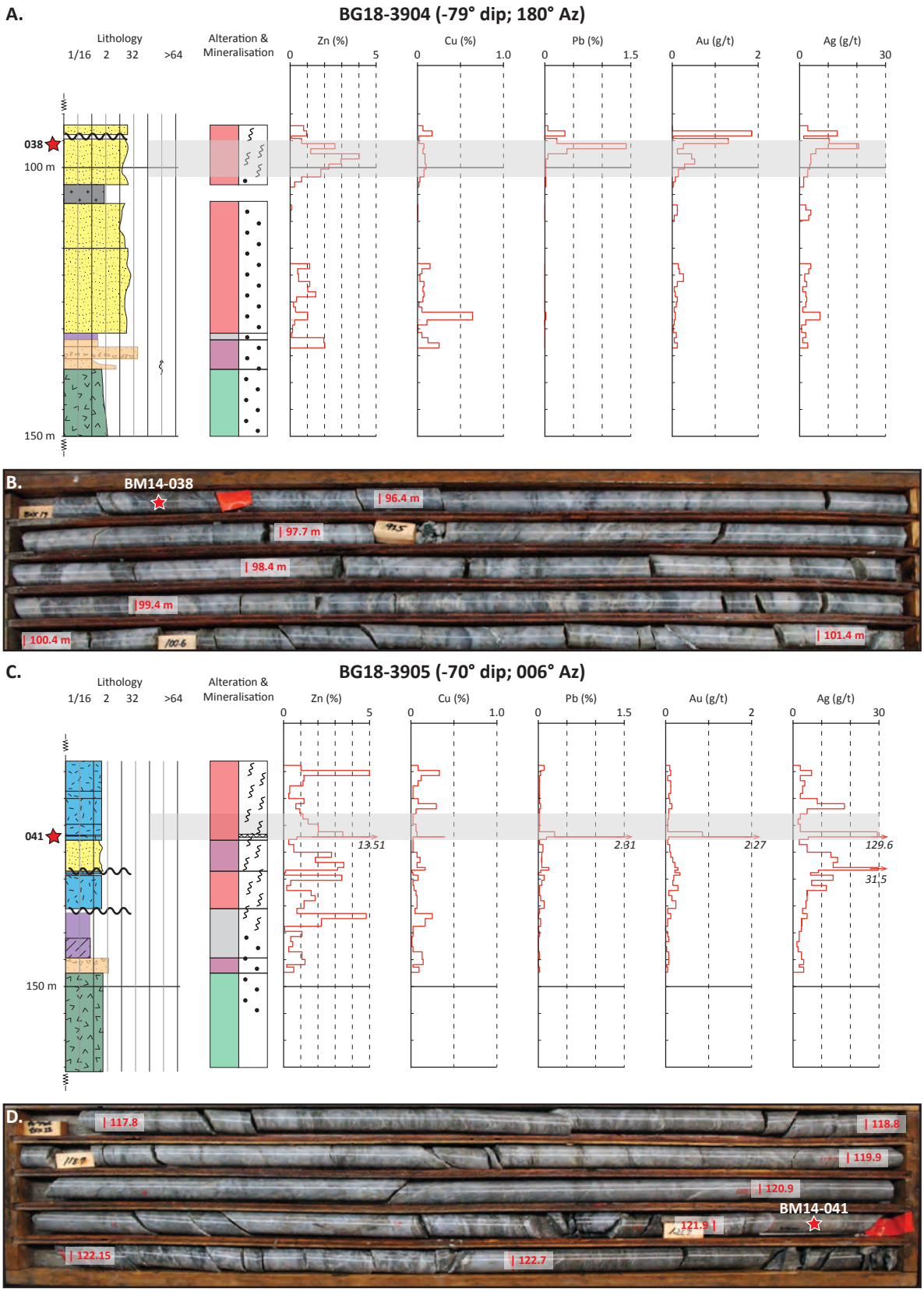

Figure 4.23 Selected graphic log interval from section 550 mE of the West Block Area showing lithology, alteration and mineralisation with Zn, Cu, Pb, Au and Ag assay results. Stratigraphic younging direction is up drill hole. A-B. Example of "upper zone" stringer-style, honey brown sphalerite in sericite-quartz altered, rhyolitic, volcaniclastic breccia. Polished thin section sample BM14-038 at 96.2 metres. C-D. Example of "upper zone" stringer and semi-massive style, honey brown sphalerite in sericite-quartz altered, quartz-phyric, coherent rhyolite. Polished thin section sample BM14-041 at 122.0 metres. See page 85 for legend.

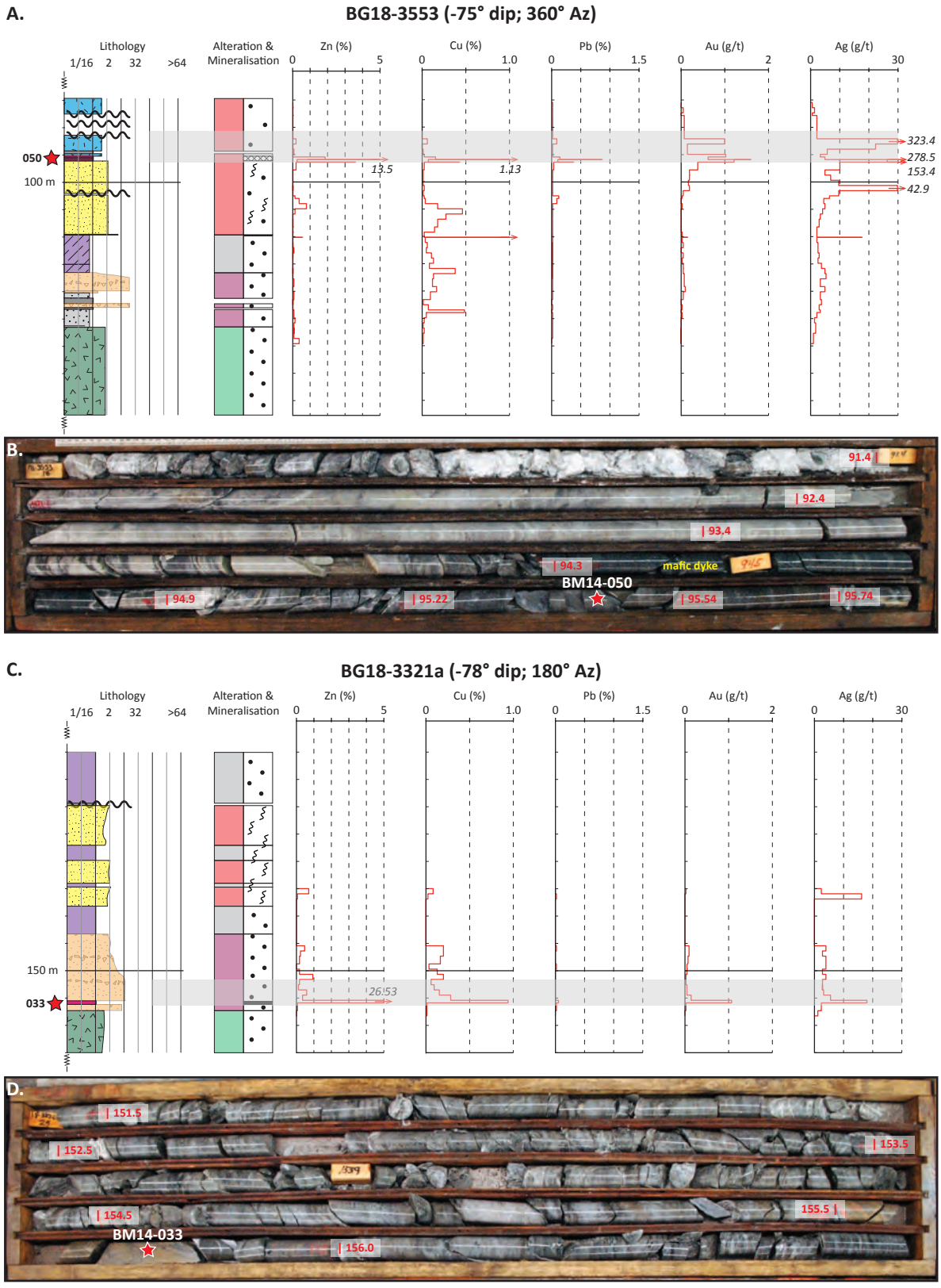

Figure 4.24 Selected graphic log intervals from section 640 mE of the West Block Area showing lithology, alteration and mineralisation with Zn, Cu, Pb, Au and Ag assay results. Stratigraphic younging direction is up drill hole. A-B. Example of "upper zone" semi-massive sphalerite from 95.22-95.74 metres located at contact between coherent rhyolite and rhyolitic, volcaniclastic breccia. Polished thin section sample BM14-050 at 95.3 metres. C-D. Example of "contact zone" massive, honey brown sphalerite from 155.5-156.6 metres within chlorite-sericite altered, Basal Volcaniclastic Unit. Polished thin section sample BM14-033 at 155.6 metres. See page 85 for legend.

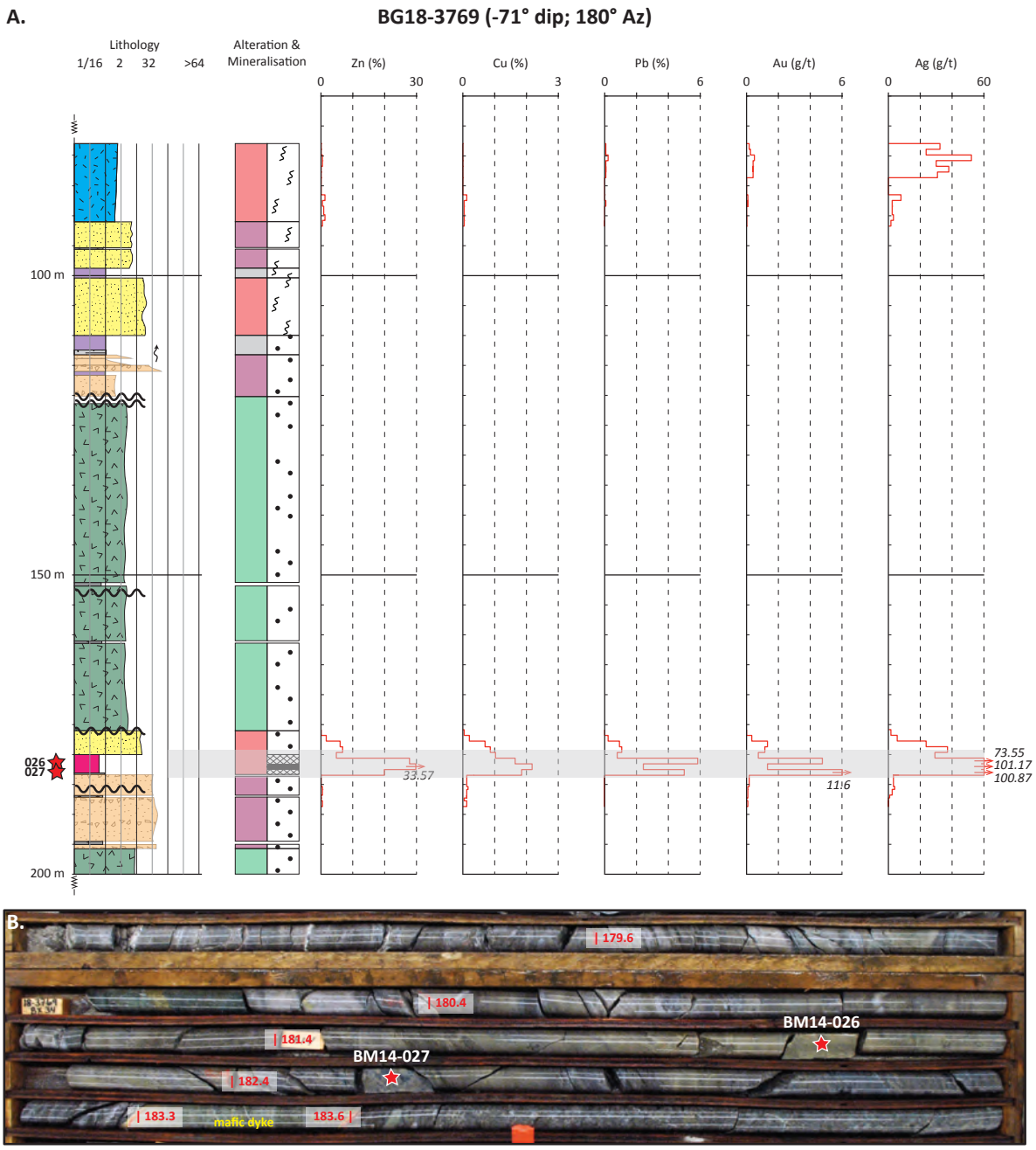

Figure 4.25 Selected graphic log interval from section 828 mE of the West Block Area showing lithology, alteration and mineralisation with Zn, Cu, Pb, Au and Ag assay results. Stratigraphic younging direction is up drill hole. A-B. Example of "contact zone" massive to semi-massive, honey brown sphalerite located at the contact between sericite-quartz altered, rhyolitic, volcaniclastic breccia and sericite-chlorite altered, Basal Volcaniclastic Unit. Polished thin section samples BM14-026 at 182.0 metres and BM14-027 at 182.6 metres. See page 85 for legend.

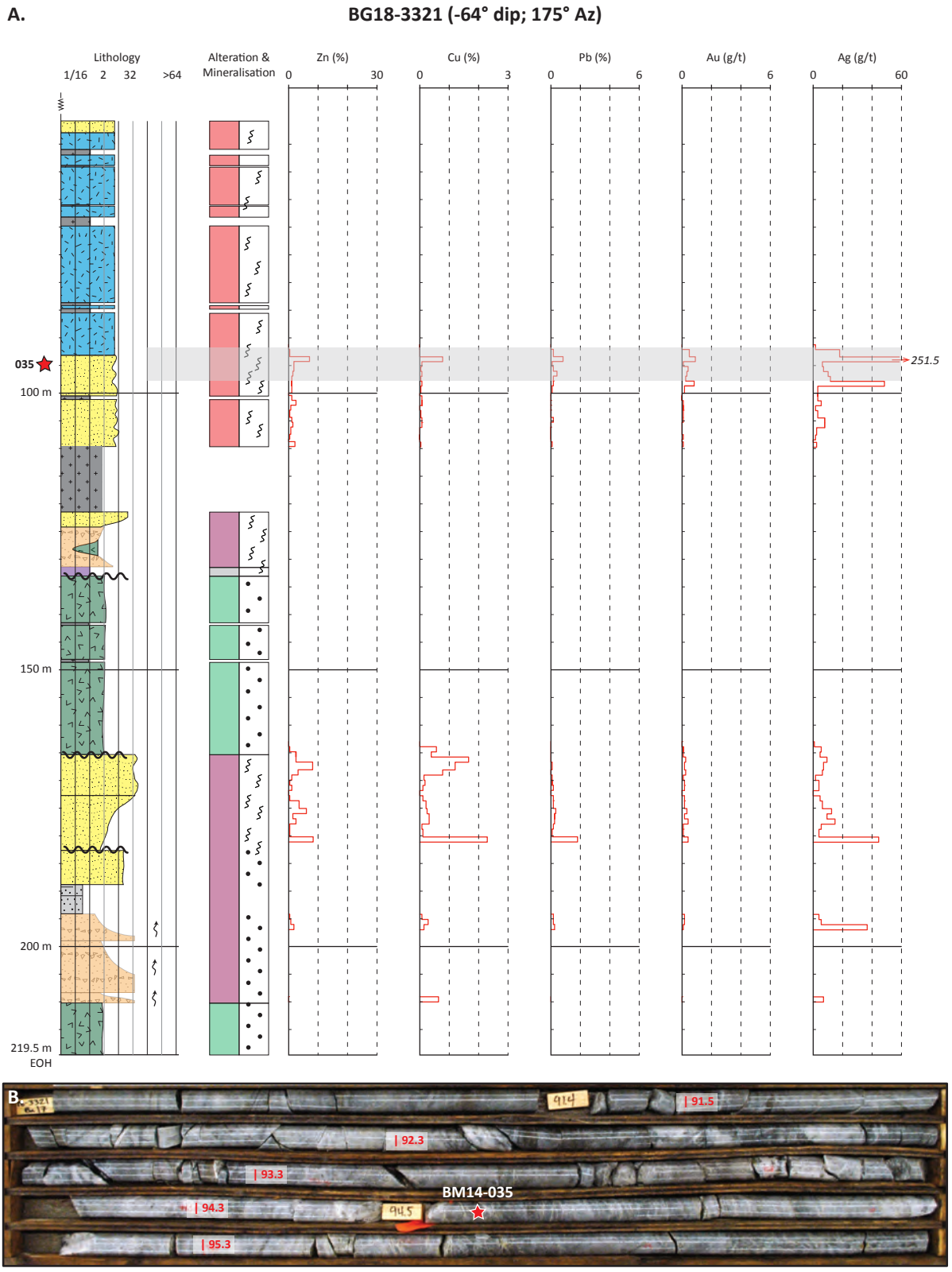

Figure 4.26 Selected graphic log interval from section 828 mE of the West Block Area showing lithology, alteration and mineralisation with Zn, Cu, Pb, Au and Ag assay results. Stratigraphic younging direction is up drill hole. A-B. Example of "upper zone" stringer-style, honey brown sphalerite located near the contact between sericite-quartz altered, rhyolitic, volcaniclastic breccia and sericite-quartz altered, quartz-phyric, coherent rhyolite. Polished thin section samples BM14-035 at 94.5 metres. See page 85 for legend.

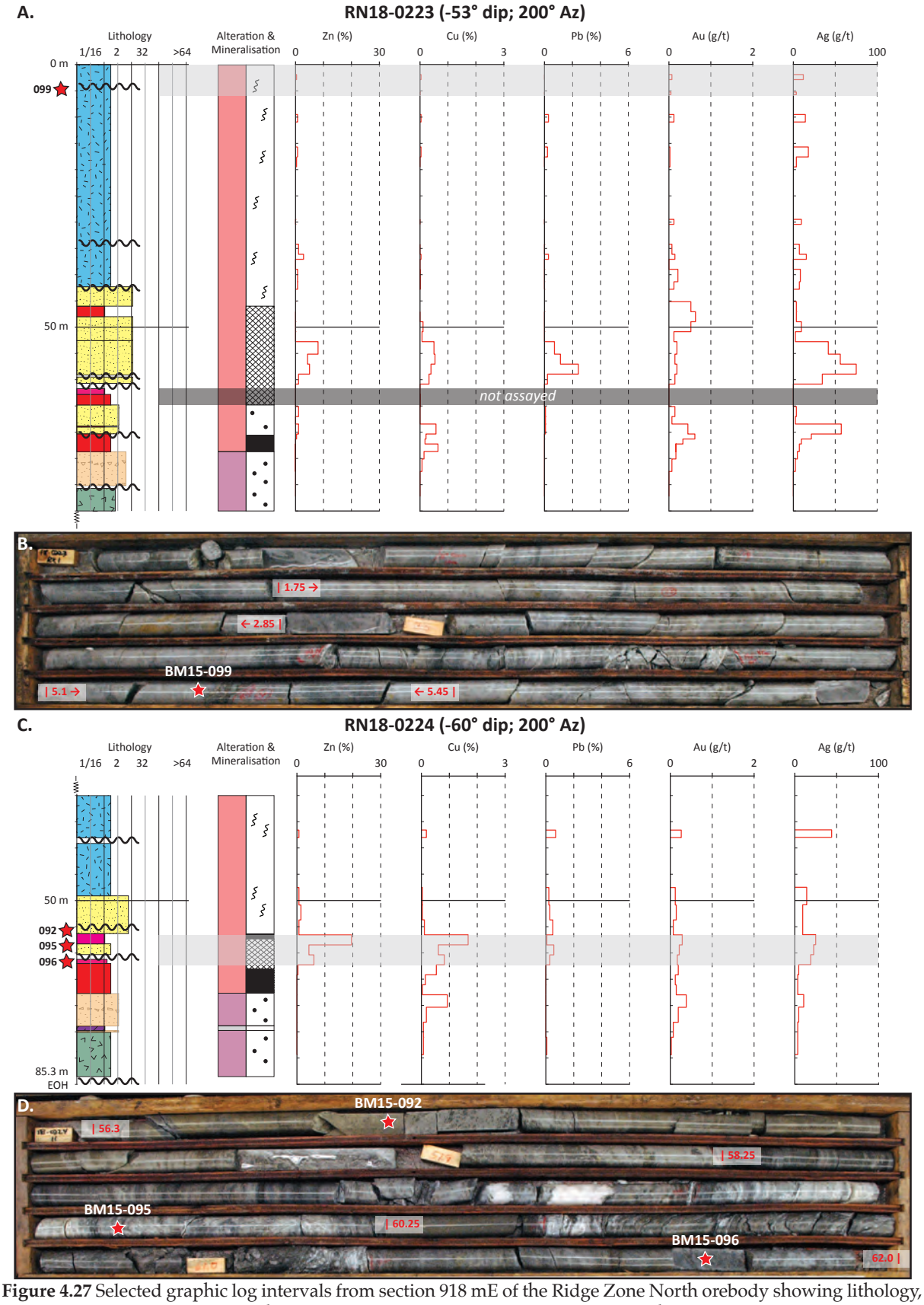

Figure 4.27 Selected graphic log intervals from section 918 mE of the Ridge Zone North orebody showing lithology, alteration and mineralisation with Zn, Cu, Pb, Au and Ag assay results. Stratigraphic younging direction is up drill hole. A-B. Example of "upper zone" stringer-style sulfide and "contact zone" massive to semi-massive, sulfide mineralisation. Polished thin section sample BM15-099 at 5.3 metres. C-D. Example of "contact zone" semi-massive and massive honey-brown, sphalerite-rich mineralisation. Polished thin section samples BM15-092 at 56.5 metres, BM15-095 at 60.0 metres, and BM15-096 at 62.0 metres. See page 85 for legend.

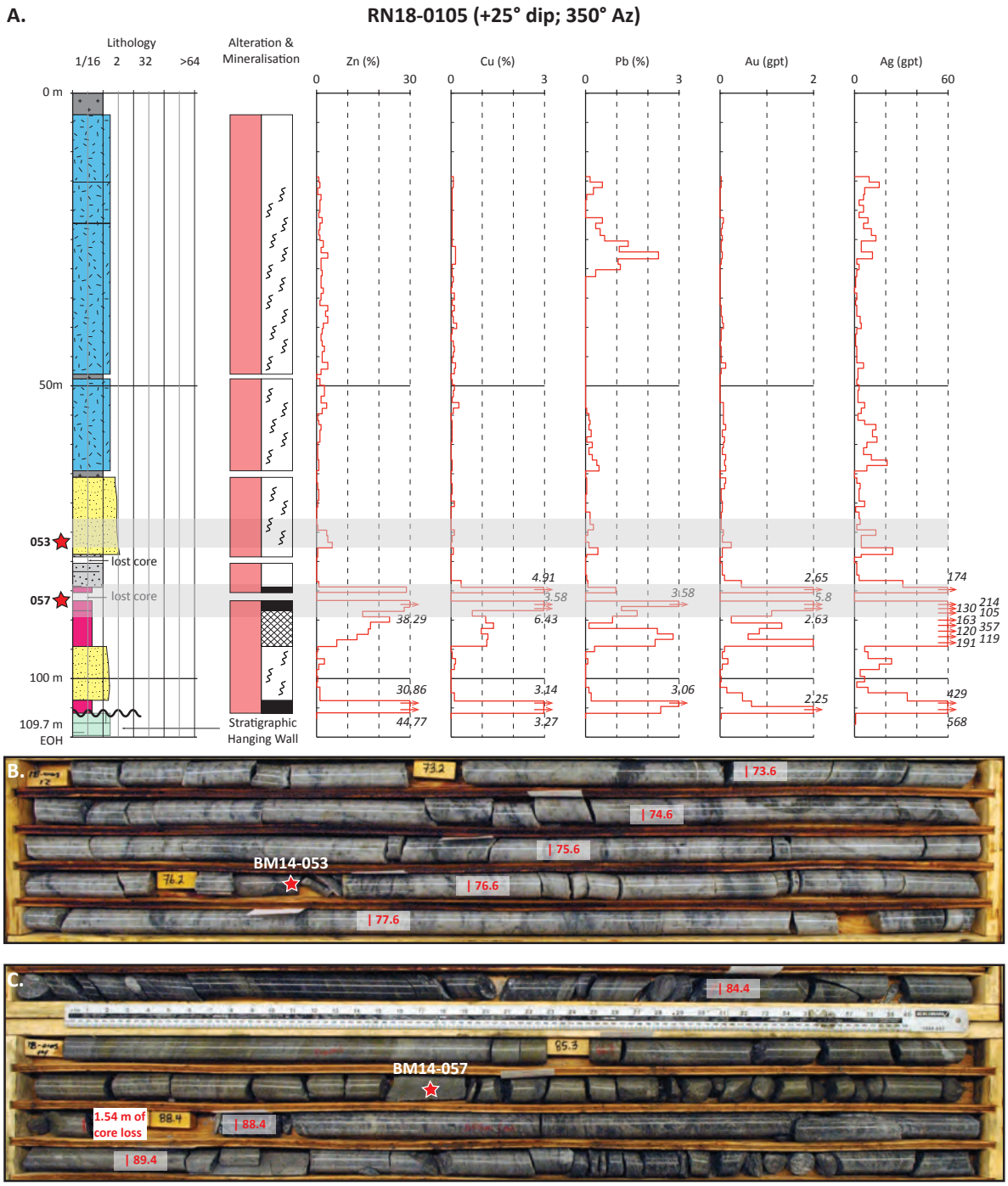

Figure 4.28 Selected graphic log interval from section 918 mE of the Ridge Zone North orebody showing lithology, alteration and mineralisation with Zn, Cu, Pb, Au and Ag assay results. A. Example of "upper zone" stringer-style and semi-massive and massive, sulfide mineralisation. B. Stinger-style, honey brown sphalerite-rich mineralisation associated with sericite-chlorite altered, rhyolitic, volcaniclastic sandstone. Polished thin section BM14-053 at 76.3 metres. C. Massive, banded, sphalerite-pyrite-chalcopyrite-galena mineralisation. Polished thin section sample BM14-057 at 87.4 metres. See page 85 for legend.

4.5 Sulfide, Sulfosalt and Telluride Mineralogy

Base and precious metal minerals were investigated from thirteen polished thin section samples. Seven samples are from the West Block Area and six samples are from the Ridge Zone North orebody (Table 4.1). Sphalerite, pyrite, chalcopyrite and galena are the dominant sulfide minerals with accessory tennantite, tetrahedrite and pearceite-polybasite sulfosalts. Precious metal-dominant phases include electrum and hessite. Sinclair (2000) documented the presence of bornite [Cu_5FeS_4], renierite [$(Cu,Zn)_{11}(Ge,As)_2Fe_4S_{16}$], anilite [$Cu_3S_4$], colusite [$Cu_3(AsGeV)S_4$], stromeyerite [AgCuS], and altaite [PbTe] in the Battle orebody. These mineral phases were not identified in the samples investigated from the West Block Area or the Ridge Zone North orebody.

Table 4.1 Identified minerals in the West Block Area and Ridge Zone North orebody samples.

Sample ID	**038**	**041**	**050**	**033**	**035**	**026**	**027**	**092**	**095**	**096**	**099**	**053**	**057**
Section (mE)	550	550	640	640	828	828	828	918	918	918	918	918	918
Area	WBA	WBA	WBA	WBA	WBA	WBA	WBA	RZN	RZN	RZN	RZN	RZN	RZN
Position	UZ	UZ	UZ	CZ	UZ	CZ	CZ	CZ	CZ	CZ	UZ	UZ	UZ
Style	STG	SMS	SMS	MS	STG	MS	SMS	SMS	SMS	SMS	STG	STG	MS
Analyses	1	2	1	1	1	1	1	2	2	1	1	1	1
precious metals													
electrum	◊	◊	◊	◊	◊						◊		
tellurides													
hessite				◊				◊		◊	◊		◊
sulfides													
pyrite	●●	●●●	●●●	●●	●●	●●	●●	●●●	●●●	●●	●●●	●●	●●
sphalerite	●●●	●●●	●●●	●●●	●●●	●●●	●●●	●●●	●●	●●●	●●●	●●●	●●●
chalcopyrite	◊	◊		●	◊	●	●●	●●	◊	●●●	◊	◊	●
galena	●●	●	●	◊	◊	◊	●●	◊	◊	◊	◊	◊	●●
sulfosalts													
tn-td	◊	●	●●	◊	◊	◊	◊	◊	◊	●	●●	◊	◊
pr-pb	◊		◊				◊						
sulfates													
barite	◊	●●●	●●			◊	◊		●●		◊	◊	◊

1 = MLA and EMP analysis
2 = MLA analysis
●●● Major mineral phase (>10%)
●● Minor mineral phase (3-10%)
● Trace mineral phase (<3%)
◊ Rare mineral phase (<<1%)
Mineral abundance estimated from Area % results from MLA SPL-lite analyses.
[CZ, contact zone; MLA, mineral liberation analysis; EMP, electron microprobe; MS, massive sulfide; pr-pb, pearciete-polybasite; SMS, semi-massive sulfide; STG, stringer-style sulfide; tn-td, tennantite-tetrahedrite; RZN, Ridge Zone North; UZ, upper zone; WBA, West Block Area]

4.5.1 Sphalerite

Sphalerite is ubiquitous in the mineralised samples from the West Block Area and Ridge Zone North orebody. Sphalerite is grey in reflected light and shows no internal zoning in transmitted light (Figure 4.29A). Sphalerite often contains variable amounts of <20 μm, irregular blebs of

chalcopyrite (Figure 4.29A-C). Zinc-rich samples contain abundant sphalerite with variable amounts of intergrown pyrite, and fine-grained, anhedral chalcopyrite and galena (Figure 4.29B-C). Electron microprobe analyses of sphalerite from the West Block Area and Ridge Zone North orebody are summarised in Table 4.2. As suggested by the honey-brown colour of sphalerite in hand sample, sphalerite from both localities is Fe-poor with typically <0.5 wt % Fe, and has between 0.27-0.33 wt % Cd (Table 4.2).

Table 4.2 Average sphalerite electron microprobe results.

Area	Style	Zone	# of PTS	n	Fe (wt%)	Zn (wt%)	S (wt%)	Cd (wt%)	Total (wt%)
WBA	stringer	upper	2	12	0.22	66.41	33.29	0.27	100.20
WBA	semi-massive	upper	1	7	0.11	67.36	33.22	0.30	101.00
WBA	semi-massive	contact	1	9	0.42	66.24	33.60	0.33	100.58
WBA	massive	contact	2	12	1.10	65.49	33.12	0.32	100.04
RZN	stringer	upper	2	9	0.11	66.46	33.10	0.27	99.94
RZN	semi-massive	contact	1	3	0.09	66.20	32.79	0.32	99.41
RZN	massive	upper	1	6	0.15	66.43	33.07	0.29	99.95

# of PTS = number of polished thin sections examined; n = number of electron microprobe analyses
Idealised mineral formula for sphalerite (Zn,Fe)S
[RZN, Ridge Zone North; WBA, West Block Area]

4.5.2 Pyrite

Pyrite occurs in a range of textures in the West Block Area and Ridge Zone North localities including euhedral, embayed, and partially annealed crystals (Figure 4.29D-I). Often more than one of these textures is present in a single sample (e.g., Figure 4.29E-F). Coarse-grained pyrite (>100 μm) typically shows evidence of multiple growth stages with spongy and inclusion-rich cores enclosed by inclusion free pyrite (e.g., Figure 4.29G-H). Embayed pyrite grains (e.g., Figure 4.29E) are abundant in massive and semi-massive sulfide mineralisation styles, as well as weakly annealed pyrite with variably developed 120º triple junctions (Figure 4.29F). Pyrite porphyroblasts are also common in samples of semi-massive and massive sulfide from the Ridge Zone North orebody (Figure 4.29I). No pyrite framboids grains were observed.

4.5.3 Chalcopyrite and galena

Chalcopyrite occurs as anhedral irregular masses associated with sphalerite, pyrite, galena and tennantite. Chalcopyrite commonly occurs as <20 μm irregular inclusions in masses of sphalerite (e.g., Figure 4.29B). Chalcopyrite is also present between pyrite grains (Figure 4.29F) and as coarse-grained masses associated with galena and sphalerite (Figure 4.29J, L).

Galena occurs as irregularly shaped masses intergrown with sphalerite, chalcopyrite and pyrite, and often shows aligned cleavage planes (Figure 4.29J-L). Galena also occurs as cuspate inclusions in massive sphalerite (Figures 4.29B). Fine- to medium-grained (5-50 μm) galena grains occur along chalcopyrite-sphalerite, sphalerite-pyrite, sphalerite-tennantite, and pyrite-tennantite mineral boundaries (e.g., Figure 4.30B-F).

4.5.4 Tennantite-tetrahedrite

Tennantite-tetrahedrite occurs in all of the samples investigated, mainly as an accessory mineral phase (Table 4.1). Tennantite is bluish-grey in reflected light and shows no zoning or internal

reflections in transmitted light (Figure 4.30A-C). Tennantite is associated with sphalerite, pyrite, galena and chalcopyrite. It occurs as coarse-grained masses with galena at the margins of sphalerite (Figure 4.30A) and is intergrown with cuspate pyrite and sphalerite with galena (Figure 4.30B). Tennantite occurs as small grains at boundaries between coarse-grained pyrite that is intergrown with masses of sphalerite (Figure 4.30C). Tetrahedrite was identified in two polished thin sections (BM14-038, BM14-027) and is an accessory mineral phase (<< 1%; Table 4.1). Tetrahedrite is light grey in reflected light and intergrown with quartz and sericite associated with fine-grained sphalerite and galena (Figure 4.30D).

Sixty-six EMP analyses of tennantite-tetrahedrite were collected from nine polished thin sections to quantify the sulfosalt mineral chemistry (Table 4.3; Figure 4.31A-D). Analyses from the West Block Area have a range of As and Sb values with elevated Ag results associated with Sb-rich analyses (Figure 4.31A-B). Analyses with less than 15 wt % As are considered tennantite, however no pure tennantite or tetrahedrite were identified (Figure 4.31A). Silver concentrations range from 0.68-3.32 wt % in tennantite and are elevated in tetrahedrite, between 8.99-17.96 wt % (Figure 4.31B). Tennantite from the Ridge Zone North orebody contain 15.09-19.30 wt % As, 0.41-6.12 wt % Sb, and 0.13-1.28 wt % Ag (Figure 4.31C-D).

Table 4.3 Average tetrahedrite-tennantite group electron microprobe results.

Area	Sample (Style)	Zone	Min	n	Cu (wt%)	Fe (wt%)	Zn (wt%)	As (wt%)	Se (wt%)	Sb (wt%)	S (wt%)	Ag (wt%)	Te (wt%)	Cd (wt%)	Total (wt%)
WBA	BM14-035 (stg)	upper	tn	6	40.77	1.49	6.97	16.58	<0.02	4.01	27.77	1.98	<0.02	0.08	99.66
WBA	BM14-038 (stg)	upper	td	6	30.06	0.49	7.11	3.17	<0.02	23.17	24.97	11.42	<0.02	0.16	100.55
WBA	BM14-050 (sm)	upper	tn	8	41.91	1.47	7.10	18.30	<0.02	1.85	28.09	0.80	<0.02	0.09	99.63
WBA	BM14-027 (sm)	contact	td	6	31.91	3.42	4.98	12.63	<0.02	8.73	26.53	11.92	<0.02	0.06	100.17
WBA	BM14-026 (m)	contact	tn	8	40.39	3.87	4.43	16.38	<0.02	4.17	27.52	2.47	0.05	0.04	99.32
RZN	BM14-053 (stg)	upper	tn	7	41.83	1.34	7.46	18.23	<0.02	1.59	28.03	0.84	<0.02	0.08	99.40
RZN	BM15-099 (stg)	upper	tn	6	41.37	0.84	7.61	16.60	<0.02	4.07	27.86	1.25	0.03	0.09	99.73
RZN	BM15-096 (sm)	contact	tn	10	42.80	1.05	7.50	18.79	<0.02	0.62	28.12	0.16	0.20	0.10	99.34
RZN	BM14-057 (m)	upper	tn	9	41.20	1.36	6.95	15.51	<0.02	5.67	27.57	1.16	0.17	0.09	99.68

# of PTS = number of polished thin sections examined; n = number of electron microprobe analyses
tennantite (tn) - tetrahedrite (td) solid solution mineral formula = $[(Cu,Ag)_{10}(Zn,Fe)_2]_{12}(Sb,As)_4(S,Se,Te)_{13}$
[m, massive; Min, Mineral; RZN, Ridge Zone North; sm, semi-massive; stg, stringer; WBA, West Block Area]

4.5.5 Pearceite-polybasite

The silver-rich sulfosalt group pearceite-polybasite (e.g., Craig and Vaughan, 1994) was identified in three polished thin sections from the West Block Area (Table 4.1). Pearceite refers to the As > Sb end member phase and polybasite is the Sb > As end member (Bindi et al., 2007). In samples BM14-027 and BM14-038 pearceite-polybasite is a trace mineral phase (Table 4.1) and occurs as <10 μm grains associated with sphalerite and galena (Appendix C). In sample BM14-050, pearceite-polybasite is grey in reflected light and occurs as 1-20 μm wide veinlets (Figure 4.30E-F). These veinlets crosscut tennantite, sphalerite, galena and pyrite and appear to have in filled brittle fractures. For example, pearceite-polybasite is infilling broken cleavage planes in galena (Figure 4.30F).

Ten EMP analyses of pearceite-polybasite were collected from three polished thin sections to determine the sulfosalt mineral chemistry (Table 4.4; Figure 4.31E-F). Based on the mineral chemistry classification of Bindi et al. (2007), five of the EMP analyses are polybasite and five are pearceite. Sample BM14-050 contains both pearceite and polybasite in crosscutting veinlets (Figures 4.30E-F; 4.31E). Compared to tennantite-tetrahedrite, pearceite and polybasite are significant silver-bearing minerals. Silver concentrations vary from 65.33-72.01 wt % in pearceite-polybasite, compared to 0.13-17.96 wt % Ag in tennantite-tetrahedrite (Figure 4.31F).

Table 4.4 West Block Area pearceite-polybasite group electron microprobe results.

Sample ID	Style	Zone	Phase	Ag (wt%)	Cu (wt%)	S (wt%)	As (wt%)	Sb (wt%)	Te (wt%)	Total (wt%)
BM14-038	stringer	upper	polybasite	70.88	3.60	15.87	2.01	7.13	0.94	100.42
BM14-038	stringer	upper	polybasite	70.48	4.77	15.46	2.26	6.61	1.33	100.92
BM14-038	stringer	upper	polybasite	69.00	4.87	15.24	2.21	6.62	1.27	99.20
BM14-050	semi-massive	upper	polybasite	71.22	5.14	16.08	3.44	4.31	0.02	100.21
BM14-050	semi-massive	upper	pearceite	68.98	7.69	17.17	5.32	2.57	0.02	101.75
BM14-050	semi-massive	upper	pearceite	72.01	5.04	16.72	5.36	2.38	0.02	101.53
BM14-050	semi-massive	upper	pearceite	65.33	8.71	17.17	4.57	3.87	0.02	99.67
BM14-050	semi-massive	upper	pearceite	71.41	4.96	16.76	5.66	1.91	0.02	100.71
BM14-050	semi-massive	upper	pearceite	70.96	5.98	16.89	5.88	1.54	0.02	101.27
BM14-027	semi-massive	contact	polybasite	70.18	2.25	17.50	2.27	9.35	0.02	101.57

Idealised formulas for pearceite $[Ag_9CuS_4][(Ag,Cu)_6(As,Sb)_2S_7]$ and polybasite $[(Ag,Cu)_6(Sb,As)_3S_7][Ag_9CuS_4]$

4.5.6 Electrum and hessite

Electrum was identified in six of the thirteen polished thin sections (Table 4.1). Electrum occurs as 1-20 μm, anhedral grains. In the West Block Area, electrum was observed along the grain boundaries between tennantite or pyrite in quartz-sericite altered host rocks (e.g., Figure 4.30G) and as inclusions in sphalerite (e.g., Figure 4.30H). In the Ridge Zone North orebody, a ~20 μm anhedral grain of electrum was observed at the grain boundary between intergrown pyrite and tennantite in a quartz-sericite altered host rock (Figure 4.30I).

Analyses of electrum from "upper zone" position samples (n=4) have gold concentrations between 55.95 and 69.48 wt % with trace amounts of Te, 0.03-0.05 wt % (Table 4.5). Electrum (n=1) from the "contact zone" position in the West Block Area has a similar gold fineness (67.48 wt % Au, 0.05 wt % Te; Table 4.5). Electrum from the Ridge Zone North orebody (n=1) has a Au concentration of 73.84 wt % with a trace amount of Te, <0.03 wt % (Table 4.5).

Hessite was identified in five of the thirteen polished thin sections (Table 4.1). Anhedral grains are 2-20 μm and occur as inclusions in sphalerite (Figure 4.30J), along the grain boundaries of tennantite and quartz (Figure 4.30K), and along grain boundaries between sphalerite, tennantite and chalcopyrite (Figure 4.30L). Hessite was observed in samples from both "contact zone" and "upper zone" positions (Table 4.1). Due to the small grain size of hessite, it was difficult to collect clean EMP analyses. As a result, the number of EMP analysis is limited (n=4). Silver concentrations vary between 60.16 and 65.12 wt % with Te contents between 34.38 wt % and 37.85 wt % (Table 4.5).

Figure 4.29 Photomicrographs of sulfide mineralogy and textures from the West Block Area and Ridge Zone North.

A. Example of massive sphalerite with <20 μm blebs of chalcopyrite (RFL). Note the relative homogenous texture with no internal zoning in plane polarised light (PPL). Polished thin section sample BM14-033; "contact zone" massive sulfide mineralisation from the West Block Area (Figure 4.24).

B. Example of massive sphalerite with <20 μm blebs of chalcopyrite and irregular shaped, coarser-grained galena and pyrite. Polished thin section sample BM14-038; stringer-style "upper zone" sulfide mineralisation from the West Block Area (Figure 4.23)

C. Example of massive sphalerite with <20 μm blebs of chalcopyrite and >100 μm anhedral masses of chalcopyrite and subhedral pyrite. Sulfide minerals are intergrown with quartz and minor barite. Polished thin section sample BM14-026; "contact zone" massive sulfide mineralisation from the West Block Area (Figure 4.25).

D. Example of disseminated, euhedral pyrite intergrown with sphalerite, in a quartz and white mica altered matrix. Polished thin section sample BM14-035; stringer-style "upper zone" sulfide mineralisation from the West Block Area (Figure 4.26).

E. Example of embayed, irregular shaped, pyrite in sphalerite. Polished thin section sample BM15-092; "contact zone" semi-massive sulfide mineralisation from the Ridge Zone North orebody (Figure 4.27).

F. Example of coarse-grained pyrite with chalcopyrite and sphalerite, interstitial between pyrite grain boundaries. Note pyrite mineral boundaries are near 120°, which indicates a degree of recrystallisation. Polished thin section sample BM15-092; "contact zone" semi-massive sulfide mineralisation from the Ridge Zone North orebody (Figure 4.27).

G. Example of pyrite grain with an inclusion-rich, spongy core. Polished thin section sample BM14-026; "contact zone" massive sulfide mineralisation from the West Block Area (Figure 4.25).

H. Example of circular shaped, pyrite core with inclusions enclosed by clean, pyrite rim associated with chalcopyrite, sphalerite and minor galena. Polished thin section sample BM14-057; "upper zone" massive sulfide mineralisation from the Ridge Zone North orebody (Figure 4.26).

I. Example of pyrite porphyroblast with chalcopyrite and rare sphalerite. Polished thin section sample BM15-092; "contact zone" semi-massive sulfide mineralisation from the Ridge Zone North orebody (Figure 4.27).

J. Example of coarse-grained, anhedral masses of chalcopyrite intergrown with galena and sphalerite in a quartz-sericite matrix. Polished thin section sample BM14-027; "contact zone" semi-massive sulfide mineralisation from the West Block Area (Figure 4.25).

K. Example of coarse-grained, anhedral masses of galena intergrown with embayed, coarse-grained pyrite and irregular masses of sphalerite. Sulfide minerals in a quartz-sericite matrix. Polished thin section sample BM14-038; stringer-style "upper zone" sulfide mineralisation from the West Block Area (Figure 4.23A-B).

L. Example of coarse-grained, anhedral chalcopyrite on the margins of sphalerite with abundant <20 μm blebs of chalcopyrite. Polished thin section sample BM15-096; "contact zone" semi-massive sulfide mineralisation from the Ridge Zone North orebody (Figure 4.27).

[cpy, chalcopyrite; gn, galena; PPL, plane polarised light; py, pyrite; qtz, quartz; sp, sphalerite; wm, white-mica; XPL, cross polarised light]

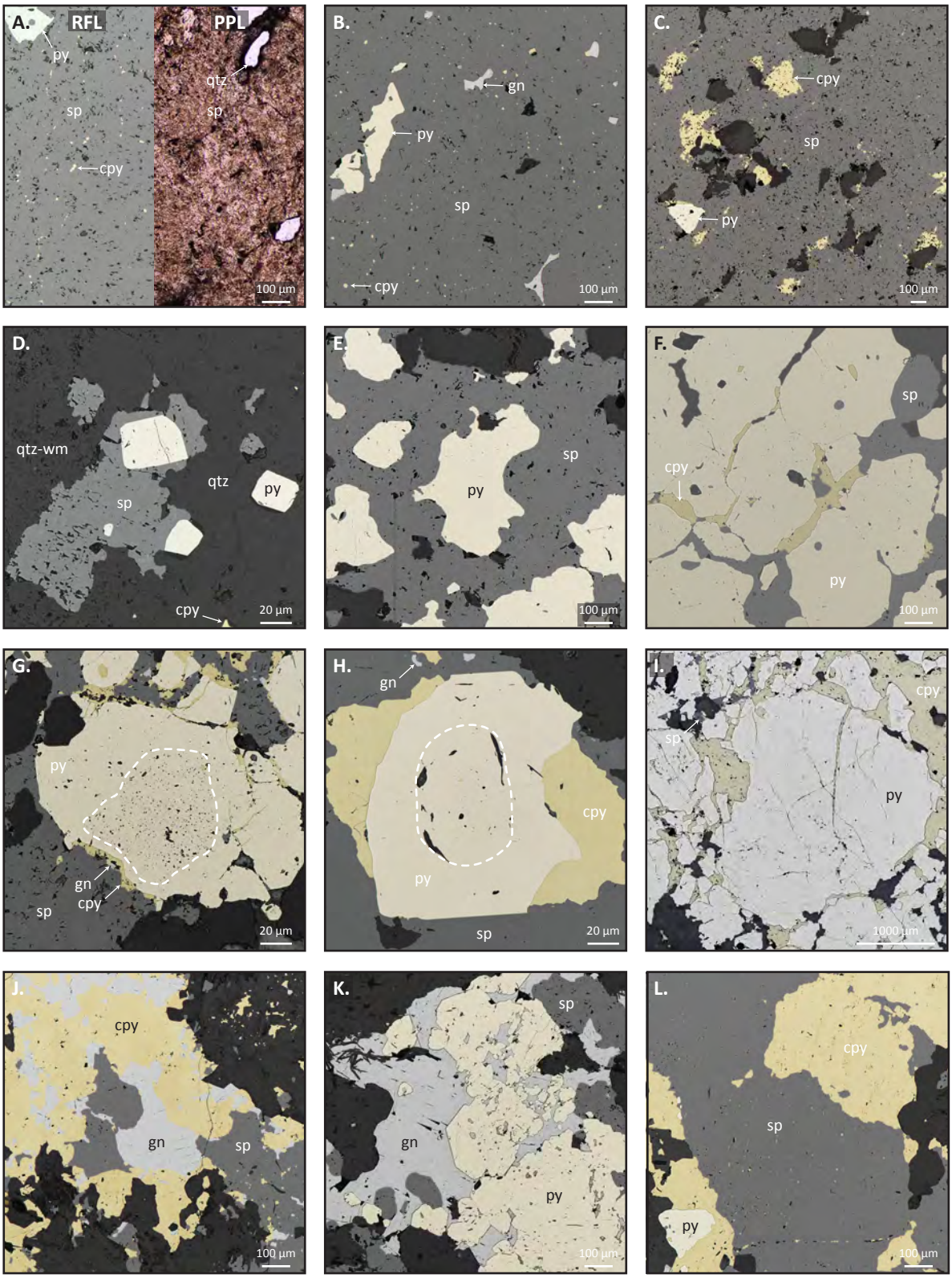
A.
RFL
PPL
py
qtz
sp
sp
cpy
100 µm
B.
gn
py
sp
cpy
100 µm
C.
cpy
sp
py
100 µm
D.
qtz-wm
qtz
py
sp
cpy
20 µm
E.
sp
py
100 µm
F.
sp
cpy
py
100 µm
G.
py
gn
cpy
sp
20 µm
H.
gn
cpy
py
sp
20 µm
I.
cpy
sp
py
1000 µm
J.
cpy
gn
sp
100 µm
K.
sp
gn
py
100 µm
L.
cpy
sp
py
100 µm

Figure 4.30 Photomicrographs and backscatter electron images of sulfosalts, electrum and tellurides from the West Block Area and Ridge Zone North orebody. Tetrahedrite, tennantite, pearceite-polybasite and hessite minerals confirmed with a combination of EMP and EDS analysis.

A. Example of coarse-grained tennantite intergrown with sphalerite-pyrite and galena with <10 μm chalcopyrite along margins of anhedral galena grains (RFL). Polished thin section BM14-050; "upper zone" semi-massive sulfide mineralisation from the West Block Area (Figure 4.24).

B. Example of anhedral mass of tennantite with inclusions of embayed pyrite and sphalerite and anhedral grains of galena (RFL). Polished thin section BM14-050; "upper zone" semi-massive sulfide mineralisation from the West Block Area (Figure 4.24).

C. Example of tennantite with pyrite porphyroblasts and anhedral chalcopyrite and galena (RFL). Polished thin section sample BM14-057; "upper zone" massive sulfide mineralisation from the Ridge Zone North orebody (Figure 4.28).

D. Example of irregular-shaped tetrahedrite associated with anhedral galena and sphalerite in a quartz-sericite-rutile matrix (RFL). Polished thin section sample BM14-038; stringer-style "upper zone" sulfide mineralisation from the West Block Area (Figure 4.23).

E. Example of pearceite-polybasite crosscutting intergrown mass of tennantite-sphalerite-galena (RFL). The planar, crosscutting nature of this mineral phase indicates a later precipitation timing relative to the host mineral phases, possibly related to metamorphism. Polished thin section BM14-050; "upper zone" semi-massive sulfide mineralisation from the West Block Area (Figure 4.24). White dashed lines outline pearceite-polybasite veinlets.

F. Example of pearceite-polybasite crosscutting tennantite, sphalerite, pyrite and galena (RFL). Note how the pearceite-polybasite crosscuts the galena grain along broken cleavage plains. Polished thin section BM14-050; "upper zone" semi-massive sulfide mineralisation from the West Block Area (Figure 4.24A-B). White dashed lines outline pearceite-polybasite veinlets.

G. Example of electrum between tennantite and quartz mineral boundaries (RFL). Polished thin section BM14-050; "upper zone" semi-massive sulfide mineralisation from the West Block Area (Figure 4.24).

H. Example of massive sphalerite with inclusions of electrum, quartz and galena (RFL). Polished thin section sample BM14-035; stringer-style "upper zone" sulfide mineralisation from the West Block Area (Figure 4.26).

I. Example of electrum at the margins of pyrite and tennantite with quartz (RFL). Polished thin section sample BM15-099; stringer-style "upper zone" sulfide mineralisation from the Ridge Zone North orebody (Figure 4.27).

J. Example of small inclusion of hessite in sphalerite (BSE). Polished thin section sample BM14-033; "contact zone" massive sulfide mineralisation from the West Block Area (Figure 4.24).

K. Example of small grain of hessite between tennantite and quartz mineral boundaries (BSE). Polished thin section sample BM15-096; "contact zone" semi-massive sulfide mineralisation from the Ridge Zone North orebody (Figure 4.27).

L. Example of hessite between chalcopyrite-sphalerite and chalcopyrite-sphalerite-tennantite mineral boundaries (BSE). Polished thin section sample BM14-057; "upper zone" massive sulfide mineralisation from the Ridge Zone North orebody (Figure 4.28).

[BSE, backscatter electron; cpy, chalcopyrite; EDS, energy-dispersive x-ray spectroscopy; el, electrum; EMP, electron microprobe; gn, galena; hs, hessite; pr-pb, pearceite-polybasite; py, pyrite; qtz, quartz; sp, sphalerite; RFL, reflected light; rt, rutile; td, tetrahedrite; tn, tennantite; wm, white-mica]

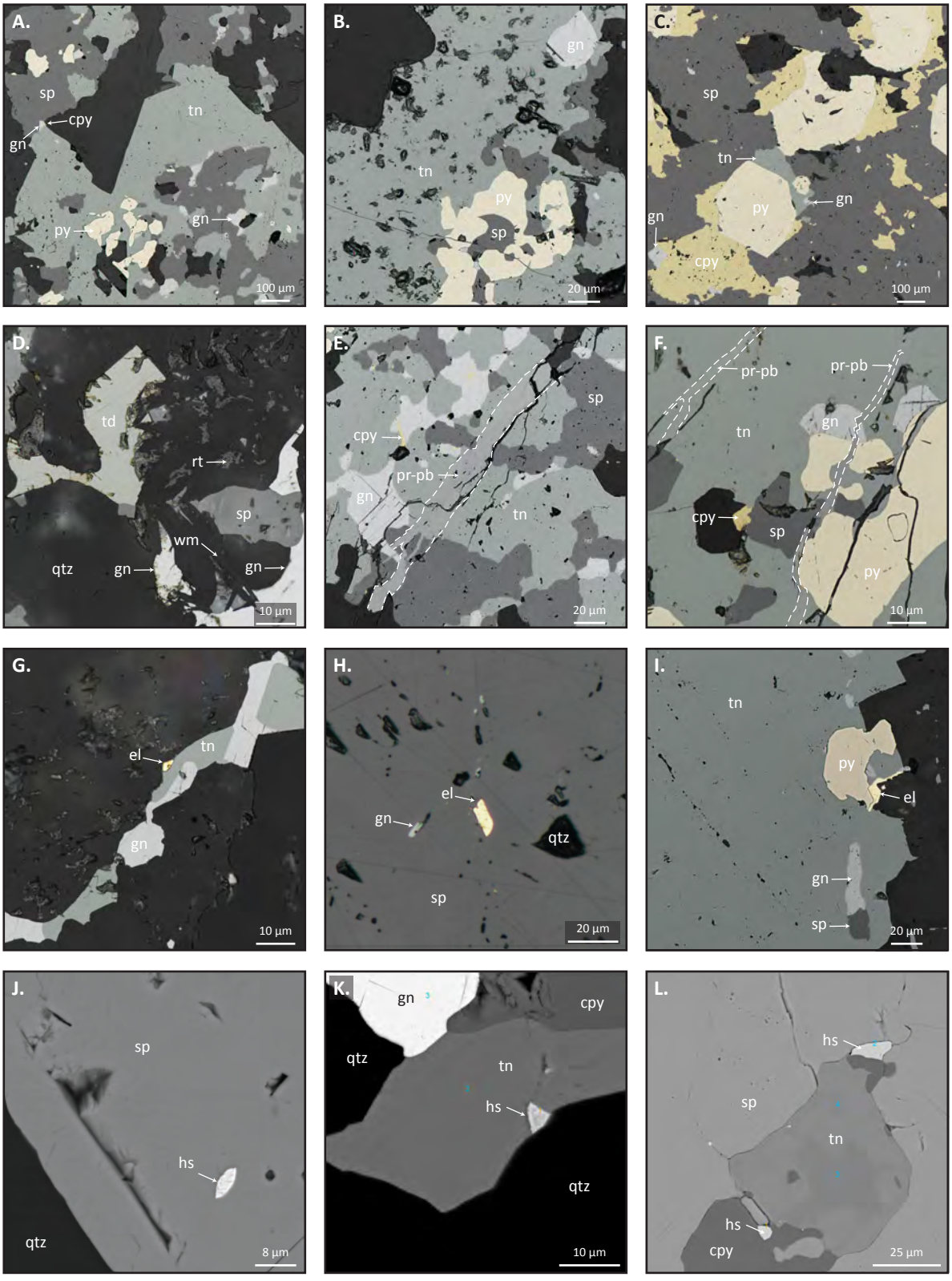
A.
sp
cpy
gn
tn
py
gn
100 µm
B.
gn
tn
py
sp
20 µm
C.
sp
tn
gn
py
gn
cpy
100 µm
D.
td
rt
sp
wm
qtz
gn
gn
10 µm
E.
sp
cpy
pr-pb
gn
tn
20 µm
F.
pr-pb
pr-pb
tn
gn
cpy
sp
py
10 µm
G.
el
tn
gn
10 µm
H.
el
gn
qtz
sp
20 µm
I.
tn
py
el
gn
sp
20 µm
J.
sp
hs
qtz
8 µm
K.
gn
cpy
qtz
tn
hs
qtz
10 µm
L.
hs
sp
tn
hs
cpy
25 µm

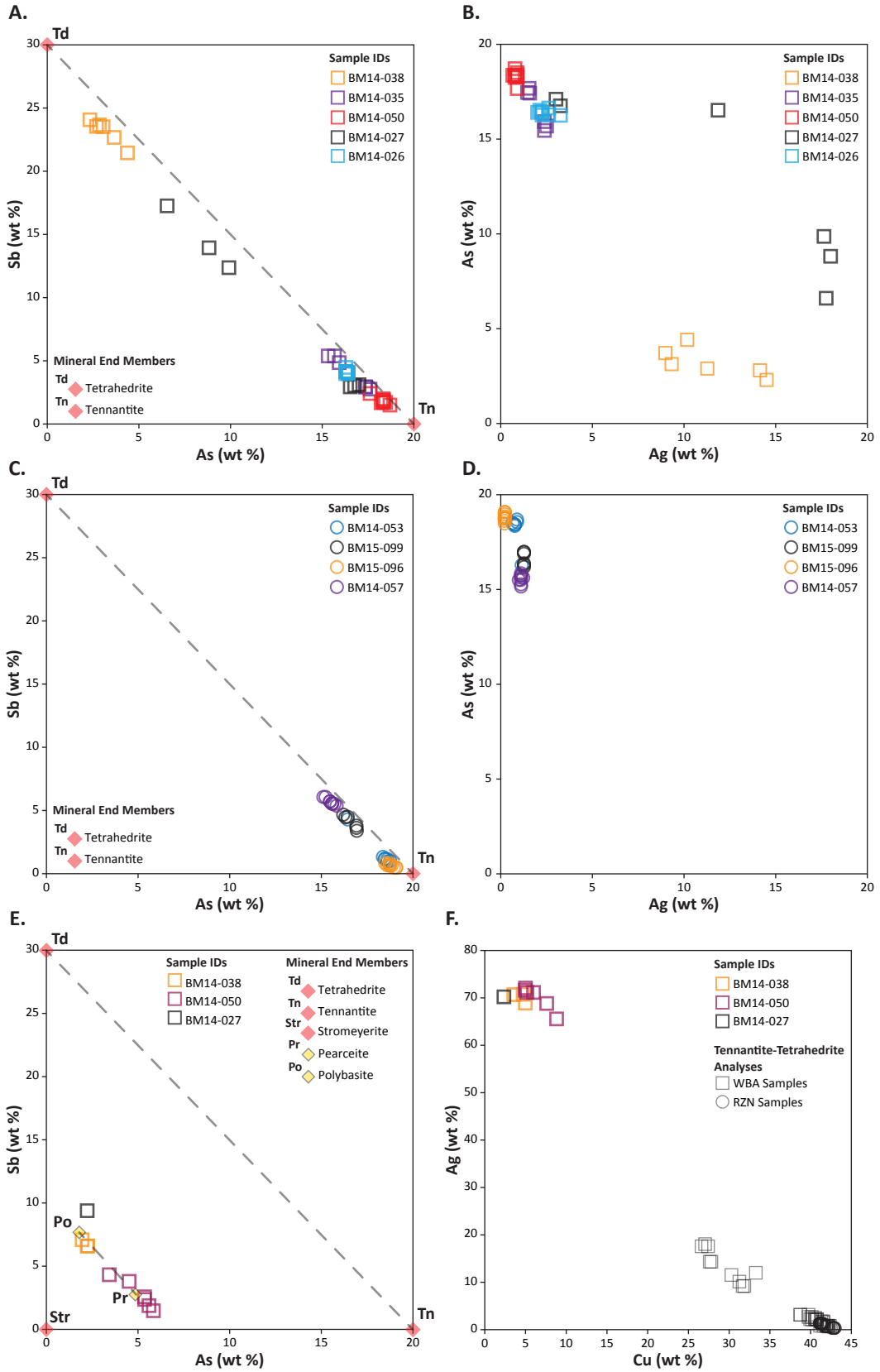

Figure 4.31 Major composition of tennantite and tetrahedrite (A-D; n=34) and pearceite-polybasite (E-F; n=10) analysed by EMP analysis. A-B. Analyses from the West Block Area. A. As vs Sb plot of tennantite and tetrahedrite chemistry. B. Ag vs As plot illustrating that the samples with lower As have higher Ag contents. C-D. Analyses from the Ridge Zone North orebody (n=32). C. As vs Sb plot showing that the samples are characterised by tennantite. D. Ag vs As plot showing the association of low Ag with high As abundance in tennantite. E. As vs Sb plot showing chemical range of pearceite-polybasite and tennantite-tetrahedrite. F. Cu vs Ag plot illustrating the silver-rich nature of pearceite-polybasite relative to tennantite-tetrahedrite.

Table 4.5 Electrum and hessite electron microprobe results.

Sample ID	Area	Style	Zone	Mineral	Au (wt%)	Ag (wt%)	Te (wt%)	Total (wt%)
BM14-035	WBA	stringer	upper	electrum	66.25	33.30	0.05	99.60
BM14-035	WBA	stringer	upper	electrum	64.18	37.45	0.04	101.67
BM14-050	WBA	semi-massive	upper	electrum	55.95	35.97	0.03	91.95
BM14-050	WBA	semi-massive	upper	electrum	69.18	33.17	<0.03	102.35
BM14-033	WBA	massive	contact	electrum	67.48	32.81	0.05	100.34
BM15-099	RZN	stringer	upper	electrum	73.84	28.23	<0.03	102.07
BM14-033	WBA	massive	contact	hessite	0.14	60.16	35.38	95.68
BM15-099	RZN	stringer	upper	hessite	<0.06	65.12	34.38	99.50
BM15-099	RZN	stringer	upper	hessite	0.08	63.03	35.63	98.75
BM14-057	RZN	massive	upper	hessite	<0.06	62.75	37.85	100.60

Idealised formulas for electrum (Au, Ag) and hessite Ag_2Te
[RZN, Ridge Zone North; WBA, West Block Area]

4.5.7 Paragenesis of sulfide mineralisation

In the West Block Area, stringer-style, semi-massive and massive sulfide mineralisation are polymetallic and sphalerite-dominant (Table 4.1). Pyrite is ubiquitous thought the study area. Pyrite textures include anhedral, resorbed and subhedral grains, zoned pyrite, and pyrite porphyroblasts (Figure 4.29). Zoned pyrite suggests at least two stages of pyrite growth: (1) early, spongy and inclusion-rich pyrite and (2) clean, inclusion-free pyrite (Figure 4.29G-H). No, obvious, framboidal pyrite textures were observed; however the spongy and inclusion-rich pyrite cores may reflect relict pyrite framboids. While sulfide mineralisation in the West Block Area is sphalerite-dominant; pyrite, chalcopyrite, and galena are present. Pyrite, chalcopyrite and galena often coexist as irregular-shaped intergrowths with sphalerite (Figure 4.29A-C), as well as anhedral sphalerite intergrown with euhedral pyrite (Figure 4.29D).

Pyrite porphyroblasts were observed in pyrite-rich, massive sulfide samples from the Ridge Zone North orebody (Figure 4.22K). In thin section, pyrite porphyroblasts commonly display brittle fractures filled with chalcopyrite (Figure 4.29I). Partial annealing of pyrite with interstitial chalcopyrite and sphalerite (Figure 4.29F), as well as subhedral pyrite grains with inclusions of galena and sphalerite (Figure 4.29K), suggest some degree of recrystallisation. However, monomineralic, completely annealed pyrite masses were not observed in either the West Block Area or Ridge Zone North orebody samples. Rather, coarse pyrite textures comprise inclusion-rich cores enclosed by "clean", inclusion-free pyrite rims (Figure 4.29G-H).

Coarse, anhedral masses of galena and chalcopyrite were also observed. In general, chalcopyrite and galena occur at the margins of anhedral sphalerite masses (Figure 4.29J, L). This texture could indicate co-precipitation and/or modification of sphalerite. Tennantite-tetrahedrite is typically associated with galena, sphalerite and lesser pyrite and chalcopyrite (Figure 4.30). In some cases, tennantite-tetrahedrite appears to be replacing sphalerite (Figure 4.30A-B).

Pearceite-polybasite veinlets crosscut sulfide and sulfosalt mineralisation at an "upper zone" position, in the West Block Area. Pearceite-polybasite veinlets are 1-20 μm wide and crosscut intergrown masses of sphalerite and tennantite (Figure 4.30E), as well as masses of intergrown tennantite, pyrite, sphalerite, and galena (Figure 4.30F). The veinlets appear to be brittle-fracture fills, and in one example pearceite-polybasite is infilling broken cleavage planes

of galena (Figure 4.30F). Electrum and hessite are rare mineral phases and often occur on the margins of tennantite-tetrahedrite, pyrite, sphalerite, and silicates (Figure 4.30G, I, K, L).

Four paragenetic stages of mineralisation are proposed for the study area based on the described petrographic textures (Figure 4.32). Stage-1 includes early, inclusion-rich pyrite. Stage-2 consists of inclusion-free pyrite rimming Stage-1 pyrite and accompanied by the precipitation of sphalerite with minor galena-chalcopyrite-barite ± tennantite and tetrahedrite. As the VHMS hydrothermal system evolved, Stage-3 mineralisation results in the modification to Stage 2 mineral phases, likely in the form of zone-refining (e.g., Eldridge et al., 1983). This modification is characterised by grain coarsening, the homogenisation of sphalerite, and the local remobilisation of hypogene sulfide and sulfosalt phases. Stage-4 comprises the precipitation of precious metal mineral phases, interpreted to be the result of later, regional metamorphism. Stage-4 includes the formation of pearceite-polybasite veinlets crosscutting hypogene mineral assemblages. The precipitation of electrum and hessite could have occurred during either or both of Stages-3 and -4.

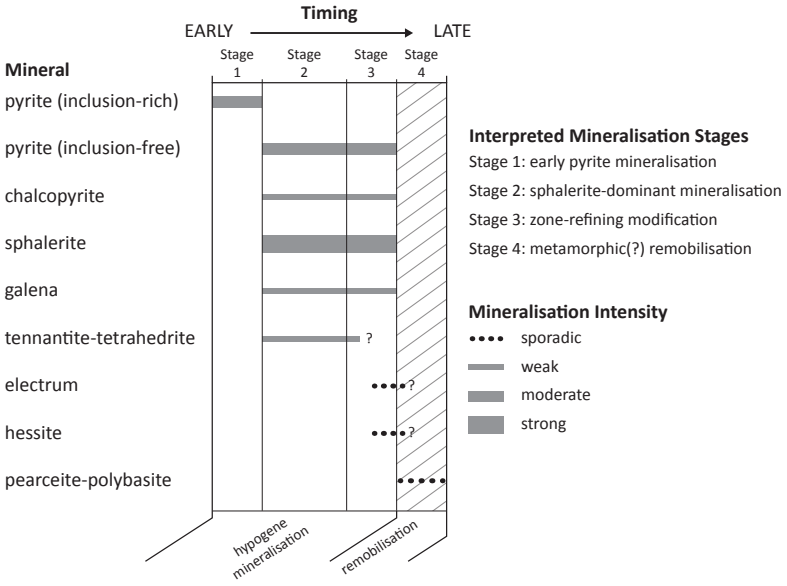

Figure 4.32 Paragenetic chart showing the interpreted timing of precipitation for the most abundant metal sulfide, sulfosalt and precious metal minerals in the West Block Area and Ridge Zone North orebody.

Regional metamorphism of VHMS deposits typically results in ore mineralogy and textural changes that are largely isochemical (e.g., Vokes, 1966; Stanton, 1972; Spry et al., 2000; Vikentyev et al., 2017). In the case of VHMS deposits affected by lower greenschist facies metamorphism, the VHMS hydrothermal and subsequent metamorphic temperature conditions overlap (e.g., Craig and Vaughan, 1994). As a result, distinguishing hypogene mineralisation features from secondary metamorphic features can be ambiguous. The homogenisation of sphalerite and the segregation of electrum and tellurides from hypogene mineral phases could be attributed to zone-refinement by a late-stage, low-temperature hydrothermal fluid, or by prehnite-pumpellyite up to greenschist facies metamorphism (e.g., Craig and Vokes, 1993; Huston et al., 1996; Huston, 2000; Vikentyev, 2006).

4.6 West Block Area Alteration

Alteration mineral facies were described and documented on detailed graphic logs (Figures 4.23-4.28). The spatial distribution and association to sulfide mineralisation of the identified

alteration mineral assemblages where then assessed on detailed cross-section interpretations (Figures 4.3B-4.6B). Alteration minerals include sericite (fine-grained white mica), chlorite, quartz, epidote, calcite and pyrite. Relative alteration intensities vary from weak to strong in the West Block Area.

4.6.1 Chlorite-calcite-pyrite alteration

Chlorite-calcite-pyrite alteration affects andesitic rocks of the Price Formation. Pervasive, fine-grained chlorite and calcite throughout the groundmass results in a medium green to dark green rock (Figures 4.33A-B). Typically, 5-10% disseminated, fine-grained pyrite is associated with chlorite ± calcite alteration. In thin section chlorite, calcite, and pyrite are interstitial with albite and quartz to form a mosaic-textured groundmass (Figures 4.34A-B). Locally, mafic mineral phenocrysts, likely pyroxene, are selectively replaced by chlorite (Figure 4.34B).

In the West Block Area this alteration is ubiquitous throughout the Price Formation (Figures 4.3B-4.5B). Andesite, immediately below the Myra Formation contact, is typically dark green and contains up to 15% disseminated pyrite (Figure 4.33B). With increasing depth from the lower Myra Formation contact, the Price Formation becomes medium green and contains <5% disseminated pyrite (Figure 4.33A).

4.6.2 Chlorite-sericite-pyrite alteration

Chlorite-sericite alteration is fine-grained, pervasive to patchy, and affects the groundmass of coherent rocks and matrix of clastic rocks. This alteration manifests as a light green to grey colouration. Chlorite and sericite alters the groundmass of Price Formation coherent andesite (Figure 4.33C), the matrix of polylithic volcaniclastic rocks of the Basal Volcaniclastic Unit (Figure 4.33D-E) and of rhyolitic, volcaniclastic siltstone and sandstone of the HW Rhyolite (Figure 4.33F). Fine- to medium-grained, 5-15%, disseminated pyrite is common with this alteration. In thin section, volcaniclastic lithic fragments are supported by fine-grained intergrowths of chlorite and sericite (Figure 4.34C-D).

In the West Block Area chlorite-sericite alteration is pervasive in the Basal Volcaniclastic Unit, and locally present in the Price Formation, and sporadically distributed in the HW Rhyolite (Figure 4.3B). Unlike the chlorite ± calcite and pyrite alteration that affects the Price Formation, chlorite-sericite alteration affects multiple rock types and is discordant to lithological contacts. This alteration type is spatially associated with "contact zone" position, massive sulfide mineralisation (Figures 4.4B-4.5B).

4.6.3 Sericite-quartz-pyrite alteration

Sericite-quartz-pyrite alteration is pervasive in the HW Rhyolite. It is characterised by moderate to strong, sericite and quartz alteration to the groundmass of coherent quartz and feldspar-phyric rhyolite, and the matrix of rhyolitic volcaniclastic siltstone, sandstone and breccia. Sericite-quartz alteration results in a white to grey rock (Figure 4.33G). Fine-grained, disseminated pyrite is commonly associated with this alteration (Figure 4.33H), as well as pyrite-rich stringers. In thin section, the altered groundmass of coherent rhyolite has a mosaic texture, defined by interlocking quartz, albite and pyrite (Figures 4.34E-F). Feldspar phenocrysts are variably altered by sericite (Figure 4.34E), and quartz phenocrysts often have secondary quartz on their margins (Figure 4.11H). In felsic volcaniclastic rocks, the matrix is altered to sericite and is commonly associated with disseminated pyrite (Figure 4.34G).

Figure 4.33 BQ drill core photograph examples of identified alteration facies in drill core from the West Block Area.

A. Example of chlorite-calcite-pyrite altered feldspar-phyric andesite of the Price Formation. Photograph from BG18-3902 at 150.5 metres (Figure 4.3B).

B. Example of chlorite-calcite-pyrite altered andesite of the Price Formation. Photograph from BG18-3769 at 130.0 metres (Figure 4.5B).

C. Example of chlorite-sericite-pyrite altered andesite of the Price Formation. Photograph from BG18-3904 at 149.4 metres (Figure 4.3B).

D. Example of chlorite-sericite-pyrite altered, polylithic, volcaniclastic conglomerate of the Basal Volcaniclastic Unit. Photograph from BG18-3903 at 139.7 metres (Figure 4.3B).

E. Example of chlorite-sericite-pyrite altered, polylithic, volcaniclastic sandstone of the Basal Volcaniclastic Unit. Photograph from BG18-3321 at 175.6 metres (Figure 4.5B).

F. Example of chlorite-sericite altered, rhyolitic, volcaniclastic sandstone of the HW Rhyolite. Photograph from BG18-3902 at 109.9 metres (Figure 4.3B).

G. Example of sericite-quartz-pyrite altered, quartz-phyric, coherent rhyolite of the HW Rhyolite. Photograph from BG18-3905 at 117.1 metres (Figure 4.3B).

H. Example of sericite-quartz-pyrite altered, rhyolitic, volcaniclastic sandstone of the HW Rhyolite. Photograph from BG18-3952 at 104.3 metres.

I. Example of bedded chert and argillite with coarse-grained chalcopyrite and pyrite. Photograph from BG18-3550 at 106.5 metres (Figure 4.4B).

J. Example of rare, and discontinuous, chlorite-sericite-pyrite alteration of andesitic, volcaniclastic sandstone of the Hanging Wall Andesite member. Photograph from BG18-3902 at 61.8 metres (Figure 4.3B).

K. Example of chlorite-calcite-epidote altered, coherent, andesite lava flow. Photograph from BG18-3905 at 76.4 metres (Figure 4.3B).

L. Example of pervasive chlorite-calcite alteration of andesitic, volcaniclastic breccia of the Hanging Wall Andesite member. Photograph from BG18-3298 at 45.2 metres (Figure 4.4B).

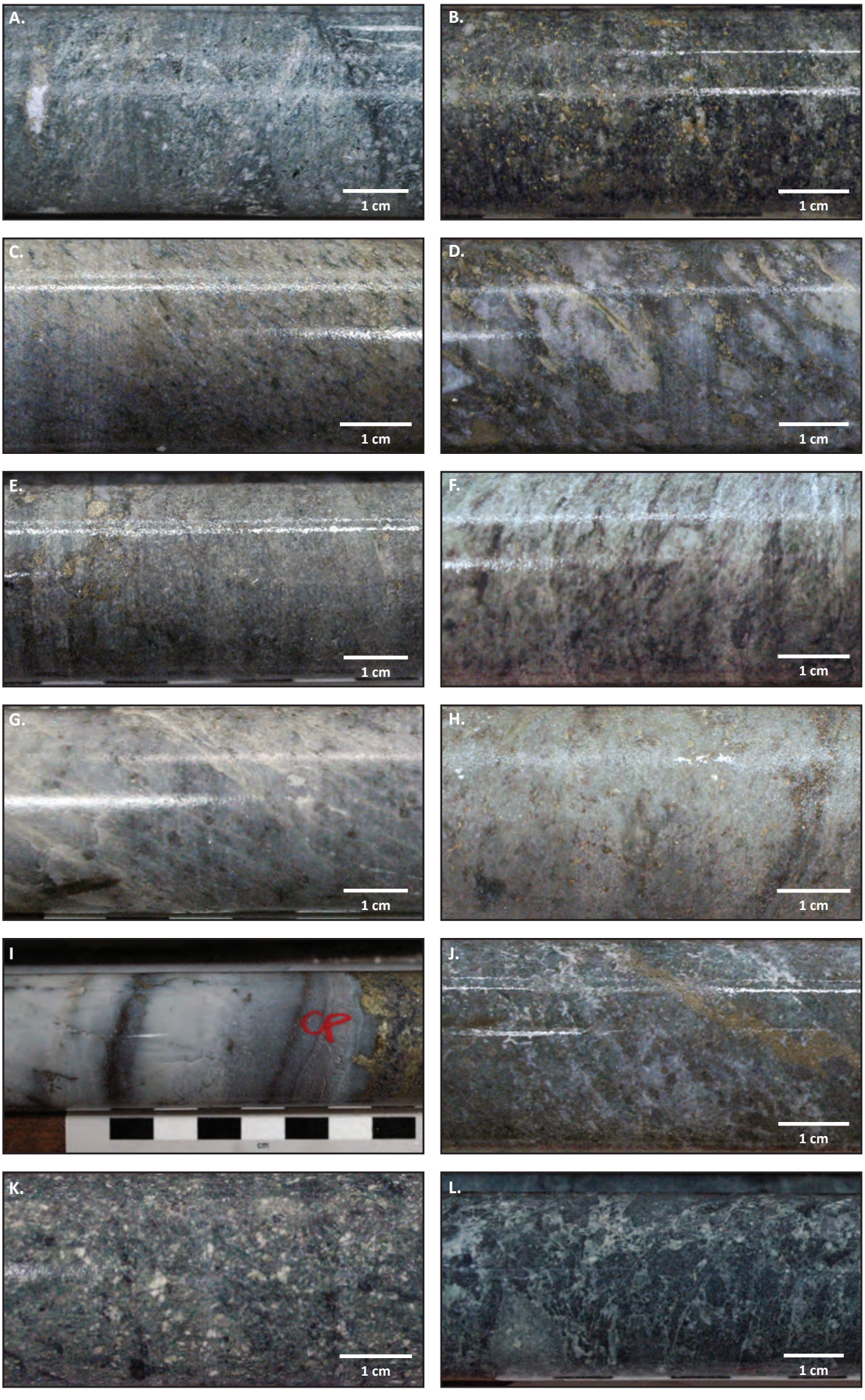
A.
1 cm
B.
1 cm
C.
1 cm
D.
1 cm
E.
1 cm
F.
1 cm
G.
1 cm
H.
1 cm
I
CP
J.
1 cm
K.
1 cm
L.
1 cm

Figure 4.34 Photomicrographs of alteration facies identified from drill core logging in the West Block Area and Ridge Zone North localities.

A. Example of moderate chlorite with interstitial albite alteration of fine-grained groundmass of feldspar-phyric [F], andesite of the Price Formation. Polished thin section sample BM14-042 from BG18-3905 at 188.0 metres.

B. Example of strong chlorite with interstitial albite and quartz, and lesser sericite, alteration of fine-grained groundmass in feldspar-phyric [F], andesite of the Price Formation. Tabular masses of chlorite after primary mafic phenocrysts(?). Note that the opaque minerals are pyrite. Polished thin section sample BM14-029 from BG18-3769 at 203.0 metres.

C. Example of strong chlorite-sericite alteration of Basal Volcaniclastic Unit associated with disseminated pyrite. Altered volcaniclastic matrix supports subangular lithics [L]. Polished thin section sample BM14-023 from BG18-3769 at 115.9 metres.

D. Example of strong sericite alteration of Basal Volcaniclastic Unit associated with disseminated pyrite and chalcopyrite. Altered volcaniclastic matrix supports subangular lithics [L]. Polished thin section sample BM14-023 from BG18-3769 at 115.9 metres.

E. Example of sericite-quartz alteration of fine-grained groundmass of quartz [Q] and feldspar-phyric [F], coherent rhyolite. Note that primary feldspar phenocrysts are weakly altered. Opaque minerals are pyrite. Polished thin section sample UPB08 from BG18-3952 at 76.0 metres.

F. Example of strong sericite-quartz alteration of fine-grained groundmass of quartz-phyric, coherent rhyolite. Opaque cubic minerals are pyrite. Polished thin section sample UPB05 from RN18-0224 at 7.0 metres.

G. Example sericite-quartz alteration in rhyolitic, volcaniclastic sandstone. Strong sericite alteration of volcaniclastic matrix associated with disseminated pyrite. Altered matrix supports quartz-rich felsic lithics [L]. Polished thin section sample BM14-070 from BG18-3534 at 45.5 metres.

H. Example of chlorite-calcite-epidote alteration in feldspar-phyric [F], andesitic lava flow. Patchy chlorite and calcite alteration of groundmass with disseminated fine-grained epidote. Polished thin section BM14-012 from BG18-3903 at 78.6 metres.

I. Example of chlorite-calcite alteration in andesitic volcaniclastic sandstone of the Hanging Wall Andesite member. Pervasive chlorite and calcite alteration of volcaniclastic matrix. Polished thin section BM14-001 from BG18-3902 at 21.2 metres.

[alb, albite; ca, calcite; chl, chlorite; cpy, chalcopyrite; ep, epidote; F, feldspar phenocryst; L, lithic; PPL, plane polarised light; py, pyrite; Q, quarts phenocryst/crystal; qtz; fine-grained quartz; RFL, reflected light; wm, white mica (sericite); XPL, cross polarised light]

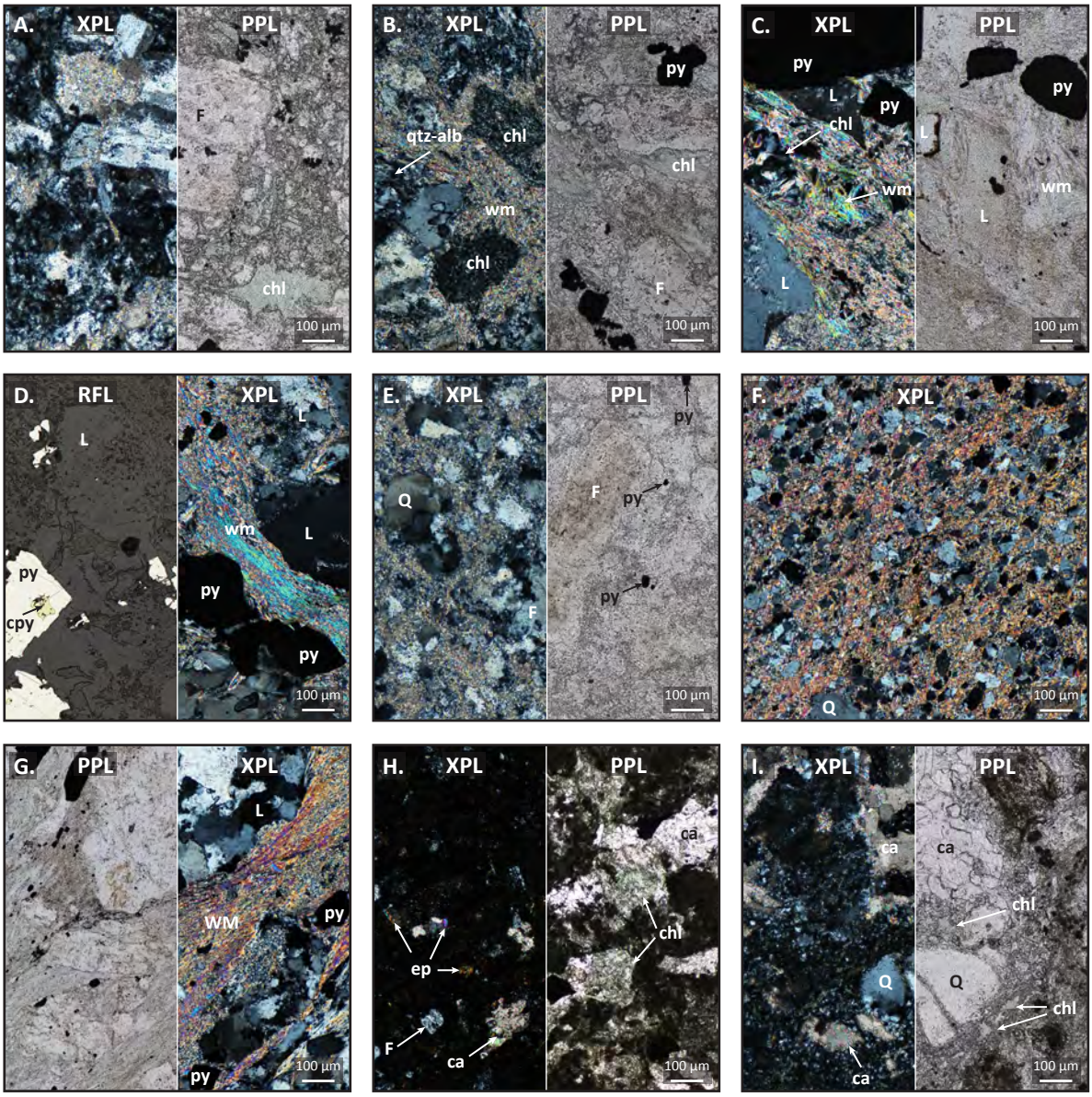
A.
XPL
PPL
F
chl
100 µm
B.
XPL
PPL
py
qtz-alb
chl
wm
chl
chl
F
100 µm
C.
XPL
PPL
py
L
py
chl
wm
L
py
L
wm
L
100 µm
D.
RFL
XPL
L
L
wm
L
py
cpy
py
py
100 µm
E.
XPL
PPL
py
Q
F
py
F
py
100 µm
F.
XPL
Q
100 µm
G.
PPL
XPL
L
WM
py
py
100 µm
H.
XPL
PPL
ca
chl
ep
F
ca
100 µm
I.
XPL
PPL
ca
ca
chl
Q
Q
chl
ca
100 µm

In the West Block Area, sericite-quartz alteration is pervasive throughout the felsic volcanic stratigraphy of the HW Rhyolite (Figures 4.3B-4.4B). This alteration is associated with "upper zone" position, semi-massive and stringer-style sulfide mineralisation (Figures 4.3B-4.4B).

4.6.4 Quartz (silicification) alteration

Zones of intense quartz alteration manifest as 1 to 10's of metre-thick beds of silicified mudstone (chert) intercalated with rhyolitic sandstones of the HW Rhyolite (Figure 4.33I). Chert is white to grey, and locally massive or interbedded with argillite (Figure 4.9). Chert is typically located on top of the Basal Volcaniclastic Unit (Figure 4.3B). Non-silicified argillite, locally, overlies the Basal Volcaniclastic Unit with zones of chert intercalated with rhyolitic volcaniclastic rocks up section (e.g., Figure 4.5B). In the West Block Area, the presence of chert is only sporadically coincident with "contact zone" position, massive sulfide mineralisation (Figure 4.4B).

4.6.5 Hanging Wall Andesite member alteration

Alteration of the Hanging Wall Andesite member in the West Block Area is characterised by: (1) sericite-calcite-pyrite; (2) chlorite-calcite-epidote; and (3) chlorite-calcite. Compared to the HW Rhyolite and the Price Formation stratigraphy, the Hanging Wall Andesite member is only weakly altered.

Locally, the matrix of volcaniclastic rocks is moderately altered to sericite-calcite-pyrite (Figure 4.33J). This alteration facies is light green to grey, with up to 10% disseminated fine-grained pyrite, and typically occurs as less than 10-centimetre-thick intervals. Due to the sporadic nature and limited intersections in drill core, the spatial distribution of this alteration assemblage is unknown.

Chlorite-calcite-epidote alteration affects coherent andesite overlying the HW Rhyolite (Figures 4.3B-4.4B). Feldspar and pyroxene phenocrysts are typically preserved in a fine-grained groundmass (Figure 4.33K). The groundmass is weakly altered to calcite, chlorite, and epidote. In thin section, the groundmass comprises patches of chlorite and calcite with disseminated, 10-20 μm, euhedral epidote (Figure 4.34H).

Chlorite-calcite alteration is characterised by light green rocks. Pyrite is rarely observed. With the exception of chlorite-calcite-epidote altered coherent andesite, this is the most common alteration facies observed in the Hanging Wall Andesite member (Figures 4.3B-4.5B). In thin section, chlorite and calcite are disseminated throughout the volcaniclastic matrix (Figure 4.34I).

4.6.6 Ridge Zone North orebody alteration

The Price Formation and H-W member strata in the Ridge Zone North orebody are affected by some of the same alteration facies documented in the West Block Area. However, unlike the West Block Area, hydrothermal alteration appears less restricted to lithology. Alteration types include: (1) chlorite-calcite-pyrite; (2) chlorite-sericite; and (3) sericite-quartz (Figure 4.35). The interpreted distribution of hydrothermal alteration in the Ridge Zone North orebody is shown on Figure 4.6B.

Both chlorite-calcite-pyrite and chlorite-sericite alteration facies are present in the Price Formation, below massive and semi-massive, sulfide mineralisation. Andesite located below the Basal Volcaniclastic Unit is altered to chlorite-sericite with 10-15% disseminated pyrite

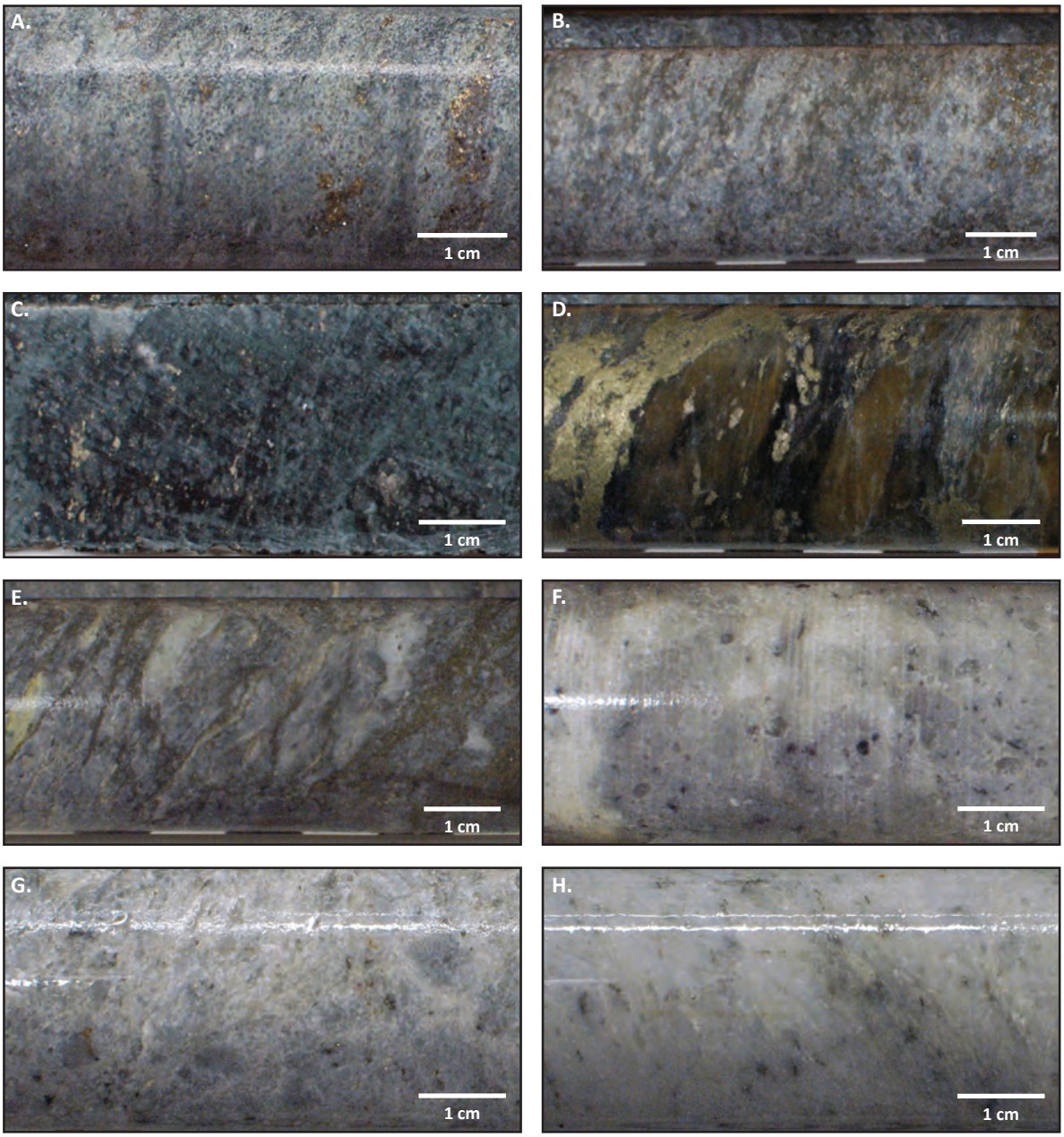

Figure 4.35 BQ drill core photograph examples of identified alteration facies in drill core from the Ridge Zone North orebody. A. Example of chlorite-sericite altered, coherent andesite of the Price Formation. Photograph from RN18-0223 at 85.5 metres (Figure 4.6B). B. Example of chlorite-sericite altered, coherent andesite of the Price Formation. Photograph from RN18-0224 at 78.3 metres (Figure 4.6B). C. Example of chlorite-pyrite-calcite altered, coherent andesite of the Price Formation. Photograph from RN18-0224 at 83.1 metres. D. Example of intense chlorite-sericite-pyrite altered, polylithic, volcaniclastic breccia of the Basal Volcaniclastic Unit. Photograph from RN18-0224 at 67.8 metres (Figure 4.6B). E. Example of quartz-sericite-pyrite altered, rhyolitic, volcaniclastic breccia of the HW Rhyolite. Photograph from RN18-0224 at 55.8 metres (Figure 4.6B). F. Example of quartz-sericite-pyrite altered, quartz and feldspar-phyric, coherent rhyolite of the HW Rhyolite. Photograph from RN18-0224 at 33.2 metres (Figure 4.6B). G. Example of quartz-sericite-pyrite altered, rhyolite autobreccia of the HW Rhyolite. Photograph from RN18-0223 at 7.4 metres (Figure 4.6B). H. Example of quartz-sericite-pyrite altered, quartz-phyric, coherent rhyolite of the HW Rhyolite. Photograph from RN18-0223 at 2.1 metres (Figure 4.6B).

(Figure 4.6B). This alteration results in a grey-green rock (Figure 4.25A-B). With increasing depth, alteration grades into chlorite-calcite-pyrite, which manifests as a medium to dark green rock (Figure 4.35C).

Chlorite-sericite alteration is pervasive in the Basal Volcaniclastic Unit (Figure 4.6B; 4.35D). Similar to the West Block Area, chlorite-sericite alteration is discordant to lithological contacts, and is coincident with "contact zone" position, semi-massive and massive sulfide mineralisation (Figure 4.6B). Sericite-quartz alteration is dominant in the felsic volcaniclastic and coherent rhyolite stratigraphy above "contact zone" position mineralisation (Figure 4.35E-H). "Upper zone" position, semi-massive and massive zinc-rich, sulfide mineralisation is hosted in sericite-quartz altered, felsic volcaniclastic rocks below coherent rhyolite (Figure 4.6B).

4.7 Summary

Stratigraphy of the West Block Area comprises coherent, volcaniclastic and marine sedimentary rocks of the Price and lower Myra Formations. Polymetallic, sulfide mineralisation is hosted in the felsic stratigraphy of the lower Myra Formation. In the West Block Area, the Price Formation comprises a submarine, extrusive sequence of coherent, andesitic lavas and related breccias, at least 80 metres in thickness.

The 150-175 metres-thick H-W member of the lower Myra Formation consists of syn- and post-eruptive volcanic and marine-sedimentary rocks. Polylithic siltstone, sandstone, and conglomerate of the Basal Volcaniclastic Unit marks the base of the lower Myra Formation. The Basal Volcaniclastic Unit is overlain by intercalated argillite and chert of the Caprocks unit. The HW Rhyolite comprises felsic volcaniclastic rocks, which are overlain by coherent, quartz and feldspar-phyric rhyolite (10-40 m-thick). A 10 to 50 metres-thick, plagioclase and pyroxene-phyric coherent andesite flow, is the youngest unit of the H-W member and overlies the HW Rhyolite stratigraphy. The Hanging Wall Andesite member overlies the H-W member and consists of polylithic volcaniclastic sandstone and conglomerate.

The stratigraphy in the West Block Area is dissected by moderate dipping planar structures with minor gouge and shallow-to-moderate dipping, gouge-rich, wavy structures. Identified structures can have thrust or normal apparent-senses of movement, with displacements up to 50 metres. These structures likely correspond to the D_4 and D_5 brittle structures identified by Jones et al. (2006a). The inferred open upright fold patterns, identified in cross-section interpretations of the West Block Area and Ridge Zone North orebody, are consistent with observations of Jones et al. (2006a) for the Battle orebody. These parasitic fold structures developed subparallel to the northwest-trending Myra Anticline, which was the result of northeast-southwest compression (D_1) during the Middle Permian to pre-Middle Triassic (Muller, 1980; Massey, 1992b; Jones et al., 2006a).

Styles of sulfide mineralisation in the West Block Area include disseminated, stringer, semi-massive, and massive sulfides. Disseminated sulfide is pyrite-rich, and is associated with altered, andesite of the Price Formation and all rock types of the H-W member. Sphalerite-rich and pyrite-dominant stringer-style mineralisation is associated with altered H-W member rock types; in particular, coherent and volcaniclastic rhyolite. Less common in the West Block Area are semi-massive and massive, zinc-rich, polymetallic sulfide mineralisation styles. These styles of sulfide mineralisation are associated with sericite-quartz-pyrite altered coherent

rhyolite and autobreccias, and chlorite-sericite altered, polylithic conglomerate of the Basal Volcaniclastic Unit. Sulfide mineralisation styles in the Ridge Zone North orebody are similar to those identified in the West Block Area, however zinc-rich, polymetallic sulfide mineralisation is significantly more developed.

Sulfide mineralisation is located at two stratigraphic positions in the West Block Area and the Ridge Zone North orebody. The nomenclature of Sinclair (2000) is used to describe the two positions. "Upper zone" position refers to stringer-style, semi-massive and massive sulfide mineralisation 30 to 75 metres above the Price Formation contact. Whereas "contact zone" position refers to semi-massive and massive sulfide mineralisation at or near the Price Formation contact.

Petrographic and micro-analytical analysis of mineralised samples indicates a number of sulfide, sulfosalt and precious metal-bearing minerals. Fe-poor sphalerite, pyrite, chalcopyrite and galena are the dominant sulfide minerals with accessory tennantite, tetrahedrite and pearceite-polybasite sulfosalts. Precious metal mineral phases include electrum and hessite. Based on the petrographic textures of these minerals, four paragenetic stages of mineralisation are proposed for the study area:

- Stage-1: early, inclusion-rich pyrite;
- Stage-2: inclusion-free pyrite rimming Stage-1 pyrite and the precipitation of sphalerite with less abundant galena-chalcopyrite-barite ± tennantite and tetrahedrite;
- Stage-3: modification of Stage-2 mineral phases resulting in the coarsening of sulfide grains, homogenisation of sphalerite(?), and local remobilisation of sulfide and sulfosalt phases.
- Stage-4: metamorphic remobilisation recorded by planar, pearceite-polybasite veinlets crosscutting previous mineralisation stages;
- The timing of electrum and hessite precipitation is unclear, and could have occurred during Stages-3 and -4.

Hydrothermal alteration facies in the West Block Area and the Ridge Zone North orebody were identified based on mineral assemblages. The spatial distribution and association to sulfide mineralisation of alteration facies in the Price Formation and H-W member stratigraphy were assessed with detailed cross-section interpretations. Alteration facies include:

- Chlorite-calcite-pyrite alteration of Price Formation andesite is semi-conformable, pervasive, and decreases in intensity with depth from the lower Myra Formation contact.
- Chlorite-sericite alteration affects the Price Formation and H-W member, is discordant to lithological contacts, and is associated with "contact zone" position sulfide mineralisation.
- Sericite-quartz-pyrite alteration is pervasive throughout the coherent rhyolite and felsic volcaniclastic stratigraphy, and is associated "upper zone" position sulfide mineralisation.
- Quartz (silicification) alteration results in 1 to 10's of metre-thick beds of chert intercalated with rhyolitic siltstone of the HW Rhyolite and in the West Block Area is locally coincident with "contact zone" position sulfide mineralisation.

Chapter 5:

Mineral & Whole-Rock Chemistry of VHMS Host Rocks

Determining the intensity, zonation and extent of hydrothermal alteration associated with volcanic-hosted massive sulfide (VHMS) deposits can provide important implications for exploration (Franklin et al., 1981; Large, 1992). At a local scale, favourable alteration factors may include texturally destructive alteration of volcanic rocks, broad sodium-depletion halos, and elevated whole-rock geochemical alteration indices (e.g., Galley, 1995; Large et al., 2001c; Franklin et al., 2005; Galley et al., 2007). The reaction of hot, mildly acidic to neutral, hydrothermal fluids with volcanic rocks results in the breakdown of primary feldspar and volcanic glass (e.g., Gifkins et al., 2005). This alteration process leads to the formation of secondary minerals. In the case of ancient VHMS deposits, hosted in greenschist facies or lower metamorphic rocks, this process typically manifests as white mica- and chlorite-dominant alteration zones (e.g., Large, 1977; Franklin et al., 1981).

Previous mineralogical and whole-rock geochemical studies of altered host rocks at Myra Falls have focused on the footwall and hanging wall stratigraphy within ~100 metres of massive sulfide ore lenses (e.g., Robinson et al., 1996; Sinclair, 2000; Jones et al., 2005). These studies have characterised the proximal (within 100 metres) alteration halos of the HW and Battle orebodies. The aim of this study is to characterise the distal hydrothermal environment, within 500 metres, to massive sulfide mineralisation. New data from the West Block Area is presented and compiled with previous data from the Battle orebody to identify hydrothermal up-flow zones in the Price Formation as a vector to overlying sulfide deposits. A combination of electron microprobe (EMP), whole-rock lithogeochemistry, and shortwave infrared (SWIR) analytical methods were used to assess the mineralogy and chemistry of altered Price Formation andesite. In addition to samples collected by the candidate, representative samples of Price Formation andesite were selected from previous studies on the Battle and Ridge Zone West orebodies available from the CODES rock catalogue.

5.1 Review of Previous Alteration Studies at Myra Falls

A number of alteration studies have been completed at Myra Falls, specifically focusing on the H-W member VHMS deposits. Jones (2001) used a combination of SWIR and white mica

EMP analyses to map out distinct alteration patterns in H-W member stratigraphy above the Battle orebody. Whereas Robinson (1994) and Sinclair (2000) used whole-rock geochemistry to assess lithogeochemical trends in altered Price Formation andesite and volcanic and marine-sedimentary rocks of the lower Myra Formation. In addition, Sinclair (2000) combined SWIR and EMP analyses to assess changes in chlorite chemistry in variably altered andesite of the Price Formation. For the Ridge Zone West orebody, Chong (2004) completed EMP analyses of white mica to assess potential mineralogical changes in altered argillite and polylithic conglomerate units proximal to semi-massive sulfide mineralisation. The following is a compilation and review of these datasets for the Battle and Ridge Zone West orebodies.

5.1.1 Mineral chemistry

Jones (2001) and Chong (2004) investigated white mica chemistry with EMP analysis from a combined twelve rock samples. Samples included chert, argillite and polylithic conglomerate of the lower Myra Formation. Nine samples are from the Battle orebody, two are from the Ridge Zone West orebody, and one sample is from the Thelwood Valley. These studies documented that; in general, altered marine-sedimentary rocks of the H-W member within 100 metres of massive sulfide mineralisation, contain muscovite with Fe+Mg <0.2 apfu and Al^{vi} >3.7 apfu. While distal H-W member stratigraphy, located >100 metres from massive sulfide mineralisation, have phengitic K-mica, with Fe+Mg >0.4 apfu and Al^{vi} <3.5 apfu (Jones, 2001; Chong, 2004).

Sinclair (2000) investigated chlorite chemistry with EMP analysis from three samples of andesite of the Price Formation. One sample is from the Thelwood Valley, and two samples are located below massive sulfide mineralisation in the Battle orebody. Chlorite-calcite-epidote altered andesite from the Thelwood Valley has intermediate chlorite compositions, with Fe/Fe+Mg ratios of 0.45 (Sinclair, 2000). Whereas chlorite associated with texture destructive, sericite-quartz-pyrite altered andesite, within 50 metres of massive sulfide mineralisation, is Mg-rich with Fe/Fe+Mg ratios between 0.07 and 0.18 (Sinclair, 2000).

5.1.2 Whole-rock geochemical trends

Studies by Robinson (1994), Sinclair (2000) and Jones (2001) used whole-rock geochemistry to assess the Battle orebody VHMS hydrothermal system. Jones (2001) focused on chert and argillite from the H-W member; while Robinson (1994) and Sinclair (2000) examined samples of the H-W member and the Price Formation. This chapter focuses on assessing the nature of hydrothermal alteration in the West Block Area affecting the Price Formation. As such, a compilation of whole-rock geochemical data from the previously analysed Price Formation samples of Robinson (1994) and Sinclair (2000) is reviewed. These samples include, least-altered andesite from the Thelwood Valley and hydrothermally altered andesite from below the Battle orebody (Figure 5.1).

Price Formation andesite (n=52) has intermediate to mafic Ti/Zr ratios (average of 62.0). Least-altered andesite from the Thelwood Valley has Na_2O concentrations greater than 3.0 wt. %, no sulfur (Figure 5.1A), and Rb/Sr <0.1. Intensely altered andesite, from ≤50 metres below the Battle orebody, is depleted in Na_2O and variably enriched in sulfur (Figure 5.1A) with Rb/Sr >1.0. Sinclair (2000) attributed these whole-rock chemical trends to the alteration of primary plagioclase phenocrysts (depletion of sodium) by white mica and the addition of pyrite (enrichment in sulfur). Similarly, on the K-Ca-Na molar element ratio diagram after Warren

et al. (2007), least-altered andesite samples plot near the albite-plagioclase node, whereas the majority of altered andesite samples plot near the K-mica node (Figure 5.1B). The predominant alteration minerals observed in andesite of the Price Formation are white mica, chlorite and pyrite (e.g., Juras, 1987; Robinson, 1994; Sinclair, 2000). The alteration box plot after Large et al. (2001) utilises alteration indices calculated from whole-rock geochemical data appropriate for this alteration mineral assemblage. Samples from the Thelwood Valley plot in the least-altered andesite field whereas altered andesite from near the Battle orebody form an array between white mica- and chlorite-pyrite-dominant alteration end members (Figure 5.1C).

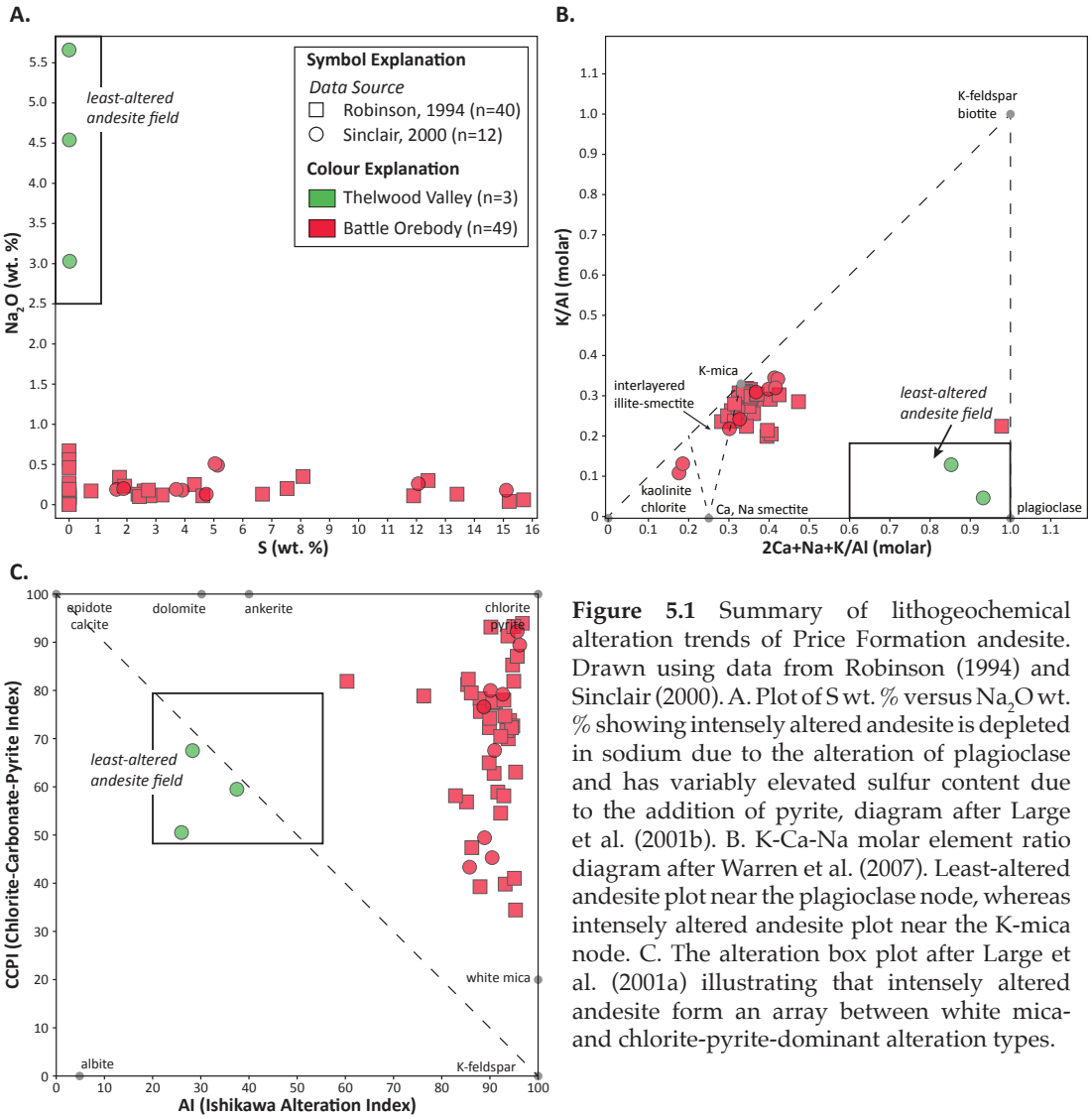

Figure 5.1 Summary of lithogeochemical alteration trends of Price Formation andesite. Drawn using data from Robinson (1994) and Sinclair (2000). A. Plot of S wt. % versus Na_2O wt. % showing intensely altered andesite is depleted in sodium due to the alteration of plagioclase and has variably elevated sulfur content due to the addition of pyrite, diagram after Large et al. (2001b). B. K-Ca-Na molar element ratio diagram after Warren et al. (2007). Least-altered andesite plot near the plagioclase node, whereas intensely altered andesite plot near the K-mica node. C. The alteration box plot after Large et al. (2001a) illustrating that intensely altered andesite form an array between white mica- and chlorite-pyrite-dominant alteration types.

5.1.3 SWIR spectral characterisation

The first SWIR spectroscopy studies at Myra Falls were completed by Sinclair (2000) and Jones (2001) and utilised a PIMA-II spectrometer. Jones et al. (2005) demonstrated how SWIR analysis could be used to identify trends in mineral compositions that could then be applied to assessing mine-scale vectors to sulfide mineralisation. Utilising spectral parameter maps, zones of intense hydrothermal alteration in felsic stratigraphy above the Battle and HW orebodies were identified, and characterised by AlOH and FeOH absorption wavelengths <2,197 nm and <2,240 nm, respectively (Jones et al., 2005).

5.2 Alteration Facies of the Price Formation Footwall

Alteration below the H-W member VHMS deposits is mineralogically and texturally diverse. The following section is a compilation of previous alteration studies at Myra Falls (Sinclair, 2000; Chong, 2004) with the detailed description of the West Block Area (*see Chapter 4*) to define several alteration facies in the Price Formation (Table 5.1).

Table 5.1 Mineralogy of alteration facies of the Price Formation andesite

	Weak alteration	**Moderate alteration**		**Intense alteration**		
	Chl-Ca ± Ep	Chl-Ca-Py	Chl-Ser	Ser-Qtz-Py	Chl-rich	Chl-Ser-Py
	TV	WBA, RZW	WBA, RZW	Battle, RZN	Battle	RZN, Battle
†Quartz	●	●	●	●●●	●●●	●●
†Plagioclase	●●●	●●				
†Amygdales	● to ●●	●				
†Sericite	●		●●●	●●●●	● to ●●	●●●
†Chlorite	●●	●●	●●●	● to ●●	●●●●	●●●
†Calcite	●●	●●	●	●	●	●
†Epidote	● to ●●					
†Pyrite		●●	● to ●●	●●●	●●●	●●●
◊Apatite	●●	● to ●●	● to ●●	●●●	●●●	●●●
◊Rutile	●●	●●	●●	●●●	●●●	●●●

† = mineral identified in hand sample and thin section; ◊ = mineral identified in thin section.
Symbols: ● = rare; ●● = common; ●●● = abundant; ●●●● = dominant
[Ca, calcite; Chl, chlorite; Ep, epidote; Qtz, quartz; RZN, Ridge Zone North; RZW; Ridge Zone West; Ser, sericite; TV, Thelwood Valley;]

Weak alteration consists of a pervasive, chlorite-calcite ± epidote alteration facies. In general, this alteration facies is not texturally destructive (Figure 5.2A-B). Chlorite and calcite are prominent in hand samples of Price Formation andesite from the Thelwood Valley, while epidote is commonly present in thin section (Sinclair, 2000). This alteration facies is considered least-altered and represents the background mineralogy and lithogeochemical signature of the Price Formation andesite (Sinclair, 2000).

Moderate alteration consists of pervasive, texturally non-destructive, chlorite-calcite-pyrite and chlorite-sericite alteration facies (Table 5.1). Chong (2004) documented semi-conformable, chlorite-calcite-pyrite and chlorite-sericite alteration facies in Price Formation andesite 75-100 metres below "upper zone" semi-massive sulfide mineralisation in the Ridge Zone West orebody. Both alteration facies occur below sporadic sulfide mineralisation in the West Block Area (*see Chapter 4*). Representative cross-sections through the West Block Area (Figure 5.3) illustrate the distribution of these alteration facies. Chlorite-calcite-pyrite footwall alteration consists predominately of fine-grained chlorite and calcite throughout the groundmass, with 5-20% pyrite, in hand sample (Figure 5.2C-D). Chlorite-sericite alteration facies occurs in coherent and clastic rocks of the Price and lower Myra Formations (*see Chapter 4*). Fine-grained, chlorite and sericite with 5-10% disseminated pyrite is characteristic of altered Price Formation andesite (Figure 5.2E-F). Preserved, primary volcanic textures include amygdales and plagioclase phenocrysts (*see Chapter 4*, Figure 4.7).

Intense alteration is texture destructive and confined to the footwall, immediately below semi-massive to massive sulfide mineralisation near the Battle and Ridge Zone North orebodies (Figure 5.3C-D). The footwall alteration consists predominately of feldspar-destructive, sericite-

quartz-pyrite, chlorite-rich and chlorite-sericite-pyrite alteration facies (Figure 5.2G-L; Table 5.1). In the Battle orebody, sericite-quartz-pyrite alteration forms a semi-conformable blanket at the top of the Price Formation, whereas chlorite-pyrite alteration has a domainal distribution (Sinclair, 2000; Figure 5.3D). Chlorite-sericite-pyrite alteration is pervasive (*see Chapter 4*) and occurs immediately below massive and semi-massive sulfide mineralisation in the Ridge Zone North orebody (Figure 5.3C). In hand sample, primary volcanic textures such as amygdales are not preserved (Figure 5.2G-L).

5.3 Price Formation Andesite Samples

Nineteen samples were collected to determine the alteration mineral chemistry and lithogeochemical signatures of altered andesite of the Price Formation (Table 5.2). The West Block Area, including the Ridge Zone North orebody, was the primary focus of this study (n=14). Samples from the Thelwood Valley (n=1), Battle orebody (n=2) and Ridge Zone West (n=2) were selected from the rock catalogues of Sinclair (2000) and Chong (2004) for comparison. Sample photographs are provided in Appendix E.

5.3.1 Thelwood Valley sample

Sample 143640 is an example of pervasive, chlorite-calcite-epidote altered Price Formation andesite from the Thelwood Valley. The sample was collected by Sinclair (2000) and is from a regional exploration drill hole, approximately 5 km to the east of the West Block Area and at least 2 km away from the HW orebody (Table 5.2). New EMP and SWIR analyses were collected, while whole-rock geochemical data were available from Sinclair (2000). This sample is considered least-altered and represents the background mineralogy and lithogeochemistry of the Price Formation andesite.

5.3.2 Battle orebody samples

Samples 143682 and 143700 are examples of strong and pervasive sericite-quartz-pyrite altered Price Formation andesite from below the Battle orebody. These samples were collected by Sinclair (2000) and are from resource delineation drill holes (Table 5.2). New EMP and SWIR analyses were collected, while whole-rock geochemical results were compiled from Sinclair (2000). These samples are intensely altered and located proximal (10-25 metres) to massive, polymetallic sulfide mineralisation.

5.3.3 West Block Area and Ridge Zone North orebody samples

Thirteen samples of Price Formation andesite were collected from the West Block Area, and one sample was selected from the Ridge Zone North orebody. The majority of samples consist of pervasive, chlorite-pyrite-calcite altered groundmass of coherent andesite (Table 5.2). Samples TS-1180 and TS-345 are of pervasive, chlorite-sericite-pyrite altered andesite. Sample TS-1180 is located below semi-massive, polymetallic sulfide mineralisation of the Ridge Zone North orebody, whereas TS-345 is located below the Myra Formation contact in the West Block Area.

5.3.4 Ridge Zone West orebody samples

Samples MF18853 and MF19908 are examples of moderate and pervasive chlorite-pyrite-calcite altered Price Formation andesite from below the Ridge Zone West orebody, and were collected by Chong (2004). New EMP analyses were collected. Semi-massive, polymetallic sulfide mineralisation is located 100 to 130 metres above these samples.

Figure 5.2 Textures and mineralogy of least-altered andesite of the Price Formation and the prominent alteration facies in the footwall of the West Block Area, Ridge Zone North orebody and Battle orebody.

A-B. Example of weak, chlorite-calcite-epidote alteration facies from the Thelwood Valley. A. Pervasive chlorite and patchy calcite and epidote alteration to andesite groundmass. B. BSE image showing primary albite phenocryst (white dashed-line) with chlorite-white mica-epidote alteration, and disseminated chlorite and epidote throughout the groundmass. Sample 143640 is from drill hole PR-0123 at 206.3 metres and was collected by Sinclair (2000). BSE image collected by the candidate.

C-D. Example of moderate, chlorite-calcite-pyrite alteration facies in the West Block Area. C. Pervasive chlorite with disseminated calcite and pyrite alteration to andesite groundmass. Photograph from drill hole BG18-3769 at 130.0 metres, cross-section 828 mE (*see Chapter 4*, Figure 4.5). D. BSE image showing abundant calcite associated with altered, primary albite phenocrysts and intergrown chlorite-white mica with accessory apatite and rutile. Sample TS-722 is from drill hole BG18-3554 at 202.7 metres, cross-section 640 mE (Figure 5.3B).

E-F. Example of moderate, chlorite-sericite-pyrite alteration facies in the West Block Area. E. Pervasive chlorite-sericite with disseminated, fine-grained pyrite alteration to andesite groundmass resulting in pseudoclastic texture. Note the lack of feldspar phenocrysts in hand sample. F. BSE image showing fine-grained chlorite altered groundmass with pyrite and accessory apatite and quartz. Sample TS-345 is from drill hole BG18-3904 at 149.4 metres, cross-section 550 mE (Figure 5.3A).

G-H. Example of intense, chlorite-sericite-pyrite alteration facies from below the Ridge Zone North orebody. G. Pervasive chlorite-sericite with abundant disseminated, medium-grained pyrite alteration to andesite groundmass. Note no obvious feldspar phenocrysts. H. BSE image showing fine- to medium-grained white-mica intergrown with quartz-pyrite and accessory apatite and rutile. Sample TS-1180 is from drill hole RN18-0224 at 78.3 metres, cross-section 918 mE (Figure 5.3C).

I-J. Example of intense, sericite-quartz-pyrite alteration facies from below the Battle orebody. I. Pervasive sericite-pyrite-quartz with minor chlorite alteration to andesite groundmass. Note no feldspar phenocrysts in hand sample. J. BSE image showing medium-grained white mica and quartz altered groundmass with minor intergrown chlorite and accessory apatite and rutile. Sample 143682 is from drill hole BG18-0981 at 122.3 metres, cross-section 1420 mE (Figure 5.3D). Sample was collected by Sinclair (2000). BSE image collected by the candidate.

K-L. Example of intense, chlorite-rich alteration facies. Pervasive chlorite alteration to andesite groundmass with disseminated pyrite and patchy quartz, and no preserved primary feldspar. Sample 143689 (K) is from drill hole BG18-1003 at 105.2 metres and sample 143701 (L) is from BG18-1006 at 124.9 metres, cross-section 1420 mE (Figure 5.3D). Chlorite is magnesium-rich and samples were collected by Sinclair (2000).

[alb, albite; ap, apatite; ca, calcite; chl, chlorite; ep, epidote; F, feldspar crystal; py, pyrite; qtz, quartz; rt, rutile; wm, white mica]

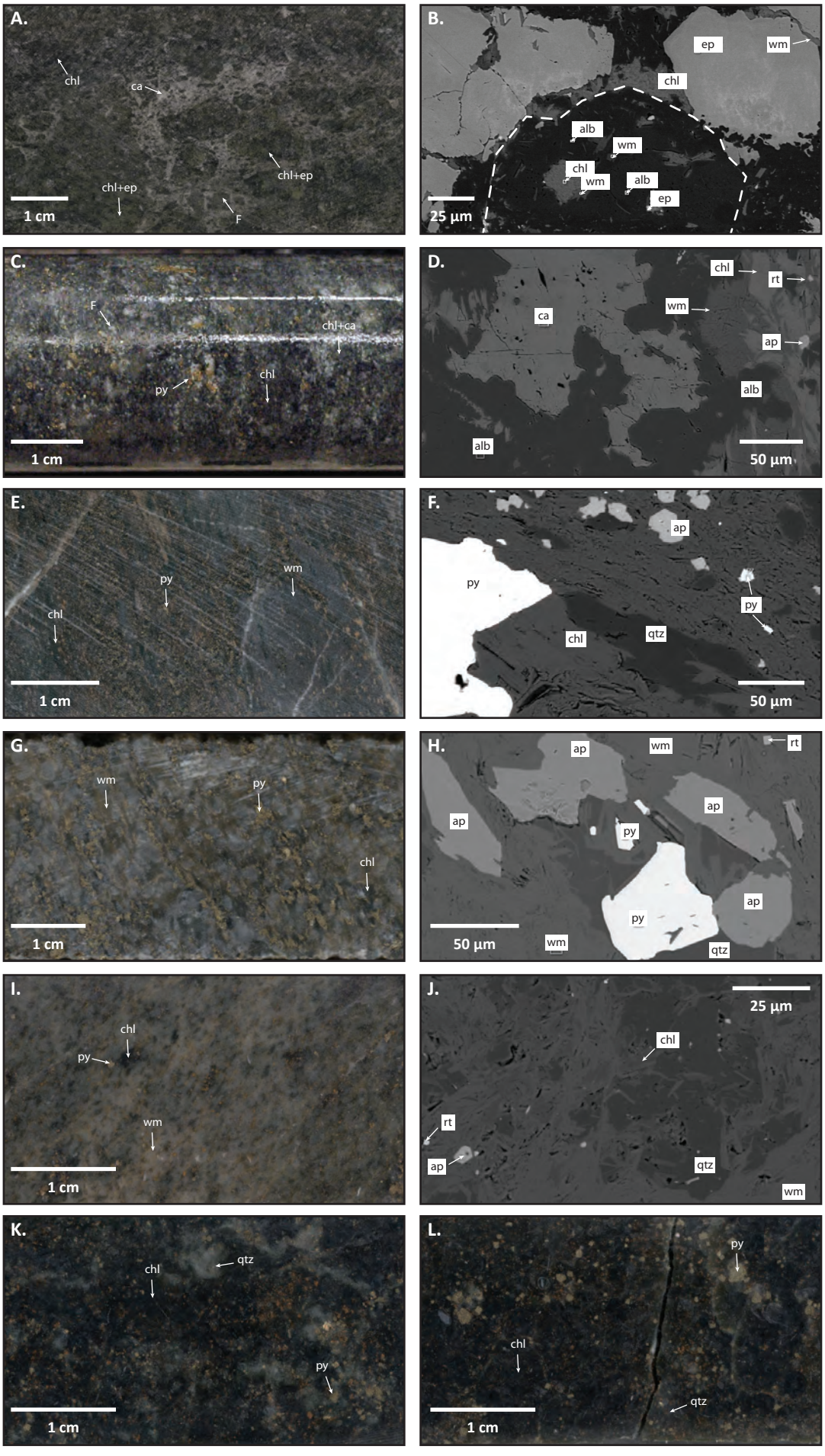
A.
chl
ca
chl+ep
chl+ep
F
1 cm
B.
ep
wm
chl
alb
wm
chl
wm
alb
ep
25 µm
C.
F
chl+ca
py
chl
1 cm
D.
chl
rt
ca
wm
ap
alb
alb
50 µm
E.
py
wm
chl
1 cm
F.
ap
py
py
chl
qtz
50 µm
G.
wm
py
chl
1 cm
H.
ap
wm
rt
ap
ap
py
ap
py
50 µm
wm
qtz
I.
chl
py
wm
1 cm
J.
25 µm
chl
rt
ap
qtz
wm
K.
chl
qtz
py
1 cm
L.
py
chl
qtz
1 cm

Figure 5.3 Distribution of Price Formation footwall alteration facies in cross-sections through the West Block Area, Ridge Zone North orebody and Battle orebody. Cross-sections show detailed geology (patterns), alteration (colours) and sulfide mineralisation textures (symbols) interpreted from detailed graphic logging (red drill hole stems) and historic drill logs (grey drill hole stems). The top of the Price Formation is highlighted by a thick, blue-line, and the cross-sections only display alteration facies identified in the footwall. New data from underground drill hole samples are presented in the results section, and red stars indicate sample locations. Refer to the plan map in the legend for the locations of cross-sections.

A. Cross-section interpretation 550 mE of the West Block Area, looking west.

B. Cross-section interpretation 640 mE of the West Block Area, looking west.

C. Cross-section interpretation 918 mE of the Ridge Zone North orebody, looking west.

D. Cross-section interpretation 1420 mE of the Battle orebody, looking west. Geology, alteration and mineralisation interpretations adapted from Sinclair (2000) and Jones (2001).

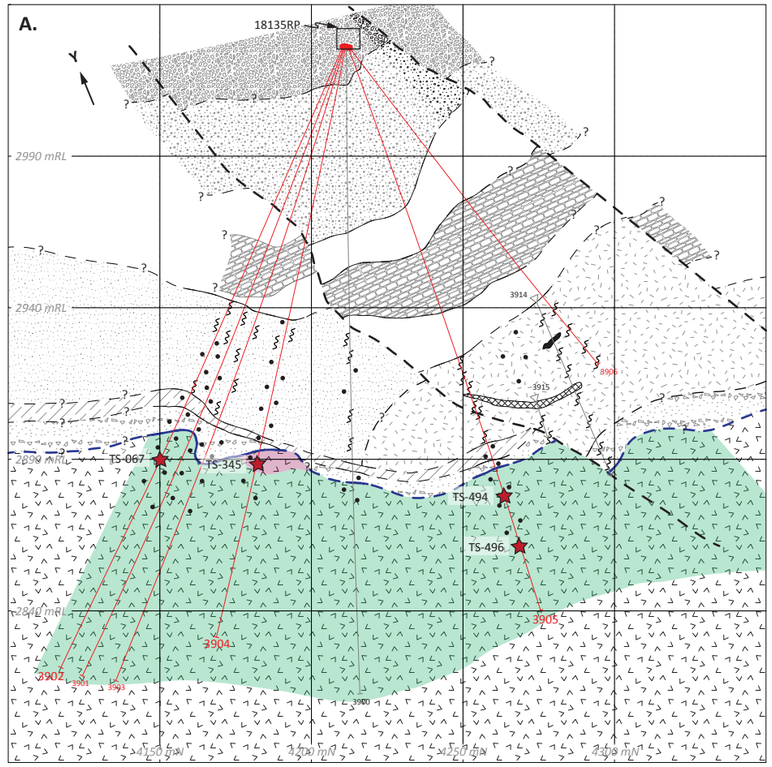

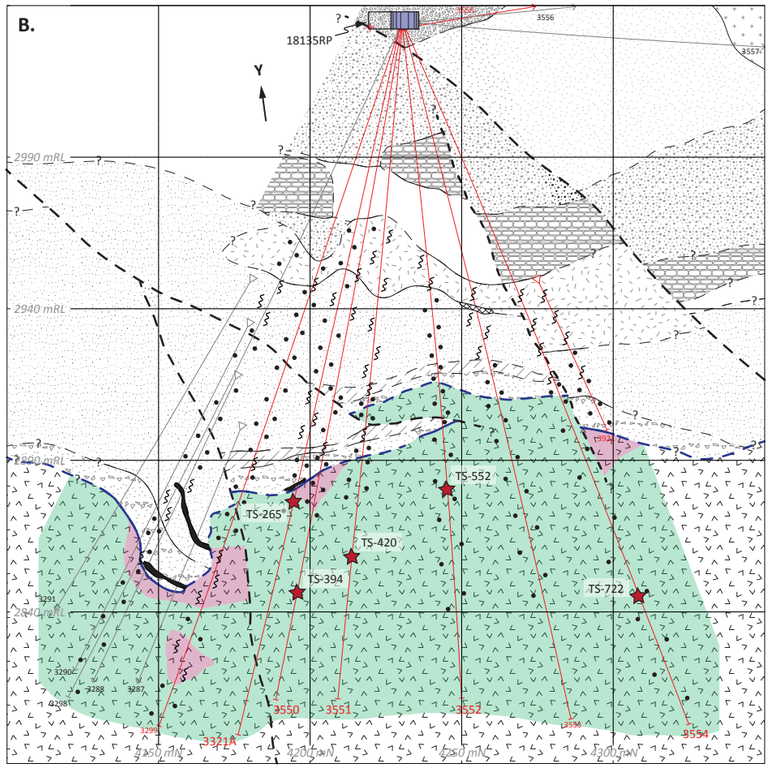

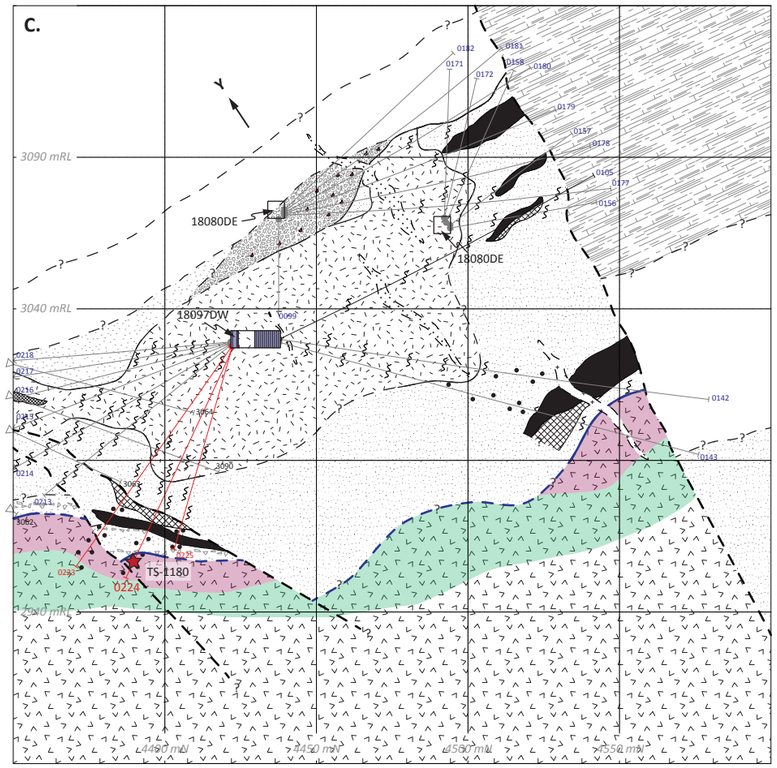

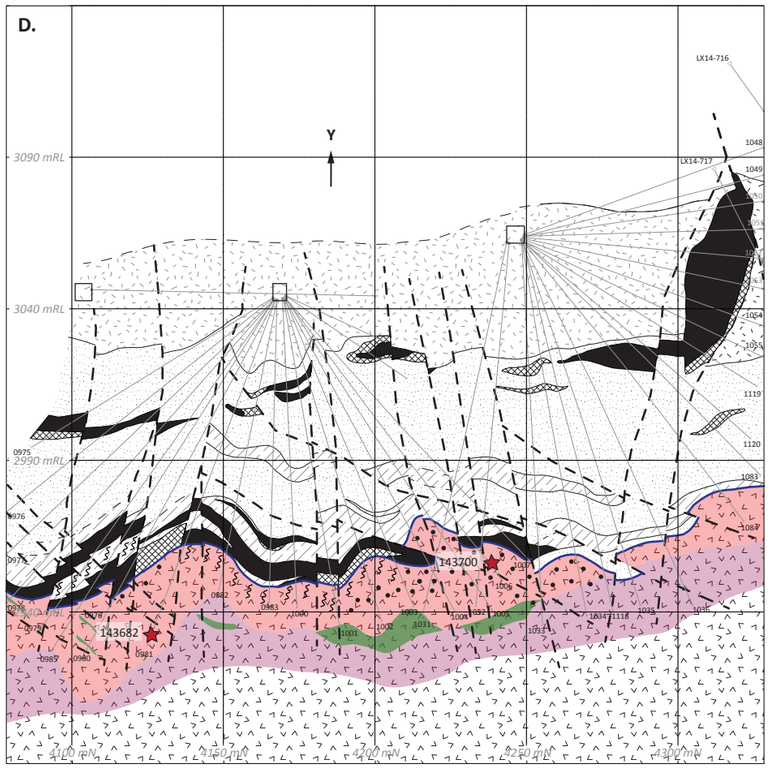

Figure 5.3:
Price Formation Footwall Alteration Facies
Cross-Section Interpretations

Lithology

- mafic dyke
- *Hanging Wall Andesite Member*
  - andesitic siltstone-sandstone
  - massive andesitic sandstone
  - polylithic volcaniclastic conglomerate
  - polylithic volcaniclastic sandstone
  - polylithic volcaniclastic conglomerate w/ sulfide clasts
  - massive siltstone
- *H-W Member*
  - coherent andesite
  - coherent rhyolite
  - rhyolitic volcaniclastic siltstone, sandstone and autobreccia
  - bedded, massive chert and argillite
  - laminated to thinly bedded argillite
  - polylithic volcaniclastic sandstone and conglomerate
- *Price Formation*
  - andesite
- *interpreted top of Price Formation contact*

Mineralisation Textures

- disseminated sulfide
- stringer-style sulfide
- semi-massive (50-75% sulfide)
- massive (>75% sulfide)

Footwall Alteration Facies

- chlorite-sericite ± pyrite
- chlorite-calcite-pyrite
- sericite-quartz-pyrite
- chlorite-rich

Cross-Section Location Map

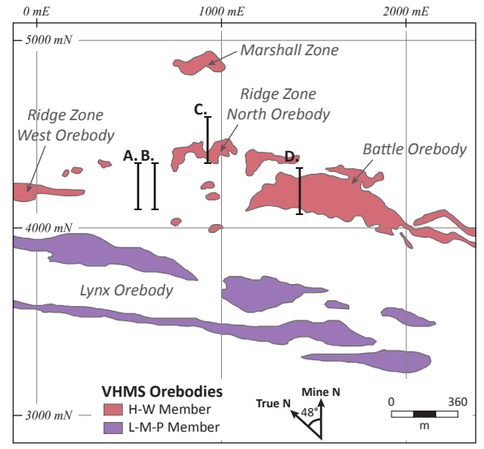

Annotations

- EMP & lithogeochemistry sample location (*this study*)
- younging direction
- interpreted contact
- interpreted fault
- *Underground Drill Holes*
  - SWIR analysed drill holes (*this study*)
- *Underground Workings*
  - 18135RP
- *Section Layout and Orientation*
  - 0 30 metres
  - True N, Mine N, 48°, W, E, S

Table 5.2 Price Formation andesite sample set summary.

Sample ID	Area	Section (mE)	Alteration Facies	Analyses	Normative Mineralogy
143640	TV	5880	chl-ca-ep	SWIR; EMP; WR*	yes
143682	B	1420	ser-qtz-py	SWIR; EMP; WR*	yes
143700	B	1420	ser-qtz-py	SWIR; EMP; WR*	no
TS-1180	RZN	918	chl-ser-py	SWIR; EMP; WR	yes
BM14-029	WBA	828	chl-ca-py	SWIR; WR	no
TS-971	WBA	700	chl-ca-py	SWIR; WR	no
TS-265	WBA	640	chl-ca-py	SWIR; EMP; WR	yes
TS-394	WBA	640	chl-ca-py	SWIR; EMP; WR	yes
TS-420	WBA	640	chl-ca-py	SWIR; EMP; WR	yes
TS-552	WBA	640	chl-ca-py	SWIR; EMP; WR	yes
TS-722	WBA	640	chl-ca-py	SWIR; EMP; WR	yes
TS-683	WBA	585	chl-ca-py	SWIR; EMP; WR	yes
TS-788	WBA	585	chl-ca-py	SWIR; EMP; WR	yes
TS-345	WBA	550	chl-ser-py	SWIR; EMP; WR	yes
TS-067	WBA	550	chl-ca-py	SWIR; EMP; WR	yes
TS-494	WBA	550	chl-ca-py	SWIR; EMP; WR	yes
TS-496	WBA	550	chl-ca-py	SWIR; EMP; WR	yes
MF18853	RZW	25	chl-ca-py	SWIR; EMP	no
MF19908	RZW	-60	chl-ca-py	SWIR; EMP	no

WR*, whole-rock geochemistry data from Sinclair (2000).
[B, Battle; ca, calcite; ch, chlorite; EMP, electron microprobe; py, pyrite; RZN, Ridge Zone North; RZW, Ridge Zone West; ser, sericite; SWIR, shortwave infrared; TV, Thelwood Valley; WBA, West Block Area; WR, whole-rock geochemistry]

5.4 Analytical Methods

5.4.1 EMP analysis

Prior to EMP analysis, samples were examined with a petrographic microscope, from which areas of interest were selected for scanning electron microscopy (SEM). Samples were then imaged with a Hitachi SU-70 field emission scanning electron microscope (FE-SEM) at the CSL, University of Tasmania. Petrographic mineral identifications were confirmed by semi-quantitative energy dispersive X-ray spectral (EDS) analysis. Chlorite, white mica, and carbonate minerals greater than 15 μm in size were prioritised for EMP analysis.

Mineral chemistry data were acquired on a Cameca SX100 TCP/IP Socket electron microprobe equipped with five tunable wavelength dispersive spectrometers (WDS) at the CSL, University of Tasmania. Operating conditions were a beam diameter of 10 μm at a 40° take off angle with an energy of 15 keV and current of 10 nA. For details on analytical standards, measurement count times, and data corrections refer to Appendix E.

Electron microprobe measurements were completed on 17 samples (Table 5.2) over the course of five analytical sessions. Dr K. Goemann of the CSL prepared the microprobe analytical program and completed the initial raw data processing. For each EMP analysis, a BSE image was collected to document the beam location for each measurement (Appendix E). All EMP data are included in Appendix E. The quality of each EMP analysis was scrutinised by interrogating the oxide results and the analysis spot location. Results that had either textural

or chemical evidence for mineral inclusions were removed from the final dataset. Chlorite analyses were included in the dataset if: SiO_2 = 24-30%; TiO_2 <0.5%; K_2O <0.25%; total MgO-FeO >35%; Al_2O_3 = 18-24%; and if total oxides ≥86%. White mica analyses were included in the dataset if: SiO_2 = 44.5-53%; TiO_2 <0.5%; K_2O = 8-12%; total MgO-FeO <8%; Al_2O_3 = 28-38%; and if total oxides ≥93.5%. Carbonate analyses were not rejected from the dataset if: SiO_2 <0.1%; CO_2 = 38-52%; and if total oxides ≥98%.

5.4.2 Whole-rock geochemistry

Major and trace element lithogeochemistry was collected for 14 samples of Price Formation andesite (Table 5.2) to investigate bulk rock chemical changes due to alteration using calculated alteration indices. A single batch of samples were analysed at ALS, Perth, WA, Australia (Appendix F). X-ray fluorescence (XRF) with a lithium borate fusion was used to measure the major oxides. Trace elements were analysed by inductively coupled plasma atomic emission spectroscopy (ICP-MS) of a lithium borate fused bead. Total sulfur, total carbon, and loss on ignition (LOI) were measured by Leco and TGA furnace, respectively.

5.4.3 Quantitative mineralogy

Mineral abundances were determined from whole-rock geochemical and EMP data from 14 samples (Table 5.2) to assess mineralogical changes between footwall alteration facies. The mineral assemblage of each sample was determined from reflected light, transmitted light, and scanning electron microscope analysis. Quantitative mineralogy calculations were completed following the procedure of Herrmann and Berry (2002). Mineral compositions used in the calculations included measured mineral chemistries from new EMP results and end-member mineral compositions provided in the MINSQ method (Herrmann and Berry, 2002).

5.4.4 SWIR spectroscopy

Shortwave infrared measurements were obtained from 949 samples from underground drill holes from the West Block Area and Ridge Zone North orebody with a TerraSpec™ Standard Res Mineral Analyzer. Samples were collected at a down-hole sampling interval of approximately 3 metres. Shortwave infrared spectroscopy was completed at CODES, University of Tasmania.

Shortwave infrared spectrometry examines the infrared (1,300-2,500-nm wavelength) radiation reflected from an illuminated geological sample. Light interacting with the molecular bonds of a sample is either absorbed or reflected in discrete portions of the SWIR range, which results in unique spectral absorption responses that reflect the mineralogy of the sample (Figure 5.4). The OH, H_2O, CO_3, AlOH, FeOH, and MgOH molecular bonds produce diagnostic absorption features in SWIR spectra (Thompson et al., 1999). In particular, the AlOH (~2,185-2,225 nm) and FeOH (~2,235-2,255 nm) absorption features are useful for the identification of white mica and chlorite phyllosilicate minerals (Figure 5.5; e.g., Pontual et al., 1997).

Spectra were acquired on the clean, flat surface of dry drill core samples using a contact probe with a 10 mm diameter spot size. Prior to sample analysis and after every hour of machine runtime, the analyser was calibrated with a Spectralon® disk. Care was taken to analyse representative portions of the sample as opposed to unique or uncommon geological features. Where possible, portions of the sample that contained abundant sulfide were avoided to minimise spectral interference. The TerraSpec™ Standard Res Mineral Analyzer acquires data between 1,000-2,500 nm wavelengths. The analyser has a spectral resolution of 6 nm, sampling

interval of 2 nm, and a wavelength accuracy of ±1.0 nm (*per. com. Malvern Panalytical 2018*). Each spectrum acquired from the drill core samples consists of an average of 150 consecutive measurements. Spectra absorption features were processed using TSG® analysis software. Spectral parameters such as the wavelength position and depth of absorption features were extracted from Hull quotient corrected spectra (e.g., Figure 5.4B).

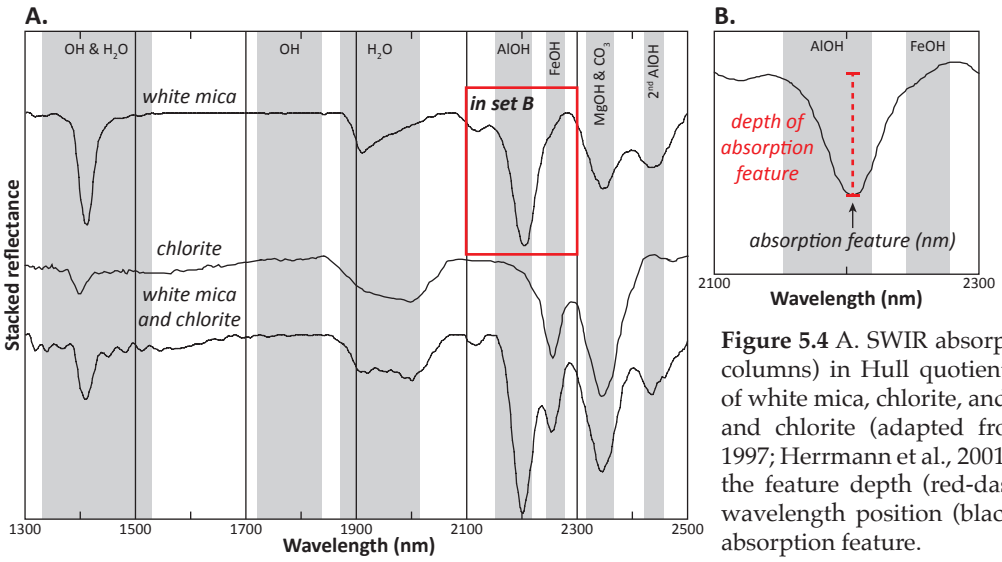

Figure 5.4 A. SWIR absorption features (grey columns) in Hull quotient corrected spectra of white mica, chlorite, and mixed white mica and chlorite (adapted from Pontual et al., 1997; Herrmann et al., 2001). B. In set showing the feature depth (red-dashed line) and the wavelength position (black arrow) of AlOH absorption feature.

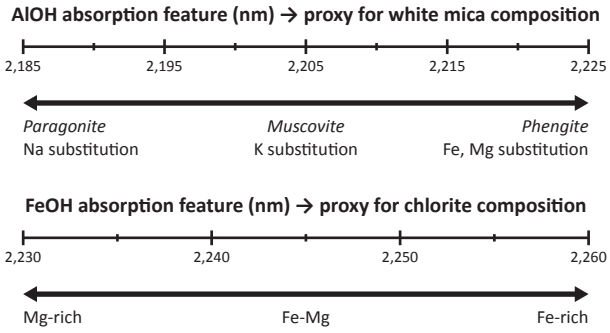

Figure 5.5 White mica (A) and chlorite (B) mineral composition proxies based on wavelength position of AlOH and FeOH absorption features in SWIR spectra of phyllosilicate minerals (adapted from Pontual et al., 1997).

5.5 Alteration Mineral Chemistry

Electron microprobe analysis was completed on seventeen samples to assess the chemistry of alteration minerals in andesite from Myra Falls (Table 5.2). Samples are from the West Block Area (n=13), Ridge Zone North (n=1), Ridge Zone West (n=2), Battle (n=2), and the Thelwood Valley (n=1).

Average chlorite EMP results from 16 samples (120 points) are presented in Table 5.3. Based on the classification diagram of Si^{iv} versus Fe/Fe+Mg (Hey, 1954), chlorites have ripidolite (n=14) and sheridanite (n=2) mineral compositions (Figure 5.6A). Analysed chlorites define an array from intermediate Fe-Mg chlorite to Mg-rich chlorite (Figure 5.6B). Chlorite was too fine-grained (<15 μm) in the Ridge Zone North orebody sample to analyse by EMP. Chlorite in andesite of the Price Formation from the West Block Area (n=11) is intermediate in composition, with Fe/Fe+Mg ratios between 0.27 and 0.49. Below the Battle orebody, chlorite in andesite of

Figure 5.6 Plots showing the variation in the composition of chlorite (A-B), white mica (C-D), and carbonate (E-F) based on EMP analyses from altered andesite of the Price Formation. Samples are from the Thelwood Valley, Battle orebody, West Block Area, Ridge Zone North, and Ridge Zone West. Smaller and transparent symbols are single analyses, whereas the larger and opaque symbols are the sample average.

A. Chlorite composition diagram from Hey (1954). The majority of chlorite analysed are ripidolite and two are sheridanite.

B. Ternary plot showing variations in chlorite composition. Note the variation in Mg and Fe in the dataset. Mg-rich chlorite is associated with intensely altered samples, proximal to sulfide mineralisation.

C. Diagram illustrating the variation in K-mica composition with muscovite and phengite end-members.

D. Muscovite-phengite-paragonite mineral composition diagram for K-micas. Note that analysed white mica is Na-poor, muscovitic with minor phengite substitution.

E. Carbonate mineral composition ternary diagram. Altered andesite samples have calcite and dolomite mineral compositions. Samples TS-1180 and TS-788 have both calcite and dolomite carbonate mineral chemistries.

F. Diagram illustrating the variation of MnO contents in carbonate analyses.

[apfu, atoms per formula unit; BR, brunsvigite; CC, clinochore; CP, corundophilite; PC, pynochlorite; PT, pseuothuringite; RP, ripidolite]

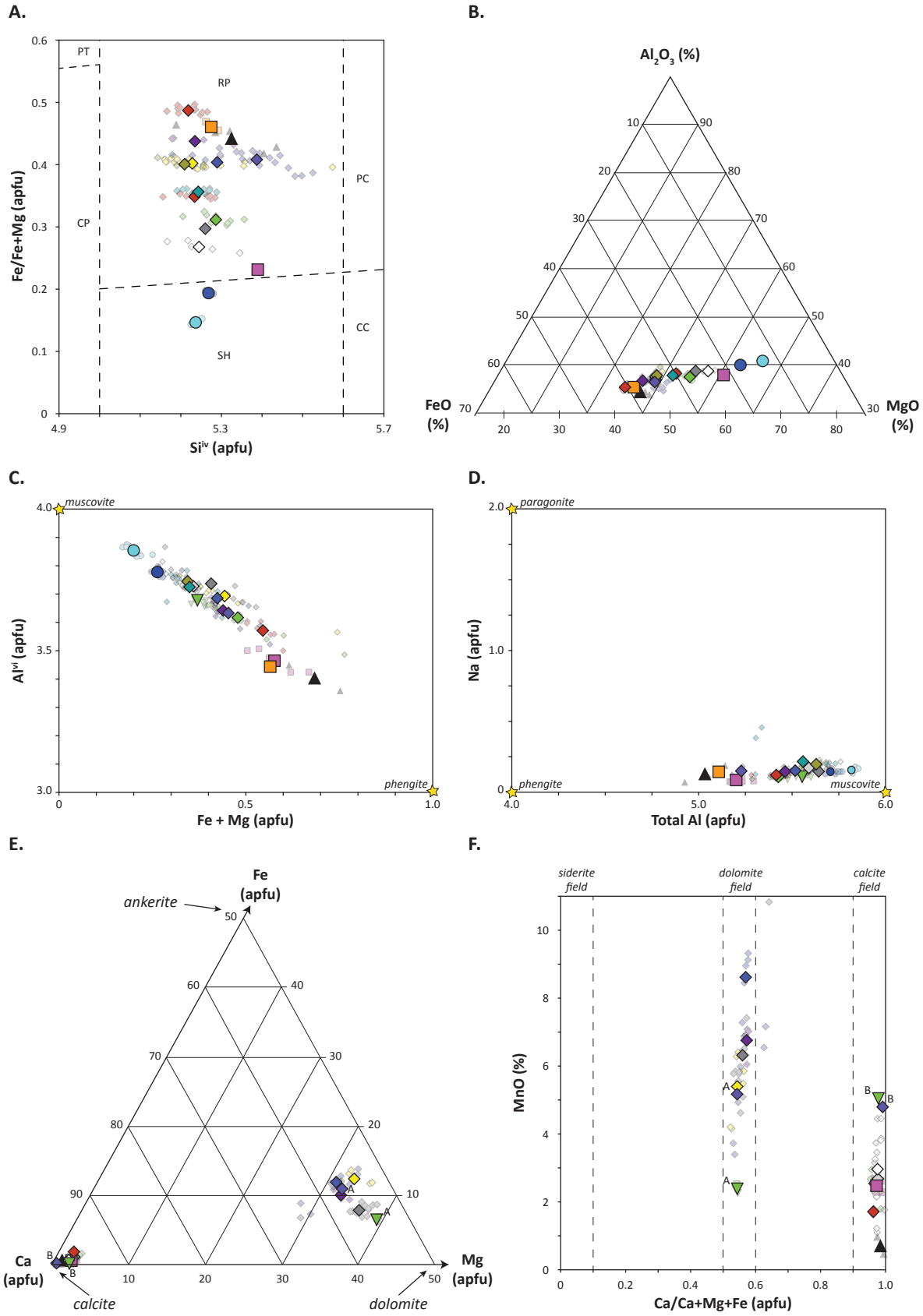
A.
PT
RP
PC
CP
CC
SH
Fe/Fe+Mg (apfu)
Si^iv (apfu)
B.
Al2O3 (%)
FeO (%)
MgO (%)
C.
muscovite
phengite
Al^vi (apfu)
Fe + Mg (apfu)
D.
paragonite
muscovite
phengite
Na (apfu)
Total Al (apfu)
E.
Fe (apfu)
ankerite
Ca (apfu)
Mg (apfu)
calcite
dolomite
F.
siderite field
dolomite field
calcite field
MnO (%)
Ca/Ca+Mg+Fe (apfu)
Thelwood Valley
143640 (5880 mE)
Battle Orebody
143682 (1420 mE)
143700 (1420 mE)
Ridge Zone North
TS-1180 (918 mE)
A - dolomite
B - calcite
TS-265 (640 mE)
TS-394 (640 mE)
TS-420 (640 mE)
TS-552 (640 mE)
TS-722 (640 mE)
West Block Area
TS-683 (585 mE)
TS-788 (585 mE)
A - dolomite
B - calcite
TS-067 (550 mE)
TS-494 (550 mE)
TS-496 (550 mE)
TS-345 (550 mE)
Ridge Zone West
MF18853 (25 mE)
MF19908 (-60 mE)

the Price Formation (n=2) is Mg-rich, with Fe/Fe+Mg ratios of 0.15 and 0.20. Chlorite from below the Ridge Zone West orebody (n=2) is both, Mg-rich and intermediate in composition with Fe/Fe+Mg ratios of 0.23 and 0.46. Price Formation andesite from the Thelwood Valley contains intermediate chlorite, with an average Fe/Fe+Mg ratio of 0.44.

Average white mica EMP results from 16 samples (116 points) of the Price Formation are presented in Table 5.4. Analysed white micas are K-mica in composition with K >1.50-apfu (Table 5.4) and Al^{iv}, Fe, Mg, and Na apfu values that indicate limited phengite and no paragonite substitution (Figure 5.6C-D). White mica from the West Block Area (n=10) has Fe/Fe+Mg ratios between 0.36 and 0.69. White mica in the stratigraphic footwall of the Ridge Zone North orebody (n=1) has a Fe/Fe+Mg ratio of 0.37. Below the Battle orebody (n=2), white mica has Fe/Fe+Mg ratios of 0.23 and 0.33, while samples from below the Ridge Zone West orebody (n=2) are 0.32 and 0.45. Price Formation andesite from the Thelwood Valley contains white mica, with an average Fe/Fe+Mg ratio of 0.51.

Average carbonate EMP results from 12 samples (n=84) of the Price Formation are presented in Table 5.5 and Figure 5.6E-F. Samples from the West Block Area and Ridge Zone North orebody have calcite or dolomite carbonate compositions, with both calcite and dolomite present in samples TS-788 and TS-1180. Sample TS-788, from the West Block Area, has FeO-MnO value of 12.79 wt. % for dolomite and 5.06 wt. % for calcite (Table 5.5). Sample TS-1180, from the Ridge Zone North orebody, has average total FeO-MnO concentrations of 7.21 wt. % for dolomite and 5.38 wt. % for calcite (Table 5.5). Below the Ridge Zone West orebody (n=1), calcite has an average total FeO-MnO concentration of 3.02 wt. %. Price Formation andesite from the Thelwood Valley has calcite with low iron and manganese; total FeO-MnO value of 1.28 wt. %.

5.6 Alteration Trends From Whole-Rock Geochemistry

Alteration indices were calculated from major oxide results to assess geochemical signatures of altered Price Formation andesite at Myra Falls (Table 5.6). The new lithogeochemical results are graphically displayed on Figure 5.7 with the previously published data of Robinson (1994) and Sinclair (2000).

Figure 5.7A illustrates the alteration of plagioclase as a function of depleted Na_2O wt. % and the addition of pyrite as a function of elevated S wt. % (e.g., Large et al., 2001b). The K-Ca-Na molar element ratio plot (Figure 5.7B) shows the alteration trend of primary plagioclase progressively replaced by white mica (e.g., Warren et al., 2007). The alteration box plot of Large et al. (2001a), combines the Ishikawa Alteration Index (AI) and the Chlorite-Carbonate-Pyrite Index (CCPI) to characterise the nature and degree of alteration of volcanic rocks (Figure 5.7C). The AI and CCPI indices, were developed to quantify the intensity of white mica, chlorite, carbonate, and pyrite alteration of feldspar and glass in volcanic rocks associated with VHMS hydrothermal systems (Ishikawa et al., 1976; Lentz, 1999; Large et al., 2001a). Calculated AI and CCPI values for the West Block Area and Ridge Zone North orebody dataset are shown in Table 5.6.

On all three plots, a significant number of the West Block Area samples plot within or near the least-altered andesite fields and form trends toward the intensely altered Ridge Zone North and Battle orebody samples (Figure 5.7). The West Block Area lacks significant sodium depletion and only minor additions of sulfur, with Rb/Sr ratios from 0.21-0.92 (Figure 5.7A;

Table 5.6). The K-Ca-Na molar element ratio diagram illustrates two alteration trends: (1) least-altered andesite to K-mica-dominant alteration and (2) least-altered andesite to mixed white mica and chlorite alteration (Figure 5.7). Similarly, on the alteration box plot, the results form an array from least-altered andesite towards white mica and chlorite-pyrite alteration signatures (Figure 5.6C). A sample of intensely altered Price Formation andesite from below the "contact zone" sulfide mineralisation position in the Ridge Zone North orebody has the most extreme lithogeochemical alteration signatures, which plot within the intensely altered Battle orebody sample set fields, and has a Rb/Sr ratio of 1.67 (Figure 5.7; Table 5.6).

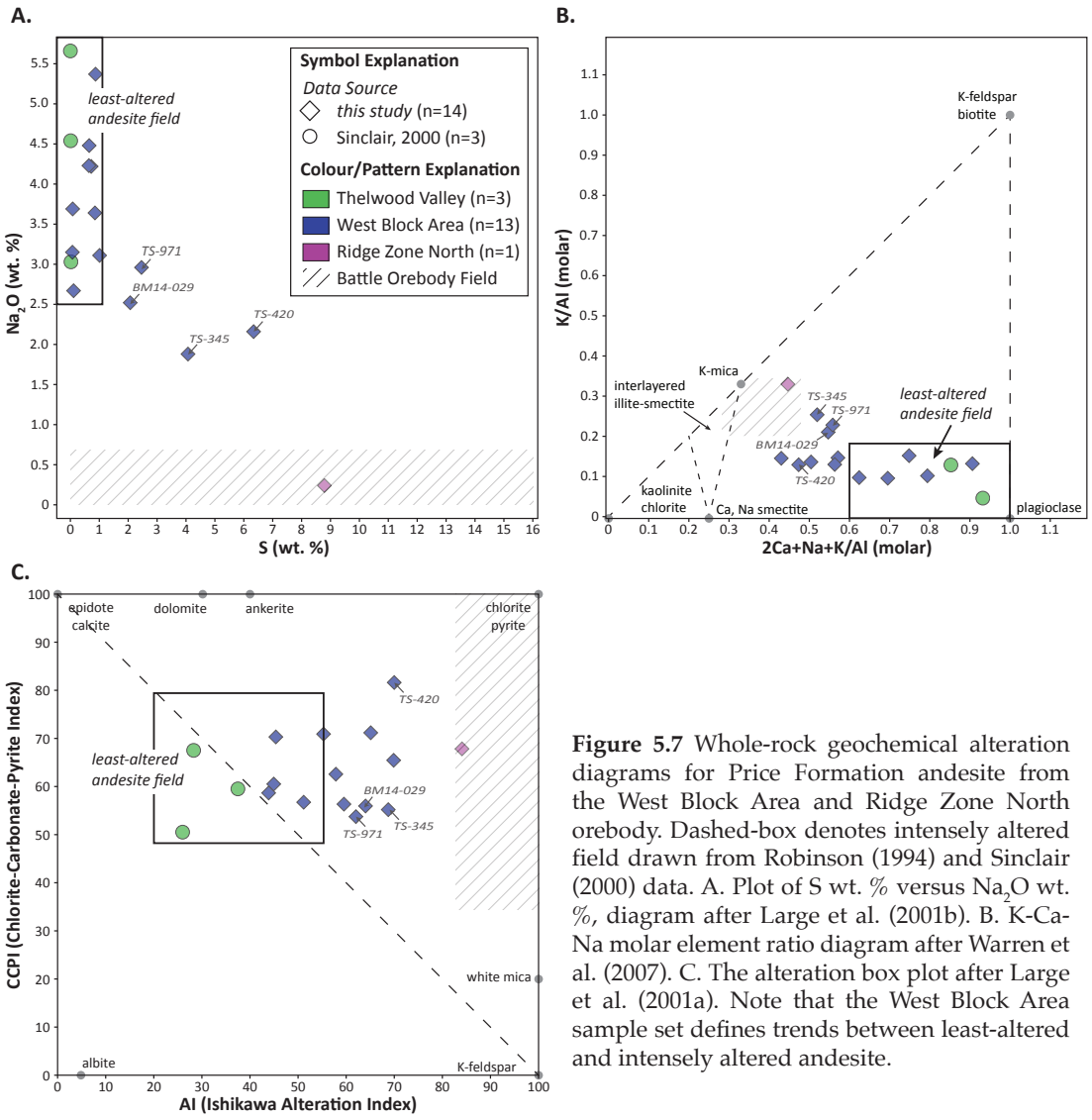

Figure 5.7 Whole-rock geochemical alteration diagrams for Price Formation andesite from the West Block Area and Ridge Zone North orebody. Dashed-box denotes intensely altered field drawn from Robinson (1994) and Sinclair (2000) data. A. Plot of S wt. % versus Na_2O wt. %, diagram after Large et al. (2001b). B. K-Ca-Na molar element ratio diagram after Warren et al. (2007). C. The alteration box plot after Large et al. (2001a). Note that the West Block Area sample set defines trends between least-altered and intensely altered andesite.

5.7 Quantitative Mineralogy

The most common alteration minerals identified in hand samples from the footwall alteration facies include chlorite, white mica, quartz and pyrite (Table 5.1). With respect to alteration intensity, the lack of feldspar phenocrysts is most evident in samples proximal to sulfide zones in the Ridge Zone North and Battle orebodies (Figure 5.2E-L). To constrain the mineralogical changes due to alteration, quantitative mineralogy was calculated for 14 samples of Price

Formation andesite (Table 5.7; Figure 5.8). Weak, chlorite-calcite ± epidote altered andesite has albite concentrations >35 wt. %. While, moderate, chlorite-calcite-pyrite altered andesite has albite concentrations between 44.5 wt. % and 17.1 wt. %. Intense, sericite-quartz-pyrite and chlorite-sericite-pyrite altered andesite have no albite. A decrease in albite abundance is associated with elevated total chlorite and white mica, and generally coincident with elevated pyrite values (Figure 5.8). The abundance of chlorite and white mica is variable in samples of altered andesite. Calculated chlorite concentrations are between 0.0-30.3 wt. %, and white mica abundances range from 0.0-57.0 wt. % (Table 5.7). The calculated mineralogy is in agreement with the visual assessment of footwall alteration facies, and indicates that intense alteration facies are characterised by elevated white mica and chlorite concentrations with depleted albite and elevated pyrite concentrations (Figure 5.8).

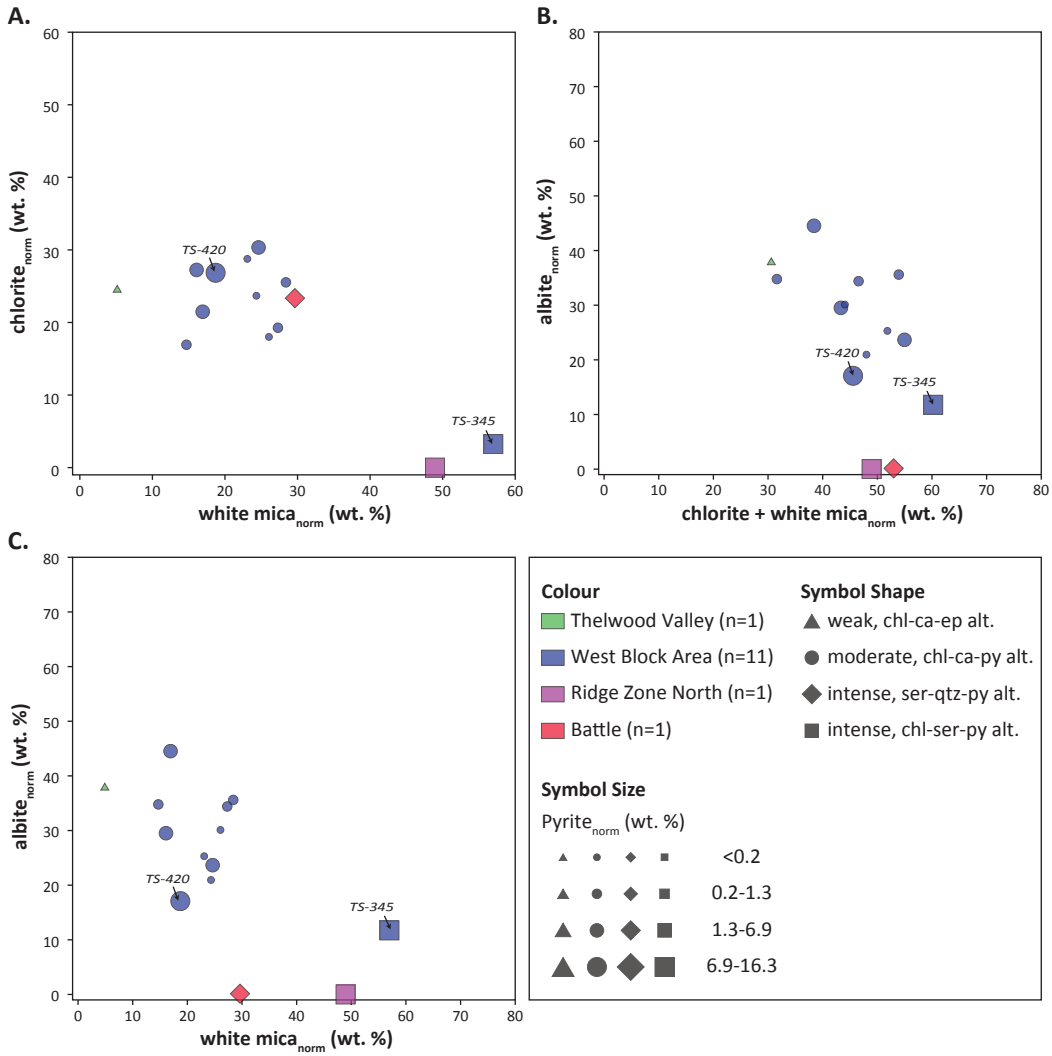

Figure 5.8 Modal mineralogy of variably altered andesite of the Price Formation from whole-rock geochemistry and mineral chemistry data. A. Alteration of andesite comprises the addition of white mica and chlorite. B. Altered andesite have elevated total white mica and chlorite normative concentrations, coupled with reduced albite concentrations. C. The concentrations of normative pyrite are generally higher in samples with elevated white mica and reduced albite.

5.8 Alteration Characterisation by SWIR Spectroscopy

Fine-grained, chlorite and sericite alteration facies are prevalent in all rock types in the West Block Area (*see Chapter 4*). Systematic SWIR spectral analysis was used to identify, quantify, and characterise phyllosilicate mineralogy from 23 drill holes in the West Block Area and 3 drill holes in the Ridge Zone North orebody. The dataset was used to: (1) identify SWIR-active minerals in rocks of the Price Formation, H-W member, and Hanging Wall Andesite member; (2) assess the spatial relationship of the white mica and chlorite AlOH and FeOH absorption feature wavelengths to lithology and sulfide mineralisation; and (3) determine alteration domains with SWIR-active minerals in the West Block Area and Ridge Zone North orebody. The term "SWIR-active mineral" in this study refers to minerals with OH bonds that register a unique response in the SWIR spectrum. Specific to the Myra Falls dataset, these minerals include chlorite, white mica and epidote (Figure 5.9).

5.8.1 Results

Shortwave infrared spectroscopy was collected from 949 samples (West Block Area = 825; Ridge Zone North orebody = 124; Appendix G). The dataset comprises 637 analyses of felsic and andesitic rocks of the H-W member and the Hanging Wall Andesite member, plus 227 analyses of the Price Formation. Typical SWIR spectra of drill core samples are shown in Figure 5.9. Shortwave infrared results (Figure 5.10) include samples with white mica (n=413), mixed chlorite and white mica (n=311), chlorite (n=104), and mixed chlorite and epidote (n=95).

5.8.2 Relationship between SWIR identified mineralogy and lithology

Figure 5.11 shows the variation of the AlOH and FeOH absorption wavelengths with lithology. In the West Block Area, the Hanging Wall Andesite member is weakly altered and has no appreciable concentrations of sulfide. Chlorite is the dominant alteration mineral and is characterised by FeOH absorption feature wavelengths between 2,247 nm and 2,257 nm, suggesting intermediate Fe-Mg chlorite compositions (Figure 5.11B).

Moderate to intense alteration of marine-sedimentary and volcanic rocks of the H-W member are host to VHMS mineralisation in the West Block Area and Ridge Zone North orebody (*see Chapter 4*). The SWIR results suggest a range of muscovitic white mica compositions, independent of lithology (Figure 5.11C-D). FeOH absorption feature wavelengths are between 2,245 nm and 2,255 nm in samples of the Basal Volcaniclastic Unit (Figure 5.11D) and are <2,242 nm for samples of coherent rhyolite and felsic volcaniclastic rocks (Figure 5.11D). The longer FeOH wavelengths suggest intermediate, Fe-Mg chlorite compositions, whereas the shorter wavelengths suggest Mg-rich chlorite (Figure 5.5).

Samples of the Price Formation andesite, which form the stratigraphic footwall to the VHMS deposits at Myra Falls, have a range of AlOH and FeOH absorption features that mirror those of the H-W member (Figure 5.11E-F). The majority of andesite samples have an AlOH absorption feature between 2,195 nm and 2,207 nm (Figure 5.11E). Whereas chlorite FeOH absorption feature wavelengths suggests intermediate Fe-Mg chlorite (2,245-2,255 nm; n=176) and Mg-rich chlorite mineral compositions (<2,242 nm; n=15).

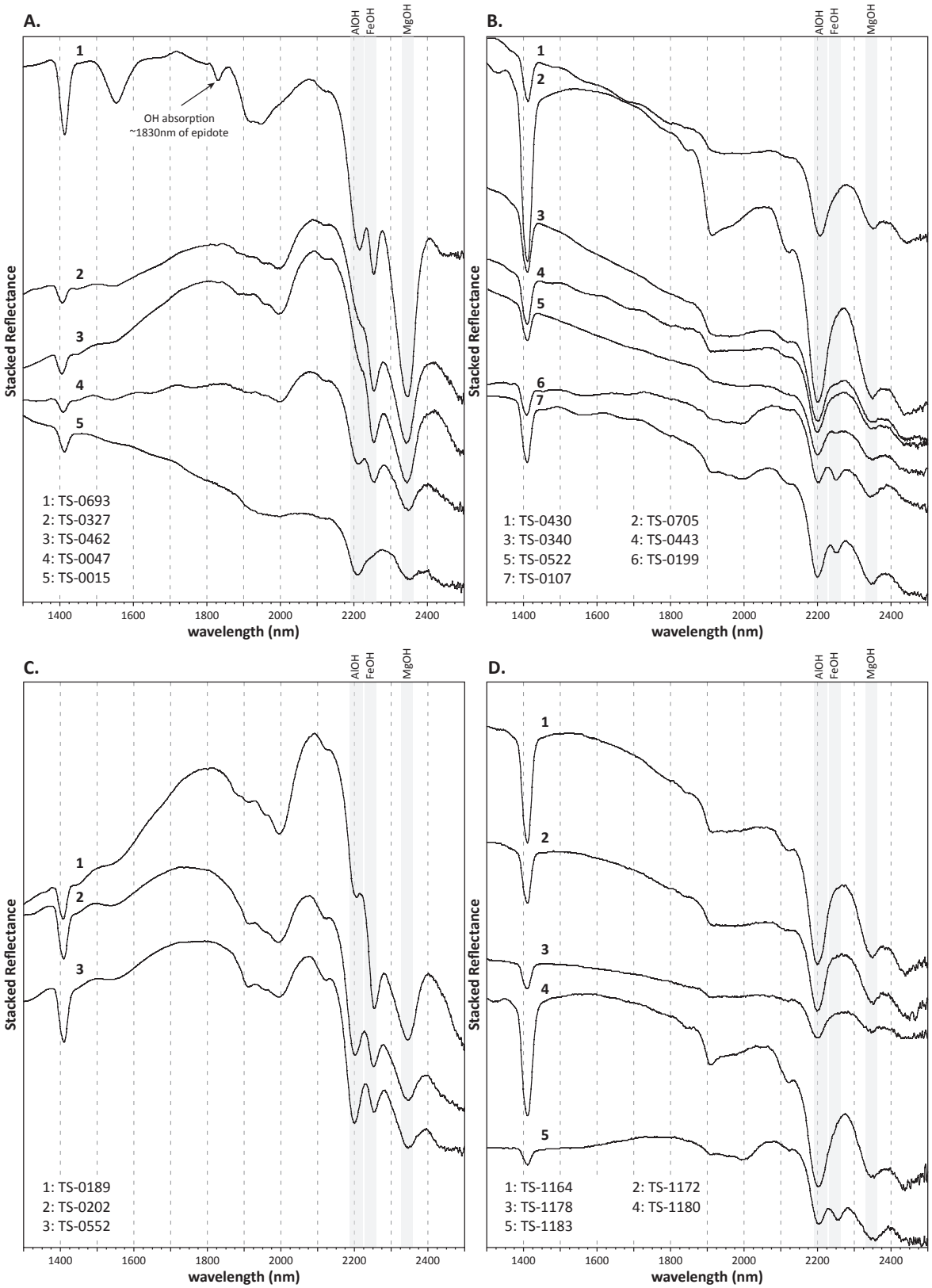

Figure 5.9 Typical SWIR spectra of drill core samples from the West Block Area (A-C) and Ridge Zone North orebody (D). A. SWIR spectra of andesitic rocks of the lower Myra Formation – chlorite-epidote (1); chlorite (2-3); chlorite and white mica (4); and white mica (5). B. SWIR spectra of felsic rocks of the H-W member – white mica in coherent rhyolite (1-2); white mica in rhyolitic volcaniclastic sandstone (3-4): white mica in chert (5); chlorite and white mica in the Basal Volcaniclastic Unit (6-7). C. SWIR spectra of andesitic rocks of the Price Formation – chlorite (1); chlorite and white mica (2-3). D. SWIR spectra from the Ridge Zone North orebody – white mica in coherent rhyolite (1); white mica in rhyolitic volcaniclastic breccia (2); white mica in the Basal Volcaniclastic Unit (3); white mica in Price Formation andesite (4); chlorite and white mica in Price Formation andesite (5).

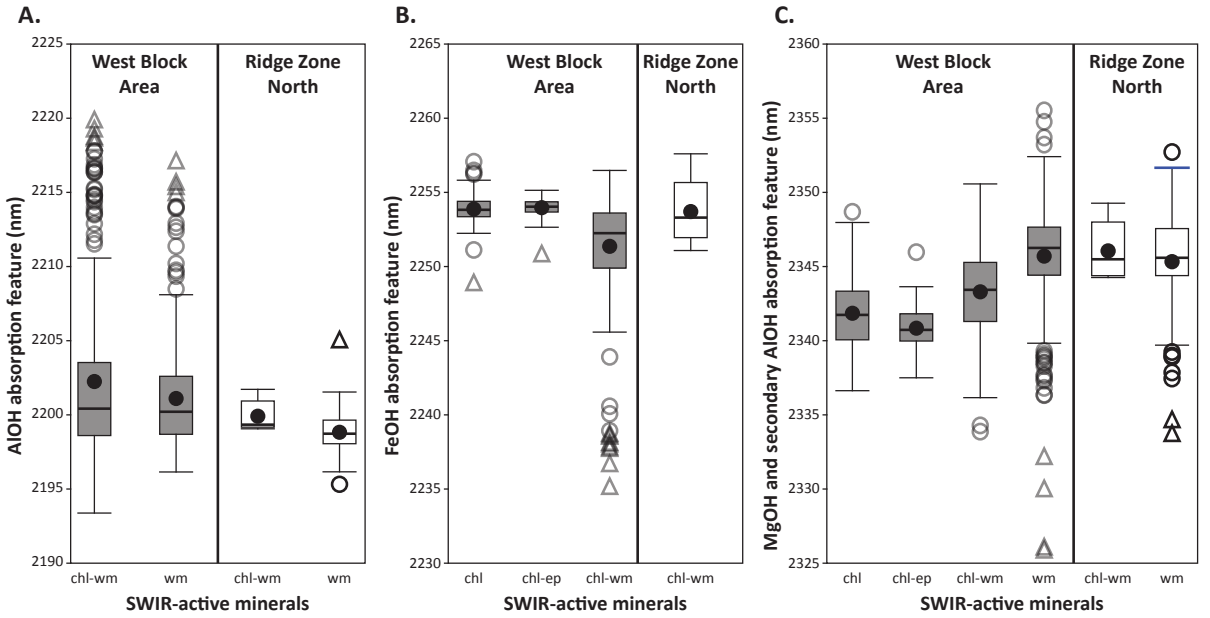

Figure 5.10 Tukey box and whisker plots for SWIR spectral results of samples from the West Block Area and Ridge Zone North. A. AlOH absorption features for TSG® identified mixed chlorite and white mica, and white mica dominant SWIR assemblages. B. FeOH absorption features for TSG® identified chlorite dominant, chlorite-epidote, and mixed chlorite and white mica SWIR assemblages. C. MgOH and secondary AlOH absorption features for TSG® identified chlorite dominant, chlorite-epidote, mixed chlorite and white mica, and white mica dominant SWIR assemblages. Note the triangle and circle symbols denote data outliers and not rock type. [chl, chlorite; ep, epidote; wm, white mica]

5.8.3 SWIR down-hole profiles

Figure 5.12 illustrates the down-hole variation of the AlOH and FeOH absorption feature wavelengths of white mica and chlorite in the West Block Area and the Ridge Zone North orebody.

Drill hole BG18-3904 is from the West Block Area and is located on cross-section 550 mE (Figure 5.3A). Chlorite-calcite, chlorite-calcite-epidote, and patchy sericite altered volcaniclastic and coherent rocks of the Hanging Wall Andesite member are characterised by AlOH and FeOH absorption wavelengths of >2,205 nm and ~2,254 nm, respectively (Figure 5.12A). Sericite-quartz-pyrite altered, felsic volcaniclastic rocks of the H-W member, host disseminated sphalerite-pyrite and sphalerite stringer-style sulfide mineralisation. These rocks have AlOH absorption wavelengths between 2,197 nm and 2,200 nm (Figure 5.12A). Disseminated pyrite ± sphalerite-chalcopyrite mineralisation is associated with chlorite-sericite-pyrite altered rocks of the Basal Volcaniclastic Unit, which has AlOH and FeOH absorption wavelengths of ~2,199 nm and ~2,238 nm, respectively (Figure 5.12A). Disseminated pyrite associated with chlorite-calcite altered andesite of the Price Formation is characterised by AlOH and FeOH absorption wavelengths of ~2,200 nm and <2,245 nm, respectively (Figure 5.12A). Chlorite-calcite altered andesite, below 165 metres, has AlOH and FeOH absorption wavelengths of >2,200 nm and >2,250 nm, respectively (Figure 5.12A).

Drill hole BG18-3321a is from the West Block Area and is located on cross-section 640 mE (Figure 5.3B). Chlorite-calcite altered volcaniclastic and coherent rocks of the Hanging Wall Andesite member are characterised by FeOH absorption wavelengths of >2,250 nm (Figure 5.12B). Disseminated sphalerite-pyrite and stringer-style sphalerite sulfide mineralisation is hosted in sericite-quartz-pyrite altered, coherent rhyolite and felsic volcaniclastic sandstone

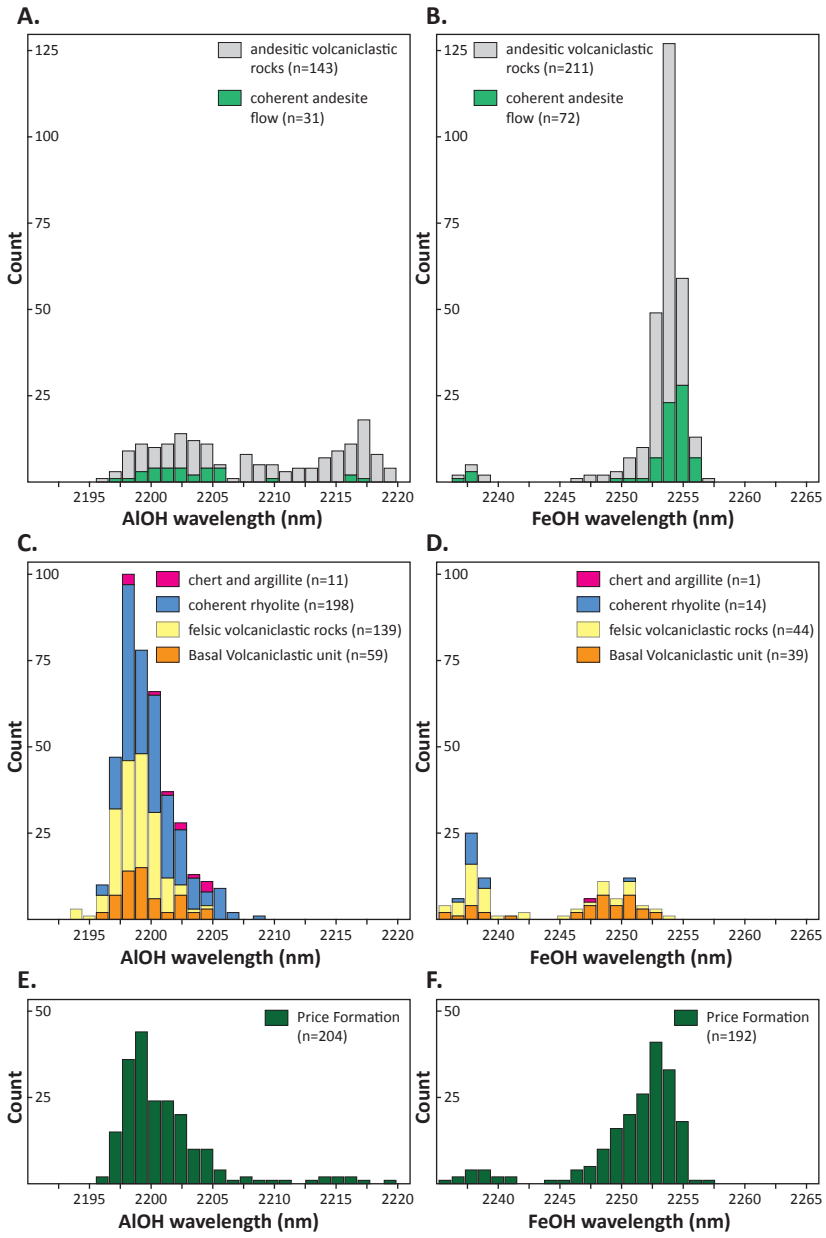

Figure 5.11 Histogram plots for SWIR spectral results of samples from the West Block Area and Ridge Zone North orebody. A-B. Distribution of the AlOH and FeOH absorption feature wavelengths for samples of the Hanging Wall Andesite member and coherent andesite flow of the H-W member. C-D. Distribution of the AlOH and FeOH absorption feature wavelengths for samples of chert and argillite, coherent rhyolite, felsic volcaniclastic rocks and the Basal Volcaniclastic Unit of the H-W member. E-F. Distribution of the AlOH and FeOH absorption feature wavelengths for samples of Price Formation andesite.

of the H-W member. These rocks have AlOH absorption wavelengths between 2,197 nm and 2,201 nm and there appears to be a subtle, down-hole shift to shorter AlOH absorption wavelengths (Figure 5.12B). Massive sphalerite mineralisation from 95.22-95.74 metres is hosted in chlorite-sericite-pyrite altered rocks of the Basal Volcaniclastic Unit characterised by AlOH and FeOH absorption features of <2,199 nm and 2,246-2,251 nm, respectively (Figure 5.12B). Chlorite-calcite-pyrite altered andesite of the Price Formation is characterised by AlOH and FeOH absorption wavelengths from 2,197 nm to 2,202 nm and from 2,249 nm to 2,250 nm, respectively (Figure 5.12B).

Drill hole RN18-0223 is from the Ridge Zone North orebody, located on cross-section 918 mE (Figure 5.3C). This drill hole intersected intense sericite-quartz-pyrite altered coherent rhyolite and felsic volcaniclastic sandstone of the H-W member (Figure 5.12C). A 15-metre-thick interval of semi-massive sphalerite mineralisation is hosted in felsic volcaniclastic rocks below coherent rhyolite. Sericite-quartz-pyrite altered rocks are characterised by AlOH absorption wavelengths between 2,196 nm and 2,200 nm (Figure 5.12C). Sericite-quartz-pyrite

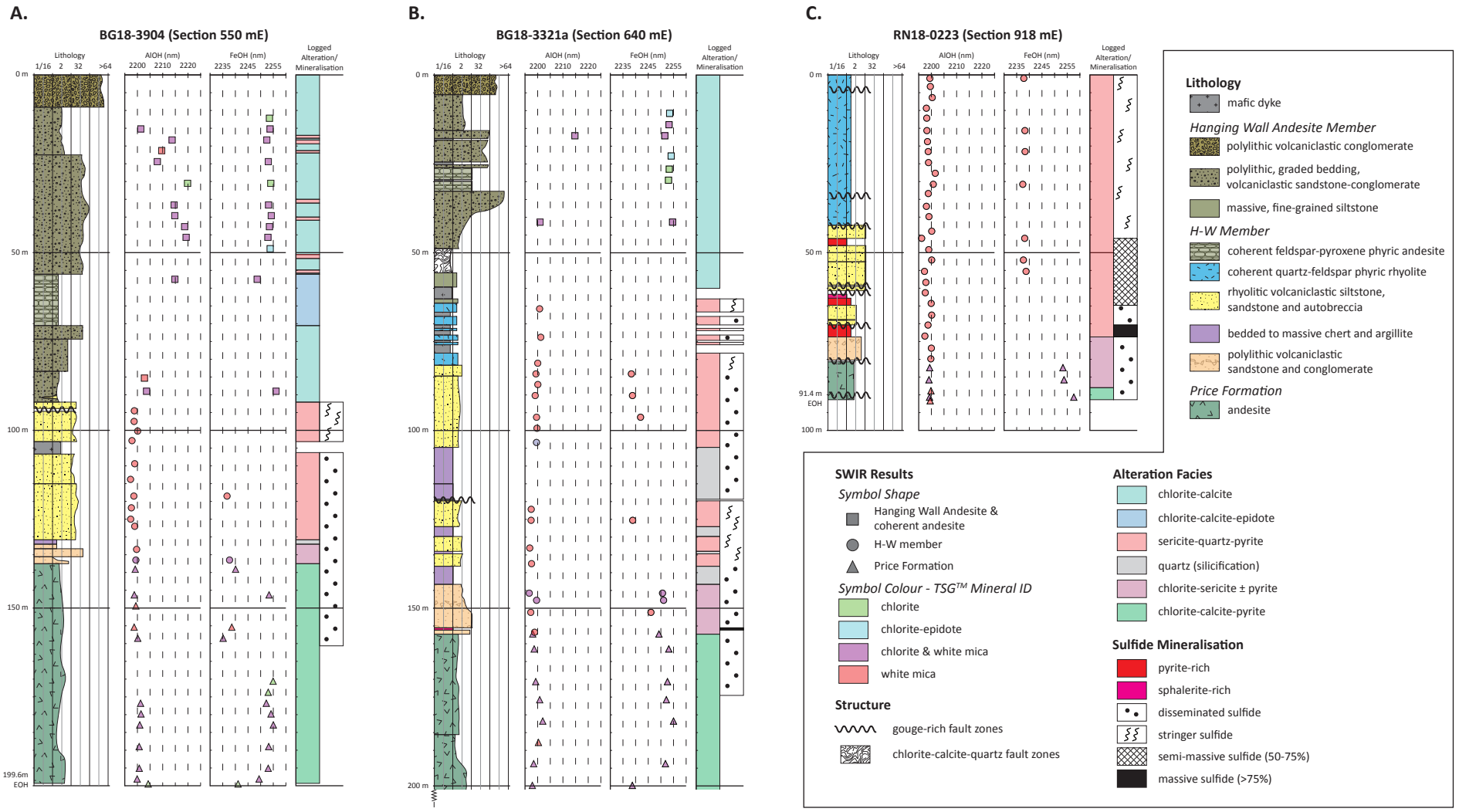

Figure 5.12 Graphic logs with lithology, alteration, mineralisation and SWIR down-hole profiles showing the relationship between lithology, logged alteration and the AlOH and FeOH absorption feature of white mica and chlorite. A. Underground drill hole BG18-3904 is from the West Block Area, cross-section 550 mE. B. Underground drill hole BG18-3221a is from the West Block Area, cross-section 640 mE. Underground drill hole RN18-0223 is from the Ridge Zone North orebody, cross-section 918 mE.

altered rocks of the Basal Volcaniclastic Unit, below massive pyrite mineralisation, has AlOH absorption wavelengths between 2,199 nm and 2,200 nm (Figure 5.12C). Chlorite-sericite-pyrite altered Price Formation andesite, immediately below the Myra Formation, is characterised by AlOH and FeOH absorption wavelengths of 2,199-2,200 nm and <2,554 nm, respectively (Figure 5.12C).

5.8.4 Comparison of SWIR results with EMP analyses of chlorite and white mica

Electron microprobe analyses indicate that chlorites range from Mg-rich to intermediate Fe-Mg compositions (Figure 5.6A-B) and white micas are K-micas, ranging from muscovitic to phengitic compositions (Figure 5.6C-D). Pontual et al. (1997) observed that the position of the FeOH absorption feature is related to the Fe-Mg composition of chlorite (Figure 5.5). In general, Mg-rich chlorite has short wavelengths (<2,240 nm) and Fe-rich chlorite has long wavelengths (>2,260 nm). Herrmann et al. (2001) demonstrated that the wavelength of the AlOH absorption feature of white mica decreases with increasing Na and decreasing Fe-Mg substitutions in K-micas. Typically, phengite (K-mica with elevated Fe-Mg) has long wavelengths (>2,220 nm) and paragonite (K-mica with elevated Na) has short wavelengths (<2,190 nm), with wavelengths between 2,200-2,220 nm representing muscovite (Figure 5.5). Mineral chemistry from chlorite and white mica analyses are compared with SWIR analyses from samples of Price Formation andesite on Figure 5.13.

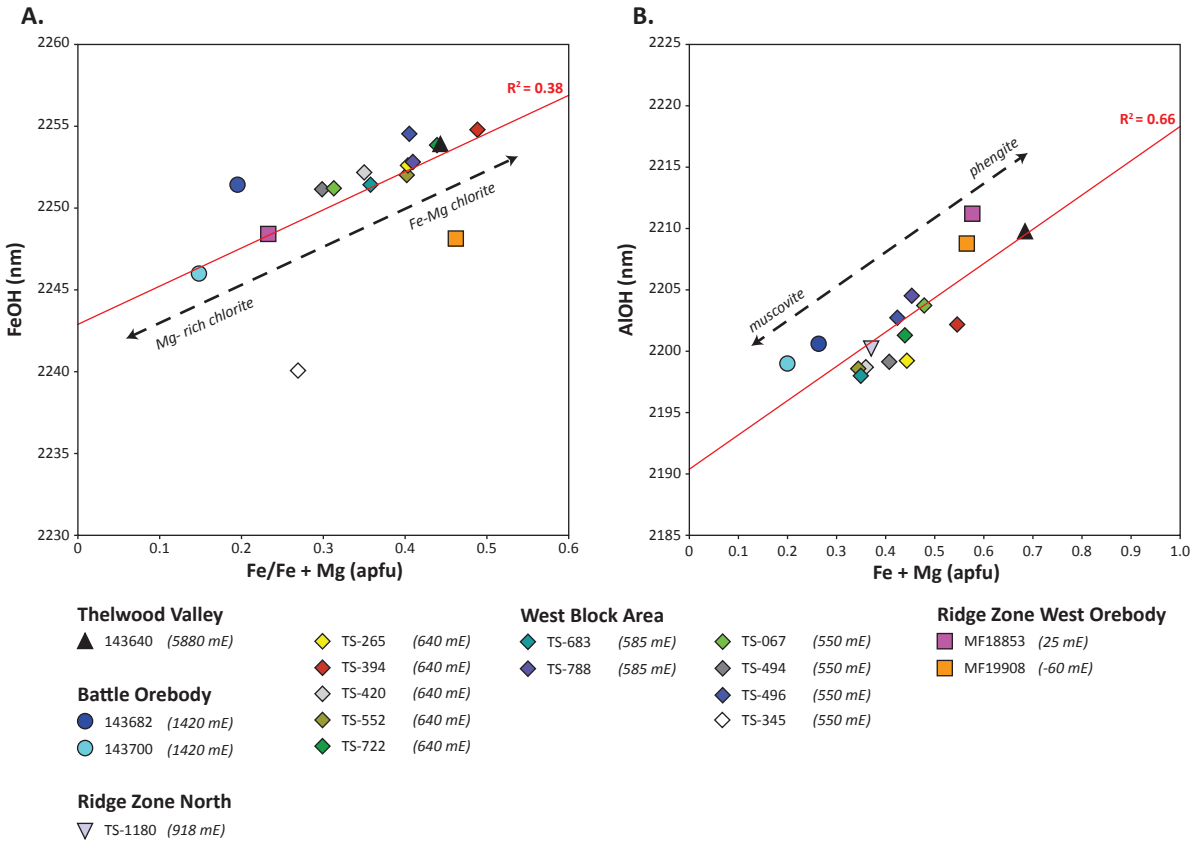

Figure 5.13 Plots illustrating the relationship between SWIR absorption feature wavelengths and EMP mineral chemistry. Each point represents an average of chlorite (A) and white mica (B) compositions from EMP results. A. Chlorite Fe/(Fe+Mg) versus FeOH absorption feature wavelength. Mg-rich chlorites generally have FeOH absorption features with short wavelengths and intermediate Fe-Mg chlorites have longer wavelengths. B. White mica Fe+Mg versus AlOH absorption feature wavelength. Muscovitic K-micas have low Fe+Mg concentrations and AlOH absorption features with short wavelengths and phengitic K-micas have elevated Fe-Mg with longer AlOH absorption feature wavelengths. [apfu, atoms per formula unit]

The Fe and Mg concentrations in chlorite are shown as the Fe/Fe+Mg ratio, with values <0.3 indicating Mg-rich chlorite and values between 0.3-0.6 indicating intermediate Fe-Mg chlorite (Figure 5.13A). No paragonite was identified in the EMP dataset (Figure 5.6C); therefore the phengite-muscovite substitution is assessed using total Fe-Mg apfu values (Figure 5.13B). There is a moderate, positive correlation between the Fe/Fe+Mg ratio of chlorite and the FeOH absorption feature wavelength for samples of Price Formation andesite; R^2=0.38 (Figure 5.13A). For the white mica dataset, there is a strong, positive R^2 value of 0.66 for the total Fe-Mg in K-micas and the AlOH absorption feature wavelength. These results, illustrate that SWIR analysis can be used to assess chemical changes in chlorite and K-mica at Myra Falls, which is in agreement with the findings of Jones et al. (2005).

5.8.5 SWIR alteration mineral domains

While the wavelength position of the AlOH and FeOH absorption features reflect the composition of white mica and chlorite present in the sample, the depth of the AlOH, FeOH and MgOH absorption features are a relative measure of mineral abundance (e.g., Thompson et al., 1999). Samples with deep AlOH absorption features are enriched in white mica and samples with deep FeOH absorption features are enriched in chlorite; whereas samples with deep 2,320 nm absorption features can be enriched in either white mica, chlorite or carbonate minerals (Clark et al., 1990; Pontual et al., 1997).

Based on the depth ratio of the 2,200 nm AlOH and 2,320 nm MgOH absorption features, three SWIR alteration mineral domains were identified for the study area (Figure 5.14). Samples that are white mica-dominant are characterised by a depth ratio ≥1.8, whereas a depth ratio ≤0.45 is indicative of chlorite-dominant samples (Figure 5.14). Depth ratios between 1.8 and 0.45 define mixed chlorite and white mica samples (Figure 5.14). The AlOH and MgOH depth ratio successfully distinguishes white mica, chlorite, and mixtures of chlorite and white mica. However, chlorite and epidote do not have an AlOH absorption feature and their diagnostic MgOH absorption features overlap (Pontual et al., 1997). As such, the AlOH and MgOH depth ratio does not distinguish between chlorite-dominant and mixed chlorite-epidote samples.

5.8.6 SWIR signatures for the West Block Area and Ridge Zone North orebody

The SWIR dataset was used to evaluate the alteration facies and their interpreted spatial distribution (Figures 5.15-5.18). Three-dimensional, numerical models of the AlOH and FeOH absorption feature wavelengths, and the AlOH to MgOH depth ratio were generated in Leapfrog® using the *numerical model* function. It is important to note that the data points used in these models are from the red drill stems only. Base data layers for each cross-section include the interpreted geology, structure, and distribution of sulfide mineralisation (*see Chapter 4*).

In general, the Hanging Wall Andesite member in the West Block Area is characterised by phengitic K-mica SWIR compositions with AlOH absorption wavelengths >2,210 nm (Figure 5.16A-C) and intermediate Fe-Mg chlorite with FeOH absorption wavelengths >2,250 nm (Figure 5.17A-C). Both chlorite-dominant and mixed chlorite-white mica alteration domains are present in the Hanging Wall Andesite member (Figure 5.18A-C). No samples were available from the Hanging Wall Andesite member above the Ridge Zone North orebody for comparison.

The H-W member in the West Block Area and Ridge Zone North localities is characterised by muscovitic K-mica SWIR compositions with AlOH absorption wavelengths <2,205 nm (Figure 5.16). Semi-massive and massive sulfide mineralisation coincides with white mica

AlOH absorption feature wavelengths from 2,197.5-2,200.0 nm (Figure 5.16C-D) and in some cases wavelengths <2,197.5 nm (Figure 5.16B). SWIR results for chlorite from the H-W member indicate intermediate Fe-Mg chlorite (FeOH >2,245 nm) and Mg-rich chlorite (FeOH <2,245 nm) compositions. Semi-massive and massive sulfide mineralisation is coincident with both chlorite compositions (Figure 5.17A-C). Figure 5.18 illustrates the distribution of the SWIR alteration mineral domains for the West Block Area and Ridge Zone North localities. The H-W member is characterised by the white mica-dominant alteration domain on cross-sections 550 mE and 918 mE (Figure 5.18A, D). On cross-sections 640 mE and 828 mE, both white mica-dominant and mixed chlorite-white mica alteration domains are present (Figure 5.18B-C). Semi-massive and massive sulfide mineralisation is coincident with both SWIR alteration mineral domains.

Shortwave infrared white mica compositions in the Price Formation andesite are muscovitic (2,202.5-2,197.5 nm; Figure 5.16) and locally phengitic; AlOH absorption wavelengths of >2,210 nm (Figure 5.16A-B). Chlorite SWIR results are predominately intermediate Fe-Mg in composition (FeOH >2,245 nm) with local zones of Mg-rich chlorite (FeOH <2,245 nm; Figure 5.17). There is no clear correlation between chlorite SWIR compositions in the Price Formation with proximity to massive and semi-massive sulfide mineralisation. Both white mica-dominant and mixed chlorite-white mica alteration domains are present in the Price Formation andesite (Figure 5.18). Notably, in the Ridge Zone North orebody, altered andesite is characterised by white mica-dominant alteration (Figure 5.18D). To the west of cross-section 918 mE, there is a progressive change from white mica-dominant to mixed chlorite-white mica alteration in the Price Formation andesite (Figure 5.18).

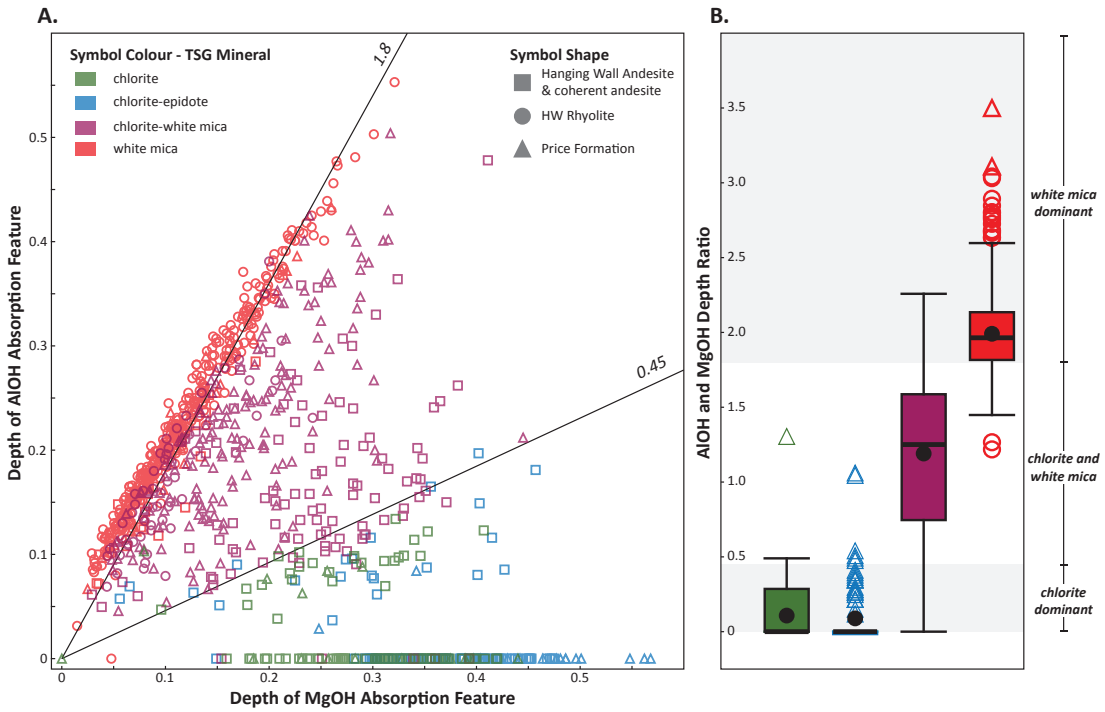

Figure 5.14 MgOH and AlOH absorption feature depth ratio diagrams. A. MgOH depth vs AlOH depth showing SWIR active mineral alteration trends in the West Block Area and Ridge Zone North orebody (modified from Cloutier and Piercey, 2017). B. Tukey box and whisker plots showing the distribution of AlOH and MgOH depth ratios relative to TSG identified mineral groups. Note the triangle and circle symbols (B) denote data outliers and not rock type. The AlOH and MgOH depth ratio distinguishes white mica dominant, chlorite dominant and mixed alteration trends, but is unable to separate chlorite dominant from mixed chlorite-epidote spectral signatures.

Figure 5.15 Distribution of alteration facies in cross-sections through the West Block Area and Ridge Zone North orebody (*see Chapter 4*). Cross-sections show detailed geology (patterns), alteration (colours) and sulfide mineralisation textures (symbols) interpreted from detailed graphic logging (red drill hole stems) and historic drill logs (grey drill hole stems). Refer to the plan map in the legend for the locations of cross-sections.

A. Cross-section interpretation 550 mE of the West Block Area, looking west.

B. Cross-section interpretation 640 mE of the West Block Area, looking west.

C. Cross-section interpretation 828 mE of the West Block Area, looking west.

D. Cross-section interpretation 918 mE of the Ridge Zone North orebody, looking west.

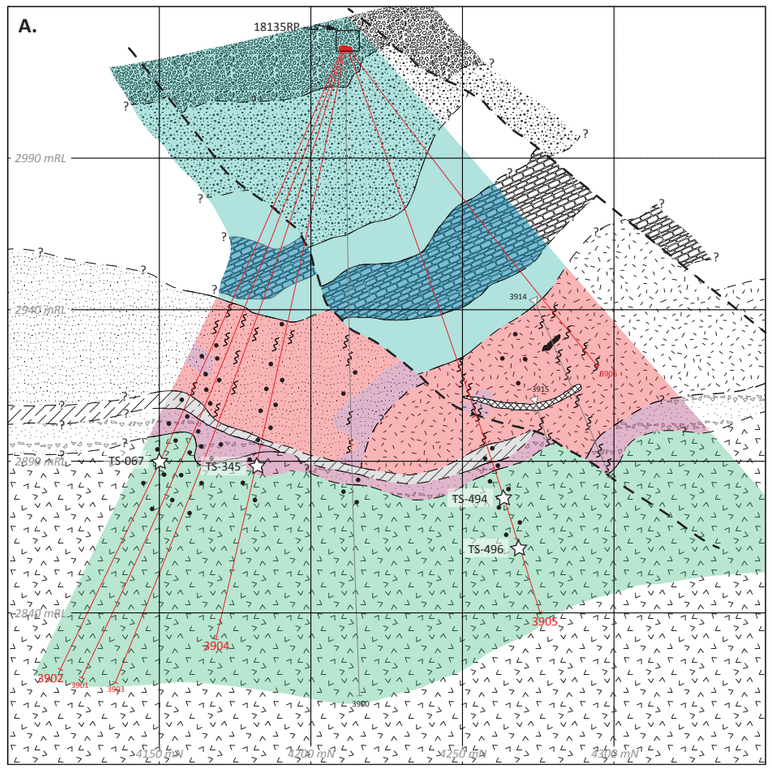

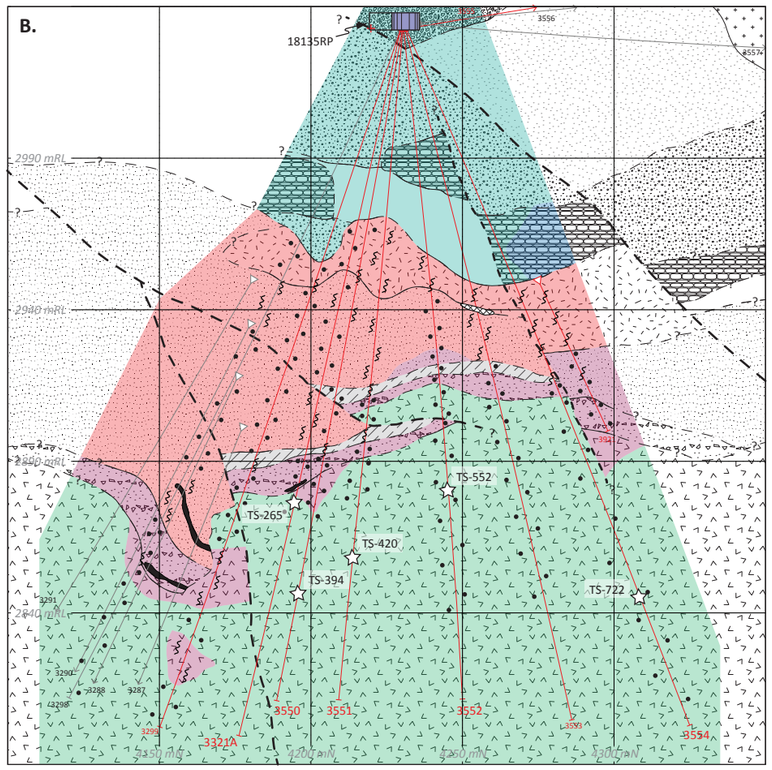

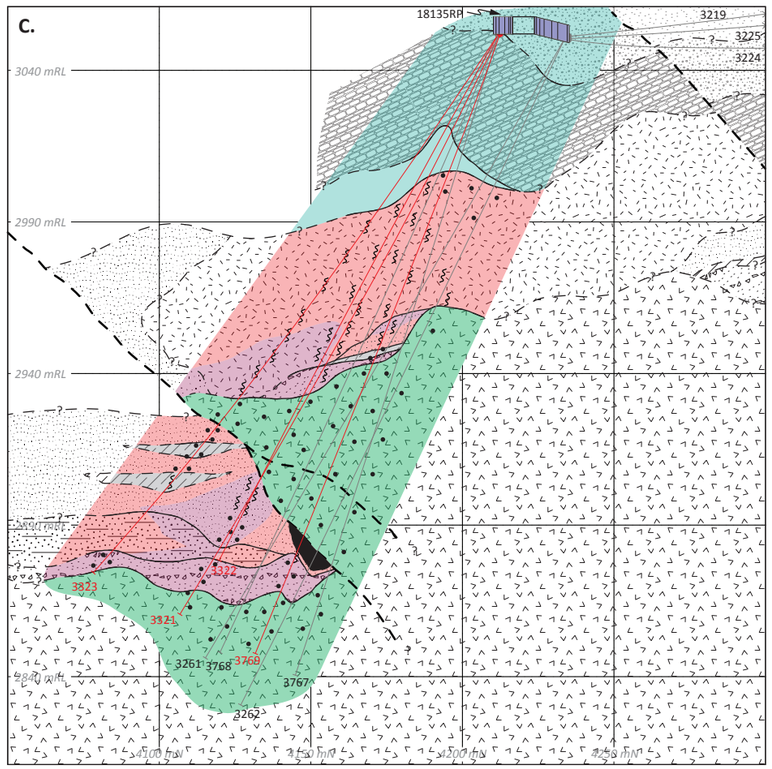

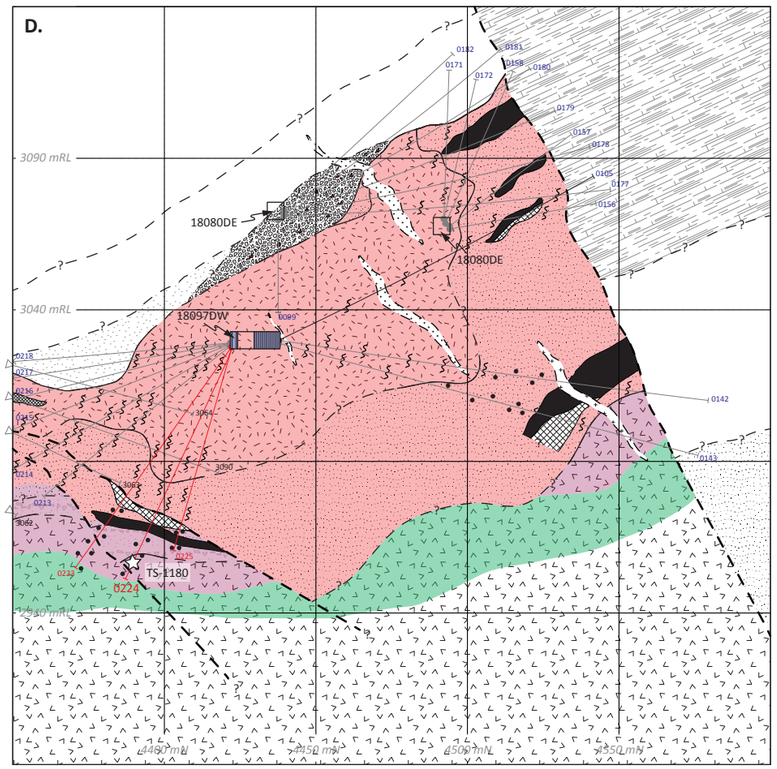

Figure 5.15:
Alteration Facies Cross-Section Interpretations

Lithology

- mafic dyke

Hanging Wall Andesite Member

- andesitic siltstone-sandstone
- massive andesitic sandstone
- polylithic volcaniclastic conglomerate
- polylithic volcaniclastic sandstone
- polylithic volcaniclastic conglomerate w/ sulfide clasts
- massive siltstone

Price Formation

- andesite

H-W Member

- coherent andesite
- coherent rhyolite
- rhyolitic volcaniclastic siltstone, sandstone and autobreccia
- bedded, massive chert and argillite
- laminated to thinly bedded argillite
- polylithic volcaniclastic sandstone and conglomerate

Mineralisation Textures

- disseminated sulfide
- stringer-style sulfide
- semi-massive (50-75% sulfide)
- massive (>75% sulfide)

Alteration Facies

- chlorite-calcite
- chlorite-calcite-epidote
- sericite-quartz-pyrite
- quartz (silicification)
- chlorite-sericite ± pyrite
- chlorite-calcite-pyrite
- chlorite-rich

Cross-Section Location Map

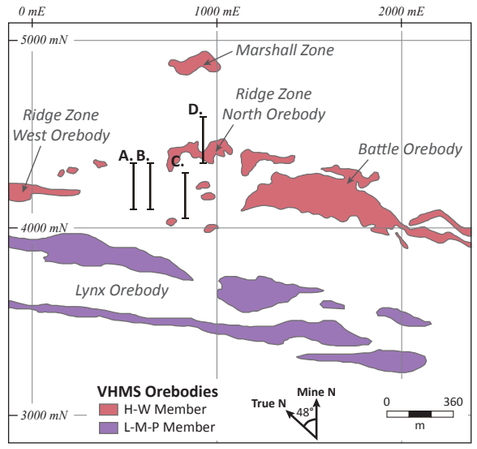

Annotations

- EMP & lithogeochemistry sample location (*this study*)
- younging direction
- interpreted contact
- interpreted fault

Underground Drill Holes

- SWIR analysed drill holes (*this study*)

Underground Workings

- 18135RP

Section Layout and Orientation

0 30 metres

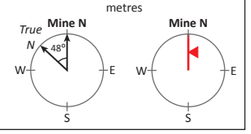

Figure 5.16 Numerical model interpretation of the white mica AlOH absorption feature wavelength. The wavelength position of the AlOH absorption feature is a proxy for K-mica composition (Figure 5.13B). In general, short AlOH wavelengths of less than 2,190 nm suggest paragonite, while wavelengths between 2,190-2,215 suggest muscovite, and long AlOH wavelengths of >2,215 nm suggest phengite (Pontual et al., 1997). Cross-sections show detailed geology (patterns) and sulfide mineralisation textures (symbols) interpreted from detailed graphic logs (red drill hole stems) and historic drill logs (grey drill hole stems). Data for the numerical model are from red drill stems only. Refer to the plan map in the legend for the locations of cross-sections.

A. Cross-section interpretation 550 mE of the West Block Area, looking west.

B. Cross-section interpretation 640 mE of the West Block Area, looking west.

C. Cross-section interpretation 828 mE of the West Block Area, looking west.

D. Cross-section interpretation 918 mE of the Ridge Zone North orebody, looking west.

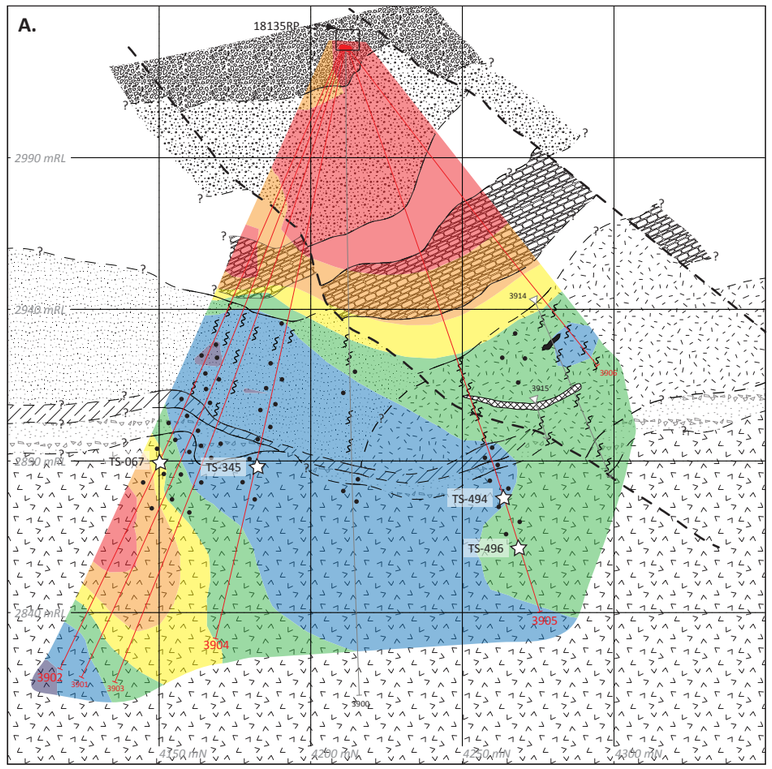

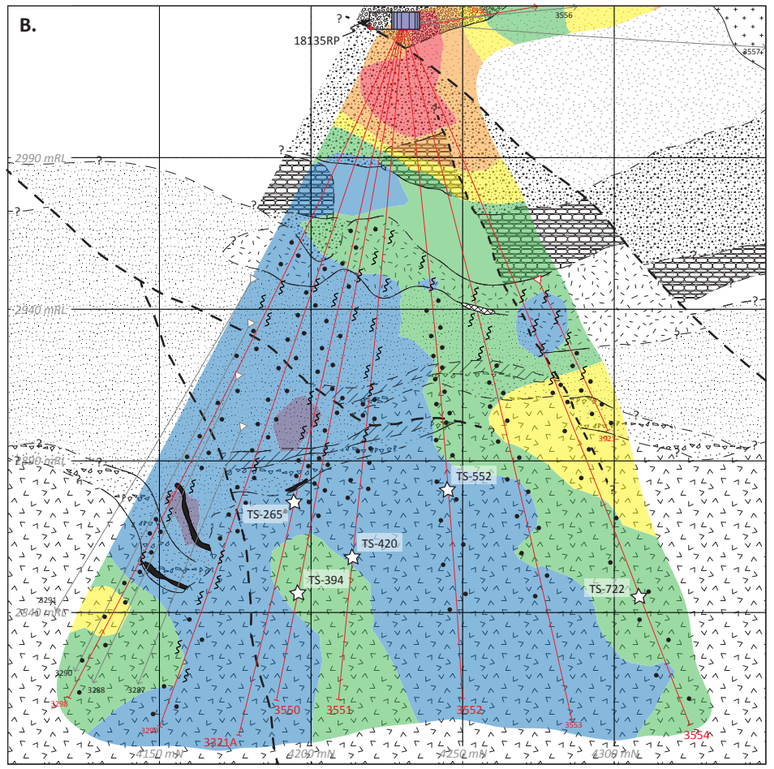

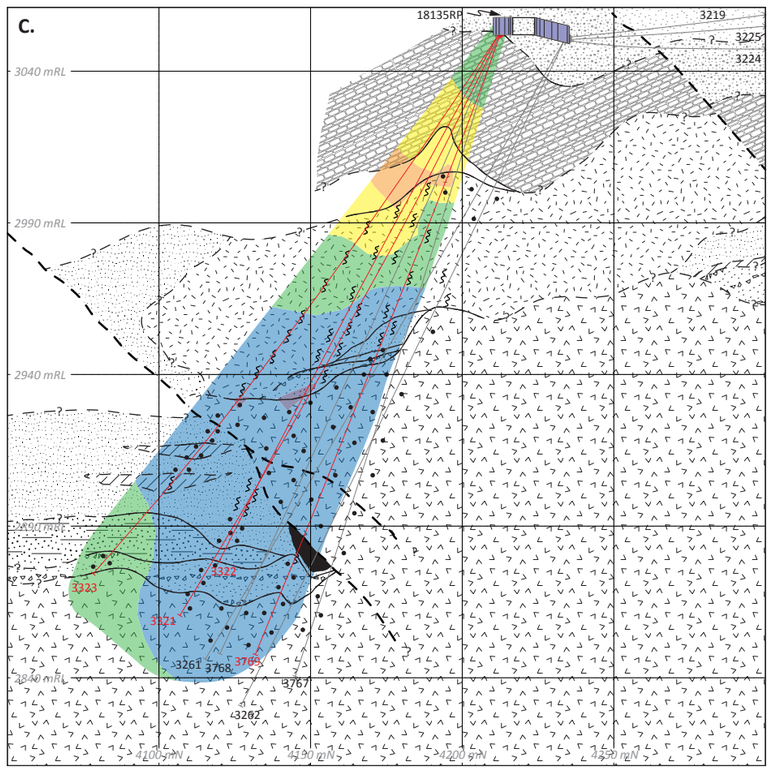

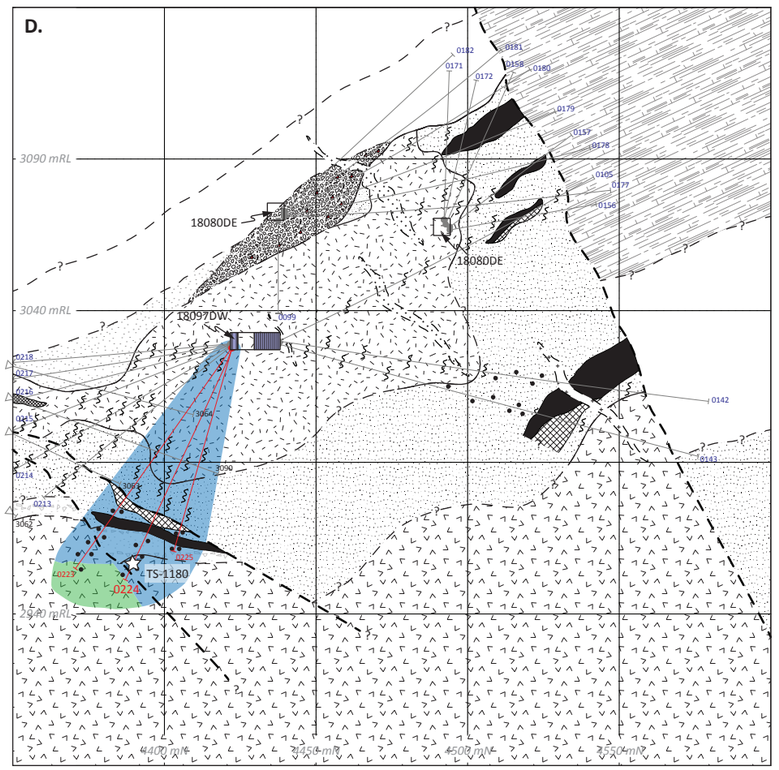

Figure 5.16:
Distribution of AlOH Absorption Feature Wavelength

Lithology

- mafic dyke

Hanging Wall Andesite Member

- andesitic siltstone-sandstone
- massive andesitic sandstone
- polylithic volcaniclastic conglomerate
- polylithic volcaniclastic sandstone
- polylithic volcaniclastic conglomerate w/ sulfide clasts
- massive siltstone

Price Formation

- andesite

H-W Member

- coherent andesite
- coherent rhyolite
- rhyolitic volcaniclastic siltstone, sandstone and autobreccia
- bedded, massive chert and argillite
- laminated to thinly bedded argillite
- polylithic volcaniclastic sandstone and conglomerate

Mineralisation Textures

- disseminated sulfide
- stringer-style sulfide
- semi-massive (50-75% sulfide)
- massive (>75% sulfide)

AlOH Absorption Feature Wavelength

- <2,197.5 nm
- 2,197.5 - 2,200.0 nm
- 2,200.0 - 2,202.5 nm
- 2,202.5 - 2,205.0 nm
- 2,205.0 - 2,210.0 nm
- >2,210.0 nm

Cross-Section Location Map

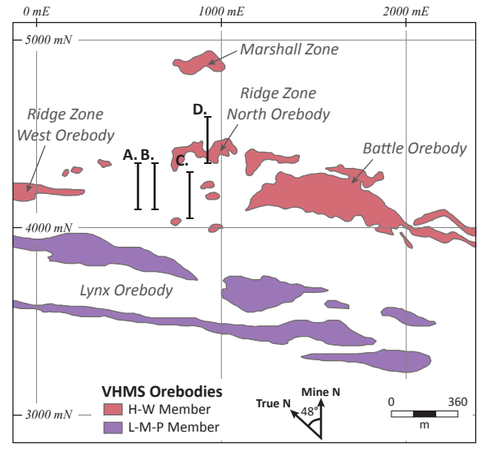

Annotations

- EMP & lithogeochemistry sample location (*this study*)
- younging direction
- interpreted contact
- interpreted fault

Underground Drill Holes

- SWIR analysed drill holes (*this study*)

Underground Workings

- 18135RP

Section Layout and Orientation

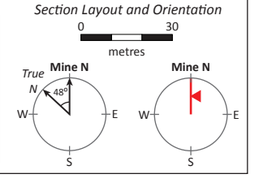

Figure 5.17 Numerical model interpretation of the chlorite FeOH absorption feature wavelength. The wavelength position of the FeOH absorption feature is a proxy for chlorite composition (Figure 5.13A). In general, FeOH absorption feature wavelengths <2,240 nm suggest Mg-rich chlorite, wavelengths between 2,240-2,255 nm suggest intermediate Fe-Mg chlorite, and wavelengths >2,255 nm suggest Fe-rich chlorite mineral compositions (Pontual et al., 1997). Cross-sections show detailed geology (patterns) and sulfide mineralisation textures (symbols) interpreted from detailed graphic logs (red drill hole stems) and historic drill logs (grey drill hole stems). Data for the numerical model are from red drill stems only. Refer to the plan map in the legend for the locations of cross-sections.

A. Cross-section interpretation 550 mE of the West Block Area, looking west.

B. Cross-section interpretation 640 mE of the West Block Area, looking west.

C. Cross-section interpretation 828 mE of the West Block Area, looking west.

D. Cross-section interpretation 918 mE of the Ridge Zone North orebody, looking west.
Insufficient data for numerical model.

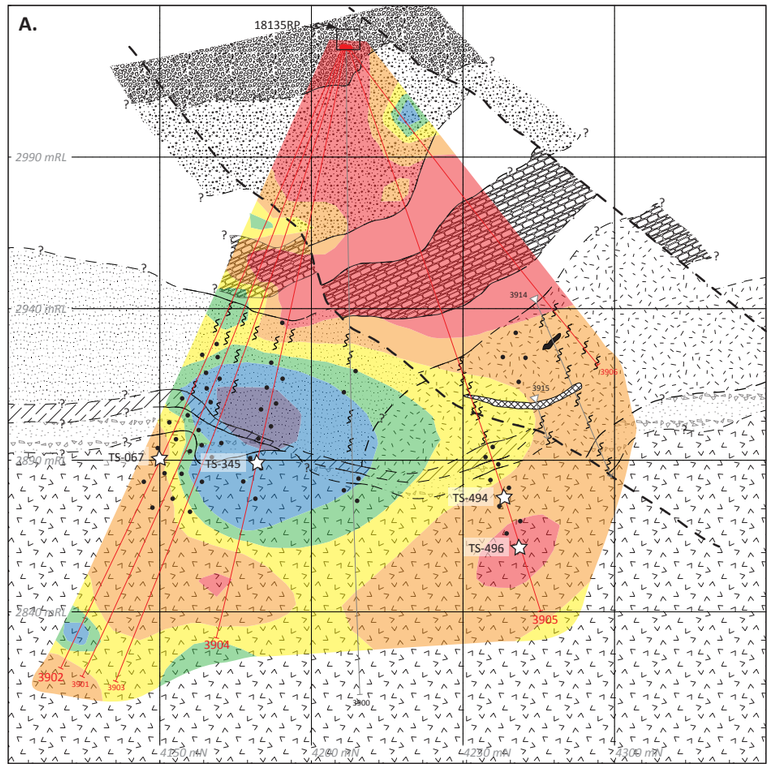

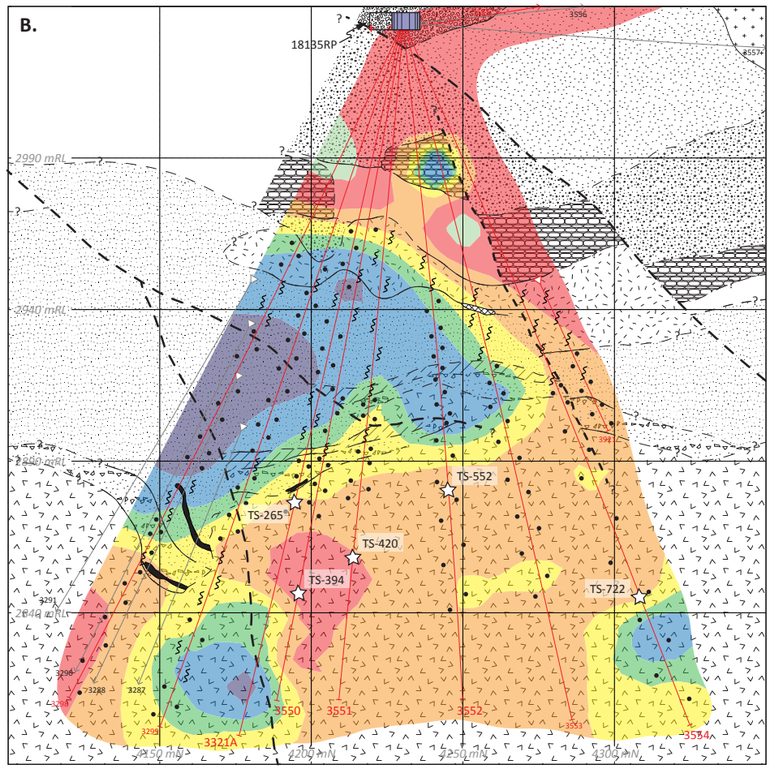

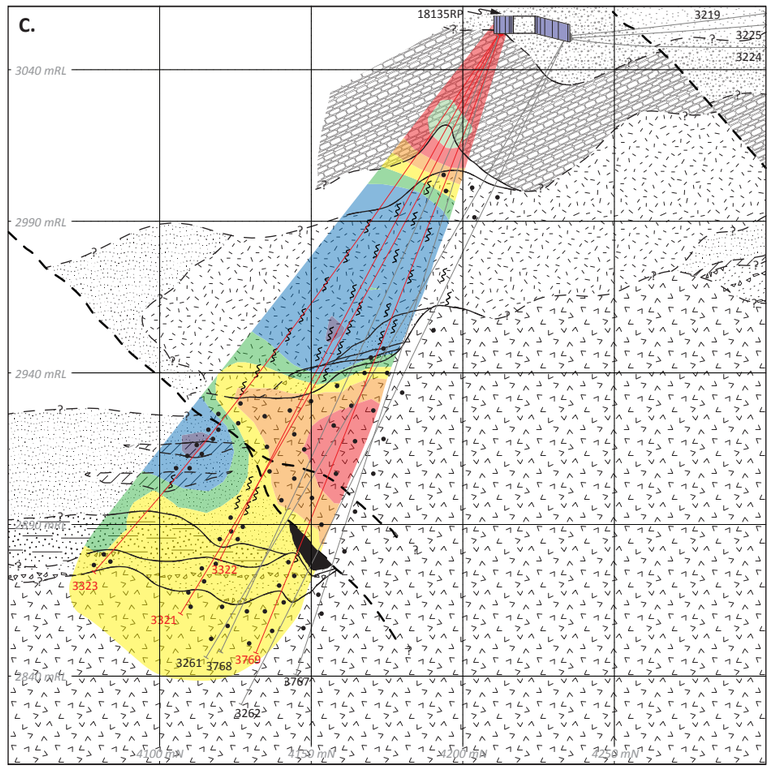

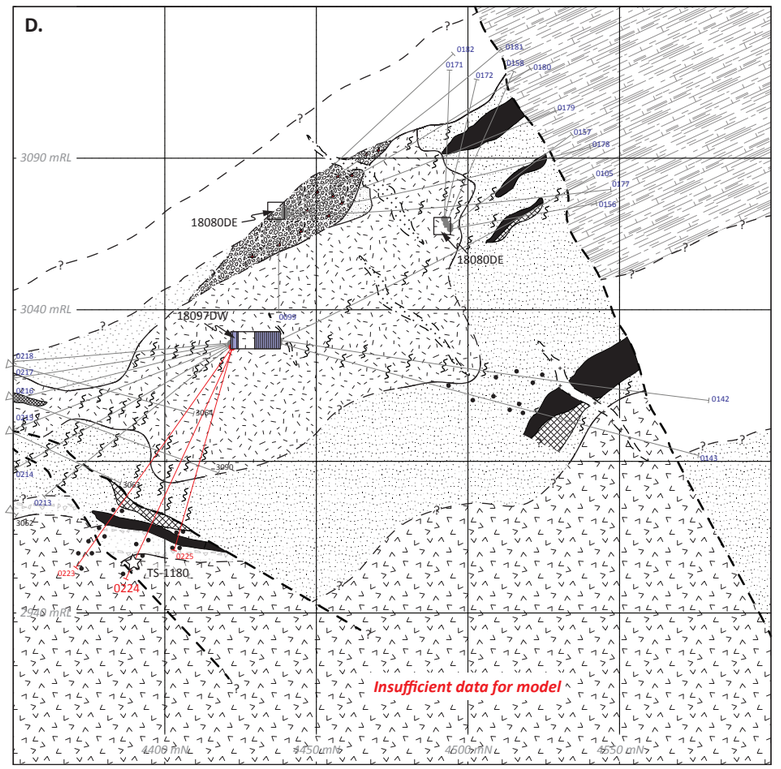

Figure 5.17:
Distribution of FeOH Absorption Feature Wavelength

Lithology

- mafic dyke
- *Hanging Wall Andesite Member*
  - andesitic siltstone-sandstone
  - massive andesitic sandstone
  - polylithic volcaniclastic conglomerate
  - polylithic volcaniclastic sandstone
  - polylithic volcaniclastic conglomerate w/ sulfide clasts
  - massive siltstone
- *Price Formation*
  - andesite
- *H-W Member*
  - coherent andesite
  - coherent rhyolite
  - rhyolitic volcaniclastic siltstone, sandstone and autobreccia
  - bedded, massive chert and argillite
  - laminated to thinly bedded argillite polylithic volcaniclastic sandstone and conglomerate

Mineralisation Textures

- disseminated sulfide
- stringer-style sulfide
- semi-massive (50-75% sulfide)
- massive (>75% sulfide)

FeOH Absorption Feature Wavelength

- 2,235.0 - 2,240.0 nm
- 2,240.0 - 2,245.0 nm
- 2,245.0 - 2,247.5 nm
- 2,247.5 - 2,250.0 nm
- 2,250.0 - 2,252.5 nm
- 2,252.5 - 2,255.0 nm

Cross-Section Location Map

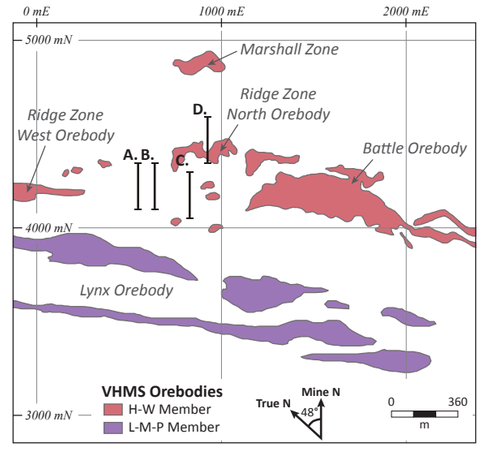

Annotations

- EMP & lithogeochemistry sample location (*this study*)
- younging direction
- interpreted contact
- interpreted fault
- *Underground Drill Holes*
  - SWIR analysed drill holes (*this study*)
- *Underground Workings*
  - 18135RP
- *Section Layout and Orientation*
  - 0 30 metres
  - True N, Mine N, 48°
  - W, E, S

Figure 5.18 Identified SWIR alteration mineral domains. Numerical model interpretation of the AlOH to MgOH depth ratio. The depth ratio is a proxy for chlorite and white mica mineral abundance (Clark et al., 1990; Pontual et al., 1997; Thompson et al., 1999; Figure 5.14) and used to map chlorite-dominant, white mica-dominant, and mixed chlorite-white mica alteration domains. Cross-sections show detailed geology (patterns) and sulfide mineralisation textures (symbols) interpreted from detailed graphic logs (red drill hole stems) and historic drill logs (grey drill hole stems). Data for the numerical model are from red drill stems only. Refer to the plan map in the legend for the locations of cross-sections.

A. Cross-section interpretation 550 mE of the West Block Area, looking west.

B. Cross-section interpretation 640 mE of the West Block Area, looking west.

C. Cross-section interpretation 828 mE of the West Block Area, looking west.

D. Cross-section interpretation 918 mE of the Ridge Zone North orebody, looking west.

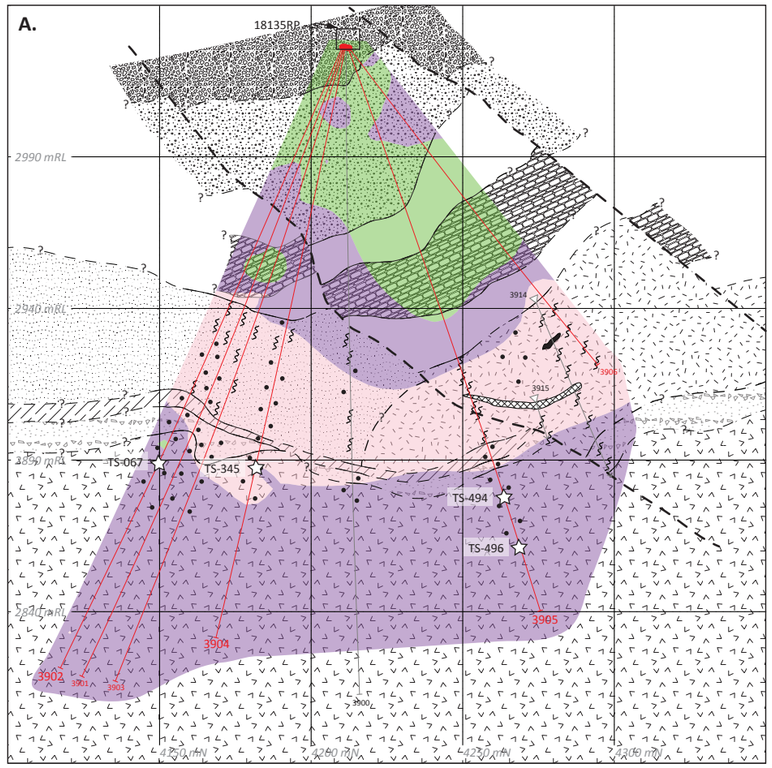

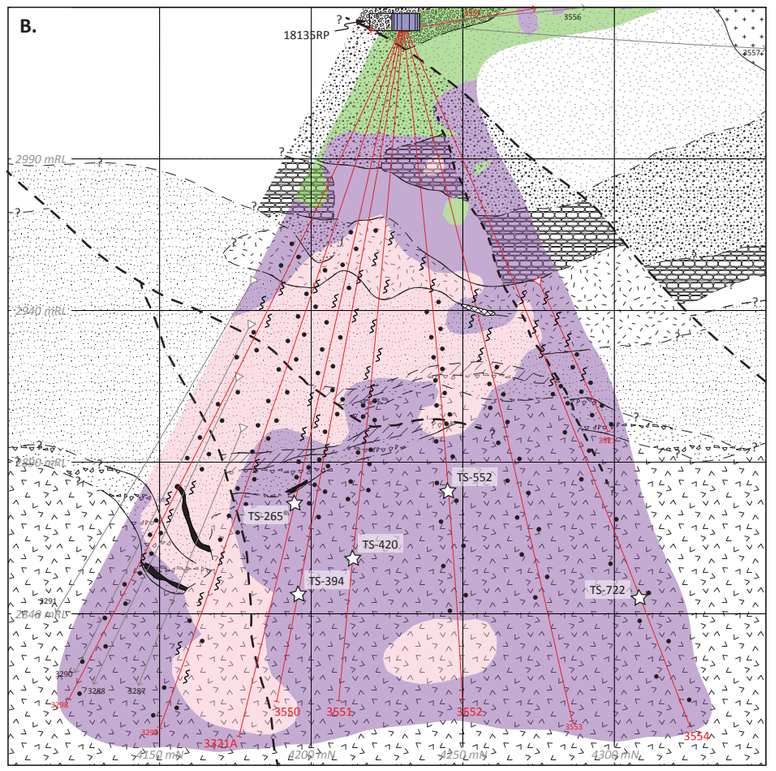

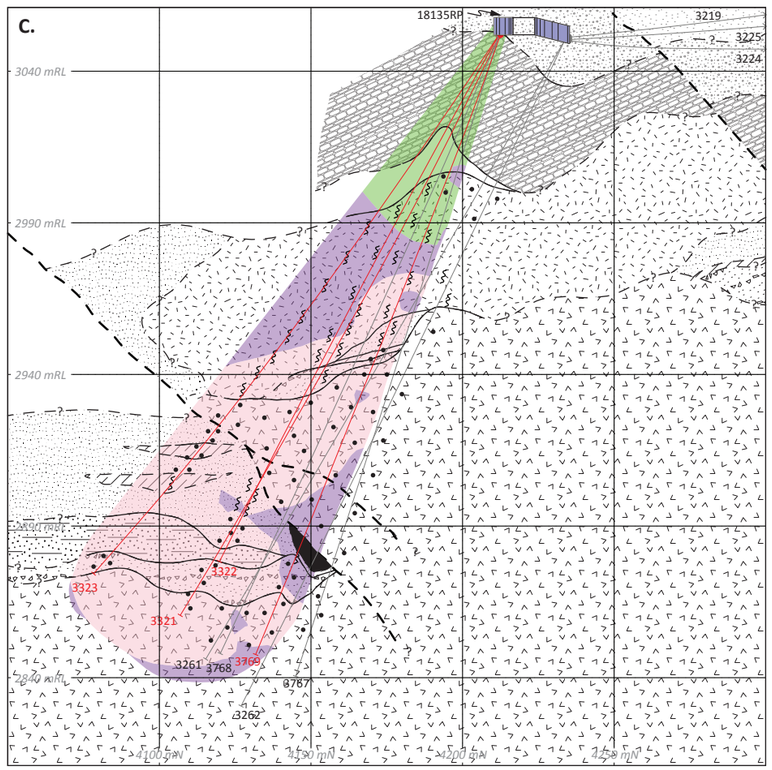

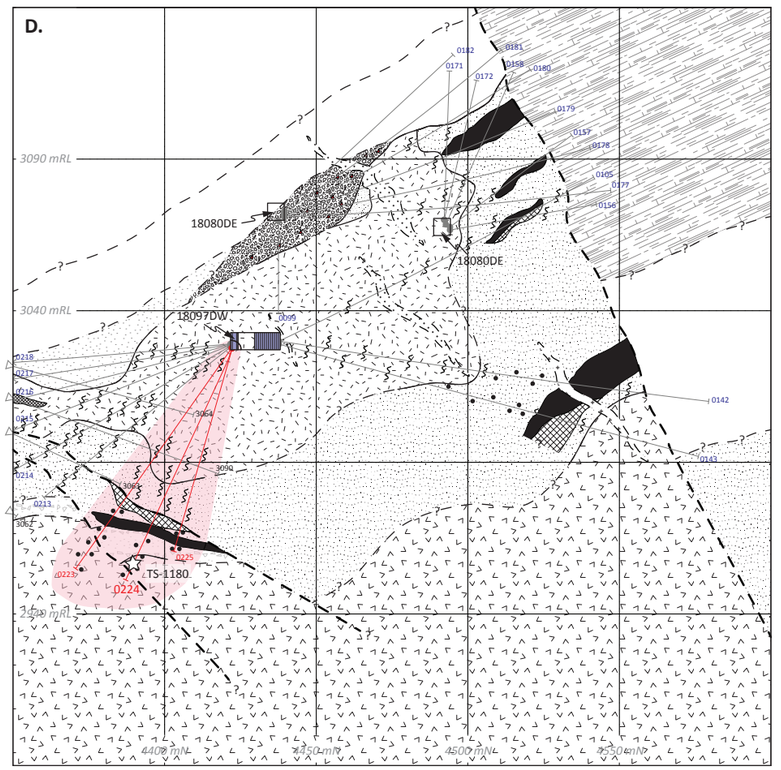

Figure 5.18:
Distribution of SWIR-Active Mineral Domain

Lithology

- mafic dyke

Hanging Wall Andesite Member

- andesitic siltstone-sandstone
- massive andesitic sandstone
- polylithic volcaniclastic conglomerate
- polylithic volcaniclastic sandstone
- polylithic volcaniclastic conglomerate w/ sulfide clasts
- massive siltstone

Price Formation

- andesite

H-W Member

- coherent andesite
- coherent rhyolite
- rhyolitic volcaniclastic siltstone, sandstone and autobreccia
- bedded, massive chert and argillite
- laminated to thinly bedded argillite
- polylithic volcaniclastic sandstone and conglomerate

Mineralisation Textures

- disseminated sulfide
- stringer-style sulfide
- semi-massive (50-75% sulfide)
- massive (>75% sulfide)

SWIR Alteration Mineral Domains

2,200 depth / 2,320 depth (AlOH and MgOH depth ratio)

- <0.45 → chlorite dominant
- >1.8 → white mica dominant
- 0.45-1.8 → chlorite & white mica

Cross-Section Location Map

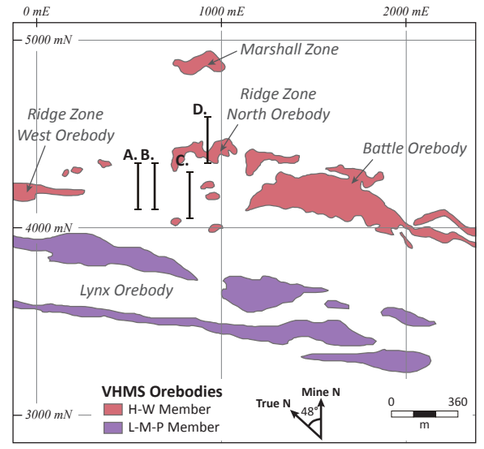

Annotations

- EMP & lithogeochemistry sample location (*this study*)
- younging direction
- interpreted contact
- interpreted fault

Underground Drill Holes

- SWIR analysed drill holes (*this study*)

Underground Workings

- 18135RP

Section Layout and Orientation

0 30 metres

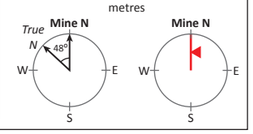

5.9 Discussion

5.9.1 Footwall alteration zone mineralogical and geochemical proximity indicators

A laterally continuous (~1,500 metres), footwall alteration zone extends beneath the West Block Area and the Battle and Ridge Zone North orebodies. The alteration of the Price Formation andesite comprises a variety of phyllosilicate-dominant alteration facies with a range of mineralogical and whole-rock geochemical signatures.

Least-altered andesite is characterised by pervasive, texturally non-destructive, chlorite-calcite ± epidote alteration, which is emblematic of metamorphic and/or diagenetic alteration of the paleo-seafloor (e.g., Dimroth and Lichtblau, 1979; Gifkins, 2001). Moderate alteration of andesite, defined from the West Block Area, consists of pervasive, chlorite-calcite-pyrite and chlorite-sericite alteration facies. Whilst, intense hydrothermal alteration of the immediate footwall to the Ridge Zone North and Battle orebodies comprise feldspar destructive, sericite-quartz-pyrite, chlorite-rich and chlorite-sericite-pyrite alteration facies. The observed breakdown of primary feldspar and addition of phyllosilicates and sulfides in the Price Formation footwall alteration zone is typical of circulating, hot, mildly acidic fluids in VHMS hydrothermal systems (e.g., Large, 1977; Franklin et al., 1981; Gifkins et al., 2005).

Some mineralogical parameters show well-constrained correlations with proximity to "contact zone" position sulfide mineralisation at Myra Falls. For example, the Fe/Fe+Mg ratio of chlorite decreases from 0.49-0.27 to <0.20 with proximity to ore (Figure 5.19). While, in general, K-mica compositions shift from phengitic to muscovitic with proximity to ore, with corresponding Fe+Mg values of >0.6 to <0.4, respectively (Figure 5.19). Carbonates do not show a systematic change in mineralogy or chemistry (Table 5.5) with proximity to ore and, therefore, are not considered a robust exploration indicator at Myra Falls.

The SWIR signatures also vary with proximity, with short AlOH and FeOH absorption feature wavelengths associated with intense footwall alteration immediately below the Battle and the Ridge Zone North orebodies (Figure 5.19). With increasing distance from ore, the AlOH and FeOH absorption features become longer (Figure 5.19). At Myra Falls, SWIR spectral results correlate with EMP mineral chemistry. For white mica, the AlOH wavelength strongly correlates with Fe+Mg values and the FeOH wavelength moderately correlates with the Fe/Fe+Mg ratio of chlorite (Figure 5.13). Therefore, inferred alteration mineral chemistry from systematic SWIR analysis of altered Price Formation can be used to map prospective VHMS hydrothermal alteration facies. The investigation by Jones et al. (2005) of the alteration zone above the Battle and HW orebodies recognised a similar application with assessing hydrothermally altered rocks of the H-W member.

It appears that the most robust proximity indicators from the footwall alteration zone are lithogeochemical. These include elevated CCPI, AI, Rb/Sr, S and depleted Na_2O values (Figure 5.7; Table 5.6). For example, the AI values increase from background values of <40 to values >80 in altered andesite within 50 metres below the Battle and Ridge Zone North orebodies (Figure 5.19). Similarly, Rb/Sr ratios increase from <0.1 to >1.0 with proximity to "contact zone" position, massive sulfide mineralisation (Figure 5.19). Significant, depletion of Na_2O and varied enrichment of S relative to background values are typical of andesite proximal to ore (Figure 5.19). Portable-XRF (pXRF) analysers are now providing a rapid and inexpensive alternative for the acquisition of lithogeochemical data (e.g., Peter et al., 2009). In Chapter 6, pXRF analysis is investigated to discriminate protolith using immobile elements.

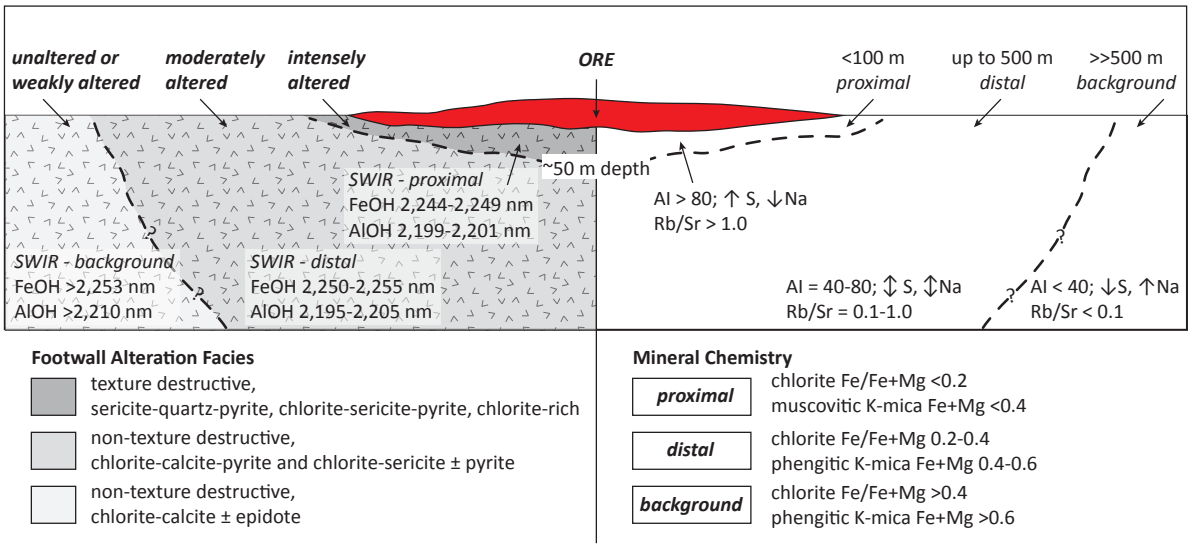

Figure 5.19 Summary of mineralogical and geochemical proximity indicators to "contact zone" position massive sulfide mineralisation of the Battle and Ridge Zone North orebodies. The Alteration Index and Rb/Sr values from whole-rock geochemistry produce the most robust results, while the SWIR and mineral chemistry show overlapping trends. Proximal and distal alteration halos can be distinguished in the footwall alteration zone of the Price Formation andesite. Background mineralogical and geochemical signatures are defined form the Thelwood Valley samples, signatures inferred to be within 500 metres of ore are defined form the West Bock Area, and signatures within 100 metres to ore are defined from below the Battle and Ridge Zone North orebodies. [geochemical changes are relative to the background samples = ↑, elevated; ↓, depleted; ↕, variable]

5.9.2 Application of SWIR spectroscopy

Although, whole-rock geochemistry and mineral chemistry provide robust proximity indicators at Myra Falls, these methods suffer from high analytical cost and extensive time lag between sample collection and results. Shortwave infrared spectroscopy of host rocks in VHMS deposits has been utilised to map fine-grained and, sometimes, cryptic alteration facies. For example, the wavelength of the AlOH absorption feature has been used to identify spatial relationships of ore with the composition of white mica (Huston et al., 1999) and the AlOH to FeOH depth ratio has been used as a proxy for white mica and chlorite alteration intensities (Herrmann et al., 2001). Jones et al. (2005) identified zones of intense hydrothermal alteration in felsic stratigraphy above the Battle and HW orebodies. These zones are characterised by AlOH and FeOH absorption features of <2,197 nm and <2,240 nm, respectively. Similar results for altered Price Formation andesite and felsic stratigraphy of the H-W member are reported in this study for the West Block Area and the Ridge Zone North orebody.

Electron microprobe results from this study, and those from Jones et al. (2005), illustrate that SWIR spectroscopy can be used as a proxy to infer phyllosilicate mineral chemistry. Samples with muscovitic K-mica have SWIR AlOH absorption features <2,201 nm and Mg-rich chlorite has FeOH wavelengths <2,250 nm (Figure 5.13). In addition, SWIR spectroscopy can be used to go beyond phyllosilicate mineral identification at Myra Falls. The depth ratio of the AlOH to MgOH absorption features is used as a proxy for phyllosilicate mineral abundance (Figure 5.14). The relative abundance of white mica to chlorite combined with the SWIR inferred mineral chemistry of phyllosilicate alteration minerals, is a new and an important exploration tool at Myra Falls (Figure 5.20).

"Upper zone" position sulfide mineralisation is hosted in variably altered, felsic volcanic and volcaniclastic rocks, with zones of massive sulfide coincident with autoclastic rhyolite

stratigraphy at the base of coherent rhyolite (*see Chapter 4*). Sericite-quartz-pyrite alteration facies is ubiquitous, however SWIR results vary with proximity. Within 100 metres of "upper zone" position sulfide mineralisation, FeOH and AlOH absorption features are <2,240 nm and <2,197 nm, and have white mica dominant AlOH/MgOH depth ratio values >1.8 (Figure 5.20). Up to 500 metres away from "upper zone" position sulfide mineralisation the FeOH and AlOH absorption wavelengths become longer and AlOH/MgOH depth ratio values remain white mica dominant (Figure 5.20).

"Contact zone" position sulfide mineralisation is associated with the top of the Price Formation andesite and massive sulfide zones are capped by fine-grained felsic volcaniclastic rocks and chert (*see Chapter 4*). Sericite-quartz-pyrite and chlorite-sericite-pyrite alteration facies occur in the immediate footwall of the Battle and Ridge Zone North orebodies, respectively. Within 100 metres of "contact zone" position sulfide mineralisation, FeOH and AlOH absorption wavelengths are <2,249 nm and <2,201 nm, respectively (Figure 5.20). With increasing distance away from "contact zone" position sulfide mineralisation, the FeOH and AlOH wavelengths become longer in altered andesite of the Price Formation (Figure 5.20). The AlOH/MgOH depth ratio shows that proximal to "contact zone" position sulfide mineralisation white mica is dominant (depth ratio >1.8) while in the distal environment, chlorite and white mica are mixed (depth ratio from 0.45-1.8) in andesite of the footwall alteration zone (Figure 5.20).

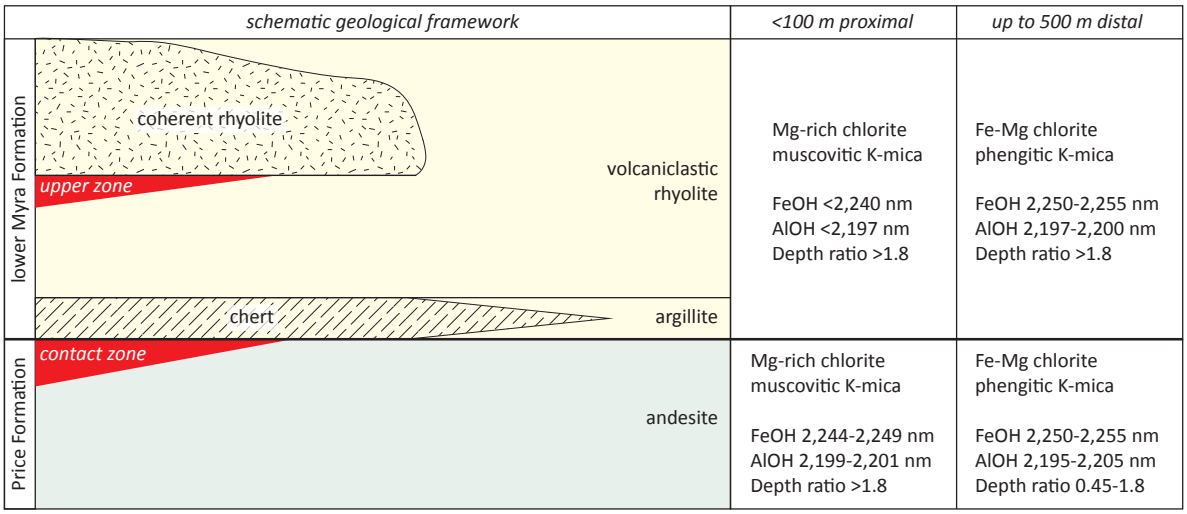

Figure 5.20 Summary of SWIR spectral signatures with proximity to "contact zone" position and "upper zone" position massive sulfide mineralisation. Proximal SWIR signatures are defined from new data from the Ridge Zone North orebody and the published data from the Battle orebody (Jones et al., 2005). Distal SWIR signatures are defined from new data from the West Block Area. Depth ratios of the AlOH (2,200 nm) and MgOH (2,320 nm) absorption features; <0.45 = chlorite dominant, 0.45-1.8 = mixed chlorite and white mica, and >1.8 = white mica dominant.

5.10 Summary

The Price Formation andesite footwall alteration zone comprises a number of phyllosilicate-dominant alteration facies with a range of mineralogical and lithogeochemical characteristics. As these mineralogical and lithogeochemical alteration trends change systematically relative to the position of ore, they can be used in the exploration for other VHMS deposits within the Myra Falls district.

Three alteration intensities were identified in the footwall alteration zone:

- Weak alteration is characterised by a pervasive, texturally non-destructive, chlorite-calcite ± epidote alteration facies; prominent in samples from the Thelwood Valley.
- Moderate alteration consists of pervasive, texturally non-destructive, chlorite-calcite-pyrite and chlorite-sericite alteration facies; both facies are prominent in andesite below sporadic sulfide mineralisation in the West Block Area.
- Intense alteration comprises feldspar-destructive, sericite-quartz-pyrite, chlorite-rich and chlorite-sericite pyrite alteration facies; prominent in andesite below semi-massive and massive sulfide mineralisation in the Battle and Ridge Zone North orebodies.

Ore proximity indicators from mineral chemistry of the footwall alteration zone include:

- The Fe/Fe+Mg of chlorite decreases from 0.49-0.27 in least to moderately altered andesite to <0.20 in intensely altered andesite immediately below ore.
- In general, K-mica compositions shift from phengitic in least-altered andesite to muscovitic in intensely altered andesite proximal to ore.

Ore proximity indicators from lithogeochemistry of the footwall alteration zone include:

- Least-altered footwall alteration has elevated Na_2O, Rb/Sr <0.1, and moderate AI and CCPI values that plot in the diagenetic field of the alteration box plot.
- Proximal, within 100 metres to ore, footwall alteration has depleted Na_2O (≤0.75 wt. %), variably elevated S (<16.0 wt. %), Rb/Sr >1.0, AI values >80, and CCPI values from 35-95.
- Distal, up to 500 metres away from ore, footwall alteration has variable Na_2O and S values, and Rb/Sr from 0.1-1.0. The AI and CCPI values plot in the hydrothermal alteration field on the alteration box plot and form an array from the least-altered andesite field to the chlorite-pyrite and white mica fields.

The mineral chemistry and whole-rock geochemistry results of the Price Formation footwall alteration zone provide proximity to ore indicators at Myra Falls. However, these methods are time consuming and expensive. Portable-XRF analysers provide an opportunity to acquire rapid and cost-effective lithogeochemical data, and is assessed in Chapter 6. Results from systematic SWIR spectroscopy, illustrate the potential application of SWIR combined with alteration facies logging and mapping.

Inferred mineral chemistry from SWIR analysis:

- Chlorite EMP results have a moderate, positive correlation with chlorite FeOH absorption wavelengths from SWIR analysis. Chlorite with FeOH wavelengths <2,249 nm from Myra Falls are considered Mg-rich chlorite, while wavelengths >2,249 nm are inferred as intermediate Fe-Mg chlorite.
- White mica EMP results have a strong, positive correlation with white mica AlOH absorption wavelengths from SWIR analysis. White mica with AlOH wavelengths <2,200 nm are considered muscovitic K-mica, while wavelengths >2,200 nm are inferred as phengitic K-mica.

Ore proximity indicators from SWIR spectroscopy include:

- Proximal, within 100 metres to ore, H-W member alteration has chlorite FeOH wavelength <2,240 nm (Mg-rich chlorite), white mica AlOH wavelength <2,197 nm (muscovitic K-mica), and AlOH/MgOH depth ratio values >1.8 (white mica dominant SWIR results).
- Distal, up to 500 metres to ore, H-W member alteration has chlorite FeOH wavelengths from 2,250-2,255 nm (intermediate Fe-Mg chlorite), white mica AlOH wavelengths from 2,197-2,200 nm (muscovitic K-mica), and AlOH/MgOH depth ratio values >1.8 (white mica dominant SWIR results).
- Proximal, within 100 metres to ore, Price Formation alteration has chlorite FeOH wavelengths from 2,244-2,249 nm (Mg-rich chlorite), white mica AlOH wavelengths from 2,199-2,201 nm (muscovitic K-mica), and AlOH/MgOH depth ratio values >1.8 (white mica dominant SWIR results).
- Distal, up to 500 metres to ore, Price Formation alteration has chlorite FeOH wavelengths from 2,250-2,255 nm (intermediate Fe-Mg chlorite), white mica AlOH wavelengths from 2,195-2,205 nm (muscovitic to phengitic K-mica), and AlOH/MgOH depth ratio values from 0.45-1.8 (mixed chlorite and white mica SWIR results).

Table 5.3 Price Formation andesite average chlorite EMP results.

Sample ID	**143640**	**143682**	**143700**	**TS-265**	**TS-394**	**TS-420**	**TS-552**	**TS-722**
Section (mE)	5880	1420	1420	640	640	640	640	640
Area	Thelwood	Battle	Battle	WBA	WBA	WBA	WBA	WBA
n	5	2	2	26	12	11	5	4
Reformatted oxide percentages based on 28 oxygens (with Fe^{2+}/Fe^{3+} and OH calculated assuming full site occupancy)								
SiO_2	25.45	26.74	27.30	25.71	24.65	25.72	25.21	25.16
TiO_2	0.04	0.02	0.00	0.05	0.06	0.05	0.03	0.07
Al_2O_3	21.07	23.18	23.74	23.24	21.94	23.12	23.01	22.50
Cr_2O_3	0.01	0.02	0.00	0.01	0.01	0.01	0.02	0.01
Fe_2O_3	0.02	0.65	0.87	0.28	0.02	0.39	0.32	0.17
FeO	23.44	10.06	7.52	21.00	25.14	18.08	20.43	22.47
MnO	0.35	0.63	0.61	0.48	0.42	0.56	0.54	0.67
MgO	16.67	24.62	26.80	17.64	14.85	19.21	17.33	16.22
ZnO	0.06	0.13	0.04	0.13	0.21	0.11	0.17	0.31
CaO	0.11	0.03	0.01	0.01	0.02	0.01	0.02	0.04
Na_2O	0.06	0.02	0.01	0.06	0.02	0.02	0.05	0.03
K_2O	0.03	0.02	0.01	0.03	0.04	0.02	0.06	0.06
BaO	0.01	0.05	0.04	0.01	0.01	0.01	0.02	0.01
F	0.09	0.30	0.47	0.05	0.03	0.09	0.04	0.04
Cl	0.01	0.01	0.01	0.01	0.00	0.00	0.02	0.02
H_2O	11.33	11.78	11.89	11.71	11.27	11.65	11.52	11.45
Total	98.71	98.13	99.11	100.39	98.69	99.03	98.78	99.20
Number of ions on the basis of 28 oxygens								
Si $^{(iv)}$	5.33	5.27	5.24	5.23	5.22	5.24	5.21	5.24
Al $^{(iv)}$	2.67	2.73	2.76	2.77	2.78	2.76	2.79	2.76
Al $^{(vi)}$	2.54	2.68	2.65	2.82	2.71	2.80	2.83	2.77
Ti	0.01	0.00	0.00	0.01	0.01	0.01	0.01	0.01
Cr	0.00	0.00	0.00	0.00	0.00	0.00	0.00	0.00
Fe^{3+}	0.00	0.10	0.12	0.04	0.00	0.06	0.05	0.03
Fe^{2+}	4.14	1.66	1.21	3.58	4.47	3.08	3.54	3.91
Mn	0.06	0.10	0.10	0.08	0.08	0.10	0.09	0.12
Mg	5.20	7.23	7.67	5.35	4.69	5.83	5.34	5.03
Zn	0.01	0.02	0.01	0.02	0.03	0.02	0.03	0.05
Ca	0.03	0.01	0.00	0.00	0.00	0.00	0.00	0.01
Na	0.05	0.02	0.01	0.05	0.01	0.01	0.04	0.02
K	0.02	0.01	0.01	0.01	0.02	0.01	0.03	0.03
Ba	0.00	0.01	0.01	0.00	0.00	0.00	0.00	0.00
Total	20.05	19.84	19.78	19.96	20.04	19.92	19.97	19.98
F	0.12	0.37	0.57	0.06	0.04	0.12	0.05	0.06
Cl	0.00	0.00	0.01	0.01	0.00	0.00	0.01	0.01
OH	15.88	15.63	15.42	15.93	15.96	15.88	15.93	15.93
Fe/Fe+Mg	0.44	0.20	0.15	0.40	0.49	0.35	0.40	0.44
Mineral	ripidolite	sheridanite	sheridanite	ripidolite	ripidolite	ripidolite	ripidolite	ripidolite

Table 5.3 Continued.

Sample ID	**TS-683**	**TS-788**	**TS-067**	**TS-345**	**TS-494**	**TS-496**	**MF18853**	**MF19908**
Section (mE)	585	585	550	550	550	550	25	-60
Area	WBA	WBA	WBA	WBA	WBA	WBA	RZW	RZW
n	14	17	9	5	1	4	1	2
Reformatted oxide percentages based on 28 oxygens (with Fe^{2+}/Fe^{3+} and OH calculated assuming full site occupancy)								
SiO_2	25.61	26.01	26.30	26.02	26.50	25.93	26.91	24.80
TiO_2	0.04	0.04	0.03	0.06	0.02	0.04	0.05	0.09
Al_2O_3	22.85	21.74	22.68	22.89	23.54	22.56	22.07	21.51
Cr_2O_3	0.01	0.01	0.00	0.01	0.00	0.00	0.02	0.02
Fe_2O_3	0.32	0.62	0.21	0.41	0.35	0.42	0.28	0.00
FeO	18.52	20.64	16.78	14.09	15.83	20.89	12.49	23.66
MnO	0.45	0.59	0.56	0.46	0.51	0.69	0.50	0.41
MgO	18.94	17.17	20.92	22.04	21.28	17.54	23.58	15.52
ZnO	0.23	0.15	0.12	0.12	0.14	0.23	0.07	0.14
CaO	0.02	0.03	0.05	0.00	0.01	0.01	0.02	0.07
Na_2O	0.02	0.02	0.00	0.02	0.04	0.03	0.00	0.06
K_2O	0.04	0.05	0.02	0.00	0.07	0.05	0.08	0.10
BaO	0.01	0.02	0.02	0.02	0.00	0.00	0.01	0.02
F	0.08	0.09	0.12	0.19	0.08	0.11	0.09	0.00
Cl	0.01	0.01	0.01	0.00	0.03	0.01	0.00	0.01
H_2O	11.59	11.44	11.77	11.65	11.95	11.59	11.85	11.24
Total	98.68	98.58	99.56	97.92	100.29	100.06	97.98	97.66
Number of ions on the basis of 28 oxygens								
$Si^{(iv)}$	5.24	5.39	5.29	5.25	5.26	5.29	5.39	5.28
$Al^{(iv)}$	2.76	2.61	2.71	2.75	2.74	2.71	2.61	2.72
$Al^{(vi)}$	2.77	2.72	2.67	2.71	2.79	2.74	2.61	2.68
Ti	0.01	0.01	0.01	0.01	0.00	0.01	0.01	0.01
Cr	0.00	0.00	0.00	0.00	0.00	0.00	0.00	0.00
Fe^{3+}	0.05	0.10	0.03	0.06	0.05	0.06	0.04	0.00
Fe^{2+}	3.17	3.58	2.82	2.38	2.63	3.57	2.09	4.23
Mn	0.08	0.10	0.10	0.08	0.09	0.12	0.09	0.07
Mg	5.78	5.30	6.27	6.62	6.30	5.34	7.04	4.92
Zn	0.03	0.02	0.02	0.02	0.02	0.04	0.01	0.02
Ca	0.00	0.01	0.01	0.00	0.00	0.00	0.00	0.02
Na	0.01	0.02	0.00	0.01	0.03	0.03	0.00	0.05
K	0.02	0.03	0.01	0.00	0.03	0.03	0.04	0.05
Ba	0.00	0.00	0.00	0.00	0.00	0.00	0.00	0.00
Total	19.94	19.88	19.95	19.90	19.94	19.92	19.95	20.06
F	0.11	0.11	0.15	0.24	0.09	0.14	0.11	0.00
Cl	0.01	0.01	0.01	0.00	0.02	0.01	0.00	0.01
OH	15.88	15.88	15.84	15.76	15.89	15.85	15.89	15.99
Fe/Fe+Mg	0.36	0.41	0.31	0.27	0.30	0.41	0.23	0.46
Mineral	ripidolite	ripidolite	ripidolite	ripidolite	ripidolite	ripidolite	ripidolite	ripidolite

[Fm, formation; mbr, member; RZN, RZW, Ridge Zone West; WBA, West Block Area]

Table 5.4 Price Formation andesite average white mica EMP results.

Sample ID	143640	143682	143700	TS-1180	TS-265	TS-394	TS-420	TS-552
Section (mE)	5880	1420	1420	918	640	640	640	640
Area	Thelwood	Battle	Battle	RZN	WBA	WBA	WBA	WBA
n	2	8	9	6	8	7	11	4
SiO_2	47.02	44.91	45.43	45.21	45.93	45.19	45.92	45.70
TiO_2	0.12	0.15	0.09	0.25	0.18	0.29	0.17	0.18
Al_2O_3	31.53	35.80	37.14	34.78	35.67	33.72	35.49	35.68
FeO	3.07	0.77	0.41	1.20	2.27	3.29	1.54	1.57
MnO	0.02	0.01	0.02	0.01	0.02	0.02	0.02	0.01
MgO	1.66	0.87	0.78	1.16	0.96	0.84	0.94	0.84
CaO	0.06	0.01	0.02	0.02	0.01	0.00	0.01	0.01
Na_2O	0.49	0.55	0.61	0.42	0.64	0.46	0.67	0.76
K_2O	10.33	10.44	10.37	10.27	9.68	9.98	9.82	9.63
SrO	0.00	0.01	0.00	0.00	0.01	0.01	0.01	0.00
BaO	0.66	0.45	0.31	0.93	0.34	0.44	0.31	0.32
ZnO	0.00	0.01	0.02	0.02	0.02	0.03	0.02	0.01
F	0.14	0.14	0.15	0.25	0.04	0.08	0.09	0.04
Cl	0.00	0.00	0.01	0.02	0.00	0.00	0.00	0.00
Cr_2O_3	0.00	0.01	0.01	0.01	0.01	0.01	0.00	0.02
H_2O*	4.36	4.37	4.44	4.30	4.49	4.36	4.44	4.46
O=F,Cl	0.06	0.06	0.07	0.11	0.02	0.03	0.04	0.02
Total	99.46	98.52	99.81	98.86	100.27	98.72	99.45	99.24
Number of ions on the basis of 28 oxygens								
Si	6.37	6.07	6.04	6.12	6.10	6.16	6.14	6.12
Al $^{(iv)}$	1.63	1.93	1.96	1.88	1.90	1.84	1.86	1.88
Al $^{(vi)}$	3.40	3.78	3.85	3.68	3.69	3.57	3.73	3.74
Ti	0.01	0.02	0.01	0.03	0.02	0.03	0.02	0.02
Cr	0.00	0.00	0.00	0.00	0.00	0.00	0.00	0.00
Fe	0.35	0.09	0.05	0.14	0.25	0.38	0.17	0.18
Mn	0.00	0.00	0.00	0.00	0.00	0.00	0.00	0.00
Mg	0.34	0.18	0.15	0.23	0.19	0.17	0.19	0.17
Zn	0.00	0.00	0.00	0.00	0.00	0.00	0.00	0.00
Ca	0.01	0.00	0.00	0.00	0.00	0.00	0.00	0.00
Na	0.13	0.14	0.16	0.11	0.17	0.12	0.17	0.20
K	1.79	1.80	1.76	1.78	1.64	1.73	1.67	1.64
Sr	0.00	0.00	0.00	0.00	0.00	0.00	0.00	0.00
Ba	0.04	0.02	0.02	0.05	0.02	0.02	0.02	0.02
OH*	3.94	3.94	3.93	3.89	3.98	3.97	3.96	3.98
F	0.06	0.06	0.06	0.11	0.02	0.03	0.04	0.02
Cl	0.00	0.00	0.00	0.00	0.00	0.00	0.00	0.00
Total	18.06	18.03	18.00	18.02	17.99	18.03	17.97	17.97
Na/Na+K	0.07	0.07	0.08	0.06	0.09	0.07	0.09	0.11
Fe/Fe+Mg	0.51	0.33	0.23	0.37	0.57	0.69	0.48	0.51
Mineral	phengitic	muscovitic	muscovitic	muscovitic	phengitic	phengitic	phengitic	phengitic

Table 5.4 Continued.

Sample ID	TS-722	TS-683	TS-788	TS-067	TS-494	TS-496	MF18853	MF19908
Section (mE)	640	585	585	550	550	550	25	-60
Area	WBA	WBA	WBA	WBA	WBA	WBA	RZW	RZW
n	8	13	5	13	7	6	8	1
SiO_2	45.68	46.05	47.84	46.22	45.95	46.15	45.90	46.24
TiO_2	0.21	0.15	0.11	0.28	0.21	0.16	0.40	0.38
Al_2O_3	34.25	35.21	33.13	34.37	36.09	35.01	32.33	31.62
FeO	2.52	1.64	1.44	1.98	1.38	1.91	1.61	2.22
MnO	0.01	0.01	0.03	0.02	0.04	0.02	0.02	0.01
MgO	0.77	0.83	1.46	1.28	1.29	1.06	1.93	1.52
CaO	0.05	0.02	0.10	0.01	0.04	0.01	0.02	0.07
Na_2O	0.56	0.83	0.58	0.42	0.57	0.59	0.33	0.54
K_2O	9.91	9.52	8.83	10.18	9.36	9.66	10.81	10.41
SrO	0.01	0.01	0.01	0.00	0.00	0.01	0.01	0.05
BaO	0.46	0.38	0.39	0.29	0.35	0.43	0.35	0.40
ZnO	0.03	0.02	0.03	0.03	0.03	0.02	0.02	0.00
F	0.10	0.09	0.16	0.10	0.07	0.12	0.10	0.00
Cl	0.01	0.00	0.00	0.00	0.01	0.01	0.00	0.09
Cr_2O_3	0.00	0.01	0.01	0.01	0.01	0.01	0.01	0.00
H_2O*	4.38	4.43	4.40	4.43	4.49	4.43	4.34	0.02
O=F,Cl	0.05	0.04	0.07	0.04	0.03	0.05	0.04	0.04
Total	98.94	99.22	98.53	99.60	99.87	99.59	98.18	97.88
Number of ions on the basis of 28 oxygens								
Si	6.18	6.17	6.40	6.19	6.09	6.17	6.26	6.34
Al $^{(iv)}$	1.82	1.83	1.60	1.81	1.91	1.83	1.74	1.66
Al $^{(vi)}$	3.64	3.72	3.63	3.62	3.74	3.69	3.46	3.44
Ti	0.02	0.02	0.01	0.03	0.02	0.02	0.04	0.04
Cr	0.00	0.00	0.00	0.00	0.00	0.00	0.00	0.00
Fe	0.28	0.18	0.16	0.22	0.15	0.21	0.18	0.25
Mn	0.00	0.00	0.00	0.00	0.00	0.00	0.00	0.00
Mg	0.15	0.17	0.29	0.26	0.25	0.21	0.39	0.31
Zn	0.00	0.00	0.00	0.00	0.00	0.00	0.00	0.00
Ca	0.01	0.00	0.01	0.00	0.01	0.00	0.00	0.01
Na	0.15	0.22	0.15	0.11	0.15	0.15	0.09	0.14
K	1.71	1.63	1.51	1.74	1.58	1.65	1.88	1.82
Sr	0.00	0.00	0.00	0.00	0.00	0.00	0.00	0.00
Ba	0.02	0.02	0.02	0.02	0.02	0.02	0.02	0.02
OH*	3.95	3.96	3.93	3.96	3.97	3.95	3.96	3.96
F	0.04	0.04	0.07	0.04	0.03	0.05	0.04	0.04
Cl	0.00	0.00	0.00	0.00	0.00	0.00	0.00	0.00
Total	17.99	17.96	17.80	17.99	17.93	17.96	18.08	18.05
Na/Na+K	0.08	0.12	0.09	0.06	0.08	0.08	0.04	0.07
Fe/Fe+Mg	0.65	0.52	0.36	0.46	0.38	0.50	0.32	0.45
Mineral	phengitic	phengitic	muscovitic	phengitic	muscovitic	phengitic	muscovitic	phengitic

Calculations for H_2O* and OH* after Tindle and Webb (1990).
[Fm, formation; mbr, member; RZN, Ridge Zone North; RZW, Ridge Zone West; WBA, West Block Area]

Table 5.5 Price Formation andesite average carbonate EMP results.

Sample ID	143640	TS-1180		TS-394	TS-420	TS-552	TS-722
Section (mE)	5880	918		640	640	640	640
Area	Thelwood	RZN		WBA	WBA	WBA	WBA
n	3	3	3	2	4	6	8
SiO_2 (%)	<0.04	<0.04	<0.04	<0.04	<0.04	0.04	<0.04
FeO (%)	0.58	4.82	0.33	1.38	6.64	8.30	0.52
MnO (%)	0.70	2.39	5.05	1.71	6.76	5.40	2.68
MgO (%)	0.30	15.56	0.69	0.63	11.85	12.28	0.58
CaO (%)	53.78	30.05	51.49	50.11	29.03	28.04	50.45
SrO (%)	0.05	0.09	0.19	0.05	0.05	0.07	0.06
BaO (%)	<0.07	<0.07	<0.07	<0.07	<0.07	<0.07	<0.07
CO_2 (%)	44.05	46.22	43.23	44.33	44.98	45.04	44.22
ZnO (%)	<0.07	<0.07	<0.07	<0.07	<0.07	<0.07	<0.07
Total	99.46	99.12	101.04	98.21	99.31	99.16	98.50
Number of ions on the basis of 3 oxygens							
Si	0.00	0.00	0.00	0.00	0.00	0.00	0.00
Fe^{2+}	0.01	0.06	0.00	0.02	0.09	0.11	0.01
Mn	0.01	0.03	0.07	0.02	0.09	0.08	0.04
Mg	0.01	0.37	0.02	0.02	0.29	0.30	0.01
Ca	0.96	0.51	0.92	0.90	0.51	0.49	0.91
Sr	0.00	0.00	0.00	0.00	0.00	0.00	0.00
Ba	0.00	0.00	0.00	0.00	0.00	0.00	0.00
C	1.01	1.01	0.99	1.02	1.01	1.01	1.02
Zn	0.00	0.00	0.00	0.00	0.00	0.00	0.00
Total	1.99	1.99	2.01	1.98	1.99	1.99	1.98
FeO+MnO	1.28	7.21	5.38	3.09	13.40	13.69	3.20
Mineral	calcite	dolomite	calcite	calcite	dolomite	dolomite	calcite

Table 5.5 Continued.

Sample ID	TS-788		TS-067	TS-494	TS-496	TS-345	MF18853
Section (mE)	585		550	550	550	550	25
Area	WBA		WBA	WBA	WBA	WBA	RZW
n	6	1	8	13	6	12	9
SiO_2 (%)	<0.04	<0.04	<0.04	0.04	0.06	<0.04	<0.04
FeO (%)	7.50	0.26	0.91	5.33	7.57	0.58	0.54
MnO (%)	5.29	4.80	2.54	6.32	8.62	2.96	2.48
MgO (%)	11.73	0.09	0.80	13.38	10.88	0.63	0.78
CaO (%)	29.33	49.05	51.61	28.94	27.84	52.49	52.58
SrO (%)	0.05	0.05	0.06	0.05	<0.05	0.05	0.05
BaO (%)	<0.07	<0.07	<0.07	<0.07	<0.07	<0.07	<0.07
CO_2 (%)	45.08	44.01	43.85	45.35	44.47	43.63	43.74
ZnO (%)	<0.07	<0.07	<0.07	<0.07	<0.07	<0.07	<0.07
Total	99.03	98.26	99.76	99.41	99.44	100.35	100.16
Number of ions on the basis of 3 oxygens							
Si	0.00	0.00	0.00	0.00	0.00	0.00	0.00
Fe^{2+}	0.10	0.00	0.01	0.07	0.10	0.01	0.01
Mn	0.07	0.07	0.04	0.09	0.12	0.04	0.04
Mg	0.29	0.00	0.02	0.32	0.27	0.02	0.02
Ca	0.52	0.89	0.93	0.50	0.49	0.94	0.94
Sr	0.00	0.00	0.00	0.00	0.00	0.00	0.00
Ba	0.00	0.00	0.00	0.00	0.00	0.00	0.00
C	1.01	1.02	1.00	1.01	1.00	1.00	1.00
Zn	0.00	0.00	0.00	0.00	0.00	0.00	0.00
Total	1.99	1.98	2.00	1.99	1.99	2.00	2.00
FeO+MnO	12.79	5.06	3.45	11.65	16.19	3.55	3.02
Mineral	dolomite	calcite	calcite	dolomite	dolomite	calcite	calcite

[Fm, formation; mbr, member; RZN, Ridge Zone North; RZW, Ridge Zone West; WBA, West Block Area]

Table 5.6 Price Formation andesite whole-rock geochemical results.

Sample ID	TS-067	TS-345	TS-494	TS-496	TS-683	TS-788	TS-420
Section (mE)	550	550	550	550	585	585	640
Area	WBA	WBA	WBA	WBA	WBA	WBA	WBA
Rock Type	andesite	andesite	andesite	andesite	andesite	andesite	andesite
SiO_2 (wt %)	52.69	51.99	57.19	54.88	60.01	50.66	48.54
Al_2O_3 (wt %)	20.53	22.65	19.56	17.71	18.17	21.83	16.08
$Fe_2O_3^{tot}$ (wt %)	5.25	7.21	3.99	8.4	5.48	7.51	13.84
CaO (wt %)	2.91	1.61	1.23	1.84	0.43	1.15	1.09
MgO (wt %)	4.6	2.37	4.59	5.19	4.75	5.11	5.66
Na_2O (wt %)	4.23	1.88	3.69	3.64	2.67	4.48	2.16
K_2O (wt %)	2.88	5.31	2.65	1.59	2.44	2.62	1.92
MnO (wt %)	0.28	0.1	0.27	0.57	0.13	0.29	0.36
TiO_2 (wt %)	0.97	1.02	0.82	0.81	0.77	1.1	0.71
P_2O_5 (wt %)	0.27	0.29	0.29	0.47	0.2	0.42	0.16
BaO (wt %)	0.08	0.19	0.1	0.07	0.09	0.12	0.06
SrO (wt %)	0.01	0.01	0.01	0.01	<0.01	0.01	<0.01
Cr_2O_3 (wt %)	0.01	<0.01	<0.01	<0.01	<0.01	<0.01	<0.01
LOI (wt %)	6.23	6.11	4.62	5.45	3.81	4.09	8.17
Total (wt %)	100.94	100.74	99.01	100.63	98.95	99.39	98.75
Total S (wt %)	0.64	4.07	0.08	0.85	0.11	0.65	6.34
Total C (wt %)	0.67	0.31	0.35	0.5	0.06	0.21	0.37
Zr (ppm)	79	94	127	73	114	98	65
Cr (ppm)	40	10	10	10	10	10	10
V (ppm)	304	289	124	222	214	287	238
Cu (ppm)	7	25	238	30	5	648	169
Pb (ppm)	6	51	23	10	6	11	10
Zn (ppm)	165	97	717	1010	1360	2710	213
Ti/Zr	73.6	65.1	38.7	66.5	40.5	67.3	65.5
Rb/Sr	0.34	0.92	0.42	0.26	0.54	0.35	0.57
AI	51	69	60	55	70	58	70
CCPI	57	55	56	71	65	63	82

Table 5.6 Continued.

Sample ID	TS-265	TS-394	TS-552	TS-722	TS-971	BM14-029	TS-1180
Section (mE)	640	640	640	640	700	828	918
Area	WBA	WBA	WBA	WBA	WBA	WBA	RZN
Rock Type	andesite	andesite	andesite	andesite	andesite	andesite	andesite
SiO_2 (wt %)	50.86	47.56	58.67	55.82	51.77	55.17	54.79
Al_2O_3 (wt %)	20.67	19.28	15.96	19.46	22.78	20.79	17.26
$Fe_2O_3^{tot}$ (wt %)	9.27	9.23	5.53	7.07	7.33	5.66	12.1
CaO (wt %)	1.37	5.36	2.26	1.56	1.46	1.57	0.89
MgO (wt %)	5.76	4.72	3.79	3.7	2.42	3.24	0.71
Na_2O (wt %)	3.11	3.15	4.22	5.37	2.96	2.52	0.24
K_2O (wt %)	2.6	2.35	1.5	1.72	4.8	4.04	5.26
MnO (wt %)	0.23	0.31	0.46	0.21	0.19	0.2	0.05
TiO_2 (wt %)	0.91	0.83	0.64	0.82	1	0.91	0.76
P_2O_5 (wt %)	0.4	0.24	0.23	0.39	0.17	0.13	0.25
BaO (wt %)	0.09	0.1	0.05	0.08	0.23	0.43	0.51
SrO (wt %)	0.01	0.02	0.01	0.01	0.01	0.01	0.01
Cr_2O_3 (wt %)	<0.01	0.01	<0.01	<0.01	<0.01	0.01	<0.01
LOI (wt %)	5.53	7.56	5.51	3.85	4.85	4.75	8.03
Total (wt %)	100.81	100.72	98.83	100.06	99.97	99.43	100.86
Total S (wt %)	1.01	0.07	0.72	0.87	2.46	2.07	8.79
Total C (wt %)	0.32	1.14	0.79	0.24	0.32	0.51	0.2
Zr (ppm)	80	72	99	78	90	82	114
Cr (ppm)	10	20	10	10	10	10	10
V (ppm)	282	259	103	233	364	301	114
Cu (ppm)	8	3	124	277	67	62	620
Pb (ppm)	9	7	6	4	4	8	604
Zn (ppm)	315	527	1020	1150	314	223	1740
Ti/Zr	68.2	69.1	38.8	63.0	66.6	66.5	40.0
Rb/Sr	0.41	0.27	0.21	0.28	0.82	0.71	1.67
AI	65	45	45	44	62	64	84
CCPI	71	70	61	59	54	56	68

[AI, Ishikawa Alteration Index; CCPI, Chlorite-Carbonate-Pyrite Index; Fm, formation; mbr, member; RZN, Ridge Zone North; RZW, WBA, West Block Area]

Table 5.7 Price Formation andesite MINSQ quantitative mineralogy results.

Sample ID	143640*	143682*	TS-1180	TS-265	TS-394	TS-420	TS-552
Section (mE)	5880	1420	918	640	640	640	640
Area	Thelwood	Battle	RZN	WBA	WBA	WBA	WBA
Alteration Indices							
AI	28	93	84	65	45	70	45
CCPI	66	79	68	71	70	82	61
Normative Mineralogy from MINSQ (wt. %)							
quartz	9.4	36.8	31.8	15.0	12.4	21.4	23.6
albite	38.0	0.1	-	23.7	25.3	17.1	34.8
k-feldspar	-	0.7	-	0.7	-	-	0.4
clinozoisite	3.0	n/a	n/a	n/a	n/a	n/a	n/a
muscovite	n/a	29.6	49.0	24.6	23.1	18.7	14.7
phengite	6.0	n/a	n/a	n/a	n/a	n/a	n/a
chlorite	24.6	23.4	-	30.3	28.8	26.9	16.9
apatite	0.6	0.2	0.6	0.6	0.6	0.4	0.5
calcite	9.2	-	-	1.3	9.4	-	0.5
dolomite	-	1.7	1.5	1.0	-	3.1	6.0
rutile	0.7	0.5	0.6	0.8	0.5	0.7	0.6
titanite	n/a	n/a	n/a	n/a	n/a	n/a	n/a
barite	-	-	-	-	-	-	0.2
epidote	7.1	-	-	-	-	-	-
pyrite	-	6.9	16.3	2.0	-	11.1	1.2
chalcopyrite	-	-	0.1	-	-	-	0.1
galena	-	-	-	-	-	0.1	-
sphalerite	-	-	0.1	-	-	0.3	0.2
Total	98.6	100.0	100.0	100.0	100.0	99.6	99.6
Residual SSQ	0.1	0.0	0.1	0.1	0.4	0.3	0.0

Table 5.7 Continued.

Sample ID	TS-722	TS-683	TS-788	TS-067	TS-345	TS-494	TS-496
Section (mE)	640	585	585	550	550	550	550
Area	WBA	WBA	WBA	WBA	WBA	WBA	WBA
Alteration Indices							
AI	44	70	58	51	69	60	55
CCPI	59	65	63	57	55	56	71
Normative Mineralogy from MINSQ (wt. %)							
quartz	12.0	28.0	5.6	11.2	17.7	19.2	20.1
albite	44.5	20.9	35.6	34.4	11.8	30.1	29.5
k-feldspar	-	0.6	-	-	-	0.9	-
clinozoisite	n/a	n/a	n/a	n/a	n/a	n/a	n/a
muscovite	16.9	24.3	28.4	27.3	57.0	26.1	16.1
phengite	n/a	n/a	n/a	n/a	n/a	n/a	n/a
chlorite	21.5	23.7	25.5	19.3	3.2	18.0	27.2
apatite	0.9	0.1	0.9	0.4	-	0.7	0.8
calcite	1.9	0.4	0.5	4.9	1.6	-	0.9
dolomite	-	0.3	1.0	0.5	-	2.8	3.0
rutile	0.7	0.7	1.0	0.8	-	0.8	0.7
titanite	n/a	n/a	n/a	n/a	1.2	n/a	-
barite	-	-	-	-	-	0.6	-
epidote	-	-	-	-	-	-	-
pyrite	1.5	0.1	1.2	1.3	7.5	0.2	1.8
chalcopyrite	-	-	-	-	-	-	-
galena	-	-	-	-	-	-	-
sphalerite	-	0.2	0.2	-	-	0.1	-
Total	100.0	99.2	100.0	100.0	100.0	99.3	100.0
Residual SSQ	0.1	0.0	0.1	0.1	1.5	0.0	0.2

*whole rock data from Sinclair (2000).
[AI, Ishikawa Alteration Index; CCPI, Chlorite-Carbonate-Pyrite Index; Fm, formation; RZN, Ridge Zone North; WBA, West Block Area]

Chapter 6:

Lithological discrimination of altered volcanic rocks – Application of systematic pXRF analysis of drill core

Lithological discrimination of altered volcanic rocks based on systematic portable X-ray fluorescence analysis of drill core at the Myra Falls VHMS deposit, Canada.

Published in full: McNulty, B.A., Fox, N., Berry, R.F., Gemmell, J.B., (2018), *Journal of Geochemical Exploration*, v 193, 1-21.

Lithogeochemistry is an effective tool used widely in petrologic, chemostratigraphic and hydrothermal alteration studies of the host rocks to VHMS deposits, with significant implications for exploration (MacLean and Barrett, 1993; Barrett and MacLean, 1999; Large et al., 2001c; Franklin et al., 2005; Galley et al., 2007; Piercey, 2010). Conventional laboratory-based X-ray fluorescence (XRF) analysis is an accepted technique for the acquisition of accurate and precise lithogeochemical data from bulk samples. However, this and other lab-based methods suffer from poor spatial resolution due to the high analytical costs, extensive time lag between sample collection and obtaining laboratory results, and the destructive nature of the sample preparation. Field-portable X-ray fluorescence (pXRF) analysers allow rapid, nondestructive analysis of drill core materials and are proving to be an effective, on site tool for the fit-for-purpose acquisition of lithogeochemical data in the mineral exploration industry (e.g., Morris, 2009; Peter et al., 2009; Gazley et al., 2011; Ross et al., 2014b; Le Vaillant et al., 2014).

Numerous investigations have been focused on the development of pXRF as an analytical tool in the field of lithogeochemistry. Specifically, studies have aimed to better understand the effect of grain size on analytical results (e.g., Potts et al., 1997; Forster et al., 2011); test the performance of different brands and models of pXRF analysers (e.g., Goodale et al., 2012; Brand and Brand, 2014; Ross et al., 2014a); and evaluate the application of pXRF in discriminating lithology, alteration and mineralisation in ore deposits (e.g., Morris, 2009; Gazley et al., 2011; Gazley et al., 2014; Le Vaillant et al., 2014; Mauriohooho et al., 2016).

Recent studies have focused on documenting the operation, calibration, data quality, and

independent testing of pXRF analysers in the mineral exploration industry (e.g., Fisher et al., 2014; Hall et al., 2014). The majority of previous pXRF studies were conducted on powdered rock samples, a sample preparation step that is time and labour consuming. A small number of studies have examined the applicability of pXRF analysis in VHMS deposits (Peter et al., 2009; Sack and Lewis, 2013; Piercey and Devine, 2014; Ross et al., 2014b; Ross et al., 2016); with only a few studies focused on the acquisition of pXRF lithogeochemical data from unprepared drill core samples. Bourke and Ross (2015) compared pXRF measurements on drill core samples with measurements on the corresponding drill core powders for 27 samples of fine- to medium-grained, mafic to felsic, unmineralised Precambrian volcanic and intrusive rocks from the Abitibi Greenstone Belt of Canada. Their study confirmed that averaging multiple measurements on different spots of the sample yielded, after correction, accurate and precise elemental results for many geological applications.

In this study, conventional XRF lithogeochemical results are compared with data collected with a pXRF instrument from both powdered samples and the surface of drill core from the H-W member of the Myra Falls VHMS district, Canada. A routine pXRF sampling methodology and data processing procedure is proposed, and estimates of correlation with each sample medium are presented to demonstrate that analysis from the surface of drill core samples produces accurate concentrations for some key lithogeochemical elements. Results are based on selected immobile elements and indicate that pXRF analysis can discriminate the protolith of hydrothermally altered volcanic rock types, and provide increased spatial resolution from systematic pXRF down-hole analyses with direct applications to mineral exploration.

6.1 Stratigraphic Relationships of the H-W Member

Simplified summaries of stratigraphic relationships for the H-W member in Figure 6.1 are based on a compilation of new and published lithological descriptions and geochemical data (Barrett and Sherlock, 1996; Robinson et al., 1996; Barrett and MacLean, 2000; Sinclair, 2000; Jones, 2001; Chong, 2004; Jones et al., 2006b; *Chapter 4*). A number of submarine coherent volcanic units are present in the lower Myra Formation and are included in the stratigraphic sequence. Representative, least-altered examples of rock types from the West Block Area are shown on Figure 6.2. The reader is referred to *Chapter 4* for more detail on the West Block Area stratigraphy.

The overall stratigraphic relationships are similar from east to west across the district. The top of the Price Formation marks the stratigraphic footwall to the H-W member. The Price Formation has a minimum thickness of 300 metres and is characterised by feldspar and pyroxene-phyric, amygdaloidal mafic lavas and associated autobreccias (Figure 6.2A-B; Juras, 1987). The lower Myra Formation is 50 to 250-metres-thick and consists of felsic volcanic and volcano-sedimentary rocks characterised by interlayered argillite, chert and felsic volcaniclastic rocks at its base with variably thick coherent rhyolite lavas and associated felsic volcaniclastic rocks towards the top (Figure 6.2D-F; Juras, 1987; Barrett and Sherlock, 1996; Sinclair, 2000; Jones, 2001). An exception to this "normal" stratigraphic sequence occurs in the West Block Area and Ridge Zone West localities. Here, the base of the Myra Formation is marked by a 10 to 90-metres-thick unit of graded sandstone to conglomerate, intercalated with polylithic volcaniclastic beds, referred to as the Basal Volcaniclastic Unit (Figure 6.2C; Chong, 2004). This unit is not observed near the Battle and HW orebodies, but has been noted in historic drill logs from the Marshall Zone orebody (Figure 6.1).

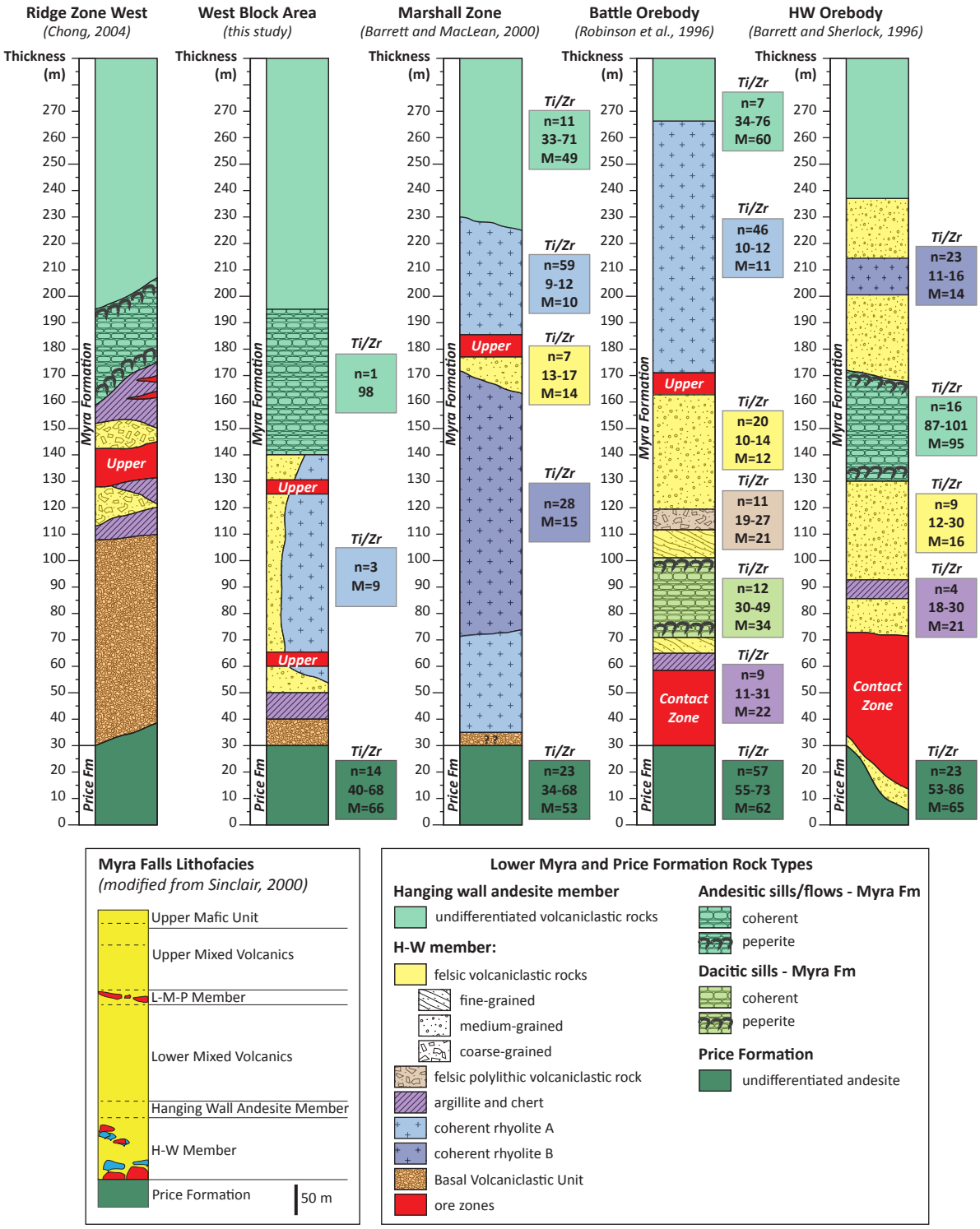

Figure 6.1 Simplified stratigraphic columns of the lower Myra Formation. Note the stratigraphic positions of "contact zone" position and "upper zone" position sulfide mineralisation and the east to west transition of coherent rhyolite and felsic volcaniclastic stratigraphy of the H-W member. [n, number of samples; M, median; Fm, formation]

The H-W member of the lower Myra Formation is laterally continuous for at least 5 kilometres. The felsic stratigraphy near the HW orebody is dominated by volcaniclastic and sedimentary rocks with less abundant coherent rhyolite (Juras, 1987). Whereas massive, coherent rhyolite flows and associated volcaniclastic rocks are present near the Battle orebody and West Block Area (Robinson et al., 1996; Sinclair, 2000; *Chapter 4*). The lower Myra Formation

thins to the west (50-100 m thick) and becomes increasingly interlayered with argillite, chert and felsic volcaniclastic rocks, with no coherent rhyolite near the Ridge Zone West orebody (Chong, 2004). The Marshall Zone orebody is located approximately 500 metres to the north of the West Block Area. Here the H-W member consists of stacked coherent, massive rhyolitic flows separated by felsic volcaniclastic rocks (Figure 6.1; Barrett and MacLean, 2000).

The Hanging Wall Andesite, the youngest member in the lower Myra Formation, is characterised by relatively unaltered, bedded, feldspar-crystal-rich volcaniclastic rocks with an andesitic composition (Sinclair, 2000). This lithofacies is observed immediately above the H-W member in the HW and Battle orebodies, and Marshall Zone orebody (Figure 6.1) and is characterised by polylithic pebblestone intercalated with intervals of normal to reverse graded pebbly sandstone and thickly bedded to laminated sandstone (Figure 6.2I-J). Lithic components are subangular to sub-rounded andesite with lesser rhyolite, argillite, chert and rare sulfide clasts (Juras, 1987; Barrett and MacLean, 2000; Sinclair, 2000).

A number of submarine volcanic sills and flows are present in the lower Myra Formation. Andesitic sills and flows are characterised by massive, feldspar and pyroxene-phyric cores with up to 15-metre-thick jig-saw-fit, curviplanar fragmental margins (Figure 6.2G-H). Near the HW orebody and the Ridge Zone West orebody, a series of andesitic units have 5 to 10-metre-thick peperitic margins and are interpreted to be sills (Juras, 1987; Barrett and Sherlock, 1996; Chong, 2004). Near the HW orebody a sill intrudes the H-W member while at the Ridge Zone West orebody, the sill intrudes at the contact between the H-W member and the Hanging Wall Andesite member. In the West Block Area, a 10 to 50-metre-thick andesitic flow, with a 5 to 10-metre-thick carapace of jig-saw-fit, curviplanar autoclastic breccia is observed at the contact between the H-W member and the Hanging Wall Andesite member.

Near the Battle orebody are a number of sericite-pyrite-quartz altered sills. Upper and lower contacts are peperitic. The 5 to 30-metre-thick sills intrude the H-W member and, locally, the Price Formation (Robinson et al., 1996). These sills have a dacitic composition.

6.2 Previous Myra Falls Lithogeochemistry

A compilation of conventional XRF geochemical data collected during previous studies was used to assess the Ti/Zr ratios of key stratigraphic units prior to pXRF data collection (Appendix H). Datasets from Juras (1987), Robinson (1994), Barrett and Sherlock (1996), Sinclair (2000), and Barrett and MacLean (2000) consist of whole-rock geochemical analyses of volcanic rocks from the Price Formation; coherent, volcaniclastic and volcano-sedimentary rocks of the H-W member; and volcaniclastic rocks of the Hanging Wall Andesite member. To assess lithogeochemical signatures of key rock types, bivariate and histogram plots were generated. Ti/Zr signatures for each rock group were assigned from median values and the first to third quartile range were defined from Tukey box and whisker plots (Figure 6.3).

The Price Formation samples (Figure 6.3A-B) are distinctly elevated compared to the Myra Formation samples (Figure 6.3C-F), with a median Ti/Zr ratio of 62.5 and a first to third quartile range of 51.4 to 77.0. Coherent rhyolites from the Myra Formation are characterised by a median Ti/Zr ratio of 11.3 with a range of 10.2 to 14.4 (Figure 6.3C-D). Barrett and MacLean (2000) identified two types of rhyolite based on lithogeochemistry and mineralogy near the Marshall Zone orebody: (1) Rhyolite A – quartz and feldspar-phyric rhyolite with an average Ti/Zr ratio of 10.6 and (2) Rhyolite B – feldspar-phyric rhyolite with an average Ti/Zr ratio of 15.5

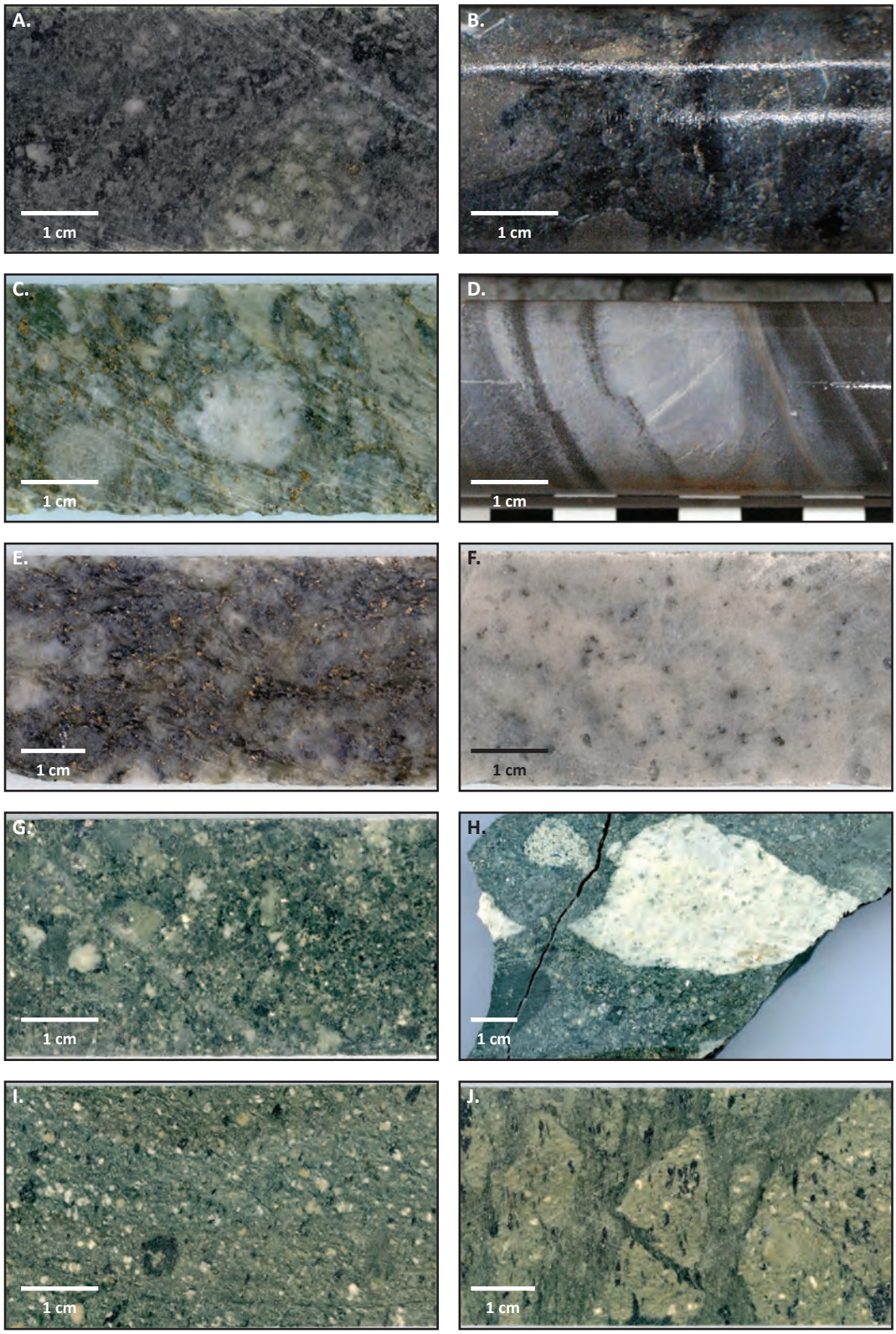

Figure 6.2 Photographs of least-altered rock types in the West Block Area. A. Feldspar-phyric, chlorite and carbonate altered andesite of the Price Formation. B. Chlorite-pyrite altered andesitic breccia of the Price Formation. C-F. Examples of H-W member rock types. C. Polylithic, pyrite and chlorite altered Basal Volcaniclastic Unit. D. Interbedded chert and argillite. E. Pyrite and sericite altered, medium-grained felsic volcaniclastic rock. F. Sericite and quartz altered, quartz-phyric coherent rhyolite. G-H. Examples of Hanging Wall Andesite member rock types. G. Medium-grained andesitic polylithic volcaniclastic rock. H. Coarse-grained andesitic polylithic volcaniclastic rock. I-J. Examples of coherent andesite flow. I. Feldspar and pyroxene-phyric, massive, coherent andesite lava. J. Example of jig-saw-fit, hyaloclastite with feldspar and pyroxene-phyric andesitic clasts separated by fine-grained matrix of the same composition.

(Figure 6.3D). The lithogeochemical classification of Barrett and MacLean (2000) was applied to the available whole-rock geochemical data and is presented on the summary stratigraphic columns (Figure 6.1). Felsic volcaniclastic rocks have a similar Ti/Zr signature to the coherent rhyolite (11.3-16.1) while polylithic felsic volcaniclastic rocks with 5% exotic lithic clasts have a range of 19.1 to 26.9 (Figure 6.3E-F). Argillite and chert samples have Ti/Zr ratios between 14.4 and 29.8 (Figure 6.3E-F). Andesitic sills and flows have a median Ti/Zr ratio of 95.5 with a range of 81.3 to 101.3. This is a comparatively tight range of Ti/Zr ratios compared to the volcaniclastic rocks of the Hanging Wall Andesite member, 34.0-72.5 (Figure 6.3G-H). Dacitic sills have a median Ti/Zr ratio of 33.9, with a range of 30.2 to 49.0 (Figure 6.3G-H).

The available geochemistry shows discrete lithogeochemical variations between rock types. In particular, distinct Ti/Zr trends for andesite of the Price Formation, coherent rhyolite of the H-W member, and coherent andesitic and dacitic sills. These ratios have the potential to be used to discriminate rock types at Myra Falls. However the Ti/Zr ratios for volcaniclastic and sedimentary rock types are less distinctive, probably due to the incorporation of several sources into these rock types, and this should be considered when collecting samples.

6.3 Methodology

6.3.1 Instrument

Field-portable X-ray fluorescence data was collected at CODES, University of Tasmania using an Olympus Innov-X Delta Premium energy dispersive pXRF analyser with a rhodium X-ray tube (max voltage of 40 kV and 4 W power; 20 mm^2 detector window). Analyses were completed in SOIL MODE with 40 kV beams-1 and -2 (U, Sr, Zr, Th, Mo, Ag, Cd, Sn, Sb, Fe, Co, Ni, Cu, Zn, W, Hg, As, Se, Pb, Bi, Rb, and *Ti, V, and Cr*), and 15 kV beam-3 (P, S, Cl, K, Ca, Ti, V, Cr, Mn, and *Fe*). In some cases an element is detected from multiple beam settings. Elements listed in italics are those detected by non-primary beam settings. Elemental results are only reported from their primary beam setting. The Innov-X Delta Advance PC software utilises a Compton normalisation algorithm to calculate element abundances with detection limits in the ppm range (Jenkins, 1999; Innov-X Systems Inc, 2010; Hall et al., 2013). The total measurement integration time-interval was 210 seconds (70 s per beam with a ~55-60 s per beam active runtime). The total 3-spot pXRF measurement runtime is approximately 11 minutes per drill core sample.

6.3.2 Sample preparation

Analyses were collected from drill core powders (n=18) and the surface of drill core samples (n=483). Drill core powders were prepared at ALS to 85% passing 75 microns with a low-Cr steel ring mill. Prior to pXRF analysis, powders were prepared into pills at CODES. Approximately 10-15 grams of sample material was pressed into a pill for each sample using an automated hydraulic press at 10 tons for 1 minute. No binding solution was added to the dry powders prior to pressing. Each sample was analysed once. Three analyses were collected from the clean, dry, free from dust flat, cut surface of drill core samples. Analyses were carried out on the sawn, flat surface of halved drill core samples to avoid diffraction of X-rays from the detector

Figure 6.3 Published conventional XRF lithogeochemistry for Myra Falls. Drawn using data from Juras (1987), Robinson (1994), Barrett and Sherlock (1996), Barrett and MacLean (2000), and Sinclair (2000). Note the two samples with Ti/Zr ratios >100 in the dataset are likely samples of intensely altered mafic rocks miss-logged as felsic in composition.

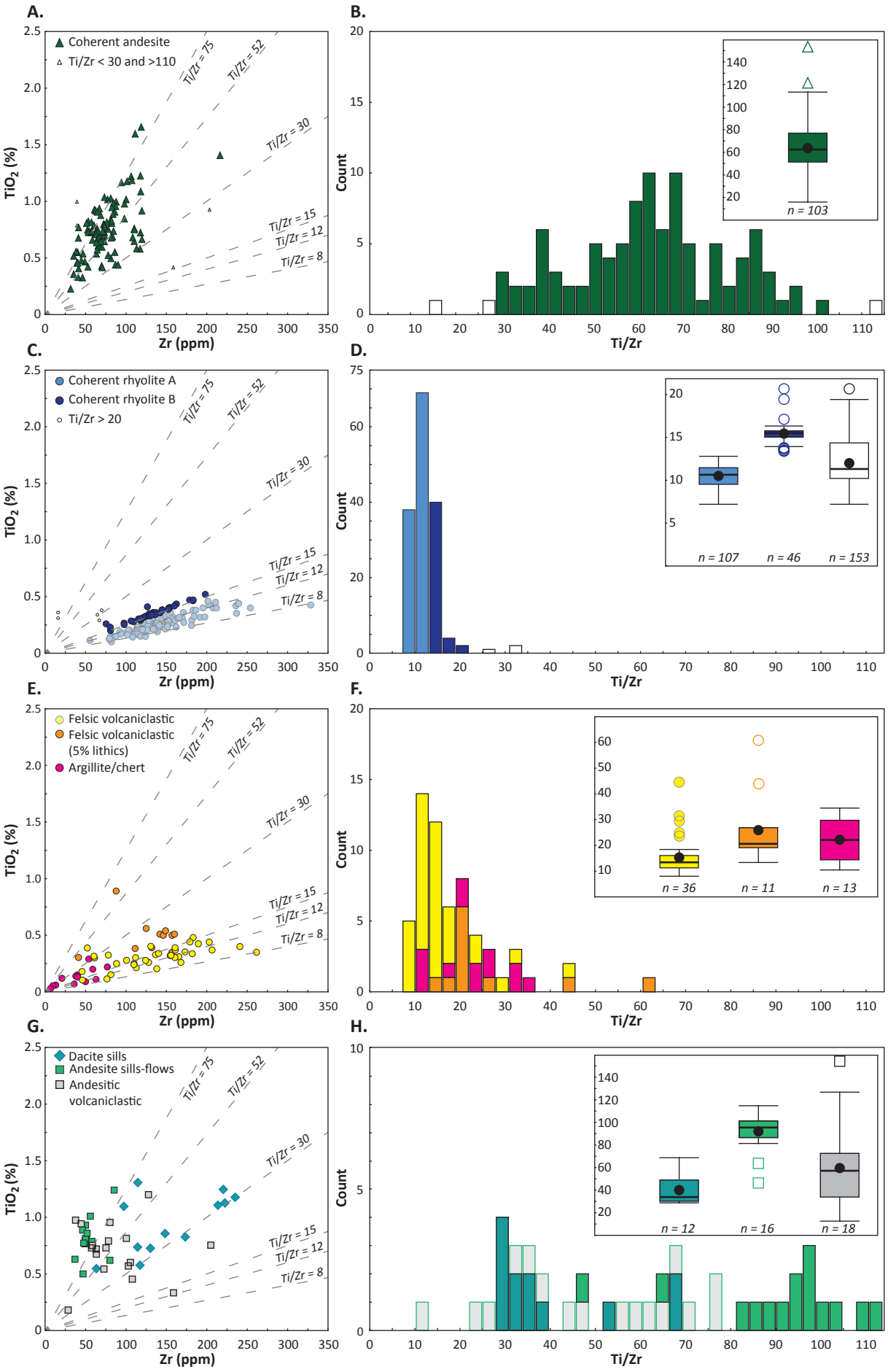
A.
Coherent andesite
Ti/Zr < 30 and >110
Ti/Zr = 75
Ti/Zr = 52
Ti/Zr = 30
Ti/Zr = 15
Ti/Zr = 12
Ti/Zr = 8
TiO2 (%)
Zr (ppm)
B.
Count
Ti/Zr
n = 103
C.
Coherent rhyolite A
Coherent rhyolite B
Ti/Zr > 20
D.
n = 107
n = 46
n = 153
E.
Felsic volcaniclastic
Felsic volcaniclastic (5% lithics)
Argillite/chert
F.
n = 36
n = 11
n = 13
G.
Dacite sills
Andesite sills-flows
Andesitic volcaniclastic
H.
n = 12
n = 16
n = 18

(e.g., Morris 2009). For coherent rocks, the groundmass was the focal area of analysis whereas for volcaniclastic rocks, the matrix was targeted.

6.3.3 Instrument calibration

To optimise the acquisition of lithogeochemical data from unprepared drill core samples a calibration method was developed using standard reference materials. When developing a calibration it requires standard reference materials that: (1) include all the elements of interest in the sample material; (2) have a range of concentrations for those elements of interest; and (3) have a similar matrix to the samples. Matrix matching the standards and sample material is important because the density, chemical composition and crystal structure of a material will effect how X-rays attenuate, refract and absorb. Ideally, the sample preparation of the standard reference material would be the same as for the unknown sample material. This is a challenge with analysing unprepared drill cores.

Four pressed powder pill reference standards (TasBas, TasGran, TasMonz, W2; Table 6.1) were analysed at the beginning of each analytical session and after every fifth unknown sample. A minimum of three measurements of each reference standard was collected during each analytical session. The reference standards were selected based on their variation in Ti and Zr concentrations (Table 6.1). Measuring the pressed powder pill standard reference materials with a small amount of polyvinyl acetate binder was considered an adequate representation of the intact rock and preferred over loose powders. The use of loose powder with Mylar® films is known to have a significant effect on the analytical results and therefore was avoided as a standard (e.g., Bourke and Ross, 2015).

Table 6.1 Standard reference values.

Element	TasBas[a]	TasGran[a]	TasMonz[a]	W2[b]
Ti (ppm)	13,908	1,739	3,717	6,355
Fe (ppm)	88,410	15,738	38,330	75,750
Mn (ppm)	1,317	310	1,007	1,293
Ca (ppm)	56,032	13,079	40,309	77,616
K (ppm)	16,022	38,104	24,739	5,197
Cr (ppm)	181	9	61	93
Zr (ppm)	259	160	154	92
Rb (ppm)	16	251	110	21
Sr (ppm)	1,008	147	345	196

[a] Values are for in-house University of Tasmania - CODES standard reference materials (analytical procedure in Falloon et al., 2007)
[b] Values are for USGS certified reference material (diabase)

Element specific calibration factors were calculated from a least-squares linear model (calibration-line) using the pXRF-measured value (x) to predict the certified value (y) of the standard (Figure 6.4). Upper and lower confidence limits of the linear model were calculated and used to determine the limit of detection (LOD) and limit of quantification (LOQ) for each element after the method described by Meier and Zünd (1993; Figure 6.4). A horizontal line defined by the intercept of the upper confidence limit with the y-axis is used to determine the LOD and LOQ for each element (Meier and Zünd, 1993). The LOD is equal to the x-axis value at the intercept of the horizontal line with the calibration line. The LOQ is equal to the x-axis value at the intercept of the horizontal line with the lower confidence limit. This calibration method was completed for each analytical session (Figure 6.5).

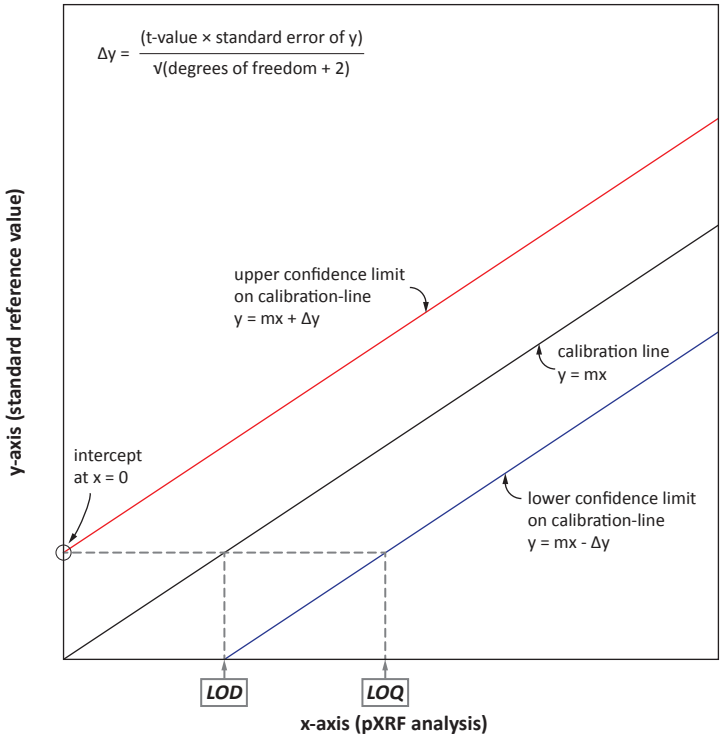

Figure 6.4 Explanation for the determination of an element specific calibration-line, upper and lower confidence limits on the calibration-line, and the definition of the limit of detection (LOD) and limit of quantitation (LOQ) from Meier and Zünd (1993).

6.3.4 Instrument precision and accuracy

Portable-XRF analyses of drill core samples were collected during 15 analytical sessions during which the standard reference pressed powder pills TasBas, TasGran, TasMonz and W2 were analysed 63 times. The percent relative standard deviation (RSD; Barford, 1985) of each reference material for selected elements are presented in Table 6.2. The RSD of Ti for each standard reference material range from 0.22% to 2.01%, with an average RSD of 1.29%. For Zr, the range is 3.86% to 4.43% RSD, and the average is 4.05% RSD. If an element of interest is above the LOQ, then the instrument precision is excellent for RSD of 0-3%, very good to good for RSD of 3-7%, good for RSD of 7-10%, and not precise for RSD >10% (Jenner, 1996; Piercey, 2014). The instrument precision of Ti and Zr using this proposed pXRF methodology is therefore excellent to very good (Table 6.2). Instrument precision by pXRF is excellent for Sr; very good for Fe and Rb; good for Mn, K, and Cr; but not precise for Ca (Table 6.2).

Accuracy of the instrument and calibration-line method was assessed by the root mean squared (RSM) error of the regression (Barford, 1985). Measurements of the reference standards by the proposed pXRF method yielded RSMs of 1.98% to 14.14%, with an average of 8.12% for Ti and a range from 3.88% to 10.12%, with an average of 5.6% for Zr (Table 6.2). Results with RSM values from 0-3% have excellent accuracy, values from 3-7% have very good accuracy, values from 7-10% have good accuracy, and values >10% are not accurate (Jenner, 1996; Piercey, 2014). Thus the accuracy of the instrument and calibration-line method is good for Ti and very good for Zr. In addition the instrument and calibration-line method accuracy is excellent for Sr, good for Mn, and not accurate for Fe, Ca, K, Cr, and Rb (Table 6.2).

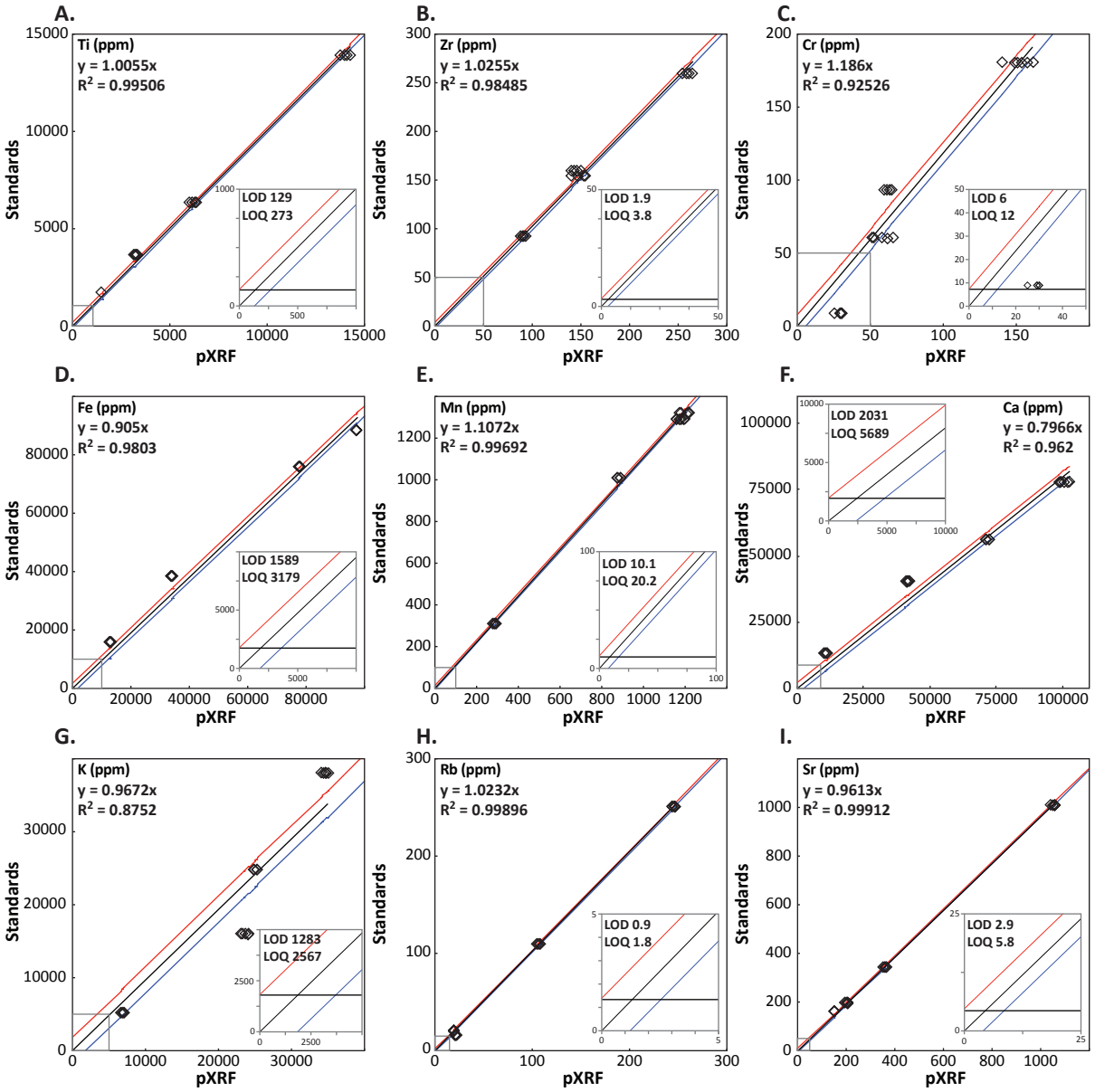

Figure 6.5 Example of calculated calibration factors, upper and lower confidence limits, and limit of quantitation (LOQ) values for one analytical session. Four standard reference materials were analysed 6 times, for a total of 28 measurements. In set graphs are expanded field of views of the origin to illustrate the determination of the LOQ. Note that calibration factors were calculated for Ti, Zr, Cr, Fe, Mn, Ca, K, Rb and Sr; however this chapter will only discuss the Ti, Zr and Cr results as they pertain to identifying protolith geochemical signatures.

6.3.5 Sampling precision and measurement uncertainty

The raw pXRF elemental data were multiplied by their respective calibration factor prior to sample averaging. Where applicable, elemental results were converted to their major oxide equivalents. Sampling precision was estimated from the RSD of the three-pXRF measurements for each element. The sampling precision is in effect an estimate of the heterogeneity of the rock sample (e.g., Markowicz, 2008). Total measurement uncertainty ($\%G_{tot}$) for calibrated pXRF results were calculated by the square root of the sum of squares of the RSD and RSM of the instrument, and the RSD of the sample (Barford, 1985).

To assess the proposed pXRF methodology and its application to discriminating rock types based on lithogeochemical criteria, two experiments were developed. First, two sample sets with conventional XRF results were analysed by pXRF and compared. Second, the proposed

Table 6.2 Range of precision expressed as %RSD and accuracy expressed as %RSM for various elements by pXRF.

Element	%RSD					%RSM				
	TasBas	TasGran	TasMonz	W2	Average	TasBas	TasGran	TasMonz	W2	Average
Ti	0.22	2.01	1.70	1.22	1.29	1.98	11.63	14.14	4.73	8.12
Fe	3.39	3.56	3.27	3.43	3.41	8.49	21.99	13.39	3.50	11.84
Mn	7.03	7.18	6.86	6.59	6.91	7.71	7.67	8.94	7.87	8.05
Ca	17.11	17.16	17.03	16.81	17.03	25.75	28.49	17.49	26.03	24.44
K	9.26	8.94	9.42	10.89	9.63	36.39	18.34	11.79	26.41	23.33
Cr	9.91	9.11	10.38	9.77	9.79	11.48	275.12	12.03	25.01	80.91
Zr	3.86	4.43	3.99	3.93	4.05	3.88	10.12	4.47	3.93	5.60
Rb	5.53	1.74	1.67	3.22	3.04	40.58	1.79	2.04	5.38	12.45
Sr	1.38	2.11	1.77	1.80	1.77	1.40	3.64	1.87	2.26	2.29

$$\%RSD = \frac{\left(\sqrt{\frac{\Sigma\left(x - \bar{x}\right)^2}{n}} - 1\right)}{\bar{x}} \times 100$$

where: x = pXRF measurement; x-bar = mean of the pXRF measured data; n = number of measurements.

$$\%RSM = \frac{\left(\sqrt{\frac{\Sigma\left(x - X\right)^2}{n}} - 1\right)}{X} \times 100$$

where: x = pXRF measurement; X = standard reference value of element; n = number of measurements.

sampling method was applied to variably hydrothermally altered, halved drill core samples to test if the method successfully discriminated between the andesite of the Price Formation, the coherent rhyolite of the H-W member, and the coherent andesite flow in the West Block Area using Ti/Zr ratios.

6.3.5.1 Powders vs. drill core analyses

Eighteen samples from the West Block Area were analysed (14 coherent andesite of the Price Formation; 3 coherent rhyolite of the H-W member; 1 coherent andesite flow). Three pXRF measurements were collected from the flat surface of halved drill core samples, up to 3 x 6 cm in size with sample weights between 25 to 375 grams, prior to conventional XRF analysis (Appendix I). A single pXRF measurement was later collected from the 85% passing 75 micron reject material (Appendix I). Raw pXRF results from drill core and pressed powdered samples were processed per the above described calibration and data reduction methods. Major oxides were measured from a fused disc by XRF and trace elements were measured from a lithium borate fused bead by ICP-MS by ALS in Perth, WA, Australia (Appendix F).

6.3.5.2 Three-spot pXRF analysis of drill core

To validate the three-spot pXRF analysis method, 47 drill core samples were analysed and compared to a conventional XRF dataset collected by Sinclair (2000) of the same samples (Table 6.3). Pressed powdered pills and fused discs for laboratory XRF analyses were prepared from 0.2 to 0.5 metre drill core sample lengths (pulverised by tungsten-carbide mill) and analysed at CODES, University of Tasmania. Three pXRF measurements were collected from each of the flat surface of 5 to 10-centimetre-long, representative drill core off-cuts. Analysed rock types included: Price Formation coherent andesite (n=14), H-W member argillite and chert (n=8), H-W member felsic volcaniclastic rocks (n=10), H-W member coherent rhyolite (n=8), and andesitic volcaniclastic rocks of the Hanging Wall Andesite member (n=7).

Table 6.3 Results from three-spot pXRF analysis of drill core compared to conventional XRF analyses by Sinclair (2000) of the same sample set.

Sample	Formation/ member	Rock type	Facies	Three-spot pXRF result				Conventional XRF result			
				TiO_2 (%)	Zr (ppm)	Ti/Zr	Cr (ppm)	TiO_2 (%)	Zr (ppm)	Ti/Zr	Cr (ppm)
143652	Price Fm	Andesite	Coherent	0.50	58	51	6	0.58	66	52	6
143653	Price Fm	Andesite	Coherent	0.25	37	41	25	0.34	42	48	7
143668	Price Fm	Andesite	Coherent	0.41	50	49	26	0.48	46	64	5
143670	Price Fm	Andesite	Coherent	0.42	35	71	49	0.56	41	82	57
143681	Price Fm	Andesite	Coherent	1.26	124	61	38	1.20	110	65	10
143682	Price Fm	Andesite	Coherent	0.59	68	52	38	0.63	70	54	28
143689	Price Fm	Andesite	Coherent	0.85	83	62	6	0.96	84	68	8
143690	Price Fm	Andesite	Coherent	0.28	47	35	27	0.44	71	37	6
143700	Price Fm	Andesite	Coherent	1.02	104	59	39	1.24	121	61	10
143701	Price Fm	Andesite	Coherent	0.94	89	64	6	1.01	90	67	8
143640	Price Fm	Andesite	Coherent	0.68	80	51	18	0.69	81	51	39
143641	Price Fm	Andesite	Coherent	0.65	142	27	16	0.65	130	30	1
143645	Price Fm	Andesite	Coherent	0.65	81	48	68	0.82	95	51	106
143646	Price Fm	Andesite	Coherent	0.56	122	27	23	0.66	138	29	1
143671	H-W Mbr	Chert	Sedimentary	0.07	13	31	15	0.06	13	27	16
143680	H-W Mbr	Chert	Sedimentary	0.10	7	84	37	0.06	10	33	17
143688	H-W Mbr	Chert	Sedimentary	0.23	105	13	40	0.03	7	26	15
143699	H-W Mbr	Chert	Sedimentary	0.12	20	37	33	0.12	21	34	40
143687	H-W Mbr	Argillite	Sedimentary	0.30	147	12	44	0.21	142	9	1
143635	H-W Mbr	Argillite	Sedimentary	0.52	74	42	36	0.57	80	42	39
143643	H-W Mbr	Argillite	Sedimentary	0.46	54	51	34	0.48	60	47	35
143644	H-W Mbr	Argillite	Sedimentary	0.69	73	56	40	0.65	72	54	34
143649	H-W Mbr	Felsic	Volcaniclastic	0.76	208	22	84	0.44	184	14	1
143650	H-W Mbr	Felsic	Volcaniclastic	0.32	107	18	56	0.31	165	11	3
143679	H-W Mbr	Felsic	Volcaniclastic	0.25	116	13	43	0.22	116	11	12
143684	H-W Mbr	Felsic	Volcaniclastic	0.43	157	16	55	0.37	212	11	2
143685	H-W Mbr	Felsic	Volcaniclastic	0.14	71	12	41	0.12	78	9	2
143686	H-W Mbr	Felsic	Volcaniclastic	0.39	235	10	44	0.35	268	8	5
143692	H-W Mbr	Felsic	Volcaniclastic	0.48	192	15	62	0.26	172	9	2
143695	H-W Mbr	Felsic	Volcaniclastic	0.14	60	15	17	0.11	47	13	5
143696	H-W Mbr	Felsic	Volcaniclastic	0.35	128	16	37	0.33	160	12	6
143637	H-W Mbr	Felsic	Volcaniclastic	0.91	85	65	53	0.83	89	55	14
143647	H-W Mbr	Rhyolite A	Coherent	0.59	208	17	83	0.36	243	9	2
143648	H-W Mbr	Rhyolite A	Coherent	0.23	86	16	43	0.17	119	8	2
143683	H-W Mbr	Rhyolite A	Coherent	0.21	83	16	37	0.13	82	9	1
143704	H-W Mbr	Rhyolite A	Coherent	0.27	144	11	60	0.25	136	11	31
143705	H-W Mbr	Rhyolite A	Coherent	0.18	112	9	27	0.20	122	10	9
143636	H-W Mbr	Rhyolite A	Coherent	0.27	118	14	27	0.26	133	11	3
143638	H-W Mbr	Rhyolite A	Coherent	0.37	164	13	42	0.33	191	10	1
143639	H-W Mbr	Rhyolite A	Coherent	0.21	108	11	18	0.26	135	11	3
143654	Hanging Wall Mbr	Andesitic	Volcaniclastic	0.77	86	54	13	0.61	108	34	7
143656	Hanging Wall Mbr	Andesitic	Volcaniclastic	0.31	168	11	10	0.34	163	12	2
143657	Hanging Wall Mbr	Andesitic	Volcaniclastic	0.84	68	74	14	0.80	80	59	8
143702	Hanging Wall Mbr	Andesitic	Volcaniclastic	0.49	61	48	9	0.72	65	67	9
143703	Hanging Wall Mbr	Andesitic	Volcaniclastic	0.73	66	66	6	0.76	60	75	6
143634	Hanging Wall Mbr	Andesitic	Volcaniclastic	0.76	62	73	6	0.69	62	67	14
143642	Hanging Wall Mbr	Andesitic	Volcaniclastic	0.66	63	63	11	0.77	65	72	23

Fm, formation; Mbr, member

6.4 Results

6.4.1 Instrument performance

The pXRF results for pressed powders and drill cores and conventional XRF results for Ti, Zr and Cr are compared in Figure 6.6. The Spearman rank correlation coefficient method (r_s) was used to evaluate the correlation between methods and sample media. The Pearson product-moment coefficient of linear correlation (r) is also presented for comparison, however the Spearman rank coefficient is preferred as it is more robust against data outliers (Rollinson, 1993).

6.4.1.1 Powders vs. drill core analyses - Ti and Zr results

The pXRF results of sample powders for TiO_2 and Zr correlate well with conventional geochemical XRF results (TiO_2 r_s = 0.80; Zr r_s = 0.99; Figure 6.6A-B). The average three-spot pXRF measurement results of drill core samples for TiO_2 and Zr also correlate well, with r_s values of 0.71 and 0.93, respectively (Figure 6.6D-E). The Ti/Zr pXRF results from pressed powders and drill core samples correlate very well with the conventional XRF results (r_s = 0.88; Figure 6.6C, F).

This outcome is in agreement with previous publications that document homogenisation by crushing and pulverising a sample prior to pXRF analysis produces robust geochemical

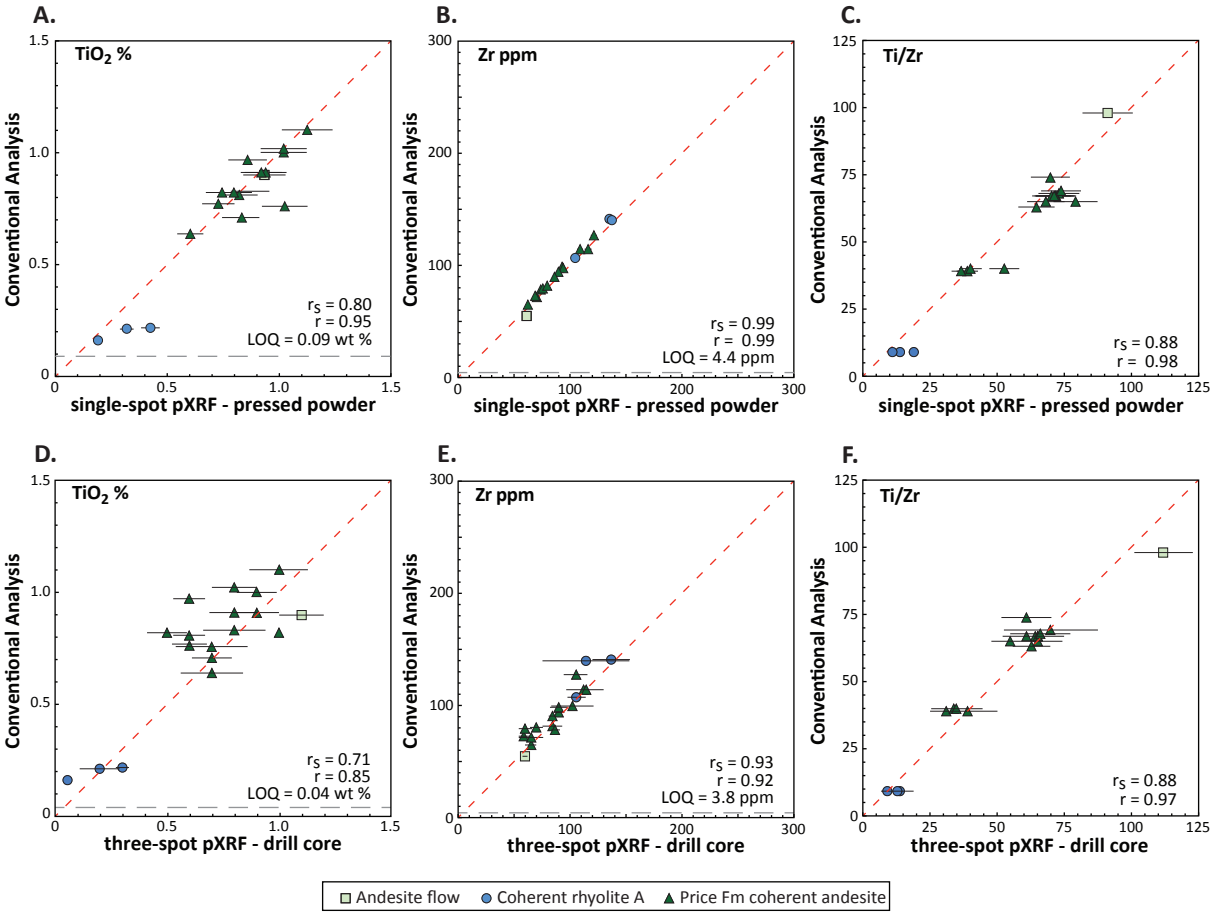

Figure 6.6 Panel of correlation plots demonstrating the correlation between the conventional XRF/ICP-MS results by ALS (y-axis) and single-spot pXRF analysis of pressed powders (x-axis; A-C) and three-spot pXRF analysis of drill core samples (x-axis; D-F). Note the strong correlation between methods. Error bars are the total measurement uncertainty ($\%G_{tot}$) for pXRF measurements, x-axis. [Fm, formation]

results (e.g., Figueroa-Cisterna et al., 2011; Hall et al., 2013; Piercey and Devine, 2014). What is encouraging is that the three-spot pXRF measurement method from the surface of drill core yielded well-correlated results for Ti and Zr with the conventional XRF results. Furthermore, the strong, positive correlation of the Ti/Zr ratio results by this method compared to the conventional XRF results indicates that the proposed method is practical for collecting meaningful lithogeochemical data at Myra Falls. These results are in agreement with those of Bourke and Ross (2015), which showed that robust TiO_2 and Zr results were achievable by collecting multiple pXRF measurements from unprepared drill core samples.

6.4.1.2 Three-spot pXRF analysis of drill core - Ti and Zr results

A comparison of the three-spot pXRF and conventional XRF results of 47 samples show that the two methods produce similar results (Figure 6.7; Table 6.4). TiO_2 and Zr are well correlated, with r_s values of 0.93 and 0.92, respectively (Figure 6.7A-B). The Ti/Zr ratio results have a strong, positive correlation between both analytical methods ($r_s = 0.87$; Figure 6.7C). Subdividing the dataset by logged lithology illustrates the challenge of geological heterogeneity and visual discrimination between volcaniclastic rocks and coherent rocks. Coherent rock samples have high r_s values of 0.95, 0.94 and 0.91 for TiO_2, Zr and Ti/Zr, respectively (Table 6.4). Felsic and andesitic volcaniclastic rocks have an r_s value of 0.94 for Zr (Table 6.4). However, the r_s value for TiO_2 is not as strong as the results for coherent rock types ($r_s = 0.88$; Table 6.4). Consequently, the Ti/Zr correlation value is not as high, $r_s = 0.81$ (Table 6.4). Chert and argillite rock samples show a strong correlation for TiO_2 and good correlation for Ti/Zr (Table 6.4). Only eight samples were available for comparison and the poor correlation ($r_s = 0.5$) for Zr is strongly controlled by one sample (Sample 143688). This sample has a conventional XRF result for Zr of 7 ppm and reported three-spot pXRF result of 105 ppm (Table 6.4; Figure 6.6). Removing this anomalous sample from the Spearman correlation calculations yields pXRF Zr results that correlate with the conventional XRF results ($r_s = 1.00$).

Table 6.4 Comparison of correlation between three-spot pXRF analysis of drill core and conventional XRF by Sinclair (2000) of the same sample set.

Element/Ratio	All n=47	Coherent n=22	Volcaniclastic n=17	Chert/argillite n=8
Ti	0.93	0.95	0.88	0.83
Zr	0.92	0.94	0.94	0.5
Ti/Zr	0.87	0.91	0.81	0.76
Cr	-0.06	0.22	-0.52	-0.55

$$r_s = 1 - \left(\frac{6 \Sigma D^2}{n\left(n^2 - 1\right)} \right)$$

where: D = the difference in ranking between the x and y values; n = the number of pairs.

6.4.1.3 Sample heterogeneity

For coherent volcanic rocks the sample heterogeneity is a function of mineral grain size. For volcaniclastic rocks the sample heterogeneity is more complex, and is a function of both mineral grain size and the composition of the lithic components. For samples with uniform grain size (this would be the ideal scenario), the variability between separate analyses is inversely proportional to the number of particles sampled (Wilson, 1964). This is the fundamental reason for crushing, pulverising and homogenising samples prior to analysis.

Yet the Spearman rank coefficient comparisons between conventional XRF analysis with single-spot pXRF analysis of sample powders and three-spot pXRF analysis of drill core samples illustrates that the powder method is not significantly better for TiO_2 and Zr results and the proposed three-spot pXRF method is sufficient. It is important to assess the sample precision of each three-point pXRF measurement, as results with greater variability are a function of grain size heterogeneity and therefore, may produce spurious results and lead to inappropriate lithological interpretations.

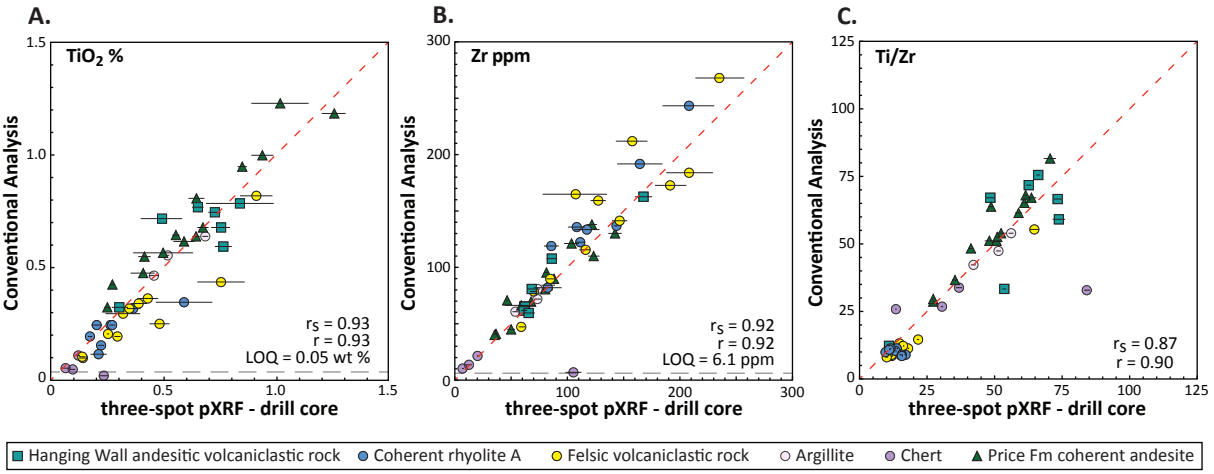

Figure 6.7 Panel of correlation plots demonstrating the fit between the conventional XRF results by CODES (y-axis; Sinclair, 2000) and three-spot pXRF analysis of drill core (x-axis). Note the strong, positive correlation between methods for TiO_2, Zr, and Ti/Zr. Error bars are the total measurement uncertainty ($\%G_{tot}$) for pXRF measurements, x-axis. [Fm, formation]

6.4.1.4 Chromium results

Spearman rank correlation values for Cr reported by pXRF compared to conventional XRF indicate that for these samples, the two analytical methods do not correlate. The calculated LOD and LOQ for Cr range from 6-6.1 ppm and 12.0-12.2 ppm, respectively (Figure 6.8A-C). The TasGran standard reference material has Cr and Mn concentrations of 11 ppm and 343 ppm, respectively (Table 6.1). Chromium concentrations by pXRF are overestimated by 300% for the TasGran standard reference material (181 ppm Cr). This trend occurs in both sample set comparisons, where 47 of the 65 samples have conventional XRF values of Cr below the LOQ and the majority of these samples have over-reported three-spot pXRF values (Figure 6.8A-C). Some samples have three-spot pXRF results that over-report Cr with conventional XRF values greater than the LOQ (Figure 6.8A-C). These discrepancies may be the result of the sample being below the Cr limit of quantitation and/or a potential Cr and Mn peak energy overlap. Chromium has Kα and Kβ peaks at 5.415 kV and 5.947 kV and manganese has Kα and Kβ peaks at 5.899 kV and 6.490 kV (Bearden, 1967). Figure 6.8D-I presents pXRF spectral results for samples with overestimated Cr values and Mn/Cr ratios between 3 and 65.

Previous studies have shown that pXRF analysis for Cr can be reliable and a useful lithological discriminator in ore deposit geology. Bourke and Ross (2015) compared pXRF performance on powdered and non-powdered drill core samples from Precambrian volcanic and intrusive rocks, using the same instrument model used in this study. They found that pXRF measurements on drill core samples of basaltic andesite produced fit-for-purpose Cr data with an instrument precision of 8.9% and sample precision of 15.2% from an average of five-spot

measurements. Gazley et al. (2011) utilised systematic down-hole pXRF measurements on sample powders to identify individual lava flows of metabasalt stratigraphy at the Plutonic Gold Mine, WA, Australia. Here, the metabasalt has Cr concentrations from 100 to 1,300 ppm. As a result, even with a pXRF average relative error of 19.4% (Gazley et al., 2011), the significant range in Cr concentrations of individual lava flows could be identified with pXRF analysis. The intermediate to mafic volcanic rocks at Myra Falls are low in Cr (<100 ppm) and based on the data in this study the effective detection limit for Cr using the three-spot pXRF protocols is approximately 50 ppm (Figure 6.8).

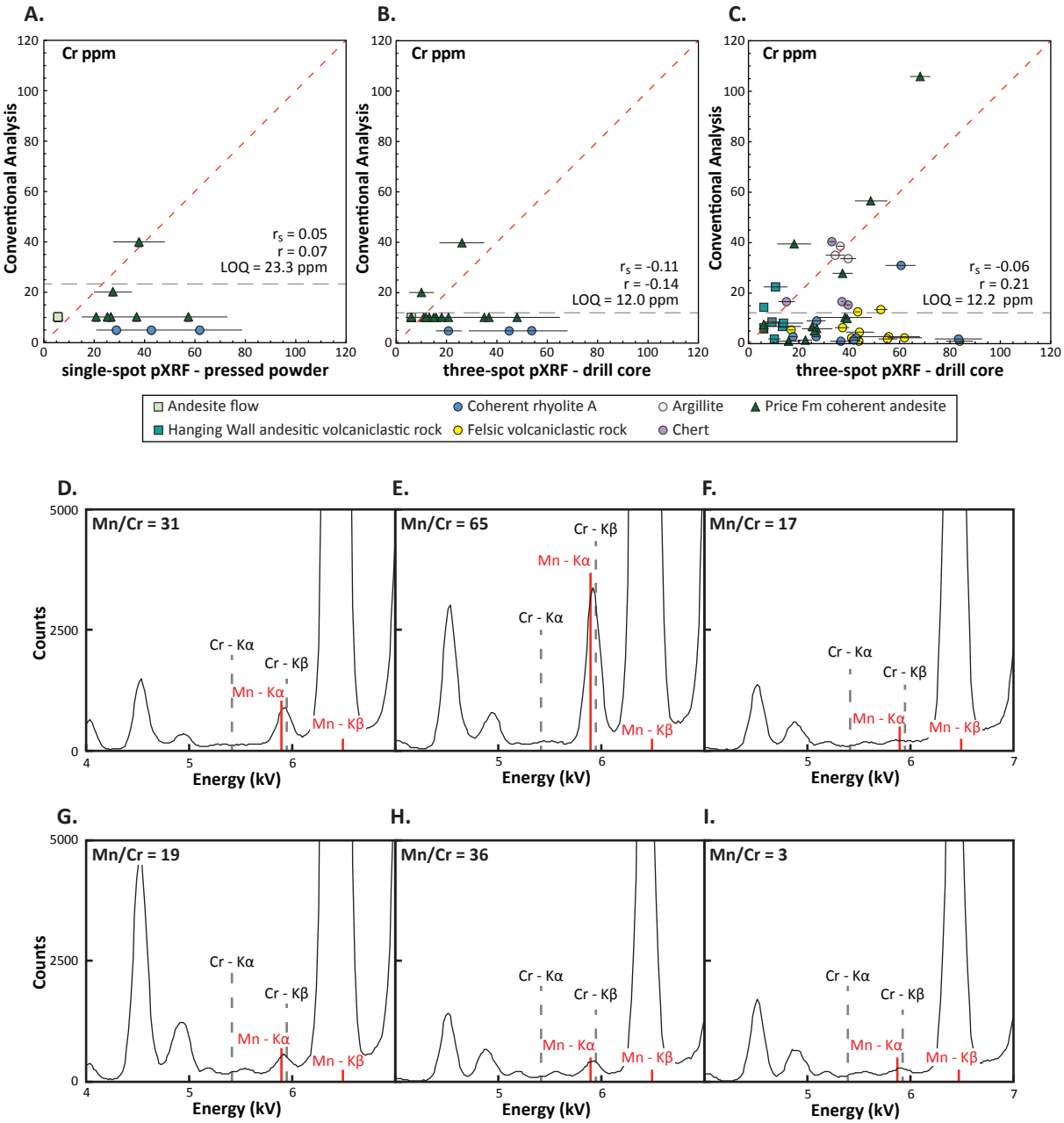

Figure 6.8 A-C. Panel of correlation plots for Cr (ppm) demonstrating the lack of correlation between the conventional XRF/ICP-MS results by ALS (y-axis; A-B) and conventional XRF results by CODES (y-axis; C; Sinclair, 2000) with single-spot pXRF analysis of pressed powders (x-axis, A) and three-spot pXRF analysis of drill core samples (x-axis, B-C). Error bars are the total measurement uncertainty ($\%G_{tot}$) for pXRF measurements, x-axis. D-I. Examples of 40 kV beam-2 pXRF spectra from SOIL MODE analyses of Sinclair (2000) sample set. Mn/Cr ratios are calculated from lab XRF results of Sinclair (2000). D. TasGran standard reference sample. E. Coherent andesite from Price Formation, sample 143682. F. Chert from Myra Formation, sample 143688. G-H. Felsic volcaniclastic rocks from Myra Formation, sample 143637 and sample 143679. I. Coherent rhyolite Myra Formation, sample 143704.

6.4.2 West Block Area lithogeochemistry by pXRF

A total of 418 drill core samples were analysed by the three-spot pXRF methodology (Appendix I). These samples were from underground drill holes in the West Block Area of Myra Falls. The instrument precision and calibration error are much smaller than the sample precision (RSD) for Ti and Zr. This is a function of sample heterogeneity. The RSD of a sample's three-spot pXRF measurements is controlled by geological variability between spot measurements. Using a ratio, rather than absolute element abundances, assists in minimising the effect of sample heterogeneity. Based on the expected Ti/Zr ranges for each rock type from the published conventional XRF data, a total measurement uncertainty threshold was used to reduce the dataset. The distribution of the three-spot pXRF Ti/Zr $\%G_{tot}$ by rock type is shown on Figure 6.9; 65% of coherent rock types analysed have Ti/Zr $\%G_{tot}$ <10%, compared to 52% of volcaniclastic/sedimentary rock types sampled. Based on this, a <10%G_{tot} thresh hold was selected to remove potential spurious results from the pXRF drill core dataset.

Bivariate Zr vs TiO_2 plots and Ti/Zr histograms were used to classify rock types in the West Block Area. Figure 6.10 presents the results for all 418 samples analysed. The Ti/Zr trends mirror those from the conventional XRF datasets (Figure 6.4). The pXRF data are more variable, therefore results with $\%G_{tot}$ <10% for Ti/Zr were used to assign Ti/Zr lithogeochemical signatures for the West Block Area (Figure 6.11). Tukey box and whisker plots define the Ti/Zr medians and first to third quartile ranges for each logged rock type.

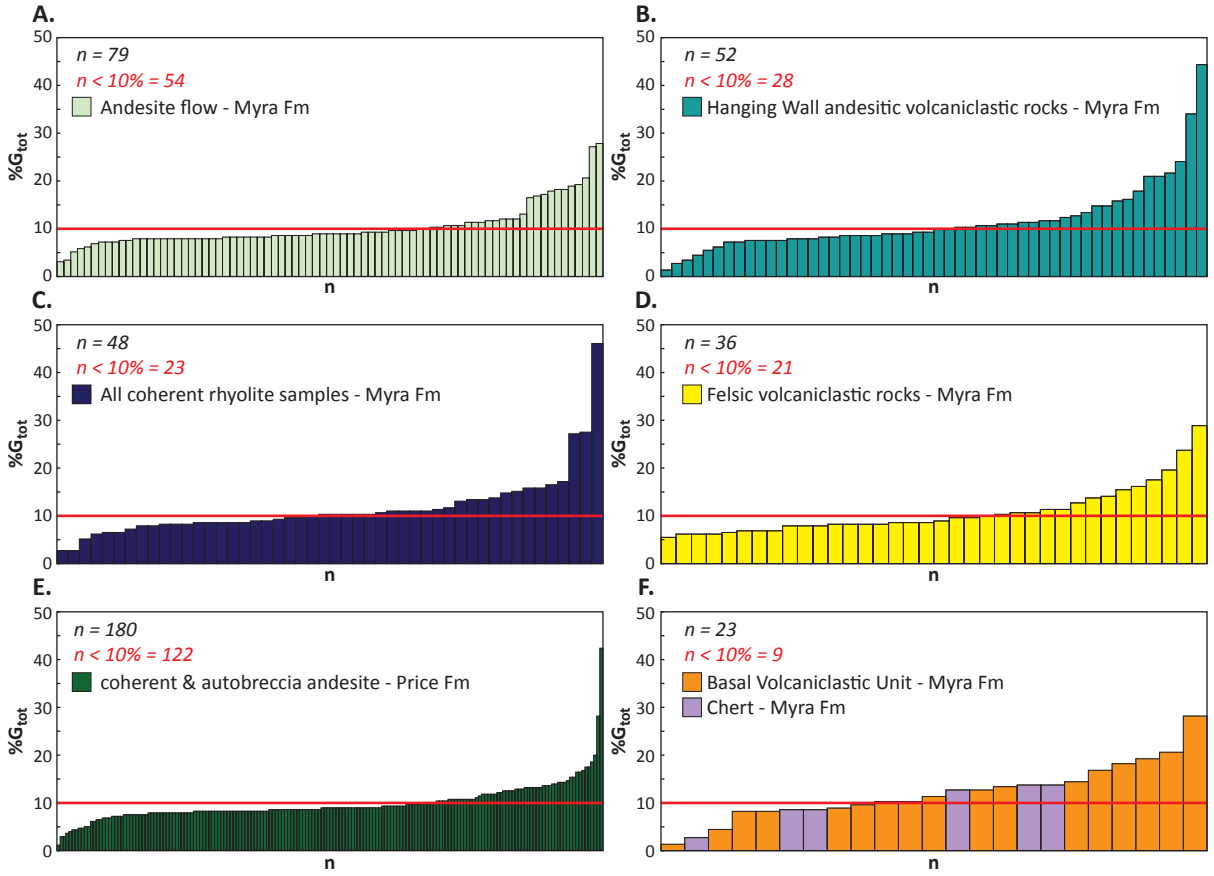

Figure 6.9 Distribution of the total measurement uncertainty ($\%G_{tot}$) for the 418 samples analysed from the West Block Area. Samples have been subdivided by their logged lithology. A. Coherent andesite flow from the H-W member. B. Andesitic volcaniclastic rocks of the Hanging Wall Andesite member. C. Coherent rhyolite of the H-W member. D. Felsic volcaniclastic rocks of the H-W member. E. Coherent and autobreccia andesite of the Price Formation. F. Polylithic, Basal Volcaniclastic Unit (orange) and chert/argillite (purple) samples of the H-W member.

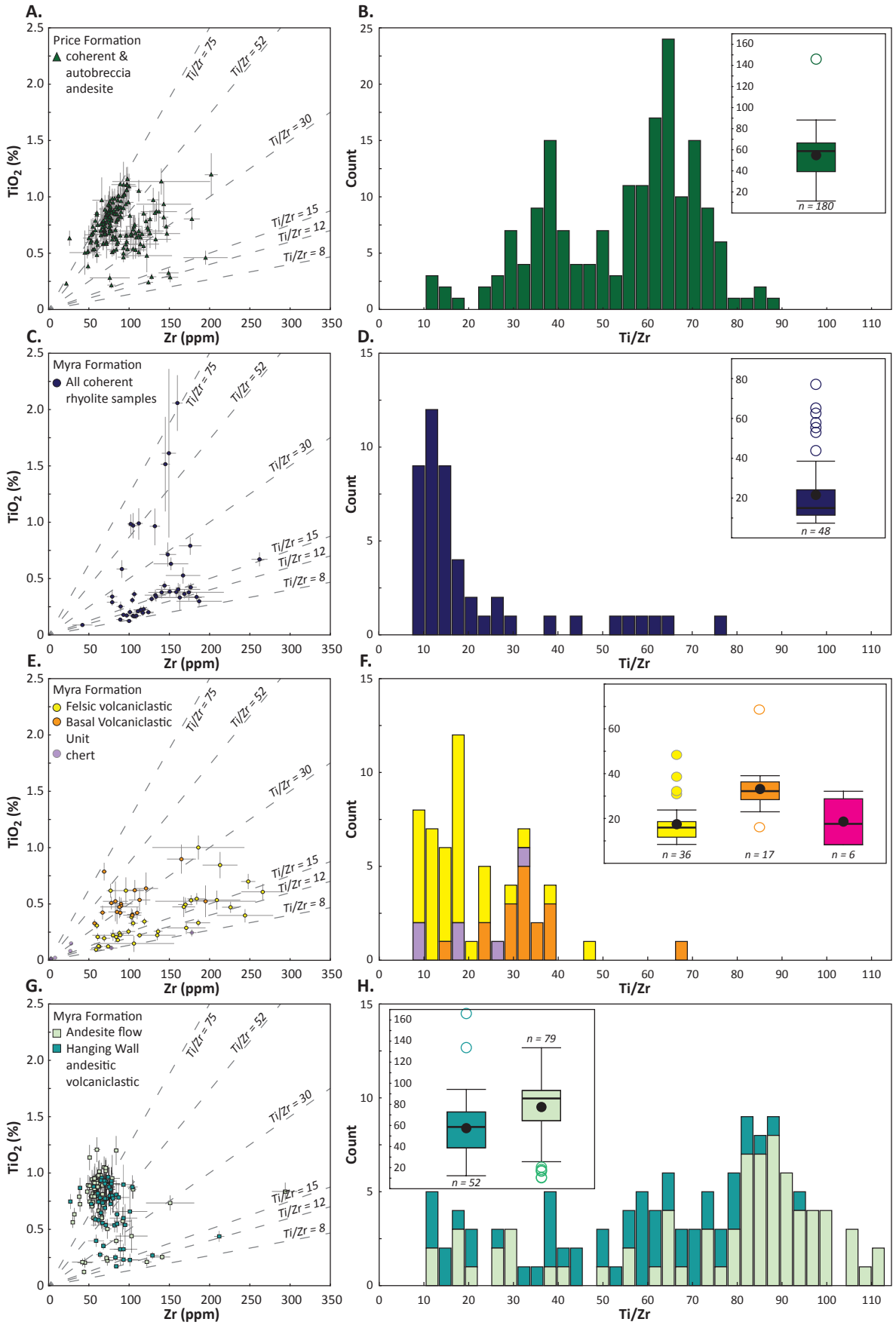

Figure 6.10 Summary of immobile element discrimination plots, histograms, and Tukey box and whisker plots for down-hole three-spot pXRF analyses. A-B. Coherent and autobreccia andesite of the Price Formation. C-D. Coherent rhyolite of the H-W member. E-F. Volcaniclastic and sedimentary rock samples of the H-W member. G-H. Coherent andesite flow (H-W member) and andesitic volcaniclastic rocks of the Hanging Wall Andesite member. Error bars are the total measurement uncertainty ($\%G_{tot}$) for each average three-spot measurement.

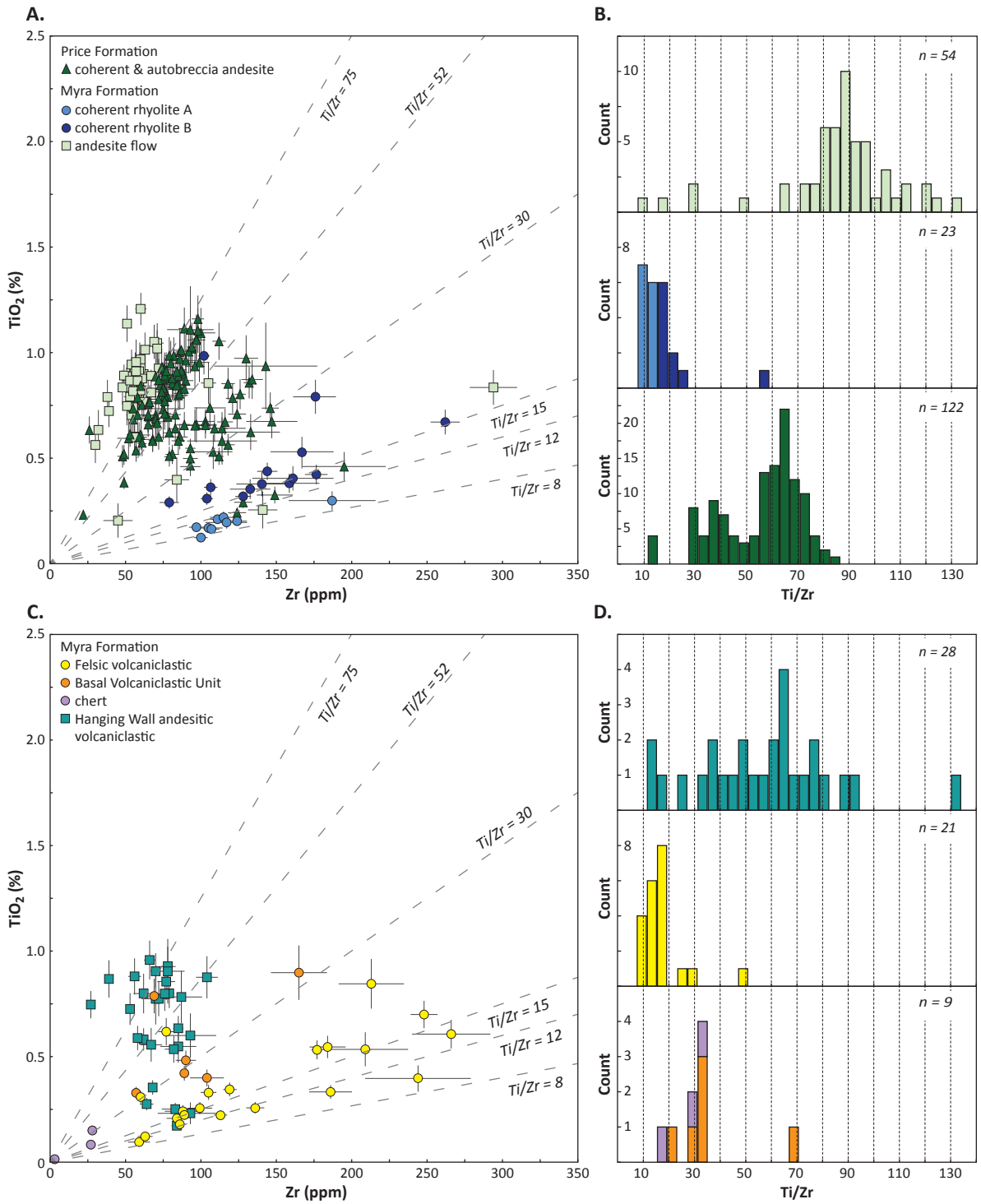

Figure 6.11 Summary of immobile element discrimination plots and histograms after the removal of data points with $\%G_{tot}$ >10%. Results are subdivide by coherent (A-B) and volcaniclastic/sedimentary rock facies (C-D). Error bars are the total measurement uncertainty ($\%G_{tot}$) for each average three-spot measurement.

The 122 analysed samples of andesite of the Price Formation have a median Ti/Zr ratio of 61 and a first to third quartile range of 42 to 67. Further inspection of the Ti/Zr histogram (Figure 6.9B) indicates two modes centred about Ti/Zr values of 37 and 65 for andesite in the Price Formation. Coherent rhyolite of the H-W member (n=23) is characterised by a median Ti/Zr ratio of 15 with a range of 10 to 18. Felsic volcaniclastic rocks of the H-W member (n=21) have Ti/Zr ratios that overlap with the coherent rhyolite samples, 12 to 18. Samples of the Basal Volcaniclastic Unit (n=6) have elevated Ti/Zr ratios between 27 and 43. Argillite and chert

samples (n=3) have a range of Ti/Zr ratios between 18 and 32. Coherent andesite flow (n=54) has a median Ti/Zr ratio of 88 with a range of 64 to 97, whereas andesitic volcaniclastic rocks of the Hanging Wall Andesite member (n=28) have a range from 39 to 76 (Figure 6.11).

6.5 Application to Chemostratigraphy

To illustrate the potential utilisation of pXRF data in a spatial context, down-hole profiles of three-spot pXRF data, with an average sample spacing of 6 metres, for selected drill holes are shown in Figure 6.12. Drill holes BG18-3952 and BG18-3907 are from the West Block Area and intersect a complete section of the H-W member. Drill hole RN18-0224 is from the Ridge Zone North orebody, and was chosen because the hole intersects hydrothermally altered H-W member and stratigraphic footwall andesite of the Price Formation.

Grade control drill holes at Myra Falls are normally BQ size (36.5 mm core diameter). This limits the observations site geologists can make while logging drill core. As a result colour, phenocryst mineralogy and rock texture are the primary features used in rock identification. This classification scheme becomes difficult when secondary effects such as hydrothermal alteration and metamorphism obscure primary volcanic textures. Data presented here indicates that lithology logging can be improved by combining systematic pXRF analysis with traditional drill core observations.

Typical examples of drill core from BG18-3907, BG18-3952 and RN18-0224 are shown in Figures 6.13-6.14. A coherent andesite flow is identified by its green to grey mottled texture, feldspar ± pyroxene phenocrysts, and massive to autobrecciated texture (Figure 6.13A). In addition to these physical properties, this rock type has elevated Ti/Zr ratios, typically above 70 (Figure 6.11B). Coherent rhyolite of the H-W member is identified in drill core by its massive texture and presence of quartz ± feldspar phenocrysts (Figure 6.13B). This rock type is typically intensely altered to a sericite-quartz + sulfide mineral assemblage. Margins of phenocrysts become fuzzy with increased alteration intensity and crosscutting sulfide stringer veins with patchy alteration domains, which produces pseudo-breccia textures. As a result, accurate identification of coherent rhyolite from volcaniclastic rocks becomes very difficult by visual observation. Ti/Zr ratios, from pXRF analysis, successfully distinguish units with felsic compositions (Ti/Zr < 20) from intermediate to mafic composition rocks (Ti/Zr > 30).

Barrett and MacLean (2000) identified two types of rhyolite based on Ti/Zr ratios in the Marshall Zone orebody (Figure 6.1). Rhyolite A is characterised by Ti/Zr ratios less than 15 and Rhyolite B has Ti/Zr ratios greater than 15. Sulfide mineralisation in the Marshall Zone orebody is present in felsic volcaniclastic rocks located at the upper contact of Rhyolite B (Figure 6.1). The pXRF results indicate the presence of Rhyolite A and B south of the Marshall Zone orebody in the Ridge Zone North and West Block Area localities (Figure 6.12). Massive sulfide mineralisation is present in felsic volcaniclastic rocks at the base of coherent rhyolite, which has a Ti/Zr signature of Rhyolite B (drill hole RN18-0224; Figure 6.11) from the Ridge Zone North orebody. Conversely, coherent rhyolite in the West Block Area (drill hole BG18-3952; Figure 6.11) has a Ti/Zr signature equal to that of Rhyolite A. The lithogeochemical distinction using pXRF between different coherent rhyolite bodies and their spatial distribution relative

Figure 6.12 Summary of immobile element down-hole profiles for drill holes RN18-0224, BG18-3952 and BG18-3907. Data from the <10%G_{tot} subset. Error bars are the total measurement uncertainty (%G_{tot}) for each average three-spot measurement.

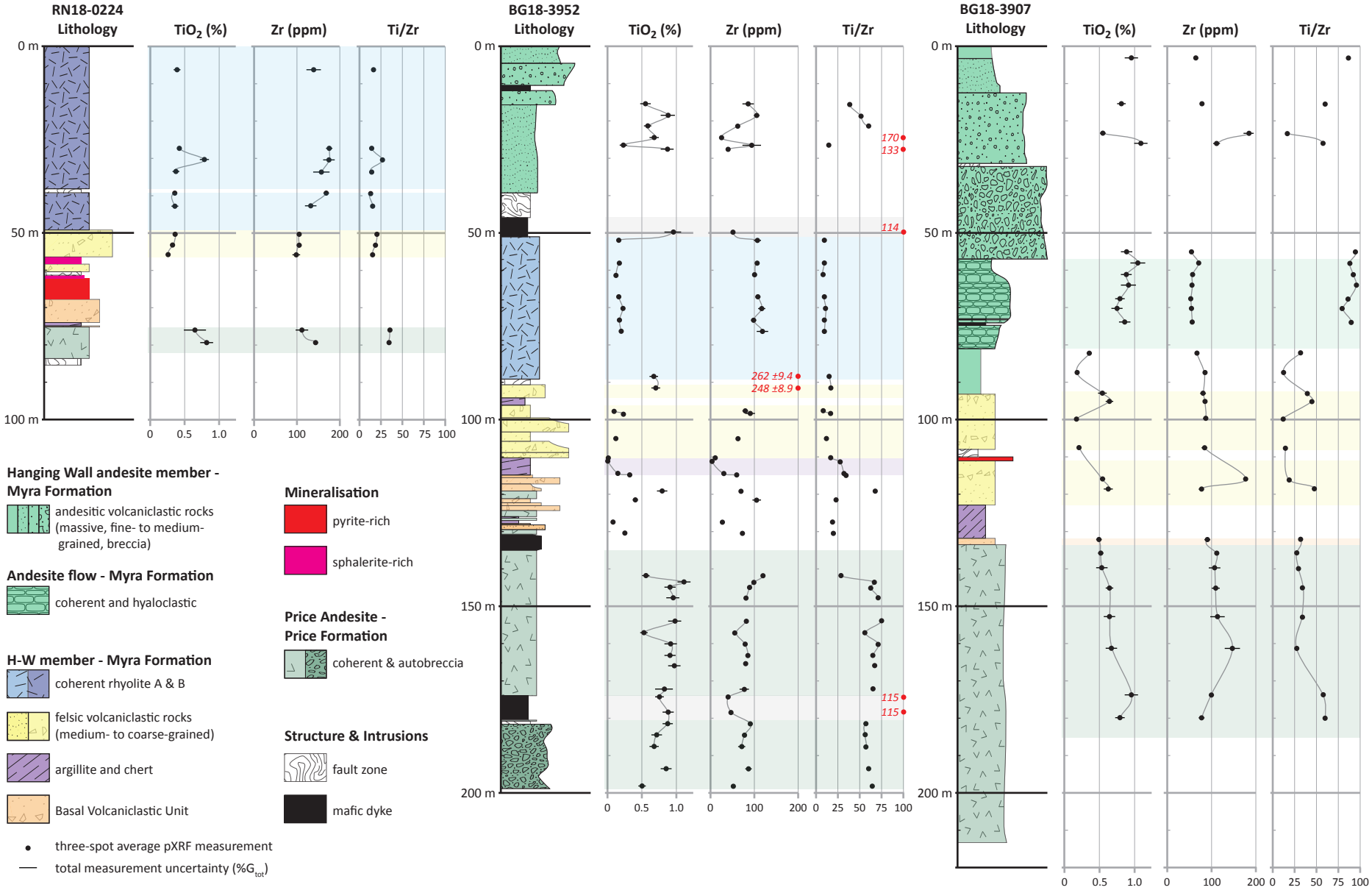
RN18-0224
Lithology
TiO2 (%)
Zr (ppm)
Ti/Zr
0 m
50 m
100 m
0 0.5 1.0
0 100 200
0 25 50 75 100
BG18-3952
Lithology
TiO2 (%)
Zr (ppm)
Ti/Zr
0 m
50 m
100 m
150 m
200 m
170
133
114
262 ±9.4
248 ±8.9
115
115
0 0.5 1.0
0 100 200
0 25 50 75 100
BG18-3907
Lithology
TiO2 (%)
Zr (ppm)
Ti/Zr
0 m
50 m
100 m
150 m
200 m
0 0.5 1.0
0 100 200
0 25 50 75 100
Hanging Wall andesite member - Myra Formation
andesitic volcaniclastic rocks (massive, fine- to medium-grained, breccia)
Andesite flow - Myra Formation
coherent and hyaloclastic
H-W member - Myra Formation
coherent rhyolite A & B
felsic volcaniclastic rocks (medium- to coarse-grained)
argillite and chert
Basal Volcaniclastic Unit
Mineralisation
pyrite-rich
sphalerite-rich
Price Andesite - Price Formation
coherent & autobreccia
Structure & Intrusions
fault zone
mafic dyke
three-spot average pXRF measurement
total measurement uncertainty (%G$_{tot}$)

to sulfide mineralisation in the H-W member will improve volcano-stratigraphic models and assist in exploring for VHMS mineralisation at Myra Falls.

Volcano-sedimentary rock types in the West Block Area change abruptly with depth down-hole. In one example, medium-grained felsic volcaniclastic, bedded argillite-chert, and normally graded Basal Volcaniclastic Unit rocks are encountered over an 8-metre interval (Figure 6.13C). Volcaniclastic rock types pose the greatest challenge in pXRF analysis due to their natural heterogeneity and variable grain size. However, overall, felsic volcaniclastic samples mirror the Ti/Zr signatures of the coherent rhyolite, argillite and chert samples with Ti/Zr ratios ranging between 10 and 30, and the Basal Volcaniclastic Unit has Ti/Zr ratios >30 (BG18-3952; Figure 6.12).

Figure 6.13 BQ drill core photographs. Red circles are locations of three-spot pXRF measured samples with Ti/Zr results in red text. Measurements were taken from the flat, sawn surface of drill core samples. In some cases in the drill core photograph the core is rotated and appears whole, and in other cases the core photograph was taken prior to cutting. A. Interval of coherent to fragmental andesite flow from drill hole BG18-3907. B. Interval of quartz-sericite-pyrite altered coherent rhyolite from drill hole BG18-3952. C. Interval of felsic volcaniclastic, bedded chert and argillite, and graded Basal Volcaniclastic Unit rocks from drill hole BG18-3952. [Fvc, felsic volcaniclastic rocks; Arg, bedded argillite-chert; Bvc, Basal Volcaniclastic Unit]

In the West Block Area, the Price Formation has a bimodal Ti/Zr signature. The top 5 to 30-metres of Price Formation has an intermediate composition with Ti/Zr ratios between 30 and 45 (Figure 6.12). The Ti/Zr ratios change with increasing depth to values more typical of mafic compositions (Ti/Zr 50-65; Figure 6.12). This lithogeochemical feature is shown on the Ti/Zr profiles for drill holes BG18-3952 and BG18-3907; where a lithological contact was not visually observed in the drill core but is indicated by abrupt change in Ti/Zr ratios near 145 metres and 170 metres depth, respectively.

A significant challenge at Myra Falls is accurately identifying the contact between the H-W member and the Price Formation. This contact is important as it marks the base of known mineralised stratigraphy in the district. Moderate to intense chlorite-quartz ± sulfide alteration is texture destructive and results in a darkening of the drill core. This effect resulted in a number of drill holes ending in H-W member stratigraphy, being incorrectly logged as Price Formation, in the Marshall Zone locality (Barrett and MacLean, 2000). Sulfide lenses in the Marshall Zone orebody are located at an "upper zone" position and the potential for "contact zone" position sulfide mineralisation remains untested. Sericite-quartz ± sulfide alteration results in a rock colour change to white-light grey, regardless of protolith. This phenomenon is illustrated in Figure 6.14 where andesite of the Price Formation at the contact with the H-W member is hydrothermally altered. Though the physical appearance of the drill core is drastically different at the top of the interval and the bottom, pXRF Ti/Zr ratios are consistent (RN18-0224, BG18-3907; Figures 6.12; 6.14) and indicate an intermediate composition (Ti/Zr of 30-35).

Figure 6.14 BQ drill core photographs. Red circles are locations of three-spot pXRF measured samples with Ti/Zr results in red text. A-B. Intervals of sericite-quartz-pyrite altered Price Formation andesite transitioning down-hole to chlorite-quartz-pyrite altered, from drill holes RN18-0224 and BG18-3907, respectively.

6.6 Discussion

Whilst it is common industry practice to prepare powdered samples prior to analysis by pXRF, this preparation method is sample destructive, expensive, and time-consuming. Bourke and Ross (2015) demonstrated that pXRF instrument precision and data accuracy are not significantly improved with powdered samples, relative to drill core surface measurements of fine- to medium-grained volcanic and intrusive rocks. This study confirms this, specifically for elements significant for lithogeochemistry including Ti, Zr, Mn, Rb and Sr (Table 6.2). The calibration-line and sampling procedure provided here illustrates that the pXRF analysis, can produce robust lithogeochemical discrimination data, particularly the immobile elements Ti and Zr (Table 6.2).

Previous studies have shown that pXRF analyses can produce precise and accurate results for Cr, which is a useful immobile element for lithogeochemical discrimination of mafic volcanic rock types with variable Cr concentrations (e.g., Gazley et al. 2011). The average instrument precision of 9.79 % RSD for Cr analyses in this study is similar to other studies (Gazley et al. 2011; Bourke and Ross 2015; Le Vaillant et al., 2014). However, in this study the conventional XRF Cr results could not be reproduced (Table 6.2). This appears to be a function of low Cr concentrations and possibly sample heterogeneity of the Myra Falls rock types. In general Cr concentrations are <100 ppm at Myra Falls. This combined with an effective detection limit of ~50 ppm indicates that Cr is not as effective as a lithogeochemical discriminator as Ti and Zr at Myra Falls.

Key limiting factors to the effectiveness of pXRF analysis on drill core samples are count rates (i.e., beam run-time) and sample volume (i.e., sample window size and penetration depth). Previous studies have reported a range of optimal beam times of pXRF analysis. Le Vaillant et al. (2014) demonstrated that a beam run-time as short as 20 seconds was sufficient. While Ross et al. (2014a) and Bourke and Ross (2015) concluded that 30 seconds per beam (1.5 min total in SOIL MODE, and 1 min total in MINING PLUS mode) was sufficient for both major and trace element analysis using an Olympus Innov-X Delta Premium analyser for routine *in situ* measurements. Mauriohooho et al. (2016) determined that a total beam runtime of 1 minute in GEOCHEM MODE with an Olympus Innov-X Delta 50 kV analyser was optimal for analysing rock chip cuttings with an average sample grain size between 1 and 6 mm.

A longer total beam runtime of 3.5 minutes was used because the expected concentrations for Zr were <200 ppm. The objective of the proposed methodology was to replicate conventional XRF whole-rock analysis for Ti and Zr. The key factor identified in this study effecting Ti and Zr results was not the pXRF analyser but geological sample heterogeneity. To improve effects of sampling precision more analyses per sample could be measured or an increased density of samples could be collected. One alternative pXRF analysis method is to collect more samples (e.g., one measurement every 30 cm versus 3 measurements every 3 metres) at shorter beam runtimes and calculate a 3-point moving average (e.g., Ross et al., 2014).

The second critical factor for acquiring robust pXRF measurements from the surface of drill core samples is the number of particles (mineral grains) analysed, which is a function of grain size. For fine-grained rock samples this is less of an issue than for coarse-grained rocks (e.g., Potts et al., 1997; Forster et al., 2011). Recent developments in pXRF analysers are producing larger sample windows, such as the Olympus Vanta 50 kV M-Series analyser that has a detector window area of approximately 38 mm^2. This detector window has almost twice

the area compared to the analyser used in this study. As a result, the larger detector window would double the number of particles analysed per measurement from drill core samples in this study. This has the potential to improve measurement variability without adding additional analysis time.

The successful implementation of a pXRF sampling protocol is dependent on rock type, grain size and the intended application of the acquired geochemical data. Therefore the appropriate beam runtime, mode setup, reference standards, and sample measurements will be site and objective specific and should be tested on a series of representative samples prior to the implementation of a routine logging procedure (e.g., Andrew and Barker, 2017; Ryan et al., 2017). In this study, a calibrated average result from three-spot analyses collected from the clean, flat surface of drill core with an Olympus Innov-X Delta Premium analyser in SOIL MODE reproduced conventional XRF Ti/Zr lithogeochemical signatures. No significant improvement in accuracy or precision between drill core powders and unprepared drill core samples was observed. Sampling precision could be improved by increasing the number of analyses. Without adding additional time to the analytical method, this could be achieved by reducing the beam-run time to 30 seconds and either increasing the spot measurements to six per sample or by collecting twice as many rock samples using the three-spot measurement technique.

Correct identification of volcanic rock types in hydrothermally altered and metamorphosed environments, such as VHMS systems, can be challenging. In particular, at Myra Falls the manifestation of this challenge is presented in the Barrett and MacLean (2000) study of the Marshall Zone orebody. The recognition and confirmation of unintentionally stopping exploration drill holes short of the Price Formation contact due to the misidentification of fine-grained and hydrothermally altered volcanic rocks was not revealed until after a conventional lithogeochemical study. The results of this study show that pXRF analysis of unprepared drill core samples can produce robust, on site, and near real-time Ti/Zr results that the exploration geologist can use to inform drilling and targeting decisions. This has applications beyond Myra Falls, where this method can be used to improve the protolith recognition of volcanic rocks in other VHMS environments, specifically altered stratigraphy. The benefits of applying routine pXRF analysis are that it is inexpensive, fast, and adaptable to the desired geochemical outputs (e.g., whole-rock geochemistry or grade control). A previous perceived weakness of pXRF analysis was that to acquire robust data sample preparation required pulverising the rock sample. However, this study shows that with fine- to medium-grained rocks samples, fit-for-purpose pXRF data is achievable by averaging of three-spot pXRF measurements from the flat, clean surface of drill core. This technique can be expanded from drill core samples to rock outcrop samples, providing the exploration geologist with the means to acquire important lithogeochemical data that can be incorporated in the assessment of mineral exploration targets.

Additionally, immobile element geochemistry can be used to assess magmatic affinity of volcanic and intrusive rocks (e.g., MacLean and Barrett, 1993; Piercey, 2010), as well as major element oxide geochemistry to characterise hydrothermal alteration trends (e.g., Large et al., 2001a; Warren et al., 2007). These particular aspects of lithogeochemistry were not assessed in this study. However, the acquisition of major oxide and trace element data using systematic pXRF from either drill core or rock outcrop could be applied to assess these lithogeochemical features in a mineral exploration context (e.g., komatiite-hosted Ni deposits – Le Vaillant et al., 2014; Pb-Zn skarn deposits – Yuan et al., 2014; banded iron formation – Lawley et al., 2015; and

base metal SEDEX deposits – Andrew and Barker, 2017).

6.7 Portable XRF Considerations

Factors that users should consider when developing and implementing a fit-for-purpose pXRF analysis protocol include: (1) major vs. trace element data; (2) immobile vs. mobile elements (alteration characterisation vs. protolith discrimination); (3) sample grain size (sample heterogeneity); (4) sampling material (drill core, out crop, coarse rejects, powders etc.); and (5) standard reference materials.

For the analysis of drill core samples, it is recommended that the samples be sawn to allow for a flat measurement surface (e.g., Morris 2009; Le Vaillant et al., 2014). These samples can then be archived to preserve a record of the drill hole and/or analysed with other nondestructive methods, such as shortwave infrared, magnetic susceptibility or density. Instrument set-up is contingent upon the desired lithogeochemical data (major vs. trace elements), with the instrumental precision a function of beam-run time (e.g., Fisher et al., 2014; Le Vaillant et al., 2014; Ross et al., 2014a). Sample precision is a function of grain size and heterogeneity of the sample (e.g., Potts et al., 1997; Forster et al., 2011). In general, coarser-grained samples will require more analyses than finer-grained samples. Instrument optimisation testing (beam-run time and number of analyses per sample) on a representative sample set prior to routine analysis is encouraged. To obtain appropriate calibration equations; the standard reference materials need to be selected carefully based on the elements of interest and the composition of the samples to be analysed.

Geologic variability (volcaniclastic vs. coherent volcanic rocks) must always be considered when developing an analytical protocol and interpreting the results. Portable-XRF lithogeochemical data should be integrated with geological observations, not used in isolation. VHMS deposits form in submarine volcanic depositional settings, that are preserved in variably metamorphosed and hydrothermally altered rocks. The combination of detailed graphic logs with near-real time, down-hole pXRF chemistry provides the exploration geologist with a robust dataset to make informed decisions for identifying and testing of drill hole targets in the field.

6.8 Summary

An investigation of the available whole-rock geochemistry for the H-W member confirmed sufficient elemental variation to discriminate mafic, intermediate and felsic rock types at Myra Falls. Specifically, Ti/Zr ratios are a robust lithogeochemical discriminator and can be used to confidently identify hydrothermally altered volcanic rock types at Myra Falls. This includes andesite of the Price Formation (51.4-77.0), and coherent rhyolite (10.2-14.4), andesite sills and flows (81.3-101.3), and dacite sills (30.2-49.0) of the lower Myra Formation. Two types of rhyolite were identified by Barrett and MacLean (2000) near the Marshall Zone orebody based on Ti/Zr ratios: (1) Rhyolite A – quartz and feldspar-phyric rhyolite with an average Ti/Zr ratio of 10.6 and (2) Rhyolite B – feldspar-phyric rhyolite with an average Ti/Zr ratio of 15.5.

Based on these conventional geochemical results, a three-spot pXRF methodology was proposed and developed to provide a time- and cost-effective alternative to conventional XRF techniques. A comparison of pXRF results utilising calibrated and average three-spot analysis of intact drill core samples with corresponding conventional XRF/ICP-MS results, indicated that pXRF Ti/Zr ratios provide a fit-for-purpose solution to improving the identification of

hydrothermally altered rock types at Myra Falls. The down-hole profile results illustrate that the acquisition of systematic pXRF lithogeochemistry combined with detailed lithofacies graphic logs at Myra Falls can improve lithology logging.

In summary it is suggested that pXRF analyses should become a routine part of lithology logging as its application can support geologic and lithostratigraphic interpretations at Myra Falls and elsewhere. In particular, the use of immobile elements in regional greenschist to amphibolite facies metamorphosed stratigraphy and hydrothermally altered rocks in VHMS, SEDEX, and orogenic gold mineral deposit exploration.

Chapter 7:

Myra Falls Sicker Group Geochronology

The duration, nature and geochemistry of volcanic and volcano-sedimentary rocks in VHMS settings are important controlling factors on the location of syngenetic sulfide mineralisation (e.g., Mortensen et al., 2015). Understanding these factors at deposit and regional scales are crucial for developing new lithological frameworks to assist mineral exploration in mature districts. Previous attempts to date the duration of volcanic activity at Myra Falls by Juras (1987), Brandon et al. (1986), Parrish and McNicoll (1992), Barrett and Sherlock (1996) and Ruks (2015) have resulted in relatively imprecise crystallisation ages, which overlap in error, and do not resolve the temporal relationship between the L-M-P and H-W members that host two distinct VHMS horizons. Additionally, the crystallisation age of the Price Formation andesite, the footwall stratigraphy to the H-W member, is not known. New geochronology data presented in this chapter was collected in an effort to refine the temporal relationships between the two VHMS-hosting felsic volcanic members of the Myra Formation at Myra Falls, and compare these results with the mineralised felsic volcanic units in the Cowichan Lake uplift.

7.1 Vancouver Island Sicker Group Age Constraints and Correlations

The oldest stratigraphy identified in the Wrangellia Terrane is the mid-Paleozoic Sicker Group on Vancouver Island (Figure 7.1). Paleozoic stratigraphy is exposed in several northwest-trending basement highs that are the result of both Middle Jurassic accretion of Wrangellia to the Laurentian margin and Eocene deformation related to the Cowichan fold and thrust belt (Muller, 1980; England and Calon, 1991; Yorath et al., 1999). Regional metamorphism of the Sicker Group is characterised by lower- to upper-greenschist facies (Juras, 1987; Greenwood et al., 1991).

Volcanic-hosted massive sulfide mineralisation occurs throughout Vancouver Island (Figure 7.1), with the most economically significant deposits hosted in the felsic volcanic stratigraphy of the Sicker Group (*see Chapter 2*). The Myra Falls VHMS district is hosted in the Devonian felsic volcanic and volcano-sedimentary rocks of the Myra Formation. The Lara, Lenora and Jane VHMS occurrences are located in the Cowichan Lake uplift and are associated

with Devonian felsic volcanic rocks of the McLaughlin Ridge Formation (Figure 7.1; Massey and Friday, 1987). Yorath et al. (1999) determined that the Myra Formation is a regional correlate with the McLaughlin Ridge Formation (Figure 7.2).

The oldest Sicker Group rocks exposed in the Buttle Lake uplift comprise basaltic to andesitic lavas and breccias of the Price Formation (Juras, 1987). The Price Formation is at least Late Devonian in age based on the crystallisation age of 366 ± 4 Ma (Brandon et al., 1986) for coherent rhyolite in the overlying Myra Formation. The Myra Formation comprises rhyolite and rhyolitic volcaniclastic rocks, and andesitic volcaniclastic rocks, basalt, and marine sedimentary rocks (Juras, 1987; Sinclair, 2000). The Thelwood Formation overlies (locally unconformably) the Myra Formation, and consists of volcaniclastic rocks intruded by mafic sills. Early Mississippian radiolaria are reported from the base of the Thelwood Formation immediately above the Myra Formation (Figure 7.2; Jones, 2001). A maximum $^{207}Pb/^{206}Pb$ zircon age of 320 ± 7 Ma for andesitic volcaniclastic rocks indicates an Early Mississippian to Pennsylvanian age for the lower Thelwood Formation (Figure 7.2; Juras, 1987). The Flower Ridge Formation conformably overlies the Thelwood Formation, and consists of basaltic volcaniclastic and coherent rocks, with less abundant mudstone of unknown age (Juras, 1987).

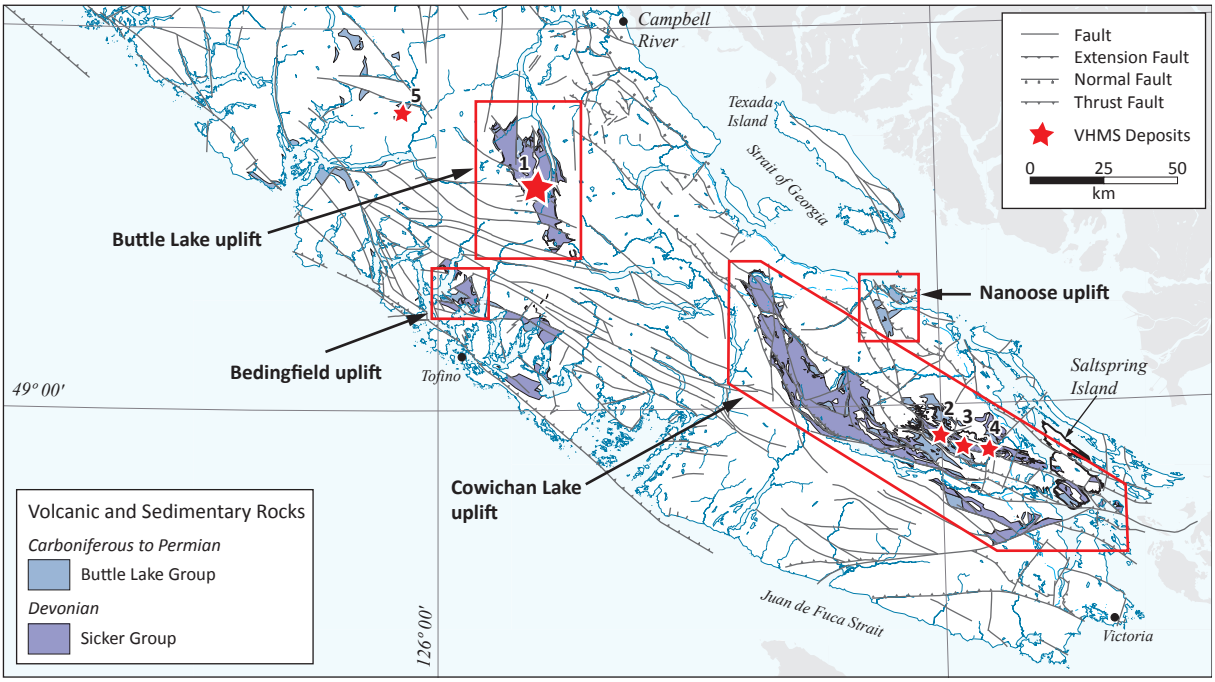

Figure 7.1 Location of Paleozoic strata of the Sicker and Buttle Lake Groups on Vancouver Island (modified from Massey et al., 2005). [VHMS deposits: 1, Myra Falls; 2, Lara; 3, Lenora; 4, Jane; 5, Dragon property]

In the Cowichan Lake uplift, the lowermost Sicker Group rock units are Middle Devonian basaltic to andesitic volcanic rocks of the Duck Lake Formation (Massey, 1995). A dacite flow, intercalated with basalt flows assigned to the Duck Lake Formation, yielded a U-Pb zircon age of 366.6 ± 0.7 Ma (Figure 7.2; Ruks, 2015). Chert at the base of the Duck Lake Formation contains radiolarian assemblages suggesting a Middle or Late Devonian age (Ruks, 2015). Submarine mafic volcanic and volcaniclastic rocks of the Nitinat Formation overlie the Duck Lake Formation (Yorath et al., 1999). Radiolarian biochronology of chert within the McLaughlin Ridge Formation yield Late Devonian ages, suggesting that the underlying Nitinat and Duck Lake Formations are pre-Late Devonian in age (Ruks, 2015). The Duck Lake and Nitinat

Formations are interpreted to be regional equivalents to the Price Formation in the Buttle Lake uplift (Figure 7.2; Yorath et al., 1999).

The Late Devonian McLaughlin Ridge Formation overlies the Nitinat Formation in the Cowichan Lake uplift (Yorath et al., 1999). Felsic volcanic rocks of the McLaughlin Ridge Formation range in age from 364.8 ± 1.3 Ma to 353.1 ± 3.4 Ma (Figure 7.2; U-Pb zircon ages; Sluggett, 2003; Ruks, 2015). Quartz-feldspar porphyritic intrusions of the Saltspring Intrusive Suite in the Cowichan Lake uplift range in age from 360.7 ± 2.4 Ma to 355.0 ± 1.5 Ma, suggesting they are coeval with the rhyolitic volcanic rocks of the McLaughlin Ridge Formation (U-Pb zircon ages; Sluggett, 2003; Ruks, 2015).

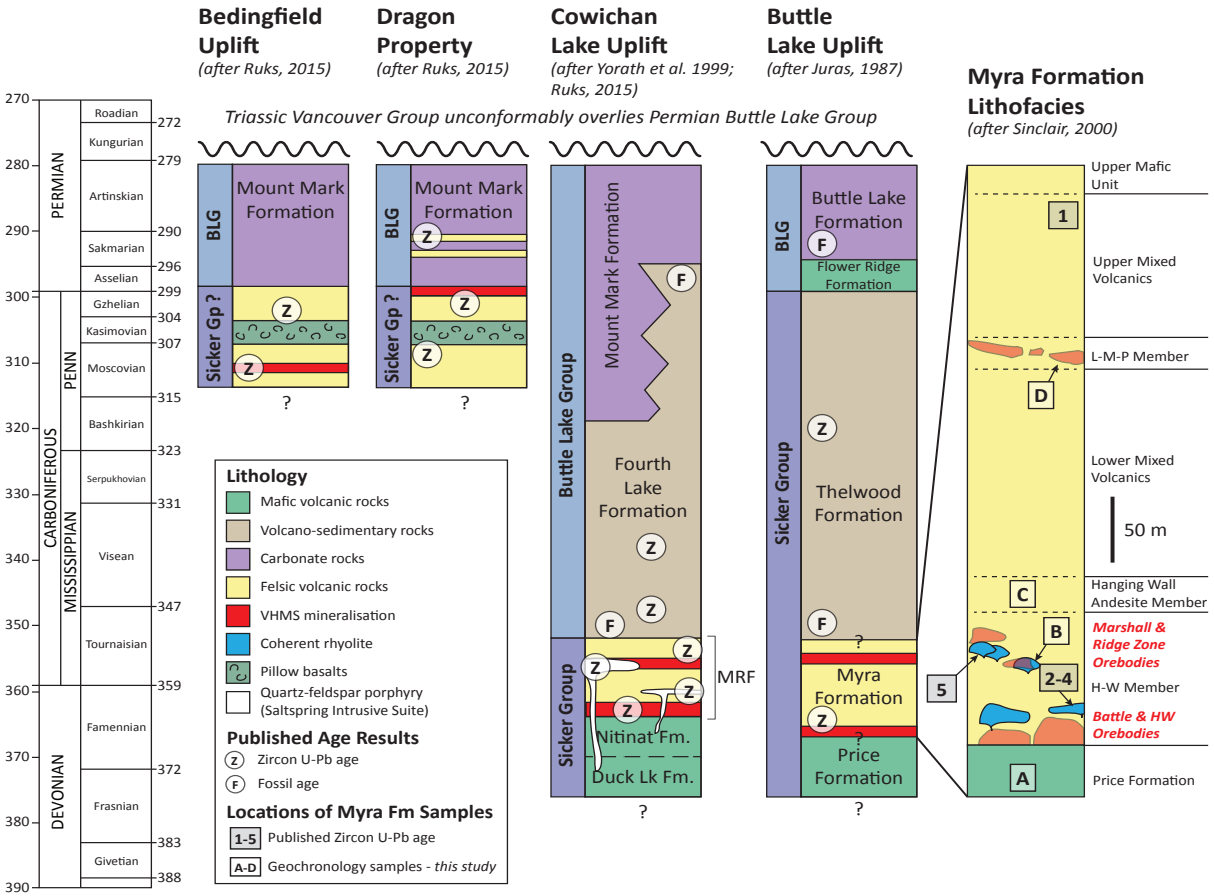

Figure 7.2 Comparative chronostratigraphic columns illustrating the temporal relationships of the Paleozoic rocks of Vancouver Island (modified from Massey, 1992; Juras, 1987; Sinclair, 2000; Ruks, 2015) with the location of published age constraints and new geochronology samples at Myra Falls. Selected zircon and fossil ages from Parrish and McNicoll (1992), Barrett and Sherlock (1996), Jones (2001), Katvala (2006) and Ruks (2015). Geologic time scale from Walker et al. (2012). [BLG, Buttle Lake Group; Fm, Formation; Lk, Lake; MRF, McLaughlin Ridge Formation]

The Buttle Lake Group overlies the Sicker Group (Figure 7.2). In the Cowichan Lake uplift, rocks of the Fourth Lake Formation are the oldest stratigraphic unit of the Buttle Lake Group, and comprise Mississippian through Early Permian marine sedimentary rocks, reworked felsic volcaniclastic rocks, and minor rhyolite porphyries (Yorath et al., 1999; Ruks, 2015). New U-Pb zircon age constraints by Ruks (2015) of reworked felsic volcaniclastic rocks and rhyolite porphyries yielded ages from 347.2 ± 2.3 Ma through 340.7 ± 1.7 Ma and 338.2 ± 3.5 Ma to 335.3 ± 2.5 Ma, respectively (Figure 7.2). Fossil ages for the Fourth Lake Formation strata range from Early Mississippian to Early Permian (Figure 7.2; Yorath et al., 1999; Katvala and Henderson,

2002; Ruks, 2015). The Middle Pennsylvanian through Early Permian Mount Mark Formation limestone overlies the Fourth Lake Formation (Yorath et al., 1999; Katvala and Henderson, 2002). The Fourth Lake and Mount Mark Formations are correlated with the Thelwood and Buttle Lake Formations in the Buttle Lake uplift (Figure 7.2) by Yorath et al. (1999).

Numerous studies have used U-Pb zircon geochronology to decipher chronostratigraphic relationships between lithostratigraphic units and sulfide mineralisation at Myra Falls (Figure 7.3). The first age constraint for the Myra Formation comes from a maximum zircon age of ca. 370 Ma for the Upper Rhyolite volcaniclastic unit of the Myra Formation (Juras, 1987). Further geochronological studies at Myra Falls have focused on determining the igneous crystallisation age of the HW Rhyolite unit above the HW orebody. Minimum modelled U-Pb ages of approximately 370 Ma (2 zircon grains) and 366 ± 4 Ma (5 zircon fractions) from coherent rhyolite samples were reported by Brandon et al. (1986) and Parrish and McNicoll (1992). More recently, Barrett and Sherlock (1996) reported a rhyolite crystallisation age of 365 ± 4 Ma (weighted average $^{206}Pb/^{238}U$ ages from 5 zircon fractions). These results are consistent with the Late Devonian age for the Myra Formation identified by Juras (1987), however, these results are spatially restricted and have relatively large errors. The most recent age constraint for the Myra Formation is from a sample of HW Rhyolite collected from the Marshall Zone orebody. This hydrothermally altered and mineralised sample yielded a $^{206}Pb/^{238}U$ zircon age of 361.5 ± 2.5 Ma (Ruks, 2015).

7.2 Geochronology Samples

The geology of the Myra Falls VHMS district and the locations of U-Pb geochronology samples from this study are summarised in a stylized stratigraphic column (Figure 7.2). A total of twenty-six samples were collected for U-Pb analyses, of which ten samples were dated (Table 7.1). The primary objective of this study was to investigate the crystallisation and depositional history of andesitic and rhyolitic volcanic stratigraphy using U-Pb zircon dating techniques. However, zircons were difficult to locate in all samples and no zircons were found in most of the andesite samples. As a result, U-Th-Pb monazite dating was attempted on one sample from the Price Formation and U-Pb apatite on one sample of coherent andesite from the H-W member to investigate the age of these units.

7.2.1 Sample preparation and automated mineral identification

Samples were prepared in three ways at the University of Tasmania (UTAS). Samples consisted of zircon mounts of handpicked grains from heavy mineral separates, grain mounts from heavy mineral fractions, and rock chip mounts. Heavy mineral fractions for U-Pb zircon and apatite dating were prepared by crushing 200-400 g of sample in a Cr-steel ring mill to a grain size <400 μm. Heavy mineral fractions were separated using a standard plastic pan and warm water. Further agitation of the heavy mineral fraction on a watch glass resulted in the removal of a residual light fraction. Magnetic material was removed using a Fe-B-Nd hand magnet. For pyrite-rich samples, the heavy mineral fraction was roasted in an oven at 350°C for 2 hr, which partially oxidised the pyrite allowing it to be removed with a hand magnet. Zircons were picked from the nonmagnetic, heavy mineral fraction under a petrographic microscope and placed individually onto doubled-sided sticky tape. Heavy mineral fractions for U-Pb apatite dating were poured onto double-sided sticky tape. Mineral grains were then mounted in 2.5 cm diameter moulds, and encased in an epoxy resin. Mounts were dried in an oven at 60°C for 4 hr, polished using clean sandpaper and a polishing lap, and washed in distilled water in an

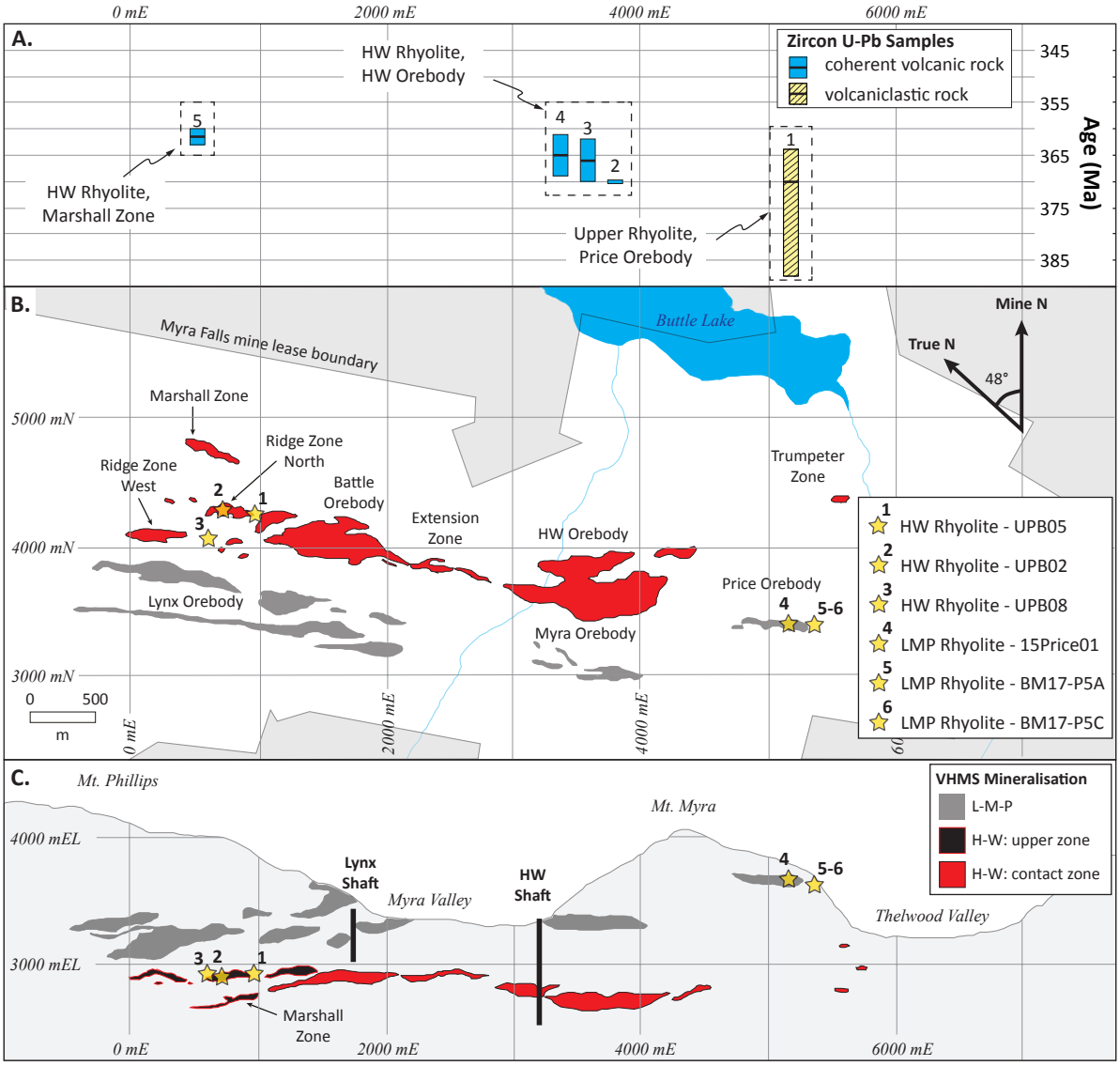

Figure 7.3 Summary of published geochronology and sample locations from this study. A. Summary of U-Pb zircon age constraints for the Sicker Group at Myra Falls. (1) Age constraint from felsic volcaniclastic rock from Price Mine (Juras, 1987). (2) Age constraint from coherent rhyolite from above the HW orebody, no reported error (Brandon et al., 1986). (3) Age constraint from coherent rhyolite above HW orebody (Parrish and McNicoll, 1992). (4) Age constraint from coherent rhyolite above HW orebody (Barrett and Sherlock, 1996). (5) Age constraint from mineralised coherent rhyolite from Marshall Zone orebody (Ruks, 2015). B. Map of Myra Falls VHMS district showing two camp-scale ore horizons (after Jones et al. 2006b), the location of the contact and upper zone mineralisation styles, and the location of zircon U-Pb dating samples of coherent rhyolite of the HW Rhyolite and rhyolite volcaniclastic rocks from the LMP Rhyolite from this study. C. Composite cross-section of Myra Falls (after Jones et al. 2006a) with relative location of zircon U-Pb geochronology samples.

ultrasonic bath. Rock chips were mounted in 2.5 cm diameter epoxy resin moulds, polished, and washed with distilled water in an ultrasonic bath. These mounts were used for scanning electron microscopy (SEM) and *in situ* U-Pb zircon and monazite dating.

Prior to U-Th-Pb analysis, mineral and rock chip mounts prepared at UTAS were carbon coated and imaged by SEM and cathodoluminescence (CL). Zircon and monazite in polished rock chip mounts and apatite in polished grain mounts were identified using a FEI MLA650 environmental SEM operated by an automated software package (Mineral Liberation Analyser or MLA; Gu 2003) at the Central Science Laboratory (CSL), UTAS. Sack et al. (2011) developed

a protocol that utilises automated SEM, energy-dispersive X-ray spectrum-based searching method to locate minerals for geochronology research. For each sample, a high-resolution back-scattered electron (BSE) sample mosaic was collected and integrated with the MLA mineral identification RGB image to create a digital, mineral of interest sample map. Typical MLA run time was 1 to 2 hr per sample, with up to 13 samples analysed in a session.

Table 7.1 Summary of collected Myra Falls geochronology samples.

Sample Id	Rock type	Lithofacies	Sample type	Mineral	Method	Mineral Id	U-Th-Pb analysis	# of analyses
BM14-029	And	Price Fm	DC: BG18-3769	z	min sep	N		
				a	SEM-MLA[2]	Y		
BM14-043	And	Price Fm	DC: BG18-3905	z	min sep	N		
				a	SEM-MLA[2]	Y		
BM14-074	And	Price Fm	DC: BG18-3517	z	min sep	N		
				a	SEM-MLA[2]	Y		
UPB06A	And	Price Fm	DC: RN18-0224	z	SEM-MLA[1]	Y	*in situ* LA-ICPMS	3
UPB06B	And	Price Fm	DC: RN18-0224	z	SEM-MLA[1]	Y		
UPB07A	And	Price Fm	DC: RN18-0224	z	SEM-MLA[1]	Y	*in situ* LA-ICPMS	3
UPB07B	And	Price Fm	DC: RN18-0224	z	SEM-MLA[1]	Y		
UPB10A	And	Price Fm	DC: BG18-3952	z	SEM-MLA[1]	Y	*in situ* LA-ICPMS	5
UPB10B	And	Price Fm	DC: BG18-3952	z	SEM-MLA[1]	Y	*in situ* LA-ICPMS	6
				m	SEM-MLA[1]	Y	*in situ* LA-ICPMS	20
TS-076	And	Price Fm	DC: BG18-3902	z	SEM-MLA[1]	Y		
TS-182	And	Price Fm	DC: BG18-3769	z	SEM-MLA[1]	N		
TS-192	And	Price Fm	DC: BG18-3769	z	SEM-MLA[1]	N		
TS-717	And	Price Fm	DC: BG18-3554	z	SEM-MLA[1]	Y		
TS-721	And	Price Fm	DC: BG18-3554	z	SEM-MLA[1]	N		
BM17-P13A	And	Price Fm	Surface	z	min sep	N		
BM17-P13B	And	Price Fm	Surface	z	min sep	N		
UPB02	Rhy	HW Rhyolite	Under ground	z	min sep	Y	LA-ICPMS	20
				z	UBC	Y	CA-ID-TIMS	5
UPB05	Rhy	HW Rhyolite	DC: RN18-0224	z	min sep	Y	LA-ICPMS	7
				z	UBC	Y	CA-ID-TIMS	5
UPB08	Rhy	HW Rhyolite	DC: BG18-3952	z	min sep	Y	LA-ICPMS	23
15RN04	Rhy	HW Rhyolite	Under ground	z	min sep	N		
UPB12	And	HW Member	DC: BG18-3921	z	min sep	N		
				a	SEM-MLA[2]	Y	LA-ICPMS	15
UPB12A	And	HW Member	DC: BG18-3921	z	SEM-MLA[1]	N		
UPB12B	And	HW Member	DC: BG18-3921	z	SEM-MLA[1]	N		
15Price01	Rhy	LMP Rhyolite	Under ground	z	min sep	N		
				z	UBC	Y	CA-ID-TIMS	2
BM17-P5A	Rhy	LMP Rhyolite	Surface	z	min sep	Y	LA-ICPMS	13
BM17-P5B	Rhy	LMP Rhyolite	Surface	z	min sep	N		
BM17-P5C	Rhy	LMP Rhyolite	Surface	z	min sep	Y	LA-ICPMS	23
BM17-P5D	Rhy	LMP Rhyolite	Surface	z	min sep	N		
BM17-P5E	Rhy	LMP Rhyolite	Surface	z	min sep	N		

SEM-MLA[1] = mineral search on rock chip mounts
SEM-MLA[2] = mineral search on grain mounts
[And, andesite; Rhy, rhyolite; DC, drill core; min sep, mineral separate; Y, yes; N, no; a, apatite; m, monazite; z, zircon]

Back-scattered electron images of monazite and zircon grains selected for *in situ* U-Th-Pb analysis were collected on a Hitachi SU-70 field emission scanning electron microscope (FE-SEM) at the CSL, UTAS. Sample compositional zoning was investigated by semi-quantitative energy dispersive X-ray spectral (EDS) analysis. Back-scattered electron images of apatite grains were collected on a FEI MLA650 SEM to document crystal morphologies and textures prior to U-Pb LA-ICPMS analysis. Cathodoluminescence images of zircon grains were also collected on a FEI MLA650 SEM to document internal structure, morphology and zoning to provide a context for the U-Pb age results.

At the University of British Columbia (UBC), Canada, zircons from 0.5-1 kg rock samples were separated using conventional crushing, grinding, wet shaking table, heavy liquid, and magnetic separation techniques by H. Lin. Zircons were then handpicked from the heavy mineral fraction in alcohol for CA-ID-TIMS analysis at the Pacific Centre for Isotopic and Geochemical Research (PCIGR) facility at UBC by Dr R. Friedman.

7.2.2 Price Formation samples

The Price Formation in the West Block Area is a feldspar-phyric, amygdaloidal and massive andesite with a fine- to medium-grained groundmass. It is variably chlorite- and muscovite-altered, with up to 15% disseminated sulfide (pyrite-dominant). Price Formation andesite from the Price Hillside near the Price orebody is feldspar-phyric, amygdaloidal and massive with a fine- to medium-grained groundmass. Dark green, chlorite altered pyroxene phenocrysts are common along with a variably chlorite and carbonate altered groundmass. Thirteen samples of the Price Formation were collected for U-Th-Pb geochronology (Table 7.1). Eleven samples were from the West Block Area and two samples were from the Price Hillside, with only samples from the West Block Area analysed (Figure 7.4A-F).

Samples BM14-029, BM14-043 and BM14-074 were collected for conventional heavy mineral fraction separation of zircon, but unfortunately, no zircons were recovered. Polished grain mounts made from the heavy mineral fraction of these samples were investigated for apatite, however the apatite grains identified were of insufficient size and quantity to analyse. Samples BM17-P13A and BM17-P13B were collected from the Price Hillside for conventional heavy mineral fraction separation of zircon, no zircon were recovered.

Eight samples (11 rock chip mounts) were collected to locate and analyse small zircon grains for *in situ* U-Pb dating analysis after the technique described by Sack et al. (2011). No zircons were identified with a MLA mineral search on samples TS-182, TS-192, and TS-721. Small zircons, no greater than 10 μm, were located in samples UPB06, UPB07, UPB10, TS-076 and TS-717 (Table 7.1). A total of two, 4 μm zircon grains were identified in samples TS-076 and TS-717, but were too small to be analysed. Zircons were analysed from samples UPB06A, UPB07A, UPB10A, and UPB10B. Monazite was identified in all 11 rock chip mounts and U-Th-Pb monazite dating was attempted on sample UPB10B.

7.2.3 HW Rhyolite samples

The HW Rhyolite in the West Block Area is characterised by a muscovite-quartz altered fine-grained groundmass with 5-10% (1-3 mm) quartz and 2-5% (1-2 mm) feldspar phenocrysts. In both drill core and underground exposures, coherent rhyolite is white and massive in texture. Coherent rhyolite is up to 50-metres-thick in the West Block Area and locally is host to polymetallic sulfide mineralisation. Four samples of coherent rhyolite were collected to

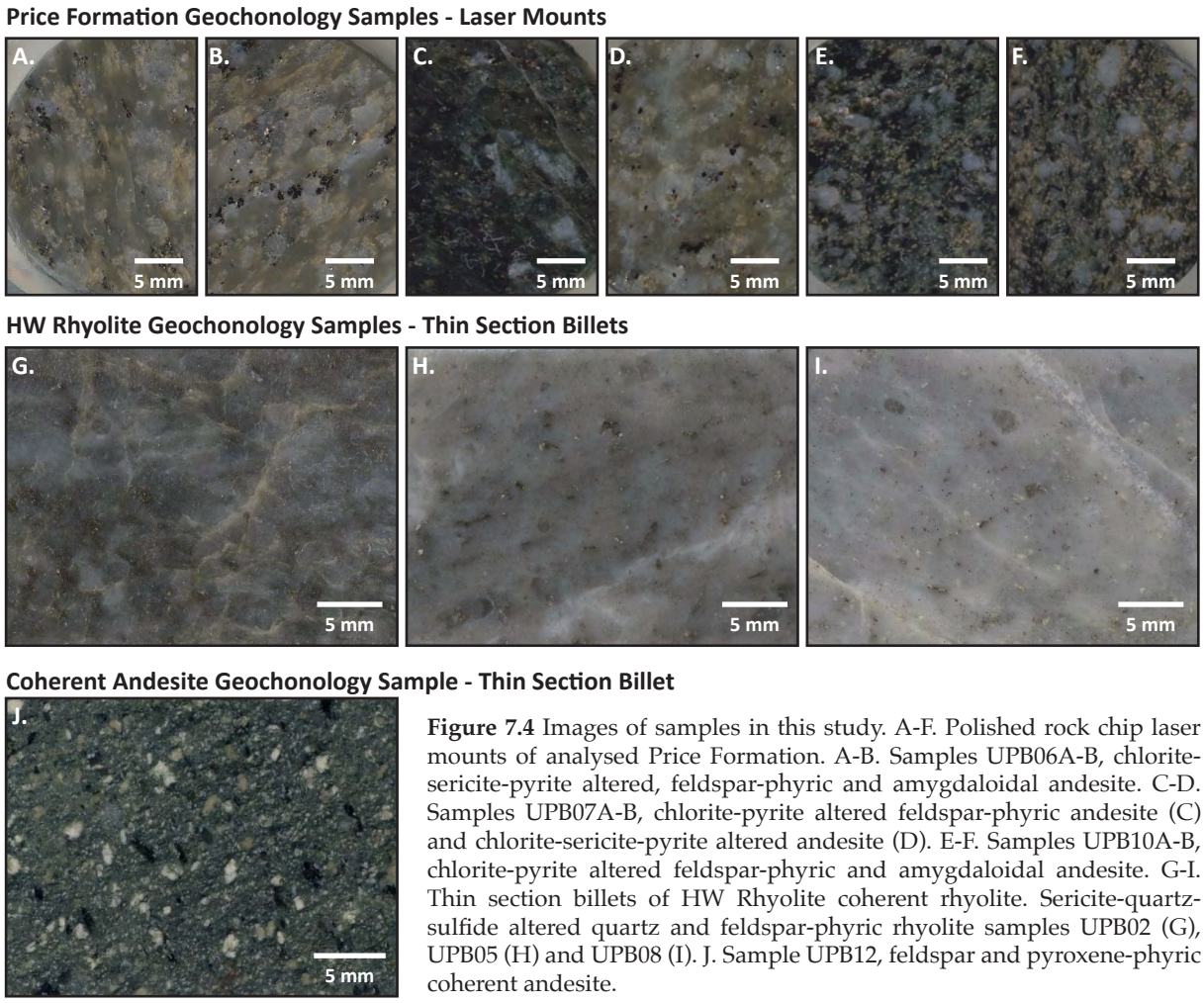

Figure 7.4 Images of samples in this study. A-F. Polished rock chip laser mounts of analysed Price Formation. A-B. Samples UPB06A-B, chlorite-sericite-pyrite altered, feldspar-phyric and amygdaloidal andesite. C-D. Samples UPB07A-B, chlorite-pyrite altered feldspar-phyric andesite (C) and chlorite-sericite-pyrite altered andesite (D). E-F. Samples UPB10A-B, chlorite-pyrite altered feldspar-phyric and amygdaloidal andesite. G-I. Thin section billets of HW Rhyolite coherent rhyolite. Sericite-quartz-sulfide altered quartz and feldspar-phyric rhyolite samples UPB02 (G), UPB05 (H) and UPB08 (I). J. Sample UPB12, feldspar and pyroxene-phyric coherent andesite.

constrain the temporal relationships of the polymetallic sulfide host rocks in the West Block Area (Table 7.1). Zircons for LA-ICPMS and CA-ID-TIMS U-Pb analysis were successfully extracted from samples UPB02, UPB05, and UPB08 (Figure 7.4G-I). Sample 15RN04 proved difficult to extract zircons from, as pyrite and barite were abundant in the heavy mineral fraction. As a result, this sample was not analysed.

7.2.4 Coherent andesite samples

In the West Block Area, a 10-30 metre in thickness andesite lava flow is present at the upper contact with the HW Rhyolite and the Hanging Wall Andesite member. The unit is massive, light green, and has a fine-grained groundmass. It has 5-10% feldspar phenocrysts and ≤5% pyroxene phenocrysts. The unit is weakly altered to chlorite-carbonate ± epidote (Figure 7.4J). Heavy mineral fraction separates were prepared from multiple samples, however no zircons were identified. Polished grain mounts of the heavy mineral fraction were investigated for apatite using an MLA mineral search. Fifteen apatites of sufficient size were identified and analysed. In addition, two rock chip mounts were made (UPB12A and UPB12B) and investigated for *in situ* small zircons using an MLA mineral search; no zircons were identified.

7.2.5 LMP Rhyolite samples

Five samples of muscovite-quartz-sulfide altered, rhyolitic volcaniclastic sandstone from the LMP Rhyolite member were collected from surface near the Price Mine Level 5 adit (Figure 7.5). Zircons suitable for U-Pb LA-ICPMS analysis were extracted from two of the five samples (Table 7.1). One underground sample was collected from Level 4 of the Price Mine (Figure 7.5D). Sample 15Price01 is strongly altered and is characterised by intense and pervasive muscovite and disseminated to stringer sulfide. This sample proved difficult to separate zircons from, as pyrite was abundant in the heavy mineral fraction. Unfortunately no zircons were extracted at UTAS. However, small zircons were successfully extracted from one sample sent to UBC for CA-ID-TIMS analysis (Table 7.1).

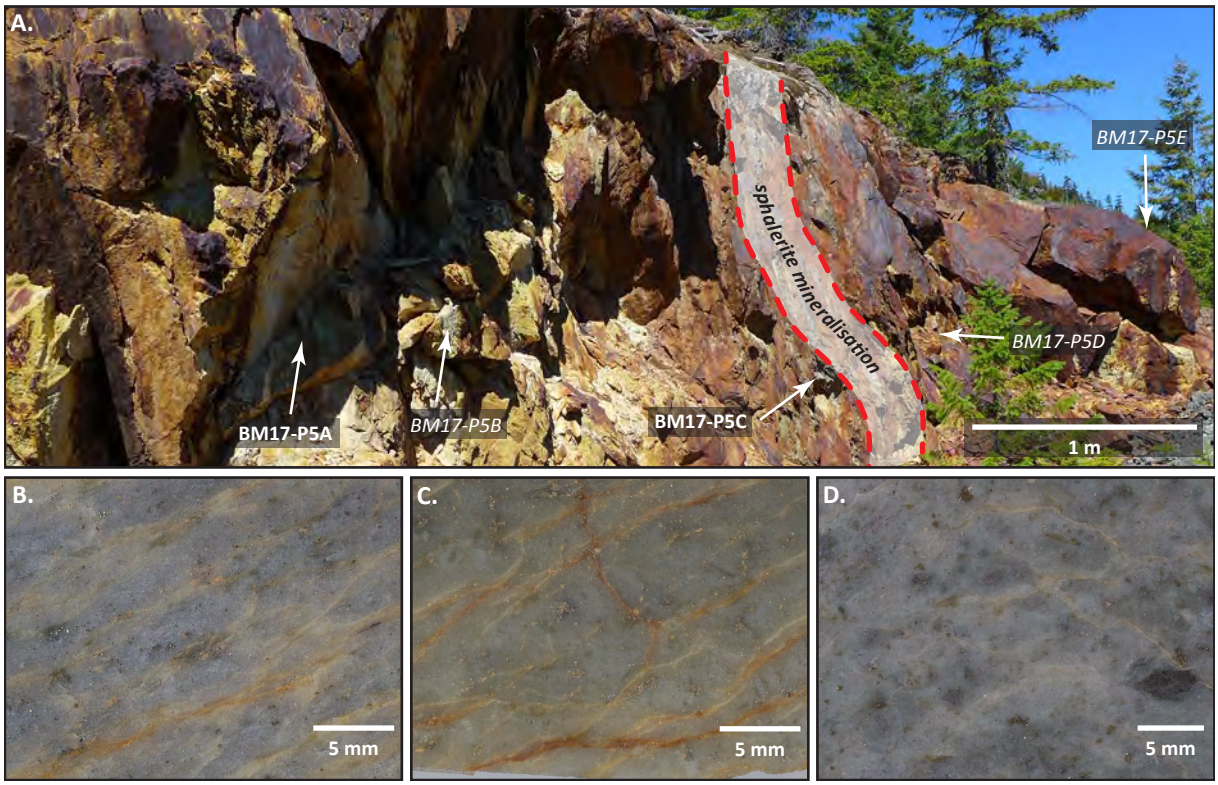

Figure 7.5 Samples from the L-M-P member near the Price orebody. A. Outcrop of L-M-P member volcaniclastic rhyolite near the Price Mine Level 5 adit. B-C. Thin section billets of LMP Rhyolite. B. Sample BM17-P5A, quartz-sericite-pyrite altered rhyolitic volcaniclastic sandstone. C. Sample BM17-P5C, quartz-sericite-pyrite altered rhyolitic volcaniclastic sandstone. D. Sample 15Price01, quartz-sericite-barite-sulfide altered rhyolitic volcaniclastic sandstone, was collected from the Price Mine Level 4.

7.3 Analytical Methods

7.3.1 LA-ICPMS U-Th-Pb analysis

Uranium-thorium-lead analyses were performed on an Agilent 7900 quadrupole ICPMS with a 193 nm Coherent Ar-F excimer laser using the Resonetics S155 ablation cell at CODES, UTAS. Each analysis area was pre-ablated with 2-3 laser pulses before a 30 s blank gas measurement that was followed by 30 s of mineral ablation at 5 Hz and ~2 J/cm^2. Spot sizes ranged from 9 to 29 μm. The ablation spot was enclosed in helium carrier gas (flow rate of 0.35 l/min) that transported ablated particles out of the sample chamber to be mixed with argon gas prior to transfer to the plasma. Elements measured are listed in Table 7.2, and were sequentially measured in a 0.17 s sweep, with longer count times for Pb isotopes. The mass bias correction

factor for the $^{207}Pb/^{206}Pb$ ratio was calculated from 29 μm spot analyses of the NIST610 glass standard throughout the analytical sessions and corrected using the values recommended by Baker et al. (2004). The down hole fractionation, instrument drift, and mass bias correction factors for Pb/U and Pb/Th ratios were calculated by analysing standard reference materials. Two analyses on a primary standard and one analysis on each of the secondary standards at the beginning of the measurement session and after every 15 unknown measurements were completed using the same spot size and analytical conditions as used on the unknown mineral (Table 7.2). In the case of zircon analyses, additional secondary zircon standards (Mud Tank of Black and Gulson, 1978; Plesovice of Slama et al., 2008; Penglai of Li et al., 2010) were also analysed. Data collection and reduction were completed using the method described in Halpin et al. (2014) by the author and J. Thompson from CODES, UTAS.

Table 7.2 Summary of zircon, monazite, and apatite analytical standards and measured isotopes.

Mineral	Beam (μm)	Primary standard	Secondary standard	Primary isotopes measured	Additional isotopes measured
zircon[1]	9, 19, 29	91500 of Wiedenbeck et al. (1995)	TEMORA of Black et al. (2003) JG1 of Jackson et al. (2004)	^{49}Ti, ^{56}Fe, ^{90}Zr, ^{178}Hf, ^{202}Hg, ^{204}Pb, ^{206}Pb, ^{207}Pb, ^{208}Pb, ^{232}Th, ^{235}U, ^{238}U	^{31}P, ^{89}Y, ^{93}Nb, ^{139}La, ^{140}Ce, ^{141}Pr, ^{146}Nd, ^{147}Sm, ^{153}Eu, ^{157}Gd, ^{159}Tb, ^{163}Dy, ^{165}Ho, ^{166}Er, ^{169}Tm, ^{172}Yb, ^{175}Lu, ^{181}Ta
zircon[2]	9	91500 of Wiedenbeck et al. (1995)	TEMORA of Black et al. (2003) JG1 of Jackson et al. (2004)	^{49}Ti, ^{56}Fe, ^{90}Zr, ^{178}Hf, ^{202}Hg, ^{204}Pb, ^{206}Pb, ^{207}Pb, ^{208}Pb, ^{232}Th, ^{235}U, ^{238}U	not measured
monazite[2]	9	14971 Monazite (UTAS in house)	RGL4B of Rubatto et al. (2001) Banaeira monazite of Gonçlaves et al. (2016)	^{31}P, ^{139}La, ^{140}Ce, ^{204}Pb, ^{206}Pb, 207Pb, ^{208}Pb, ^{232}Th, ^{235}U, ^{238}U	^{89}Y, ^{141}Pr, ^{146}Nd, ^{147}Sm, ^{153}Eu, ^{157}Gd, ^{159}Tb, ^{163}Dy, ^{165}Ho, ^{166}Er, ^{169}Tm, ^{172}Yb, ^{175}Lu, ^{202}Hg
apatite[2]	29	Acropolis OD306 Apatite (UTAS in house)	Kovdor apatite of Amelin & Zaitsev (2002) McClure Mt apatite of Schoene & Bowring (2006) Otter Lake apatite of Barfod et al. (2005)	^{31}P, ^{43}Ca, ^{56}Fe, ^{140}Ce, ^{202}Hg, ^{204}Pb, ^{206}Pb, ^{207}Pb, ^{208}Pb, ^{232}Th, ^{238}U	not measured

[1] grain mount; [2] rock chip mount *in situ*

7.3.2 CA-ID-TIMS zircon U-Pb analysis

The CA-ID-TIMS analysis procedure used at the PCIGR is described here and modified after Mundil et al. (2004), Mattinson (2005), and Scoates and Friedman (2008). The clearest, crack- and inclusion-free zircons were selected, photographed, and then annealed in quartz glass crucibles at 900°C for 60 hr. Annealed grains were transferred into 3.5 mL PFA screw top beakers, ultrapure HF (up to 50% strength, 500 μL) and HNO_3 (up to 14N, 50μL) were added and caps were closed finger tight. The beakers were placed in 125 mL PTFE liners with approximately 2 mL HF and 0.2 mL HNO_3 added to the liners. The liners were then placed into stainless steel Parr™ high pressure dissolution devices, which were sealed and brought up to a maximum temperature of 200°C for 8-16 hr. Beakers were removed from liners and zircons were separated from leachate. Zircons were rinsed with >18 MΩ.cm water and sub-boiled acetone. Then, 2 mL of sub-boiled 6N HCl was added and beakers were set on a hotplate at 80-130˚C for 30 min, and finally rinsed with water and acetone.

Masses were estimated from volumes of individual grains. Single grains were transferred into clean 300 mL PFA microcapsules, and 50 mL of 50% HF and 5 mL of 14 N HNO_3 were added. Each was spiked with a $^{233\text{-}235}U\text{-}^{205}Pb$ tracer solution (EARTHTIME ET535), capped, and again placed in a Parr™ liner. Hydrofluoric and nitric acids in a 10:1 ratio were added to the liner, which was then placed in a Parr™ high-pressure device and dissolved at 220˚C for 40 hr. The resulting solutions were dried on a hotplate at 130˚C; 50 mL 6 N HCl was then added to microcapsules and fluorides were dissolved in high-pressure Parr™ devices for 12 hr at 180˚C. Hydrochloric solutions were transferred into clean 7 mL PFA beakers and dried with 2 mL of 0.5 N H_3PO_4. Samples were loaded onto degassed, zone-refined Re filaments in 2 mL of silicic acid emitter (Gerstenberger and Haase, 1997).

Isotopic ratios were measured by a modified single collector 354S thermal ionization mass spectrometer (TIMS) with Sector 54 electronics equipped with analogue Daly photomultipliers. Analytical blanks were 0.1 pg for U and up to 1.7 pg for Pb. The U-fractionation was determined directly on individual runs using the EARTHTIME ET535 mixed $^{233\text{-}235}U\text{-}^{205}Pb$ isotopic tracer and Pb isotopic ratios were corrected for fractionation of 0.25 ± 0.04%/amu based on replicate analyses of NBS-982 reference material and the values recommended by Thirlwall (2000). Data reduction employed the Microsoft Excel® based program of Schmitz and Schoene (2007). Unless otherwise noted, all errors were quoted at 2-sigma or 95% level of confidence. Isotopic dates were calculated with the delay constants $l_{238} = 1.55125x10^{-10}$ and $l_{235} = 9.8485x10^{-10}$ (Jaffey et al., 1971). EARTHTIME U-Pb synthetic solutions were analysed on an on-going basis to monitor the accuracy of results. T. Ockerman conducted activities in the clean lab and C. Wall, H. Lin and N. Moerhius assisted with mass spectrometry. Dr R. Friedman completed the data reduction.

7.3.3 LA-ICPMS data reduction and reproducibility

Data reduction calculations and error propagations were completed in Microsoft Excel® via macros, developed at UTAS, using techniques summarised by Meffre et al. (2008), Sack et al. (2011), and Halpin et al. (2014). Time-resolved isotopic ratios for each analysis were investigated on concordia diagrams to assess the presence of common Pb and Pb-loss. Analyses were excluded from the dataset where a combination of these trends was detected. Uncertainties were calculated using the methods of Halpin et al. (2014).

Analytical results for primary and secondary zircon, monazite and apatite standards are summarised in Table 7.3. ^{207}Pb corrected zircon $^{206}Pb/^{238}U$ age results for primary and secondary standards are in agreement with published results (Table 7.3), with larger analytical errors coincident with smaller beam size measurements. Monazite and apatite, primary and secondary $^{206}Pb/^{238}U$ age standards are also in agreement with reported standard results (Table 7.3).

Table 7.3 Primary and secondary zircon, monazite, and apatite analytical standard values and mean session measurements.

Standard	Comment	Beam (μm)	Sample session	n	$^{206}Pb/^{238}U^{*}$ Age (Ma) mean	±	MSWD	Standard value	±	$^{207}Pb/^{206}Pb$ Ratio mean	±	MSWD	Standard value	±
zircon analyses														
91500	Pb/U primary standard	9	UPB05	7	1,065.0	27.0	0.48	1062.4	0.4					
91500	Pb/U primary standard	19	UPB02 UPB08	4	1,065.0	14.0	0.11	1062.4	0.4					
91500	Pb/U primary standard	29	UPB02	16	1,061.9	6.7	0.92	1062.4	0.4					
91500	Pb/U primary standard	9	PA	10	1,057.0	16.0	0.22	1062.4	0.4					
NIST610	Pb isotopes & trace element primary standard	9	UPB05	4						0.9093	0.0032	0.08	0.90986	0.0001
NIST610	Pb isotopes & trace element primary standard	19	UPB02 UPB08	2						0.9097	0.0043	0.01	0.90986	0.0001
NIST610	Pb isotopes & trace element primary standard	29	UPB02	16						0.9093	0.0014	0.62	0.90986	0.0001
NIST610	Pb isotopes & trace element primary standard	9	PA	4						0.9093	0.0029	0.12	0.90986	0.0001
GJ1	Secondary standard	9	UPB05	3	593.0	18.0	0.07	600.4	2					
Plesovice	Secondary standard	19	UPB02 UPB08	3	339.0	4.5	0.48	337.13	0.37					
Temora	Secondary standard	19	UPB02 UPB08	3	419.7	8.9	1.04	416.8	1.1					
Mudtank	Secondary standard	29	UPB02	5	709.0	13.0	0.13	732	5					
Plesovice	Secondary standard	29	UPB02	5	337.9	3.7	0.48	337.13	0.37					
Temora	Secondary standard	29	UPB02	5	416.1	5.0	0.29	416.8	1.1					
Plesovice	Secondary standard	9	PA	6	340.9	7.6	1.40	337.13	0.37					
Temora	Secondary standard	9	PA	6	419.3	9.9	0.18	416.8	1.1					

Table 7.3 Continued.

Standard	Comment	Beam (μm)	Sample session	n	$^{206}Pb/^{238}U^{*}$ Age (Ma) mean	±	MSWD	Standard value	±	$^{207}Pb/^{206}Pb$ Ratio mean	±	MSWD	Standard value	±
monazite analyses														
14971Mon	Pb/U primary standard	9	PA	8	908.6	6.8	1.10	909	2.9					
NIST610Mon	Pb isotopes & trace element primary standard	9	PA	6						0.9088	0.0027	1.20	0.90986	0.0001
RGBL4	Secondary standard	9	PA	5	1,575	17	0.32	1,566	3					
Banaeira	Secondary standard	9	PA	5	507.4	8.1	1.70	507.7	1.3					
apatite analyses														
OD306	Pb/U primary standard	29	UPB12	12	1,597.5	9.3	0.82	1,595.9	5.9					
NIST610Ap	Pb isotopes & trace element primary standard	29	UPB12	9						0.9083	0.0016	0.53	0.90986	0.0001
Kovdor	Secondary standard	29	UPB12	5	387.9	6.1	0.64	377.5	3.5					
McClure Mt	Secondary standard	29	UPB12	6	523.1	6.9	0.06	523.98	0.12					
Otter Lake	Secondary standard	29	UPB12	5	927.6	6.9	1.06	913	7.0					

7.4 Zircon Petrography and Mineral Chemistry

The morphology and texture of zircons identified from a MLA mineral search and analysed from the Price Formation (sample UPB10B) are summarised in Figure 7.6. Zircons are less than 9 μm, irregular masses intergrown with fine-grained chlorite, muscovite, albite, and quartz with minor rutile. High-resolution BSE images of MLA-identified zircons reveal a complex mixture of bright mineral phases (Figure 7.6A). Semi-quantitative EDS spectra (Figure 7.6E-H) of these phases indicate zircon is the abundant mineral phase with minor xenotime (YPO_4). The irregular masses of zircon-xenotime show an intricate radial growth or cauliflower texture (Figure 7.6A-D). This texture is not indicative of igneous zircon precipitation, but rather secondary modification and/or precipitation (Corfu et al., 2003).

The morphology, texture, and beam spot locations of the 69 zircons analysed from the HW Rhyolite (n=48) and LMP Rhyolite (n=21) by LA-ICPMS at UTAS are summarised in Figures 7.7-7.11. Zircons analysed range in size from 10 to 60 μm. Crystal morphologies vary from euhedral (Figures 7.7P; 7.9M, W; 7.10A-B; 7.11I, K), to subhedral with weakly resorbed margins (Figures 7.7C, Q; 7.8A, G; 7.9Q, V), to crystal fragments (Figures 7.7R; 7.8C, F; 7.9C, F, T; 7.10C, H; 7.11D-E, L). Zircons have predominantly an oscillatory zoning texture (e.g., Figures 7.7G; 7.8G; 7.9U; 7.11B), and to a lesser degree sector zoning (e.g., Figures 7.7C; 7.8D; 7.9H). Zircons also display sector-zoned cores with oscillatory-zoned rims (e.g., Figures 7.7J, S; 7.9W). In addition to investigating zircon morphology and texture, CL imaging was used to document fractures in zircon grains so that, where possible, these could be avoided during LA-ICPMS analysis (e.g., Figure 7.7N).

Rare earth element (REE) and Y concentrations were measured to characterise zircons analysed from the HW Rhyolite by LA-ICPMS (Table 7.4). Trace element data were collected on 39 zircons (UPB02=10; UPB05=7; UPB08=22) during U-Pb analysis. Average Ce abundances for the analysed samples are less than 50 ppm (13.1 to 17.0 ppm; Table 7.4) and suggest an igneous provenance (Hoskin and Schaltegger, 2003). Altered zircons or accidental mineral inclusion in zircon analyses typically have ΣREE+Y abundances significantly higher than 1 wt. % (Hoskin and Schaltegger, 2003). Average ΣREE+Y abundances for samples UPB02, UPB05 and UPB08 are 0.44 wt. %, 0.38 wt. % and 0.37 wt. %, respectively (Table 7.4), with chondrite normalised LREE depleted patterns (chondrite reference values from McDonough and Sun 1995), and positive Ce and negative Eu anomalies. Together, these data suggest that the analysed zircons are unaltered and of igneous origin (Figure 7.12; Hoskin and Schaltegger, 2003).

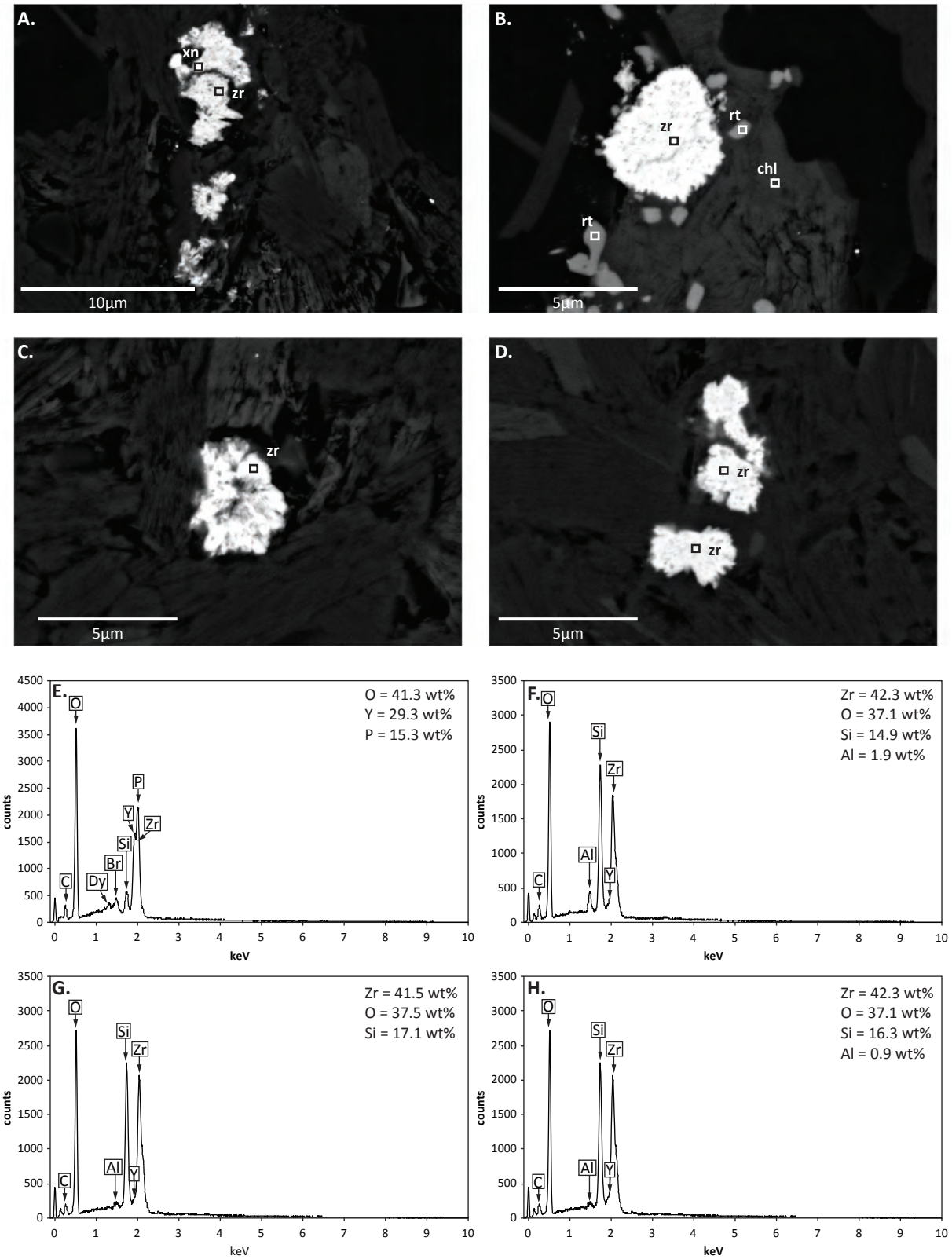

Figure 7.6 Examples of small, *in situ* zircons from Price Formation andesite sample UPB10B. A-D. High resolution, BSE images showing secondary precipitation, cauliflower textures of zircon. No EDS spectra shown for figure D. Note in all cases, sub-micron inclusions of dark phase minerals, likely silicates. Xenotime was identified in one sample and forms a discontinuous brighter rim around secondary zircon (A). E-H. Examples of EDS spectra and semi-quantitative element concentrations of zircon and xenotime. E-F. EDS spectra for annotated square in figure A. F. EDS spectra for labeled zircon in figure B. G. EDS spectra for labeled zircon in figure C. [xn, xenotime; zr, zircon; rt, rutile; chl, chlorite]

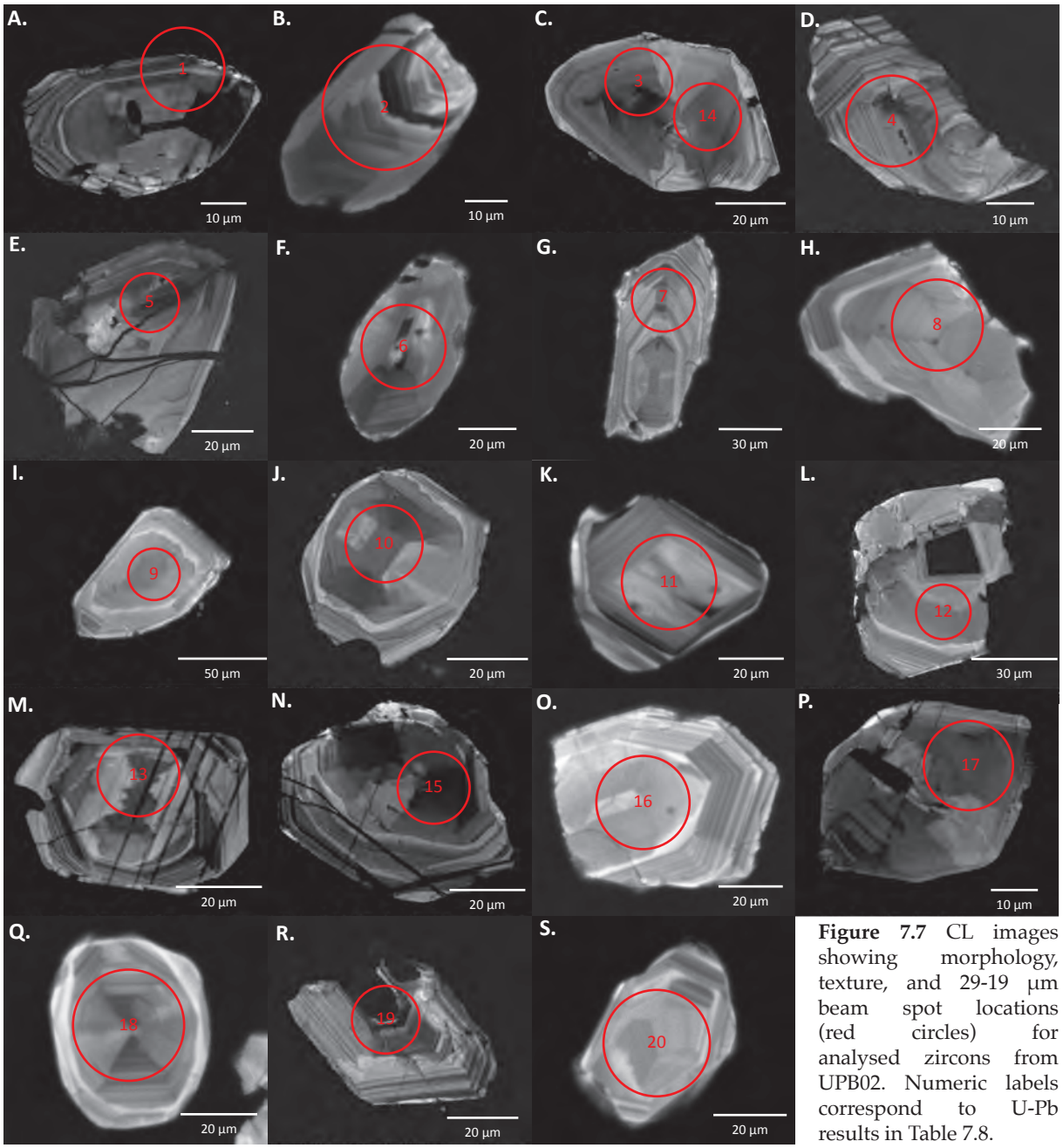

Figure 7.7 CL images showing morphology, texture, and 29-19 µm beam spot locations (red circles) for analysed zircons from UPB02. Numeric labels correspond to U-Pb results in Table 7.8.

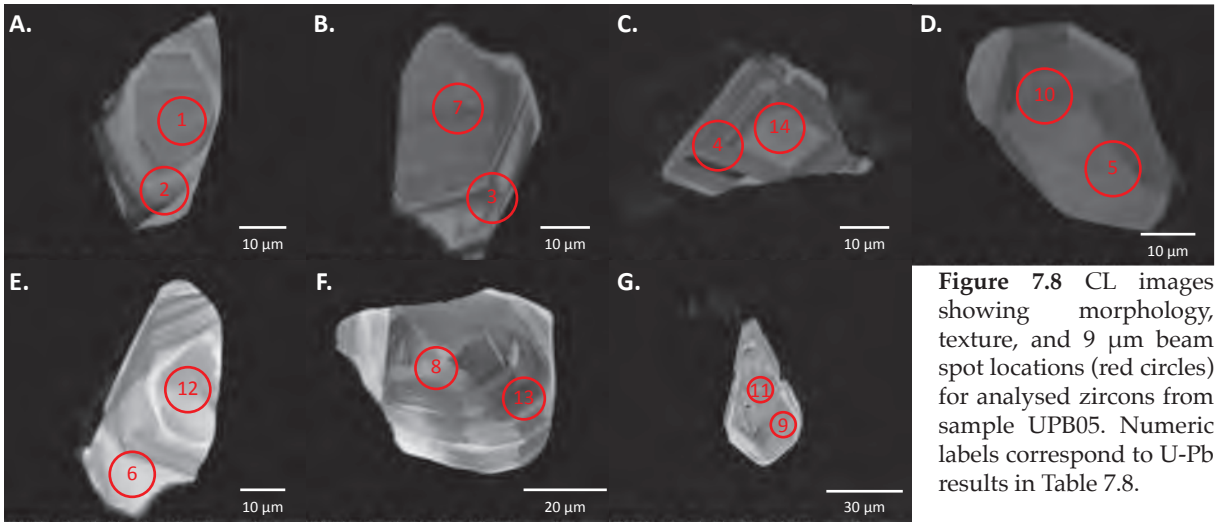

Figure 7.8 CL images showing morphology, texture, and 9 µm beam spot locations (red circles) for analysed zircons from sample UPB05. Numeric labels correspond to U-Pb results in Table 7.8.

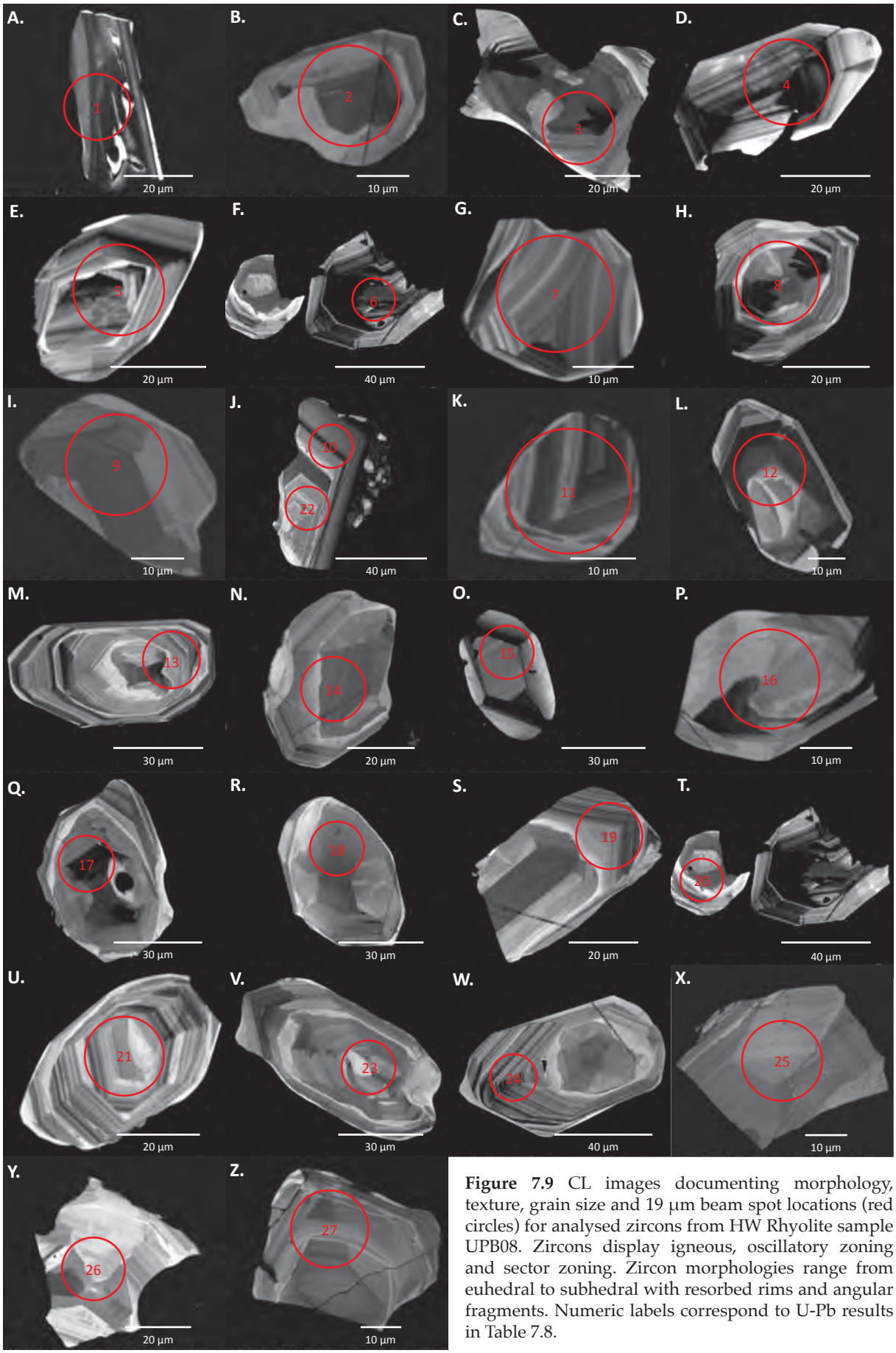

Figure 7.9 CL images documenting morphology, texture, grain size and 19 µm beam spot locations (red circles) for analysed zircons from HW Rhyolite sample UPB08. Zircons display igneous, oscillatory zoning and sector zoning. Zircon morphologies range from euhedral to subhedral with resorbed rims and angular fragments. Numeric labels correspond to U-Pb results in Table 7.8.

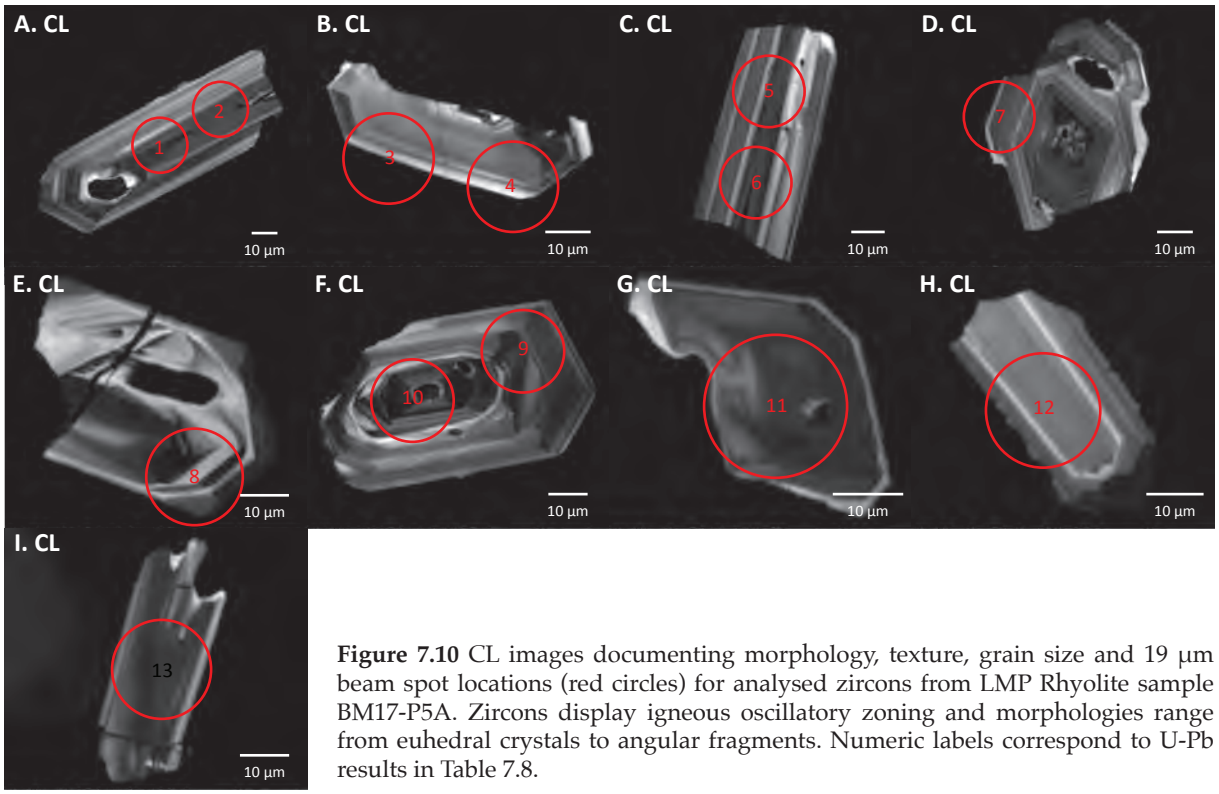

Figure 7.10 CL images documenting morphology, texture, grain size and 19 µm beam spot locations (red circles) for analysed zircons from LMP Rhyolite sample BM17-P5A. Zircons display igneous oscillatory zoning and morphologies range from euhedral crystals to angular fragments. Numeric labels correspond to U-Pb results in Table 7.8.

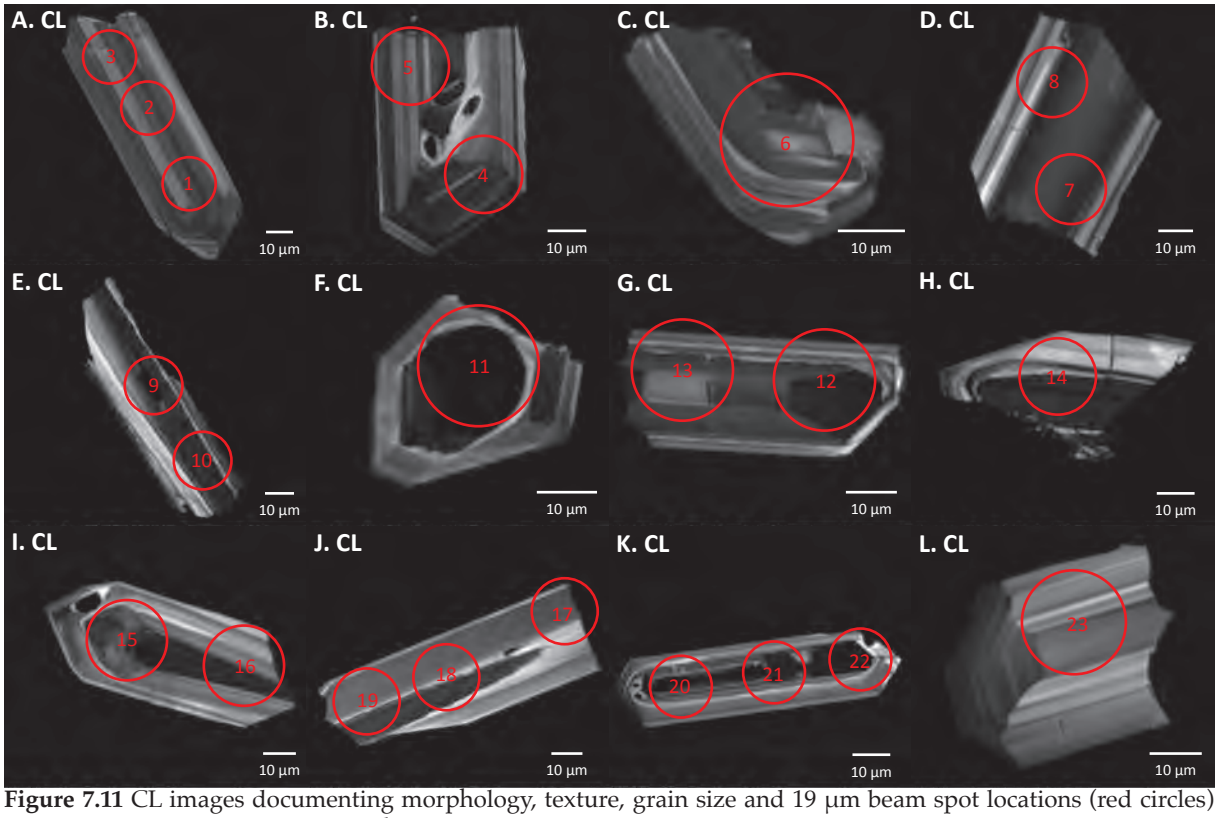

Figure 7.11 CL images documenting morphology, texture, grain size and 19 µm beam spot locations (red circles) for analysed zircons from LMP Rhyolite sample BM17-P5C. Zircons display igneous oscillatory zoning and morphologies range from euhedral crystals to angular fragments. Numeric labels correspond to U-Pb results in Table 7.8.

Table 7.4 Zircon average REE and Y composition by LA-ICPMS analyses on HW Rhyolite samples UPB02, UPB05, and UPB08.

Element	UPB02			UPB05			UPB08		
beam (μm)	19			9			19		
ppm	n=10	±1 σ	N	n=13	±1 σ	N	n=22	±1 σ	N
Y	2480	88	1579	2363	114	1505	2050	78	1306
La	0.1	0.05	0.5	1.1	0.35	4.7	1.9	0.26	8.1
Ce	14.1	0.75	23.1	13.1	1.65	21.4	17.0	1.03	27.7
Pr	0.2	0.04	1.6	0.6	0.23	6.1	0.6	0.10	7.0
Nd	2.4	0.37	5.2	4.5	1.43	9.9	4.4	0.63	9.7
Sm	6.0	0.68	40.2	4.7	1.39	31.6	5.2	0.61	35.2
Eu	1.4	0.16	24.0	1.8	0.57	32.6	1.0	0.13	17.2
Gd	42.2	2.33	212.0	30.1	4.14	151.1	33.3	1.95	167.4
Tb	15.4	0.69	426.6	12.1	1.17	333.8	12.3	0.58	341.0
Dy	209.7	8.03	852.5	163.1	11.84	663.1	169.2	6.83	687.6
Ho	82.8	3.07	1,517.2	62.8	4.18	1,150.5	68.2	2.66	1,249.4
Er	425.8	15.14	2,661.2	325.9	21.03	2,036.8	352.3	13.46	2,201.6
Tm	92.8	3.35	3,639.6	66.0	4.33	2,589.6	77.9	3.00	3,055.8
Yb	880.4	31.93	5,468.3	628.6	39.72	3,904.0	739.7	28.44	4,594.3
Lu	169.4	5.88	6,887.8	149.1	9.43	6,059.7	145.2	5.33	5,903.6
$(Sm/La)_N$	78			7			4		
$(Lu/Gd)_N$	32			40			35		
Ce_N/Ce_N^*	25			4			4		
Eu_N/Eu_N^*	0.1			0.5			0.1		
ΣREE + Y (%)	0.44			0.38			0.37		

N = chondrite normalised with values from McDonough and Sun (1995)
$Ce_N/Ce_N^* = Ce/\sqrt{(La \times Pr)}$
$Eu_N/Eu_N^* = Eu/\sqrt{(Sm \times Gd)}$

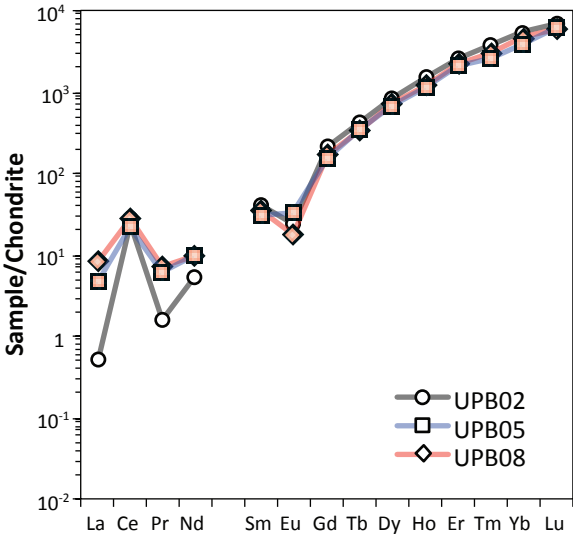

Figure 7.12 Compilation of chondrite normalised REE patterns for UPB02, UPB05 and UPB08 zircon. Chondrite normalised with values from McDonough and Sun (1995).

7.5 Monazite and Apatite Petrography and Mineral Chemistry

The morphology, texture and compositional zoning of monazite from sample UPB10B were investigated with a Hitachi SU-70 FE-SEM (Figure 7.13). In total 18 of the 20 monazites analysed were BSE imaged prior to U-Th-Pb analysis. These monazites are irregular in shape, 5 to 9 μm, and are associated with muscovite, albite, quartz, chlorite, and less abundant rutile and calcite. The monazite textures display spongy, inclusion-rich cores rimmed by brighter, inclusion-free monazite (e.g., Figure 7.13I-K). In some cases, monazite is uniformly bright and homogenous in the BSE images (Figure 7.13C-D). Semi-quantitative EDS analysis indicated no significant compositional zoning of Th between the inclusion-rich cores and brighter, homogenous rims (e.g., Figure 7.13B-C).

Monazites from the Price Formation sample contain low Th (av. 0.4%), U (av. 33 ppm) and Y (av. 0.6%) concentrations (Table 7.5). These geochemical features likely represent monazite crystallisation under low temperature conditions (e.g., Williams et al., 2007) and when combined with petrographic observations, suggest that they are hydrothermal/metamorphic in origin.

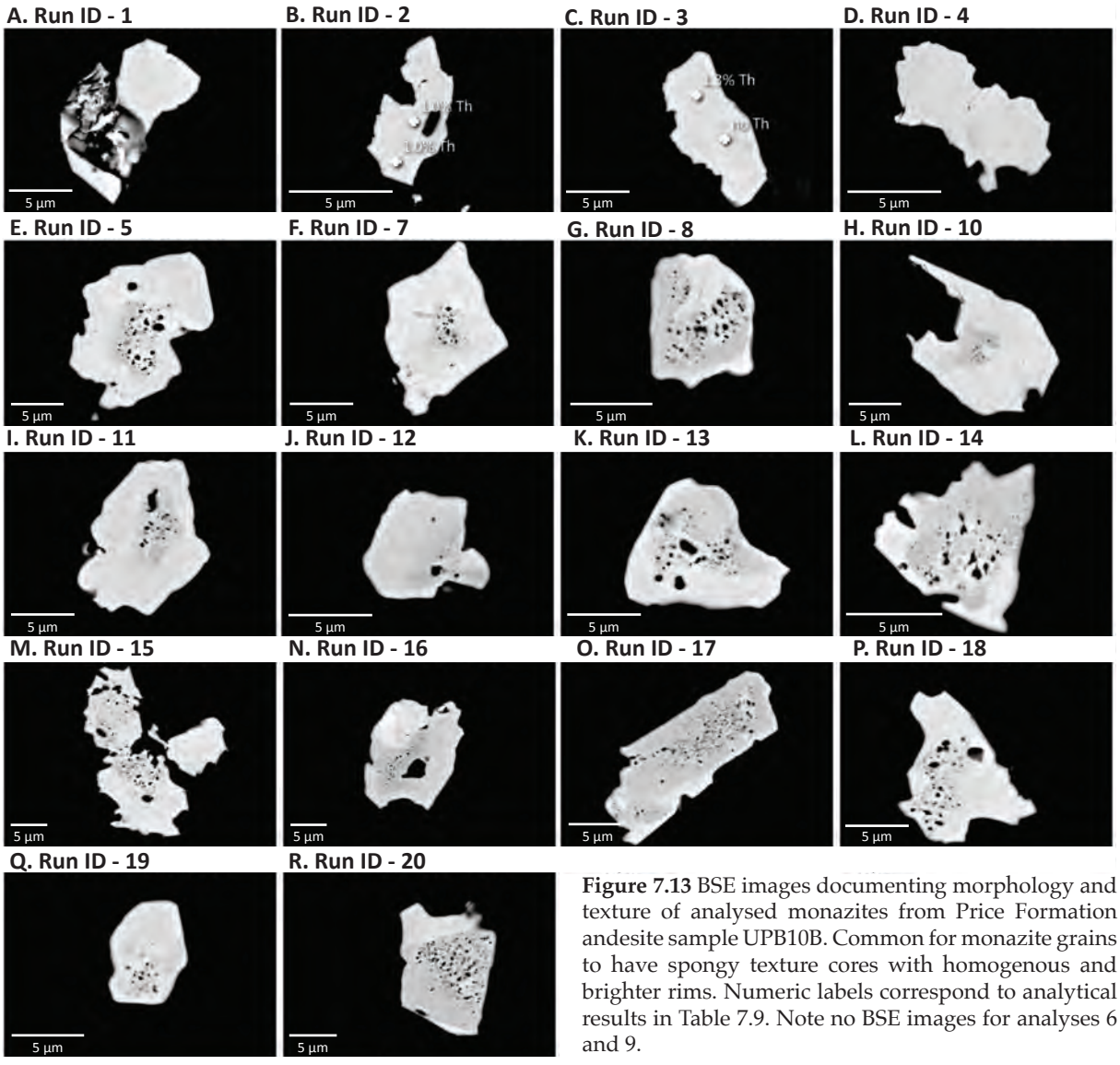

Figure 7.13 BSE images documenting morphology and texture of analysed monazites from Price Formation andesite sample UPB10B. Common for monazite grains to have spongy texture cores with homogenous and brighter rims. Numeric labels correspond to analytical results in Table 7.9. Note no BSE images for analyses 6 and 9.

Three samples of Price Formation andesite (BM14-029, BM14-074, BM14-043) and one sample of coherent andesite from the H-W member (UPB12) were investigated for U-Pb apatite geochronology. The Price Formation samples contain abundant apatite associated with fine-grained chlorite, muscovite, quartz, albite, rutile, and less abundant pyrite, sphalerite and chalcopyrite (Figure 7.14). Apatite grains are subhedral to irregular in shape and up to 50 μm, though the average grain size is less than 25 μm. Due to the small grain size, morphology and association with secondary minerals, U-Pb apatite dating analysis was not attempted on the Price Formation samples. It is unlikely that these apatites represent igneous crystallisation, but rather secondary growth from hydrothermal and/or metamorphic fluids.

Apatites from coherent andesite of the H-W member (sample UPB12) are subhedral in shape, 30 to 60 μm, and are associated with albite, chlorite, and pyrite (Figure 7.15). These apatites were of sufficient size and quantity for U-Pb dating analysis and have low concentrations of Th (av. 1.9 ppm), U (av. 1.4 ppm), and moderate Ce (av. 383.1 ppm); summarised in Table 7.6.

Table 7.5 Monazite mineral chemistry from LA-ICPMS of Price Formation andesite sample UPB10B.

Run Id	1		2		3		4		5		6		7	
Analysis #	NO90B058		NO90B087		NO90B066		NO90B083		NO90B065		NO90B075		NO90B080	
Beam (μm)	9		9		9		9		9		9		9	
	result	±1 σ	result	±1 σ	result	±1 σ	result	±1 σ	result	±1 σ	result	±1 σ	result	±1 σ
P (wt %)	18.4	0.9	17.3	1.0	16.9	0.7	19.5	0.8	16.2	0.9	16.9	0.8	18.2	0.9
La (wt %)	13.7	0.7	13.7	0.8	13.5	0.4	13.7	0.5	13.5	0.8	13.5	0.5	13.5	0.7
Ce (wt %)	29.5	1.4	29.5	1.8	29.5	0.9	29.5	1.0	29.5	1.4	29.5	1.2	29.5	1.3
Y (wt %)	0.3	0.0	0.5	0.0	0.4	0.0	0.5	0.0	0.5	0.0	0.4	0.0	0.4	0.0
Eu (wt %)	0.8	0.0	0.9	0.1	0.8	0.0	0.8	0.0	0.8	0.0	0.8	0.0	0.9	0.0
Th (wt %)	0.7	0.0	1.1	0.1	1.0	0.0	0.4	0.0	0.2	0.0	0.4	0.0	0.6	0.0
U (ppm)	21.20	1.15	38.42	2.61	35.27	1.76	35.62	1.27	24.22	1.33	19.89	1.05	22.37	0.91

Run Id	8		9		10		11		12		13		14	
Analysis #	NO90B074		NO90B076		NO90B081		NO90B088		NO90B084		NO90B072		NO90B063	
Beam (μm)	9		9		9		9		9		9		9	
	result	±1 σ	result	±1 σ	result	±1 σ	result	±1 σ	result	±1 σ	result	±1 σ	result	±1 σ
P (wt %)	17.0	0.9	18.1	0.8	16.9	0.9	19.6	1.0	17.7	1.1	18.1	1.0	15.9	1.5
La (wt %)	14.3	0.7	13.6	0.5	13.5	0.7	13.5	0.7	13.9	0.9	14.8	0.8	13.2	1.3
Ce (wt %)	29.5	1.6	29.5	1.2	29.5	1.4	29.5	1.5	29.5	1.8	29.5	1.5	29.5	2.9
Y (wt %)	0.9	0.1	0.6	0.0	0.6	0.0	0.7	0.0	0.7	0.1	0.5	0.0	0.6	0.1
Eu (wt %)	0.7	0.0	0.7	0.0	0.8	0.0	0.7	0.0	0.8	0.0	0.7	0.0	0.7	0.1
Th (wt %)	0.1	0.0	0.1	0.0	0.8	0.0	0.2	0.0	0.5	0.0	0.4	0.0	0.3	0.0
U (ppm)	31.25	1.39	28.16	1.06	27.35	1.29	31.71	1.80	39.30	2.78	28.37	2.08	23.03	2.15

Run Id	15		16		17		18		19		20		**Average (n = 20)**	
Analysis #	NO90B052		NO90B059		NO90B073		NO90B079		NO90B061		NO90B078			
Beam (μm)	9		9		9		9		9		9			
	result	±1 σ	result	±1 σ	result	±1 σ	result	±1 σ	result	±1 σ	result	±1 σ	result	±1 σ
P (wt %)	15.9	0.9	17.7	1.1	15.8	1.6	18.8	1.2	16.5	1.2	16.1	1.1	17.4	1.0
La (wt %)	13.5	0.8	13.9	0.9	13.4	1.3	14.6	0.9	13.7	1.0	11.7	0.7	13.6	0.8
Ce (wt %)	29.5	1.7	29.5	2.0	29.5	3.0	29.5	2.0	29.5	2.3	29.5	1.9	29.5	1.7
Y (wt %)	0.4	0.0	1.2	0.1	0.8	0.1	0.4	0.0	0.6	0.0	0.7	0.0	0.6	0.0
Eu (wt %)	0.8	0.0	1.0	0.1	0.5	0.0	1.0	0.1	0.8	0.1	0.4	0.0	0.8	0.0
Th (wt %)	0.5	0.0	0.1	0.0	0.0	0.0	1.0	0.1	0.2	0.0	0.0	0.0	0.4	0.0
U (ppm)	20.42	1.16	128.59	8.70	32.11	2.53	25.67	1.58	30.70	2.58	17.14	1.31	33.04	2.02

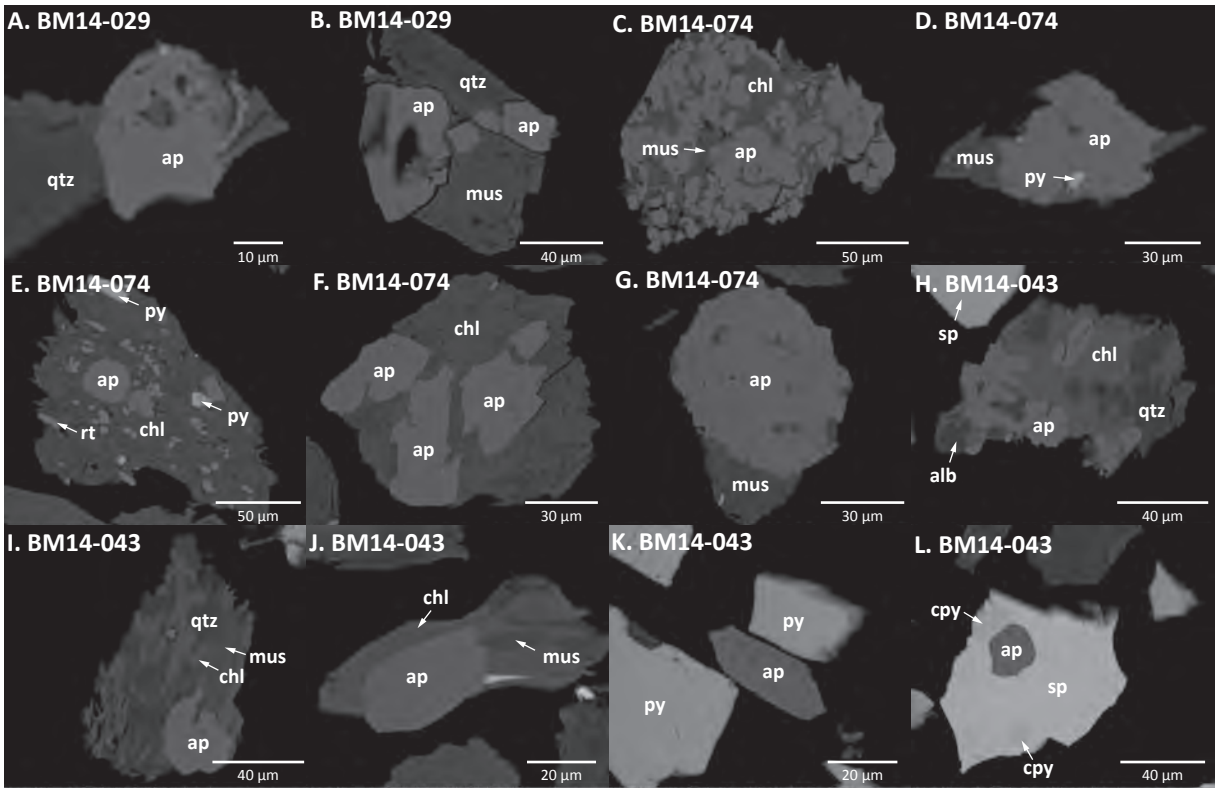

Figure 7.14 BSE images documenting morphology, texture, size and associated minerals with apatite from Price Formation andesite samples that were not analysed. Apatite is typically associated with quartz, muscovite, and chlorite with lesser pyrite, rutile, sphalerite and chalcopyrite. Apatite grains were too small for analysis. [qtz, quartz; ap, apatite; mus, muscovite; chl, chlorite; rt, rutile; py, pyrite; alb, albite; sp, sphalerite; cpy, chalcopyrite]

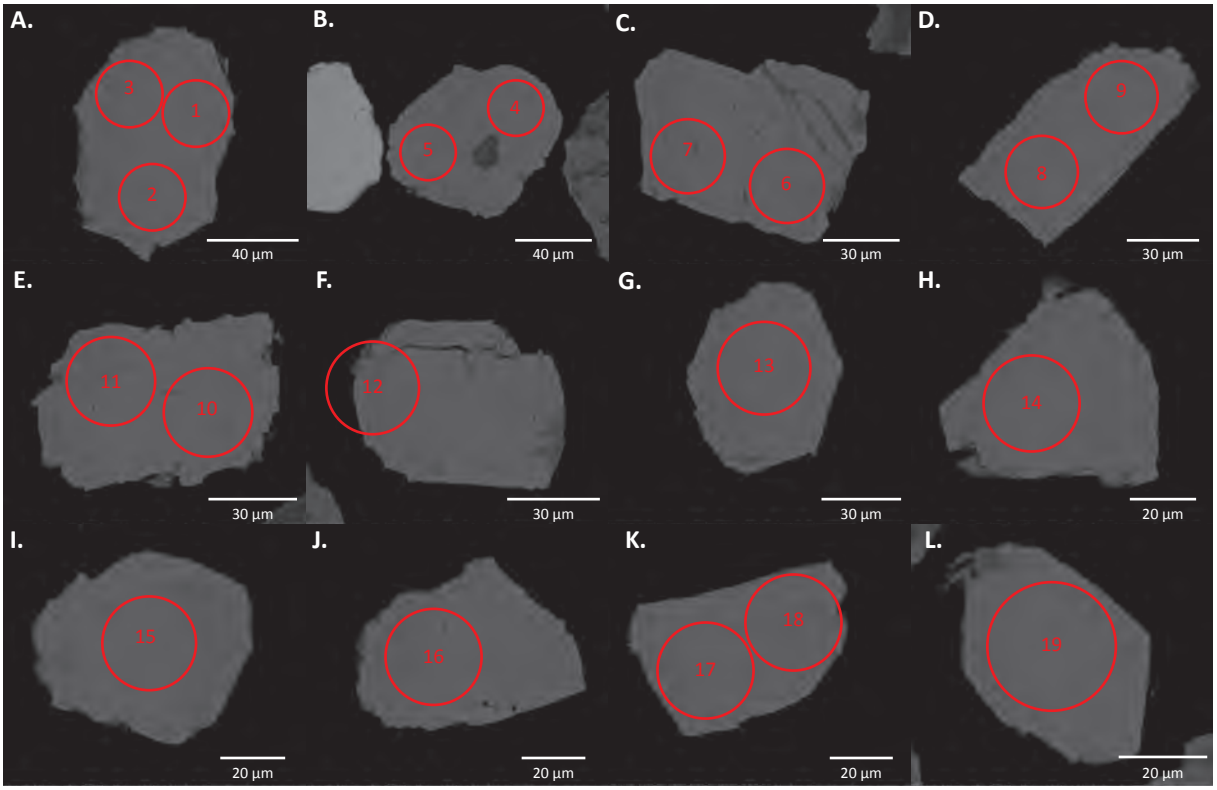

Figure 7.15 BSE images documenting morphology, texture, grain size and beam spot locations (red circles) for analysed apatites from coherent andesite sample UPB12 polished grain mount. Alpha-numeric labels correspond to U-Pb results in Table 7.11.

Table 7.6 Apatite mineral chemistry from LA-ICPMS of coherent andesite sample UPB12.

Run Id	1		2		3		4		5		6		7	
Analysis #	NO23A081		NO23A080		NO23A082		NO23A084		NO23A083		NO23A086		NO23A085	
Beam (μm)	29		29		29		29		29		29		29	
	result	±1 σ	result	±1 σ	result	±1 σ	result	±1 σ	result	±1 σ	result	±1 σ	result	±1 σ
P (wt %)	22.7	1.4	22.3	1.4	22.8	1.4	22.0	1.6	21.7	1.4	22.6	1.4	22.6	1.4
Ca (wt %)	39.4	0.4	39.4	0.5	39.4	0.4	39.4	0.5	39.4	0.4	39.4	0.4	39.4	0.4
Ce (ppm)	429.0	3.5	392.8	3.0	480.3	7.6	403.1	3.4	347.1	3.7	365.5	2.9	385.1	3.0
Th (ppm)	1.8	0.0	1.7	0.0	2.0	0.0	1.8	0.0	1.5	0.0	1.8	0.0	1.8	0.0
U (ppm)	1.9	0.0	1.2	0.0	1.8	0.1	0.9	0.0	0.8	0.0	0.7	0.0	0.8	0.0

Run Id	8		9		10		11		12		13		14	
Analysis #	NO23A087		NO23A088		NO23A089		NO23A095		NO23A096		NO23A097		NO23A098	
Beam (μm)	29		29		29		29		29		29		29	
	result	±1 σ	result	±1 σ	result	±1 σ	result	±1 σ	result	±1 σ	result	±1 σ	result	±1 σ
P (wt %)	21.1	1.4	22.4	1.4	22.3	1.4	22.0	1.4	22.2	1.4	21.6	1.4	18.7	1.5
Ca (wt %)	39.4	0.4	39.4	0.4	39.4	0.4	39.4	0.4	39.4	0.4	39.4	0.5	39.4	0.5
Ce (ppm)	333.4	4.8	416.1	3.4	366.7	3.2	411.4	3.1	425.9	3.5	346.1	2.9	240.5	2.6
Th (ppm)	1.8	0.0	2.0	0.0	1.9	0.0	2.1	0.0	2.0	0.0	2.1	0.0	1.5	0.0
U (ppm)	0.7	0.0	0.8	0.0	3.7	0.0	1.0	0.0	1.6	0.0	1.7	0.0	1.3	0.0

Run Id	15		16		17		18		19		**average (n = 19)**	
Analysis #	NO23A099		NO23A100		NO23A101		NO23A102		NO23A103			
Beam (μm)	29		29		29		29		29			
	result	±1 σ	result	±1 σ	result	±1 σ	result	±1 σ	result	±1 σ	result	±1 σ
P (wt %)	21.6	1.4	21.4	1.5	18.5	1.4	18.2	1.4	21.7	1.4	16.1	1.1
Ca (wt %)	39.4	0.4	39.4	0.5	39.4	0.5	39.4	0.5	39.4	0.4	11.7	0.7
Ce (ppm)	417.6	3.3	382.7	3.8	399.3	3.2	382.1	3.1	353.9	2.7	29.5	1.9
Th (ppm)	1.9	0.0	2.1	0.0	1.8	0.0	1.8	0.0	1.9	0.0	0.7	0.0
U (ppm)	2.2	0.0	1.1	0.0	0.8	0.0	0.8	0.0	2.3	0.0	0.4	0.0

7.6 Geochronology Results

New geochronology results are presented in ascending stratigraphic order. Zircon, monazite and apatite U-Th-Pb age results are summarised in Tables 7.7-7.10.

7.6.1 Price Formation – sample UPB06A

UPB06A is from the Ridge Zone North orebody and was collected from drill hole RN18-0224 at 918 mE, 4,385 mN, 2,895 mEL. This sample is strongly altered by muscovite with lesser chlorite and pyrite. Massive polymetallic sulfide mineralisation is located <10 metres above the sample location. Nine zircons (6-10 μm) were identified with an MLA mineral search and were analysed *in situ* with a 9 μm beam. Only three zircons analysed were successfully ablated. These zircons yielded $^{206}Pb/^{238}U$ ages between 110.3 ± 5.5 Ma to 183.1 ± 19.5 Ma (Table 7.7; Figure 7.16).

7.6.2 Price Formation – sample UPB07A

UPB07A is from the Ridge Zone North orebody and was collected from drill hole RN18-0224 at 918 mE, 4,383 mN, 2,954 mEL. The sample is strongly altered by chlorite with less abundant pyrite and muscovite. Massive polymetallic sulfide mineralisation is located 15 metres above the sample location. Three zircons (4-10 μm) were identified with an MLA mineral search and were analysed *in situ* with a 9 μm beam. All three zircons were successfully ablated and yielded $^{206}Pb/^{238}U$ ages between 108.9 ± 7.3 Ma to 140.7 ± 26.4 Ma (Table 7.7; Figure 7.16).

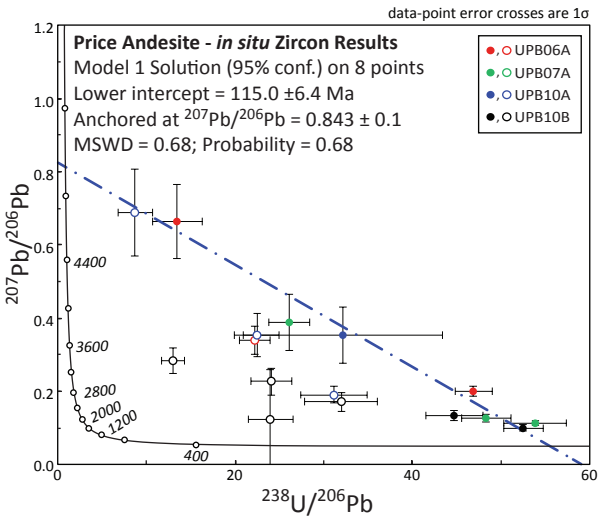

Figure 7.16 Tera-Wasserburg U-Pb concordia diagram for *in situ* LA-ICPMS analyses of zircons from the Price Formation andesite. Solid symbols are results used in the lower intercept age determination. Open symbols were rejected.

7.6.3 Price Formation – sample UPB10A-B

Samples UPB10A and UPB10B are from the West Block Area and were collected from drill hole BG18-3952 at 700 mE, 4,265 mN, 2,897 mEL. These samples are weakly altered, feldspar-phyric, and amygdaloidal andesite, characterised by a chlorite-calcite alteration with rare, fine-grained disseminated pyrite. The samples are located approximately 30 metres below the lower Myra Formation contact. A total of 18 zircons (4-8 μm) were identified with an MLA mineral search and were analysed *in situ* with a 9 μm beam. Five zircons from UPB10A and six zircons from UPB10B were successfully ablated and yielded $^{206}Pb/^{238}U$ ages between 108.9 ± 7.3 Ma to 176.4 ± 28.1 Ma and 113.9 ± 5.0 Ma to 347.0 ± 40.0 Ma, respectively (Table 7.7; Figure 7.16).

Thirty-five monazites (4-10 μm) were selected from an MLA mineral search of sample UPB10B, thirty of which were ablated *in situ* with a 9 μm beam. Five monazite analyses were unsuccessfully ablated, ten monazite analyses were rejected because of their small grain size and low U and Pb concentrations, and twenty monazite analyses were ablated successfully. $^{206}Pb/^{238}U$ age results are highly variable, have significant analytical error, and are affected by common Pb. Monazite $^{208}Pb/^{232}Th$ ages, when corrected for common Pb after the method described by Berry et al. (2016), range from 147.5 ± 10.4 Ma to 260.7 ± 15.0 Ma with a dominant peak at ca. 170 Ma (Table 7.8; Figure 7.17).

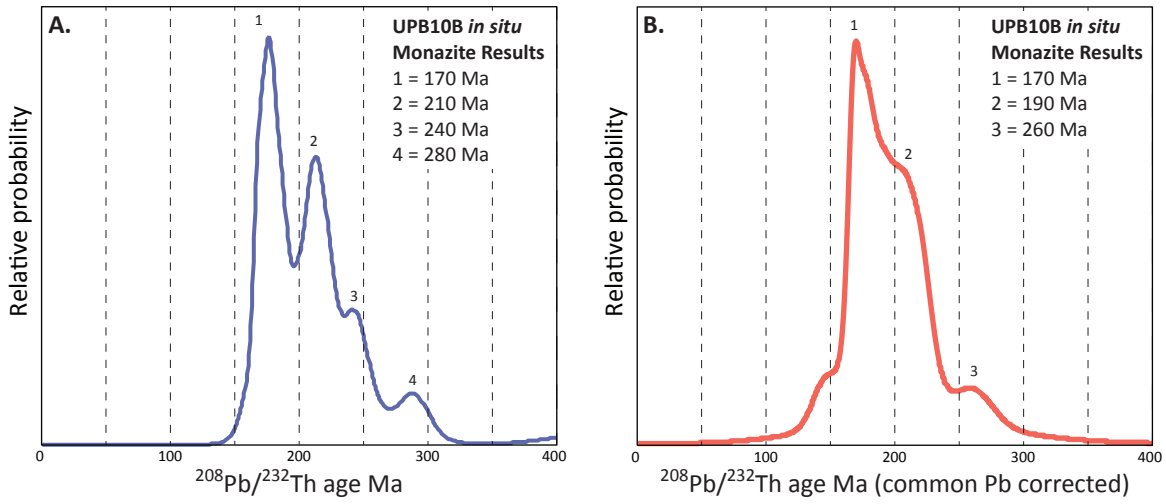

Figure 7.17 Relative probability plot of $^{208}Pb/^{232}Th$ age results for in situ LA-ICPMS analyses of monazites from the Price Formation andesite. A. Uncorrected common Pb age results. B. Corrected common Pb age results.

7.6.4 HW Rhyolite – sample UPB02

Sample UPB02 is of quartz and feldspar-phyric rhyolite from the Ridge Zone North orebody and was collected from underground development at 855 mE, 4,495 mN, 3,060 mEL. The sample is muscovite-quartz-pyrite altered with less abundant chlorite-barite-sphalerite-galena-chalcopyrite. Semi-massive to massive, polymetallic sulfide mineralisation is located immediately above the sample location. A total of twenty zircons were analysed from two LA-ICPMS analytical sessions (Table 7.8). One session utilised a 29 μm beam (n=9) and the second session used a 19 μm beam (n=11) and measured REE in addition to U-Pb isotopes. Zircons from sample UPB02 yielded individual $^{206}Pb/^{238}U$ ages between 308.0 ± 6.9 Ma to 371.6 ± 6.0 Ma (Table 7.8), with a weighted average age of 363.7 ± 2.6 Ma (n=16, MSWD=0.67; Figure 7.18A-B). Four zircon analyses were excluded from the weighted average age calculation due to discordance attributed to post-crystallisation Pb loss (Figure 7.18A-B).

A total of five zircons were analysed from sample UPB02 by CA-ID-TIMS (Table 7.10) to confirm the LA-ICPMS geochronology results presented above. Three of the five analyses yielded overlapping concordant results with a weighted average $^{206}Pb/^{238}U$ age of 362.32 ± 0.74 Ma (MSWD=0.07; Figure 7.19A-B). The high precision CA-ID-TIMS result is in agreement with the LA-ICPMS result. Two analyses give younger $^{206}Pb/^{238}U$ ages (Table 7.10) and are attributed to post-crystallisation Pb loss and were rejected from the reported weighted average age.

7.6.5 HW Rhyolite – sample UPB05

Sample UPB05 is of quartz and feldspar-phyric rhyolite from the Ridge Zone North orebody and was collected from drill hole RN18-0224 at 918 mE, 4,420 mN, 3,022 mEL. The sample is muscovite-quartz altered with minor, fine-grained disseminated pyrite. Massive polymetallic sulfide mineralisation is present approximately 50 metres below the location of sample UPB05. Seven zircons were analysed twice (n=14) with a 9 μm beam. Individual $^{206}Pb/^{238}U$ ages are between 330.6 ± 13.8 Ma and 371.5 ± 14.6 Ma (Table 7.8). The youngest age results (UPB08-1: 330.6 ± 13.8 Ma) falls off the concordia and is interpreted to have suffered Pb loss and was excluded from the weighted average age calculation (Figure 7.18C-D). This sample yielded a weighted average age of 355.1 ± 7.5 Ma (n=13; MSWD=0.38; Figure 7.18D).

A total of five zircons were analysed by CA-ID-TIMS to confirm and better constrain the indicated age of sample UPB05 by LA-ICPMS (Table 7.10). Four of the analyses yielded overlapping concordant results with a weighted average $^{206}Pb/^{238}U$ age of 362.5 ± 0.6 Ma (MSWD=0.71; Figure 7.19C-D). The LA-ICPMS results suggested a younger crystallisation age with significant error (± 7.3 Ma) for sample UPB05. However, the CA-ID-TIMS results yielded an older age that overlaps in error with both the LA-ICPMS results for UPB05 and the CA-ID-TIMS results for sample UPB02. One zircon analysis produced a younger $^{206}Pb/^{238}U$ age (Table 7.10) and is attributed to post-crystallisation Pb loss.

7.6.6 HW Rhyolite – sample UPB08

Sample UPB08 is of quartz and feldspar-phyric rhyolite from the West Block Area and was collected from drill hole BG18-3952 at 700 mE, 4,240 mN, 2,977 mEL. The sample is muscovite-quartz altered with rare, fine-grained disseminated pyrite. Semi-massive polymetallic sulfide mineralisation is present approximately 40 metres below and 60 metres to the west of the sample location. Twenty-seven zircons were analysed with a 19 μm beam and yielded $^{206}Pb/^{238}U$ ages from 310.0 ± 4.1 Ma to 367.7 ± 6.0 Ma (Table 7.7). Six analyses plot off concordia due to Pb loss,

three of which yielded anomalously young $^{206}Pb/^{238}U$ ages (310.0 ± 4.1 Ma, 312.0 ± 5.7 Ma, and 313.5 ± 5.1 Ma; Figure 7.18E). These six analyses were excluded from the weighted average $^{206}Pb/^{238}U$ age calculation of 359.4 ± 2.4 Ma (n=21, MSWD=0.59; Figure 7.18F).

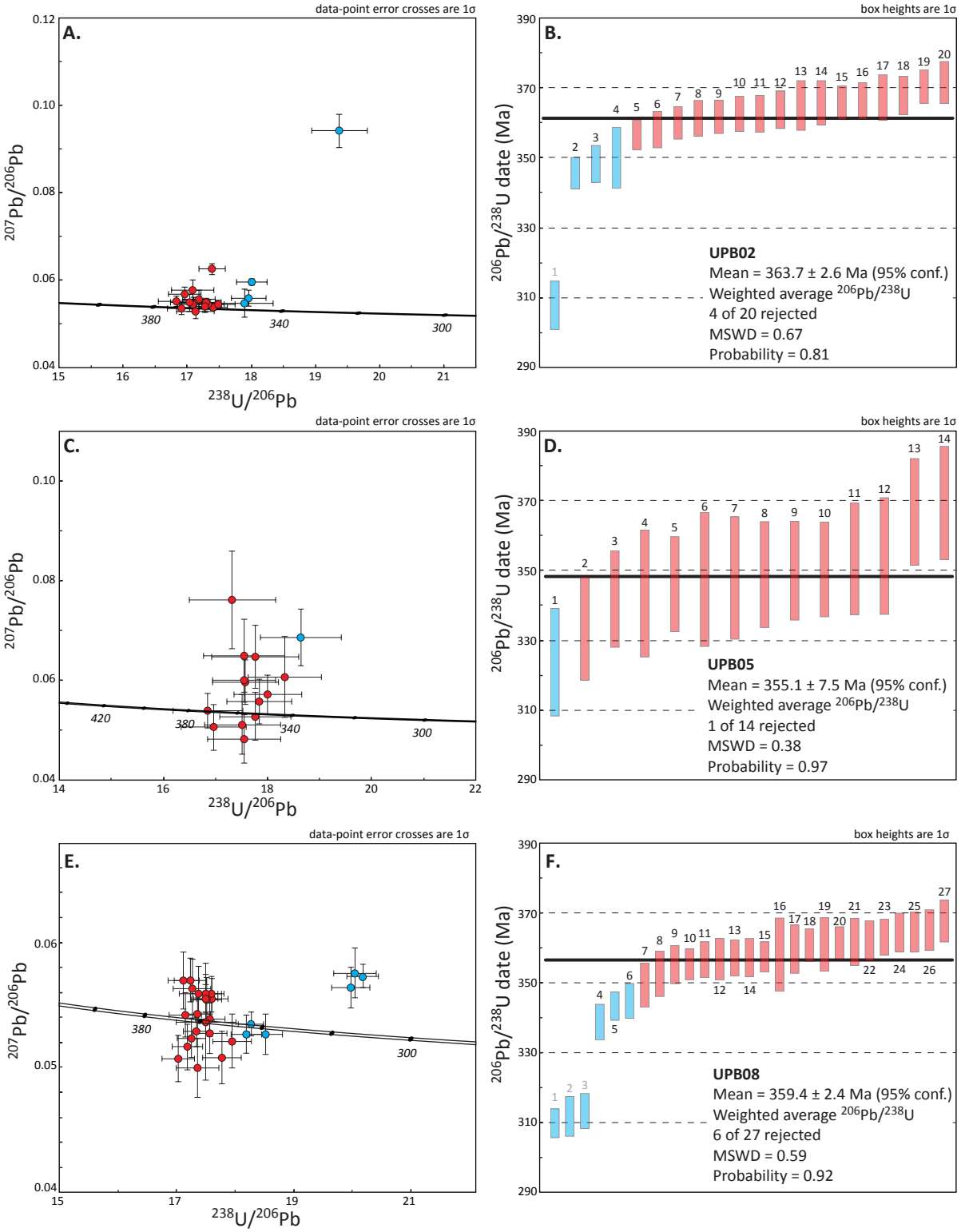

Figure 7.18 Tera-Wasserburg U-Pb concordia and $^{206}Pb/^{238}U$ age diagrams for LA-ICPMS analyses of zircons from the HW Rhyolite. A-B. Sample UPB02. C-D. Sample UPB05. E-F. Sample UPB08. Red symbols are analyses selected fro the weighted average age calculation. Blue symbols are single analyses that have been rejected due to Pb loss. Numeric labels correspond to the zircon grain labels for Figures 7.7-7.9 and U-Pb results in Table 7.8.

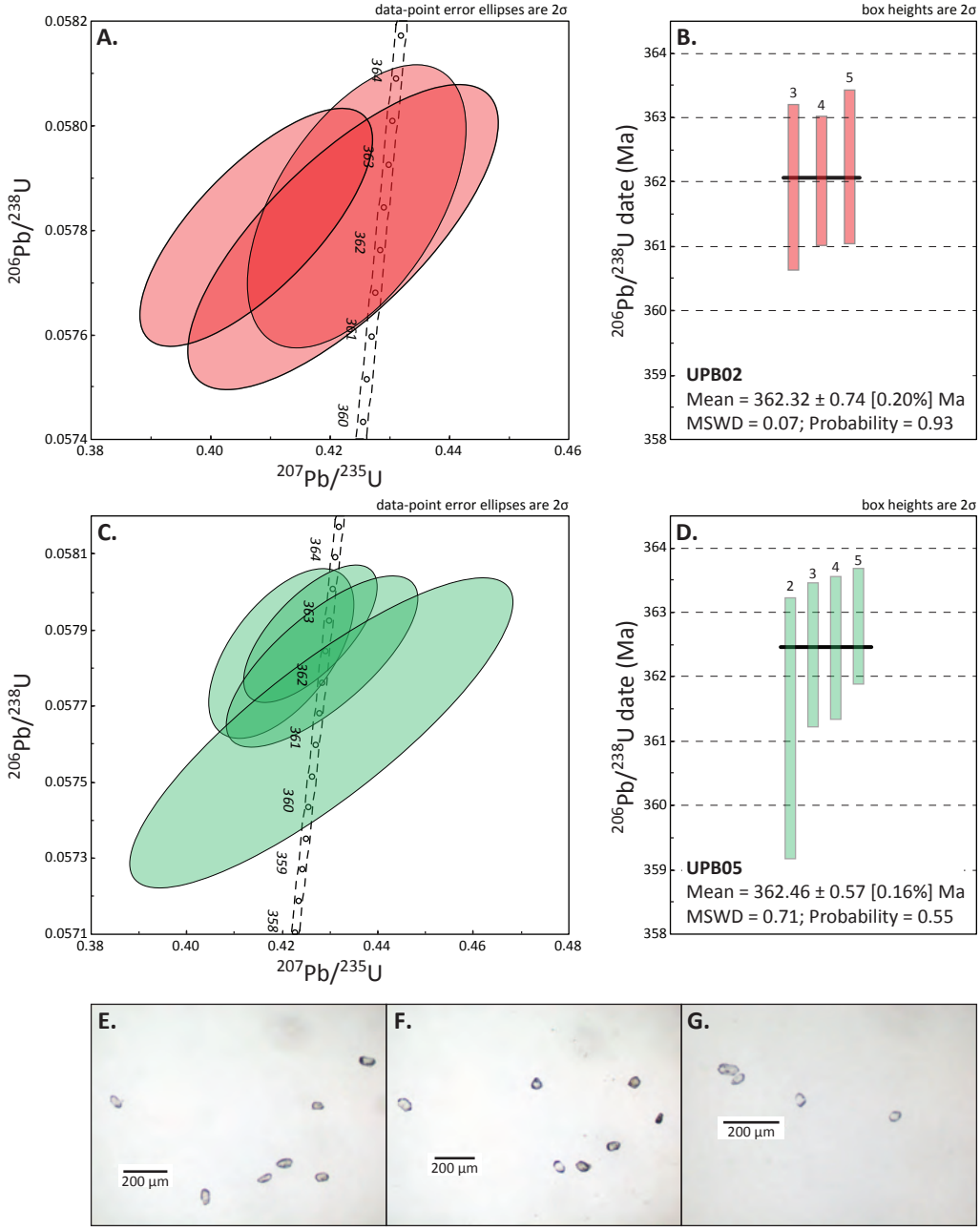

Figure 7.19 Wetherill U-Pb concordia and $^{206}Pb/^{238}U$ age diagrams for CA-ID-TIMS analyses of zircons from the HW Rhyolite. A-B. Sample UPB02. C-D. Sample UPB05. Numeric labels correspond to U-Pb results in Table 7.10. E-G. Plane polarized light photomicrographs of picked zircons for CA-ID-TIMS analysis. E. Zircons from sample UPB02. F. Zircons from sample UPB05. G. Zircons from sample 15Price01.

7.6.7 Coherent andesite – sample UPB12

UPB12 was collected from drill hole BG18-3921 at 587 mE, 4,270 mN, 2,963 mEL. Twenty U-Pb apatite analyses by LA-ICPMS with a 29 µm beam were collected (Table 7.11). Individual results form an off concordia array on the Tera-Wasserberg plot (Figure 7.20). The array yields a lower intercept age of 327 ± 22 Ma (n=19, MSWD=1.00; Figure 7.20).

7.6.8 LMP Rhyolite – sample BM17-P5A

BM17-P5A is from the Price orebody and was collected from surface outcrop near the Price Level 5 adit at 5,514 mE, 3,374 mN, 3,620 mEL (Figure 7.5A). This sample is of a quartz-muscovite-pyrite altered rhyolitic volcaniclastic sandstone. Semi-massive polymetallic sulfide

mineralisation is located 3 meters to the north of the sample location. Nine zircon grains were analysed with a 19 μm beam (n=13) and yielded $^{206}Pb/^{238}U$ ages from 305.7 ± 9.5 Ma to 369.1 ± 3.8 Ma (Table 7.8). Seven analyses plot off concordia due to common Pb and were excluded from the weighted average age calculation (Figure 7.21A-B). This sample yielded a weighted average age of 359.4 ± 7.9 Ma (n=6; MSWD=2.9; Figure 7.21B).

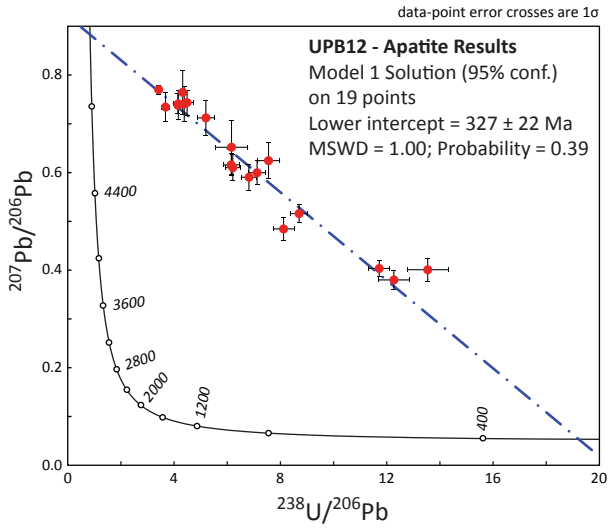

Figure 7.20 Tera-Wasserburg U-Pb concordia diagram for LA-ICPMS analyses of apatites from coherent andesite sample UPB12. Note no single analyses plots near concordia and the results appear to reflect contributions of common Pb, interpreted to be the result of secondary re-crystallisation.

7.6.9 LMP Rhyolite – sample BM17-P5C

BM17-P5C is from the Price orebody and was collected from surface outcrop near the Price Level 5 adit at 5,517 mE, 3,369 mN, 3,620 mEL (Figure 7.5A). This sample is of a quartz-muscovite-pyrite altered, rhyolitic volcaniclastic sandstone. Semi-massive polymetallic sulfide mineralisation is immediately above the sample location. Twelve zircon grains were analysed with a 19 μm beam (n=23) and yielded $^{206}Pb/^{238}U$ ages from 288.2 ± 4.0 Ma to 369.0 ± 3.9 Ma (Table 7.8). Thirteen of the twenty-three analyses were excluded from the weighted average age calculation (Figure 7.21C-D). Analyses 1-3 are from the same zircon grain, have young $^{206}Pb/^{238}U$ age results, and form an array below and off the concordia, that is interpreted to be the result Pb loss. Analyses 6, 8, 11, 13, 16, 17, 21 and 22 are discordant as a result of common Pb and Pb loss. Analyses 9 and 10 are from a small zircon grain that had low counts as result of epoxy dilution during analysis. This sample yielded a weighted average age of 355.5 ± 2.8 Ma (n=10; MSWD=0.89; Figure 7.21D).

7.6.10 LMP Rhyolite – sample 15Price01

A 1-2 kg hand specimen of sample 15Price01 was sent to UBC for CA-ID-TIMS analysis. This sample was collected from Level 4 underground workings of the Price Mine at 4,498 mE, 3,390 mN, 3,680 mEL (Figure 7.5D). Two clear, <15 μm zircons (Figure 7.17) were analysed. The sample yielded very young $^{206}Pb/^{238}U$ ages of 68.5 ± 0.6 Ma and 70.8 ± 1.1 Ma (Table 7.10). These age results are attributed to significant post-crystallisation Pb loss, a challenge with sub 10 μm zircon analyses (Ault et al., 2012), and are unlikely to represent the timing of igneous crystallisation.

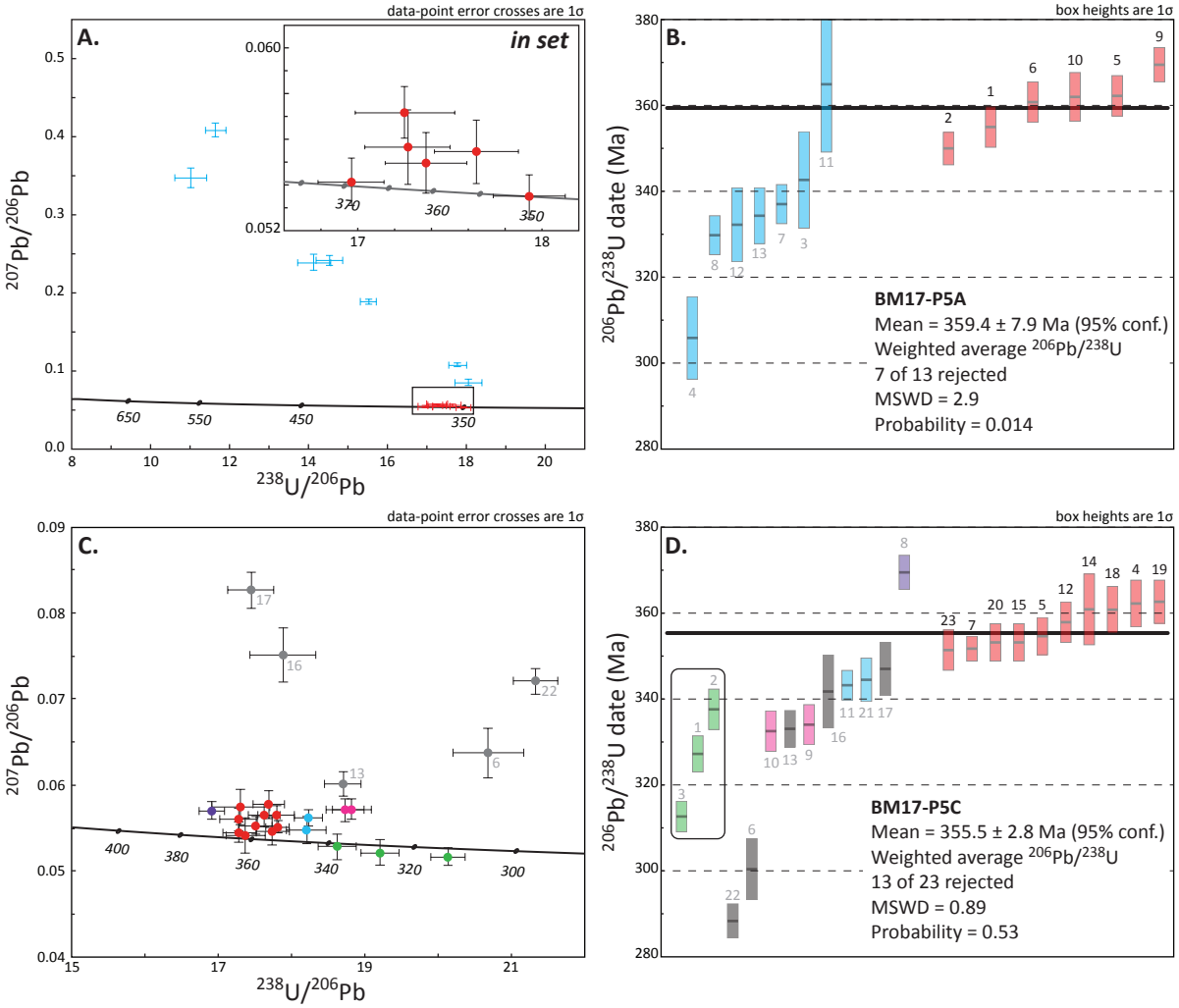

Figure 7.21 Tera-Wasserburg U-Pb concordia and $^{206}Pb/^{238}U$ age diagrams for LA-ICPMS analyses of zircons from the LMP Rhyolite. A-B. Sample BM17-P5A. Red symbols are analyses selected for the weighed average age calculation. Blue symbols are analysis effected by common Pb. C-D. Sample BM17-P5C. Red symbols were selected for the weighted average age calculation. All other measurements were rejected. Green symbols are analyses from one zircon grain interpreted to suffer from Pb loss. Grey symbols are individual spot analysis effected by common Pb. Pink symbols are two analyses from one zircon grain that had low counts from epoxy dilution during analysis. Blue symbols are single spot analysis effected by common Pb and laser miss-fire. Purple symbol is an individual analysis that is effected by common Pb. Numeric labels correspond to the zircon grain labels for figures 7.10-7.11 and U-Pb results in Table 7.8.

7.7 Discussion

Attempts to obtain crystallisation ages for andesite of the Price Formation at Myra Falls were unsuccessful. Analysis of sub 10 μm, *in situ* zircons, yielded anomalously young ages that form an array between radiogenic and common Pb sources with a lower intercept age of 115.0 ± 6.4 Ma (Figure 7.16). Petrographic examination of the analysed zircons revealed cauliflower textured, anhedral grains with inclusions and intergrowths of xenotime and silicates. This texture suggests secondary modification or precipitation of zircon (Corfu et al., 2003) within the Price Formation andesite. The lower intercept age does not directly correspond with a known igneous or metamorphic event reported for the Wrangellia Terrane. Extensive magmatism during the Jurassic (ca. 177-160 Ma) records the collision of the Wrangellia-Alexander Terrane with the Laurentian continental margin (Nelson and Colpron, 2007). Cretaceous intrusions of the Island Plutonic Suite are widespread throughout the Buttle Lake uplift along with

subordinate Triassic intrusions of the Mt. Washington Intrusive Suite (Yorath et al., 1999). The origin of these secondary zircon growths, and their significance, was not resolved in this study.

In situ LA-ICPMS analysis of monazite was attempted to establish U-Th-Pb age constraints on the crystallisation of andesite of the Price Formation. Common Pb corrected $^{208}Pb/^{232}Th$ results yielded an age population at ca. 170 Ma (Figure 7.17B). Igneous monazite has not been reported in primary lavas or plutons with a mafic composition (Mungall and Martin, 1996). This is a function of the relatively high CaO contents of mafic melts and as a result promotes the stability of LREE-bearing apatite (phosphate-group) and allanite (epidote-group) over monazite (Watt and Harley, 1993; Meyer et al., 1994). Monazites analysed from the andesite of the Price Formation have geochemical features (av. 0.4 wt. % Th; av. 33 ppm U; av. 0.6 wt. % Y) consistent with low temperature crystallisation (e.g., Williams et al., 2007) and petrographic textures and mineral relationships that suggest a hydrothermal/metamorphic origin. The ca. 170 Ma age of crystallisation for monazite in the Price Formation may record a metamorphic event related to the accretion of the Wrangellia-Alexander Terrane to the Laurentian continental margin. The oldest $^{208}Pb/^{232}Th$ monazite age population is ca. 260 Ma and is coincident with the inferred timing of regional greenschist metamorphism of the Sicker Group (Brandon et al., 1986; Greenwood et al., 1991).

Based on stratigraphic relationships (Figure 7.2), coherent andesite of the H-W member in the West Block Area is younger than the coherent rhyolite of the HW Rhyolite. Apatite U-Pb analyses yielded a $^{238}U/^{206}Pb$ lower intercept age of 326 ± 22 Ma (Figure 7.16). This age result is in agreement with the apparent depositional timing of the andesite lava flow based on geologic observations. However, individual results plot well off concordia. The large error of the lower intercept age result does not provide a precise age constraint. Estimated closure temperatures of apatite vary from 350-500ºC (e.g., Krogstad and Walker, 1993), whereas lower greenschist facies metamorphism ranges from 200-350ºC (e.g., Spear, 1993). Apatite grains show some petrographic evidence of re-crystallisation and this age result could reflect a partial metamorphic U-Pb re-setting. Additional U-Pb apatite analyses could provide a more precise, lower intercept age for apatite in coherent andesite of the H-W member.

New zircon U-Pb age determinations from this study are plotted together with previously available zircon and fossil age constraints for the Sicker Group in Figure 7.22. Results of this study provide a precise age for the HW Rhyolite of the Ridge Zone North orebody in the H-W member. This unit is host to semi-massive, polymetallic sulfide mineralisation and has an interpreted crystallisation age of 362.4 ± 0.7 Ma. The high precision CA-ID-TIMS results for coherent rhyolite overlap in error with the LA-ICPMS U-Pb zircon crystallisation age of 361.5 ± 2.5 Ma (Ruks, 2015) for coherent rhyolite from the Marshall Zone orebody (Figure 7.22). Due to the similar stratigraphic relationships and age results, coherent rhyolite from the Ridge Zone North and Marshall Zone orebodies are interpreted to be coeval. A crystallisation age of 365 ± 4 Ma from Barrett and Sherlock (1996) for coherent rhyolite located 140 metres above the Price Formation contact near the HW orebody, overlaps in error with the CA-ID-TIMS results. It is likely that coherent rhyolite near the HW orebody is coeval with rhyolite of the Ridge Zone North and Marshall Zone orebodies (Figure 7.22). This study yielded a LA-ICPMS U-Pb zircon crystallisation age of 359.4 ± 2.4 Ma for coherent rhyolite located 60 metres above the Price Formation contact in the West Block Area. This result overlaps in error with the CA-ID-TIMS ages from this study. There is potential for multiple felsic volcanic events during the deposition of the H-W member at Myra Falls. However, the overlap in errors of the published

and new U-Pb zircon data do not resolve the potential for different crystallisation ages of coherent rhyolite in the H-W member.

Based on stratigraphic relationships (Figure 7.2), the LMP Rhyolite is younger than the HW Rhyolite in the Myra Formation. New LA-ICPMS U-Pb age results of zircon from rhyolitic volcaniclastic sandstone of the LMP Rhyolite provide a maximum age of deposition (Figure 7.22). Sample BM17-5PC yielded a weighted average age of 355.5 ± 2.8 Ma (Figure 7.22). Unfortunately, efforts to date the LMP Rhyolite by CA-ID-TIMS were unsuccessful. The top of the Myra Formation is constrained by Early Mississippian (~350 Ma) radiolarian fossils found in the base of the Thelwood Formation (Jones, 2001).

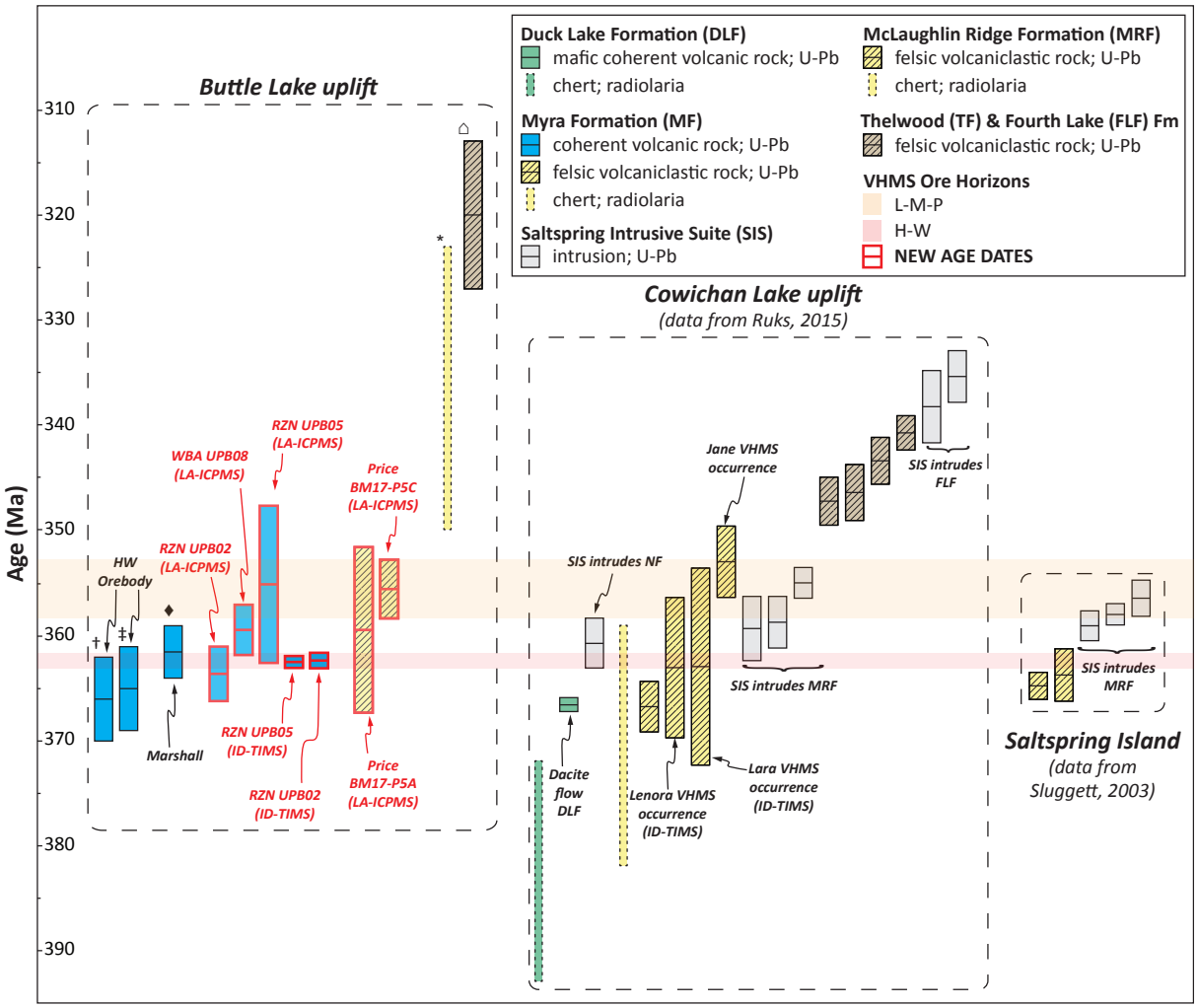

Figure 7.22 Compilation of selected previously available U-Pb zircon age constraints and biochronology ages together, with the results of this study (Ridge Zone North* and WBA*), showing new constraints on the timing of felsic volcanism within the Myra Formation. Previous age constrains from Brandon et al. (1986), Juras (1987), Parrish and McNicoll (1992), Barrett and Sherlock (1996), Jones (2001), Sluggett (2003), and Ruks (2015).

7.7.1 Implications for timing of VHMS deposit formation at Myra Falls

The new U-Pb zircon ages, combined with previously available geologic and age data, constrain the timing of the two felsic volcanism events at Myra Falls, recognised by Juras (1987). The felsic host rocks to the H-W member and L-M-P member VHMS deposits are separated by approximately 7 million years (Figure 7.23).

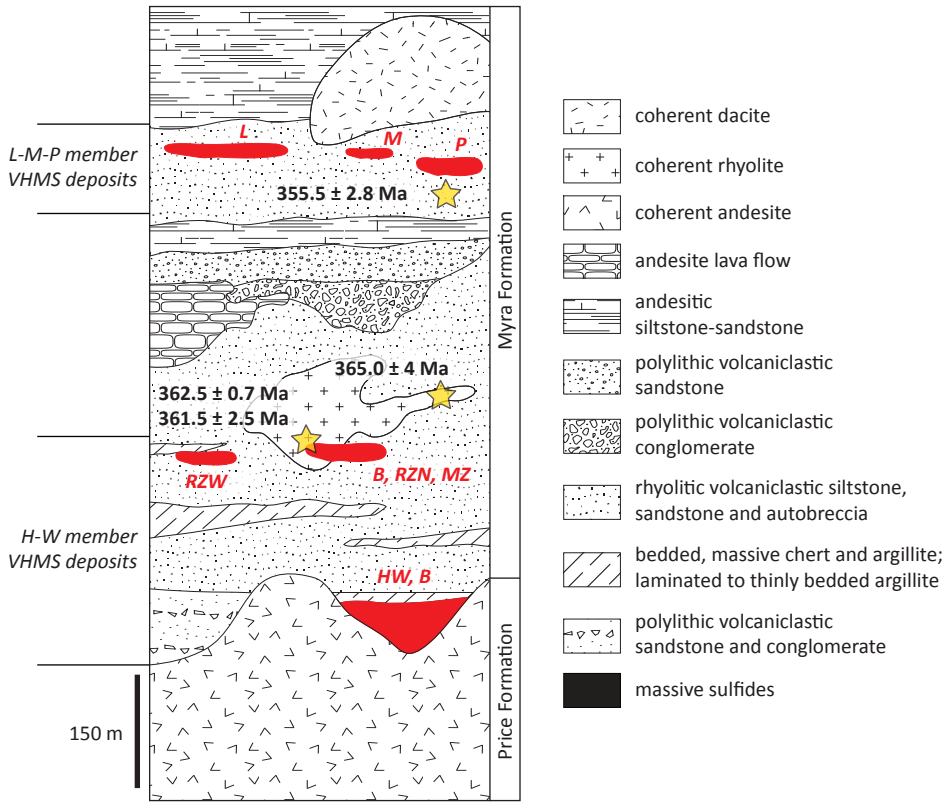

Figure 7.23 Stratigraphic reconstruction of Myra Falls district, showing the new age constraints from this study and previous age results. [B, Battle; L, Lynx; M, Myra; MZ, Marshall Zone; P, Price; RZN, Ridge Zone North; RZW, Ridge Zone West]

The VHMS deposits of the H-W member occur in the lower Myra Formation, and sulfide mineralisation is hosted in two stratigraphic positions in the HW Rhyolite. "Contact zone" position is characterised by massive sulfide located at the contact between the Price and Myra Formations and includes the HW orebody and Battle Main Lens (Figure 7.23). "Upper zone" position consists of semi-massive to massive sulfide hosted in HW Rhyolite rocks 50 to 150 metres above the contact between the Price and Myra Formations. These include upper lenses of the Battle orebody and the Gap Zone, Ridge Zone North, Ridge Zone West, and the Marshall Zone orebodies (Figure 7.23). The L-M-P member is up to 500 metres above the Price and Myra Formation contact and includes the Lynx, Myra and Price orebodies.

High precision CA-ID-TIMS results indicate that VHMS mineralisation in the Ridge Zone North orebody is hosted in 362.4 ± 0.7 Ma coherent rhyolite. Mineralised coherent rhyolite from the Marshall Zone orebody overlaps with the CA-ID-TIMS results, 361.5 ± 2.5 Ma (Ruks, 2015). Hydrothermally altered, 359.4 ± 2.4 Ma coherent rhyolite from the West Block Area suggests that VHMS mineralisation could have formed as late as ca. 357 Ma. The timing of VHMS mineralisation, is currently, only constrained by the age of the host rocks. Based on the CA-ID-TIMS results, VHMS mineralisation in the Ridge Zone North orebody formed after ca. 362 Ma. The timing of mineralisation in the HW orebody is empirically constrained by the 365 ± 4 Ma crystallisation age for hydrothermally altered rhyolite (Barrett and Sherlock 1996), located 140 metres above the HW orebody. A maximum depositional age of 355.5 ± 2.8 Ma is proposed for the deposition of the LMP Rhyolite, which hosts the Price orebody.

Compared to the Cowichan Lake uplift, the constraints on zircon U-Pb crystallisation ages of felsic volcanic rocks is more robust at Myra Falls. Prior to the work of Ruks (2015), the age constraints on VHMS occurrences in the Cowichan Lake uplift were based solely on stratigraphic relationships. There is considerable overlap in error, but the age results of Ruks (2015), suggest a H-W member equivalent in the Cowichan Lake uplift with the ~363 Ma host rocks for the Lenora and Lara VHMS occurrences (Figure 7.22). The Jane VHMS felsic volcaniclastic host rocks are within error of the maxim depositional age proposed for the Price orebody host rocks, which suggests that the Jane VHMS occurrence host rocks are a regional correlative to the L-M-P member (Figure 7.22).

Recognising the specific chronostratigraphic intervals and geologic settings of VHMS deposits is important for exploration models. The duration of VHMS hydrothermal systems can be episodic or singular in nature. For example, the VHMS deposits within the Finlayson Lake district of the Yukon, Canada. Four discrete VHMS events have been recognised, spanning a 90 million year period: the ~365 Ma Fyre Lake, ~360 Ma Kudz Ze Kayah, ~348 Ma Wolverine, and ~275 Ma Ice VHMS deposits (Mortensen, 1992a, b; Murphy et al., 2006; Piercey et al., 2008). However, Mortensen et al. (2015) validated the concept of a "Holy Host" for VHMS mineralisation within the Mount Read Volcanic Belt of Tasmania, Australia. They demonstrated that the VHMS deposits, though hosted by sequences that differ in composition and in volcanic lithofacies, within the Mount Lyell, Roseberry-Hercules, and Que-Hellyer districts formed within a narrow time interval at ~500 ± 1 Ma. Conversely, McNicoll et al. (2014) identified periodic VHMS events in the Blake River Group of the Abitibi greenstone belt of Quebec Canada. For example, the Horne, Aldermac, LaRonde-Penna and Bouchar-Hébert VHMS deposits occur at ca. 2-million year intervals between 2702 Ma and 2696 Ma.

The compilation of previous and new geochronological constraints of Sicker Group stratigraphy from the Buttle Lake and Cowichan Lake uplifts illustrates that VHMS mineralisation was episodic and associated with felsic volcanism and sedimentation over a period of ca. ~7-m.y. (Figure 7.22). There are two VHMS mineralisation events at ~362 Ma and ~355 Ma, associated with the lower and upper Myra Formation in the Buttle Lake uplift (Figure 7.23). A Pennsylvanian, third VHMS mineralisation event was recognised by Ruks (2015) in the Bedingfield uplift and Dragon area (Figures 7.1-7.2). These deposits are poorly understood, and are hosted in ~310-300 Ma felsic volcanic rocks near the base of the Mount Mark Formation. Future mineral exploration for VHMS deposits on Vancouver Island should not be limited to the ~362 Ma felsic stratigraphy, but rather also target younger, ~355 Ma and ~310-300 Ma felsic stratigraphy of the Sicker Group.

7.8 Summary

The new U-Pb zircon CA-ID-TIMS results from the HW Rhyolite and LA-ICPMS results from the LMP Rhyolite, combined with previous age constraints and stratigraphic relationships, confirm at least two phases of felsic volcanism at Myra Falls that were episodic over a period of approximately 7-million year (Figures 7.22-7.23). Attempts to determine the igneous crystallisation age of the Price Formation were, however, unsuccessful. Secondary, hydrothermal/metamorphic zircon and monazite were identified in the Price Formation and may provide an opportunity to better constrain the timing of the VHMS hydrothermal system and regional metamorphism at Myra Falls. Apatite U-Pb results from coherent andesite of the H-W member in the West Block Area were inconclusive. Further LA-ICPMS U-Pb analyses of

apatite are required to determine the significance and application of apatite geochronology at Myra Falls.

New U-Pb zircon ages of felsic stratigraphy have produced new and precise geochronological constraints for the deposition of important host rocks at Myra Falls:

- New CA-ID-TIMS results for coherent rhyolite of the H-W member near the Ridge Zone North orebody yielded a crystallisation age of 362.4 ± 0.7 Ma.
- New LA-ICPMS results for rhyolitic volcaniclastic rocks of the L-M-P member near the Price orebody yielded a maximum depositional age of 355.5 ± 2.8 Ma.
- Published age results for the Cowichan Lake uplift Lara and Lenora VHMS occurrence host rocks overlap and are within error of the age results for the H-W member of this study.
- Published age results for the Cowichan Lake uplift Jane VHMS occurrence host rocks overlap and are within error of the age results for the L-M-P member of this study.
- These results suggest that:
    1. The host rocks to the H-W and L-M-P member VHMS deposits are separated by ~7 million years.
    2. VHMS deposits of the H-W member are regional time correlatives with the Lara and Lenora VHMS occurrences.
    3. VHMS deposits of the L-M-P member are regional time correlatives with the Jane VHMS occurrence.
- VHMS mineral exploration in the Sicker Group on Vancouver Island should consider:
    1. ~362 Ma felsic stratigraphy located within 200 metres of the upper contact of the Price and Nitinat Formations. Within this stratigraphic sequence: (1) seafloor exhalative sulfide mineralisation is associated with the top of the Price/Nitinat Formation contact hosted in fine-grained felsic volcaniclastic rocks capped by chert and (2) sub-seafloor sulfide mineralisation is hosted in coarse-grained volcaniclastic rocks proximal to coherent rhyolite domes.
    2. ~355 Ma felsic stratigraphy located in the upper 100 metres of the Myra and McLaughlin Ridge Formations near the contact with the Thelwood and Fourth Lake Formations. Massive sulfide mineralisation is associated with distal, felsic volcaniclastic lithofacies.
    3. ~310 Ma to 300 Ma felsic stratigraphy below the Mount Mark Formation (Ruks, 2015).

Table 7.7 *In situ* zircon U-Pb age results by LA-ICPMS.

			Radiogenic isotope ratios							Isotopic ages (Ma)					
Run Id	**Analysis #**	**Beam (μm)**	**$^{206}Pb/^{238}U$**	**±1 σ**	**$^{208}Pb/^{232}Th$**	**±1 σ**	**$^{207}Pb/^{206}Pb$**	**±1 σ**	**Pb^{u}**	**$^{207}Pb/^{206}Pb$**	**±1 σ**	**$^{208}Pb/^{232}Th$**	**±1 σ**	**$^{206}Pb/^{238}U^{*}$**	**±1 σ**
UPB06A zircon — *massive andesite (Price Formation)*															
1	MY18A013	9	0.0213	4.5%	0.0165	8.1%	0.2000	6.9%	0.8445	330.9	26.7	2,826.4	112.2	**110.3**	**5.5**
2	MY18A019	9	0.0741	20.8%	0.1400	19.5%	0.6622	15.2%	0.8669	2,648.3	515.5	4,650.7	219.6	**118.5**	**63.1**
3	MY18A015	9	0.0450	7.8%	0.0820	9.0%	0.3388	11.3%	0.8544	1,592.8	143.8	3,657.4	173.0	**183.1**	**19.5**
UPB07A zircon — *massive andesite (Price Formation)*															
1	MY18A054	9	0.0207	5.8%	0.0100	6.9%	0.1254	7.9%	0.8442	201.4	14.0	2,033.8	139.4	**119.4**	**7.1**
2	MY18A053	9	0.0382	8.9%	0.0433	9.9%	0.3884	19.9%	0.8516	857.4	85.1	3,864.8	300.0	**140.7**	**26.4**
3	MY18A055	9	0.0186	6.6%	0.0106	6.3%	0.1138	6.2%	0.8433	213.3	13.5	1,861.7	111.2	**108.9**	**7.3**
UPB10A zircon — *massive andesite (Price Formation)*															
1	MY18A032	9	0.0311	35.0%	0.0115	23.2%	0.3531	21.8%	0.8486	231.9	53.8	3,720.5	331.1	**123.0**	**46.8**
2	MY18A026	9	0.0321	11.9%	0.0241	12.8%	0.1906	12.0%	0.8490	481.1	61.5	2,747.6	197.9	**168.1**	**20.7**
3	MY18A030	9	0.1142	22.2%	0.1859	28.3%	0.6868	17.2%	0.8845	3,446.2	975.4	4,703.3	247.4	**172.0**	**108.8**
4	MY18A029	9	0.0445	11.1%	0.0526	11.7%	0.3525	16.5%	0.8542	1,035.2	121.1	3,717.7	251.3	**176.4**	**28.1**
UPB10A zircon — *massive andesite (Price Formation)*															
1	MY18A047	9	0.0190	4.3%	0.0124	7.2%	0.0989	8.6%	0.8435	248.6	18.0	1,603.2	160.5	**113.9**	**5.0**
2	MY18A050	9	0.0223	7.1%	0.0132	7.8%	0.1337	10.4%	0.8449	265.4	20.7	2,147.0	182.2	**127.4**	**9.4**
3	MY18A049	9	0.0313	12.9%	0.0257	14.6%	0.1710	15.4%	0.8486	512.7	75.0	2,567.8	257.7	**168.6**	**22.5**
4	MY18A043	9	0.0415	9.6%	0.0428	10.5%	0.2258	16.5%	0.8530	846.4	88.9	3,022.6	264.9	**205.8**	**23.1**
5	MY18A045	9	0.0417	10.7%	0.0571	10.2%	0.1238	108.2%	0.8530	1,121.6	114.5	2,011.0	1,920.1	**239.7**	**50.3**
6	MY18A046	9	0.0769	10.0%	0.1461	11.3%	0.2825	12.6%	0.8681	2,755.8	312.2	3,376.6	196.7	**347.0**	**40.0**

Pb^{u} = common Pb at age of zircon; $^{206}Pb/^{238}U^{*}$ = corrected common Pb age result

Table 7.8 Zircon U-Pb age results by LA-ICPMS.

				Radiogenic isotope ratios							Isotopic ages (Ma)					
Run Id	**Grain Id**	**Analysis #**	**Beam (μm)**	**$^{206}Pb/^{238}U$**	**±1 σ**	**$^{208}Pb/^{232}Th$**	**±1 σ**	**$^{207}Pb/^{206}Pb$**	**±1 σ**	**Pb^{u}**	**$^{207}Pb/^{206}Pb$**	**±1 σ**	**$^{208}Pb/^{232}Th$**	**±1 σ**	**$^{206}Pb/^{238}U$***	**±1 σ**
UPB02 zircon — *coherent rhyolite (HW Rhyolite, lower Myra Formation)*																
*1	A	AU05A429	19	0.0516	2.2%	0.0201	4.4%	0.0942	4.0%	0.8572	402.5	17.5	1,511.3	76.2	**308.0**	**6.9**
*2	B	JL03A009	29	0.0555	1.3%	0.0175	1.7%	0.0596	1.3%	0.8589	350.4	5.9	587.4	27.4	**345.7**	**4.5**
*3	C	AU05A427	19	0.0557	1.5%	0.0169	4.4%	0.0560	3.3%	0.8590	337.8	14.8	450.5	74.4	**348.3**	**5.3**
14		AU05A426	19	0.0584	1.7%	0.0183	3.9%	0.0529	3.4%	0.8601	365.6	14.4	326.4	77.1	**365.8**	**6.3**
*4	D	AU05A419	19	0.0559	2.5%	0.0163	6.1%	0.0547	5.8%	0.8591	326.5	20.0	400.1	129.0	**350.1**	**8.7**
5	E	AU05A422	19	0.0575	1.2%	0.0195	2.1%	0.0625	1.9%	0.8598	390.8	8.3	691.6	41.5	**356.7**	**4.2**
6	R	JL03A013	29	0.0572	1.5%	0.0176	2.1%	0.0544	1.8%	0.8596	353.2	7.3	386.9	40.2	**358.1**	**5.2**
7	G	JL03A008	29	0.0575	1.3%	0.0180	1.7%	0.0539	1.5%	0.8597	361.4	6.3	365.8	34.5	**360.1**	**4.6**
8	H	JL03A011	29	0.0577	1.4%	0.0175	1.8%	0.0546	1.4%	0.8598	351.3	6.3	395.4	32.4	**361.3**	**5.1**
9	I	JL03A016	29	0.0578	1.3%	0.0185	2.1%	0.0549	1.8%	0.8599	371.4	7.9	407.3	40.0	**361.8**	**4.7**
10	J	AU05A423	19	0.0579	1.4%	0.0178	3.2%	0.0541	2.7%	0.8599	357.2	11.3	373.2	59.9	**362.6**	**5.0**
11	K	JL03A015	29	0.0579	1.5%	0.0174	2.7%	0.0540	1.9%	0.8599	349.7	9.5	369.1	41.7	**362.6**	**5.2**
12	L	AU05A420	19	0.0582	1.5%	0.0195	4.5%	0.0557	3.8%	0.8601	389.9	17.7	440.4	84.6	**363.8**	**5.3**
13	M	AU05A428	19	0.0585	1.9%	0.0177	4.8%	0.0578	3.9%	0.8602	354.1	17.0	521.0	86.2	**365.0**	**7.1**
15	N	AU05A425	19	0.0584	1.3%	0.0175	3.0%	0.0547	2.4%	0.8602	351.5	10.5	400.5	54.8	**365.8**	**4.8**
16	O	JL03A010	29	0.0585	1.4%	0.0207	2.3%	0.0545	2.0%	0.8602	414.5	9.3	392.4	43.9	**366.3**	**5.2**
17	P	AU05A424	19	0.0587	1.8%	0.0182	3.3%	0.0549	3.7%	0.8603	364.1	12.2	407.1	82.1	**367.3**	**6.5**
18	Q	JL03A012	29	0.0589	1.5%	0.0185	2.7%	0.0569	2.6%	0.8604	370.1	9.9	487.6	56.5	**367.8**	**5.5**
19	R	AU05A421	19	0.0591	1.3%	0.0177	3.1%	0.0535	2.6%	0.8605	354.6	11.1	348.4	58.5	**370.4**	**4.8**
20	S	JL03A014	29	0.0594	1.6%	0.0179	2.8%	0.0552	2.1%	0.8606	358.5	10.0	418.8	46.1	**371.6**	**6.0**
UPB05 zircon — *coherent rhyolite (HW Rhyolite, lower Myra Formation)*																
*1	A	NO09A028	9	0.0537	4.2%	0.0181	13.0%	0.0687	8.3%	0.8581	362.1	47.1	888.6	171.6	**330.6**	**13.8**
2		NO09A031	9	0.0545	3.9%	0.0155	10.6%	0.0607	13.3%	0.8585	310.1	32.9	628.6	287.6	**339.2**	**13.3**
3	B	NO09A033	9	0.0555	3.6%	0.0146	10.0%	0.0571	6.9%	0.8589	293.8	29.4	496.7	152.9	**346.8**	**12.4**
7		NO09A032	9	0.0570	4.4%	0.0160	14.8%	0.0649	11.2%	0.8595	320.1	47.4	772.1	236.3	**352.2**	**15.7**
4	C	NO09A027	9	0.0563	4.7%	0.0166	9.9%	0.0647	9.8%	0.8592	332.3	33.0	766.0	206.4	**348.2**	**16.3**
14		NO09A026	9	0.0593	4.0%	0.0163	10.6%	0.0539	6.5%	0.8605	327.8	34.8	364.8	145.7	**371.5**	**14.6**
5	D	NO09A041	9	0.0561	3.5%	0.0146	10.7%	0.0558	8.0%	0.8591	293.6	31.4	442.9	178.6	**350.6**	**12.2**
10		NO09A040	9	0.0570	3.5%	0.0149	10.4%	0.0600	7.3%	0.8595	298.1	31.1	604.1	157.7	**354.4**	**12.2**

Table 7.8 Continued.

				Radiogenic isotope ratios							Isotopic ages (Ma)					
Run Id	**Grain Id**	**Analysis #**	**Beam (μm)**	**$^{206}Pb/^{238}U$**	**±1 σ**	**$^{208}Pb/^{232}Th$**	**±1 σ**	**$^{207}Pb/^{206}Pb$**	**±1 σ**	**Pb^{u}**	**$^{207}Pb/^{206}Pb$**	**±1 σ**	**$^{208}Pb/^{232}Th$**	**±1 σ**	**$^{206}Pb/^{238}U$***	**±1 σ**
6	E	NO09A037	9	0.0577	4.8%	0.0272	20.6%	0.0761	12.9%	0.8598	542.0	111.5	1,099.0	259.0	**351.9**	**17.2**
12		NO09A036	9	0.0571	4.2%	0.0184	13.1%	0.0512	11.7%	0.8596	369.2	48.2	248.5	268.6	**357.9**	**15.0**
8	F	NO09A038	9	0.0563	3.9%	0.0116	9.6%	0.0528	9.1%	0.8592	234.1	22.5	318.5	207.3	**353.1**	**13.7**
13		NO09A039	9	0.0589	3.7%	0.0177	8.5%	0.0506	9.1%	0.8604	353.9	29.9	222.2	210.8	**369.2**	**13.7**
9	G	NO09A034	9	0.0569	3.6%	0.0159	9.9%	0.0596	7.5%	0.8595	317.9	31.4	590.5	161.6	**354.1**	**12.7**
11		NO09A035	9	0.0570	4.0%	0.0140	11.0%	0.0482	10.0%	0.8595	281.4	30.9	110.3	235.5	**357.2**	**14.4**
UPB08 zircon — *coherent rhyolite (HW Rhyolite, lower Myra Formation)*																
*1	A	AU05A448	19	0.0496	1.3%	0.0136	2.4%	0.0573	1.6%	0.8564	272.5	6.6	502.8	35.9	**310.0**	**4.1**
*2	B	AU05A454	19	0.0499	1.8%	0.0132	4.0%	0.0575	3.5%	0.8565	264.9	10.7	511.7	76.3	**312.0**	**5.7**
*3	C	AU05A449	19	0.0501	1.6%	0.0151	3.4%	0.0564	2.9%	0.8566	303.4	10.4	466.2	63.7	**313.5**	**5.1**
*4	D	AU05A452	19	0.0540	1.5%	0.0156	2.8%	0.0526	3.0%	0.8582	313.8	8.7	312.9	69.1	**338.8**	**5.1**
*5	E	AU05A440	19	0.0547	1.2%	0.0159	2.1%	0.0535	1.8%	0.8586	319.2	6.8	348.3	40.0	**343.4**	**4.0**
*6	F	AU05A438	19	0.0550	1.4%	0.0162	3.1%	0.0526	2.9%	0.8587	325.0	10.2	313.1	65.2	**344.9**	**5.0**
7	G	AU05A441	19	0.0557	1.8%	0.0174	5.3%	0.0521	4.2%	0.8590	349.6	18.5	289.7	95.4	**349.4**	**6.3**
8	H	AU05A460	19	0.0562	1.8%	0.0176	3.6%	0.0508	4.1%	0.8592	352.4	12.8	230.8	95.5	**352.7**	**6.5**
9	I	AU05A459	19	0.0568	1.5%	0.0189	3.8%	0.0554	3.1%	0.8594	378.0	14.5	430.3	68.3	**355.3**	**5.4**
10	J	AU05A447	19	0.0568	1.2%	0.0174	3.0%	0.0559	2.6%	0.8595	347.9	10.5	446.7	57.3	**355.4**	**4.4**
22		AU05A446	19	0.0580	1.6%	0.0181	3.4%	0.0570	3.1%	0.8600	362.8	12.4	489.6	67.8	**362.1**	**5.7**
11	K	AU05A462	19	0.0569	1.5%	0.0185	3.1%	0.0538	2.5%	0.8595	370.7	11.4	363.8	57.4	**356.7**	**5.1**
12	L	AU05A456	19	0.0569	1.7%	0.0164	3.6%	0.0527	3.0%	0.8595	329.4	11.9	315.8	68.7	**356.8**	**5.9**
13	M	AU05A444	19	0.0571	1.5%	0.0168	3.0%	0.0554	3.2%	0.8596	336.0	10.0	429.7	70.5	**357.2**	**5.2**
14	N	AU05A443	19	0.0571	1.5%	0.0170	3.3%	0.0559	2.8%	0.8596	340.6	11.2	448.1	62.6	**357.3**	**5.4**
15	O	AU05A436	19	0.0571	1.2%	0.0175	2.3%	0.0555	2.0%	0.8596	351.4	8.1	432.3	43.8	**357.4**	**4.3**
16	P	AU05A437	19	0.0571	2.9%	0.0191	12.5%	0.0536	8.7%	0.8596	383.4	48.0	355.2	197.1	**358.1**	**10.5**
17	Q	AU05A461	19	0.0575	1.9%	0.0169	4.8%	0.0559	3.9%	0.8598	339.1	16.1	448.1	87.0	**359.7**	**6.9**
18	R	AU05A455	19	0.0576	1.3%	0.0179	2.9%	0.0543	2.4%	0.8598	358.8	10.4	381.4	53.0	**360.9**	**4.6**
19	S	AU05A442	19	0.0576	2.1%	0.0168	5.1%	0.0499	4.7%	0.8598	336.1	17.1	192.2	109.9	**361.0**	**7.7**
20	T	AU05A439	19	0.0577	1.3%	0.0184	2.7%	0.0528	2.3%	0.8598	369.2	10.0	322.2	51.4	**361.5**	**4.6**
21	U	AU05A453	19	0.0579	1.9%	0.0184	5.3%	0.0563	4.2%	0.8599	368.9	19.6	463.9	93.0	**361.7**	**6.7**
23	V	AU05A451	19	0.0579	1.4%	0.0181	3.4%	0.0523	3.0%	0.8599	361.6	12.3	300.6	68.1	**363.1**	**5.2**

Table 7.8 Continued.

Run Id	Grain Id	Analysis #	Beam (μm)	Radiogenic isotope ratios							Isotopic ages (Ma)					
				$^{206}Pb/^{238}U$	±1 σ	$^{208}Pb/^{232}Th$	±1 σ	$^{207}Pb/^{206}Pb$	±1 σ	Pb^{u}	$^{207}Pb/^{206}Pb$	±1 σ	$^{208}Pb/^{232}Th$	±1 σ	$^{206}Pb/^{238}U^{*}$	±1 σ
24	W	AU05A450	19	0.0582	1.5%	0.0175	4.1%	0.0516	3.6%	0.8600	351.5	14.4	269.5	81.9	**364.4**	**5.5**
25	X	AU05A457	19	0.0584	1.6%	0.0174	4.4%	0.0569	4.0%	0.8601	349.1	15.3	489.1	89.0	**364.6**	**5.7**
26	Y	AU05A445	19	0.0583	1.6%	0.0177	3.5%	0.0542	3.3%	0.8601	353.8	12.4	378.9	73.1	**365.1**	**5.8**
27	Z	AU05A458	19	0.0587	1.6%	0.0189	4.6%	0.0507	3.7%	0.8603	379.0	17.3	227.5	84.7	**367.7**	**6.0**
BM17-P5A zircon — rhyolite volcaniclastic sandstone *(LMP Rhyolite, upper Myra Formation)*																
1	A	OC05A0038	19	0.0567	1.3%	0.0180	2.6%	0.0555	2.5%	0.8594	430.8	56.0	360.9	9.6	**354.6**	**4.6**
2		OC05A0039	19	0.0558	1.1%	0.0174	1.7%	0.0535	1.8%	0.8590	350.2	39.9	349.4	6.1	**349.8**	**3.8**
*3	B	OC05A0040	19	0.0707	3.0%	0.0584	4.7%	0.2389	4.1%	0.8654	3,112.9	66.0	1,148.0	53.7	**342.5**	**11.5**
*4		OC05A0041	19	0.0859	2.3%	0.0900	2.6%	0.4085	2.3%	0.8720	3,940.5	33.9	1,742.1	45.6	**305.7**	**9.5**
5	C	OC05A0042	19	0.0579	1.4%	0.0178	2.5%	0.0557	2.9%	0.8599	438.7	65.2	356.7	8.8	**362.0**	**4.9**
6		OC05A0043	19	0.0576	1.3%	0.0167	2.4%	0.0550	2.4%	0.8598	411.2	54.1	333.8	7.9	**360.3**	**4.6**
*7	D	OC05A0044	19	0.0644	1.3%	0.0545	2.1%	0.1883	1.7%	0.8627	2,727.7	28.7	1,071.8	22.3	**337.0**	**4.7**
*8	E	OC05A0045	19	0.0563	1.3%	0.0254	2.3%	0.1078	2.0%	0.8592	1,762.2	37.0	506.3	11.6	**329.5**	**4.3**
9	F	OC05A0046	19	0.0589	1.0%	0.0185	2.1%	0.0541	1.9%	0.8604	376.7	43.0	371.1	7.9	**369.1**	**3.8**
10		OC05A0047	19	0.0579	1.6%	0.0171	1.9%	0.0572	2.0%	0.8599	498.5	43.3	343.7	6.7	**361.7**	**5.6**
*11	G	OC05A0048	19	0.0907	3.6%	0.1162	5.1%	0.3477	3.7%	0.8741	3,697.1	56.8	2,221.2	112.2	**364.8**	**15.9**
*12	H	OC05A0049	19	0.0688	2.3%	0.0649	3.1%	0.2417	2.7%	0.8646	3,131.2	42.5	1,270.4	39.6	**331.9**	**8.4**
*13	I	OC05A0050	19	0.0554	1.9%	0.0210	3.4%	0.0853	4.9%	0.8589	1,323.4	95.0	419.7	14.4	**334.0**	**6.6**
BM17-P5C zircon — rhyolite volcaniclastic sandstone *(LMP Rhyolite, upper Myra Formation)*																
*1		OC05A0009	19	0.0521	1.3%	0.0162	2.7%	0.0522	2.8%	0.8574	292.5	64.4	324.4	8.7	**327.2**	**4.3**
*2	A	OC05A0010	19	0.0537	1.4%	0.0172	2.5%	0.0528	2.8%	0.8581	320.5	64.0	343.8	8.7	**337.2**	**4.8**
*3		OC05A0011	19	0.0497	1.2%	0.0151	2.2%	0.0517	2.0%	0.8564	270.3	45.8	303.4	6.6	**312.6**	**3.6**
4	B	OC05A0012	19	0.0579	1.5%	0.0183	2.4%	0.0560	2.4%	0.8599	452.3	52.4	366.2	8.6	**361.8**	**5.3**
5		OC05A0013	19	0.0567	1.2%	0.0177	2.0%	0.0565	2.3%	0.8594	470.3	51.1	354.3	7.2	**354.4**	**4.3**
*6	C	OC05A0014	19	0.0483	2.3%	0.0151	3.0%	0.0637	4.5%	0.8558	732.8	96.4	303.5	9.0	**300.2**	**6.9**
7	D	OC05A0015	19	0.0562	0.9%	0.0172	1.7%	0.0551	1.3%	0.8592	417.8	29.4	345.0	5.7	**351.5**	**3.0**
*8		OC05A0016	19	0.0591	1.1%	0.0203	2.1%	0.0570	1.8%	0.8605	491.2	40.1	405.5	8.6	**369.0**	**3.9**
*9	E	OC05A0017	19	0.0534	1.4%	0.0166	3.5%	0.0571	2.3%	0.8580	494.6	51.6	333.4	11.5	**333.8**	**4.6**
*10		OC05A0018	19	0.0532	1.4%	0.0163	4.0%	0.0572	2.1%	0.8579	497.6	46.5	326.8	13.1	**332.2**	**4.7**
*11	F	OC05A0019	19	0.0549	1.1%	0.0166	1.8%	0.0562	1.8%	0.8586	460.6	38.9	332.0	5.9	**343.1**	**3.6**

Table 7.8 Continued.

				Radiogenic isotope ratios							Isotopic ages (Ma)					
Run Id	**Grain Id**	**Analysis #**	**Beam (μm)**	**$^{206}Pb/^{238}U$**	**±1 σ**	**$^{208}Pb/^{232}Th$**	**±1 σ**	**$^{207}Pb/^{206}Pb$**	**±1 σ**	**Pb^{u}**	**$^{207}Pb/^{206}Pb$**	**±1 σ**	**$^{208}Pb/^{232}Th$**	**±1 σ**	**$^{206}Pb/^{238}U^{*}$**	**±1 σ**
12	G	OC05A0020	19	0.0571	1.3%	0.0169	2.0%	0.0553	1.9%	0.8596	424.2	43.1	339.4	6.9	**357.4**	**4.7**
*13		OC05A0021	19	0.0535	1.3%	0.0158	2.0%	0.0601	2.3%	0.8580	606.3	50.5	317.6	6.4	**333.0**	**4.4**
14	H	OC05A0022	19	0.0578	2.3%	0.0178	3.2%	0.0574	3.7%	0.8599	508.2	80.6	356.4	11.4	**360.5**	**8.1**
15	I	OC05A0023	19	0.0564	1.3%	0.0160	2.5%	0.0546	3.1%	0.8593	396.9	68.4	320.9	8.1	**353.0**	**4.5**
*16		OC05A0024	19	0.0559	2.5%	0.0205	6.0%	0.0752	4.2%	0.8591	1,072.6	84.9	410.7	24.4	**341.5**	**8.4**
*17		OC05A0025	19	0.0573	1.8%	0.0225	2.5%	0.0826	2.5%	0.8597	1,260.4	49.2	449.7	11.2	**346.6**	**6.1**
18	J	OC05A0026	19	0.0576	1.5%	0.0178	3.5%	0.0542	3.8%	0.8598	377.6	86.0	356.0	12.6	**360.6**	**5.5**
19		OC05A0027	19	0.0578	1.4%	0.0176	3.0%	0.0545	2.1%	0.8599	391.5	47.0	351.9	10.7	**362.2**	**4.8**
20		OC05A0028	19	0.0566	1.2%	0.0171	2.6%	0.0577	2.7%	0.8594	518.0	60.3	343.3	9.0	**352.9**	**4.3**
*21	K	OC05A0029	19	0.0549	1.5%	0.0160	3.0%	0.0548	2.9%	0.8587	402.7	65.4	321.2	9.6	**344.2**	**5.1**
*22		OC05A0030	19	0.0469	1.4%	0.0159	1.8%	0.0721	2.1%	0.8552	988.3	43.1	319.5	5.7	**288.2**	**4.0**
23	L	OC05A0037	19	0.0562	1.4%	0.0168	2.5%	0.0565	2.1%	0.8592	470.1	46.5	336.4	8.3	**351.3**	**4.8**

*Analysis excluded from weighted average age calculation; Pb^{u} = common Pb at age of zircon; $^{206}Pb/^{238}U^{*}$ = corrected common Pb age result.

Table 7.9 Monazite U-Th-Pb age results by *in situ* LA-ICPMS.

				Radiogenic isotope ratios							Isotopic ages (Ma)							
Run Id	**Grain Id**	**Analysis #**	**Beam (μm)**	**$^{206}Pb/^{238}U$**	**±1 σ**	**$^{208}Pb/^{232}Th$**	**±1 σ**	**$^{207}Pb/^{206}Pb$**	**±1 σ**	**Pb^{u}**	**$^{206}Pb/^{238}U$***	**±1 σ**	**$^{208}Pb/^{232}Th$**	**±1 σ**	**$^{207}Pb/^{206}Pb$**	**±1 σ**	**$^{208}Pb/^{232}Th$***	**±1 σ**
UPB10B monazite — *massive andesite (Price Formation)*																		
1	A	NO90B058	9	0.0647	20.1%	0.0097	3.0%	0.5975	112.0%	0.8628	134.5	338.2	194.8	5.9	4,502.0	1,628.5	**189.5**	**8.8**
2	B	NO90B087	9	0.0418	16.4%	0.0087	3.1%	0.3050	234.7%	0.8530	181.0	236.2	175.8	5.5	3,495.9	3,629.1	**173.7**	**7.9**
3	C	NO90B066	9	0.0546	17.6%	0.0093	2.4%	0.4315	203.6%	0.8585	183.4	375.2	186.3	4.4	4,022.7	3,040.4	**182.3**	**10.2**
4	D	NO90B083	9	0.0337	10.1%	0.0084	2.2%	0.0953	27.4%	0.8496	201.7	21.2	168.6	3.7	1,533.9	515.2	**167.7**	**3.7**
5	E	NO90B065	9	0.0537	14.8%	0.0101	3.5%	0.3072	18.4%	0.8581	232.1	41.3	203.3	7.2	3,507.0	284.1	**195.1**	**7.4**
6	na	NO90B075	9	0.0599	18.4%	0.0105	3.1%	0.3634	22.7%	0.8608	232.7	57.1	211.0	6.5	3,763.9	345.3	**206.1**	**6.6**
7	F	NO90B080	9	0.0444	15.8%	0.0088	2.3%	0.1797	311.6%	0.8542	236.2	197.3	177.1	4.0	2,650.3	5,169.6	**175.9**	**6.1**
8	G	NO90B074	9	0.0705	15.9%	0.0118	20.2%	0.4001	19.2%	0.8654	254.8	57.6	237.9	48.0	3,909.4	288.1	**181.3**	**50.2**
9	na	NO90B076	9	0.0642	12.3%	0.0123	5.3%	0.3360	11.8%	0.8626	263.3	37.5	246.9	13.0	3,644.9	180.3	**219.5**	**13.9**
10	H	NO90B081	9	0.0834	20.0%	0.0087	3.8%	0.4382	21.4%	0.8709	277.8	81.0	174.2	6.7	4,045.8	319.6	**168.3**	**6.9**
11	I	NO90B088	9	0.0736	9.5%	0.0121	3.5%	0.3691	9.3%	0.8667	283.4	32.9	242.6	8.4	3,787.7	141.3	**221.9**	**8.9**
12	J	NO90B084	9	0.0616	18.4%	0.0111	3.4%	0.2535	21.3%	0.8615	291.8	58.8	222.2	7.6	3,206.7	337.3	**217.2**	**7.8**
13	K	NO90B072	9	0.0629	23.1%	0.0105	3.4%	0.2601	96.4%	0.8621	294.8	138.5	211.4	7.2	3,247.6	1,519.3	**206.1**	**9.5**
14	L	NO90B063	9	0.0981	29.4%	0.0082	5.3%	0.4778	15.0%	0.8774	299.2	101.5	164.6	8.7	4,174.1	221.8	**147.5**	**10.4**
15	M	NO90B052	9	0.0639	19.8%	0.0091	3.3%	0.2539	154.9%	0.8625	302.2	201.3	182.5	6.1	3,209.5	2,448.1	**179.6**	**8.1**
16	N	NO90B059	9	0.0560	9.7%	0.0144	4.1%	0.1368	20.6%	0.8591	315.3	32.4	288.8	12.0	2,187.3	358.0	**260.7**	**15.0**
17	O	NO90B073	9	0.0863	12.5%	0.0506	12.9%	0.3525	11.2%	0.8722	343.8	49.4	997.3	128.3	3,717.7	170.5	**231.8**	**191.2**
18	P	NO90B079	9	0.2959	16.6%	0.0109	3.5%	0.7894	12.2%	0.9691	364.0	201.7	219.7	7.8	4,902.8	174.6	**189.9**	**10.0**
19	Q	NO90B061	9	0.0804	45.7%	0.0115	9.9%	0.2087	415.5%	0.8696	407.2	554.8	231.2	22.9	2,895.3	6,740.0	**220.0**	**64.4**
20	R	NO90B078	9	0.1530	12.3%	0.0221	8.8%	0.4076	15.5%	0.9019	553.6	95.7	441.2	38.9	3,937.3	232.0	**237.7**	**58.5**

Pb^{u} = common Pb at age of zircon; $^{206}Pb/^{238}U$* = corrected common Pb age result; $^{208}Pb/^{232}Th$* = corrected common Pb age result by the method described by Berry et al. (2016).

Table 7.10 Zircon U-Pb age results by CA-ID-TIMS.

	Compositional parameters								Radiogenic isotope ratios									Isotopic ages (Ma)					
Run Id	Wt	U	Pb	Th/U	$^{206}Pb^*$	$^{206}Pb^*$	Pb^*/Pb_c	Pb_c	$^{206}Pb/^{204}Pb$	$^{208}Pb/^{206}Pb$	$^{207}Pb/^{206}Pb$	err	$^{207}Pb/^{235}U$	err	$^{206}Pb/^{238}U$	err	corr. coef.	$^{207}Pb/^{206}Pb$	±	$^{207}Pb/^{235}U$	±	$^{206}Pb/^{238}U$	±
	µg	ppm	ppm		x10^{-13} mol	mol%		pg				%		%		%							
(a)	(b)	(c)	(c)	(d)	(e)	(e)	(e)	(e)	(f)	(g)	(g)	(h)	(g)	(h)	(g)	(h)		(j)	(h)	(j)	(h)	(j)	(h)
UPB02 zircon — *coherent rhyolite (HW Rhyolite, lower Myra Formation)*																							
*1	0.7	93	5.0	0.378	0.1188	94.59	5	0.56	342	0.120	0.05351	3.51	0.33029	3.71	0.04477	0.38	0.570	351	79	289.8	9.4	**282.3**	**1.1**
*2	0.7	87	6.6	0.494	0.1117	84.23	2	1.72	117	0.156	0.05505	5.70	0.34421	6.05	0.04535	0.43	0.840	414	127	300.4	15.7	**285.9**	**1.2**
3	0.4	106	8.3	0.422	0.1093	91.40	3	0.85	215	0.133	0.05298	4.71	0.42210	5.01	0.05779	0.41	0.748	328	107	357.6	15.1	**362.2**	**1.4**
4	0.5	83	5.8	0.361	0.1022	94.37	5	0.50	328	0.114	0.05114	3.65	0.40764	3.88	0.05781	0.32	0.737	247	84	347.2	11.4	**362.3**	**1.1**
5	0.3	144	10.0	0.442	0.0984	94.90	6	0.43	363	0.139	0.05321	3.31	0.42438	3.51	0.05785	0.38	0.547	338	75	359.2	10.6	**362.5**	**1.3**
UPB05 zircon — *coherent rhyolite (HW Rhyolite, lower Myra Formation)*																							
*1	0.4	249	9.8	0.299	0.1337	91.36	3	1.04	214	0.095	0.05140	5.47	0.21386	5.80	0.03017	0.42	0.809	259	126	196.8	10.4	**191.6**	**0.8**
2	0.9	59	4.2	0.428	0.1293	94.56	5	0.61	340	0.135	0.05387	7.14	0.42809	7.61	0.05763	0.57	0.844	366	161	361.8	23.2	**361.2**	**2.0**
3	1.1	55	4.2	0.396	0.1509	91.66	3	1.13	222	0.125	0.05372	3.58	0.42824	3.80	0.05782	0.32	0.738	359	81	361.9	11.6	**362.3**	**1.1**
4	0.7	106	7.0	0.408	0.1743	96.34	8	0.54	506	0.129	0.05264	2.77	0.41975	2.94	0.05784	0.31	0.577	313	63	355.9	8.8	**362.5**	**1.1**
5	0.8	90	6.0	0.388	0.1639	96.06	7	0.55	469	0.122	0.05335	2.50	0.42581	2.67	0.05789	0.25	0.683	344	57	360.2	8.1	**362.8**	**0.9**
15Price01 zircon — *rhyolite (LMP Rhyolite, upper Myra Formation)*																							
*1	0.3	138	2.8	0.559	0.0209	80.74	1	0.41	96	0.179	0.05177	13.73	0.07626	14.43	0.01068	0.89	0.794	275	314	74.6	10.4	**68.5**	**0.6**
*2	0.5	79	2.1	0.439	0.0186	71.19	1	0.62	64	0.141	0.04489	28.45	0.06840	29.43	0.01105	1.54	0.648	-62	694	67.2	19.1	**70.8**	**1.1**

(a) 1, 2 etc. are labels for fractions composed of single zircon grain; all fractions annealed and chemically abraded after Mattinson (2005) and Scoates and Friedman (2008)
(c) Nominal U and total Pb concentrations subject to uncertainty in photomicrographic estimation of weight (b) and partial dissolution during chemical abrasion
(d) Model Th/U ratio calculated from radiogenic $^{208}Pb/^{206}Pb$ ratio and $^{207}Pb/^{235}U$ age
(e) Pb* and Pbc represent radiogenic and common Pb, respectively; mol% $^{206}Pb^*$ with respect to radiogenic, blank and initial common Pb
(f) Measured ratio corrected for spike and fractionation only; mass discrimination of 0.25 ±0.04%/amu based on analysis of NBS-982, all Daly analyses
(g) Corrected for fractionation and spike; common Pb was assumed to be procedural blank: $^{206}Pb/^{204}Pb$=18.50 ±1.0%; $^{207}Pb/^{204}Pb$=15.50 ±1.0%; $^{208}Pb/^{204}Pb$=38.40 ± 1.08% (uncertainties 1σ)
(h) Errors are 2σ, propagated using the algorithms of Crowley et al. (2007) and Schmitz and Schoene (2007)
(i) Calculations are based on the decay constants of Jaffey et al. (1971); $^{206}Pb/^{238}U$ and $^{207}Pb/^{206}Pb$ ages corrected for initial disequilibrium in $^{230}Th/^{238}U$ using Th/U [magma] = 3

Table 7.11 Apatite U-Pb age results by LA-ICPMS.

				Radiogenic isotope ratios							Isotopic ages (Ma)					
Run Id	**Grain Id**	**Analysis #**	**Beam (μm)**	**$^{206}Pb/^{238}U$**	**±1 σ**	**$^{208}Pb/^{232}Th$**	**±1 σ**	**$^{207}Pb/^{206}Pb$**	**±1 σ**	**Pb^{u}**	**$^{207}Pb/^{206}Pb$**	**±1 σ**	**$^{208}Pb/^{232}Th$**	**±1 σ**	**$^{206}Pb/^{238}U^{*}$**	**±1 σ**
UPB12 apatite — *coherent andesite (lower Myra Formation)*																
1		NO23A081	29	0.1149	3.8%	0.1782	3.5%	0.5152	3.7%	0.8848	3314.5	117.3	4285.4	54.6	**321.0**	**20.8**
2	A	NO23A080	29	0.1468	4.4%	0.1626	3.8%	0.5904	4.6%	0.8991	3046.0	116.9	4484.5	67.4	**336.5**	**33.4**
3		NO23A082	29	0.1627	4.9%	0.1931	4.6%	0.6153	3.7%	0.9063	3568.7	162.6	4544.4	53.3	**348.3**	**32.4**
4	B	NO23A084	29	0.1623	10.2%	0.1316	6.9%	0.6512	8.3%	0.9062	2498.2	171.3	4626.6	120.2	**305.2**	**71.3**
5		NO23A083	29	0.2401	4.4%	0.2456	3.9%	0.7381	4.2%	0.9424	4438.3	172.2	4806.7	59.9	**346.4**	**55.1**
6	C	NO23A086	29	0.2716	4.9%	0.1890	3.9%	0.7340	4.1%	0.9575	3498.8	135.4	4798.8	59.2	**419.7**	**60.9**
7		NO23A085	29	0.1961	7.1%	0.1380	5.1%	0.6150	6.8%	0.9218	2613.4	132.3	4543.7	98.1	**432.9**	**65.5**
8	D	NO23A087	29	0.1923	6.3%	0.1399	4.9%	0.7117	5.1%	0.9200	2646.5	129.2	4754.5	73.8	**290.8**	**54.5**
9		NO23A088	29	0.1607	4.6%	0.0941	4.5%	0.6098	4.5%	0.9054	1817.5	81.2	4531.6	64.9	**349.8**	**36.2**
10	E	NO23A089	29	0.0739	5.9%	0.1583	7.0%	0.3999	6.2%	0.8668	2971.1	209.2	3908.6	92.7	**267.1**	**21.1**
11		NO23A095	29	0.1401	4.6%	0.1067	4.2%	0.5987	4.3%	0.8961	2049.1	86.9	4505.0	62.0	**310.9**	**30.5**
12	F	NO23A096	29	0.1233	5.0%	0.1189	5.1%	0.4837	4.9%	0.8885	2271.1	115.0	4192.3	73.0	**374.4**	**28.8**
13	G	NO23A097	29	0.0815	4.8%	0.0726	5.3%	0.3798	5.6%	0.8701	1416.9	74.9	3830.9	84.2	**307.4**	**19.8**
14	H	NO23A098	29	0.2403	4.7%	0.3918	4.2%	0.7404	2.9%	0.9425	6681.6	282.4	4811.3	41.3	**342.7**	**41.0**
15	I	NO23A099	29	0.1324	5.9%	0.2361	5.6%	0.6244	6.1%	0.8926	4284.7	239.4	4565.7	88.7	**266.6**	**41.1**
16	J	NO23A100	29	0.2225	5.6%	0.2216	4.3%	0.7434	3.5%	0.9341	4045.3	172.5	4817.0	50.2	**303.0**	**45.7**
17	K	NO23A101	29	0.2307	3.9%	0.1925	4.1%	0.7638	6.0%	0.9380	3557.9	144.1	4855.7	86.2	**285.9**	**76.5**
18		NO23A102	29	0.2283	5.0%	0.1953	4.0%	0.7407	4.8%	0.9369	3605.1	143.7	4811.7	68.9	**318.6**	**60.4**
19	L	NO23A103	29	0.0853	3.5%	0.1111	3.9%	0.4030	4.3%	0.8718	2129.3	83.8	3920.1	65.0	**307.3**	**15.7**

Pb^{u} = common Pb at age of zircon; $^{206}Pb/^{238}U^{*}$ = corrected common Pb age result.

Chapter 8:

Discussion

The lithofacies and styles of sulfide mineralisation from the HW, Battle, West Block Area, Ridge Zone North and Ridge Zone West orebodies are reviewed and a genetic model is proposed for the formation of the H-W member VHMS deposits. The depositional history of the Myra Formation is discussed and updated with new geochronological constraints for the H-W and L-M-P members. To conclude, implications for mineral exploration in the Myra Falls district and on Vancouver Island are presented.

8.1 H-W Member VHMS Deposits Host Lithofacies

Deciphering how a VHMS deposit formed requires identifying the nature and deposition mechanism of the host facies, and the paleo-seafloor position where mineralisation was focused. The host facies to the H-W member VHMS deposits vary across the Myra Falls district and sulfide mineralisation occurs at two stratigraphic positions.

Massive sulfide mineralisation in the HW orebody occurs on top of andesite of the Price Formation and is overlain by argillite (Figure 8.1; Barrett and Sherlock, 1996). This mineralisation position is referred to as "contact zone". Above the argillite, the sequence transitions into normally graded, intercalated argillite and rhyolitic volcaniclastic siltstone and sandstone beds, with coherent rhyolite prominent at the top of the sequence north of the HW orebody (Figure 8.1; Juras, 1987; Barrett and Sherlock, 1996). In contrast, "contact zone" position massive sulfide mineralisation in the Battle orebody is immediately overlain by white chert (Figure 8.1; Robinson et al., 1996). Jones et al. (2006b) determined that chert was the result of replacement of pre-existing sediments. The 3-5 metre-thick chert extends 100 to 150 metres laterally from massive sulfide mineralisation. Distally, this unit grades to black chert and eventually to unaltered argillite (Jones et al., 2006b). Similar to the HW orebody host facies, the Battle orebody host rocks transition up stratigraphy from chert to intercalated argillite, chert and rhyolitic volcaniclastic siltstone and sandstone beds (Figure 8.1; Sinclair, 2000). At the top of the host sequence is a coherent rhyolite flow with massive sulfide mineralisation associated with autoclastic breccias along its base and margins (Figure 8.1; Robinson et al., 1996; Sinclair, 2000). Sulfide mineralisation at this higher stratigraphic position is referred to as "upper zone".

Massive sulfide mineralisation in the Ridge Zone West orebody does not occur in a "contact zone" position, but rather near the top of the H-W member in an "upper zone" position (Figure 8.1; Chong, 2004). In contrast to the Battle and HW orebody localities, polylithic conglomerate to sandstone beds overly the Price Formation andesite in the Ridge Zone West (Figure 8.1; Chong, 2004). The Basal Volcaniclastic Unit is up to 90 metres in thickness, and is overlain by interlayered argillite, chert and rhyolitic volcaniclastic breccia and sandstone, with no coherent rhyolite facies (Figure 8.1). "Upper zone" position mineralisation is associated with coarse-grained rhyolitic volcaniclastic rocks and chert in the Ridge Zone West orebody (Figure 8.1; Chong, 2004). The intercalated nature of chert and argillite beds, preservation of bedding, and the spatial association of chert with massive sulfide mineralisation suggest that chert near the Ridge Zone West orebody is the result of the silicification of argillite beds, comparable to the process proposed by Jones et al. (2006b) for the Battle orebody (Chong, 2004).

Comparable to the Battle orebody, sulfide mineralisation occurs in "contact zone" and "upper zone" positions in the West Block Area (Figure 8.1). However, with the exception of the Ridge Zone North orebody, semi-massive and massive sulfide mineralisation in the West Block Area is sporadic and discontinuous (*Chapter 4*). Nevertheless, the West Block Area provides important lithofacies links between the Battle and Ridge Zone West orebodies. The base of the H-W member in the West Block Area is marked by a 10 to 30 metre-thick sequence of polylithic conglomerate to sandstone beds of the Basal Volcaniclastic Unit, which correlate with the Ridge Zone West orebody stratigraphy (Figure 8.1). Overlying the Basal Volcaniclastic Unit are intercalated chert, argillite and rhyolitic volcaniclastic siltstone and sandstone beds (Figure 8.1). The top of the H-W member in the West Block Area is marked by coherent rhyolite with associated autobreccia at its base and southern margins, comparable to the Battle orebody stratigraphy (Figure 8.1).

The volcano-sedimentary units of the H-W member have excellent east-west continuity for over 5 kilometres in the Myra Falls district (Figure 8.1). However, in the north-south direction, facies changes are rapid and this is interpreted to define an east-west elongated and north-south restricted seafloor basin (e.g., Juras, 1987; Barrett and Sherlock, 1996). Marine sedimentary lithofacies dominate the H-W member stratigraphic sequence in the southern margin of the basin. Re-worked, polylithic volcaniclastic mass-flow deposits of the Basal Volcaniclastic Unit mark the base of the H-W member in the Ridge Zone West and West Block Area localities (Figure 8.1A-B). This unit defines a south thickening, east thinning depocentre with a source direction to the west (e.g., Chong, 2004). Argillite and chert (silicified argillite) mark the base of the H-W member near the Battle and HW orebodies (Figure 8.1C-D). These fine-grained sediments were deposited in depocentres within paleotopographic lows of the basin and have sedimentalogical features that suggest deposition occurred below storm wave base, >200 metres (e.g., Juras, 1987; Barrett and Sherlock, 1996; Jones et al., 2006b). Coherent and volcaniclastic rocks dominate the H-W member stratigraphy in the northern margin of the basin (Figure 8.1D). Juras (1987) inferred that coherent rhyolite north of the HW orebody was the source of the felsic volcaniclastic mass flow deposits of the H-W member. Robinson et al. (1996) and Sinclair (2000) confirmed this interpretation by identifying and increasing

Figure 8.1 Stratigraphic columns of the H-W member across the Myra Falls VHMS district with 3D lithofacies interpretations. A. Ridge Zone West orebody locality (diagram drawn from data of Chong, 2004). B. The West Block Area and Ridge Zone North orebody (this study). C. The Battle orebody (diagram drawn from data of Sinclair, 2000 and Jones, 2001). D. The HW orebody (diagram drawn from data of Juras, 1987 and Barrett and Sherlock, 1996). The Hanging Wall Andesite member is removed from the lithofacies interpretations. [CZ, contact zone; UZ, upper zone]

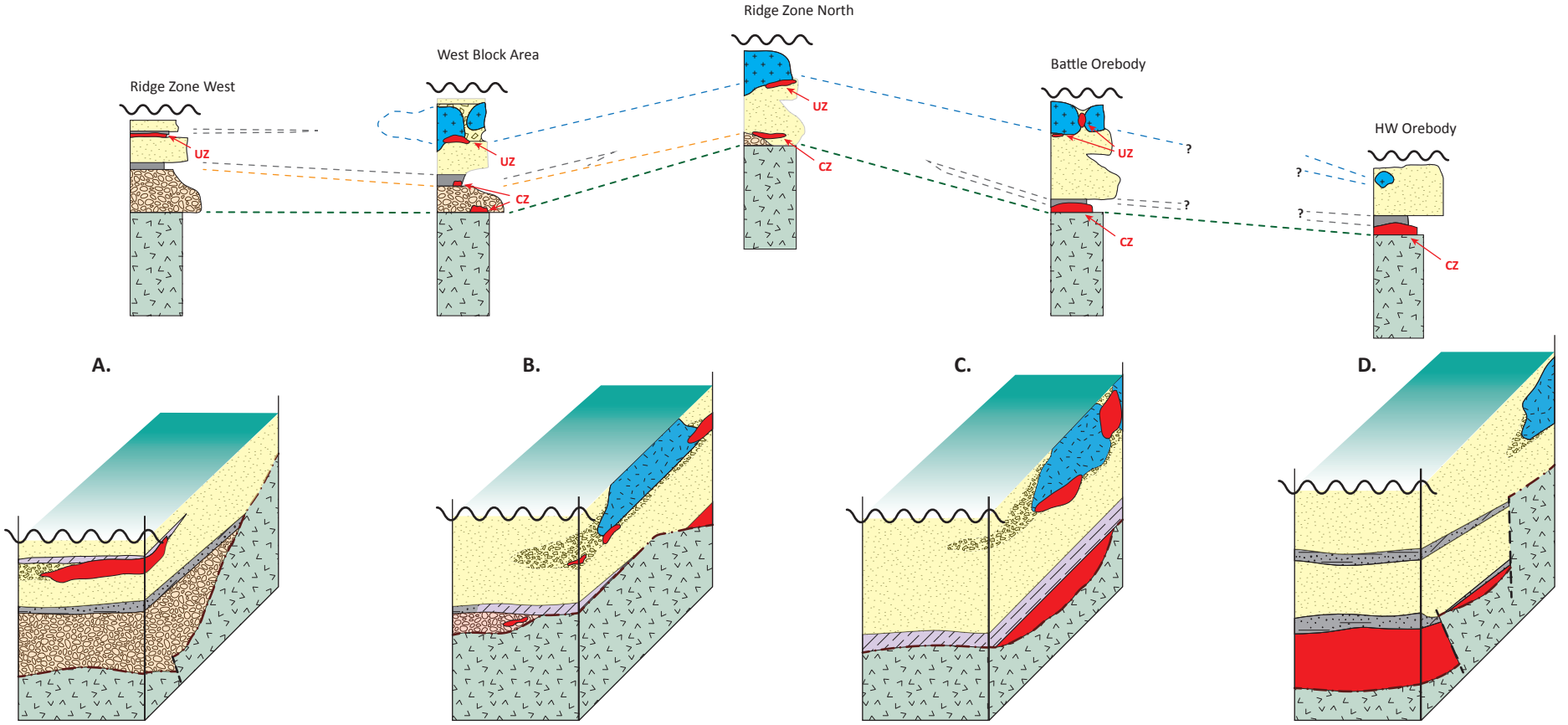

H-W Member Lithofacies

- rhyolitic volcaniclastic siltstone, sandstone
- rhyolitic volcaniclastic breccia
- laminated to thinly bedded argillite
- chert (silicified argillite)
- coherent rhyolite
- Basal Volcaniclastic Unit

Price Formation Lithofacies

- coherent andesite

Mineralisation

- sulfide
- UZ Upper Zone
- CZ Contact Zone

Contacts & Structure

- top of Price Formation andesite
- growth fault
- erosional contact between H-W member and overlying Hanging Wall Andesite member
- Lower surface of Hanging Wall Andesite member

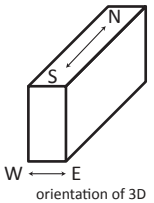

orientation of 3D lithofacies interpretations

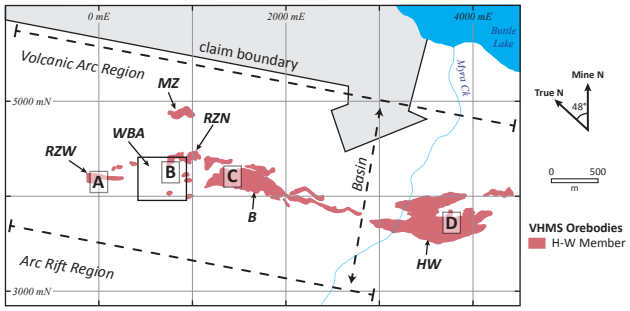

the spatial extent of coherent rhyolite and related felsic volcaniclastic mass flow deposits in the Battle orebody locality (Figure 8.1C). In the West Block Area and at the Ridge Zone North orebody, coherent rhyolite transitions to coarse- and fine-grained rhyolitic volcaniclastic rocks southward (Figure 8.1B). The lack of coherent rhyolite rock types in the Ridge Zone West orebody suggests that the felsic stratigraphy of the H-W member is thinning to the west (Chong, 2004).

8.2 Modes of Sulfide Emplacement

Based on studies of ancient VHMS deposits and investigations of active seafloor hydrothermal vents, VHMS deposits are widely accepted to form from the exhalation of metalliferous fluids onto the seafloor and by the replacement of sediments in the sub-seafloor environment (e.g., Large, 1992; Doyle and Allen, 2003; Franklin et al., 2005; Hannington et al., 2005). Evidence for sulfide accumulation on the seafloor environment includes (e.g., Doyle and Allen, 2003): (1) sedimentary clastic sulfide textures; (2) sulfide chimney textures; (3) exhalative rocks associated with sulfide mineralisation; (4) fossil tube worms and bivalves; (5) slowly accumulated host rock facies; and (6) strong stratigraphic footwall alteration relative to weaker stratigraphic hanging wall alteration patterns. Distinguishing features for replacement-style sulfide mineralisation in the sub-seafloor environment include (Doyle and Allen, 2003): (1) relicts of host facies within the mineralised deposit; (2) enclosure of mineralised horizons by rapidly emplaced volcanic or sedimentary facies; (3) replacement fronts between the deposit and host lithofacies; (4) discordance of sulfide mineralisation to bedding, and (5) strong hanging wall alteration without an abrupt break in intensity. In the H-W member, sulfide zones in the VHMS deposits are located at similar stratigraphic positions within locally variable host rocks, with evidence for both seafloor accumulation and sub-seafloor replacement sulfide deposition (Figure 8.2).

The stratigraphy of the lower Myra Formation in the West Block Area, Ridge Zone West and Battle orebodies consists of marine sedimentary and coherent and volcaniclastic felsic rocks. “Upper zone” position sulfide mineralisation is hosted in volcaniclastic breccias at the base and margins of submarine, coherent rhyolite lava flows; whilst “contact zone” position sulfide mineralisation is capped by chert (silicified argillite) and quartz-sericite-pyrite altered felsic volcaniclastic siltstone-sandstone or hosted in chlorite-sericite-pyrite altered polylithic volcaniclastic sandstone-conglomerate beds (Figure 8.2A-C; Robinson, 1994; Sinclair, 2000; Chong, 2004; *Chapter 4*). Clasts of quartz-phyric rhyolite and lithic clasts of rhyolitic siltstone are commonly found in “upper zone” position semi-massive sulfide and “contact zone” position massive sulfide ores, respectively (e.g., Sinclair, 2000). Sulfide mineralisation in the Ridge Zone West orebody is hosted in quartz-sericite-pyrite altered rhyolitic volcaniclastic breccia and capped by chert (silicified argillite). Here, the sulfide zone is 30 to 60 metres above the Price Formation contact and is interpreted to be in an “upper zone” position (Figure 8.2C; Chong, 2004). Hydrothermal alteration patterns are discordant to stratigraphic units and are pervasive throughout the footwall (Price Formation) and hanging wall (H-W member) strata (Figure 8.2A-C; Robinson, 1994; Sinclair, 2000; Chong, 2004; *Chapters 4-5*). The intimate association of “upper zone” position sulfide mineralisation with rapidly emplaced volcanic lithofacies, the silicification of argillite to form chert above “contact zone” position sulfide mineralisation, pervasive hydrothermal alteration to the felsic stratigraphy above sulfide zones, and the laterally extensive footwall alteration zone suggests that sulfide precipitated from metal-bearing fluid in a sub-seafloor environment (Figure 8.2A-C).

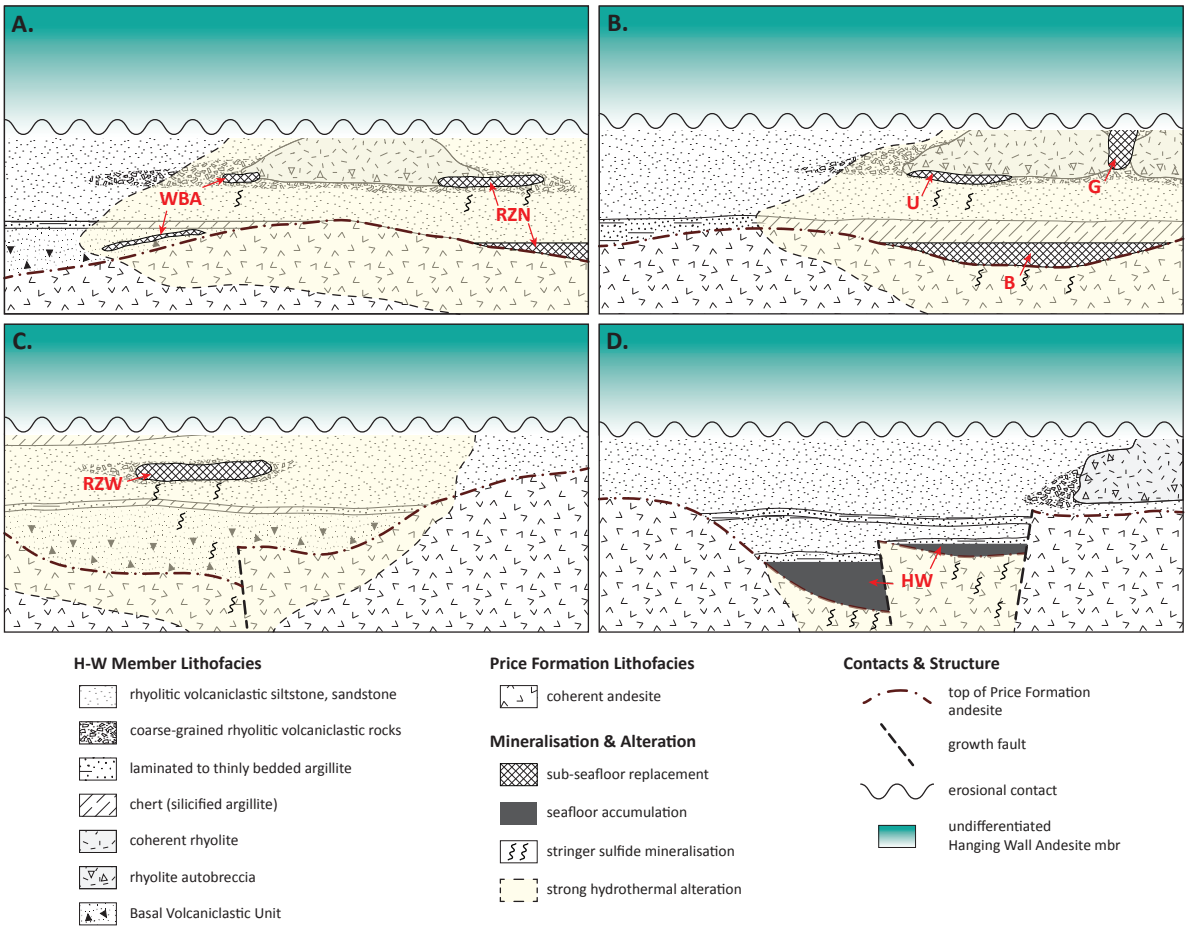

Figure 8.2 Lithofacies models for the depositional environment of selected VHMS orebodies of the H-W member. A. West Block Area (this study). B. Battle orebody (diagram adapted from Sinclair 2000, Jones 2001). C. Ridge Zone West orebody (diagram adapted from Chong, 2004). D. HW orebody (diagram adapted from Chong 2004, Jones 2001). Models are oriented south-north looking west, mine co-coordinates. [B, Battle orebody; G, Gap Zone orebody; HW, HW orebody; RZN, Ridge Zone North orebody; RZW, Ridge Zone West orebody; U, Upper Zone; WBA, West Block Area]

In contrast, "contact zone" position sulfide mineralisation in the HW orebody is typically overlain by black mudstones with intercalated felsic siltstones or by rhyolitic, volcaniclastic mass flow deposits separated by thin beds of black mudstone (Figure 8.2D; Barrett and Sherlock, 1996). Locally, laterally discontinuous massive sulfide breccias with a mudstone matrix overlie massive sulfide and possibly represent mass wasting deposits on the flanks of an ancient seafloor vent system (e.g., Barrett and Sherlock, 1996). Unlike the H-W member VHMS deposits to the west, the HW orebody has a well-developed alteration pipe in the stratigraphic footwall and relatively unaltered rocks in the stratigraphic hanging wall (Figure 8.2D). The footwall alteration pipe is characterised by intense sericite-quartz-pyrite altered andesite of the Price Formation (Juras, 1987; Barrett and Sherlock, 1996). The strong stratigraphic footwall alteration zone relative to the weakly altered stratigraphic hanging wall, as well as the association of slowly deposited mudstone with "contact zone" position massive sulfide mineralisation suggests that the HW orebody formed from the exhalation of metalliferous, hydrothermal fluid onto the seafloor (Figure 8.2D).

8.3 Sulfide Mineralisation

Metal-bearing fluids in VHMS hydrothermal systems generally evolve from high-temperature to low-temperature solutions resulting in base metal sulfide zoning (Figure 8.3A; e.g., Large,

1977; Large, 1992). Further segregation of Cu, Zn and Pb, in the form of chalcopyrite, sphalerite and galena, is accommodated by the process of zone-refining (Eldridge et al., 1983). The circulation of hot, buoyant, fluids through the sulfide mound results in the coarsening of initial, fine-grained sulfides and the homogenisation of intergrown pyrite, sphalerite, galena, tennantite-tetrahedrite and chalcopyrite to produce pyrite-, chalcopyrite-, and sphalerite-dominant zones (Figure 8.3B; Eldridge et al., 1983). Initial Pb- and Zn-bearing sulfide / sulfosalts are dissolved by hot, Cu-bearing hydrothermal fluids; chalcopyrite and pyrite precipitate and the residual Pb-Zn-bearing fluid rises, and sphalerite and galena precipitate as the fluid cools (Figure 8.3B; e.g., Large, 1977; Eldridge et al., 1983).

Further modification of hypogene sulfide mineralisation in VHMS deposits is complicated by post-mineralisation, regional metamorphism (Vokes, 1966; Stanton, 1972; Spry et al., 2000; Vikentyev et al., 2017). Greenschist facies and higher-grade regional metamorphism can result

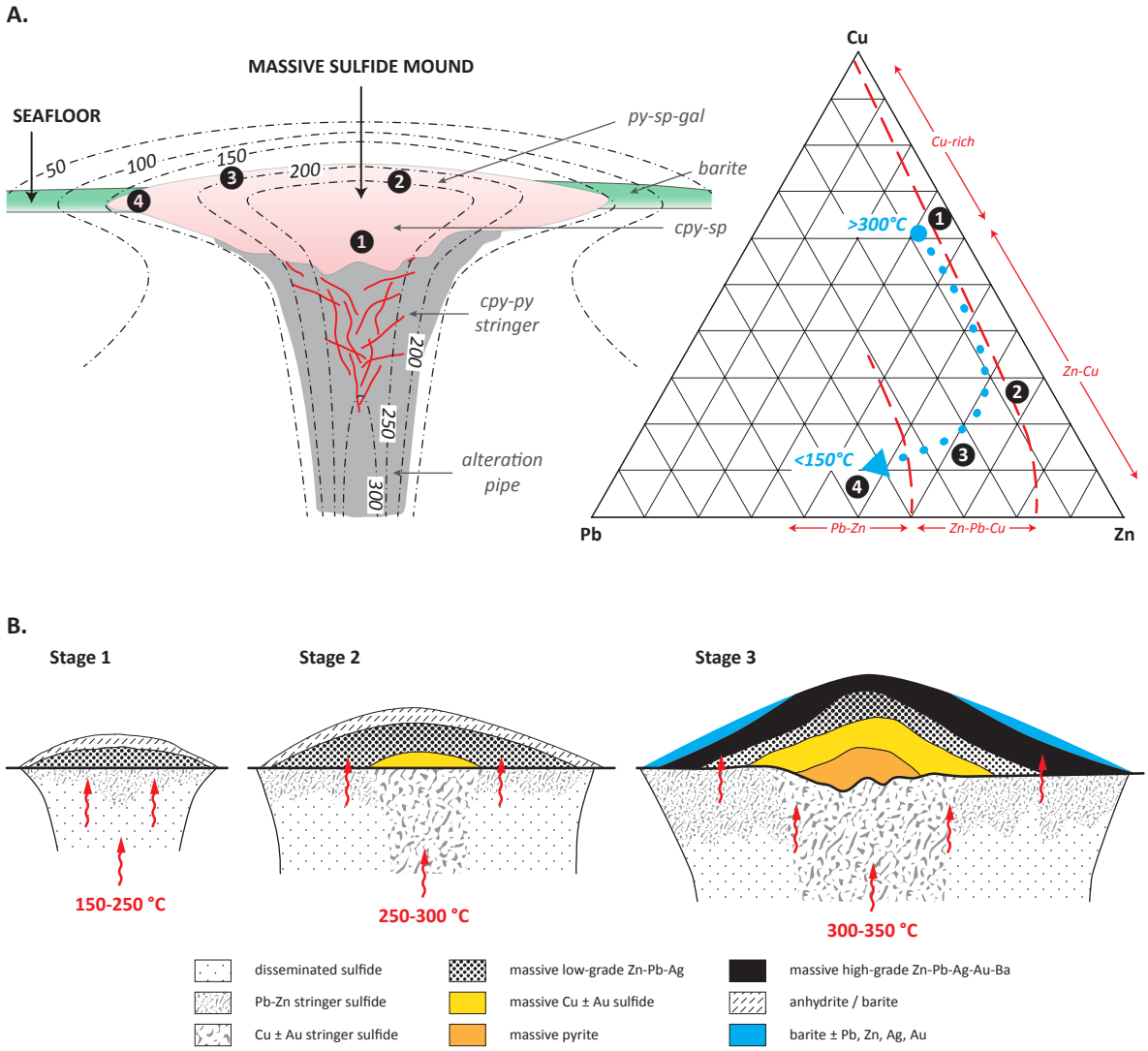

Figure 8.3 Schematic diagrams for VHMS deposit growth as a function of fluid temperature and zone-refining. A. Idealised VHMS deposit illustrating a stratabound lens of massive sulfide overlying an alteration pipe with stringer-style sulfide mineralisation (modified from Large, 1977; Gibson et al., 2007). The Cu-Pb-Zn triangle diagram schematically shows the evolution from copper-rich to lead-zinc-rich sulfides as the hydrothermal fluid cools. B. Idealised zone-refining model of a massive sulfide lens (after Eldridge et al., 1983; Large, 1992). Further sulfide segregation and grain coarsening in VHMS deposits is attributed to temperature-solubility relationships where circulating, hotter fluids dissolve lead-zinc, precipitate copper, and as the fluid rises up through the mound it cools and precipitates lead-zinc (e.g. Eldridge et al., 1983).

in the coarsening and annealing of sulfide minerals. Under these metamorphic conditions, mineralogical and textural changes are typically the result of isochemical processes, where pyrite displays brittle behaviour and sphalerite, chalcopyrite and galena behave in a ductile manner (e.g., Craig and Vaughan, 1994). For example, the migration of chalcopyrite, sphalerite and galena to the boundaries of euhedral or annealed pyrite grains is typically attributed to metamorphism rather than hypogene hydrothermal processes in VHMS deposits (e.g., Stanton, 1972; Spry et al., 2000). However, distinguishing hypogene mineralisation features from secondary metamorphic features in rocks affected by lower greenschist facies metamorphism can be ambiguous, as the metamorphic thermal conditions overlap with the VHMS hydrothermal conditions (e.g., Huston, 2000; Vikentyev et al., 2017).

Figure 8.4 shows the base metal classification for the HW, Battle, Ridge Zone West and Ridge Zone North orebodies using pre-mining geological resource values provided by Nyrstar Myra Falls Operation. The HW orebody is Cu-rich relative to the other deposits. The Battle and Ridge Zone West orebodies have Zn-Cu-rich sulfide ores, while the Ridge Zone North orebody has Zn-Pb-Cu-rich ores (Figure 8.4). This district-scale base metal zoning suggests a hydrothermal fluid gradient, with ~300°C metal-bearing fluid for the HW orebody and cooler, <250°C metal-bearing fluid for the orebodies to the west (e.g., Large, 1992; Ohmoto, 1996). In addition to temperature, other important factors are host stratigraphy and mode of sulfide emplacement for the distribution and preservation of sulfide mineralisation in VHMS deposits. Schardt and Large (2009) suggested that the presence of sizeable barite caps found in VHMS deposits might prevent the "wash-out" of Zn during hydrothermal zone-refining. The Zn-Cu-rich Battle orebody and Ridge Zones formed in a sub-seafloor hydrothermal setting with zones of massive sulfide mineralisation overlain by relatively impermeable rock types (e.g., silicified argillite and coherent rhyolite). The HW orebody formed on the seafloor and lacks an impermeable cap, which in addition to hydrothermal temperature may also explain its Cu-rich tenor.

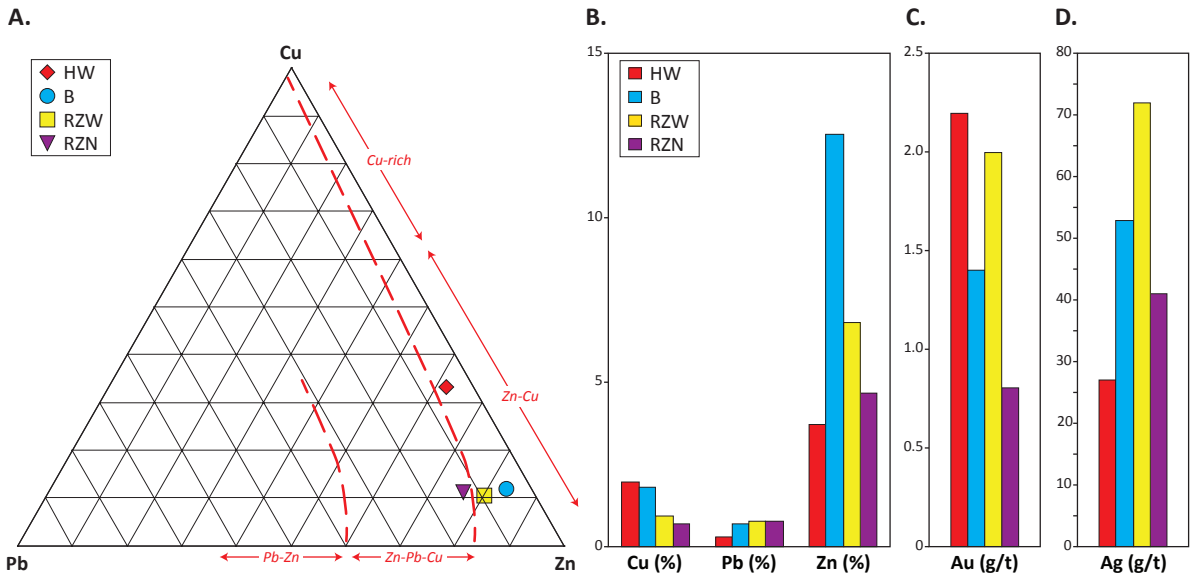

Figure 8.4 Summary of base and precious metal concentrations for selected H-W member VHMS deposits. A. Cu-Pb-Zn base metal classification diagram after Galley et al. (2007) for the HW, Battle, Ridge Zone North and Ridge Zone West orebodies. B. Distribution of copper, lead and zinc grades for the HW, Battle, Ridge Zone North and Ridge Zone West orebodies. C-D. Precious metals gold and silver concentrations for the HW, Battle, Ridge Zone North and Ridge Zone West orebodies. Diagrams drawn with Nyrstar Myra Falls Operation provided data (Chapter 3). [B, Battle orebody; HW; HW orebody; RZN, Ridge Zone North orebody; RZW, Ridge Zone West orebody]

Within individual VHMS deposits at Myra Falls, zone-refining is also a significant factor in the concentration and distribution of base metals. In the HW orebody, the base of massive sulfide lenses typically consists of coarse-grained pyrite, with rare base-metal sulfides (e.g., Barrett and Sherlock, 1996). Above this interval is a thick zone of massive pyrite with lesser chalcopyrite, sphalerite, and tennantite interstitial to coarse-grained pyrite (e.g., Barrett and Sherlock, 1996). Lateral and upper margins of "contact zone" position massive sulfide lenses generally contain more sphalerite, galena and barite and locally, barite-rich mudstone beds, 1-2 metres in thickness, cap massive sulfide ore (e.g., Barrett and Sherlock, 1996). The spatial distribution of sulfide minerals is indicative of zone-refining and the most prominent example of this process in the H-W member VHMS deposits.

There is chemical and sulfide textural evidence which indicates that both primary zone-refining and secondary metamorphic modification have occurred in the Battle, Ridge Zones and the West Block Area VHMS deposits (Sinclair, 2000; Chong, 2004; *Chapter 4*). In particular, zone-refining appears to be a significant factor in the Battle orebody where a clear segregation of Fe, Cu and Zn manifests as pyrite-dominant, chalcopyrite-dominant and sphalerite-dominant mineralised zones (Sinclair, 2000). The Ridge Zone North orebody, locally, has intervals of pyrite-dominant massive sulfide with sphalerite-dominant massive and semi-massive sulfide up stratigraphy, suggesting some degree of zone-refining. While the West Block Area (*Chapter 4*) and Ridge Zone West orebody (Chong, 2004) are sphalerite-dominant and lack any significant Fe-Cu-Zn zoning, suggesting that zone-refining was minor.

Sulfide textures that are interpreted to be indicative of zone-refining include resorbed pyrite grains, bornite replacing chalcopyrite, chalcopyrite replacing sphalerite, tennantite-tetrahedrite replacing sphalerite, and zoned pyrite (Sinclair, 2000; *Chapter 4*). Pyrite porphyroblasts, partially annealed pyrite masses, migration of chalcopyrite and galena to the margins of pyrite grains, and texturally and chemically homogenised sphalerite are interpreted to represent metamorphic modification, as opposed to zone-refinement. Crosscutting pearceite-polybasite and stromeyerite veinlets in the West Block Area and Battle orebody are likely the product of metamorphic remobilisation (Sinclair, 2000; *Chapter 4*). Texturally, electrum and tellurides appear late in the mineralisation paragenesis (*Chapter 4*). The segregation of gold and tellurides from hypogene sulfide and sulfosalt phases could have occurred during zone-refining and/or post-deposition, low grade regional metamorphism (e.g., Craig and Vokes, 1993; Huston et al., 1996; Huston, 2000; Vikentyev, 2006). Alternatively, Marshall et al. (2018) proposed a shallow-water depth (15-125 m) epithermal-boiling model for the precipitation of late-gold in the Battle and Ridge Zone West orebodies.

Sinclair (2000) identified three ore mineral assemblages for the Battle orebody, which include: (1) a Cu-Pb-Zn-Fe-rich assemblage of sphalerite-pyrite-chalcopyrite-galena and tennantite; (2) a Cu-rich assemblage of bornite and anilite with accessory renierite and electrum modifying Assemblage 1 chalcopyrite; and (3) a Au-Ag-rich assemblage of stromeyerite and electrum with minor chalcopyrite, which overprints Assemblage 1 and 2 sulfides. In the Battle orebody, ores with Assemblage 1 mineralogy occur at "contact zone" and "upper zone" positions. However, ores constituting Assemblage 2 and 3 mineralogy are restricted to the "upper zone" position.

Using the mineral assemblage nomenclature of Sinclair (2000) and based on the work of Chong (2004), the Ridge Zone West orebody mineralisation is characterised by a Cu-Pb-Zn-Fe-rich assemblage of sphalerite-pyrite-chalcopyrite-galena and Ag-rich tennantite. Barite is

ubiquitous, and is associated with sphalerite and galena (Chong, 2004). Assemblage 1 semi-massive and massive sulfide ore occur in the "upper zone" position.

Two ore mineral assemblages are present in the West Block Area and Ridge Zone North orebody (*Chapter 4*), based on the classification scheme of Sinclair (2000): (1) a Cu-Pb-Zn-Fe-rich assemblage of sphalerite-pyrite-chalcopyrite-galena and tennantite-tetrahedrite and (2) a Au-Ag-rich assemblage of pearceite-polybasite, electrum and hessite. No Cu-rich mineral assemblage consisting of bornite-anilite and renierite was observed in the West Block Area. Assemblage 1 sulfide zones are present in both "contact zone" and "upper zone" positions. Similar to the Ridge Zone West orebody, sphalerite-rich mineralisation is most abundant. However, like the Battle orebody, there is a distinct, late Ag-rich phase. In the case of the West Block Area, no stromeyerite was identified. However, pearceite-polybasite present in the West Block Area likely represents an Sb-As bearing equivalent phase to stromeyerite identified by Sinclair (2000) in the Battle orebody. Pearceite-polybasite was not observed in the Ridge Zone North orebody samples, but electrum and hessite were identified. Electrum and hessite in both the West Block Area and Ridge Zone North orebody, appear late in the mineralisation paragenesis as they often occur between the mineral boundaries of other sulfide-sulfosalt and silicate minerals.

8.4 Genesis of the H-W Member VHMS Deposits

A genetic model for the formation of the H-W member VHMS deposits is shown in a series of south to north orientated illustrations in Figure 8.5. The model integrates lithofacies and mineralisation observations from the HW (Juras, 1987; Barrett and Sherlock, 1996), Battle (Robinson et al., 1996; Sinclair, 2000; Jones et al., 2006b), West Block Area/Ridge Zone North (*Chapters 4-5*) and the Ridge Zone West (Chong, 2004) orebodies. A series of events are proposed to explain the evolution of the deposits, beginning with the formation of sub-basin depocentres and ending with the deposition of the Hanging Wall Andesite and Lower Mixed Volcanics members.

Stage-1: Sub-basin development

A series of sub-basins in a district-wide seafloor basin formed as a result of normal movement along growth faults. These sub-basins provided local depocentres for the accumulation of seafloor massive sulfide mineralisation (HW orebody) or sub-seafloor replacement sulfide mineralisation (Battle, Ridge Zones). In the HW orebody, significant marine sedimentation did not occur until after the deposition of massive sulfide mineralisation.

Prior to the initiation of hydrothermal activity in the Battle and Ridge Zone localities, the depocentres were filled with a combination of re-worked volcanic material and marine sediments. In the Battle and Ridge Zone North localities, the onset of rhyolitic volcanism produced reworked, syn-eruptive mass flow deposits sourced from the Volcanic Arc Region. In the Ridge Zone West and West Block Area, the basin is filled with polylithic, graded, volcaniclastic conglomerate and sandstone sourced from the West-G Seamount. A period of volcanic quiescence followed the deposition of these units and is recorded by the local deposition of several meters of finely laminated muds, silts, and minor interbedded turbidites (precursors to chert and argillite).

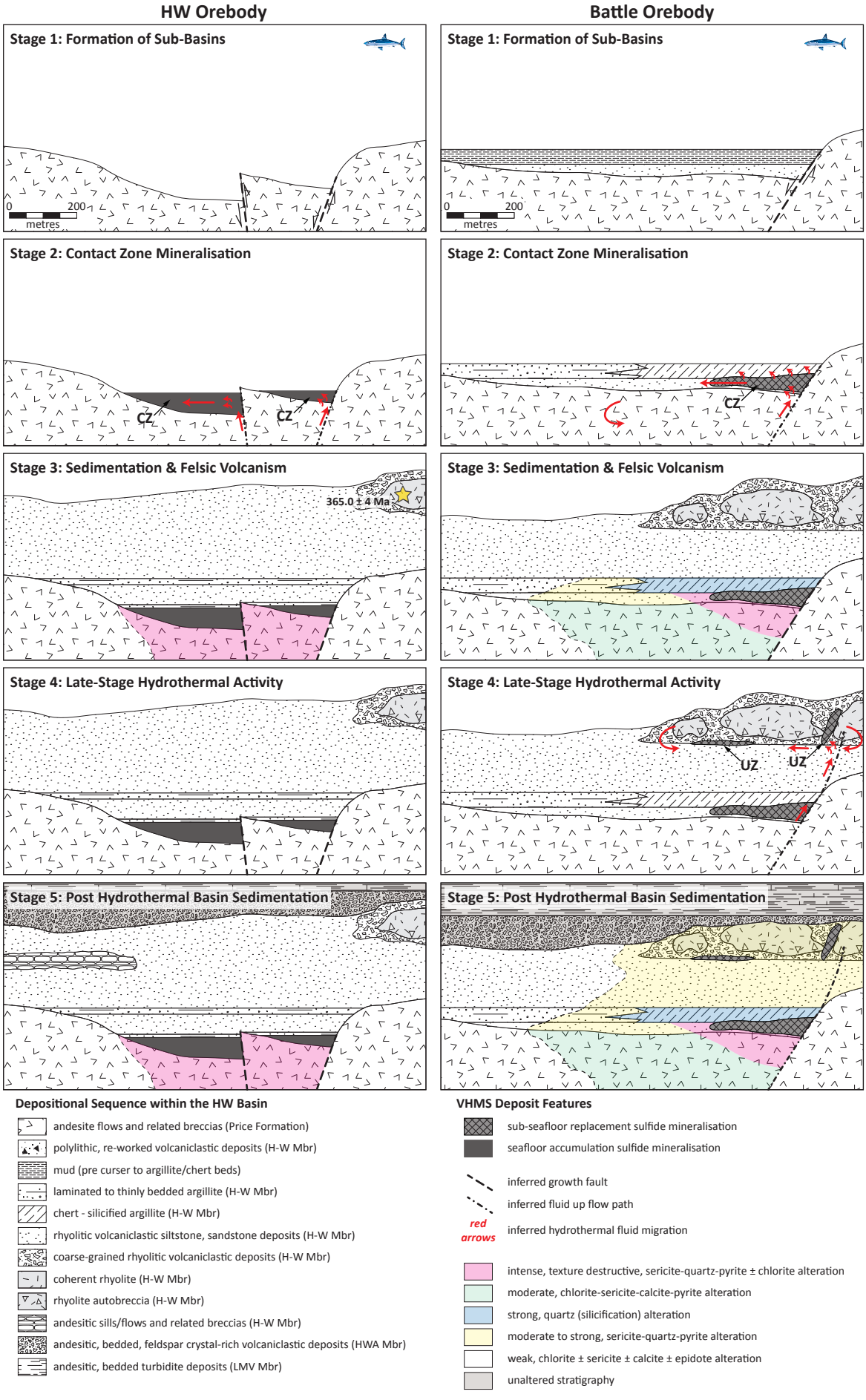
HW Orebody
Battle Orebody
Stage 1: Formation of Sub-Basins
0
200
metres
Stage 2: Contact Zone Mineralisation
CZ
Stage 3: Sedimentation & Felsic Volcanism
365.0 ± 4 Ma
Stage 4: Late-Stage Hydrothermal Activity
UZ
Stage 5: Post Hydrothermal Basin Sedimentation
Depositional Sequence within the HW Basin
andesite flows and related breccias (Price Formation)
polylithic, re-worked volcaniclastic deposits (H-W Mbr)
mud (pre curser to argillite/chert beds)
laminated to thinly bedded argillite (H-W Mbr)
chert - silicified argillite (H-W Mbr)
rhyolitic volcaniclastic siltstone, sandstone deposits (H-W Mbr)
coarse-grained rhyolitic volcaniclastic deposits (H-W Mbr)
coherent rhyolite (H-W Mbr)
rhyolite autobreccia (H-W Mbr)
andesitic sills/flows and related breccias (H-W Mbr)
andesitic, bedded, feldspar crystal-rich volcaniclastic deposits (HWA Mbr)
andesitic, bedded turbidite deposits (LMV Mbr)
VHMS Deposit Features
sub-seafloor replacement sulfide mineralisation
seafloor accumulation sulfide mineralisation
inferred growth fault
inferred fluid up flow path
red arrows
inferred hydrothermal fluid migration
intense, texture destructive, sericite-quartz-pyrite ± chlorite alteration
moderate, chlorite-sericite-calcite-pyrite alteration
strong, quartz (silicification) alteration
moderate to strong, sericite-quartz-pyrite alteration
weak, chlorite ± sericite ± calcite ± epidote alteration
unaltered stratigraphy

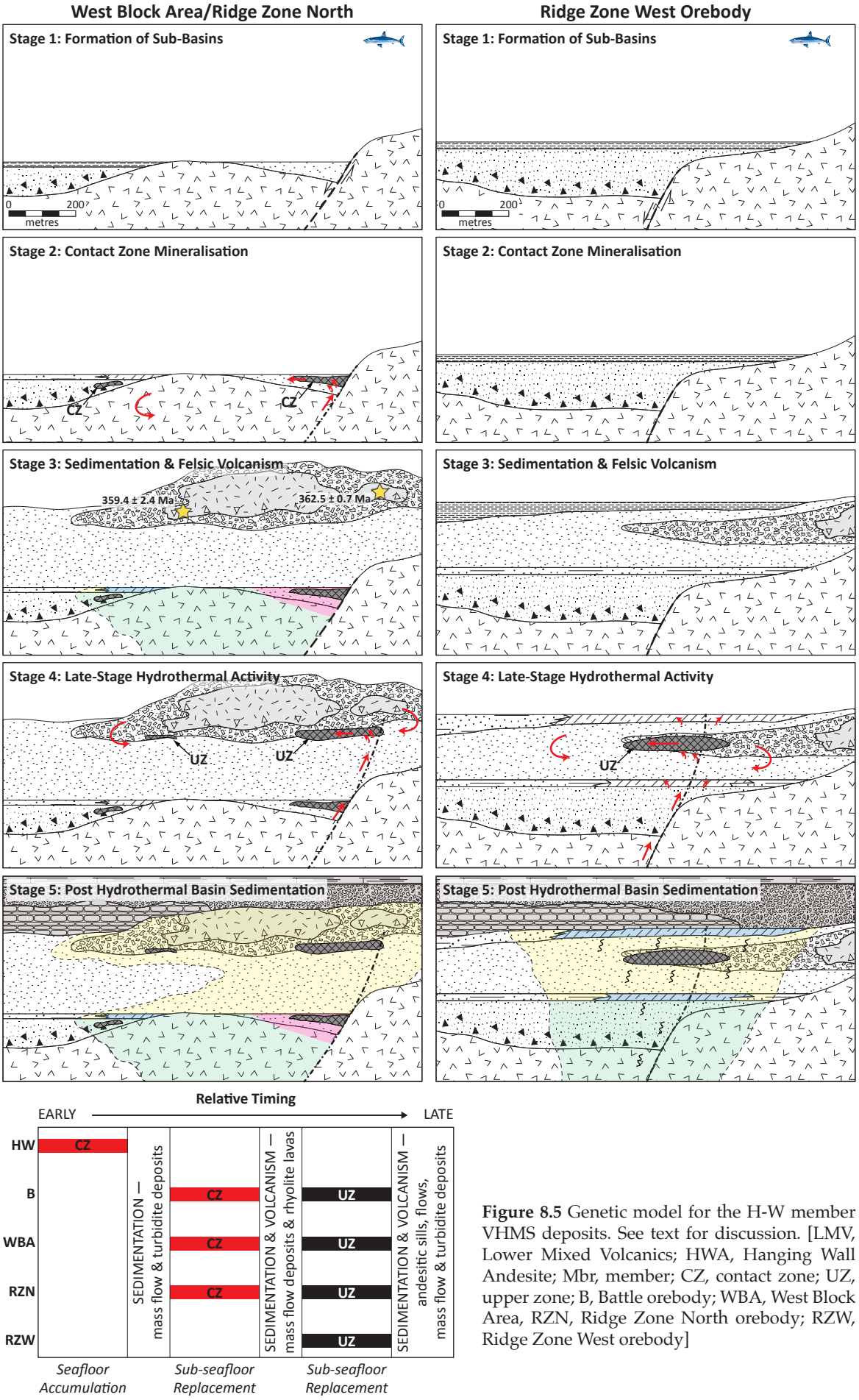

Figure 8.5 Genetic model for the H-W member VHMS deposits. See text for discussion. [LMV, Lower Mixed Volcanics; HWA, Hanging Wall Andesite; Mbr, member; CZ, contact zone; UZ, upper zone; B, Battle orebody; WBA, West Block Area, RZN, Ridge Zone North orebody; RZW, Ridge Zone West orebody]

Stage-2: Contact zone mineralisation

It is inferred that the H-W member VHMS orebodies were concentrated around several hydrothermal centres with buoyant, metalliferous hydrothermal fluids focused upward through pre-existing growth fault structures. The initiation of hydrothermal activity produced "contact zone" position sulfide mineralisation throughout the Myra Falls district.

In the HW orebody, hydrothermal fluids rising up growth faults exhaled onto the seafloor to produce massive sulfide mounds. The relatively rapid ascent of focused hydrothermal fluids through the paleo-seafloor resulted in a restricted alteration pipe immediately below the massive sulfide mound. Massive sulfide of the HW orebody is abruptly overlain by argillite, which indicates that the hydrothermal system had ceased prior to sedimentation.

In the Battle and Ridge Zone North orebodies, hydrothermal fluids rising up growth faults interacted with unconsolidated, porous beds of volcanic mass flow deposits and seafloor muds. Lateral, hydrothermal fluid flow through the sediments was diffuse and unfocused and produced sub-seafloor replacement sulfide mineralisation as well as a broad, semi-conformable footwall alteration zone. Continued lateral hydrothermal activity resulted in the silicification of unconsolidated muds to form chert above the Battle orebody, which extends into the West Block Area, but not in the Ridge Zone North orebody. The gradual transition from chert to sericite-quartz ± pyrite altered argillite to unaltered argillite marks the lateral extent of circulating hydrothermal fluids.

Stage-3: Sedimentation and felsic volcanism

The formation of the "contact zone" position sulfide ores and chert was followed by another episode of rhyolitic volcanism. Re-worked, syn-eruptive rhyolitic mass flows were deposited onto the seafloor, which was followed by the emplacement of coherent rhyolite lavas at the top of the rhyolitic volcanic sequence. In the Ridge Zone West orebody, rhyolitic mass flow deposits predominate and the top of the rhyolitic volcanic sequence is marked by several metres of finely laminated muds and silts (precursors to chert and argillite).

Stage-4: Late-stage hydrothermal activity

There is evidence for very limited "upper zone" position mineralisation in the HW orebody, with silicified argillite forming in a few localised zones. These zones represent the waning stages of hydrothermal activity in the HW orebody. However, while the HW orebody hydrothermal system was shutting down, hydrothermal activity persisted westward.

In the Battle and Ridge Zone North orebodies, hydrothermal fluids percolated up through the porous and permeable volcaniclastic beds producing a broad, discordant sericite-quartz-pyrite alteration zone. Lateral fluid flow at the base of rhyolite lavas produced sub-seafloor replacement sulfide mineralisation in the Battle and Ridge Zone North orebodies. Locally, hydrothermal fluids where focused along reactivated growth faults to produce sub-seafloor replacement sulfide mineralisation within rhyolite lavas (Gap Zone of the Battle orebody). In the Ridge Zone West orebody, hydrothermal fluids rising up through growth faults interacted with unconsolidated, porous volcanic mass flow deposits and seafloor muds. Circulation of hydrothermal fluids through the volcanic pile produced sub-seafloor replacement sulfide mineralisation with semi-conformable alteration zones and chert horizons after the silicification of argillite and seafloor muds on the paleo-seafloor.

Stage-5: Post hydrothermal sedimentation

Andesitic volcanism followed after the cessation of the VHMS hydrothermal system. Locally, andesitic sills and flows were emplaced along with related breccias. Volcaniclastic rocks at the base of the Hanging Wall Andesite member contain clasts of altered rhyolitic sandstone, siltstone, porphyritic rhyolite, massive sulfide, and chert from the underlying H-W member, indicating some degree of post-mineral erosion. Continued deposition of multi-sourced, volcanic detritus into the basin is recorded by the formation of the Lower Mixed Volcanics member. Importantly, these rocks are not hydrothermally altered and therefore post-date the hydrothermal system responsible for the H-W member VHMS deposits.

8.5 Myra Formation Volcanic and Depositional History

The Myra Formation was deposited as a series of submarine volcanic and marine sedimentary events (Figure 8.6). New zircon U-Pb age results (*Chapter 7*) combined with temporal constraints based on stratigraphic relationships (*Chapters 3-4*) help constrain the depositional history of the Myra Formation. The onset of rhyolitic volcanism (H-W member) resulted in early basin infill of coarse, proximal volcanic deposits along the north-eastern margin of the basin with fine-grained, distal volcaniclastic deposits and bedded argillite to the southwest (Figure 8.6B; e.g., Juras, 1987; Sinclair, 2000; Jones et al., 2006b). Deposition of the H-W member was followed by the eruption and deposition of the Hanging Wall Andesite member, likely sourced from the West-G Seamount, which resulted in the local erosion of the H-W member (Figure 8.6C; e.g., Juras, 1987). The deposition of polylithic reworked mass flow deposits and andesitic turbidites of the Lower Mixed Volcanics member records an active submarine edifice on the south-eastern margin of the basin, following the deposition of the Hanging Wall Andesite member (Figure 8.6C). Renewed felsic volcanism from the Volcanic Arc Region and the Price Seamount produced reworked, syn-eruptive, rhyolitic mass flow deposits with less abundant, proximal coherent and volcaniclastic facies of the L-M-P member (Figure 8.6D; Juras, 1987). Felsic volcanism was then followed by mafic volcanism sourced from the West-G Seamount and the deposition of polylithic, bedded to massive turbidites of the Upper Mixed Volcanic member (Figure 8.6D; Juras, 1987).

Volcanic-hosted massive sulfide deposits are restricted to two cycles of felsic volcanism in the Myra Falls VHMS district (e.g., Juras, 1987). The high precision CA-ID-TIMS results for coherent rhyolite in the Ridge Zone North orebody of the H-W member overlap in error with less precise crystallisation ages of coherent rhyolite in the Marshall Zone, West Block Area and HW orebody (*Chapter 7*). These coherent rhyolite lavas are interpreted to be coeval with a depositional age of ca. 362 Ma. New LA-ICPMS U-Pb age results of zircon from rhyolitic volcaniclastic sandstone of the L-M-P member provide a maximum age of deposition of ca. 355 Ma (*Chapter 7*). The new age constraints show that the H-W and L-M-P members are separated by approximately 7 million years (Figure 8.6D). This is a significant result as it indicates the VHMS deposits of the H-W and L-M-P members are not coeval, but rather likely formed from temporally distinct hydrothermal events.

8.6 Vancouver Island Sicker Group Stratigraphic Relationships

No new age constraints for the Price Formation were obtained in this study, but the Price Formation is considered be a lithostratigraphic correlative of the Duck Lake and Nitinat Formations in the Cowichan Lake uplift (Figure 8.7; Yorath et al., 1999; *Chapter 2*). Ruks (2015) analysed a dacite flow assigned to the Duck Lake Formation that yielded an age of 366.6 ± 0.7 Ma.

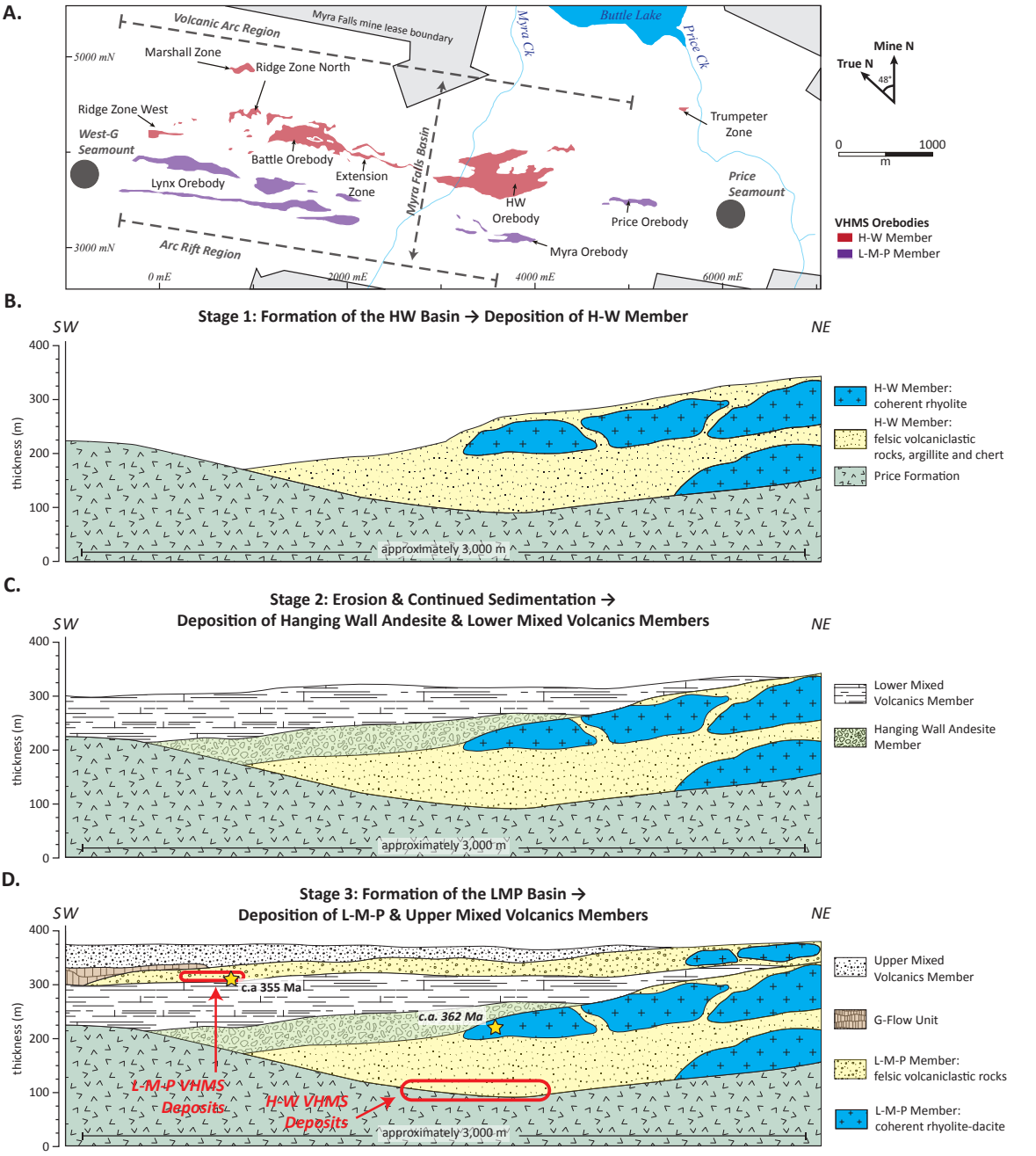

Figure 8.6 Schematic diagram of the pre-deformation depositional sequence of the Myra Formation in the Myra Falls VHMS district adapted from previous models of Juras (1987), Robinson et al. (1996), Sinclair (2000), Chong (2004), Jones et al. (2006b). A. Map of the Myra Falls VHMS district showing the source areas of volcanic material from (Juras, 1987) and the distribution of the L-M-P and H-W member VHMS deposits projected to surface (adapted from Jones et al., 2006a). B. Deposition of the H-W member on a paleo-seafloor comprised of andesite of the Price Formation. Crystallisation age of the Price Formation is unknown, minimum age is constrained by zircon U-Pb crystallisation age of coherent rhyolite of the H-W member of ca. 362 Ma (this study). C. Following a period of erosion, reworked, volcano-sedimentary mass flow deposits of the Hanging Wall Andesite member and mass flows and turbidites of the Lower Mixed Volcanics member were deposited on the of the H-W member. This succession records multi-source input of volcanic detritus into the basin as a result of an active submarine volcanic edifice (Juras, 1987; Robinson et al., 1996; Sinclair, 2000; Chong, 2004). D. Deposition of reworked, syn-eruptive, mass flow deposits with minor coherent rhyolite of the L-M-P member representing a distal volcanic edifice depositional setting compared the H-W member (Seraphim, 1980; Juras, 1987). New zircon U-Pb age of rhyolitic volcaniclastic sandstone provided a maximum age constraint of 355.5 ± 2.8 Ma for the L-M-P member. Intercalated with the L-M-P member are submarine, basalt lava flows of the G-Flow Unit. Deposited on top of the L-M-P member are reworked, felsic to mafic, polylithic volcaniclastic rocks, intercalated with laminated argillite and chert of the Upper Mixed Volcanics member as a result of resumption of rift basin-infilling with local quiescent in volcanic activity (Juras, 1987; Sinclair, 2000; Jones, 2001). Volcanic-hosted massive sulfide deposits are hosted in sub-basins in the district basin, and associated with felsic volcaniclastic rocks separated by ca. ~7 million years of the H-W and L-M-P members.

The Nitinat Formation has not been directly dated, however, crosscutting quartz and feldspar-phyric rhyolite porphyries assigned to the Saltspring Intrusive Suite provide minimum age constraints. A 360.7 ± 2.2 Ma Saltspring intrusion crosscuts clinopyroxene-phyric mafic volcanic rocks of the Nitinat Formation in the Cowichan Lake uplift (Ruks, 2015). On Saltspring Island, mafic volcanic rocks of the Nitinat Formation are crosscut by Saltspring intrusions ranging in age from 358 ± 1.0 Ma through 356.5 Ma (Sluggett, 2003). These crosscutting relationships confirm a Late Devonian age for the Nitinat Formation.

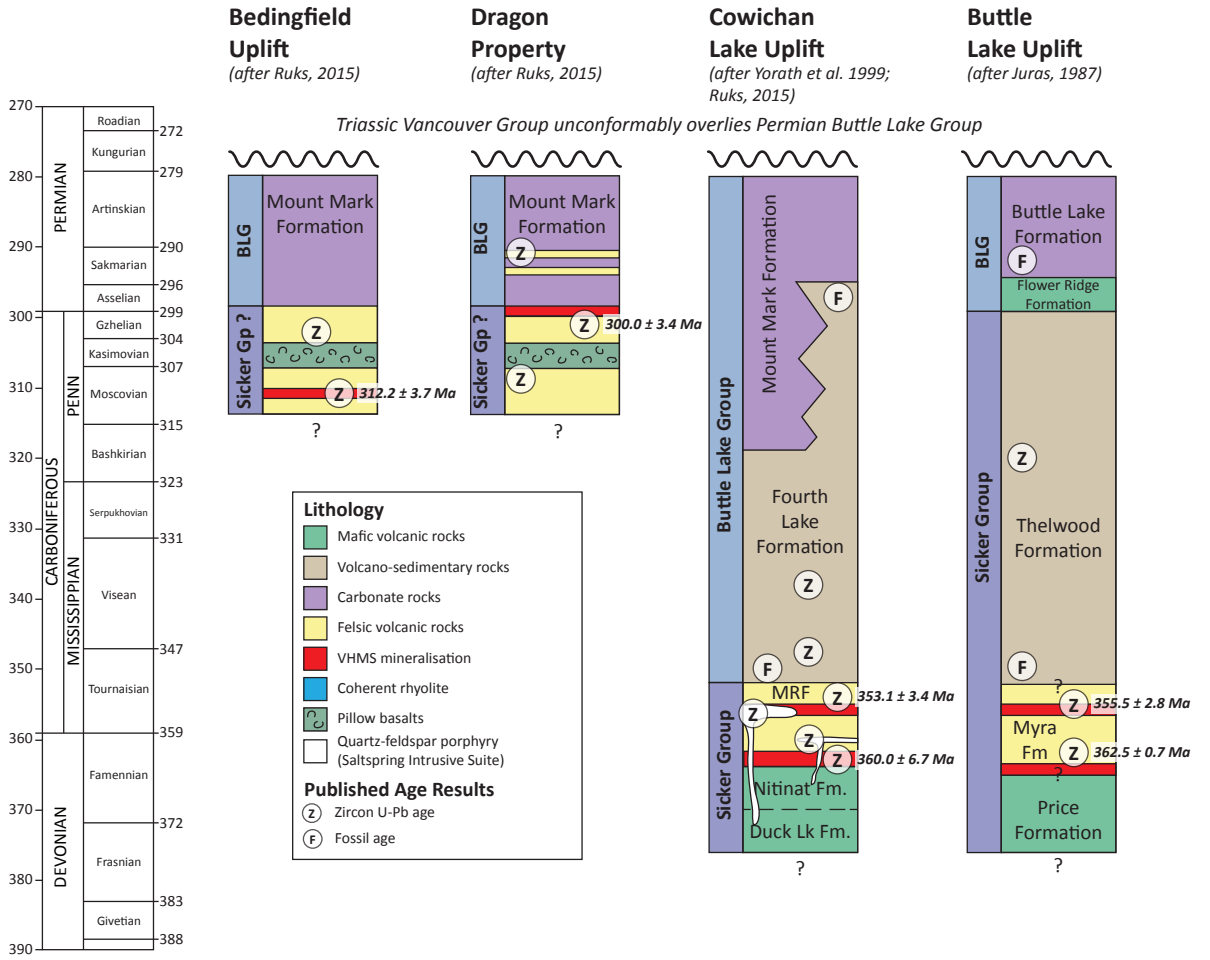

Figure 8.7 Comparative chronostratigraphic columns with updated geochronology results, illustrating the temporal relationships of the Paleozoic rocks of Vancouver Island. Modified from Massey (1992), Juras (1987), Sinclair (2000) and Ruks (2015). Selected zircon and fossil ages from Parrish and McNicoll (1992), Barrett and Sherlock (1996), Jones (2001), Katvala (2006) and Ruks (2015). Geologic time scale from Walker et al. (2012).

McLaughlin Ridge Formation felsic volcaniclastic host rocks of the Lara and Lenora VHMS occurrences yielded U-Pb zircon age results of 362.6 ± 9.4 Ma and 363.0 ± 6.7 Ma, respectively (Ruks, 2015). These results overlap with the known crystallisation age range for the HW Rhyolite of the Myra Formation (*Chapter 7*). Chert interbedded with felsic volcaniclastic stratigraphy of the McLaughlin Ridge Formation has a Late Devonian radiolaria age (Ruks, 2015), and chert immediately above the HW and Battle orebodies has a Mississippian radiolaria age (Jones, 2001). The McLaughlin Ridge Formation felsic volcaniclastic host rocks to the Jane VHMS occurrence yielded a U-Pb zircon age of 353.1 ± 3.4 Ma (Figure 8.7; Ruks, 2015). This age result overlaps with the 355.5 ± 2.8 Ma age result of the LMP Rhyolite for this study (Figure 8.7; *Chapter 7*). This suggests that the felsic volcaniclastic stratigraphy that hosts the Jane VHMS occurrence in the Cowichan Lake uplift and the Lynx, Myra and Price orebodies

in the Buttle Lake uplift are regional correlatives. On Saltspring Island, felsic volcanic rocks of the McLaughlin Ridge Formation have U-Pb zircon ages of 364.8 ± 1.3 Ma and 363.8 ± 2.5 Ma and quartz-feldspar porphyry Saltspring intrusions range in age from 359.1 ± 1.4 Ma through 356.5 ± 1.7 Ma (Sluggett, 2003). Felsic volcanic rocks on Saltspring Island are the oldest known rocks of the McLaughlin Ridge Formation and overlap in age and error with the oldest rocks of the HW Rhyolite. No intrusions assigned to the Saltspring Intrusive Suite have been identified in the Buttle Lake uplift.

In addition to the two Late Devonian felsic volcanic cycles that host VHMS deposits in the Myra Falls district and the Cowichan Lake uplift, a third cycle of felsic volcanism was recognised by Ruks (2015) in the Bedingfield uplift and Dragon area (*Chapter 2*, Figure 8.7). These VHMS deposits are poorly understood, and are hosted by Pennsylvanian, ~310-300 Ma felsic volcanic rocks near the base of the Mount Mark Formation (Figure 8.7).

8.7 Implications for Mineral Exploration

Lithofacies mapping of the H-W member continues to be a fundamental and important exercise for understanding the depositional environment in the Myra Falls district, which will aid in the future identification of prospective exploration targets. It is critical that exploration drill holes intersect the complete H-W member, as VHMS orebodies are located near the top and at the base of this sequence. Portable-XRF analysis is a robust and time efficient tool in discriminating volcanic protolith with immobile element ratios. This combined with lithofacies mapping will assist geologists in identifying rock types where primary textures and minerals are obscured or destroyed by hydrothermal alteration.

In addition to lithofacies mapping, attention to hydrothermal alteration mineral assemblages is significant. For example, the Price Formation andesite footwall alteration zone extends from the Battle orebody to the Ridge Zone West orebody. Mineralogical and lithogeochemical alteration trends change systematically relative to the position of ore within this large-scale, semi-conformable alteration zone, and can be used to aid in mineral exploration. Changes in phyllosilicate mineral chemistry can be inferred with SWIR analysis, which is a rapid and robust tool for mapping alteration halos associated with VHMS orebodies in the Myra Falls district. Useful whole-rock hydrothermal alteration geochemical indicators include Na_2O and S concentrations, Rb/Sr ratios, and the Alteration Index and Chlorite-Carbonate-Pyrite Index petrochemical alteration indices. In addition to assessing immobile element ratios for protolith discrimination, pXRF analysis could be used to acquire mobile element data, such as Rb and Sr, to discriminate hydrothermal alteration trends.

New U-Pb zircon age constraints, combined with previous age constraints and stratigraphic relationships indicate that felsic volcanism at Myra Falls was episodic over a period of approximately 7 million years. Published age results for felsic volcanic rocks that host VHMS deposits elsewhere on Vancouver Island overlap with the age constraints for the Myra Falls VHMS district. Therefore, regional-scale VHMS mineral exploration on Vancouver Island should consider: (1) ~362 Ma felsic stratigraphy located within 200 metres of the upper contact of the Price and Nitinat Formations; and (2) ~355 Ma felsic stratigraphy located in the upper 100 metres of the Myra and McLaughlin Ridge Formations near the contact with the Thelwood and Fourth Lake Formations. In addition, a new and emergent chronostratigraphic interval for VHMS deposit exploration, identified by Ruks (2015), includes felsic stratigraphy below the Mount Mark formation with depositional ages between ca. 310-300 Ma.

Chapter 9:

Conclusion

Myra Falls is a series of polymetallic, volcanic-hosted massive sulfide (VHMS) deposits located in central Vancouver Island, 90 km southwest of Campbell River, British Columbia, Canada. As of April 2013, production has exceeded 30 Mt of ore at average grades of 5.5% Zn, 1.6% Cu, 0.6% Pb, 2.0 g/t Au and 54.0 g/t Ag. In this area, ten VHMS deposits are spatially and temporally related to Devonian to Late Carboniferous felsic volcanism of the Sicker Group, which defines two district-scale stratigraphic members. The near surface L-M-P member is host to the Lynx, Myra, and Price orebodies. In contrast, the HW, Trumpeter Zone, Battle, Extension Zone, Ridge Zone West, Ridge Zone North, and Marshall Zone orebodies are hosted in the lower H-W member.

The geology of Vancouver Island principally consists of mid-Paleozoic to Early Mesozoic Wrangellia stratigraphy of the Insular Terrane (Nelson and Colpron, 2007). The Wrangellia Terrane on Vancouver Island is comprised of the Devonian Sicker Group, the Permian Buttle Lake Group, the Upper Triassic Vancouver Group, and the Lower Jurassic Bonanza Group (Muller, 1980; Yorath et al., 1999; Nixon and Orr, 2007). The Paleozoic Sicker Group represents the oldest rocks identified in the Wrangellia Terrane and are exposed in several northwest trending uplifts on Vancouver Island (Muller, 1980; England and Calon, 1991; Yorath et al., 1999). The Sicker and Buttle Lake Groups record the evolution of a Late Devonian through Early Permian island arc and arc-back arc complex.

9.1 Geochronology and Myra Formation Depositional History

Previous attempts to date zircon from the two primary felsic volcanic cycles at Myra Falls have resulted in relatively imprecise ages that do not resolve the temporal relationship between L-M-P and H-W members. New, high precision CA-ID-TIMS and LA-ICPMS results, combined with published age constraints and stratigraphic relationships, confirm at least two phases of episodic felsic volcanism at Myra Falls.

Prior to the geochronological work presented in this thesis, the understanding of the temporal evolution of the Myra Formation was primarily based on field observations. The Myra Formation was deposited as a series of submarine volcanic and marine sedimentary

events within an elongated and northeast-southwest restricted basin. The onset of rhyolitic volcanism (recorded as the H-W member) resulted in early basin infill of coarse, proximal volcanic deposits along the north-eastern margin of the basin with fine-grained, distal volcaniclastic deposits and bedded argillite to the southwest (Juras, 1987; Sinclair, 2000; Jones et al., 2006b). Felsic volcanism was followed by an andesitic volcanic event sourced from the West-G Seamount, which resulted in local erosion of the H-W member and deposition of the Hanging Wall Andesite member (e.g., Juras, 1987). An active submarine volcanic edifice on the south-eastern margin of the basin is recorded by the deposition of polylithic, reworked mass flow deposits and andesitic turbidites (Lower Mixed Volcanics member). Renewed felsic volcanism sourced from the Volcanic Arc Region and the Price Seamount deposited reworked, syn-eruptive, rhyolitic mass flows and less abundant proximal volcanic lithofacies of the L-M-P member (Juras, 1987). Felsic volcanism was followed by mafic volcanism sourced from the West-G Seamount and the deposition of polylithic, bedded to massive turbidites of the Upper Mixed Volcanic member ensued (Juras, 1987).

Volcanic-hosted massive sulfide deposits are restricted to the H-W and L-M-P members. The high precision CA-ID-TIMS results for coherent rhyolite in the Ridge Zone North orebody of the H-W member, overlap in error with less precise crystallisation ages of coherent rhyolite in the Marshall Zone, West Block Area and HW orebody. These coherent rhyolite lavas are interpreted to be coeval with a depositional age of ca. 362 Ma. Zircon U-Pb LA-ICPMS age results from rhyolitic volcaniclastic sandstone of the L-M-P member indicate a maximum deposition age of ca. 355 Ma. The new age constraints indicate a period of approximately 7 million years between the H-W and L-M-P members. This finding contributes a significant change in the understanding of the formation of the Myra Falls district and indicates that the VHMS deposits of the H-W and L-M-P members are not coeval, but rather likely formed from temporally distinct hydrothermal events.

9.2 West Block Area Geology

The research presented in this thesis has documented, in detail, the geology of the West Block Area, which was previously poorly understood. Stratigraphy in the West Block Area comprises coherent, volcaniclastic and marine sedimentary rocks of the Price and lower Myra Formations. The Price Formation, at least 80 metres-thick, is characterised by a submarine, extrusive sequence of coherent, andesitic lavas and related breccias. The 150 to 175 metres-thick H-W member consists of syn- and post-eruptive volcanic and marine-sedimentary rocks. Polylithic siltstones, sandstones and conglomerates of the Basal Volcaniclastic Unit mark the base of the H-W member and extend west over 500 metres to the Ridge Zone West orebody. The Basal Volcaniclastic Unit is overlain by intercalated argillite and chert of the Caprocks unit. The overlying HW Rhyolite comprises felsic volcaniclastic rocks, which are overlain by coherent, quartz and feldspar-phyric rhyolite, 10 to 40 metres in thickness. Coherent rhyolite domes of the West Block Area extend east over 500 metres to the Battle orebody and north over 250 metres to the Ridge Zone North orebody. The youngest extrusive unit of the H-W member is a 10 to 50 metre-thick, plagioclase and pyroxene-phyric andesitic lava flow. This unit overlies the HW Rhyolite and extends >500 metres to the west, above the Ridge Zone West orebody. The Hanging Wall Andesite member unconformably overlies the H-W member and consists of polylithic, volcaniclastic sandstone and conglomerate, locally with clasts of massive sulfide and chert.

In the West Block Area, sulfide mineralisation is in altered andesite of the Price Formation

(footwall) and the rhyolite-dominant, volcano-sedimentary sequence of the H-W member. Styles of sulfide mineralisation are disseminated, stringer, semi-massive and massive. Disseminated sulfide is pyrite-rich, and occurs in altered, Price Formation andesite and all rock types of the H-W member. Sphalerite-rich and pyrite-dominant stringer-style mineralisation is present in altered coherent and volcaniclastic rhyolite of the HW Rhyolite. Although less common in the West Block Area, semi-massive and massive Zn-rich, polymetallic sulfide mineralisation styles are hosted in altered coherent rhyolite and autobreccias of the HW Rhyolite, and polylithic conglomerate of the Basal Volcaniclastic Unit.

Volcanic-hosted massive sulfide mineralisation is located at two stratigraphic positions: (1) upper zone and (2) contact zone. The "upper zone" position is characterised by stringer-style, semi-massive and massive sulfide mineralisation occurring 30 to 75 metres above the Price Formation contact. The "contact zone" position comprises semi-massive and massive sulfide mineralisation at or near the Price Formation contact. Sulfide mineralisation consists of sphalerite, pyrite, chalcopyrite, and galena with accessory tennantite-tetrahedrite and pearceite-polybasite. Precious metal mineralisation includes, primarily, electrum and hessite. Four paragenetic stages of mineralisation are proposed. Stage-1 includes early, inclusion-rich pyrite. Stage-2 consists of inclusion-free pyrite rimming Stage-1 pyrite and accompanied by the precipitation of sphalerite with minor galena-chalcopyrite-barite ± tennantite and tetrahedrite. Stage-3 is characterised by the modification of Stage-2 mineral phases in the form of grain coarsening, homogenisation of sphalerite(?), and local remobilisation of sulfide and sulfosalt phases. The timing of electrum and hessite precipitation is unresolved, but likely occurred during Stage-3. Pearceite-polybasite veinlets, though rare, crosscut Stages 1-3 mineral phases. Therefore, Stage-4 metamorphic remobilisation event is proposed for the precipitation of pearceite-polybasite mineralisation.

9.3 Hydrothermal Alteration

A laterally continuous footwall alteration zone extends beneath the West Block Area and the Battle, Ridge Zone North and Ridge Zone West orebodies for >1,500 metres. Alteration of the Price Formation is mineralogically and texturally diverse. Weak alteration, defined by the Thelwood Valley locality, consists of a pervasive, texturally non-destructive, chlorite-calcite ± epidote alteration. Moderate alteration, defined from the West Block Area, consists of pervasive, texturally non-destructive, chlorite-calcite-pyrite and chlorite-sericite alteration. Intense alteration occurs in the footwall below the Ridge Zone North and Battle orebodies, and consists of feldspar-destructive, sericite-quartz-pyrite, chlorite-rich, and chlorite-sericite-pyrite alteration.

Footwall alteration associated with the West Block Area, Ridge Zone North and Battle orebodies has several mineralogical and geochemical characteristics that show systematic changes with increasing proximity to ore. The Fe/Fe+Mg values in chlorite decrease from 0.49-0.27 in least to moderately altered andesite to <0.20 in intensely altered andesite immediately below ore. In general, K-mica compositions shift from phengitic in least-altered andesite to muscovitic in intensely altered andesite proximal to ore. Using whole-rock lithogeochemical trends, least-altered footwall alteration is characterised by elevated Na_2O, Rb/Sr <0.1, and moderate Alteration Index (AI) and Chlorite-Carbonate-Pyrite Index (CCPI) values that plot in the diagenetic field of the alteration box plot. Proximal (within 100 m of ore) lithogeochemical trends include depleted Na_2O (≤0.75 wt. %), variably elevated S (up to 16.0 wt. %), Rb/Sr >1.0, AI values >80, and CCPI values from 35-95. Distal (up to 500 m away from ore) lithogeochemical

signatures are characterised by variable Na_2O and S values, and Rb/Sr from 0.1-1.0. Alteration Index and CCPI values that plot in the hydrothermal alteration field on the alteration box plot form an array from the least-altered andesite field to the chlorite-pyrite and white mica fields. As these mineralogical and lithogeochemical alteration trends change systematically relative to the position of ore, they can be used in the exploration for other VHMS deposits within the Myra Falls district.

9.4 Lithogeochemical Discrimination of Volcanic Rocks

This research produced a new method for the lithological discrimination of altered volcanic rocks based on systematic portable X-ray fluorescence (pXRF) analysis of drill core. Calibration, estimation of total measurement uncertainty, and data reduction procedures for systematic three-spot pXRF analysis of drill core samples were developed to improve lithological logging of altered volcanic rocks using Ti/Zr ratios. Portable-XRF analysis, combined with detailed logging of volcanic lithofacies, can improve geological interpretations, particularly in areas where alteration obscures the protolith. Rapid field determinations using these procedures are vital for developing mineral exploration models for VHMS deposits at Myra Falls.

9.5 Future Work

Further geochronology studies are recommended as a result of this research. Advancements in LA-ICPMS analysis provide an opportunity to constrain the timing of hydrothermal and metamorphic minerals at Myra Falls. Zircons were difficult to locate in coherent, andesitic rocks at Myra Falls. Monazite and apatite, however, are abundant and could provide additional constraints on the timing of hydrothermal activity and/or metamorphism. The Price Formation remains undated and a search of least-altered, coarse-grained andesite in the Thelwood Valley or Price Hillside may provide appropriate zircons for future U-Pb analysis. The new age constraint provided by this research for the L-M-P member should be followed up with samples of felsic volcanic rocks from the Lynx Mine. Finally, a detrital zircon study on the various turbidite beds throughout the Myra Formation may provide additional information regarding provenance and periods of depositional quiescence in the Myra Falls district.

9.6 Summary

This research advances the overall understanding of the H-W member stratigraphy, the nature of hydrothermal alteration, and the temporal relationship of felsic host rocks at Myra Falls. The integration of these datasets and observations has resulted in the first district-scale synthesis of the H-W member VHMS deposits. The H-W member VHMS deposits represent an active seafloor hydrothermal environment interacting with different, sub-basin sedimentation regimes to form seafloor sulfide and sub-seafloor sulfide replacement VHMS orebodies. These advancements have implications for mineral exploration within the H-W member and throughout the Myra Falls district.

Published age results for felsic volcanic stratigraphy elsewhere on Vancouver Island overlap with the age constraints for the Myra Falls VHMS district. Future VHMS mineral exploration on Vancouver Island should consider: (1) ~362 Ma felsic stratigraphy located within 200 metres of the upper contact of the Price and Nitinat Formations; (2) ~355 Ma felsic stratigraphy located in the top 100 metres of the Myra and McLaughlin Ridge Formations; and (3) the emergent, VHMS prospective chronostratigraphic interval of felsic volcanic rocks, ca. 310-300 Ma, below the Mount Mark Formation, identified by Ruks (2015).

References:

Amelin, Y., and Zaitsev, A., 2002, Precise geochronology of phoscorites and carbonatites: The critical role of U-series disequilibrium in age interpretations: Geochimica et Cosmochimica Acta, v. 66, no. 13, p. 2399–2419.

Andrew, B.S., and Barker, S., 2017, Determination of carbonate vein chemistry using portable X-ray fluorescence and its application to mineral exploration: Geochemistry: Exploration, Environment, Analysis, v. 18, no. 1, p. 85–93.

Andrew, A., and Godwin, C.I., 1989, Lead- and strontium-isotope geochemistry of Paleozoic Sicker Group and Jurassic Bonanza group volcanic rocks and Island Intrusions, Vancouver Island, British Columbia: Canadian Journal of Earth Sciences, v. 26, no. 5, p. 894–907.

Armstrong, J.T., 1988, Quantitative analysis of silicates and oxide minerals: Comparison of Monte-Carlo, ZAF and Phi-Rho-Z procedures: Microbeam Analysis, p. 239–246.

Bacon, C.R., Vazquez, J.A., and Wooden, J.L., 2012, Peninsular terrane basement ages recorded by Paleozoic and Paleoproterozoic zircon in gabbro xenoliths and andesite from Redoubt volcano, Alaska: Bulletin of the Geological Society of America, v. 124, p. 24–34.

Baker, J., Peate, D., Waight, T., and Meyzen, C., 2004, Pb isotopic analysis of standards and samples using a 207Pb – 204Pb double spike and thallium to correct for mass bias with a double-focusing MC-ICP-MS: Chemical Geology, v. 211, p. 275–303.

Barfod, G., Krogstad, E., Frei, R., and Albarede, F., 2005, Lu-Hf and PbSL geochronology of apatites from Proterozoic terranes: A first look at Lu-Hf isotopic closure in metamorphic apatite: Geochimica et Cosmochimica Acta, v. 69, no. 7, p. 1847–1859.

Barford, N.C., 1985, Experimental Measurements: Precision, Error and Truth: John Wiley & Sons, Inc., 159 p.

Barrett, T.J., and MacLean, W.H., 2000, Chemostratigraphy, Petrography and Alteration of the Marshall Zone, Myra Falls, Vancouver Island, B.C.: Internal Company Report.

Barrett, T.J., and MacLean, W.H., 1999, Volcanic Sequence, Lithogeochemistry, and

Hydrothermal Alteration in Some Bimodal Volcanic-Associated Massive Sulfide Systems, in Barrett, T.J. and Hannington, M.D. eds., Volcanic Associated Massive Sulfide Deposits: Processes and Examples in Modern and Ancient Settings, Society of Economic Geologists, p. 101–131.

Barrett, T.J., and Sherlock, R.L., 1996, Volcanic Stratigraphy, Lithogeochemistry, and Seafloor Setting of the H-W Massive Sulfide Deposit, Myra Falls, Vancouver Island, British Columbia: Exploration and Mining Geology, v. 5, no. 4, p. 421–458.

Barrie, C.T., 2012, Volcanogenic Massive Sulfide Occurrence Model: Economic Geology, v. 107, p. 1073–1073.

Barrie, T., Amelin, Y., and Pascual, E., 2002, U-Pb Geochronology of VMS mineralization in the Iberian Pyrite Belt: Mineralium Deposita, v. 37, no. 8, p. 684–703.

Barrie, C.T., and Hannington, M.D., 1999, Classification of Volcanic-Associated Massive Sulfide Deposits Based on Host-Rock Composition, in Barrie, C.T. and Hannington, M.D. eds., Reviews in Economic Geology Volume 8, Society of Economic Geologists, p. 1–11.

Bazard, D.R., Butler, R.F., Gehrels, G.E., and Soja, C.M., 1995, Early Devonian paleomagnetic data from the Lower Devonian Karheen Formation suggest Laurentia-Baltica connection for the Alexander terrane: Geology, v. 23, no. 8, p. 707–710.

Bearden, J.A., 1967, X-Ray Wavelength: Reviews of Modern Physics, v. 30, no. 1, p. 78–124.

Beranek, L.P., Staal, C.R. Van, McClelland, W.C., Israel, S., and Mihalynuk, M.G., 2013, Baltican crustal provenance for Cambrian–Ordovician sandstones of the Alexander terrane, North American Cordillera: evidence from detrital zircon U–Pb geochronology and Hf isotope geochemistry: Journal of the Geological Society, v. 170, no. 2006, p. 7–18.

Beranek, L.P., van Staal, C.R., McClelland, W.C., Joyce, N., and Israel, S., 2014, Late Paleozoic assembly of the Alexander-Wrangellia-Peninsular composite terrane, Canadian and Alaskan Cordillera: Geological Society of America Bulletin, v. 126, no. 11–12, p. 1531–1550.

Berg, H.C., Jones, D.L., and Coney, P.J., 1978, Map showing pre-Cenozoic Tectonostratigraphic Terranes of Southeastern Alaska and Adjacent Areas: US Geological Survey Open-File Report 78-1085.

Berry, R., 2000, Structural geology of the Myra Falls Operation: Internal Company Report, 16 p.

Berry, R., Thompson, J., Meffre, S., and Goemann, K., 2016, U-Th-Pb monazite dating and the timing of arc-continent collision in East Timor: Australian Journal of Earth Sciences, v. 63, no. 4, p. 367–377.

Bindi, L., Evain, M., Spry, P.G., and Menchetti, S., 2007, The pearceite-polybasite group of minerals: Crystal chemistry and new nomenclature rules: American Mineralogist, v. 92, p. 918–925.

Black, L.P., and Gulson, B.L., 1978, The age of the Mud tank Carbonatite, Strangways Range, Northern Territory: BMR Journal of Australian Geology and Geophysics, v. 3, p. 227–232.

Black, L.P., Kamo, S.L., Allen, C.M., Aleinikoff, J.N., Davis, D.W., Korsch, R.J., and Foudoulis, C., 2003, TEMORA 1: a new zircon standard for Phanerozoic U – Pb geochronology: Chemical Geology, v. 200, p. 155–170.

Blodgett, B.R.B., and Sralla, B., 2006, A Major Unconformity Between Permian and Triassic Strata at Cape Kekurnoi, Alaska Peninsula: Old and New Observations on Stratigraphy and Hydrocarbon Potential: U.S. Geological Survey Professional Paper 1739–E, 13 p.

Bourke, A., and Ross, P., 2015, Portable X-ray fluorescence measurements on exploration drill-cores : comparing performance on unprepared cores and powders for 'whole-rock' analysis: Geochemistry: Exploration, Environment, Analysis, v. 16, no. 2, p. 147–157.

Brand, N.W., and Brand, C.J., 2014, Performance comparison of portable XRF instruments: Geochemistry: Exploration, Environment, Analysis, v. 14, p. 125–138.

Brandon, M.T., 1989, Deformational styles in a sequence of olistostromal mélanges, Pacific Rim Complex, western Vancouver Island, Canada: GSA Bulletin, v. 101, p. 1520–1542.

Brandon, M.T., Orchard, M.J., Parrish, R.R., Sutherland Brown, A., and Yorath, C.J., 1986, Fossil ages and isotopic dates from the Paleozoic Sicker Group and associated intrusive rocks, Vancouver Island, British Columbia: Geological Survey of Canada Paper, , no. 86–1A, p. 683–696.

Canil, D., Styan, J., Larocque, J., Bonnet, E., and Kyba, J., 2010, Thickness and composition of the Bonanza arc crustal section, Vancouver Island, Canada: GSA Bulletin, v. 122, p. 1094–1105.

Carvalho, I.G., 1979, Geology of the Western Mines District, Vancouver Island, British Columbia: University of Western Ontario, Unpublished PhD Thesis.

Chong, A.G., 2004, Geology and Genesis of the Polymetallic Ridge Zone West VHMS Deposit, Myra Falls, Vancouver Island, British Columbia, Canada: University of Tasmania, Unpublished MSc Thesis, 210 p.

Chryssoullis, S.L., 1989, Determination of invisible gold in flotation products and four our types from the HW mine, British Columbia: Internal Company Report.

Clapp, C.H., 1912, Southern Vancouver Island: Geological Survey of Canada, Memoir 13, 208 p.

Clark, R.N., King, T., Klejwa, M., Swayze, G.A., and Vergo, N., 1990, High spectral resolution reflectance spectroscopy of minerals: Journal of Geophysical Research, v. 95, p. 12,653-12,680.

Cloutier, J., and Piercey, S.J., 2017, Hyperspectral reflectance in mineral exploration: example from the Northwest Zone of the Lemarchant VMS deposit, Canada: in Proceedings of the 14th SGA Biennial Meeting, 20-23 August 2017, Quebec City, Canada, p. 1127–1130.

Colpron, M., and Nelson, J.L., 2009, A Palaeozoic Northwest Passage: incursion of Caledonian, Baltican and Siberian terranes into eastern Panthalassa, and the early evolution of the North American Cordillera: Geological Society, London, Special Publications, v. 318, no. June, p. 273–307.

Colpron, M., Nelson, J.L., and Murphy, D.C., 2007, Northern Cordilleran terranes and their interactions through time: GSA Today, v. 17, no. 4, p. 4–10.

Corfu, F., Hanchar, J.M., Hoskin, P.W.O., and Kinny, P., 2003, Atlas of zircon textures, in Hanchar, J.M. and Hosking, P.W.O. eds., Reviews in mineralogy and geochemistry, 53, The

Mineralogical Society of America, Washington, DC, USA, p. 469–500.

Craig, J.R., and Vaughan, D.J., 1994, Ore Microscopy and Ore Petrography: John Wiley & Sons, Inc., 434 p.

Craig, J., and Vokes, F.M., 1993, The metamorphism of pyrite and pyritic ores: an overview: Mineralogical Magazine, v. 57, no. 286, p. 3–18.

Creswell, S.D., 1997, A study of the Upper Zone Mineralisation of the H-Zone of Westmin Resources Ltd., Myra Falls Operation, Vancouver Island, British Columbia, Canada: University of Exeter, Unpublished MSc Thesis, 112 p.

Crowley, J.L., Schoene, B., and Bowring, S.A., 2007, U-Pb dating of zircon in the Bishop Tuff at the millennial scale: Geology, v. 35, no. 12, p. 1123–1126.

Davies, M., 2017, Myra Falls re-opening gets a timeline: Campbell River Mirror, December 13.

Dimroth, E., and Lichtblau, A.P., 1979, Metamorphic evolution of Archaean hyaloclastites, Noranda area. Part 1: Comparison of Archaean and Cenozoic sea-floor metamorphism: Canadian Journal of Earth Sciences, v. 16, p. 1315–1340.

Dishaw, G., 1998, Price Orebody: University of Manitoba, Unpublished BSc Honours Thesis.

Donovan, J.J., Snyder, D.A., and Rivers, M.L., 1993, An improved interference correction for trace element analysis: Microbeam Analysis, v. 2, p. 23–28.

Doyle, M.G., and Allen, R.L., 2003, Subsea-floor replacement in volcanic- hosted massive sulfide deposits: Ore Geology Reviews, v. 23, p. 183–222.

Duncan, D.N., and Ord, R.S., 1987, Geological, geochemical, geophysical and diamond drilling work conducted on the Cypres claims, Bedingfield Range, Vancouver Island, British Columbia: British Columbia Ministry of Energy, Mines and Petroleum Resources, Assessment Report 16742.

Eldridge, C.S., Barton, P.. J., and Ohmoto, H., 1983, Mineral textures and their bearing on formation of the Kuroko orebodies, in Economic Geology Monograph 5, Economic Geology, p. 241–281.

England, T.D.J., and Calon, T.J., 1991, The Cowichan fold and thrust system, Vancouver Island, southwestern British Columbia: Geological Society of America Bulletin, v. 103, no. 3, p. 336–362.

Epstein, A.G., Epstein, J.B., and Harris, L.D., 1977, Conodont color alteration - an index to organic metamorphism: USGS Professional Paper, v. 995, 27 p.

Fairchild, L.H., and Cowan, D.S., 1982, Structure, petrology, and tectonic history of the Leech River Complex northwest of Victoria, Vancouver Island: Can. J. Earth Sci, v. 19, no. 9, p. 1817–1835.

Falloon, T.J., Danyushevsky, L. V., Crawford, T.J., Maas, R., Woodhead, J.D., Eggins, S.M., Bloomer, S.H., Wright, D.J., Zlobin, S.K., and Stacey, A.R., 2007, Multiple mantle plume components involved in the petrogenesis of subduction-related lavas from the northern termination of the Tonga Arc and northern Lau Basin: Evidence from the geochemistry of arc and backarc submarine volcanics: Geochemistry, Geophysics, Geosystems, v. 8, no. 9, p. 1–45.

Figueroa-Cisterna, J., Bagur-Gonzalez, M.G., Morales-Ruano, S., Carrillo-Rosua, J., and Martin-Peinado, F., 2011, The use of combined portable X-ray fluorescence and multivariate statistical methods to assess a validated macroscopic rock samples classification in an ore exploration survey: Talanta, v. 85, p. 2307–2315.

Fisher, L., Gazley, M.F., Baensch, A., Barnes, S.J., Cleverly, J., and Duclaux, G., 2014, Resolution of geochemical and lithostratigraphic complexity: a workflow for application of portable X-ray fluorescence to mineral exploration: Geochemistry: Exploration, Environment, Analysis, v. 14, p. 149–159.

Forster, N., Grave, P., Vicker, N., and Kealhofer, L., 2011, Non-destructive analysis using PXRF: methodology and application to archaeological ceramics: X-Ray Spectrometry, v. 40, p. 389–398.

Francheteau, J., Needham, H.D., Choukroune, P., Juteau, T., Séguret, M., Ballard, R.D., Fox, P.J., Normark, W., Carranza, A., Cordoba, D., Guerrero, J., Rangin, C., Bougault, H., Cambon, P., et al., 1979, Massive deep-sea sulphide ore deposits discovered on the East Pacific Rise: Nature, v. 277, no. 5697, p. 523–528.

Franklin, J.M., Gibson, H.L., Jonasson, I.R., and Galley, A.G., 2005, Volcanogenic Massive Sulfide Deposits: Economic Geology, v. 100th Anniversary, p. 523–560.

Franklin, J.M., Lydon, J.W., and Sangster, D.F., 1981, Volcanic-associated massive sulfide deposits: Economic Geology, v. 75th Anniversary, p. 485–627.

Freeze, A.C., 1986, Assessment report geology of the Bedingfield 1-15, Cypres 1 Mineral Claims, Alberni Mining Division, Tofino Area, British Columbia: British Columbia Ministry of Energy, Mines and Petroleum Resources, Assessment Report 14500.

Fyles, J.T., 1955, Geology of the Cowichan Lake area, Vancouver Island, British Columbia: British Columbia Ministry of Energy, Mines and Petroleum Resources Bulletin 37, 79 p.

Gabrielse, H., Monger, J.W.H., Wheeler, J.O., and Yorath, C.J., 1991, Tectonic Framework Part A: Morphogeological belts, tectonic assemblages and terranes, in Gabrielse, H. and Yorath, C.J. eds., Geology of the Cordilleran Orogen in Canada, Geological Survey of Canada, Geology of Canada, no. 4, p. 15–28.

Galley, A.G., 1995, Target vectoring using lithogeochemistry: Applications to the exploration for volcanic-hosted massive sulphide deposits: CIM Bulletin, v. 88, no. 990, p. 15–27.

Galley, A.G., Hannington, M.D., and Jonasson, I.R., 2007, Volcanogenic Massive Sulphide Deposits, in Goodfellow, W.D. eds., Mineral Deposits of Canada: A Synthesis of Major Deposit Types, District Metallogeny, the Evolution of Geological Province and Exploration Methods, Geological Association of Canada, Mineral Deposits Division, Special Publication No. 5, p. 141–161.

Galley, A.G., Watkinson, D.H., Jonasson, I.R., and Riverin, G., 2006, The Subsea-Floor Formation of Volcanic-Hosted Massive Sulfide: Evidence from the Ansil Deposit, Rouyn-Noranda, Canada: Economic Geology, v. 90, p. 2006–2017.

Gardner, M.C., Bergman, S.C., Cushing, G.W., MacKevett, E.M.J., Plafker, G., Campbell, R.B., Dodds, C.J., McClelland, W.C., and Mueller, P.A., 1988, Pennsylvanian pluton stitching of Wrangellia and the Alexander terrane, Wrangell Mountains, Alaska: Geology, v. 16, p. 967–

971.

Gazley, M.F., Duclaux, G., Fisher, L.A., Tutt, C.M., Latham, A.R., Hough, R.M., Beer, S.J. De, and Taylor, M.D., 2014, A comprehensive approach to understanding ore deposits using portable X-ray fluorescence (pXRF) data at the Plutonic Gold Mine, Western Australia: Geochemistry: Exploration, Environment, Analysis, v. 15, p. 113–124.

Gazley, M.F., Vry, J.K., Du Plessis, E., and Handler, M.R., 2011, Application of portable X-ray fluorescence analyses to metabasalt stratigraphy, Plutonic Gold Mine, Western Australia: Journal of Geochemical Exploration, v. 110, no. 2, p. 74–80.

Gehrels, G.E., 1990, Late Proterozoic-Cambrian metamorphic basement of the Alexander terrane on Long and Dall Islands, southeast Alaska: Geological Society of America Bulletin, v. 102, p. 760–767.

Gehrels, G.E., and Berg, H.C., 1994, Geology of southeastern Alaska, in Plafker, G. and Berg, H.C. eds., The Geology of Alaska, Geological Society of America, Boulder, CO, USA, p. 451–468.

Gehrels, G.E., Butler, R.F., and Bazard, D.R., 1996, Detrital zircon geochronology of the Alexander terrane, southeastern Alaska: GSA Bulletin, v. 108, no. 6, p. 722–734.

Gehrels, E., and Saleeby, B., 1987, Geologic Framework, Tectonic Evolution and Displacement History of the Alexander Terrane: Tectonics, v. 6, no. 2, p. 151–173.

Gerstenberger, H., and Haase, G., 1997, A highly effective emitter substance for mass spectrometric Pb isotope ratio determinations: Chemical Geology, v. 136, p. 309–312.

Gibson, H.L., Allen, R.L., Riverin, G., and Lane, T.E., 2007, The VMS Model: Advances and Application to Exploration Targeting: in Proceedings of Exploration 07: Fifth Decennial International Conference on Mineral Exploration, Milkereit, B., eds., p. 713–730.

Gifkins, C.C., and Allen, R.L., 2001, Textural and Chemical Characteristics of Diagenetic and Hydrothermal Alteration in Glassy Volcanic Rocks: Examples from the Mount Read Volcanics, Tasmania: Economic Geology, v. 96, no. 5, p. 973–1002.

Gifkins, C.C., Herrmann, W., and Large, R.R., 2005, Altered volcanic rocks: A guide to description and interpretation: Centre for Ore Deposit Research, University of Tasmania Australia, Hobart, 275 p.

Godwin, C.I., and Robinson, M., 1996, Galena Lead Isotopes, Buttle Lake Mining Camp, Vancouver Island, British Columbia, Canada: Geology, v. 91, p. 549–562.

Gonçalves, G.O., Lana, C., Scholz, R., Buick, I.S., Gerdes, A., Kamo, S.L., Corfu, F., Marinho, M.M., Chaves, A.O., Valeriano, C., and Nalini, H.A., 2016, An assessment of monazite from the Itambé pegmatite district for use as U–Pb isotope reference material for microanalysis and implications for the origin of the "Moacyr" monazite: Chemical Geology, v. 424, p. 30–50.

Goodale, N., Bailey, D.G., Jones, G.T., Prescott, C., Scholz, E., Stagliano, N., and Lewis, C., 2012, pXRF: a study of inter-instrument performance: Journal of Archaeological Science, v. 39, p. 875–883.

Gordey, S.P., Geldsetzer, H.H.J., Morrow, D.W., Bamber, E.W., Henderson, C.M., Richards, B.C.,

Mcgugan, A., Gibson, D.W., and Poulton, T.P., 1991, Upper Devonian to Middle Jurassic Assemblages (H. Gabrielse & C. J. Yorath, eds.): Geology of the Cordilleran Orogen in Canada, p. 221–328.

Greene, A., 2010, The architecture of oceanic plateaus revealed by the volcanic stratigraphy of the accreted Wrangellia oceanic plateau: Geosphere, v. 6, no. 1, p. 47–73.

Greene, A.R., Nixon, G.T., Scoates, J.S., and Massey, N.W.D., 2008, A Field Trip Guide to Wrangellia Flood Basalts on Vancouver Island: An Accreted Late Triassic Oceanic Plateau: Goldschmidt 2008 Conference, Vancouver, B.C., Canada, 25 p.

Greenwood, H.J., Woodworth, G.J., Read, P.B., Ghent, E.D., and Evenchick, C.A., 1991, Metamorphism, in Gabrielse, H. and Yorath, C.J. eds., Geology of the Cordilleran Orogen in Canada, Geological Survey of Canada, Geology of Canada, p. 533–570.

Groome, W.G., Thorkelson, D.J., Friedman, R.M., Mortensen, J.K., and Marshall, D.D., 2003, Magmatic and tectonic history of the Leech River Complex, Vancouver Island, British Columbia: Evidence for ridge-trench intersection and accretion of the Crescent terrane: Geological Society of America Special Papers, v. 371, p. 327–353.

Gu, Y., 2003, Automated scanning electron microscope based mineral liberation analysis: Journal of Minerals and Materials Characterization and Engineering, v. 2, p. 33–41.

Gunning, H.C., 1931, Buttle Lake map-area, Vancouver Island, British Columbia: Geological Survey of Canada, Summary Report 1930, p. 56-78.

Hall, G.E.M., Bonham-carter, G.F., and Buchar, A., 2014, Evaluation of portable X-ray fluorescence (pXRF) in exploration and mining: Phase 1, control reference materials: Geochemistry: Exploration, Environment, Analysis, v. 14, p. 99–123.

Hall, G.E.M., Buchar, A., and Bonham-Carter, G., 2013, Quality control assessment of portable XRF analysers: development of standard operating procedures, performance on variable media and recommended uses: CAMIRO Project 10E01 Report, 112 p.

Halpin, J.A., Jensen, T., Mcgoldrick, P., Meffre, S., Berry, R.F., Everard, J.L., Calver, C.R., Thompson, J., Goemann, K., and Whittaker, J.M., 2014, Authigenic monazite and detrital zircon dating from the Proterozoic Rocky Cape Group, Tasmania: Links to the Belt-Purcell Supergroup, North America: Precambrian Research, v. 250, p. 50–67.

Hannington, M.D., Poulsen, K.H., Thompson, J.F.H., and Sillitoe, R.H., 1999, Volcanogenic gold in the massive sulfide environment, in Barrie, C.T. and Hannington, M.D. eds., Volcanic-associated massive sulfide deposits: processes and examples in modern and ancient settings, vol 8, Society of Economic Geologists, Boulder, CO, USA, p. 325–351.

Hannington, M.D., De Ronde, C.E., and Oetersen, S., 2005, Sea-Floor Tectonics and Submarine Hydrothermal Systems: Economic Geology, p. 111–141.

Hannington, M.D., and Scott, S.D., 1989, Sulfidation equilibria as guides to gold mineralization in volcanogenic massive sulfides; evidence from sulfide mineralogy and the composition of sphalerite: Economic Geology, v. 84, p. 1978–1995.

Hart, T.R., Gibson, H.L., and Lesher, C.M., 2004, Trace element geochemistry and petrogenesis of felsic volcanic rocks associated with volcanogenic massive Cu-Zn-Pb sulfide deposits: Economic Geology, v. 99, p. 1003–1013.

Herrmann, W., and Berry, R.F., 2002, MINSQ – a least squares spreadsheet method for calculating mineral proportions from whole rock major element analyses: Geochemistry: Exploration, Environment, Analysis, v. 2, no. 4, p. 361–368.

Herrmann, W., Blake, M., Doyle, M., Huston, D.L., Kamprad, J., Merry, N., and Pontual, S., 2001, Short Wavelength Infrared (SWIR) Spectral Analysis of Hydrothermal Alteration Zones Associated with Base Metal Sulfide Deposits at Rosebery and Western Tharsis, Tasmania, and Highway-Reward, Queensland: Economic Geology, v. 96, p. 939–955.

Hey, M.H., 1954, A New Review of the Chlorites: Mineralogical Magazine, v. 30, no. 224, p. 277–292.

Van der Heyden, P., 1992, A Middle Jurassic to Early Tertiary Andean-Sierran arc model for the Coast Belt of British Columbia: Tectonics, v. 11, p. 82–97.

Hoskin, P.W.O., and Schaltegger, U., 2003, The composition of zircon and igneous and metamorphic petrogenesis, in Reviews in mineralogy and geochemistry, 53, The Mineralogical Society of America, Washington, DC, USA, p. 27–55.

Huston, D., 2000, Gold in volcanic-hosted massive sulfide deposits: distribution, genesis, and exploration, in Hagemann, S. and Brown, P. eds., Reviews in Economic Geology: Gold in 2000, vol 13, Society of Economic Geologists, Boulder, CO, USA, p. 401–426.

Huston, D., Jablonski, W., and Sie, S., 1996, The distribution and mineral hosts of silver in Eastern Australia Volcanogenic Massive Sulfide Deposits: Canadian Mineralogist, v. 34, p. 529–546.

Huston, D.L., Kamprad, J., and Brauhart, C., 1999, Definition of high-temperature alteration zones with PIMA: an example from the Panorama VHMS district, central Pilbara Craton: AGSO Research Newsletter, v. 30, p. 1–3.

Huston, D.L., and Large, R.R., 1987, Genetic and exploration significance of the zinc ratio (100 Zn/(Zn + Pb)) in massive sulfide systems: Economic Geology, v. 82, no. 6, p. 1521–1539.

Huston, D.L., Pehrsson, S., Eglington, B.M., and Zaw, K., 2010, The geology and metallogeny of volcanic-hosted massive sulfide deposits: Variations through geologic time and with tectonic setting: Economic Geology, v. 105, p. 571–591.

Ishikawa, Y., Sawaguchi, T., Shin-ichi, I., and Horiuchi, M., 1976, Delineation of Prospecting Targets for Kuroko Deposits Based on Modes of Volcanism and underlying Dacite and Alteration Haloes: Mining Geology, v. 26, p. 105–117.

Israel, S., Beranek, L., Friedman, R.M., and Crowley, J.L., 2014, New ties between the Alexander terrane and Wrangellia and implications for North America Cordilleran evolution: Lithosphere, v. 6, no. 4, p. 270–276.

Jackson, S.E., Pearson, N.J., Griffin, W.L., and Belousova, E.A., 2004, The application of laser ablation-inductively coupled plasma-mass spectrometry to in situ U–Pb zircon geochronology: Chemical Geology, v. 211, p. 47–69.

Jaffey, A.H., Flynn, K.F., Glendenin, L.E., Bentley, W.C., and Essling, A.M., 1971, Precision measurement of half-lives and specific activities of 235U and 238U: Physical Review, v. 4, no. 5, p. 1889–1906.

Jeffery, W.G., 1970, Buttle Lake: British Columbia Ministry of Energy, Mines and Petroleum Resources, Annual Report.

Jeletzky, I.A., 1976, Mesozoic and Tertiary Rocks of Quatsino Sound, Vancouver Island, British Columbia: Geological Survey of Canada, Bulletin 242, 243 p.

Jenkins, R., 1999, X-Ray Fluorescence Spectrometry: John Wiley & Sons, Inc, New York, 207p.

Jenner, G.A., 1996, Trace element geochemistry of igneous rocks: geochemical nomenclature and analytical geochemistry, in Wyman, D.A. eds., Trace element geochemistry of volcanic rocks: applications for massive sulfide exploration, Geological Association of Canada, p. 51–77.

Johnston, S.T., and Acton, S., 2003, The Eocene Southern Vancouver Island Orocline—a response to seamount accretion and the cause of fold-and-thrust belt and extensional basin formation: Tectonophysics, v. 365, p. 165–183.

Jones, M.I., 1997, 1996-1997 Assessment report, Dragon property: Diamond drilling; Alberni and Nanaimo Mining Divisions, NTS map areas 92E/16E: British Columbia Ministry of Energy, Mines and Petroleum Resources, Assessment Report 24895, 189 p.

Jones, S.A., 2001, Geology and Geochemistry of the "Caprocks" above VHMS Deposits at Myra Falls, Vancouver Island, British Columbia: University of Tasmania, Unpublished PhD Thesis, 410 p.

Jones, S., Berry, R., and Sinclair, B., 2006a, Multiple deformation episodes at Myra Falls volcanic-hosted massive sulfide camp, central Vancouver Island, British Columbia, Canada: Canadian Journal of Earth Sciences, v. 43, no. 11, p. 1711–1732.

Jones, S., Gemmell, J.B., and Davidson, G.J., 2006b, Petrographic, geochemical, and fluid inclusion evidence for the origin of siliceous cap rocks above volcanic-hosted massive sulfide deposits at Myra Falls, Vancouver Island, British Columbia, Canada: Economic Geology, v. 101, p. 555–584.

Jones, S., Herrmann, W., and Gemmell, B.J., 2005, Short Wavelength Infrared Spectral Characteristics of the HW Horizon: Implications for Exploration in the Myra Falls Volcanic-Hosted Massive Sulfide Camp, Vancouver Island, British Columbia, Canada: Economic Geology, v. 100, p. 273–294.

Jones, D.L., Silberling, N.J., Coney, P.J., and Plafker, G., 1984, Part A - Lithotectonic terrane map of Alaska (west of the 141st Meridian), in Jones, D.L. and Silberling, N.J. eds., Lithotectonic Terrane Maps of North American Cordillera, p. A1–A12.

Jones, D.L., Silberling, N.J., and Hillhouse, J., 1977, Wrangellia—A displaced terrane in northwestern North America: Canadian Journal of Earth Sciences, v. 14, no. 11, p. 2565–2577.

Juras, S.J., 1987, Geology of the polymetallic volcanogenic Buttle Lake Camp, with emphasis on the Price Hillside, central Vancouver Island, British Columbia, Canada: University of British Columbia, Unpublished PhD Thesis, 196 p.

Juras, S.G., and Pearson, C.A., 1990, Mineral deposits of the southern Canadian Cordillera, in Guidebook for Field Trip B2, Geological Association of Canada-Mineral Association of Canada, 21 p.

Katnick, D.C., and Mustard, P.S., 2003, Geology of Denman and Hornby islands, British Columbia: implications for Nanaimo Basin evolution and formal definition of the Geoffrey and Spray formations, Upper Cretaceous Nanaimo Group: Can. J. Earth Sci, v. 40, p. 375–393.

Katvala, E.C., 2006, Re-examining the stratigraphic and palaeontologic definition of Wrangellia, in GSA: Wrangellia Tectonics and Metallogeny, 30 Years of Progress, Geological Society of America, Anchorage, Alaska, 24 p.

Katvala, E.C., and Henderson, C.M., 2002, Conodont Sequence Biostratigraphy and Paleogeography of the Pennsylvanian-Permian Mount Mark Formation, southern Vancouver Island: Memoir-Canadian Society of Petroleum Geologists, v. 19, p. 461–478.

Kemp, R., and Gill, G., 1993, Geological, geochemical and diamond drilling report on the Specogna-Muchalat property (92E/16, Alberni Mining Division): British Columbia Ministry of Energy, Mines and Petroleum Resources, Assessment Report 23125, 48 p.

Krogstad, E.J., and Walker, R.J., 1994, High closure temperatures of the U-Pb system in large apatites from the Tin Mountain pegmatite, Black Hills, South Dakota, USA: Geochimica et Cosmochimica Acta, v. 58, no. 18, p. 3845–3853.

Large, R.R., 1992, Australian Massive Sulfide Deposits: Features, Styles, and Genetic Models: Economic Geology, v. 87, p. 471–510.

Large, R.R., 1977, Chemical Evolution and Zonation of Massive Sulfide Deposits in Volcanic Terrains: Economic Geology, v. 72, p. 549–572.

Large, R.R., Gemmell, B.J., and Paulick, H., 2001a, The Alteration Box Plot : A Simple Approach to Understanding the Relationship between Alteration Mineralogy and Lithogeochemistry Associated with Volcanic-Hosted Massive Sulfide Deposits: Economic Geology, v. 96, p. 957–971.

Large, R.R., Allen, R.L., Blake, M., and Herrmann, W., 2001b, Hydrothermal Alteration and Volatile Element Halos for the Rosebery K Lens Volcanic-Hosted Massive Sulfide Deposit, Western Tasmania: Economic Geology, v. 96, no. 1981, p. 1055–1072.

Large, R.R., McPhie, J., Gemmell, B.J., Herrmann, W., and Davidson, G.J., 2001c, The Spectrum of Ore Deposit Types, Volcanic Environments, Alteration Halos, and Related Exploration Vectors in Submarine Volcanic Successions: Some Examples from Australia: Economic Geology, v. 96, p. 913–938.

Lawley, C.J.M., Dubé, B., Mercier-Langevin, P., Kjarsgaard, B., Knight, R., and Vaillancourt, D., 2015, Defining and mapping hydrothermal footprints at the BIF-hosted Meliadine gold district, Nunavut, Canada: Journal of Geochemical Exploration, v. 155, p. 33–55.

Lentz, D.R., 1998, Petrogenetic evolution of felsic volcanic sequences associated with Phanerozoic volcanic-hosted massive sulphide systems: the role of extensional geodynamics: Ore Geology Reviews, v. 12, p. 289–327.

Lentz, D.R., 1999, Petrology, geochemistry, and oxygen isotope interpretation of felsic volcanic and related rocks hosting the Brunswick 6 and 12 massive sulfide deposits (Brunswick Belt), Bathurst Mining Camp, New Brunswick, Canada: Economic Geology, v. 94, p. 57–86.

Lesher, C.M., and Campbell, I.H., 1987, Trace-element geochemistry of ore-associated and

barren, felsic metavolcanic rocks in the Superior Province, Canada: Reply: Canadian Journal of Earth Sciences, v. 24, no. 7, p. 1500–1501.

Li, X., Long, W., Li, Q., Liu, Y., and Zheng, Y., 2010, Penglai Zircon Megacrysts : A Potential New Working Reference Material for Microbeam Determination of Hf--O Isotopes and U--Pb Age: Geostandars and Geoanalytical Research, v. 34, no. 2, p. 117–134.

Lydon, J.W., 1984, Volcanogenic massive sulphide deposits. Part 1: a descriptive model: Geoscience Canada, v. 11, no. 4, p. 195–202.

Lydon, J.W., 1988, Volcanogenic massive sulphide deposits. Part 2: genetic models: Geoscience Canada, v. 15, no. 1, p. 43–65.

Maas, K.M., Bittenbender, P.E., and Still, J.C., 1995, Mineral Investigations in the Ketchikan Mining District: US Department of the Interior Bureau of Mines, Open File Report 11-95, 619 p.

Mackie, D.C., 2002, An integrated structural and hydrogeologic investigation of the fracture system in the Upper Cretaceous Nanaimo Group, southern Gulf Islands, British Columbia: Simon Fraser University, Unpublished MSc Thesis, 716 p.

MacLean, W.H., and Barrett, T.J., 1993, Lithogeochemical techniques using immobile elements: Journal of Geochemical Exploration, v. 48, p. 109–133.

MacLean, W.H., and Kranidiotis, P., 1987, Immobile Elements as Monitors of Mass Transfer in Hydrothermal Alteration: Phelps Dodge Massive Sulfide Deposit, Matagami, Quebec: Economic Geology, v. 82, p. 951–962.

Markowicz, A.A., 2008, Quantification and Correction Procedures, in Potts, P.J. and West, M. eds., Portable X-ray Fluorescence Spectrometry: Capabilities for In Situ Analysis, RSC Publishing, Cambridge, p. 13–38.

Marshall, D., Nicol, C.-A., Greene, R., Sawyer, R., Stansell, A., and Easterbrook, R., 2018, Precious Metal Enrichment at the Myra Falls VMS Deposit, British Columbia, Canada: Geosciences, v. 8, no. 11, 13 p.

Massey, N.W.D., 1992a, Geology and Mineral Resources of the Alberni-Nanaimo Lakes Sheet, Vancouver Island (92F/1W, 92F/2E, 92F/7E): British Columbia Ministry of Energy, Mines and Petroleum Resources, Paper 1992-2, 144 p.

Massey, N.W.D., 1992b, Geology and mineral resources of the Duncan sheet, Vancouver Island (92B/13): British Columbia Ministry of Energy, Mines and Petroleum Resources, 57 p.

Massey, N.W.D., 1995, Geology and mineral resources of the Duncan sheet, Vancouver Island 92B/13: Ministry of Energy, Mines and Petroleum Resources, Mineral Resources Division, Geological Survey Branch, 57 p.

Massey, N.W.D., 1986, Metchosin igneous complex, southern Vancouver Island: Ophiolite stratigraphy developed in an emergent island setting: Geology, v. 14, p. 602–605.

Massey, N.W.D., Desjardin, P.J., and Cooney, R.T., 2005, Digital map of British Columbia: Tile NM10 Southwest B.C.: British Columbia Ministry of Energy, Mines and Petroleum Resources, GeoFile 2005-3.

Massey, N.W.D., and Friday, S.J., 1988, Geology of the Cheminus River-Duncan area, Vancouver

Island (92 C/16; 92 B/13): British Columbia Ministry of Energy, Mines and Petroleum Resources, Paper 1988-1, p. 81-91.

Massey, N.W.D., and Friday, S.J., 1987, Geology of the Cowichan Lake Area, Vancouver Island (92C/16): British Columbia Ministry of Energy, Mines and Petroleum Resources Bulletin, Paper 1987, p. 223–229.

Massey, N.W.D., Friday, S.J., Riddell, J.M., and Dumais, S.E., 1991, Geology of the Port Alberni-Nanaimo Lakes area: British Columbia Ministry of Energy, Mines and Petroleum Resources, Geoscience Map 1991-1.

Mattinson, J.M., 2005, Zircon U–Pb chemical abrasion ("CA-TIMS") method: Combined annealing and multi-step partial dissolution analysis for improved precision and accuracy of zircon ages: Chemical Geology, v. 220, p. 47–66.

Mauriohooho, K., Barker, S.L.L., and Rae, A., 2016, Mapping lithology and hydrothermal alteration in geothermal systems using portable X-ray fluorescence (pXRF): A case study from the Tauhara geothermal system, Taupo Volcanic Zone: Geothermics, v. 64, p. 125–134.

McClelland, W.C., Gehrels, G.E., and Saleeby, J.B., 1992, Upper Jurassic-Lower Cretaceous basinal strata along the Cordilleran Margin: Implications for the accretionary history of the Alexander-Wrangellia-Peninsular Terrane: Tectonics, v. 11, no. 4, p. 823–835.

McDonough, W.F., and Sun, S.-S., 1995, The composition of the Earth: Chemical Geology, v. 120, p. 223–253.

McNicoll, V., Goutier, J., Dube, B., Mercier-Langevin, P., Ross, P.-S., Dion, C., Monecke, T., Legault, M., Percival, J., and Gibson, H., 2014, U-Pb Geochronology of the Blake River Group, Abitibi Greenstone Belt, Quebec, and Implications for Base Metal Exploration: Economic Geology, v. 109, no. 1, p. 27–59.

McPhie, J., and Allen, R.L., 1992, Facies Architecture of Mineralized Submarine Volcanic Sequences: Cambrian Mount Read Volcanics, Western Tasmania: Economic Geology, v. 87, p. 587–596.

Meffre, S., Large, R.R., Scott, R., Woodhead, J., Chang, Z., Gilbert, S.E., Danyushevsky, L. V, Maslennikov, V., and Hergt, J.M., 2008, Age and pyrite Pb-isotopic composition of the giant Sukhoi Log sediment-hosted gold deposit, Russia: Geochimica et Cosmochimica Acta, v. 72, p. 2377–2391.

Meier, P.C., and Zund, R.E., 1993, Statistical Methods in Analytical Chemistry (J. D. Winefordner & I. M. Kolthoff, eds.): John Wiley & Sons, Inc, New York, 321 p.

Mercier-Langevin, P., Hannington, M.D., Dubé, B., and Bécu, V., 2010, The gold content of volcanogenic massive sulfide deposits: Mineralium Deposita, v. 46, no. 5–6, p. 509–539.

Meyer, F.M., Robb, L.J., Reimonld, W.U., and de Bruiyn, H., 1994, Contrasting low- and high-Ca granites in the Archean Barberton Mountain Land, Southern Africa: Lithos, v. 32, p. 63–76.

Mihalynuk, M.G., Smith, M.T., MacIntyre, D.G., and Deschenes, M., 1992, Tatsenshini Project Part B: Stratigraphic and magmatic setting of mineral occurrences: British Columbia Ministry of Energy, Mines and Petroleum Resources, Paper 1993-1, p. 189-229.

Monger, J.W.H., Price, R. a., and Tempelman-Kluit, D.J., 1982, Tectonic accretion and the origin of the two major metamorphic and plutonic welts in the Canadian Cordillera: Geology, v. 10, no. 2, p. 70–75.

Morris, P.A., 2009, Field-portable X-ray fluorescence analysis and its application in GSWA: Geological Survey of Western Australia, Paper 2009/7, 23 p.

Mortensen, J.K., 1992a, New U-Pb ages for the Slide Mountain Terrane in southeastern Yukon Territory, in Radiogenic and isotopic studies, Report 5 (91-2), Geological Survey of Canada, Ottawa, ON, Canada, p. 167–173.

Mortensen, J.K., 1992b, Pre-mid-Mesozoic Tectonic Evolution of the Yukon-Tanana Terrane, Yukon and Alaska: Tectonics, v. 11, no. 4, p. 836–853.

Mortensen, J.K., Gemmell, J.B., McNeill, A.W., and Friedman, R.M., 2015, High-Precision U-Pb Zircon Chronostratigraphy of the Mount Read Volcanic Belt in Western Tasmania , Australia : Implications for VHMS Deposit Formation: Economic Geology, v. 110, p. 445–468.

Mortensen, J.K., and Israel, S., 2006, Is the Windy-McKinley terrane a displaced fragment of Wrangellia? Evidence from new geological, geochemical and geochronological studies in western Yukon, in Geological Society of American Abstract with Programs, Geological Society of America, Anchorage, Alaska, 93 p.

Morton, R.L., Walker, J.S., Hudak, G.J., and Franklin, J.M., 1991, The early development of an Archean submarine caldera complex with emphasis on the Mattabi ash-flow tuff and its relationship to the Mattabi massive sulfide deposit: Economic Geology, v. 86, no. 5, p. 1002–1011.

Mosier, D.L., Berger, V.I., and Singer, D.A., 2009, Volcanogenic massive sulfide deposits of the world; databse and grade and tonnage models: U.S. Geological Survey, Open-File Report 2009-1034, 46 p.

Muller, J.E., 1977, Geology of Vancouver Island (Map): Geological Survey of Canada, Open File 463.

Muller, J.E., 1980, The Paleozoic Sicker Group of Vancouver Island, British Columbia: Geological Survey of Canada, Paper 79-30, 22 p.

Muller, J.E., Cameron, B.E.B., and Northcote, K.E., 1981, Geology and mineral deposits of Nootka Sound Map-Area (92 E) Vancouver Island, British Columbia: Geological Survey of Canada, Paper 80-16, 53 p.

Muller, J.E., and Jeletzky, I.A., 1970, Geology of the Upper Cretaceous Nanaimo Group, Vancouver Island and Gulf Islands, British Columbia: Geological Survey of Canada, Paper 69-25, 77 p.

Mundil, R., Ludwig, K.R., Metcalfe, I., and Renne, P.R., 2004, Age and Timing of the Permian Mass Extinctions: U/Pb Dating of Closed-System Zircons: Science, v. 305, p. 1760–1763.

Murphy, D.C., Mortensen, J.K., Piercey, S.J., Orchard, M.J., and Gehrels, G.E., 2006, Tectonostratigraphic evolution of Yukon-Tanana Terrane, Finlayson Lake massive sulphide district, southeastern Yukon, in Special Paper 45, Geological Association of Canada, St. John's, Newfoundland, p. 75–106.

Nelson, J., and Colpron, M., 2007, Tectonics and metallogeny of the British Columbia, Yukon and Alaskan Cordillera, 1.8 Ga to present (W. Goodfellow, eds.): Mineral Deposits of Canada: A Synthesis of Major Deposit Types, District Metallogeny, the Evolution of Geological Province and Exploration Methods, p. 755–791.

Nixon, G.T., Hammack, J.L., Koyanagi, V.M., Payie, G.J., Panteleyev, A., Massey, N.W.D., Hamilton, J.V., and Haggart, J., 1994, Preliminary geology of the Quatsino - Port McNeill map areas, Northern Vancouver Island: British Columbia Geological Survey, Fieldwork Report 1994-1, p. 63-86.

Nixon, G.T., Hammack, J.L., Payie, G.J., Snyder, L.D., ARchibald, D.A., and Barron, D.J., 1995, Quatsino - San Josef Map Area, Northern Vancouver Island: Geological Overview (92L/12W, 102I/8, 9): British Columbia Geological Survey, Fieldwork Report 1995-1, p. 9-21.

Nixon, G.T., Kelman, M.C., Stevenson, D., Stokes, L.A., and Johnston, K.A., 2006, Preliminary geology of the Nimpkish map area (NTS 092L/07), northern Vancouver Island, British Columbia, in Grant, B. and Newell, J.M. eds., Geological Fieldwork 2005, Ministry of Energy, Mines and Petroleum Resources.

Nixon, G.T., and Orr, A.J., 2007, Recent Revisions to the Early Mesozoic Stratigraphy of Northern Vancouver Island (NTS 102I ; 092L) and Metallogenic Implications, British Columbia: British Columbia Geological Survey, Fieldwork Report 2007-1, p. 163–178.

Nowak, M., Johnson, M., Van Der Heever, D., and Arseneau, G., 2011, Mineral resource estimation Niblack polymetallic sulphide project, Alaska, USA 43-101 Report: Heatherdale Resources Ltd. & Niblack Mineral Development Inc., 94 p.

Nyrstar 2017 Mineral Resource and Mineral Reserve Statement, 2018, Nyrstar News Release, p. 1–9.

Ohmoto, H., 1996, Formation of volcanogenic massive sulfide deposits: The Kuroko perspective: Ore Geology Reviews, v. 10, p. 135–177.

Ohmoto, H., Mizukami, M., Drummon, S.E., Eldridge, C.S., and Lenagh, T.C., 1983, Chemical Processes of Kuroko Formation, in Ohmoto, H. and Skinner, B.J. eds., The Kuroko and Related Volcanogenic Massive Sulfide Deposits, Economic Geology, p. 570–604.

Ohmoto, H., and Rye, R.O., 1974, Hydrogen and oxygen isotopic compositions of fluid inclusions in the Kuroko deposits, Japan: Economic Geology, v. 69, p. 947–953.

Oliver, J., Roberts, K., and Friedman, R., 2011, The Niblack Mine: A Neoproterozoic, precious metals enhanced, volcanic hosted massive sulphide, Prince of Wales Island, Alaska, in Mining From Prospect to Feasibility, AMA Conference, Anchorage, Alaska, p. 60–62.

Parrish, R.R., and McNicoll, V.J., 1992, U-Pb age determinations from the southern Vancouver Island area, British Columbia. Radiogenic Age and Isotopic Studies: Report 5: Geological Survey of Canada, Paper 91-2, p. 79-86.

Peter, J.M., Mercier-Langevin, P., and Chapman, J.B., 2009, Application of field-portable x-ray fluorescence spectrometers in mineral exploration, with examples from the Abitibi Greenstone Belt, in 24th IAGS, p. 83–86.

Peter, J.M., and Scott, S.D., 1999, Windy Craggy, Northwestern British Columbia: The World's Largest Besshi-Type Deposit, in Barrie, C.T. and Hannington, M.D. eds., Volcanic Associated

Massive Sulfide Deposits: Processes and Examples in Modern and Ancient Settings, Society of Economic Geologists, Littleton, CO, p. 261–295.

Piercey, S.J., 2010, An overview of petrochemistry in the regional exploration for volcanogenic massive sulphide (VMS) deposits: Geochemistry: Exploration, Environment, Analysis, v. 10, p. 119–136.

Piercey, S.J., 2014, Modern Analytical Facilities 2. A Review of Quality Assurance and Quality Control (QA / QC) Procedures for Lithogeochemical Data: Geoscience Canada, v. 41, p. 1–14.

Piercey, S.J., 2011, The setting, style, and role of magmatism in the formation of volcanogenic massive sulfide deposits: Mineralium Deposita, v. 46, no. 5–6, p. 449–471.

Piercey, S.J., and Devine, M.C., 2014, Analysis of powdered reference materials and known samples with a benchtop, field portable X-ray fluorescence (pXRF) spectrometer: evaluation of performance and potential applications for exploration lithogeochemistry: Geochemistry: Exploration, Environment, Analysis, v. 14, p. 139–148.

Piercey, S.J., Peter, J.M., Mortensen, J.K., Paradis, S., Murphy, D.C., and Tucker, T.L., 2008, Petrology and U-Pb geochronology of footwall porphyritic rhyolites from the Wolverine volcanogenic massive sulfide deposit, Yukon, Canada: Implications for the genesis of massive sulfide deposits in continental margin environments: Economic Geology, v. 103, p. 5–33.

Plafker, G., Nokleberg, W.J., and Lull, J.S., 1989, Bedrock geology and tectonic evolution of the Wrangellia, Peninsular, and Chugach terranes along the Trans-Alaska crustal transect in the Chugach Mountains and southern Copper River Basin, Alaska: Journal of Geophysical Research, v. 94, no. 84, p. 4255–4295.

Pontual, S., Merry, N., and Gamson, P., 1997, GMEX Volume 1: Spectral interpretation field manual: Ausspec International Pty. Ltd., Kew, Victoria 3101, Australia, 169 p.

Potts, P.J., Williams-Thorpe, O., and Webb, P.C., 1997, The Bulk Analysis of Silicate Rocks by Portable X-Ray Fluorescence: Effect of Sample Mineralogy in Relation to the Size of the Excited Volume: Journal of Geostandards and Geoanalysis, v. 21, p. 29–41.

Read, P.B., and Monger, J.W.H., 1976, Pre-Cenozoic Volcanic Assemblages of the Kluane and Alsek Ranges, Southwestern Yukon Territory: Geological Survey of Canada, Open File Report 381, 96 p.

Reid, R.R., 1993, Westmin Structure 18 and 20 level data: Westmin Resources Ltd, Internal Company Report, 48 p.

Rejebian, V.A., Harris, A.G., and Huebner, J.., 1987, Conodont color and textural alteration - An index to regional metamorphism, contact metamorphism, and hydrothermal alteration: Geological Society of America Bulletin, v. 99, p. 471–479.

Relvas, J.M.R.S., Barriga, F.J.A.S., and Longstaffe, F.J.., 2006, Hydrothermal Alteration and Mineralization in the Neves-Corvo Volcanic-Hosted Massive Sulfide Deposit, Portugal. II. Oxygen, hydrogen, and carbon isotopes: Economic Geology, v. 101, p. 791–804.

Richter, D.H., 1976, Geologic map of the Nabesna Quadrangle, Alaska: US Geological Survey, Map 1-932.

Rioux, M., Hacker, B., Mattinson, J., Kelemen, P., Blusztajn, J., and Gehrels, G., 2007, Magmatic development of an intra-oceanic arc: High-precision U-Pb zircon and whole-rock isotopic analyses from the accreted Talkeetna arc, south-central Alaska: Bulletin of the Geological Society of America, v. 119, no. 9–10, p. 1168–1184.

Robinson, M., 1994, Geology, Mineralization and Alteration of the Battle Zone, Buttle Lake Camp, Central Vancouver Island, Southwestern British Columbia: University of British Columbia, Unpublished MSc Thesis, 246 p.

Robinson, M., Godwin, C.I., and Stanley, C.R., 1996, Geology, lithogeochemistry, and alteration of the battle volcanogenic massive sulfide zone, Buttle Lake mining camp, Vancouver Island, British Columbia: Economic Geology, v. 91, no. 3, p. 527–548.

Rollinson, H., 1993, Using Geochemical Data: evaluation, presentation, interpretation: Pearson Education Limited, Harlow, Essex England, 352 p.

Ross, P., Bourke, A., and Fresia, B., 2014a, Improving lithological discrimination in exploration drill-cores using portable X-ray fluorescence measurements: (1) testing three Olympus Innov-X analysers on unprepared cores: Geochemistry: Exploration, Environment, Analysis, v. 14, p. 171–185.

Ross, P., Bourke, A., and Fresia, B., 2014b, Improving lithological discrimination in exploration drill-cores using portable X-ray fluorescence measurements: (2) applications to the Zn-Cu Matagami mining camp, Canada: Geochemistry: Exploration, Environment, Analysis, v. 14, p. 187–196.

Ross, P.S., Bourke, A., Mercier-Langevin, P., Lépine, S., Leclerc, F., and Boulerice, A., 2016, High-resolution physical properties, geochemistry, and alteration mineralogy for the host rocks of the Archean Lemoine auriferous volcanogenic massive sulfide deposit, Canada: Economic Geology, v. 111, no. 7, p. 1561–1574.

Rubatto, D., Williams, I.S., and Buick, I.S., 2001, Zircon and monazite response to prograde metamorphism in the Reynolds Range, central Australia: Contributions to Mineralogy and Petrology, v. 140, p. 458–468.

Ruks, T.W., 2015, Stratigraphic and paleotectonic studies of Paleozoic Wrangellia and its contained volcanogenic massive sulfide (VMS) occurrences, Vancouver Island, British Columbia, Canada: University of British Columbia, Unpublished PhD Thesis, 186 p.

Ruks, T., and Mortensen, J.K., 2007, Geological Setting of Volcanogenic Massive Sulphide Occurrences in the Middle Paleozoic Sicker Group of the Southeastern Cowichan Lake Uplift, Southern Vancouver Island: Geoscience BC, Paper 2007-1, p. 381-394.

Ruks, T., Mortensen, J.K., and Cordey, F., 2009, New Results of Geological Mapping and Micropaleontological and Lead Isotopic Studies of Volcanogenic Massive Sulphide-Hosting Stratigraphy of the Middle and Late Paleozoic Sicker and Buttle Lake Groups on Vancouver Island, British Columbia (NTS 92B/13, 92): Geoscience BC, Report 2010-1 p. 149-170.

Rusmore, M.E., and Cowan, D.S., 1985, Jurassic-Cretaceous rock units along the southern edge of the Wrangellia terrane on Vancouver Island: Can. J. Earth Sci, v. 22, no. 8, p. 1223–1232.

Sack, P.J., Berry, R.F., Meffre, S., Falloon, T.J., Gemmell, J.B., and Friedman, R.M., 2011, In situ location and U-Pb dating of small zircon grains in igneous rocks using laser ablation-

inductively coupled plasma-quadrupole mass spectrometry: Geochemistry Geophysics Geosystems, v. 12, 23 p.

Sack, P.J., and Lewis, L.L., 2013, Field-portable x-ray fluorescence spectrometer use in volcanogenic massive sulphide exploration with examples from the Touleary occurrence (MINFILE Occurrence 115O 176) in west-central Yukon, in MacFarlane, K.E., Norling, M.G., and Sack, P.J. eds., Yukon Exploration and Geology 2012, Yukon Geological Survey, p. 115–131.

Saleeby, J.B., 2000, Geochronologic investigations along the Alexander-Taku terrane boundary, southern Revillagigedo Island to Cape Fox areas, southeast Alaska, in Stowell, H.H. and McClelland, W.C. eds., Tectonics of the Coast Mountains, southeastern Alaska and British Columbia, Geological Society of America, p. 107–143.

Samson, S.D., McClelland, W.C., Patchett, P.J., Gehrels, G.E., and Anderson, R.G., 1989, Evidence from neodymium isotopes for mantle contributions to Phanerozoic crustal genesis in the Canadian Cordillera: Nature, v. 337, p. 705–709.

Samson, S.D., Patchett, P.J., McClelland, W.C., and Gehrels, G.E., 1991, Nd isotopic characterization of metamorphic rocks in the Coast Mountains, Alaskan and Canadian Cordillera: Ancient crust bounded by juvenile terranes: Tectonics, v. 10, no. 4, p. 770–780.

Schardt, C., and Large, R.R., 2009, New insights into the genesis of volcanic-hosted massive sulfide deposits on the seafloor from numerical modelling studies: Ore Geology Reviews, v. 35, p. 333–351.

Schmitz, M.D., and Schoene, B., 2007, Derivation of isotope ratios, errors, and error correlations for U-Pb geochronology using 205Pb-235U-(233U)-spiked isotope dilution thermal ionization mass spectrometric data: Geochemistry Geophysics Geosystems, v. 8, no. 8, p. 1–20.

Schoene, B., and Bowring, S.A., 2006, U–Pb systematics of the McClure Mountain syenite: thermochronological constraints on the age of the 40Ar / 39Ar standard MMhb: Contributions to Mineralogy and Petrology, v. 151, p. 615–630.

Scoates, J.S., and Friedman, R.M., 2008, Precise age of the platiniferous Merensky Reef, Bushveld Complex, South Africa, by the U-Pb zircon chemical abrasion ID-TIMS technique: Economic Geology, v. 103, no. 3, p. 465–471.

Seraphim, R.H., 1980, Western Mines - Myra, Lynx and Price deposits: CIM Bulletin, , no. December, p. 71–86.

Sinclair, B.J., 2000, Geology and genesis of the Battle Zone VHMS deposits, Myra Falls District, British Columbia, Canada: University of Tasmania, Unpublished PhD Thesis, 313 p.

Slack, J.F., Shanks III, W.C., Karl, S.M., Gemery, P.A., Bittenbender, P.E., and Ridley, W.I., 2005, Geochemical and sulfur-isotopic signatures of volcanogenic massive sulfide deposits on Prince of Wales Island and vicinity, southeastern Alaska: U.S. Geological Survey Professional Paper, v. 1732–C, p. 1–37.

Slama, J., Kosler, J., Condon, D.J., Crowley, J.L., Gerdes, A., Hanchar, J.M., Horstwood, M.S.A., Morris, G.A., Nasdala, L., Norberg, N., Schaltegger, U., Schoene, B., Tubrett, M., and Whitehouse, M.J., 2008, Plešovice zircon — A new natural reference material for U–Pb and

Hf isotopic microanalysis: Chemical Geology, v. 249, p. 1–35.

Sluggett, C.L., 2003, Uranium-lead age and geochemical constraints on Paleozoic and Early Mesozoic magmatism in Wrangellia Terrane, Saltspring Island, British Columbia: University of British Columbia, Unpublished BSc Honours Thesis, 56 p.

Smith, J.G., and MacKevett, E.M.J., 1970, The Skolai Group in the McCarthy B-4, C-4, C-5 Quadrangles, Wrangell Mountains, Alaska: US Geological Survey Bulletin 1274-Q, 26 p.

Soja, C.M., and Antoshkina, A.I., 1997, Coeval development of Silurian stromatolite reefs in Alaska and the Ural Mountains: Implications for paleogeography of the Alexander terrane: Geology, v. 25, no. 6, p. 539–542.

Solomon, M., 1976, "Volcanic" massive sulphide deposits and their host rocks: a review and an explanation, in Wolf, K.H. eds., Handbook of stratabound and stratiform ore deposits, Elsevier Scientific Publishing Company, Amsterdam, The Netherlands, p. 21–54.

Solomon, M., and Walshe, J.L., 1976, The Formation of Massive Sulfide Deposits on the Sea: Economic Geology, v. 74, p. 797–813.

Spear, F.S., 1993, Metamorphic Phase Equilibria and Pressure-Temperature-Time Paths: Mineralogical Society of America Monograph, 799 p.

Spry, P.G., Marshall, B., and Vokes, F.M. (eds.), 2000, Metamorphosed and Metamorphogenic Ore Deposits, in Reviews in Economic Geology Volume 11, Society of Economic Geologists, p. 310.

van Staal, C.R., Israel, S., McClelland, W.C., Mihalynuk, M.G., Nelson, J., and Joyce, N., 2010, New data and ideas on the Paleozoic-Triassic evolution of the insular superterrane of the North American Cordillera, in 2010 GSA Denver Annual Meeting, Geological Society of America, Denver, 54 p.

Stanton, R.L., 1972, Ore Petrology: McGraw-Hill Companies, 713 p.

Sunit, K.A., and Peter, J.M., 1977, Origin of Massive Sulfide Deposits at Ducktown, Tennessee: An oxygen, carbon and hydrogen isotope study: Economic Geology, v. 72, p. 1245–1268.

Taylor, C.D., Premo, W.R., Meier, A.L., and Taggart, J.J.E., 2008, The metallogeny of Late Triassic rifting of the Alexander terrane in southeastern Alaska and northwestern British Columbia: Economic Geology, v. 103, p. 89–115.

Templeman-Kluit, D.J., 1974, Reconnaissance geology of Aishihik Lak, Snag and part of Stewart River map-areas, west-central Yukon: Geological Survey of Canada, Paper 73-41, 97 p.

Thirlwall, M.F., 2000, Inter-laboratory and other errors in Pb isotope analyses investigated using a 207Pb–204Pb double spike: Chemical Geology, v. 163, no. 1–4, p. 299–322.

Thompson, A.J., Hauff, P.L., and Robitaille, A.J., 1999, SEG Newsletter - Alteration Mapping in Exploration: Application of Short-Wave Infrared (SWIR) Spectroscopy: SEG Newsletter, v. 39, no. October, p. 1, 16–27.

Tindle, A.G., and Webb, P.C., 1990, Estimation of lithium contents in trioctahedral micas using microprobe data : application to micas from granitic rocks: European Journal of Mineralogy, v. 2, p. 595–610.

Le Vaillant, M., Barnes, S.J., Fisher, L., Fiorentini, M.L., and Caruso, S., 2014, Use and calibration of portable X-Ray fluorescence analysers: application to lithogeochemical exploration for komatiite-hosted nickel sulphide deposits: Geochemistry: Exploration, Environment, Analysis, v. 14, no. 3, p. 199–209.

Vikentyev, I. V., 2006, Precious metal and telluride mineralogy of large volcanic-hosted massive sulfide deposits in the Urals: Mineralogy and Petrology, v. 87, p. 305–326.

Vikentyev, I. V., Belogub, E. V., Novoselov, K.A., and Moloshag, V.P., 2017, Metamorphism of volcanogenic massive sulphide deposits in the Urals. Ore geology: Ore Geology Reviews, v. 85, p. 30–63.

Vokes, F.M., 1966, On the possible modes of origin of the Caledonian sulfide ore deposit at Bleikvassli, Norland, Norway: Economic Geology, v. 61, p. 1130–1139.

Walker, R.R., 1985, Westmin Resources' Massive Sulphide Deposits, Vancouver Island, in Geological Society of America, Cordillerian Section Meeting, Geological Society of America, 13 p.

Walker, J.D., Geissman, J.W., Bowring, S.A., and Babcok, L.E., 2012, GSA Geologic time scale v. 4.0: Geological Society of America.

Warren, I., Simmons, S.F., and Mauk, J.L., 2007, Whole-Rock Geochemical Techniques for Evaluating Hydrothermal Alteration, Mass Changes, and Compositional Gradients Associated with Epithermal Au-Ag Mineralization: Economic Geology, v. 102, p. 923–948.

Watt, G.R., and Harley, S.L., 1993, Accessory phase controls on the geochemistry of crustal melts and restites produced during water-undersaturated partial melting: Contributions to Mineralogy and Petrology, v. 114, p. 550–566.

Welford, J.K., Clowes, R.M., Ellis, R.M., Spence, G.D., Asudeh, I., and Hajnal, Z., 2001, Lithospheric structure across the craton – Cordilleran transition of northeastern British Columbia 1: Can. J. Earth Sci, v. 1189, no. 38, p. 1169–1189.

Wheeler, J.O., and McFeely, P., 1991, Tectonic Assemblage Map of the Canadian Cordillera and adjacent parts of the United States of American: Geological Survey of Canada, Map 1712A.

Wiedenbeck, M., Alle, P., Corfu, F., Griffin, W.L., Meier, M., Oberli, F., Von Quadt, A., Roddick, J.C., and Spiegel, W., 1995, Three natural zircon standards for U-Th-Pb, Lu-Hf, Trace element and REE analyses: Geostandards Newsletter, v. 19, no. 1, p. 1–23.

Williams, M.L., Jercinovic, M.J., and Hetherington, C.J., 2007, Microprobe Monazite Geochronology: Understanding Geologic Processes by Integrating Composition and Chronology: Annu. Rev. Earth Planet. Sci, v. 35, p. 137–175.

Wilson, G., 1993, Mineralogy of sulphide ores from the H-W Kuroko deposit, British Columbia, Part II: multi-element analysis of the ore minerals: Westmin Resources Ltd., Internal Company Report, 42 p.

Wilson, A.D., 1964, The sampling of silicate rock powders for chemical analysis: Analyst, v. 89, p. 18–30.

Yole, R.W., 1969, Upper Paleozoic stratigraphy of Vancouver Island, British Columbia, in Geological Association of Canada, p. 30–40.

Yorath, C.J., 1991, Upper Jurassic To Paleogene Assemblages, in Gabrielse, H. and Yorath, C.J. eds., Geology of the Cordilleran Orogen in Canada, Geological Survey of Canada, p. 331–371.

Yorath, C.J., Brown, A.S., and Massey, N.W.D., 1999, Lithoprobe, Southern Vancouver Island, British Columbia: Geology: Geological Survey of Canada, Bulletin 498, 145 p.

Yuan, Z., Cheng, Q., Xia, Q., Yao, L., Chen, Z., Zuo, R., and Xu, D., 2014, Spatial patterns of geochemical elements measured on rock surfaces by portable X-ray fluorescence: application to hand specimens and rock outcrops: Geochemistry: Exploration, Environment, Analysis, v. 14, no. 3, p. 265–276.

Appendix A:

Sample Catalogue

This section provides a list of collected samples, including a general rock description and summary of sample preparations. Table A.1 presents samples collected from drill core and Table A.2 is a list of samples collected from underground and surface exposures. Sample locations for drill core samples include the drill hole number and down hole depth in metres. Sample locations for underground and surface samples are presented in mine co-ordinates (mE and mN) and elevation is in metres above sea level.

Table A.1 Drill Hole Sample Catalogue

Field ID	UTAS ID	Area	Rock Code	Strat Member	DDH	Depth (m)	Preparation
TS-001	182296	WBA	Avc	Hanging Wall And	BG18-3901	3.0	R; SWIR
TS-002	182297	WBA	Avc	Hanging Wall And	BG18-3901	8.0	R; SWIR
TS-003	182298	WBA	Avc	Hanging Wall And	BG18-3901	15.2	R; SWIR
TS-004	182299	WBA	Avc	Hanging Wall And	BG18-3901	18.3	R; SWIR
TS-005	182300	WBA	Avc	Hanging Wall And	BG18-3901	21.3	R; SWIR
TS-006	182301	WBA	Avc	Hanging Wall And	BG18-3901	24.4	R; SWIR
TS-007	182302	WBA	Avc	Hanging Wall And	BG18-3901	27.4	R; SWIR
TS-008	182303	WBA	Avc	Hanging Wall And	BG18-3901	30.5	R; SWIR
TS-009	182304	WBA	Avc	Hanging Wall And	BG18-3901	33.5	R; SWIR
TS-010	182305	WBA	Avc	Hanging Wall And	BG18-3901	36.6	R; SWIR
TS-011	182306	WBA	Avc	Hanging Wall And	BG18-3901	39.6	R; SWIR
TS-012	182307	WBA	Avc	Hanging Wall And	BG18-3901	42.7	R; SWIR
TS-013	182308	WBA	Avc	Hanging Wall And	BG18-3901	45.7	R; SWIR
TS-014	182309	WBA	Avc	Hanging Wall And	BG18-3901	48.7	R; SWIR
TS-015	182310	WBA	Avc	Hanging Wall And	BG18-3901	51.8	R; SWIR
TS-016	182311	WBA	Avc	Hanging Wall And	BG18-3901	55.0	R; SWIR
TS-017	182312	WBA	Avc	Hanging Wall And	BG18-3901	58.1	R; SWIR
TS-018	182313	WBA	Avc	Hanging Wall And	BG18-3901	80.9	R; SWIR
TS-019	182314	WBA	Af	H-W	BG18-3901	70.1	R; pXRF; SWIR
TS-020	182315	WBA	Af	H-W	BG18-3901	73.2	R; pXRF; SWIR
TS-021	182316	WBA	Af	H-W	BG18-3901	82.3	R; pXRF; SWIR
TS-022	182317	WBA	Af	H-W	BG18-3901	85.3	R; pXRF; SWIR
TS-023	182318	WBA	Af	H-W	BG18-3901	89.2	R; pXRF; SWIR
TS-024	182319	WBA	Avc	Hanging Wall And	BG18-3901	91.6	R; SWIR
TS-025	182320	WBA	Fvc	H-W	BG18-3901	97.5	R; SWIR
TS-026	182321	WBA	Fvc	H-W	BG18-3901	101.6	R; SWIR
TS-027	182322	WBA	Fvc	H-W	BG18-3901	107.0	R; SWIR
TS-028	182323	WBA	Fvc	H-W	BG18-3901	110.0	R; SWIR
TS-029	182324	WBA	Fvc	H-W	BG18-3901	115.8	R; SWIR
TS-030	182325	WBA	Fvc	H-W	BG18-3901	119.0	R; SWIR
TS-031	182326	WBA	Fvc	H-W	BG18-3901	134.1	R; SWIR
TS-032	182327	WBA	PA	Price Andesite	BG18-3901	140.2	R; pXRF; SWIR
TS-033	182328	WBA	PA	Price Andesite	BG18-3901	159.5	R; pXRF; SWIR
TS-034	182329	WBA	PA	Price Andesite	BG18-3901	203.7	R; pXRF; SWIR
TS-035	182330	WBA	Avc	Hanging Wall And	BG18-3902	9.7	R; pXRF; SWIR
TS-036	182331	WBA	Avc	Hanging Wall And	BG18-3902	13.9	R; pXRF; SWIR
TS-037	182332	WBA	Avc	Hanging Wall And	BG18-3902	17.3	R; pXRF; SWIR
TS-038	182333	WBA	Avc	Hanging Wall And	BG18-3902	20.6	R; pXRF; SWIR
TS-039	182334	WBA	Avc	Hanging Wall And	BG18-3902	25.1	R; pXRF; SWIR
TS-040	182335	WBA	Avc	Hanging Wall And	BG18-3902	29.2	R; pXRF; SWIR
TS-041	182336	WBA	Avc	Hanging Wall And	BG18-3902	33.5	R; pXRF; SWIR
TS-042	182337	WBA	Avc	Hanging Wall And	BG18-3902	37.0	R; pXRF; SWIR
TS-043	182338	WBA	Avc	Hanging Wall And	BG18-3902	40.3	R; pXRF; SWIR
TS-044	182339	WBA	Avc	Hanging Wall And	BG18-3902	45.7	R; pXRF; SWIR
TS-045	182340	WBA	Avc	Hanging Wall And	BG18-3902	50.0	R; pXRF; SWIR
TS-046	182341	WBA	Avc	Hanging Wall And	BG18-3902	54.4	R; pXRF; SWIR
TS-047	182342	WBA	Avc	Hanging Wall And	BG18-3902	60.0	R; pXRF; SWIR
TS-048	182343	WBA	Avc	Hanging Wall And	BG18-3902	61.1	R; pXRF; SWIR
TS-049	182344	WBA	Avc	Hanging Wall And	BG18-3902	70.6	R; pXRF; SWIR
TS-050	182345	WBA	Af	H-W	BG18-3902	77.5	R; pXRF; SWIR
TS-051	182346	WBA	Af	H-W	BG18-3902	80.2	R; LM; pXRF; SWIR
TS-052	182347	WBA	Fvc	H-W	BG18-3902	91.4	R; pXRF; SWIR
TS-053	182348	WBA	Fvc	H-W	BG18-3902	95.5	R; pXRF; SWIR

Table A.1 Continued.

Field ID	UTAS ID	Area	Rock Code	Strat Member	DDH	Depth (m)	Preparation
TS-054	182349	WBA	Fvc	H-W	BG18-3902	102.3	R; pXRF; SWIR
TS-055	182350	WBA	Fvc	H-W	BG18-3902	103.6	R; pXRF; SWIR
TS-056	182351	WBA	Fvc	H-W	BG18-3902	106.7	R; pXRF; SWIR
TS-057	182352	WBA	Fvc	H-W	BG18-3902	109.7	R; pXRF; SWIR
TS-058	182353	WBA	Fvc	H-W	BG18-3902	112.8	R; pXRF; SWIR
TS-059	182354	WBA	Fvc	H-W	BG18-3902	116.5	R; pXRF; SWIR
TS-060	182355	WBA	Fvc	H-W	BG18-3902	119.4	R; pXRF; SWIR
TS-061	182356	WBA	Fvc	H-W	BG18-3902	122.0	R; pXRF; SWIR
TS-062	182357	WBA	Fvc	H-W	BG18-3902	130.5	R; pXRF; SWIR
TS-063	182358	WBA	Bvc	H-W	BG18-3902	133.3	R; pXRF; SWIR
TS-064	182359	WBA	Bvc	H-W	BG18-3902	135.0	R; pXRF; SWIR
TS-065	182360	WBA	Bvc	H-W	BG18-3902	138.2	R; pXRF; SWIR
TS-066	182361	WBA	PA	Price Andesite	BG18-3902	142.9	R; pXRF; SWIR
TS-067	182362	WBA	PA	Price Andesite	BG18-3902	148.4	PD, LM, WR; pXRF; SWIR
TS-068	182363	WBA	PA	Price Andesite	BG18-3902	156.5	R; pXRF; SWIR
TS-069	182364	WBA	PA	Price Andesite	BG18-3902	164.6	R; pXRF; SWIR
TS-070	182365	WBA	PA	Price Andesite	BG18-3902	169.6	R; pXRF; SWIR
TS-071	182366	WBA	PA	Price Andesite	BG18-3902	176.4	R; pXRF; SWIR
TS-072	182367	WBA	PA	Price Andesite	BG18-3902	183.6	R; pXRF; SWIR
TS-073	182368	WBA	PA	Price Andesite	BG18-3902	191.3	R; pXRF; SWIR
TS-074	182369	WBA	PA	Price Andesite	BG18-3902	201.2	R; pXRF; SWIR
TS-075	182370	WBA	PA	Price Andesite	BG18-3902	213.4	R; pXRF; SWIR
TS-076	182371	WBA	PA	Price Andesite	BG18-3902	222.0	R; pXRF; SWIR
TS-077	182372	WBA	Avc	Hanging Wall And	BG18-3903	12.7	R; SWIR
TS-078	182373	WBA	Avc	Hanging Wall And	BG18-3903	17.3	R; SWIR
TS-079	182374	WBA	Avc	Hanging Wall And	BG18-3903	19.3	R; SWIR
TS-080	182375	WBA	Avc	Hanging Wall And	BG18-3903	21.5	R; SWIR
TS-081	182376	WBA	Avc	Hanging Wall And	BG18-3903	24.4	R; SWIR
TS-082	182377	WBA	Avc	Hanging Wall And	BG18-3903	27.4	R; SWIR
TS-083	182378	WBA	Avc	Hanging Wall And	BG18-3903	30.0	R; SWIR
TS-084	182379	WBA	Avc	Hanging Wall And	BG18-3903	34.8	R; SWIR
TS-085	182380	WBA	Avc	Hanging Wall And	BG18-3903	40.0	R; SWIR
TS-086	182381	WBA	Avc	Hanging Wall And	BG18-3903	42.7	R; SWIR
TS-087	182382	WBA	Avc	Hanging Wall And	BG18-3903	45.5	R; SWIR
TS-088	182383	WBA	Avc	Hanging Wall And	BG18-3903	48.9	R; SWIR
TS-089	182384	WBA	Avc	Hanging Wall And	BG18-3903	52.8	R; SWIR
TS-090	182385	WBA	Avc	Hanging Wall And	BG18-3903	61.5	R; SWIR
TS-091	182386	WBA	Avc	Hanging Wall And	BG18-3903	64.0	R; SWIR
TS-092	182387	WBA	Avc	Hanging Wall And	BG18-3903	67.5	R; SWIR
TS-093	182388	WBA	Af	H-W	BG18-3903	74.2	R; pXRF; SWIR
TS-094	182389	WBA	Af	H-W	BG18-3903	79.0	R; pXRF; SWIR
TS-095	182390	WBA	Af	H-W	BG18-3903	82.1	R; pXRF; SWIR
TS-096	182391	WBA	Af	H-W	BG18-3903	85.7	R; pXRF; SWIR
TS-097	182392	WBA	Af	H-W	BG18-3903	90.7	R; pXRF; SWIR
TS-098	182393	WBA	Fvc	H-W	BG18-3903	92.1	R; SWIR
TS-099	182394	WBA	Fvc	H-W	BG18-3903	94.5	R; SWIR
TS-100	182395	WBA	Fvc	H-W	BG18-3903	98.5	R; SWIR
TS-101	182396	WBA	Fvc	H-W	BG18-3903	100.3	R; SWIR
TS-102	182397	WBA	Fvc	H-W	BG18-3903	107.9	R; SWIR
TS-103	182398	WBA	Fvc	H-W	BG18-3903	112.2	R; SWIR
TS-104	182399	WBA	Fvc	H-W	BG18-3903	118.3	R; SWIR
TS-105	182400	WBA	Fvc	H-W	BG18-3903	131.1	R; SWIR
TS-106	182401	WBA	Fvc	H-W	BG18-3903	134.1	R; SWIR

Table A.1 Continued.

Field ID	UTAS ID	Area	Rock Code	Strat Member	DDH	Depth (m)	Preparation
TS-107	182402	WBA	Fvc	H-W	BG18-3903	137.2	R; SWIR
TS-108	182403	WBA	Fvc	H-W	BG18-3903	140.2	R; SWIR
TS-109	182404	WBA	Fvc	H-W	BG18-3903	143.3	R; SWIR
TS-110	182405	WBA	Fvc	H-W	BG18-3903	145.1	R; SWIR
TS-111	182406	WBA	Avc	Hanging Wall And	BG18-3298	9.3	R; SWIR
TS-112	182407	WBA	Avc	Hanging Wall And	BG18-3298	11.7	R; SWIR
TS-113	182408	WBA	Avc	Hanging Wall And	BG18-3298	13.6	R; SWIR
TS-114	182409	WBA	Avc	Hanging Wall And	BG18-3298	16.5	R; SWIR
TS-115	182410	WBA	Avc	Hanging Wall And	BG18-3298	19.3	R; SWIR
TS-116	182411	WBA	Avc	Hanging Wall And	BG18-3298	20.7	R; SWIR
TS-117	182412	WBA	Avc	Hanging Wall And	BG18-3298	23.0	R; SWIR
TS-118	182413	WBA	Avc	Hanging Wall And	BG18-3298	27.3	R; SWIR
TS-119	182414	WBA	Avc	Hanging Wall And	BG18-3298	29.2	R; SWIR
TS-120	182415	WBA	Avc	Hanging Wall And	BG18-3298	32.2	R; SWIR
TS-121	182416	WBA	Avc	Hanging Wall And	BG18-3298	34.5	R; SWIR
TS-122	182417	WBA	Avc	Hanging Wall And	BG18-3298	37.8	R; SWIR
TS-123	182418	WBA	Avc	Hanging Wall And	BG18-3298	44.0	R; SWIR
TS-124	182419	WBA	Avc	Hanging Wall And	BG18-3298	46.8	R; SWIR
TS-125	182420	WBA	Af	H-W	BG18-3298	63.7	R; pXRF; SWIR
TS-126	182421	WBA	Af	H-W	BG18-3298	70.6	R; pXRF; SWIR
TS-127	182422	WBA	QFP	H-W	BG18-3298	152.4	R; SWIR
TS-128	182423	WBA	QFP	H-W	BG18-3298	155.8	R; SWIR
TS-129	182424	WBA	Fvc	H-W	BG18-3298	158.6	R; SWIR
TS-130	182425	WBA	Fvc	H-W	BG18-3298	161.5	R; SWIR
TS-131	182426	WBA	Fvc	H-W	BG18-3298	164.6	R; SWIR
TS-132	182427	WBA	Fvc	H-W	BG18-3298	167.7	R; SWIR
TS-133	182428	WBA	Bvc	H-W	BG18-3298	173.4	R; SWIR
TS-134	182429	WBA	Bvc	H-W	BG18-3298	176.8	R; SWIR
TS-135	182430	WBA	Bvc	H-W	BG18-3298	180.0	R; SWIR
TS-136	182431	WBA	Bvc	H-W	BG18-3298	183.3	R; SWIR
TS-137	182432	WBA	Bvc	H-W	BG18-3298	186.0	R; SWIR
TS-138	182433	WBA	PA	Price Andesite	BG18-3298	201.2	R; pXRF; SWIR
TS-139	182434	WBA	PA	Price Andesite	BG18-3298	207.4	R; pXRF; SWIR
TS-140	182435	WBA	PA	Price Andesite	BG18-3298	210.5	R; pXRF; SWIR
TS-141	182436	WBA	PA	Price Andesite	BG18-3298	222.4	R; pXRF; SWIR
TS-142	182437	WBA	PA	Price Andesite	BG18-3298	234.7	R; pXRF; SWIR
TS-143	182438	WBA	Bvc	H-W	BG18-3299	178.3	R; SWIR
TS-144	182439	WBA	Bvc	H-W	BG18-3299	181.6	R; SWIR
TS-145	182440	WBA	Bvc	H-W	BG18-3299	184.5	R; SWIR
TS-146	182441	WBA	Bvc	H-W	BG18-3299	187.2	R; SWIR
TS-147	182442	WBA	Bvc	H-W	BG18-3299	196.6	R; SWIR
TS-148	182443	WBA	Bvc	H-W	BG18-3299	199.5	R; SWIR
TS-149	182444	WBA	PA	Price Andesite	BG18-3299	202.6	R; pXRF; SWIR
TS-150	182445	WBA	PA	Price Andesite	BG18-3299	205.7	R; pXRF; SWIR
TS-151	182446	WBA	PA	Price Andesite	BG18-3299	211.8	R; pXRF; SWIR
TS-152	182447	WBA	PA	Price Andesite	BG18-3299	214.9	R; pXRF; SWIR
TS-153	182448	WBA	PA	Price Andesite	BG18-3299	223.9	R; pXRF; SWIR
TS-154	182449	WBA	PA	Price Andesite	BG18-3299	228.6	R; pXRF; SWIR
TS-155	182450	WBA	PA	Price Andesite	BG18-3299	231.6	R; pXRF; SWIR
TS-156	182451	WBA	Af	H-W	BG18-3769	3.0	R; pXRF; SWIR
TS-157	182452	WBA	Af	H-W	BG18-3769	6.1	R; pXRF; SWIR
TS-158	182453	WBA	Af	H-W	BG18-3769	12.1	R; pXRF; SWIR
TS-159	182454	WBA	Af	H-W	BG18-3769	15.2	R; pXRF; SWIR

Table A.1 Continued.

Field ID	UTAS ID	Area	Rock Code	Strat Member	DDH	Depth (m)	Preparation
TS-160	182455	WBA	Af	H-W	BG18-3769	21.4	R; pXRF; SWIR
TS-161	182456	WBA	Af	H-W	BG18-3769	24.4	R; pXRF; SWIR
TS-162	182457	WBA	Af	H-W	BG18-3769	29.2	R; pXRF; SWIR
TS-163	182458	WBA	Af	H-W	BG18-3769	33.2	R; pXRF; SWIR
TS-164	182459	WBA	Avc	Hanging Wall And	BG18-3769	38.6	R; pXRF; SWIR
TS-165	182460	WBA	QFP	H-W	BG18-3769	51.8	R; pXRF; SWIR
TS-167	182461	WBA	QFP	H-W	BG18-3769	54.9	R; pXRF; SWIR
TS-168	182462	WBA	QFP	H-W	BG18-3769	58.1	R; pXRF; SWIR
TS-169	182463	WBA	QFP	H-W	BG18-3769	61.0	R; pXRF; SWIR
TS-170	182464	WBA	QFP	H-W	BG18-3769	64.0	R; pXRF; SWIR
TS-171	182465	WBA	QFP	H-W	BG18-3769	68.5	R; pXRF; SWIR
TS-172	182466	WBA	QFP	H-W	BG18-3769	71.7	R; pXRF; SWIR
TS-173	182467	WBA	QFP	H-W	BG18-3769	75.7	R; pXRF; SWIR
TS-174	182468	WBA	QFP	H-W	BG18-3769	77.7	R; pXRF; SWIR
TS-175	182469	WBA	QFP	H-W	BG18-3769	81.0	R; pXRF; SWIR
TS-176	182470	WBA	QFP	H-W	BG18-3769	83.8	R; pXRF; SWIR
TS-177	182471	WBA	QFP	H-W	BG18-3769	87.0	R; pXRF; SWIR
TS-178	182472	WBA	Fvc	H-W	BG18-3769	96.0	R; pXRF; SWIR
TS-179	182473	WBA	Fvc	H-W	BG18-3769	102.1	R; pXRF; SWIR
TS-180	182474	WBA	Fvc	H-W	BG18-3769	105.4	R; pXRF; SWIR
TS-181	182475	WBA	Fvc	H-W	BG18-3769	108.2	R; pXRF; SWIR
TS-182	182476	WBA	PA	Price Andesite	BG18-3769	123.4	R; LM; pXRF; SWIR
TS-183	182477	WBA	PA	Price Andesite	BG18-3769	126.6	R; pXRF; SWIR
TS-184	182478	WBA	PA	Price Andesite	BG18-3769	129.7	R; pXRF; SWIR
TS-185	182479	WBA	PA	Price Andesite	BG18-3769	132.8	R; pXRF; SWIR
TS-186	182480	WBA	PA	Price Andesite	BG18-3769	135.6	R; pXRF; SWIR
TS-187	182481	WBA	PA	Price Andesite	BG18-3769	138.7	R; pXRF; SWIR
TS-188	182482	WBA	PA	Price Andesite	BG18-3769	141.6	R; pXRF; SWIR
TS-189	182483	WBA	PA	Price Andesite	BG18-3769	144.7	R; pXRF; SWIR
TS-190	182484	WBA	PA	Price Andesite	BG18-3769	148.0	R; pXRF; SWIR
TS-191	182485	WBA	PA	Price Andesite	BG18-3769	150.9	R; LM; pXRF; SWIR
TS-192	182486	WBA	PA	Price Andesite	BG18-3769	159.0	R; pXRF; SWIR
TS-193	182487	WBA	PA	Price Andesite	BG18-3769	163.2	R; pXRF; SWIR
TS-194	182488	WBA	PA	Price Andesite	BG18-3769	167.4	R; pXRF; SWIR
TS-195	182489	WBA	PA	Price Andesite	BG18-3769	170.5	R; pXRF; SWIR
TS-196	182490	WBA	PA	Price Andesite	BG18-3769	175.2	R; pXRF; SWIR
TS-197	182491	WBA	Bvc	H-W	BG18-3769	187.6	R; pXRF; SWIR
TS-198	182492	WBA	Bvc	H-W	BG18-3769	190.5	R; pXRF; SWIR
TS-199	182493	WBA	Bvc	H-W	BG18-3769	193.5	LM; pXRF; SWIR
TS-200	182494	WBA	PA	Price Andesite	BG18-3769	205.7	R; pXRF; SWIR
TS-201	182495	WBA	PA	Price Andesite	BG18-3769	211.8	R; pXRF; SWIR
TS-202	182496	WBA	PA	Price Andesite	BG18-3769	217.9	R; pXRF; SWIR
TS-203	182497	RZN	QFP	H-W	RN18-0104	3.1	R; SWIR
TS-204	182498	RZN	QFP	H-W	RN18-0104	6.2	R; SWIR
TS-205	182499	RZN	QFP	H-W	RN18-0104	9.2	R; SWIR
TS-206	182500	RZN	QFP	H-W	RN18-0104	12.2	R; SWIR
TS-207	182501	RZN	QFP	H-W	RN18-0104	15.2	R; SWIR
TS-208	182502	RZN	QFP	H-W	RN18-0104	16.5	R; SWIR
TS-209	182503	RZN	QFP	H-W	RN18-0104	18.4	R; SWIR
TS-210	182504	RZN	QFP	H-W	RN18-0104	21.3	R; SWIR
TS-211	182505	RZN	QFP	H-W	RN18-0104	25.6	R; SWIR
TS-212	182506	RZN	QFP	H-W	RN18-0104	28.4	R; SWIR
TS-213	182507	RZN	QFP	H-W	RN18-0104	31.0	R; SWIR

Table A.1 Continued.

Field ID	UTAS ID	Area	Rock Code	Strat Member	DDH	Depth (m)	Preparation
TS-214	182508	RZN	QFP	H-W	RN18-0104	33.5	R; SWIR
TS-215	182509	RZN	QFP	H-W	RN18-0104	36.6	R; SWIR
TS-216	182510	RZN	QFP	H-W	RN18-0104	39.7	R; SWIR
TS-217	182511	RZN	QFP	H-W	RN18-0104	42.7	R; SWIR
TS-218	182512	RZN	QFP	H-W	RN18-0104	45.7	R; SWIR
TS-219	182513	RZN	QFP	H-W	RN18-0104	52.3	R; SWIR
TS-220	182514	RZN	QFP	H-W	RN18-0104	57.6	R; SWIR
TS-221	182515	RZN	Fvc	H-W	RN18-0104	62.5	R; SWIR
TS-222	182516	RZN	Fvc	H-W	RN18-0104	65.5	R; SWIR
TS-223	182517	RZN	Fvc	H-W	RN18-0104	68.5	R; SWIR
TS-224	182518	RZN	QFP	H-W	RN18-0104	71.6	R; SWIR
TS-225	182519	RZN	QFP	H-W	RN18-0104	74.7	R; SWIR
TS-226	182520	RZN	QFP	H-W	RN18-0104	80.7	R; SWIR
TS-227	182521	RZN	Fvc	H-W	RN18-0104	83.7	R; SWIR
TS-228	182522	RZN	Fvc	H-W	RN18-0104	87.0	R; SWIR
TS-229	182523	RZN	Fvc	H-W	RN18-0104	94.0	R; SWIR
TS-230	182524	RZN	Fvc	H-W	RN18-0104	102.2	R; SWIR
TS-231	182525	RZN	Fvc	H-W	RN18-0104	105.3	R; SWIR
TS-232	182526	RZN	Avc	Hanging Wall And	RN18-0104	113.8	R; SWIR
TS-233	182527	RZN	Avc	Hanging Wall And	RN18-0104	118.6	R; SWIR
TS-234	182528	RZN	Avc	Hanging Wall And	RN18-0104	122.1	R; SWIR
TS-235	182529	RZN	Avc	Hanging Wall And	RN18-0104	129.5	R; SWIR
TS-236	182530	RZN	Avc	Hanging Wall And	RN18-0104	132.6	R; SWIR
TS-237	182531	RZN	Avc	Hanging Wall And	RN18-0104	135.6	R; SWIR
TS-238	182532	RZN	Avc	Hanging Wall And	RN18-0104	146.5	R; SWIR
TS-239	182533	WBA	Avc	Hanging Wall And	BG18-3321a	10.5	R; SWIR
TS-240	182534	WBA	Avc	Hanging Wall And	BG18-3321a	13.7	R; SWIR
TS-241	182535	WBA	Avc	Hanging Wall And	BG18-3321a	16.8	R; SWIR
TS-242	182536	WBA	Avc	Hanging Wall And	BG18-3321a	22.5	R; SWIR
TS-243	182537	WBA	Avc	Hanging Wall And	BG18-3321a	26.2	R; SWIR
TS-244	182538	WBA	Af	H-W	BG18-3321a	29.3	R; SWIR
TS-245	182539	WBA	Avc	Hanging Wall And	BG18-3321a	41.1	R; SWIR
TS-246	182540	WBA	QFP	H-W	BG18-3321a	65.5	R; SWIR
TS-247	182541	WBA	QFP	H-W	BG18-3321a	73.5	R; SWIR
TS-248	182542	WBA	QFP	H-W	BG18-3321a	80.8	R; SWIR
TS-249	182543	WBA	Fvc	H-W	BG18-3321a	83.8	R; SWIR
TS-250	182544	WBA	Fvc	H-W	BG18-3321a	86.8	R; SWIR
TS-251	182545	WBA	Fvc	H-W	BG18-3321a	89.9	R; SWIR
TS-252	182546	WBA	Fvc	H-W	BG18-3321a	96.0	R; SWIR
TS-253	182547	WBA	Fvc	H-W	BG18-3321a	99.1	R; SWIR
TS-254	182548	WBA	Fvc	H-W	BG18-3321a	103.1	R; SWIR
TS-255	182549	WBA	Fvc	H-W	BG18-3321a	121.9	R; SWIR
TS-256	182550	WBA	Fvc	H-W	BG18-3321a	125.0	R; SWIR
TS-257	182551	WBA	Fvc	H-W	BG18-3321a	132.8	R; SWIR
TS-258	182552	WBA	Fvc	H-W	BG18-3321a	137.2	R; SWIR
TS-259	182553	WBA	Fvc	H-W	BG18-3321a	145.5	R; SWIR
TS-260	182554	WBA	Fvc	H-W	BG18-3321a	147.5	R; SWIR
TS-261	182555	WBA	Fvc	H-W	BG18-3321a	150.9	R; SWIR
TS-262	182556	WBA	Fvc	H-W	BG18-3321a	156.5	R; SWIR
TS-263	182557	WBA	PA	Price Andesite	BG18-3321a	157.0	R; pXRF; SWIR
TS-264	182558	WBA	PA	Price Andesite	BG18-3321a	161.2	R; pXRF; SWIR
TS-265	182559	WBA	PA	Price Andesite	BG18-3321a	170.4	PD; LM; WR; pXRF; SWIR
TS-266	182560	WBA	PA	Price Andesite	BG18-3321a	175.5	R; pXRF; SWIR

Table A.1 Continued.

Field ID	UTAS ID	Area	Rock Code	Strat Member	DDH	Depth (m)	Preparation
TS-267	182561	WBA	PA	Price Andesite	BG18-3321a	181.5	LM; pXRF; SWIR
TS-268	182562	WBA	PA	Price Andesite	BG18-3321a	187.5	R; pXRF; SWIR
TS-269	182563	WBA	PA	Price Andesite	BG18-3321a	193.5	R; pXRF; SWIR
TS-270	182564	WBA	PA	Price Andesite	BG18-3321a	199.6	R; pXRF; SWIR
TS-271	182565	WBA	PA	Price Andesite	BG18-3321a	206.0	R; pXRF; SWIR
TS-272	182566	WBA	PA	Price Andesite	BG18-3321a	211.8	R; pXRF; SWIR
TS-273	182567	WBA	PA	Price Andesite	BG18-3321a	218.9	R; pXRF; SWIR
TS-274	182568	WBA	PA	Price Andesite	BG18-3321a	227.1	R; pXRF; SWIR
TS-275	182569	WBA	PA	Price Andesite	BG18-3321a	233.2	R; pXRF; SWIR
TS-276	182570	WBA	PA	Price Andesite	BG18-3321a	239.2	R; pXRF; SWIR
TS-277	182571	WBA	Af	H-W	BG18-3321	4.5	R; pXRF; SWIR
TS-278	182572	WBA	Af	H-W	BG18-3321	10.1	R; pXRF; SWIR
TS-279	182573	WBA	Af	H-W	BG18-3321	15.2	R; pXRF; SWIR
TS-280	182574	WBA	Af	H-W	BG18-3321	18.3	R; pXRF; SWIR
TS-281	182575	WBA	Af	H-W	BG18-3321	21.4	R; pXRF; SWIR
TS-282	182576	WBA	Af	H-W	BG18-3321	24.6	R; pXRF; SWIR
TS-283	182577	WBA	Af	H-W	BG18-3321	27.6	R; SWIR
TS-284	182578	WBA	Af	H-W	BG18-3321	30.5	R; SWIR
TS-285	182579	WBA	Af	H-W	BG18-3321	44.2	R; SWIR
TS-286	182580	WBA	Af	H-W	BG18-3321	48.8	R; SWIR
TS-287	182581	WBA	Af	H-W	BG18-3321	51.7	R; SWIR
TS-288	182582	WBA	QFP	H-W	BG18-3321	54.8	R; SWIR
TS-289	182583	WBA	QFP	H-W	BG18-3321	58.9	R; SWIR
TS-290	182584	WBA	QFP	H-W	BG18-3321	61.0	R; SWIR
TS-291	182585	WBA	QFP	H-W	BG18-3321	65.0	R; SWIR
TS-292	182586	WBA	QFP	H-W	BG18-3321	68.1	R; SWIR
TS-293	182587	WBA	QFP	H-W	BG18-3321	70.4	R; SWIR
TS-294	182588	WBA	QFP	H-W	BG18-3321	73.4	R; SWIR
TS-295	182589	WBA	QFP	H-W	BG18-3321	79.5	R; SWIR
TS-296	182590	WBA	QFP	H-W	BG18-3321	81.2	R; SWIR
TS-297	182591	WBA	QFP	H-W	BG18-3321	88.5	R; SWIR
TS-298	182592	WBA	QFP	H-W	BG18-3321	91.4	R; SWIR
TS-299	182593	WBA	QFP	H-W	BG18-3321	95.0	R; SWIR
TS-300	182594	WBA	Fvc	H-W	BG18-3321	97.5	R; SWIR
TS-301	182595	WBA	Fvc	H-W	BG18-3321	100.4	R; SWIR
TS-302	182596	WBA	Fvc	H-W	BG18-3321	106.7	R; SWIR
TS-303	182597	WBA	Fvc	H-W	BG18-3321	108.2	R; SWIR
TS-304	182598	WBA	Fvc	H-W	BG18-3321	122.9	R; SWIR
TS-305	182599	WBA	Fvc	H-W	BG18-3321	125.0	R; SWIR
TS-306	182600	WBA	PA	Price Andesite	BG18-3321	138.0	R; pXRF; SWIR
TS-307	182601	WBA	PA	Price Andesite	BG18-3321	140.2	R; pXRF; SWIR
TS-308	182602	WBA	PA	Price Andesite	BG18-3321	147.3	R; pXRF; SWIR
TS-309	182603	WBA	PA	Price Andesite	BG18-3321	159.0	R; pXRF; SWIR
TS-310	182604	WBA	PA	Price Andesite	BG18-3321	163.0	R; pXRF; SWIR
TS-311	182605	WBA	Bvc	H-W	BG18-3321	166.0	R; SWIR
TS-312	182606	WBA	Bvc	H-W	BG18-3321	167.6	R; SWIR
TS-313	182607	WBA	Bvc	H-W	BG18-3321	170.7	R; SWIR
TS-314	182608	WBA	Bvc	H-W	BG18-3321	173.9	R; SWIR
TS-315	182609	WBA	Bvc	H-W	BG18-3321	175.8	R; SWIR
TS-316	182610	WBA	Bvc	H-W	BG18-3321	180.0	R; SWIR
TS-317	182611	WBA	Bvc	H-W	BG18-3321	185.8	R; SWIR
TS-318	182612	WBA	Bvc	H-W	BG18-3321	188.0	R; SWIR
TS-319	182613	WBA	Avc	Hanging Wall And	BG18-3904	12.2	R; SWIR

Table A.1 Continued.

Field ID	UTAS ID	Area	Rock Code	Strat Member	DDH	Depth (m)	Preparation
TS-320	182614	WBA	Avc	Hanging Wall And	BG18-3904	15.2	R; SWIR
TS-321	182615	WBA	Avc	Hanging Wall And	BG18-3904	18.3	R; SWIR
TS-322	182616	WBA	Avc	Hanging Wall And	BG18-3904	21.3	R; SWIR
TS-323	182617	WBA	Avc	Hanging Wall And	BG18-3904	24.4	R; SWIR
TS-324	182618	WBA	Avc	Hanging Wall And	BG18-3904	30.5	R; SWIR
TS-325	182619	WBA	Avc	Hanging Wall And	BG18-3904	36.6	R; SWIR
TS-326	182620	WBA	Avc	Hanging Wall And	BG18-3904	39.6	R; SWIR
TS-327	182621	WBA	Avc	Hanging Wall And	BG18-3904	42.7	R; SWIR
TS-328	182622	WBA	Avc	Hanging Wall And	BG18-3904	45.7	R; SWIR
TS-329	182623	WBA	Avc	Hanging Wall And	BG18-3904	48.9	R; SWIR
TS-330	182624	WBA	Avc	Hanging Wall And	BG18-3904	57.5	R; SWIR
TS-331	182625	WBA	Avc	Hanging Wall And	BG18-3904	85.3	R; SWIR
TS-332	182626	WBA	Avc	Hanging Wall And	BG18-3904	89.0	R; SWIR
TS-333	182627	WBA	Fvc	H-W	BG18-3904	94.5	R; SWIR
TS-334	182628	WBA	Fvc	H-W	BG18-3904	97.5	R; SWIR
TS-335	182629	WBA	Fvc	H-W	BG18-3904	100.2	R; SWIR
TS-336	182630	WBA	Fvc	H-W	BG18-3904	102.9	R; SWIR
TS-337	182631	WBA	Fvc	H-W	BG18-3904	109.4	R; SWIR
TS-338	182632	WBA	Fvc	H-W	BG18-3904	113.8	R; SWIR
TS-339	182633	WBA	Fvc	H-W	BG18-3904	118.5	R; SWIR
TS-340	182634	WBA	Fvc	H-W	BG18-3904	121.8	R; SWIR
TS-341	182635	WBA	Fvc	H-W	BG18-3904	125.0	R; SWIR
TS-342	182636	WBA	Fvc	H-W	BG18-3904	127.0	R; SWIR
TS-343	182637	WBA	Fvc	H-W	BG18-3904	133.5	R; SWIR
TS-344	182638	WBA	Fvc	H-W	BG18-3904	136.5	R; SWIR
TS-345	182639	WBA	PA	Price Andesite	BG18-3904	139.1	R; PD; LM; WR; pXRF; SWIR
TS-346	182640	WBA	PA	Price Andesite	BG18-3904	146.3	R; pXRF; SWIR
TS-347	182641	WBA	PA	Price Andesite	BG18-3904	149.4	R; pXRF; SWIR
TS-348	182642	WBA	PA	Price Andesite	BG18-3904	155.4	R; pXRF; SWIR
TS-349	182643	WBA	PA	Price Andesite	BG18-3904	158.5	R; pXRF; SWIR
TS-350	182644	WBA	PA	Price Andesite	BG18-3904	170.6	R; pXRF; SWIR
TS-351	182645	WBA	PA	Price Andesite	BG18-3904	173.7	R; pXRF; SWIR
TS-352	182646	WBA	PA	Price Andesite	BG18-3904	176.8	R; pXRF; SWIR
TS-353	182647	WBA	PA	Price Andesite	BG18-3904	179.8	R; pXRF; SWIR
TS-354	182648	WBA	PA	Price Andesite	BG18-3904	182.9	R; LM; pXRF; SWIR
TS-355	182649	WBA	PA	Price Andesite	BG18-3904	189.0	R; pXRF; SWIR
TS-356	182650	WBA	PA	Price Andesite	BG18-3904	195.1	R; pXRF; SWIR
TS-357	182651	WBA	PA	Price Andesite	BG18-3904	198.1	R; pXRF; SWIR
TS-358	182652	WBA	PA	Price Andesite	BG18-3904	199.5	R; pXRF; SWIR
TS-359	182653	WBA	Avc	Hanging Wall And	BG18-3550	10.7	R; SWIR
TS-360	182654	WBA	Avc	Hanging Wall And	BG18-3550	13.6	R; SWIR
TS-361	182655	WBA	Avc	Hanging Wall And	BG18-3550	16.9	R; SWIR
TS-362	182656	WBA	Avc	Hanging Wall And	BG18-3550	23.2	R; SWIR
TS-363	182657	WBA	Avc	Hanging Wall And	BG18-3550	28.0	R; SWIR
TS-364	182658	WBA	Avc	Hanging Wall And	BG18-3550	32.0	R; SWIR
TS-365	182659	WBA	Avc	Hanging Wall And	BG18-3550	35.0	R; SWIR
TS-366	182660	WBA	Avc	Hanging Wall And	BG18-3550	38.3	R; SWIR
TS-367	182661	WBA	Avc	Hanging Wall And	BG18-3550	41.5	R; SWIR
TS-368	182662	WBA	Avc	Hanging Wall And	BG18-3550	44.3	R; SWIR
TS-369	182663	WBA	Avc	Hanging Wall And	BG18-3550	47.2	R; SWIR
TS-370	182664	WBA	Avc	Hanging Wall And	BG18-3550	49.8	R; SWIR
TS-371	182665	WBA	Avc	Hanging Wall And	BG18-3550	53.3	R; SWIR
TS-372	182666	WBA	QFP	H-W	BG18-3550	64.5	R; SWIR

Table A.1 Continued.

Field ID	UTAS ID	Area	Rock Code	Strat Member	DDH	Depth (m)	Preparation
TS-373	182667	WBA	QFP	H-W	BG18-3550	68.0	R; SWIR
TS-374	182668	WBA	QFP	H-W	BG18-3550	71.2	R; SWIR
TS-375	182669	WBA	QFP	H-W	BG18-3550	77.7	R; SWIR
TS-376	182670	WBA	QFP	H-W	BG18-3550	80.8	R; SWIR
TS-377	182671	WBA	Fvc	H-W	BG18-3550	84.0	R; SWIR
TS-378	182672	WBA	Fvc	H-W	BG18-3550	90.0	R; SWIR
TS-379	182673	WBA	Fvc	H-W	BG18-3550	93.0	R; SWIR
TS-380	182674	WBA	Fvc	H-W	BG18-3550	97.0	R; SWIR
TS-381	182675	WBA	Fvc	H-W	BG18-3550	99.1	R; SWIR
TS-382	182676	WBA	Fvc	H-W	BG18-3550	105.1	R; SWIR
TS-383	182677	WBA	A	H-W	BG18-3550	108.2	R; SWIR
TS-384	182678	WBA	Fvc	H-W	BG18-3550	112.8	R; SWIR
TS-385	182679	WBA	Fvc	H-W	BG18-3550	136.2	R; SWIR
TS-386	182680	WBA	Fvc	H-W	BG18-3550	143.3	R; SWIR
TS-387	182681	WBA	Bvc	H-W	BG18-3550	146.0	R; SWIR
TS-388	182682	WBA	Bvc	H-W	BG18-3550	148.0	R; SWIR
TS-389	182683	WBA	PA	Price Andesite	BG18-3550	158.5	R; pXRF; SWIR
TS-390	182684	WBA	PA	Price Andesite	BG18-3550	164.6	R; pXRF; SWIR
TS-391	182685	WBA	PA	Price Andesite	BG18-3550	170.7	R; pXRF; SWIR
TS-392	182686	WBA	PA	Price Andesite	BG18-3550	176.8	R; pXRF; SWIR
TS-393	182687	WBA	PA	Price Andesite	BG18-3550	182.9	R; pXRF; SWIR
TS-394	182688	WBA	PA	Price Andesite	BG18-3550	189.0	PD; LM; WR; pXRF; SWIR
TS-395	182689	WBA	PA	Price Andesite	BG18-3550	195.1	R; pXRF; SWIR
TS-396	182690	WBA	PA	Price Andesite	BG18-3550	204.2	PD; LM; WR; pXRF; SWIR
TS-397	182691	WBA	PA	Price Andesite	BG18-3550	210.3	R; pXRF; SWIR
TS-398	182692	WBA	PA	Price Andesite	BG18-3550	216.4	R; pXRF; SWIR
TS-399	182693	WBA	PA	Price Andesite	BG18-3550	219.5	R; pXRF; SWIR
TS-400	182694	WBA	PA	Price Andesite	BG18-3550	223.0	R; pXRF; SWIR
TS-401	182695	WBA	Avc	Hanging Wall And	BG18-3551	6.1	R; SWIR
TS-402	182696	WBA	Avc	Hanging Wall And	BG18-3551	15.2	R; SWIR
TS-403	182697	WBA	Avc	Hanging Wall And	BG18-3551	18.3	R; SWIR
TS-404	182698	WBA	Avc	Hanging Wall And	BG18-3551	21.3	R; SWIR
TS-405	182699	WBA	Avc	Hanging Wall And	BG18-3551	24.4	R; SWIR
TS-406	182700	WBA	Avc	Hanging Wall And	BG18-3551	27.4	R; SWIR
TS-407	182701	WBA	Avc	Hanging Wall And	BG18-3551	30.5	R; SWIR
TS-408	182702	WBA	Avc	Hanging Wall And	BG18-3551	42.7	R; SWIR
TS-409	182703	WBA	QFP	H-W	BG18-3551	55.0	R; SWIR
TS-410	182704	WBA	QFP	H-W	BG18-3551	61.0	R; SWIR
TS-411	182705	WBA	QFP	H-W	BG18-3551	67.1	R; SWIR
TS-412	182706	WBA	QFP	H-W	BG18-3551	73.5	R; SWIR
TS-413	182707	WBA	QFP	H-W	BG18-3551	76.2	R; SWIR
TS-414	182708	WBA	QFP	H-W	BG18-3551	85.3	R; SWIR
TS-415	182709	WBA	Fvc	H-W	BG18-3551	91.2	R; SWIR
TS-416	182710	WBA	Bvc	H-W	BG18-3551	123.3	R; SWIR
TS-417	182711	WBA	PA	Price Andesite	BG18-3551	128.0	R; SWIR
TS-418	182712	WBA	Bvc	H-W	BG18-3551	143.0	R; SWIR
TS-419	182713	WBA	PA	Price Andesite	BG18-3551	158.5	R; pXRF; SWIR
TS-420	182714	WBA	PA	Price Andesite	BG18-3551	173.7	PD; LM; WR; pXRF; SWIR
TS-421	182715	WBA	PA	Price Andesite	BG18-3551	183.0	R; LM; pXRF; SWIR
TS-422	182716	WBA	PA	Price Andesite	BG18-3551	192.0	R; pXRF; SWIR
TS-423	182717	WBA	PA	Price Andesite	BG18-3551	205.2	R; pXRF; SWIR
TS-424	182718	WBA	PA	Price Andesite	BG18-3551	216.4	R; pXRF; SWIR
TS-425	182719	WBA	PA	Price Andesite	BG18-3551	222.5	R; pXRF; SWIR

Table A.1 Continued.

Field ID	UTAS ID	Area	Rock Code	Strat Member	DDH	Depth (m)	Preparation
TS-426	182720	WBA	QFP	H-W	BG18-3322	60.5	R; pXRF; SWIR
TS-427	182721	WBA	QFP	H-W	BG18-3322	64.0	R; pXRF; SWIR
TS-428	182722	WBA	QFP	H-W	BG18-3322	67.7	R; pXRF; SWIR
TS-429	182723	WBA	QFP	H-W	BG18-3322	70.7	R; pXRF; SWIR
TS-430	182724	WBA	QFP	H-W	BG18-3322	73.2	R; pXRF; SWIR
TS-431	182725	WBA	QFP	H-W	BG18-3322	76.2	R; pXRF; SWIR
TS-432	182726	WBA	QFP	H-W	BG18-3322	78.5	R; pXRF; SWIR
TS-433	182727	WBA	QFP	H-W	BG18-3322	82.3	R; pXRF; SWIR
TS-434	182728	WBA	QFP	H-W	BG18-3322	86.8	R; pXRF; SWIR
TS-435	182729	WBA	QFP	H-W	BG18-3322	90.9	R; pXRF; SWIR
TS-436	182730	WBA	QFP	H-W	BG18-3322	94.0	R; pXRF; SWIR
TS-437	182731	WBA	QFP	H-W	BG18-3322	98.8	R; pXRF; SWIR
TS-438	182732	WBA	Fvc	H-W	BG18-3322	101.4	R; pXRF; SWIR
TS-439	182733	WBA	Fvc	H-W	BG18-3322	103.4	R; pXRF; SWIR
TS-440	182734	WBA	Fvc	H-W	BG18-3322	106.8	R; pXRF; SWIR
TS-441	182735	WBA	Fvc	H-W	BG18-3322	109.7	R; pXRF; SWIR
TS-442	182736	WBA	Fvc	H-W	BG18-3322	122.3	R; pXRF; SWIR
TS-443	182737	WBA	Fvc	H-W	BG18-3322	126.1	R; pXRF; SWIR
TS-444	182738	WBA	Fvc	H-W	BG18-3322	129.8	R; pXRF; SWIR
TS-445	182739	WBA	Fvc	H-W	BG18-3322	133.1	R; pXRF; SWIR
TS-446	182740	WBA	Fvc	H-W	BG18-3322	139.5	R; pXRF; SWIR
TS-447	182741	WBA	PA	Price Andesite	BG18-3322	145.0	R; pXRF; SWIR
TS-448	182742	WBA	PA	Price Andesite	BG18-3322	148.4	R; pXRF; SWIR
TS-449	182743	WBA	PA	Price Andesite	BG18-3322	152.4	R; pXRF; SWIR
TS-450	182744	WBA	PA	Price Andesite	BG18-3322	156.4	R; pXRF; SWIR
TS-451	182745	WBA	Fvc	H-W	BG18-3322	159.8	R; pXRF; SWIR
TS-452	182746	WBA	Fvc	H-W	BG18-3322	162.1	R; pXRF; SWIR
TS-453	182747	WBA	Fvc	H-W	BG18-3322	166.0	R; pXRF; SWIR
TS-454	182748	WBA	Fvc	H-W	BG18-3322	167.6	R; pXRF; SWIR
TS-455	182749	WBA	Fvc	H-W	BG18-3322	172.0	R; pXRF; SWIR
TS-456	182750	WBA	Fvc	H-W	BG18-3322	175.2	R; pXRF; SWIR
TS-457	182751	WBA	Fvc	H-W	BG18-3322	179.4	R; pXRF; SWIR
TS-458	182752	WBA	Fvc	H-W	BG18-3322	180.6	R; pXRF; SWIR
TS-459	182753	WBA	Avc	Hanging Wall And	BG18-3905	12.4	R; SWIR
TS-460	182754	WBA	Avc	Hanging Wall And	BG18-3905	18.0	R; SWIR
TS-461	182755	WBA	Avc	Hanging Wall And	BG18-3905	21.3	R; SWIR
TS-462	182756	WBA	Avc	Hanging Wall And	BG18-3905	24.4	R; SWIR
TS-463	182757	WBA	Avc	Hanging Wall And	BG18-3905	29.2	R; SWIR
TS-464	182758	WBA	Avc	Hanging Wall And	BG18-3905	30.5	R; SWIR
TS-465	182759	WBA	Avc	Hanging Wall And	BG18-3905	33.5	R; SWIR
TS-466	182760	WBA	Avc	Hanging Wall And	BG18-3905	45.7	R; SWIR
TS-467	182761	WBA	Avc	Hanging Wall And	BG18-3905	49.0	R; SWIR
TS-468	182762	WBA	Af	H-W	BG18-3905	54.9	R; pXRF; SWIR
TS-469	182763	WBA	Af	H-W	BG18-3905	58.5	R; pXRF; SWIR
TS-470	182764	WBA	Af	H-W	BG18-3905	61.0	R; pXRF; SWIR
TS-471	182765	WBA	Af	H-W	BG18-3905	64.0	R; pXRF; SWIR
TS-472	182766	WBA	Af	H-W	BG18-3905	67.1	R; pXRF; SWIR
TS-473	182767	WBA	Af	H-W	BG18-3905	70.1	R; pXRF; SWIR
TS-474	182768	WBA	Af	H-W	BG18-3905	73.2	R; pXRF; SWIR
TS-475	182769	WBA	Af	H-W	BG18-3905	76.4	R; pXRF; SWIR
TS-476	182770	WBA	Af	H-W	BG18-3905	79.2	R; pXRF; SWIR
TS-477	182771	WBA	Af	H-W	BG18-3905	82.3	R; pXRF; SWIR
TS-478	182772	WBA	Af	H-W	BG18-3905	85.3	R; pXRF; SWIR

Table A.1 Continued.

Field ID	UTAS ID	Area	Rock Code	Strat Member	DDH	Depth (m)	Preparation
TS-479	182773	WBA	Af	H-W	BG18-3905	88.9	R; pXRF; SWIR
TS-480	182774	WBA	Af	H-W	BG18-3905	91.6	R; pXRF; SWIR
TS-481	182775	WBA	Af	H-W	BG18-3905	95.0	R; pXRF; SWIR
TS-482	182776	WBA	Md		BG18-3905	103.6	R; SWIR
TS-483	182777	WBA	Avc	Hanging Wall And	BG18-3905	106.7	R; SWIR
TS-484	182778	WBA	QFP	H-W	BG18-3905	110.7	R; SWIR
TS-485	182779	WBA	QFP	H-W	BG18-3905	113.8	R; SWIR
TS-486	182780	WBA	QFP	H-W	BG18-3905	115.8	R; SWIR
TS-487	182781	WBA	QFP	H-W	BG18-3905	119.3	R; SWIR
TS-488	182782	WBA	QFP	H-W	BG18-3905	123.0	R; SWIR
TS-489	182783	WBA	Fvc	H-W	BG18-3905	125.0	R; SWIR
TS-490	182784	WBA	QFP	H-W	BG18-3905	128.7	R; SWIR
TS-491	182785	WBA	QFP	H-W	BG18-3905	131.8	R; SWIR
TS-492	182786	WBA	QFP	H-W	BG18-3905	134.0	R; SWIR
TS-493	182787	WBA	C	H-W	BG18-3905	144.9	R; SWIR
TS-494	182788	WBA	PA	Price Andesite	BG18-3905	155.4	PD; LM; WR; pXRF; SWIR
TS-495	182789	WBA	PA	Price Andesite	BG18-3905	158.5	R; pXRF; SWIR
TS-496	182790	WBA	PA	Price Andesite	BG18-3905	170.7	PD; LM; WR; pXRF; SWIR
TS-497	182791	WBA	PA	Price Andesite	BG18-3905	182.9	R; pXRF; SWIR
TS-498	182792	WBA	PA	Price Andesite	BG18-3905	185.9	R; pXRF; SWIR
TS-499	182793	WBA	Af	H-W	BG18-3323	42.7	R; SWIR
TS-500	182794	WBA	Af	H-W	BG18-3323	45.7	R; SWIR
TS-501	182795	WBA	QFP	H-W	BG18-3323	76.0	R; SWIR
TS-502	182796	WBA	QFP	H-W	BG18-3323	79.4	R; SWIR
TS-503	182797	WBA	QFP	H-W	BG18-3323	86.0	R; SWIR
TS-504	182798	WBA	QFP	H-W	BG18-3323	91.4	R; SWIR
TS-505	182799	WBA	QFP	H-W	BG18-3323	94.5	R; SWIR
TS-506	182800	WBA	QFP	H-W	BG18-3323	97.5	R; SWIR
TS-507	182801	WBA	QFP	H-W	BG18-3323	99.5	R; SWIR
TS-508	182802	WBA	QFP	H-W	BG18-3323	109.7	R; SWIR
TS-509	182803	WBA	QFP	H-W	BG18-3323	113.6	R; SWIR
TS-510	182804	WBA	QFP	H-W	BG18-3323	117.2	R; SWIR
TS-511	182805	WBA	QFP	H-W	BG18-3323	119.2	R; SWIR
TS-512	182806	WBA	QFP	H-W	BG18-3323	121.9	R; SWIR
TS-513	182807	WBA	QFP	H-W	BG18-3323	127.0	R; SWIR
TS-514	182808	WBA	QFP	H-W	BG18-3323	130.2	R; SWIR
TS-515	182809	WBA	QFP	H-W	BG18-3323	131.4	R; SWIR
TS-516	182810	WBA	QFP	H-W	BG18-3323	136.8	R; SWIR
TS-517	182811	WBA	QFP	H-W	BG18-3323	141.0	R; SWIR
TS-518	182812	WBA	QFP	H-W	BG18-3323	144.6	R; SWIR
TS-519	182813	WBA	Fvc	H-W	BG18-3323	153.4	R; SWIR
TS-520	182814	WBA	Fvc	H-W	BG18-3323	159.0	R; SWIR
TS-521	182815	WBA	Fvc	H-W	BG18-3323	161.5	R; SWIR
TS-522	182816	WBA	C	H-W	BG18-3323	164.6	R; SWIR
TS-523	182817	WBA	C	H-W	BG18-3323	167.6	R; SWIR
TS-524	182818	WBA	Fvc	H-W	BG18-3323	176.8	R; SWIR
TS-525	182819	WBA	PA	Price Andesite	BG18-3323	189.0	R; SWIR
TS-526	182820	WBA	A	H-W	BG18-3323	195.8	R; SWIR
TS-527	182821	WBA	A	H-W	BG18-3323	207.2	R; SWIR
TS-528	182822	WBA	Fvc	H-W	BG18-3323	216.4	R; SWIR
TS-529	182823	WBA	Fvc	H-W	BG18-3323	220.0	R; SWIR
TS-530	182824	WBA	Avc	Hanging Wall And	BG18-3552	5.8	R; SWIR
TS-531	182825	WBA	Avc	Hanging Wall And	BG18-3552	8.2	R; SWIR

Table A.1 Continued.

Field ID	UTAS ID	Area	Rock Code	Strat Member	DDH	Depth (m)	Preparation
TS-532	182826	WBA	Avc	Hanging Wall And	BG18-3552	10.7	R; SWIR
TS-533	182827	WBA	Avc	Hanging Wall And	BG18-3552	13.7	R; SWIR
TS-534	182828	WBA	Avc	Hanging Wall And	BG18-3552	16.8	R; SWIR
TS-535	182829	WBA	Avc	Hanging Wall And	BG18-3552	19.5	R; SWIR
TS-536	182830	WBA	Avc	Hanging Wall And	BG18-3552	44.8	R; SWIR
TS-537	182831	WBA	Avc	Hanging Wall And	BG18-3552	47.2	R; SWIR
TS-538	182832	WBA	QFP	H-W	BG18-3552	77.0	R; SWIR
TS-539	182833	WBA	QFP	H-W	BG18-3552	80.8	R; SWIR
TS-540	182834	WBA	QFP	H-W	BG18-3552	83.8	R; SWIR
TS-541	182835	WBA	Fvc	H-W	BG18-3552	89.9	R; SWIR
TS-542	182836	WBA	Fvc	H-W	BG18-3552	96.2	R; SWIR
TS-543	182837	WBA	Fvc	H-W	BG18-3552	99.1	R; SWIR
TS-544	182838	WBA	Fvc	H-W	BG18-3552	102.1	R; SWIR
TS-545	182839	WBA	Fvc	H-W	BG18-3552	105.2	R; SWIR
TS-546	182840	WBA	Bvc	H-W	BG18-3552	117.8	R; SWIR
TS-547	182841	WBA	PA	Price Andesite	BG18-3552	121.0	R; SWIR
TS-548	182842	WBA	PA	Price Andesite	BG18-3552	126.5	R; SWIR
TS-549	182843	WBA	Bvc	H-W	BG18-3552	129.5	R; SWIR
TS-550	182844	WBA	PA	Price Andesite	BG18-3552	138.7	R; pXRF; SWIR
TS-551	182845	WBA	PA	Price Andesite	BG18-3552	147.8	R; pXRF; SWIR
TS-552	182846	WBA	PA	Price Andesite	BG18-3552	152.9	PD; LM; WR; pXRF; SWIR
TS-553	182847	WBA	PA	Price Andesite	BG18-3552	159.0	R; pXRF; SWIR
TS-554	182848	WBA	PA	Price Andesite	BG18-3552	163.1	R; pXRF; SWIR
TS-555	182849	WBA	PA	Price Andesite	BG18-3552	169.2	R; LM; pXRF; SWIR
TS-556	182850	WBA	PA	Price Andesite	BG18-3552	172.2	R; pXRF; SWIR
TS-557	182851	WBA	PA	Price Andesite	BG18-3552	178.3	R; pXRF; SWIR
TS-558	182852	WBA	PA	Price Andesite	BG18-3552	193.5	R; pXRF; SWIR
TS-559	182853	WBA	PA	Price Andesite	BG18-3552	205.7	R; pXRF; SWIR
TS-560	182854	WBA	PA	Price Andesite	BG18-3552	217.9	R; pXRF; SWIR
TS-561	182855	WBA	Avc	Hanging Wall And	BG18-3906	9.1	R; SWIR
TS-562	182856	WBA	Avc	Hanging Wall And	BG18-3906	12.2	R; SWIR
TS-563	182857	WBA	Avc	Hanging Wall And	BG18-3906	15.2	R; SWIR
TS-564	182858	WBA	Avc	Hanging Wall And	BG18-3906	21.3	R; SWIR
TS-565	182859	WBA	Avc	Hanging Wall And	BG18-3906	27.4	R; SWIR
TS-566	182860	WBA	Avc	Hanging Wall And	BG18-3906	35.1	R; SWIR
TS-567	182861	WBA	Avc	Hanging Wall And	BG18-3906	38.1	R; SWIR
TS-568	182862	WBA	Af	H-W	BG18-3906	41.1	R; pXRF; SWIR
TS-569	182863	WBA	Af	H-W	BG18-3906	44.2	R; pXRF; SWIR
TS-570	182864	WBA	Af	H-W	BG18-3906	49.4	R; pXRF; SWIR
TS-571	182865	WBA	Avc	Hanging Wall And	BG18-3906	62.6	R; SWIR
TS-572	182866	WBA	Avc	Hanging Wall And	BG18-3906	65.5	R; SWIR
TS-573	182867	WBA	Avc	Hanging Wall And	BG18-3906	76.2	R; SWIR
TS-574	182868	WBA	Avc	Hanging Wall And	BG18-3906	79.2	R; SWIR
TS-575	182869	WBA	Avc	Hanging Wall And	BG18-3906	85.3	R; SWIR
TS-576	182870	WBA	Avc	Hanging Wall And	BG18-3906	88.4	R; SWIR
TS-577	182871	WBA	Avc	Hanging Wall And	BG18-3906	93.5	R; SWIR
TS-578	182872	WBA	Avc	Hanging Wall And	BG18-3906	99.0	R; SWIR
TS-579	182873	WBA	Avc	Hanging Wall And	BG18-3906	103.6	R; SWIR
TS-580	182874	WBA	QFP	H-W	BG18-3906	106.7	R; SWIR
TS-581	182875	WBA	QFP	H-W	BG18-3906	109.9	R; SWIR
TS-582	182876	WBA	QFP	H-W	BG18-3906	112.8	R; SWIR
TS-583	182877	WBA	QFP	H-W	BG18-3906	115.8	R; SWIR
TS-584	182878	WBA	QFP	H-W	BG18-3906	118.9	R; SWIR

Table A.1 Continued.

Field ID	UTAS ID	Area	Rock Code	Strat Member	DDH	Depth (m)	Preparation
TS-585	182879	WBA	QFP	H-W	BG18-3906	122.4	R; SWIR
TS-586	182880	WBA	QFP	H-W	BG18-3906	124.8	R; SWIR
TS-587	182881	WBA	Qtz vn				R
TS-613	182882	WBA	Avc	Hanging Wall And	BG18-3553	6.9	R; SWIR
TS-614	182883	WBA	Avc	Hanging Wall And	BG18-3553	9.1	R; SWIR
TS-615	182884	WBA	Avc	Hanging Wall And	BG18-3553	12.2	R; SWIR
TS-616	182885	WBA	Avc	Hanging Wall And	BG18-3553	15.2	R; SWIR
TS-617	182886	WBA	Avc	Hanging Wall And	BG18-3553	18.4	R; SWIR
TS-618	182887	WBA	Avc	Hanging Wall And	BG18-3553	21.5	R; SWIR
TS-619	182888	WBA	Avc	Hanging Wall And	BG18-3553	24.4	R; SWIR
TS-620	182889	WBA	Avc	Hanging Wall And	BG18-3553	27.4	R; SWIR
TS-621	182890	WBA	Af	H-W	BG18-3553	33.6	R; pXRF; SWIR
TS-623	182891	WBA	Af	H-W	BG18-3553	36.8	R; pXRF; SWIR
TS-624	182892	WBA	Af	H-W	BG18-3553	39.6	R; pXRF; SWIR
TS-625	182893	WBA	Af	H-W	BG18-3553	42.7	R; pXRF; SWIR
TS-626	182894	WBA	Af	H-W	BG18-3553	46.8	R; pXRF; SWIR
TS-627	182895	WBA	Af	H-W	BG18-3553	48.8	R; pXRF; SWIR
TS-628	182896	WBA	Af	H-W	BG18-3553	60.0	R; pXRF; SWIR
TS-629	182897	WBA	Avc	Hanging Wall And	BG18-3553	71.3	R; SWIR
TS-630	182898	WBA	QFP	H-W	BG18-3553	84.9	R; SWIR
TS-631	182899	WBA	QFP	H-W	BG18-3553	85.5	R; SWIR
TS-632	182900	WBA	QFP	H-W	BG18-3553	92.6	R; SWIR
TS-633	182901	WBA	Fvc	H-W	BG18-3553	97.5	R; SWIR
TS-634	182902	WBA	Fvc	H-W	BG18-3553	100.6	R; SWIR
TS-635	182903	WBA	Fvc	H-W	BG18-3553	104.1	R; SWIR
TS-636	182904	WBA	Fvc	H-W	BG18-3553	106.5	R; SWIR
TS-637	182905	WBA	Bvc	H-W	BG18-3553	116.8	R; SWIR
TS-638	182906	WBA	Bvc	H-W	BG18-3553	118.9	R; SWIR
TS-639	182907	WBA	Bvc	H-W	BG18-3553	122.3	R; SWIR
TS-640	182908	WBA	PA	Price Andesite	BG18-3553	131.1	R; pXRF; SWIR
TS-641	182909	WBA	PA	Price Andesite	BG18-3553	134.1	R; pXRF; SWIR
TS-642	182910	WBA	PA	Price Andesite	BG18-3553	149.4	R; pXRF; SWIR
TS-643	182911	WBA	PA	Price Andesite	BG18-3553	155.4	R; pXRF; SWIR
TS-644	182912	WBA	PA	Price Andesite	BG18-3553	170.7	R; pXRF; SWIR
TS-645	182913	WBA	PA	Price Andesite	BG18-3553	179.8	R; pXRF; SWIR
TS-646	182914	WBA	PA	Price Andesite	BG18-3553	183.2	R; pXRF; SWIR
TS-647	182915	WBA	PA	Price Andesite	BG18-3553	192.0	R; pXRF; SWIR
TS-648	182916	WBA	PA	Price Andesite	BG18-3553	215.9	R; pXRF; SWIR
TS-649	182917	WBA	PA	Price Andesite	BG18-3553	231.6	R; pXRF; SWIR
TS-650	182918	WBA	Avc	Hanging Wall And	BG18-3907	3.0	R; pXRF; SWIR
TS-651	182919	WBA	Avc	Hanging Wall And	BG18-3907	6.0	R; pXRF; SWIR
TS-652	182920	WBA	Avc	Hanging Wall And	BG18-3907	12.2	R; pXRF; SWIR
TS-653	182921	WBA	Avc	Hanging Wall And	BG18-3907	15.2	R; pXRF; SWIR
TS-654	182922	WBA	Avc	Hanging Wall And	BG18-3907	21.2	R; pXRF; SWIR
TS-655	182923	WBA	Avc	Hanging Wall And	BG18-3907	23.1	R; pXRF; SWIR
TS-656	182924	WBA	Fd		BG18-3907	26.0	R; pXRF; SWIR
TS-657	182925	WBA	Avc	Hanging Wall And	BG18-3907	36.8	R; pXRF; SWIR
TS-658	182926	WBA	Avc	Hanging Wall And	BG18-3907	45.5	R; pXRF; SWIR
TS-659	182927	WBA	Avc	Hanging Wall And	BG18-3907	48.8	R; pXRF; SWIR
TS-660	182928	WBA	Avc	Hanging Wall And	BG18-3907	51.9	R; pXRF; SWIR
TS-661	182929	WBA	Avc	Hanging Wall And	BG18-3907	54.9	R; pXRF; SWIR
TS-662	182930	WBA	Af	H-W	BG18-3907	57.9	LM; pXRF; SWIR
TS-663	182931	WBA	Af	H-W	BG18-3907	61.0	R; pXRF; SWIR

Table A.1 Continued.

Field ID	UTAS ID	Area	Rock Code	Strat Member	DDH	Depth (m)	Preparation
TS-664	182932	WBA	Af	H-W	BG18-3907	64.0	R; pXRF; SWIR
TS-665	182933	WBA	Af	H-W	BG18-3907	67.5	R; pXRF; SWIR
TS-666	182934	WBA	Af	H-W	BG18-3907	70.3	R; pXRF; SWIR
TS-667	182935	WBA	Af	H-W	BG18-3907	73.8	R; pXRF; SWIR
TS-668	182936	WBA	Af	H-W	BG18-3907	77.0	R; pXRF; SWIR
TS-669	182937	WBA	Avc	Hanging Wall And	BG18-3907	82.3	R; pXRF; SWIR
TS-670	182938	WBA	Avc	Hanging Wall And	BG18-3907	87.4	R; pXRF; SWIR
TS-671	182939	WBA	Avc	Hanging Wall And	BG18-3907	92.8	R; pXRF; SWIR
TS-672	182940	WBA	Avc	Hanging Wall And	BG18-3907	95.0	R; pXRF; SWIR
TS-673	182941	WBA	Fvc	H-W	BG18-3907	99.5	R; pXRF; SWIR
TS-674	182942	WBA	Fvc	H-W	BG18-3907	100.6	R; pXRF; SWIR
TS-675	182943	WBA	Fvc	H-W	BG18-3907	107.4	R; pXRF; SWIR
TS-676	182944	WBA	Fvc	H-W	BG18-3907	115.8	R; pXRF; SWIR
TS-677	182945	WBA	Fvc	H-W	BG18-3907	118.7	R; pXRF; SWIR
TS-678	182946	WBA	C	H-W	BG18-3907	126.1	R; pXRF; SWIR
TS-679	182947	WBA	Bvc	H-W	BG18-3907	132.1	R; pXRF; SWIR
TS-680	182948	WBA	PA	Price Andesite	BG18-3907	135.9	R; pXRF; SWIR
TS-681	182949	WBA	PA	Price Andesite	BG18-3907	139.6	R; pXRF; SWIR
TS-682	182950	WBA	PA	Price Andesite	BG18-3907	145.3	R; pXRF; SWIR
TS-683	182951	WBA	PA	Price Andesite	BG18-3907	152.7	PD; LM; WR; pXRF; SWIR
TS-684	182952	WBA	PA	Price Andesite	BG18-3907	161.3	R; pXRF; SWIR
TS-685	182953	WBA	PA	Price Andesite	BG18-3907	173.7	R; pXRF; SWIR
TS-686	182954	WBA	PA	Price Andesite	BG18-3907	179.8	R; pXRF; SWIR
TS-687	182955	WBA	PA	Price Andesite	BG18-3907	185.9	R; pXRF; SWIR
TS-688	182956	WBA	Avc	Hanging Wall And	BG18-3554	10.7	R; pXRF; SWIR
TS-689	182957	WBA	Avc	Hanging Wall And	BG18-3554	13.7	R; pXRF; SWIR
TS-690	182958	WBA	Avc	Hanging Wall And	BG18-3554	16.5	R; pXRF; SWIR
TS-691	182959	WBA	Avc	Hanging Wall And	BG18-3554	19.8	R; pXRF; SWIR
TS-692	182960	WBA	Avc	Hanging Wall And	BG18-3554	23.0	R; pXRF; SWIR
TS-693	182961	WBA	Avc	Hanging Wall And	BG18-3554	25.9	R; pXRF; SWIR
TS-694	182962	WBA	Avc	Hanging Wall And	BG18-3554	29.7	R; pXRF; SWIR
TS-695	182963	WBA	Avc	Hanging Wall And	BG18-3554	35.1	R; pXRF; SWIR
TS-696	182964	WBA	Avc	Hanging Wall And	BG18-3554	38.1	R; pXRF; SWIR
TS-697	182965	WBA	Avc	Hanging Wall And	BG18-3554	44.2	R; pXRF; SWIR
TS-698	182966	WBA	Avc	Hanging Wall And	BG18-3554	50.3	R; pXRF; SWIR
TS-699	182967	WBA	Avc	Hanging Wall And	BG18-3554	54.2	R; pXRF; SWIR
TS-700	182968	WBA	Avc	Hanging Wall And	BG18-3554	71.6	R; pXRF; SWIR
TS-701	182969	WBA	Avc	Hanging Wall And	BG18-3554	77.7	R; pXRF; SWIR
TS-702	182970	WBA	QFP	H-W	BG18-3554	95.0	R; pXRF; SWIR
TS-703	182971	WBA	QFP	H-W	BG18-3554	98.0	R; pXRF; SWIR
TS-704	182972	WBA	QFP	H-W	BG18-3554	102.1	R; pXRF; SWIR
TS-705	182973	WBA	QFP	H-W	BG18-3554	105.4	R; pXRF; SWIR
TS-706	182974	WBA	QFP	H-W	BG18-3554	107.6	R; pXRF; SWIR
TS-707	182975	WBA	QFP	H-W	BG18-3554	111.4	R; pXRF; SWIR
TS-708	182976	WBA	QFP	H-W	BG18-3554	114.3	R; pXRF; SWIR
TS-709	182977	WBA	QFP	H-W	BG18-3554	119.3	R; pXRF; SWIR
TS-710	182978	WBA	Bvc	H-W	BG18-3554	127.0	R; pXRF; SWIR
TS-711	182979	WBA	Bvc	H-W	BG18-3554	128.0	R; pXRF; SWIR
TS-712	182980	WBA	Bvc	H-W	BG18-3554	129.5	R; pXRF; SWIR
TS-713	182981	WBA	PA	Price Andesite	BG18-3554	136.7	R; pXRF; SWIR
TS-714	182982	WBA	PA	Price Andesite	BG18-3554	154.9	R; LM; pXRF; SWIR
TS-715	182983	WBA	PA	Price Andesite	BG18-3554	159.0	R; pXRF; SWIR
TS-716	182984	WBA	PA	Price Andesite	BG18-3554	163.1	R; pXRF; SWIR

Table A.1 Continued.

Field ID	UTAS ID	Area	Rock Code	Strat Member	DDH	Depth (m)	Preparation
TS-717	182985	WBA	PA	Price Andesite	BG18-3554	172.2	R; LM; pXRF; SWIR
TS-718	182986	WBA	PA	Price Andesite	BG18-3554	181.4	R; pXRF; SWIR
TS-719	182987	WBA	PA	Price Andesite	BG18-3554	184.4	R; pXRF; SWIR
TS-720	182988	WBA	PA	Price Andesite	BG18-3554	190.5	R; pXRF; SWIR
TS-721	182989	WBA	PA	Price Andesite	BG18-3554	196.6	R; LM; pXRF; SWIR
TS-722	182990	WBA	PA	Price Andesite	BG18-3554	202.7	PD; LM; WR; pXRF; SWIR
TS-723	182991	WBA	PA	Price Andesite	BG18-3554	214.9	R; pXRF; SWIR
TS-724	182992	WBA	PA	Price Andesite	BG18-3554	224.0	R; pXRF; SWIR
TS-725	182993	WBA	PA	Price Andesite	BG18-3554	230.1	R; pXRF; SWIR
TS-726	182994	WBA	PA	Price Andesite	BG18-3554	233.2	R; pXRF; SWIR
TS-727	182995	WBA	Avc	Hanging Wall And	BG18-3555	4.6	R; SWIR
TS-728	182996	WBA	Avc	Hanging Wall And	BG18-3555	10.5	R; SWIR
TS-729	182997	WBA	Avc	Hanging Wall And	BG18-3555	13.2	R; SWIR
TS-730	182998	WBA	Avc	Hanging Wall And	BG18-3555	19.8	R; SWIR
TS-731	182999	WBA	Avc	Hanging Wall And	BG18-3555	25.9	R; SWIR
TS-732	183000	WBA	Avc	Hanging Wall And	BG18-3555	32.2	R; SWIR
TS-733	183001	WBA	Avc	Hanging Wall And	BG18-3555	38.2	R; SWIR
TS-734	183002	WBA	Avc	Hanging Wall And	BG18-3555	41.1	R; SWIR
TS-735	183003	WBA	Avc	Hanging Wall And	BG18-3555	44.2	R; SWIR
TS-736	183004	WBA	Avc	Hanging Wall And	BG18-3555	47.2	R; SWIR
TS-737	183005	WBA	Avc	Hanging Wall And	BG18-3555	53.3	R; SWIR
TS-738	183006	WBA	Avc	Hanging Wall And	BG18-3555	56.4	R; SWIR
TS-739	183007	WBA	Avc	Hanging Wall And	BG18-3555	59.4	R; SWIR
TS-740	183008	WBA	Avc	Hanging Wall And	BG18-3555	62.5	R; SWIR
TS-741	183009	WBA	Avc	Hanging Wall And	BG18-3555	71.6	R; SWIR
TS-742	183010	WBA	Avc	Hanging Wall And	BG18-3555	74.7	R; SWIR
TS-743	183011	WBA	Avc	Hanging Wall And	BG18-3555	80.0	R; SWIR
TS-744	183012	WBA	Avc	Hanging Wall And	BG18-3555	83.8	R; SWIR
TS-745	183013	WBA	Avc	Hanging Wall And	BG18-3555	86.9	R; SWIR
TS-746	183014	WBA	Avc	Hanging Wall And	BG18-3555	89.9	R; SWIR
TS-747	183015	WBA	Avc	Hanging Wall And	BG18-3555	151.2	R; SWIR
TS-748	183016	WBA	Avc	Hanging Wall And	BG18-3555	156.0	R; SWIR
TS-749	183017	WBA	Avc	Hanging Wall And	BG18-3555	162.0	R; SWIR
TS-750	183018	WBA	Avc	Hanging Wall And	BG18-3555	166.1	R; SWIR
TS-751	183019	WBA	Avc	Hanging Wall And	BG18-3555	172.2	R; SWIR
TS-752	183020	WBA	Avc	Hanging Wall And	BG18-3555	178.0	R; SWIR
TS-753	183021	WBA	Avc	Hanging Wall And	BG18-3555	183.0	R; SWIR
TS-754	183022	WBA	Avc	Hanging Wall And	BG18-3555	189.1	R; SWIR
TS-755	183023	WBA	Avc	Hanging Wall And	BG18-3555	195.1	R; SWIR
TS-756	183024	WBA	Avc	Hanging Wall And	BG18-3555	201.1	R; SWIR
TS-757	183025	WBA	Avc	Hanging Wall And	BG18-3555	207.5	R; SWIR
TS-758	183026	WBA	Avc	Hanging Wall And	BG18-3555	210.3	R; SWIR
TS-759	183027	WBA	Avc	Hanging Wall And	BG18-3555	216.4	R; SWIR
TS-760	183028	WBA	Avc	Hanging Wall And	BG18-3555	222.5	R; SWIR
TS-761	183029	WBA	Avc	Hanging Wall And	BG18-3555	225.6	R; SWIR
TS-762	183030	WBA	Avc	Hanging Wall And	BG18-3555	232.6	R; SWIR
TS-763	183031	WBA	Avc	Hanging Wall And	BG18-3908	6.1	R; SWIR
TS-764	183032	WBA	Avc	Hanging Wall And	BG18-3908	18.3	R; SWIR
TS-765	183033	WBA	Avc	Hanging Wall And	BG18-3908	21.3	R; SWIR
TS-766	183034	WBA	Avc	Hanging Wall And	BG18-3908	24.4	R; SWIR
TS-767	183035	WBA	Avc	Hanging Wall And	BG18-3908	27.4	R; SWIR
TS-768	183036	WBA	Avc	Hanging Wall And	BG18-3908	32.2	R; SWIR
TS-769	183037	WBA	Avc	Hanging Wall And	BG18-3908	42.7	R; SWIR

Table A.1 Continued.

Field ID	UTAS ID	Area	Rock Code	Strat Member	DDH	Depth (m)	Preparation
TS-770	183038	WBA	Af	H-W	BG18-3908	45.7	R; pXRF; SWIR
TS-771	183039	WBA	Af	H-W	BG18-3908	54.9	R; pXRF; SWIR
TS-772	183040	WBA	Af	H-W	BG18-3908	57.9	R; pXRF; SWIR
TS-773	183041	WBA	Af	H-W	BG18-3908	64.0	R; pXRF; SWIR
TS-774	183042	WBA	Af	H-W	BG18-3908	70.1	R; pXRF; SWIR
TS-775	183043	WBA	Avc	Hanging Wall And	BG18-3908	85.9	R; SWIR
TS-776	183044	WBA	QFP	H-W	BG18-3908	94.5	R; SWIR
TS-777	183045	WBA	QFP	H-W	BG18-3908	97.5	R; SWIR
TS-778	183046	WBA	QFP	H-W	BG18-3908	180.7	R; SWIR
TS-779	183047	WBA	QFP	H-W	BG18-3908	106.3	R; SWIR
TS-780	183048	WBA	QFP	H-W	BG18-3908	109.7	R; SWIR
TS-781	183049	WBA	QFP	H-W	BG18-3908	112.8	R; SWIR
TS-782	183050	WBA	QFP	H-W	BG18-3908	118.9	R; SWIR
TS-783	183051	WBA	QFP	H-W	BG18-3908	125.5	R; SWIR
TS-784	183052	WBA	QFP	H-W	BG18-3908	127.7	R; SWIR
TS-785	183053	WBA	PA	Price Andesite	BG18-3908	140.2	R; pXRF; SWIR
TS-786	183054	WBA	PA	Price Andesite	BG18-3908	143.3	R; pXRF; SWIR
TS-787	183055	WBA	PA	Price Andesite	BG18-3908	158.5	R; pXRF; SWIR
TS-788	183056	WBA	PA	Price Andesite	BG18-3908	161.5	PD; LM; WR; pXRF; SWIR
TS-789	183057	WBA	PA	Price Andesite	BG18-3908	173.7	R; pXRF; SWIR
TS-790	183058	WBA	PA	Price Andesite	BG18-3908	179.8	R; pXRF; SWIR
TS-791	183059	WBA	PA	Price Andesite	BG18-3908	195.1	R; pXRF; SWIR
TS-913	183060	WBA	Avc	Hanging Wall And	BG18-3952	12.2	R; pXRF; SWIR
TS-914	183061	WBA	Avc	Hanging Wall And	BG18-3952	15.2	R; pXRF; SWIR
TS-915	183062	WBA	Avc	Hanging Wall And	BG18-3952	18.3	R; pXRF; SWIR
TS-916	183063	WBA	Avc	Hanging Wall And	BG18-3952	21.3	R; pXRF; SWIR
TS-917	183064	WBA	Md		BG18-3952	24.4	R; pXRF; SWIR
TS-918	183065	WBA	Avc	Hanging Wall And	BG18-3952	26.3	R; pXRF; SWIR
TS-919	183066	WBA	Avc	Hanging Wall And	BG18-3952	27.5	R; pXRF; SWIR
TS-920	183067	WBA	Avc	Hanging Wall And	BG18-3952	30.5	R; pXRF; SWIR
TS-921	183068	WBA	Avc	Hanging Wall And	BG18-3952	34.0	R; pXRF; SWIR
TS-922	183069	WBA	Avc	Hanging Wall And	BG18-3952	36.6	R; pXRF; SWIR
TS-923	183070	WBA	Md		BG18-3952	49.6	R; pXRF; SWIR
TS-924	183071	WBA	QFP	H-W	BG18-3952	51.8	R; pXRF; SWIR
TS-925	183072	WBA	QFP	H-W	BG18-3952	54.9	R; pXRF; SWIR
TS-926	183073	WBA	QFP	H-W	BG18-3952	57.9	R; pXRF; SWIR
TS-927	183074	WBA	QFP	H-W	BG18-3952	61.0	R; pXRF; SWIR
TS-928	183075	WBA	QFP	H-W	BG18-3952	64.0	R; pXRF; SWIR
TS-929	183076	WBA	QFP	H-W	BG18-3952	67.1	R; pXRF; SWIR
TS-930	183077	WBA	QFP	H-W	BG18-3952	70.1	R; pXRF; SWIR
TS-931	183078	WBA	QFP	H-W	BG18-3952	73.2	R; pXRF; SWIR
TS-932	183079	WBA	QFP	H-W	BG18-3952	76.2	R; pXRF; SWIR
TS-933	183080	WBA	QFP	H-W	BG18-3952	79.2	R; pXRF; SWIR
TS-934	183081	WBA	QFP	H-W	BG18-3952	82.3	R; pXRF; SWIR
TS-935	183082	WBA	QFP	H-W	BG18-3952	85.3	R; pXRF; SWIR
TS-936	183083	WBA	QFP	H-W	BG18-3952	88.4	R; pXRF; SWIR
TS-937	183084	WBA	Fvc	H-W	BG18-3952	91.4	R; pXRF; SWIR
TS-938	183085	WBA	Fvc	H-W	BG18-3952	95.0	R; pXRF; SWIR
TS-939	183086	WBA	C	H-W	BG18-3952	97.5	R; pXRF; SWIR
TS-940	183087	WBA	Fvc	H-W	BG18-3952	98.2	R; pXRF; SWIR
TS-941	183088	WBA	Fvc	H-W	BG18-3952	99.1	R; pXRF; SWIR
TS-942	183089	WBA	Fvc	H-W	BG18-3952	102.1	R; pXRF; SWIR
TS-943	183090	WBA	Fvc	H-W	BG18-3952	105.2	R; pXRF; SWIR

Table A.1 Continued.

Field ID	UTAS ID	Area	Rock Code	Strat Member	DDH	Depth (m)	Preparation
TS-944	183091	WBA	Fvc	H-W	BG18-3952	108.1	R; pXRF; SWIR
TS-945	183092	WBA	C	H-W	BG18-3952	110.1	R; pXRF; SWIR
TS-946	183093	WBA	C	H-W	BG18-3952	111.3	R; pXRF; SWIR
TS-947	183094	WBA	C	H-W	BG18-3952	114.3	R; pXRF; SWIR
TS-948	183095	WBA	Bvc	H-W	BG18-3952	114.7	R; pXRF; SWIR
TS-949	183096	WBA	Bvc	H-W	BG18-3952	115.3	R; pXRF; SWIR
TS-950	183097	WBA	Bvc	H-W	BG18-3952	117.3	R; pXRF; SWIR
TS-951	183098	WBA	Bvc	H-W	BG18-3952	119.2	R; pXRF; SWIR
TS-952	183099	WBA	PA	Price Andesite	BG18-3952	119.7	R; pXRF; SWIR
TS-953	183100	WBA	Bvc	H-W	BG18-3952	121.4	R; pXRF; SWIR
TS-954	183101	WBA	Bvc	H-W	BG18-3952	122.8	R; pXRF; SWIR
TS-955	183102	WBA	Bvc	H-W	BG18-3952	124.6	R; pXRF; SWIR
TS-956	183103	WBA	PA	Price Andesite	BG18-3952	126.5	R; pXRF; SWIR
TS-957	183104	WBA	C	H-W	BG18-3952	127.4	R; pXRF; SWIR
TS-958	183105	WBA	PA	Price Andesite	BG18-3952	129.5	R; pXRF; SWIR
TS-959	183106	WBA	Md		BG18-3952	130.3	R; pXRF; SWIR
TS-960	183107	WBA	Md		BG18-3952	132.6	R; pXRF; SWIR
TS-961	183108	WBA	PA	Price Andesite	BG18-3952	135.6	R; pXRF; SWIR
TS-962	183109	WBA	PA	Price Andesite	BG18-3952	138.7	R; pXRF; SWIR
TS-963	183110	WBA	PA	Price Andesite	BG18-3952	141.7	R; pXRF; SWIR
TS-964	183111	WBA	PA	Price Andesite	BG18-3952	143.4	R; pXRF; SWIR
TS-965	183112	WBA	PA	Price Andesite	BG18-3952	144.8	R; pXRF; SWIR
TS-966	183113	WBA	PA	Price Andesite	BG18-3952	147.7	R; pXRF; SWIR
TS-967	183114	WBA	PA	Price Andesite	BG18-3952	150.9	R; pXRF; SWIR
TS-968	183115	WBA	PA	Price Andesite	BG18-3952	153.9	R; pXRF; SWIR
TS-969	183116	WBA	PA	Price Andesite	BG18-3952	157.0	R; pXRF; SWIR
TS-970	183117	WBA	PA	Price Andesite	BG18-3952	160.0	R; pXRF; SWIR
TS-971	183118	WBA	PA	Price Andesite	BG18-3952	163.1	PD; LM; WR; pXRF; SWIR
TS-972	183119	WBA	PA	Price Andesite	BG18-3952	165.2	R; pXRF; SWIR
TS-973	183120	WBA	PA	Price Andesite	BG18-3952	166.1	R; pXRF; SWIR
TS-974	183121	WBA	PA	Price Andesite	BG18-3952	169.2	R; pXRF; SWIR
TS-975	183122	WBA	PA	Price Andesite	BG18-3952	172.2	R; pXRF; SWIR
TS-976	183123	WBA	Md		BG18-3952	174.4	R; pXRF; SWIR
TS-977	183124	WBA	Md		BG18-3952	178.3	R; pXRF; SWIR
TS-978	183125	WBA	PA	Price Andesite	BG18-3952	181.4	R; pXRF; SWIR
TS-979	183126	WBA	PA	Price Andesite	BG18-3952	184.4	R; pXRF; SWIR
TS-980	183127	WBA	PA	Price Andesite	BG18-3952	187.5	R; pXRF; SWIR
TS-981	183128	WBA	PA	Price Andesite	BG18-3952	190.5	R; pXRF; SWIR
TS-982	183129	WBA	PA	Price Andesite	BG18-3952	193.5	R; pXRF; SWIR
TS-983	183130	WBA	PA	Price Andesite	BG18-3952	196.6	R; pXRF; SWIR
TS-984	183131	WBA	PA	Price Andesite	BG18-3952	198.1	R; pXRF; SWIR
TS-1055	183132	WBA	Avc	Hanging Wall And	BG18-3921	3.0	R; SWIR
TS-1056	183133	WBA	Avc	Hanging Wall And	BG18-3921	6.1	R; SWIR
TS-1057	183134	WBA	Md		BG18-3921	9.1	R; SWIR
TS-1058	183135	WBA	Avc	Hanging Wall And	BG18-3921	12.5	R; SWIR
TS-1059	183136	WBA	Avc	Hanging Wall And	BG18-3921	15.2	R; SWIR
TS-1060	183137	WBA	Md		BG18-3921	21.3	R; SWIR
TS-1061	183138	WBA	Avc	Hanging Wall And	BG18-3921	22.7	R; SWIR
TS-1062	183139	WBA	Md		BG18-3921	24.8	R; SWIR
TS-1063	183140	WBA	Avc	Hanging Wall And	BG18-3921	26.0	R; SWIR
TS-1064	183141	WBA	Avc	Hanging Wall And	BG18-3921	28.0	R; SWIR
TS-1065	183142	WBA	Fd		BG18-3921	33.6	R; SWIR
TS-1066	183143	WBA	Fd		BG18-3921	35.0	R; SWIR

Table A.1 Continued.

Field ID	UTAS ID	Area	Rock Code	Strat Member	DDH	Depth (m)	Preparation
TS-1067	183144	WBA	Avc	Hanging Wall And	BG18-3921	36.3	R; SWIR
TS-1068	183145	WBA	Md		BG18-3921	39.6	R; SWIR
TS-1069	183146	WBA	Avc	Hanging Wall And	BG18-3921	42.7	R; SWIR
TS-1070	183147	WBA	Avc	Hanging Wall And	BG18-3921	43.5	R; SWIR
TS-1071	183148	WBA	Avc	Hanging Wall And	BG18-3921	45.5	R; SWIR
TS-1072	183149	WBA	Avc	Hanging Wall And	BG18-3921	49.0	R; SWIR
TS-1073	183150	WBA	Avc	Hanging Wall And	BG18-3921	51.5	R; SWIR
TS-1074	183151	WBA	Avc	Hanging Wall And	BG18-3921	54.1	R; SWIR
TS-1075	183152	WBA	Af	H-W	BG18-3921	55.9	R; pXRF; SWIR
TS-1076	183153	WBA	Af	H-W	BG18-3921	57.9	R; pXRF; SWIR
TS-1077	183154	WBA	Af	H-W	BG18-3921	70.0	R; pXRF; SWIR
TS-1078	183155	WBA	Af	H-W	BG18-3921	61.0	R; pXRF; SWIR
TS-1079	183156	WBA	Af	H-W	BG18-3921	62.4	R; pXRF; SWIR
TS-1080	183157	WBA	Af	H-W	BG18-3921	64.0	R; SWIR
TS-1081	183158	WBA	Af	H-W	BG18-3921	64.9	R; pXRF; SWIR
TS-1082	183159	WBA	Af	H-W	BG18-3921	66.8	R; pXRF; SWIR
TS-1083	183160	WBA	Af	H-W	BG18-3921	67.8	R; pXRF; SWIR
TS-1084	183161	WBA	Af	H-W	BG18-3921	69.1	R; pXRF; SWIR
TS-1085	183162	WBA	Af	H-W	BG18-3921	70.5	R; pXRF; SWIR
TS-1086	183163	WBA	Af	H-W	BG18-3921	74.7	R; LM; pXRF; SWIR
TS-1087	183164	WBA	Af	H-W	BG18-3921	75.1	R; pXRF; SWIR
TS-1088	183165	WBA	Md		BG18-3921	78.2	R; pXRF; SWIR
TS-1089	183166	WBA	Af	H-W	BG18-3921	81.0	R; pXRF; SWIR
TS-1090	183167	WBA	QFP	H-W	BG18-3921	83.1	R; SWIR
TS-1091	183168	WBA	QFP	H-W	BG18-3921	85.0	R; SWIR
TS-1092	183169	WBA	Md		BG18-3921	86.7	R; SWIR
TS-1093	183170	WBA	Md		BG18-3921	89.4	R; SWIR
TS-1094	183171	WBA	QFP	H-W	BG18-3921	90.2	R; SWIR
TS-1095	183172	WBA	QFP	H-W	BG18-3921	92.8	R; SWIR
TS-1096	183173	WBA	QFP	H-W	BG18-3921	95.0	R; SWIR
TS-1097	183174	WBA	QFP	H-W	BG18-3921	98.4	R; SWIR
TS-1098	183175	WBA	QFP	H-W	BG18-3921	100.3	R; SWIR
TS-1099	183176	WBA	QFP	H-W	BG18-3921	102.1	R; SWIR
TS-1100	183177	WBA	QFP	H-W	BG18-3921	105.4	R; SWIR
TS-1101	183178	WBA	QFP	H-W	BG18-3921	108.3	R; SWIR
TS-1102	183179	WBA	QFP	H-W	BG18-3921	110.0	R; SWIR
TS-1103	183180	WBA	QFP	H-W	BG18-3921	111.3	R; SWIR
TS-1104	183181	WBA	QFP	H-W	BG18-3921	113.8	R; SWIR
TS-1105	183182	WBA	QFP	H-W	BG18-3921	114.3	R; SWIR
TS-1106	183183	WBA	QFP	H-W	BG18-3921	116.1	R; SWIR
TS-1107	183184	WBA	Fvc	H-W	BG18-3921	119.4	R; SWIR
TS-1108	183185	WBA	Fvc	H-W	BG18-3921	120.6	R; SWIR
TS-1109	183186	WBA	Fvc	H-W	BG18-3921	122.7	R; SWIR
TS-1110	183187	WBA	Fvc	H-W	BG18-3921	125.4	R; SWIR
TS-1111	183188	WBA	Fvc	H-W	BG18-3921	126.5	R; SWIR
TS-1112	183189	WBA	Fvc	H-W	BG18-3921	128.3	R; SWIR
TS-1113	183190	WBA	Md		BG18-3921	129.4	R; SWIR
TS-1114	183191	WBA	Fvc	H-W	BG18-3921	130.5	R; SWIR
TS-1115	183192	WBA	Bvc	H-W	BG18-3921	132.7	R; SWIR
TS-1116	183193	WBA	Bvc	H-W	BG18-3921	134.0	R; SWIR
TS-1117	183194	WBA	Bvc	H-W	BG18-3921	135.6	R; SWIR
TS-1118	183195	WBA	Bvc	H-W	BG18-3921	137.4	R; SWIR
TS-1119	183196	WBA	Bvc	H-W	BG18-3921	139.7	R; SWIR

Table A.1 Continued.

Field ID	UTAS ID	Area	Rock Code	Strat Member	DDH	Depth (m)	Preparation
TS-1120	183197	WBA	Bvc	H-W	BG18-3921	141.8	R; SWIR
TS-1121	183198	WBA	Bvc	H-W	BG18-3921	143.9	R; SWIR
TS-1122	183199	WBA	Bvc	H-W	BG18-3921	145.5	R; SWIR
TS-1123	183200	WBA	Bvc	H-W	BG18-3921	146.1	R; SWIR
TS-1124	183201	RZN	QFP	H-W	RN18-0223	0.7	R; SWIR
TS-1125	183202	RZN	QFP	H-W	RN18-0223	3.0	R; SWIR
TS-1126	183203	RZN	QFP	H-W	RN18-0223	6.1	R; SWIR
TS-1127	183204	RZN	QFP	H-W	RN18-0223	9.1	R; SWIR
TS-1128	183205	RZN	QFP	H-W	RN18-0223	11.9	R; SWIR
TS-1129	183206	RZN	QFP	H-W	RN18-0223	15.4	R; SWIR
TS-1130	183207	RZN	QFP	H-W	RN18-0223	18.5	R; SWIR
TS-1131	183208	RZN	QFP	H-W	RN18-0223	21.3	R; SWIR
TS-1132	183209	RZN	QFP	H-W	RN18-0223	24.4	R; SWIR
TS-1133	183210	RZN	QFP	H-W	RN18-0223	27.4	R; SWIR
TS-1134	183211	RZN	QFP	H-W	RN18-0223	30.5	R; SWIR
TS-1135	183212	RZN	QFP	H-W	RN18-0223	33.1	R; SWIR
TS-1136	183213	RZN	QFP	H-W	RN18-0223	36.7	R; SWIR
TS-1137	183214	RZN	QFP	H-W	RN18-0223	39.6	R; SWIR
TS-1138	183215	RZN	Fvc	H-W	RN18-0223	43.7	R; SWIR
TS-1139	183216	RZN	Fvc	H-W	RN18-0223	45.7	R; SWIR
TS-1140	183217	RZN	Fvc	H-W	RN18-0223	48.9	R; SWIR
TS-1141	183218	RZN	Fvc	H-W	RN18-0223	51.8	R; SWIR
TS-1142	183219	RZN	Fvc	H-W	RN18-0223	55.0	R; SWIR
TS-1143	183220	RZN	Fvc	H-W	RN18-0223	58.1	R; SWIR
TS-1144	183221	RZN	Fvc	H-W	RN18-0223	61.0	R; SWIR
TS-1145	183222	RZN	Fvc	H-W	RN18-0223	64.0	R; SWIR
TS-1146	183223	RZN	Fvc	H-W	RN18-0223	67.3	R; SWIR
TS-1147	183224	RZN	Fvc	H-W	RN18-0223	70.1	R; SWIR
TS-1148	183225	RZN	Bvc	H-W	RN18-0223	73.2	R; SWIR
TS-1149	183226	RZN	Bvc	H-W	RN18-0223	76.6	R; SWIR
TS-1150	183227	RZN	Bvc	H-W	RN18-0223	79.6	R; SWIR
TS-1151	183228	RZN	PA	Price Andesite	RN18-0223	82.1	R; SWIR
TS-1152	183229	RZN	PA	Price Andesite	RN18-0223	85.5	R; pXRF; SWIR
TS-1153	183230	RZN	PA	Price Andesite	RN18-0223	88.6	R; pXRF; SWIR
TS-1154	183231	RZN	PA	Price Andesite	RN18-0223	90.4	R; pXRF; SWIR
TS-1155	183232	RZN	PA	Price Andesite	RN18-0223	91.4	R; pXRF; SWIR
TS-1156	183233	RZN	QFP	H-W	RN18-0224	1.5	R; pXRF; SWIR
TS-1157	183234	RZN	QFP	H-W	RN18-0224	6.3	R; pXRF; SWIR
TS-1158	183235	RZN	QFP	H-W	RN18-0224	9.1	R; pXRF; SWIR
TS-1159	183236	RZN	QFP	H-W	RN18-0224	13.3	R; pXRF; SWIR
TS-1160	183237	RZN	QFP	H-W	RN18-0224	15.2	R; pXRF; SWIR
TS-1161	183238	RZN	QFP	H-W	RN18-0224	18.3	R; pXRF; SWIR
TS-1162	183239	RZN	QFP	H-W	RN18-0224	21.3	R; pXRF; SWIR
TS-1163	183240	RZN	QFP	H-W	RN18-0224	24.4	R; pXRF; SWIR
TS-1164	183241	RZN	QFP	H-W	RN18-0224	27.3	R; pXRF; SWIR
TS-1165	183242	RZN	QFP	H-W	RN18-0224	30.5	R; pXRF; SWIR
TS-1166	183243	RZN	QFP	H-W	RN18-0224	33.5	R; pXRF; SWIR
TS-1167	183244	RZN	QFP	H-W	RN18-0224	36.6	R; pXRF; SWIR
TS-1168	183245	RZN	QFP	H-W	RN18-0224	39.3	R; pXRF; SWIR
TS-1169	183246	RZN	QFP	H-W	RN18-0224	42.7	R; pXRF; SWIR
TS-1170	183247	RZN	QFP	H-W	RN18-0224	45.7	R; pXRF; SWIR
TS-1171	183248	RZN	QFP	H-W	RN18-0224	49.0	R; pXRF; SWIR
TS-1172	183249	RZN	QFP	H-W	RN18-0224	51.8	R; pXRF; SWIR

Table A.1 Continued.

Field ID	UTAS ID	Area	Rock Code	Strat Member	DDH	Depth (m)	Preparation
TS-1173	183250	RZN	Fvc	H-W	RN18-0224	54.5	R; pXRF; SWIR
TS-1174	183251	RZN	Fvc	H-W	RN18-0224	57.9	R; SWIR
TS-1175	183252	RZN	sulfide ore	H-W	RN18-0224	61.5	R; SWIR
TS-1176	183253	RZN	Fvc	H-W	RN18-0224	64.0	R; SWIR
TS-1177	183254	RZN	Fvc	H-W	RN18-0224	67.1	R; SWIR
TS-1178	183255	RZN	Bvc	H-W	RN18-0224	69.9	R; SWIR
TS-1179	183256	RZN	Bvc	H-W	RN18-0224	73.2	R; SWIR
TS-1180	183257	RZN	PA	Price Andesite	RN18-0224	76.2	PD; LM; WR; pXRF; SWIR
TS-1181	183258	RZN	PA	Price Andesite	RN18-0224	79.2	R; pXRF; SWIR
TS-1182	183259	RZN	PA	Price Andesite	RN18-0224	82.3	R; pXRF; SWIR
TS-1183	183260	RZN	PA	Price Andesite	RN18-0224	83.3	R; SWIR
TS-1184	183261	RZN	QFP	H-W	RN18-0225	2.4	R; SWIR
TS-1185	183262	RZN	QFP	H-W	RN18-0225	4.6	R; SWIR
TS-1186	183263	RZN	QFP	H-W	RN18-0225	8.5	R; SWIR
TS-1187	183264	RZN	QFP	H-W	RN18-0225	10.7	R; SWIR
TS-1188	183265	RZN	QFP	H-W	RN18-0225	13.7	R; SWIR
TS-1189	183266	RZN	QFP	H-W	RN18-0225	16.4	R; SWIR
TS-1190	183267	RZN	QFP	H-W	RN18-0225	18.2	R; SWIR
TS-1191	183268	RZN	QFP	H-W	RN18-0225	19.2	R; SWIR
TS-1192	183269	RZN	Md		RN18-0225	20.5	R; SWIR
TS-1193	183270	RZN	QFP	H-W	RN18-0225	22.9	R; SWIR
TS-1194	183271	RZN	QFP	H-W	RN18-0225	26.2	R; SWIR
TS-1195	183272	RZN	QFP	H-W	RN18-0225	29.0	R; SWIR
TS-1196	183273	RZN	QFP	H-W	RN18-0225	32.0	R; SWIR
TS-1197	183274	RZN	QFP	H-W	RN18-0225	34.2	R; SWIR
TS-1198	183275	RZN	Fvc	H-W	RN18-0225	36.4	R; SWIR
TS-1199	183276	RZN	Fvc	H-W	RN18-0225	39.3	R; SWIR
TS-1200	183277	RZN	Fvc	H-W	RN18-0225	41.1	R; SWIR
TS-1201	183278	RZN	Fvc	H-W	RN18-0225	44.1	R; SWIR
TS-1202	183279	RZN	Fvc	H-W	RN18-0225	47.5	R; SWIR
TS-1203	183280	RZN	Fvc	H-W	RN18-0225	50.3	R; SWIR
TS-1204	183281	RZN	Fvc	H-W	RN18-0225	53.3	R; SWIR
TS-1205	183282	RZN	Fvc	H-W	RN18-0225	56.0	R; SWIR
TS-1206	183283	RZN	Fvc	H-W	RN18-0225	59.4	R; SWIR
TS-1207	183284	RZN	Fvc	H-W	RN18-0225	62.2	R; SWIR
TS-1208	183285	RZN	Fvc	H-W	RN18-0225	63.1	R; SWIR
TS-1209	183286	RZN	Fvc	H-W	RN18-0225	63.7	R; SWIR
TS-1210	183287	RZN	sulfide ore	H-W	RN18-0225	65.5	R; SWIR
TS-1211	183288	RZN	Bvc	H-W	RN18-0225	67.8	R; SWIR
BM14-001	183289	WBA	Avc	Hanging Wall And	BG18-3902	21.1	R; TS; PB
BM14-012	183290	WBA	Af	H-W	BG18-3903	78.6	R; TS; PB
BM14-021	183291	WBA	QFP	H-W	BG18-3769	62.0	R; TS; PB
BM14-023	183292	WBA	Bvc	H-W	BG18-3769	115.9	R; TS; PB
BM14-024	183293	WBA	PA	Price Andesite	BG18-3769	131.6	R; TS; PB
BM14-029	183294	WBA	PA	Price Andesite	BG18-3769	203.0	R; PD; TS; PB; LM; WR; G
BM14-037	183295	WBA	Md		BG18-3321	111.9	R; TS; PB
BM14-043	183296	WBA	PA	Price Andesite	BG18-3905	188.0	R; TS; PB; LM; G
BM14-052	183297	WBA	QFP	H-W	BG18-3907	31.9	R; TS; PB
BM14-060	183298	WBA	QFP	H-W	BG18-3554	103.6	R; TS; PB
BM14-070	183299	WBA	Fvc	H-W	BG18-3534	45.4	R; TS; PB
BM14-074	183300	WBA	PA	Price Andesite	BG18-3517	24.5	R; TS; PB; LM; G
UPB-03	183302	WBA	Id		BG18-3555	120.0	R; TS; PB
UPB-08	183303	WBA	QFP	H-W	BG18-3952	76.0	R; PD; TS; PB; LM; WR; G

Table A.1 Continued.

Field ID	UTAS ID	Area	Rock Code	Strat Member	DDH	Depth (m)	Preparation
UPB-13	183305	WBA	QFP	H-W	BG18-3921	101.0	R; TS; PB; G
UPB-05	183309	RZN	QFP	H-W	RN18-0224	8.0	R; PD; TS; PB; LM; WR; G
UPB-12	183310	WBA	Af	H-W	BG18-3921	59.0	R; PD; TS; PB; LM; WR; G
BM14-035	183311	WBA	sulfide ore	H-W	BG18-3321	94.5	R; TS; PB; MLA; EMPA
BM14-038	183312	WBA	sulfide ore	H-W	BG18-3904	96.2	TS; PB; MLA; EMPA
BM14-041	183313	WBA	sulfide ore	H-W	BG18-3905	122.0	R; TS; PB; MLA; EMPA
BM14-050	183314	WBA	sulfide ore	H-W	BG18-3553	95.3	TS; PB; MLA; EMPA
BM14-027	183315	WBA	sulfide ore	H-W	BG18-3769	182.6	TS; PB; MLA; EMPA
BM14-033	183316	WBA	sulfide ore	H-W	BG18-3321a	155.6	R; TS; PB; MLA; EMPA
BM14-026	183317	WBA	sulfide ore	H-W	BG18-3769	182.0	TS; PB; MLA; EMPA
BM14-053	183318	RZN	sulfide ore	H-W	RN18-0105	76.2	R; TS; PB; MLA; EMPA
BM15-099	183319	RZN	sulfide ore	H-W	RN18-0223	5.3	TS; PB; MLA; EMPA
BM14-057	183320	RZN	sulfide ore	H-W	RN18-0105	86.3	TS; PB; MLA; EMPA
BM15-096	183321	RZN	sulfide ore	H-W	RN18-0224	61.3	R; TS; PB; MLA; EMPA
BM15-095	183322	RZN	sulfide ore	H-W	RN18-0224	59.8	TS; PB; MLA; EMPA
BM15-092	183323	RZN	sulfide ore	H-W	RN18-0224	56.7	R; TS; PB; MLA; EMPA
MF18853	183328	RZW	PA	Price Andesite	LX10-2048	609.6	LM; SWIR
MF19908	183329	RZW	PA	Price Andesite	LX10-2040	572.5	LM; SWIR
UPB-06	183330	RZN	PA	Price Andesite	RN18-0224	78.0	R; LM; G
UPB-07	183331	RZN	PA	Price Andesite	RN18-0224	82.5	R; LM; G
UPB-10	183332	WBA	PA	Price Andesite	BG18-3952	146.5	R; LM; G

Area – RZN, Ridge Zone North; RZW, Ridge Zone West; WBA, West Block Area
Rock Code – A; argillite; Af, andesite flow; Avc, andesite volcaniclastics; Bvc, basal volcaniclastics; C; chert; Fd, felsic dyke; Fvc, felsic volcaniclastics; Id, intermediate dyke; Md, mafic dyke; PA, Price andesite; QFP, quartz and feldspar-phyric rhyolite; Qtz vn, quartz vein
Depth – reported in metres down hole
Preparation – R, rock sample, PD, powder sample; TS, polished thin section; PB, polished off-cut; LM, laser mount; MLA, Mineral Liberation Analysis; EMPA, electron microprobe analysis; WR, whole-rock geochemistry; G, geochronology; pXRF, portable X-ray fluorescence analysis; SWIR, shortwave infrared spectral analysis

Table A.2 Underground and Surface Sample Catalogue

Field ID	UTAS ID	Area	Rock Code	Strat Member	Type	mN	mE	Elv (m)	Preparation
UPB-02	183301	RZN	QFP	H-W	U	4495.0	855.0	12.49	R; TS; PB; LM; G
15Price02	183304	PM	Md		U	3373.0	4498.0	632.49	R; PD; TS; PB; WR; G
15Price01	183306	PM	Fvc	L-M-P	U	3390.0	4498.0	632.49	R; TS; PB; LM; G
15RN04	183307	RZN	Fvc	H-W	U	4465.0	1010.0	2.48	R; TS; PB; LM; G
15Price03	183308	PM	Md		U	3396.0	4498.0	632.49	R; TS; PB; LM; G
MF-2017-772	183324	PM	Fvc	L-M-P	S	3374.0	5514.0	572.49	R; TS; PB; LM; G
MF-2017-774	183325	PM	Fvc	L-M-P	S	3369.0	5517.0	572.49	R; TS; PB; LM; G
MF-2017-777	183326	PM	PA	Price Andesite	S	3505.2	5928.4	230.49	R; PD; TS; PB; WR; G
MF-2017-778	183327	PM	PA	Price Andesite	S	3505.2	5958.8	230.49	R; PD; TS; PB; WR; G
BM17-P5-B	183333	PM	Fvc	L-M-P	S	3372.0	5515.0	572.49	R; PD; LM; WR; G
BM17-P5-D	183334	PM	Fvc	L-M-P	S	3366.0	5519.0	572.49	R; PD; ; WR; G
BM17-P5-E	183335	PM	Fvc	L-M-P	S	3361.0	5521.0	572.49	R; LM; G

Area – PM, Pirce Mine; RZN, Ridge Zone North;
Rock Code – Fvc, felsic volcaniclastics; Md, mafic dyke; PA, Price andesite; QFP, quartz and feldspar-phyric rhyolite
Type – U, underground; S, surface
mN & mE – reported in mine coordinate system
Elv (m) – reported in metres above sea level
Preparation – R, rock sample, PD, powder sample; TS, polished thin section; PB, polished off-cut; LM, laser mount; WR, whole-rock geochemistry; G, geochronology

Appendix B:

Detailed Graphic Logs

This section provides a selection of detailed graphic logs produced and used in this study. Table B.1 presents the drill hole names, lengths, areas and section locations.

Table B.1 List of provided detailed graphic logs.

DDH	Length (m)	Area	Section (mE)	Pages
BG18-3901	225.0	WBA	550	2
BG18-3902	225.0	WBA	550	2
BG18-3903	225.0	WBA	550	2
BG18-3904	199.6	WBA	550	2
BG18-3905	196.6	WBA	550	2
BG18-3906	133.2	WBA	550	2
BG18-3907	213.4	WBA	585	2
BG18-3321a	239.3	WBA	640	2
BG18-3550	255.6	WBA	640	2
BG18-3551	255.6	WBA	640	2
BG18-3552	226.0	WBA	640	2
BG18-3553	245.0	WBA	640	2
BG18-3554	248.4	WBA	640	2
BG18-3921	146.3	WBA	640	2
BG18-3555	435.9	WBA	640	4
BG18-3952	198.1	WBA	700	2
BG18-3323	226.0	WBA	828	2
BG18-3322	226.0	WBA	828	2
BG18-3321	219.5	WBA	828	2
BG18-3769	220.0	WBA	828	2
RN18-0223	91.4	RZN	918	1
RN18-0224	85.3	RZN	918	1
RN18-0225	70.1	RZN	918	1
RN18-0105	118.0	RZN	918	1
RN18-0104	150.9	RZN	957	1

Area – RZN, Ridge Zone North;
WBA, West Block Area

BG18-3901 page 1 of 2

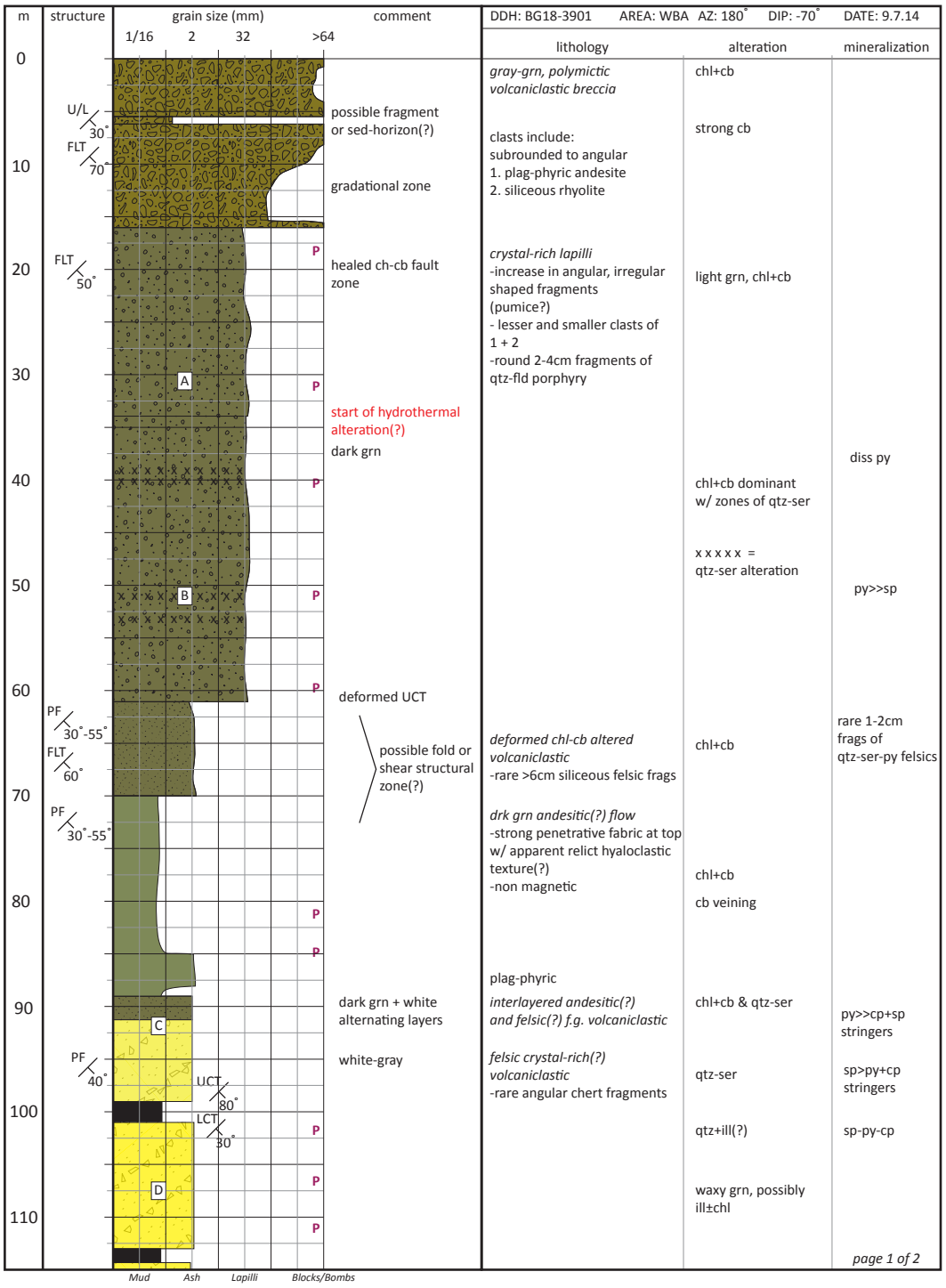

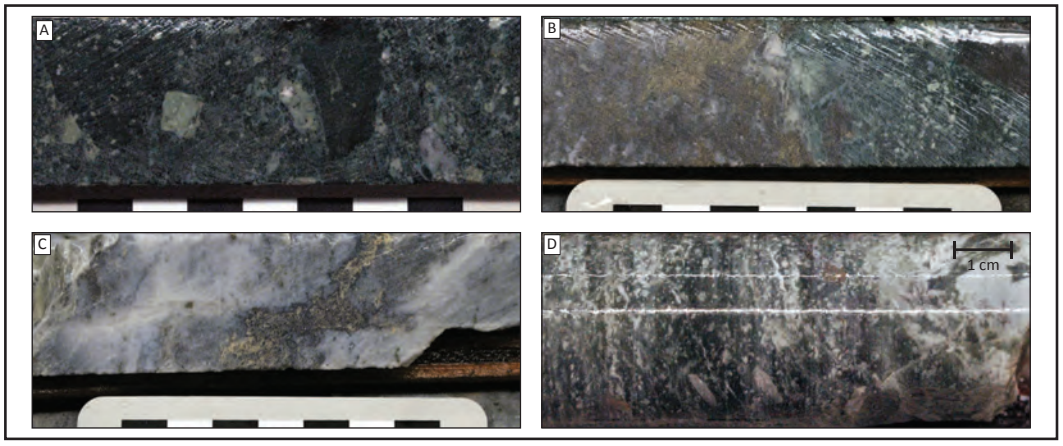

BG18-3901 page 2 of 2

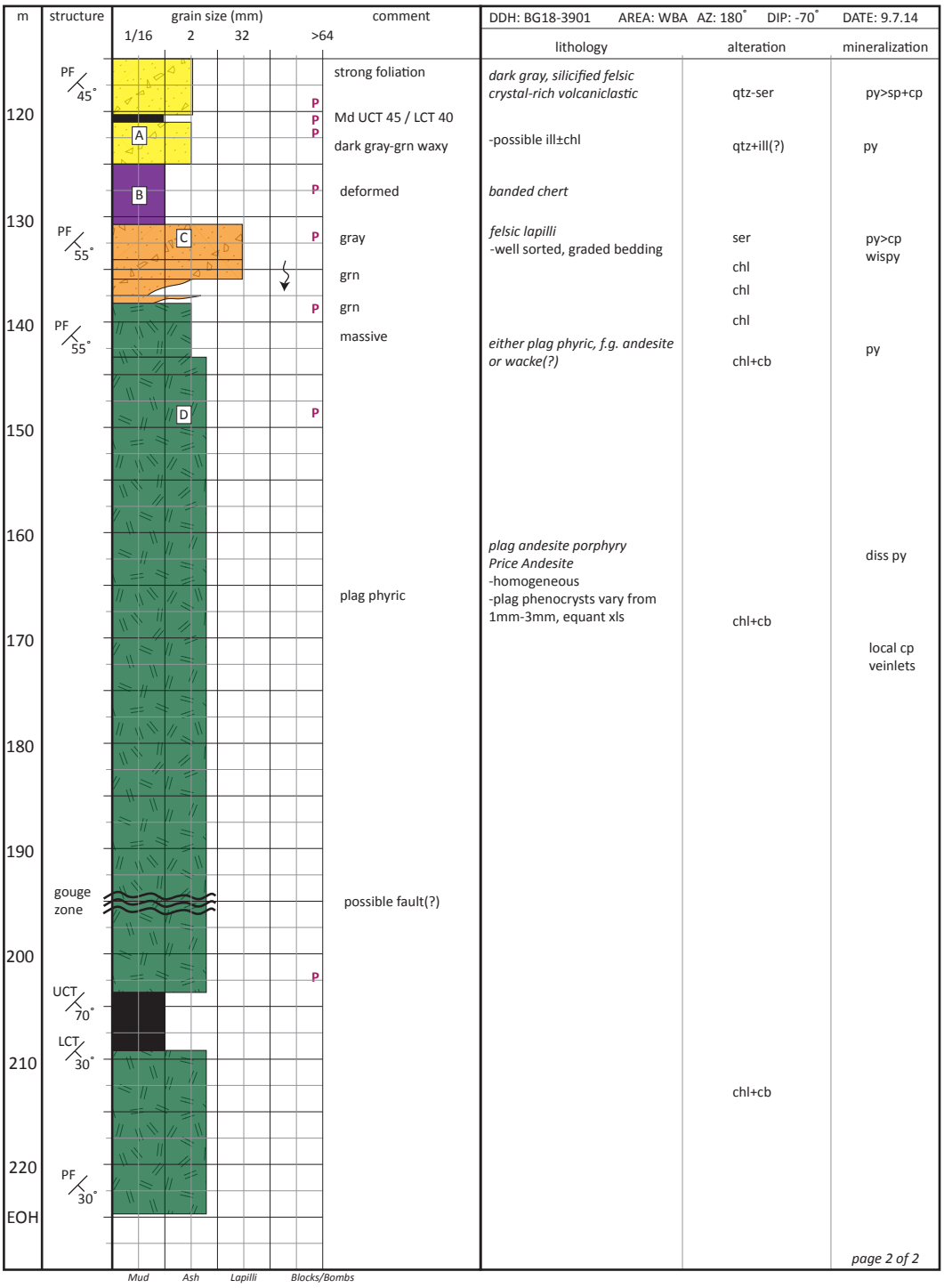

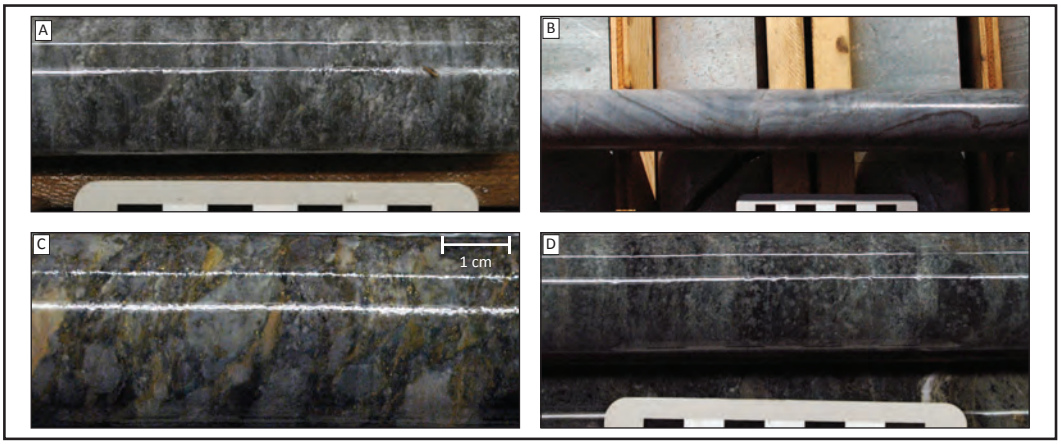

BG18-3902 page 1 of 2

DDH: BG18-3902 AREA: WBA AZ: 180° DIP: 60° DATE: 9.9.14

m	structure	grain size (mm) 1/16 2 32 >64	comment	lithology	alteration	mineralization
0			dark gray to grn	*polymictic andesite breccia* -same as top of BG18-3901	metamorphic(?) chl+cb	
10				*andesite crystal-rich lapilli* -on av. 2mm crystal-rich matrix -lack qtz => intermediate comp -5-10% angular felsic(?) lithics		
20	PF 65° A	P	light gray to grn BM14-001 @ 21.1m		metamorphic(?) chl+cb	
30	B	P P	dark gray to grn	5-10%, 3-6cm angular to sub-angular clasts of: 1. fsp-phyric rhyolite 2. siliceous rhyolite 3. plag phyric andesite 4. chert (rare).	metamorphic(?) chl+cb	
40			start of hydrothermal alteration(?) dark grn			
50		P			chl+cb+py	diss py
60	PF 35° PF 55°	P	dark grn locally white-gray Fault zone: broken core	*crystal-rich andesitic lapilli* -less than 1% lithics *andesitic f.g. volcaniclastic(?)*	x x x x x = qtz+ser	diss py local py stringers
70		P		*massive, light grn andesite flow(?)* -local hyaloclastic texture	chl+cb+py cb+chl	
80		P P		plag phyric unit, part of flow or dike(?)		
90	C PF 70° PF 75° UCT 40° LCT 60°	P P	possible shear zone(?) stringer sulfide	*andesitic f.g. volcaniclastic*	chl±ser+qtz qtz+ser	diss py
100	PF 70° PF 70°	P		*intensely altered rhyolite* -locally massive - possibly a coherent rhyolite or rhyolite volcaniclastic breccia(?)	qtz+ser	sp+py±gn stringers
110	PF 70° PF 60° D	P	"ill" altered "ill" altered	*chert, massive*	ill(?)	py py

Mud Ash Lapilli Blocks/Bombs

page 1 of 2

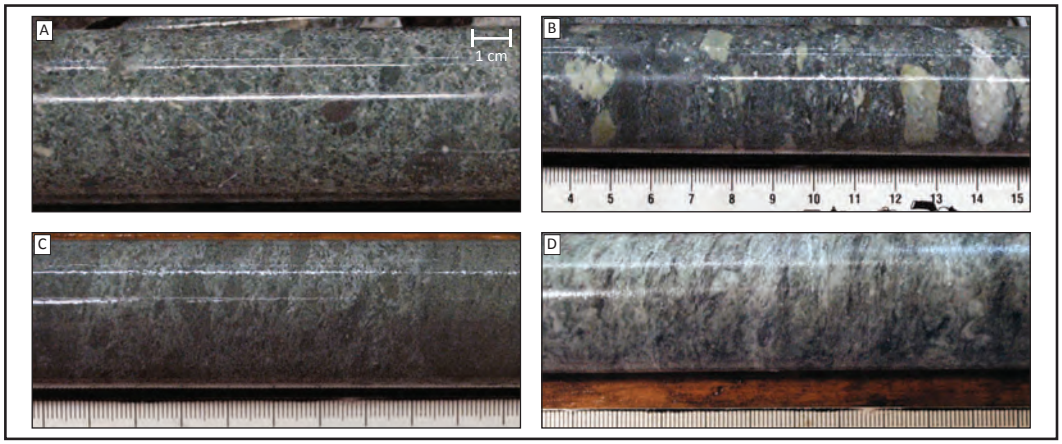

BG18-3902 page 2 of 2

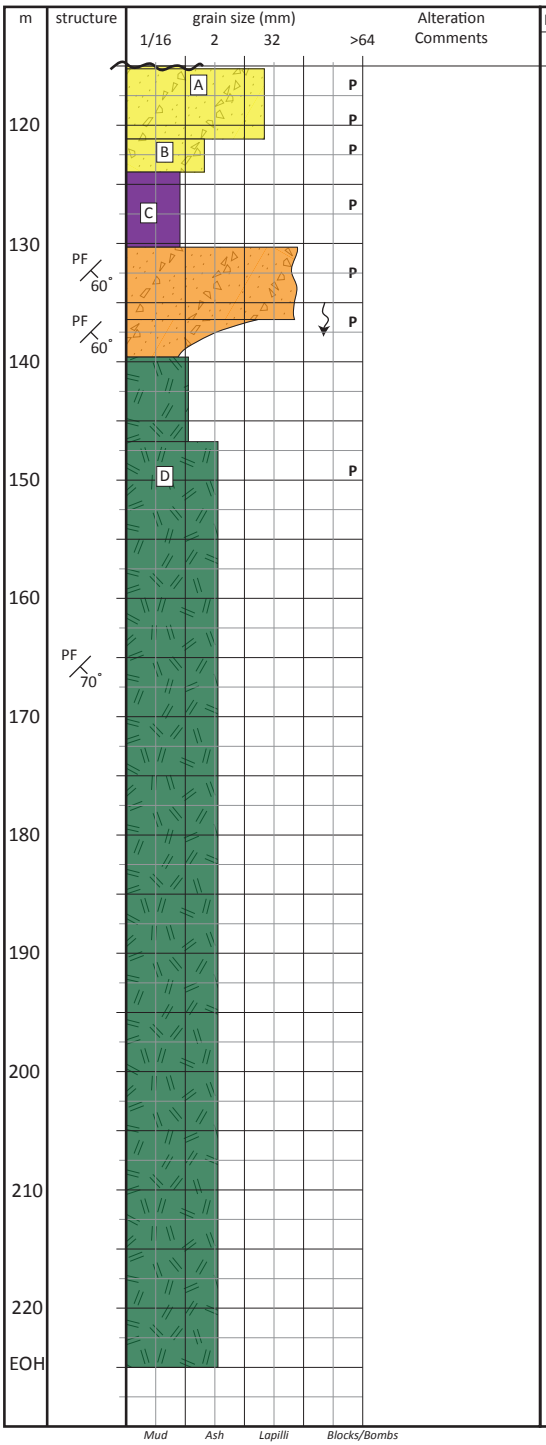

DDH: BG18-3902 AREA: WBA AZ: 180° DIP: -60° DATE: 9.9.14

lithology	alteration	mineralization
intense alteration of a polymictic feslic matrix fragmental (?) f.g. felsic volcaniclastic	silica-f.g. sulfide silicification	f.g. sulfide
massive to deformed, thin bedded chert	qtz+ser	sp>py stringers/ net texture
andesite(?)-rhyolite lapilli volcaniclastic -well sorted clast size -fines down hole to wacke-sandstone grain size	ser+chl+py	py diss
altered andesite could be sedimentary rock or chill margin (?)	chl+cb	
altered, massive andeiste -plag phyric -ghost plag phenos common -possible flow(?) local patchy, mottled texture -minor diss pyrite	chl+cb	

page 2 of 2

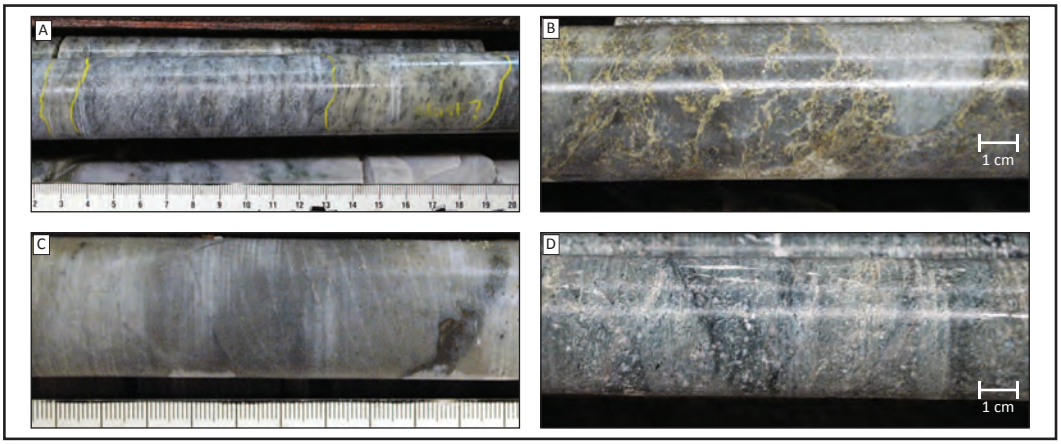

BG18-3903 page 1 of 2

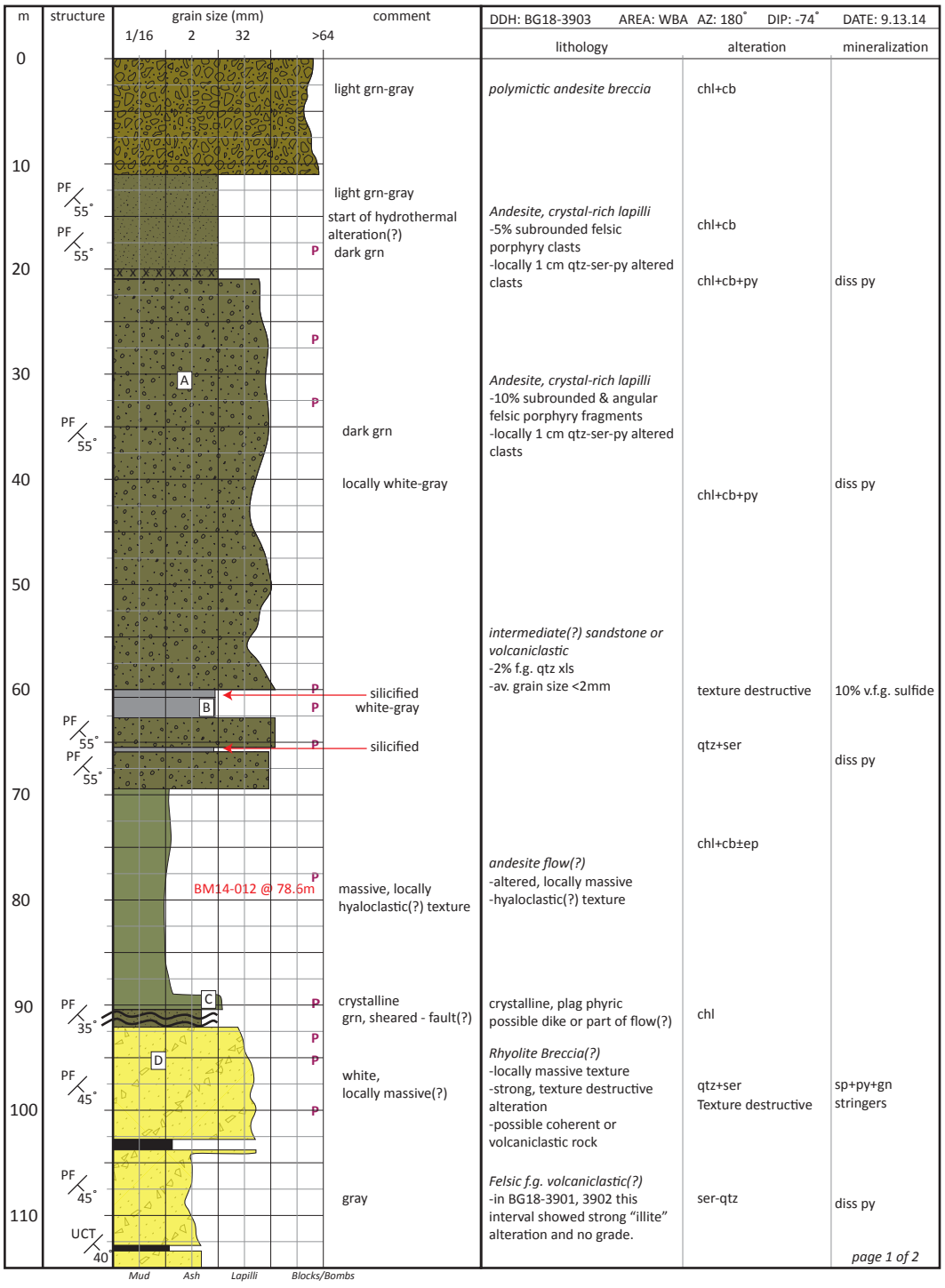

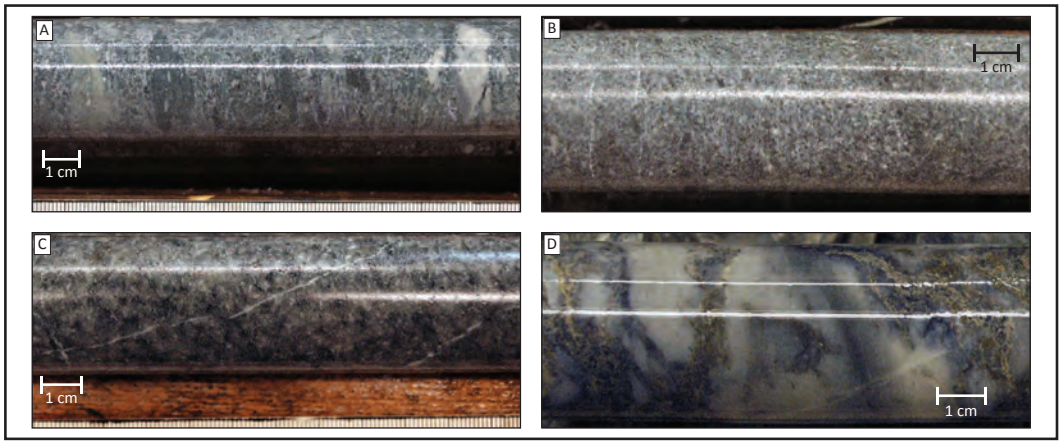

BG18-3903 page 2 of 2

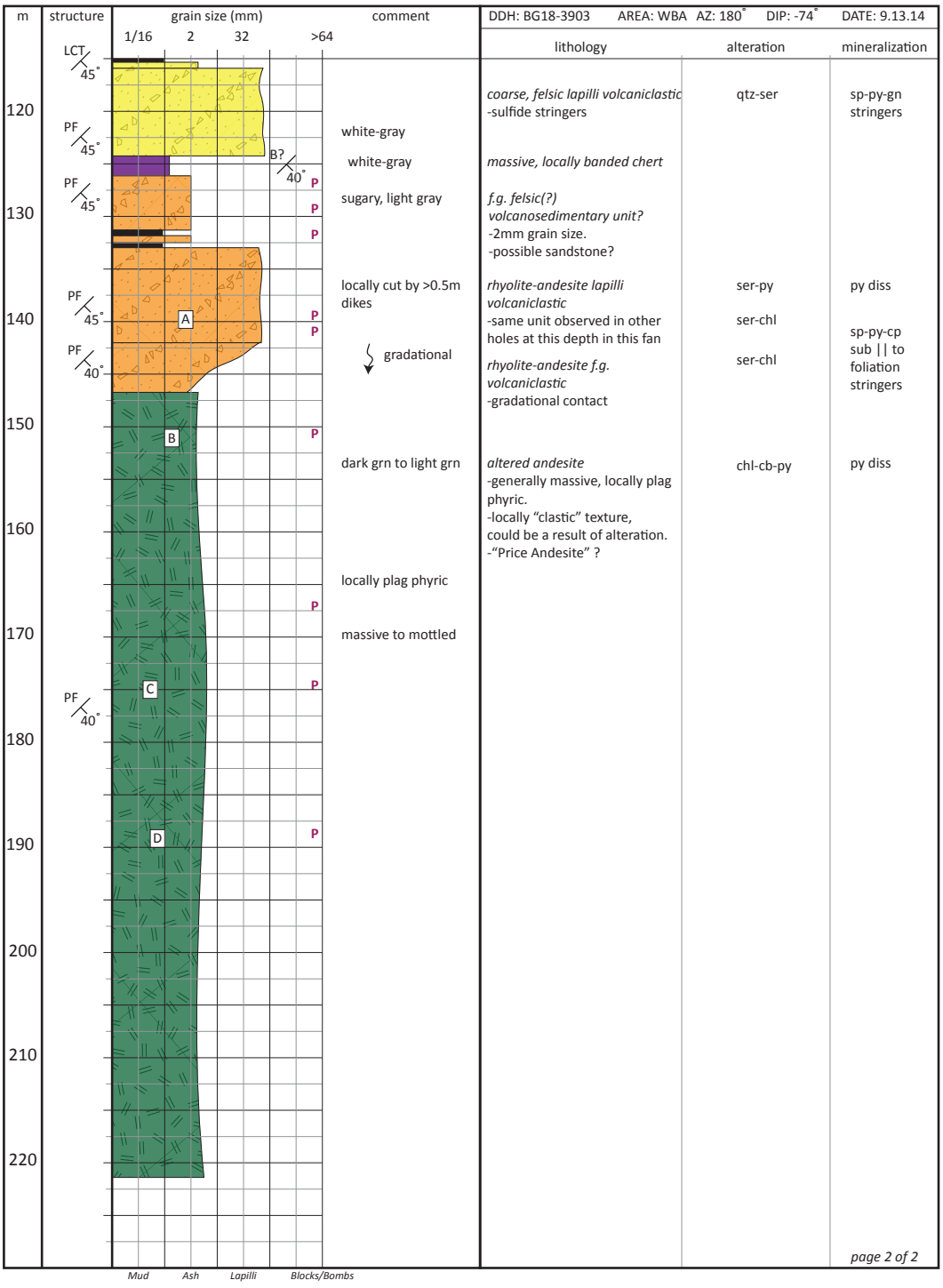

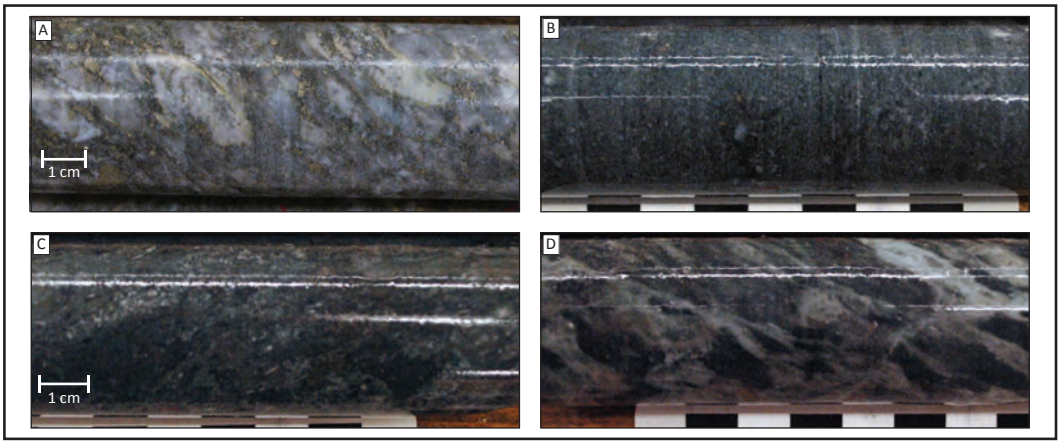

BG18-3904 page 1 of 2

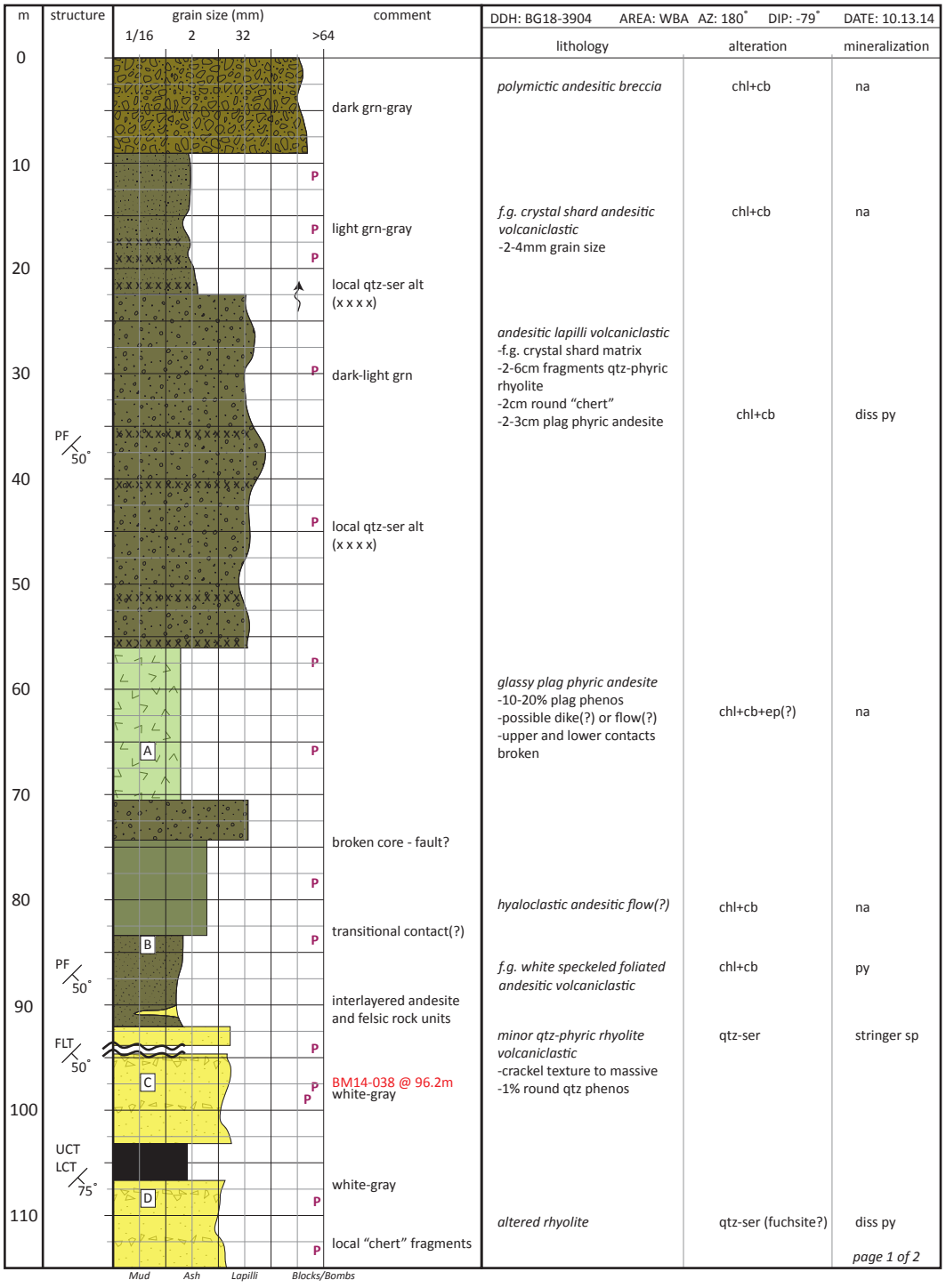

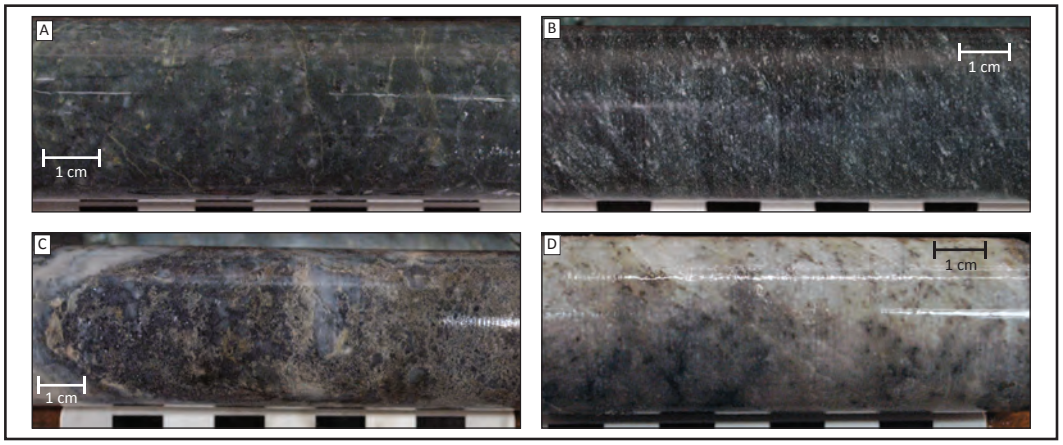

BG18-3904 page 2 of 2

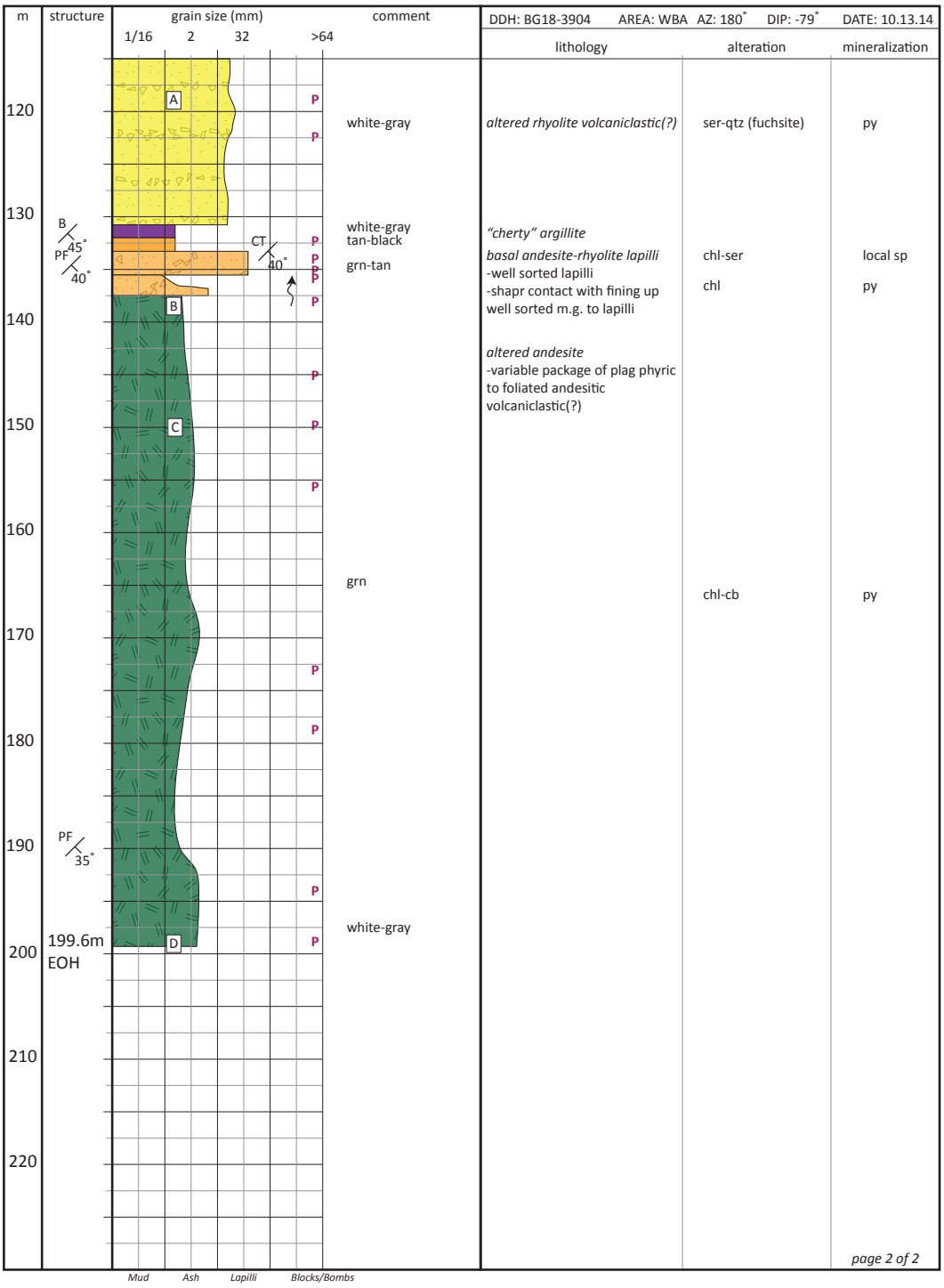

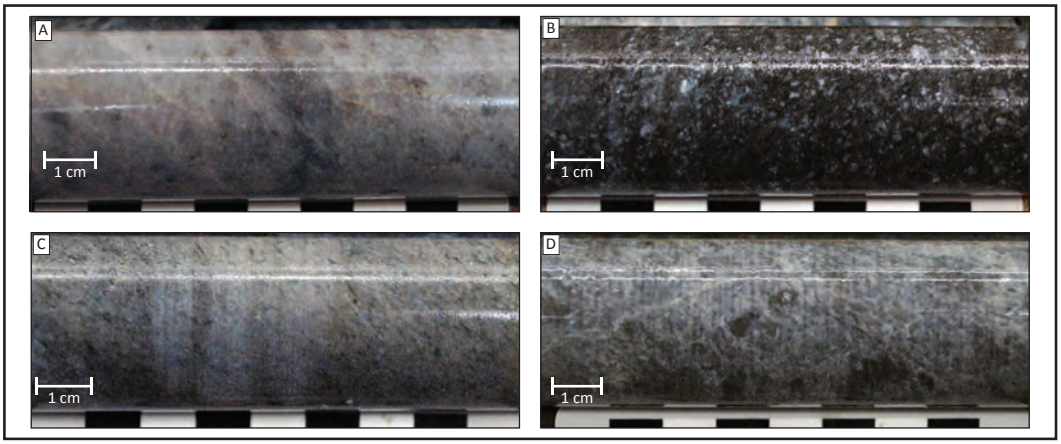

BG18-3905 page 1 of 2

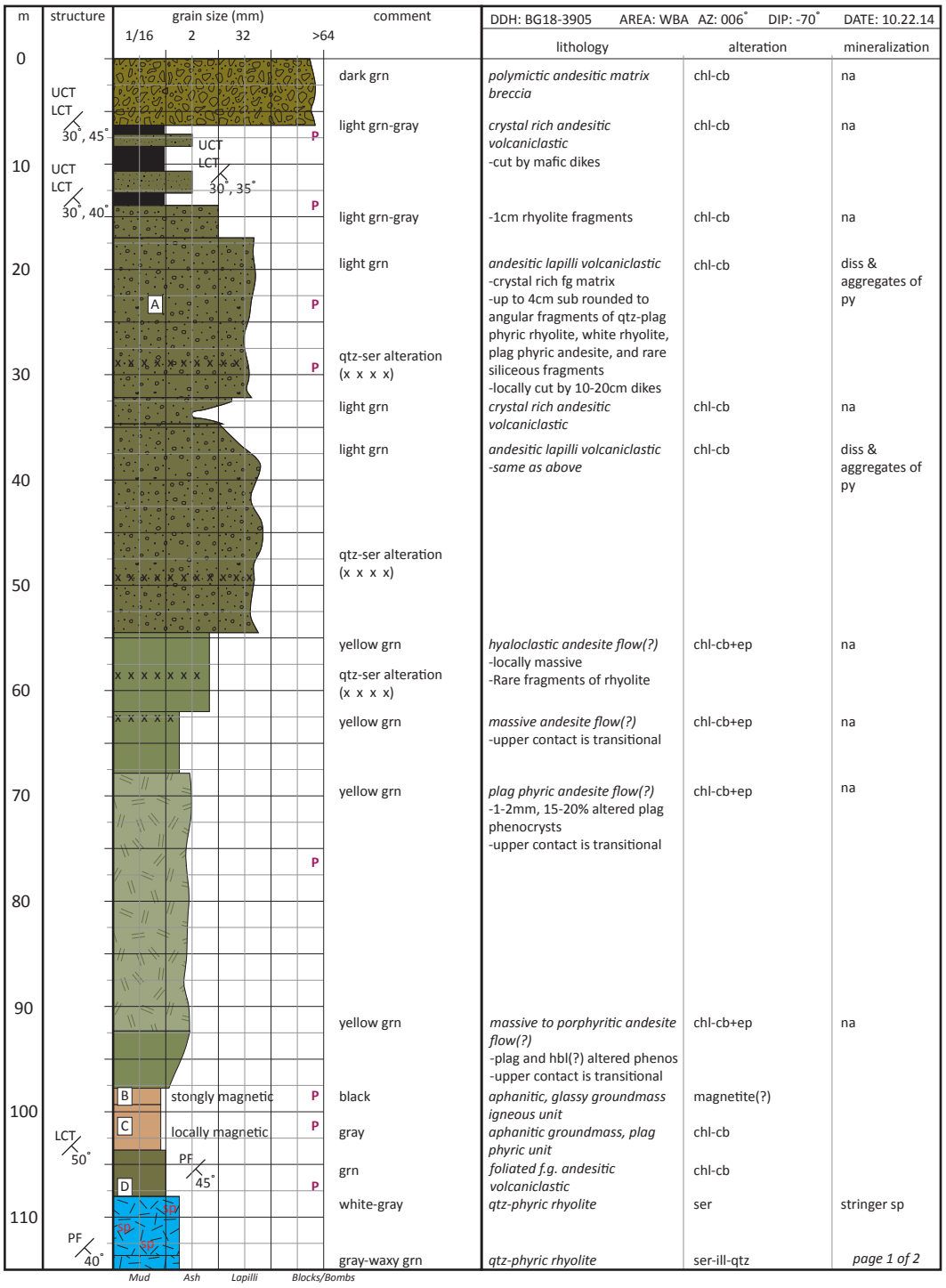

DDH: BG18-3905 AREA: WBA AZ: 006˚ DIP: -70˚ DATE: 10.22.14

comment	lithology	alteration	mineralization
dark grn	*polymictic andesitic matrix breccia*	chl-cb	na
light grn-gray	*crystal rich andesitic volcaniclastic* -cut by mafic dikes	chl-cb	na
light grn-gray	-1cm rhyolite fragments	chl-cb	na
light grn	*andesitic lapilli volcaniclastic* -crystal rich fg matrix -up to 4cm sub rounded to angular fragments of qtz-plag phyric rhyolite, white rhyolite, plag phyric andesite, and rare siliceous fragments -locally cut by 10-20cm dikes	chl-cb	diss & aggregates of py
qtz-ser alteration (x x x x)			
light grn	*crystal rich andesitic volcaniclastic*	chl-cb	na
light grn	*andesitic lapilli volcaniclastic* *-same as above*	chl-cb	diss & aggregates of py
qtz-ser alteration (x x x x)			
yellow grn	*hyaloclastic andesite flow(?)* -locally massive -Rare fragments of rhyolite	chl-cb+ep	na
qtz-ser alteration (x x x x)			
yellow grn	*massive andesite flow(?)* -upper contact is transitional	chl-cb+ep	na
yellow grn	*plag phyric andesite flow(?)* -1-2mm, 15-20% altered plag phenocrysts -upper contact is transitional	chl-cb+ep	na
yellow grn	*massive to porphyritic andesite flow(?)* -plag and hbl(?) altered phenos -upper contact is transitional	chl-cb+ep	na
black	*aphanitic, glassy groundmass igneous unit*	magnetite(?)	
gray	*aphanitic groundmass, plag phyric unit*	chl-cb	
grn	*foliated f.g. andesitic volcaniclastic*	chl-cb	
white-gray	*qtz-phyric rhyolite*	ser	stringer sp
gray-waxy grn	*qtz-phyric rhyolite*	ser-ill-qtz	*page 1 of 2*

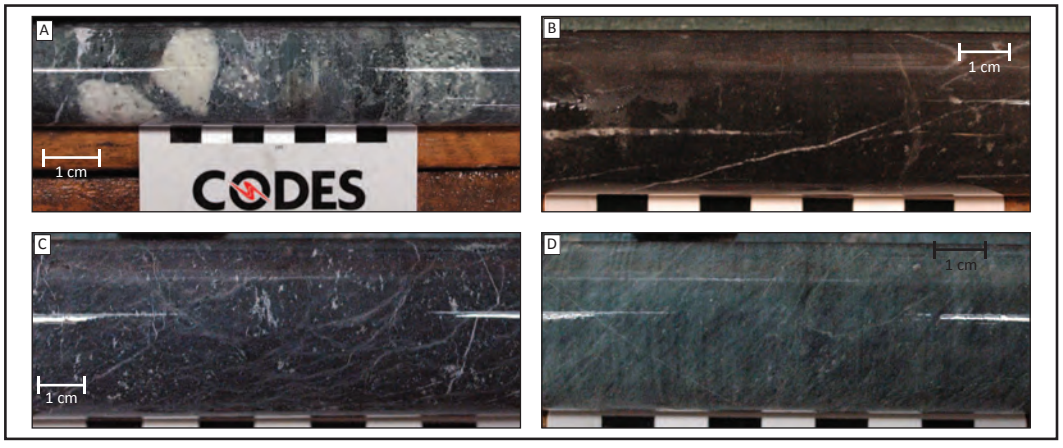

BG18-3905 page 2 of 2

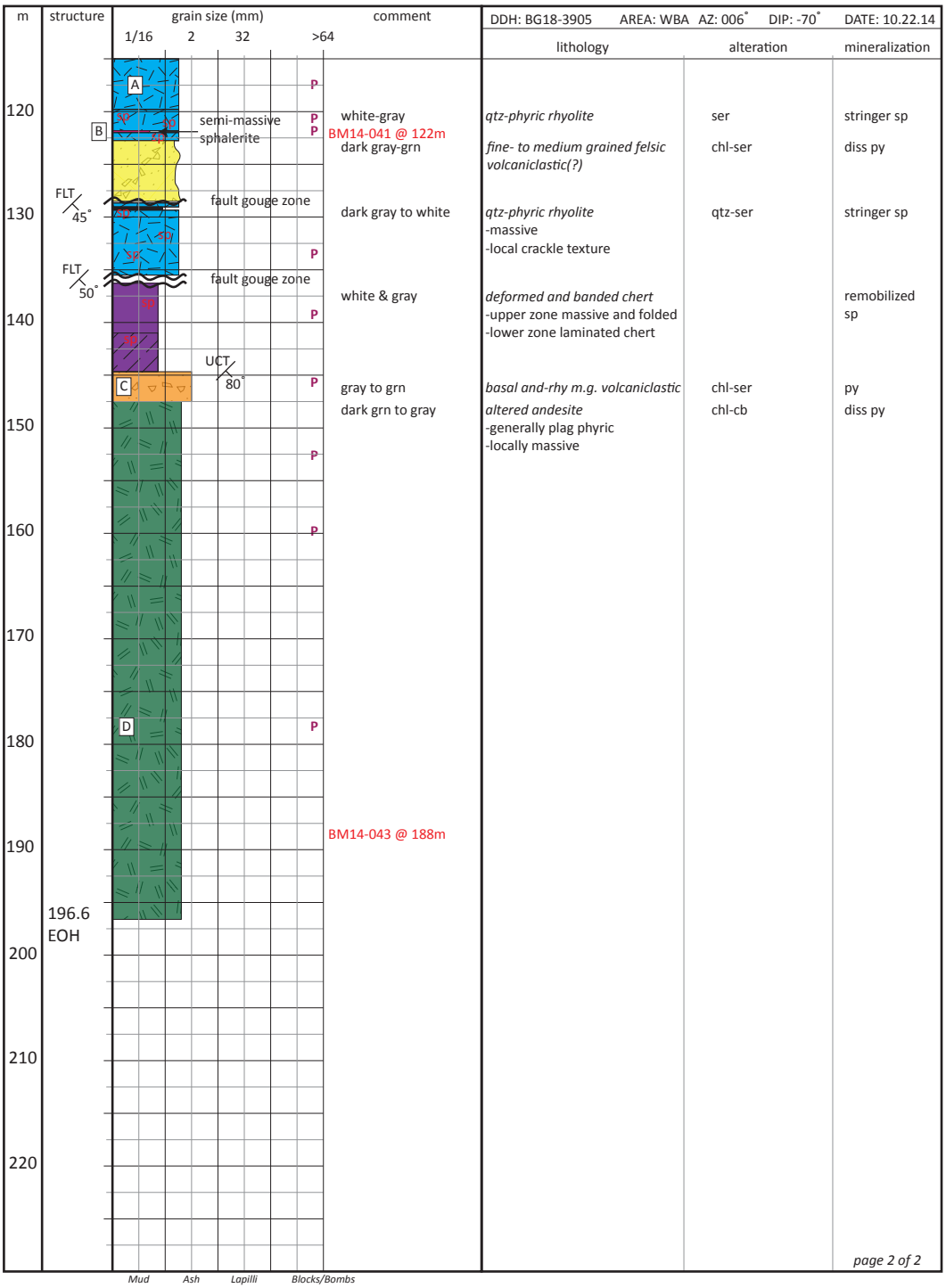

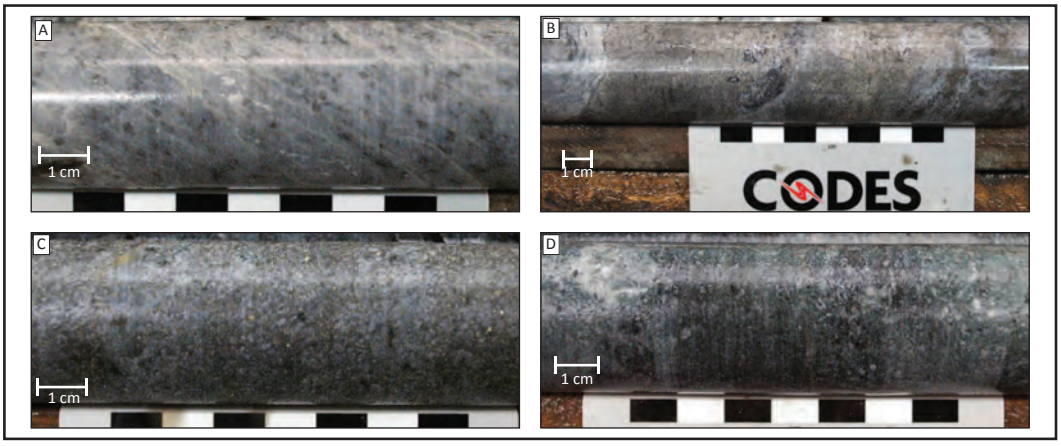

BG18-3906 page 1 of 2

DDH: BG18-3906 AREA: WBA AZ: 000° DIP: -54° DATE: 10.25.14

m	structure	grain size (mm) 1/16 2 32 >64	comment	lithology	alteration	mineralization
0		A P	dark grn	*andesitic polymictic breccia* -crystal shard matrix -20% blocks of rhy and andesite	chl-cb	na
	PF 75°	UCT LCT 30° P	light grn to gray	*andesitic volcaniclastic* -crystal shard matrix -up to 5% 0.5cm in size lithics	chl-cb	na
10		P	light grn to gray	-increase in fragments, 30% angular rhy-and fragments -upper contact is gradational	chl-cb	na
			black	*fine-grained mafic dike*		
20	LCT 40°		dark grn	-alt change, same unit as above	chl-ep	na
		UCT LCT 35°	black	*fine-grained mafic dike*		
			gray	*texture destructive altered andesite(?)*	silicification	f.g. sulfide
30		B P	dark grn	-alt change, same unit as above	chl-ep	minor py
			gray	*texture destructive altered andesite(?)*	silicification	f.g. sulfide
			dark grn	-alt change, same unit as above	chl-ep	minor py
40		P	dark grn & yellow grn	*hyaloclastic andesite flow(?)* -rare fragments of rhyolite	chl-cb	minor py
		qtz-ser alt (x x x) P	dark grn	*massive andesite flow(?)* -locally plag phyric	chl-cb	minor py
50	UCT 40°		gray	*texture destructive altered andesite(?)*	silicification	f.g. sulfide
			dark grn	*massive andesite flow(?)* -locally plag phyric	chl-cb	minor py
60		P	yellow grn	*massive andesite flow(?)* -locally plag phyric	chl-ep	minor py
	UCT 45°		yellow grn	*massive andesite flow(?)* -locally plag phyric	chl-ep	minor py
	UCT LCT 25°		black	*fine-grained mafic dike*		
70		P				
			yellow grn	*massive andesite flow(?)*	chl-ep	minor py
80		P				
90			grn	*massive andesite flow(?)*	chl-cb	minor py
		C P	gray	*texture destructive altered andesite(?)*	silicification	f.g. sulfide
			grn	*massive andesite flow(?)*	chl-cb	minor py
100		P	gray	*texture destructive altered andesite(?)*	silicification	f.g. sulfide
			gray	*texture destructive altered andesite(?)*	silicification	f.g. sulfide
		sp D sp P				
110		sp sp sp sp	white to gray	*qtz-fsp rhyolite* -massive, locally contains up to 10% fsp and qtz phenocrysts -local crackle texture	qtz-ser	polymetallic sulfide stringers sphalerite-rich

page 1 of 2

Mud Ash Lapilli Blocks/Bombs

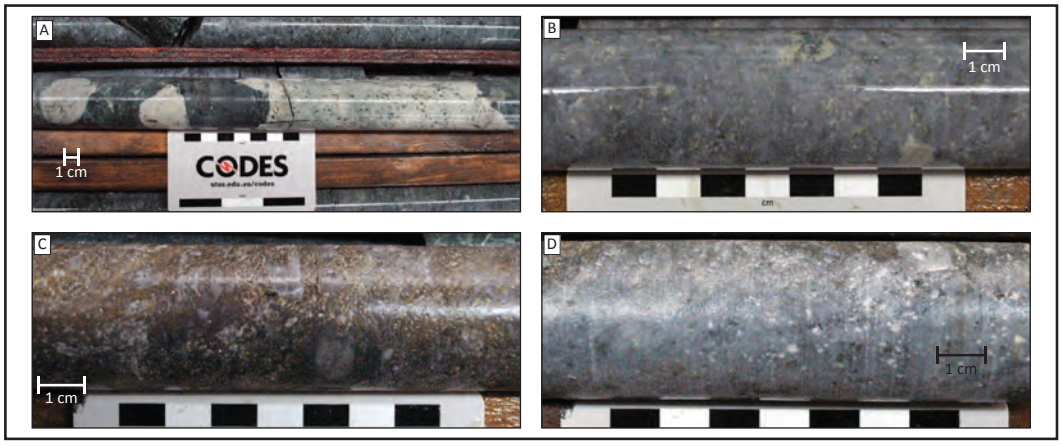

BG18-3906 page 2 of 2

DDH: BG18-3906 AREA: WBA AZ: 000° DIP: -54° DATE: 10.25.14

m	structure	grain size (mm) 1/16 2 32 >64	comment	lithology	alteration	mineralization
120		A: sp; B: sp; sp; sp; P; P	white to gray	*qtz-fsp rhyolite* -massive, locally contains up to 10% fsp and qtz phenocrysts -local crackle texture	qtz-ser	polymetallic sulfide stringers sphalerite-rich
	PF 15°					
	LCT 35°		dark green	*fine-grained mafic dike*		
130	C: sp+cpy	P	white	*massive quartz ± calcite vein*		sphalerite-chalcopyrite
	133.2 EOH					
140						
150						
160						
170						
180						
190						
200						
210						
220						

Mud Ash Lapilli Blocks/Bombs

page 2 of 2

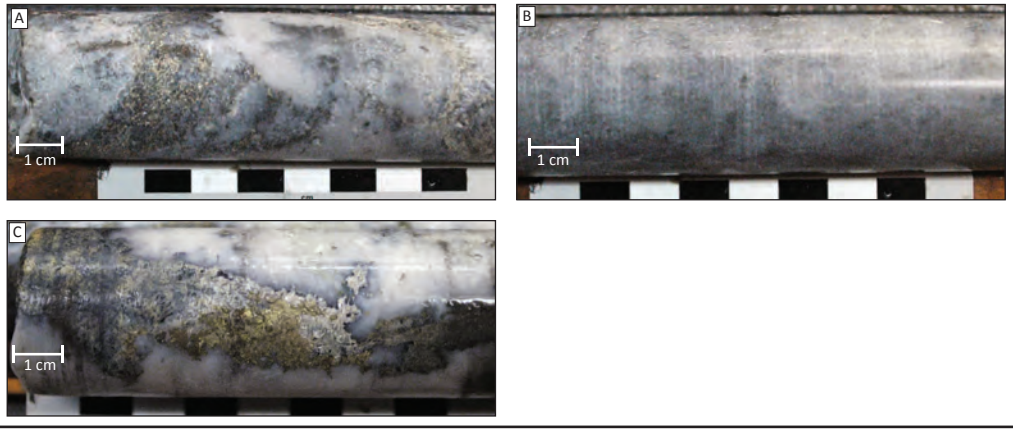

BG18-3321A page 1 of 2

DDH: BG18-3321A AREA: WBA AZ: 180° DIP: -77.6° DATE: 10.13.14

m	structure	comment	lithology	alteration	mineralization
0		dark gray-grn	*polymictic andesitic breccia*	chl+cb	na
			andesitic f.g. volcaniclastic -crystal shard-rich matrix -5%, 1.5cm rhyolite fragments	chl+cb	na
10		gray-grn			
	UCT LCT 35°		*andesitic lapilli volcaniclastic* -crystal shard-rich matrix -5-10%, 2-6cm qtz-phyric rhyolite -1% plag phyric andesite	chl+cb	py
20		dark-medium grn			
	UCT LCT 50°				
	UCT LCT 45°, 50° A	possible hyaloclastite(?)	-dark grn flattened "fragments" -yellow-green "matrix"	chl+cb	na
30		light-dark grn	-5% blocks of qtz-fsp rhyolite -fine grained green matrix		
40					
	PF 45°		-fines down hole -f.g. foliated andesitic volcaniclastic	chl+cb	na
50	FLT 40° B	healed shear zone(?)	-folded & detached chlorite-carbonate veins -foliated fine grained andesitic volcaniclastic		remobilized py-cp
	PF 40°			chl+cb	
60	BK BK				
	UCT LCT UCT 50°	gray-white	*qtz-phyric rhyolite* -upper interval crackle texture -lower interval coherent	ser-qtz±chl	diss & stringer pyrite
70	LCT 75° UCT LCT 70° C BK				
	UCT LCT 40°			ser-qtz±chl	py
80					
	PF 75°	white-gray	*f.g. rhyolite volcaniclastic* -upper interval crackle texture -lower interval coherent	qtz-ser	stringer py
90		white-gray	*altered, massive rhyolite* -no obvious qtz phenocrysts	qtz-ser	stringer py
100					
	D	white-gray-grn	*banded chert & altered argillite* -upper interval massive to banded gray-white "chert" -lower interval interlayered, gray-grn, soft mudstone-siltstone-sandstone		
110	B? 75°	sandstone interval(?)			

grain size (mm): 1/16 | 2 | 32 | >64

Mud | Ash | Lapilli | Blocks/Bombs

page 1 of 2

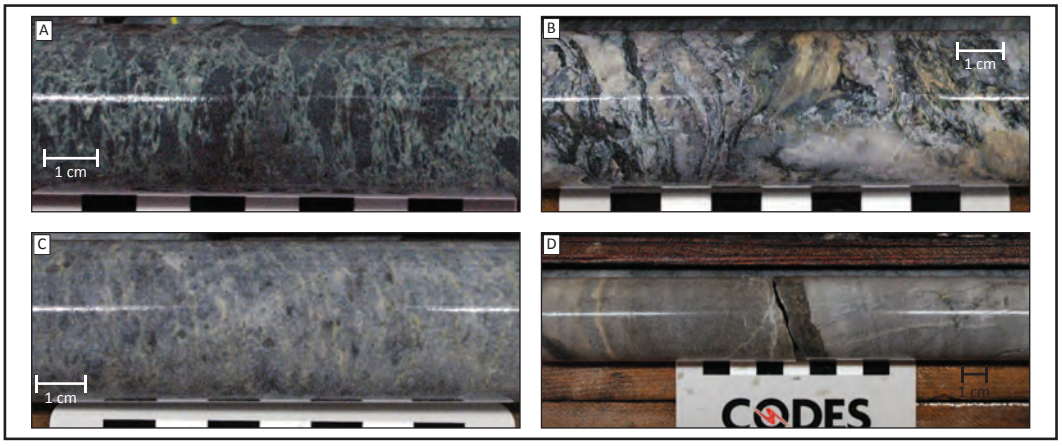

BG18-3321A page 2 of 2

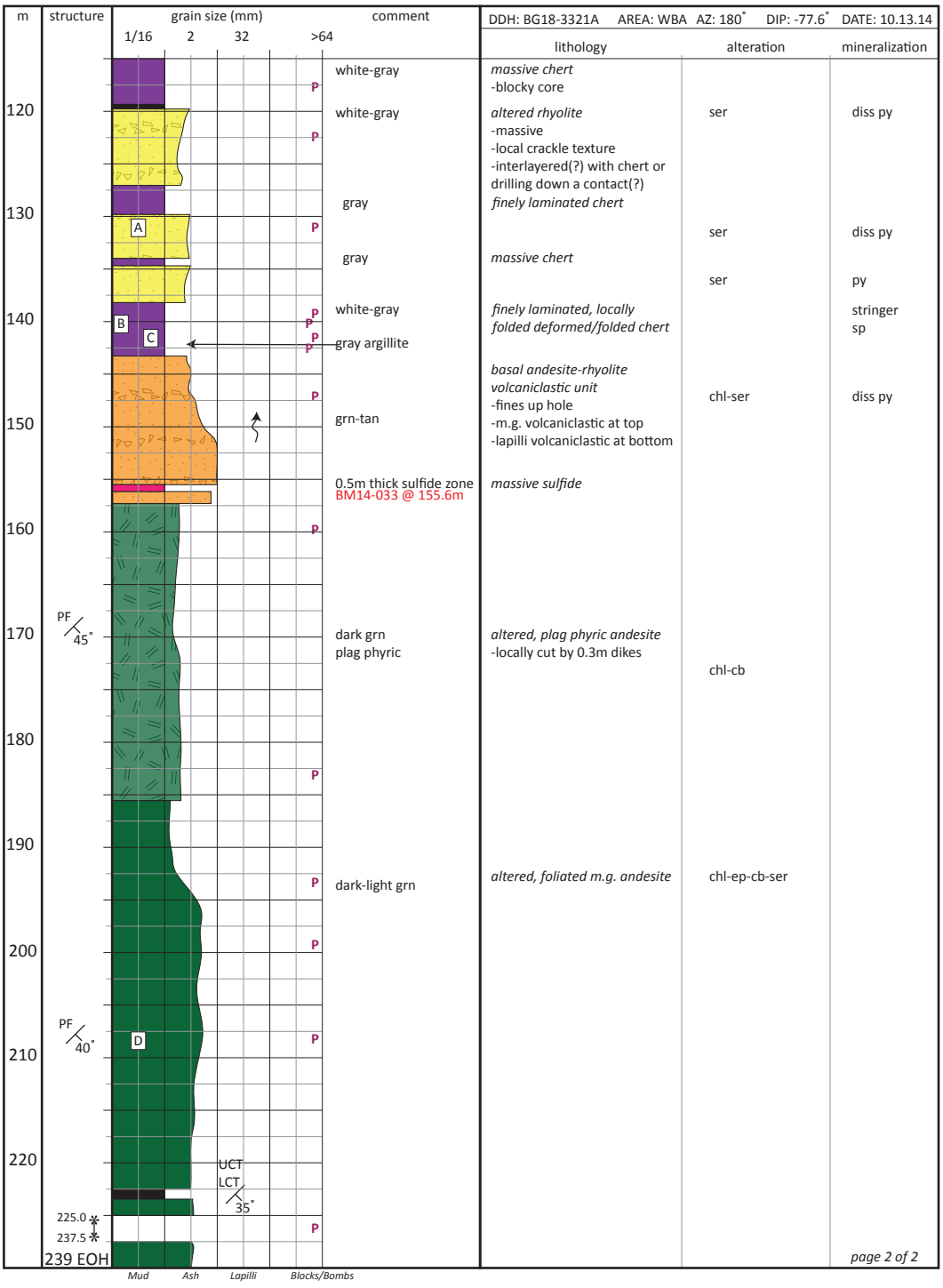

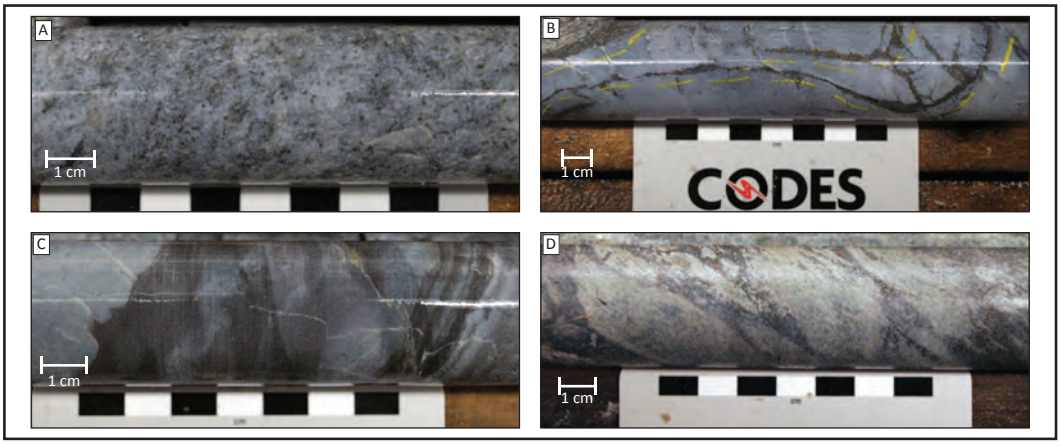

BG18-3550 page 1 of 2

DDH: BG18-3550 AREA: WBA AZ: 180° DIP: -80° DATE: 10.18.14

m	structure	grain size (mm) 1/16 2 32 >64	comment	lithology	alteration	mineralization
0			dark grn	*polymictic andesitic breccia* -blocks of rhyolite & andesite	chl-cb	na
	UCT LCT 40°		light gray-grn	*andesitic crystal shard volcaniclastic* -2-4 mm matrix -rare subrounded 2cm fragments of rhyolite and andesite -well sorted	chl-cb	na
10		P				
	UCT LCT 30°	A	light gray-grn	*andesitic crystal shard volcaniclastic* -2-4 mm matrix -10% rhyolite and plag phyric andesite fragments, 2-4cm	chl-cb	diss py
20		P				
	UCT LCT 45°					
	UCT LCT 50°	B	dark grn, yellow grn	-dark grn flattened "fragments" -yellow-grn f.g. "matrix"	chl	trace py
30		P	UCT healed fault(?)	-potential hyaloclastic(?)		
			dark grn	-dark grn f.g matrix -20% blocks of rhyolite and smaller fragments of plag phyric andesite	chl-cb	diss py
40		P				
	PF 40°		dark-med grn w/ white speckles	*foliated andesitic fine grained volcaniclastic* -local intervals of healed, deformed chl-cb-qtz-hm faults	chl-cb	diss py
	HFLT 45°					
50		P				
	PF 40°					
	HFLT 20°					
60	PF 40°					
	FLT 35°		chl-cb-qtz healed fault			
	PF 45°		gray-white	*qtz-phyric rhyolite* -5-10% qtz phenocrysts -crackle texture, locally massive -possible rhyolite autobreccia(?)	ser-qtz±chl	diss & stringer py locally remobilized cpy
70	UCT LCT 35° C	P				
			gray-white			
80		P				
			gray-white	*f.g. - m.g. felsic volcaniclastic(?)* -penetrative fabric defined by sericite alteration -local, near the end of interval, "cherty" fragments, 5cm	qtz-ser	stringer py local stringer sp
90		P				
	UCT LCT 35°					
100	B? 50°					
	B? 50° D		white and gray	*interlayered chert & mudstone*	locally siliceous	local remobilized cpy "veins"
		P				
110		P	medium grn to gray	*m.g. felsic volcaniclastic*	ser-ill±chl	na
		P				

Mud Ash Lapilli Blocks/Bombs

page 1 of 2

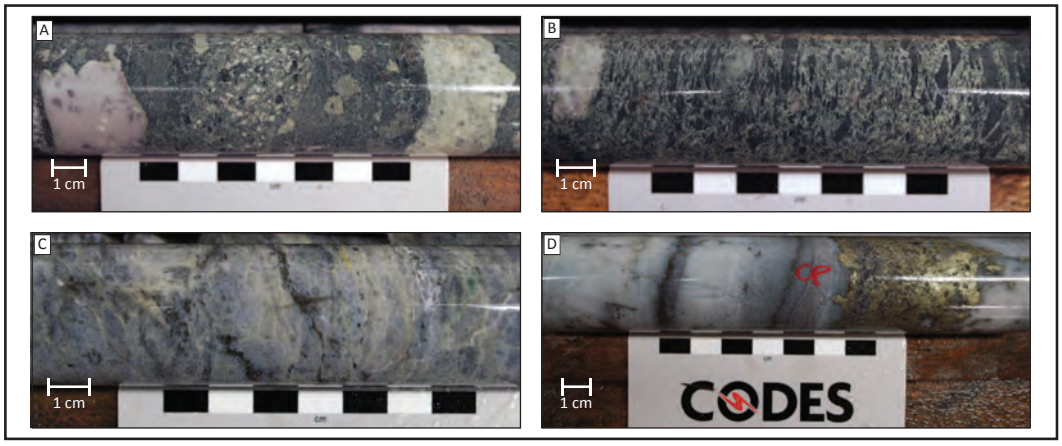

BG18-3550 page 2 of 2

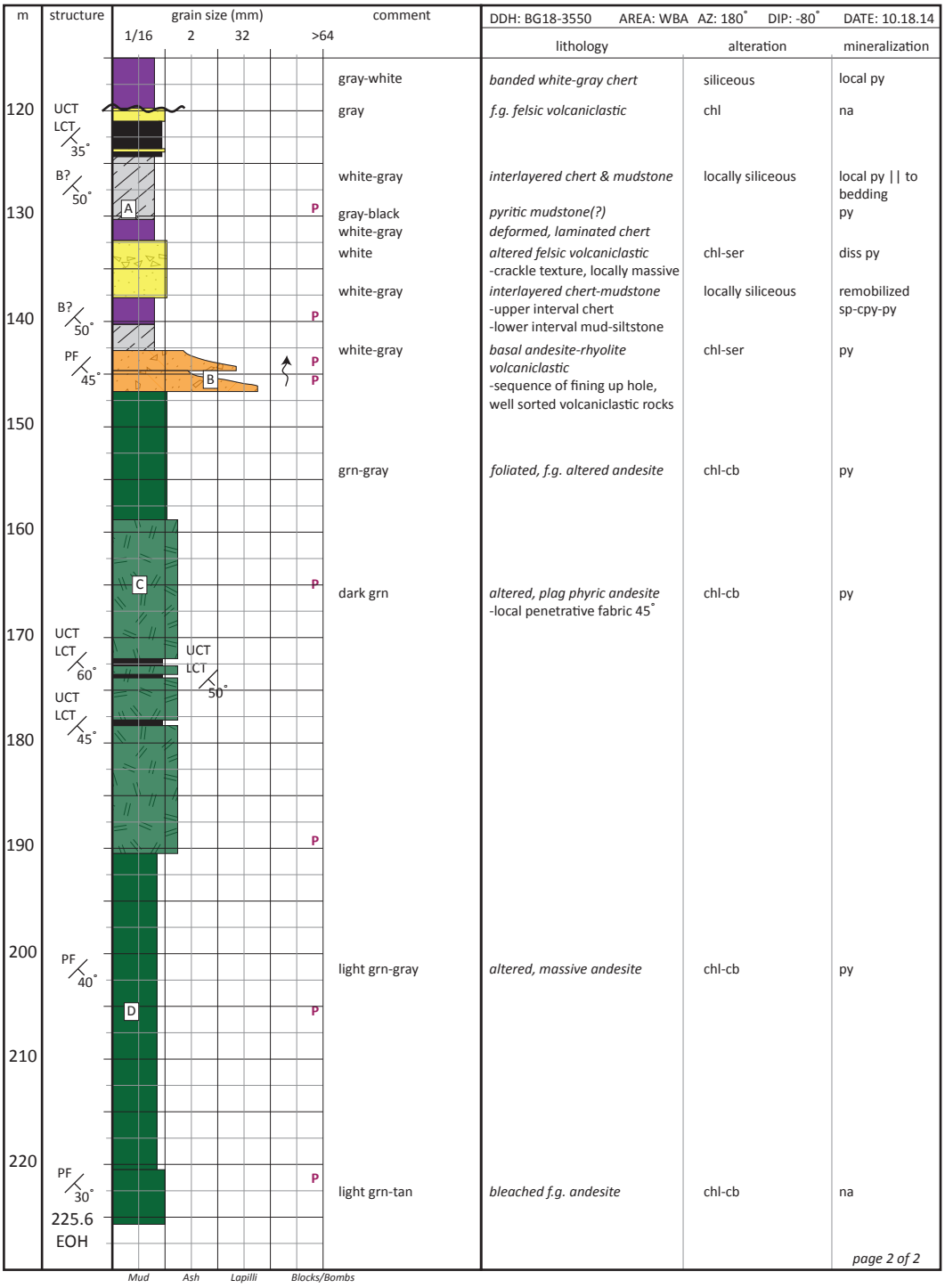

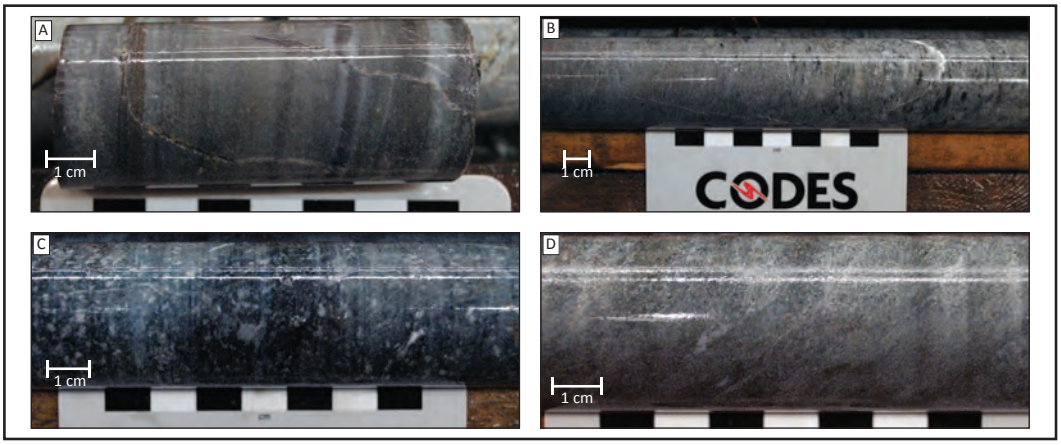

BG18-3551 page 1 of 2

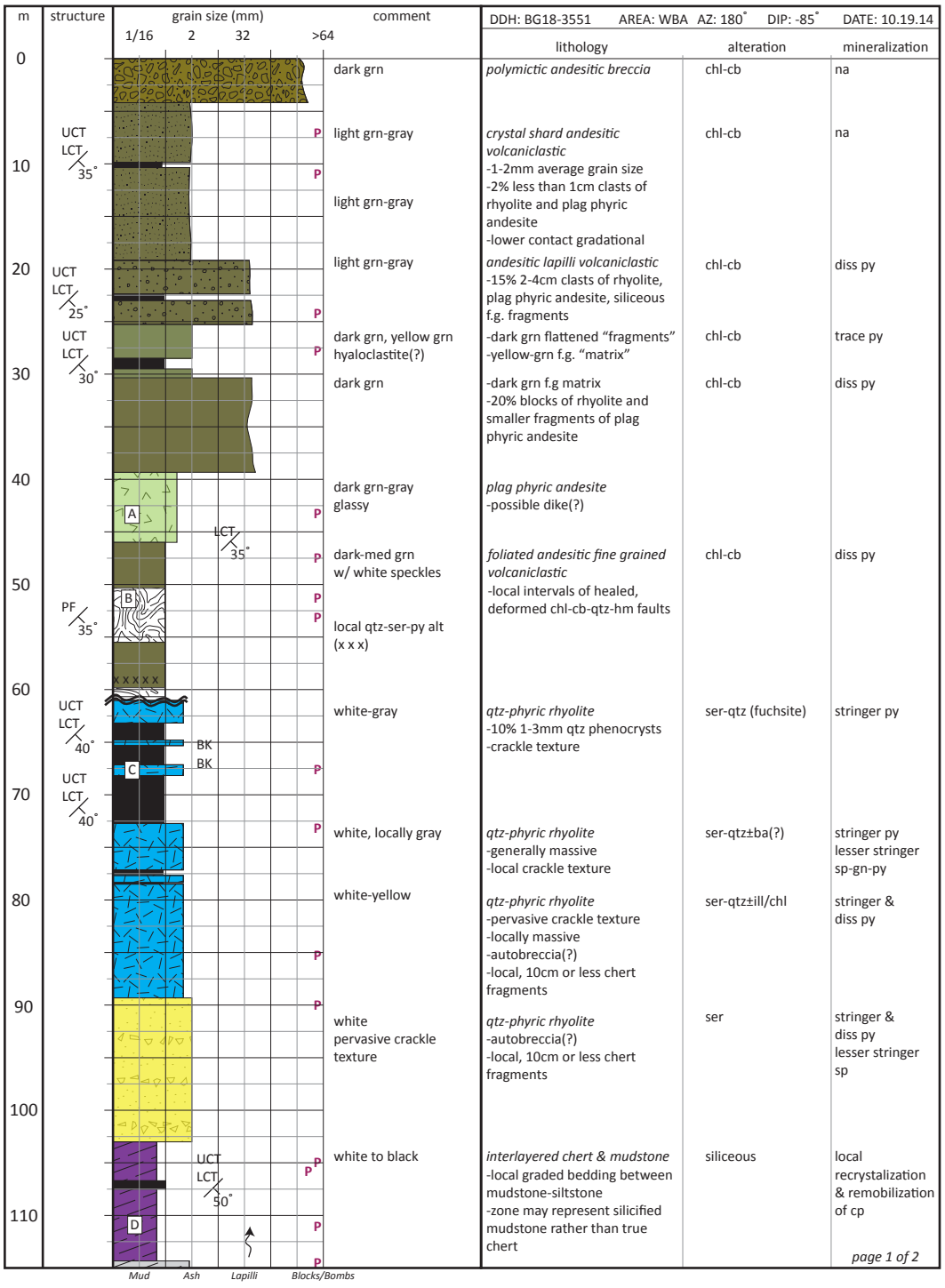

DDH: BG18-3551 AREA: WBA AZ: 180° DIP: -85° DATE: 10.19.14

lithology	alteration	mineralization
dark grn *polymictic andesitic breccia*	chl-cb	na
light grn-gray *crystal shard andesitic volcaniclastic* -1-2mm average grain size -2% less than 1cm clasts of rhyolite and plag phyric andesite -lower contact gradational	chl-cb	na
light grn-gray *andesitic lapilli volcaniclastic* -15% 2-4cm clasts of rhyolite, plag phyric andesite, siliceous f.g. fragments	chl-cb	diss py
dark grn, yellow grn hyaloclastite(?) -dark grn flattened "fragments" -yellow-grn f.g. "matrix"	chl-cb	trace py
dark grn -dark grn f.g matrix -20% blocks of rhyolite and smaller fragments of plag phyric andesite	chl-cb	diss py
dark grn-gray glassy *plag phyric andesite* -possible dike(?)		
dark-med grn w/ white speckles *foliated andesitic fine grained volcaniclastic* -local intervals of healed, deformed chl-cb-qtz-hm faults	chl-cb	diss py
local qtz-ser-py alt (x x x)		
white-gray *qtz-phyric rhyolite* -10% 1-3mm qtz phenocrysts -crackle texture	ser-qtz (fuchsite)	stringer py
white, locally gray *qtz-phyric rhyolite* -generally massive -local crackle texture	ser-qtz±ba(?)	stringer py lesser stringer sp-gn-py
white-yellow *qtz-phyric rhyolite* -pervasive crackle texture -locally massive -autobreccia(?) -local, 10cm or less chert fragments	ser-qtz±ill/chl	stringer & diss py
white pervasive crackle texture *qtz-phyric rhyolite* -autobreccia(?) -local, 10cm or less chert fragments	ser	stringer & diss py lesser stringer sp
white to black *interlayered chert & mudstone* -local graded bedding between mudstone-siltstone -zone may represent silicified mudstone rather than true chert	siliceous	local recrystalization & remobilization of cp

page 1 of 2

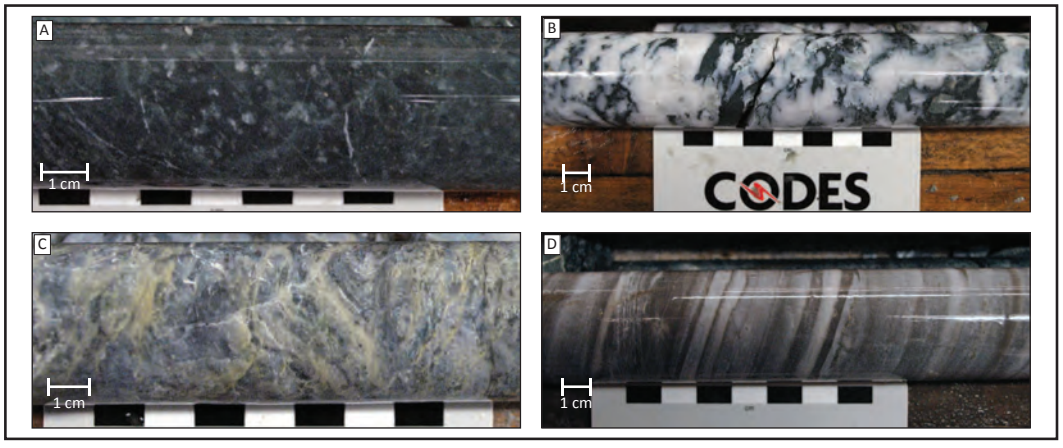

BG18-3551 page 2 of 2

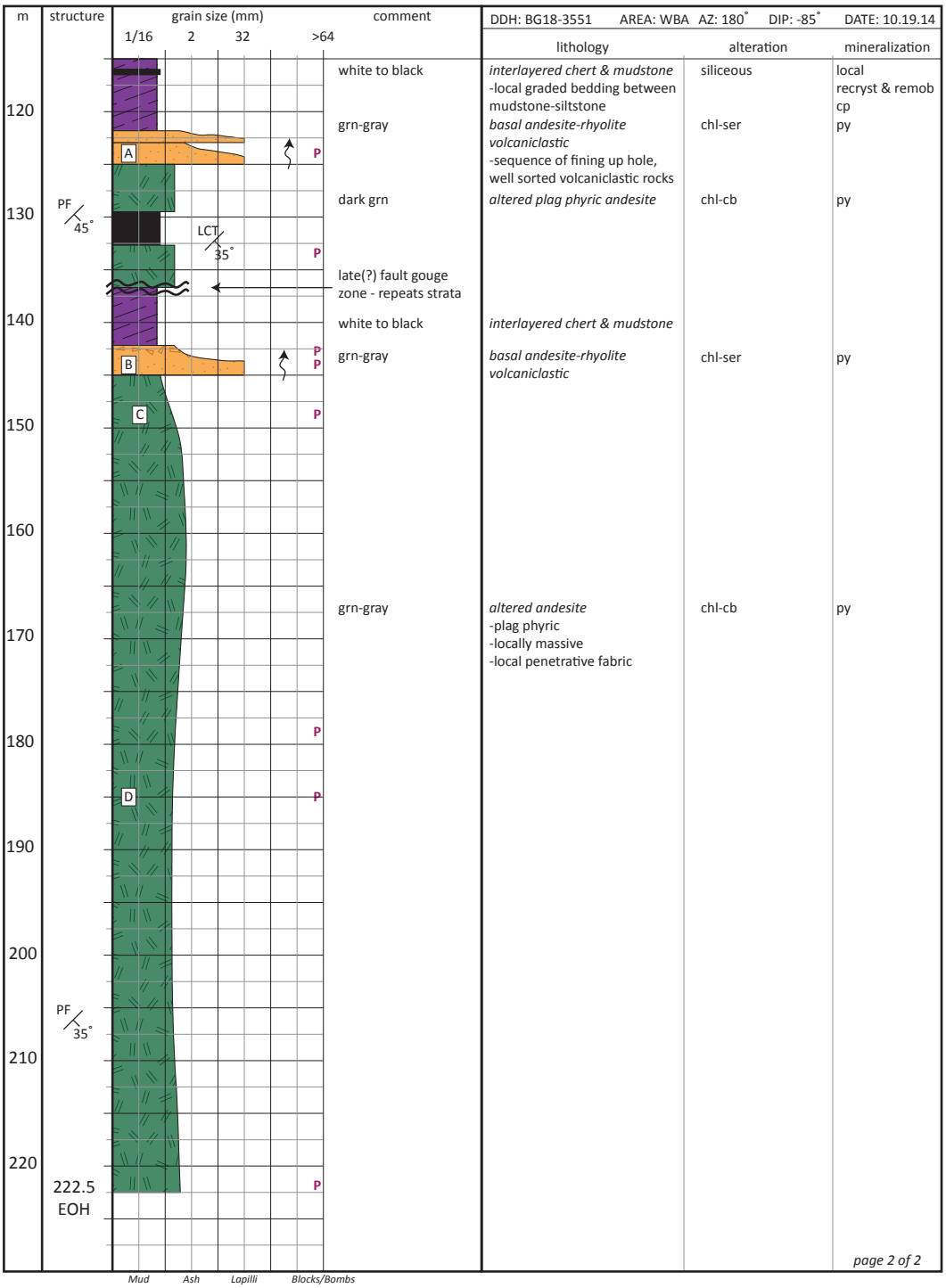

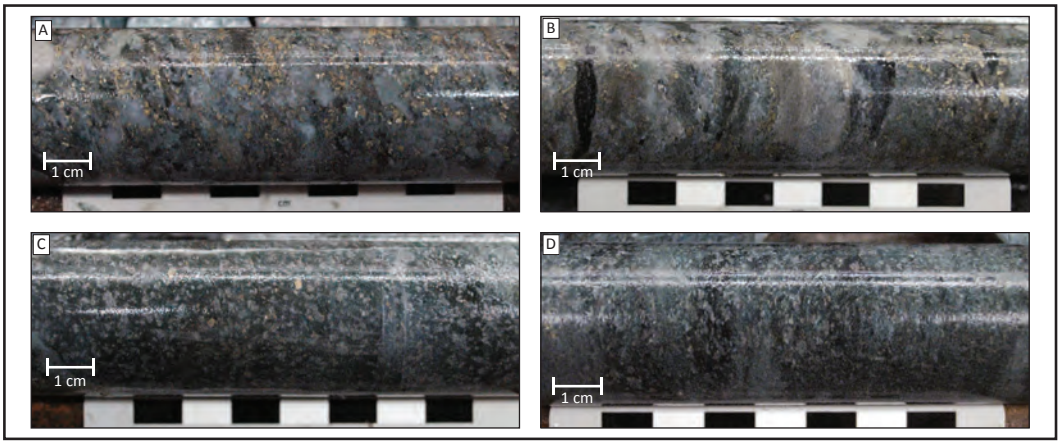

BG18-3552 page 1 of 2

DDH: BG18-3552 AREA: WBA AZ: 354° DIP: -83.5° DATE: 11.2.14

m	structure	grain size (mm) 1/16 2 32 >64	comment	lithology	alteration	mineralization
0			light grn to gray	*andesitic m.g. crystal-shard volcaniclastic* -2mm average grain size -local grading to f.g. volcaniclastic -weak alignment of grains at 50°	chl-cb	na
10	PF 50°		light grn to gray	*andesitic crystal-shard lapilli volcaniclastic* -10% angular to subrounded lithics -average lithic size 1 cm	chl-cb	na
20	A		dark grn	*andesitic crystal-shard lapilli volcaniclastic* -lithcs up to 3 cm in size	chl-cb	minor py
			dark grn, yellow grn hyaloclastite(?)	-dark grn flattened "fragments" -yellow-grn f.g. "matrix"	chl-cb	trace py
30			dark grn	-dark grn f.g matrix -20% blocks of rhyolite and smaller fragments of plag phyric andesite	chl-cb	diss py
40			dark grn	-generally massive -local zones show clastic texture -local qtz-ser-py alteration -unclear lithofacies	chl-cb	
50	B MPY clasts		*chl-qtz-cb-mag healed fault*			
	HFLT HFLT 20° 35°		dark grn	*f.g. andesitic(?) volcaniclastic* -massive to foliated -fine grained unit -local healed fault zones	chl-cb	minor py
60						
70						
80	C		white to gray	*qtz-phyric rhyolite* -massive -coherent volcanic rock	qtz-ser	minor pyritic stringers
90			white to gray	*qtz-phyric rhyolite breccia* -pervasive crackle texture -1-3 mm qtz phenocrysts -no accessory or exotic lithics -cut by mafic dikes -possible rhyolite flow breccia(?)	qtz-ser-illite(?)	minor diss sphalerite
100			gray	*f.g. to m.g. felsic volcaniclastic?* -normal graded bedding -well sorted -cut by mafic dike	chl-ser	diss py
110	B? 80° D		gray to white	*interlayered mud-silt-sandstone* -locally silicified "chert) layers -normal graded bedding	silicified	

Mud Ash Lapilli Blocks/Bombs

page 1 of 2

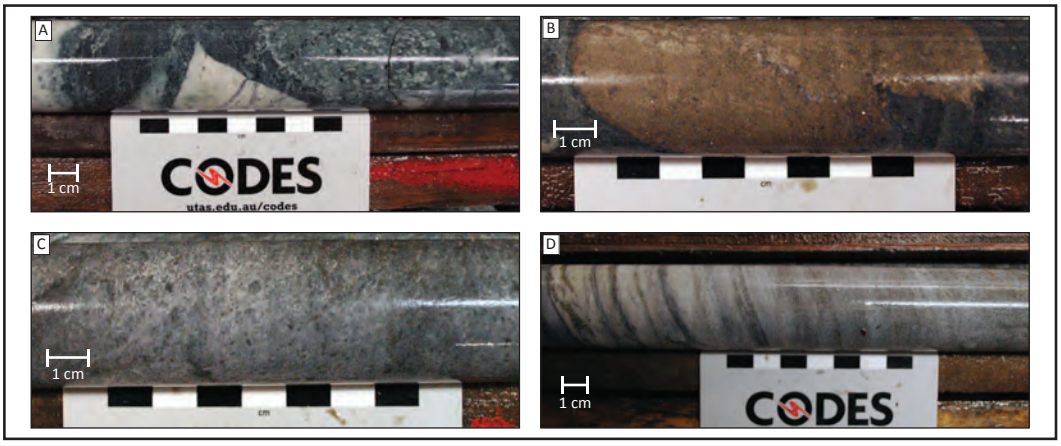

BG18-3552 page 2 of 2

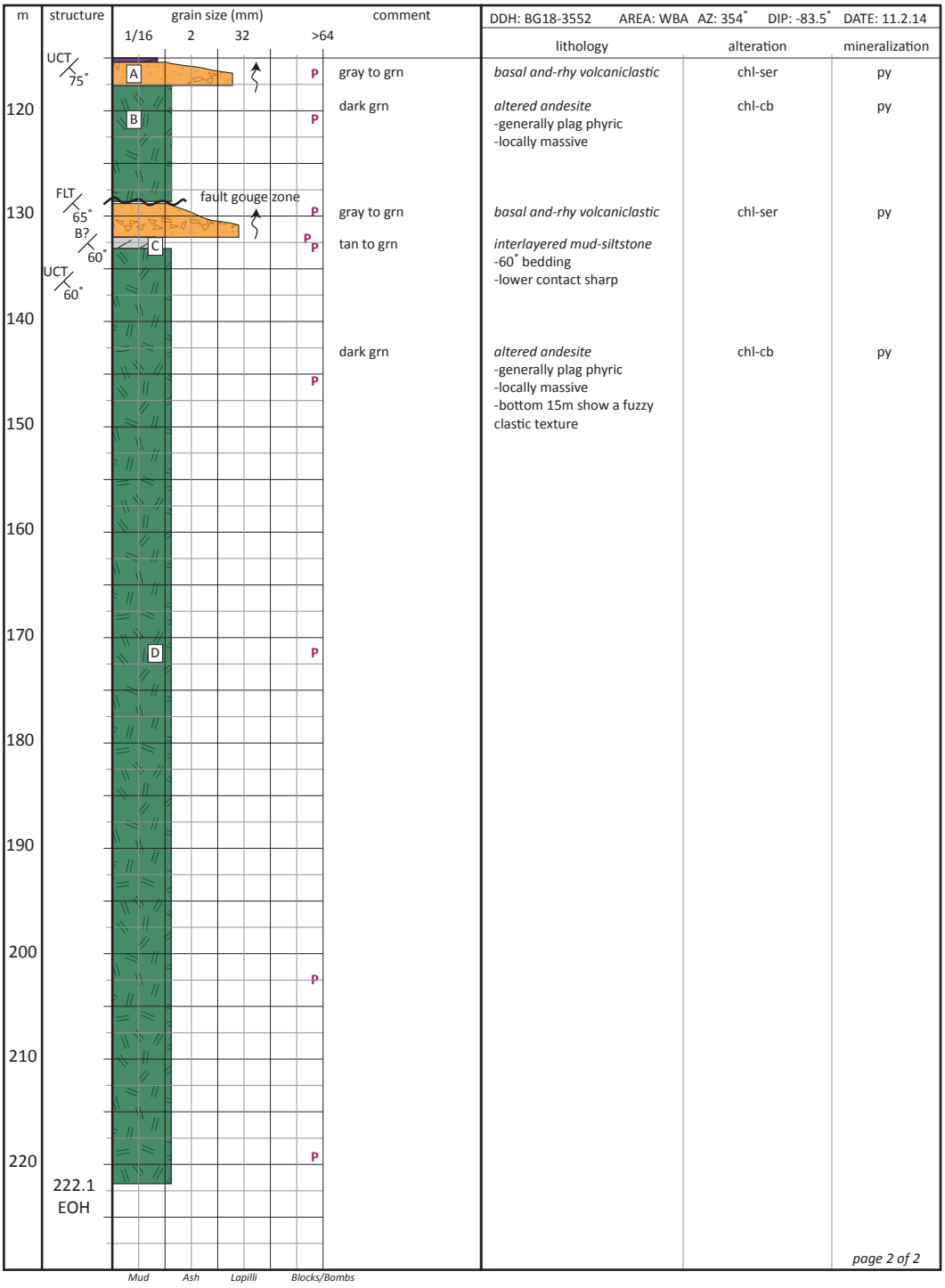

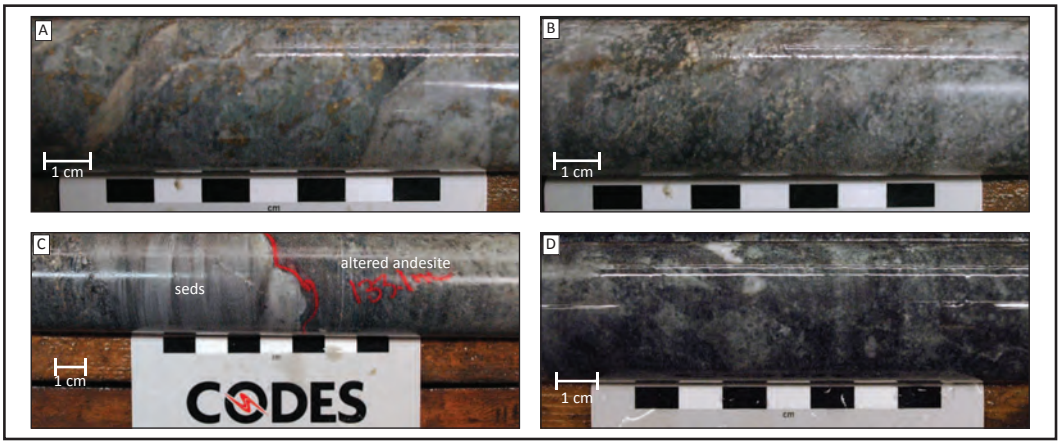

BG18-3553 page 1 of 2

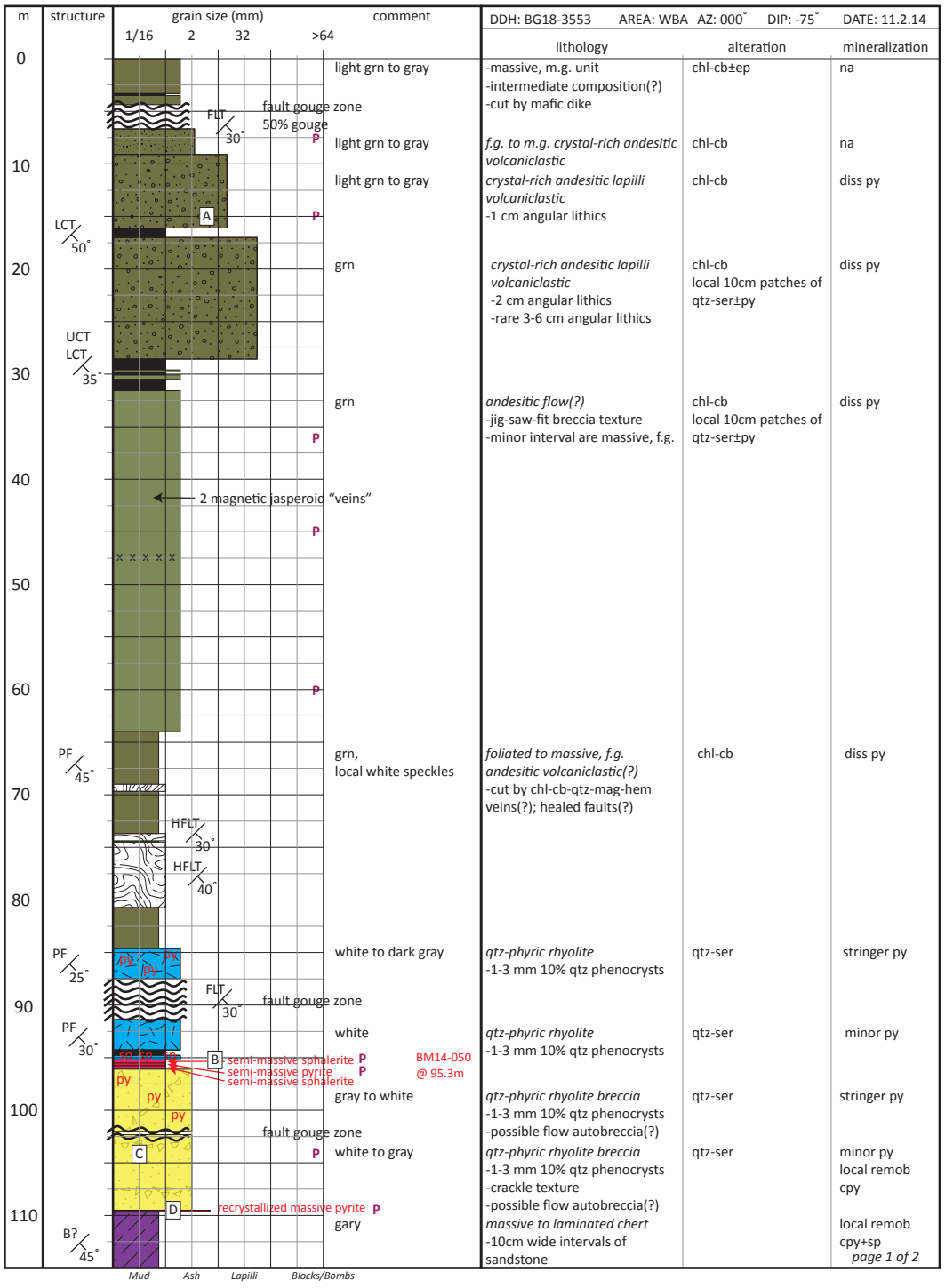

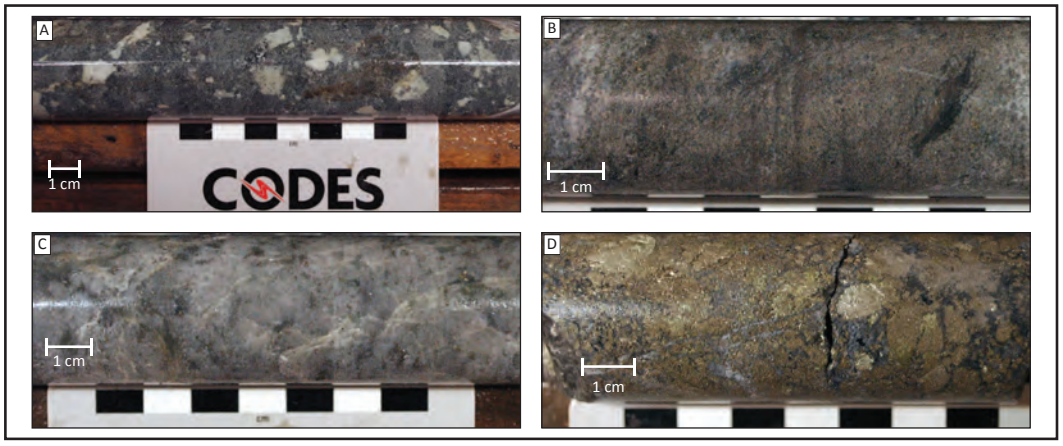

BG18-3553 page 2 of 2

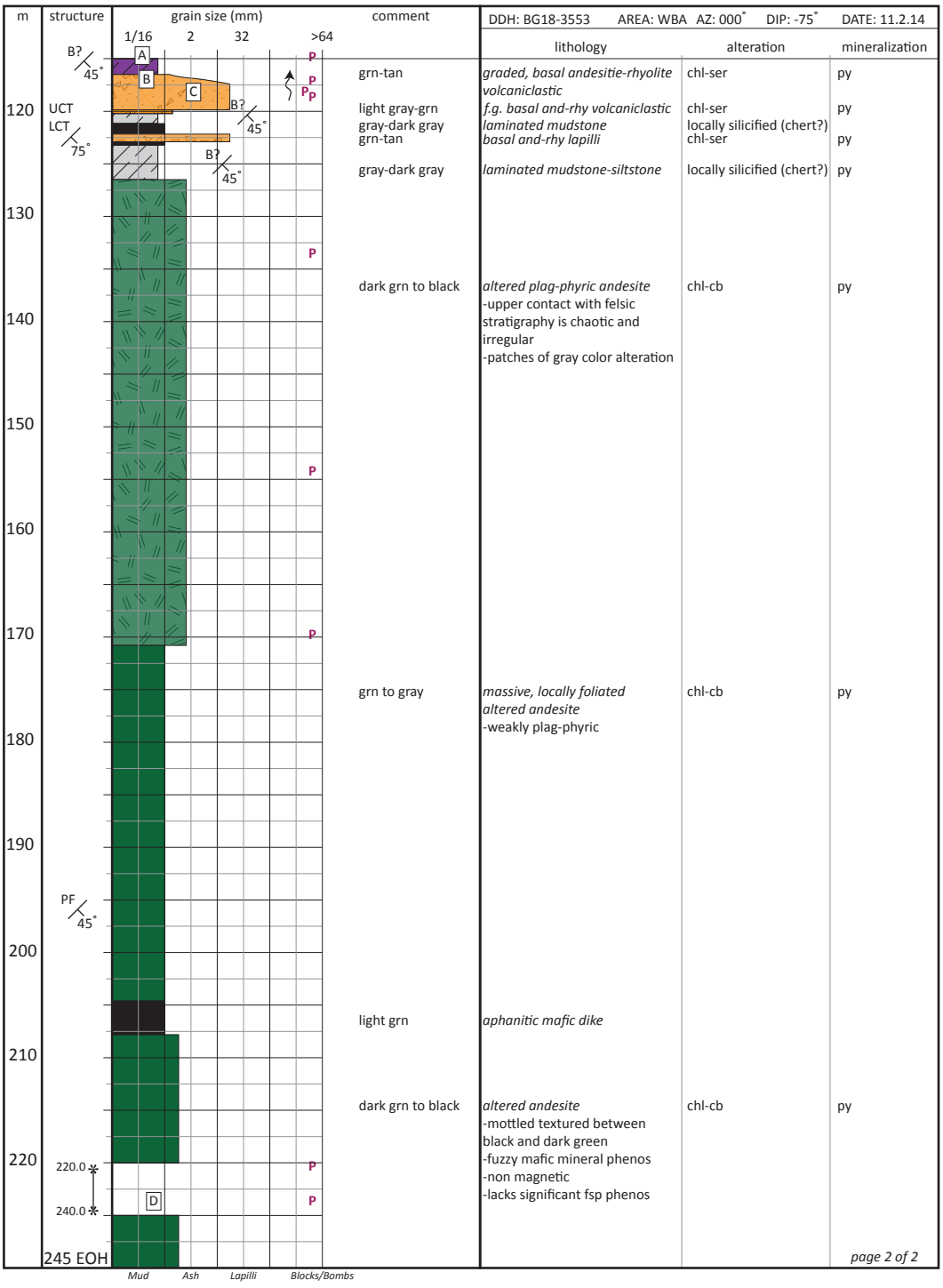

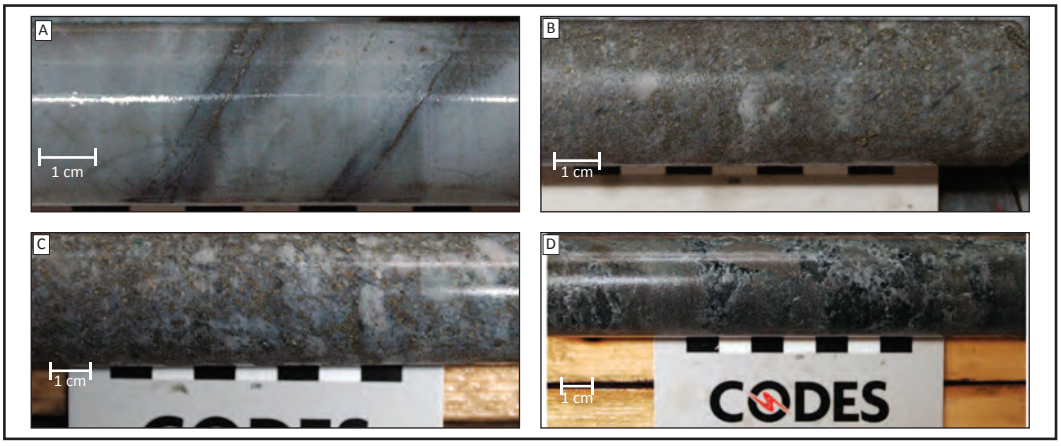

BG18-3554 page 1 of 2

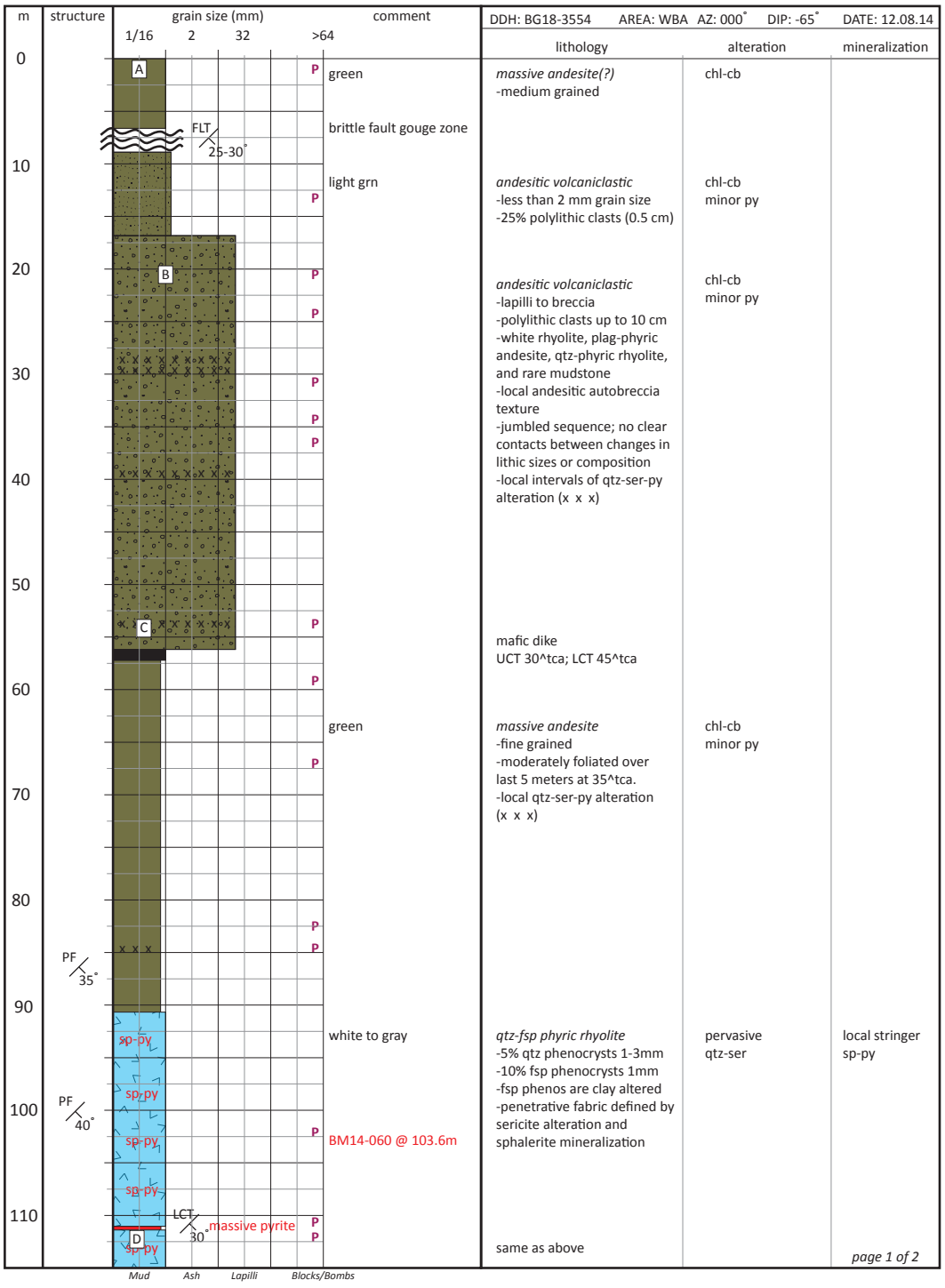

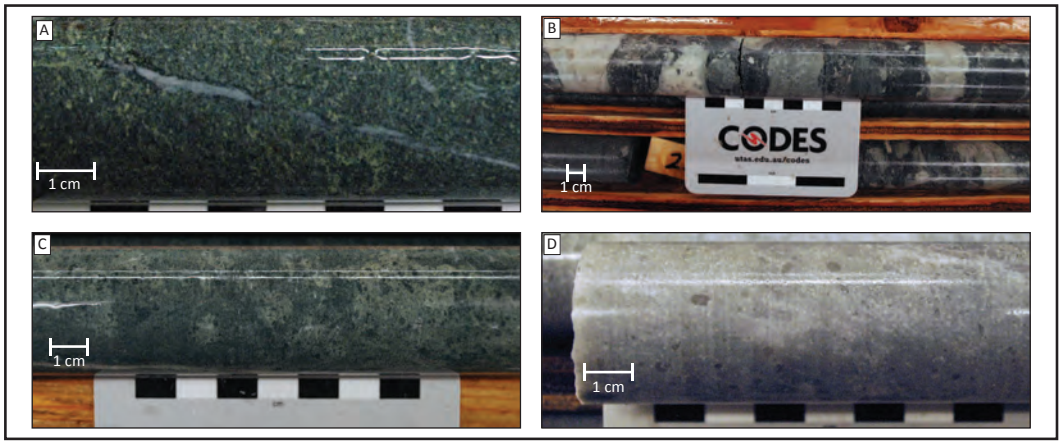

BG18-3554 page 2 of 2

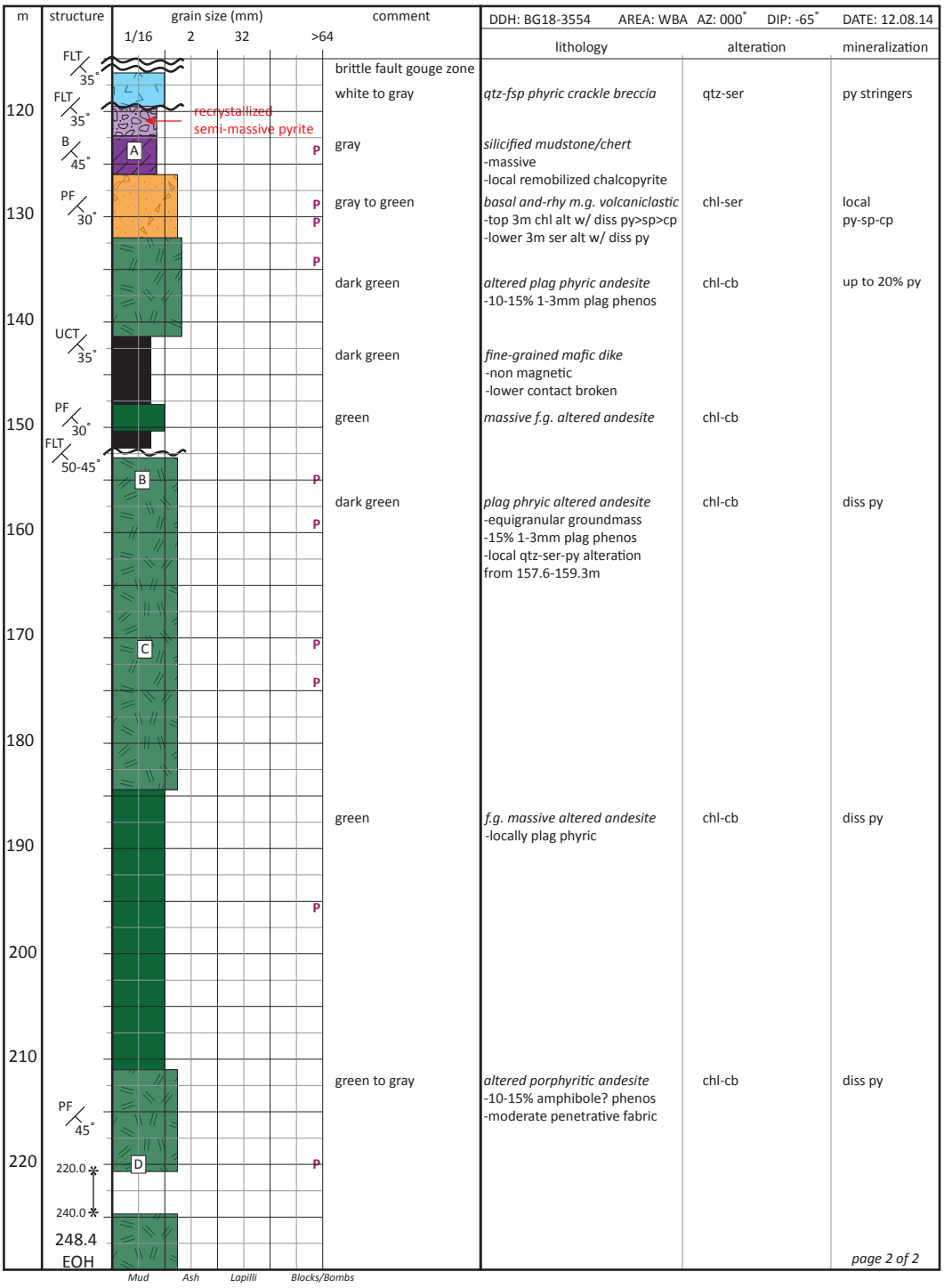

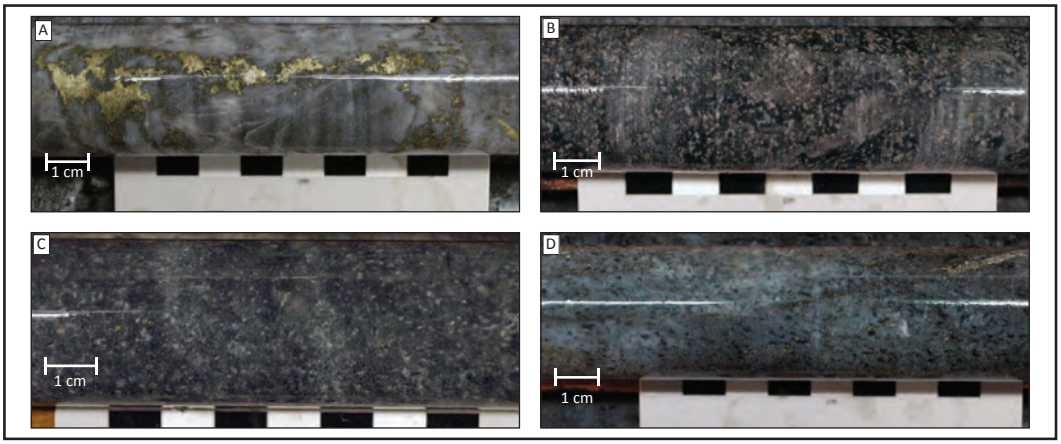

BG18-3921 page 1 of 2

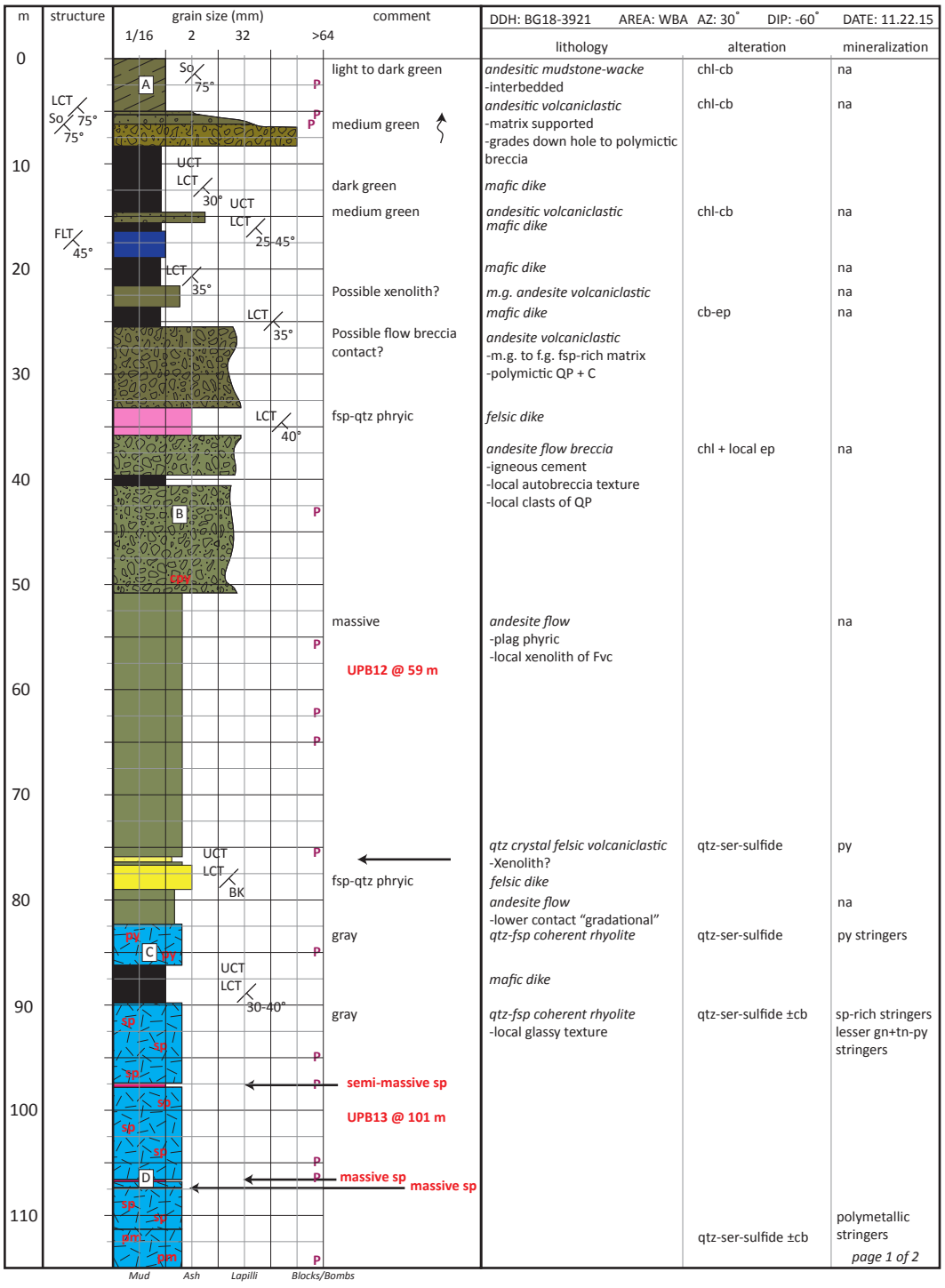

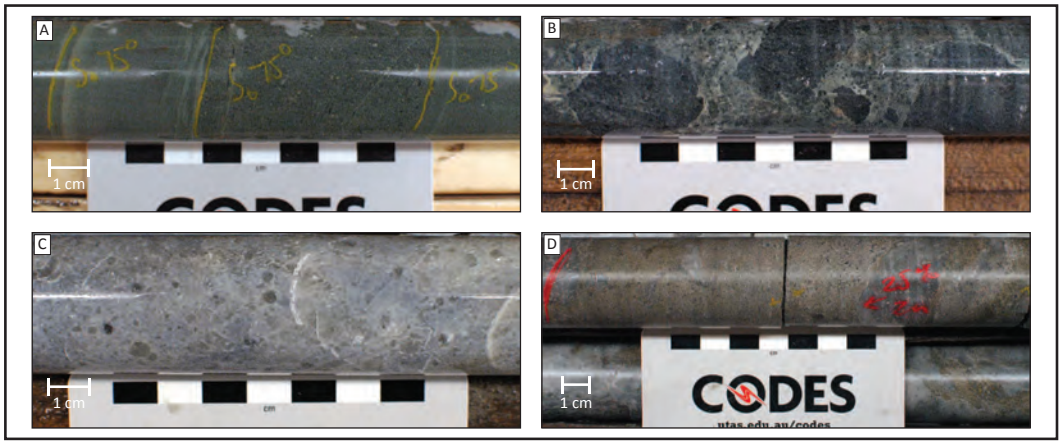

BG18-3921 page 2 of 2

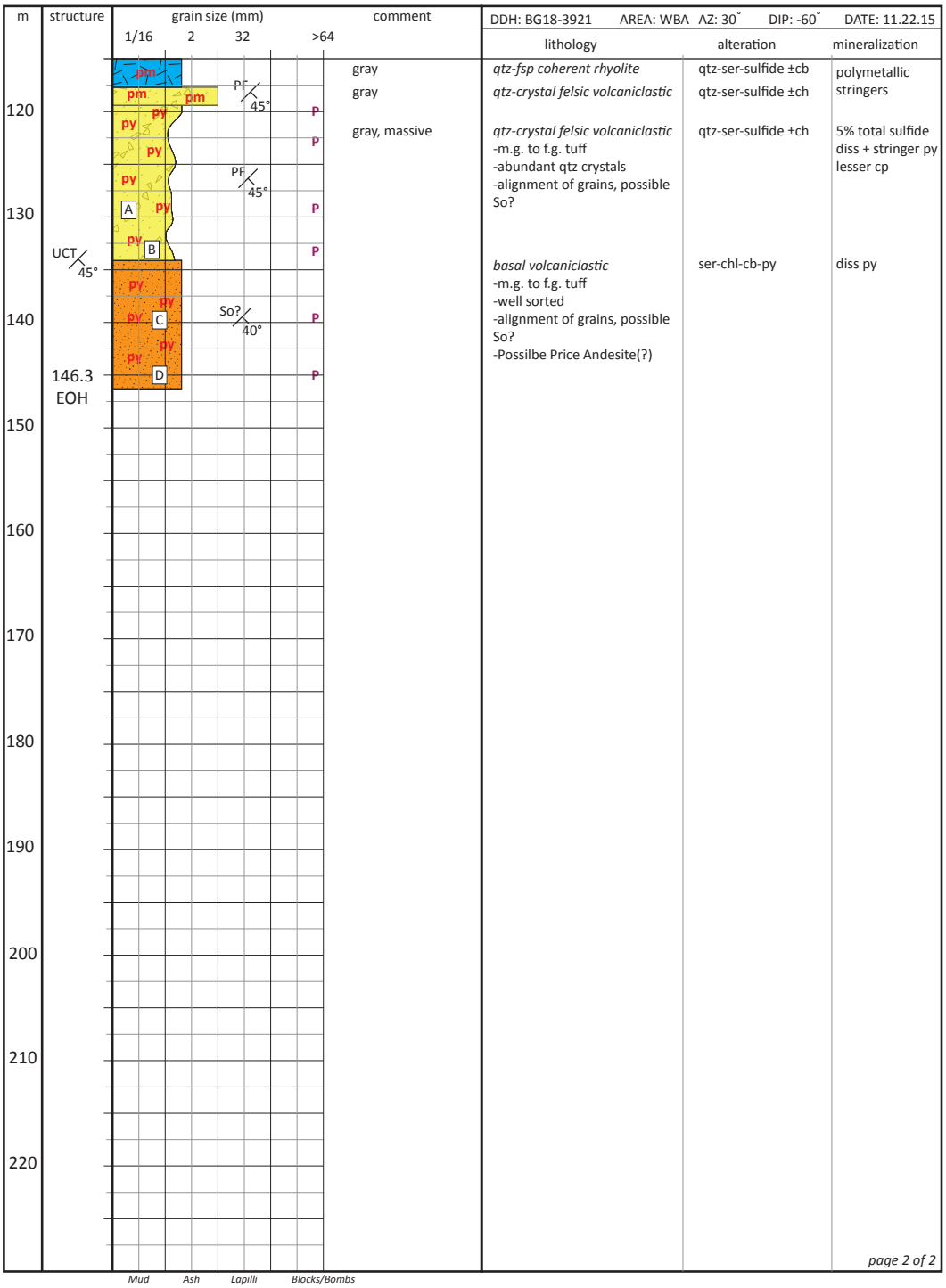

DDH: BG18-3921 AREA: WBA AZ: 30° DIP: -60° DATE: 11.22.15

lithology	alteration	mineralization
qtz-fsp coherent rhyolite	qtz-ser-sulfide ±cb	polymetallic stringers
qtz-crystal felsic volcaniclastic	qtz-ser-sulfide ±ch	
qtz-crystal felsic volcaniclastic -m.g. to f.g. tuff -abundant qtz crystals -alignment of grains, possible So?	qtz-ser-sulfide ±ch	5% total sulfide diss + stringer py lesser cp
basal volcaniclastic -m.g. to f.g. tuff -well sorted -alignment of grains, possible So? -Possilbe Price Andesite(?)	ser-chl-cb-py	diss py

page 2 of 2

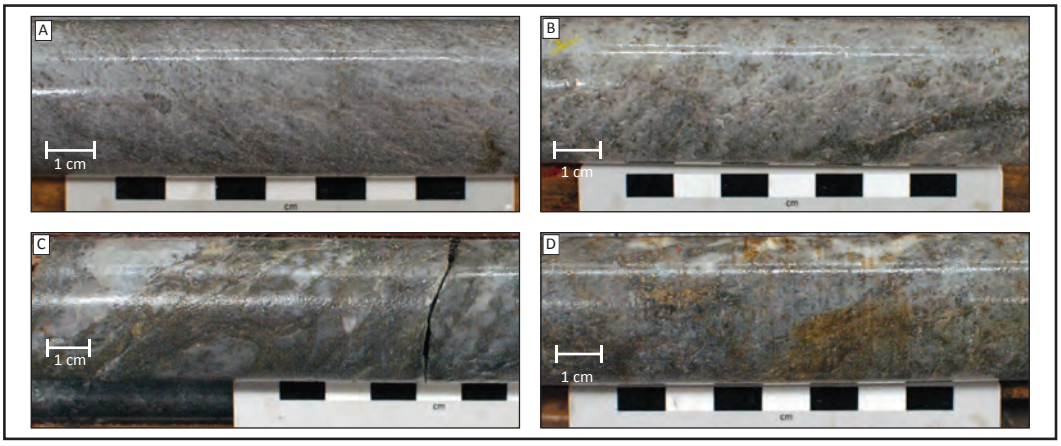

BG18-3555 page 1 of 4

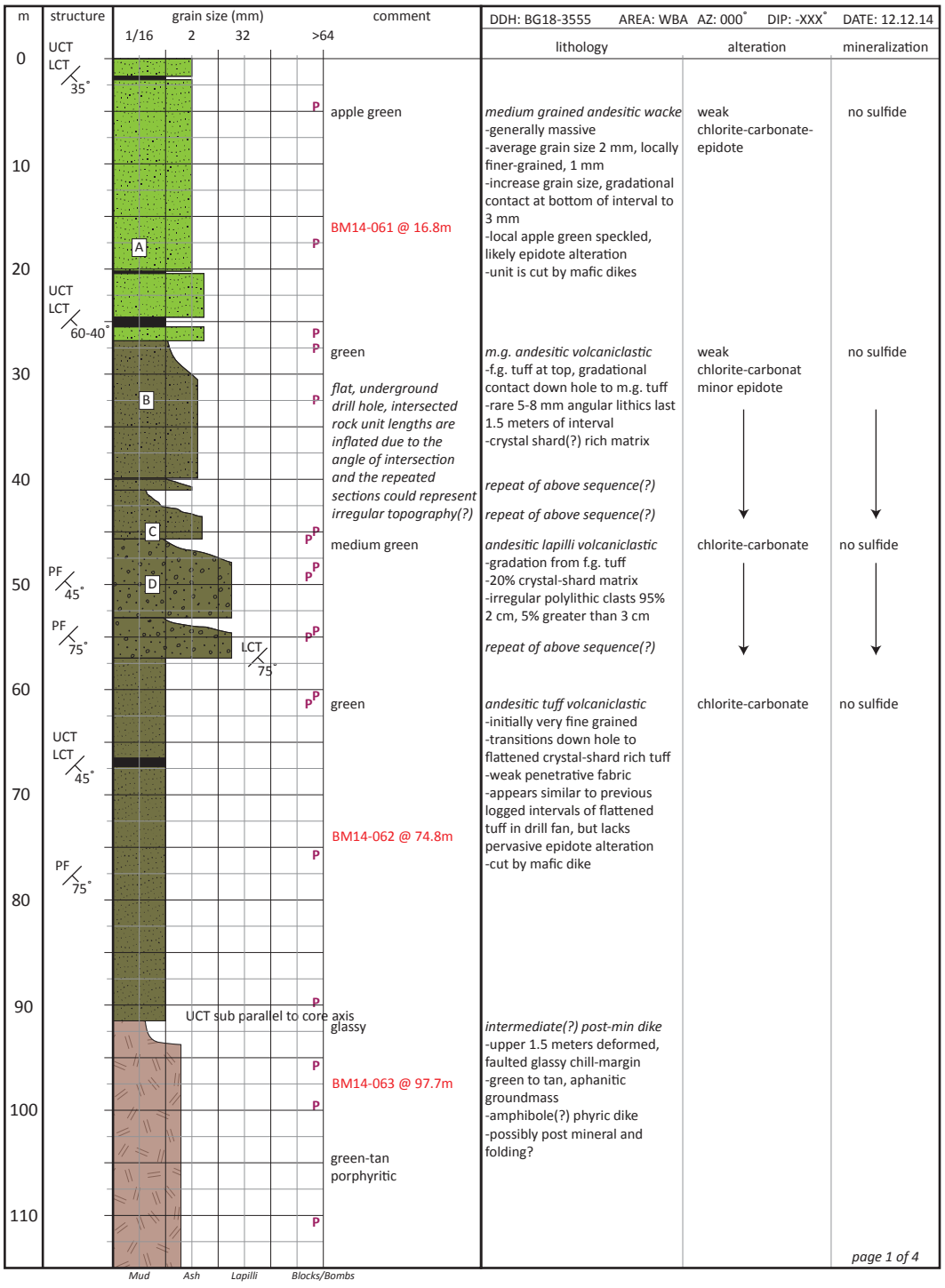

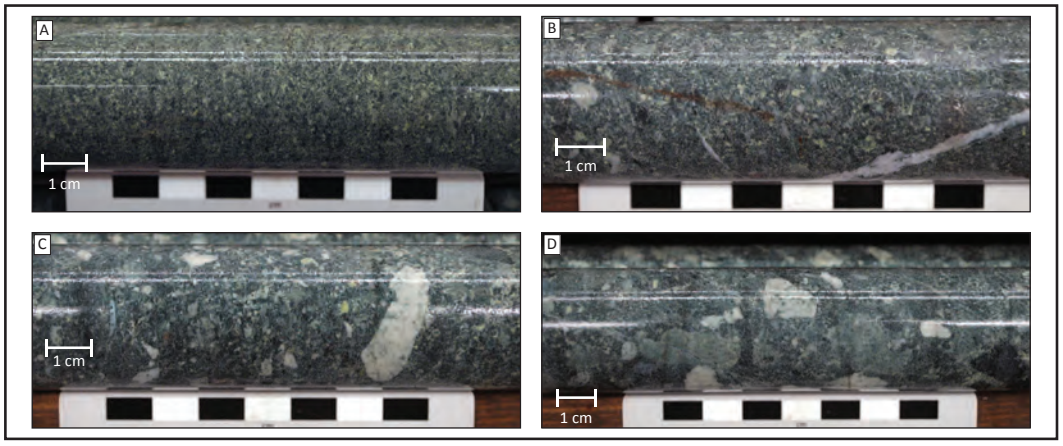

BG18-3555 page 2 of 4

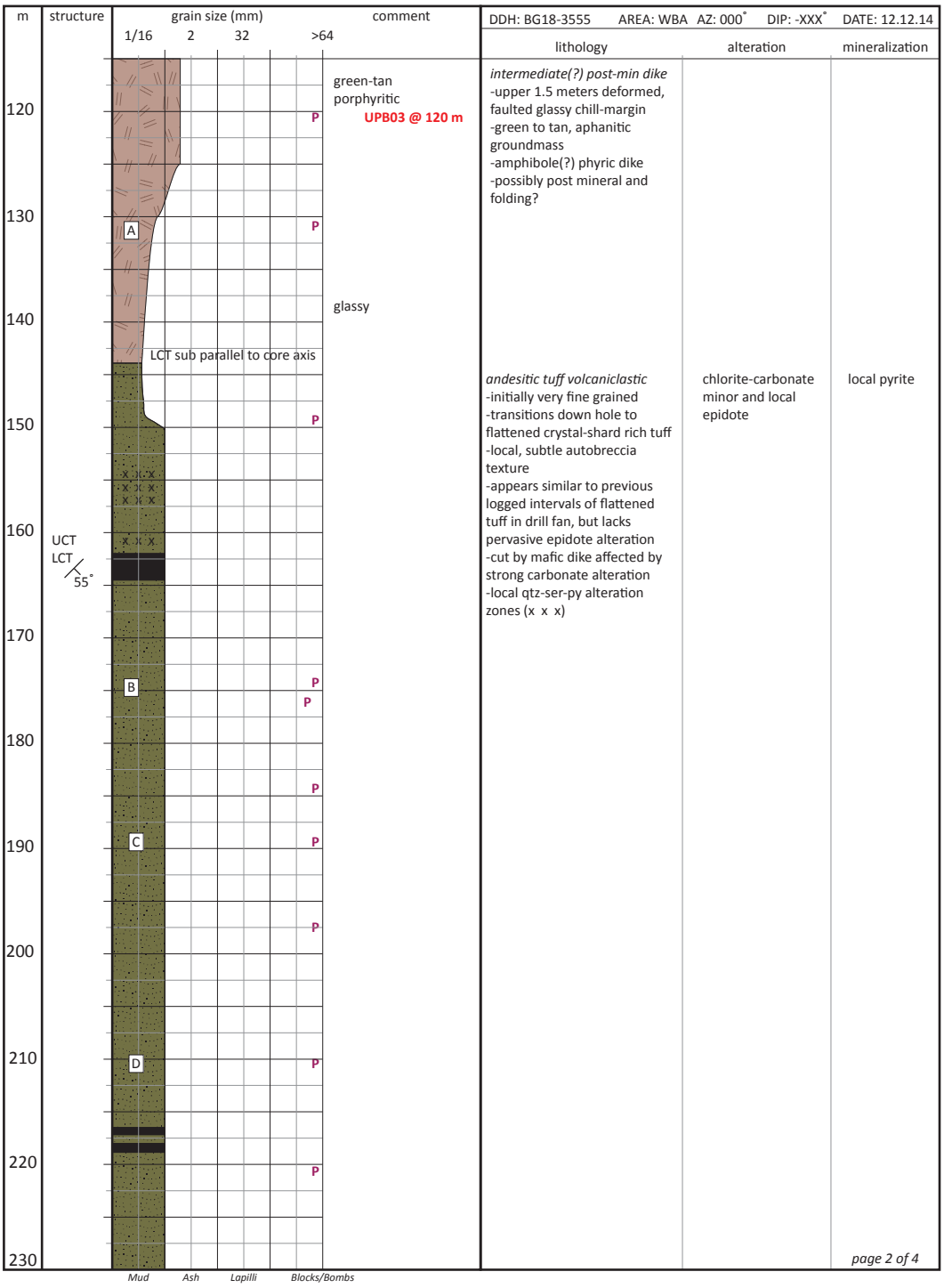

DDH: BG18-3555 AREA: WBA AZ: 000° DIP: -XXX° DATE: 12.12.14

lithology	alteration	mineralization
intermediate(?) post-min dike -upper 1.5 meters deformed, faulted glassy chill-margin -green to tan, aphanitic groundmass -amphibole(?) phyric dike -possibly post mineral and folding?		
andesitic tuff volcaniclastic -initially very fine grained -transitions down hole to flattened crystal-shard rich tuff -local, subtle autobreccia texture -appears similar to previous logged intervals of flattened tuff in drill fan, but lacks pervasive epidote alteration -cut by mafic dike affected by strong carbonate alteration -local qtz-ser-py alteration zones (x x x)	chlorite-carbonate minor and local epidote	local pyrite

page 2 of 4

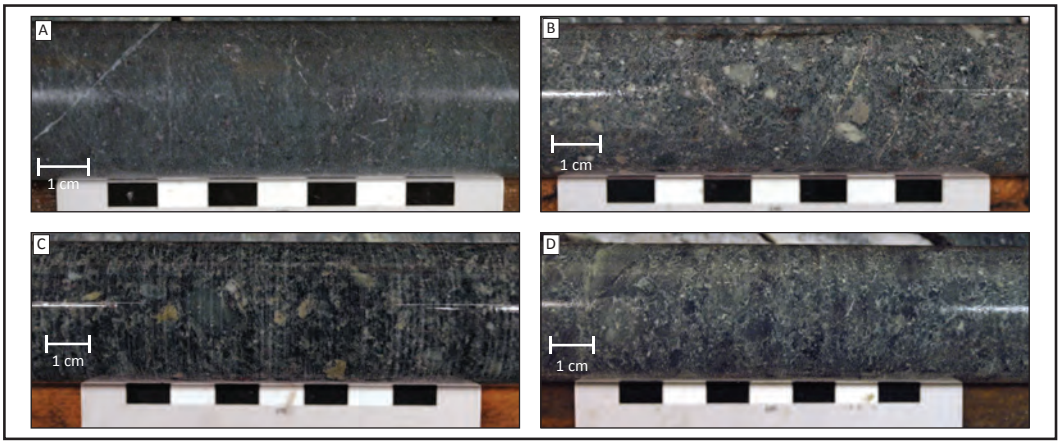

BG18-3555 page 3 of 4

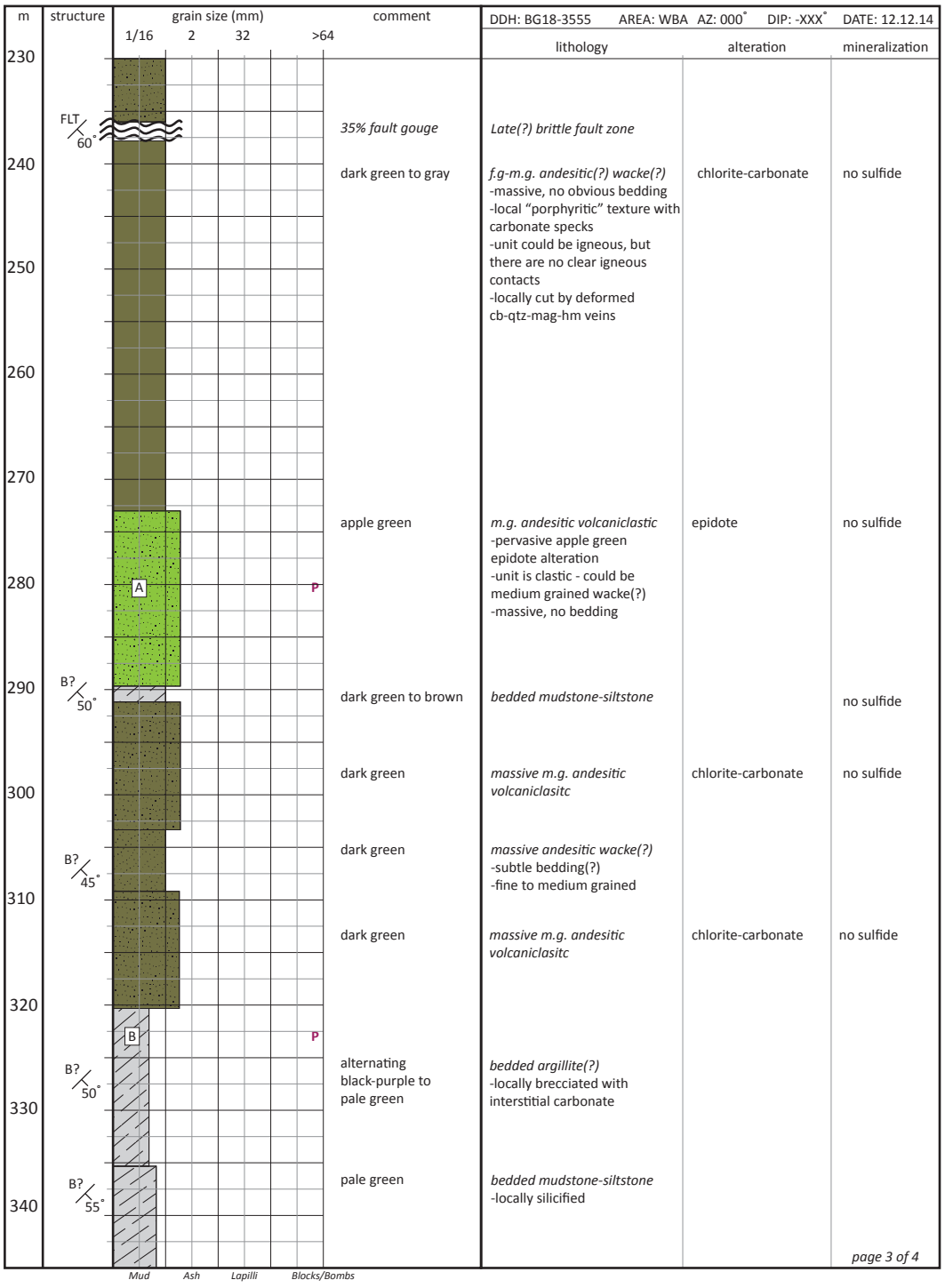

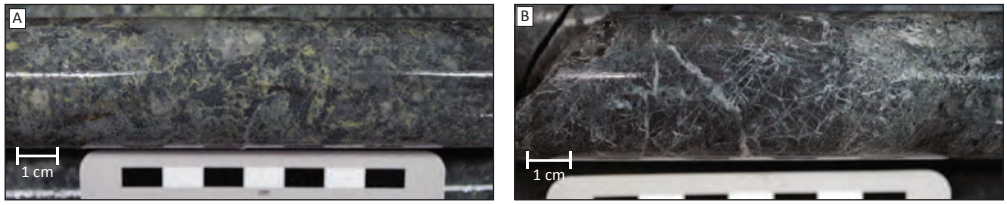

BG18-3555 page 3 of 4

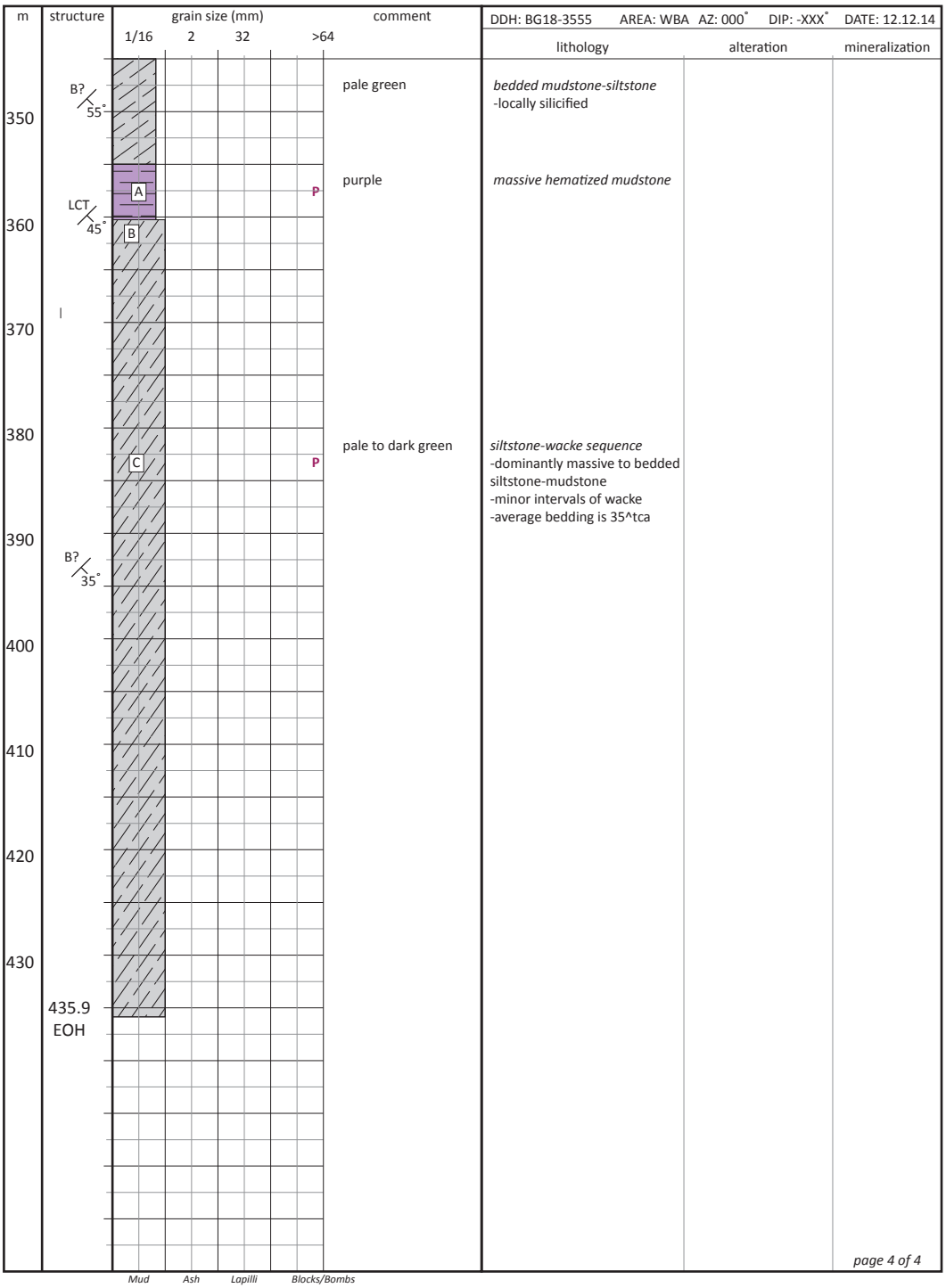

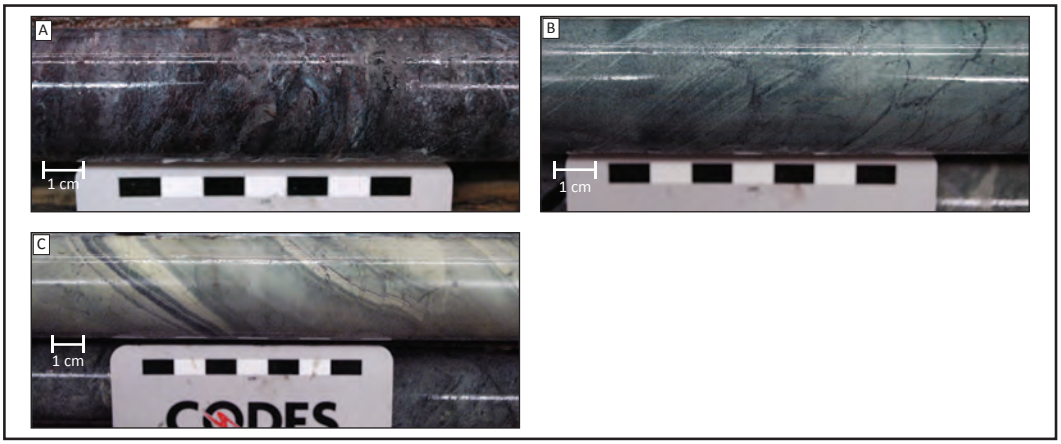

BG18-3952 page 1 of 2

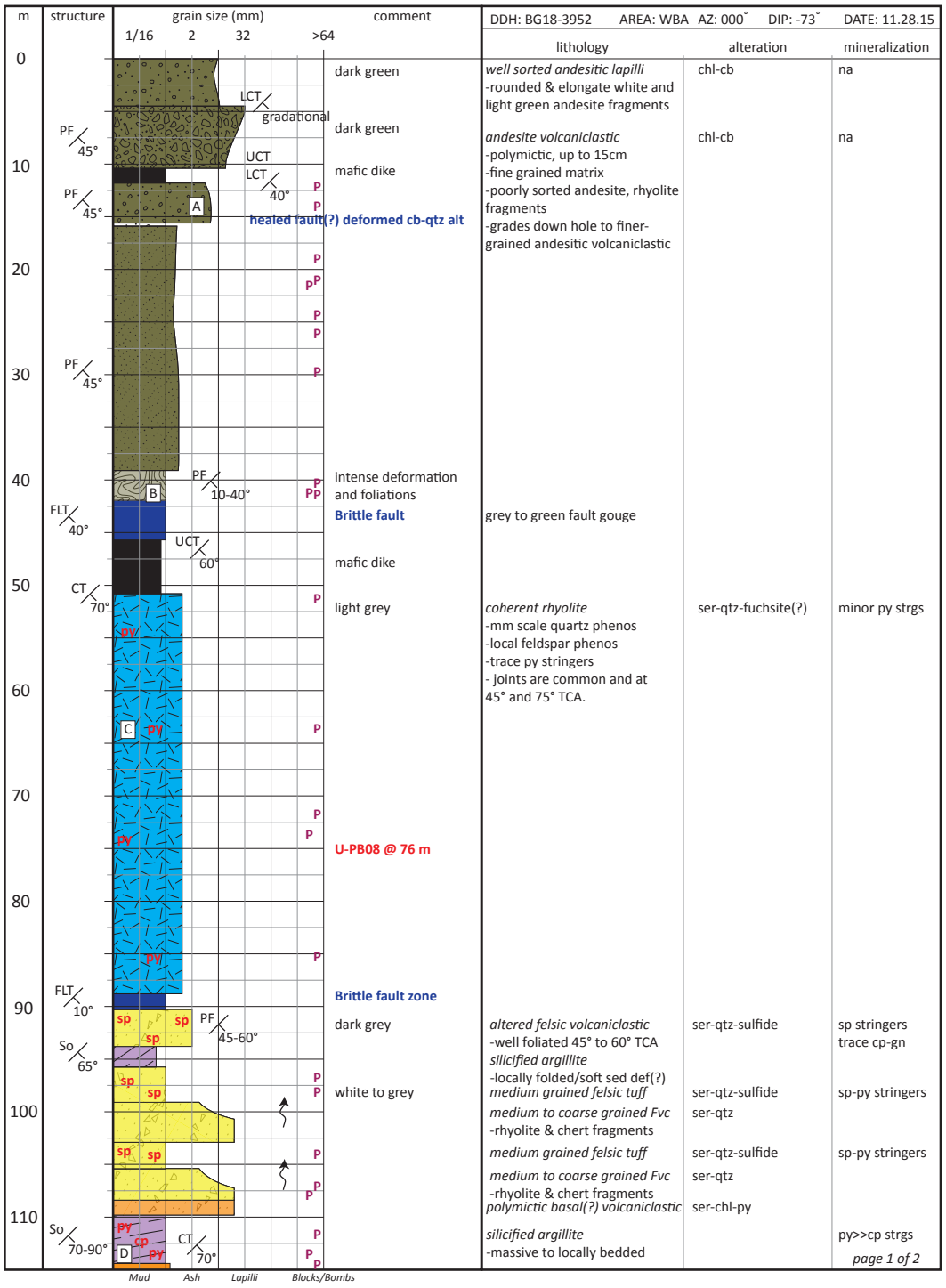

DDH: BG18-3952 AREA: WBA AZ: 000° DIP: -73° DATE: 11.28.15

lithology	alteration	mineralization
well sorted andesitic lapilli -rounded & elongate white and light green andesite fragments	chl-cb	na
andesite volcaniclastic -polymictic, up to 15cm -fine grained matrix -poorly sorted andesite, rhyolite fragments -grades down hole to finer-grained andesitic volcaniclastic	chl-cb	na
grey to green fault gouge		
coherent rhyolite -mm scale quartz phenos -local feldspar phenos -trace py stringers - joints are common and at 45° and 75° TCA.	ser-qtz-fuchsite(?)	minor py strgs
altered felsic volcaniclastic -well foliated 45° to 60° TCA	ser-qtz-sulfide	sp stringers trace cp-gn
silicified argillite -locally folded/soft sed def(?)		
medium grained felsic tuff	ser-qtz-sulfide	sp-py stringers
medium to coarse grained Fvc -rhyolite & chert fragments	ser-qtz	
medium grained felsic tuff	ser-qtz-sulfide	sp-py stringers
medium to coarse grained Fvc -rhyolite & chert fragments	ser-qtz	
polymictic basal(?) volcaniclastic	ser-chl-py	
silicified argillite -massive to locally bedded		py>>cp strgs

page 1 of 2

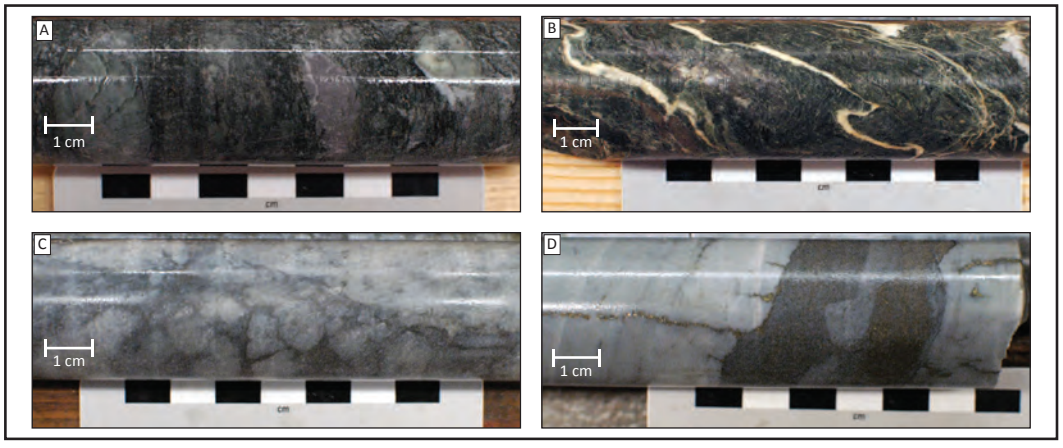

BG18-3952 page 2 of 2

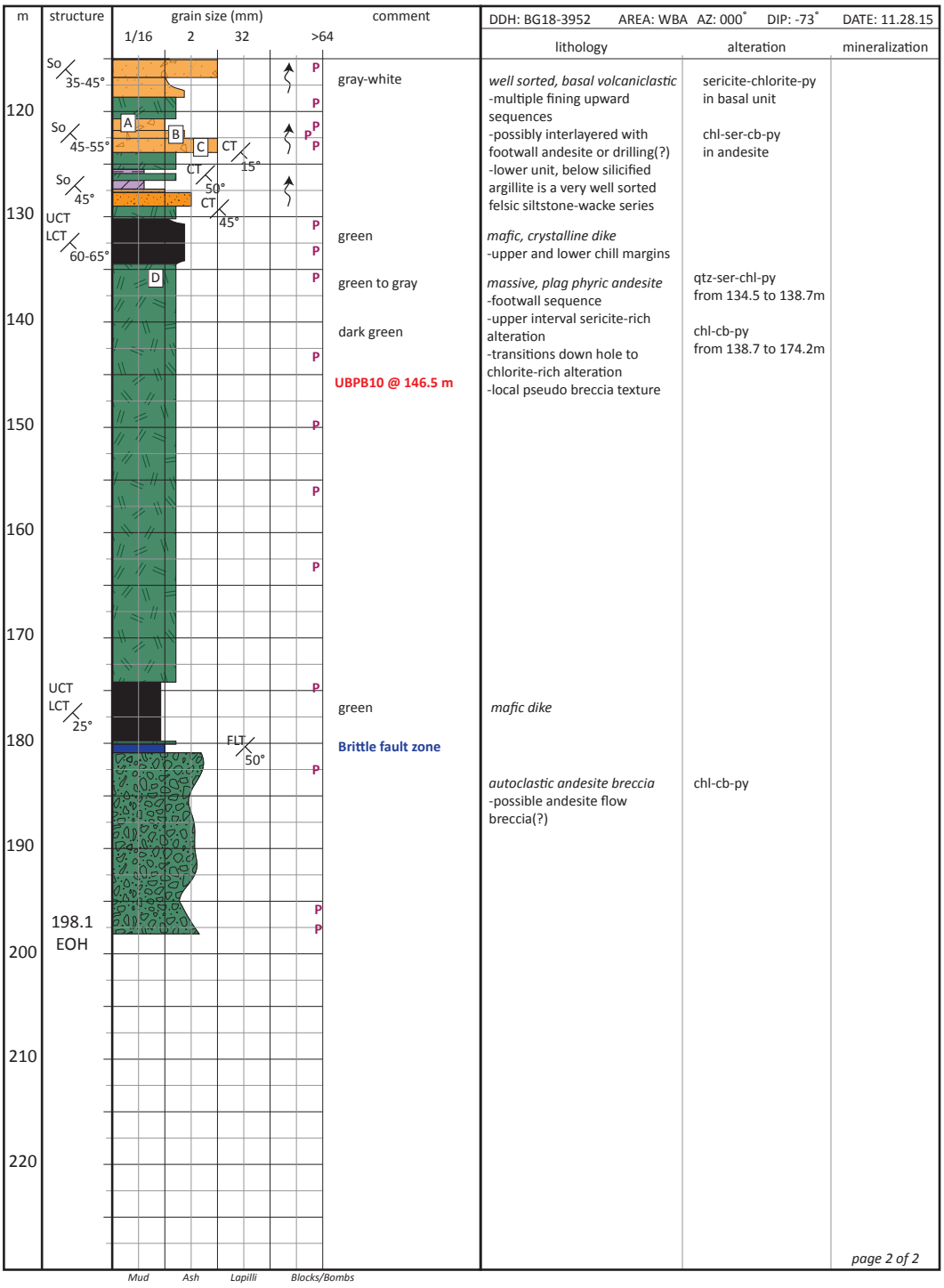

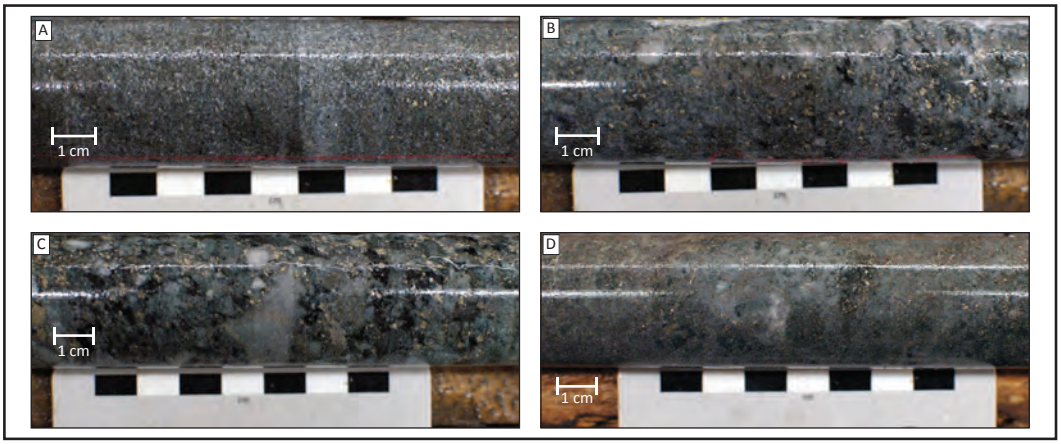

BG18-3323 page 1 of 2

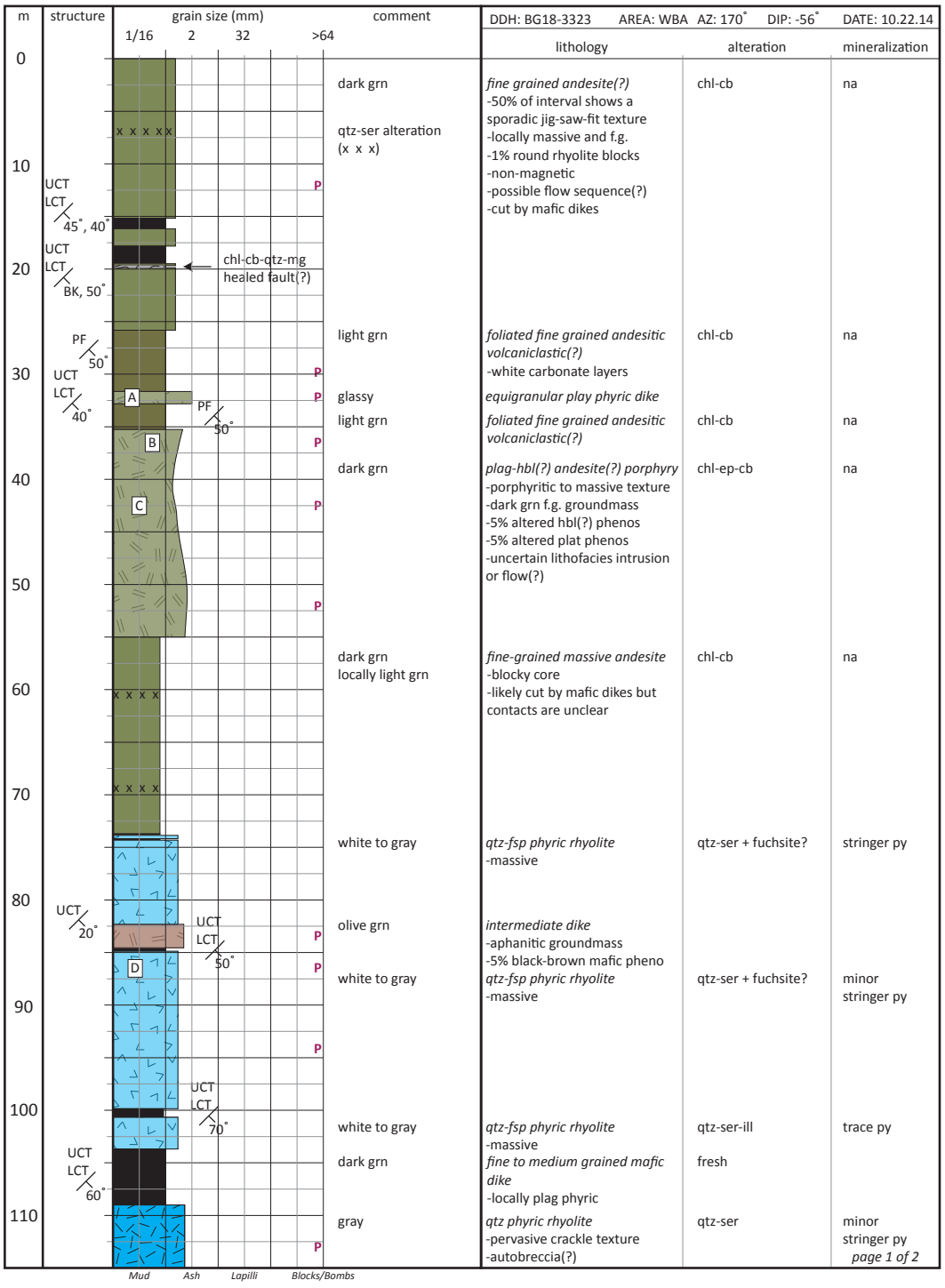

DDH: BG18-3323 AREA: WBA AZ: 170° DIP: -56° DATE: 10.22.14

lithology	alteration	mineralization
fine grained andesite(?) -50% of interval shows a sporadic jig-saw-fit texture -locally massive and f.g. -1% round rhyolite blocks -non-magnetic -possible flow sequence(?) -cut by mafic dikes	chl-cb	na
foliated fine grained andesitic volcaniclastic(?) -white carbonate layers	chl-cb	na
equigranular play phyric dike		
foliated fine grained andesitic volcaniclastic(?)	chl-cb	na
plag-hbl(?) andesite(?) porphyry -porphyritic to massive texture -dark grn f.g. groundmass -5% altered hbl(?) phenos -5% altered plat phenos -uncertain lithofacies intrusion or flow(?)	chl-ep-cb	na
fine-grained massive andesite -blocky core -likely cut by mafic dikes but contacts are unclear	chl-cb	na
qtz-fsp phyric rhyolite -massive	qtz-ser + fuchsite?	stringer py
intermediate dike -aphanitic groundmass -5% black-brown mafic pheno		
qtz-fsp phyric rhyolite -massive	qtz-ser + fuchsite?	minor stringer py
qtz-fsp phyric rhyolite -massive	qtz-ser-ill	trace py
fine to medium grained mafic dike -locally plag phyric	fresh	
qtz phyric rhyolite -pervasive crackle texture -autobreccia(?)	qtz-ser	minor stringer py

page 1 of 2

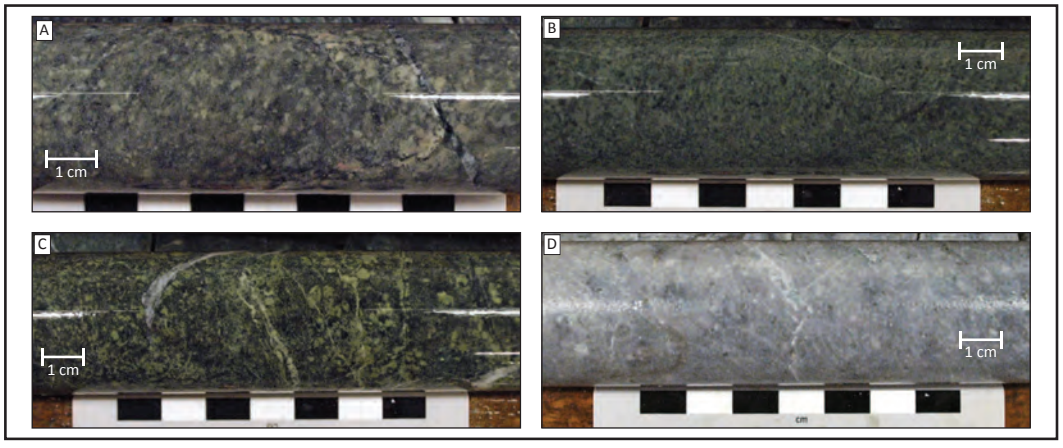

BG18-3323 page 2 of 2

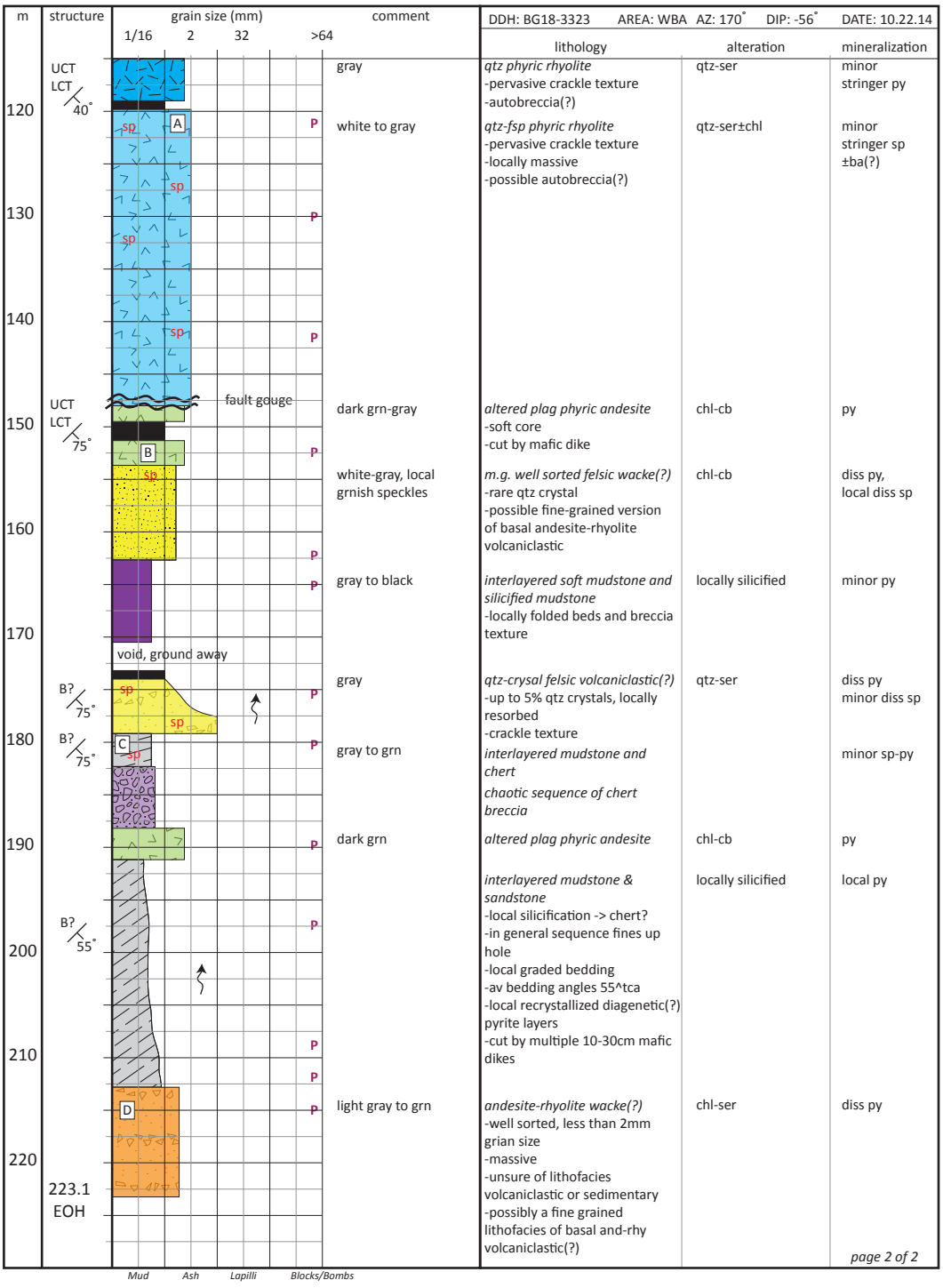

DDH: BG18-3323 AREA: WBA AZ: 170° DIP: -56° DATE: 10.22.14

comment	lithology	alteration	mineralization
gray	*qtz phyric rhyolite* -pervasive crackle texture -autobreccia(?)	qtz-ser	minor stringer py
white to gray	*qtz-fsp phyric rhyolite* -pervasive crackle texture -locally massive -possible autobreccia(?)	qtz-ser±chl	minor stringer sp ±ba(?)
dark grn-gray	*altered plag phyric andesite* -soft core -cut by mafic dike	chl-cb	py
white-gray, local grnish speckles	*m.g. well sorted felsic wacke(?)* -rare qtz crystal -possible fine-grained version of basal andesite-rhyolite volcaniclastic	chl-cb	diss py, local diss sp
gray to black	*interlayered soft mudstone and silicified mudstone* -locally folded beds and breccia texture	locally silicified	minor py
gray	*qtz-crysal felsic volcaniclastic(?)* -up to 5% qtz crystals, locally resorbed -crackle texture	qtz-ser	diss py minor diss sp
gray to grn	*interlayered mudstone and chert* *chaotic sequence of chert breccia*		minor sp-py
dark grn	*altered plag phyric andesite*	chl-cb	py
	interlayered mudstone & sandstone -local silicification -> chert? -in general sequence fines up hole -local graded bedding -av bedding angles 55^tca -local recrystallized diagenetic(?) pyrite layers -cut by multiple 10-30cm mafic dikes	locally silicified	local py
light gray to grn	*andesite-rhyolite wacke(?)* -well sorted, less than 2mm grian size -massive -unsure of lithofacies volcaniclastic or sedimentary -possibly a fine grained lithofacies of basal and-rhy volcaniclastic(?)	chl-ser	diss py

page 2 of 2

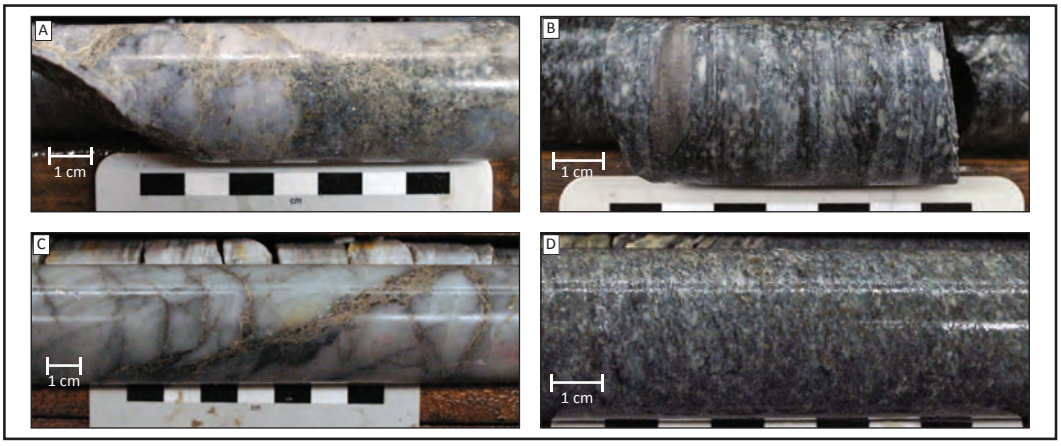

BG18-3322 page 1 of 2

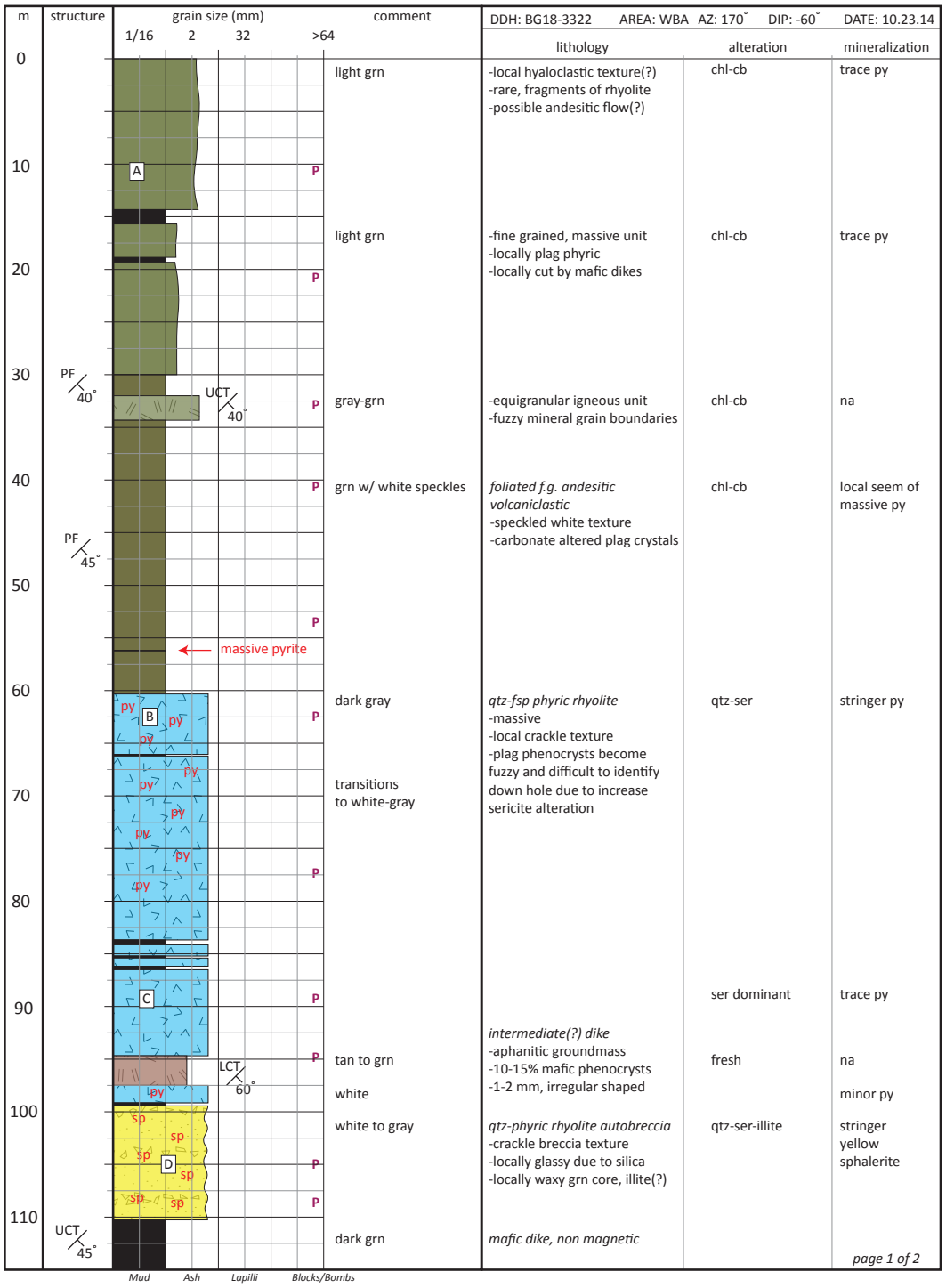

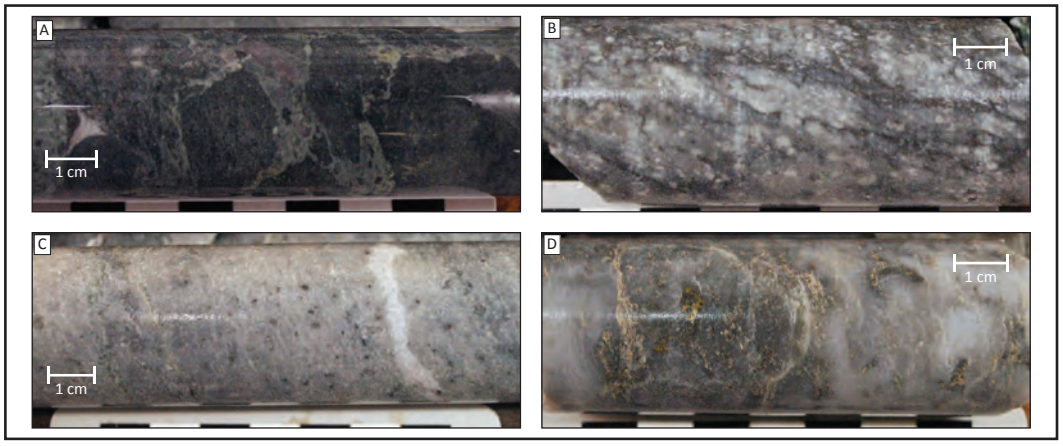

BG18-3322 page 2 of 2

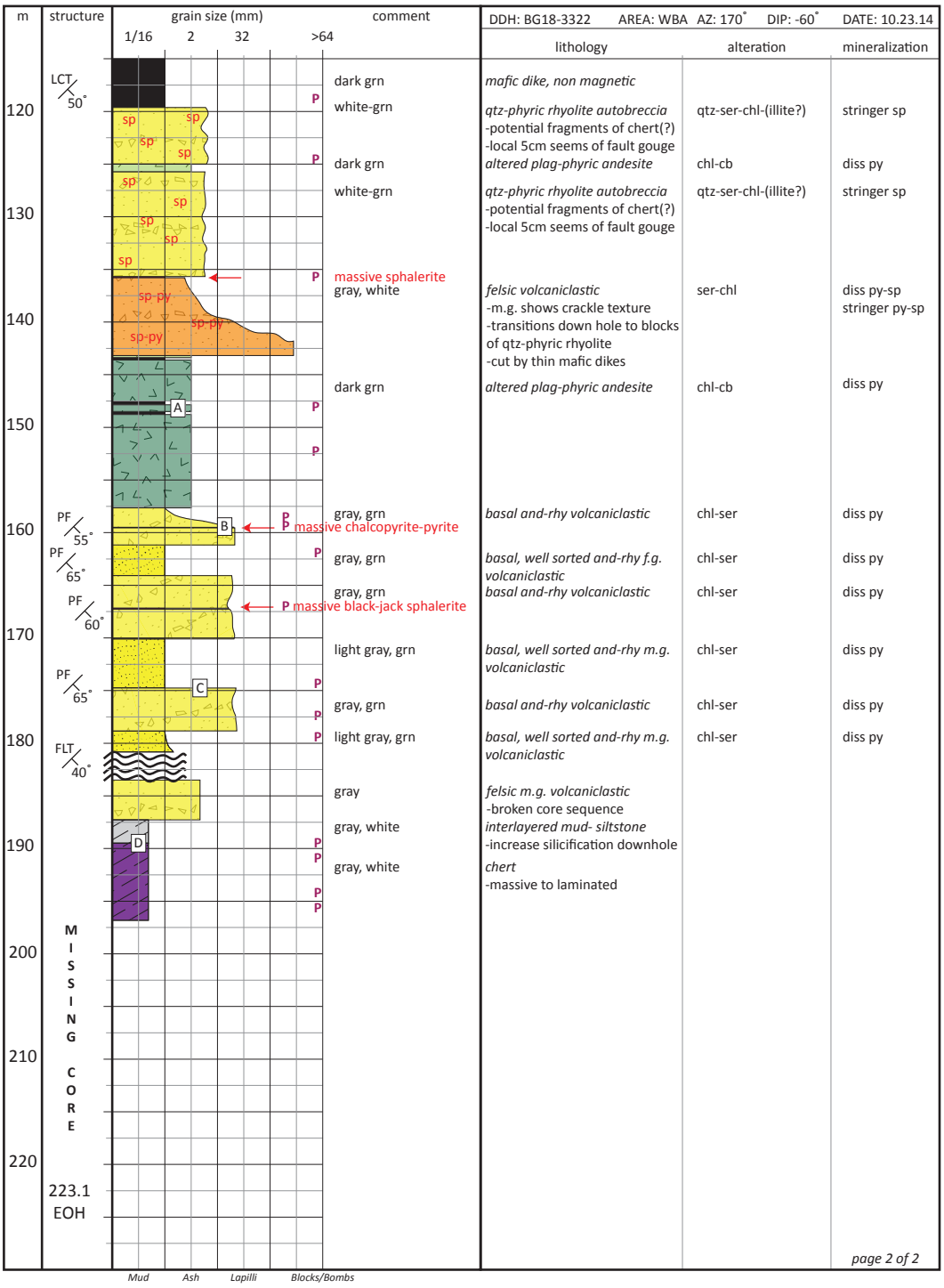

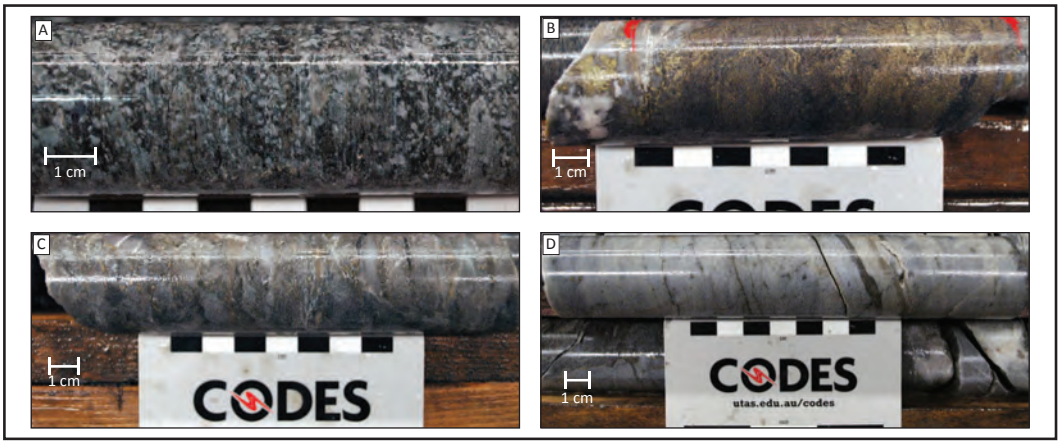

BG18-3321 page 1 of 2

DDH: BG18-3321 AREA: WBA AZ: 170° DIP: -64° DATE: 10.18.14

m	structure	grain size (mm) 1/16 2 32 >64	comment	lithology	alteration	mineralization
0			light grn	-local hyaloclastic texture(?) -rare, fragments of rhyolite -possible andesitic flow(?)	chl-cb	trace py
10		A	P			
			P			
20						
			P light grn local 10 cm intervals of qtz-ser-py alt	-fine grained, massive unit -locally plag phyric -possibly cut by mafic dikes but contacts are broken	chl-cb	local remobilized py-cp
30						
			gray-grn same unit noted at base of flow in G5	-equigranular igneous unit -intrusive contact obscure -fuzzy mineral grain boundaries -feldspar-amphibole(?) crystic	chl-cb	na
			P			
40			P			
	PF 40°		grn w/ white speckles	*foliated f.g. andesitic volcaniclastic* -speckled white texture -carbonate altered plag crystals -local 10cm zones of qtz-ser alt	chl-cb cb-hm veinlets	local remobilized py-cp
50	PF 45°	B	P white-gray	*altered rhyolite* -massive w/ local crackle texture	ser	stringer py
	UCT		gray			
	LCT 45°		gray	*qtz-fsp phyric rhyolite* -massive -coherent volcanic rock		
60		C	P			
			gray		ser	stringer & diss py
		UCT 80° LCT 60°				
70			P			
	PF 50°		gray	-moderate penetrative fabric	ser	stringer & diss py
80						
	PF 45°		grn, speckled white	*altered plag phyric andesite*	chl-cb	na
			gray-white	*qtz-fsp phyric coherent rhyolite*	ser	stringer sp
90						
			P BM14-035 @ 94.5m gray-white autobreccia(?)	*locally qtz phyric rhyolite* -crackle breccia texture -lacks fsp crystals -dome/flow margin(?) -local silicified zone alteration or "chert" fragments(?).	ser-qtz ser-sp define crackle texture	stringer-net textured sp +gray sulfide
100						
	UCT 30°					
110		D	P BM14-037 @ 111.9m tan-grn post min-deformation(?)	*intermediate(?) dike* -aphanitic groundmass -10-15% mafic phenocrysts -1-2 mm, irregular shaped	fresh	na

Mud Ash Lapilli Blocks/Bombs

page 1 of 2

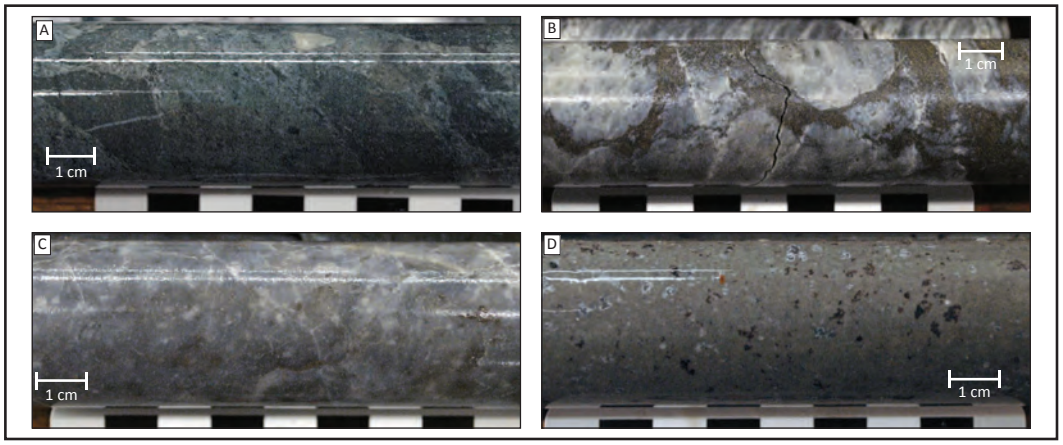

BG18-3321 page 2 of 2

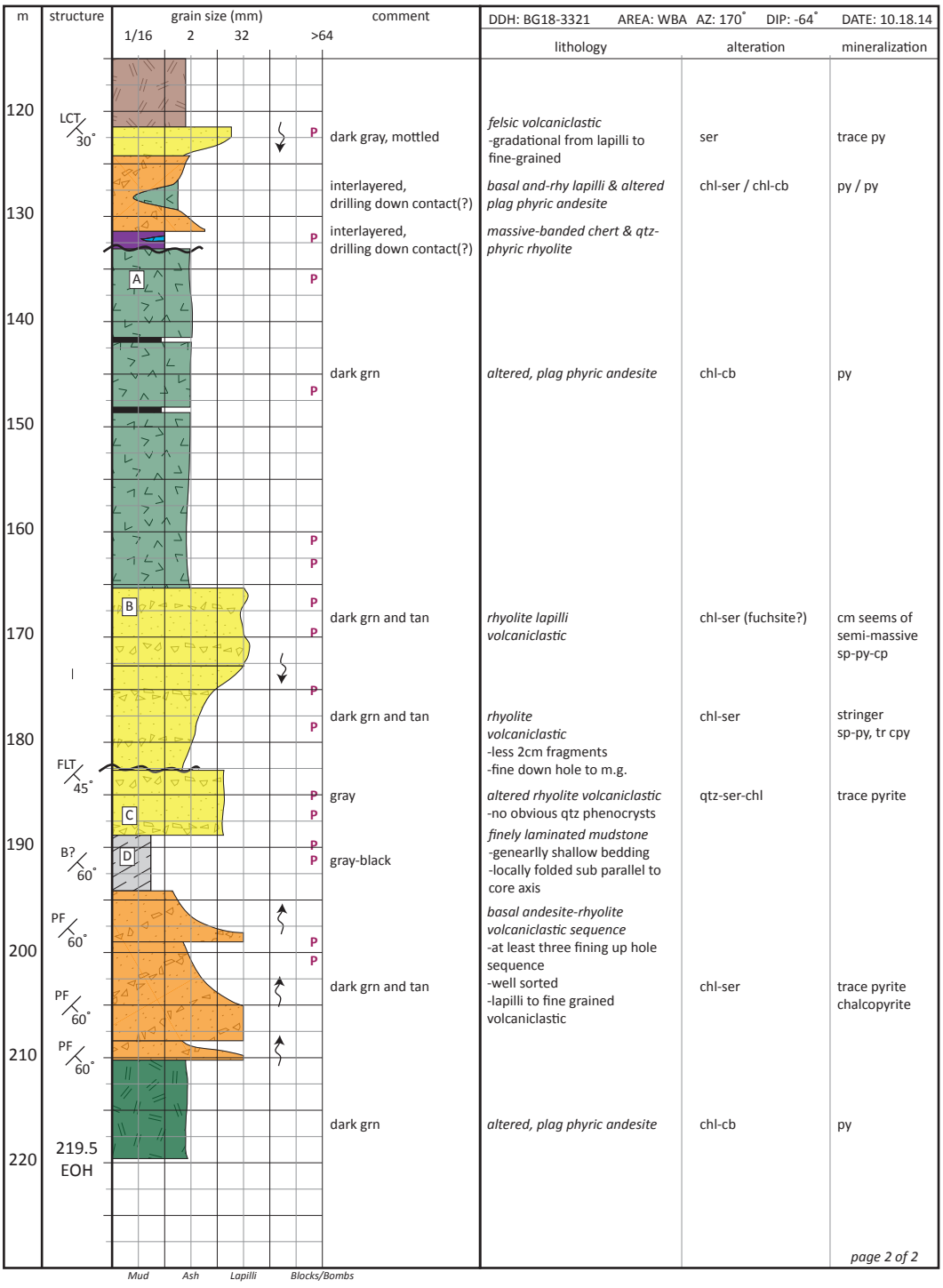

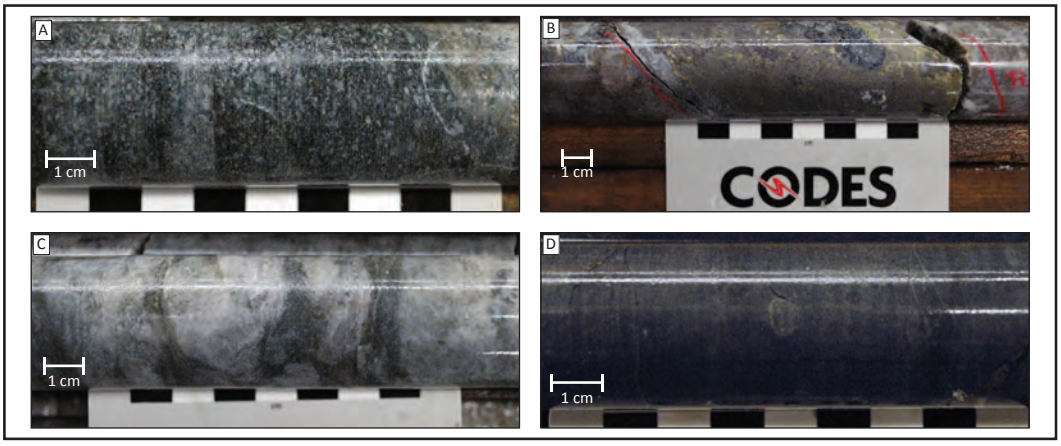

BG18-3769 page 1 of 2

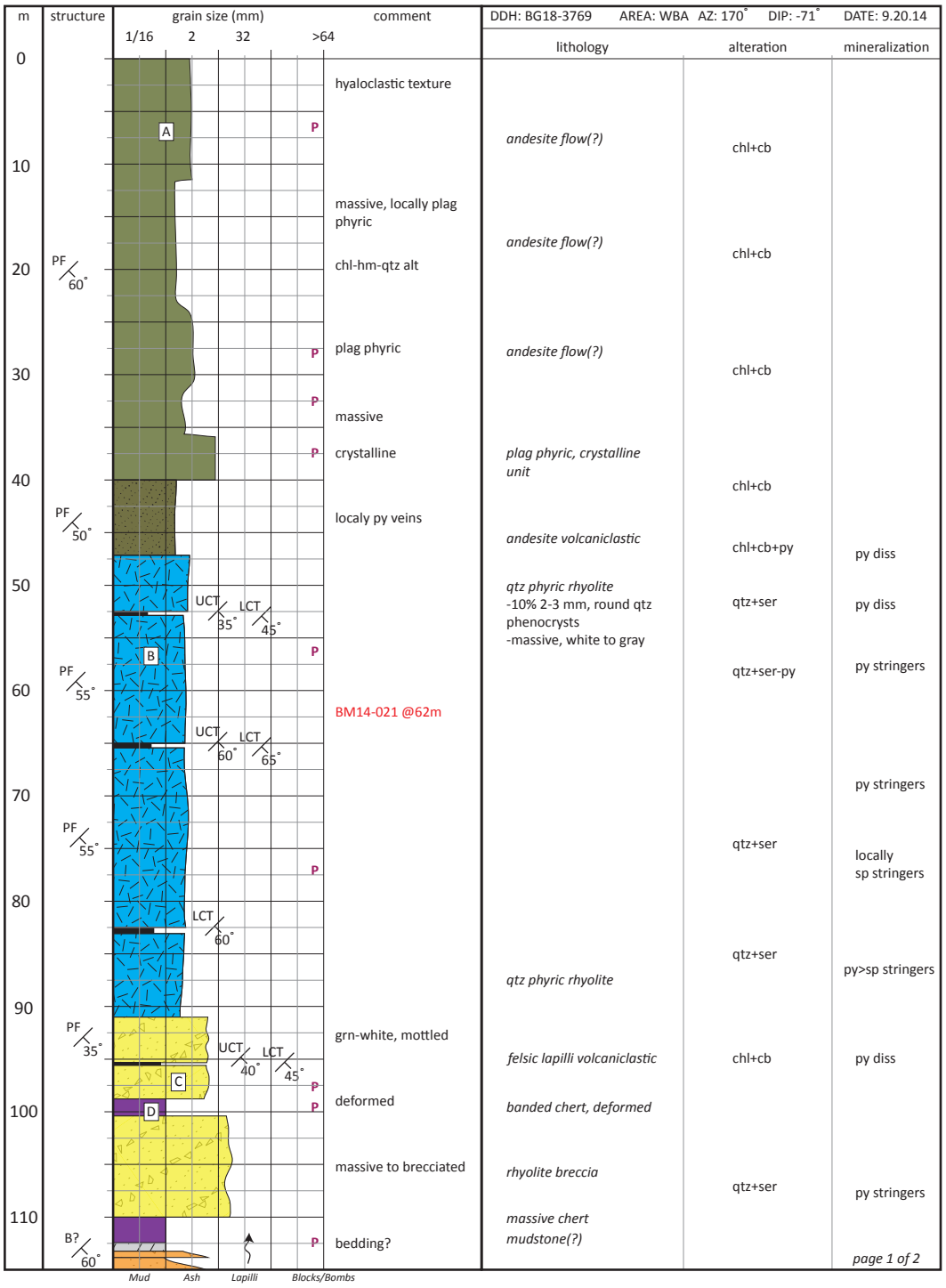

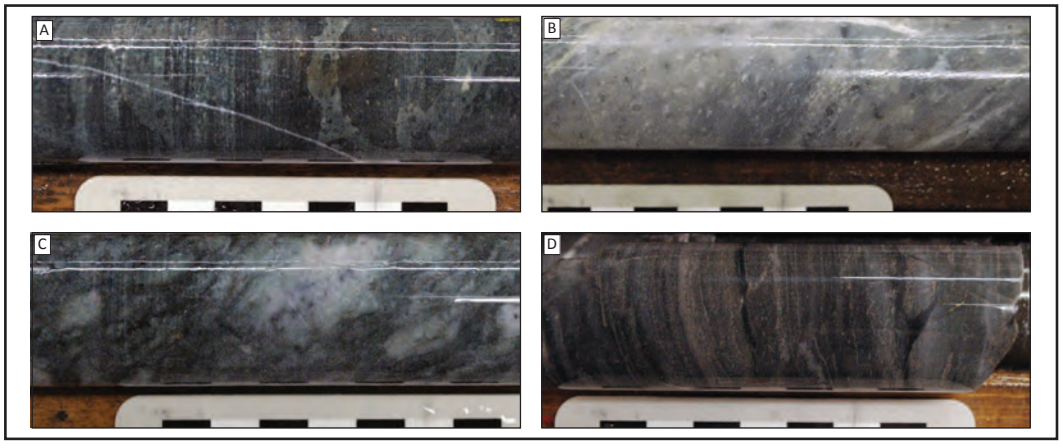

BG18-3769 page 2 of 2

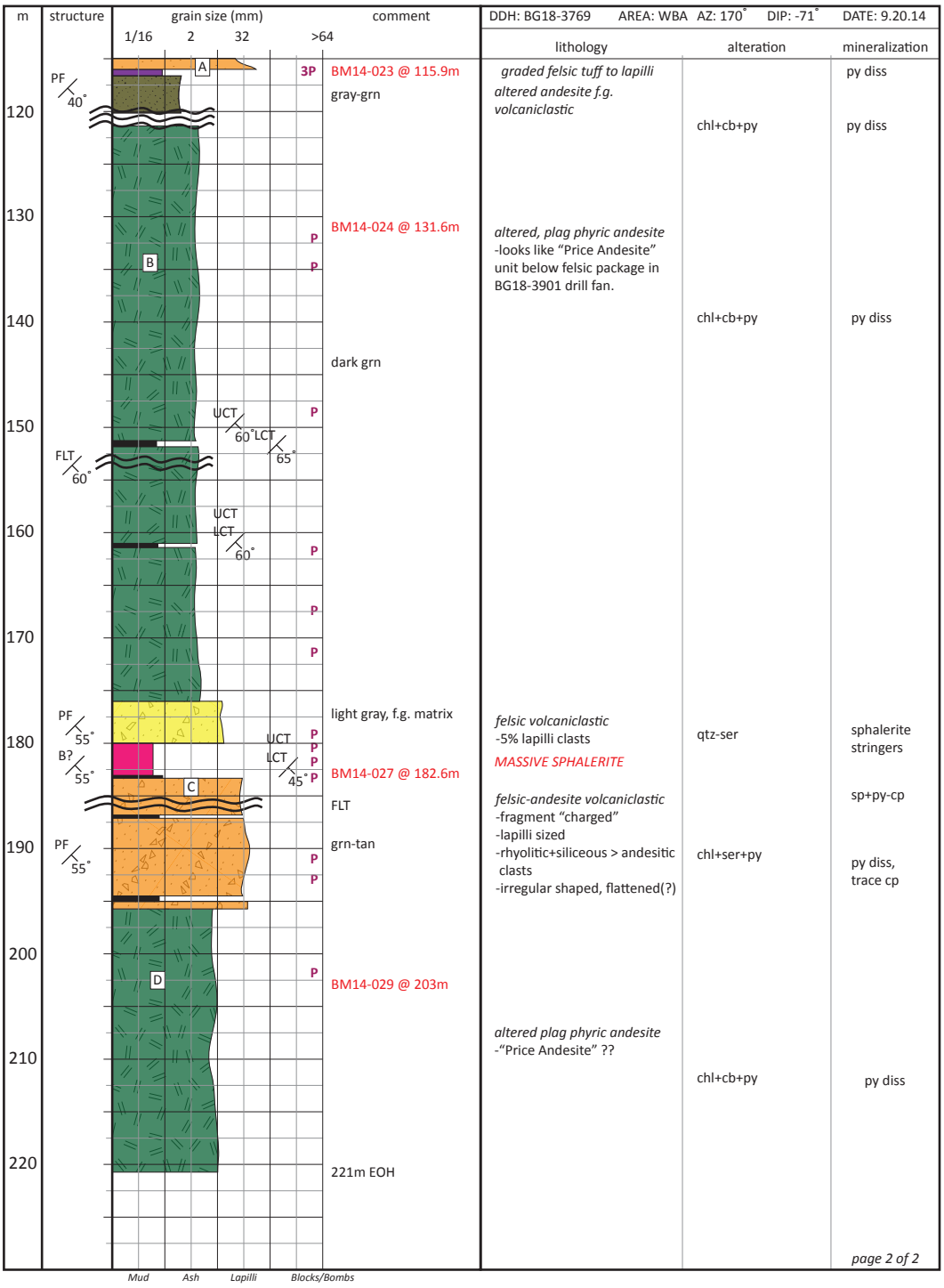

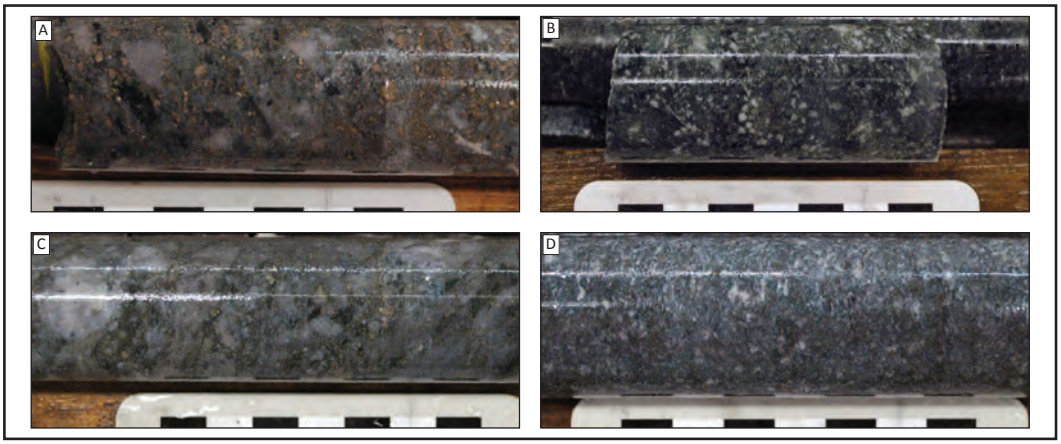

RN18-0223 page 1 of 1

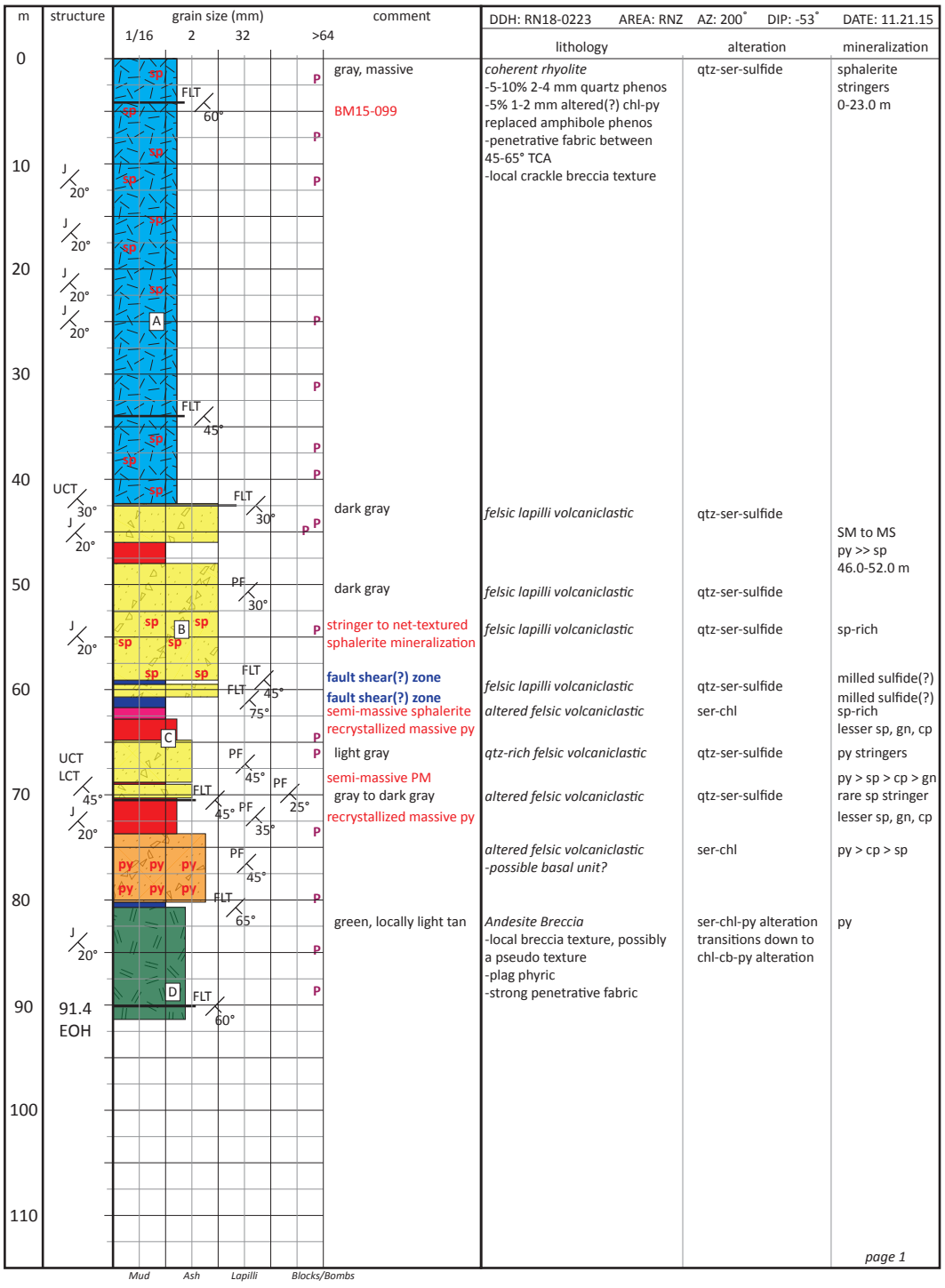

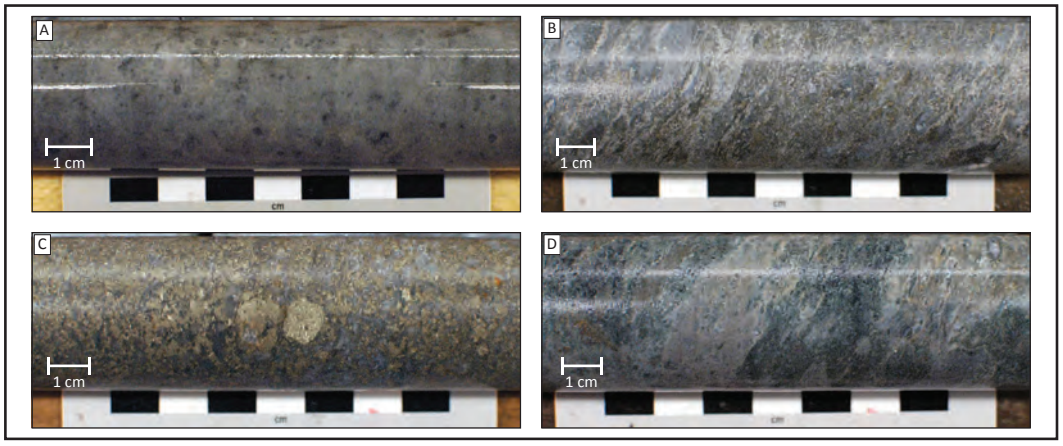

RN18-0224 page 1 of 1

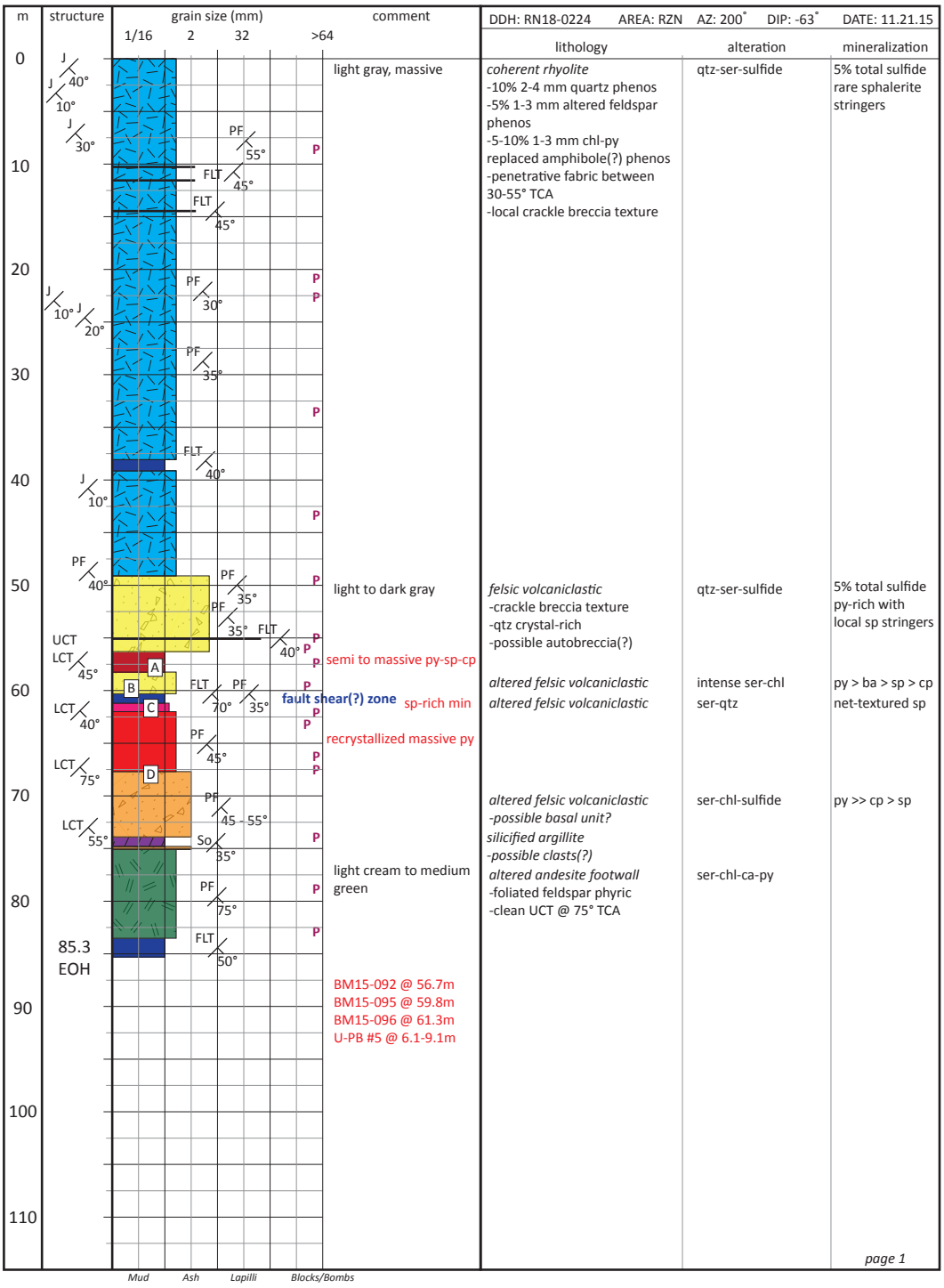

DDH: RN18-0224 AREA: RZN AZ: 200° DIP: -63° DATE: 11.21.15

lithology	alteration	mineralization
coherent rhyolite -10% 2-4 mm quartz phenos -5% 1-3 mm altered feldspar phenos -5-10% 1-3 mm chl-py replaced amphibole(?) phenos -penetrative fabric between 30-55° TCA -local crackle breccia texture	qtz-ser-sulfide	5% total sulfide rare sphalerite stringers
felsic volcaniclastic -crackle breccia texture -qtz crystal-rich -possible autobreccia(?)	qtz-ser-sulfide	5% total sulfide py-rich with local sp stringers
altered felsic volcaniclastic	intense ser-chl	py > ba > sp > cp
altered felsic volcaniclastic	ser-qtz	net-textured sp
altered felsic volcaniclastic *-possible basal unit?* *silicified argillite* *-possible clasts(?)*	ser-chl-sulfide	py >> cp > sp
altered andesite footwall -foliated feldspar phyric -clean UCT @ 75° TCA	ser-chl-ca-py	

page 1

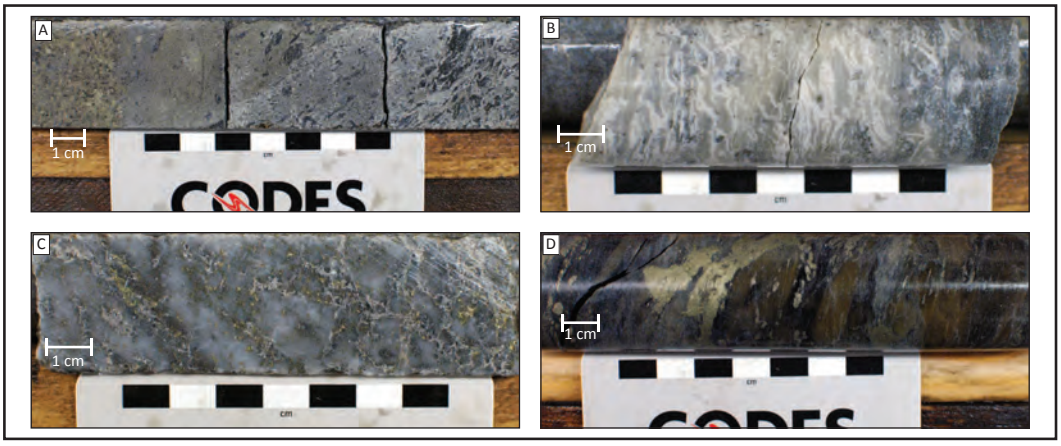

RN18-0225 page 1 of 1

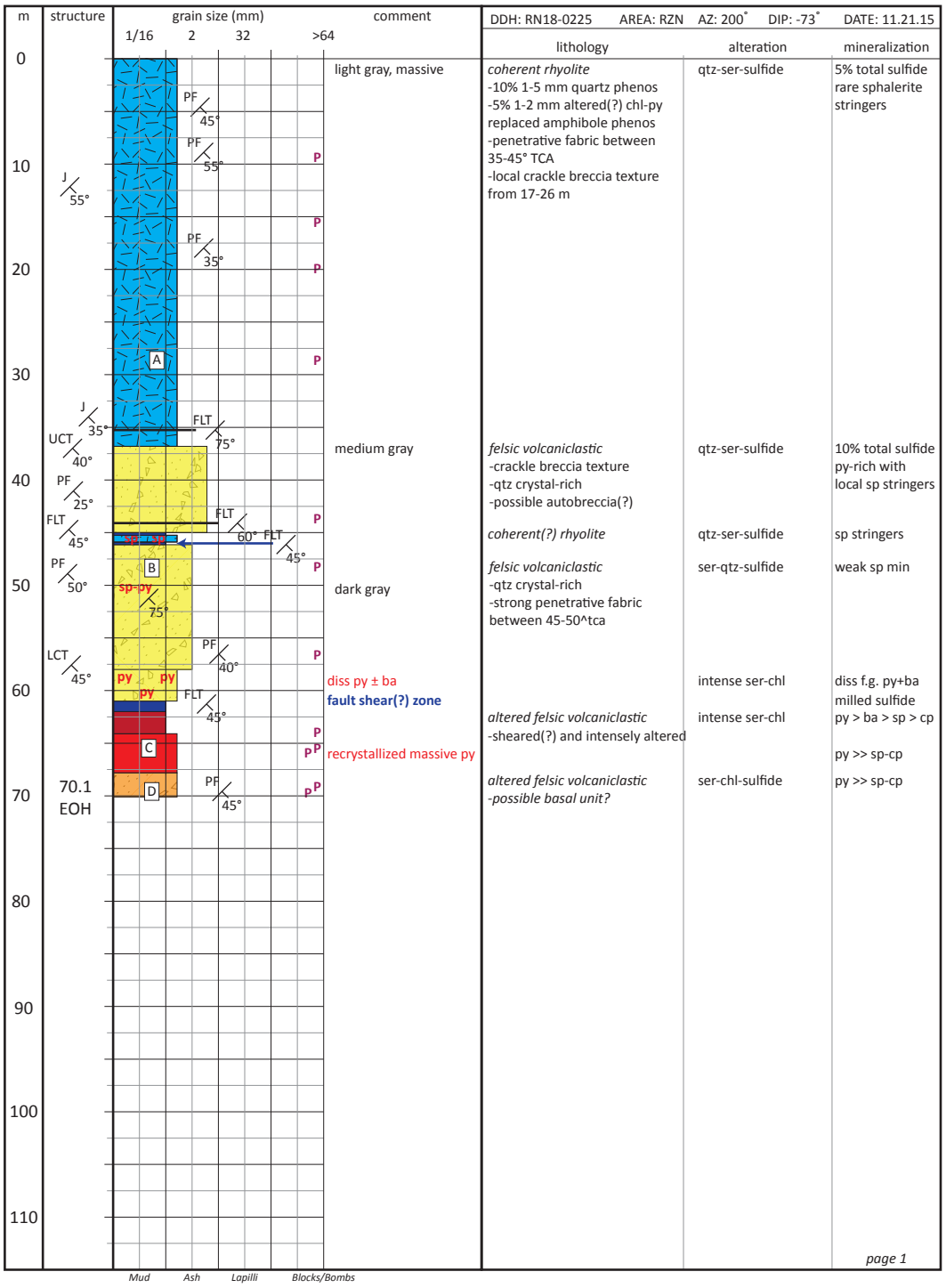

DDH: RN18-0225 AREA: RZN AZ: 200° DIP: -73° DATE: 11.21.15

lithology	alteration	mineralization
coherent rhyolite -10% 1-5 mm quartz phenos -5% 1-2 mm altered(?) chl-py replaced amphibole phenos -penetrative fabric between 35-45° TCA -local crackle breccia texture from 17-26 m	qtz-ser-sulfide	5% total sulfide rare sphalerite stringers
felsic volcaniclastic -crackle breccia texture -qtz crystal-rich -possible autobreccia(?)	qtz-ser-sulfide	10% total sulfide py-rich with local sp stringers
coherent(?) rhyolite	qtz-ser-sulfide	sp stringers
felsic volcaniclastic -qtz crystal-rich -strong penetrative fabric between 45-50^tca	ser-qtz-sulfide	weak sp min
	intense ser-chl	diss f.g. py+ba milled sulfide
altered felsic volcaniclastic -sheared(?) and intensely altered	intense ser-chl	py > ba > sp > cp py >> sp-cp
altered felsic volcaniclastic *-possible basal unit?*	ser-chl-sulfide	py >> sp-cp

page 1

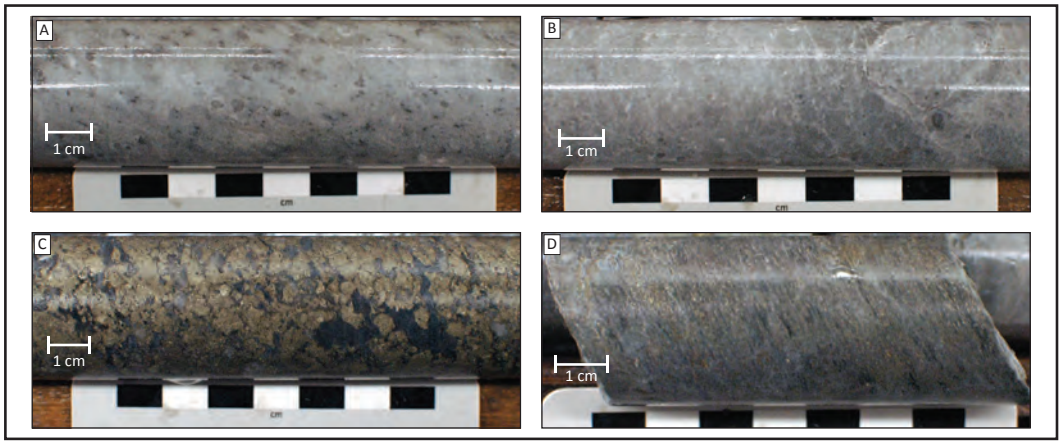

RN18-0105 page 1 of 1

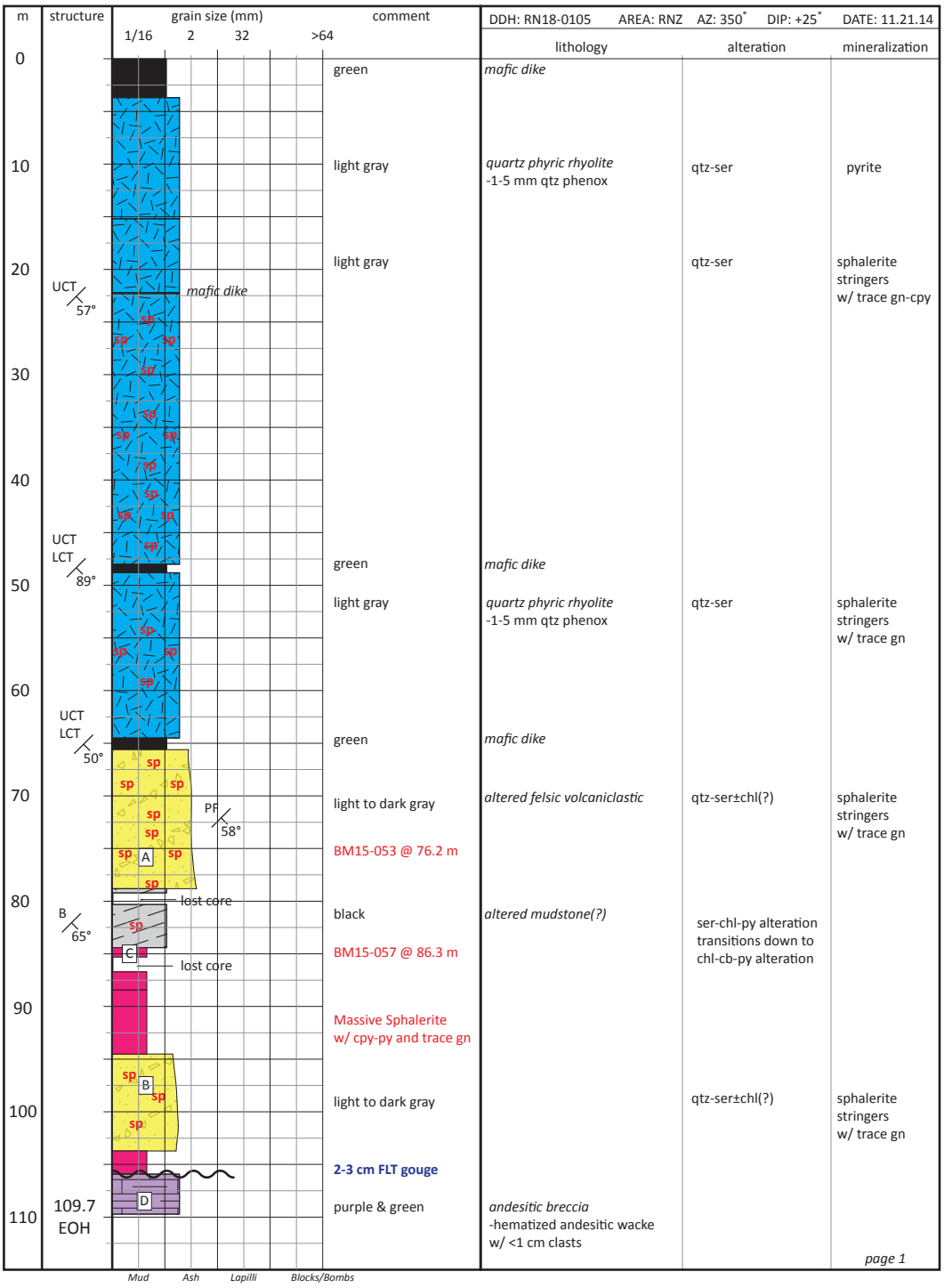

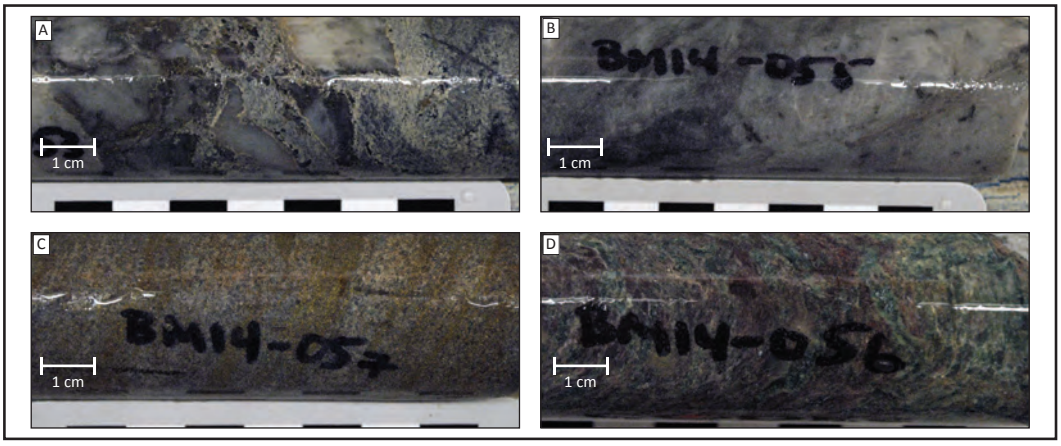

RN18-0104 page 1 of 1

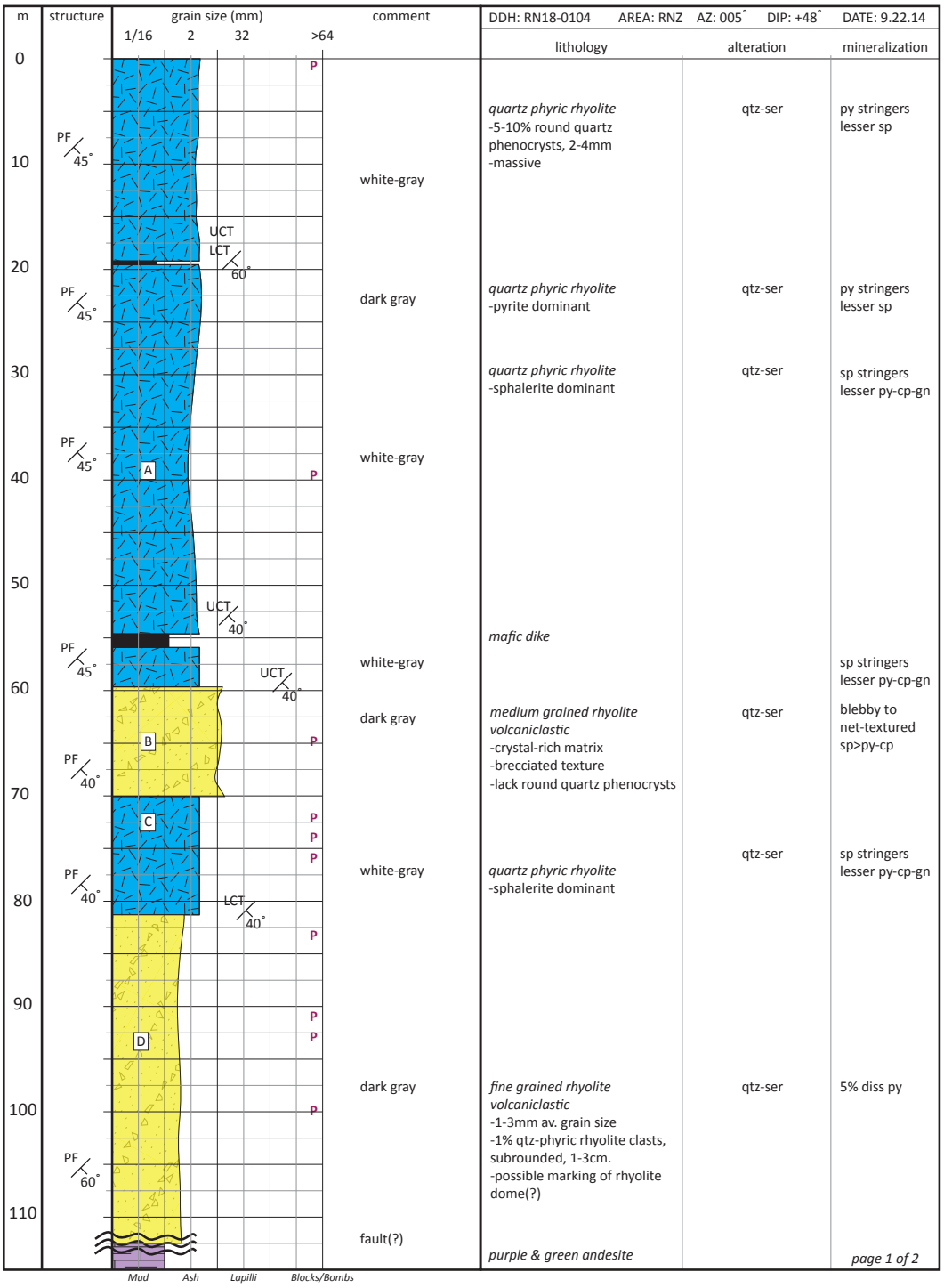

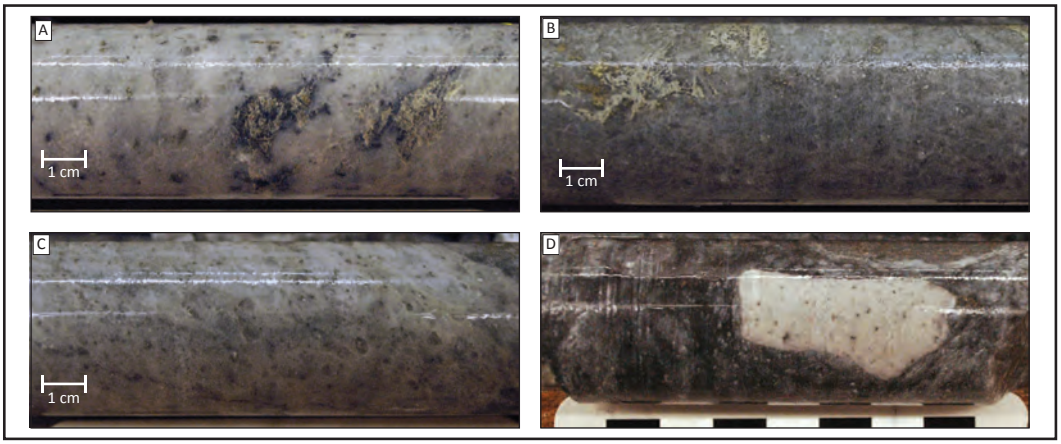

Appendix C:

Electron Microprobe Analytical Method and Results for sulfide, sulfosalts, tellurides and electrum

Analyses were acquired on a JEOL JXA 8530F Plus electron microprobe with 5 tunable wavelength dispersive spectrometers. Operational conditions were 40º takeoff angle, and a beam energy of 20 keV at 30 nA with a 2 μm diameter. Elements were acquired using analysing crystals LIFL for V-Kα, Mn-Kα, Fe-Kα, Co-Kα, Ni-Kα; LiFL for Cu-Kα, Zn-Kα, Ge-Kα, Au-Lγ, Bi-Lγ; PETL for Cd-Lγ, In-Lγ, Sn-Lγ, Sb-Lγ, Te-Lγ, S-Kα, Hg-Mγ, Pb-Mγ, Ag-Lγ; and TAP for Se-Lγ, As-Lγ.

The standards were cassiterite (SnO_2) for Sn; hessite for Ag; galena for Pb; gallium arsenide (GaAs) for As; greenockite (CdS) for Cd; sphalerite (ZnS) for Zn; zinc selenide (ZnSe) for Se; indium antimonide (InSb) for In; manganese metal for Mn; pentlandite astimex for Ni; stibnite astimex for Sb; bismuth selenide astimex for Bi; gold metal for Au; cobalt metal for Co; pyrite Peru CODES for S, Fe; tellurium metal natural for Te; vanadium metal Aldrich for V; cinnabar for Hg; germanium sulfide MAC 11389 for Ge; and chalcocite Geller for Cu. Counting times were: 20 s for Fe, Ni, Cu, Zn, Ag, Cd, Sn, Sb, Te, In; 30 s for Mn, S, Co, Au, Bi, Ge, V; 40 s for Se, As; and 60 s for Hg, Pb. Off peak counting times were: 20 s for Fe, Ni, Cu, Zn, Ag, Cd, Sn, Sb, Te, In; 30 s for Mn, S, Co, Au, Bi, Ge, V; 40 s for Se, As; and 60 s for Hg, Pb.

A multipoint off peak correction method was used for all elements. Unknown and standard intensities were corrected for deadtime and standard intensities were corrected for standard drift over time. Interference corrections were applied to: (1) V for interference by Hg, Te; (2) Mn for interference by Hg; (3) Fe for interference by Mn; (4) Co for interference by Fe; (5) Zn for interference by Cu; (6) Se for interference by As; (7) Cd for interference by Ag, Pb, Bi; (8) Sn for interference by Ag, Cd, Sb, Co; (9) Sb for interference by Cd, Te, Sn; (10) Te for interference by Ag, Sn; (11) Au for interference by Zn; (12) Hg for interference by Au, Pb; (13) Pb for interference by S; and (14) Bi for interference by As, Pb (Donovan et al., 1993). The matrix correction method was ZAF or Phi-Rho-Z calculations with mass absorption coefficients of FFAST Chantler (NIST v2.1, 2005). The ZAF or Phi-Rho-Z algorithm utilised was the Armstrong/Love Scott (Armstrong, 1988). Results are from single point analysis (Table C.1; Figures C.1-C.5).

Table C.1 EMP results for all sulfide, sulfosalt, telluride and electrum analyses

Sample	Analysis Number	Area	Mineral	Note	S wt %	Fe wt %	Cu wt %	Zn wt %	Pb wt %	As wt %	Sb wt %	Cd wt %	Se wt %
BM14-050	1	WBA	el	R	0.19	0.21	<0.02	7.13	<0.05	<0.02	0.04	0.07	<0.02
BM14-050	2	WBA	sp	A	33.26	0.10	0.02	67.49	<0.03	<0.02	<0.02	0.27	<0.02
BM14-050	3	WBA	el	A	2.14	0.16	4.93	0.94	<0.05	1.31	0.28	0.05	<0.02
BM14-050	4*	WBA	tn	A	28.22	1.29	41.17	7.12	<0.03	17.63	2.43	0.10	<0.02
BM14-050	5	WBA	gn	A	13.32	<0.02	0.08	0.03	86.49	<0.02	<0.03	<0.06	<0.02
BM14-050	6	WBA	el	A	0.08	0.06	0.35	0.08	<0.06	<0.02	0.05	<0.05	<0.02
BM14-050	7	WBA	pr-pb	A	16.08	<0.02	5.14	0.14	<0.03	3.44	4.31	<0.04	<0.02
BM14-050	8	WBA	tn	A	27.97	1.43	42.11	7.15	<0.03	18.30	2.09	0.04	<0.02
BM14-050	9	WBA	tn	A	28.02	1.57	42.13	7.07	<0.03	18.31	1.96	0.10	<0.02
BM14-050	10	WBA	sp	A	33.18	0.07	0.24	67.41	<0.03	<0.02	<0.02	0.25	<0.02
BM14-050	11	WBA	pr-pb	A	17.17	0.10	7.69	0.48	<0.03	5.32	2.57	<0.04	<0.02
BM14-050	12	WBA	pr-pb	A	16.72	0.05	5.04	0.12	<0.03	5.36	2.38	<0.04	<0.02
BM14-050	13	WBA	tn	A	28.17	1.47	41.53	7.05	<0.03	18.24	1.67	0.07	<0.02
BM14-050	14	WBA	pr-pb	A	17.17	0.21	8.71	0.90	<0.03	4.57	3.87	<0.04	<0.02
BM14-050	15	WBA	gn	A	13.21	<0.02	0.07	0.04	86.29	<0.02	<0.03	0.08	<0.02
BM14-050	16	WBA	pr-pb	A	16.76	<0.02	4.96	0.88	<0.03	5.66	1.91	<0.04	<0.02
BM14-050	17	WBA	gn	A	13.28	<0.02	0.18	0.22	86.50	0.14	<0.03	0.10	<0.02
BM14-050	18	WBA	tn	A	28.12	1.35	41.87	7.15	<0.03	18.38	1.72	0.14	<0.02
BM14-050	19	WBA	pr-pb	A	16.89	0.06	5.98	0.23	<0.03	5.88	1.54	<0.04	<0.02
BM14-050	20	WBA	sp	A	33.28	0.10	0.17	67.33	<0.03	0.05	<0.02	0.30	<0.02
BM14-050	21	WBA	gn	A	13.20	0.10	0.14	0.03	86.58	0.04	<0.03	<0.06	<0.02
BM14-050	22	WBA	py	A	52.90	46.22	0.09	0.09	<0.03	<0.02	<0.02	<0.03	<0.01
BM14-050	23	WBA	gn	A	13.27	<0.02	0.02	0.11	86.31	0.02	<0.03	0.06	0.02
BM14-050	24	WBA	sp	A	33.10	0.15	0.04	67.68	<0.03	<0.02	<0.02	0.33	<0.02
BM14-050	25	WBA	tn	A	28.13	1.51	41.97	7.22	<0.03	18.49	1.68	0.10	<0.02
BM14-050	26	WBA	sp	A	33.24	0.13	0.19	67.39	<0.03	<0.02	<0.02	0.27	<0.02
BM14-050	27	WBA	gn	R	13.31	<0.02	0.04	2.05	87.39	<0.02	<0.03	<0.06	0.03
BM14-050	28	WBA	sp	A	33.32	0.12	0.05	67.41	<0.03	<0.02	<0.02	0.34	<0.02
BM14-050	29	WBA	tn	A	28.03	1.59	42.18	7.04	<0.03	18.36	1.81	0.10	<0.02
BM14-050	30	WBA	gn	A	13.32	<0.02	0.04	<0.02	86.97	0.02	<0.03	<0.06	0.03
BM14-050	31	WBA	py	A	52.79	46.38	0.11	0.06	<0.03	<0.02	<0.02	0.05	<0.01
BM14-050	32	WBA	gn	A	14.21	<0.02	0.02	<0.02	86.15	0.04	<0.03	<0.06	0.02
BM14-050	33	WBA	sp	A	33.16	0.12	0.35	66.84	<0.03	<0.02	<0.02	0.32	<0.02
BM14-050	34	WBA	tn	A	28.09	1.56	42.32	7.03	<0.03	18.67	1.46	0.07	<0.02
BM14-033	35	WBA	el	A	0.23	1.25	0.07	0.73	<0.06	<0.02	0.07	0.10	<0.02
BM14-033	36	WBA	py	A	54.07	46.51	0.03	0.35	<0.03	<0.02	<0.02	<0.03	<0.01
BM14-033	37	WBA	py	A	33.64	1.92	0.25	64.76	<0.03	<0.02	<0.02	0.31	<0.02
BM14-033	38	WBA	hs	R	1.10	0.15	<0.02	6.40	<0.03	<0.03	<0.03	<0.04	0.06
BM14-033	39	WBA	sp	A	33.56	1.71	<0.02	65.03	<0.03	<0.02	<0.02	0.32	<0.02
BM14-033	40	WBA	hs	A	0.64	0.11	0.06	3.84	0.77	<0.03	<0.03	<0.04	0.07
BM14-033	41	WBA	sp	A	33.45	1.50	0.20	65.03	<0.03	<0.02	<0.02	0.33	<0.02
BM14-033	42	WBA	gn	R	9.58	2.12	<0.02	0.58	64.32	<0.02	<0.03	<0.05	0.38
BM14-033	43	WBA	sp	A	33.47	1.30	0.13	64.77	<0.03	<0.02	<0.02	0.34	<0.02
BM14-033	44	WBA	hs	A	1.06	0.18	<0.02	3.63	0.53	<0.03	<0.03	<0.04	0.15
BM14-033	45	WBA	gn	R	13.39	0.15	<0.02	2.14	86.97	<0.02	<0.03	<0.06	0.46
BM14-033	46	WBA	py	R	53.52	46.78	0.45	0.38	<0.03	<0.02	<0.02	<0.03	<0.01
BM14-033	47	WBA	cpy	A	35.03	30.28	33.86	0.31	<0.03	<0.02	<0.02	0.04	<0.02
BM14-033	48	WBA	py	A	53.80	47.03	<0.01	0.30	<0.03	<0.02	<0.02	0.03	0.01
BM14-033	49	WBA	sp	A	33.28	2.15	0.02	64.82	<0.03	<0.02	<0.02	0.28	<0.02
BM14-033	50	WBA	py	A	54.06	46.98	<0.01	0.50	<0.03	<0.02	<0.02	<0.03	<0.01
BM14-033	51	WBA	sp	A	33.54	1.61	<0.01	65.33	<0.03	<0.02	<0.02	0.32	<0.02
BM14-033	52	WBA	sp	A	33.50	1.38	0.22	65.23	<0.03	<0.02	<0.02	0.34	<0.02
BM14-038	53	WBA	gn	A	13.52	1.42	<0.02	0.34	86.31	<0.02	<0.03	<0.06	<0.02

Table C.1 EMP results for all sulfide, sulfosalt, telluride and electrum analyses

Analysis Number	Au wt %	Ag wt %	Te wt %	V wt %	Mn wt %	Co wt %	Ni wt %	Ge wt %	In wt %	Sn wt %	Hg wt %	Bi wt %	Total wt %
1	64.97	36.72	<0.03	<0.02	0.02	<0.01	<0.02	-	-	<0.03	<0.04	<0.1	109.35
2	<0.05	<0.04	<0.02	<0.02	<0.01	<0.01	<0.02	-	-	<0.02	<0.03	<0.08	101.14
3	55.95	35.97	0.03	<0.02	<0.02	<0.01	<0.02	-	-	<0.03	<0.04	<0.1	101.77
4	<0.05	0.87	<0.02	<0.02	<0.01	<0.01	<0.02	-	-	<0.02	<0.03	<0.08	98.84
5	<0.05	0.09	<0.03	<0.02	<0.02	<0.01	<0.02	-	-	<0.03	<0.03	<0.1	100.01
6	69.18	33.17	<0.03	<0.02	<0.02	<0.01	<0.02	-	-	<0.03	<0.04	<0.1	102.97
7	0.06	71.22	<0.03	<0.02	<0.02	<0.01	<0.02	-	-	<0.03	<0.03	<0.09	100.39
8	<0.05	0.80	<0.02	<0.01	<0.02	<0.01	<0.02	-	-	<0.02	<0.03	<0.08	99.89
9	<0.05	0.87	<0.02	<0.01	<0.01	<0.01	<0.02	-	-	0.02	<0.03	<0.08	100.06
10	<0.05	<0.03	<0.02	<0.01	<0.01	<0.01	<0.01	-	-	<0.02	<0.03	<0.08	101.14
11	<0.05	68.98	<0.03	<0.02	<0.02	<0.01	<0.02	-	-	<0.03	<0.03	<0.09	102.31
12	<0.05	72.01	<0.03	<0.02	<0.02	<0.01	<0.02	-	-	<0.03	<0.03	<0.09	101.69
13	<0.05	0.86	<0.02	<0.01	<0.01	<0.01	<0.02	-	-	<0.02	<0.03	<0.08	99.06
14	<0.05	65.33	<0.03	<0.02	0.02	<0.01	<0.02	-	-	<0.03	<0.03	<0.09	100.78
15	<0.05	<0.06	<0.04	<0.02	<0.02	<0.01	<0.02	-	-	<0.04	<0.03	<0.1	99.69
16	<0.05	71.41	<0.03	<0.02	<0.02	<0.01	<0.02	-	-	<0.03	<0.03	<0.09	101.57
17	0.08	0.10	0.05	<0.02	<0.02	<0.01	<0.02	-	-	<0.03	<0.03	<0.1	100.65
18	<0.05	0.68	<0.02	<0.02	<0.02	<0.01	<0.02	-	-	<0.02	<0.03	<0.08	99.40
19	<0.05	70.96	<0.03	<0.02	<0.02	<0.01	<0.02	-	-	<0.03	<0.03	<0.09	101.55
20	<0.05	<0.03	<0.02	<0.02	<0.02	<0.01	<0.01	-	-	<0.02	<0.03	<0.08	101.23
21	<0.06	0.15	0.06	<0.02	<0.02	<0.01	<0.02	-	-	<0.03	<0.03	<0.1	100.29
22	0.05	<0.03	<0.02	0.02	<0.01	<0.01	0.02	-	-	<0.02	<0.03	<0.08	99.40
23	<0.06	<0.05	<0.03	0.02	0.02	<0.01	<0.02	-	-	<0.03	<0.03	<0.1	99.87
24	<0.05	<0.04	<0.02	<0.02	<0.02	<0.01	<0.02	-	-	<0.02	<0.03	<0.08	101.29
25	<0.05	0.84	<0.02	<0.02	<0.01	<0.01	<0.02	-	-	<0.02	<0.03	<0.08	99.95
26	<0.05	<0.04	<0.02	<0.02	<0.02	<0.01	<0.02	-	-	<0.02	<0.03	<0.08	101.22
27	0.07	0.06	0.04	<0.02	<0.02	<0.01	<0.02	-	-	<0.03	<0.03	<0.1	103.00
28	<0.05	<0.03	<0.02	<0.02	<0.02	<0.01	<0.01	-	-	<0.02	<0.03	<0.08	101.25
29	<0.05	0.79	<0.02	<0.02	<0.02	<0.01	<0.02	-	-	<0.02	<0.03	<0.08	99.89
30	0.06	<0.05	<0.03	<0.02	<0.02	<0.01	<0.02	-	-	<0.03	0.03	<0.1	100.47
31	<0.04	<0.03	<0.02	<0.01	<0.01	<0.01	<0.02	-	-	<0.02	<0.03	<0.08	99.40
32	<0.06	<0.05	0.07	<0.02	<0.02	<0.01	<0.02	-	-	<0.03	<0.03	<0.1	100.52
33	<0.05	<0.03	<0.02	<0.01	<0.02	<0.01	<0.01	-	-	<0.02	<0.03	<0.08	100.80
34	<0.05	0.73	<0.02	<0.02	<0.01	<0.01	<0.02	-	-	<0.02	<0.03	<0.08	99.93
35	67.48	32.81	0.05	<0.02	<0.02	<0.01	<0.02	-	-	<0.03	0.27	<0.1	103.07
36	<0.04	<0.03	<0.02	0.01	<0.01	<0.01	0.07	-	-	<0.02	<0.03	<0.08	101.05
37	<0.05	<0.03	<0.02	<0.02	<0.01	<0.01	<0.01	-	-	<0.02	<0.03	<0.08	100.88
38	0.22	63.75	39.95	<0.02	<0.02	<0.01	<0.02	-	-	<0.03	<0.03	<0.1	111.65
39	<0.05	<0.03	<0.02	<0.02	0.04	<0.01	<0.01	-	-	<0.02	<0.03	<0.08	100.65
40	0.14	60.16	35.38	<0.02	<0.02	<0.01	<0.02	-	-	<0.03	<0.03	<0.09	101.17
41	<0.05	<0.03	<0.02	<0.02	<0.01	<0.01	<0.02	-	-	<0.02	<0.03	<0.08	100.51
42	<0.05	0.31	<0.04	<0.02	5.30	<0.01	<0.02	-	-	<0.03	<0.03	0.41	83.00
43	<0.05	<0.03	<0.02	<0.02	0.26	<0.01	<0.01	-	-	<0.02	<0.03	<0.08	100.26
44	0.11	60.92	36.52	<0.02	0.22	<0.01	<0.02	-	-	<0.03	<0.03	<0.1	103.31
45	<0.06	0.37	0.07	<0.02	0.23	<0.01	<0.02	-	-	<0.03	<0.03	0.38	104.14
46	<0.04	<0.03	<0.02	<0.01	<0.01	0.02	<0.02	-	-	<0.02	<0.03	<0.08	101.16
47	<0.05	<0.03	<0.02	<0.01	<0.01	<0.01	<0.02	-	-	<0.02	<0.03	<0.08	99.53
48	0.05	<0.03	<0.02	<0.01	<0.01	0.02	<0.02	-	-	<0.02	<0.03	<0.08	101.23
49	<0.05	<0.03	<0.02	<0.02	0.02	<0.01	<0.01	-	-	<0.02	<0.03	<0.08	100.57
50	<0.04	<0.03	<0.02	0.02	<0.01	0.05	0.07	-	-	<0.02	<0.03	<0.08	101.67
51	<0.05	<0.03	<0.02	<0.02	0.03	<0.01	<0.02	-	-	<0.02	<0.03	<0.08	100.82
52	<0.05	<0.03	<0.02	<0.02	<0.02	<0.01	<0.01	-	-	<0.02	<0.03	<0.08	100.66
53	0.10	<0.05	0.04	<0.02	<0.02	<0.01	<0.02	-	-	<0.03	<0.03	<0.1	101.74

Table C.1 Continued.

Sample	Analysis Number	Area	Mineral	Note	S wt %	Fe wt %	Cu wt %	Zn wt %	Pb wt %	As wt %	Sb wt %	Cd wt %	Se wt %
BM14-038	54	WBA	py	A	53.69	47.63	<0.01	0.06	<0.03	<0.02	<0.02	<0.03	<0.01
BM14-038	55	WBA	sp	A	33.38	1.05	<0.01	65.63	<0.03	<0.02	<0.02	0.26	<0.02
BM14-038	56	WBA	py	A	53.67	47.65	<0.01	0.06	<0.03	<0.02	<0.02	<0.03	<0.01
BM14-038	57	WBA	sp	A	34.04	0.28	<0.02	66.82	<0.03	<0.02	<0.02	0.28	<0.02
BM14-038	58	WBA	py	A	53.70	47.12	<0.01	0.27	<0.03	<0.02	<0.02	<0.03	<0.01
BM14-038	59	WBA	pr-pb	R	16.47	0.03	4.88	5.01	<0.03	2.45	6.76	<0.04	<0.02
BM14-038	60	WBA	gn	R	14.16	<0.02	0.73	8.79	77.38	0.12	0.47	<0.05	<0.02
BM14-038	61	WBA	sp	A	33.52	0.08	0.02	67.13	<0.03	<0.02	<0.02	0.32	<0.02
BM14-038	62	WBA	td	A	24.42	0.45	27.59	6.94	<0.03	2.32	24.05	0.17	<0.02
BM14-038	63	WBA	td	A	24.53	0.49	27.84	6.92	0.03	2.72	23.54	0.19	<0.02
BM14-038	64	WBA	gn	A	13.46	<0.02	<0.02	<0.02	86.53	<0.02	<0.03	<0.06	<0.02
BM14-038	65	WBA	ac	R	10.76	0.02	0.03	3.70	0.04	0.02	<0.03	<0.04	<0.02
BM14-038	66	WBA	ac	R	13.08	<0.02	0.04	3.85	<0.03	<0.02	<0.02	<0.04	<0.02
BM14-038	67	WBA	el	R	9.48	0.08	0.23	4.98	0.17	<0.02	<0.03	<0.04	<0.02
BM14-038	68	WBA	pr-pb	A	15.87	1.34	3.60	0.02	0.03	2.01	7.13	<0.04	<0.02
BM14-038	69	WBA	pr-pb	R	17.29	3.65	4.41	0.03	0.16	2.01	6.87	<0.04	<0.02
BM14-038	70	WBA	py	A	53.86	47.29	0.02	<0.02	<0.03	<0.02	<0.02	<0.03	<0.01
BM14-038	71	WBA	gn	A	13.43	0.67	<0.02	0.31	87.11	<0.02	<0.03	<0.06	<0.02
BM14-038	72	WBA	gn	R	13.66	<0.02	<0.02	2.27	87.84	<0.02	<0.03	<0.06	<0.02
BM14-038	73	WBA	sp	A	33.47	0.08	<0.01	66.85	<0.03	<0.02	<0.02	0.26	<0.02
BM14-038	74	WBA	gn	A	13.42	<0.02	<0.02	1.00	86.44	<0.02	<0.03	<0.06	<0.02
BM14-038	75	WBA	py	A	53.79	47.52	<0.01	0.25	<0.03	<0.02	<0.02	<0.03	<0.01
BM14-038	76	WBA	td	A	25.00	0.47	30.19	7.13	<0.03	2.88	23.72	0.15	0.02
BM14-038	77	WBA	td	A	25.17	0.55	31.23	7.17	<0.03	4.35	21.45	0.14	<0.02
BM14-038	78	WBA	cpy	A	35.11	30.09	33.89	0.16	<0.03	0.02	<0.02	<0.03	<0.02
BM14-038	79	WBA	gn	A	13.34	0.04	0.28	0.40	86.53	0.03	<0.03	<0.06	<0.02
BM14-038	80	WBA	pr-pb	A	15.46	<0.02	4.77	0.07	<0.03	2.26	6.61	<0.04	<0.02
BM14-038	81	WBA	pr-pb	A	15.24	<0.02	4.87	0.20	<0.03	2.21	6.62	<0.04	<0.02
BM14-038	82	WBA	sp	A	33.43	0.08	<0.01	66.43	<0.03	<0.02	<0.02	0.29	<0.02
BM14-038	83	WBA	gn	A	13.31	<0.02	<0.02	0.03	86.53	<0.02	<0.03	<0.06	<0.02
BM14-038	84	WBA	td	A	25.38	0.49	31.92	7.22	<0.03	3.65	22.69	0.19	<0.02
BM14-038	85	WBA	td	A	25.32	0.47	31.61	7.27	<0.03	3.08	23.57	0.10	<0.02
BM14-038	86	WBA	sp	A	33.58	0.09	0.05	66.13	<0.03	<0.02	<0.02	0.31	0.02
BM14-027	87	WBA	pr-pb	A	17.50	0.03	2.25	1.02	<0.03	2.27	9.35	<0.04	<0.02
BM14-027	88	WBA	gn	A	16.77	0.08	0.08	13.48	67.05	<0.02	<0.03	0.13	<0.02
BM14-027	89	WBA	sp	A	33.44	0.37	<0.01	65.69	<0.03	<0.02	<0.02	0.36	<0.02
BM14-027	90	WBA	tn	A	27.99	4.88	38.62	4.88	<0.03	16.80	3.07	0.03	<0.02
BM14-027	91	WBA	py	A	54.26	46.44	0.05	0.02	<0.03	<0.02	<0.02	<0.03	<0.01
BM14-027	92	WBA	tn	A	28.21	5.08	38.76	4.87	<0.03	17.08	3.06	0.07	<0.02
BM14-027	93	WBA	py	A	54.22	46.42	0.02	<0.02	<0.03	0.02	<0.02	<0.03	<0.01
BM14-027	94	WBA	cpy	A	35.10	29.94	34.03	<0.02	<0.03	<0.02	<0.02	0.06	<0.02
BM14-027	95	WBA	td	A	25.29	2.65	26.95	5.10	<0.03	8.86	13.89	0.07	<0.02
BM14-027	96	WBA	tn	A	27.12	3.27	33.19	4.57	<0.03	16.50	2.86	0.05	<0.02
BM14-027	97	WBA	td	A	25.59	2.46	27.43	5.09	<0.03	9.93	12.33	<0.04	<0.02
BM14-027	98	WBA	td	A	24.98	2.16	26.53	5.39	<0.03	6.59	17.19	0.09	<0.02
BM14-027	99	WBA	aspy	A	20.16	34.08	1.33	0.17	<0.03	44.20	0.05	<0.03	<0.02
BM14-027	100	WBA	cpy	A	35.20	29.89	33.90	0.03	<0.03	<0.02	<0.02	<0.03	0.02
BM14-027	101	WBA	gn	A	13.45	0.02	0.31	0.09	86.02	<0.02	0.06	<0.06	0.02
BM14-027	102	WBA	sp	A	33.44	0.36	<0.01	66.22	<0.03	<0.03	<0.02	0.32	<0.02
BM14-027	103	WBA	sp	A	33.48	0.39	0.02	66.24	<0.03	<0.03	<0.02	0.31	<0.02
BM14-027	104	WBA	sp	A	33.47	0.37	0.03	66.13	<0.03	0.03	<0.02	0.31	<0.02
BM14-027	105	WBA	sp	A	33.85	0.41	<0.01	66.86	<0.03	<0.03	<0.02	0.36	<0.02
BM14-027	106	WBA	cpy	A	35.55	29.37	33.94	1.19	<0.03	<0.02	<0.02	<0.03	<0.02

Table C.1 Continued.

Analysis Number	Au wt %	Ag wt %	Te wt %	V wt %	Mn wt %	Co wt %	Ni wt %	Ge wt %	In wt %	Sn wt %	Hg wt %	Bi wt %	Total wt %
54	<0.04	<0.03	<0.02	<0.01	<0.01	0.01	0.02	-	-	<0.02	<0.03	<0.08	101.41
55	<0.05	<0.03	<0.02	<0.02	<0.02	<0.01	<0.02	-	-	<0.02	0.03	<0.08	100.35
56	<0.04	<0.03	<0.02	<0.02	<0.01	<0.01	<0.02	-	-	<0.02	<0.03	<0.08	101.38
57	<0.05	<0.03	<0.02	<0.02	<0.01	<0.01	<0.01	-	-	<0.02	<0.03	<0.08	101.41
58	0.04	<0.03	<0.02	<0.01	<0.01	<0.01	<0.02	-	-	<0.02	<0.03	<0.08	101.13
59	<0.05	68.22	1.13	<0.02	<0.02	<0.01	<0.02	-	-	<0.03	<0.03	<0.09	104.94
60	<0.06	4.43	0.15	<0.02	<0.02	<0.01	<0.02	-	-	<0.03	<0.03	<0.1	106.22
61	<0.05	<0.03	<0.02	<0.02	<0.02	<0.01	<0.02	-	-	<0.02	<0.03	<0.08	101.07
62	<0.05	14.49	<0.02	<0.02	<0.02	<0.01	<0.02	-	-	<0.02	<0.03	0.09	100.52
63	<0.05	14.18	<0.02	<0.02	<0.02	<0.01	<0.02	-	-	<0.02	<0.03	<0.09	100.44
64	0.06	0.08	0.05	<0.02	<0.02	<0.01	<0.02	-	-	<0.03	<0.03	0.10	100.28
65	<0.05	72.16	<0.03	<0.02	<0.02	<0.01	<0.02	-	-	<0.03	<0.03	<0.09	86.74
66	<0.05	74.49	<0.02	<0.02	<0.02	<0.01	<0.02	-	-	<0.02	<0.03	<0.1	91.46
67	12.32	61.19	0.04	<0.02	<0.02	<0.01	<0.02	-	-	<0.03	<0.03	<0.09	88.50
68	<0.05	70.88	0.94	<0.02	<0.02	<0.01	<0.02	-	-	<0.03	<0.03	<0.09	101.81
69	<0.05	65.28	0.90	<0.02	<0.02	<0.01	<0.02	-	-	<0.03	<0.03	<0.09	100.59
70	0.04	<0.03	<0.02	<0.01	<0.01	<0.01	<0.02	-	-	<0.02	<0.03	<0.08	101.21
71	<0.06	0.08	<0.03	<0.02	<0.02	<0.01	<0.02	-	-	<0.03	<0.03	<0.1	101.59
72	<0.06	0.16	<0.03	<0.02	<0.02	<0.01	<0.02	-	-	<0.03	<0.03	<0.1	103.92
73	<0.05	<0.03	<0.02	<0.01	<0.02	<0.01	<0.01	-	-	<0.02	<0.03	<0.08	100.66
74	0.06	<0.05	0.05	<0.02	<0.02	<0.01	<0.02	-	-	<0.03	<0.03	<0.1	100.97
75	<0.04	<0.03	<0.02	<0.01	<0.01	0.02	<0.02	-	-	<0.02	<0.03	<0.08	101.58
76	<0.05	11.32	<0.02	<0.02	<0.02	<0.01	<0.02	-	-	<0.02	<0.03	<0.09	100.87
77	<0.05	10.20	<0.02	0.02	<0.02	<0.01	<0.02	-	-	<0.02	<0.03	<0.09	100.27
78	0.05	<0.03	<0.02	<0.01	<0.01	<0.01	<0.02	-	-	<0.02	<0.03	<0.08	99.33
79	0.06	0.08	<0.03	<0.02	<0.02	<0.01	<0.02	-	-	<0.03	<0.03	0.11	100.87
80	0.06	70.48	1.33	<0.02	<0.02	<0.01	<0.02	-	-	<0.03	<0.03	<0.09	101.04
81	0.05	69.00	1.27	<0.02	<0.02	<0.01	<0.02	-	-	<0.03	<0.03	<0.09	99.45
82	<0.05	<0.03	<0.02	<0.01	<0.01	<0.01	<0.01	-	-	<0.02	<0.03	0.09	100.32
83	<0.05	0.06	<0.03	<0.02	<0.02	<0.01	<0.02	-	-	<0.03	<0.03	<0.1	99.93
84	<0.05	8.99	<0.02	<0.02	<0.02	<0.01	<0.02	-	-	<0.02	<0.03	<0.09	100.54
85	<0.05	9.37	<0.02	<0.02	<0.02	<0.01	0.02	-	-	<0.02	<0.03	<0.09	100.81
86	<0.05	<0.03	<0.02	<0.02	<0.02	<0.01	<0.02	-	-	<0.02	<0.03	<0.08	100.18
87	0.07	70.18	<0.03	<0.02	0.05	<0.01	<0.02	-	-	<0.03	<0.03	0.10	102.82
88	<0.06	0.16	<0.03	<0.02	0.04	<0.01	<0.02	-	-	<0.03	<0.03	<0.1	97.79
89	<0.05	<0.03	<0.02	<0.02	0.04	<0.01	<0.01	-	-	<0.02	<0.03	<0.08	99.90
90	<0.05	3.22	<0.02	<0.02	<0.01	<0.01	<0.02	-	-	<0.02	<0.03	<0.08	99.50
91	0.06	<0.03	<0.02	<0.02	<0.02	<0.01	0.13	-	-	<0.02	<0.03	0.08	101.05
92	<0.05	3.02	<0.02	<0.02	<0.02	<0.01	<0.02	-	-	<0.02	<0.03	<0.08	100.14
93	<0.04	<0.03	<0.02	<0.02	<0.02	<0.01	<0.02	-	-	<0.02	<0.03	<0.08	100.69
94	0.05	<0.03	<0.02	<0.02	<0.02	<0.01	<0.02	-	-	<0.02	<0.03	<0.08	99.17
95	<0.05	17.96	<0.02	<0.02	<0.02	<0.01	<0.02	-	-	<0.03	<0.03	<0.09	100.76
96	<0.05	11.88	<0.02	<0.02	<0.02	<0.01	<0.02	-	-	<0.02	<0.03	<0.09	99.44
97	<0.05	17.70	<0.02	<0.02	<0.02	<0.01	<0.02	-	-	<0.03	<0.03	<0.09	100.52
98	<0.05	17.73	<0.02	<0.02	<0.02	<0.01	<0.02	-	-	<0.03	<0.03	0.11	100.76
99	0.05	<0.04	<0.02	<0.02	<0.02	<0.01	<0.02	-	-	<0.02	<0.03	<0.08	100.04
100	<0.04	<0.03	<0.02	<0.02	<0.02	<0.01	<0.02	-	-	<0.02	<0.03	<0.08	99.04
101	<0.05	0.16	0.06	0.03	<0.02	<0.02	<0.03	-	-	<0.03	<0.03	<0.1	100.22
102	<0.05	<0.04	<0.02	<0.02	<0.02	<0.01	<0.02	-	-	<0.02	<0.03	<0.08	100.33
103	<0.05	<0.04	<0.02	<0.02	0.02	<0.01	<0.02	-	-	<0.02	<0.03	<0.08	100.45
104	<0.05	<0.04	<0.02	<0.02	<0.02	<0.01	<0.02	-	-	<0.02	<0.03	<0.08	100.33
105	<0.05	<0.04	<0.02	<0.02	<0.02	0.01	<0.02	-	-	<0.02	<0.03	<0.08	101.49
106	<0.05	<0.03	<0.02	<0.02	<0.02	<0.01	<0.02	-	-	<0.02	<0.03	<0.08	100.06

Table C.1 Continued.

Sample	Analysis Number	Area	Mineral	Note	S wt %	Fe wt %	Cu wt %	Zn wt %	Pb wt %	As wt %	Sb wt %	Cd wt %	Se wt %
BM14-027	107	WBA	sp	A	33.55	0.68	0.22	66.35	<0.03	<0.02	<0.02	0.31	<0.02
BM14-027	108	WBA	py	A	54.07	46.14	0.05	0.88	<0.03	<0.02	<0.02	<0.03	<0.01
BM14-027	109	WBA	gn	A	13.40	0.05	0.07	<0.02	86.26	<0.02	<0.03	<0.06	<0.02
BM14-027	110	WBA	gn	A	13.43	0.41	0.66	<0.02	86.71	0.02	<0.03	<0.06	<0.02
BM14-027	111	WBA	gn	A	13.37	<0.02	<0.02	<0.02	86.32	<0.02	0.07	<0.06	0.02
BM14-027	112	WBA	gn	A	13.36	<0.02	<0.02	0.05	86.01	<0.02	0.03	<0.06	0.03
BM14-027	113	WBA	sp	A	33.50	0.34	<0.02	65.02	0.04	<0.03	<0.02	0.31	<0.02
BM14-027	114	WBA	cpy	A	35.21	29.97	33.95	0.08	<0.03	<0.02	<0.02	<0.03	<0.02
BM14-027	115	WBA	sp	A	33.62	0.39	<0.01	66.77	<0.03	<0.03	<0.02	0.34	<0.02
BM14-027	116	WBA	sp	A	34.04	0.44	0.06	66.86	<0.03	<0.02	<0.02	0.32	<0.02
BM14-035	117*	WBA	el	A	0.00	0.61	1.18	0.00	<0.05	<0.03	<0.04	<0.06	<0.03
BM14-035	118*	WBA	el	A	0.00	<0.02	<0.02	0.00	0.07	<0.03	<0.04	<0.06	<0.03
BM14-035	119	WBA	tn	A	27.79	1.57	41.54	6.80	<0.03	17.63	2.74	0.06	<0.03
BM14-035	120	WBA	tn	A	27.93	1.55	41.41	6.77	<0.03	17.38	2.89	0.10	<0.02
BM14-035	121	WBA	tn	A	27.92	1.60	41.58	6.81	<0.03	17.43	2.84	0.08	<0.02
BM14-035	122	WBA	sp	A	32.92	0.12	0.05	66.67	<0.03	<0.02	<0.02	0.25	<0.02
BM14-035	123	WBA	sp	A	32.97	0.15	0.04	66.76	<0.03	<0.02	<0.02	0.30	<0.02
BM14-035	124	WBA	sp	A	32.82	0.12	0.15	66.60	<0.03	0.02	<0.02	0.27	<0.02
BM14-035	125	WBA	tn	A	27.80	1.38	40.07	7.28	<0.03	15.91	4.88	0.09	<0.02
BM14-035	126	WBA	tn	A	27.63	1.37	40.14	7.11	<0.03	15.72	5.33	0.08	<0.02
BM14-035	127	WBA	tn	A	27.56	1.49	39.90	7.08	<0.03	15.41	5.40	0.06	<0.02
BM14-035	128	WBA	sp	A	32.90	0.36	0.56	65.67	<0.03	<0.02	<0.02	0.30	<0.02
BM14-035	129	WBA	sp	A	33.15	0.13	0.54	66.11	<0.03	<0.02	<0.02	0.24	<0.02
BM14-035	130	WBA	sp	A	33.32	0.13	0.31	66.15	<0.03	<0.02	<0.02	0.21	<0.02
BM14-053	131	RZN	tn	A	28.18	1.48	41.91	7.06	<0.03	18.45	1.13	0.08	<0.02
BM14-053	132	RZN	tn	A	28.14	1.39	42.00	7.30	0.04	18.38	1.34	0.07	<0.03
BM14-053	133	RZN	tn	A	28.06	1.39	42.07	7.09	0.05	18.66	0.93	0.06	<0.03
BM14-053	134	RZN	gn	A	13.35	<0.02	0.12	0.16	86.27	<0.02	<0.03	<0.06	0.02
BM14-053	135	RZN	gn	A	13.44	0.06	0.32	0.38	87.09	<0.02	<0.03	<0.05	0.03
BM14-053	136	RZN	sp	A	33.20	0.13	0.03	66.14	<0.03	<0.02	<0.02	0.27	<0.02
BM14-053	137	RZN	sp	A	33.18	0.06	<0.02	66.66	0.03	<0.02	<0.02	0.29	<0.02
BM14-053	138	RZN	sp	A	33.08	0.07	<0.02	66.70	<0.03	<0.02	<0.02	0.28	<0.02
BM14-053	139	RZN	sp	A	32.97	0.13	0.10	66.11	<0.03	<0.02	<0.02	0.32	<0.02
BM14-053	140	RZN	sp	A	33.10	0.17	0.19	66.41	<0.03	<0.02	<0.02	0.30	<0.02
BM14-053	141	RZN	tn	A	28.19	1.34	41.81	8.03	<0.03	18.44	1.15	0.11	<0.03
BM14-053	142	RZN	tn	A	27.71	1.17	41.24	7.86	<0.03	16.39	4.40	0.05	<0.02
BM14-053	143	RZN	tn	A	28.12	1.36	41.94	7.67	<0.03	18.70	1.02	0.10	<0.03
BM14-053	144	RZN	sp	A	33.01	0.10	0.18	66.29	<0.03	<0.02	<0.02	0.29	<0.02
BM14-053	145	RZN	tn	A	27.80	1.29	41.82	7.19	<0.03	18.60	1.19	0.07	0.02
BM15-099	146	RZN	el	A	0.00	0.27	0.22	0.00	0.07	0.03	<0.03	<0.05	<0.02
BM15-099	147	RZN	hs	A	0.00	0.03	1.37	0.00	<0.03	0.06	<0.03	<0.04	0.05
BM15-099	148	RZN	hs	A	1.08	1.08	1.45	0.24	<0.03	0.15	<0.03	0.04	0.09
BM15-099	149	RZN	hs	R	6.72	0.28	10.02	1.83	0.18	5.86	0.79	0.07	0.05
BM15-099	150	RZN	tn	A	27.90	0.88	41.38	7.51	<0.03	16.92	3.51	0.08	<0.02
BM15-099	151	RZN	tn	A	27.79	0.87	41.30	7.48	<0.03	16.87	3.76	0.07	<0.02
BM15-099	152	RZN	tn	A	27.90	0.87	41.33	7.46	<0.03	16.95	3.66	0.07	<0.02
BM15-099	153	RZN	sp	A	33.08	0.09	0.05	66.60	<0.03	<0.02	<0.02	0.23	<0.02
BM15-099	154	RZN	sp	A	33.10	0.13	0.05	66.56	<0.03	<0.02	<0.02	0.22	<0.02
BM15-099	155	RZN	sp	A	33.19	0.13	0.12	66.68	<0.03	<0.02	<0.02	0.23	<0.02
BM15-099	156	RZN	tn	A	27.82	0.81	41.20	7.88	<0.03	16.38	4.47	0.11	<0.02
BM15-099	157	RZN	tn	A	27.92	0.79	41.49	7.71	<0.03	16.20	4.59	0.09	<0.03
BM15-099	158	RZN	tn	A	27.82	0.80	41.55	7.65	<0.03	16.26	4.44	0.09	<0.02
BM14-057	159	RZN	hs	A	0.00	<0.02	<0.02	0.00	<0.03	<0.03	<0.03	<0.04	<0.02

Table C.1 Continued.

Analysis Number	Au wt %	Ag wt %	Te wt %	V wt %	Mn wt %	Co wt %	Ni wt %	Ge wt %	In wt %	Sn wt %	Hg wt %	Bi wt %	Total wt %
107	<0.05	<0.04	<0.02	<0.02	<0.02	<0.01	<0.02	-	-	<0.02	<0.03	<0.08	101.11
108	<0.04	<0.03	<0.02	<0.02	<0.02	0.06	0.07	-	-	<0.02	<0.03	<0.08	101.27
109	0.08	0.19	<0.03	<0.03	0.03	<0.02	<0.02	-	-	<0.03	<0.03	<0.1	100.09
110	<0.06	0.18	0.05	0.03	0.05	<0.02	<0.03	-	-	<0.03	<0.03	<0.1	101.55
111	<0.05	<0.06	0.05	0.04	<0.02	<0.02	<0.02	-	-	<0.03	<0.03	0.10	99.96
112	<0.05	0.13	0.04	<0.02	<0.02	<0.02	<0.03	-	-	<0.03	<0.03	<0.1	99.65
113	<0.05	<0.03	<0.02	<0.02	<0.02	<0.01	<0.02	-	-	<0.02	<0.03	<0.08	99.21
114	<0.05	<0.03	<0.02	<0.02	<0.02	<0.01	<0.02	-	-	<0.02	<0.03	<0.08	99.22
115	<0.05	<0.04	<0.02	0.02	<0.02	<0.01	<0.02	-	-	<0.02	<0.03	<0.08	101.13
116	<0.05	<0.04	<0.02	<0.02	<0.02	<0.01	<0.01	-	-	<0.02	<0.03	<0.08	101.72
117	66.25	33.30	0.05	<0.02	<0.02	<0.02	<0.02	0.10	<0.03	<0.04	<0.05	<0.15	101.49
118	64.18	37.45	0.04	<0.02	<0.02	<0.02	<0.02	0.11	<0.03	<0.04	<0.05	<0.14	101.85
119	<0.06	1.54	<0.02	<0.01	<0.01	<0.01	<0.01	<0.02	<0.02	<0.02	<0.03	<0.1	99.65
120	<0.06	1.55	<0.02	<0.01	<0.01	<0.01	<0.01	<0.02	<0.02	<0.02	<0.03	<0.1	99.57
121	<0.06	1.53	<0.02	<0.01	<0.01	<0.01	<0.01	<0.02	<0.02	<0.02	<0.03	<0.1	99.78
122	<0.06	<0.03	<0.02	<0.01	<0.01	<0.01	<0.01	<0.02	<0.02	<0.02	<0.03	<0.1	100.01
123	<0.06	<0.03	<0.02	<0.01	<0.01	<0.01	<0.01	<0.02	<0.02	<0.02	<0.03	<0.1	100.22
124	<0.06	<0.03	<0.02	<0.01	<0.01	<0.01	<0.01	<0.02	<0.02	<0.02	<0.03	<0.1	99.98
125	<0.06	2.39	<0.02	<0.01	<0.01	<0.01	<0.01	<0.02	<0.02	<0.02	<0.03	<0.1	99.78
126	<0.06	2.46	<0.02	<0.01	<0.01	<0.01	<0.01	<0.02	<0.02	<0.02	<0.03	<0.1	99.83
127	<0.06	2.42	<0.02	<0.01	<0.01	<0.01	<0.01	<0.02	<0.02	<0.02	<0.03	<0.1	99.33
128	<0.06	<0.03	<0.02	<0.01	<0.01	<0.01	<0.01	<0.02	<0.02	<0.02	<0.03	<0.1	99.79
129	<0.05	<0.03	<0.02	<0.01	<0.01	<0.01	<0.01	<0.02	<0.02	<0.02	<0.03	0.10	100.27
130	<0.06	<0.03	<0.02	<0.01	<0.01	<0.01	<0.01	<0.02	<0.02	<0.02	<0.03	<0.1	100.13
131	<0.06	0.73	<0.02	<0.01	<0.01	<0.01	<0.01	<0.02	<0.02	<0.02	<0.03	<0.1	99.02
132	<0.06	0.75	<0.02	<0.01	<0.01	<0.01	<0.01	<0.02	<0.02	<0.02	<0.03	<0.1	99.40
133	<0.06	0.71	<0.02	<0.01	<0.01	<0.01	<0.01	<0.02	<0.02	<0.02	<0.03	<0.1	99.00
134	<0.07	<0.05	0.04	<0.02	<0.01	<0.01	<0.02	<0.03	<0.03	<0.03	<0.03	<0.12	99.95
135	<0.07	<0.05	0.06	<0.02	<0.01	<0.01	<0.02	<0.03	<0.03	<0.03	<0.03	<0.12	101.38
136	<0.06	<0.03	<0.02	<0.01	<0.01	<0.01	<0.01	<0.02	<0.02	<0.02	<0.03	<0.1	99.77
137	<0.06	<0.03	<0.02	<0.01	<0.01	<0.01	<0.01	<0.02	<0.02	<0.02	<0.03	<0.1	100.22
138	<0.06	<0.03	<0.02	<0.01	0.01	<0.01	<0.01	<0.02	<0.02	<0.02	<0.03	<0.1	100.15
139	<0.05	<0.03	<0.02	<0.01	0.01	<0.01	<0.01	<0.02	<0.02	<0.02	<0.03	<0.1	99.65
140	<0.06	<0.03	<0.02	<0.01	<0.01	<0.01	<0.01	<0.02	<0.02	<0.02	<0.03	<0.1	100.16
141	<0.06	0.81	<0.02	<0.01	<0.01	0.01	<0.01	<0.02	<0.02	<0.02	<0.03	<0.1	99.90
142	<0.06	1.14	<0.02	<0.01	<0.01	<0.01	<0.01	<0.02	<0.02	<0.02	<0.03	<0.1	99.97
143	<0.06	0.88	<0.02	<0.01	<0.01	<0.01	<0.01	<0.02	<0.02	<0.02	<0.03	<0.1	99.80
144	<0.05	<0.03	<0.02	<0.01	<0.01	<0.01	<0.01	<0.02	<0.02	<0.02	<0.03	<0.1	99.87
145	<0.06	0.88	<0.02	<0.01	<0.01	<0.01	<0.01	<0.02	<0.02	<0.02	<0.03	<0.1	98.87
146	73.84	28.23	<0.03	<0.02	<0.01	<0.01	<0.02	0.09	<0.03	<0.03	<0.04	<0.12	102.75
147	<0.06	65.12	34.38	<0.02	<0.01	<0.01	<0.02	<0.03	<0.02	<0.03	<0.03	<0.11	101.00
148	0.08	63.03	35.63	<0.02	<0.01	<0.01	<0.02	<0.03	<0.02	<0.02	<0.03	<0.11	102.88
149	<0.06	49.30	26.06	<0.01	<0.01	<0.01	<0.02	<0.03	<0.02	<0.02	<0.03	<0.11	101.15
150	<0.06	1.26	0.03	<0.01	<0.01	<0.01	<0.01	<0.02	<0.02	<0.02	<0.03	<0.1	99.47
151	<0.06	1.23	0.03	<0.01	<0.01	0.01	<0.01	<0.02	<0.02	<0.02	<0.03	<0.1	99.42
152	<0.06	1.24	0.04	<0.01	<0.01	<0.01	<0.01	<0.02	<0.02	<0.02	<0.03	<0.1	99.52
153	<0.06	<0.03	<0.02	<0.01	<0.01	<0.01	<0.01	<0.02	<0.02	<0.02	<0.03	<0.1	100.05
154	<0.06	<0.03	<0.02	<0.01	<0.01	<0.01	<0.01	<0.02	<0.02	<0.02	<0.03	<0.1	100.05
155	<0.06	<0.03	<0.02	<0.01	<0.01	<0.01	<0.01	<0.02	<0.02	<0.02	<0.03	<0.1	100.35
156	<0.06	1.28	0.03	<0.01	<0.01	<0.01	<0.01	<0.02	<0.02	<0.02	<0.03	<0.1	99.98
157	<0.06	1.26	0.02	<0.01	<0.01	<0.01	<0.01	<0.02	<0.02	<0.02	<0.03	<0.1	100.08
158	<0.06	1.25	0.06	<0.01	<0.01	<0.01	<0.01	<0.02	<0.02	<0.02	<0.03	<0.1	99.91
159	<0.06	62.75	37.85	<0.02	<0.01	<0.01	<0.02	<0.03	<0.02	<0.02	<0.03	<0.11	100.60

Table C.1 Continued.

Sample	Analysis Number	Area	Mineral	Note	S wt %	Fe wt %	Cu wt %	Zn wt %	Pb wt %	As wt %	Sb wt %	Cd wt %	Se wt %
BM14-057	160	RZN	strom	R	20.81	0.38	1.88	0.12	<0.03	<0.02	<0.02	<0.04	0.23
BM14-057	161	RZN	tn	A	27.70	1.32	41.28	6.98	<0.03	15.63	5.48	0.07	<0.02
BM14-057	162	RZN	tn	A	27.69	1.29	41.17	6.98	<0.03	15.71	5.51	0.06	<0.02
BM14-057	163	RZN	tn	A	27.64	1.36	41.16	7.01	<0.03	15.81	5.44	0.10	<0.02
BM14-057	164	RZN	sp	A	33.33	0.10	0.09	66.56	<0.03	<0.02	<0.02	0.27	<0.02
BM14-057	165	RZN	sp	A	33.15	0.10	0.02	66.61	<0.03	<0.02	<0.02	0.32	<0.02
BM14-057	166	RZN	sp	A	33.14	0.41	0.45	65.82	<0.03	<0.02	<0.02	0.30	<0.02
BM14-057	167	RZN	tn	A	27.63	1.28	41.33	7.08	<0.03	15.48	5.74	0.12	<0.02
BM14-057	168	RZN	tn	A	27.51	1.26	41.29	7.06	<0.03	15.09	6.12	0.12	<0.02
BM14-057	169	RZN	tn	A	27.42	1.29	41.23	7.00	<0.03	15.18	6.04	0.08	<0.02
BM14-057	170	RZN	tn	A	27.49	1.54	41.08	6.79	<0.03	15.59	5.50	0.11	<0.02
BM14-057	171	RZN	tn	A	27.57	1.43	41.15	6.83	<0.03	15.64	5.53	0.05	<0.02
BM14-057	172	RZN	tn	A	27.46	1.49	41.14	6.78	<0.03	15.48	5.64	0.10	<0.02
BM14-057	173	RZN	sp	A	32.90	0.09	<0.01	66.36	<0.03	<0.02	<0.02	0.30	<0.02
BM14-057	174	RZN	sp	A	32.95	0.11	<0.01	66.55	<0.03	<0.02	<0.02	0.27	<0.02
BM14-057	175	RZN	sp	A	32.94	0.09	<0.02	66.71	<0.03	<0.02	<0.02	0.29	<0.02
BM15-096	176	RZN	tn	A	27.89	1.00	42.73	7.51	<0.03	18.85	0.61	0.12	0.03
BM15-096	177	RZN	tn	A	28.28	1.10	42.82	7.66	<0.03	18.67	0.63	0.10	<0.03
BM15-096	178	RZN	tn	A	28.16	1.02	42.73	7.48	<0.03	18.51	0.91	0.14	<0.03
BM15-096	179	RZN	tn	A	28.18	1.13	42.79	7.40	<0.03	18.78	0.62	0.10	<0.03
BM15-096	180	RZN	tn	A	28.10	1.13	43.01	7.44	<0.03	18.68	0.75	0.11	<0.03
BM15-096	181	RZN	tn	A	28.04	1.10	42.76	7.50	<0.03	18.68	0.72	0.11	<0.03
BM15-096	182	RZN	sp	A	32.74	0.11	0.07	66.13	<0.03	<0.02	<0.02	0.32	<0.02
BM15-096	183	RZN	sp	A	32.81	0.09	0.04	66.13	<0.03	<0.02	<0.02	0.34	<0.02
BM15-096	184	RZN	sp	A	32.82	0.08	0.04	66.35	<0.03	<0.02	<0.02	0.31	<0.02
BM15-096	185	RZN	tn	A	28.07	1.03	42.53	7.42	<0.03	18.63	0.59	0.07	0.03
BM15-096	186	RZN	tn	A	28.13	1.00	41.73	7.33	<0.03	18.74	0.54	0.08	<0.02
BM15-096	187	RZN	hs	R	14.95	0.04	0.07	37.44	<0.03	<0.03	<0.02	0.13	<0.02
BM15-096	188	RZN	tn	A	28.16	1.01	42.86	7.49	<0.03	19.03	0.48	0.09	<0.03
BM15-096	189	RZN	tn	A	28.09	1.01	42.81	7.49	<0.03	18.96	0.50	0.11	<0.02
BM15-096	190	RZN	tn	A	28.19	0.99	42.91	7.58	<0.03	19.13	0.41	0.08	<0.02
BM14-026	191	WBA	tn	A	27.38	3.68	40.55	4.82	<0.03	16.43	4.07	<0.03	<0.02
BM14-026	192	WBA	tn	A	27.57	3.66	40.70	4.48	<0.03	16.46	4.17	0.04	<0.02
BM14-026	193	WBA	tn	A	27.53	3.64	40.58	4.52	<0.03	16.35	4.22	0.04	<0.02
BM14-026	194	WBA	sp	A	32.77	0.55	<0.01	65.94	<0.03	<0.02	<0.02	0.34	<0.02
BM14-026	195	WBA	sp	A	32.79	0.56	<0.01	65.85	<0.03	<0.02	<0.02	0.36	<0.02
BM14-026	196	WBA	sp	A	32.82	0.57	0.02	65.93	0.03	<0.02	<0.02	0.33	<0.02
BM14-026	197	WBA	tn	A	27.52	3.65	40.70	4.31	<0.03	16.27	4.47	0.07	<0.02
BM14-026	198	WBA	tn	A	27.60	3.75	40.71	4.53	<0.03	16.34	4.15	0.05	<0.02
BM14-026	199	WBA	tn	A	27.42	4.32	39.70	3.85	<0.03	16.31	4.02	0.06	<0.02
BM14-026	200	WBA	tn	A	27.59	4.28	39.77	4.89	<0.03	16.57	4.06	0.04	<0.02
BM14-026	201	WBA	tn	A	27.53	3.99	40.43	4.01	<0.03	16.31	4.17	0.04	<0.02
BM14-026	202	WBA	sp	A	32.71	0.63	0.05	65.99	<0.03	<0.02	<0.02	0.31	<0.02
BM14-026	203	WBA	sp	A	32.79	0.60	0.04	65.95	<0.03	<0.02	<0.02	0.28	<0.02
BM14-026	204	WBA	sp	A	32.81	0.65	0.06	66.00	<0.03	<0.02	<0.02	0.33	<0.02

Analysis Number – refers to spot number on BSE images; red = rejected analysis, black or white = accepted analysis
Area – RZN, Ridge Zone North; WBA, West Block Area
Mineral – ac; acanthite; aspy, arsenopyrite; cpy, chalcopyrite; el, electrum; gn; galena; hs, hessite; pr-pb, pearceite-polybasite; py, pyrite; sp, sphalerite; strom, stromeyerite; td, tetrahedrite; tn, tennantite
Note – R, rejected analysis; A, accepted analysis
*no BSE image

Table C.1 Continued.

Analysis Number	Au wt %	Ag wt %	Te wt %	V wt %	Mn wt %	Co wt %	Ni wt %	Ge wt %	In wt %	Sn wt %	Hg wt %	Bi wt %	Total wt %
160	0.08	66.61	0.17	0.05	<0.01	<0.01	<0.02	9.31	<0.02	0.02	<0.03	<0.11	99.66
161	<0.06	1.21	0.18	0.01	0.01	<0.01	<0.01	<0.02	<0.02	<0.02	<0.03	<0.1	99.87
162	<0.06	1.17	0.17	<0.01	<0.01	<0.01	<0.01	<0.02	<0.02	<0.02	<0.03	<0.1	99.75
163	<0.06	1.05	0.17	<0.01	<0.01	<0.01	<0.01	<0.02	<0.02	<0.02	<0.03	<0.1	99.75
164	<0.06	<0.03	<0.02	<0.01	<0.01	<0.01	<0.01	<0.02	0.02	<0.02	<0.03	<0.1	100.38
165	<0.06	<0.03	<0.02	<0.01	0.01	<0.01	<0.01	<0.02	<0.02	<0.02	<0.03	<0.1	100.21
166	<0.05	<0.03	<0.02	<0.01	<0.01	<0.01	<0.01	<0.02	<0.02	<0.02	<0.03	<0.1	100.11
167	<0.06	1.08	0.18	<0.01	<0.01	<0.01	<0.01	<0.02	<0.02	<0.02	<0.03	<0.1	99.92
168	<0.06	1.18	0.17	<0.01	<0.01	<0.01	<0.01	<0.02	<0.02	<0.02	<0.03	<0.1	99.79
169	<0.06	1.19	0.17	<0.01	<0.01	<0.01	<0.01	<0.02	<0.02	<0.02	<0.03	<0.1	99.59
170	<0.06	1.23	0.16	<0.01	<0.01	<0.01	<0.01	<0.02	<0.02	<0.02	<0.03	<0.1	99.50
171	<0.06	1.16	0.18	<0.01	<0.01	<0.01	<0.01	<0.02	<0.02	<0.02	<0.03	<0.1	99.54
172	<0.06	1.21	0.17	<0.01	<0.01	<0.01	<0.01	<0.02	<0.02	<0.02	<0.03	<0.1	99.46
173	<0.06	<0.03	<0.02	<0.01	0.01	<0.01	<0.01	<0.02	<0.02	<0.02	<0.03	0.11	99.77
174	<0.06	<0.03	<0.02	<0.01	<0.01	<0.01	<0.01	<0.02	<0.02	<0.02	<0.03	<0.1	99.87
175	<0.06	<0.03	<0.02	<0.01	0.01	<0.01	<0.01	<0.02	<0.02	<0.02	<0.03	<0.1	100.05
176	<0.06	0.20	0.20	<0.01	<0.01	<0.01	<0.01	<0.02	<0.02	<0.02	<0.03	<0.1	99.14
177	<0.06	0.15	0.18	<0.01	<0.01	<0.01	<0.01	<0.02	<0.02	<0.02	<0.03	<0.1	99.58
178	<0.06	0.21	0.38	<0.01	<0.01	<0.01	<0.01	<0.02	<0.02	<0.02	<0.03	<0.1	99.54
179	<0.06	0.18	0.24	<0.01	<0.01	0.01	<0.01	<0.02	<0.02	<0.02	<0.03	<0.1	99.42
180	<0.06	0.17	0.27	<0.01	<0.01	<0.01	<0.01	<0.02	<0.02	<0.02	<0.03	<0.1	99.66
181	<0.06	0.15	0.31	<0.01	<0.01	<0.01	<0.01	<0.02	<0.02	<0.02	<0.03	<0.1	99.37
182	<0.05	<0.03	<0.02	<0.01	<0.01	<0.01	<0.01	<0.02	<0.02	<0.02	<0.03	<0.1	99.36
183	<0.06	<0.03	<0.02	<0.01	<0.01	<0.01	<0.01	<0.02	<0.02	<0.02	<0.03	<0.1	99.41
184	<0.05	<0.03	<0.02	<0.01	<0.01	<0.01	<0.01	<0.02	<0.02	<0.02	<0.03	<0.1	99.60
185	<0.06	0.13	0.19	<0.01	<0.01	<0.01	<0.01	<0.02	<0.02	<0.02	<0.03	<0.1	98.70
186	<0.06	0.17	0.14	<0.01	<0.01	<0.01	<0.01	<0.02	<0.02	<0.02	<0.03	<0.1	97.87
187	<0.06	34.30	13.60	<0.01	<0.01	<0.01	0.01	<0.03	<0.02	<0.02	<0.03	<0.1	100.56
188	<0.06	0.14	0.07	<0.01	0.01	<0.01	<0.01	<0.02	<0.02	<0.02	<0.03	<0.1	99.35
189	<0.06	0.16	0.08	<0.01	<0.01	<0.01	<0.01	<0.02	<0.02	<0.02	<0.03	<0.1	99.22
190	<0.06	0.16	0.06	<0.01	<0.01	<0.01	<0.01	<0.02	<0.02	<0.02	<0.03	<0.1	99.50
191	<0.06	2.30	0.06	<0.01	<0.01	<0.01	<0.01	<0.02	<0.02	<0.02	<0.03	<0.1	99.29
192	<0.06	2.22	0.05	<0.01	<0.01	<0.01	<0.01	<0.02	<0.02	<0.02	<0.03	<0.1	99.36
193	<0.06	2.27	0.09	<0.01	<0.01	<0.01	<0.01	<0.02	<0.02	<0.02	<0.03	<0.1	99.22
194	<0.05	<0.03	<0.02	<0.01	0.02	<0.01	<0.01	<0.02	<0.02	<0.02	<0.03	<0.1	99.62
195	<0.05	<0.03	<0.02	<0.01	<0.01	<0.01	<0.01	<0.02	<0.02	<0.02	<0.03	<0.1	99.57
196	<0.05	<0.03	<0.02	<0.01	0.01	<0.01	<0.01	<0.02	<0.02	<0.02	<0.03	0.10	99.80
197	<0.06	2.26	0.02	<0.01	<0.01	<0.01	<0.01	<0.02	<0.02	<0.02	<0.03	<0.1	99.27
198	<0.06	2.09	<0.02	<0.01	<0.01	<0.01	<0.01	<0.02	<0.02	<0.02	<0.03	<0.1	99.21
199	<0.06	3.32	<0.02	<0.01	<0.01	0.01	<0.01	<0.02	<0.02	<0.02	<0.03	<0.1	99.03
200	<0.06	2.65	0.07	<0.01	<0.01	<0.01	<0.01	<0.02	<0.02	<0.02	<0.03	<0.1	99.92
201	<0.06	2.63	0.09	<0.01	<0.01	<0.01	<0.01	<0.02	<0.02	<0.02	<0.03	<0.1	99.21
202	<0.06	<0.03	<0.02	<0.01	0.01	<0.01	<0.01	<0.02	<0.02	<0.02	<0.03	<0.1	99.69
203	<0.06	<0.03	<0.02	<0.01	0.02	<0.01	<0.01	<0.02	<0.02	<0.02	<0.03	<0.1	99.67
204	<0.05	<0.03	<0.02	<0.01	<0.01	<0.01	0.01	<0.02	<0.02	<0.02	<0.03	<0.1	99.86

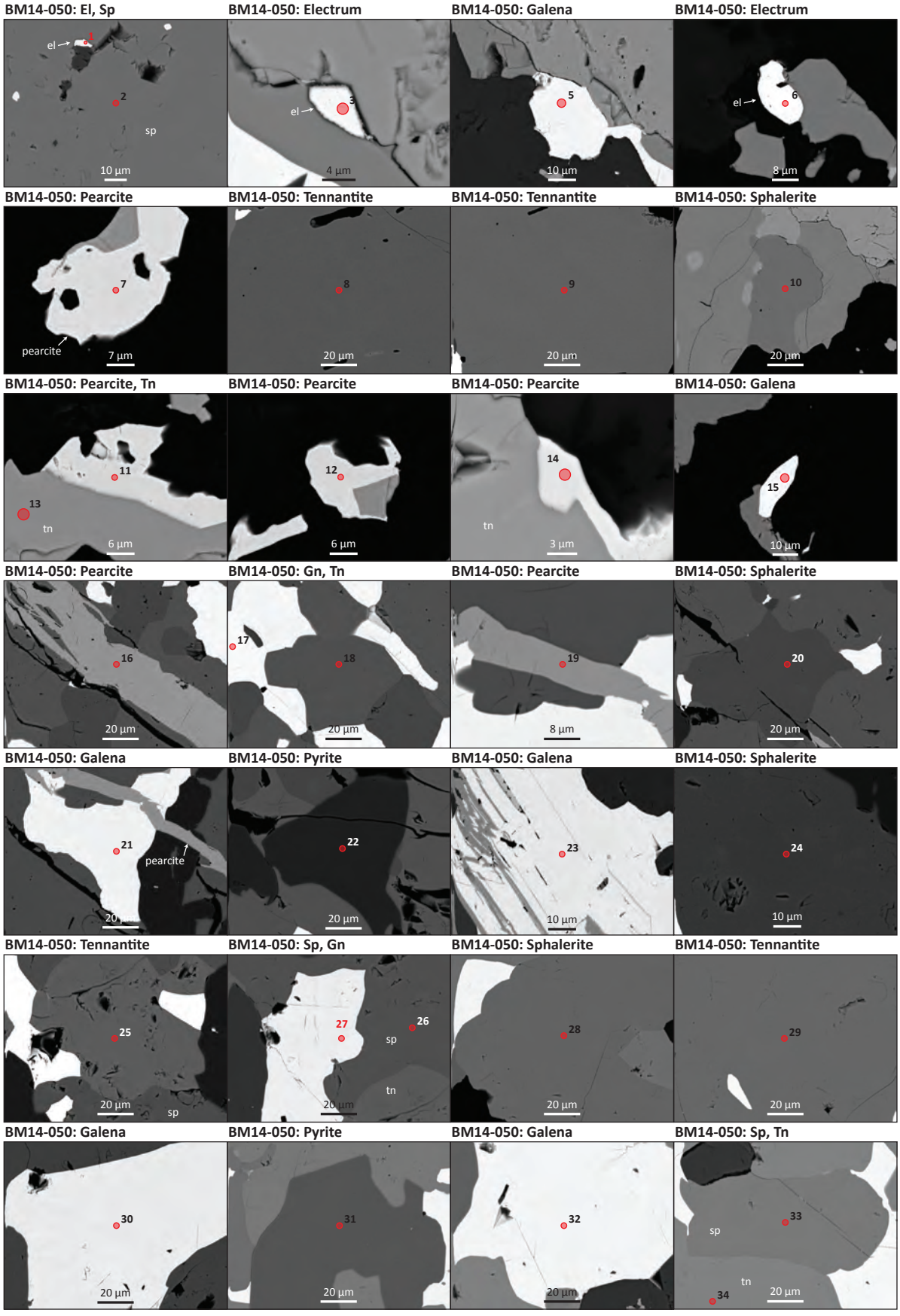

Figure C.1 Summary of electron microprobe analysis numbers 1-34.

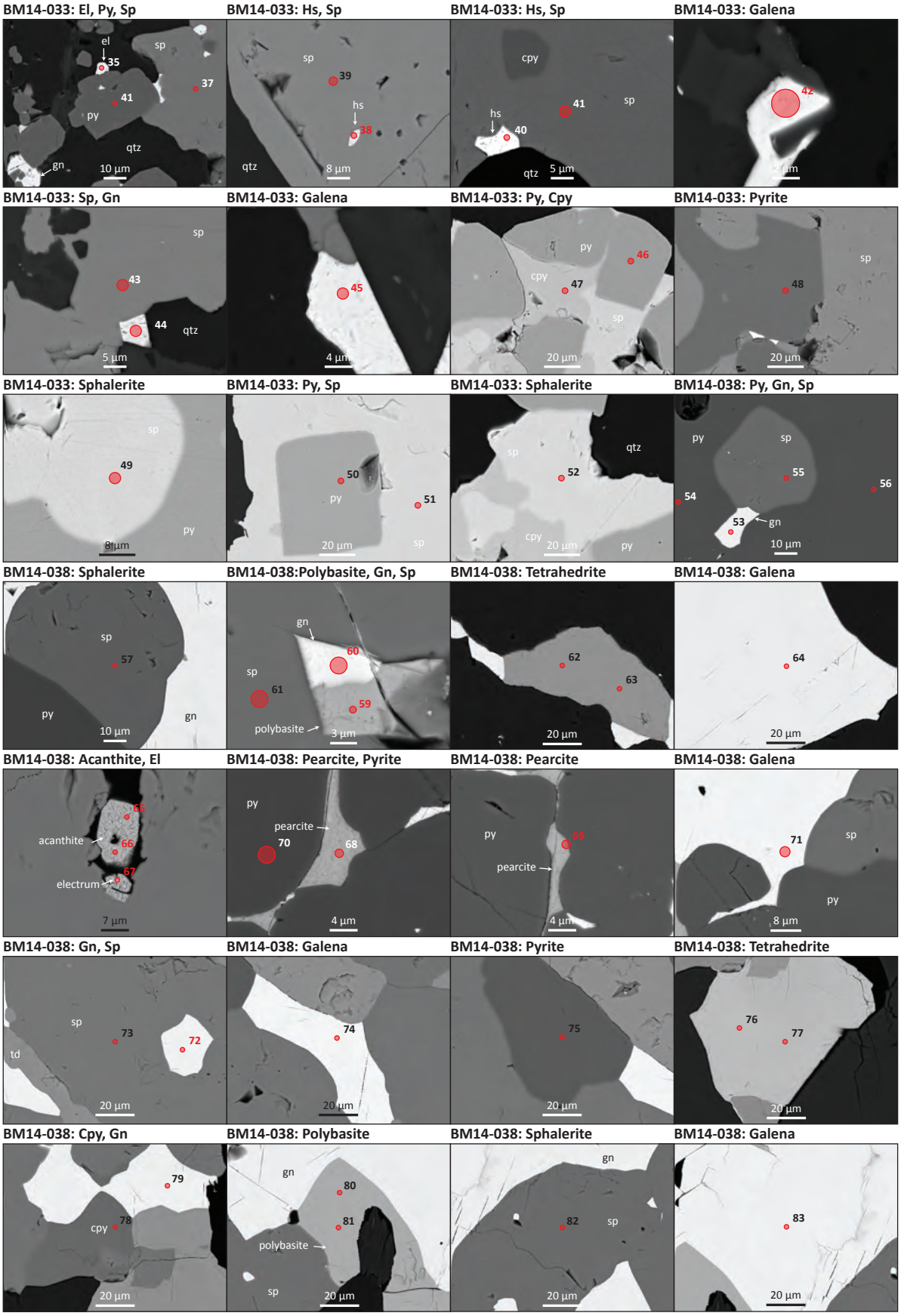

Figure C.2 Summary of electron microprobe analysis numbers 35-83.

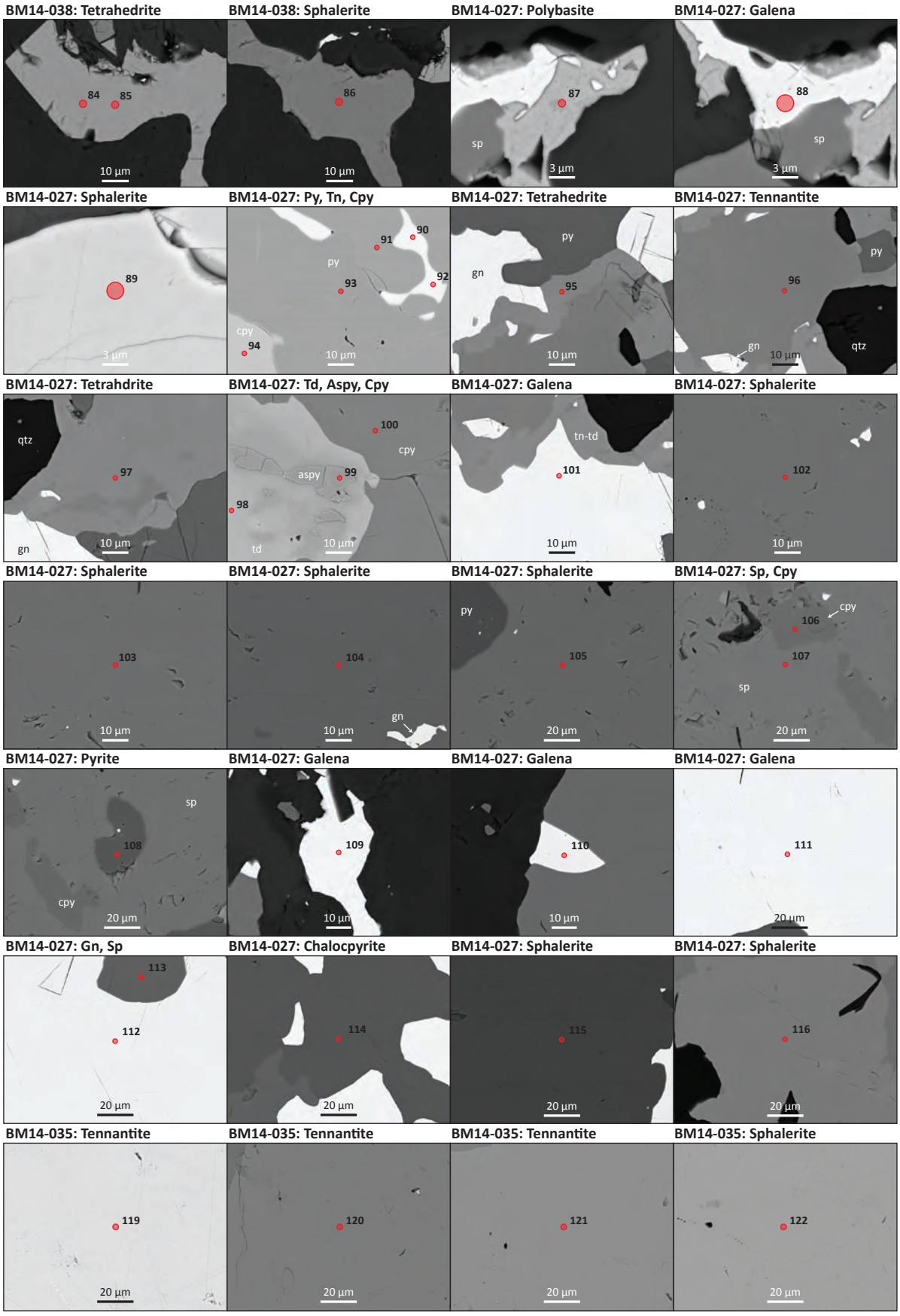

Figure C.3 Summary of electron microprobe analysis numbers 84-122.

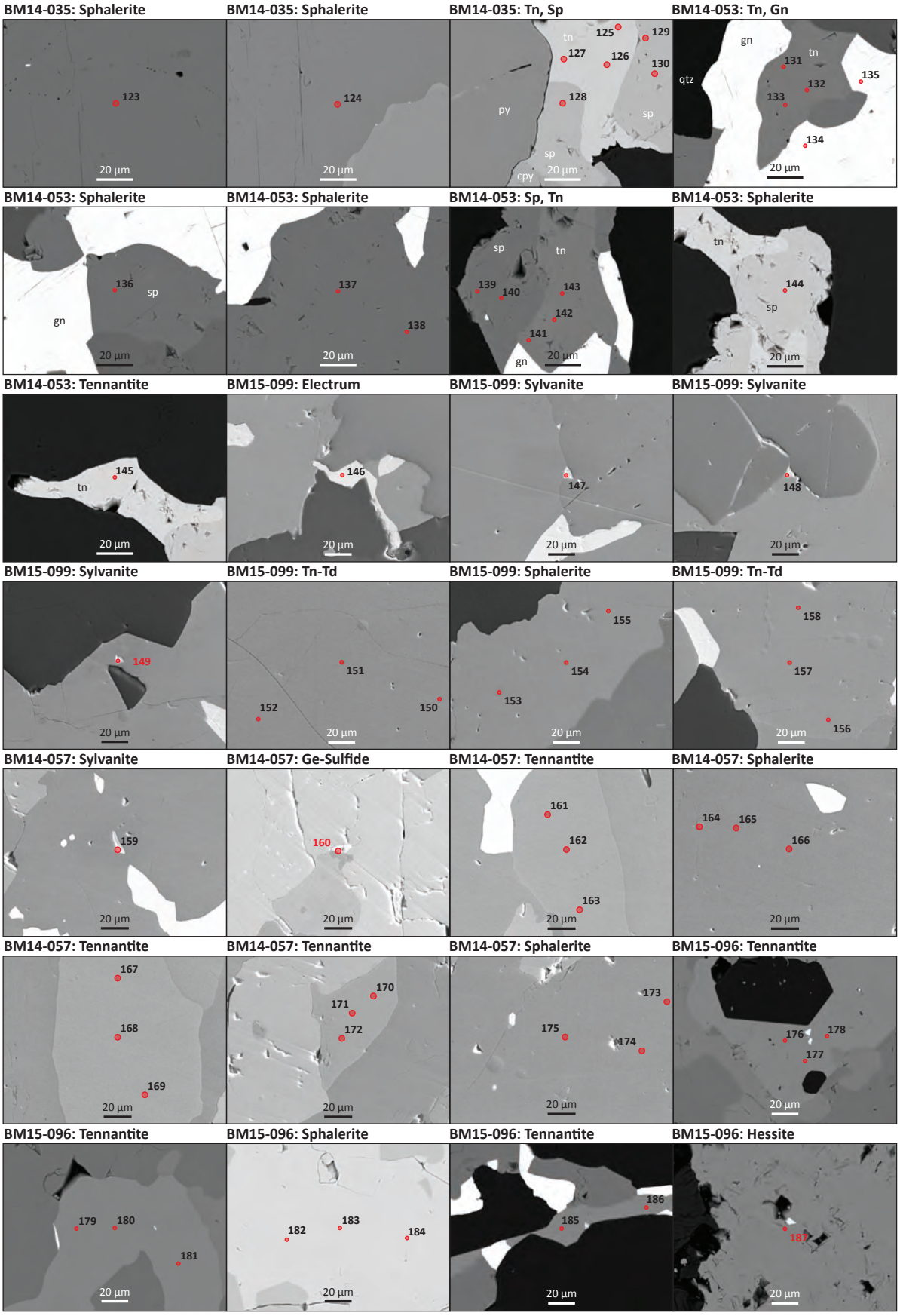

Figure C.4 Summary of electron microprobe analysis numbers 123-187.

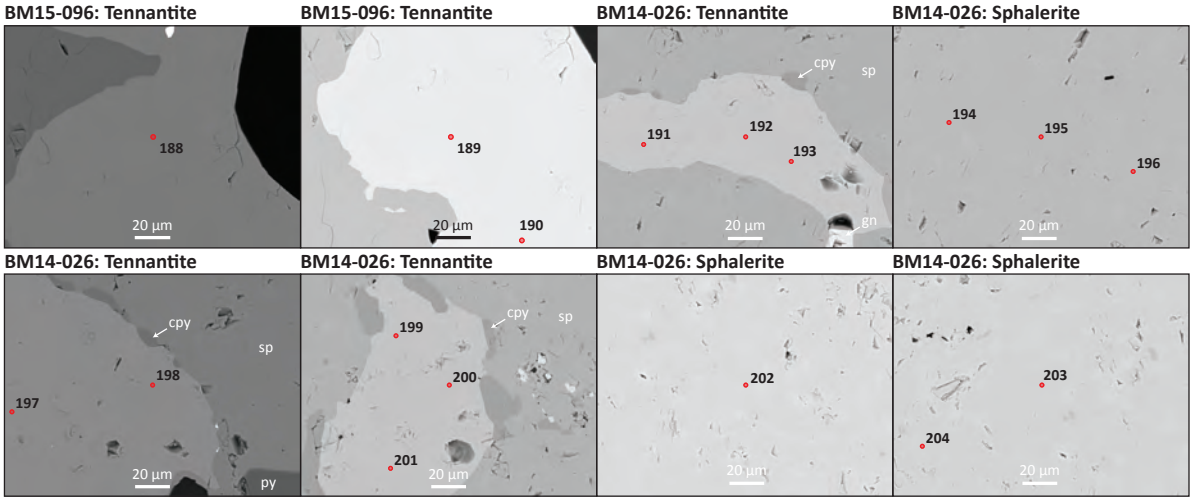

Figure C.5 Summary of electron microprobe analysis numbers 188-204.

Appendix D:

Additional Geology Cross-Section Interpretations

Eight cross-section interpretations were generated by integrating the lithofacies framework identified in this study from the West Block Area with descriptions from historic logs. Cross-sections 550 mE, 640 mE, 828 mE and 918 mE were presented and discussed in detail in Chapter 4. Cross-sections 585 mE, 700 mE, 880 mE and 957 mE are presented here (Figures D.2-D.5). The cross-sections are oriented south-to-north looking west in the mine grind co-ordinate system (Figure D.1). The vertical (2,790-3,140 metre relative level) and horizontal (4,000-4,650 metre north) extents are uniform for the set of sections. To simplify the lithological interpretations, individual rock types were grouped into one of five stratigraphic units: (1) Price Formation; (2) Basal Volcaniclastic Unit; (3) undifferentiated HW Rhyolite; (4) undifferentiated Hanging Wall Andesite member; and (5) mafic dykes. In addition to the 31 logged drill holes, 124 underground drill holes from Level 18 were re-coded using the above stratigraphic classification. Re-coding of drill core intervals was completed based on the assessment of historic drill core logs.

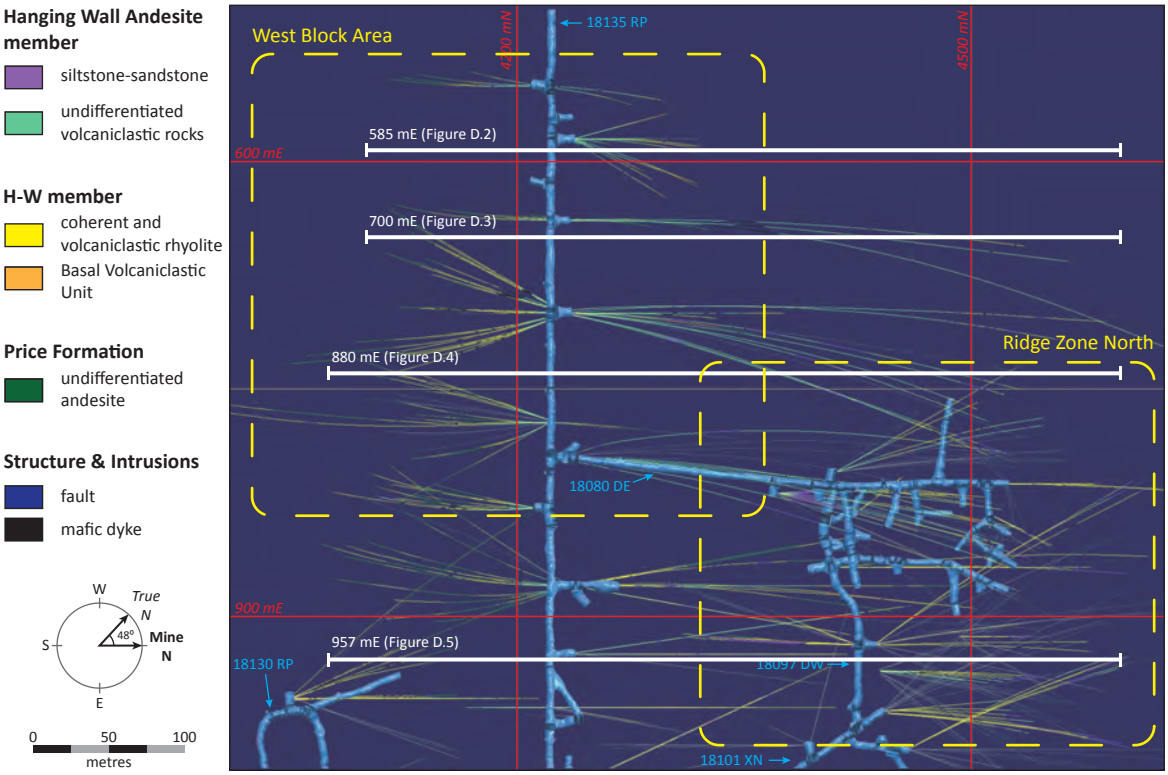

Figure D.1 Plan view at 3,140 m relative level showing the West Block Area and Ridge Zone North localities and the locations of geology cross-section interpretations at 585 mE, 700 mE, 880 mE and 957 mE (Figures D.2-D.5).

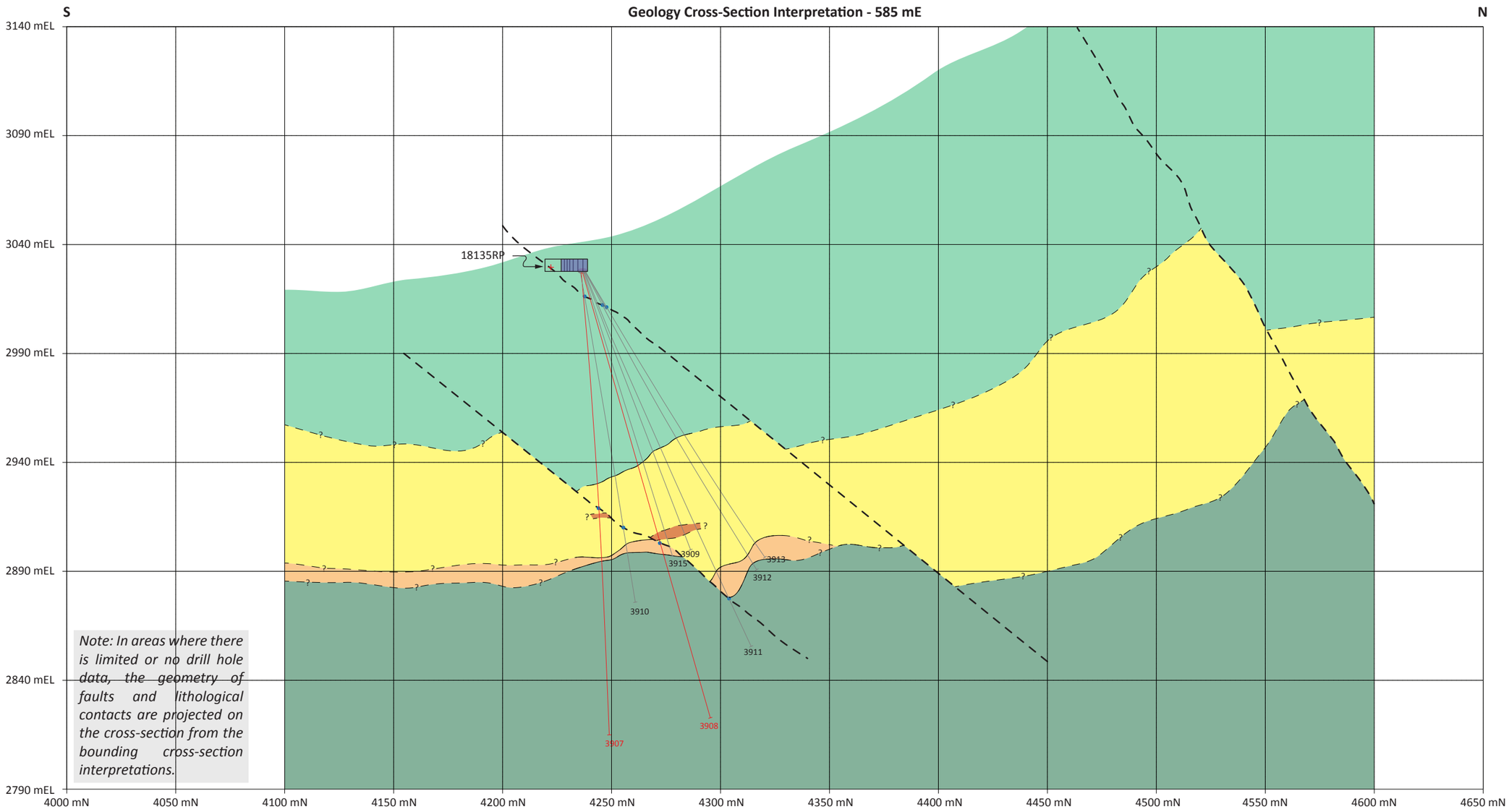

Underground Drill Holes

- Re-coded drill holes
- Logged drill holes
- Fault interval
- Projected fault interval

Underground Workings

18135RP

Geology Legend

- Hanging Wall Andesite Member - undifferentiated
- HW Rhyolite Member - undifferentiated
- HW Rhyolite Member - Basal Volcaniclastic Unit
- Price Formation - undifferentiated
- Mafic dyke
- Zinc assay ≥ 5%
- Lithology contact
- Inferred lithology contact
- Interpreted fault

Section Layout

Scale: 1:2,000

0 25 50 m

Section Orientation (±7 mE)

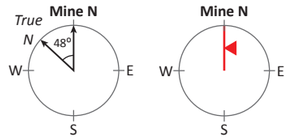

Underground Drill Holes (7 holes total)

BG18-3907
BG18-3908
BG18-3909
BG18-3910
BG18-3911
BG18-3912
BG18-3913

red = logged drill holes

Figure D.2 585 mE cross-section interpretation.

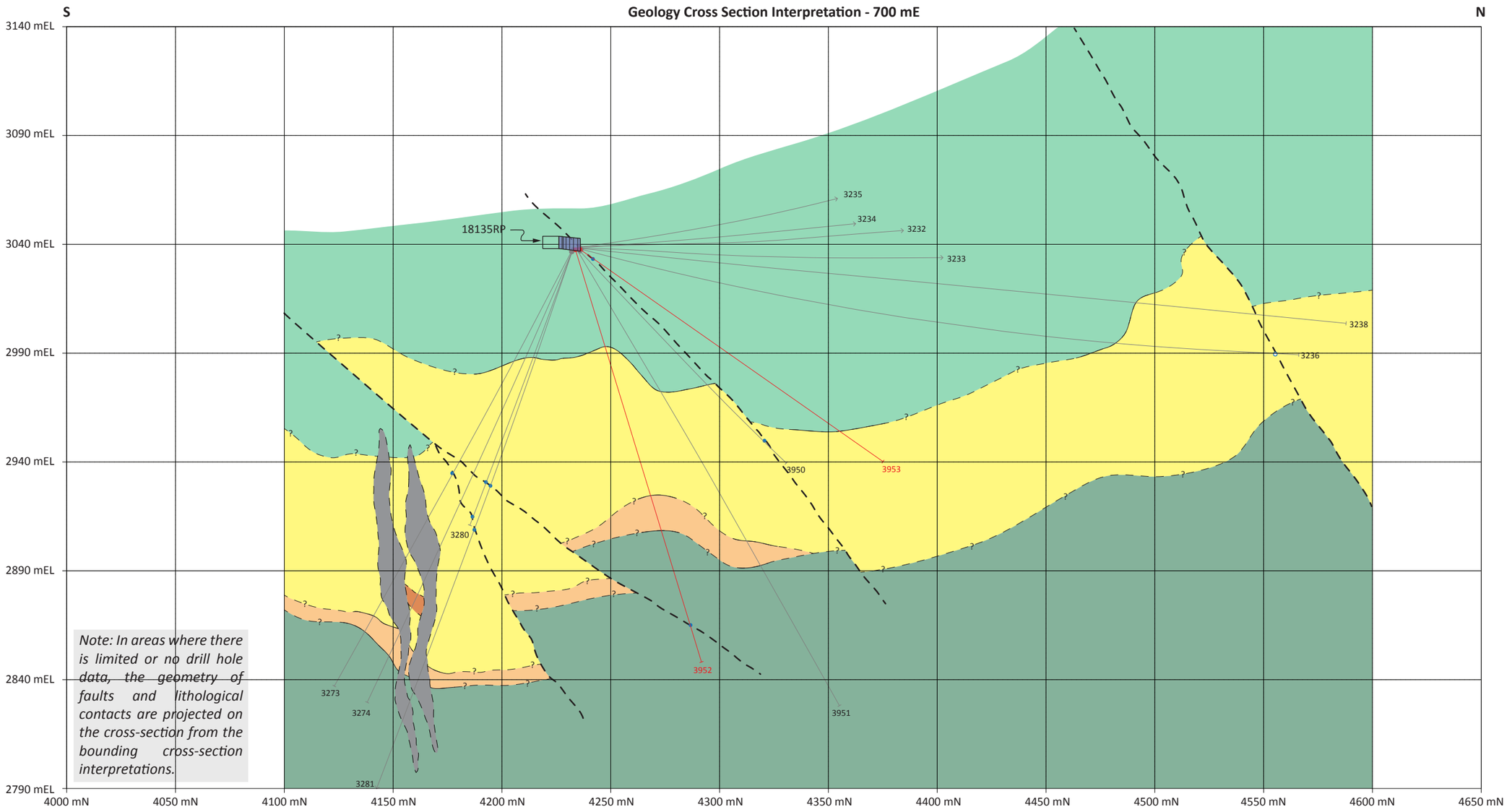

Underground Drill Holes

- Re-coded drill holes
- Logged drill holes
- Fault interval
- Projected fault interval

Underground Workings

18135RP

Geology Legend

- Hanging Wall Andesite Member - undifferentiated
- HW Rhyolite Member - undifferentiated
- HW Rhyolite Member - Basal Volcaniclastic Unit
- Price Formation - undifferentiated
- Mafic dyke
- Zinc assay ≥ 5%
- Lithology contact
- Inferred lithology contact
- Interpreted fault

Section Layout

Scale: 1:2,000

0 25 50 m

Section Orientation (±10 mE)

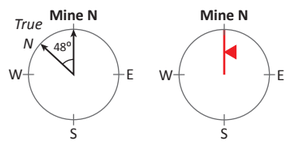

Underground Drill Holes (14 holes total)

BG18-3232
BG18-3233
BG18-3234
BG18-3235
BG18-3236
BG18-3238
BG18-3273
BG18-3274
BG18-3280
BG18-3281
BG18-3950
BG18-3951
BG18-3952
BG18-3953

red = logged drill holes

Figure D.3 700 mE cross-section interpretation.

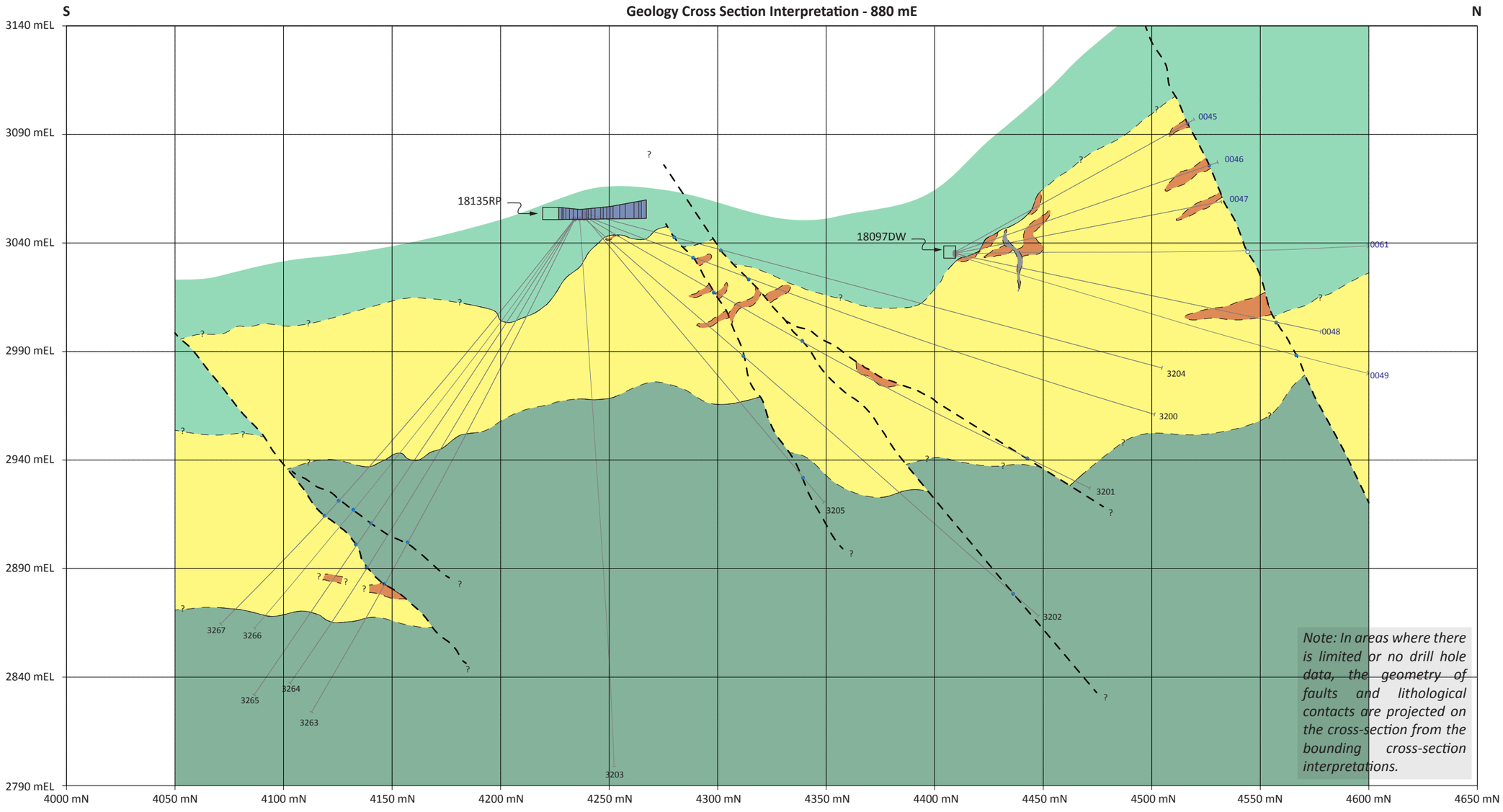

Underground Drill Holes

- Re-coded drill holes
- Logged drill holes
- Fault interval
- Projected fault interval

Underground Workings

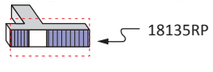

Geology Legend

- Hanging Wall Andesite Member - undifferentiated
- HW Rhyolite Member - undifferentiated
- HW Rhyolite Member - Basal Volcaniclastic Unit
- Price Formation - undifferentiated
- Mafic dyke
- Zinc assay ≥ 5%
- Lithology contact
- Inferred lithology contact
- Interpreted fault

Section Layout

Scale: 1:2,000

0 25 50 m

Section Orientation (±15 mE)

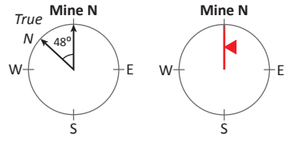

Underground Drill Holes (16 holes total)

BG18-3200	RN18-0045 (12 m)
BG18-3201	RN18-0046 (12 m)
BG18-3202	RN18-0047 (12 m)
BG18-3203	RN18-0048 (12 m)
BG18-3204	RN18-0049 (12 m)
BG18-3205	RN18-0061 (8 m)
BG18-3263	
BG18-3264	
BG18-3266	
BG18-3267	

red = logged drill holes

Figure D.4 880 mE cross-section interpretation.

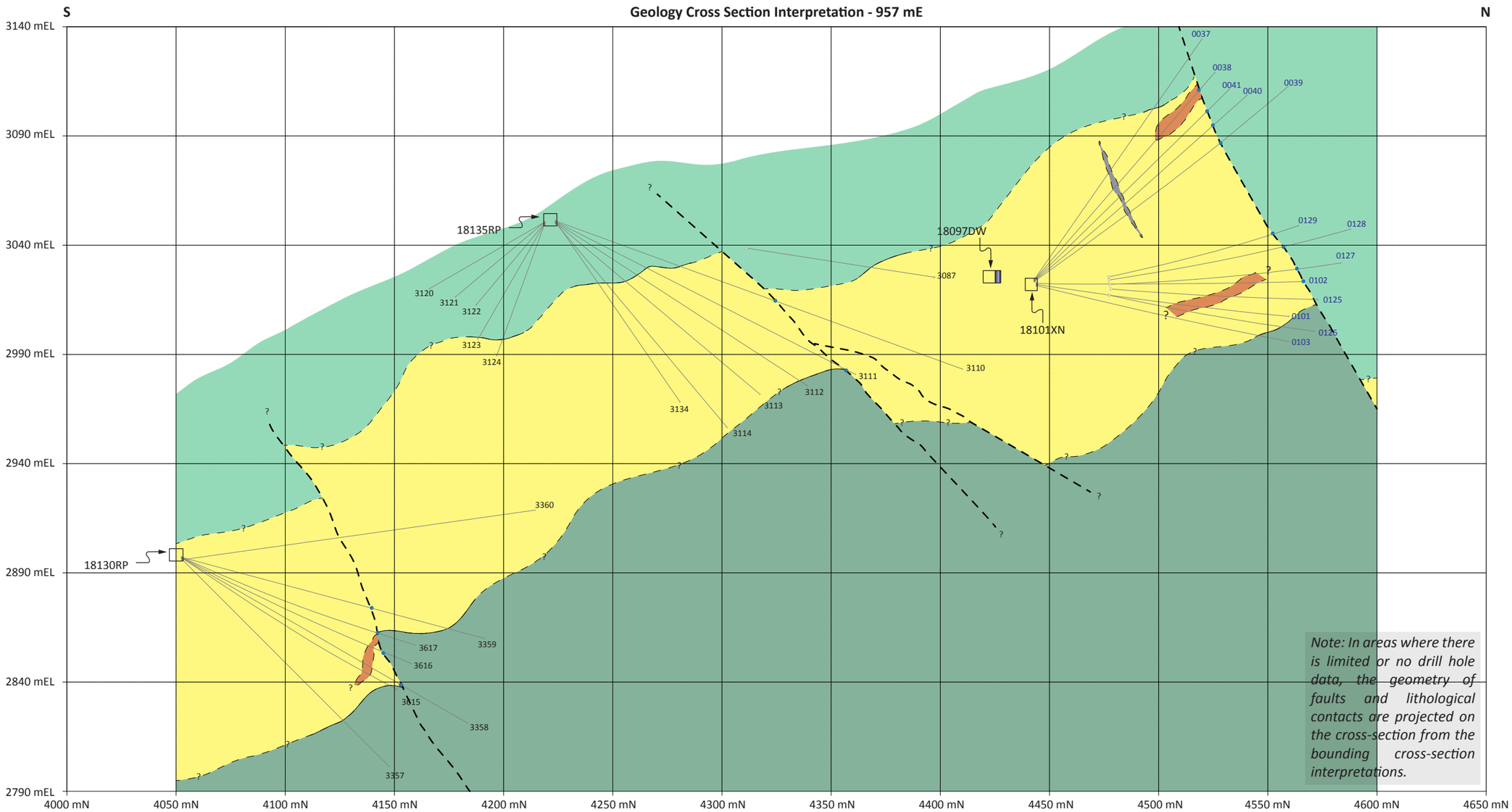

Underground Drill Holes

- Re-coded drill holes
- Logged drill holes
- Fault interval
- Projected fault interval

Underground Workings

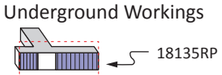

Geology Legend

- Hanging Wall Andesite Member - undifferentiated
- HW Rhyolite Member - undifferentiated
- HW Rhyolite Member - Basal Volcaniclastic Unit
- Price Formation - undifferentiated
- Mafic dyke
- Zinc assay ≥ 5%
- Lithology contact
- Inferred lithology contact
- Interpreted fault

Section Layout

Scale: 1:2,000

0 25 50 m

Section Orientation (±10 mE)

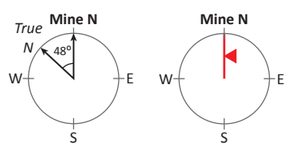

Underground Drill Holes (32 holes total)

BG18-3357 (2 m)	BG18-3112 (3 m)	RN18-0125
BG18-3358 (2 m)	BG18-3113 (3 m)	RN18-0126
BG18-3359 (2 m)	BG18-3114 (3 m)	RN18-0127
BG18-3360 (2 m)	BG18-3134 (3 m)	RN18-0128
BG18-3615 (1 m)	BG18-3087	RN18-0129
BG18-3616 (1 m)		
BG18-3617 (1 m)	RN18-0037	
BG18-3120 (3 m)	RN18-0038 (3 m)	
BG18-3121 (3 m)	RN18-0039 (5 m)	
BG18-3122 (3 m)	RN18-0040 (4 m)	
BG18-3123 (3 m)	RN18-0041 (4 m)	
BG18-3124 (3 m)	RN18-0101 (6 m)	
BG18-3110 (3 m)	RN18-0102 (6 m)	
BG18-3111 (3 m)	RN18-0103 (6 m)	

red = logged drill holes

Figure D.5 957 mE cross-section interpretation.

Appendix E:

Electron Microprobe Analytical Method and Results for silicates and carbonates

Analyses were acquired on a Cameca SX100 TCP/IP Socket electron microprobe with 5 tunable wavelength dispersive spectrometers. Operational conditions were 40° takeoff angle, and a beam energy of 15 keV at 10 nA with a 10 μm diameter. Elements were acquired using analysing crystals LLIF for Mn-Kα, Fe-Kα, Ti-Kα, V-Kα, Cr-Kα, Ba-Lγ, Zn-Kα; LPET for Ca-Kα, Cl-Kα, Sr-Lγ, K-Kα; TAP for Si-Kα, Al-Kα, Mg-Kα, Na-Kα; and PC0 for F-Kα. Silicate and carbonate minerals were analysed during the same session using the below procedure.

The standards were rutile (TiO_2) for Ti; $SrTiO_3$ for Sr; rhodonite ($MnSiO_3$) for Mn; eskolaite for Cr; jadeite for Na; barite (Ba_SO_4) for Ba; orthoclase for K; hematite Harvard for Fe; tugtupite astimex for Cl; plagioclase Lake County NMNH 115900 for Al; gahnite Brazil NMNH 145883 for Zn; wollastonite UNE for Ca, Si; periclase UNE for Mg; vanadium metal Aldrich for V; and topaz (UTAS4 block) for F. The counting times were: 10 s for Si, Cl; 20 s for Na, Mn, Al, Mg, Ti, Cr, Fe, K, Ca; 30 s for V, F, Sr, Zn; and 40 s for Ba. Off peak counting time were: 4 s for Si; 10 s for Na, Fe, Al, Mg, Cl, K; 20 s for Cr, Mn, Ti, Ca; 30 s for V, F, Sr, Zn; and 40 s for Ba.

The intensity data were corrected for Time Dependent Intensity (TDI) loss (or gain) using a self-calibrated correction for Mn, Fe, Mg, and Ca. The off peak correction method was Linear for elements Fe, Si, Mg, Ca, Ba, Sr, Zn; and was Slope for Mn. Unknown and standard intensities were corrected for deadtime.

Oxygen was calculated by cation stoichiometry and included in the matrix correction. Carbon was calculated by stoichiometry to oxygen with 0.333333 atoms C relative to 1.0 atom O. The matrix correction method was ZAF or Phi-Rho-Z calculations with mass absorption coefficients of LINEMU Henke (LBL, 1985). The ZAF or Phi-Rho-Z algorithm utilised was the Armstrong/Love Scott (Armstrong, 1988). Sample photographs are shown in Figure E.1. Results are from single point analysis (Table E.1) and Figures E.2-E.12 document the location of each EMP analysis.

Figure E.1 Photographs of electron microprobe analysed samples. Red circles denote areas on the laser mount that were analysed. Sample photographs 143640 (A), 143682 (B) UPB12 (S) are of the thin section off-cut.

A. Sample 143640 is of Price Formation andesite from the Thelwood Valley. This sample is an example of weak, chlorite-calcite-epidote alteration facies of the footwall alteration zone.

B. Sample 143682 is of Price Formation andesite from the Battle orebody. This sample is an example of intense, sericite-quartz-pyrite alteration facies of the footwall alteration zone.

C. Sample 143700 is of Price Formation andesite from the Battle orebody. This sample is an example of intense, sericite-quartz-pyrite alteration facies of the footwall alteration zone.

D. Sample TS-1180 is of Price Formation andesite from the Ridge Zone North oreobdy. This sample is an example of intense, chlorite-sericite-pyrite alteration of the footwall alteration zone.

E. Sample TS-265 is of Price Formation andesite from the West Block Area. This sample is an example of moderate, chlorite-calcite-pyrite alteration facies of the footwall alteration zone.

F. Sample TS-394 is of Price Formation andesite from the West Block Area. This sample is an example of moderate, chlorite-calcite-pyrite alteration facies of the footwall alteration zone.

G. Sample TS-420 is of Price Formation andesite from the West Block Area. This sample is an example of moderate, chlorite-calcite-pyrite alteration facies of the footwall alteration zone.

H. Sample TS-552 is of Price Formation andesite from the West Block Area. This sample is an example of moderate, chlorite-calcite-pyrite alteration facies of the footwall alteration zone.

I. Sample TS-722 is of Price Formation andesite from the West Block Area. This sample is an example of moderate, chlorite-calcite-pyrite alteration facies of the footwall alteration zone.

J. Sample TS-683 is of Price Formation andesite from the West Block Area. This sample is an example of moderate, chlorite-calcite-pyrite alteration facies of the footwall alteration zone.

K. Sample TS-788 is of Price Formation andesite from the West Block Area. This sample is an example of moderate, chlorite-calcite-pyrite alteration facies of the footwall alteration zone.

L. Sample TS-345 is of Price Formation andesite from the West Block Area. This sample is an example of moderate, chlorite-sericite-pyrite alteration facies of the footwall alteration zone.

M. Sample TS-067 is of Price Formation andesite from the West Block Area. This sample is an example of moderate, chlorite-calcite-pyrite alteration facies of the footwall alteration zone.

N. Sample TS-494 is of Price Formation andesite from the West Block Area. This sample is an example of moderate, chlorite-calcite-pyrite alteration facies of the footwall alteration zone.

O. Sample TS-496 is of Price Formation andesite from the West Block Area. This sample is an example of moderate, chlorite-calcite-pyrite alteration facies of the footwall alteration zone.

P. Sample MF18853 is of Price Formation andesite from the Ridge Zone West orebody. This sample is an example of moderate, chlorite-calcite-pyrite alteration facies of the footwall alteration zone.

Q. Sample FM19908 is of Price Formation andesite from the Ridge Zone West orebody. This sample is an example of moderate, chlorite-calcite-pyrite alteration facies of the footwall alteration zone.

R-S. Samples TS-1086 and UPB12 are of coherent andesite flow from the hanging wall of the West Block Area. These samples are examples of weak, chlorite-calcite-epidote alteration facies the result of greenschist facie metamorphism.

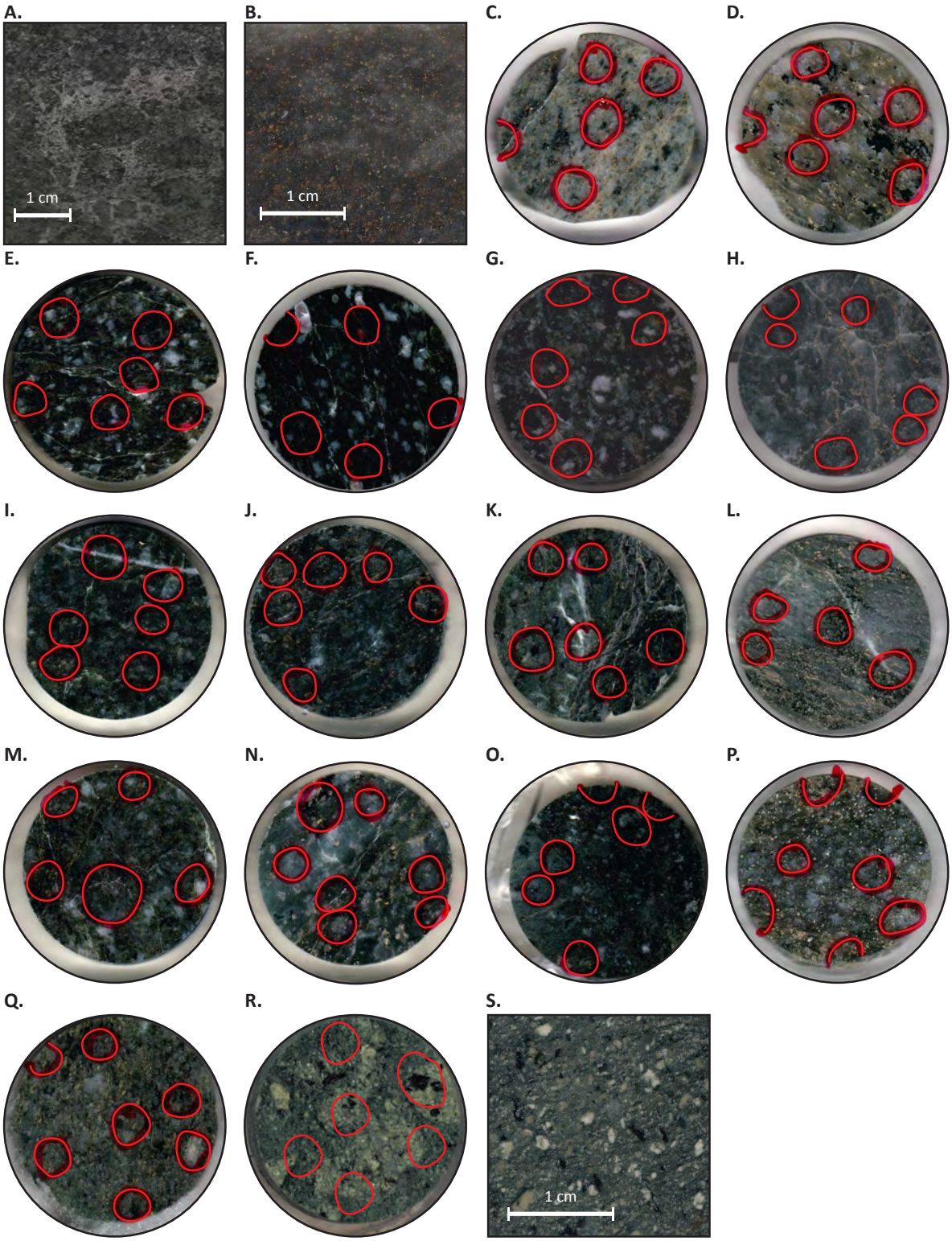
A.
1 cm
B.
1 cm
C.
D.
E.
F.
G.
H.
I.
J.
K.
L.
M.
N.
O.
P.
Q.
R.
S.
1 cm

Table E.1 EMP results for all silicate and carbonate analyses

Sample	Analysis Number	Area	Min.	Note	Si wt %	Al wt %	Ca wt %	Na wt %	K wt %	Mg wt %	Fe wt %	Ti wt %	Zn wt %	V wt %	Cr wt %	Mn wt %	Sr wt %	Ba wt %	Cl wt %	F wt %	O wt %	H wt %	Total wt %
143640	1	TV	ep	A	17.32	12.46	16.12	<0.03	<0.02	<0.03	9.61	<0.04	<0.06	0.07	<0.03	0.14	0.99	<0.07	<0.02	<0.05	41.88	0.21	98.79
143640	2	TV	ep	A	17.02	12.27	15.93	<0.03	<0.02	<0.03	10.06	<0.04	<0.06	0.06	<0.03	0.13	1.41	<0.07	<0.02	<0.05	41.52	0.20	98.60
143640	3	TV	ep	R	17.33	11.85	16.13	0.08	<0.02	<0.02	10.51	<0.04	<0.06	<0.03	<0.03	0.12	0.83	<0.07	<0.02	<0.05	41.60	0.20	98.65
143640	4	TV	ep	A	17.35	12.71	15.98	0.03	<0.02	<0.03	9.39	<0.04	<0.06	<0.03	<0.03	0.28	1.11	<0.07	0.03	<0.05	42.10	0.21	99.20
143640	5	TV	ep	A	17.15	12.31	16.24	<0.03	<0.02	<0.02	9.51	<0.04	<0.06	0.09	<0.03	0.12	0.97	<0.07	<0.02	<0.05	41.64	0.21	98.25
143640	6	TV	ep	A	17.14	12.27	16.12	<0.05	<0.02	<0.02	9.79	<0.04	<0.06	0.09	<0.03	0.11	1.18	<0.07	<0.02	<0.05	41.57	0.20	98.47
143640	7	TV	cb	R	0.28	-	37.79	-	-	0.25	0.77	-	<0.06	-	-	0.36	0.04	<0.07	-	-	48.06	-	99.59
143640	8	TV	chl	A	12.07	10.74	0.27	0.07	<0.02	10.57	17.26	0.04	0.06	0.04	<0.03	0.19	<0.05	<0.06	<0.02	0.11	45.73	1.30	98.46
143640	9	TV	chl	A	11.79	10.94	0.05	0.05	0.02	9.90	18.64	<0.04	<0.06	0.07	<0.03	0.29	<0.05	<0.07	<0.02	0.10	45.37	1.29	98.51
143640	10	TV	wm	A	22.12	16.27	0.02	0.19	8.67	1.17	2.45	<0.03	<0.05	0.20	<0.03	<0.03	<0.05	0.65	<0.02	0.16	47.05	0.50	99.45
143640	11	TV	ep	A	17.37	12.80	16.69	<0.03	<0.02	<0.02	9.16	0.06	<0.06	0.09	<0.03	0.09	0.39	<0.08	<0.02	<0.05	42.28	0.21	99.13
143640	12	TV	ep	A	17.38	13.08	16.58	<0.04	<0.02	<0.02	9.03	<0.04	<0.06	0.11	<0.03	0.15	0.50	<0.08	<0.02	<0.05	42.50	0.21	99.54
143640	13	TV	ep	A	17.41	12.80	16.59	<0.04	<0.02	<0.02	9.16	<0.04	<0.06	0.12	<0.03	0.11	0.42	<0.08	<0.02	<0.05	42.31	0.21	99.14
143640	14*	TV	chl	A	12.13	10.98	0.04	0.09	<0.02	10.22	17.59	<0.03	0.08	0.05	<0.03	0.25	<0.04	<0.06	<0.02	0.07	45.82	1.30	98.60
143640	15	TV	chl	R	12.22	11.72	0.06	0.20	<0.02	9.74	18.43	<0.04	0.08	0.06	<0.03	0.24	0.04	<0.07	<0.02	0.06	46.51	1.29	100.66
143640	16	TV	cb	A	<0.02	-	37.82	-	-	0.28	0.72	-	<0.06	-	-	0.75	<0.04	<0.08	-	-	47.77	-	99.37
143640	17	TV	cb	A	<0.02	-	38.29	-	-	0.19	0.47	-	<0.06	-	-	0.52	<0.04	<0.06	-	-	47.77	-	99.26
143640	18	TV	cb	A	<0.02	-	39.21	-	-	0.06	0.17	-	<0.06	-	-	0.36	0.08	<0.07	-	-	47.85	-	99.76
143640	19	TV	ep	A	17.28	12.17	15.93	0.04	<0.02	<0.03	9.79	0.04	<0.06	0.08	<0.03	0.12	1.49	0.07	<0.02	<0.06	41.69	0.20	98.89
143640	20	TV	wm	A	21.84	17.10	0.06	0.53	8.49	0.84	2.32	0.11	<0.05	0.13	<0.03	<0.03	<0.05	0.54	<0.02	0.11	47.35	0.50	99.90
143640	21	TV	chl	A	11.67	11.78	<0.01	<0.03	0.07	9.66	19.06	<0.04	<0.06	0.06	<0.03	0.30	<0.04	<0.06	<0.02	0.09	45.92	1.29	99.90
143640	22	TV	chl	A	11.82	11.32	0.04	0.03	<0.02	9.92	18.62	<0.04	0.06	0.05	<0.03	0.31	<0.05	<0.07	<0.02	0.07	45.78	1.29	99.30
143682	23	B	wm	A	20.89	18.82	<0.01	0.38	8.63	0.50	0.58	0.10	<0.06	0.05	<0.03	<0.03	<0.04	0.44	<0.02	0.17	48.09	0.50	99.16
143682	24	B	wm	A	20.94	18.87	<0.01	0.41	8.73	0.48	0.58	0.08	<0.06	0.04	0.03	<0.03	<0.05	0.45	<0.02	0.11	47.32	1.32	99.37
143682	25	B	wm	R	20.78	18.90	<0.01	0.40	8.64	0.53	0.59	0.04	<0.06	0.04	<0.03	<0.03	<0.05	0.46	<0.02	0.10	48.02	0.50	99.02
143682	26	B	chl	R	12.30	12.23	0.02	<0.03	0.02	14.66	8.16	0.06	0.09	<0.03	<0.03	0.52	<0.04	<0.07	0.03	0.30	48.26	0.51	97.16
143682	27	B	wm	A	21.29	19.02	<0.01	0.37	8.64	0.52	0.60	0.10	<0.06	0.06	<0.03	<0.03	<0.04	0.44	<0.02	0.16	47.14	1.32	99.66
143682	28	B	chl	A	12.49	12.33	0.05	<0.03	0.03	14.81	8.37	<0.04	0.12	<0.03	<0.03	0.46	<0.04	<0.07	<0.02	0.31	48.24	0.51	97.72
143682	29	B	wm	A	21.12	19.10	<0.01	0.48	8.66	0.55	0.66	0.06	<0.05	<0.03	<0.03	<0.03	<0.04	0.29	<0.02	0.10	47.88	0.50	99.41
143682	30	B	chl	R	13.36	12.67	0.02	0.04	0.57	14.26	7.78	<0.04	0.06	<0.03	<0.03	0.43	<0.04	<0.06	<0.02	0.35	47.28	0.50	97.33
143682	31	B	wm	A	20.83	18.97	0.02	0.36	8.72	0.50	0.60	0.11	<0.05	0.04	<0.03	<0.03	<0.04	0.45	<0.02	0.13	46.98	1.32	99.06
143682	32	B	wm	A	20.89	18.87	<0.01	0.46	8.64	0.54	0.60	0.11	<0.05	0.07	<0.03	<0.03	<0.05	0.37	<0.02	0.15	46.56	1.32	98.59

Table E.1 Continued.

Sample	Analysis Number	Area	Min.	Note	Si wt %	Al wt %	Ca wt %	Na wt %	K wt %	Mg wt %	Fe wt %	Ti wt %	Zn wt %	V wt %	Cr wt %	Mn wt %	Sr wt %	Ba wt %	Cl wt %	F wt %	O wt %	H wt %	Total wt %
143682	33	B	wm	A	20.88	19.13	<0.01	0.41	8.62	0.52	0.62	0.08	<0.06	0.08	<0.03	<0.03	<0.05	0.39	<0.02	0.14	46.94	1.32	99.14
143682	34	B	wm	A	21.10	18.77	<0.01	0.40	8.67	0.59	0.55	0.09	<0.06	0.07	<0.03	<0.03	<0.05	0.37	<0.02	0.19	47.45	0.50	98.76
143682	35	B	chl	R	12.17	12.24	0.03	<0.03	0.02	14.50	8.30	0.04	0.09	<0.03	0.04	0.53	<0.04	<0.06	<0.02	0.32	47.42	0.51	96.21
143682	36	B	chl	R	12.19	12.11	0.03	<0.03	0.03	14.42	8.54	<0.04	0.08	<0.03	<0.03	0.50	<0.05	<0.07	<0.02	0.37	46.77	1.32	96.36
143682	37	B	chl	R	12.43	12.29	0.03	<0.03	0.18	14.42	8.43	0.06	0.10	0.04	0.07	0.51	<0.04	<0.06	<0.02	0.34	46.90	1.32	97.10
143682	38	B	chl	R	12.26	11.90	0.01	<0.03	0.06	14.77	8.22	<0.03	0.12	<0.03	0.03	0.47	<0.04	<0.06	<0.02	0.33	47.80	1.34	97.33
143682	39	B	chl	A	12.50	12.20	<0.01	<0.03	<0.02	14.88	8.17	<0.03	0.08	<0.03	<0.03	0.51	<0.04	0.08	<0.02	0.29	47.71	0.50	96.94
143682	40	B	chl	R	12.27	12.41	<0.01	<0.03	<0.02	14.58	8.59	<0.03	<0.06	<0.03	<0.03	0.43	<0.04	<0.06	<0.02	0.30	48.06	0.51	97.14
143682	41	B	chl	R	12.05	12.39	<0.01	<0.03	<0.02	14.41	8.44	<0.04	0.09	<0.03	<0.03	0.48	<0.04	<0.07	<0.02	0.29	46.89	0.50	95.55
143682	42	B	chl	R	12.27	12.31	<0.01	<0.03	<0.02	14.82	8.36	<0.04	0.11	<0.03	<0.03	0.47	<0.04	<0.07	<0.02	0.25	49.97	0.52	99.08
143700	43	B	wm	A	21.31	19.47	<0.01	0.42	8.59	0.52	0.34	0.05	<0.05	<0.03	<0.03	0.03	<0.05	0.32	<0.02	0.12	48.00	0.51	99.67
143700	44	B	wm	A	21.08	19.61	<0.01	0.38	8.55	0.60	0.36	0.04	<0.05	<0.03	0.04	<0.03	<0.05	0.24	<0.02	0.25	47.82	0.50	99.48
143700	45	B	wm	A	21.57	19.57	<0.01	0.42	8.72	0.47	0.39	0.06	<0.06	<0.03	<0.03	0.04	<0.04	0.32	<0.02	0.15	48.35	0.51	100.57
143700	46	B	wm	A	21.12	19.60	<0.01	0.44	8.67	0.50	0.32	0.07	<0.05	<0.03	<0.03	<0.03	<0.04	0.27	<0.02	0.13	47.89	0.51	99.52
143700	47	B	chl	R	12.46	13.26	<0.01	<0.03	0.16	15.11	7.33	<0.03	<0.06	<0.03	<0.03	0.43	<0.04	<0.07	0.02	0.29	49.05	1.38	99.49
143700	48	B	chl	A	12.87	12.66	<0.01	<0.03	0.02	16.09	6.65	<0.04	<0.06	0.03	<0.03	0.47	<0.04	<0.06	<0.02	0.47	49.34	1.38	99.97
143700	49	B	chl	A	12.65	12.47	<0.01	<0.04	<0.02	16.24	6.25	<0.03	<0.06	<0.03	<0.03	0.48	<0.04	<0.06	<0.02	0.47	48.90	1.38	98.83
143700	50	B	wm	A	21.35	19.82	0.04	0.45	8.55	0.42	0.23	0.12	<0.06	0.05	<0.03	<0.03	<0.05	0.31	<0.02	0.12	48.31	0.51	100.27
143700	51	B	wm	A	21.18	19.73	0.09	0.51	8.60	0.46	0.28	0.04	<0.05	0.06	<0.03	<0.03	<0.05	0.21	<0.02	0.16	48.07	0.51	99.90
143700	52	B	wm	A	21.13	19.64	<0.01	0.45	8.61	0.39	0.35	0.07	<0.05	0.05	<0.03	<0.03	<0.05	0.27	<0.02	0.16	47.86	0.51	99.50
143700	53	B	chl	R	13.20	13.35	0.01	<0.03	0.54	15.31	5.76	0.04	<0.05	0.04	<0.03	0.58	<0.04	<0.06	<0.02	0.37	49.86	1.39	100.44
143700	54	B	wm	A	21.21	19.71	<0.01	0.51	8.48	0.43	0.32	0.05	<0.06	<0.03	<0.03	<0.03	<0.05	0.25	0.03	0.15	48.02	0.51	99.67
143700	55	B	wm	A	21.15	19.75	<0.01	0.48	8.68	0.41	0.32	<0.04	<0.06	0.07	<0.03	0.03	<0.05	0.33	<0.02	0.13	47.98	0.50	99.84
143700	56	B	chl	R	12.77	12.86	<0.01	0.05	0.03	15.59	6.94	<0.04	0.10	<0.03	<0.03	0.45	<0.04	<0.06	0.02	0.44	49.18	1.38	99.80
MF18853	57	RZW	cb	R	0.60	-	37.87	-	-	0.07	0.06	-	<0.06	-	-	1.01	<0.04	<0.07	-	-	48.37	-	100.07
MF18853	58	RZW	wm	R	21.43	16.95	0.02	0.16	8.93	1.06	1.03	0.20	<0.05	0.04	<0.03	<0.03	<0.05	0.33	<0.02	0.07	46.11	1.32	97.65
MF18853	59	RZW	wm	R	21.27	16.87	<0.01	0.22	9.10	1.11	1.06	0.20	<0.06	0.06	0.03	<0.03	<0.05	0.25	<0.02	<0.05	46.97	0.51	97.64
MF18853	60	RZW	cb	R	0.30	-	37.42	-	-	0.28	0.37	-	<0.06	-	-	1.54	<0.04	<0.07	-	-	48.06	-	100.00
MF18853	61	RZW	cb	A	0.04	-	36.87	-	-	0.54	0.49	-	<0.06	-	-	1.85	<0.04	<0.08	-	-	47.79	-	99.58
MF18853	62	RZW	chl	R	12.61	11.82	<0.01	<0.03	0.28	13.95	9.57	0.04	0.08	<0.03	<0.03	0.46	<0.05	<0.07	<0.02	0.16	46.81	0.50	96.29
MF18853	63	RZW	wm	A	21.48	17.30	<0.01	0.22	8.99	1.18	1.25	0.25	<0.06	0.11	<0.03	<0.03	<0.05	0.31	<0.02	0.10	47.06	0.50	98.75
MF18853	64	RZW	chl	A	12.58	11.68	0.01	<0.03	0.07	14.22	9.91	<0.04	<0.06	<0.03	<0.03	0.39	<0.05	<0.06	<0.02	0.09	46.08	1.30	96.32

Table E.1 Continued.

Sample	Analysis Number	Area	Min.	Note	Si wt %	Al wt %	Ca wt %	Na wt %	K wt %	Mg wt %	Fe wt %	Ti wt %	Zn wt %	V wt %	Cr wt %	Mn wt %	Sr wt %	Ba wt %	Cl wt %	F wt %	O wt %	H wt %	Total wt %
MF18853	65	RZW	wm	A	21.23	17.37	<0.01	0.22	9.04	1.10	1.12	0.23	<0.05	0.04	<0.03	<0.03	<0.04	0.36	<0.02	0.07	46.59	0.50	97.87
MF18853	66	RZW	wm	A	21.52	16.95	<0.01	0.21	9.06	1.25	1.04	0.17	<0.06	0.09	<0.03	<0.03	<0.05	0.32	<0.02	0.09	46.39	1.30	98.40
MF18853	67	RZW	wm	A	21.43	17.18	<0.01	0.28	8.96	1.07	0.97	0.26	<0.05	0.08	<0.03	<0.03	<0.04	0.37	<0.02	0.10	47.21	0.50	98.40
MF18853	68	RZW	wm	A	21.57	17.33	<0.01	0.20	9.04	1.17	1.18	0.30	<0.05	0.07	<0.03	<0.03	<0.05	0.20	<0.02	0.13	47.11	0.50	98.80
MF18853	69	RZW	wm	A	21.38	17.00	<0.01	0.20	8.94	1.40	1.34	0.20	<0.06	0.05	<0.03	<0.03	<0.04	0.31	<0.02	0.11	46.22	1.30	98.45
MF18853	70	RZW	chl	R	12.45	11.76	<0.01	<0.03	<0.02	14.09	9.89	<0.04	0.09	<0.03	<0.03	0.47	<0.04	0.07	<0.02	0.10	46.03	1.29	96.26
MF18853	71	RZW	cb	A	<0.02	-	37.35	-	-	0.55	0.47	-	<0.06	-	-	2.05	0.04	<0.07	-	-	47.81	-	100.19
MF18853	72	RZW	cb	A	<0.02	-	37.70	-	-	0.21	0.18	-	<0.06	-	-	1.77	0.05	<0.07	-	-	47.70	-	99.58
MF18853	73	RZW	cb	A	<0.02	-	38.22	-	-	0.23	0.28	-	<0.06	-	-	2.03	0.12	<0.07	-	-	47.77	-	100.53
MF18853	74	RZW	wm	A	21.40	17.03	0.04	0.20	9.12	1.24	1.37	0.28	<0.06	0.06	<0.03	0.04	<0.05	0.26	<0.02	0.12	46.63	1.31	99.09
MF18853	75	RZW	cb	A	<0.02	-	37.81	-	-	0.61	0.50	-	<0.06	-	-	1.99	<0.04	0.06	-	-	47.90	-	100.77
MF18853	76	RZW	cb	A	<0.02	-	37.32	-	-	0.57	0.46	-	<0.06	-	-	1.91	0.04	<0.07	-	-	47.80	-	100.05
MF18853	77	RZW	cb	A	<0.02	-	37.34	-	-	0.52	0.45	-	<0.06	-	-	1.93	<0.03	<0.07	-	-	47.81	-	100.00
MF18853	78	RZW	cb	A	<0.02	-	38.06	-	-	0.53	0.48	-	<0.06	-	-	1.96	<0.04	<0.07	-	-	47.94	-	100.85
MF18853	79	RZW	cb	A	<0.02	-	37.52	-	-	0.47	0.47	-	<0.06	-	-	1.78	0.06	<0.07	-	-	47.76	-	99.99
MF19908	80	RZW	cb	R	2.45	-	31.58	-	-	1.22	1.94	-	<0.06	-	-	1.98	0.07	<0.07	-	-	50.23	-	101.80
MF19908	81	RZW	wm	R	20.88	16.95	0.04	0.39	8.85	1.00	2.06	0.31	<0.06	0.03	<0.03	<0.03	<0.05	0.41	<0.02	0.08	47.41	1.32	99.72
MF19908	82	RZW	cb	R	0.44	-	34.99	-	-	0.89	1.75	-	<0.06	-	-	1.73	0.21	<0.07	-	-	48.14	-	100.19
MF19908	83	RZW	chl	A	11.72	11.57	0.04	0.05	0.15	9.46	18.12	<0.04	0.14	<0.03	<0.03	0.27	<0.05	<0.07	<0.02	<0.06	47.44	0.50	99.46
MF19908	84	RZW	chl	R	11.46	11.25	0.04	0.10	0.02	9.24	18.42	<0.04	0.07	<0.03	<0.03	0.37	<0.04	<0.06	<0.02	<0.05	47.50	0.50	98.98
MF19908	85	RZW	chl	R	11.53	10.91	0.07	0.13	<0.02	9.26	18.22	0.06	0.13	<0.03	<0.03	0.37	<0.04	<0.07	<0.02	<0.05	47.22	0.50	98.40
MF19908	86	RZW	chl	A	11.47	11.20	0.05	<0.03	0.02	9.26	18.66	0.08	0.09	<0.03	0.03	0.36	<0.05	<0.06	0.02	<0.05	46.67	1.32	99.22
MF19908	87	RZW	wm	R	20.59	16.90	0.05	0.34	8.67	1.03	1.89	0.24	<0.06	0.04	0.04	<0.03	<0.05	0.38	<0.02	0.12	46.16	1.30	97.74
MF19908	88	RZW	wm	R	21.38	17.21	0.02	0.16	8.82	0.99	1.35	0.19	0.06	0.04	0.04	<0.03	<0.05	0.28	<0.02	0.07	45.82	1.30	97.70
MF19908	89	RZW	wm	R	20.87	16.94	<0.01	0.18	8.86	1.03	1.81	0.30	<0.05	0.07	<0.03	<0.03	<0.05	0.46	<0.02	0.06	47.38	0.50	98.47
MF19908	90	RZW	wm	A	21.61	16.74	0.05	0.40	8.64	0.92	1.73	0.23	<0.06	0.07	<0.03	<0.03	<0.04	0.36	<0.02	0.09	47.37	0.50	98.71
MF19908	91	RZW	wm	R	20.58	16.37	0.07	0.40	8.32	1.18	2.22	0.29	<0.06	<0.03	<0.03	<0.03	<0.04	0.30	<0.02	0.10	45.97	1.31	97.10
MF19908	92	RZW	chl	R	11.31	11.12	0.10	0.03	<0.02	9.38	18.49	<0.03	0.10	0.03	<0.03	0.39	<0.04	<0.07	0.02	<0.05	46.00	1.31	98.27
TS-067	93	WBA	chl	A	12.51	11.77	<0.010	<0.029	<0.015	12.78	13.32	<0.037	0.09	<0.032	<0.033	0.45	<0.036	<0.064	<0.018	0.14	47.62	1.33	100.00
TS-067	94	WBA	chl	R	13.95	13.08	<0.012	0.06	1.36	10.76	11.30	0.07	0.07	0.04	<0.027	0.34	<0.042	0.08	<0.019	0.09	49.03	1.35	101.59
TS-067	95	WBA	chl	A	12.41	11.81	<0.011	<0.032	<0.017	12.96	13.14	<0.034	0.11	0.04	<0.028	0.45	<0.039	<0.070	<0.017	0.14	47.66	1.33	100.05
TS-067	96	WBA	wm	A	21.97	17.85	<0.012	0.27	8.61	0.89	1.84	0.18	<0.057	0.08	<0.029	0.03	<0.042	0.26	<0.018	0.13	47.99	0.50	100.59

Table E.1 Continued.

Sample	Analysis Number	Area	Min.	Note	Si wt %	Al wt %	Ca wt %	Na wt %	K wt %	Mg wt %	Fe wt %	Ti wt %	Zn wt %	V wt %	Cr wt %	Mn wt %	Sr wt %	Ba wt %	Cl wt %	F wt %	O wt %	H wt %	Total wt %
TS-067	97	WBA	chl	R	14.33	13.52	0.06	0.09	1.77	10.06	10.51	0.06	<0.059	0.06	<0.026	0.37	<0.038	<0.065	<0.019	<0.054	49.37	1.36	101.56
TS-067	98	WBA	chl	R	17.40	15.33	0.04	0.18	4.10	6.62	7.34	0.13	<0.058	0.05	<0.027	0.22	<0.043	0.08	<0.018	0.09	51.99	1.39	104.94
TS-067	99	WBA	cb	R	0.05	-	37.73	-	-	0.21	0.38	-	<0.06	-	-	1.33	0.04	0.07	-	-	47.73	-	99.52
TS-067	100	WBA	cb	R	0.03	-	37.95	-	-	0.18	0.40	-	<0.06	-	-	1.33	0.06	<0.06	-	-	47.74	-	99.68
TS-067	101	WBA	cb	A	0.02	-	37.07	-	-	0.62	0.77	-	<0.06	-	-	2.05	<0.04	<0.08	-	-	47.85	-	100.32
TS-067	102	WBA	cb	A	<0.02	-	36.48	-	-	0.57	0.87	-	<0.06	-	-	2.10	<0.03	<0.07	-	-	47.72	-	99.71
TS-067	103	WBA	cb	A	<0.02	-	36.23	-	-	0.66	0.95	-	<0.06	-	-	2.07	0.06	<0.07	-	-	47.68	-	99.62
TS-067	104	WBA	wm	A	21.13	17.73	0.03	0.30	8.28	1.00	1.79	0.13	<0.058	0.09	<0.029	<0.030	<0.046	0.18	<0.018	0.06	46.92	0.50	98.16
TS-067	105	WBA	wm	A	21.59	18.25	<0.012	0.31	8.48	0.64	1.40	0.19	<0.058	0.06	<0.029	<0.029	<0.044	0.25	<0.018	0.10	47.62	0.50	99.38
TS-067	106	WBA	wm	A	21.78	18.32	<0.012	0.29	8.42	0.68	1.42	0.11	<0.056	0.08	0.03	<0.031	<0.043	0.28	<0.019	0.13	47.90	0.50	99.95
TS-067	107	WBA	wm	A	21.53	18.32	<0.012	0.32	8.47	0.59	1.38	0.19	<0.055	0.08	<0.028	0.03	<0.044	0.30	<0.017	0.07	47.65	0.50	99.46
TS-067	108	WBA	chl	A	12.10	12.07	0.01	<0.028	<0.015	12.27	13.55	<0.035	0.06	<0.027	<0.027	0.42	<0.036	<0.063	<0.017	0.06	47.20	1.33	99.07
TS-067	109	WBA	chl	A	12.16	12.15	0.03	<0.030	0.09	12.25	13.19	<0.038	0.11	<0.028	<0.030	0.39	<0.039	<0.066	0.02	0.12	47.21	1.33	99.04
TS-067	110	WBA	cb	A	0.04	-	37.77	-	-	0.19	0.38	-	<0.06	-	-	1.78	0.05	<0.07	-	-	47.75	-	99.93
TS-067	111	WBA	cb	A	<0.02	-	38.43	-	-	0.18	0.37	-	<0.06	-	-	1.39	0.07	<0.08	-	-	47.82	-	100.20
TS-067	112	WBA	cb	A	<0.02	-	36.32	-	-	0.60	0.87	-	<0.06	-	-	2.28	0.07	0.07	-	-	47.67	-	99.82
TS-067	113	WBA	chl	A	12.44	12.00	0.12	<0.027	0.02	12.82	12.79	<0.035	0.11	<0.029	<0.029	0.45	<0.040	<0.060	0.03	0.14	47.73	1.34	99.97
TS-067	114	WBA	chl	A	12.10	12.26	0.06	<0.033	<0.016	12.51	13.32	0.04	0.08	0.04	<0.030	0.50	<0.043	<0.071	<0.017	0.12	47.48	1.33	99.83
TS-067	115	WBA	wm	A	21.73	18.24	0.01	0.28	8.63	0.80	1.43	0.20	<0.055	0.07	<0.030	<0.030	<0.043	0.30	<0.018	0.11	47.94	0.50	100.25
TS-067	116	WBA	wm	A	21.92	18.21	<0.013	0.30	8.62	0.85	1.45	0.12	<0.054	0.09	<0.027	<0.032	<0.043	0.21	<0.018	0.11	48.12	0.50	100.51
TS-067	117	WBA	cb	A	<0.02	-	36.47	-	-	0.54	0.78	-	<0.06	-	-	2.02	0.05	<0.07	-	-	47.69	-	99.54
TS-067	118	WBA	cb	A	0.04	-	36.28	-	-	0.49	0.64	-	<0.06	-	-	2.06	0.06	<0.07	-	-	47.65	-	99.23
TS-067	119	WBA	cb	R	0.05	-	31.79	-	-	1.75	1.36	-	<0.06	-	-	3.70	0.05	<0.07	-	-	47.63	-	98.43
TS-067	120	WBA	cb	R	0.02	-	36.37	-	-	0.47	0.69	-	<0.06	-	-	1.94	0.09	<0.06	-	-	47.62	-	99.20
TS-067	121	WBA	chl	A	12.30	12.00	0.06	<0.035	<0.016	12.87	13.08	<0.035	0.07	0.04	<0.031	0.44	<0.036	<0.067	<0.018	0.10	47.65	1.33	99.92
TS-067	122	WBA	chl	A	12.39	11.91	0.03	<0.034	0.03	12.71	13.09	<0.038	0.11	<0.030	<0.028	0.45	<0.043	<0.059	<0.016	0.10	47.57	1.33	99.72
TS-067	123	WBA	wm	A	21.66	18.40	<0.012	0.33	8.48	0.68	1.52	0.16	<0.052	0.06	<0.029	0.03	<0.046	0.28	<0.015	0.11	47.90	0.50	100.13
TS-067	124	WBA	wm	A	21.68	18.16	<0.013	0.31	8.49	0.66	1.53	0.13	<0.057	0.06	<0.031	<0.031	<0.042	0.20	<0.018	0.08	47.66	0.50	99.47
TS-067	125	WBA	wm	A	21.57	18.32	<0.013	0.35	8.48	0.63	1.37	0.13	<0.055	0.08	<0.028	<0.033	<0.046	0.27	<0.018	0.09	47.65	0.50	99.45
TS-067	126	WBA	wm	A	21.83	18.31	<0.012	0.29	8.49	0.66	1.29	0.16	<0.056	0.08	<0.026	<0.030	<0.049	0.24	<0.018	0.10	47.92	0.50	99.86
TS-067	127	WBA	wm	A	20.85	18.03	<0.012	0.31	7.89	1.33	2.18	0.22	<0.056	0.08	<0.031	0.05	<0.039	0.36	<0.017	<0.049	47.20	0.50	98.99
TS-067	128	WBA	wm	A	21.61	18.34	<0.013	0.33	8.50	0.64	1.43	0.21	<0.057	0.10	<0.028	<0.032	<0.046	0.22	<0.016	0.15	47.76	0.50	99.79

Table E.1 Continued.

Sample	Analysis Number	Area	Min.	Note	Si wt %	Al wt %	Ca wt %	Na wt %	K wt %	Mg wt %	Fe wt %	Ti wt %	Zn wt %	V wt %	Cr wt %	Mn wt %	Sr wt %	Ba wt %	Cl wt %	F wt %	O wt %	H wt %	Total wt %
TS-067	129*	WBA	chl	A	12.26	12.06	0.02	<0.032	<0.015	12.39	13.25	<0.035	0.15	0.03	<0.026	0.37	<0.045	<0.075	<0.018	0.14	47.35	1.33	99.34
TS-1086	130	WBA	chl	R	12.07	10.98	0.02	<0.03	0.02	9.98	17.71	<0.04	<0.06	<0.03	<0.03	0.29	<0.04	<0.06	<0.02	0.07	45.57	1.30	98.01
TS-1086	131	WBA	ap	R	0.72	0.63	36.40	<0.04	<0.02	0.69	1.73	<0.04	<0.06	<0.04	<0.03	0.07	<0.04	<0.08	0.34	3.39	22.88	0.94	67.80
TS-1086	132	WBA	ap	R	0.63	0.09	37.74	<0.04	<0.02	0.35	1.42	<0.05	<0.06	<0.03	<0.03	0.12	0.08	<0.07	0.59	2.91	22.66	0.94	67.52
TS-1086	133	WBA	cb	A	<0.02	-	38.24	-	-	0.09	0.26	-	<0.06	-	-	0.36	<0.03	<0.07	-	-	47.73	-	98.75
TS-1086	134	WBA	cb	A	0.05	-	38.07	-	-	0.11	0.29	-	<0.06	-	-	0.36	<0.03	0.06	-	-	47.73	-	98.74
TS-1086	135	WBA	chl	A	12.01	10.95	0.04	0.09	0.03	10.13	17.78	<0.04	<0.06	<0.03	<0.03	0.34	<0.04	<0.06	0.02	<0.05	45.66	1.30	98.35
TS-1086	136	WBA	chl	A	12.07	10.86	0.04	0.05	0.02	10.29	18.07	<0.04	0.06	0.04	<0.03	0.29	<0.04	<0.07	0.04	<0.05	45.79	1.30	98.92
TS-1086	137	WBA	chl	R	12.40	10.70	0.03	<0.04	<0.02	10.43	17.73	<0.04	<0.06	<0.03	0.03	0.27	<0.05	<0.07	0.02	0.06	46.01	1.30	98.98
TS-1086	138	WBA	chl	A	12.39	10.59	0.02	<0.03	<0.02	10.61	17.36	<0.03	<0.06	<0.03	<0.03	0.28	<0.05	<0.07	<0.02	<0.05	45.95	1.31	98.50
TS-1086	139	WBA	chl	R	13.52	10.59	0.15	<0.04	<0.02	9.78	17.47	<0.04	<0.06	<0.03	<0.03	0.31	<0.04	<0.06	<0.02	<0.05	46.81	1.31	99.94
TS-1086	140	WBA	chl	A	12.27	10.80	0.03	<0.04	<0.02	10.39	18.00	<0.04	<0.06	0.04	<0.03	0.30	<0.05	0.06	<0.02	0.07	45.98	1.30	99.24
TS-265	141	WBA	wm	A	21.72	18.98	0.02	0.46	8.05	0.48	1.42	0.13	<0.059	0.05	<0.030	<0.028	<0.047	0.34	<0.015	<0.050	48.33	0.50	100.51
TS-265	142	WBA	wm	A	21.65	18.71	<0.012	0.48	8.08	0.51	1.58	0.12	<0.056	0.10	<0.028	<0.031	<0.043	0.23	<0.018	<0.051	48.07	0.50	100.05
TS-265	143	WBA	wm	A	21.58	18.99	<0.012	0.50	8.02	0.43	1.66	0.14	0.07	0.06	<0.028	<0.029	<0.043	0.27	<0.018	0.06	48.20	0.50	100.48
TS-265	144	WBA	wm	A	21.56	18.83	<0.012	0.42	8.16	0.54	1.62	0.08	<0.055	0.06	<0.027	<0.030	<0.040	0.28	<0.018	<0.048	48.06	0.50	100.11
TS-265	145	WBA	wm	A	21.40	18.87	<0.012	0.51	8.08	0.49	1.51	0.09	<0.056	0.07	<0.029	<0.029	<0.046	0.32	<0.016	0.06	47.86	0.50	99.74
TS-265	146	WBA	chl	A	13.18	12.04	<0.012	0.60	0.08	10.28	15.47	<0.032	0.10	0.04	<0.030	0.41	<0.041	<0.065	<0.018	0.08	47.76	1.32	101.35
TS-265	147	WBA	chl	A	12.34	12.06	<0.012	0.24	0.02	10.41	16.22	<0.040	0.14	<0.030	<0.028	0.37	<0.042	<0.073	<0.019	0.09	46.90	1.31	100.09
TS-265	148	WBA	chl	A	11.88	12.57	<0.012	<0.027	0.02	10.57	16.77	<0.032	0.08	<0.029	<0.026	0.36	<0.040	<0.060	<0.020	<0.050	47.01	1.31	100.56
TS-265	149	WBA	chl	A	12.22	12.33	<0.011	0.06	0.19	10.52	16.02	<0.040	0.12	<0.031	<0.025	0.38	<0.039	<0.067	<0.017	0.06	47.02	1.31	100.24
TS-265	150	WBA	chl	A	11.77	12.44	0.01	<0.034	0.02	10.51	16.69	<0.033	0.13	<0.028	<0.026	0.36	<0.038	<0.066	0.02	<0.053	46.72	1.31	99.98
TS-265	151	WBA	chl	A	12.01	12.47	<0.011	<0.029	0.03	10.47	16.66	<0.032	0.11	<0.031	<0.027	0.33	<0.043	<0.070	<0.019	<0.051	46.97	1.31	100.35
TS-265	152	WBA	chl	A	12.01	12.42	0.01	<0.036	0.02	10.66	16.39	<0.035	0.10	0.03	<0.031	0.31	<0.045	<0.056	0.02	0.06	46.95	1.31	100.29
TS-265	153	WBA	chl	A	12.18	12.43	0.02	<0.032	0.02	10.77	16.39	<0.038	0.11	<0.034	<0.027	0.35	<0.037	<0.071	<0.019	<0.052	47.28	1.31	100.87
TS-265	154	WBA	chl	A	11.97	12.13	<0.012	<0.031	<0.016	10.91	16.38	<0.037	0.07	<0.029	<0.031	0.42	<0.042	<0.073	<0.020	<0.052	46.83	1.31	100.00
TS-265	155	WBA	chl	R	12.42	12.53	0.02	0.04	0.28	10.36	15.96	<0.042	<0.059	<0.032	<0.026	0.37	<0.042	<0.067	<0.018	0.08	47.26	1.32	100.63
TS-265	156	WBA	chl	R	12.21	12.56	<0.012	0.03	0.27	10.36	16.09	<0.035	0.15	0.05	<0.028	0.36	<0.039	<0.068	<0.017	0.11	47.10	1.31	100.61
TS-265	157	WBA	wm	R	21.32	19.10	<0.013	0.40	8.18	0.50	1.88	0.18	<0.055	0.09	<0.029	<0.030	<0.046	0.28	<0.019	0.06	48.12	0.50	100.61
TS-265	158	WBA	wm	R	22.34	18.19	<0.011	0.43	7.52	0.91	1.93	0.08	<0.058	0.08	<0.026	<0.031	<0.043	0.21	<0.017	<0.048	48.60	0.51	100.80
TS-265	159	WBA	wm	A	21.03	18.87	<0.012	0.51	7.51	1.12	2.65	0.11	<0.057	0.09	<0.029	<0.032	<0.047	0.37	<0.016	<0.048	48.07	0.50	100.82
TS-265	160	WBA	chl	A	11.97	12.31	<0.012	<0.039	<0.015	10.73	16.69	<0.036	0.09	<0.031	<0.029	0.39	<0.038	<0.067	<0.018	<0.052	46.93	1.31	100.43

Table E.1 Continued.

Sample	Analysis Number	Area	Min.	Note	Si wt %	Al wt %	Ca wt %	Na wt %	K wt %	Mg wt %	Fe wt %	Ti wt %	Zn wt %	V wt %	Cr wt %	Mn wt %	Sr wt %	Ba wt %	Cl wt %	F wt %	O wt %	H wt %	Total wt %
TS-265	161	WBA	chl	A	11.84	12.35	0.02	<0.029	<0.017	10.66	16.62	<0.035	0.09	0.04	<0.031	0.33	<0.043	<0.059	<0.017	<0.051	46.80	1.31	100.07
TS-265	162	WBA	chl	A	11.87	12.42	<0.011	<0.030	<0.016	10.55	16.79	<0.035	0.12	<0.030	<0.028	0.32	<0.039	<0.062	<0.017	<0.054	46.85	1.31	100.22
TS-265	163	WBA	chl	A	11.94	12.53	<0.012	<0.031	<0.015	10.51	16.98	<0.033	0.14	0.04	<0.033	0.40	<0.041	<0.070	<0.016	<0.051	47.04	1.31	100.87
TS-265	164	WBA	chl	A	11.89	12.47	0.02	<0.029	<0.017	10.49	16.66	<0.036	0.08	<0.032	<0.026	0.40	<0.048	<0.064	<0.017	<0.051	46.87	1.31	100.19
TS-265	165	WBA	chl	A	11.89	12.41	<0.011	<0.034	<0.016	10.61	16.96	0.04	0.07	<0.032	<0.030	0.41	<0.045	<0.073	<0.017	<0.049	46.93	1.31	100.62
TS-265	166	WBA	wm	A	21.47	18.86	<0.012	0.44	8.19	0.61	1.95	0.12	<0.058	<0.033	<0.029	<0.032	<0.041	0.32	<0.018	0.06	48.11	0.50	100.64
TS-265	167	WBA	chl	A	11.86	12.18	<0.012	0.04	<0.015	10.70	16.58	0.05	0.16	<0.028	<0.029	0.36	<0.044	<0.065	<0.017	<0.053	46.71	1.31	99.94
TS-265	168	WBA	chl	A	11.85	12.24	<0.012	<0.030	<0.014	10.65	16.88	<0.034	0.08	<0.029	<0.027	0.42	<0.045	<0.065	<0.018	<0.053	46.78	1.31	100.20
TS-265	169	WBA	chl	A	12.32	11.86	<0.012	0.03	<0.016	10.77	16.33	0.04	0.12	0.04	<0.031	0.44	<0.042	<0.066	0.02	0.08	46.92	1.31	100.28
TS-265	170	WBA	chl	A	12.06	11.94	<0.012	<0.030	<0.016	10.97	16.53	<0.037	0.14	<0.029	<0.030	0.42	<0.041	<0.064	<0.018	0.09	46.82	1.31	100.28
TS-265	171	WBA	chl	A	12.03	11.86	<0.012	<0.031	<0.016	11.11	16.50	<0.037	0.14	0.04	<0.029	0.44	<0.039	<0.064	<0.018	0.12	46.81	1.31	100.36
TS-265	172	WBA	wm	A	21.34	18.90	<0.012	0.50	8.20	0.47	1.71	0.10	<0.056	0.08	<0.028	<0.031	<0.044	0.27	<0.017	0.06	47.88	0.50	99.99
TS-265	173	WBA	chl	A	11.85	12.31	<0.012	<0.037	0.02	10.53	16.53	0.05	0.10	0.05	<0.028	0.34	<0.039	<0.068	<0.016	0.08	46.66	1.31	99.83
TS-265	174	WBA	chl	A	11.83	12.38	<0.011	<0.033	<0.017	10.69	16.69	0.06	0.12	<0.031	<0.027	0.34	<0.042	<0.067	<0.020	0.07	46.84	1.31	100.33
TS-265	175	WBA	chl	A	11.95	12.54	<0.012	<0.030	<0.017	10.51	16.72	0.05	0.10	<0.028	<0.030	0.37	<0.042	<0.062	<0.018	<0.052	47.03	1.31	100.58
TS-265	176	WBA	wm	R	20.85	18.92	<0.012	0.47	7.56	1.00	2.47	0.12	<0.057	0.05	<0.028	<0.030	<0.047	0.33	0.03	<0.048	47.76	0.50	100.07
TS-265	177	WBA	chl	R	12.17	12.70	<0.011	<0.031	0.26	10.48	16.08	0.08	0.12	0.03	<0.031	0.34	<0.041	<0.065	0.03	<0.050	47.30	1.31	100.90
TS-265	178	WBA	chl	A	11.90	12.24	0.02	<0.027	<0.018	10.77	16.35	<0.036	0.12	<0.028	<0.030	0.33	<0.045	<0.069	<0.017	<0.049	46.76	1.31	99.81
TS-265	179	WBA	chl	A	11.94	12.26	<0.012	<0.033	0.02	10.75	16.50	0.05	0.06	<0.033	<0.031	0.40	<0.043	<0.067	<0.019	0.07	46.83	1.31	100.19
TS-265	180	WBA	chl	A	11.83	12.60	<0.011	<0.031	0.06	10.48	16.35	<0.037	0.13	<0.030	<0.030	0.33	<0.038	0.06	<0.018	<0.050	46.83	1.31	99.98
TS-394	181	WBA	chl	R	12.67	11.73	0.03	0.20	0.52	8.36	17.99	0.04	0.19	0.04	<0.03	0.31	<0.04	0.07	<0.02	<0.05	46.19	1.30	99.63
TS-394	182	WBA	cb	R	0.85	-	35.76	-	-	0.16	0.61	-	<0.06	-	-	0.72	<0.04	<0.08	-	-	48.41	-	98.77
TS-394	183	WBA	cb	R	0.04	-	35.90	-	-	0.36	0.95	-	<0.06	-	-	1.19	<0.03	<0.06	-	-	47.52	-	98.06
TS-394	184	WBA	chl	A	11.62	11.56	0.03	0.06	0.02	9.03	19.67	0.04	0.18	0.04	<0.03	0.32	<0.04	<0.08	<0.02	<0.05	45.48	1.28	99.33
TS-394	185	WBA	chl	A	11.44	11.73	<0.01	<0.03	0.02	8.86	19.53	0.06	0.16	<0.03	<0.03	0.36	<0.04	<0.07	<0.02	<0.05	45.27	1.28	98.73
TS-394	186	WBA	chl	A	11.52	11.69	<0.01	<0.04	<0.02	8.91	19.81	0.07	0.21	0.05	<0.03	0.32	<0.04	<0.07	0.02	0.08	45.38	1.28	99.34
TS-394	187*	WBA	chl	A	11.65	11.74	<0.01	<0.04	0.06	9.03	19.70	<0.04	0.21	<0.03	<0.03	0.30	<0.04	<0.07	<0.02	<0.05	45.63	1.28	99.61
TS-394	188	WBA	wm	R	20.04	16.99	<0.01	0.29	7.34	1.44	4.22	0.14	<0.06	0.06	<0.03	<0.03	<0.04	0.33	<0.02	<0.05	45.77	0.49	97.11
TS-394	189	WBA	wm	A	21.15	17.26	<0.01	0.34	8.22	0.57	2.75	0.22	<0.06	0.10	<0.03	0.04	<0.05	0.44	<0.02	0.13	46.57	0.50	98.29
TS-394	190	WBA	wm	R	20.78	17.00	<0.01	0.37	8.10	0.55	2.95	0.17	<0.06	0.08	<0.03	<0.03	<0.04	0.38	<0.02	0.06	45.91	0.50	96.84
TS-394	191	WBA	chl	R	11.79	11.64	<0.01	<0.04	0.14	8.88	19.57	0.05	0.17	<0.03	<0.03	0.31	<0.04	<0.06	0.02	0.08	45.58	1.28	99.51
TS-394	192	WBA	chl	A	11.68	11.79	<0.01	<0.03	0.15	8.88	19.20	<0.04	0.18	<0.03	<0.03	0.31	<0.04	<0.07	<0.02	<0.05	45.56	1.29	99.04

Table E.1 Continued.

Sample	Analysis Number	Area	Min.	Note	Si wt %	Al wt %	Ca wt %	Na wt %	K wt %	Mg wt %	Fe wt %	Ti wt %	Zn wt %	V wt %	Cr wt %	Mn wt %	Sr wt %	Ba wt %	Cl wt %	F wt %	O wt %	H wt %	Total wt %
TS-394	193	WBA	chl	A	11.64	11.62	<0.01	<0.04	0.02	9.06	19.52	0.04	0.11	<0.03	<0.03	0.31	<0.05	<0.07	<0.02	<0.05	45.50	1.28	99.10
TS-394	194	WBA	chl	A	11.60	11.60	<0.01	<0.04	0.05	9.12	19.30	<0.04	0.14	<0.03	<0.03	0.29	<0.04	<0.07	<0.02	<0.06	45.44	1.29	98.82
TS-394	195	WBA	wm	A	20.94	18.08	<0.01	0.37	8.25	0.57	2.38	0.12	<0.06	0.06	<0.03	<0.03	<0.04	0.40	<0.02	0.07	46.89	0.50	98.63
TS-394	196	WBA	wm	A	21.00	17.78	<0.01	0.36	8.31	0.47	2.77	0.19	<0.06	0.05	<0.03	<0.03	<0.05	0.34	<0.02	<0.05	46.80	0.50	98.56
TS-394	197	WBA	wm	A	21.02	17.77	<0.01	0.32	8.28	0.49	2.79	0.17	<0.06	0.08	<0.03	<0.03	<0.04	0.37	<0.02	0.07	46.82	0.50	98.68
TS-394	198	WBA	wm	A	21.03	17.98	<0.01	0.32	8.36	0.45	2.40	0.18	<0.06	0.06	<0.03	<0.03	<0.05	0.36	<0.02	0.07	46.88	0.50	98.58
TS-394	199	WBA	cb	A	<0.02	-	35.72	-	-	0.39	1.10	-	<0.06	-	-	1.25	0.07	<0.07	-	-	47.48	-	98.12
TS-394	200	WBA	cb	A	<0.02	-	35.91	-	-	0.37	1.04	-	<0.06	-	-	1.40	<0.03	<0.08	-	-	47.51	-	98.32
TS-394	201	WBA	cb	R	<0.02	-	35.69	-	-	0.37	1.03	-	<0.06	-	-	1.27	0.05	<0.06	-	-	47.45	-	97.97
TS-394	202	WBA	wm	R	20.65	17.03	<0.01	0.31	8.26	0.53	2.51	0.16	<0.06	0.09	<0.03	<0.03	<0.05	0.35	<0.02	0.10	45.65	0.50	96.14
TS-394	203	WBA	wm	R	20.81	17.32	<0.01	0.39	8.26	0.42	2.45	0.08	<0.06	0.09	<0.03	<0.03	<0.04	0.38	<0.02	0.10	45.97	0.50	96.76
TS-394	204	WBA	wm	R	21.06	17.28	0.01	0.34	8.30	0.45	2.23	0.10	<0.05	0.05	<0.03	<0.03	<0.04	0.42	<0.02	0.06	46.21	0.50	97.00
TS-394	205	WBA	chl	A	11.41	11.27	0.03	<0.03	<0.02	8.88	19.69	<0.04	0.17	0.06	<0.03	0.32	<0.05	<0.07	<0.02	0.06	44.84	1.28	98.01
TS-394	206	WBA	chl	A	11.44	11.41	0.02	0.04	0.09	8.71	19.65	<0.04	0.19	<0.03	<0.03	0.35	<0.04	<0.07	<0.02	0.06	44.90	1.28	98.15
TS-394	207	WBA	chl	A	11.29	11.30	<0.01	<0.03	<0.02	8.86	19.69	<0.04	0.20	<0.03	<0.02	0.34	<0.04	<0.07	<0.02	<0.06	44.71	1.28	97.66
TS-394	208	WBA	wm	A	21.47	18.01	<0.01	0.30	8.24	0.50	2.51	0.21	<0.06	0.09	<0.03	0.04	<0.04	0.42	<0.01	0.06	47.51	0.50	99.85
TS-394	209	WBA	wm	A	21.23	18.04	<0.01	0.37	8.34	0.49	2.32	0.15	0.08	0.07	<0.03	<0.03	<0.05	0.41	<0.02	0.10	47.18	0.50	99.28
TS-394	210	WBA	chl	A	11.49	11.83	0.02	<0.03	0.02	9.01	19.28	0.06	0.12	<0.03	<0.03	0.37	<0.04	<0.06	<0.02	<0.05	45.49	1.29	98.97
TS-394	211	WBA	chl	A	11.48	11.81	0.03	<0.04	<0.02	9.13	19.62	<0.04	0.18	<0.03	<0.03	0.34	<0.04	<0.06	<0.02	<0.05	45.57	1.28	99.43
TS-420	212	WBA	cb	R	4.69	-	18.46	-	-	6.45	4.28	-	0.06	-	-	5.80	<0.04	<0.07	-	-	53.60	-	106.00
TS-420	213	WBA	wm	A	21.42	18.79	<0.01	0.48	8.20	0.61	1.20	0.11	<0.06	0.10	<0.03	<0.03	<0.04	0.30	<0.02	0.08	47.82	0.50	99.62
TS-420	214	WBA	wm	A	21.23	19.40	<0.01	0.62	8.10	0.40	1.01	0.06	<0.06	0.07	<0.03	<0.03	<0.04	0.26	<0.02	0.07	47.95	0.51	99.67
TS-420	215	WBA	cb	A	<0.02	-	20.48	-	-	7.47	4.85	-	<0.06	-	-	5.33	<0.03	<0.07	-	-	48.82	-	99.25
TS-420	216	WBA	wm	A	21.42	18.80	<0.01	0.40	8.02	0.77	1.37	0.09	<0.06	0.05	<0.03	0.04	<0.05	0.33	<0.02	0.09	47.89	0.50	99.76
TS-420	217	WBA	wm	A	20.99	18.35	0.02	0.46	7.81	0.76	1.62	0.08	<0.06	0.05	<0.03	<0.03	<0.05	0.20	<0.02	0.10	47.03	0.50	97.97
TS-420	218	WBA	cb	R	0.10	-	20.52	-	-	6.60	4.42	-	<0.06	-	-	6.38	<0.03	<0.07	-	-	48.48	-	98.78
TS-420	219	WBA	chl	A	11.83	12.35	<0.01	<0.03	0.02	11.72	14.38	0.04	0.11	<0.03	<0.03	0.47	<0.04	<0.06	<0.02	0.09	46.99	1.32	99.32
TS-420	220	WBA	chl	A	12.25	12.34	<0.01	<0.03	0.02	11.70	14.46	<0.04	0.08	<0.03	0.03	0.42	<0.05	<0.07	<0.02	<0.05	47.48	1.33	100.10
TS-420	221	WBA	cb	A	<0.02	-	20.55	-	-	7.12	4.85	-	<0.06	-	-	5.49	<0.04	<0.07	-	-	48.68	-	98.99
TS-420	222	WBA	wm	A	21.37	18.88	<0.01	0.51	8.27	0.49	1.11	0.12	<0.05	0.05	<0.03	<0.03	<0.05	0.26	<0.02	0.05	47.79	0.50	99.41
TS-420	223	WBA	wm	A	21.48	18.69	<0.01	0.43	8.26	0.52	1.10	0.14	<0.06	0.09	<0.03	<0.03	0.07	0.29	<0.02	0.12	47.73	0.50	99.42
TS-420	224	WBA	wm	A	21.76	18.52	<0.01	0.48	8.20	0.68	1.38	0.12	<0.06	0.08	<0.03	<0.03	<0.04	0.30	<0.02	0.13	48.06	0.50	100.21

Table E.1 Continued.

Sample	Analysis Number	Area	Min.	Note	Si wt %	Al wt %	Ca wt %	Na wt %	K wt %	Mg wt %	Fe wt %	Ti wt %	Zn wt %	V wt %	Cr wt %	Mn wt %	Sr wt %	Ba wt %	Cl wt %	F wt %	O wt %	H wt %	Total wt %
TS-420	225	WBA	wm	A	21.66	18.52	<0.01	0.41	8.26	0.60	1.17	0.08	<0.06	0.06	<0.03	<0.03	<0.04	0.30	<0.02	0.11	47.81	0.50	99.50
TS-420	226	WBA	wm	A	21.63	19.00	<0.01	0.57	8.18	0.44	1.11	0.11	<0.06	0.05	<0.03	<0.03	<0.04	0.31	<0.02	0.13	48.10	0.50	100.13
TS-420	227	WBA	chl	A	12.05	12.32	<0.01	<0.03	<0.02	11.59	14.25	0.04	0.07	0.05	<0.03	0.45	<0.04	<0.07	<0.02	0.12	47.07	1.33	99.34
TS-420	228	WBA	chl	A	11.84	12.26	<0.01	<0.04	<0.02	11.51	14.43	<0.04	0.09	0.03	<0.03	0.42	<0.04	<0.07	<0.02	0.06	46.79	1.33	98.76
TS-420	229	WBA	cb	A	<0.02	-	21.17	-	-	7.20	5.44	-	<0.06	-	-	4.68	<0.04	<0.07	-	-	48.81	-	99.57
TS-420	230	WBA	cb	A	0.02	-	20.79	-	-	6.80	5.51	-	<0.06	-	-	5.44	0.04	<0.07	-	-	48.55	-	99.38
TS-420	231	WBA	chl	A	12.11	12.04	0.04	0.03	0.05	11.74	14.20	<0.04	0.06	0.05	<0.03	0.44	<0.04	<0.06	<0.02	0.10	46.99	1.33	99.17
TS-420	232	WBA	chl	A	11.98	12.03	<0.01	<0.03	<0.02	11.49	14.19	0.04	0.09	<0.03	0.03	0.40	<0.05	<0.07	<0.02	0.09	46.69	1.33	98.36
TS-420	233	WBA	chl	A	12.03	12.20	<0.01	<0.03	0.04	11.45	14.49	0.04	<0.06	<0.03	<0.03	0.46	<0.04	<0.07	<0.02	0.14	46.89	1.32	99.06
TS-420	234	WBA	cb	R	11.88	-	0.06	-	-	12.03	13.07	-	0.08	-	-	0.38	<0.04	<0.07	-	-	61.83	-	113.03
TS-420	235	WBA	cb	R	11.49	-	0.08	-	-	12.47	13.21	-	0.13	-	-	0.38	<0.04	<0.06	-	-	61.59	-	112.99
TS-420	236	WBA	wm	A	21.62	18.56	<0.01	0.43	8.26	0.55	1.04	0.10	<0.06	0.07	<0.03	<0.03	<0.05	0.26	<0.02	0.08	47.74	0.51	99.21
TS-420	237	WBA	wm	A	21.55	19.08	0.02	0.65	8.10	0.42	1.04	0.11	<0.06	0.05	<0.03	<0.03	<0.04	0.23	<0.02	0.08	48.08	0.51	99.89
TS-420	238	WBA	chl	A	12.16	12.25	0.01	<0.03	0.05	11.56	14.10	0.04	0.09	<0.03	<0.03	0.40	<0.04	<0.06	<0.02	0.06	47.12	1.33	99.18
TS-420	239	WBA	chl	A	12.05	12.25	0.01	<0.03	<0.02	11.57	14.52	<0.04	0.08	<0.03	<0.03	0.41	<0.05	<0.06	<0.02	0.12	47.02	1.32	99.35
TS-420	240	WBA	chl	A	11.95	12.29	0.02	<0.03	<0.02	11.58	14.29	<0.03	0.11	<0.03	<0.03	0.44	<0.04	<0.06	<0.02	0.09	46.95	1.33	99.06
TS-420	241	WBA	chl	A	11.99	12.27	<0.01	<0.03	<0.02	11.51	14.32	0.03	0.12	0.03	<0.03	0.44	<0.04	<0.06	<0.02	0.09	46.94	1.33	99.07
TS-494	242	WBA	wm	A	21.47	18.90	0.06	0.37	7.96	1.09	1.20	0.13	<0.056	0.04	<0.029	0.05	<0.047	0.27	<0.015	0.13	48.20	0.50	100.36
TS-494	243	WBA	wm	A	21.02	19.32	0.05	0.42	7.68	0.87	1.29	0.13	<0.053	0.06	<0.030	0.04	<0.044	0.29	<0.017	0.07	47.95	0.50	99.68
TS-494	244	WBA	cb	A	<0.02	-	20.36	-	-	8.39	4.21	-	<0.06	-	-	4.29	0.05	<0.06	-	-	49.30	-	99.05
TS-494	245	WBA	cb	A	0.02	-	20.71	-	-	8.11	4.03	-	<0.06	-	-	5.00	0.06	<0.06	-	-	49.22	-	99.53
TS-494	246	WBA	cb	A	0.02	-	20.85	-	-	7.82	4.05	-	<0.06	-	-	5.35	<0.03	<0.06	-	-	49.08	-	99.50
TS-494	247	WBA	cb	A	<0.02	-	20.55	-	-	8.28	4.54	-	<0.06	-	-	4.47	<0.04	<0.07	-	-	49.27	-	99.50
TS-494	248	WBA	cb	A	<0.02	-	20.19	-	-	8.52	4.60	-	<0.06	-	-	4.52	0.05	<0.06	-	-	49.31	-	99.57
TS-494	249	WBA	cb	A	0.02	-	20.01	-	-	8.65	4.64	-	<0.06	-	-	4.47	0.05	<0.07	-	-	49.40	-	99.65
TS-494	250	WBA	cb	R	2.70	-	17.65	-	-	7.37	4.08	-	<0.06	-	-	4.17	<0.04	<0.07	-	-	51.60	-	100.42
TS-494	251	WBA	wm	R	20.58	18.16	0.02	0.36	6.82	2.42	2.59	0.07	<0.054	<0.031	<0.027	0.10	<0.043	0.24	0.02	<0.051	47.54	0.50	99.40
TS-494	252	WBA	wm	A	21.73	19.17	0.04	0.43	8.12	0.59	0.86	0.13	<0.058	<0.030	<0.028	<0.032	<0.047	0.36	0.02	<0.048	48.38	0.51	100.32
TS-494	253	WBA	wm	A	21.74	19.36	0.03	0.46	6.58	0.49	0.86	0.17	0.06	0.04	<0.029	<0.030	<0.049	0.30	<0.018	0.06	48.30	0.51	98.97
TS-494	254	WBA	cb	R	0.27	-	21.24	-	-	6.00	3.31	-	<0.06	-	-	7.70	<0.03	0.06	-	-	48.48	-	99.27
TS-494	255	WBA	cb	A	<0.02	-	20.52	-	-	8.45	4.33	-	<0.06	-	-	4.31	<0.04	<0.06	-	-	49.35	-	99.38
TS-494	256	WBA	chl	R	12.71	12.42	0.01	0.03	0.33	12.53	12.07	<0.033	0.13	<0.027	<0.031	0.46	<0.039	0.07	<0.019	0.11	48.11	1.34	100.34

Table E.1 Continued.

Sample	Analysis Number	Area	Min.	Note	Si wt %	Al wt %	Ca wt %	Na wt %	K wt %	Mg wt %	Fe wt %	Ti wt %	Zn wt %	V wt %	Cr wt %	Mn wt %	Sr wt %	Ba wt %	Cl wt %	F wt %	O wt %	H wt %	Total wt %
TS-494	257	WBA	wm	A	21.59	18.83	<0.012	0.38	7.91	0.95	1.09	0.13	<0.054	<0.031	<0.027	0.04	<0.042	0.32	<0.019	0.07	48.18	0.51	100.00
TS-494	258	WBA	cb	A	0.02	-	20.74	-	-	7.98	3.90	-	<0.06	-	-	5.04	<0.04	<0.06	-	-	49.15	-	99.22
TS-494	259	WBA	cb	R	0.08	-	20.49	-	-	8.50	4.72	-	<0.06	-	-	4.18	<0.03	<0.07	-	-	49.48	-	99.85
TS-494	260	WBA	chl	R	12.42	12.45	0.02	0.06	0.23	12.54	11.99	<0.039	0.10	<0.027	<0.030	0.42	<0.042	<0.069	0.04	0.15	47.73	1.34	99.50
TS-494	261	WBA	chl	A	12.39	12.46	<0.011	0.03	0.05	12.83	12.55	<0.035	0.11	<0.030	<0.031	0.40	<0.034	<0.070	0.03	0.08	48.00	1.34	100.26
TS-494	262	WBA	cb	A	<0.02	-	20.63	-	-	8.12	4.83	-	0.07	-	-	4.52	0.05	<0.07	-	-	49.21	-	99.77
TS-494	263	WBA	wm	A	21.40	19.15	<0.012	0.48	8.21	0.51	0.91	0.04	<0.059	0.04	0.03	<0.029	<0.041	0.30	<0.016	<0.048	47.94	0.51	99.52
TS-494	264	WBA	wm	A	21.39	18.96	0.03	0.42	7.96	0.93	1.29	0.14	<0.059	0.05	0.03	0.03	<0.044	0.32	<0.018	0.06	48.15	0.50	100.27
TS-494	265	WBA	cb	A	<0.02	-	21.26	-	-	5.80	3.21	-	<0.06	-	-	8.39	0.09	<0.07	-	-	48.08	-	98.98
TS-494	266	WBA	cb	A	<0.02	-	20.56	-	-	7.61	3.93	-	<0.06	-	-	5.74	<0.04	<0.06	-	-	48.91	-	99.10
TS-494	267	WBA	cb	A	0.04	-	21.32	-	-	8.49	3.74	-	0.09	-	-	3.94	0.04	<0.07	-	-	49.55	-	99.66
TS-494	268	WBA	cb	A	0.03	-	21.21	-	-	8.70	3.82	-	0.08	-	-	3.58	0.07	<0.06	-	-	49.61	-	99.56
TS-494	269	WBA	chl	R	13.06	13.12	<0.012	0.07	0.78	11.69	11.29	<0.036	0.12	0.03	<0.029	0.36	<0.041	<0.067	0.02	<0.054	48.53	1.35	100.42
TS-496	270	WBA	chl	R	11.70	12.42	<0.012	0.05	<0.017	10.30	16.90	<0.037	0.25	<0.030	<0.029	0.47	<0.043	<0.070	<0.018	0.09	46.53	1.30	100.01
TS-496	271	WBA	chl	R	11.61	12.23	0.01	<0.032	<0.016	10.05	16.81	<0.035	0.17	<0.030	<0.031	0.54	<0.041	<0.068	0.02	0.11	46.05	1.30	98.91
TS-496	272	WBA	chl	R	11.73	12.22	<0.012	0.06	<0.016	10.35	16.62	0.04	0.21	<0.028	<0.025	0.46	<0.039	<0.076	<0.021	<0.054	46.42	1.31	99.41
TS-496	273	WBA	chl	R	11.69	12.20	0.03	<0.034	<0.016	10.27	16.54	<0.034	0.21	0.05	<0.030	0.53	<0.045	<0.064	0.02	0.06	46.25	1.31	99.15
TS-496	274	WBA	cb	A	0.03	-	19.92	-	-	6.59	5.84	-	<0.06	-	-	6.63	<0.03	<0.06	-	-	48.28	-	99.43
TS-496	275	WBA	cb	A	<0.02	-	19.94	-	-	6.68	6.02	-	<0.06	-	-	6.54	0.06	<0.07	-	-	48.32	-	99.68
TS-496	276	WBA	cb	A	0.03	-	19.79	-	-	6.45	5.46	-	0.08	-	-	7.07	<0.04	<0.07	-	-	48.21	-	99.24
TS-496	277	WBA	cb	R	0.34	-	20.28	-	-	6.02	5.61	-	<0.06	-	-	6.61	<0.04	<0.06	-	-	48.41	-	99.43
TS-496	278	WBA	cb	A	0.04	-	19.87	-	-	6.33	5.73	-	<0.06	-	-	7.22	<0.04	<0.06	-	-	48.16	-	99.47
TS-496	279	WBA	cb	R	0.35	-	20.28	-	-	4.70	4.52	-	<0.06	-	-	10.31	<0.04	<0.07	-	-	47.76	-	99.89
TS-496	280	WBA	chl	R	11.85	12.41	0.02	0.04	0.13	10.15	16.55	<0.037	0.22	0.03	<0.027	0.48	<0.036	<0.068	<0.018	0.08	46.57	1.31	99.85
TS-496	281	WBA	chl	R	12.61	11.80	0.03	0.08	0.33	10.34	15.90	<0.036	0.16	<0.031	<0.027	0.46	<0.040	<0.060	0.04	0.13	46.87	1.31	100.06
TS-496	282	WBA	chl	A	12.08	12.04	<0.011	<0.032	0.02	10.65	16.82	<0.033	0.17	<0.030	<0.030	0.50	<0.044	<0.069	<0.017	0.08	46.84	1.30	100.53
TS-496	283	WBA	chl	R	11.98	12.35	0.02	0.05	0.03	10.30	16.66	<0.034	0.15	0.06	<0.028	0.47	<0.048	<0.057	<0.018	<0.055	46.80	1.31	100.18
TS-496	284	WBA	wm	A	21.33	18.91	<0.012	0.47	8.11	0.40	1.41	0.12	<0.055	0.10	<0.027	<0.030	<0.045	0.44	0.02	0.08	47.76	0.50	99.66
TS-496	285	WBA	wm	A	21.33	19.15	<0.012	0.54	7.94	0.42	1.32	0.05	<0.057	0.08	<0.030	<0.033	<0.045	0.37	0.02	0.09	47.86	0.50	99.68
TS-496	286	WBA	wm	A	21.68	18.63	0.02	0.41	8.03	0.51	1.38	0.13	<0.055	0.12	<0.028	0.04	<0.048	0.38	<0.015	0.09	47.95	0.50	99.87
TS-496	287	WBA	chl	R	11.18	11.75	0.02	0.04	0.09	9.70	16.60	<0.032	0.29	<0.031	<0.027	0.58	<0.038	<0.062	0.02	0.08	44.93	1.30	96.58
TS-496	288	WBA	chl	R	11.62	11.91	0.02	<0.033	<0.016	10.23	16.84	0.03	0.70	0.03	<0.028	0.58	<0.043	<0.056	<0.019	0.11	46.03	1.30	99.41

Table E.1 Continued.

Sample	Analysis Number	Area	Min.	Note	Si wt %	Al wt %	Ca wt %	Na wt %	K wt %	Mg wt %	Fe wt %	Ti wt %	Zn wt %	V wt %	Cr wt %	Mn wt %	Sr wt %	Ba wt %	Cl wt %	F wt %	O wt %	H wt %	Total wt %
TS-496	289	WBA	chl	R	11.71	12.06	0.05	0.04	0.02	10.11	16.89	<0.034	0.47	0.04	<0.025	0.56	<0.044	<0.068	0.02	0.09	46.18	1.30	99.53
TS-496	290	WBA	chl	A	11.80	12.11	<0.012	0.04	0.03	10.12	16.50	0.04	0.21	0.05	<0.030	0.57	<0.042	<0.059	0.02	0.07	46.21	1.31	99.06
TS-496	291	WBA	chl	A	11.81	12.15	<0.012	0.04	0.03	10.44	17.01	<0.037	0.21	<0.031	<0.031	0.60	<0.045	<0.071	<0.019	0.09	46.53	1.30	100.23
TS-496	292	WBA	cb	R	0.39	-	19.79	-	-	5.72	5.20	-	<0.06	-	-	8.29	0.06	<0.06	-	-	48.24	-	99.79
TS-496	293	WBA	cb	R	0.03	-	19.62	-	-	6.57	5.90	-	<0.06	-	-	6.60	0.05	<0.07	-	-	48.23	-	99.17
TS-496	294	WBA	cb	A	<0.02	-	19.76	-	-	6.54	5.75	-	<0.06	-	-	6.93	0.04	<0.06	-	-	48.22	-	99.39
TS-496	295	WBA	cb	A	0.04	-	20.11	-	-	6.80	6.49	-	0.10	-	-	5.64	0.04	<0.07	-	-	48.43	-	99.79
TS-496	296	WBA	chl	R	12.00	12.37	<0.012	<0.033	0.24	10.06	16.21	<0.039	0.13	<0.030	<0.032	0.55	<0.047	<0.070	<0.017	0.06	46.56	1.31	99.48
TS-496	297	WBA	chl	A	12.78	11.45	0.02	<0.036	0.08	11.11	15.79	<0.036	0.15	0.04	<0.030	0.47	<0.032	<0.075	<0.020	0.19	47.15	1.31	100.56
TS-496	298	WBA	wm	A	22.77	17.07	0.01	0.30	7.93	1.16	1.29	0.06	<0.055	0.09	<0.026	<0.028	<0.040	0.35	<0.019	0.20	48.06	0.51	99.80
TS-496	299	WBA	wm	R	21.55	17.47	0.03	0.38	7.96	0.80	1.31	0.07	<0.054	0.06	<0.028	<0.030	<0.045	0.41	<0.019	0.13	46.83	0.50	97.49
TS-496	300	WBA	wm	A	21.31	18.77	<0.012	0.41	8.06	0.58	1.73	0.13	0.06	0.06	<0.026	<0.031	<0.043	0.45	<0.017	0.13	47.77	0.50	99.95
TS-496	301	WBA	wm	A	21.00	18.64	<0.012	0.48	8.03	0.76	1.76	0.07	<0.056	0.04	<0.027	<0.028	<0.042	0.35	<0.019	0.11	47.39	0.50	99.14
TS-552	302	WBA	cb	A	<0.02	-	20.10	-	-	7.15	6.82	-	<0.06	-	-	4.96	0.08	<0.07	-	-	48.59	-	99.88
TS-552	303	WBA	cb	A	0.04	-	19.66	-	-	7.06	6.99	-	<0.06	-	-	4.86	0.10	<0.06	-	-	48.50	-	99.42
TS-552	304	WBA	cb	R	0.10	-	20.81	-	-	7.57	6.54	-	<0.06	-	-	3.41	0.04	<0.07	-	-	49.02	-	99.80
TS-552	305	WBA	cb	R	0.60	-	18.76	-	-	7.23	6.97	-	<0.06	-	-	4.92	0.07	<0.07	-	-	49.13	-	99.97
TS-552	306	WBA	chl	A	11.83	12.66	0.02	<0.03	0.06	10.26	15.63	0.04	0.15	<0.03	<0.03	0.38	<0.04	<0.07	0.02	0.06	46.60	1.32	99.03
TS-552	307	WBA	chl	R	12.13	12.59	<0.01	<0.03	0.27	10.07	15.38	<0.04	0.18	<0.03	<0.03	0.41	<0.04	<0.07	0.02	0.09	46.73	1.32	99.17
TS-552	308	WBA	wm	A	21.48	19.18	<0.01	0.61	8.09	0.41	0.93	0.08	<0.06	<0.03	<0.03	<0.03	<0.05	0.29	<0.02	0.06	48.04	0.51	99.67
TS-552	309	WBA	wm	A	21.57	18.63	<0.01	0.53	8.10	0.51	1.16	0.15	<0.06	<0.03	<0.03	<0.03	<0.05	0.27	<0.02	<0.05	47.81	0.51	99.22
TS-552	310	WBA	chl	A	11.56	12.04	0.01	0.14	<0.02	10.40	16.49	<0.03	0.12	<0.03	0.04	0.41	<0.04	<0.07	0.06	<0.05	46.04	1.31	98.63
TS-552	311	WBA	chl	R	12.72	12.61	0.03	0.06	0.81	9.33	14.83	<0.04	0.12	<0.03	<0.03	0.38	<0.04	<0.07	<0.02	0.09	46.92	1.32	99.24
TS-552	312	WBA	chl	A	11.82	12.12	<0.01	<0.03	<0.01	10.52	16.39	<0.04	0.18	<0.03	<0.03	0.39	<0.04	<0.07	<0.02	0.10	46.39	1.31	99.20
TS-552	313	WBA	chl	A	11.84	11.92	0.02	<0.04	0.03	10.68	16.07	<0.04	0.10	<0.03	<0.03	0.47	<0.04	<0.06	<0.02	<0.06	46.33	1.31	98.78
TS-552	314	WBA	chl	A	11.88	12.15	<0.01	<0.03	0.12	10.41	15.95	<0.03	0.11	<0.03	<0.03	0.45	<0.05	<0.06	<0.02	<0.05	46.38	1.31	98.76
TS-552	315	WBA	cb	A	<0.02	-	20.50	-	-	6.99	6.22	-	0.08	-	-	4.25	0.03	<0.06	-	-	48.56	-	98.91
TS-552	316	WBA	cb	A	<0.02	-	19.80	-	-	8.10	6.23	-	<0.06	-	-	3.22	0.04	<0.07	-	-	49.06	-	98.87
TS-552	317	WBA	cb	A	0.03	-	20.32	-	-	6.89	6.07	-	<0.06	-	-	4.53	0.05	<0.07	-	-	48.51	-	98.69
TS-552	318	WBA	wm	R	20.90	18.48	0.05	0.51	8.19	0.42	1.28	0.12	<0.06	0.05	<0.03	<0.03	<0.05	0.47	<0.02	0.06	46.90	0.50	97.93
TS-552	319	WBA	chl	R	12.48	12.09	0.02	0.30	0.05	10.26	15.69	0.05	0.13	<0.03	<0.03	0.36	<0.04	<0.07	0.03	0.11	46.91	1.32	99.81
TS-552	320	WBA	chl	R	12.23	11.65	0.59	0.21	0.06	9.91	15.16	<0.03	0.11	<0.03	<0.03	0.34	<0.04	<0.07	0.02	0.16	46.00	1.32	97.76

Table E.1 Continued.

Sample	Analysis Number	Area	Min.	Note	Si wt %	Al wt %	Ca wt %	Na wt %	K wt %	Mg wt %	Fe wt %	Ti wt %	Zn wt %	V wt %	Cr wt %	Mn wt %	Sr wt %	Ba wt %	Cl wt %	F wt %	O wt %	H wt %	Total wt %
TS-552	321	WBA	chl	R	12.02	11.84	0.03	<0.04	0.09	10.10	15.58	<0.04	0.15	0.04	<0.03	0.37	<0.05	<0.07	0.03	<0.05	35.50	0.00	85.75
TS-552	322	WBA	cb	A	0.04	-	19.84	-	-	8.23	6.35	-	<0.06	-	-	3.25	0.05	<0.07	-	-	49.16	-	99.31
TS-552	323	WBA	cb	R	0.44	-	19.25	-	-	7.29	6.10	-	<0.06	-	-	4.70	<0.04	<0.06	-	-	49.05	-	99.21
TS-552	324	WBA	wm	A	21.40	19.00	<0.01	0.60	7.98	0.48	1.15	0.09	<0.06	<0.03	<0.03	<0.03	<0.04	0.32	<0.02	0.05	47.87	0.51	99.44
TS-552	325	WBA	wm	A	20.99	18.73	<0.01	0.52	7.81	0.64	1.63	0.11	<0.06	<0.03	<0.03	<0.03	<0.04	0.27	<0.02	<0.05	47.36	0.50	98.59
TS-552	326	WBA	wm	R	20.22	18.25	<0.01	0.51	7.04	1.52	3.00	0.10	<0.06	0.04	<0.03	0.03	<0.05	0.25	<0.02	0.06	46.82	0.50	98.36
TS-683	327	WBA	chl	A	12.15	12.31	<0.01	0.03	0.05	11.62	14.73	<0.04	0.20	<0.03	<0.03	0.35	<0.04	<0.07	<0.02	<0.05	47.32	1.32	100.08
TS-683	328	WBA	wm	A	21.66	18.82	<0.01	0.45	8.01	0.57	1.30	0.05	<0.06	0.06	<0.03	<0.03	<0.04	0.42	<0.02	0.12	48.02	0.50	99.99
TS-683	329	WBA	wm	A	22.28	18.00	0.02	1.11	7.15	0.69	1.47	0.09	0.08	0.05	<0.03	<0.03	<0.04	0.29	<0.02	0.06	48.26	0.51	100.06
TS-683	330	WBA	chl	A	12.00	12.43	<0.01	<0.04	<0.02	11.42	14.83	<0.04	0.20	0.03	<0.03	0.33	<0.04	<0.07	<0.02	<0.05	47.14	1.32	99.70
TS-683	331	WBA	wm	A	21.45	18.98	<0.01	0.47	7.98	0.57	1.66	0.11	<0.06	0.05	<0.03	<0.03	<0.04	0.34	<0.02	<0.05	48.09	0.50	100.21
TS-683	332	WBA	wm	A	21.23	19.17	<0.01	0.60	8.07	0.46	1.33	0.09	<0.06	0.06	<0.03	<0.03	<0.04	0.31	<0.02	0.07	47.88	0.50	99.77
TS-683	333	WBA	wm	A	21.63	19.13	<0.01	0.54	8.02	0.42	1.15	0.15	<0.06	0.05	<0.03	<0.03	<0.05	0.34	<0.02	0.07	48.24	0.51	100.25
TS-683	334	WBA	wm	A	20.90	19.02	<0.01	0.57	7.85	0.45	1.31	0.05	<0.06	0.06	<0.03	<0.03	<0.05	0.28	<0.02	0.09	47.28	0.50	98.39
TS-683	335	WBA	wm	A	21.18	18.83	<0.01	0.54	8.16	0.42	1.16	0.12	<0.06	0.04	<0.03	<0.03	<0.04	0.37	<0.02	0.06	47.45	0.50	98.83
TS-683	336	WBA	chl	A	11.92	12.23	<0.01	<0.04	<0.02	11.58	14.85	0.04	0.20	<0.03	0.03	0.32	<0.04	0.07	<0.02	0.09	46.98	1.32	99.63
TS-683	337	WBA	chl	A	11.90	12.00	<0.01	<0.04	<0.02	11.41	14.57	0.05	0.17	<0.03	<0.03	0.37	<0.04	<0.07	<0.02	0.12	46.56	1.32	98.46
TS-683	338	WBA	chl	A	11.95	12.21	<0.01	<0.03	<0.02	11.53	14.92	<0.04	0.23	<0.03	<0.03	0.34	<0.05	<0.06	<0.02	0.11	46.94	1.32	99.55
TS-683	339	WBA	chl	A	11.99	12.17	0.02	<0.03	0.12	11.31	14.42	0.05	0.18	<0.03	<0.03	0.35	<0.04	<0.06	<0.02	0.09	46.77	1.32	98.80
TS-683	340	WBA	chl	A	12.14	12.01	<0.01	<0.03	<0.02	11.48	14.57	<0.04	0.24	<0.03	<0.03	0.35	<0.05	<0.07	<0.02	0.12	46.90	1.32	99.13
TS-683	341	WBA	chl	R	13.43	12.71	<0.01	0.06	1.05	9.86	13.13	<0.04	0.18	<0.03	<0.03	0.31	<0.04	<0.06	<0.02	0.14	47.80	1.34	100.01
TS-683	342	WBA	wm	A	21.35	18.91	<0.01	0.54	8.10	0.41	1.24	0.11	<0.06	0.05	<0.03	<0.03	<0.05	0.32	<0.02	0.09	47.71	0.50	99.33
TS-683	343	WBA	wm	A	21.97	17.65	0.08	0.36	7.78	0.80	1.16	0.06	<0.06	0.08	<0.03	<0.03	<0.05	0.34	0.02	0.14	47.42	0.51	98.35
TS-683	344	WBA	wm	A	22.28	18.03	<0.01	1.31	7.38	0.41	1.06	0.07	<0.06	0.05	<0.03	<0.03	<0.04	0.39	<0.02	0.11	48.06	0.51	99.66
TS-683	345	WBA	chl	R	11.63	11.91	<0.01	<0.04	0.10	11.15	14.04	<0.04	0.21	0.03	<0.03	0.32	<0.04	<0.07	<0.02	0.14	45.88	1.33	96.73
TS-683	346	WBA	wm	R	21.11	18.13	0.05	0.67	7.94	0.37	1.12	0.08	<0.06	0.08	<0.03	<0.03	<0.05	0.41	0.02	0.16	46.68	0.50	97.32
TS-683	347	WBA	wm	R	20.87	18.62	<0.01	0.57	8.08	0.38	1.25	0.11	<0.05	0.06	<0.03	<0.03	<0.05	0.40	<0.02	0.11	46.89	0.50	97.84
TS-683	348	WBA	wm	R	27.82	13.73	<0.01	0.38	6.06	0.35	0.88	0.05	<0.06	<0.03	<0.03	<0.03	<0.06	0.24	0.02	0.08	49.97	0.52	100.11
TS-683	349	WBA	wm	A	21.49	18.62	<0.01	0.56	8.05	0.39	1.28	0.12	<0.06	0.06	<0.03	<0.03	<0.04	0.31	<0.02	0.07	47.63	0.50	99.09
TS-683	350	WBA	chl	A	12.00	12.02	<0.01	<0.03	0.05	11.35	14.51	0.05	0.13	<0.03	<0.03	0.38	<0.05	<0.06	<0.02	0.11	46.65	1.32	98.57
TS-683	351	WBA	chl	R	13.90	11.32	0.02	<0.03	0.02	10.86	13.96	0.04	0.13	<0.03	<0.03	0.36	<0.04	<0.07	<0.02	0.09	47.85	1.34	99.88
TS-683	352	WBA	wm	A	21.61	18.41	<0.01	0.45	8.02	0.53	1.14	0.10	<0.06	0.08	<0.03	<0.03	<0.05	0.35	<0.02	0.12	47.58	0.51	98.89

Table E.1 Continued.

Sample	Analysis Number	Area	Min.	Note	Si wt %	Al wt %	Ca wt %	Na wt %	K wt %	Mg wt %	Fe wt %	Ti wt %	Zn wt %	V wt %	Cr wt %	Mn wt %	Sr wt %	Ba wt %	Cl wt %	F wt %	O wt %	H wt %	Total wt %
TS-683	353	WBA	wm	A	20.82	18.71	<0.01	0.56	8.13	0.40	1.28	0.08	<0.06	0.05	<0.03	<0.03	<0.04	0.39	<0.02	0.13	46.92	0.50	97.97
TS-683	354	WBA	wm	R	20.96	18.18	<0.01	0.51	8.07	0.42	1.34	0.09	<0.06	0.08	<0.03	<0.03	<0.05	0.32	<0.02	0.13	46.62	0.50	97.22
TS-683	355	WBA	chl	A	11.87	11.90	<0.01	<0.04	0.12	11.18	14.55	<0.03	0.17	<0.03	<0.03	0.37	<0.04	<0.07	<0.02	<0.05	46.32	1.33	97.80
TS-683	356	WBA	chl	A	11.82	12.03	0.02	<0.03	<0.02	11.41	14.40	<0.04	0.17	<0.03	<0.03	0.33	<0.04	<0.07	<0.02	<0.06	46.49	1.33	98.00
TS-683	357	WBA	chl	A	11.85	11.96	0.01	<0.04	<0.01	11.35	14.45	<0.04	0.17	0.04	<0.03	0.35	<0.04	<0.07	0.03	0.06	46.43	1.33	98.02
TS-683	358	WBA	chl	A	12.12	12.18	0.01	<0.04	<0.02	11.42	14.67	<0.04	0.18	<0.03	<0.03	0.34	<0.04	<0.08	0.02	0.10	46.98	1.33	99.35
TS-683	359	WBA	chl	A	12.02	12.09	0.04	<0.04	<0.02	11.44	14.36	<0.04	0.18	<0.03	<0.03	0.37	<0.04	<0.06	<0.02	0.14	46.72	1.32	98.69
TS-683	360	WBA	chl	R	11.83	11.74	<0.01	<0.03	<0.02	11.09	14.79	<0.04	0.19	<0.03	<0.03	0.37	<0.04	<0.07	<0.02	0.11	46.06	1.32	97.50
TS-683	361	WBA	chl	A	11.84	11.78	0.01	<0.03	<0.02	11.41	14.79	<0.04	0.16	<0.03	<0.03	0.35	<0.05	<0.07	<0.02	0.06	46.33	1.32	98.06
TS-683	362	WBA	chl	R	11.86	11.69	<0.01	<0.03	0.09	11.16	14.67	<0.04	0.16	<0.03	<0.03	0.34	<0.04	<0.07	<0.02	0.07	46.11	1.32	97.45
TS-683	363	WBA	wm	R	21.17	18.41	<0.01	0.50	8.09	0.48	0.97	<0.04	0.06	0.04	<0.03	<0.03	<0.04	0.28	<0.02	0.10	46.97	0.51	97.58
TS-683	364	WBA	wm	R	21.27	18.28	0.01	0.56	7.94	0.51	1.07	0.08	<0.06	0.09	<0.03	<0.03	<0.04	0.35	<0.02	0.11	47.06	0.50	97.84
TS-722	365	WBA	cb	A	0.02	-	34.66	-	-	0.31	0.51	-	<0.06	-	-	3.44	0.09	<0.06	-	-	47.28	-	98.34
TS-722	366	WBA	cb	A	<0.02	-	36.46	-	-	0.26	0.43	-	<0.06	-	-	1.97	0.07	<0.07	-	-	47.51	-	98.73
TS-722	367	WBA	cb	A	<0.02	-	35.57	-	-	0.36	0.52	-	<0.06	-	-	2.68	0.06	<0.06	-	-	47.43	-	98.65
TS-722	368	WBA	cb	A	<0.02	-	35.35	-	-	0.39	0.59	-	<0.06	-	-	2.89	0.05	<0.08	-	-	47.43	-	98.73
TS-722	369	WBA	cb	A	<0.02	-	36.90	-	-	0.53	0.13	-	<0.06	-	-	0.85	0.03	<0.06	-	-	47.73	-	98.32
TS-722	370	WBA	cb	A	<0.02	-	36.82	-	-	0.57	0.11	-	<0.06	-	-	0.94	<0.03	<0.07	-	-	47.77	-	98.36
TS-722	371	WBA	wm	A	21.12	17.96	0.17	0.50	8.20	0.44	1.84	0.16	<0.06	0.08	<0.03	<0.03	<0.05	0.38	0.09	0.21	46.81	0.50	98.45
TS-722	372	WBA	chl	R	12.35	12.22	0.03	0.06	0.58	8.99	16.80	0.05	0.18	0.05	<0.03	0.45	<0.04	0.09	0.03	<0.05	46.39	1.30	99.56
TS-722	373	WBA	wm	R	21.01	17.80	0.02	0.35	8.23	0.44	1.97	0.17	<0.06	0.09	<0.03	<0.04	<0.05	0.26	0.03	0.05	46.59	0.50	97.52
TS-722	374	WBA	cb	A	0.02	-	35.24	-	-	0.35	0.87	-	<0.06	-	-	2.44	<0.04	<0.07	-	-	47.40	-	98.38
TS-722	375	WBA	cb	R	<0.02	-	34.67	-	-	0.47	1.06	-	<0.06	-	-	2.62	0.05	<0.07	-	-	47.35	-	98.28
TS-722	376	WBA	cb	R	0.10	-	34.53	-	-	0.40	1.02	-	<0.06	-	-	2.77	0.04	<0.07	-	-	47.41	-	98.35
TS-722	377	WBA	chl	A	11.96	11.63	0.02	<0.04	0.07	9.91	17.30	0.07	0.26	0.04	<0.03	0.55	<0.04	<0.07	<0.02	<0.05	46.08	1.30	99.19
TS-722	378	WBA	chl	R	12.09	12.08	0.04	0.07	0.32	9.40	16.87	<0.04	0.23	0.05	<0.03	0.51	<0.04	<0.06	0.03	<0.06	46.22	1.30	99.22
TS-722	379	WBA	wm	A	21.38	18.02	0.01	0.40	8.30	0.46	1.88	0.15	<0.06	0.09	<0.03	<0.03	<0.04	0.40	<0.02	0.09	47.21	0.50	98.89
TS-722	380	WBA	wm	A	21.20	18.27	0.02	0.45	8.22	0.48	1.73	0.08	<0.06	0.06	<0.03	0.04	<0.04	0.42	<0.02	0.14	47.11	0.50	98.72
TS-722	381	WBA	cb	A	<0.02	-	37.45	-	-	0.03	0.11	-	<0.06	-	-	1.37	<0.03	<0.07	-	-	47.57	-	98.60
TS-722	382	WBA	cb	R	0.27	-	37.34	-	-	0.08	0.18	-	<0.06	-	-	0.46	<0.03	<0.07	-	-	47.89	-	98.39
TS-722	383	WBA	cb	R	0.20	-	37.04	-	-	0.44	0.16	-	<0.06	-	-	0.88	<0.03	<0.06	-	-	47.95	-	98.81
TS-722	384	WBA	chl	R	13.07	11.95	0.04	<0.04	1.03	8.84	15.72	<0.04	0.18	<0.03	<0.03	0.45	<0.04	<0.07	<0.02	<0.06	46.67	1.32	99.26

Table E.1 Continued.

Sample	Analysis Number	Area	Min.	Note	Si wt %	Al wt %	Ca wt %	Na wt %	K wt %	Mg wt %	Fe wt %	Ti wt %	Zn wt %	V wt %	Cr wt %	Mn wt %	Sr wt %	Ba wt %	Cl wt %	F wt %	O wt %	H wt %	Total wt %
TS-722	385	WBA	chl	R	12.38	12.64	0.03	0.05	0.69	8.79	16.59	0.06	0.15	<0.03	0.04	0.41	<0.04	0.07	0.02	<0.05	46.63	1.31	99.85
TS-722	386	WBA	chl	A	11.64	12.05	0.02	<0.04	0.03	9.78	17.79	0.05	0.22	<0.03	<0.03	0.45	<0.04	<0.06	<0.02	0.07	46.03	1.29	99.44
TS-722	387	WBA	chl	R	13.38	12.87	0.02	0.05	1.49	8.15	15.17	0.07	0.22	0.04	<0.03	0.40	<0.04	0.12	<0.02	0.08	47.41	1.32	100.78
TS-722	388	WBA	wm	A	21.60	17.94	<0.01	0.35	8.28	0.49	2.15	0.13	<0.06	0.06	<0.03	<0.03	<0.04	0.45	<0.02	0.06	47.44	0.50	99.46
TS-722	389	WBA	wm	A	21.45	18.29	0.02	0.42	8.15	0.42	1.91	0.17	0.06	0.10	<0.03	<0.03	<0.04	0.42	<0.02	0.11	47.50	0.50	99.53
TS-722	390	WBA	wm	A	21.35	18.15	0.01	0.42	8.15	0.46	1.82	0.08	<0.06	0.06	<0.03	<0.03	<0.05	0.41	<0.02	0.05	47.22	0.50	98.69
TS-722	391	WBA	cb	R	0.68	-	36.98	-	-	0.09	0.27	-	0.14	-	-	0.96	<0.03	<0.06	-	-	48.32	-	99.57
TS-722	392	WBA	cb	R	3.40	-	33.12	-	-	0.11	0.36	-	0.16	-	-	1.23	<0.04	<0.07	-	-	51.05	-	101.96
TS-722	393	WBA	chl	A	11.69	12.28	<0.01	<0.03	0.06	9.66	17.62	<0.04	0.23	0.04	<0.03	0.51	<0.04	<0.06	<0.02	0.06	46.16	1.30	99.62
TS-722	394	WBA	chl	A	11.74	11.68	0.06	0.05	0.03	9.78	17.62	0.04	0.29	<0.03	<0.03	0.56	<0.04	<0.07	0.05	<0.06	45.82	1.30	99.01
TS-722	395	WBA	wm	A	21.32	18.26	<0.01	0.41	8.28	0.46	2.07	0.12	<0.06	0.08	<0.03	<0.03	<0.04	0.44	<0.02	0.07	47.38	0.50	99.38
TS-722	396	WBA	wm	A	21.38	18.13	0.02	0.35	8.20	0.47	2.24	0.12	<0.06	0.09	<0.03	<0.03	<0.05	0.41	<0.02	0.07	47.37	0.50	99.37
TS-788	397	WBA	chl	A	11.88	11.71	0.04	<0.04	<0.02	10.19	16.52	0.05	0.11	0.04	<0.03	0.48	<0.04	<0.06	<0.02	0.10	45.97	1.31	98.41
TS-788	398	WBA	chl	A	12.20	11.12	0.04	<0.05	0.02	10.56	16.41	0.05	0.14	<0.03	<0.03	0.43	<0.04	0.07	0.02	0.10	46.00	1.31	98.47
TS-788	399	WBA	chl	A	12.11	11.66	0.02	<0.03	0.04	10.32	16.40	<0.03	0.10	<0.03	<0.03	0.50	<0.04	<0.07	<0.02	0.17	46.18	1.31	98.83
TS-788	400	WBA	cb	A	0.02	-	20.20	-	-	7.59	7.40	-	<0.06	-	-	2.89	0.04	<0.07	-	-	48.85	-	99.31
TS-788	401	WBA	cb	R	0.77	-	19.74	-	-	7.24	6.27	-	<0.06	-	-	3.98	0.05	<0.06	-	-	49.50	-	99.93
TS-788	402	WBA	cb	A	<0.02	-	20.35	-	-	7.46	6.41	-	<0.06	-	-	3.82	<0.04	<0.06	-	-	48.78	-	99.12
TS-788	403	WBA	chl	A	12.11	11.31	<0.01	<0.04	<0.02	10.70	16.82	<0.04	0.10	0.04	<0.03	0.49	<0.04	<0.07	<0.02	0.07	46.23	1.31	99.17
TS-788	404	WBA	chl	A	12.24	11.31	<0.01	<0.04	<0.02	10.86	16.55	<0.04	0.15	<0.03	<0.03	0.51	<0.04	<0.07	<0.02	0.10	46.39	1.31	99.41
TS-788	405	WBA	cb	A	<0.02	-	20.43	-	-	7.68	7.02	-	<0.06	-	-	2.63	0.06	0.07	-	-	48.90	-	99.13
TS-788	406	WBA	cb	R	0.13	-	20.27	-	-	7.41	6.00	-	<0.06	-	-	4.44	<0.04	0.06	-	-	48.89	-	99.49
TS-788	407	WBA	cb	A	0.02	-	20.18	-	-	7.27	5.98	-	<0.06	-	-	4.63	0.07	<0.07	-	-	48.69	-	99.14
TS-788	408	WBA	chl	A	12.31	11.47	<0.01	<0.03	0.07	10.44	16.75	<0.04	0.20	0.04	<0.02	0.45	<0.04	<0.06	<0.02	0.06	46.47	1.31	99.55
TS-788	409	WBA	chl	A	12.14	11.76	0.07	<0.03	0.11	9.85	16.29	<0.04	0.11	0.03	<0.03	0.41	<0.04	<0.07	<0.02	0.10	46.04	1.31	98.23
TS-788	410	WBA	chl	A	12.31	11.93	0.02	<0.04	0.19	9.81	15.97	<0.04	0.11	0.03	<0.03	0.42	<0.04	<0.07	<0.02	<0.06	46.36	1.32	98.48
TS-788	411	WBA	chl	R	12.58	11.86	0.04	<0.04	0.23	9.82	15.71	<0.04	0.13	<0.03	<0.03	0.39	<0.04	<0.07	<0.02	0.06	46.54	1.32	98.68
TS-788	412	WBA	chl	A	12.15	11.70	0.02	<0.03	0.08	10.06	16.54	<0.04	0.06	0.03	<0.03	0.44	<0.04	<0.06	<0.02	0.09	46.17	1.31	98.64
TS-788	413	WBA	chl	A	11.88	11.58	0.03	<0.04	<0.02	10.01	16.70	0.04	0.16	<0.03	<0.03	0.42	<0.04	<0.07	<0.02	<0.05	45.75	1.31	97.85
TS-788	414	WBA	chl	A	11.79	11.57	0.05	<0.03	<0.02	10.18	16.67	<0.04	0.10	0.04	<0.03	0.45	<0.04	<0.07	<0.02	0.08	45.76	1.31	97.99
TS-788	415	WBA	cb	A	0.02	-	22.31	-	-	5.97	4.45	-	<0.06	-	-	5.55	0.04	<0.07	-	-	48.35	-	98.92
TS-788	416	WBA	cb	A	<0.02	-	22.32	-	-	6.47	3.72	-	<0.06	-	-	5.07	0.06	<0.07	-	-	48.59	-	98.56

Table E.1 Continued.

Sample	Analysis Number	Area	Min.	Note	Si wt %	Al wt %	Ca wt %	Na wt %	K wt %	Mg wt %	Fe wt %	Ti wt %	Zn wt %	V wt %	Cr wt %	Mn wt %	Sr wt %	Ba wt %	Cl wt %	F wt %	O wt %	H wt %	Total wt %
TS-788	417	WBA	cb	R	0.02	-	32.95	-	-	0.18	0.34	-	<0.06	-	-	5.50	0.06	<0.07	-	-	46.94	-	97.98
TS-788	418	WBA	cb	A	<0.02	-	35.05	-	-	0.05	0.20	-	<0.06	-	-	3.71	0.04	<0.07	-	-	47.19	-	98.27
TS-788	419	WBA	wm	A	21.79	18.01	0.05	0.36	7.55	0.71	1.18	0.09	<0.06	0.06	<0.03	<0.03	<0.04	0.42	<0.02	0.12	47.47	0.51	98.32
TS-788	420	WBA	wm	A	22.69	17.72	0.06	0.52	7.11	0.86	0.91	<0.04	<0.06	0.06	<0.03	<0.03	<0.04	0.25	<0.02	0.14	48.19	0.51	99.03
TS-788	421	WBA	wm	A	22.35	17.47	0.08	0.47	7.38	0.80	1.10	0.07	<0.06	0.08	<0.03	<0.03	<0.04	0.38	<0.02	0.18	47.64	0.51	98.51
TS-788	422	WBA	wm	A	22.89	17.27	0.11	0.45	6.80	1.19	1.04	0.06	<0.06	0.06	<0.03	0.04	<0.04	0.25	<0.02	0.14	48.23	0.51	99.04
TS-788	423	WBA	wm	A	22.09	17.18	0.06	0.34	7.80	0.86	1.35	0.10	<0.06	0.04	<0.03	<0.03	<0.05	0.46	<0.02	0.21	47.20	0.50	98.20
TS-788	424	WBA	chl	A	12.63	11.09	<0.01	<0.03	0.02	11.03	16.00	<0.04	0.16	<0.03	<0.03	0.48	<0.04	<0.07	<0.02	0.09	46.68	1.31	99.50
TS-788	425	WBA	chl	A	12.49	11.17	<0.01	<0.04	0.02	10.98	16.44	<0.04	0.16	<0.03	<0.03	0.51	<0.04	<0.06	<0.02	0.08	46.68	1.31	99.84
TS-788	426	WBA	chl	A	12.31	10.75	0.04	0.08	<0.02	11.10	15.73	<0.04	0.13	<0.03	<0.03	0.43	<0.04	<0.07	0.03	0.17	45.95	1.31	98.04
TS-788	427	WBA	chl	A	12.12	11.87	0.02	<0.04	0.06	10.03	16.60	0.06	0.09	0.03	<0.03	0.45	<0.04	<0.07	<0.02	0.09	46.30	1.31	99.04
TS-788	428	WBA	chl	A	12.16	11.79	<0.01	<0.04	0.05	9.98	16.77	<0.03	0.12	0.03	<0.03	0.43	<0.04	<0.06	<0.02	0.07	46.27	1.31	98.98
TS-788	429	WBA	chl	A	11.83	11.76	<0.01	<0.03	0.04	9.91	16.94	0.04	0.07	0.04	<0.03	0.43	<0.04	0.07	<0.02	0.06	45.86	1.31	98.35
TS-788	430	WBA	wm	R	19.53	16.49	0.03	0.29	6.19	2.77	4.92	0.09	<0.06	0.06	<0.03	0.11	<0.04	0.35	0.02	0.14	45.56	0.49	97.05
TS-1180	431	RZN	wm	A	21.21	18.64	0.02	0.36	8.50	0.65	0.96	0.28	<0.06	0.03	<0.03	<0.03	<0.05	0.99	<0.02	0.23	46.27	1.29	99.44
TS-1180	432	RZN	wm	R	20.36	17.71	0.02	0.33	8.49	0.62	0.87	0.14	<0.06	<0.03	<0.03	<0.03	<0.05	0.63	<0.02	0.23	45.90	1.30	96.60
TS-1180	433	RZN	wm	R	19.80	18.08	<0.01	0.28	8.72	0.53	0.85	0.15	<0.05	0.06	<0.03	<0.03	<0.04	0.70	<0.02	0.26	45.66	1.30	96.39
TS-1180	434	RZN	wm	R	19.91	17.70	<0.01	0.35	8.48	0.66	0.78	0.08	<0.06	<0.03	<0.03	<0.03	<0.04	0.70	<0.02	0.24	45.79	1.29	95.99
TS-1180	435	RZN	wm	R	19.77	17.84	<0.01	0.33	8.51	0.65	0.75	0.07	<0.05	<0.03	<0.03	<0.03	<0.05	0.62	<0.02	0.23	46.01	1.29	96.07
TS-1180	436	RZN	wm	R	19.91	17.69	0.02	0.32	8.50	0.58	0.88	0.10	<0.06	0.03	<0.03	<0.03	<0.05	0.75	<0.02	0.18	45.60	1.29	95.85
TS-1180	437	RZN	wm	A	21.28	18.07	0.02	0.24	8.54	0.73	0.95	0.09	<0.05	0.04	<0.03	<0.04	<0.05	0.62	<0.02	0.24	46.11	1.30	98.23
TS-1180	438	RZN	wm	R	20.74	17.92	<0.01	0.33	8.53	0.78	1.00	0.17	<0.06	<0.03	<0.03	<0.03	<0.05	1.08	<0.02	0.27	45.72	1.29	97.83
TS-1180	439	RZN	wm	R	20.49	18.13	0.05	0.35	8.06	0.73	0.97	0.12	<0.05	0.04	<0.03	<0.03	<0.05	1.03	0.03	0.28	45.86	1.29	97.44
TS-1180	440	RZN	cb	A	<0.02	-	21.60	-	-	9.26	3.78	-	<0.05	-	-	1.75	0.08	<0.07	-	-	49.95	-	99.05
TS-1180	441	RZN	cb	A	<0.02	-	21.34	-	-	9.43	3.90	-	<0.05	-	-	1.84	0.07	<0.07	-	-	50.01	-	99.21
TS-1180	442	RZN	wm	A	21.27	18.39	0.04	0.31	8.47	0.69	1.10	0.17	<0.05	0.03	<0.03	0.03	<0.05	0.89	0.03	0.26	46.21	1.30	99.18
TS-1180	443	RZN	wm	A	20.99	18.59	0.01	0.30	8.47	0.75	0.98	0.14	<0.06	<0.03	<0.03	<0.03	<0.05	1.13	0.03	0.25	45.71	1.29	98.64
TS-1180	444	RZN	wm	A	21.22	18.55	0.01	0.34	8.55	0.68	0.76	0.09	<0.06	0.05	<0.03	<0.03	<0.05	0.53	<0.02	0.28	45.04	1.30	97.39
TS-1180	445	RZN	wm	A	20.83	18.23	<0.01	0.31	8.64	0.71	0.83	0.12	<0.06	<0.03	<0.03	<0.03	<0.05	0.85	0.02	0.24	45.33	1.30	97.41
TS-1180	446	RZN	wm	R	20.48	18.27	0.03	0.34	8.68	0.79	0.83	0.15	<0.06	0.03	<0.03	<0.03	<0.05	0.93	<0.02	0.32	43.41	1.34	95.59
TS-1180	447	RZN	wm	R	20.32	18.16	<0.01	0.26	8.92	0.59	0.89	0.09	<0.06	<0.03	<0.03	<0.03	<0.05	0.62	<0.02	0.23	46.43	1.30	97.80
TS-1180	448	RZN	cb	A	<0.02	-	21.49	-	-	9.45	3.55	-	<0.06	-	-	1.95	0.07	<0.07	-	-	50.03	-	99.17

Table E.1 Continued.

Sample	Analysis Number	Area	Min.	Note	Si wt %	Al wt %	Ca wt %	Na wt %	K wt %	Mg wt %	Fe wt %	Ti wt %	Zn wt %	V wt %	Cr wt %	Mn wt %	Sr wt %	Ba wt %	Cl wt %	F wt %	O wt %	H wt %	Total wt %
TS-1180	449	RZN	cb	A	0.02	-	36.80	-	-	0.42	0.26	-	<0.06	-	-	3.91	0.16	<0.07	-	-	47.68	-	101.05
TS-345	450	WBA	wm	R	20.61	17.99	0.08	0.50	7.66	1.03	1.08	0.09	<0.06	0.06	<0.03	<0.03	<0.05	0.18	<0.02	0.15	47.63	0.50	97.57
TS-345	451	WBA	wm	R	19.75	17.45	0.05	0.46	7.28	1.75	1.73	0.10	<0.05	0.08	<0.03	0.04	<0.05	0.22	0.02	0.12	45.88	1.33	96.26
TS-345	452	WBA	cb	A	<0.02	-	37.72	-	-	0.39	0.49	-	<0.06	-	-	1.95	<0.04	<0.08	-	-	47.81	-	100.28
TS-345	453	WBA	cb	A	0.02	-	37.38	-	-	0.62	0.62	-	<0.06	-	-	1.81	0.05	<0.07	-	-	47.88	-	100.32
TS-345	454	WBA	cb	A	<0.02	-	37.74	-	-	0.42	0.53	-	<0.06	-	-	1.66	<0.04	<0.06	-	-	47.83	-	100.13
TS-345	455	WBA	cb	A	0.04	-	37.76	-	-	0.42	0.49	-	<0.06	-	-	1.67	0.08	<0.07	-	-	47.86	-	100.26
TS-345	456	WBA	cb	A	<0.02	-	37.63	-	-	0.35	0.41	-	<0.06	-	-	2.13	<0.04	<0.08	-	-	47.76	-	100.20
TS-345	457	WBA	cb	A	0.02	-	37.57	-	-	0.53	0.51	-	<0.06	-	-	2.52	0.05	<0.07	-	-	47.87	-	100.96
TS-345	458	WBA	cb	A	<0.02	-	38.10	-	-	0.36	0.45	-	<0.06	-	-	2.21	0.06	<0.07	-	-	47.86	-	100.91
TS-345	459	WBA	cb	A	0.03	-	38.10	-	-	0.32	0.43	-	<0.06	-	-	2.30	0.07	<0.08	-	-	47.86	-	100.99
TS-345	460	WBA	cb	A	<0.02	-	37.58	-	-	0.56	0.60	-	<0.06	-	-	1.88	0.04	<0.07	-	-	47.86	-	100.44
TS-345	461	WBA	chl	R	17.27	16.42	<0.01	0.24	4.67	6.22	5.58	0.06	0.07	<0.03	<0.03	0.17	<0.05	0.11	<0.02	0.08	46.68	0.50	98.07
TS-345	462	WBA	chl	R	21.23	19.08	<0.01	0.52	8.69	0.57	0.80	0.12	<0.06	0.03	<0.03	<0.03	<0.04	0.37	<0.02	0.11	46.65	1.32	99.49
TS-345	463	WBA	chl	R	12.03	11.90	<0.01	<0.03	0.02	13.28	10.98	<0.04	<0.06	<0.03	<0.02	0.31	<0.04	<0.06	<0.02	0.24	47.85	1.34	97.94
TS-345	464	WBA	chl	A	11.89	12.23	<0.01	0.04	<0.02	13.11	11.51	<0.04	0.12	<0.03	<0.03	0.35	<0.04	<0.06	<0.02	0.17	47.58	0.51	97.51
TS-345	465	WBA	chl	R	12.16	12.01	0.02	<0.03	<0.02	13.20	11.12	<0.03	0.09	<0.03	<0.03	0.31	<0.05	0.06	<0.02	0.21	46.92	0.50	96.60
TS-345	466	WBA	cb	A	<0.02	-	36.46	-	-	0.18	0.31	-	<0.06	-	-	3.45	0.05	<0.07	-	-	47.48	-	99.82
TS-345	467	WBA	cb	A	<0.02	-	37.04	-	-	0.17	0.31	-	<0.06	-	-	2.99	<0.03	<0.08	-	-	47.58	-	100.00
TS-345	468	WBA	cb	A	<0.02	-	37.13	-	-	0.20	0.31	-	<0.06	-	-	2.96	0.04	0.07	-	-	47.59	-	100.17
TS-345	469	WBA	chl	R	11.95	12.24	<0.01	<0.03	<0.02	13.27	11.08	<0.04	0.11	<0.03	<0.03	0.32	<0.04	<0.06	<0.02	0.12	46.62	0.50	96.20
TS-345	470	WBA	chl	A	12.25	12.01	<0.01	<0.03	<0.02	13.41	11.07	0.06	<0.06	<0.03	<0.03	0.32	<0.04	<0.07	<0.02	0.20	46.32	1.33	96.96
TS-345	471	WBA	chl	A	12.56	12.04	<0.01	<0.03	<0.02	13.56	10.84	0.04	0.10	<0.03	<0.03	0.35	<0.05	<0.07	<0.02	0.21	46.49	1.33	97.51
TS-345	472	WBA	chl	A	12.02	12.13	<0.01	<0.03	<0.02	13.05	11.56	0.04	0.12	<0.03	<0.03	0.40	<0.05	0.08	<0.02	0.16	46.43	1.33	97.33
TS-345	473	WBA	chl	R	11.95	11.98	<0.01	<0.03	<0.02	13.07	11.46	<0.04	0.12	<0.03	<0.03	0.41	<0.04	<0.08	<0.02	0.17	46.98	1.33	97.46
TS-345	474	WBA	chl	R	12.02	11.86	<0.01	<0.03	<0.02	12.98	11.56	<0.03	0.10	<0.03	<0.03	0.43	<0.04	<0.07	<0.02	0.22	46.72	1.32	97.21
TS-345	475	WBA	chl	R	12.02	11.87	<0.01	<0.03	<0.02	13.09	11.36	<0.03	0.10	<0.03	<0.03	0.39	<0.04	<0.06	<0.02	0.14	46.06	1.32	96.35
TS-345	476	WBA	chl	A	12.11	12.16	<0.01	<0.03	<0.02	13.32	11.22	<0.03	0.11	<0.03	<0.03	0.36	<0.04	<0.06	<0.02	0.20	46.33	1.32	97.13
UPB12	477	WBA	cb	A	<0.02	-	39.85	-	-	<0.02	0.04	-	<0.06	-	-	0.06	<0.04	<0.07	-	-	47.92	-	99.88
UPB12	478	WBA	cb	A	<0.02	-	39.71	-	-	<0.02	<0.04	-	<0.06	-	-	0.09	<0.04	<0.07	-	-	47.91	-	99.73
UPB12	479	WBA	chl	R	11.92	10.64	0.04	0.07	0.05	9.66	17.94	<0.04	0.08	<0.03	<0.03	0.33	<0.04	<0.06	0.04	<0.05	45.04	1.30	97.09
UPB12	480	WBA	chl	A	12.13	10.45	0.02	0.06	<0.02	10.05	18.09	<0.04	<0.06	<0.03	<0.03	0.31	<0.05	0.09	0.05	<0.05	45.33	1.30	97.88

Table E.1 Continued.

Sample	Analysis Number	Area	Min.	Note	Si wt %	Al wt %	Ca wt %	Na wt %	K wt %	Mg wt %	Fe wt %	Ti wt %	Zn wt %	V wt %	Cr wt %	Mn wt %	Sr wt %	Ba wt %	Cl wt %	F wt %	O wt %	H wt %	Total wt %
UPB12	481	WBA	chl	R	11.64	9.93	0.01	<0.04	<0.02	9.96	14.21	<0.04	<0.06	0.03	<0.02	0.27	<0.04	<0.06	<0.02	0.09	43.41	1.34	90.88
UPB12	482	WBA	chl	R	12.63	10.95	0.02	0.06	0.03	10.18	18.05	<0.03	<0.06	<0.03	<0.03	0.33	<0.04	<0.07	0.05	<0.05	46.43	1.30	100.02
UPB12	483	WBA	cb	A	<0.02	-	39.55	-	-	<0.02	0.08	-	<0.06	-	-	<0.04	<0.04	<0.06	-	-	47.86	-	99.51
UPB12	484	WBA	cb	A	<0.02	-	39.98	-	-	<0.02	<0.04	-	<0.06	-	-	0.04	<0.03	<0.08	-	-	47.96	-	99.99
UPB12	485	WBA	cb	A	<0.02	-	39.70	-	-	<0.02	0.06	-	<0.06	-	-	0.05	<0.04	<0.07	-	-	47.91	-	99.74
UPB12	486	WBA	chl	R	12.53	10.67	0.08	<0.03	<0.02	10.18	18.91	0.04	<0.06	<0.03	<0.03	0.31	<0.04	<0.08	<0.02	<0.05	46.27	1.29	100.28
UPB12	487	WBA	chl	R	12.32	10.78	0.08	<0.03	<0.02	9.99	18.27	0.05	<0.06	<0.03	<0.03	0.33	<0.04	<0.07	0.03	<0.05	45.90	1.30	99.04
UPB12	488	WBA	cb	A	<0.02	-	39.76	-	-	<0.02	0.15	-	<0.06	-	-	0.07	<0.04	<0.07	-	-	47.89	-	99.87
UPB12	489	WBA	chl	A	12.29	10.49	0.02	<0.03	0.02	10.16	18.31	<0.03	<0.06	<0.03	<0.03	0.31	<0.05	<0.06	<0.02	<0.05	45.66	1.30	98.56
UPB12	490	WBA	chl	A	12.24	10.95	0.02	0.04	<0.02	9.79	18.40	<0.04	<0.06	<0.03	<0.03	0.31	<0.04	<0.06	0.02	<0.05	45.79	1.29	98.86
UPB12	491	WBA	chl	A	12.35	10.64	0.05	<0.03	0.02	10.17	18.61	0.07	0.07	<0.03	<0.03	0.34	<0.04	<0.08	<0.02	<0.05	46.01	1.29	99.63
UPB12	492	WBA	chl	A	12.06	10.79	0.04	0.04	<0.02	9.88	18.75	<0.04	<0.06	0.03	<0.03	0.36	<0.04	<0.06	0.02	<0.05	45.60	1.29	98.86
UPB12	493	WBA	chl	A	12.61	10.43	0.02	<0.03	<0.02	10.29	18.22	0.07	<0.06	<0.03	0.04	0.32	<0.04	<0.07	<0.02	<0.05	46.11	1.30	99.41
UPB12	494	WBA	chl	A	12.20	10.63	0.02	<0.03	<0.02	10.01	18.79	<0.03	0.07	<0.03	<0.03	0.38	<0.04	<0.07	<0.02	<0.05	45.72	1.29	99.11
UPB12	495	WBA	chl	A	12.24	10.70	<0.01	<0.04	<0.02	10.14	18.77	<0.04	0.06	0.03	<0.03	0.33	<0.04	<0.07	<0.02	0.07	45.86	1.29	99.49
UPB12	496	WBA	chl	R	12.71	10.37	<0.01	<0.03	<0.02	10.44	18.25	<0.04	0.07	<0.03	<0.03	0.32	<0.04	<0.06	<0.02	<0.05	46.21	1.30	99.66
UPB12	497	WBA	chl	A	12.16	10.57	<0.01	<0.04	<0.02	10.07	18.89	0.04	0.08	0.04	<0.03	0.35	<0.05	<0.06	<0.02	<0.05	45.71	1.29	99.21

Analysis Number – refers to spot number on BSE images; red = rejected analysis, black = accepted analysis
Area – B, Battle orebody; RZN, Ridge Zone North; TV, Thelwood Valley; WBA, West Block Area
Min. (Mineral) – ap, apatite; cb, carbonate; chl, chlorite; ep, epidote; wm, white mica
Note – R, rejected analysis; A, accepted analysis
*no BSE image

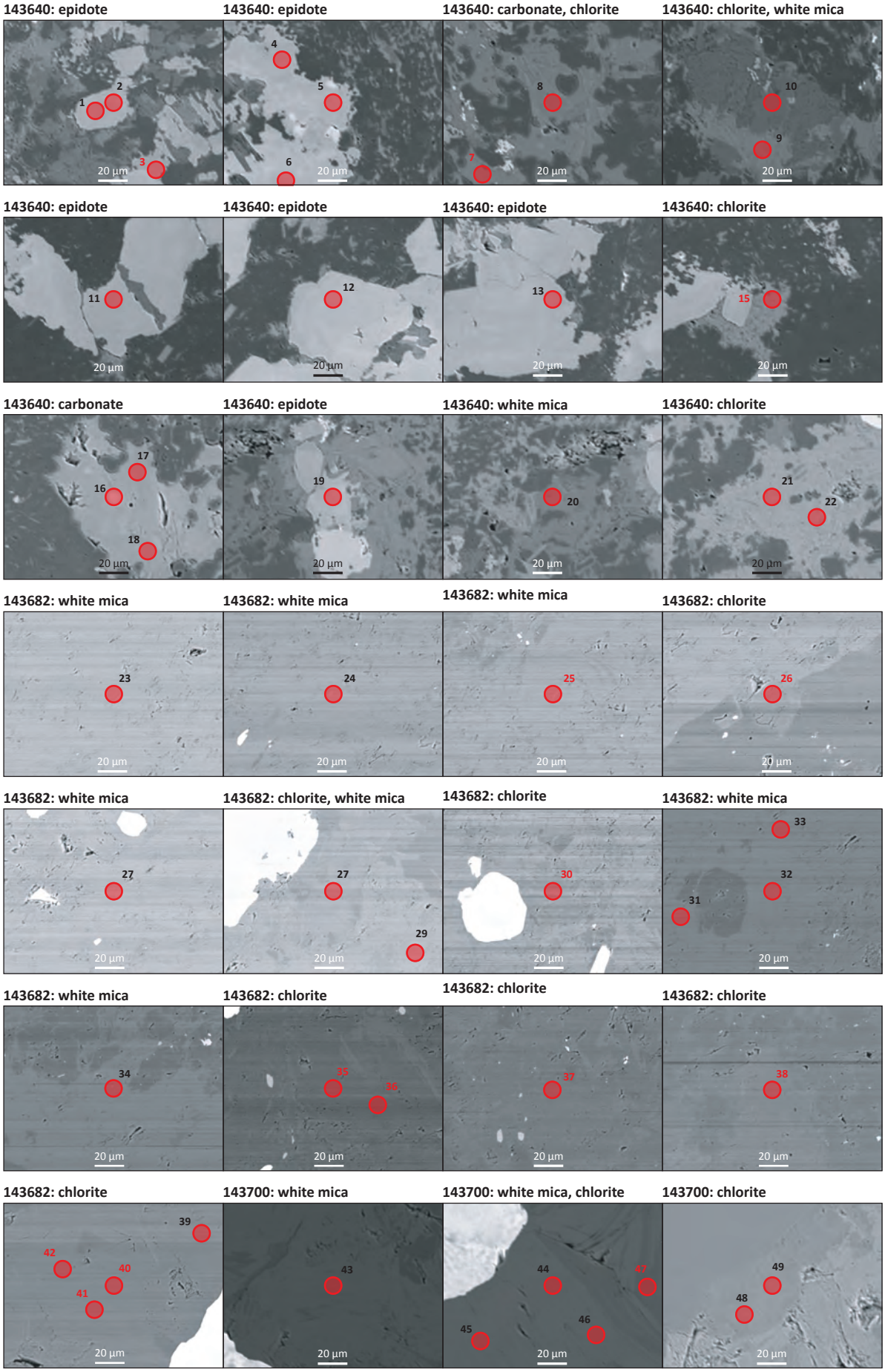

Figure E.2 Summary of electron microprobe analysis numbers 1-49.

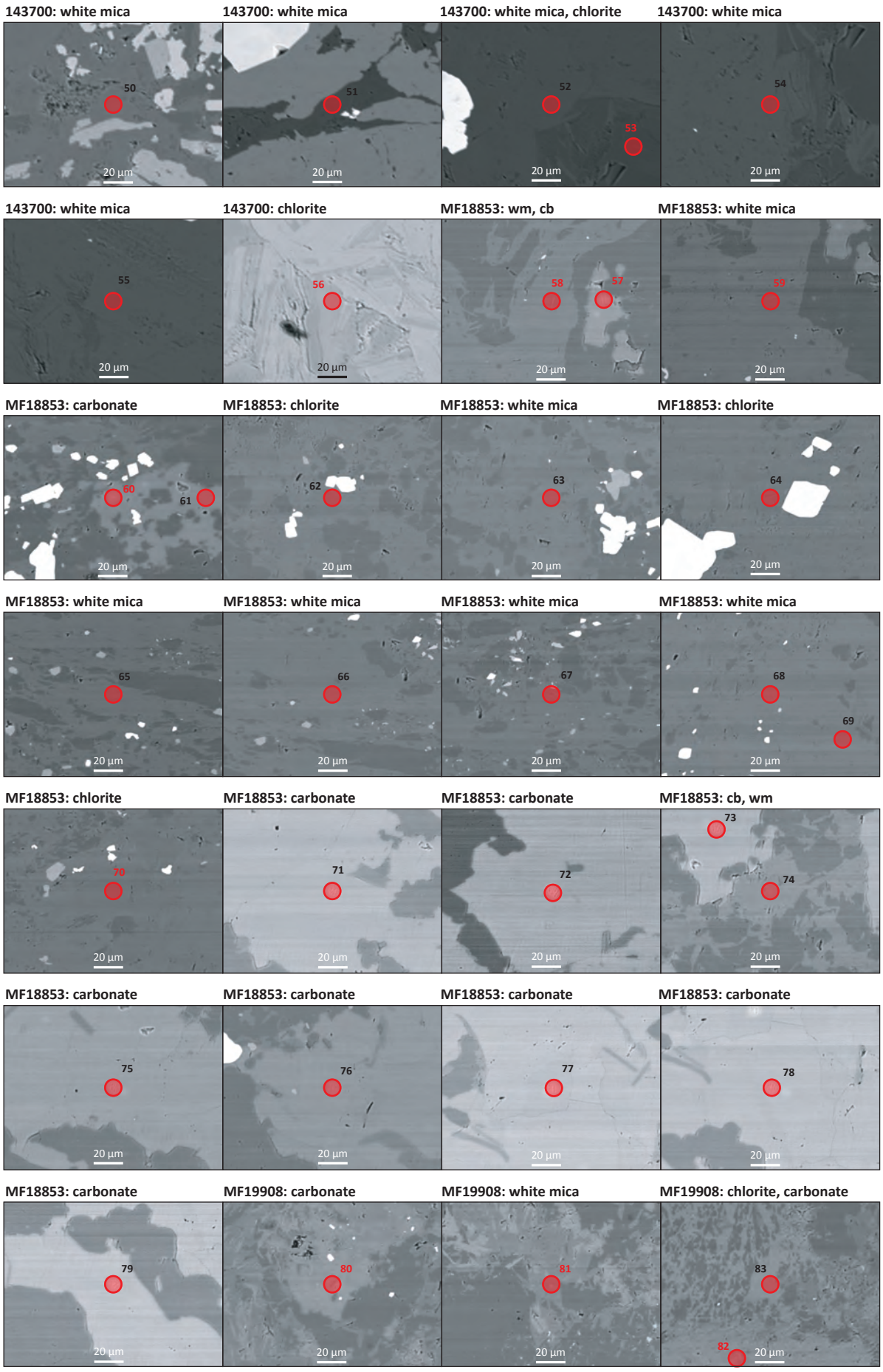

Figure E.3 Summary of electron microprobe analysis numbers 50-83.

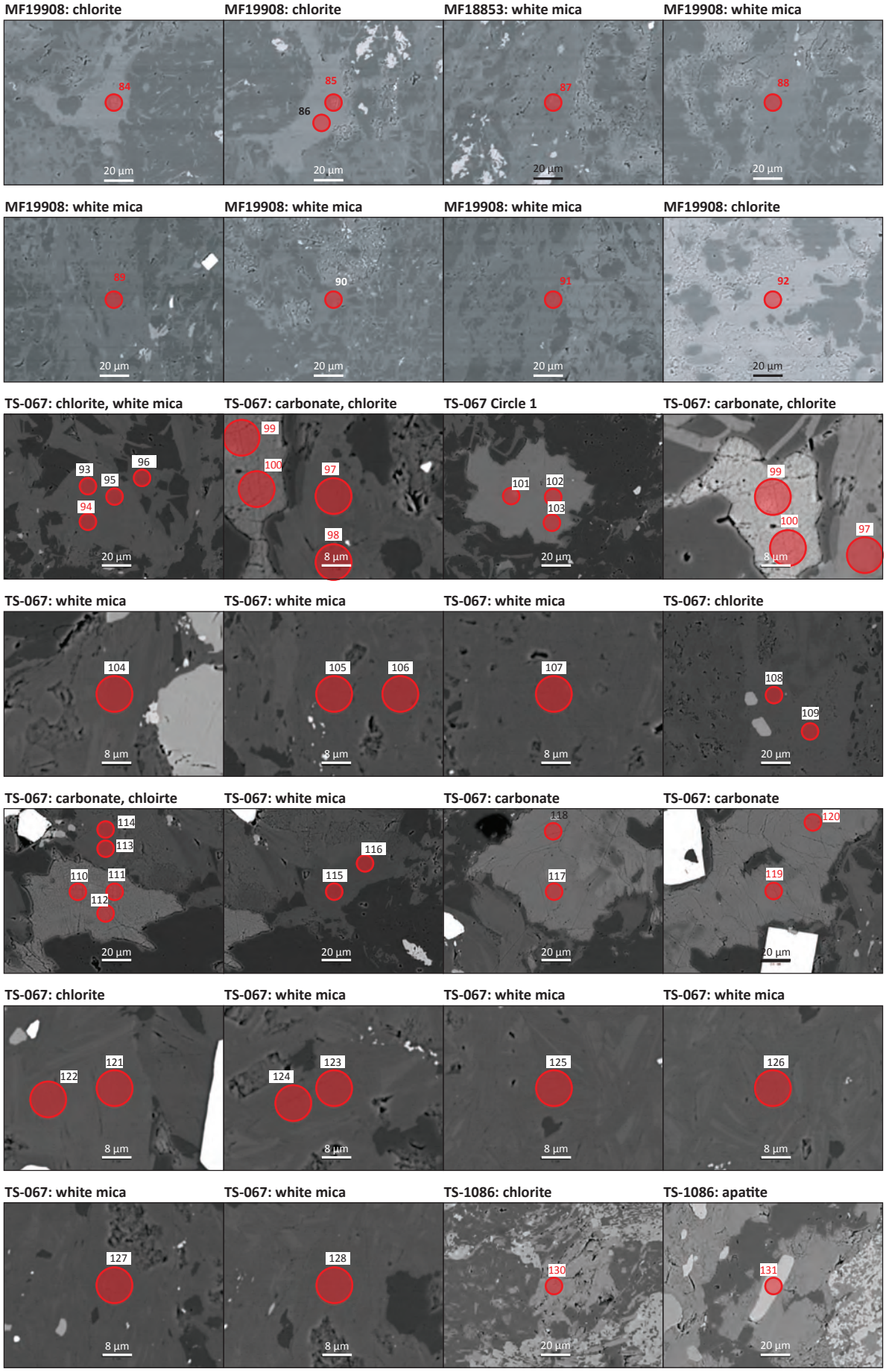

Figure E.4 Summary of electron microprobe analysis numbers 84-131.

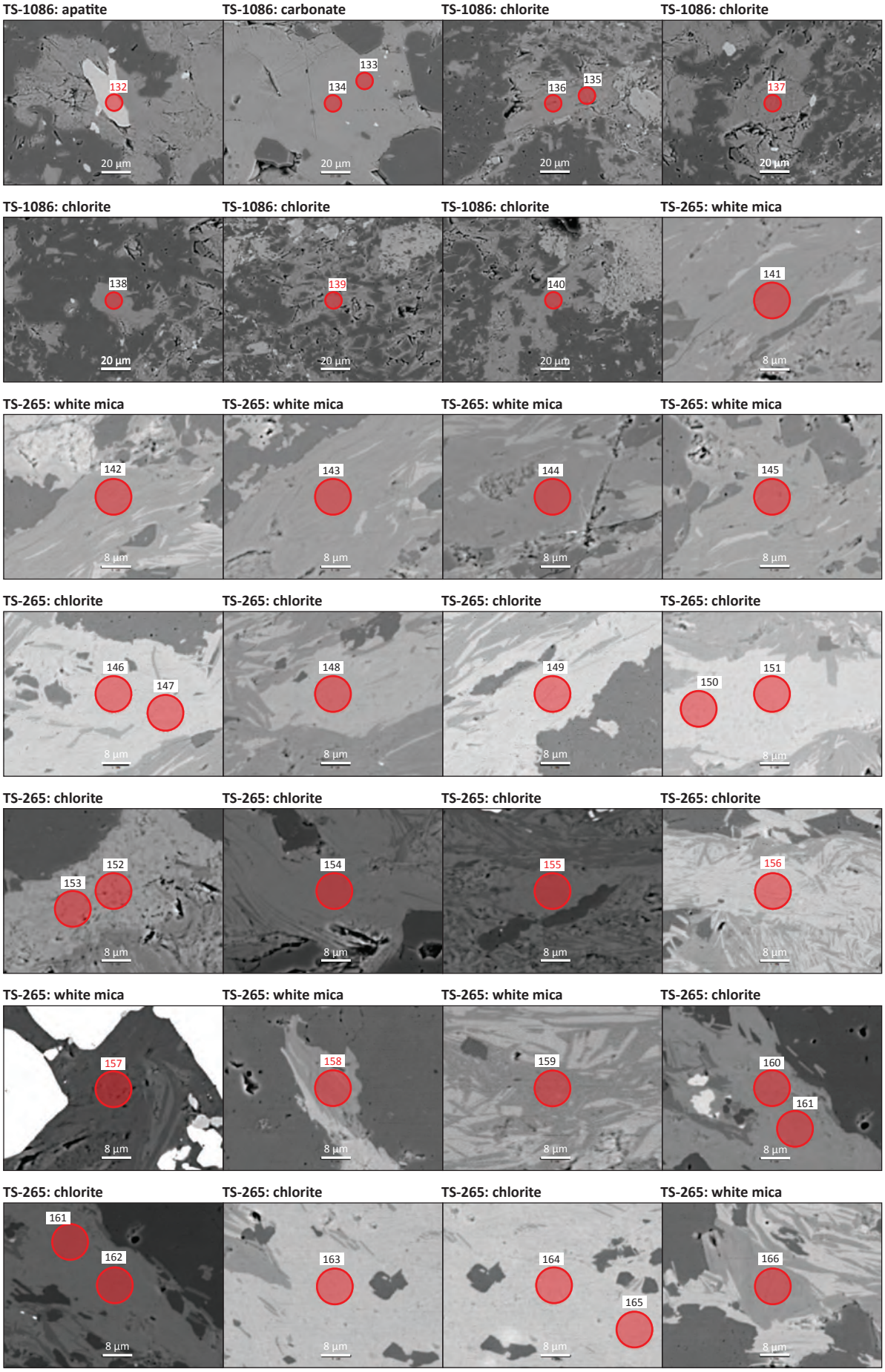

Figure E.5 Summary of electron microprobe analysis numbers 132-166.

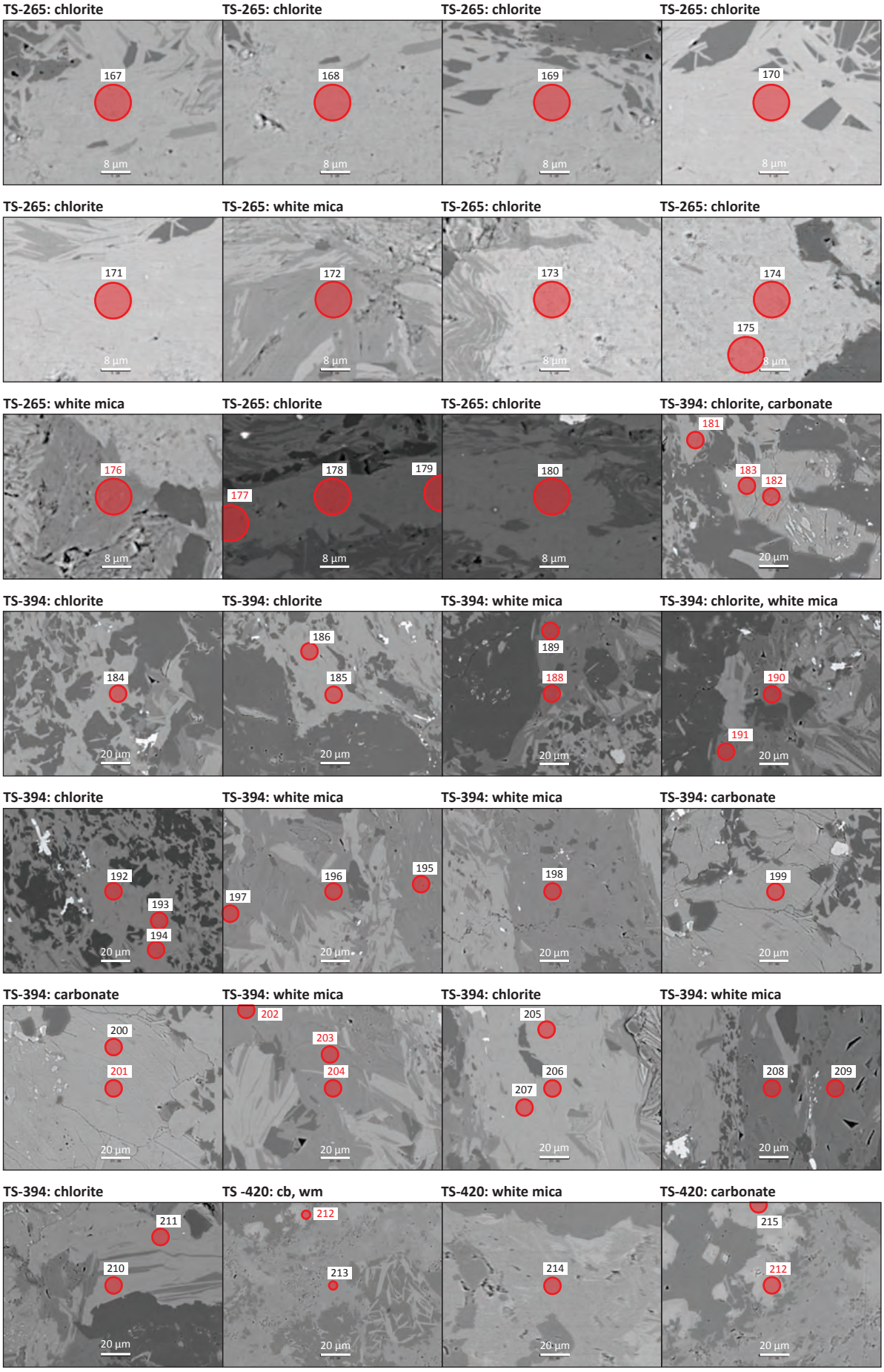

Figure E.6 Summary of electron microprobe analysis numbers 167-215.

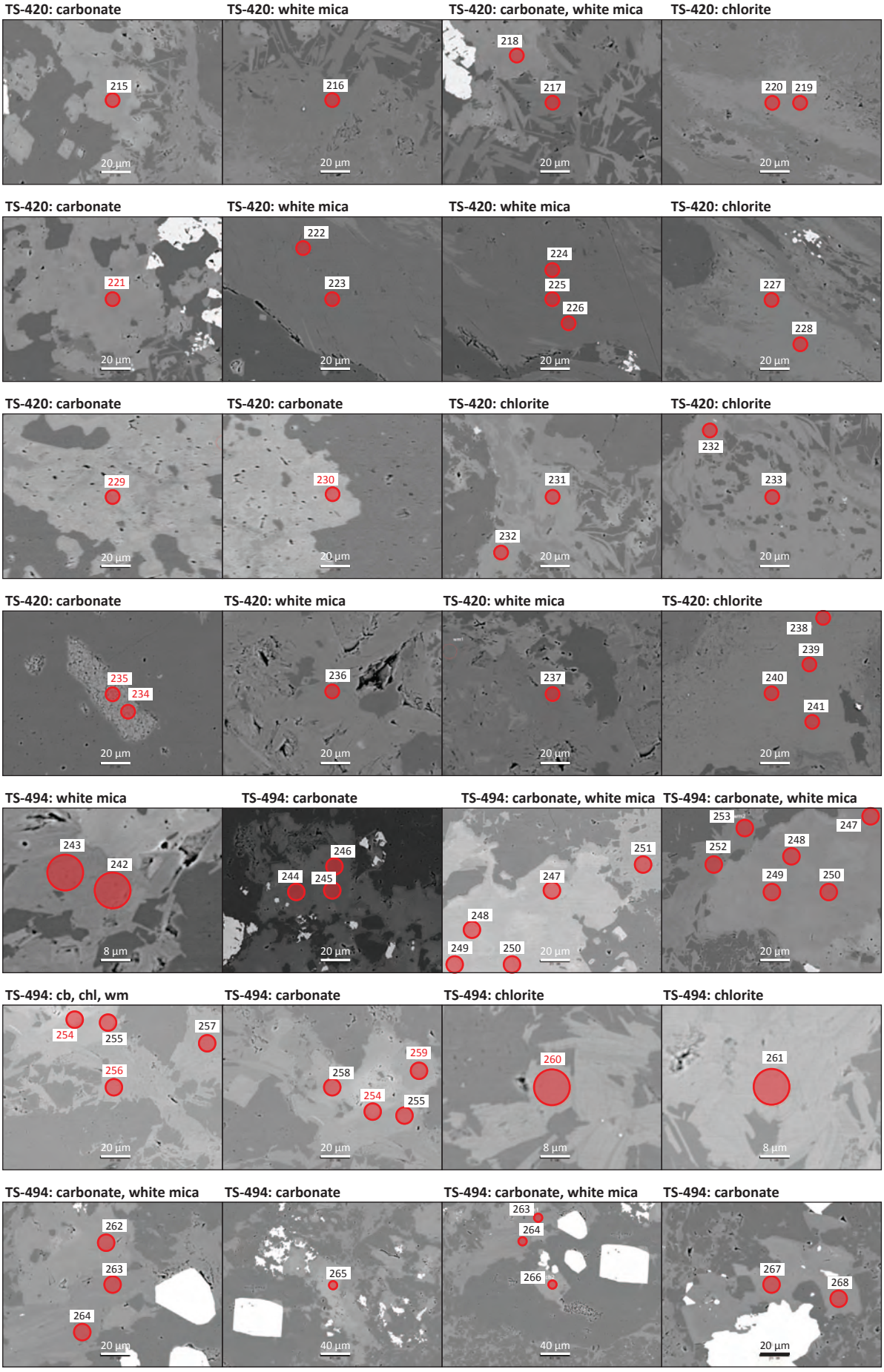

Figure E.7 Summary of electron microprobe analysis numbers 216-268.

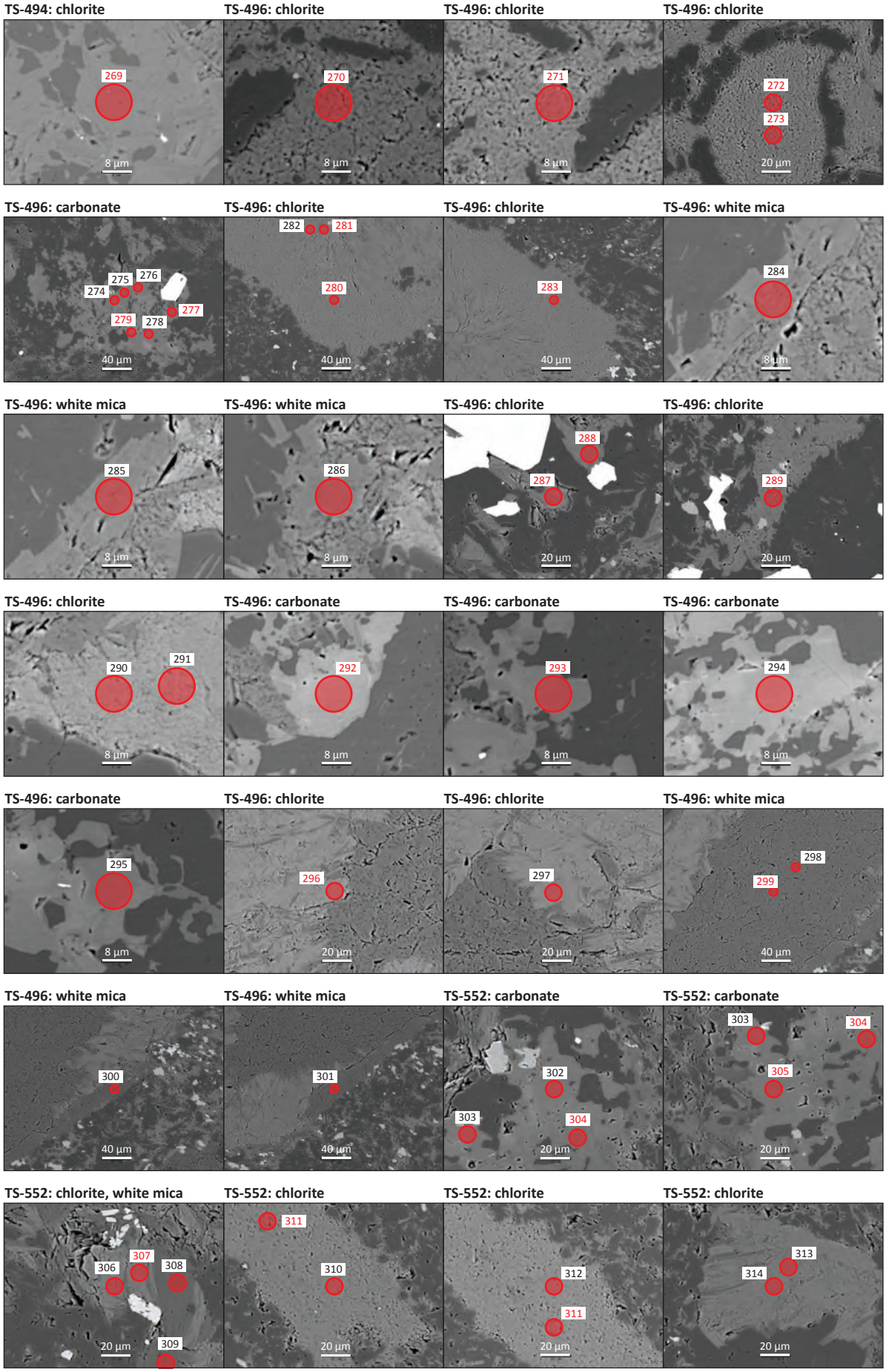

Figure E.8 Summary of electron microprobe analysis numbers 269-314.

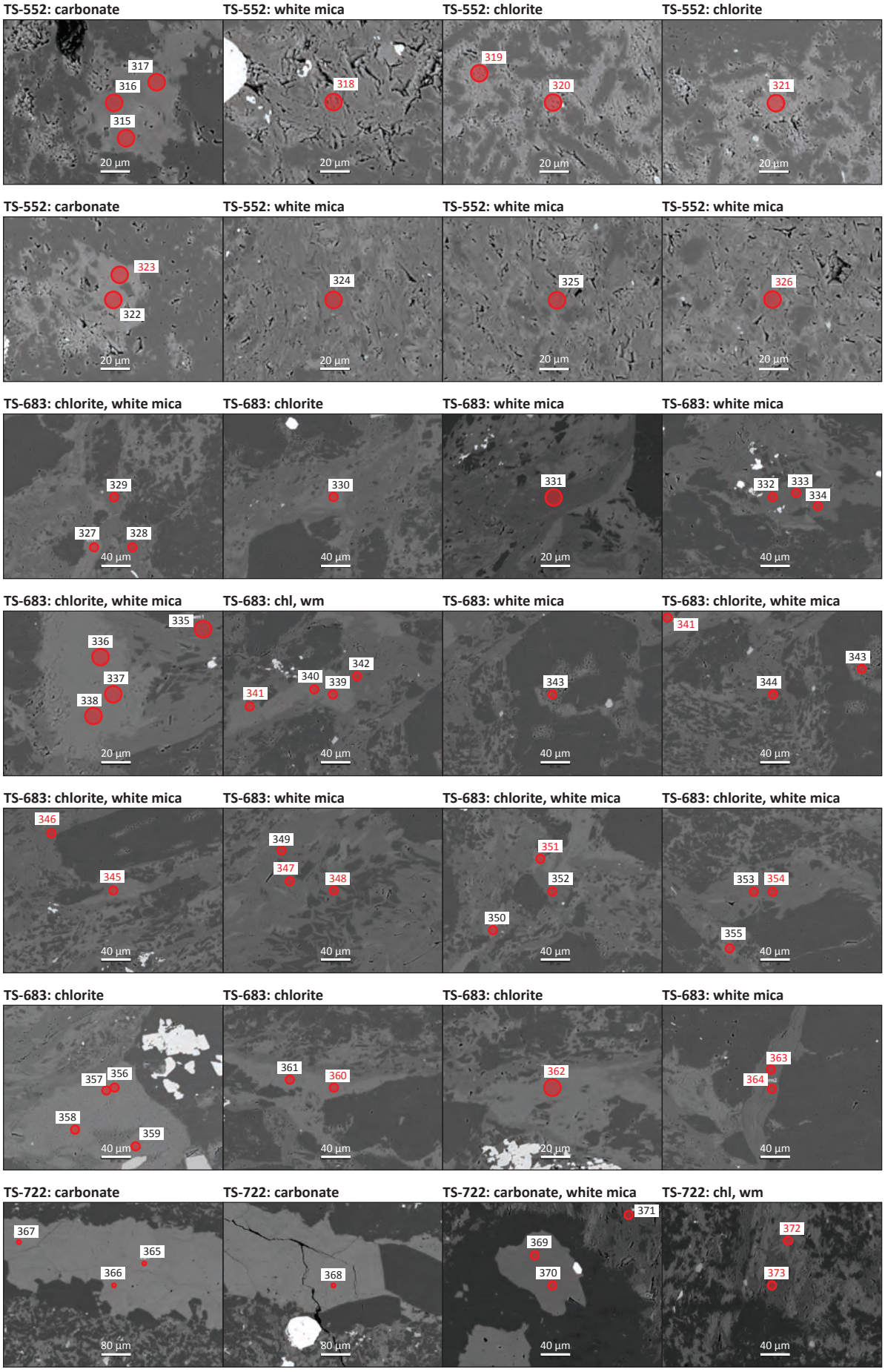

Figure E.9 Summary of electron microprobe analysis numbers 315-373.

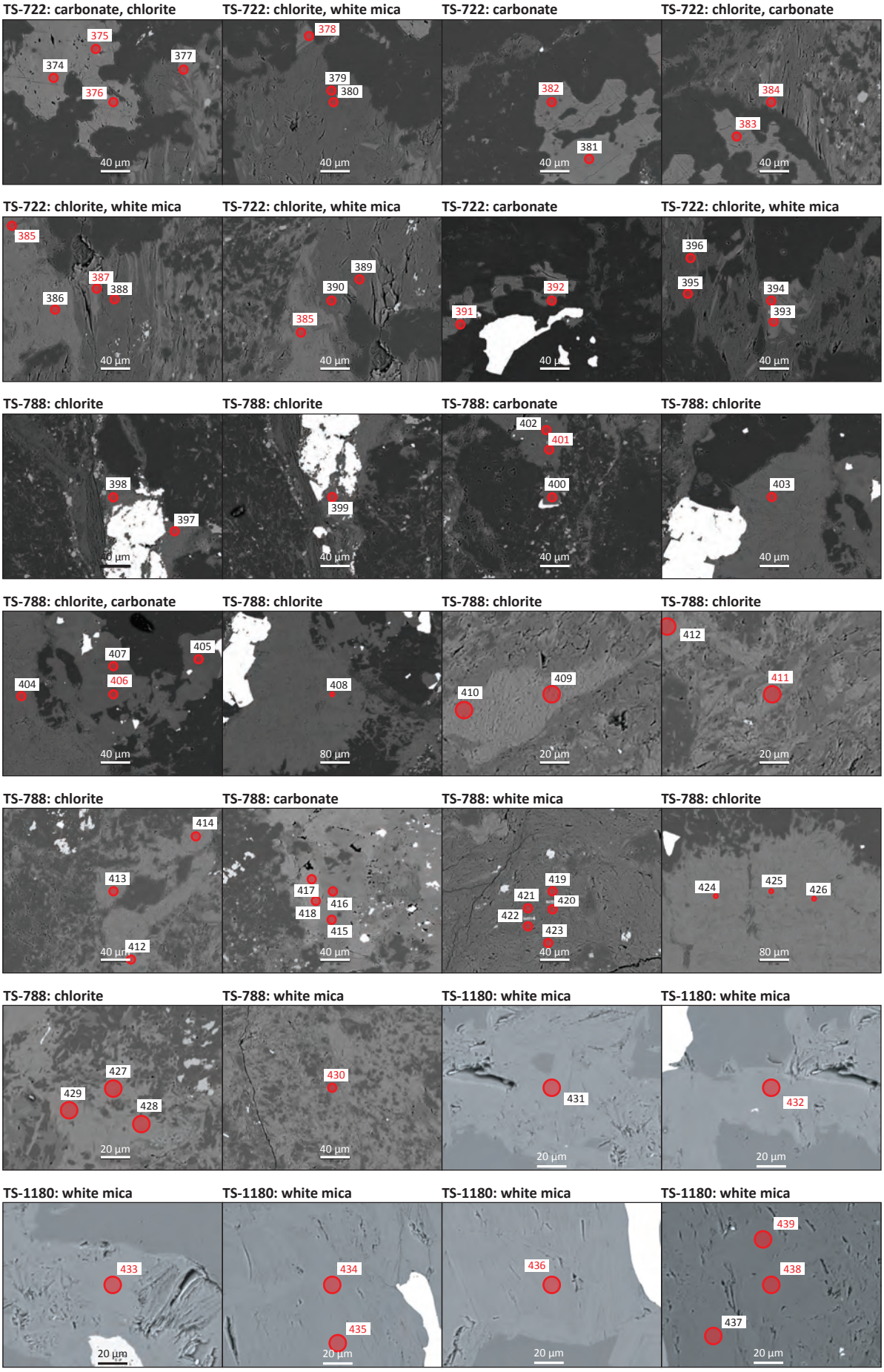

Figure E.10 Summary of electron microprobe analysis numbers 374-439.

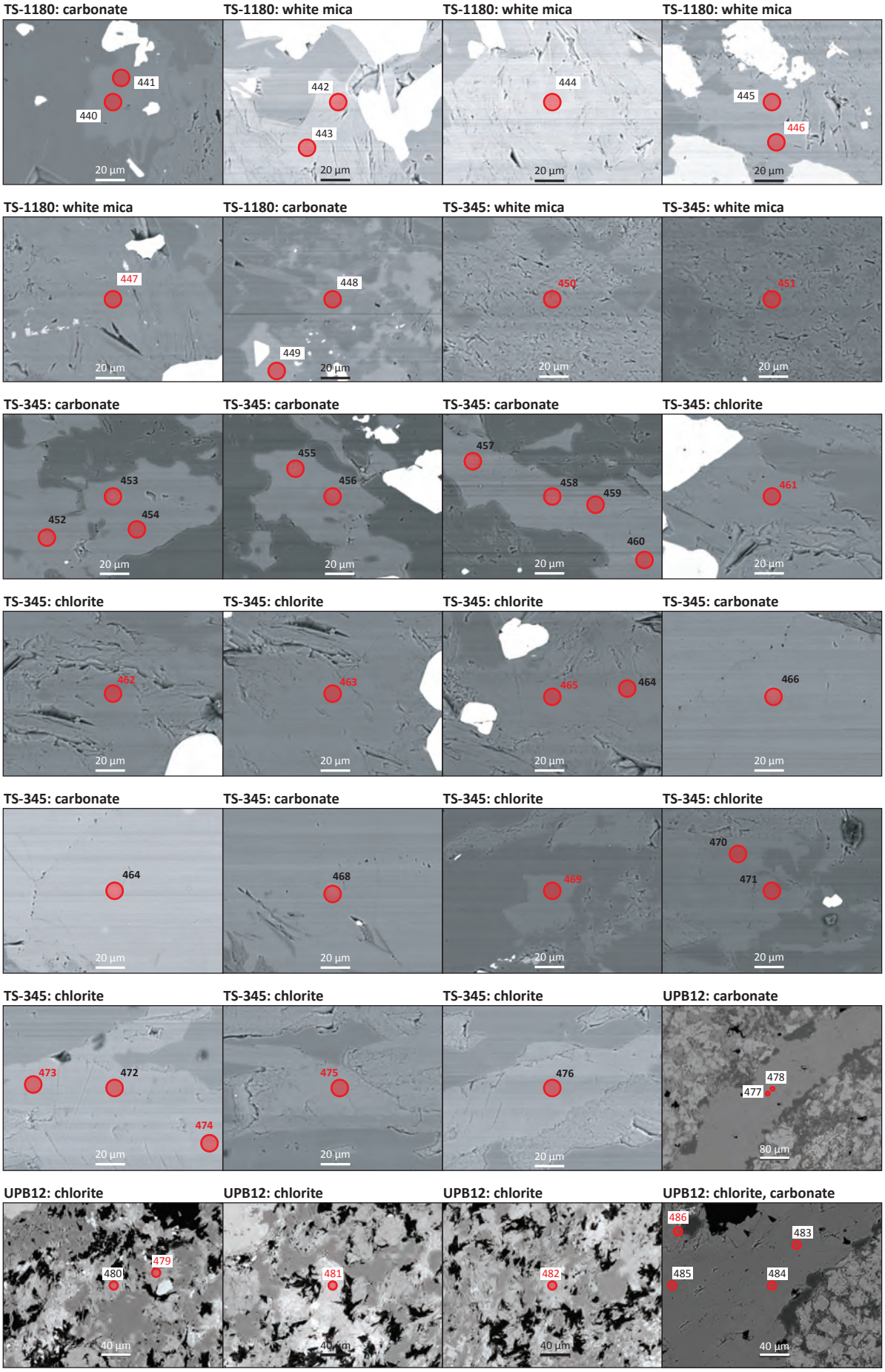

Figure E.11 Summary of electron microprobe analysis numbers 440-486.

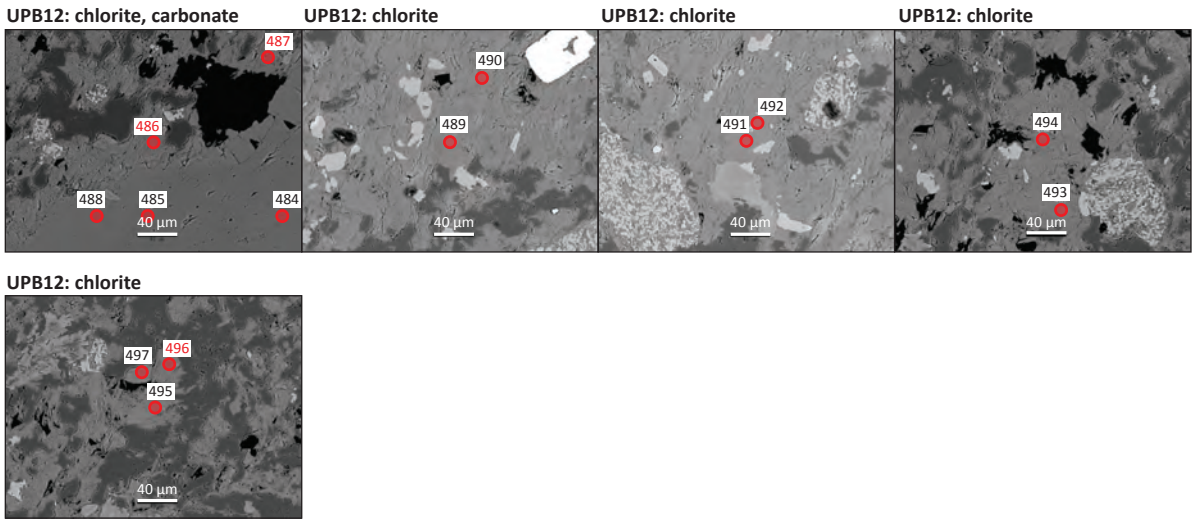

Figure E.12 Summary of electron microprobe analysis numbers 487-497.

Appendix F:

Whole-Rock Chemistry Methods and Results

Nineteen samples from the West Block Area (n=15), Ridge Zone North (n=3) and Price orebody (n=1) were analysed for whole-rock geochemistry by ALS, Perth, WA, Australia (Figure F.1; Table F.1). Sample preparation included a course crush of 70% less than 2 mm, followed by complete sample pulverised to 85% passing 75 microns. The pulverisers were cleaned with "barren" material after every sample preparation.

Table F.1 Whole-rock geochemistry sample set summary.

Sample ID	ALS ID	DDH	Depth (m)	Section (mE)	mN	mE	Elv (m)	Area	Rock Code	Weight (g)
TS-067	MFO-2017-01	BG18-3902	148.4	550				WBA	PA	61
TS-345	MFO-2017-02	BG18-3904	139.1	550				WBA	PA	38
TS-494	MFO-2017-03	BG18-3905	155.4	550				WBA	PA	31
TS-496	MFO-2017-04	BG18-3905	170.7	550				WBA	PA	43
TS-683	MFO-2017-05	BG18-3907	152.7	550				WBA	PA	49
TS-788	MFO-2017-06	BG18-3908	161.5	550				WBA	PA	27
TS-420	MFO-2017-07	BG18-3551	173.7	640				WBA	PA	43
TS-265	MFO-2017-08	BG18-3321a	170.4	640				WBA	PA	44
TS-394	MFO-2017-09	BG18-3550	189	640				WBA	PA	38
TS-552	MFO-2017-10	BG18-3552	152.9	640				WBA	PA	35
TS-722	MFO-2017-11	BG18-3554	202.7	640				WBA	PA	60
TS-971	MFO-2017-12	BG18-3952	163.1	700				WBA	PA	64
BM14-029	MFO-2017-13	BG18-3769	203.0	828				WBA	PA	185
TS-1180	MFO-2017-14	RN18-0224	76.2	918				RZN	PA	70
UPB12	MFO-2017-15	BG18-3921	57.9 to 59.9	585				WBA	Af	105
UPB02	MFO-2017-16	underground			4495.0	855.0	12.5	RZN	QFP	375
UPB05	MFO-2017-17	RN18-0224	6.1 to 9.1	918				RZN	QFP	200
UPB08	MFO-2017-18	BG18-3952	75.2 to 77	700				WBA	QFP	139
15PRICE01	MFO-2017-19	underground			3390.0	4498.0	632.5	PM	Fvc	410

ALS ID – lab sample identification number
mN and mE – reported in mine co-ordinate system
Elv – reported in metres above sea level
Area – PM; Price Mine; RZN, Ridge Zone North; WBA, West Block Area
Rock Code – Af, andesite flow; Fvc, felsic volcaniclastics; PA, Price andesite; QFP, quartz and feldspar-phyric rhyolite

Figure F.1 Photographs of samples selected for whole-rock geochemistry.

A. Sample TS-067 is of Price Formation andesite from the West Block Area. This sample is an example of moderate, chlorite-calcite-pyrite alteration facies of the footwall alteration zone.

B. Sample TS-345 is of Price Formation andesite from the West Block Area. This sample is an example of moderate, chlorite-sericite-pyrite alteration facies of the footwall alteration zone.

C. Sample TS-494 is of Price Formation andesite from the West Block Area. This sample is an example of moderate, chlorite-calcite-pyrite alteration facies of the footwall alteration zone.

D. Sample TS-496 is of Price Formation andesite from the West Block Area. This sample is an example of moderate, chlorite-calcite-pyrite alteration facies of the footwall alteration zone.

E. Sample TS-683 is of Price Formation andesite from the West Block Area. This sample is an example of moderate, chlorite-calcite-pyrite alteration facies of the footwall alteration zone.

F. Sample TS-788 is of Price Formation andesite from the West Block Area. This sample is an example of moderate, chlorite-calcite-pyrite alteration facies of the footwall alteration zone.

G. Sample TS-420 is of Price Formation andesite from the West Block Area. This sample is an example of moderate, chlorite-calcite-pyrite alteration facies of the footwall alteration zone.

H. Sample TS-265 is of Price Formation andesite from the West Block Area. This sample is an example of moderate, chlorite-calcite-pyrite alteration facies of the footwall alteration zone.

I. Sample TS-394 is of Price Formation andesite from the West Block Area. This sample is an example of moderate, chlorite-calcite-pyrite alteration facies of the footwall alteration zone.

J. Sample TS-552 is of Price Formation andesite from the West Block Area. This sample is an example of moderate, chlorite-calcite-pyrite alteration facies of the footwall alteration zone.

K. Sample TS-722 is of Price Formation andesite from the West Block Area. This sample is an example of moderate, chlorite-calcite-pyrite alteration facies of the footwall alteration zone.

L. Sample TS-971 is of Price Formation andesite from the West Block Area. This sample is an example of moderate, chlorite-calcite-pyrite alteration facies of the footwall alteration zone.

M. Sample BM14-029 is of Price Formation andesite from the West Block Area. This sample is an example of moderate, chlorite-calcite-pyrite alteration facies of the footwall alteration zone.

N. Sample TS-1180 is of Price Formation andesite from the Ridge Zone North oreobdy. This sample is an example of intense, chlorite-sericite-pyrite alteration of the footwall alteration zone.

O. Sample UPB12 is of coherent andesite flow from the hanging wall of the West Block Area. This sample is an example of weak, chlorite-calcite-epidote alteration facies a result of greenschist facies metamorphism.

P. Sample UPB02 is of coherent rhyolite from of the HW Rhyolite from the Ridge Zone North orebody. This sample is an example of strong, quartz-sericite-pyrite alteration.

Q. Sample UPB05 is of coherent, quartz and feldspar-phyric rhyolite of the HW Rhyolite from the Ridge Zone orebody. This sample is an example of strong, quartz-sericite-pyrite alteration.

R. Sample UP08 is of coherent, quartz and feldspar-phyric rhyolite of the HW Rhyolite from the West Block Area. This sample is an example of moderate, quartz-sericite-pyrite alteration.

S. Sample 15PRICE01 is of rhyolitic, volcaniclastic sandstone of the LMP Rhyolite from the Price orebody. This sample is an example of strong, quartz-sericite-pyrite alteration.

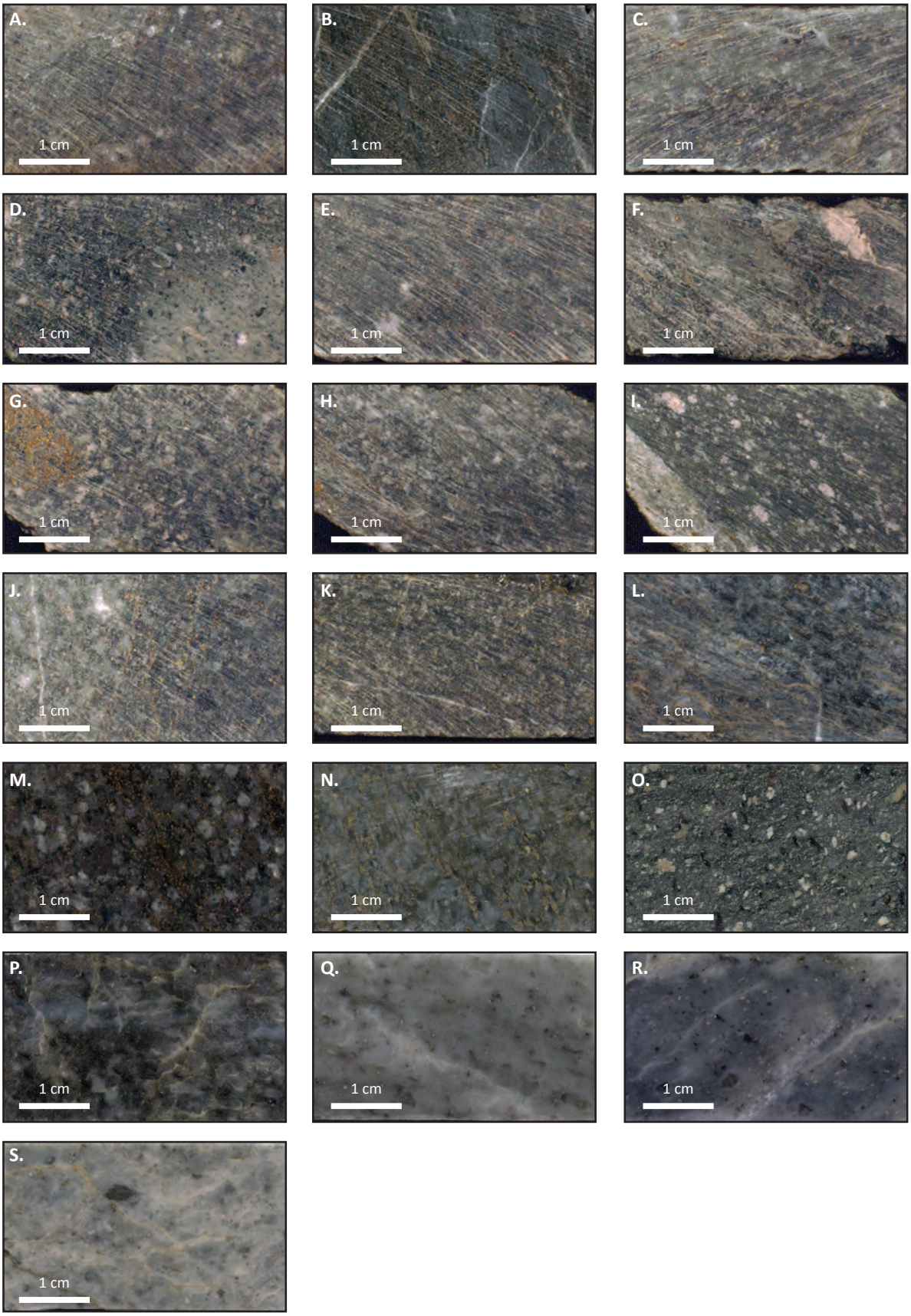
A.
1 cm
B.
1 cm
C.
1 cm
D.
1 cm
E.
1 cm
F.
1 cm
G.
1 cm
H.
1 cm
I.
1 cm
J.
1 cm
K.
1 cm
L.
1 cm
M.
1 cm
N.
1 cm
O.
1 cm
P.
1 cm
Q.
1 cm
R.
1 cm
S.
1 cm

The "Complete Characterisation Package" (ALS analytical code CCP-PKG03; Table F.2) combines a number of analytical methods to obtain a complete whole-rock lithogeochemical characterisation. The analytical package utilises XRF of a lithium borate fused disk to measure major oxides (Table F.3). Trace elements, including the full rare earth element suites are reported from three digestions: (1) a lithium borate fusion with a ICP-MS finish for the resistive elements (Table F.4); (2) a four acid digestion with a ICP-AES finish for the base metals (Table F.5); and (3) an aqua regia digestion with a ICP-MS finish for the volatile gold related trace elements (Table F.6). Total sulfur, carbon, and loss on ignition (LOI) were measured by Leco and TGA furnace, respectively (Table F.7).

Table F.2 Summary of ALS Laboratory range of detection for analytes.

Analytes and ranges								**Analytical Code**
SiO_2	0.01-100%	MgO	0.01-100%	TiO_2	0.01-100%	BaO	0.01-100%	ME-XRF26 *ME-GRA05
Al_2O_3	0.01-100%	Na_2O	0.01-100%	MnO	0.01-100%	LOI*	0.01-100%	
Fe_2O_3	0.01-100%	K_2O	0.01-100%	P_2O_5	0.01-100%			
CaO	0.01-100%	Cr_2O_3	0.01-100%	SrO	0.01-100%			
Ba	0.5-10,000	Gd	0.05-1,000	Sm	0.03-1,000	W	1-10,000	ME-MS81
Ce	0.5-10,000	Hf	0.2-10,000	Sn	1-10,000	Y	0.5-10,000	
Cr	10-10,000	Ho	0.01-1,000	Sr	0.1-10,000	Yb	0.03-1,000	
Cs	0.01-10,000	La	0.5-10,000	Ta	0.1-2,500	Zr	2-10,000	
Dy	0.05-1,000	Lu	0.01-1,000	Tb	0.01-1,000			
Er	0.03-1,000	Nb	0.2-2,500	Th	0.05-1,000			
Eu	0.03-1,000	Nd	0.1-10,000	Tm	0.01-1,000			
Ga	0.1-1,000	Pr	0.03-1,000	U	0.05-1,000			
Ge	5-1,000	Rb	0.2-10,000	V	5-10,000			
Ag	0.5-100	Cu	1-10,000	Ni	1-10,000	Zn	2-10,000	ME-4ACD81
Cd	0.5-1,000	Li	10-10,000	Pb	2-10,000			
Co	1-10,000	Mo	1-10,000	Sc	1-10,000			
As	0.1-250	In	0.005-250	Se	0.2-250			ME-MS42
Bi	0.01-250	Re	0.001-250	Te	0.01-250			
Hg	0.005-25	Sb	0.05-250	Tl	0.02-250			
S	0.01-50%							S-IR08
C	0.01-50%							C-IR07

Analytes and ranges – ppm for all analytes not reported in percent

Table F.3 Major oxide results from XRF analysis of lithium borate fused disk.

Sample ID	Al_2O_3 wt %	BaO wt %	CaO wt %	Cr_2O_3 wt %	Fe_2O_3 wt %	K_2O wt %	MgO wt %	MnO wt %	Na_2O wt %	P_2O_5 wt %	SiO_2 wt %	SrO wt %	TiO_2 wt %
TS-067	20.53	0.08	2.91	0.01	5.25	2.88	4.60	0.28	4.23	0.27	52.69	0.01	0.97
TS-345	22.65	0.19	1.61	<0.01	7.21	5.31	2.37	0.10	1.88	0.29	51.99	0.01	1.02
TS-494	19.56	0.10	1.23	<0.01	3.99	2.65	4.59	0.27	3.69	0.29	57.19	0.01	0.82
TS-496	17.71	0.07	1.84	<0.01	8.40	1.59	5.19	0.57	3.64	0.47	54.88	0.01	0.81
TS-683	18.17	0.09	0.43	<0.01	5.48	2.44	4.75	0.13	2.67	0.20	60.01	<0.01	0.77
TS-788	21.83	0.12	1.15	<0.01	7.51	2.62	5.11	0.29	4.48	0.42	50.66	0.01	1.10
TS-420	16.08	0.06	1.09	<0.01	13.84	1.92	5.66	0.36	2.16	0.16	48.54	<0.01	0.71
TS-265	20.67	0.09	1.37	<0.01	9.27	2.60	5.76	0.23	3.11	0.40	50.86	0.01	0.91
TS-394	19.28	0.10	5.36	0.01	9.23	2.35	4.72	0.31	3.15	0.24	47.56	0.02	0.83
TS-552	15.96	0.05	2.26	<0.01	5.53	1.50	3.79	0.46	4.22	0.23	58.67	0.01	0.64
TS-722	19.46	0.08	1.56	<0.01	7.07	1.72	3.70	0.21	5.37	0.39	55.82	0.01	0.82
TS-971	22.78	0.23	1.46	<0.01	7.33	4.80	2.42	0.19	2.96	0.17	51.77	0.01	1.00
BM14-029	20.79	0.43	1.57	0.01	5.66	4.04	3.24	0.20	2.52	0.13	55.17	0.01	0.91
TS-1180	17.26	0.51	0.89	<0.01	12.10	5.26	0.71	0.05	0.24	0.25	54.79	0.01	0.76
UPB12	18.39	0.02	9.92	<0.01	11.44	0.09	4.54	0.18	1.80	0.26	49.84	0.09	0.90
UPB02	14.22	0.33	0.05	<0.01	2.15	3.70	0.43	<0.01	0.41	0.01	74.67	<0.01	0.21
UPB05	13.19	0.53	0.07	<0.01	1.46	3.54	0.50	0.01	0.31	0.04	77.89	0.01	0.22
UPB08	10.04	0.19	3.25	0.01	0.69	1.40	0.12	0.04	3.17	0.03	78.18	0.02	0.16
15PRICE01	4.92	5.58	0.53	<0.01	3.28	1.23	0.48	0.03	0.13	0.01	78.32	0.06	0.15

Table F.4 Rare earth element results from ICP-MS of lithium borate fused bead.

Sample ID	Ba ppm	Ce ppm	Cr ppm	Cs ppm	Dy ppm	Er ppm	Eu ppm	Ga ppm	Gd ppm	Ge ppm	Hf ppm	Ho ppm	La ppm	Lu ppm	Nb ppm
TS-067	665	22.4	40	0.50	3.750	2.350	1.090	20.400	3.560	<5	2.4	0.77	9.5	0.40	3.5
TS-345	1615	35.1	10	0.92	5.210	3.160	1.460	21.800	4.980	<5	2.7	1.09	16.3	0.49	4.3
TS-494	876	35.4	10	0.38	5.660	3.570	1.640	19.600	5.490	<5	3.7	1.17	16.0	0.59	5.5
TS-496	610	39.5	10	0.35	5.370	2.990	2.020	16.300	5.800	<5	2.1	1.10	18.1	0.44	3.4
TS-683	813	38.0	10	0.44	3.580	2.270	1.350	19.400	3.980	<5	3.6	0.75	17.9	0.39	5.4
TS-788	968	45.1	10	1.72	6.110	3.640	1.960	20.100	5.920	<5	2.8	1.26	20.5	0.57	4.7
TS-420	503	29.9	10	0.29	3.610	2.100	1.310	14.900	3.880	<5	1.8	0.71	14.1	0.32	3.1
TS-265	733	31.2	10	0.54	4.000	2.390	1.480	18.900	4.260	<5	2.4	0.81	14.2	0.37	3.8
TS-394	861	27.6	20	0.40	4.180	2.530	1.470	19.000	4.250	<5	2.1	0.88	12.7	0.39	3.5
TS-552	465	37.5	10	0.29	4.520	2.910	1.570	15.400	4.890	<5	2.8	0.99	17.6	0.46	4.1
TS-722	622	30.9	10	0.28	4.690	3.010	1.330	17.100	4.630	<5	2.3	1.00	13.8	0.45	3.6
TS-971	1805	30.7	10	0.63	4.720	2.920	1.400	20.500	4.460	<5	2.5	1.00	14.4	0.46	4.0
BM14-029	3430	28.0	10	0.62	4.330	2.550	1.250	20.000	4.300	<5	2.4	0.84	12.8	0.40	3.7
TS-1180	3880	58.0	10	0.49	5.500	3.210	1.550	16.700	6.070	<5	3.1	1.10	28.3	0.49	5.1
UPB12	160.5	22.9	10	0.05	4.050	2.470	1.330	18.800	3.950	<5	1.6	0.86	10.0	0.37	2.1
UPB02	2740	31.1	<10	0.58	2.060	1.530	0.790	14.100	2.160	7	3.8	0.46	15.1	0.33	4.9
UPB05	4260	40.6	<10	0.47	3.250	2.210	0.940	12.400	3.030	<5	3.8	0.70	21.5	0.43	4.8
UPB08	1555	32.2	<10	0.13	2.040	1.110	0.730	4.800	2.300	<5	2.8	0.41	18.3	0.15	3.6
15PRICE01	>10000	19.6	<10	0.35	2.190	1.390	1.090	8.900	1.910	6	1.4	0.46	9.8	0.31	2.3

Table F.4 Continued.

Sample ID	Nd ppm	Pr ppm	Rb ppm	Sm ppm	Sn ppm	Sr ppm	Ta ppm	Tb ppm	Th ppm	Tm ppm	U ppm	V ppm	W ppm	Y ppm	Yb ppm	Zr ppm
TS-067	14.1	3.16	40.7	3.41	1	120.0	0.2	0.60	1.75	0.35	2.43	304	1	21.0	2.44	79
TS-345	20.5	4.74	77.9	4.95	1	84.4	0.3	0.82	2.20	0.47	0.85	289	5	31.4	3.01	94
TS-494	20.6	4.86	41.3	5.05	1	98.8	0.4	0.93	2.96	0.53	1.71	124	2	33.5	3.69	127
TS-496	23.6	5.39	25.0	6.02	1	97.8	0.2	0.90	1.63	0.45	0.61	222	2	32.2	2.86	73
TS-683	21.2	5.04	38.8	4.66	1	72.2	0.3	0.59	3.23	0.37	1.05	214	2	20.3	2.40	114
TS-788	26.1	5.82	42.1	6.20	1	121.5	0.3	0.94	2.39	0.55	1.33	287	6	35.9	3.56	98
TS-420	17.3	3.99	30.7	3.85	1	53.4	0.2	0.55	1.55	0.32	0.60	238	2	20.8	2.11	65
TS-265	18.8	4.23	39.1	4.43	1	96.4	0.2	0.69	1.88	0.36	0.76	282	2	22.3	2.26	80
TS-394	16.1	3.70	37.2	4.02	1	139.0	0.2	0.67	1.66	0.40	0.57	259	1	26.0	2.53	72
TS-552	20.4	4.86	24.4	5.02	1	118.0	0.2	0.77	2.33	0.43	1.01	103	2	28.8	2.84	99
TS-722	18.1	4.12	27.1	4.46	1	97.0	0.2	0.76	1.94	0.43	0.65	233	1	27.5	2.88	78
TS-971	18.6	4.18	74.1	4.26	1	90.1	0.2	0.72	2.05	0.45	0.92	364	3	28.9	3.01	90
BM14-029	16.3	3.76	59.8	3.96	1	83.9	0.2	0.69	1.87	0.38	2.08	301	2	23.3	2.45	82
TS-1180	29.2	6.86	68.5	6.60	1	41.0	0.3	0.91	2.81	0.45	1.59	114	6	33.0	3.04	114
UPB12	14.1	3.07	1.2	3.80	1	780.0	0.1	0.65	1.12	0.36	0.53	293	1	24.7	2.38	55
UPB02	13.7	3.53	54.4	2.92	1	61.1	0.3	0.33	4.48	0.25	1.69	27	4	13.4	1.88	140
UPB05	17.9	4.79	44.1	3.49	1	88.7	0.3	0.50	4.38	0.35	1.58	20	6	20.6	2.68	141
UPB08	12.9	3.53	12.9	2.51	<1	244.0	0.3	0.34	3.16	0.15	1.37	13	3	11.0	1.01	107
15PRICE01	9.6	2.34	17.1	2.06	<1	529.0	0.2	0.35	1.34	0.22	6.30	42	1	14.2	1.59	52

Table F.5 Base metal results from ICP-AES with four acid digest.

Sample ID	Ag ppm	Cd ppm	Co ppm	Cu ppm	Li ppm	Mo ppm	Ni ppm	Pb ppm	Sc ppm	Zn ppm
TS-067	<0.5	<0.5	20	7	10	<1	12	6	27	165
TS-345	<0.5	<0.5	15	25	10	8	5	51	23	97
TS-494	<0.5	2.3	6	238	10	<1	2	23	17	717
TS-496	<0.5	2.1	18	30	10	<1	4	10	16	1010
TS-683	<0.5	4.4	4	5	10	<1	2	6	26	1360
TS-788	0.8	9.6	21	648	10	<1	6	11	24	2710
TS-420	<0.5	<0.5	59	169	20	<1	5	10	21	213
TS-265	<0.5	<0.5	27	8	20	<1	7	9	22	315
TS-394	2.7	<0.5	9	3	10	<1	9	7	24	527
TS-552	<0.5	3.5	6	124	10	<1	1	6	13	1020
TS-722	<0.5	5.0	12	277	10	<1	7	4	20	1150
TS-971	<0.5	<0.5	27	67	10	1	7	4	31	314
BM14-029	<0.5	<0.5	20	62	10	2	10	8	27	223
TS-1180	2.8	6.7	11	620	<10	18	1	604	16	1740
UPB12	<0.5	<0.5	21	38	10	<1	2	7	30	110
UPB02	1.5	1.2	2	37	<10	1	1	478	5	266
UPB05	2.3	10.6	2	56	<10	1	1	23	6	2780
UPB08	<0.5	<0.5	1	2	<10	<1	<1	5	2	5
15PRICE01	12.2	14.3	2	1560	<10	36	13	1820	5	3120

Table F.6 Trace element results from ICP-MS with aqua regia digest.

Sample ID	As ppm	Bi ppm	Hg ppm	In ppm	Re ppm	Sb ppm	Sc ppm	Se ppm	Te ppm	Tl ppm
TS-067	1.7	0.23	0.008	0.04	0.001	0.12	10.4	0.9	0.21	0.10
TS-345	65.0	0.06	0.240	0.02	0.004	1.33	6.5	0.9	0.01	1.24
TS-494	1.2	0.01	0.092	0.06	<0.001	0.37	8.6	0.4	0.01	0.13
TS-496	3.6	0.08	0.075	0.02	<0.001	0.17	10.0	0.4	0.07	0.06
TS-683	1.4	0.02	0.101	0.08	<0.001	0.11	10.2	0.4	0.01	0.07
TS-788	33.7	0.13	0.512	0.04	<0.001	0.80	13.9	1.5	0.25	0.12
TS-420	3.2	0.08	0.006	0.03	0.001	0.53	8.2	0.7	0.03	0.07
TS-265	13.3	0.04	0.008	0.03	0.004	0.32	9.7	0.5	0.01	0.11
TS-394	3.0	0.01	0.005	0.03	<0.001	0.14	11.3	0.4	0.01	0.18
TS-552	3.4	0.03	0.134	0.04	<0.001	0.18	7.9	0.5	0.01	0.06
TS-722	0.8	0.22	0.159	0.13	<0.001	0.12	9.4	0.6	0.30	0.04
TS-971	3.1	0.25	0.035	0.03	0.001	0.23	6.2	0.5	0.23	0.48
BM14-029	9.0	0.03	0.032	0.02	0.002	0.70	4.0	0.4	0.01	0.22
TS-1180	14.2	1.88	0.384	0.18	0.002	0.65	2.1	2.5	4.51	0.35
UPB12	6.9	0.01	<0.005	0.01	0.001	0.68	6.5	0.6	0.01	<0.02
UPB02	8.1	0.03	0.065	0.01	0.001	2.86	0.4	<0.2	<0.01	0.31
UPB05	22.4	<0.01	0.160	0.04	<0.001	4.46	0.6	0.4	0.01	0.14
UPB08	0.4	<0.01	0.018	<0.005	0.001	0.15	0.7	<0.2	<0.01	0.09
15PRICE01	>250	0.02	0.176	0.05	0.015	35.70	0.8	1.5	1.03	0.78

Table F.7 Total sulfur, carbon and loss on ignition results.

Sample ID	**S** **wt %**	**C** **wt %**	**LOI** **wt %**
Analytical method	*S-IR08*	*C-IR07*	*ME-GRA05*
TS-067	0.64	0.67	6.23
TS-345	4.07	0.31	6.11
TS-494	0.08	0.35	4.62
TS-496	0.85	0.50	5.45
TS-683	0.11	0.06	3.81
TS-788	0.65	0.21	4.09
TS-420	6.34	0.37	8.17
TS-265	1.01	0.32	5.53
TS-394	0.07	1.14	7.56
TS-552	0.72	0.79	5.51
TS-722	0.87	0.24	3.85
TS-971	2.46	0.32	4.85
BM14-029	2.07	0.51	4.75
TS-1180	8.79	0.20	8.03
UPB12	0.02	0.07	3.38
UPB02	1.45	0.02	2.82
UPB05	1.18	0.02	2.5
UPB08	0.26	0.71	3.11
15PRICE01	3.63	0.21	2.7

Appendix G:

Shortwave Infrared Spectroscopy Method and Results

Shortwave infrared measurements were collected from 949 drill core samples (West Block Area = 825; Ridge Zone North = 124). Shortwave infrared spectroscopy was completed at CODES, University of Tasmania using TerraSpec™ Standard Res Mineral Analyzer.

Spectra were acquired on the clean, flat surface of dry drill core samples using a contact probe with a 10 mm diameter spot size. Prior to sample analysis and after every hour of machine runtime, the analyser was calibrated with a Spectralon® disk. Where possible, portions of the sample that contained abundant sulfide were avoided to minimise spectral interference.

The TerraSpec™ Standard Res Mineral Analyzer acquires data between 1,000-2,500 nm wavelengths. The analyser has a spectral resolution of 6 nm, sampling interval of 2 nm, and a wavelength accuracy of ±1.0 nm (*per. com. Malvern Panalytical 2018*). Each sample spectrum consists of an average of 150 consecutive measurements. Spectra absorption features were processed using TSG® analysis software and spectral parameters such as the wavelength position and depth of absorption features from Hull quotient corrected spectra were extracted (Table G.1). Digital spectral files are available electronically in *.asd* file format.

Table G.1 SWIR results for drill core samples from the West Block Area and Ridge Zone North orebody.

Sample	DDH	Depth (m)	Mineral Results	SWIR Response	Feature Position (nm)			Feature Depth			AlOHd/ MgOHd
					AlOH	FeOH	MgOH	AlOH	FeOH	MgOH	
TS-001	BG18-3901	3.0	chl-ep	mix	NUL	2254	2341	0.00	0.25	0.32	0.0
TS-002	BG18-3901	8.0	chl-wm	mix	2218	2253	2345	0.13	0.24	0.29	0.4
TS-003	BG18-3901	15.2	chl	pure	NUL	2254	2339	0.00	0.30	0.32	0.0
TS-004	BG18-3901	18.3	chl-wm	mix	2202	2254	2341	0.13	0.21	0.21	0.6
TS-005	BG18-3901	21.3	chl-wm	mix	2204	2254	2344	0.12	0.29	0.29	0.4
TS-006	BG18-3901	24.4	chl	pure	2217	2254	2343	0.10	0.30	0.33	0.3
TS-007	BG18-3901	27.4	chl-ep	mix	NUL	2254	2341	0.00	0.32	0.47	0.0
TS-008	BG18-3901	30.5	chl	pure	NUL	2254	2341	0.00	0.31	0.33	0.0
TS-009	BG18-3901	33.5	chl	pure	2218	2254	2345	0.13	0.30	0.32	0.4
TS-010	BG18-3901	36.6	chl-wm	mix	2209	2253	2341	0.18	0.26	0.32	0.6
TS-011	BG18-3901	39.6	chl	pure	2215	2249	2342	0.05	0.06	0.10	0.5
TS-012	BG18-3901	42.7	chl-wm	mix	2210	2253	2346	0.21	0.29	0.27	0.8
TS-013	BG18-3901	45.7	chl-wm	mix	2212	2254	2341	0.10	0.23	0.28	0.4
TS-014	BG18-3901	48.7	chl-wm	mix	2208	2253	2341	0.12	0.22	0.26	0.5
TS-015	BG18-3901	51.8	wm	pure	2207	NUL	2347	0.11	0.00	0.06	1.7
TS-016	BG18-3901	55.0	chl-wm	mix	2212	2254	2344	0.11	0.24	0.26	0.4
TS-017	BG18-3901	58.1	chl	pure	NUL	2255	2344	0.00	0.23	0.25	0.0
TS-018	BG18-3901	60.9	chl-wm	mix	2205	2252	2341	0.08	0.10	0.14	0.5
TS-019	BG18-3901	70.1	chl-ep	mix	2201	2254	2339	0.08	0.26	0.40	0.2
TS-020	BG18-3901	73.2	chl	pure	NUL	2256	2344	0.00	0.21	0.23	0.0
TS-021	BG18-3901	82.3	chl	pure	2216	2255	2346	0.04	0.21	0.21	0.2
TS-022	BG18-3901	85.3	chl-wm	mix	2198	2255	2347	0.23	0.12	0.15	1.5
TS-023	BG18-3901	89.2	wm	pure	2200	2237	2332	0.10	0.04	0.04	2.8
TS-024	BG18-3901	91.6	wm	pure	2199	NUL	2348	0.25	0.00	0.13	1.9
TS-025	BG18-3901	97.5	wm	pure	2200	NUL	2345	0.15	0.00	0.07	2.3
TS-026	BG18-3901	101.6	wm	pure	2199	NUL	2348	0.20	0.00	0.10	2.1
TS-027	BG18-3901	107.0	wm-chl	mix	2197	2249	2339	0.22	0.12	0.12	1.7
TS-028	BG18-3901	110.0	wm-cb	mix	2198	NUL	2337	0.11	0.00	0.05	2.3
TS-029	BG18-3901	115.8	wm	pure	2199	2239	2340	0.12	0.03	0.04	2.8
TS-030	BG18-3901	119.0	wm	pure	2200	NUL	2338	0.12	0.00	0.05	2.5
TS-031	BG18-3901	134.1	wm-cb	mix	2198	2248	2342	0.20	0.06	0.10	1.9
TS-032	BG18-3901	140.2	wm-cb	mix	2198	2247	2348	0.11	0.04	0.05	2.1
TS-033	BG18-3901	159.5	chl-wm	mix	2201	2252	2340	0.13	0.17	0.16	0.8
TS-034	BG18-3901	203.7	chl-wm	mix	2206	2253	2343	0.11	0.21	0.21	0.5
TS-035	BG18-3902	9.7	chl-ep	mix	2196	2255	2341	0.08	0.23	0.30	0.3
TS-036	BG18-3902	13.9	chl	pure	NUL	2254	2340	0.00	0.27	0.29	0.0
TS-037	BG18-3902	17.3	chl-ep	mix	2217	2254	2343	0.08	0.26	0.30	0.3
TS-038	BG18-3902	20.6	chl	pure	2205	2254	2339	0.10	0.27	0.28	0.3
TS-039	BG18-3902	25.1	chl	pure	NUL	2253	2342	0.00	0.32	0.35	0.0
TS-040	BG18-3902	29.2	chl	pure	NUL	2254	2342	0.00	0.33	0.36	0.0
TS-041	BG18-3902	33.5	chl-wm	mix	2212	2253	2343	0.11	0.23	0.25	0.4
TS-042	BG18-3902	37.0	chl-ep	mix	NUL	2254	2341	0.00	0.34	0.47	0.0
TS-043	BG18-3902	40.3	chl-ep	mix	2218	2253	2340	0.10	0.24	0.27	0.3
TS-044	BG18-3902	45.7	chl-wm	mix	2208	2252	2342	0.15	0.22	0.21	0.7
TS-045	BG18-3902	50.0	chl	pure	2211	2254	2341	0.07	0.25	0.26	0.3
TS-046	BG18-3902	54.4	chl-wm	mix	2204	2254	2345	0.12	0.21	0.23	0.5
TS-047	BG18-3902	60.0	chl-wm	mix	2208	2252	2347	0.13	0.14	0.15	0.9
TS-048	BG18-3902	61.1	wm	pure	2208	2238	2351	0.13	0.06	0.07	2.0
TS-049	BG18-3902	70.6	phn	pure	2212	NUL	2346	0.14	0.00	0.08	1.8
TS-050	BG18-3902	77.5	chl-ep	mix	NUL	2254	2340	0.00	0.28	0.41	0.0
TS-051	BG18-3902	80.2	chl-ep	mix	2216	2254	2339	0.09	0.28	0.43	0.2
TS-052	BG18-3902	91.4	wm	pure	2202	NUL	2348	0.21	0.00	0.10	2.1

Table G.1 Continued.

Sample	DDH	Depth (m)	Mineral Results	SWIR Response	Feature Position (nm)			Feature Depth			AlOHd/ MgOHd
					AlOH	FeOH	MgOH	AlOH	FeOH	MgOH	
TS-053	BG18-3902	95.5	wm	pure	2199	NUL	2338	0.22	0.00	0.10	2.2
TS-054	BG18-3902	102.3	aspectral	aspectral	2199	NUL	2340	0.11	0.00	0.04	3.2
TS-055	BG18-3902	103.6	wm	pure	2199	NUL	2348	0.20	0.00	0.09	2.3
TS-056	BG18-3902	106.7	wm-chl	mix	2194	2248	2342	0.29	0.15	0.17	1.7
TS-057	BG18-3902	109.7	wm-chl	mix	2193	2250	2341	0.38	0.12	0.20	1.9
TS-058	BG18-3902	112.8	wm-chl	mix	2196	2251	2343	0.21	0.07	0.12	1.8
TS-059	BG18-3902	116.5	wm	pure	2200	NUL	2343	0.31	0.00	0.17	1.9
TS-060	BG18-3902	119.4	wm	pure	2199	NUL	2348	0.16	0.00	0.06	2.5
TS-061	BG18-3902	122.0	wm	pure	2201	NUL	2347	0.17	0.00	0.08	2.1
TS-062	BG18-3902	130.5	wm	pure	2197	2242	2342	0.09	0.03	0.03	2.6
TS-063	BG18-3902	133.3	wm-chl	mix	2198	2250	2343	0.12	0.06	0.08	1.5
TS-064	BG18-3902	135.0	wm-chl	mix	2198	2251	2342	0.15	0.09	0.10	1.4
TS-065	BG18-3902	138.2	chl-wm	mix	2200	2249	2342	0.13	0.09	0.09	1.5
TS-066	BG18-3902	142.9	chl	pure	NUL	2252	2337	0.00	0.21	0.19	0.0
TS-067	BG18-3902	148.4	chl-wm	mix	2204	2251	2344	0.17	0.19	0.17	1.0
TS-068	BG18-3902	156.5	chl-wm	mix	2206	2252	2343	0.20	0.20	0.20	1.0
TS-069	BG18-3902	164.6	chl-wm	mix	2214	2250	2341	0.21	0.22	0.19	1.1
TS-070	BG18-3902	169.6	chl-wm	mix	2211	2252	2348	0.13	0.16	0.14	0.9
TS-071	BG18-3902	176.4	chl-wm	mix	2210	2248	2344	0.20	0.14	0.15	1.3
TS-072	BG18-3902	183.6	chl	pure	2217	2254	2343	0.08	0.26	0.26	0.3
TS-073	BG18-3902	191.3	chl-wm	mix	2207	2249	2343	0.26	0.20	0.20	1.3
TS-074	BG18-3902	201.2	chl-wm	mix	2201	2251	2344	0.24	0.19	0.18	1.4
TS-075	BG18-3902	213.4	wm-ch	mix	2198	2238	2348	0.16	0.05	0.08	2.1
TS-076	BG18-3902	222.0	chl-wm	mix	2197	2254	2343	0.21	0.20	0.17	1.2
TS-077	BG18-3903	12.7	chl	pure	2217	2254	2343	0.10	0.32	0.33	0.3
TS-078	BG18-3903	17.3	chl-wm	mix	2202	2254	2341	0.09	0.25	0.28	0.3
TS-079	BG18-3903	19.3	chl-wm	mix	2217	2254	2341	0.12	0.28	0.29	0.4
TS-080	BG18-3903	21.5	wm	pure	2204	NUL	2352	0.17	0.00	0.09	1.9
TS-081	BG18-3903	24.4	chl	pure	2219	2254	2342	0.12	0.31	0.35	0.3
TS-082	BG18-3903	27.4	chl-wm	mix	2210	2254	2341	0.15	0.30	0.37	0.4
TS-083	BG18-3903	30.0	chl-wm	mix	2215	2253	2342	0.17	0.27	0.29	0.6
TS-084	BG18-3903	34.8	chl-wm	mix	2217	2254	2343	0.12	0.25	0.27	0.4
TS-085	BG18-3903	40.0	chl-ep	mix	NUL	2254	2341	0.00	0.25	0.30	0.0
TS-086	BG18-3903	42.7	chl	pure	2217	2254	2342	0.09	0.21	0.23	0.4
TS-087	BG18-3903	45.5	chl-wm	mix	2217	2253	2342	0.13	0.27	0.26	0.5
TS-088	BG18-3903	48.9	chl-ep	mix	2218	2253	2340	0.17	0.31	0.36	0.5
TS-089	BG18-3903	52.8	chl-ep	mix	2211	2254	2344	0.10	0.22	0.28	0.3
TS-090	BG18-3903	61.5	wm	pure	2210	2239	2350	0.16	0.08	0.08	1.9
TS-1090	BG18-3921	83.1	wm	pure	2206	NUL	2349	0.31	0.00	0.16	1.9
TS-091	BG18-3903	64.0	chl	pure	2217	2254	2342	0.08	0.21	0.22	0.4
TS-1091	BG18-3921	85.0	wm	pure	2205	NUL	2346	0.29	0.00	0.17	1.7
TS-092	BG18-3903	67.5	chl-wm	mix	2208	2252	2342	0.21	0.19	0.21	1.0
TS-093	BG18-3903	74.2	chl	pure	NUL	2254	2340	0.00	0.23	0.27	0.0
TS-094	BG18-3903	79.0	chl-ep	mix	NUL	2254	2340	0.00	0.27	0.34	0.0
TS-095	BG18-3903	82.1	chl	pure	NUL	2255	2343	0.00	0.22	0.21	0.0
TS-096	BG18-3903	85.7	wm	pure	2199	2237	2342	0.15	0.04	0.05	2.7
TS-097	BG18-3903	90.7	chl	pure	2202	2256	2347	0.05	0.20	0.18	0.3
TS-098	BG18-3903	92.1	wm	pure	2199	NUL	2347	0.17	0.00	0.08	2.2
TS-099	BG18-3903	94.5	wm	pure	2197	NUL	2347	0.25	0.00	0.10	2.4
TS-100	BG18-3903	98.5	wm	pure	2200	NUL	2346	0.20	0.00	0.09	2.3
TS-101	BG18-3903	100.3	wm	pure	2198	NUL	2346	0.36	0.00	0.18	2.0
TS-102	BG18-3903	107.9	wm	pure	2200	NUL	2347	0.27	0.00	0.13	2.1

Table G.1 Continued.

Sample	DDH	Depth (m)	Mineral Results	SWIR Response	Feature Position (nm)			Feature Depth			AlOHd/ MgOHd
					AlOH	FeOH	MgOH	AlOH	FeOH	MgOH	
TS-103	BG18-3903	112.2	wm-mont	mix	2196	NUL	2344	0.31	0.00	0.15	2.1
TS-104	BG18-3903	118.3	wm	pure	2197	NUL	2342	0.30	0.00	0.14	2.1
TS-105	BG18-3903	131.1	wm-chl	mix	2201	2239	2346	0.16	0.05	0.08	2.1
TS-106	BG18-3903	134.1	wm	pure	2199	NUL	2344	0.16	0.00	0.07	2.5
TS-107	BG18-3903	137.2	wm-ch	mix	2197	2248	2344	0.20	0.08	0.10	2.0
TS-108	BG18-3903	140.2	chl-wm	mix	2199	2249	2348	0.10	0.05	0.04	2.2
TS-109	BG18-3903	143.3	wm	pure	2201	2237	2346	0.14	0.04	0.06	2.2
TS-110	BG18-3903	145.1	wm-ch	mix	2198	2238	2343	0.21	0.06	0.10	2.1
TS-111	BG18-3298	9.3	chl-ep	mix	NUL	2254	2340	0.00	0.29	0.36	0.0
TS-112	BG18-3298	11.7	chl-ep	mix	NUL	2253	2339	0.00	0.28	0.34	0.0
TS-113	BG18-3298	13.6	chl-ep	mix	NUL	2254	2341	0.00	0.24	0.30	0.0
TS-114	BG18-3298	16.5	chl-wm	mix	2214	2250	2342	0.20	0.20	0.24	0.8
TS-115	BG18-3298	19.3	ep-chl	mix	NUL	2254	2346	0.00	0.19	0.35	0.0
TS-116	BG18-3298	20.7	chl	pure	NUL	2254	2343	0.00	0.31	0.37	0.0
TS-117	BG18-3298	23.0	chl	pure	NUL	2254	2343	0.00	0.29	0.33	0.0
TS-118	BG18-3298	27.3	chl-ep	mix	NUL	2254	2340	0.00	0.30	0.39	0.0
TS-119	BG18-3298	29.2	chl-ep	mix	NUL	2254	2341	0.00	0.22	0.29	0.0
TS-120	BG18-3298	32.2	chl	pure	NUL	2254	2340	0.00	0.30	0.30	0.0
TS-121	BG18-3298	34.5	chl	pure	NUL	2254	2341	0.00	0.26	0.28	0.0
TS-122	BG18-3298	37.8	chl-wm	mix	2201	2255	2342	0.15	0.24	0.22	0.7
TS-123	BG18-3298	44.0	chl-wm	mix	2200	2256	2345	0.11	0.19	0.17	0.6
TS-124	BG18-3298	46.8	chl-wm	mix	2200	2256	2344	0.11	0.16	0.15	0.8
TS-125	BG18-3298	63.7	chl-ep	mix	NUL	2255	2339	0.00	0.28	0.37	0.0
TS-126	BG18-3298	70.6	chl-wm	mix	2200	2249	2338	0.05	0.04	0.04	1.3
TS-127	BG18-3298	152.4	wm	pure	2199	2237	2346	0.11	0.03	0.05	2.3
TS-128	BG18-3298	155.8	wm	pure	2199	NUL	2345	0.19	0.00	0.10	1.9
TS-129	BG18-3298	158.6	wm	pure	2200	NUL	2350	0.13	0.00	0.07	1.8
TS-130	BG18-3298	161.5	wm	pure	2199	NUL	2346	0.23	0.00	0.12	2.0
TS-131	BG18-3298	164.6	wm-mont	mix	2198	NUL	2344	0.35	0.00	0.18	2.0
TS-132	BG18-3298	167.7	wm	pure	2197	2238	2326	0.03	0.02	0.01	2.1
TS-133	BG18-3298	173.4	chl-wm	mix	2196	2248	2337	0.07	0.04	0.04	1.6
TS-134	BG18-3298	176.8	wm-ch	mix	2199	2248	2344	0.11	0.04	0.06	1.8
TS-135	BG18-3298	180.0	wm-ch	mix	2198	NUL	2338	0.16	0.00	0.07	2.2
TS-136	BG18-3298	183.3	wm-ch	mix	2197	2238	2345	0.22	0.07	0.11	2.0
TS-137	BG18-3298	186.0	wm-ch	mix	2198	2249	2341	0.14	0.05	0.07	2.1
TS-138	BG18-3298	201.2	chl	pure	2196	2254	2344	0.10	0.10	0.08	1.3
TS-139	BG18-3298	207.4	chl-wm	mix	2208	2251	2341	0.05	0.11	0.10	0.5
TS-140	BG18-3298	210.5	chl-wm	mix	2204	2253	2342	0.15	0.24	0.21	0.7
TS-141	BG18-3298	222.4	chl-wm	mix	2204	2254	2342	0.16	0.22	0.26	0.6
TS-142	BG18-3298	234.7	chl-wm	mix	2201	2254	2342	0.15	0.16	0.15	1.1
TS-143	BG18-3299	178.3	wm	pure	2198	NUL	2347	0.23	0.00	0.12	2.0
TS-144	BG18-3299	181.6	wm	pure	2197	NUL	2348	0.10	0.00	0.04	2.5
TS-145	BG18-3299	184.5	wm	pure	2198	NUL	2343	0.29	0.00	0.14	2.1
TS-146	BG18-3299	187.2	wm-chl	mix	2198	2253	2344	0.14	0.05	0.06	2.2
TS-147	BG18-3299	196.6	wm-chl	mix	2197	2249	2341	0.10	0.06	0.07	1.5
TS-148	BG18-3299	199.5	wm	pure	2200	NUL	2352	0.13	0.00	0.05	2.5
TS-149	BG18-3299	202.6	wm-ch	mix	2199	2246	2343	0.16	0.05	0.08	2.1
TS-150	BG18-3299	205.7	wm-chl	mix	2199	2250	2345	0.11	0.04	0.05	2.1
TS-151	BG18-3299	211.8	chl-wm	mix	2200	2255	2343	0.15	0.16	0.14	1.0
TS-152	BG18-3299	214.9	wm	pure	2200	2241	2347	0.11	0.04	0.05	2.2
TS-153	BG18-3299	223.9	wm	pure	2201	NUL	2349	0.18	0.00	0.09	2.1
TS-154	BG18-3299	228.6	wm-chl	mix	2203	2246	2344	0.14	0.06	0.08	1.8

Table G.1 Continued.

Sample	DDH	Depth (m)	Mineral Results	SWIR Response	Feature Position (nm)			Feature Depth			AlOHd/ MgOHd
					AlOH	FeOH	MgOH	AlOH	FeOH	MgOH	
TS-155	BG18-3299	231.6	wm-ch	mix	2198	NUL	2341	0.16	0.00	0.09	1.7
TS-156	BG18-3769	3.0	chl	pure	NUL	2255	2344	0.00	0.25	0.24	0.0
TS-157	BG18-3769	6.1	chl-wm	mix	2200	2255	2344	0.16	0.20	0.20	0.8
TS-158	BG18-3769	12.1	chl-wm	mix	2203	2254	2348	0.07	0.16	0.15	0.5
TS-159	BG18-3769	15.2	chl-wm	mix	2202	2255	2343	0.08	0.16	0.15	0.5
TS-160	BG18-3769	21.4	chl	pure	2200	2256	2344	0.09	0.24	0.24	0.4
TS-161	BG18-3769	24.4	chl-wm	mix	2203	2254	2345	0.11	0.13	0.12	0.9
TS-162	BG18-3769	29.2	chl	pure	NUL	2251	2337	0.00	0.16	0.18	0.0
TS-163	BG18-3769	33.2	chl	pure	NUL	2256	2348	0.00	0.20	0.20	0.0
TS-164	BG18-3769	38.6	wm	pure	2202	NUL	2347	0.25	0.00	0.14	1.8
TS-165	BG18-3769	51.8	wm	pure	2208	NUL	2346	0.24	0.00	0.15	1.7
TS-167	BG18-3769	54.9	wm	pure	2206	NUL	2348	0.32	0.00	0.19	1.7
TS-168	BG18-3769	58.1	wm	pure	2200	NUL	2346	0.23	0.00	0.11	2.0
TS-169	BG18-3769	61.0	wm	pure	2199	NUL	2345	0.17	0.00	0.07	2.5
TS-170	BG18-3769	64.0	wm	pure	2202	NUL	2344	0.15	0.00	0.07	2.3
TS-171	BG18-3769	68.5	wm	pure	2203	NUL	2345	0.21	0.00	0.11	2.0
TS-172	BG18-3769	71.7	wm	pure	2202	NUL	2347	0.24	0.00	0.12	2.0
TS-173	BG18-3769	75.7	wm	pure	2201	NUL	2346	0.30	0.00	0.16	1.9
TS-174	BG18-3769	77.7	wm	pure	2200	NUL	2350	0.21	0.00	0.10	2.1
TS-175	BG18-3769	81.0	wm	pure	2203	NUL	2346	0.21	0.00	0.11	1.9
TS-176	BG18-3769	83.8	wm	pure	2203	NUL	2349	0.21	0.00	0.11	1.9
TS-177	BG18-3769	87.0	wm	pure	2200	NUL	2346	0.20	0.00	0.10	2.0
TS-178	BG18-3769	96.0	wm-ch	mix	2198	2246	2339	0.18	0.09	0.09	2.0
TS-179	BG18-3769	102.1	wm	pure	2197	NUL	2339	0.12	0.00	0.04	3.0
TS-180	BG18-3769	105.4	wm	pure	2197	2238	2347	0.12	0.06	0.05	2.6
TS-181	BG18-3769	108.2	wm	pure	2199	NUL	2343	0.18	0.00	0.08	2.2
TS-182	BG18-3769	123.4	chl-wm	mix	2198	2253	2341	0.14	0.16	0.13	1.0
TS-183	BG18-3769	126.6	chl-wm	mix	2198	2253	2340	0.18	0.18	0.15	1.3
TS-184	BG18-3769	129.7	chl-wm	mix	2199	2253	2345	0.16	0.16	0.13	1.3
TS-185	BG18-3769	132.8	chl-wm	mix	2198	2253	2344	0.36	0.25	0.26	1.4
TS-186	BG18-3769	135.6	wm-ch	mix	2198	NUL	2346	0.43	0.00	0.24	1.8
TS-187	BG18-3769	138.7	chl-wm	mix	2199	2254	2343	0.27	0.34	0.30	0.9
TS-188	BG18-3769	141.6	wm	pure	2199	NUL	2349	0.18	0.00	0.08	2.3
TS-189	BG18-3769	144.7	chl-wm	mix	2200	2253	2341	0.13	0.26	0.22	0.6
TS-190	BG18-3769	148.0	chl-wm	mix	2199	2253	2338	0.24	0.24	0.21	1.2
TS-191	BG18-3769	150.9	chl-wm	mix	2199	2254	2342	0.07	0.12	0.13	0.6
TS-192	BG18-3769	159.0	chl-wm	mix	2199	2253	2344	0.19	0.17	0.17	1.1
TS-193	BG18-3769	163.2	chl-wm	mix	2199	2253	2343	0.28	0.19	0.19	1.5
TS-194	BG18-3769	167.4	chl-wm	mix	2199	2253	2343	0.13	0.16	0.14	1.0
TS-195	BG18-3769	170.5	chl-wm	mix	2198	2254	2345	0.15	0.15	0.13	1.2
TS-196	BG18-3769	175.2	wm	pure	2201	2247	2338	0.07	0.03	0.02	2.7
TS-197	BG18-3769	187.6	cb-wm	mix	2198	2251	2336	0.08	0.04	0.05	1.5
TS-198	BG18-3769	190.5	chl-wm	mix	2199	2251	2338	0.12	0.09	0.09	1.4
TS-199	BG18-3769	193.5	chl-wm	mix	2199	2248	2342	0.11	0.07	0.07	1.6
TS-200	BG18-3769	205.7	wm-chl	mix	2198	2248	2341	0.10	0.05	0.05	1.8
TS-201	BG18-3769	211.8	wm-ch	mix	2198	2246	2345	0.09	0.04	0.05	2.0
TS-202	BG18-3769	217.9	chl-wm	mix	2199	2250	2337	0.19	0.16	0.16	1.3
TS-203	RN18-0104	3.1	wm	pure	2198	2239	2346	0.21	0.03	0.11	2.0
TS-204	RN18-0104	6.2	wm	pure	2198	NUL	2345	0.15	NUL	0.07	2.2
TS-205	RN18-0104	9.2	wm	pure	2198	2238	2340	0.13	0.04	0.06	2.2
TS-206	RN18-0104	12.2	wm	pure	2198	NUL	2346	0.18	NUL	0.09	2.0
TS-207	RN18-0104	15.2	wm	pure	2198	NUL	2346	0.22	NUL	0.11	2.0

Table G.1 Continued.

Sample	DDH	Depth (m)	Mineral Results	SWIR Response	Feature Position (nm)			Feature Depth			AlOHd/ MgOHd
					AlOH	FeOH	MgOH	AlOH	FeOH	MgOH	
TS-208	RN18-0104	16.5	wm	pure	2198	NUL	2347	0.19	NUL	0.09	2.0
TS-209	RN18-0104	18.4	wm-mont	mix	2198	NUL	2346	0.29	NUL	0.15	2.0
TS-210	RN18-0104	21.3	wm-mont	mix	2197	NUL	2345	0.33	NUL	0.17	1.9
TS-211	RN18-0104	25.6	wm	pure	2198	2239	2347	0.15	0.03	0.07	2.1
TS-212	RN18-0104	28.4	wm	pure	2198	NUL	2345	0.26	NUL	0.14	1.9
TS-213	RN18-0104	31.0	wm	pure	2198	NUL	2348	0.18	NUL	0.09	2.0
TS-214	RN18-0104	33.5	wm	pure	2198	NUL	2348	0.17	NUL	0.08	2.0
TS-215	RN18-0104	36.6	wm	pure	2198	NUL	2346	0.21	NUL	0.11	2.0
TS-216	RN18-0104	39.7	wm	pure	2198	NUL	2343	0.15	NUL	0.07	2.3
TS-217	RN18-0104	42.7	wm	pure	2198	NUL	2347	0.11	NUL	0.05	2.4
TS-218	RN18-0104	45.7	wm	pure	2198	NUL	2346	0.21	NUL	0.10	2.1
TS-219	RN18-0104	52.3	wm	pure	2198	NUL	2343	0.13	NUL	0.05	2.4
TS-220	RN18-0104	57.6	wm	pure	2198	NUL	2346	0.13	NUL	0.06	2.3
TS-221	RN18-0104	62.5	wm	pure	2198	2238	2347	0.09	0.02	0.03	2.7
TS-222	RN18-0104	65.5	wm	pure	2198	NUL	2349	0.13	NUL	0.06	2.3
TS-223	RN18-0104	68.5	wm	pure	2200	NUL	NUL	0.07	NUL	NUL	NUL
TS-224	RN18-0104	71.6	wm	pure	2199	2238	2347	0.16	0.03	0.07	2.2
TS-225	RN18-0104	74.7	wm	pure	2198	2238	2346	0.14	0.02	0.06	2.2
TS-226	RN18-0104	80.7	wm-mont	mix	2196	2238	2346	0.14	0.02	0.06	2.5
TS-227	RN18-0104	83.7	wm	pure	2197	2237	2346	0.15	0.02	0.06	2.5
TS-228	RN18-0104	87.0	wm	pure	2197	2237	2338	0.09	0.02	0.03	2.8
TS-229	RN18-0104	94.0	wm-mont	mix	2195	2235	2340	0.14	0.02	0.05	2.8
TS-230	RN18-0104	102.2	prg	pure	2194	2238	2339	0.17	0.02	0.08	2.3
TS-231	RN18-0104	105.3	prg	pure	NUL	NUL	2344	NUL	NUL	0.05	0.0
TS-232	RN18-0104	113.8	wm-ep	mix	2216	2251	2337	0.07	0.07	0.07	1.1
TS-233	RN18-0104	118.6	chl-wm	mix	2216	2248	2332	0.06	0.07	0.07	0.8
TS-234	RN18-0104	122.1	wm-ep	mix	2216	2247	2331	0.06	0.05	0.06	1.0
TS-235	RN18-0104	129.5	chl	pure	NUL	2255	2340	NUL	0.23	0.27	0.0
TS-236	RN18-0104	132.6	chl-ep	mix	NUL	2255	2340	NUL	0.29	0.37	0.0
TS-237	RN18-0104	135.6	chl-ep	mix	NUL	2255	2343	NUL	0.31	0.40	0.0
TS-238	RN18-0104	146.5	chl	pure	NUL	2256	2341	NUL	0.23	0.30	0.0
TS-239	BG18-3321a	10.5	chl-ep	mix	NUL	2253	2342	0.00	0.24	0.31	0.0
TS-240	BG18-3321a	13.7	chl-wm	mix	NUL	2253	2344	0.00	0.30	0.34	0.0
TS-241	BG18-3321a	16.8	chl-wm	mix	2215	2252	2341	0.13	0.17	0.25	0.5
TS-242	BG18-3321a	22.5	chl-ep	mix	NUL	2254	2342	0.00	0.31	0.41	0.0
TS-243	BG18-3321a	26.2	chl	pure	NUL	2253	2342	0.00	0.23	0.23	0.0
TS-244	BG18-3321a	29.3	chl	pure	NUL	2253	2339	0.00	0.29	0.32	0.0
TS-245	BG18-3321a	41.1	chl-wm	mix	2201	2255	2346	0.13	0.17	0.17	0.8
TS-246	BG18-3321a	65.5	wm	pure	2201	NUL	2341	0.20	0.00	0.10	2.0
TS-247	BG18-3321a	73.5	wm	pure	2201	NUL	2348	0.25	0.00	0.13	1.9
TS-248	BG18-3321a	80.8	wm	pure	2200	NUL	2347	0.16	0.00	0.07	2.3
TS-249	BG18-3321a	83.8	wm	pure	2199	2238	2343	0.13	0.06	0.05	2.5
TS-250	BG18-3321a	86.8	wm	pure	2200	NUL	2344	0.18	0.00	0.09	2.0
TS-251	BG18-3321a	89.9	wm	pure	2199	2239	2346	0.22	0.05	0.11	2.0
TS-252	BG18-3321a	96.0	wm	pure	2200	2242	2352	0.10	0.03	0.05	2.2
TS-253	BG18-3321a	99.1	wm	pure	2200	NUL	2345	0.21	0.00	0.11	1.9
TS-254	BG18-3321a	103.1	wm	pure	2200	NUL	2349	0.15	0.00	0.08	2.0
TS-255	BG18-3321a	121.9	wm-mont	mix	2197	NUL	2347	0.32	0.00	0.16	2.0
TS-256	BG18-3321a	125.0	wm	pure	2197	2239	2347	0.26	0.06	0.12	2.1
TS-257	BG18-3321a	132.8	wm-mont	mix	2197	NUL	2344	0.27	0.00	0.14	2.0
TS-258	BG18-3321a	137.2	wm-mont	mix	2198	NUL	2339	0.24	0.00	0.12	2.1
TS-259	BG18-3321a	145.5	chl-wm	mix	2197	2251	2334	0.08	0.13	0.10	0.8

Table G.1 Continued.

Sample	DDH	Depth (m)	Mineral Results	SWIR Response	Feature Position (nm)			Feature Depth			AlOHd/ MgOHd
					AlOH	FeOH	MgOH	AlOH	FeOH	MgOH	
TS-260	BG18-3321a	147.5	chl-wm	mix	2200	2251	2347	0.09	0.08	0.08	1.1
TS-261	BG18-3321a	150.9	prg	pure	2197	2246	2341	0.30	0.14	0.18	1.7
TS-262	BG18-3321a	156.5	wm	pure	2199	NUL	2340	0.13	0.00	0.08	1.7
TS-263	BG18-3321a	157.0	wm-chl	mix	2198	2249	2340	0.19	0.11	0.13	1.5
TS-264	BG18-3321a	161.2	chl-wm	mix	2199	2253	2345	0.37	0.25	0.26	1.4
TS-265	BG18-3321a	170.4	chl-wm	mix	2199	2253	2343	0.11	0.10	0.10	1.1
TS-266	BG18-3321a	175.5	chl-wm	mix	2201	2252	2342	0.15	0.14	0.13	1.2
TS-267	BG18-3321a	181.5	chl-wm	mix	2202	2255	2342	0.07	0.14	0.14	0.5
TS-268	BG18-3321a	187.5	wm	pure	2200	NUL	2346	0.17	0.00	0.08	2.1
TS-269	BG18-3321a	193.5	wm-chl	mix	2198	2252	2346	0.19	0.07	0.10	1.9
TS-270	BG18-3321a	199.6	wm-chl	mix	2198	2239	2348	0.26	0.10	0.15	1.8
TS-271	BG18-3321a	206.0	wm-ch	mix	2197	2251	2348	0.27	0.08	0.14	1.9
TS-272	BG18-3321a	211.8	wm	pure	2197	NUL	2344	0.16	0.00	0.08	2.0
TS-273	BG18-3321a	218.9	wm	pure	2199	2238	2348	0.16	0.05	0.08	2.0
TS-274	BG18-3321a	227.1	wm	pure	2197	2237	2330	0.10	0.05	0.04	2.5
TS-275	BG18-3321a	233.2	wm	pure	2199	NUL	2346	0.12	0.00	0.04	2.8
TS-276	BG18-3321a	239.2	chl-wm	mix	2199	2250	2342	0.25	0.21	0.20	1.3
TS-277	BG18-3321	4.5	chl-wm	mix	2201	2255	2342	0.09	0.21	0.19	0.5
TS-278	BG18-3321	10.1	chl-wm	mix	2202	2254	2341	0.19	0.26	0.31	0.6
TS-279	BG18-3321	15.2	chl	pure	2205	2255	2340	0.07	0.17	0.18	0.4
TS-280	BG18-3321	18.3	chl	pure	NUL	2252	2339	0.00	0.23	0.24	0.0
TS-281	BG18-3321	21.4	chl-wm	mix	2198	2251	2341	0.22	0.09	0.13	1.7
TS-282	BG18-3321	24.6	chl-wm	mix	2200	2256	2345	0.10	0.22	0.22	0.4
TS-283	BG18-3321	27.6	chl	pure	2206	2255	2347	0.07	0.20	0.19	0.4
TS-284	BG18-3321	30.5	chl-wm	mix	2206	2256	NUL	0.09	0.19	0.00	NUL
TS-285	BG18-3321	44.2	chl	pure	NUL	2256	2349	0.00	0.19	0.18	0.0
TS-286	BG18-3321	48.8	wm	pure	2204	NUL	2348	0.29	0.00	0.19	1.5
TS-287	BG18-3321	51.7	wm	pure	2205	NUL	2347	0.21	0.00	0.12	1.8
TS-288	BG18-3321	54.8	wm	pure	2207	NUL	2350	0.22	0.00	0.12	1.8
TS-289	BG18-3321	58.9	wm	pure	2205	NUL	2348	0.30	0.00	0.16	1.8
TS-290	BG18-3321	61.0	wm	pure	2202	NUL	2344	0.12	0.00	0.04	2.8
TS-291	BG18-3321	65.0	wm	pure	2202	NUL	NUL	0.15	0.00	0.00	NUL
TS-292	BG18-3321	68.1	wm	pure	2204	2238	2340	0.13	0.05	0.06	2.1
TS-293	BG18-3321	70.4	wm	pure	2207	NUL	2347	0.18	0.00	0.09	2.0
TS-294	BG18-3321	73.4	wm	pure	2204	NUL	2352	0.18	0.00	0.09	2.0
TS-295	BG18-3321	79.5	wm	pure	2202	NUL	2348	0.15	0.00	0.07	2.1
TS-296	BG18-3321	81.2	wm	pure	2203	NUL	2348	0.19	0.00	0.10	2.0
TS-297	BG18-3321	88.5	wm	pure	2202	NUL	2345	0.22	0.00	0.12	1.8
TS-298	BG18-3321	91.4	wm	pure	2201	NUL	2345	0.23	0.00	0.13	1.8
TS-299	BG18-3321	95.0	wm	pure	2199	NUL	2343	0.15	0.00	0.06	2.4
TS-300	BG18-3321	97.5	wm	pure	2201	NUL	2348	0.24	0.00	0.13	1.9
TS-301	BG18-3321	100.4	wm-cb	mix	2200	2246	2340	0.26	0.07	0.20	1.3
TS-302	BG18-3321	106.7	wm	pure	2199	NUL	2346	0.23	0.00	0.12	1.9
TS-303	BG18-3321	108.2	prg	pure	2199	2238	2342	0.37	0.11	0.20	1.9
TS-304	BG18-3321	122.9	wm	pure	2198	NUL	2337	0.17	0.00	0.07	2.5
TS-305	BG18-3321	125.0	wm	pure	2197	2239	2344	0.28	0.06	0.13	2.2
TS-306	BG18-3321	138.0	chl-wm	mix	2197	2255	2340	0.34	0.26	0.24	1.4
TS-307	BG18-3321	140.2	chl-wm	mix	2197	2253	2347	0.35	0.33	0.29	1.2
TS-308	BG18-3321	147.3	chl-wm	mix	2197	2253	2342	0.40	0.31	0.31	1.3
TS-309	BG18-3321	159.0	chl-wm	mix	2197	2254	2341	0.32	0.26	0.25	1.3
TS-310	BG18-3321	163.0	wm-chl	mix	2197	2248	2340	0.40	0.18	0.23	1.7
TS-311	BG18-3321	166.0	wm-ch	mix	2198	2249	2344	0.16	0.06	0.09	1.9

Table G.1 Continued.

Sample	DDH	Depth (m)	Mineral Results	SWIR Response	Feature Position (nm)			Feature Depth			AlOHd/ MgOHd
					AlOH	FeOH	MgOH	AlOH	FeOH	MgOH	
TS-312	BG18-3321	167.6	chl-wm	mix	2198	2251	2340	0.20	0.19	0.17	1.2
TS-313	BG18-3321	170.7	chl-wm	mix	2198	2251	2341	0.23	0.27	0.24	1.0
TS-314	BG18-3321	173.9	wm	pure	2198	NUL	2342	0.16	0.00	0.07	2.3
TS-315	BG18-3321	175.8	chl-wm	mix	2200	NUL	2339	0.09	0.00	0.08	1.1
TS-316	BG18-3321	180.0	wm	pure	2199	NUL	2344	0.40	0.00	0.23	1.8
TS-317	BG18-3321	185.8	wm	pure	2198	NUL	2347	0.22	0.00	0.11	2.1
TS-318	BG18-3321	188.0	wm-chl	mix	2196	2251	2344	0.28	0.10	0.16	1.8
TS-319	BG18-3904	12.2	chl	pure	NUL	2253	2342	0.00	0.36	0.40	0.0
TS-320	BG18-3904	15.2	chl-wm	mix	2201	2254	2342	0.20	0.33	0.34	0.6
TS-321	BG18-3904	18.3	chl-wm	mix	2214	2252	2340	0.14	0.26	0.24	0.6
TS-322	BG18-3904	21.3	wm	pure	2210	NUL	2348	0.24	0.00	0.14	1.7
TS-323	BG18-3904	24.4	chl-wm	mix	2208	2253	2342	0.16	0.34	0.35	0.4
TS-324	BG18-3904	30.5	chl	pure	2220	2254	2342	0.12	0.35	0.41	0.3
TS-325	BG18-3904	36.6	chl-wm	mix	2215	2253	2339	0.17	0.28	0.33	0.5
TS-326	BG18-3904	39.6	chl-wm	mix	2215	2254	2344	0.26	0.35	0.38	0.7
TS-327	BG18-3904	42.7	chl-wm	mix	2219	2254	2342	0.12	0.23	0.29	0.4
TS-328	BG18-3904	45.7	chl-wm	mix	2219	2253	2340	0.12	0.21	0.22	0.5
TS-329	BG18-3904	48.9	chl-ep	mix	NUL	2254	2340	0.00	0.23	0.30	0.0
TS-330	BG18-3904	57.5	wm-chl	mix	2215	2249	2345	0.48	0.37	0.41	1.2
TS-331	BG18-3904	85.3	wm	pure	2203	NUL	2346	0.21	0.00	0.11	2.0
TS-332	BG18-3904	89.0	chl-wm	mix	2204	2256	2349	0.15	0.33	0.30	0.5
TS-333	BG18-3904	94.5	wm	pure	2199	NUL	2349	0.17	0.00	0.08	2.2
TS-334	BG18-3904	97.5	wm	pure	2199	NUL	2345	0.16	0.00	0.08	2.1
TS-335	BG18-3904	100.2	wm	pure	2200	NUL	2348	0.11	0.00	0.04	2.3
TS-336	BG18-3904	102.9	wm	pure	2198	NUL	2344	0.25	0.00	0.13	1.9
TS-337	BG18-3904	109.4	wm	pure	2199	NUL	2337	0.10	0.00	0.04	2.5
TS-338	BG18-3904	113.8	wm	pure	2197	NUL	2345	0.37	0.00	0.18	2.1
TS-339	BG18-3904	118.5	wm	pure	2199	2237	2344	0.12	0.02	0.05	2.5
TS-340	BG18-3904	121.8	wm	pure	2198	NUL	2344	0.16	0.00	0.07	2.2
TS-341	BG18-3904	125.0	wm	pure	2197	NUL	2344	0.18	0.00	0.08	2.2
TS-342	BG18-3904	127.0	wm	pure	2199	NUL	2349	0.23	0.00	0.11	2.0
TS-343	BG18-3904	133.5	wm	pure	2200	NUL	2345	0.18	0.00	0.09	2.0
TS-344	BG18-3904	136.5	wm-ch	mix	2199	2238	2344	0.35	0.11	0.20	1.8
TS-345	BG18-3904	139.1	wm-chl	mix	2199	2240	2340	0.14	0.04	0.08	1.7
TS-346	BG18-3904	146.3	chl-wm	mix	2199	2253	2346	0.22	0.13	0.15	1.5
TS-347	BG18-3904	149.4	wm	pure	2199	NUL	2345	0.24	0.00	0.11	2.2
TS-348	BG18-3904	155.4	wm	pure	2199	2239	2345	0.23	0.06	0.11	2.2
TS-349	BG18-3904	158.5	wm-ch	mix	2200	2235	2347	0.31	0.10	0.19	1.6
TS-350	BG18-3904	170.6	chl	pure	NUL	2255	2341	0.00	0.31	0.28	0.0
TS-351	BG18-3904	173.7	chl	pure	NUL	2253	2339	0.00	0.28	0.23	0.0
TS-352	BG18-3904	176.8	chl-wm	mix	2201	2252	2342	0.25	0.24	0.22	1.2
TS-353	BG18-3904	179.8	chl-wm	mix	2201	2254	2340	0.19	0.21	0.21	0.9
TS-354	BG18-3904	182.9	chl-wm	mix	2201	2255	2344	0.20	0.33	0.30	0.7
TS-355	BG18-3904	189.0	chl-wm	mix	2201	2253	2340	0.15	0.15	0.16	1.0
TS-356	BG18-3904	195.1	chl-wm	mix	2201	2253	2338	0.08	0.12	0.12	0.7
TS-357	BG18-3904	198.1	chl-wm	mix	2200	2249	2343	0.15	0.09	0.13	1.2
TS-358	BG18-3904	199.5	wm-cb	mix	2204	2241	2339	0.09	0.03	0.15	0.6
TS-359	BG18-3550	10.7	chl	pure	NUL	2254	2340	0.00	0.30	0.35	0.0
TS-360	BG18-3550	13.6	chl	pure	NUL	2254	2344	0.00	0.36	0.41	0.0
TS-361	BG18-3550	16.9	chl-ep	mix	2217	2253	2342	0.08	0.16	0.23	0.3
TS-362	BG18-3550	23.2	chl	pure	2217	2254	2343	0.10	0.29	0.35	0.3
TS-363	BG18-3550	28.0	chl	pure	NUL	2254	2339	0.00	0.32	0.39	0.0

Table G.1 Continued.

Sample	DDH	Depth (m)	Mineral Results	SWIR Response	Feature Position (nm)			Feature Depth			AlOHd/ MgOHd
					AlOH	FeOH	MgOH	AlOH	FeOH	MgOH	
TS-364	BG18-3550	32.0	chl-ep	mix	NUL	2254	2341	0.00	0.26	0.33	0.0
TS-365	BG18-3550	35.0	chl-wm	mix	2209	2253	2347	0.18	0.24	0.25	0.7
TS-366	BG18-3550	38.3	chl	pure	2205	2254	2343	0.08	0.22	0.26	0.3
TS-367	BG18-3550	41.5	chl-wm	mix	2202	2255	2342	0.08	0.17	0.16	0.5
TS-368	BG18-3550	44.3	chl-wm	mix	2199	2253	2344	0.29	0.20	0.20	1.5
TS-369	BG18-3550	47.2	chl-wm	mix	2198	2253	2341	0.36	0.19	0.23	1.6
TS-370	BG18-3550	49.8	chl-wm	mix	2197	2256	2344	0.20	0.18	0.17	1.2
TS-371	BG18-3550	53.3	chl-wm	mix	2197	2256	2344	0.27	0.25	0.23	1.2
TS-372	BG18-3550	64.5	wm	pure	2201	NUL	2346	0.23	0.00	0.12	1.9
TS-373	BG18-3550	68.0	wm	pure	2201	NUL	2346	0.33	0.00	0.18	1.8
TS-374	BG18-3550	71.2	wm	pure	2200	NUL	2345	0.22	0.00	0.11	2.0
TS-375	BG18-3550	77.7	wm	pure	2201	NUL	2345	0.33	0.00	0.18	1.9
TS-376	BG18-3550	80.8	wm	pure	2201	NUL	2346	0.33	0.00	0.18	1.8
TS-377	BG18-3550	84.0	wm	pure	2200	NUL	2349	0.21	0.00	0.11	1.9
TS-378	BG18-3550	90.0	wm	pure	2198	NUL	2345	0.33	0.00	0.18	1.9
TS-379	BG18-3550	93.0	wm	pure	2199	NUL	2345	0.22	0.00	0.10	2.2
TS-380	BG18-3550	97.0	wm	pure	2200	NUL	2345	0.22	0.00	0.11	2.1
TS-381	BG18-3550	99.1	wm	pure	2201	NUL	2349	0.10	0.00	0.03	3.0
TS-382	BG18-3550	105.1	wm	pure	2199	NUL	2344	0.17	0.00	0.09	2.0
TS-383	BG18-3550	108.2	wm	pure	2201	NUL	2348	0.12	0.00	0.04	3.1
TS-384	BG18-3550	112.8	wm	pure	2199	NUL	2348	0.17	0.00	0.08	2.1
TS-385	BG18-3550	136.2	wm	pure	2198	NUL	2342	0.20	0.00	0.09	2.2
TS-386	BG18-3550	143.3	wm-chl	mix	2200	2248	2346	0.11	0.05	0.06	1.7
TS-387	BG18-3550	146.0	chl-wm	mix	2199	2250	2340	0.10	0.09	0.08	1.2
TS-388	BG18-3550	148.0	chl-wm	mix	2199	2249	2339	0.11	0.06	0.06	1.7
TS-389	BG18-3550	158.5	wm-chl	mix	2200	2249	2346	0.18	0.06	0.10	1.8
TS-390	BG18-3550	164.6	chl-wm	mix	2198	2252	2343	0.26	0.24	0.21	1.2
TS-391	BG18-3550	170.7	chl-wm	mix	2202	2254	2345	0.12	0.16	0.16	0.8
TS-392	BG18-3550	176.8	chl-wm	mix	2200	2253	2344	0.14	0.15	0.14	1.0
TS-393	BG18-3550	182.9	wm	pure	2201	NUL	2345	0.30	0.00	0.16	1.9
TS-394	BG18-3550	189.0	chl-wm	mix	2202	2255	2346	0.11	0.20	0.18	0.6
TS-395	BG18-3550	195.1	chl-wm	mix	2201	2253	2346	0.14	0.08	0.10	1.4
TS-396	BG18-3550	204.2	chl-wm	mix	2198	2254	2346	0.32	0.17	0.20	1.6
TS-397	BG18-3550	210.3	chl-wm	mix	2199	2255	2344	0.15	0.09	0.11	1.4
TS-398	BG18-3550	216.4	chl-wm	mix	2198	2254	2345	0.23	0.13	0.15	1.6
TS-399	BG18-3550	219.5	wm-chl	mix	2198	2248	2344	0.24	0.09	0.13	1.8
TS-400	BG18-3550	223.0	wm	pure	2199	NUL	2346	0.27	0.00	0.14	1.9
TS-401	BG18-3551	6.1	chl	pure	NUL	2254	2344	0.00	0.32	0.37	0.0
TS-402	BG18-3551	15.2	chl-wm	mix	2220	2253	2341	0.17	0.31	0.34	0.5
TS-403	BG18-3551	18.3	chl	pure	NUL	2254	2341	0.00	0.30	0.35	0.0
TS-404	BG18-3551	21.3	chl-ep	mix	NUL	2254	2340	0.00	0.31	0.40	0.0
TS-405	BG18-3551	24.4	chl-ep	mix	NUL	2254	2342	0.00	0.26	0.32	0.0
TS-406	BG18-3551	27.4	chl	pure	NUL	2254	2340	0.00	0.26	0.32	0.0
TS-407	BG18-3551	30.5	chl-ep	mix	NUL	2254	2341	0.00	0.23	0.34	0.0
TS-408	BG18-3551	42.7	chl-wm	mix	2201	2253	2345	0.24	0.20	0.21	1.1
TS-409	BG18-3551	55.0	chl-cb	mix	NUL	2255	2337	0.00	0.11	0.20	0.0
TS-410	BG18-3551	61.0	wm	pure	2201	NUL	2346	0.16	0.00	0.08	2.1
TS-411	BG18-3551	67.1	wm	pure	2202	NUL	2347	0.30	0.00	0.17	1.8
TS-412	BG18-3551	73.5	wm	pure	2201	NUL	2346	0.18	0.00	0.09	2.1
TS-413	BG18-3551	76.2	wm	pure	2202	NUL	2349	0.23	0.00	0.13	1.9
TS-414	BG18-3551	85.3	wm	pure	2199	NUL	2341	0.12	0.00	0.06	2.2
TS-415	BG18-3551	91.2	wm	pure	2200	2239	2346	0.20	0.05	0.09	2.2

Table G.1 Continued.

Sample	DDH	Depth (m)	Mineral Results	SWIR Response	Feature Position (nm)			Feature Depth			AlOHd/ MgOHd
					AlOH	FeOH	MgOH	AlOH	FeOH	MgOH	
TS-416	BG18-3551	123.3	chl-wm	mix	2198	2250	2339	0.27	0.22	0.21	1.3
TS-417	BG18-3551	128.0	wm-chl	mix	2198	2250	2339	0.22	0.13	0.14	1.6
TS-418	BG18-3551	143.0	wm-chl	mix	2200	2249	2340	0.13	0.07	0.08	1.6
TS-419	BG18-3551	158.5	chl-wm	mix	2198	2252	2342	0.20	0.20	0.17	1.2
TS-420	BG18-3551	173.7	chl-wm	mix	2199	2252	2339	0.28	0.24	0.21	1.3
TS-421	BG18-3551	183.0	chl-wm	mix	2201	2254	2339	0.13	0.10	0.10	1.3
TS-422	BG18-3551	192.0	chl-wm	mix	2200	2253	2348	0.24	0.14	0.15	1.6
TS-423	BG18-3551	205.2	wm-chl	mix	2201	2252	2346	0.21	0.09	0.12	1.8
TS-424	BG18-3551	216.4	chl-wm	mix	2200	2252	2343	0.14	0.08	0.08	1.7
TS-425	BG18-3551	222.5	chl-wm	mix	2201	2253	2348	0.19	0.09	0.11	1.7
TS-426	BG18-3322	60.5	wm	pure	2205	NUL	2349	0.16	0.00	0.07	2.2
TS-427	BG18-3322	64.0	wm	pure	2206	NUL	2349	0.14	0.00	0.06	2.3
TS-428	BG18-3322	67.7	wm	pure	2206	NUL	2351	0.24	0.00	0.13	1.9
TS-429	BG18-3322	70.7	wm	pure	2206	NUL	2348	0.18	0.00	0.08	2.1
TS-430	BG18-3322	73.2	wm	pure	2205	NUL	2350	0.20	0.00	0.10	2.0
TS-431	BG18-3322	76.2	wm	pure	2202	NUL	2348	0.14	0.00	0.06	2.3
TS-432	BG18-3322	78.5	wm	pure	2205	NUL	2350	0.20	0.00	0.10	2.0
TS-433	BG18-3322	82.3	wm	pure	2203	NUL	2348	0.20	0.00	0.11	1.8
TS-434	BG18-3322	86.8	wm	pure	2203	NUL	2345	0.25	0.00	0.13	1.9
TS-435	BG18-3322	90.9	wm	pure	2201	NUL	2345	0.25	0.00	0.13	1.9
TS-436	BG18-3322	94.0	wm	pure	2201	NUL	2342	0.19	0.00	0.09	2.1
TS-437	BG18-3322	98.8	wm	pure	2203	NUL	2348	0.20	0.00	0.10	2.0
TS-438	BG18-3322	101.4	wm	pure	2200	NUL	2348	0.15	0.00	0.07	2.3
TS-439	BG18-3322	103.4	prg	pure	2200	NUL	2347	0.28	0.00	0.14	2.0
TS-440	BG18-3322	106.8	wm	pure	2199	NUL	2344	0.14	0.00	0.06	2.1
TS-441	BG18-3322	109.7	wm	pure	2200	NUL	2344	0.28	0.00	0.13	2.2
TS-442	BG18-3322	122.3	wm	pure	2198	NUL	2340	0.17	0.00	0.07	2.2
TS-443	BG18-3322	126.1	wm	pure	2198	NUL	2344	0.18	0.00	0.08	2.3
TS-444	BG18-3322	129.8	wm	pure	2198	NUL	2341	0.18	0.00	0.08	2.3
TS-445	BG18-3322	133.1	prg	pure	2197	NUL	2343	0.30	0.00	0.15	2.1
TS-446	BG18-3322	139.5	wm-mont	mix	2197	NUL	2347	0.20	0.00	0.09	2.3
TS-447	BG18-3322	145.0	chl-wm	mix	2197	2252	2341	0.34	0.21	0.21	1.6
TS-448	BG18-3322	148.4	chl-wm	mix	2197	2251	2344	0.36	0.19	0.22	1.7
TS-449	BG18-3322	152.4	chl-wm	mix	2200	2253	2342	0.18	0.23	0.21	0.9
TS-450	BG18-3322	156.4	wm-cb	mix	2198	2250	2342	0.16	0.05	0.08	1.9
TS-451	BG18-3322	159.8	wm-ch	mix	2197	NUL	2338	0.13	0.00	0.06	2.2
TS-452	BG18-3322	162.1	wm	pure	2198	NUL	2346	0.23	0.00	0.11	2.0
TS-453	BG18-3322	166.0	wm-chl	mix	2199	2251	2344	0.15	0.09	0.09	1.6
TS-454	BG18-3322	167.6	wm-ch	mix	2198	2248	2343	0.23	0.07	0.12	1.9
TS-455	BG18-3322	172.0	wm	pure	2198	NUL	2342	0.25	0.00	0.12	2.0
TS-456	BG18-3322	175.2	wm	pure	2198	NUL	2345	0.22	0.00	0.11	2.0
TS-457	BG18-3322	179.4	wm-ch	mix	2198	2248	2344	0.26	0.08	0.14	1.9
TS-458	BG18-3322	180.6	chl-wm	mix	2198	2250	2340	0.27	0.17	0.18	1.5
TS-459	BG18-3905	12.4	chl-ep	mix	NUL	2253	2341	0.00	0.36	0.44	0.0
TS-460	BG18-3905	18.0	chl	pure	NUL	2253	2341	0.00	0.36	0.42	0.0
TS-461	BG18-3905	21.3	chl	pure	NUL	2253	2341	0.00	0.32	0.36	0.0
TS-462	BG18-3905	24.4	chl	pure	NUL	2253	2344	0.00	0.28	0.31	0.0
TS-463	BG18-3905	29.2	wm-cb	mix	2214	NUL	2347	0.24	0.00	0.23	1.0
TS-464	BG18-3905	30.5	chl-wm	mix	2216	2252	2341	0.24	0.27	0.28	0.9
TS-465	BG18-3905	33.5	chl-ep	mix	NUL	2253	2340	0.00	0.31	0.39	0.0
TS-466	BG18-3905	45.7	chl-ep	mix	NUL	2254	2341	0.00	0.21	0.29	0.0
TS-467	BG18-3905	49.0	chl-wm	mix	NUL	2250	2340	0.00	0.15	0.15	0.0

Table G.1 Continued.

Sample	DDH	Depth (m)	Mineral Results	SWIR Response	Feature Position (nm)			Feature Depth			AlOHd/ MgOHd
					AlOH	FeOH	MgOH	AlOH	FeOH	MgOH	
TS-468	BG18-3905	54.9	chl-wm	mix	NUL	2253	2341	0.00	0.25	0.25	0.0
TS-469	BG18-3905	58.5	chl	pure	NUL	2253	2341	0.00	0.30	0.34	0.0
TS-470	BG18-3905	61.0	chl-wm	mix	NUL	2253	2340	0.00	0.32	0.39	0.0
TS-471	BG18-3905	64.0	chl-ep	mix	NUL	2254	2342	0.00	0.26	0.33	0.0
TS-472	BG18-3905	67.1	chl-ep	mix	NUL	2254	2340	0.00	0.32	0.41	0.0
TS-473	BG18-3905	70.1	chl	pure	NUL	2254	2341	0.00	0.33	0.39	0.0
TS-474	BG18-3905	73.2	chl-ep	mix	NUL	2255	2342	0.00	0.33	0.43	0.0
TS-475	BG18-3905	76.4	chl-ep	mix	NUL	2254	2340	0.00	0.35	0.45	0.0
TS-476	BG18-3905	79.2	chl	pure	NUL	2255	2344	0.00	0.32	0.42	0.0
TS-477	BG18-3905	82.3	chl-ep	mix	NUL	2254	2341	0.00	0.31	0.40	0.0
TS-478	BG18-3905	85.3	chl-ep	mix	NUL	2255	2339	0.00	0.33	0.44	0.0
TS-479	BG18-3905	88.9	chl-ep	mix	NUL	2255	2342	0.00	0.30	0.39	0.0
TS-480	BG18-3905	91.6	chl-ep	mix	NUL	2254	2340	0.00	0.31	0.45	0.0
TS-481	BG18-3905	95.0	chl	pure	NUL	2255	2342	0.00	0.27	0.33	0.0
TS-482	BG18-3905	103.6	wm	pure	2203	NUL	2349	0.10	0.00	0.05	2.0
TS-483	BG18-3905	106.7	chl-wm	mix	2202	NUL	2347	0.28	0.00	0.17	1.6
TS-484	BG18-3905	110.7	wm	pure	2200	NUL	2347	0.26	0.00	0.13	1.9
TS-485	BG18-3905	113.8	wm	pure	2203	NUL	2346	0.24	0.00	0.14	1.7
TS-486	BG18-3905	115.8	wm	pure	2203	NUL	2345	0.20	0.00	0.10	2.1
TS-487	BG18-3905	119.3	wm	pure	2199	NUL	2347	0.18	0.00	0.07	2.4
TS-488	BG18-3905	123.0	wm	pure	2202	NUL	2347	0.14	0.00	0.06	2.3
TS-489	BG18-3905	125.0	wm	pure	2199	NUL	2350	0.15	0.00	0.07	2.2
TS-490	BG18-3905	128.7	wm	pure	2203	NUL	2348	0.20	0.00	0.12	1.7
TS-491	BG18-3905	131.8	wm	pure	2200	NUL	2347	0.26	0.00	0.14	1.9
TS-492	BG18-3905	134.0	wm	pure	2201	NUL	2348	0.13	0.00	0.06	2.4
TS-493	BG18-3905	144.9	wm-ch	mix	2198	2248	2341	0.15	0.05	0.07	2.1
TS-494	BG18-3905	155.4	chl-wm	mix	2199	2251	2339	0.39	0.31	0.29	1.3
TS-495	BG18-3905	158.5	chl-wm	mix	2200	2252	2336	0.19	0.26	0.22	0.9
TS-496	BG18-3905	170.7	chl-wm	mix	2203	2255	2346	0.12	0.25	0.22	0.5
TS-497	BG18-3905	182.9	chl-wm	mix	2199	2253	2346	0.28	0.26	0.25	1.1
TS-498	BG18-3905	185.9	chl-wm	mix	2200	2254	2345	0.21	0.22	0.20	1.1
TS-499	BG18-3323	42.7	chl	pure	NUL	2255	2342	0.00	0.24	0.31	0.0
TS-500	BG18-3323	45.7	chl	pure	NUL	2255	2340	0.00	0.22	0.26	0.0
TS-501	BG18-3323	76.0	wm	pure	2202	NUL	2354	0.16	0.00	0.08	2.0
TS-502	BG18-3323	79.4	wm	pure	2206	NUL	2348	0.22	0.00	0.12	1.9
TS-503	BG18-3323	86.0	wm	pure	2201	NUL	2348	0.22	0.00	0.12	1.9
TS-504	BG18-3323	91.4	wm	pure	2202	NUL	2349	0.24	0.00	0.13	1.9
TS-505	BG18-3323	94.5	wm	pure	2200	NUL	2343	0.21	0.00	0.11	2.0
TS-506	BG18-3323	97.5	wm	pure	2201	NUL	2349	0.15	0.00	0.07	2.1
TS-507	BG18-3323	99.5	wm	pure	2203	NUL	2350	0.20	0.00	0.10	1.9
TS-508	BG18-3323	109.7	wm	pure	2200	NUL	2346	0.19	0.00	0.09	2.0
TS-509	BG18-3323	113.6	wm	pure	2200	NUL	2346	0.19	0.00	0.10	1.9
TS-510	BG18-3323	117.2	wm	pure	2200	NUL	2347	0.16	0.00	0.08	2.1
TS-511	BG18-3323	119.2	wm	pure	2198	NUL	2347	0.20	0.00	0.10	2.1
TS-512	BG18-3323	121.9	wm	pure	2199	NUL	2340	0.15	0.00	0.06	2.3
TS-513	BG18-3323	127.0	wm	pure	2199	NUL	2346	0.15	0.00	0.07	2.1
TS-514	BG18-3323	130.2	wm	pure	2198	NUL	2344	0.18	0.00	0.09	2.1
TS-515	BG18-3323	131.4	wm	pure	2199	NUL	2343	0.17	0.00	0.08	2.1
TS-516	BG18-3323	136.8	wm	pure	2199	NUL	2348	0.19	0.00	0.09	2.1
TS-517	BG18-3323	141.0	wm-mont	mix	2198	NUL	2342	0.30	0.00	0.15	2.0
TS-518	BG18-3323	144.6	wm	pure	2198	NUL	2343	0.13	0.00	0.05	2.6
TS-519	BG18-3323	153.4	chl-wm	mix	2196	2254	2340	0.21	0.20	0.18	1.2

Table G.1 Continued.

Sample	DDH	Depth (m)	Mineral Results	SWIR Response	Feature Position (nm)			Feature Depth			AlOHd/ MgOHd
					AlOH	FeOH	MgOH	AlOH	FeOH	MgOH	
TS-520	BG18-3323	159.0	wm	pure	2199	NUL	2343	0.10	0.00	0.05	2.1
TS-521	BG18-3323	161.5	wm	pure	2197	2238	2347	0.16	0.03	0.07	2.2
TS-522	BG18-3323	164.6	wm	pure	2198	NUL	2348	0.13	0.00	0.06	2.1
TS-523	BG18-3323	167.6	wm	pure	2198	NUL	2346	0.17	0.00	0.08	2.1
TS-524	BG18-3323	176.8	wm	pure	2199	2237	2344	0.12	0.03	0.05	2.4
TS-525	BG18-3323	189.0	chl-wm	mix	2198	2251	2337	0.15	0.11	0.12	1.3
TS-526	BG18-3323	195.8	wm	pure	2201	NUL	2348	0.14	0.00	0.06	2.3
TS-527	BG18-3323	207.2	wm	pure	2202	NUL	2349	0.24	0.00	0.13	1.9
TS-528	BG18-3323	216.4	wm-ch	mix	2200	2247	2347	0.16	0.06	0.10	1.7
TS-529	BG18-3323	220.0	wm-ch	mix	2200	2248	2347	0.14	0.05	0.08	1.7
TS-530	BG18-3552	5.8	chl-wm	mix	2203	2254	2344	0.16	0.21	0.24	0.7
TS-531	BG18-3552	8.2	chl-ep	mix	2198	2254	2343	0.12	0.29	0.42	0.3
TS-532	BG18-3552	10.7	chl	pure	NUL	2254	2342	0.00	0.31	0.36	0.0
TS-533	BG18-3552	13.7	chl	pure	NUL	2253	2342	0.00	0.28	0.32	0.0
TS-534	BG18-3552	16.8	chl-wm	mix	NUL	2254	2342	0.00	0.31	0.36	0.0
TS-535	BG18-3552	19.5	chl-ep	mix	NUL	2254	2342	0.00	0.24	0.30	0.0
TS-536	BG18-3552	44.8	wm	pure	2208	NUL	2347	0.22	0.00	0.13	1.7
TS-537	BG18-3552	47.2	wm	pure	2200	NUL	2345	0.16	0.00	0.08	1.9
TS-538	BG18-3552	77.0	wm-cb	mix	2201	NUL	2340	0.19	0.00	0.11	1.8
TS-539	BG18-3552	80.8	wm	pure	2202	NUL	2349	0.23	0.00	0.13	1.8
TS-540	BG18-3552	83.8	wm	pure	2198	NUL	2346	0.16	0.00	0.08	2.0
TS-541	BG18-3552	89.9	wm	pure	2201	NUL	2348	0.13	0.00	0.07	2.0
TS-542	BG18-3552	96.2	wm	pure	2201	NUL	2345	0.19	0.00	0.10	2.0
TS-543	BG18-3552	99.1	prg	pure	2201	NUL	2346	0.33	0.00	0.18	1.9
TS-544	BG18-3552	102.1	wm	pure	2201	NUL	2345	0.19	0.00	0.10	1.9
TS-545	BG18-3552	105.2	wm-ch	mix	2200	NUL	2348	0.20	0.00	0.10	2.1
TS-546	BG18-3552	117.8	wm-ch	mix	2200	2241	2345	0.10	0.04	0.06	1.8
TS-547	BG18-3552	121.0	mw-chl	mix	2202	NUL	2346	0.21	0.00	0.12	1.8
TS-548	BG18-3552	126.5	wm-ch	mix	2201	2239	2345	0.26	0.11	0.15	1.8
TS-549	BG18-3552	129.5	wm	pure	2199	2238	2339	0.08	0.03	0.03	2.7
TS-550	BG18-3552	138.7	chl-wm	mix	2201	2249	2340	0.19	0.15	0.14	1.4
TS-551	BG18-3552	147.8	chl-wm	mix	2200	2251	2340	0.24	0.25	0.21	1.1
TS-552	BG18-3552	152.9	chl-wm	mix	2199	2252	2342	0.25	0.17	0.18	1.4
TS-553	BG18-3552	159.0	chl-wm	mix	2199	2250	2343	0.25	0.16	0.19	1.3
TS-554	BG18-3552	163.1	chl-wm	mix	2199	2251	2343	0.21	0.18	0.16	1.3
TS-555	BG18-3552	169.2	chl-wm	mix	2200	2252	2342	0.30	0.29	0.26	1.2
TS-556	BG18-3552	172.2	chl-wm	mix	2197	2251	2340	0.26	0.26	0.22	1.2
TS-557	BG18-3552	178.3	wm-chl	mix	2198	2250	2346	0.35	0.16	0.21	1.7
TS-558	BG18-3552	193.5	chl-wm	mix	2198	2250	2343	0.23	0.10	0.14	1.6
TS-559	BG18-3552	205.7	wm	pure	2199	NUL	2346	0.12	0.00	0.05	2.6
TS-560	BG18-3552	217.9	chl-wm	mix	2199	2251	2345	0.19	0.10	0.12	1.5
TS-561	BG18-3906	9.1	chl-wm	mix	2209	2252	2343	0.25	0.31	0.37	0.7
TS-562	BG18-3906	12.2	chl	pure	NUL	2252	2340	0.00	0.31	0.33	0.0
TS-563	BG18-3906	15.2	chl	pure	NUL	2253	2340	0.00	0.27	0.31	0.0
TS-564	BG18-3906	21.3	chl-wm	mix	2218	2252	2340	0.17	0.24	0.28	0.6
TS-565	BG18-3906	27.4	phn	pure	2215	2239	2349	0.19	0.12	0.13	1.4
TS-566	BG18-3906	35.1	wm-chl	mix	2217	2246	2349	0.07	0.06	0.06	1.3
TS-567	BG18-3906	38.1	chl-wm	mix	2219	2251	2340	0.24	0.28	0.36	0.7
TS-568	BG18-3906	41.1	chl-ep	mix	NUL	2253	2342	0.00	0.19	0.35	0.0
TS-569	BG18-3906	44.2	chl-ep	mix	NUL	2253	2340	0.00	0.20	0.28	0.0
TS-570	BG18-3906	49.4	chl-ep	mix	NUL	2254	2340	0.00	0.28	0.37	0.0
TS-571	BG18-3906	62.6	chl-ep	mix	NUL	2254	2341	0.00	0.32	0.43	0.0

Table G.1 Continued.

Sample	DDH	Depth (m)	Mineral Results	SWIR Response	Feature Position (nm)			Feature Depth			AlOHd/ MgOHd
					AlOH	FeOH	MgOH	AlOH	FeOH	MgOH	
TS-572	BG18-3906	65.5	chl	pure	NUL	2254	2340	0.00	0.32	0.40	0.0
TS-573	BG18-3906	76.2	chl-ep	mix	NUL	2254	2340	0.00	0.33	0.48	0.0
TS-574	BG18-3906	79.2	chl-ep	mix	NUL	2254	2341	0.00	0.29	0.39	0.0
TS-575	BG18-3906	85.3	chl-ep	mix	NUL	2254	2340	0.00	0.27	0.37	0.0
TS-576	BG18-3906	88.4	chl	pure	NUL	2254	2340	0.00	0.26	0.31	0.0
TS-577	BG18-3906	93.5	wm	pure	2205	NUL	2353	0.15	0.00	0.08	2.0
TS-578	BG18-3906	99.0	wm	pure	2203	NUL	2345	0.12	0.00	0.05	2.3
TS-579	BG18-3906	103.6	wm-cb	mix	2203	NUL	2347	0.11	0.00	0.05	2.1
TS-580	BG18-3906	106.7	wm	pure	2205	NUL	2347	0.29	0.00	0.17	1.7
TS-581	BG18-3906	109.9	wm	pure	2200	NUL	2350	0.20	0.00	0.10	2.0
TS-582	BG18-3906	112.8	wm	pure	2201	NUL	2347	0.18	0.00	0.08	2.1
TS-583	BG18-3906	115.8	wm	pure	2198	NUL	2347	0.25	0.00	0.12	2.1
TS-584	BG18-3906	118.9	wm	pure	2198	NUL	2345	0.28	0.00	0.14	2.0
TS-585	BG18-3906	122.4	wm	pure	2198	NUL	2346	0.18	0.00	0.08	2.2
TS-586	BG18-3906	124.8	wm	pure	2199	NUL	2348	0.19	0.00	0.09	2.1
TS-587	BG18-3906	131.6	wm	pure	2201	NUL	2345	0.21	0.00	0.10	2.1
TS-613	BG18-3553	6.9	chl-wm	mix	2203	2254	2345	0.13	0.20	0.23	0.6
TS-614	BG18-3553	9.1	chl	pure	2217	2254	2343	0.09	0.26	0.31	0.3
TS-615	BG18-3553	12.2	chl	pure	NUL	2253	2343	0.00	0.25	0.27	0.0
TS-616	BG18-3553	15.2	chl	pure	NUL	2254	2341	0.00	0.30	0.36	0.0
TS-617	BG18-3553	18.4	chl	pure	NUL	2253	2342	0.00	0.26	0.27	0.0
TS-618	BG18-3553	21.5	chl-ep	mix	2217	2254	2342	0.09	0.26	0.35	0.2
TS-619	BG18-3553	24.4	chl-ep	mix	2218	2253	2341	0.15	0.30	0.40	0.4
TS-620	BG18-3553	27.4	chl-ep	mix	NUL	2254	2342	0.00	0.12	0.15	0.0
TS-621	BG18-3553	33.6	chl-ep	mix	2217	2254	2342	0.04	0.19	0.26	0.1
TS-623	BG18-3553	36.8	chl-wm	mix	2205	2253	2343	0.09	0.15	0.23	0.4
TS-624	BG18-3553	39.6	chl	pure	2210	2254	2341	0.08	0.22	0.22	0.3
TS-625	BG18-3553	42.7	cb-mont	mix	2205	2237	2344	0.06	0.05	0.03	2.1
TS-626	BG18-3553	46.8	wm	pure	2205	NUL	2351	0.15	0.00	0.07	2.1
TS-627	BG18-3553	48.8	wm	pure	2204	2238	2336	0.07	0.05	0.04	2.0
TS-628	BG18-3553	60.0	chl	pure	NUL	2255	2342	0.00	0.29	0.32	0.0
TS-629	BG18-3553	71.3	chl	pure	2200	2257	2347	0.10	0.25	0.21	0.5
TS-630	BG18-3553	84.9	wm	pure	2201	NUL	2346	0.27	0.00	0.13	2.1
TS-631	BG18-3553	85.5	prg	pure	2201	NUL	2348	0.31	0.00	0.15	2.1
TS-632	BG18-3553	92.6	wm	pure	2201	NUL	2346	0.32	0.00	0.16	2.0
TS-633	BG18-3553	97.5	wm	pure	2205	NUL	NUL	0.13	0.00	0.00	NUL
TS-634	BG18-3553	100.6	wm	pure	2204	NUL	2348	0.22	0.00	0.12	1.9
TS-635	BG18-3553	104.1	wm	pure	2202	NUL	2348	0.22	0.00	0.11	2.0
TS-636	BG18-3553	106.5	wm	pure	2201	NUL	2345	0.29	0.00	0.15	2.0
TS-637	BG18-3553	116.8	wm	pure	2203	NUL	2339	0.10	0.00	0.03	3.5
TS-638	BG18-3553	118.9	chl-wm	mix	2202	2248	2348	0.15	0.09	0.09	1.7
TS-639	BG18-3553	122.3	wm-ch	mix	2202	2239	2345	0.17	0.08	0.10	1.7
TS-640	BG18-3553	131.1	wm	pure	2203	NUL	2346	0.37	0.00	0.21	1.8
TS-641	BG18-3553	134.1	wm-chl	mix	2204	2249	2345	0.21	0.14	0.14	1.6
TS-642	BG18-3553	149.4	chl-wm	mix	2200	2251	2346	0.24	0.17	0.16	1.5
TS-643	BG18-3553	155.4	chl-wm	mix	2199	2251	2345	0.26	0.17	0.17	1.5
TS-644	BG18-3553	170.7	wm-ch	mix	2199	NUL	2348	0.28	0.00	0.15	1.9
TS-645	BG18-3553	179.8	chl-wm	mix	2204	2250	2334	0.05	0.06	0.05	0.8
TS-646	BG18-3553	183.2	wm-chl	mix	2199	2248	2346	0.16	0.06	0.08	1.9
TS-647	BG18-3553	192.0	chl-wm	mix	2198	2251	2342	0.30	0.18	0.19	1.5
TS-648	BG18-3553	215.9	chl-wm	mix	2200	2253	2343	0.13	0.15	0.12	1.0
TS-649	BG18-3553	231.6	chl-wm	mix	2199	2251	2344	0.17	0.18	0.16	1.0

Table G.1 Continued.

Sample	DDH	Depth (m)	Mineral Results	SWIR Response	Feature Position (nm)			Feature Depth			AlOHd/ MgOHd
					AlOH	FeOH	MgOH	AlOH	FeOH	MgOH	
TS-650	BG18-3907	3.0	chl-ep	mix	NUL	2254	2342	0.00	0.30	0.39	0.0
TS-651	BG18-3907	6.0	chl-ep	mix	NUL	2254	2343	0.00	0.30	0.39	0.0
TS-652	BG18-3907	12.2	chl	pure	NUL	2254	2343	0.00	0.27	0.27	0.0
TS-653	BG18-3907	15.2	chl	pure	NUL	2254	2343	0.00	0.28	0.31	0.0
TS-654	BG18-3907	21.2	chl-wm	mix	2218	2253	2344	0.14	0.26	0.33	0.4
TS-655	BG18-3907	23.1	phn	pure	2213	NUL	2348	0.15	0.00	0.12	1.2
TS-656	BG18-3907	26.0	phn	pure	2217	NUL	2348	0.13	0.00	0.09	1.4
TS-657	BG18-3907	36.8	wm-ep	mix	2216	2250	2341	0.06	0.07	0.13	0.5
TS-658	BG18-3907	45.5	chl	pure	NUL	2254	2339	0.00	0.26	0.31	0.0
TS-659	BG18-3907	48.8	chl	pure	NUL	2254	2341	0.00	0.26	0.31	0.0
TS-660	BG18-3907	51.9	chl-ep	mix	NUL	2254	2341	0.00	0.24	0.33	0.0
TS-661	BG18-3907	54.9	chl	pure	NUL	2254	2341	0.00	0.27	0.31	0.0
TS-662	BG18-3907	57.9	chl-ep	mix	NUL	2254	2340	0.00	0.32	0.45	0.0
TS-663	BG18-3907	61.0	chl	pure	NUL	2254	2343	0.00	0.31	0.37	0.0
TS-664	BG18-3907	64.0	chl-ep	mix	NUL	2254	2341	0.00	0.32	0.45	0.0
TS-665	BG18-3907	67.5	chl-ep	mix	NUL	2255	2340	0.00	0.31	0.42	0.0
TS-666	BG18-3907	70.3	chl-ep	mix	NUL	2254	2341	0.00	0.32	0.42	0.0
TS-667	BG18-3907	73.8	chl-ep	mix	NUL	2254	2338	0.00	0.26	0.37	0.0
TS-668	BG18-3907	77.0	chl-ep	mix	NUL	2254	2340	0.00	0.28	0.38	0.0
TS-669	BG18-3907	82.3	chl	pure	NUL	2253	2338	0.00	0.15	0.16	0.0
TS-670	BG18-3907	87.4	wm	pure	2203	NUL	2347	0.25	0.00	0.14	1.8
TS-671	BG18-3907	92.8	wm	pure	2202	NUL	2347	0.37	0.00	0.21	1.7
TS-672	BG18-3907	95.0	chl-wm	mix	2201	2253	2349	0.20	0.11	0.13	1.5
TS-673	BG18-3907	99.5	wm	pure	2201	NUL	2347	0.14	0.00	0.07	2.1
TS-674	BG18-3907	100.6	wm	pure	2200	2238	2347	0.13	0.03	0.06	2.0
TS-675	BG18-3907	107.4	wm	pure	2200	NUL	2346	0.22	0.00	0.12	1.9
TS-676	BG18-3907	115.8	wm	pure	2203	2238	2349	0.12	0.03	0.06	2.1
TS-677	BG18-3907	118.7	chl-wm	mix	2200	2249	2347	0.13	0.07	0.10	1.4
TS-678	BG18-3907	126.1	wm	pure	2199	NUL	2349	0.20	0.00	0.11	1.9
TS-679	BG18-3907	132.1	wm	pure	2198	NUL	2347	0.18	0.00	0.09	1.9
TS-680	BG18-3907	135.9	chl-wm	mix	2197	2252	2341	0.15	0.09	0.10	1.5
TS-681	BG18-3907	139.6	chl-wm	mix	2198	2251	2345	0.30	0.19	0.19	1.6
TS-682	BG18-3907	145.3	wm-ch	mix	2199	2249	2343	0.24	0.11	0.13	1.8
TS-683	BG18-3907	152.7	chl-wm	mix	2198	2251	2341	0.23	0.17	0.16	1.4
TS-684	BG18-3907	161.3	wm-chl	mix	2198	NUL	2345	0.21	0.00	0.11	1.9
TS-685	BG18-3907	173.7	chl-wm	mix	2199	2252	2346	0.27	0.23	0.22	1.3
TS-686	BG18-3907	179.8	chl-wm	mix	2200	2253	2344	0.14	0.17	0.15	0.9
TS-687	BG18-3907	185.9	chl-wm	mix	2199	2252	2341	0.25	0.20	0.18	1.4
TS-688	BG18-3554	10.7	chl	pure	NUL	2254	2342	0.00	0.26	0.30	0.0
TS-689	BG18-3554	13.7	chl-ep	mix	2218	2253	2343	0.12	0.25	0.30	0.4
TS-690	BG18-3554	16.5	chl-ep	mix	NUL	2254	2343	0.00	0.27	0.36	0.0
TS-691	BG18-3554	19.8	chl	pure	NUL	2254	2342	0.00	0.30	0.35	0.0
TS-692	BG18-3554	23.0	ep-wm	mix	2201	2255	2344	0.08	0.14	0.27	0.3
TS-693	BG18-3554	25.9	wm-ep	mix	2214	2253	2345	0.20	0.21	0.40	0.5
TS-694	BG18-3554	29.7	wm	pure	2211	NUL	2349	0.12	0.00	0.09	1.3
TS-695	BG18-3554	35.1	ep-wm	mix	2213	2254	2342	0.18	0.29	0.46	0.4
TS-696	BG18-3554	38.1	chl-ep	mix	NUL	2254	2340	0.00	0.28	0.36	0.0
TS-697	BG18-3554	44.2	wm-ch	mix	2205	NUL	2346	0.24	0.00	0.17	1.4
TS-698	BG18-3554	50.3	chl-ep	mix	NUL	2255	2341	0.00	0.29	0.40	0.0
TS-699	BG18-3554	54.2	wm-ep	mix	2206	2251	2347	0.09	0.07	0.17	0.5
TS-700	BG18-3554	71.6	chl-wm	mix	2200	2254	2345	0.21	0.13	0.15	1.4
TS-701	BG18-3554	77.7	chl-wm	mix	2201	2254	2345	0.15	0.21	0.20	0.8

Table G.1 Continued.

Sample	DDH	Depth (m)	Mineral Results	SWIR Response	Feature Position (nm)			Feature Depth			AlOHd/ MgOHd
					AlOH	FeOH	MgOH	AlOH	FeOH	MgOH	
TS-702	BG18-3554	95.0	wm	pure	2202	NUL	2347	0.21	0.00	0.12	1.8
TS-703	BG18-3554	98.0	wm	pure	2200	NUL	2345	0.28	0.00	0.15	2.0
TS-704	BG18-3554	102.1	wm-mont	mix	2198	NUL	2346	0.34	0.00	0.18	1.9
TS-705	BG18-3554	105.4	prg	pure	2199	NUL	2349	0.35	0.00	0.19	1.8
TS-706	BG18-3554	107.6	wm	pure	2200	NUL	2345	0.34	0.00	0.18	1.8
TS-707	BG18-3554	111.4	wm-mont	mix	2199	NUL	2347	0.22	0.00	0.11	2.0
TS-708	BG18-3554	114.3	wm-mont	mix	2196	NUL	2348	0.22	0.00	0.10	2.1
TS-709	BG18-3554	119.3	wm	pure	2202	NUL	NUL	0.15	0.00	0.00	NUL
TS-710	BG18-3554	127.0	wm	pure	2203	NUL	2347	0.37	0.00	0.21	1.8
TS-711	BG18-3554	128.0	wm	pure	2203	NUL	2352	0.25	0.00	0.13	1.9
TS-712	BG18-3554	129.5	wm	pure	2204	NUL	2345	0.55	0.00	0.32	1.7
TS-713	BG18-3554	136.7	wm-ch	mix	2204	2252	2349	0.13	0.08	0.09	1.4
TS-714	BG18-3554	154.9	wm	pure	2205	NUL	2346	0.20	0.00	0.12	1.8
TS-715	BG18-3554	159.0	wm	pure	2205	NUL	2344	0.15	0.00	0.08	2.0
TS-716	BG18-3554	163.1	chl-wm	mix	2202	2249	2339	0.24	0.18	0.17	1.4
TS-717	BG18-3554	172.2	chl-wm	mix	2202	2253	2340	0.22	0.27	0.24	0.9
TS-718	BG18-3554	181.4	chl-wm	mix	2203	2250	2350	0.23	0.14	0.16	1.5
TS-719	BG18-3554	184.4	chl-wm	mix	2202	2250	2346	0.28	0.19	0.21	1.3
TS-720	BG18-3554	190.5	wm-ch	mix	2200	NUL	2345	0.11	0.00	0.08	1.4
TS-721	BG18-3554	196.6	chl-wm	mix	2202	2252	2345	0.25	0.18	0.19	1.3
TS-722	BG18-3554	202.7	chl-wm	mix	2201	2254	2348	0.25	0.27	0.26	1.0
TS-723	BG18-3554	214.9	wm-cb	mix	2202	2239	2342	0.08	0.05	0.05	1.7
TS-724	BG18-3554	224.0	wm-ch	mix	2200	2244	2348	0.18	0.08	0.11	1.7
TS-725	BG18-3554	230.1	chl-wm	mix	2199	2248	2340	0.09	0.06	0.07	1.4
TS-726	BG18-3554	233.2	chl-wm	mix	2200	2249	2340	0.21	0.11	0.13	1.6
TS-727	BG18-3555	4.6	chl-ep	mix	2216	2254	2339	0.06	0.21	0.30	0.2
TS-728	BG18-3555	10.5	chl-ep	mix	NUL	2253	2338	0.00	0.25	0.41	0.0
TS-729	BG18-3555	13.2	chl-ep	mix	NUL	2253	2339	0.00	0.28	0.42	0.0
TS-730	BG18-3555	19.8	chl	pure	2202	2255	2341	0.10	0.26	0.28	0.3
TS-731	BG18-3555	25.9	chl-ep	mix	NUL	2255	2342	0.00	0.30	0.37	0.0
TS-732	BG18-3555	32.2	chl-wm	mix	2201	2255	2343	0.13	0.30	0.31	0.4
TS-733	BG18-3555	38.2	chl-wm	mix	2203	2255	2342	0.14	0.31	0.33	0.4
TS-734	BG18-3555	41.1	chl-wm	mix	2199	2255	2344	0.23	0.26	0.25	0.9
TS-735	BG18-3555	44.2	chl	pure	NUL	2254	2341	0.00	0.32	0.36	0.0
TS-736	BG18-3555	47.2	chl-wm	mix	2199	2254	2341	0.16	0.29	0.28	0.6
TS-737	BG18-3555	53.3	chl-wm	mix	2205	2253	2341	0.16	0.31	0.35	0.5
TS-738	BG18-3555	56.4	chl-wm	mix	2204	2254	2343	0.19	0.33	0.35	0.6
TS-739	BG18-3555	59.4	chl-ep	mix	NUL	2254	2341	0.00	0.36	0.42	0.0
TS-740	BG18-3555	62.5	chl	pure	NUL	2255	2343	0.00	0.32	0.37	0.0
TS-741	BG18-3555	71.6	chl-wm	mix	2202	2254	2344	0.18	0.25	0.25	0.7
TS-742	BG18-3555	74.7	chl-wm	mix	2203	2254	2345	0.14	0.27	0.25	0.6
TS-743	BG18-3555	80.0	chl	pure	NUL	2255	2344	0.00	0.26	0.25	0.0
TS-744	BG18-3555	83.8	chl-wm	mix	2199	2255	2346	0.19	0.27	0.27	0.7
TS-745	BG18-3555	86.9	chl	pure	NUL	2254	2346	0.00	0.27	0.27	0.0
TS-746	BG18-3555	89.9	chl	pure	2218	2254	2342	0.11	0.30	0.34	0.3
TS-747	BG18-3555	151.2	chl-wm	mix	2200	2254	2345	0.25	0.28	0.27	0.9
TS-748	BG18-3555	156.0	wm	pure	2199	NUL	2345	0.16	0.00	0.08	2.0
TS-749	BG18-3555	162.0	wm	pure	2203	NUL	2346	0.12	0.00	0.08	1.6
TS-750	BG18-3555	166.1	chl	pure	2216	2253	2344	0.07	0.29	0.31	0.2
TS-751	BG18-3555	172.2	chl-wm	mix	2208	2254	2342	0.10	0.24	0.25	0.4
TS-752	BG18-3555	178.0	chl	pure	NUL	2254	2344	0.00	0.31	0.34	0.0
TS-753	BG18-3555	183.0	chl	pure	2217	2254	2341	0.09	0.28	0.29	0.3

Table G.1 Continued.

Sample	DDH	Depth (m)	Mineral Results	SWIR Response	Feature Position (nm)			Feature Depth			AlOHd/ MgOHd
					AlOH	FeOH	MgOH	AlOH	FeOH	MgOH	
TS-754	BG18-3555	189.1	chl-wm	mix	2206	2250	2346	0.27	0.19	0.22	1.2
TS-755	BG18-3555	195.1	chl-wm	mix	2207	2250	2346	0.33	0.26	0.30	1.1
TS-756	BG18-3555	201.1	chl	pure	NUL	2253	2339	0.00	0.28	0.27	0.0
TS-757	BG18-3555	207.5	chl	pure	NUL	2253	2341	0.00	0.36	0.39	0.0
TS-758	BG18-3555	210.3	chl	pure	2217	2253	2343	0.09	0.30	0.32	0.3
TS-759	BG18-3555	216.4	chl-wm	mix	2213	2253	2342	0.12	0.25	0.25	0.5
TS-760	BG18-3555	222.5	chl	pure	2217	2252	2338	0.10	0.25	0.23	0.4
TS-761	BG18-3555	225.6	chl-wm	mix	2214	2252	2340	0.16	0.24	0.23	0.7
TS-762	BG18-3555	232.6	chl	pure	NUL	2253	2339	0.00	0.24	0.22	0.0
TS-763	BG18-3908	6.1	chl-ep	mix	NUL	2254	2340	0.00	0.23	0.30	0.0
TS-764	BG18-3908	18.3	chl-wm	mix	NUL	2254	2343	0.00	0.29	0.34	0.0
TS-765	BG18-3908	21.3	chl-wm	mix	2214	2252	2343	0.21	0.25	0.30	0.7
TS-766	BG18-3908	24.4	wm-cb	mix	2214	NUL	2347	0.20	0.00	0.14	1.4
TS-767	BG18-3908	27.4	chl-wm	mix	2216	2252	2345	0.10	0.14	0.17	0.6
TS-768	BG18-3908	32.2	phn	pure	2215	NUL	2351	0.13	0.00	0.08	1.6
TS-769	BG18-3908	42.7	ep	pure	2219	2251	2342	0.05	0.07	0.15	0.3
TS-770	BG18-3908	45.7	chl-ep	mix	NUL	2254	2340	0.00	0.30	0.41	0.0
TS-771	BG18-3908	54.9	chl-ep	mix	NUL	2255	2341	0.00	0.33	0.45	0.0
TS-772	BG18-3908	57.9	chl-ep	mix	NUL	2254	2340	0.00	0.34	0.47	0.0
TS-773	BG18-3908	64.0	chl-ep	mix	NUL	2255	2340	0.00	0.32	0.42	0.0
TS-774	BG18-3908	70.1	chl-ep	mix	NUL	2254	2339	0.00	0.28	0.39	0.0
TS-775	BG18-3908	85.9	wm	pure	2203	NUL	2356	0.07	0.00	0.03	2.1
TS-776	BG18-3908	94.5	wm	pure	2202	NUL	2344	0.22	0.00	0.12	1.8
TS-777	BG18-3908	97.5	wm	pure	2202	NUL	2347	0.29	0.00	0.16	1.8
TS-778	BG18-3908	100.7	wm	pure	2201	NUL	2347	0.17	0.00	0.10	1.8
TS-779	BG18-3908	106.3	wm	pure	2201	NUL	2349	0.19	0.00	0.11	1.7
TS-780	BG18-3908	109.7	prg	pure	2201	NUL	2347	0.29	0.00	0.16	1.8
TS-781	BG18-3908	112.8	wm	pure	2200	NUL	2346	0.28	0.00	0.16	1.8
TS-782	BG18-3908	118.9	wm	pure	2202	NUL	2348	0.29	0.00	0.16	1.8
TS-783	BG18-3908	125.5	wm	pure	2204	NUL	2345	0.18	0.00	0.10	1.8
TS-784	BG18-3908	127.7	wm	pure	2202	NUL	2344	0.25	0.00	0.14	1.8
TS-785	BG18-3908	140.2	wm	pure	2204	NUL	2347	0.26	0.00	0.15	1.7
TS-786	BG18-3908	143.3	wm-ch	mix	2205	NUL	2345	0.28	0.00	0.17	1.6
TS-787	BG18-3908	158.5	chl	pure	2204	2254	2341	0.08	0.21	0.20	0.4
TS-788	BG18-3908	161.5	chl-wm	mix	2205	2253	2345	0.17	0.21	0.21	0.8
TS-789	BG18-3908	173.7	prg	pure	2200	NUL	2346	0.29	0.00	0.16	1.8
TS-790	BG18-3908	179.8	chl-wm	mix	2200	2254	2347	0.09	0.09	0.09	1.0
TS-791	BG18-3908	195.1	wm	pure	2198	2238	2347	0.13	0.03	0.07	2.0
TS-913	BG18-3952	12.2	chl-wm	mix	2198	2255	2345	0.17	0.38	0.35	0.5
TS-914	BG18-3952	15.2	chl-wm	mix	2198	2255	2345	0.36	0.31	0.32	1.1
TS-915	BG18-3952	18.3	chl-wm	mix	2200	2254	2345	0.23	0.22	0.23	1.0
TS-916	BG18-3952	21.3	chl-wm	mix	2200	2255	2347	0.30	0.27	0.28	1.1
TS-917	BG18-3952	24.4	chl	pure	NUL	2253	2339	0.00	0.37	0.34	0.0
TS-918	BG18-3952	26.3	wm	pure	2199	2238	2347	0.12	0.05	0.06	1.9
TS-919	BG18-3952	27.5	chl-wm	mix	2200	2255	2344	0.20	0.29	0.29	0.7
TS-920	BG18-3952	30.5	wm-cb	mix	2198	2236	2343	0.21	0.06	0.12	1.8
TS-921	BG18-3952	34.0	chl-wm	mix	2199	2255	2344	0.31	0.27	0.27	1.1
TS-922	BG18-3952	36.6	chl-wm	mix	2198	2253	2342	0.36	0.16	0.25	1.4
TS-923	BG18-3952	49.6	chl-wm	mix	2198	2256	2344	0.21	0.29	0.29	0.7
TS-924	BG18-3952	51.8	wm	pure	2199	NUL	2346	0.47	0.00	0.27	1.8
TS-925	BG18-3952	54.9	wm	pure	2200	NUL	2346	0.48	0.00	0.28	1.7
TS-926	BG18-3952	57.9	wm	pure	2197	NUL	2340	0.32	0.00	0.18	1.8

Table G.1 Continued.

Sample	DDH	Depth (m)	Mineral Results	SWIR Response	Feature Position (nm)			Feature Depth			AlOHd/ MgOHd
					AlOH	FeOH	MgOH	AlOH	FeOH	MgOH	
TS-927	BG18-3952	61.0	wm	pure	2197	NUL	2342	0.30	0.00	0.15	2.0
TS-928	BG18-3952	64.0	wm-mont	mix	2196	NUL	2339	0.38	0.00	0.20	1.9
TS-929	BG18-3952	67.1	wm	pure	2198	NUL	2342	0.22	0.00	0.11	2.0
TS-930	BG18-3952	70.1	wm	pure	2197	NUL	2347	0.27	0.00	0.13	2.0
TS-931	BG18-3952	73.2	wm	pure	2200	NUL	2345	0.42	0.00	0.24	1.8
TS-932	BG18-3952	76.2	wm	pure	2199	NUL	2346	0.41	0.00	0.22	1.9
TS-933	BG18-3952	79.2	wm	pure	2199	NUL	2347	0.44	0.00	0.26	1.7
TS-934	BG18-3952	82.3	wm	pure	2199	NUL	2344	0.43	0.00	0.26	1.7
TS-935	BG18-3952	85.3	wm	pure	2200	NUL	2348	0.40	0.00	0.25	1.6
TS-936	BG18-3952	88.4	wm	pure	2198	NUL	2347	0.37	0.00	0.21	1.7
TS-937	BG18-3952	91.4	wm	pure	2201	NUL	2346	0.23	0.00	0.13	1.8
TS-938	BG18-3952	95.0	wm	pure	2202	NUL	2351	0.21	0.00	0.11	1.9
TS-939	BG18-3952	97.5	wm	pure	2205	NUL	2345	0.30	0.00	0.19	1.6
TS-940	BG18-3952	98.2	wm	pure	2203	NUL	2348	0.34	0.00	0.19	1.8
TS-941	BG18-3952	99.1	wm	pure	2200	NUL	2346	0.32	0.00	0.18	1.8
TS-942	BG18-3952	102.1	prg	pure	2200	NUL	2345	0.41	0.00	0.24	1.7
TS-943	BG18-3952	105.2	wm	pure	2200	NUL	2348	0.28	0.00	0.16	1.7
TS-944	BG18-3952	108.1	wm	pure	2199	NUL	2347	0.40	0.00	0.22	1.8
TS-945	BG18-3952	110.1	wm	pure	2203	NUL	2346	0.17	0.00	0.07	2.4
TS-946	BG18-3952	111.3	wm	pure	2204	NUL	2352	0.14	0.00	0.06	2.5
TS-947	BG18-3952	114.3	wm	pure	2204	NUL	2352	0.16	0.00	0.08	2.1
TS-948	BG18-3952	114.7	wm	pure	2201	NUL	2338	0.15	0.00	0.08	1.8
TS-949	BG18-3952	115.3	chl-wm	mix	2204	2253	2350	0.13	0.10	0.11	1.2
TS-950	BG18-3952	117.3	wm	pure	2203	NUL	2345	0.21	0.00	0.11	1.8
TS-951	BG18-3952	119.2	wm-chl	mix	2204	2248	2345	0.15	0.08	0.11	1.4
TS-952	BG18-3952	119.7	wm-ch	mix	2203	NUL	2349	0.25	0.00	0.18	1.4
TS-953	BG18-3952	121.4	wm	pure	2199	2253	2343	0.15	0.06	0.10	1.6
TS-954	BG18-3952	122.8	chl-wm	mix	2203	2251	2344	0.23	0.20	0.19	1.2
TS-955	BG18-3952	124.6	wm-chl	mix	2203	NUL	2351	0.19	0.00	0.10	1.9
TS-956	BG18-3952	126.5	wm-ch	mix	2202	2249	2341	0.40	0.24	0.28	1.4
TS-957	BG18-3952	127.4	wm	pure	2203	NUL	2346	0.26	0.00	0.14	1.9
TS-958	BG18-3952	129.5	wm-ch	mix	2204	2248	2346	0.36	0.19	0.25	1.4
TS-959	BG18-3952	130.3	wm-ch	mix	2203	NUL	2345	0.39	0.00	0.23	1.7
TS-960	BG18-3952	132.6	wm-ch	mix	2203	NUL	2346	0.33	0.00	0.21	1.6
TS-961	BG18-3952	135.6	wm-ch	mix	2203	2253	2344	0.21	0.12	0.14	1.5
TS-962	BG18-3952	138.7	chl-wm	mix	2203	2253	2346	0.22	0.20	0.20	1.1
TS-963	BG18-3952	141.7	chl-wm	mix	2203	2252	2345	0.28	0.32	0.29	1.0
TS-964	BG18-3952	143.4	chl-wm	mix	2202	2251	2349	0.40	0.28	0.32	1.3
TS-965	BG18-3952	144.8	wm-ch	mix	2202	NUL	2349	0.50	0.00	0.32	1.6
TS-966	BG18-3952	147.7	wm-chl	mix	2203	2247	2343	0.35	0.19	0.23	1.5
TS-967	BG18-3952	150.9	chl-wm	mix	2204	2252	2349	0.32	0.29	0.28	1.1
TS-968	BG18-3952	153.9	chl-wm	mix	2204	2253	2348	0.31	0.23	0.25	1.2
TS-969	BG18-3952	157.0	chl-wm	mix	2203	2250	2345	0.37	0.24	0.29	1.3
TS-970	BG18-3952	160.0	chl-wm	mix	2202	2251	2343	0.43	0.29	0.32	1.4
TS-971	BG18-3952	163.1	wm-ch	mix	2201	NUL	2347	0.34	0.00	0.21	1.6
TS-972	BG18-3952	165.2	wm-ch	mix	2202	2237	2346	0.20	0.08	0.12	1.6
TS-973	BG18-3952	166.1	wm-chl	mix	2201	2246	NUL	0.18	0.08	0.00	NUL
TS-974	BG18-3952	169.2	wm	pure	2202	2239	2326	0.12	0.10	0.07	1.7
TS-975	BG18-3952	172.2	wm-chl	mix	2202	2248	2345	0.31	0.17	0.22	1.4
TS-976	BG18-3952	174.4	chl-wm	mix	2205	2254	2344	0.09	0.20	0.20	0.5
TS-977	BG18-3952	178.3	chl	pure	2206	2253	2339	0.12	0.35	0.34	0.4
TS-978	BG18-3952	181.4	wm	pure	2203	2237	2343	0.16	0.06	0.10	1.7

Table G.1 Continued.

Sample	DDH	Depth (m)	Mineral Results	SWIR Response	Feature Position (nm)			Feature Depth			AlOHd/ MgOHd
					AlOH	FeOH	MgOH	AlOH	FeOH	MgOH	
TS-979	BG18-3952	184.4	chl-wm	mix	2201	2252	2342	0.34	0.20	0.24	1.4
TS-980	BG18-3952	187.5	wm	pure	2203	2249	2355	0.12	0.05	0.07	1.8
TS-981	BG18-3952	190.5	chl-wm	mix	2203	2254	2345	0.09	0.14	0.13	0.7
TS-982	BG18-3952	193.5	chl-wm	mix	2202	2249	2340	0.21	0.17	0.18	1.1
TS-983	BG18-3952	196.6	chl-wm	mix	2205	2256	2342	0.11	0.08	0.08	1.3
TS-984	BG18-3952	198.1	chl-wm	mix	2202	2250	2343	0.14	0.12	0.14	1.1
TS-1055	BG18-3921	3.0	chl-wm	mix	2216	2253	2340	0.21	0.32	0.45	0.5
TS-1056	BG18-3921	6.1	chl-ep	mix	NUL	2253	2341	0.00	0.30	0.40	0.0
TS-1057	BG18-3921	9.1	chl-wm	mix	2217	2254	2343	0.08	0.13	0.16	0.5
TS-1058	BG18-3921	12.5	chl-cb	mix	NUL	2252	2339	0.00	0.30	0.36	0.0
TS-1059	BG18-3921	15.2	chl-wm	mix	2209	2253	2340	0.19	0.26	0.30	0.6
TS-1060	BG18-3921	21.3	chl	pure	2215	2253	2344	0.07	0.20	0.21	0.3
TS-1061	BG18-3921	22.7	chl-cb	mix	NUL	2252	2345	0.00	0.23	0.26	0.0
TS-1062	BG18-3921	24.8	chl-ep	mix	NUL	2254	2340	0.00	0.29	0.39	0.0
TS-1063	BG18-3921	26.0	chl	pure	NUL	2253	2339	0.00	0.31	0.33	0.0
TS-1064	BG18-3921	28.0	chl-ep	mix	2216	2254	2340	0.08	0.26	0.34	0.2
TS-1065	BG18-3921	33.6	wm-ep	mix	2209	NUL	2346	0.25	0.00	0.22	1.1
TS-1066	BG18-3921	35.0	wm-ep	mix	2210	2239	2346	0.25	0.13	0.31	0.8
TS-1067	BG18-3921	36.3	chl-wm	mix	2215	2250	2346	0.34	0.28	0.29	1.2
TS-1068	BG18-3921	39.6	chl	pure	NUL	2254	NUL	0.00	0.32	0.00	NUL
TS-1069	BG18-3921	42.7	wm-chl	mix	2215	NUL	2345	0.15	0.00	0.13	1.1
TS-1070	BG18-3921	43.5	chl	pure	2220	2255	2346	0.09	0.29	0.29	0.3
TS-1071	BG18-3921	45.5	phn	pure	2213	NUL	2346	0.19	0.00	0.12	1.6
TS-1072	BG18-3921	49.0	chl	pure	NUL	2253	2340	0.00	0.33	0.39	0.0
TS-1073	BG18-3921	51.5	chl-ep	mix	NUL	2254	2342	0.00	0.32	0.40	0.0
TS-1074	BG18-3921	54.1	chl-ep	mix	NUL	2254	2339	0.00	0.38	0.55	0.0
TS-1075	BG18-3921	55.9	chl	pure	NUL	2254	2342	0.00	0.31	0.38	0.0
TS-1076	BG18-3921	57.9	chl	pure	NUL	2254	2340	0.00	0.37	0.44	0.0
TS-1077	BG18-3921	70.0	chl-ep	mix	NUL	2254	2341	0.00	0.40	0.56	0.0
TS-1078	BG18-3921	61.0	chl-ep	mix	NUL	2254	2338	0.00	0.40	0.57	0.0
TS-1079	BG18-3921	62.4	chl-ep	mix	NUL	2254	2342	0.00	0.37	0.49	0.0
TS-1080	BG18-3921	64.0	chl-ep	mix	NUL	2255	2343	0.00	0.34	0.46	0.0
TS-1081	BG18-3921	64.9	chl-ep	mix	NUL	2254	2341	0.00	0.34	0.44	0.0
TS-1082	BG18-3921	66.8	chl-ep	mix	NUL	2255	2339	0.00	0.37	0.48	0.0
TS-1083	BG18-3921	67.8	chl-ep	mix	NUL	2255	2343	0.00	0.34	0.43	0.0
TS-1084	BG18-3921	69.1	chl-ep	mix	NUL	2254	2342	0.00	0.37	0.50	0.0
TS-1085	BG18-3921	70.5	chl-ep	mix	NUL	2255	2340	0.00	0.36	0.48	0.0
TS-1086	BG18-3921	74.7	chl-ep	mix	NUL	2254	2340	0.00	0.36	0.50	0.0
TS-1087	BG18-3921	75.1	chl-ep	mix	NUL	2254	2341	0.00	0.36	0.49	0.0
TS-1088	BG18-3921	78.2	chl-ep	mix	2206	2255	2340	0.03	0.16	0.25	0.1
TS-1089	BG18-3921	81.0	chl	pure	2214	2255	2344	0.06	0.22	0.23	0.3
TS-1092	BG18-3921	86.7	chl-wm	mix	2206	2255	2348	0.12	0.24	0.25	0.5
TS-1093	BG18-3921	89.4	wm	pure	2201	NUL	2349	0.37	0.00	0.24	1.5
TS-1124	RN18-0223	0.7	wm-mont	mix	2199	2238	2348	0.40	0.09	0.23	1.8
TS-1125	RN18-0223	3.0	wm	pure	2200	NUL	2345	0.50	NUL	0.30	1.7
TS-1126	RN18-0223	6.1	wm	pure	2200	NUL	2345	0.37	NUL	0.21	1.7
TS-1127	RN18-0223	9.1	wm	pure	2198	NUL	2348	0.36	NUL	0.20	1.8
TS-1128	RN18-0223	11.9	wm	pure	2198	NUL	2345	0.43	NUL	0.24	1.8
TS-1129	RN18-0223	15.4	wm	pure	2198	2238	2347	0.35	0.08	0.20	1.8
TS-1130	RN18-0223	18.5	prg	pure	2198	NUL	2348	0.40	NUL	0.22	1.8
TS-1131	RN18-0223	21.3	wm	pure	2199	2238	2348	0.18	0.04	0.08	2.4
TS-1132	RN18-0223	24.4	wm	pure	2199	NUL	2349	0.43	NUL	0.25	1.7

Table G.1 Continued.

Sample	DDH	Depth (m)	Mineral Results	SWIR Response	Feature Position (nm)			Feature Depth			AlOHd/ MgOHd
					AlOH	FeOH	MgOH	AlOH	FeOH	MgOH	
TS-1133	RN18-0223	27.4	wm	pure	2202	NUL	2346	0.38	NUL	0.21	1.8
TS-1134	RN18-0223	30.5	wm	pure	2201	2237	2349	0.22	0.05	0.11	2.0
TS-1135	RN18-0223	33.1	wm	pure	2199	NUL	2345	0.33	NUL	0.19	1.7
TS-1136	RN18-0223	36.7	wm-mont	mix	2198	NUL	2344	0.39	NUL	0.21	1.9
TS-1137	RN18-0223	39.6	wm	pure	2199	NUL	2346	0.37	NUL	0.20	1.8
TS-1138	RN18-0223	43.7	wm	pure	2200	NUL	2346	0.23	NUL	0.11	2.1
TS-1139	RN18-0223	45.7	wm	pure	2196	2238	2343	0.21	0.11	0.10	2.0
TS-1140	RN18-0223	48.9	wm	pure	2199	NUL	2347	0.23	NUL	0.11	2.0
TS-1141	RN18-0223	51.8	wm	pure	2200	2238	2348	0.26	0.05	0.14	1.9
TS-1142	RN18-0223	55.0	wm	pure	2197	2239	2345	0.09	0.02	0.03	2.9
TS-1143	RN18-0223	58.1	wm	pure	2198	NUL	2345	0.24	NUL	0.12	2.0
TS-1144	RN18-0223	61.0	wm	pure	2198	NUL	2335	0.20	NUL	0.12	1.8
TS-1145	RN18-0223	64.0	wm	pure	2200	NUL	2339	0.13	NUL	0.06	2.3
TS-1146	RN18-0223	67.3	wm	pure	2200	NUL	2339	0.33	NUL	0.19	1.8
TS-1147	RN18-0223	70.1	wm	pure	2199	NUL	2338	0.26	NUL	0.14	1.9
TS-1148	RN18-0223	73.2	wm	pure	2197	NUL	2351	0.12	NUL	0.06	2.0
TS-1149	RN18-0223	76.6	wm	pure	2200	NUL	2353	0.20	NUL	0.11	1.8
TS-1150	RN18-0223	79.6	prg	pure	2200	NUL	2345	0.39	NUL	0.21	1.8
TS-1151	RN18-0223	82.1	chl-wm	mix	2199	2253	2345	0.38	0.29	0.30	1.3
TS-1152	RN18-0223	85.5	chl-wm	mix	2199	2254	2344	0.41	0.24	0.28	1.5
TS-1153	RN18-0223	88.6	wm	pure	2200	NUL	2347	0.43	NUL	0.26	1.7
TS-1154	RN18-0223	90.4	chl-wm	mix	2199	2258	2349	0.18	0.17	0.18	1.0
TS-1155	RN18-0223	91.4	wm	pure	2200	NUL	2346	0.31	NUL	0.19	1.7
TS-1156	RN18-0224	1.5	wm	pure	2199	NUL	2342	0.32	NUL	0.17	1.9
TS-1157	RN18-0224	6.3	wm	pure	2199	NUL	2347	0.34	NUL	0.20	1.8
TS-1158	RN18-0224	9.1	wm	pure	2199	NUL	2347	0.25	NUL	0.14	1.8
TS-1159	RN18-0224	13.3	prg	pure	2198	NUL	2344	0.30	NUL	0.17	1.8
TS-1160	RN18-0224	15.2	wm	pure	2198	NUL	2347	0.35	NUL	0.21	1.7
TS-1161	RN18-0224	18.3	wm	pure	2198	NUL	2348	0.31	NUL	0.18	1.7
TS-1162	RN18-0224	21.3	wm	pure	2199	NUL	2348	0.28	NUL	0.15	1.8
TS-1163	RN18-0224	24.4	wm	pure	2199	NUL	2345	0.31	NUL	0.16	1.9
TS-1164	RN18-0224	27.3	wm	pure	2199	NUL	2347	0.32	NUL	0.18	1.8
TS-1165	RN18-0224	30.5	wm-mont	mix	2199	NUL	2349	0.39	NUL	0.22	1.8
TS-1166	RN18-0224	33.5	wm	pure	2198	NUL	2347	0.36	NUL	0.19	1.9
TS-1167	RN18-0224	36.6	wm	pure	2199	NUL	2348	0.33	NUL	0.19	1.7
TS-1168	RN18-0224	39.3	wm-mont	mix	2197	NUL	2344	0.35	NUL	0.19	1.8
TS-1169	RN18-0224	42.7	wm	pure	2199	NUL	2345	0.41	NUL	0.23	1.8
TS-1170	RN18-0224	45.7	wm	pure	2198	NUL	2348	0.33	NUL	0.19	1.8
TS-1171	RN18-0224	49.0	wm	pure	2198	NUL	2346	0.29	NUL	0.17	1.7
TS-1172	RN18-0224	51.8	wm	pure	2198	NUL	2352	0.24	NUL	0.14	1.8
TS-1173	RN18-0224	54.5	wm	pure	2198	NUL	2341	0.21	NUL	0.11	1.9
TS-1174	RN18-0224	57.9	wm	pure	2200	2238	2340	0.09	0.02	0.04	2.3
TS-1175	RN18-0224	61.5	wm	pure	2201	NUL	2348	0.13	NUL	0.06	2.2
TS-1176	RN18-0224	64.0	aspectral	aspectral	2200	2238	2329	0.10	0.08	0.05	1.8
TS-1177	RN18-0224	67.1	wm	pure	2197	2237	2347	0.10	0.03	0.04	2.3
TS-1178	RN18-0224	69.9	wm	pure	2198	NUL	2347	0.20	NUL	0.10	1.9
TS-1179	RN18-0224	73.2	wm	pure	2205	2235	2337	0.15	0.05	0.07	2.1
TS-1180	RN18-0224	76.2	wm	pure	2200	NUL	2345	0.39	NUL	0.23	1.7
TS-1181	RN18-0224	79.2	wm	pure	2201	NUL	2345	0.37	NUL	0.22	1.7
TS-1182	RN18-0224	82.3	wm	pure	2200	NUL	2349	0.26	NUL	0.15	1.7
TS-1183	RN18-0224	83.3	chl-wm	mix	2202	2253	2345	0.23	0.16	0.17	1.3
TS-1184	RN18-0225	2.4	wm	pure	2199	NUL	2349	0.36	NUL	0.19	1.9

Table G.1 Continued.

Sample	DDH	Depth (m)	Mineral Results	SWIR Response	Feature Position (nm)			Feature Depth			AlOHd/ MgOHd
					AlOH	FeOH	MgOH	AlOH	FeOH	MgOH	
TS-1185	RN18-0225	4.6	wm-mont	mix	2197	NUL	2345	0.38	NUL	0.20	1.9
TS-1186	RN18-0225	8.5	wm-mont	mix	2198	NUL	2346	0.41	NUL	0.24	1.7
TS-1187	RN18-0225	10.7	wm	pure	2199	NUL	2345	0.46	NUL	0.26	1.7
TS-1188	RN18-0225	13.7	wm	pure	2200	NUL	2345	0.36	NUL	0.20	1.8
TS-1189	RN18-0225	16.4	wm	pure	2198	NUL	2344	0.35	NUL	0.20	1.7
TS-1190	RN18-0225	18.2	wm	pure	2200	NUL	2345	0.19	NUL	0.09	2.1
TS-1191	RN18-0225	19.2	wm	pure	2200	NUL	2347	0.28	NUL	0.14	1.9
TS-1192	RN18-0225	20.5	chl-wm	mix	2200	2251	2347	0.31	0.18	0.21	1.4
TS-1193	RN18-0225	22.9	wm	pure	2199	2238	2346	0.20	0.03	0.09	2.4
TS-1194	RN18-0225	26.2	wm-mont	mix	2198	NUL	2345	0.34	NUL	0.18	1.9
TS-1195	RN18-0225	29.0	wm	pure	2199	NUL	2345	0.31	NUL	0.16	2.0
TS-1196	RN18-0225	32.0	wm	pure	2199	NUL	2342	0.35	NUL	0.21	1.7
TS-1197	RN18-0225	34.2	wm-mont	mix	2198	NUL	2344	0.48	NUL	0.27	1.8
TS-1198	RN18-0225	36.4	wm-mont	mix	2198	NUL	2340	0.41	NUL	0.23	1.8
TS-1199	RN18-0225	39.3	wm	pure	2199	NUL	2346	0.29	NUL	0.17	1.7
TS-1200	RN18-0225	41.1	wm	pure	2198	NUL	2344	0.26	NUL	0.14	1.9
TS-1201	RN18-0225	44.1	wm	pure	2199	NUL	2346	0.29	NUL	0.16	1.8
TS-1202	RN18-0225	47.5	wm-mont	mix	2197	NUL	2347	0.41	NUL	0.22	1.9
TS-1203	RN18-0225	50.3	wm	pure	2197	NUL	2348	0.33	NUL	0.17	1.9
TS-1204	RN18-0225	53.3	wm	pure	2197	NUL	2349	0.24	NUL	0.13	1.8
TS-1205	RN18-0225	56.0	wm	pure	2199	NUL	2345	0.26	NUL	0.16	1.6
TS-1206	RN18-0225	59.4	wm-cb	mix	2200	2235	2334	0.17	0.03	0.11	1.6
TS-1207	RN18-0225	62.2	wm	pure	2199	NUL	2345	0.22	NUL	0.11	1.9
TS-1208	RN18-0225	63.1	wm-mont	mix	2198	NUL	2343	0.20	NUL	0.11	1.8
TS-1209	RN18-0225	63.7	wm-mont	mix	2198	NUL	2348	0.21	NUL	0.11	1.8
TS-1210	RN18-0225	65.5	wm	pure	2198	2240	2344	0.08	0.05	0.05	1.5
TS-1211	RN18-0225	67.8	wm-mont	mix	2195	2236	2339	0.22	0.12	0.14	1.6

Mineral Results – TSG identified minerals
Note – some results have more than one SWIR active mineral, these are denoted by term "mix" while samples with only one SWIR-active mineral are denoted as "pure", and samples with no SWIR-active minerals are marked as "aspectral"
Feature Position – is the wavelength position (in nm) of an absorption feature
AlOHd/MgOHd – is the ratio of the AlOH absorption feature depth and the MgOH absorption feature depth; and is used as a proxy for chlorite and white mica relative abundance. Values <0.45 denote chlorite-dominant samples, 0.45-1.8 denote mixed chlorite and white mica samples, and values >1.8 reflect white mica-dominant samples.
[cb, carbonate, chl, chlorite; ep, epidote; mont, montmorillonite; phn, phengite; prg, paragonite; wm, white mica]

Appendix H:

Compilation of Published Myra Falls Whole-Rock Chemistry

Published whole-rock geochemical data for the Myra Falls VHMS district were compiled and is presented here. Datasets are from Juras (1987), Robinson (1994), Barrett and Sherlock (1996), Sinclair (2000), and Barrett and MacLean (2000) and consist of titanium and zirconium resutls from XRF analysis of volcanic rocks from the Price Formation; coherent, volcaniclastic and volcano-sedimentary rocks of the H-W member; and volcaniclastic rocks of the Hanging Wall Andesite member. For information regarding dataset specific analytical methods refer to sited publication.

Table H.1 Published conventional XRF data results for titanium and zirconium.

DDH	Depth *m*	Lithology	Strat Member	TiO_2 *wt %*	Zr *ppm*	Ti/Zr	Source	Area
14-904	250.9	Fvc; 5% lithics	H-W	0.51	142.0	21.5	Robinson (1994)	B
14-918	297.3	Fvc; 5% lithics	H-W	0.50	146.2	20.5	Robinson (1994)	B
14-907	254.3	Fvc; 5% lithics	H-W	0.50	157.0	19.1	Robinson (1994)	B
14-906	259.8	Fvc; 5% lithics	H-W	0.56	125.0	26.9	Robinson (1994)	B
14-907	254.3	Fvc; 5% lithics	H-W	0.51	160.0	19.1	Robinson (1994)	B
14-910	295.0	Fvc; 5% lithics	H-W	0.39	132.0	17.7	Robinson (1994)	B
14-912	305.8	Fvc; 5% lithics	H-W	0.54	149.0	21.7	Robinson (1994)	B
14-905	252.3	Fvc; 5% lithics	H-W	0.35	157.0	13.4	Robinson (1994)	B
BG18-798	51.9-52.1	Fvc; 5% lithics	H-W	0.30	41.4	43.9	Sinclair (2000)	B
BG18-799	29.6-29.8	Fvc; 5% lithics	H-W	0.38	111.4	20.6	Sinclair (2000)	B
BG18-1006	49.6-49.8	Fvc; 5% lithics	H-W	0.89	87.9	60.7	Sinclair (2000)	B
W-103	454.1	A	H-W	0.29	54.0	32.2	Barrett & Sherlock (1996)	HW
W-103	469.1	A	H-W	0.15	40.0	22.5	Barrett & Sherlock (1996)	HW
W-103	481.6	A	H-W	0.22	77.0	17.1	Barrett & Sherlock (1996)	HW
W-103	549.8	A	H-W	0.20	59.0	20.3	Barrett & Sherlock (1996)	HW
14-914	262.5	C	H-W	0.07	36.0	11.7	Robinson (1994)	B
14-905	266.5	C	H-W	0.14	38.0	22.1	Robinson (1994)	B
14-906	263.7	C	H-W	0.11	63.0	10.5	Robinson (1994)	B
14-909	267.1	C	H-W	0.13	40.0	19.5	Robinson (1994)	B
14-900	255.3	C	H-W	0.09	50.0	10.8	Robinson (1994)	B
BG18-798	41.9-42.1	C	H-W	0.06	13.2	27.4	Sinclair (2000)	B
BG18-977	125.9-126.1	C	H-W	0.05	9.8	33.6	Sinclair (2000)	B
BG18-1003	83.9-84.0	C	H-W	0.03	6.8	26.4	Sinclair (2000)	B
BG18-1006	89.2-89.4	C	H-W	0.12	20.9	34.5	Sinclair (2000)	B
14-918	276.5	Ds		1.10	97.0	68.0	Robinson (1994)	B
14-918	272.3	Ds		0.55	63.0	52.3	Robinson (1994)	B
14-900	294.2	Ds		0.83	173.0	28.8	Robinson (1994)	B
14-919	264.5	Ds		1.11	213.4	31.2	Robinson (1994)	B
14-904	297.3	Ds		0.86	148.0	34.8	Robinson (1994)	B
14-904	292.7	Ds		0.58	117.0	29.7	Robinson (1994)	B
14-906	243.9	Ds		0.74	114.0	38.9	Robinson (1994)	B
14-919	276.5	Ds		0.73	129.9	33.7	Robinson (1994)	B
14-905	275.0	Ds		1.13	222.0	30.5	Robinson (1994)	B
14-904	301.2	Ds		1.25	220.0	34.1	Robinson (1994)	B
14-750	298.8	Ds		1.18	234.7	30.1	Robinson (1994)	B
14-753	268.0	Ds		1.31	114.3	68.7	Robinson (1994)	B
P13-309	255.1	Fvc	H-W	0.44	203.0	13.0	Barrett & Sherlock (1996)	HW
P13-309	359.0	Fvc	H-W	0.34	182.1	11.1	Barrett & Sherlock (1996)	HW
P13-309	426.1	Fvc	H-W	0.30	111.9	16.2	Barrett & Sherlock (1996)	HW
P13-309	434.3	Fvc	H-W	0.39	52.2	44.6	Barrett & Sherlock (1996)	HW
P13-309	452.9	Fvc	H-W	0.30	61.1	29.4	Barrett & Sherlock (1996)	HW
P13-312	286.5	Fvc	H-W	0.15	81.4	11.3	Barrett & Sherlock (1996)	HW
P13-314	302.7	Fvc	H-W	0.40	130.8	18.4	Barrett & Sherlock (1996)	HW
P13-314	396.5	Fvc	H-W	0.32	60.5	31.2	Barrett & Sherlock (1996)	HW
P13-314	403.8	Fvc	H-W	0.32	154.8	12.4	Barrett & Sherlock (1996)	HW
14-900	247.0	Fvc	H-W	0.25	110.0	13.6	Robinson (1994)	B
14-910	283.2	Fvc	H-W	0.26	128.0	12.2	Robinson (1994)	B
14-907	246.2	Fvc	H-W	0.37	161.0	13.8	Robinson (1994)	B
14-751	257.5	Fvc	H-W	0.18	45.7	23.6	Robinson (1994)	B
14-907	236.0	Fvc	H-W	0.40	241.0	9.9	Robinson (1994)	B
14-915	262.2	Fvc	H-W	0.39	160.8	14.5	Robinson (1994)	B
14-917	290.2	Fvc	H-W	0.25	88.4	17.0	Robinson (1994)	B

Table H.1 Continued.

DDH	Depth *m*	Lithology	Strat Member	TiO_2 *wt %*	Zr *ppm*	Ti/Zr	Source	Area
14-919	290.5	Fvc	H-W	0.48	183.1	15.7	Robinson (1994)	B
14-920	216.5	Fvc	H-W	0.31	165.5	11.2	Robinson (1994)	B
BG18-982	39.2-39.3	Fvc	H-W	0.37	206.6	10.7	Sinclair (2000)	B
BG18-481	16.7-16.9	Fvc	H-W	0.44	179.2	14.8	Sinclair (2000)	B
BG18-481	20.4-20.6	Fvc	H-W	0.30	160.6	11.3	Sinclair (2000)	B
BG18-481	29.8-30.1	Fvc	H-W	0.35	173.1	12.2	Sinclair (2000)	B
BG18-977	78.0-78.2	Fvc	H-W	0.21	112.7	11.4	Sinclair (2000)	B
BG18-1003	9.3-9.5	Fvc	H-W	0.11	76.5	9.0	Sinclair (2000)	B
BG18-1003	53.4-53.6	Fvc	H-W	0.35	261.5	8.0	Sinclair (2000)	B
BG18-1006	33.9-34.1	Fvc	H-W	0.10	46.2	13.6	Sinclair (2000)	B
BG18-1006	38.0-38.2	Fvc	H-W	0.32	155.7	12.5	Sinclair (2000)	B
BG18-1006	17.7-17.9	Fvc	H-W	0.26	168.0	9.3	Sinclair (2000)	B
BG18-1003	73.9-74.0	Fvc	H-W	0.20	138.2	8.8	Sinclair (2000)	B
LX10-2012	688.6	Fvc	H-W	0.33	136.7	14.4	Barrett & MacLean (2000)	M
LX10-2012	706.2	Fvc	H-W	0.43	189.6	13.4	Barrett & MacLean (2000)	M
LX10-2027	520.6	Fvc	H-W	0.34	140.4	14.5	Barrett & MacLean (2000)	M
LX10-2029	601.7	Fvc	H-W	0.24	109.9	13.1	Barrett & MacLean (2000)	M
LX10-2029	787.3	Fvc	H-W	0.28	124.3	13.4	Barrett & MacLean (2000)	M
LX10-2028	483.1	Fvc	H-W	0.28	100.8	16.6	Barrett & MacLean (2000)	M
LX10-2029	457.8	Fvc	H-W	0.33	78.2	24.9	Barrett & MacLean (2000)	M
14-916	286.3	Avc	HWA	1.20	127.9	56.2	Robinson (1994)	B
14-917	244.8	Avc	HWA	0.73	57.4	76.2	Robinson (1994)	B
BG18-486	4.2-4.4	Avc	HWA	0.60	105.5	34.2	Sinclair (2000)	B
BG18-486	20.9-21.1	Avc	HWA	0.33	158.8	12.6	Sinclair (2000)	B
BG18-486	22.3-22.5	Avc	HWA	0.79	78.4	60.5	Sinclair (2000)	B
BG18-1048	93.9-94.1	Avc	HWA	0.75	58.6	76.9	Sinclair (2000)	B
BG18-1048	49.1-49.7	Avc	HWA	0.72	63.3	68.2	Sinclair (2000)	B
LX10-2019	437.1	Avc	HWA	0.75	205.0	22.0	Barrett & MacLean (2000)	M
LX10-2019	507.5	Avc	HWA	0.45	107.9	25.2	Barrett & MacLean (2000)	M
LX10-2019	477.6	Avc	HWA	0.18	28.5	38.1	Barrett & MacLean (2000)	M
LX10-2029	467.3	Avc	HWA	0.57	103.0	33.2	Barrett & MacLean (2000)	M
LX10-2025	493.5	Avc	HWA	0.54	72.8	44.7	Barrett & MacLean (2000)	M
LX10-2019	541.9	Avc	HWA	0.73	75.3	58.1	Barrett & MacLean (2000)	M
LX10-2025	474.0	Avc	HWA	0.81	100.5	48.6	Barrett & MacLean (2000)	M
LX10-2027	485.9	Avc	HWA	0.68	63.4	63.8	Barrett & MacLean (2000)	M
LX10-2028	422.5	Avc	HWA	0.96	80.3	71.3	Barrett & MacLean (2000)	M
LX10-2025	459.9	Avc	HWA	0.98	37.7	155.0	Barrett & MacLean (2000)	M
LX10-2025	447.1	Avc	HWA	0.94	44.6	126.8	Barrett & MacLean (2000)	M
W-103	207.9	Af/s	H-W	1.24	85.4	87.0	Barrett & Sherlock (1996)	HW
W-103	213.0	Af/s	H-W	1.01	56.0	108.1	Barrett & Sherlock (1996)	HW
W-103	234.1	Af/s	H-W	0.63	37.0	102.1	Barrett & Sherlock (1996)	HW
W-103	235.0	Af/s	H-W	0.79	50.0	94.7	Barrett & Sherlock (1996)	HW
W-103	268.2	Af/s	H-W	0.62	80.2	46.3	Barrett & Sherlock (1996)	HW
W-103	275.2	Af/s	H-W	0.50	47.0	63.8	Barrett & Sherlock (1996)	HW
W-103	294.1	Af/s	H-W	0.93	50.1	111.3	Barrett & Sherlock (1996)	HW
P13-309	304.2	Af/s	H-W	0.80	50.8	94.6	Barrett & Sherlock (1996)	HW
P13-309	335.0	Af/s	H-W	0.78	54.4	86.4	Barrett & Sherlock (1996)	HW
P13-309	380.4	Af/s	H-W	0.89	46.4	114.7	Barrett & Sherlock (1996)	HW
P13-312	338.6	Af/s	H-W	0.80	49.6	96.2	Barrett & Sherlock (1996)	HW
P13-312	357.5	Af/s	H-W	0.77	49.5	92.8	Barrett & Sherlock (1996)	HW
P13-312	380.4	Af/s	H-W	0.79	58.0	81.3	Barrett & Sherlock (1996)	HW
P13-314	366.0	Af/s	H-W	0.81	50.0	97.5	Barrett & Sherlock (1996)	HW

Table H.1 Continued.

DDH	Depth *m*	Lithology	Strat Member	TiO_2 *wt %*	Zr *ppm*	Ti/Zr	Source	Area
P13-314	379.2	Af/s	H-W	0.86	52.0	99.0	Barrett & Sherlock (1996)	HW
P13-314	383.7	Af/s	H-W	0.77	47.9	96.6	Barrett & Sherlock (1996)	HW
W-103	548.6	PA	Price Andesite	0.74	84.0	52.8	Barrett & Sherlock (1996)	HW
W-103	566.3	PA	Price Andesite	0.93	61.0	91.4	Barrett & Sherlock (1996)	HW
W-103	580.6	PA	Price Andesite	0.99	84.0	70.7	Barrett & Sherlock (1996)	HW
W-103	586.1	PA	Price Andesite	1.00	39.0	153.7	Barrett & Sherlock (1996)	HW
W-103	598.9	PA	Price Andesite	0.82	57.0	86.2	Barrett & Sherlock (1996)	HW
W-103	604.1	PA	Price Andesite	0.81	82.0	59.2	Barrett & Sherlock (1996)	HW
W-103	630.9	PA	Price Andesite	1.02	77.0	79.4	Barrett & Sherlock (1996)	HW
W-103	645.8	PA	Price Andesite	0.78	73.0	64.1	Barrett & Sherlock (1996)	HW
W-103	658.9	PA	Price Andesite	0.82	76.0	64.7	Barrett & Sherlock (1996)	HW
W-103	673.3	PA	Price Andesite	0.73	73.0	59.9	Barrett & Sherlock (1996)	HW
W-103	677.5	PA	Price Andesite	0.60	70.0	51.4	Barrett & Sherlock (1996)	HW
W-103	684.5	PA	Price Andesite	0.76	110.0	41.4	Barrett & Sherlock (1996)	HW
W-103	719.3	PA	Price Andesite	0.83	53.0	93.9	Barrett & Sherlock (1996)	HW
W-103	747.3	PA	Price Andesite	0.79	60.0	78.9	Barrett & Sherlock (1996)	HW
W-103	785.7	PA	Price Andesite	0.56	38.0	88.3	Barrett & Sherlock (1996)	HW
W-103	822.0	PA	Price Andesite	0.75	52.0	86.5	Barrett & Sherlock (1996)	HW
W-110	563.5	PA	Price Andesite	0.46	39.8	69.3	Barrett & Sherlock (1996)	HW
W-110	566.3	PA	Price Andesite	0.92	119.3	46.2	Barrett & Sherlock (1996)	HW
W-110	576.3	PA	Price Andesite	1.03	80.8	76.4	Barrett & Sherlock (1996)	HW
W-110	591.0	PA	Price Andesite	0.93	203.0	27.5	Barrett & Sherlock (1996)	HW
P13-312	475.5	PA	Price Andesite	0.56	85.9	38.7	Barrett & Sherlock (1996)	HW
P13-314	436.5	PA	Price Andesite	0.76	77.6	58.6	Barrett & Sherlock (1996)	HW
P13-314	448.6	PA	Price Andesite	0.98	97.8	60.2	Barrett & Sherlock (1996)	HW
W190	824.4	PA	Price Andesite	0.83	81.7	60.9	Robinson (1994)	B
14-914	251.5	PA	Price Andesite	0.74	57.4	77.3	Robinson (1994)	B
14-908	297.6	PA	Price Andesite	0.64	63.0	60.9	Robinson (1994)	B
14-908	288.1	PA	Price Andesite	0.46	39.0	70.7	Robinson (1994)	B
14-914	288.1	PA	Price Andesite	0.68	82.0	49.7	Robinson (1994)	B
14-914	274.4	PA	Price Andesite	0.85	97.6	52.2	Robinson (1994)	B
14-909	288.4	PA	Price Andesite	0.54	63.0	51.4	Robinson (1994)	B
14-906	309.9	PA	Price Andesite	0.69	67.0	61.7	Robinson (1994)	B
14-909	303.7	PA	Price Andesite	0.47	49.0	57.5	Robinson (1994)	B
14-915	284.8	PA	Price Andesite	1.09	117.9	55.4	Robinson (1994)	B
14-909	294.2	PA	Price Andesite	0.91	64.0	85.2	Robinson (1994)	B
14-909	294.2	PA	Price Andesite	0.94	67.0	84.1	Robinson (1994)	B
14-908	276.8	PA	Price Andesite	0.36	35.0	61.7	Robinson (1994)	B
14-913	253.0	PA	Price Andesite	0.54	46.8	69.2	Robinson (1994)	B
14-913	270.4	PA	Price Andesite	0.69	83.2	49.7	Robinson (1994)	B
14-913	287.5	PA	Price Andesite	0.61	65.1	56.2	Robinson (1994)	B
14-913	287.8	PA	Price Andesite	0.65	68.1	57.2	Robinson (1994)	B
14-920	298.8	PA	Price Andesite	0.74	71.1	62.4	Robinson (1994)	B
14-920	247.3	PA	Price Andesite	0.72	62.0	69.6	Robinson (1994)	B
14-906	318.3	PA	Price Andesite	0.73	53.0	82.6	Robinson (1994)	B
14-920	268.3	PA	Price Andesite	0.50	81.0	37.0	Robinson (1994)	B
14-920	279.0	PA	Price Andesite	0.68	40.8	99.9	Robinson (1994)	B
14-920	268.6	PA	Price Andesite	0.42	70.4	35.8	Robinson (1994)	B
14-905	321.6	PA	Price Andesite	0.74	54.0	82.2	Robinson (1994)	B
14-905	307.3	PA	Price Andesite	1.22	106.0	69.0	Robinson (1994)	B
14-912	330.8	PA	Price Andesite	1.04	73.0	85.4	Robinson (1994)	B
14-907	289.6	PA	Price Andesite	1.18	101.0	70.0	Robinson (1994)	B

Table H.1 Continued.

DDH	Depth *m*	Lithology	Strat Member	TiO_2 *wt %*	Zr *ppm*	Ti/Zr	Source	Area
14-907	276.7	PA	Price Andesite	0.76	64.0	71.2	Robinson (1994)	B
14-919	309.5	PA	Price Andesite	0.89	83.6	63.8	Robinson (1994)	B
14-918	314.0	PA	Price Andesite	0.33	45.9	43.1	Robinson (1994)	B
14-910	333.7	PA	Price Andesite	0.96	87.0	66.2	Robinson (1994)	B
14-906	323.8	PA	Price Andesite	0.70	73.0	57.5	Robinson (1994)	B
14-912	317.7	PA	Price Andesite	1.17	94.0	74.6	Robinson (1994)	B
14-906	312.5	PA	Price Andesite	0.73	56.0	78.1	Robinson (1994)	B
14-918	330.8	PA	Price Andesite	0.88	68.4	77.1	Robinson (1994)	B
14-916	342.4	PA	Price Andesite	0.92	61.9	89.1	Robinson (1994)	B
14-916	305.8	PA	Price Andesite	1.02	99.8	61.3	Robinson (1994)	B
14-916	349.1	PA	Price Andesite	0.53	77.6	40.9	Robinson (1994)	B
14-916	364.6	PA	Price Andesite	0.73	64.5	67.8	Robinson (1994)	B
14-916	535.0	PA	Price Andesite	0.61	66.6	54.9	Robinson (1994)	B
14-906	286.6	PA	Price Andesite	0.41	41.0	59.9	Robinson (1994)	B
14-917	343.3	PA	Price Andesite	1.66	118.5	84.0	Robinson (1994)	B
14-906	295.7	PA	Price Andesite	0.66	58.0	68.2	Robinson (1994)	B
14-905	333.2	PA	Price Andesite	0.84	81.0	62.2	Robinson (1994)	B
14-900	259.5	PA	Price Andesite	0.23	31.2	44.2	Robinson (1994)	B
14-910	329.0	PA	Price Andesite	1.60	111.0	86.4	Robinson (1994)	B
14-910	320.7	PA	Price Andesite	1.41	216.0	39.1	Robinson (1994)	B
BG18-481	65.4-65.7	PA	Price Andesite	0.57	64.1	53.5	Sinclair (2000)	B
BG18-481	67.1-67.3	PA	Price Andesite	0.33	40.5	49.3	Sinclair (2000)	B
BG18-796	188.8-198.0	PA	Price Andesite	0.48	44.4	65.0	Sinclair (2000)	B
BG18-797	63.1-63.2	PA	Price Andesite	0.55	39.8	83.2	Sinclair (2000)	B
BG18-978	141.6-141.8	PA	Price Andesite	1.19	107.0	66.6	Sinclair (2000)	B
BG18-981	122.3-122.5	PA	Price Andesite	0.62	67.9	54.9	Sinclair (2000)	B
BG18-1003	105.1-105.3	PA	Price Andesite	0.95	82.2	69.3	Sinclair (2000)	B
BG18-1006	124.8-125.0	PA	Price Andesite	1.00	87.5	68.5	Sinclair (2000)	B
BG18-1003	112.0-112.1	PA	Price Andesite	0.43	69.5	37.3	Sinclair (2000)	B
BG18-1006	120.4-120.6	PA	Price Andesite	1.23	117.9	62.5	Sinclair (2000)	B
LX10-2008	967.8	PA	Price Andesite	0.69	108.0	38.0	Barrett & MacLean (2000)	M
LX10-2019	807.7	PA	Price Andesite	0.65	109.8	35.5	Barrett & MacLean (2000)	M
LX10-2027	827.2	PA	Price Andesite	0.59	112.8	31.2	Barrett & MacLean (2000)	M
LX10-2029	838.2	PA	Price Andesite	0.73	117.6	37.1	Barrett & MacLean (2000)	M
LX10-2029	847.4	PA	Price Andesite	0.58	117.1	29.8	Barrett & MacLean (2000)	M
LX10-2029	867.8	PA	Price Andesite	0.67	119.4	33.5	Barrett & MacLean (2000)	M
15-502	563.4	PA	Price Andesite	0.76	109.9	41.2	Barrett & MacLean (2000)	M
LX10-2008	1014.4	PA	Price Andesite	0.91	86.1	63.4	Barrett & MacLean (2000)	M
LX10-2019	861.7	PA	Price Andesite	0.67	64.3	62.6	Barrett & MacLean (2000)	M
LX10-2019	907.1	PA	Price Andesite	0.65	72.9	53.4	Barrett & MacLean (2000)	M
LX10-2027	854.4	PA	Price Andesite	0.80	72.7	65.8	Barrett & MacLean (2000)	M
LX10-2027	866.9	PA	Price Andesite	0.70	70.7	59.2	Barrett & MacLean (2000)	M
LX10-2027	894.3	PA	Price Andesite	0.73	57.0	77.0	Barrett & MacLean (2000)	M
LX10-2027	924.8	PA	Price Andesite	0.71	62.4	68.0	Barrett & MacLean (2000)	M
15-502	437.9	PA	Price Andesite	0.43	52.6	48.6	Barrett & MacLean (2000)	M
15-502	588.6	PA	Price Andesite	0.80	71.8	67.0	Barrett & MacLean (2000)	M
LX10-2027	951.6	PA	Price Andesite	0.79	39.0	121.4	Barrett & MacLean (2000)	M
LX10-2027	983.3	PA	Price Andesite	0.81	50.8	95.6	Barrett & MacLean (2000)	M
LX10-2027	1002.2	PA	Price Andesite	0.77	40.9	113.3	Barrett & MacLean (2000)	M
LX10-2027	1034.8	PA	Price Andesite	0.52	34.9	89.5	Barrett & MacLean (2000)	M
LX10-2013	822.7	PA	Price Andesite	0.44	86.6	30.7	Barrett & MacLean (2000)	M
LX10-2013	834.6	PA	Price Andesite	0.44	89.9	29.5	Barrett & MacLean (2000)	M

Table H.1 Continued.

DDH	Depth *m*	Lithology	Strat Member	TiO_2 *wt %*	Zr *ppm*	Ti/Zr	Source	Area
LX10-2008	955.6	PA	Price Andesite	0.42	158.2	16.0	Barrett & MacLean (2000)	M
W-103	353.6	QFP	H-W	0.34	136.0	15.0	Barrett & Sherlock (1996)	HW
W-103	437.1	QFP	H-W	0.30	159.0	11.3	Barrett & Sherlock (1996)	HW
W-103	440.4	QFP	H-W	0.29	67.0	25.9	Barrett & Sherlock (1996)	HW
W-103	472.4	QFP	H-W	0.38	70.0	32.5	Barrett & Sherlock (1996)	HW
W-103	494.1	QFP	H-W	0.36	155.0	13.9	Barrett & Sherlock (1996)	HW
W-103	501.1	QFP	H-W	0.29	118.0	14.7	Barrett & Sherlock (1996)	HW
W-103	513.3	QFP	H-W	0.35	129.0	16.3	Barrett & Sherlock (1996)	HW
W-103	514.5	QFP	H-W	0.17	109.0	9.3	Barrett & Sherlock (1996)	HW
W-103	514.8	QFP	H-W	0.41	126.6	19.4	Barrett & Sherlock (1996)	HW
W-110	333.4	QFP	H-W	0.26	141.2	11.0	Barrett & Sherlock (1996)	HW
W-110	341.7	QFP	H-W	0.36	133.7	16.1	Barrett & Sherlock (1996)	HW
W-110	388.6	QFP	H-W	0.34	64.7	31.5	Barrett & Sherlock (1996)	HW
W-110	404.4	QFP	H-W	0.33	147.1	13.4	Barrett & Sherlock (1996)	HW
W-110	414.5	QFP	H-W	0.18	100.0	10.8	Barrett & Sherlock (1996)	HW
W-110	416.3	QFP	H-W	0.25	124.0	12.1	Barrett & Sherlock (1996)	HW
W-110	420.9	QFP	H-W	0.21	113.0	11.1	Barrett & Sherlock (1996)	HW
W-110	441.9	QFP	H-W	0.27	137.0	11.8	Barrett & Sherlock (1996)	HW
W-110	460.8	QFP	H-W	0.29	153.0	11.4	Barrett & Sherlock (1996)	HW
W-110	489.5	QFP	H-W	0.22	116.0	11.4	Barrett & Sherlock (1996)	HW
W-110	502.6	QFP	H-W	0.36	171.0	12.6	Barrett & Sherlock (1996)	HW
W-110	527.3	QFP	H-W	0.36	136.5	15.8	Barrett & Sherlock (1996)	HW
W-110	539.5	QFP	H-W	0.31	133.0	14.0	Barrett & Sherlock (1996)	HW
W-110	539.8	QFP	H-W	0.29	127.0	13.7	Barrett & Sherlock (1996)	HW
14-720	223.5	QFP	H-W	0.15	87.6	10.3	Robinson (1994)	B
14-720	282.0	QFP	H-W	0.10	81.9	7.3	Robinson (1994)	B
14-900	282.6	QFP	H-W	0.20	81.0	14.8	Robinson (1994)	B
14-720	209.8	QFP	H-W	0.52	198.2	15.7	Robinson (1994)	B
14-904	278.4	QFP	H-W	0.19	139.0	8.2	Robinson (1994)	B
14-911	285.1	QFP	H-W	0.20	116.0	10.3	Robinson (1994)	B
14-914	186.0	QFP	H-W	0.28	109.4	15.3	Robinson (1994)	B
14-919	230.9	QFP	H-W	0.38	183.1	12.4	Robinson (1994)	B
14-918	245.4	QFP	H-W	0.46	201.4	13.7	Robinson (1994)	B
14-914	189.9	QFP	H-W	0.19	92.4	12.3	Robinson (1994)	B
14-917	572.0	QFP	H-W	0.38	186.5	12.2	Robinson (1994)	B
14-920	187.2	QFP	H-W	0.40	195.3	12.3	Robinson (1994)	B
14-753	222.0	QFP	H-W	0.21	121.2	10.4	Robinson (1994)	B
14-919	221.0	QFP	H-W	0.43	203.1	12.7	Robinson (1994)	B
14-914	193.6	QFP	H-W	0.45	210.9	12.8	Robinson (1994)	B
14-912	287.3	QFP	H-W	0.15	81.0	11.1	Robinson (1994)	B
14-905	222.6	QFP	H-W	0.42	236.0	10.7	Robinson (1994)	B
14-905	231.7	QFP	H-W	0.22	124.0	10.6	Robinson (1994)	B
14-905	231.7	QFP	H-W	0.25	145.0	10.3	Robinson (1994)	B
14-904	199.7	QFP	H-W	0.24	137.0	10.5	Robinson (1994)	B
14-909	257.6	QFP	H-W	0.27	121.0	13.4	Robinson (1994)	B
14-906	200.9	QFP	H-W	0.17	94.0	10.8	Robinson (1994)	B
14-900	227.1	QFP	H-W	0.29	161.0	10.8	Robinson (1994)	B
14-905	200.0	QFP	H-W	0.36	16.0	134.9	Robinson (1994)	B
14-904	228.0	QFP	H-W	0.27	157.0	10.3	Robinson (1994)	B
14-906	217.4	QFP	H-W	0.44	239.0	11.0	Robinson (1994)	B
14-904	234.8	QFP	H-W	0.14	85.0	9.9	Robinson (1994)	B
14-906	193.6	QFP	H-W	0.23	122.0	11.3	Robinson (1994)	B

Table H.1 Continued.

DDH	Depth *m*	Lithology	Strat Member	TiO_2 *wt %*	Zr *ppm*	Ti/Zr	Source	Area
14-907	226.2	QFP	H-W	0.40	208.0	11.5	Robinson (1994)	B
14-906	227.1	QFP	H-W	0.40	212.0	11.3	Robinson (1994)	B
14-904	184.8	QFP	H-W	0.25	128.0	11.7	Robinson (1994)	B
14-910	271.3	QFP	H-W	0.24	138.0	10.4	Robinson (1994)	B
14-908	223.8	QFP	H-W	0.26	151.0	10.3	Robinson (1994)	B
14-909	247.3	QFP	H-W	0.31	16.0	116.2	Robinson (1994)	B
14-914	163.4	QFP	H-W	0.27	148.7	10.9	Robinson (1994)	B
14-904	193.0	QFP	H-W	0.20	115.0	10.4	Robinson (1994)	B
14-904	188.1	QFP	H-W	0.18	103.0	10.5	Robinson (1994)	B
14-720	189.9	QFP	H-W	0.24	130.7	11.0	Robinson (1994)	B
14-907	231.7	QFP	H-W	0.25	133.0	11.3	Robinson (1994)	B
14-900	170.7	QFP	H-W	0.23	141.0	9.8	Robinson (1994)	B
14-753	203.7	QFP	H-W	0.26	75.5	20.6	Robinson (1994)	B
BG18-481	1.4-1.5	QFP	H-W	0.35	236.8	8.9	Sinclair (2000)	B
BG18-481	1.5-1.6	QFP	H-W	0.16	116.4	8.5	Sinclair (2000)	B
BG18-982	0.6-0.8	QFP	H-W	0.12	79.5	9.4	Sinclair (2000)	B
BG18-1054	36.9-37.2	QFP	H-W	0.25	133.1	11.3	Sinclair (2000)	B
BG18-1080	47.5-47.7	QFP	H-W	0.20	118.8	10.1	Sinclair (2000)	B
LX10-2008	944.6	QFP	H-W	0.20	136.0	9.0	Barrett & MacLean (2000)	M
LX10-2012	683.7	QFP	H-W	0.32	191.7	9.9	Barrett & MacLean (2000)	M
LX10-2012	725.7	QFP	H-W	0.26	131.9	11.8	Barrett & MacLean (2000)	M
LX10-2012	739.8	QFP	H-W	0.26	136.0	11.5	Barrett & MacLean (2000)	M
LX10-2012	763.5	QFP	H-W	0.24	125.9	11.6	Barrett & MacLean (2000)	M
LX10-2012	782.4	QFP	H-W	0.32	158.4	12.0	Barrett & MacLean (2000)	M
LX10-2012	785.2	QFP	H-W	0.11	55.4	12.2	Barrett & MacLean (2000)	M
LX10-2012	814.4	QFP	H-W	0.17	111.5	9.1	Barrett & MacLean (2000)	M
LX10-2012	830.6	QFP	H-W	0.31	169.8	10.8	Barrett & MacLean (2000)	M
LX10-2012	846.4	QFP	H-W	0.29	181.5	9.7	Barrett & MacLean (2000)	M
LX10-2012	904.7	QFP	H-W	0.22	114.9	11.3	Barrett & MacLean (2000)	M
LX10-2012	922.3	QFP	H-W	0.16	115.4	8.4	Barrett & MacLean (2000)	M
LX10-2012	936.7	QFP	H-W	0.19	122.6	9.3	Barrett & MacLean (2000)	M
LX10-2013	660.8	QFP	H-W	0.14	108.3	7.9	Barrett & MacLean (2000)	M
LX10-2013	678.5	QFP	H-W	0.13	83.1	9.5	Barrett & MacLean (2000)	M
LX10-2013	700.7	QFP	H-W	0.22	117.9	11.2	Barrett & MacLean (2000)	M
LX10-2013	774.8	QFP	H-W	0.31	164.4	11.3	Barrett & MacLean (2000)	M
LX10-2013	788.5	QFP	H-W	0.23	145.7	9.5	Barrett & MacLean (2000)	M
LX10-2013	806.5	QFP	H-W	0.22	125.0	10.5	Barrett & MacLean (2000)	M
LX10-2013	816.3	QFP	H-W	0.25	148.8	10.2	Barrett & MacLean (2000)	M
LX10-2013	825.1	QFP	H-W	0.22	129.5	10.4	Barrett & MacLean (2000)	M
LX10-2019	559.3	QFP	H-W	0.25	139.3	10.8	Barrett & MacLean (2000)	M
LX10-2019	584.9	QFP	H-W	0.23	145.8	9.5	Barrett & MacLean (2000)	M
LX10-2019	618.1	QFP	H-W	0.43	328.6	7.8	Barrett & MacLean (2000)	M
LX10-2019	654.1	QFP	H-W	0.21	103.4	11.9	Barrett & MacLean (2000)	M
LX10-2019	698.9	QFP	H-W	0.23	114.3	12.0	Barrett & MacLean (2000)	M
LX10-2019	788.2	QFP	H-W	0.18	117.6	9.3	Barrett & MacLean (2000)	M
LX10-2023	569.4	QFP	H-W	0.44	239.5	11.0	Barrett & MacLean (2000)	M
LX10-2023	598.6	QFP	H-W	0.31	155.9	11.8	Barrett & MacLean (2000)	M
LX10-2023	621.2	QFP	H-W	0.28	151.3	11.2	Barrett & MacLean (2000)	M
LX10-2023	640.7	QFP	H-W	0.27	136.9	11.6	Barrett & MacLean (2000)	M
LX10-2023	663.9	QFP	H-W	0.27	137.5	11.6	Barrett & MacLean (2000)	M
LX10-2023	680.9	QFP	H-W	0.29	152.0	11.6	Barrett & MacLean (2000)	M
LX10-2023	700.1	QFP	H-W	0.33	184.2	10.6	Barrett & MacLean (2000)	M

Table H.1 Continued.

DDH	Depth *m*	Lithology	Strat Member	TiO_2 *wt %*	Zr *ppm*	Ti/Zr	Source	Area
LX10-2025	496.2	QFP	H-W	0.21	134.0	9.5	Barrett & MacLean (2000)	M
LX10-2027	502.0	QFP	H-W	0.18	114.3	9.5	Barrett & MacLean (2000)	M
LX10-2027	534.9	QFP	H-W	0.22	114.0	11.5	Barrett & MacLean (2000)	M
LX10-2027	551.1	QFP	H-W	0.20	104.1	11.7	Barrett & MacLean (2000)	M
LX10-2027	573.0	QFP	H-W	0.27	138.8	11.6	Barrett & MacLean (2000)	M
LX10-2027	630.3	QFP	H-W	0.25	126.8	11.9	Barrett & MacLean (2000)	M
LX10-2027	793.4	QFP	H-W	0.19	121.7	9.2	Barrett & MacLean (2000)	M
LX10-2028	509.9	QFP	H-W	0.27	171.6	9.5	Barrett & MacLean (2000)	M
LX10-2028	535.2	QFP	H-W	0.23	162.1	8.6	Barrett & MacLean (2000)	M
LX10-2028	562.4	QFP	H-W	0.21	148.7	8.6	Barrett & MacLean (2000)	M
LX10-2028	606.9	QFP	H-W	0.28	152.6	11.2	Barrett & MacLean (2000)	M
LX10-2028	627.3	QFP	H-W	0.21	126.3	9.8	Barrett & MacLean (2000)	M
LX10-2028	659.0	QFP	H-W	0.15	118.1	7.6	Barrett & MacLean (2000)	M
LX10-2028	716.0	QFP	H-W	0.25	181.1	8.1	Barrett & MacLean (2000)	M
LX10-2028	855.0	QFP	H-W	0.21	120.4	10.3	Barrett & MacLean (2000)	M
LX10-2029	479.8	QFP	H-W	0.25	141.0	10.5	Barrett & MacLean (2000)	M
LX10-2029	516.0	QFP	H-W	0.32	197.5	9.7	Barrett & MacLean (2000)	M
LX10-2029	558.4	QFP	H-W	0.32	165.8	11.4	Barrett & MacLean (2000)	M
LX10-2029	649.8	QFP	H-W	0.23	114.9	12.2	Barrett & MacLean (2000)	M
LX10-2029	691.0	QFP	H-W	0.15	124.1	7.2	Barrett & MacLean (2000)	M
LX10-2029	809.9	QFP	H-W	0.16	102.1	9.6	Barrett & MacLean (2000)	M
LX10-2029	830.3	QFP	H-W	0.25	152.0	9.7	Barrett & MacLean (2000)	M
15-502	457.5	QFP	H-W	0.40	254.0	9.4	Barrett & MacLean (2000)	M
15-502	505.3	QFP	H-W	0.24	151.3	9.3	Barrett & MacLean (2000)	M
15-502	528.8	QFP	H-W	0.13	79.6	9.8	Barrett & MacLean (2000)	M
LX10-2023	590.1	QFP	H-W	0.29	128.3	13.5	Barrett & MacLean (2000)	M
LX10-2025	699.8	QFP	H-W	0.33	142.2	13.8	Barrett & MacLean (2000)	M
LX10-2012	864.7	QFP	H-W	0.46	182.9	15.2	Barrett & MacLean (2000)	M
LX10-2012	878.7	QFP	H-W	0.47	178.8	15.8	Barrett & MacLean (2000)	M
LX10-2012	890.3	QFP	H-W	0.47	183.2	15.4	Barrett & MacLean (2000)	M
LX10-2013	718.4	QFP	H-W	0.40	154.1	15.7	Barrett & MacLean (2000)	M
LX10-2013	731.5	QFP	H-W	0.36	141.9	15.0	Barrett & MacLean (2000)	M
LX10-2013	750.7	QFP	H-W	0.34	136.0	15.0	Barrett & MacLean (2000)	M
LX10-2019	754.7	QFP	H-W	0.23	80.6	17.1	Barrett & MacLean (2000)	M
LX10-2023	715.1	QFP	H-W	0.30	117.9	15.4	Barrett & MacLean (2000)	M
LX10-2025	714.8	QFP	H-W	0.44	162.4	16.1	Barrett & MacLean (2000)	M
LX10-2025	739.8	QFP	H-W	0.36	141.8	15.1	Barrett & MacLean (2000)	M
LX10-2025	761.4	QFP	H-W	0.40	152.9	15.6	Barrett & MacLean (2000)	M
LX10-2025	784.6	QFP	H-W	0.33	124.3	15.7	Barrett & MacLean (2000)	M
LX10-2025	790.4	QFP	H-W	0.31	120.9	15.5	Barrett & MacLean (2000)	M
LX10-2025	815.3	QFP	H-W	0.38	144.8	15.9	Barrett & MacLean (2000)	M
LX10-2025	842.2	QFP	H-W	0.42	159.8	15.6	Barrett & MacLean (2000)	M
LX10-2027	674.5	QFP	H-W	0.33	124.4	15.8	Barrett & MacLean (2000)	M
LX10-2027	705.9	QFP	H-W	0.29	106.4	16.1	Barrett & MacLean (2000)	M
LX10-2027	741.0	QFP	H-W	0.33	129.8	15.3	Barrett & MacLean (2000)	M
LX10-2027	767.2	QFP	H-W	0.34	132.1	15.6	Barrett & MacLean (2000)	M
LX10-2028	740.7	QFP	H-W	0.27	97.7	16.3	Barrett & MacLean (2000)	M
LX10-2028	751.3	QFP	H-W	0.30	115.6	15.7	Barrett & MacLean (2000)	M
LX10-2028	765.7	QFP	H-W	0.25	97.8	15.5	Barrett & MacLean (2000)	M
LX10-2028	794.0	QFP	H-W	0.39	152.4	15.2	Barrett & MacLean (2000)	M
LX10-2028	817.2	QFP	H-W	0.31	117.7	15.5	Barrett & MacLean (2000)	M
LX10-2028	841.3	QFP	H-W	0.34	131.7	15.4	Barrett & MacLean (2000)	M

Table H.1 Continued.

DDH	Depth *m*	Lithology	Strat Member	TiO_2 *wt %*	Zr *ppm*	Ti/Zr	Source	Area
LX10-2029	728.8	QFP	H-W	0.38	145.0	15.7	Barrett & MacLean (2000)	M
LX10-2029	749.8	QFP	H-W	0.28	109.2	15.2	Barrett & MacLean (2000)	M
LX10-2029	769.3	QFP	H-W	0.33	127.9	15.5	Barrett & MacLean (2000)	M
LX10-2025	676.7	Md		0.90	46.0	117.3	Barrett & MacLean (2000)	M
LX10-2025	693.4	Md		1.02	53.7	113.9	Barrett & MacLean (2000)	M
LX10-2027	718.4	Md		1.97	184.9	64.0	Barrett & MacLean (2000)	M
LX10-2027	1053.1	Md		1.86	106.8	104.5	Barrett & MacLean (2000)	M
LX10-2029	213.2	Md		1.46	112.4	77.9	Barrett & MacLean (2000)	M
LX10-2029	351.4	Md		2.19	63.1	207.6	Barrett & MacLean (2000)	M
LX10-2029	404.2	Md		1.15	78.2	87.9	Barrett & MacLean (2000)	M
LX10-2008	885.1	Md		0.55	13.9	238.1	Barrett & MacLean (2000)	M
LX10-2019	720.9	Md		0.54	31.8	101.4	Barrett & MacLean (2000)	M
LX10-2019	829.1	Md		0.50	11.3	262.6	Barrett & MacLean (2000)	M

Area – RZN, Ridge Zone North; RZW, Ridge Zone West; WBA, West Block Area
Lithology – A; argillite; Af/s, andesite flow/sill; Avc, andesite volcaniclastics; C; chert; Fvc, felsic volcaniclastics; Md, mafic dyke; PA, Price andesite; QFP, quartz and feldspar-phyric rhyolite
Depth – reported in metres down hole
Strat Member – HWA, Hanging Wall Andesite member
Area – B, Battle orebody; M, Marshall Zone

Appendix I:

Portable XRF Results

This section provides tables of pXRF results referenced in Chapter 6. Table I.1 presents the three-spot and singe-spot pXRF results from drill core and pressed powder samples of the same material. Table I.2 presents the three-spot pXRF results for analysed drill core samples (n=418).

Table I.1 Titanium, zirconium and chromium results from three-spot pXRF of drill core and single-spot pXRF of pressed powders.

Sample ID	DDH	Strat Member	Rock Code	*3-spot pXRF analysis of drill core*										*single-spot pXRF analysis of pressed powder*									
				Result					*Total Measurment Error*					*Result*					*Total Measurment Error*				
				Ti *ppm*	Cr *ppm*	Zr *ppm*	Ti/Zr	TiO_2 %	Ti *ppm*	Cr *ppm*	Zr *ppm*	Ti/Zr	TiO_2 %	Ti *ppm*	Cr *ppm*	Zr *ppm*	Ti/ Zr	TiO_2 %	Ti *ppm*	Cr *ppm*	Zr *ppm*	Ti/Zr	TiO_2 %
TS-067	BG18-3902	H-W	PA	3655.0	26.0	60.0	61.0	0.6	420.0	9.0	6.0	9.2	0.07	5166.8	37.9	73.8	70.0	0.9	517.7	10.2	1.9	7.2	0.09
TS-345	BG18-3904	H-W	PA	4926.0	21.0	90.0	55.0	0.8	603.0	7.0	5.0	7.4	0.10	6131.6	25.2	90.1	68.1	1.0	614.4	6.8	2.3	7.0	0.10
TS-494	BG18-3905	H-W	PA	3236.0	16.0	105.0	31.0	0.5	550.0	5.0	11.0	6.1	0.09	4463.9	5.7	121.2	36.8	0.7	447.3	1.5	3.1	3.8	0.07
TS-496	BG18-3905	H-W	PA	3590.0	6.0	59.0	61.0	0.6	423.0	2.0	5.0	8.8	0.07	4926.4	5.7	68.6	71.8	0.8	493.6	1.5	1.7	7.4	0.08
TS-683	BG18-3907	H-W	PA	3845.0	11.0	114.0	34.0	0.6	473.0	6.0	16.0	6.4	0.08	4373.3	5.7	108.8	40.2	0.7	438.2	1.5	2.7	4.2	0.07
TS-788	BG18-3908	HWA	PA	5771.0	18.0	90.0	64.0	1.0	754.0	8.0	8.0	10.3	0.13	6753.0	20.6	93.7	72.1	1.1	676.6	5.6	2.4	7.4	0.11
TS-420	BG18-3551	HWA	PA	4226.0	12.0	65.0	65.0	0.7	514.0	7.0	5.0	9.3	0.09	4968.2	5.7	62.7	79.2	0.8	497.8	1.5	1.6	8.2	0.08
TS-265	BG18-3321a	HWA	PA	4604.0	13.0	70.0	66.0	0.8	684.0	8.0	6.0	11.3	0.11	5516.3	5.7	75.5	73.1	0.9	552.7	1.5	1.9	7.5	0.09
TS-394	BG18-3550	HWA	PA	4544.0	10.0	65.0	70.0	0.8	850.0	5.0	11.0	17.5	0.14	5215.7	27.5	70.6	73.9	0.9	522.6	7.4	1.8	7.6	0.09
TS-552	BG18-3552	HWA	PA	3994.0	15.0	102.0	39.0	0.7	868.0	6.0	19.0	11.1	0.14	3616.4	5.7	92.8	39.0	0.6	362.4	1.5	2.3	4.0	0.06
TS-722	BG18-3554	HWA	PA	5486.0	6.0	87.0	63.0	1.0	534.0	1.0	4.0	7.0	0.00	4792.0	5.7	74.1	64.7	0.8	480.2	1.5	1.9	6.7	0.08
TS-971	BG18-3952	HWA	PA	5458.0	35.0	84.0	65.0	0.9	532.0	11.0	3.0	6.9	0.09	6126.5	26.4	86.0	71.2	1.0	613.9	7.1	2.2	7.4	0.10
BM14-029	BG18-3769	HWA	PA	5465.0	48.0	84.0	65.0	0.9	615.0	17.0	9.0	10.0	0.10	5624.2	36.7	79.8	70.5	0.9	563.5	9.9	2.0	7.3	0.09
TS-1180	RN18-0224	HWA	PA	3936.0	37.0	112.0	35.0	0.7	945.0	10.0	15.0	9.7	0.16	6142.8	57.4	116.4	52.8	1.0	615.5	15.5	2.9	5.5	0.10
UPB12	BG18-3921	HWA	Af	6712.0	6.0	60.0	112.0	1.1	597.0	1.0	2.0	10.9	0.10	5606.9	5.7	61.5	91.2	0.9	561.8	1.5	1.5	9.4	0.09
UPB02	underground	HWA	QFP	1484.0	45.0	114.0	13.0	0.2	519.0	16.0	39.0	6.0	0.09	1912.1	42.4	137.5	13.9	0.3	191.6	11.5	3.5	1.4	0.03
UPB05	RN18-0224	HWA	QFP	1975.0	54.0	137.0	14.0	0.3	207.0	14.0	17.0	2.3	0.03	2551.8	61.9	135.1	18.9	0.4	255.7	16.7	3.4	2.0	0.04
UPB08	BG18-3952	HWA	QFP	986.0	21.0	106.0	9.0	0.0	157.0	5.0	8.0	2.0	0.00	1139.9	28.7	104.8	10.9	0.2	114.2	7.7	2.6	1.1	0.02

Rock Code – Af, andesite flow; PA, Price andesite; QFP, quartz and feldspar-phyric rhyolite

Table I.2 Titanium, zirconium and chromium results from pXRF and conventional XRF analyses.

Sample ID	DDH	n	Strat Member	Rock Code	Ti *ppm*	Cr *ppm*	Zr *ppm*	Ti/Zr	TiO_2 %	*Total Measurment Error*				
										Ti *ppm*	Cr *ppm*	Zr *ppm*	Ti/Zr	TiO_2 %
TS-019	BG18-3901	3	H-W	Af	6110.0	6.0	71.0	1.02	86.1	569.9	1.6	2.3	8.5	0.10
TS-020	BG18-3901	3	H-W	Af	6076.0	6.0	63.0	1.01	96.4	593.5	1.6	2.5	10.2	0.10
TS-021	BG18-3901	3	H-W	Af	4611.0	6.0	71.0	0.77	64.9	559.7	1.6	2.5	8.2	0.09
TS-022	BG18-3901	3	H-W	Af	1333.0	17.0	73.0	0.22	18.3	269.7	7.6	7.7	4.2	0.04
TS-023	BG18-3901	3	H-W	Af	1225.0	23.0	45.0	0.20	27.2	276.7	7.4	9.9	8.6	0.05
TS-035	BG18-3902	3	HWA	Avc	5374.0	6.0	93.0	0.90	57.8	1071.0	1.7	11.2	13.4	0.18
TS-036	BG18-3902	3	HWA	Avc	4136.0	6.0	70.0	0.69	59.1	478.2	1.7	3.3	7.4	0.08
TS-037	BG18-3902	3	HWA	Avc	4639.0	6.0	72.0	0.77	64.4	483.4	1.7	4.1	7.7	0.08
TS-038	BG18-3902	3	HWA	Avc	5128.0	6.0	77.0	0.86	66.6	523.5	1.7	6.2	8.7	0.09
TS-039	BG18-3902	4	HWA	Avc	5565.0	6.0	78.0	0.93	71.3	575.1	1.7	5.3	8.8	0.10
TS-040	BG18-3902	3	HWA	Avc	4788.0	6.0	76.0	0.80	63.0	476.4	1.7	3.5	6.9	0.08
TS-041	BG18-3902	3	HWA	Avc	4846.0	6.0	84.0	0.81	57.7	748.7	1.7	3.6	9.2	0.12
TS-042	BG18-3902	3	HWA	Avc	1934.0	9.0	89.0	0.32	21.7	873.7	4.1	8.2	10.0	0.15
TS-043	BG18-3902	3	HWA	Avc	3335.0	6.0	67.0	0.56	49.8	478.9	1.7	6.9	8.8	0.08
TS-044	BG18-3902	3	HWA	Avc	3597.0	10.0	93.0	0.60	38.7	611.6	4.9	17.2	9.7	0.10
TS-045	BG18-3902	3	HWA	Avc	4640.0	6.0	70.0	0.77	66.3	728.0	1.7	9.7	13.9	0.12
TS-046	BG18-3902	3	HWA	Avc	4792.0	11.0	62.0	0.80	77.3	554.0	6.0	6.6	12.2	0.09
TS-047	BG18-3902	3	HWA	Avc	5543.0	38.0	71.0	0.92	78.1	1129.2	14.2	10.0	19.3	0.19
TS-048	BG18-3902	3	H-W	Fvc	1850.0	30.0	60.0	0.31	30.8	173.0	8.8	2.5	3.2	0.03
TS-049	BG18-3902	3	HWA	Avc	1649.0	42.0	64.0	0.28	25.8	182.3	13.1	4.8	3.4	0.03
TS-050	BG18-3902	3	H-W	Af	4921.0	15.0	60.0	0.82	82.0	508.5	9.8	2.6	9.2	0.08
TS-051	BG18-3902	3	H-W	Af	5334.0	6.0	64.0	0.89	83.3	656.4	1.7	3.3	11.1	0.11
TS-052	BG18-3902	3	H-W	Fvc	1334.0	38.0	80.0	0.22	16.7	284.9	13.1	25.5	6.4	0.05
TS-053	BG18-3902	3	H-W	Fvc	2066.0	75.0	119.0	0.34	17.4	193.2	22.1	4.9	1.8	0.03
TS-054	BG18-3902	3	H-W	Fvc	1174.0	32.0	69.0	0.20	17.0	209.5	9.7	7.5	3.6	0.03
TS-055	BG18-3902	3	H-W	Fvc	3637.0	74.0	266.0	0.61	13.7	422.6	21.6	26.3	2.1	0.07
TS-056	BG18-3902	3	H-W	Fvc	2822.0	118.0	226.0	0.47	12.5	327.9	50.7	11.0	1.6	0.05
TS-057	BG18-3902	3	H-W	Fvc	2969.0	45.0	170.0	0.50	17.5	373.2	13.7	8.9	2.4	0.06
TS-058	BG18-3902	3	H-W	Fvc	3205.0	41.0	209.0	0.53	15.3	497.7	12.6	29.1	3.2	0.08
TS-059	BG18-3902	3	H-W	Fvc	1725.0	64.0	171.0	0.29	10.1	328.6	18.7	24.3	2.4	0.05
TS-060	BG18-3902	3	H-W	Fvc	1535.0	31.0	136.0	0.26	11.3	151.7	9.9	5.8	1.2	0.03
TS-061	BG18-3902	3	H-W	Fvc	2430.0	38.0	104.0	0.41	23.4	299.0	12.2	6.1	3.2	0.05
TS-062	BG18-3902	3	H-W	Fvc	3708.0	120.0	96.0	0.62	38.6	712.9	43.0	22.6	11.7	0.12
TS-063	BG18-3902	3	H-W	Bvc	3141.0	62.0	195.0	0.52	16.1	853.1	19.0	62.3	6.8	0.14
TS-064	BG18-3902	3	H-W	Bvc	3001.0	23.0	90.0	0.50	33.3	361.6	6.7	15.0	6.8	0.06
TS-065	BG18-3902	3	H-W	Bvc	2528.0	51.0	110.0	0.42	23.0	342.4	15.0	5.1	3.3	0.06
TS-066	BG18-3902	3	Price Fm	PA	3795.0	537.0	26.0	0.63	146.0	397.1	161.0	1.6	17.7	0.07
TS-067	BG18-3902	3	Price Fm	PA	3655.0	26.0	60.0	0.61	60.9	420.4	9.1	5.9	9.2	0.07
TS-068	BG18-3902	3	Price Fm	PA	5048.0	51.0	60.0	0.84	84.1	495.7	16.9	4.5	10.4	0.08
TS-069	BG18-3902	3	Price Fm	PA	2760.0	15.0	195.0	0.46	14.2	398.5	7.2	27.3	2.8	0.07
TS-070	BG18-3902	3	Price Fm	PA	1449.0	13.0	124.0	0.24	11.7	135.6	5.7	5.8	1.2	0.02
TS-071	BG18-3902	3	Price Fm	PA	1744.0	23.0	128.0	0.29	13.6	167.1	7.1	6.3	1.5	0.03
TS-072	BG18-3902	3	Price Fm	PA	1719.0	13.0	151.0	0.29	11.4	256.1	4.5	10.5	1.9	0.04
TS-073	BG18-3902	3	Price Fm	PA	1950.0	12.0	149.0	0.33	13.1	237.4	4.5	12.5	1.9	0.04
TS-074	BG18-3902	3	Price Fm	PA	4234.0	94.0	83.0	0.71	51.0	396.4	27.5	3.6	5.3	0.07
TS-075	BG18-3902	3	Price Fm	PA	2907.0	66.0	60.0	0.48	48.5	437.7	21.9	5.5	8.5	0.07
TS-076	BG18-3902	3	Price Fm	PA	4223.0	11.0	58.0	0.70	72.8	700.4	5.7	8.1	15.8	0.12
TS-093	BG18-3903	3	H-W	Af	4900.0	5.0	55.0	0.82	89.1	540.3	1.3	2.7	10.8	0.09
TS-094	BG18-3903	3	H-W	Af	5191.0	5.0	59.0	0.87	88.0	541.4	1.3	3.5	10.5	0.09
TS-095	BG18-3903	3	H-W	Af	5655.0	5.0	54.0	0.94	104.7	496.9	1.3	3.3	11.2	0.08
TS-096	BG18-3903	3	H-W	Af	5005.0	58.0	294.0	0.83	17.0	481.2	15.2	15.9	1.9	0.08
TS-097	BG18-3903	3	H-W	Af	6817.0	5.0	51.0	1.14	133.7	661.7	1.3	1.8	13.8	0.11

Table I.2 Continued.

Sample ID	DDH	n	Strat Member	Rock Code	Ti *ppm*	Cr *ppm*	Zr *ppm*	Ti/Zr	TiO_2 %	*Total Measurment Error*				
										Ti *ppm*	Cr *ppm*	Zr *ppm*	Ti/Zr	TiO_2 %
TS-1075	BG18-3921	3	H-W	Af	3663.0	6.0	66.0	0.61	55.5	644.2	1.6	3.3	10.1	0.11
TS-1076	BG18-3921	3	H-W	Af	5387.0	6.0	62.0	0.90	86.9	525.5	1.6	3.6	9.9	0.09
TS-1077	BG18-3921	3	H-W	Af	5867.0	6.0	65.0	0.98	90.3	730.0	1.6	2.4	11.7	0.12
TS-1078	BG18-3921	3	H-W	Af	4742.0	6.0	53.0	0.79	89.5	590.1	1.6	4.1	13.1	0.10
TS-1079	BG18-3921	3	H-W	Af	4784.0	6.0	58.0	0.80	82.5	457.8	1.6	2.9	8.9	0.08
TS-1081	BG18-3921	3	H-W	Af	5728.0	6.0	57.0	0.96	100.5	553.2	1.6	2.1	10.4	0.09
TS-1082	BG18-3921	3	H-W	Af	5217.0	6.0	56.0	0.87	93.2	540.4	1.6	3.6	11.4	0.09
TS-1083	BG18-3921	3	H-W	Af	4948.0	6.0	59.0	0.83	83.9	503.7	1.6	3.1	9.6	0.08
TS-1084	BG18-3921	3	H-W	Af	4737.0	6.0	56.0	0.79	84.6	524.7	1.6	3.2	10.6	0.09
TS-1085	BG18-3921	3	H-W	Af	4878.0	6.0	58.0	0.81	84.1	560.2	1.6	4.2	11.4	0.09
TS-1086	BG18-3921	3	H-W	Af	4478.0	6.0	51.0	0.75	87.8	427.3	1.6	1.9	9.0	0.07
TS-1087	BG18-3921	3	H-W	Af	5194.0	6.0	58.0	0.87	89.6	575.4	1.6	2.8	10.8	0.10
TS-1088	BG18-3921	3		Md	1035.0	15.0	162.0	0.17	6.4	122.0	4.1	11.9	0.9	0.02
TS-1089	BG18-3921	3	H-W	Af	4860.0	30.0	67.0	0.81	72.5	533.0	9.0	3.3	8.7	0.09
TS-1152	RN18-0223	3	HWA	Avc	5419.0	26.0	78.0	0.90	69.5	909.3	7.8	11.3	15.4	0.15
TS-1153	RN18-0223	3	H-W	Af	3597.0	31.0	66.0	0.60	54.5	515.0	8.2	3.9	8.4	0.09
TS-1154	RN18-0223	3	H-W	Af	3997.0	21.0	62.0	0.67	64.5	498.6	9.5	2.4	8.4	0.08
TS-1155	RN18-0223	3	H-W	Af	3591.0	22.0	56.0	0.60	64.1	438.6	12.0	4.9	9.6	0.07
TS-1156	RN18-0224	3	H-W	QFP	1331.2	33.7	114.4	0.22	11.6	179.9	9.8	8.9	1.8	0.03
TS-1157	RN18-0224	3	H-W	QFP	2263.2	56.5	140.4	0.38	16.1	340.7	16.6	17.2	3.1	0.06
TS-1158	RN18-0224	3	H-W	QFP	2301.1	60.0	150.5	0.38	15.3	289.2	16.8	10.6	2.2	0.05
TS-1159	RN18-0224	3	H-W	QFP	1513.3	56.9	89.5	0.25	16.9	275.7	17.4	5.2	3.2	0.05
TS-1160	RN18-0224	3	H-W	QFP	2264.6	48.4	174.1	0.38	13.0	441.7	13.7	43.6	4.1	0.07
TS-1161	RN18-0224	3	H-W	QFP	1993.7	54.2	163.0	0.33	12.2	726.2	17.8	54.0	6.0	0.12
TS-1162	RN18-0224	3	H-W	QFP	2017.5	46.1	183.9	0.34	11.0	243.6	12.9	9.8	1.4	0.04
TS-1164	RN18-0224	3	H-W	QFP	2533.8	63.9	176.5	0.42	14.4	261.9	17.4	7.2	1.6	0.04
TS-1165	RN18-0224	3	H-W	QFP	4741.4	92.1	176.0	0.79	26.9	483.1	25.0	14.1	3.5	0.08
TS-1166	RN18-0224	3	H-W	QFP	2283.0	51.9	158.6	0.38	14.4	279.0	14.5	19.9	2.5	0.05
TS-1167	RN18-0224	3	H-W	QFP	9666.7	89.8	149.4	1.61	64.7	4490.4	24.5	8.8	30.3	0.75
TS-1168	RN18-0224	3	H-W	QFP	2175.9	43.7	168.7	0.36	12.9	237.2	12.2	6.6	1.5	0.04
TS-1169	RN18-0224	3	H-W	QFP	2116.9	51.5	132.7	0.35	16.0	291.1	14.8	13.5	2.7	0.05
TS-1170	RN18-0224	3	H-W	QFP	2033.9	54.2	133.5	0.34	15.2	248.5	14.9	6.4	2.0	0.04
TS-1171	RN18-0224	3	H-W	QFP	2169.2	56.5	106.5	0.36	20.4	228.2	15.7	4.5	2.3	0.04
TS-1172	RN18-0224	3	H-W	Fvc	1973.3	53.0	105.1	0.33	18.8	203.1	14.5	5.8	2.2	0.03
TS-1173	RN18-0224	3	H-W	Fvc	1534.1	40.6	99.3	0.26	15.5	177.8	12.4	8.5	2.2	0.03
TS-1180	RN18-0224	3	Price Fm	PA	3936.0	37.0	112.0	0.66	35.1	945.3	10.2	14.9	9.6	0.16
TS-1181	RN18-0224	3	Price Fm	PA	4914.0	43.0	143.0	0.82	34.4	561.6	13.4	5.8	4.2	0.09
TS-1182	RN18-0224	3	Price Fm	PA	4180.0	30.0	112.0	0.70	37.3	992.3	14.6	30.7	13.5	0.17
TS-138	BG18-3298	3	Price Fm	PA	4705.0	46.0	121.0	0.78	38.9	425.6	13.4	4.3	3.8	0.07
TS-139	BG18-3298	3	Price Fm	PA	4587.0	60.0	66.0	0.77	69.5	467.4	16.4	2.4	7.5	0.08
TS-140	BG18-3298	3	Price Fm	PA	4097.0	51.0	55.0	0.68	74.5	425.2	16.8	1.8	8.1	0.07
TS-141	BG18-3298	3	Price Fm	PA	4054.0	15.0	75.0	0.68	54.1	511.4	10.1	12.9	11.5	0.09
TS-142	BG18-3298	3	Price Fm	PA	3800.0	28.0	50.0	0.63	76.0	672.0	8.7	7.2	17.3	0.11
TS-149	BG18-3299	3	Price Fm	PA	6653.0	60.0	97.0	1.11	68.6	901.8	17.7	6.2	10.3	0.15
TS-150	BG18-3299	3	Price Fm	PA	5396.0	44.0	93.0	0.90	58.0	665.9	14.9	5.8	8.0	0.11
TS-151	BG18-3299	3	Price Fm	PA	3671.0	55.0	53.0	0.61	69.3	381.0	18.1	2.2	7.7	0.06
TS-152	BG18-3229	3	Price Fm	PA	4072.0	30.0	108.0	0.68	37.7	820.2	9.2	14.1	9.1	0.14
TS-153	BG18-3229	3	Price Fm	PA	3602.0	34.0	72.0	0.60	50.0	360.6	10.1	4.7	6.0	0.06
TS-154	BG18-3299	3	Price Fm	PA	3498.0	31.0	72.0	0.58	48.6	783.7	10.1	12.4	13.7	0.13
TS-155	BG18-3229	3	Price Fm	PA	1686.0	28.0	76.0	0.28	22.2	261.5	8.8	24.5	7.9	0.04
TS-156	BG18-3769	3	H-W	Af	5128.0	6.0	105.0	0.86	48.8	511.1	1.6	4.9	5.4	0.09
TS-157	BG18-3769	3	H-W	Af	5544.0	6.0	72.0	0.92	77.0	493.5	1.6	2.7	7.5	0.08

Table I.2 Continued.

Sample ID	DDH	n	Strat Member	Rock Code	Ti *ppm*	Cr *ppm*	Zr *ppm*	Ti/Zr	TiO_2 %	*Total Measurment Error*				
										Ti *ppm*	Cr *ppm*	Zr *ppm*	Ti/Zr	TiO_2 %
TS-158	BG18-3769	3	H-W	Af	4733.0	6.0	38.0	0.79	124.6	425.4	1.6	1.5	12.3	0.07
TS-159	BG18-3769	3	H-W	Af	3609.0	6.0	56.0	0.60	64.4	323.4	1.6	2.5	6.4	0.05
TS-160	BG18-3769	3	H-W	Af	5465.0	6.0	59.0	0.91	92.6	488.5	1.6	2.3	9.0	0.08
TS-161	BG18-3769	3	H-W	Af	4221.0	6.0	54.0	0.70	78.2	377.3	1.6	2.3	7.8	0.06
TS-162	BG18-3769	3	H-W	Af	3372.0	818.0	30.0	0.56	112.4	300.2	217.3	1.6	11.6	0.05
TS-163	BG18-3769	3	H-W	Af	5007.0	6.0	48.0	0.84	104.3	453.3	1.6	1.8	10.2	0.08
TS-164	BG18-3769	3	H-W	Af	1471.0	21.0	72.0	0.25	20.4	186.1	6.0	3.2	2.7	0.03
TS-165	BG18-3769	3	H-W	QFP	3782.0	89.0	152.0	0.63	24.9	348.4	23.6	21.9	4.3	0.06
TS-167	BG18-3769	3	H-W	QFP	5933.0	68.0	112.0	0.99	53.0	853.1	18.2	5.4	8.0	0.14
TS-168	BG18-3769	3	H-W	QFP	9084.0	77.0	145.0	1.52	62.6	2504.8	24.5	6.3	17.5	0.42
TS-169	BG18-3769	3	H-W	QFP	5815.0	55.0	105.0	0.97	55.4	676.5	16.0	5.8	7.1	0.11
TS-170	BG18-3769	3	H-W	QFP	1848.0	33.0	104.0	0.31	17.8	178.0	8.8	4.0	1.8	0.03
TS-171	BG18-3769	3	H-W	QFP	5902.0	79.0	102.0	0.98	57.9	545.2	23.6	4.1	5.8	0.09
TS-172	BG18-3769	3	H-W	QFP	5785.0	90.0	132.0	0.96	43.8	989.0	24.2	6.5	7.8	0.16
TS-173	BG18-3769	3	H-W	QFP	3505.0	57.0	91.0	0.58	38.5	490.4	15.3	7.2	6.2	0.08
TS-174	BG18-3769	3	H-W	QFP	2039.0	44.0	79.0	0.34	25.8	326.2	11.7	6.3	4.6	0.05
TS-175	BG18-3769	3	H-W	QFP	4280.0	74.0	148.0	0.71	28.9	635.8	20.5	10.1	4.7	0.11
TS-176	BG18-3769	3	H-W	QFP	12337.0	170.0	160.0	2.06	77.1	1475.7	48.2	6.9	9.8	0.25
TS-177	BG18-3769	3	H-W	QFP	528.0	23.0	42.0	0.09	12.6	74.7	7.4	13.0	4.3	0.01
TS-178	BG18-3769	3	H-W	Fvc	1334.0	24.0	135.0	0.22	9.9	266.6	6.8	23.2	2.6	0.04
TS-179	BG18-3769	3	H-W	Fvc	730.0	19.0	63.0	0.12	11.6	81.7	5.1	4.8	1.6	0.01
TS-180	BG18-3769	3	H-W	Fvc	893.0	18.0	106.0	0.15	8.4	437.7	7.0	50.5	5.8	0.07
TS-181	BG18-3769	3	H-W	Fvc	570.0	17.0	59.0	0.10	9.7	62.1	5.3	7.4	1.6	0.01
TS-182	BG18-3769	3	Price Fm	PA	5344.0	6.0	76.0	0.89	70.3	532.6	1.6	4.1	8.0	0.09
TS-183	BG18-3769	3	Price Fm	PA	4900.0	6.0	71.0	0.82	69.0	634.1	1.6	5.7	10.5	0.11
TS-184	BG18-3769	3	Price Fm	PA	5005.0	16.0	71.0	0.83	70.5	700.2	6.5	4.5	10.8	0.12
TS-185	BG18-3769	4	Price Fm	PA	5907.0	26.0	82.0	0.99	72.0	526.5	7.8	3.1	7.0	0.09
TS-186	BG18-3769	3	Price Fm	PA	3191.0	58.0	55.0	0.53	58.0	492.1	30.3	4.4	10.1	0.08
TS-187	BG18-3769	3	Price Fm	PA	3954.0	6.0	65.0	0.66	60.8	352.0	1.6	2.5	5.9	0.06
TS-188	BG18-3769	3	Price Fm	PA	6387.0	43.0	97.0	1.07	65.8	568.3	11.7	3.6	6.4	0.09
TS-189	BG18-3769	3	Price Fm	PA	4420.0	10.0	68.0	0.74	65.0	1089.9	4.6	10.9	19.1	0.18
TS-190	BG18-3769	3	Price Fm	PA	5218.0	12.0	72.0	0.87	72.5	590.5	6.8	5.0	9.6	0.10
TS-191	BG18-3769	3	Price Fm	PA	3438.0	9.0	61.0	0.57	56.4	361.3	3.9	3.4	6.7	0.06
TS-192	BG18-3769	3	Price Fm	PA	4194.0	28.0	65.0	0.70	64.5	425.8	9.9	4.2	7.7	0.07
TS-193	BG18-3769	3	Price Fm	PA	4990.0	14.0	75.0	0.83	66.5	538.1	5.4	4.0	8.0	0.09
TS-194	BG18-3769	3	Price Fm	PA	5120.0	12.0	81.0	0.85	63.2	465.6	7.0	5.4	7.1	0.08
TS-195	BG18-3769	3	Price Fm	PA	5558.0	6.0	75.0	0.93	74.1	735.5	1.6	6.2	11.6	0.12
TS-196	BG18-3769	3	Price Fm	PA	6647.0	29.0	93.0	1.11	71.5	1228.4	16.0	15.2	17.6	0.20
TS-197	BG18-3769	3	H-W	Bvc	3725.0	65.0	107.0	0.62	34.8	553.4	20.9	11.6	6.4	0.09
TS-198	BG18-3769	3	H-W	Bvc	3049.0	71.0	78.0	0.51	39.1	352.7	32.1	3.9	4.9	0.06
TS-199	BG18-3769	3	H-W	Bvc	2574.0	70.0	85.0	0.43	30.3	629.9	23.1	11.1	8.4	0.11
TS-200	BG18-3769	3	Price Fm	PA	5334.0	38.0	85.0	0.89	62.8	480.2	12.6	3.3	6.2	0.08
TS-201	BG18-3769	3	Price Fm	PA	4419.0	24.0	146.0	0.74	30.3	434.6	6.5	5.5	3.2	0.07
TS-202	BG18-3769	3	Price Fm	PA	6320.0	40.0	112.0	1.05	56.4	562.4	10.7	4.2	5.4	0.09
TS-263	BG18-3321A	3	Price Fm	PA	4967.0	27.0	89.0	0.83	55.8	561.9	9.6	7.2	7.8	0.09
TS-264	BG18-3221A	3	Price Fm	PA	6015.0	17.0	86.0	1.00	69.9	545.0	7.3	3.0	6.8	0.09
TS-265	BG18-3321A	3	Price Fm	PA	4604.0	13.0	70.0	0.77	65.8	684.4	7.9	6.0	11.3	0.11
TS-266	BG18-3221A	3	Price Fm	PA	4851.0	21.0	78.0	0.81	62.2	705.8	16.2	7.9	11.0	0.12
TS-267	BG18-3321A	3	Price Fm	PA	4232.0	23.0	69.0	0.71	61.3	848.7	18.3	7.7	14.1	0.14
TS-268	BG18-3221A	3	Price Fm	PA	3490.0	30.0	85.0	0.58	41.1	362.2	8.7	4.5	4.8	0.06
TS-269	BG18-3321A	3	Price Fm	PA	3923.0	22.0	96.0	0.65	40.9	465.8	7.9	8.1	6.0	0.08
TS-270	BG18-3221A	3	Price Fm	PA	4425.0	22.0	106.0	0.74	41.7	619.8	6.9	10.7	7.2	0.10

Table I.2 Continued.

Sample ID	DDH	n	Strat Member	Rock Code	Ti *ppm*	Cr *ppm*	Zr *ppm*	Ti/Zr	TiO_2 %	*Total Measurment Error*				
										Ti *ppm*	Cr *ppm*	Zr *ppm*	Ti/Zr	TiO_2 %
TS-271	BG18-3321A	3	Price Fm	PA	3193.0	20.0	84.0	0.53	38.0	540.2	7.4	11.1	8.1	0.09
TS-272	BG18-3221A	3	Price Fm	PA	5112.0	37.0	118.0	0.85	43.3	466.9	11.2	4.8	4.3	0.08
TS-273	BG18-3321A	3	Price Fm	PA	3937.0	77.0	89.0	0.66	44.2	360.8	22.8	3.6	4.4	0.06
TS-274	BG18-3221A	3	Price Fm	PA	1387.0	55.0	22.0	0.23	63.0	125.4	15.2	0.8	6.1	0.02
TS-275	BG18-3321A	3	Price Fm	PA	3110.0	123.0	49.0	0.52	63.5	281.4	33.7	1.6	6.1	0.05
TS-276	BG18-3221A	3	Price Fm	PA	3208.0	23.0	98.0	0.54	32.7	464.2	7.0	3.6	4.9	0.08
TS-277	BG18-3221	3	H-W	Af	3021.0	48.0	73.0	0.50	41.4	536.9	30.8	5.0	7.9	0.09
TS-278	BG18-3221	3	H-W	Af	7192.0	13.0	84.0	1.20	85.6	772.5	8.1	2.8	9.6	0.13
TS-279	BG18-3221	3	H-W	Af	4336.0	6.0	39.0	0.72	111.2	397.3	1.6	1.6	11.1	0.07
TS-280	BG18-3221	3	H-W	Af	3799.0	546.0	32.0	0.63	118.7	365.6	149.4	1.3	12.4	0.06
TS-281	BG18-3221	3	H-W	Af	2640.0	23.0	103.0	0.44	25.6	895.7	7.0	19.8	10.0	0.15
TS-282	BG18-3221	3	H-W	Af	4402.0	31.0	151.0	0.73	29.2	399.5	15.7	30.1	6.4	0.07
TS-306	BG18-3321	3	Price Fm	PA	5370.0	13.0	86.0	0.90	62.4	504.3	7.7	4.6	6.8	0.08
TS-307	BG18-3321	3	Price Fm	PA	4773.0	10.0	76.0	0.80	62.8	447.1	4.7	3.5	6.6	0.07
TS-308	BG18-3321	3	Price Fm	PA	4750.0	11.0	68.0	0.79	69.9	749.3	6.0	4.8	12.1	0.12
TS-309	BG18-3321	3	Price Fm	PA	5268.0	15.0	81.0	0.88	65.0	518.5	6.0	4.7	7.4	0.09
TS-310	BG18-3321	3	Price Fm	PA	5448.0	32.0	90.0	0.91	60.5	641.6	8.9	5.3	8.0	0.11
TS-345	BG18-3904	3	Price Fm	PA	4926.0	21.0	90.0	0.82	54.7	602.7	6.7	5.0	7.3	0.10
TS-346	BG18-3904	3	Price Fm	PA	4223.0	17.0	70.0	0.70	60.3	403.8	7.0	2.3	6.1	0.07
TS-347	BG18-3904	3	Price Fm	PA	3029.0	22.0	45.0	0.51	67.3	1204.1	11.6	18.9	38.9	0.20
TS-348	BG18-3904	3	Price Fm	PA	5574.0	47.0	74.0	0.93	75.3	536.6	12.2	2.7	7.7	0.09
TS-349	BG18-3904	3	Price Fm	PA	6355.0	68.0	97.0	1.06	65.5	740.4	19.5	5.9	8.6	0.12
TS-350	BG18-3904	3	Price Fm	PA	4408.0	47.0	55.0	0.74	80.1	439.2	19.1	2.7	8.9	0.07
TS-351	BG18-3904	3	Price Fm	PA	4723.0	34.0	58.0	0.79	81.4	468.6	17.4	3.1	9.2	0.08
TS-352	BG18-3904	3	Price Fm	PA	5764.0	14.0	76.0	0.96	75.8	831.1	8.9	5.0	12.0	0.14
TS-353	BG18-3904	3	Price Fm	PA	4005.0	43.0	54.0	0.67	74.2	628.5	15.6	5.4	13.8	0.10
TS-354	BG18-3904	3	Price Fm	PA	3561.0	22.0	52.0	0.59	68.5	606.2	9.8	7.4	15.2	0.10
TS-355	BG18-3904	3	Price Fm	PA	4462.0	5.0	77.0	0.74	57.9	623.0	1.3	7.4	9.8	0.10
TS-356	BG18-3904	3	Price Fm	PA	3487.0	5.0	68.0	0.58	51.3	312.3	1.3	2.8	5.1	0.05
TS-357	BG18-3904	3	Price Fm	PA	3278.0	10.0	93.0	0.55	35.2	282.0	2.7	3.1	3.2	0.05
TS-358	BG18-3904	3	Price Fm	PA	3469.0	13.0	96.0	0.58	36.1	682.7	3.8	14.3	8.9	0.11
TS-389	BG18-3550	3	Price Fm	PA	5231.0	15.0	134.0	0.87	39.0	546.8	6.3	6.9	4.6	0.09
TS-390	BG18-3550	3	Price Fm	PA	5237.0	6.0	75.0	0.87	69.8	484.8	1.6	3.8	7.4	0.08
TS-391	BG18-3550	3	Price Fm	PA	5075.0	21.0	73.0	0.85	69.5	516.6	16.2	4.8	8.4	0.09
TS-392	BG18-3550	3	Price Fm	PA	5133.0	6.0	75.0	0.86	68.4	689.3	1.6	6.0	10.7	0.11
TS-393	BG18-3550	3	Price Fm	PA	4027.0	33.0	116.0	0.67	34.7	388.9	9.9	5.2	3.7	0.06
TS-394	BG18-3550	3	Price Fm	PA	4544.0	10.0	65.0	0.76	69.9	850.1	4.8	10.9	17.5	0.14
TS-395	BG18-3550	3	Price Fm	PA	3059.0	13.0	79.0	0.51	38.7	298.4	5.8	3.6	4.2	0.05
TS-396	BG18-3550	3	Price Fm	PA	3936.0	20.0	103.0	0.66	38.2	394.1	5.9	7.1	4.7	0.07
TS-397	BG18-3550	3	Price Fm	PA	3602.0	12.0	86.0	0.60	41.9	346.8	4.4	5.4	4.8	0.06
TS-398	BG18-3550	3	Price Fm	PA	3728.0	24.0	79.0	0.62	47.2	364.9	8.0	4.0	5.2	0.06
TS-399	BG18-3550	3	Price Fm	PA	3841.0	32.0	83.0	0.64	46.3	376.0	10.8	4.1	5.1	0.06
TS-400	BG18-3550	3	Price Fm	PA	4677.0	20.0	84.0	0.78	55.7	614.5	6.0	6.3	8.4	0.10
TS-419	BG18-3551	3	Price Fm	PA	2786.0	11.0	93.0	0.46	30.0	284.6	4.0	7.1	3.8	0.05
TS-420	BG18-3551	3	Price Fm	PA	4226.0	12.0	65.0	0.70	65.0	514.4	7.0	4.9	9.3	0.09
TS-421	BG18-3551	3	Price Fm	PA	6555.0	23.0	100.0	1.09	65.6	696.7	10.7	9.9	9.5	0.12
TS-422	BG18-3551	3	Price Fm	PA	4174.0	23.0	78.0	0.70	53.5	392.4	7.0	4.8	6.0	0.07
TS-423	BG18-3551	3	Price Fm	PA	4041.0	21.0	103.0	0.67	39.2	349.3	6.6	6.1	4.1	0.06
TS-424	BG18-3551	3	Price Fm	PA	3119.0	32.0	81.0	0.52	38.5	274.6	8.8	4.4	4.0	0.05
TS-425	BG18-3551	3	Price Fm	PA	3740.0	32.0	84.0	0.62	44.5	348.3	9.8	16.8	9.8	0.06
TS-468	BG18-3905	3	H-W	Af	5802.0	6.0	60.0	0.97	96.7	514.3	1.6	2.7	9.6	0.09
TS-469	BG18-3905	3	H-W	Af	5335.0	6.0	67.0	0.89	79.6	570.3	1.6	3.7	9.6	0.10

Table I.2 Continued.

Sample ID	DDH	n	Strat Member	Rock Code	Ti *ppm*	Cr *ppm*	Zr *ppm*	Ti/Zr	TiO_2 %	*Total Measurment Error*				
										Ti *ppm*	Cr *ppm*	Zr *ppm*	Ti/Zr	TiO_2 %
TS-470	BG18-3905	3	H-W	Af	5343.0	6.0	49.0	0.89	109.0	555.1	1.6	3.4	13.6	0.09
TS-471	BG18-3905	3	H-W	Af	6301.0	6.0	69.0	1.05	91.3	571.6	1.6	3.0	9.2	0.10
TS-472	BG18-3905	3	H-W	Af	7237.0	6.0	60.0	1.21	120.6	646.2	1.6	4.1	13.6	0.11
TS-473	BG18-3905	3	H-W	Af	5859.0	6.0	62.0	0.98	94.5	788.2	1.6	3.5	13.8	0.13
TS-474	BG18-3905	3	H-W	Af	5735.0	6.0	58.0	0.96	98.9	749.4	1.6	3.8	14.4	0.12
TS-475	BG18-3905	3	H-W	Af	5140.0	6.0	58.0	0.86	88.6	537.0	1.6	4.0	11.1	0.09
TS-476	BG18-3905	3	H-W	Af	5202.0	6.0	53.0	0.87	98.2	525.6	1.6	2.5	10.9	0.09
TS-477	BG18-3905	3	H-W	Af	5509.0	6.0	56.0	0.92	98.4	476.2	1.6	2.8	9.9	0.08
TS-478	BG18-3905	3	H-W	Af	5551.0	6.0	60.0	0.93	92.5	497.5	1.6	2.6	9.2	0.08
TS-479	BG18-3905	3	H-W	Af	5321.0	6.0	51.0	0.89	104.3	475.1	1.6	4.8	13.6	0.08
TS-480	BG18-3905	3	H-W	Af	5271.0	6.0	61.0	0.88	86.4	472.4	1.6	2.7	8.7	0.08
TS-481	BG18-3905	3	H-W	Af	5699.0	6.0	57.0	0.95	100.0	661.5	1.6	2.5	12.4	0.11
TS-494	BG18-3905	3	Price Fm	PA	3236.0	16.0	105.0	0.54	30.8	549.9	5.5	10.7	6.1	0.09
TS-495	BG18-3905	3	Price Fm	PA	4248.0	6.0	124.0	0.71	34.3	395.1	1.6	5.5	3.5	0.07
TS-496	BG18-3905	3	Price Fm	PA	3590.0	6.0	59.0	0.60	60.8	423.3	1.6	4.9	8.8	0.07
TS-497	BG18-3905	3	Price Fm	PA	4122.0	16.0	70.0	0.69	58.9	676.4	6.8	9.6	12.6	0.11
TS-498	BG18-3905	3	Price Fm	PA	5290.0	10.0	78.0	0.88	67.8	492.9	4.8	3.5	7.0	0.08
TS-550	BG18-3552	3	Price Fm	PA	4057.0	20.0	126.0	0.68	32.2	784.6	5.2	15.8	7.4	0.13
TS-551	BG18-3552	3	Price Fm	PA	2992.0	9.0	93.0	0.50	32.2	303.4	4.1	4.7	3.6	0.05
TS-552	BG18-3552	3	Price Fm	PA	3994.0	15.0	102.0	0.67	39.2	868.2	6.1	18.6	11.1	0.14
TS-553	BG18-3552	3	Price Fm	PA	3912.0	17.0	80.0	0.65	48.9	525.6	7.3	4.0	7.0	0.09
TS-554	BG18-3552	3	Price Fm	PA	3940.0	9.0	97.0	0.66	40.6	483.8	4.3	13.9	7.7	0.08
TS-555	BG18-3552	3	Price Fm	PA	6163.0	6.0	94.0	1.03	65.6	653.3	1.6	3.4	7.3	0.11
TS-556	BG18-3552	3	Price Fm	PA	5063.0	11.0	84.0	0.84	60.3	502.7	6.0	4.8	6.9	0.08
TS-557	BG18-3552	3	Price Fm	PA	6027.0	17.0	92.0	1.01	65.5	641.7	7.3	4.7	7.7	0.11
TS-558	BG18-3552	3	Price Fm	PA	4508.0	75.0	61.0	0.75	73.9	434.2	26.0	3.2	8.1	0.07
TS-559	BG18-3552	3	Price Fm	PA	4995.0	38.0	101.0	0.83	49.5	692.8	10.0	5.7	7.4	0.12
TS-560	BG18-3552	3	Price Fm	PA	4670.0	42.0	72.0	0.78	64.9	468.4	12.4	7.9	9.6	0.08
TS-568	BG18-3906	3	H-W	Af	1526.0	15.0	141.0	0.25	10.8	182.2	4.5	10.4	1.5	0.03
TS-569	BG18-3906	3	H-W	Af	5712.0	6.0	79.0	0.95	72.3	1243.3	1.6	9.4	17.9	0.21
TS-570	BG18-3906	3	H-W	Af	4282.0	6.0	68.0	0.71	63.0	528.4	1.6	3.1	8.3	0.09
TS-621	BG18-3553	3	H-W	Af	3438.0	6.0	92.0	0.57	37.4	745.8	1.5	11.1	9.3	0.12
TS-623	BG18-3553	3	H-W	Af	1266.0	28.0	122.0	0.21	10.4	251.8	11.9	5.6	2.1	0.04
TS-624	BG18-3553	3	H-W	Af	4453.0	6.0	65.0	0.74	68.5	933.7	1.5	2.8	14.7	0.16
TS-625	BG18-3553	3	H-W	Af	1255.0	25.0	42.0	0.21	29.9	215.8	11.7	13.5	10.9	0.04
TS-626	BG18-3553	3	H-W	Af	2383.0	41.0	84.0	0.40	28.4	218.0	10.8	8.2	3.8	0.04
TS-627	BG18-3553	3	H-W	Af	733.0	19.0	44.0	0.12	16.7	140.0	6.0	1.5	3.2	0.02
TS-628	BG18-3553	3	H-W	Af	5467.0	6.0	60.0	0.91	91.1	610.5	1.5	1.9	10.6	0.10
TS-640	BG18-3553	3	Price Fm	PA	5612.0	53.0	143.0	0.94	39.2	1253.9	16.8	34.1	12.8	0.21
TS-641	BG18-3553	3	Price Fm	PA	3737.0	25.0	133.0	0.62	28.1	520.4	7.7	19.6	5.7	0.09
TS-642	BG18-3553	3	Price Fm	PA	5082.0	16.0	82.0	0.85	62.0	457.3	6.6	6.4	7.4	0.08
TS-643	BG18-3553	3	Price Fm	PA	4445.0	9.0	70.0	0.74	63.5	1059.4	3.7	12.0	18.6	0.18
TS-645	BG18-3553	3	Price Fm	PA	4613.0	32.0	76.0	0.77	60.7	510.7	18.4	4.9	7.8	0.09
TS-646	BG18-3553	3	Price Fm	PA	5320.0	83.0	70.0	0.89	76.0	740.9	34.8	7.9	13.6	0.12
TS-647	BG18-3553	3	Price Fm	PA	4784.0	18.0	85.0	0.80	56.3	413.6	8.6	6.9	6.7	0.07
TS-648	BG18-3553	3	Price Fm	PA	4833.0	12.0	86.0	0.81	56.2	442.1	6.8	4.3	5.9	0.07
TS-649	BG18-3553	3	Price Fm	PA	4389.0	13.0	75.0	0.73	58.5	887.9	7.9	14.0	16.1	0.15
TS-650	BG18-3907	3	HWA	Avc	5741.0	6.0	66.0	0.96	87.0	561.3	1.7	4.0	10.0	0.09
TS-651	BG18-3907	3	HWA	Avc	4461.0	6.0	62.0	0.74	72.0	572.0	1.7	3.4	10.0	0.10
TS-652	BG18-3907	3	HWA	Avc	5586.0	6.0	69.0	0.93	81.0	791.9	1.7	4.6	12.7	0.13
TS-653	BG18-3907	3	HWA	Avc	4795.0	6.0	79.0	0.80	60.7	404.8	1.7	3.6	5.8	0.07
TS-654	BG18-3907	3	HWA	Avc	3946.0	6.0	101.0	0.66	39.1	1219.1	1.7	22.1	14.8	0.20

Table I.2 Continued.

Sample ID	DDH	n	Strat Member	Rock Code	Ti *ppm*	Cr *ppm*	Zr *ppm*	Ti/Zr	TiO_2 %	*Total Measurment Error*				
										Ti *ppm*	Cr *ppm*	Zr *ppm*	Ti/Zr	TiO_2 %
TS-655	BG18-3907	3	H-W	Fvc	3271.0	62.0	184.0	0.55	17.8	301.4	18.1	11.7	2.0	0.05
TS-656	BG18-3907	3		Md	6532.0	72.0	112.0	1.09	58.3	545.2	21.0	6.9	6.1	0.09
TS-657	BG18-3907	3	HWA	Avc	3235.0	18.0	95.0	0.54	34.1	1121.6	8.0	6.6	12.0	0.19
TS-658	BG18-3907	3	HWA	Avc	4678.0	6.0	64.0	0.78	73.1	603.5	1.7	3.5	10.2	0.10
TS-659	BG18-3907	3	HWA	Avc	5602.0	6.0	65.0	0.93	86.2	496.9	1.7	8.8	14.0	0.08
TS-660	BG18-3907	3	HWA	Avc	4408.0	6.0	67.0	0.74	65.8	599.9	1.7	2.0	9.2	0.10
TS-661	BG18-3907	3	HWA	Avc	5276.0	6.0	56.0	0.88	94.2	510.1	1.7	4.5	11.9	0.09
TS-662	BG18-3907	3	H-W	Af	6265.0	6.0	71.0	1.05	88.2	602.3	1.7	4.5	10.1	0.10
TS-663	BG18-3907	3	H-W	Af	5266.0	6.0	57.0	0.88	92.4	445.9	1.7	2.6	8.9	0.07
TS-664	BG18-3907	3	H-W	Af	5465.0	6.0	57.0	0.91	95.9	609.0	1.7	3.1	11.9	0.10
TS-665	BG18-3907	3	H-W	Af	4753.0	6.0	54.0	0.79	88.0	405.2	1.7	1.6	8.0	0.07
TS-666	BG18-3907	3	H-W	Af	4440.0	6.0	55.0	0.74	80.7	494.8	1.7	4.3	11.0	0.08
TS-667	BG18-3907	3	H-W	Af	5155.0	6.0	57.0	0.86	90.4	495.6	1.7	2.7	9.7	0.08
TS-668	BG18-3907	3	H-W	Af	4823.0	6.0	59.0	0.80	81.7	505.8	1.7	1.4	8.8	0.08
TS-669	BG18-3907	3	HWA	Avc	2120.0	137.0	68.0	0.35	31.2	197.4	55.5	1.9	3.0	0.03
TS-670	BG18-3907	3	HWA	Avc	1034.0	24.0	84.0	0.17	12.3	105.9	7.2	3.4	1.4	0.02
TS-671	BG18-3907	3	HWA	Avc	3208.0	33.0	82.0	0.54	39.1	370.9	10.5	6.2	5.4	0.06
TS-672	BG18-3907	3	HWA	Avc	3802.0	25.0	85.0	0.63	44.7	332.9	8.4	3.7	4.4	0.06
TS-673	BG18-3907	3	H-W	Fvc	1076.0	29.0	86.0	0.18	12.5	97.7	8.7	3.9	1.3	0.02
TS-674	BG18-3907	3	H-W	Fvc	1246.0	53.0	61.0	0.21	20.4	217.1	15.3	3.9	3.8	0.04
TS-675	BG18-3907	3	H-W	Fvc	1244.0	43.0	84.0	0.21	14.8	132.8	12.8	6.9	2.0	0.02
TS-676	BG18-3907	3	H-W	Fvc	3189.0	45.0	177.0	0.53	18.0	261.2	13.1	4.3	1.5	0.04
TS-677	BG18-3907	4	H-W	Fvc	3705.0	33.0	77.0	0.62	48.1	393.3	9.7	5.0	6.0	0.07
TS-678	BG18-3907	3	H-W	C	1470.0	33.0	178.0	0.25	8.3	195.4	11.8	6.3	1.1	0.03
TS-679	BG18-3907	3	H-W	Bvc	2892.0	78.0	90.0	0.48	32.1	262.6	35.4	7.1	3.9	0.04
TS-680	BG18-3907	3	Price Fm	PA	3050.0	12.0	112.0	0.51	27.2	248.6	4.8	2.8	2.3	0.04
TS-681	BG18-3907	3	Price Fm	PA	3178.0	15.0	108.0	0.53	29.4	482.2	7.3	13.2	5.7	0.08
TS-682	BG18-3907	3	Price Fm	PA	3840.0	21.0	109.0	0.64	35.2	381.9	6.5	9.4	4.6	0.06
TS-683	BG18-3907	3	Price Fm	PA	3845.0	11.0	114.0	0.64	33.7	472.6	6.2	16.4	6.4	0.08
TS-684	BG18-3907	3	Price Fm	PA	4040.0	29.0	147.0	0.67	27.5	472.8	8.4	16.7	4.5	0.08
TS-685	BG18-3907	3	Price Fm	PA	5717.0	11.0	99.0	0.95	57.7	543.7	6.2	6.5	6.7	0.09
TS-686	BG18-3907	3	Price Fm	PA	4736.0	11.0	78.0	0.79	60.7	396.3	5.8	7.6	7.8	0.07
TS-687	BG18-3907	3	Price Fm	PA	4385.0	6.0	67.0	0.73	65.4	650.7	1.7	4.6	10.7	0.11
TS-688	BG18-3554	3	HWA	Avc	5780.0	6.0	74.0	0.96	78.1	677.2	1.5	4.0	10.1	0.11
TS-689	BG18-3554	3	HWA	Avc	5422.0	6.0	70.0	0.90	77.5	511.1	1.5	3.8	8.4	0.09
TS-690	BG18-3554	3	HWA	Avc	3486.0	6.0	62.0	0.58	56.2	308.1	1.5	1.9	5.2	0.05
TS-691	BG18-3554	3	HWA	Avc	4645.0	6.0	80.0	0.77	58.1	776.7	1.5	3.9	10.1	0.13
TS-692	BG18-3554	3	HWA	Avc	1365.0	21.0	101.0	0.23	13.5	323.6	5.6	10.9	3.5	0.05
TS-693	BG18-3554	3	HWA	Avc	2624.0	29.0	212.0	0.44	12.4	289.3	7.7	6.4	1.4	0.05
TS-694	BG18-3554	3	HWA	Avc	1506.0	41.0	83.0	0.25	18.1	174.5	10.5	9.4	2.9	0.03
TS-695	BG18-3554	3	HWA	Avc	3216.0	6.0	71.0	0.54	45.3	299.9	1.5	18.4	12.5	0.05
TS-696	BG18-3554	3	HWA	Avc	4691.0	6.0	87.0	0.78	53.9	748.9	1.5	13.6	12.0	0.12
TS-697	BG18-3554	3	HWA	Avc	2390.0	28.0	59.0	0.40	40.5	318.8	10.2	10.2	8.8	0.05
TS-698	BG18-3554	3	HWA	Avc	3878.0	11.0	65.0	0.65	59.7	615.9	5.8	7.2	11.5	0.10
TS-699	BG18-3554	3	HWA	Avc	1608.0	25.0	129.0	0.27	12.5	202.7	6.2	7.7	1.7	0.03
TS-700	BG18-3554	3	HWA	Avc	4349.0	22.0	53.0	0.73	82.1	452.4	9.6	2.8	9.6	0.08
TS-701	BG18-3554	3	HWA	Avc	4476.0	51.0	27.0	0.75	165.8	396.8	23.4	1.1	16.2	0.07
TS-702	BG18-3554	3	H-W	QFP	1738.0	48.0	79.0	0.29	22.0	187.5	11.7	6.7	3.0	0.03
TS-703	BG18-3554	3	H-W	QFP	1912.0	47.0	128.0	0.32	14.9	169.1	11.6	5.2	1.5	0.03
TS-704	BG18-3554	3	H-W	QFP	1263.0	34.0	111.0	0.21	11.4	119.1	8.4	5.1	1.2	0.02
TS-705	BG18-3554	3	H-W	QFP	1070.0	25.0	93.0	0.18	11.5	118.6	6.1	3.7	1.4	0.02
TS-706	BG18-3554	3	H-W	QFP	1208.0	26.0	124.0	0.20	9.7	109.1	6.5	6.8	1.0	0.02

Table I.2 Continued.

Sample ID	DDH	n	Strat Member	Rock Code	Ti *ppm*	Cr *ppm*	Zr *ppm*	Ti/Zr	TiO_2 %	*Total Measurment Error*				
										Ti *ppm*	Cr *ppm*	Zr *ppm*	Ti/Zr	TiO_2 %
TS-707	BG18-3554	3	H-W	QFP	2623.0	57.0	144.0	0.44	18.2	245.5	14.2	6.9	1.9	0.04
TS-708	BG18-3554	3	H-W	QFP	3163.0	65.0	167.0	0.53	18.9	453.6	16.2	21.5	3.6	0.08
TS-709	BG18-3554	3	H-W	QFP	2424.0	61.0	161.0	0.40	15.1	355.3	14.8	27.5	3.4	0.06
TS-710	BG18-3554	3	H-W	Bvc	3141.0	25.0	83.0	0.52	37.8	1060.9	6.2	15.6	14.6	0.18
TS-711	BG18-3554	3	H-W	Bvc	5382.0	48.0	165.0	0.90	32.6	784.6	12.5	18.3	6.0	0.13
TS-712	BG18-3554	3	H-W	Bvc	2526.0	36.0	89.0	0.42	28.4	223.1	9.4	2.6	2.6	0.04
TS-713	BG18-3554	3	Price Fm	PA	5141.0	30.0	132.0	0.86	38.9	458.8	7.9	4.0	3.7	0.08
TS-714	BG18-3554	3	Price Fm	PA	4359.0	52.0	123.0	0.73	35.4	505.0	14.2	4.6	4.3	0.08
TS-715	BG18-3554	3	Price Fm	PA	3485.0	32.0	114.0	0.58	30.6	664.5	9.0	23.4	8.6	0.11
TS-716	BG18-3554	3	Price Fm	PA	4822.0	30.0	178.0	0.80	27.1	577.8	7.5	9.7	3.6	0.10
TS-717	BG18-3554	3	Price Fm	PA	6063.0	6.0	87.0	1.01	69.7	612.3	1.5	4.8	8.0	0.10
TS-718	BG18-3554	3	Price Fm	PA	6952.0	21.0	98.0	1.16	70.9	655.3	9.3	4.1	7.3	0.11
TS-719	BG18-3554	3	Price Fm	PA	3974.0	10.0	53.0	0.66	75.0	836.2	4.9	8.7	20.0	0.14
TS-720	BG18-3554	3	Price Fm	PA	5270.0	29.0	81.0	0.88	65.1	493.2	13.8	2.6	6.4	0.08
TS-721	BG18-3554	3	Price Fm	PA	6110.0	21.0	94.0	1.02	65.0	553.2	9.2	3.1	6.3	0.09
TS-722	BG18-3554	3	Price Fm	PA	5486.0	6.0	87.0	0.92	63.1	534.1	1.5	3.6	6.7	0.09
TS-723	BG18-3554	3	Price Fm	PA	2307.0	13.0	49.0	0.38	47.1	203.8	3.6	1.5	4.4	0.03
TS-724	BG18-3554	3	Price Fm	PA	3529.0	35.0	68.0	0.59	51.9	367.1	9.3	5.0	6.6	0.06
TS-725	BG18-3554	3	Price Fm	PA	4941.0	39.0	75.0	0.82	65.9	516.6	11.5	4.6	8.0	0.09
TS-726	BG18-3554	3	Price Fm	PA	3995.0	33.0	71.0	0.67	56.3	397.8	10.6	2.8	6.0	0.07
TS-770	BG18-3908	3	H-W	Af	4593.0	6.0	62.0	0.77	74.1	478.3	1.5	8.3	12.6	0.08
TS-771	BG18-3908	3	H-W	Af	5257.0	6.0	61.0	0.88	86.2	558.1	1.5	3.0	10.1	0.09
TS-772	BG18-3908	3	H-W	Af	4863.0	6.0	59.0	0.81	82.4	442.9	1.5	2.2	8.1	0.07
TS-773	BG18-3908	3	H-W	Af	4837.0	6.0	59.0	0.81	82.0	467.3	1.5	2.5	8.7	0.08
TS-774	BG18-3908	3	H-W	Af	4743.0	6.0	57.0	0.79	83.2	583.5	1.5	3.6	11.5	0.10
TS-785	BG18-3908	3	Price Fm	PA	5833.0	44.0	130.0	0.97	44.9	644.6	11.4	8.2	5.7	0.11
TS-786	BG18-3908	3	Price Fm	PA	4813.0	39.0	126.0	0.80	38.2	438.0	10.5	4.2	3.7	0.07
TS-787	BG18-3908	3	Price Fm	PA	2867.0	11.0	122.0	0.48	23.5	890.4	6.0	31.4	9.5	0.15
TS-788	BG18-3908	3	Price Fm	PA	5771.0	18.0	90.0	0.96	64.1	754.2	8.0	8.3	10.3	0.13
TS-789	BG18-3908	3	Price Fm	PA	1293.0	23.0	78.0	0.22	16.6	171.8	6.2	5.0	2.4	0.03
TS-790	BG18-3908	3	Price Fm	PA	4882.0	6.0	74.0	0.81	66.0	559.7	1.5	4.8	8.7	0.09
TS-791	BG18-3908	3	Price Fm	PA	5606.0	57.0	96.0	0.94	58.4	642.7	19.7	6.4	7.8	0.11
TS-834	BG18-3517	3	H-W	Fvc	6001.0	35.0	186.0	1.00	32.3	650.5	10.5	57.6	10.6	0.11
TS-835	BG18-3517	3	H-W	Fvc	5065.0	42.0	213.0	0.84	23.8	707.2	11.4	21.8	4.1	0.12
TS-836	BG18-3517	3	H-W	Fvc	2385.0	43.0	244.0	0.40	9.8	371.8	13.2	35.1	2.1	0.06
TS-837	BG18-3517	3	H-W	Fvc	2841.0	36.0	168.0	0.47	16.9	551.4	11.4	14.5	3.6	0.09
TS-838	BG18-3517	3	H-W	Fvc	2299.0	28.0	103.0	0.38	22.3	471.1	9.0	6.0	4.8	0.08
TS-839	BG18-3517	3	Price Fm	PA	5152.0	12.0	60.0	0.86	85.9	612.2	4.9	3.0	11.0	0.10
TS-840	BG18-3517	3	Price Fm	PA	5522.0	29.0	76.0	0.92	72.7	485.2	7.9	2.8	6.9	0.08
TS-841	BG18-3517	3	Price Fm	PA	5820.0	5.0	66.0	0.97	88.2	1219.1	1.3	11.5	24.0	0.20
TS-842	BG18-3517	3	Price Fm	PA	6679.0	33.0	89.0	1.11	75.0	596.3	9.0	4.0	7.5	0.10
TS-843	BG18-3517	3	Price Fm	PA	6818.0	20.0	140.0	1.14	48.7	707.2	10.6	61.2	21.9	0.12
TS-913	BG18-3952	3	HWA	Avc	4353.0	6.0	77.0	0.73	56.5	593.6	1.6	4.1	8.3	0.10
TS-914	BG18-3952	3	HWA	Avc	3286.0	6.0	85.0	0.55	38.7	472.7	1.6	12.3	7.9	0.08
TS-915	BG18-3952	3	HWA	Avc	5251.0	35.0	104.0	0.88	50.5	610.0	11.5	7.3	6.8	0.10
TS-916	BG18-3952	3	HWA	Avc	3526.0	21.0	58.0	0.59	60.8	328.8	6.2	2.1	6.1	0.05
TS-917	BG18-3952	3		Md	4084.0	371.0	24.0	0.68	170.2	451.0	97.8	1.3	20.9	0.08
TS-918	BG18-3952	3	HWA	Avc	1387.0	30.0	93.0	0.23	14.9	305.7	8.3	21.6	4.8	0.05
TS-919	BG18-3952	3	HWA	Avc	5204.0	28.0	39.0	0.87	133.4	548.1	7.6	1.4	14.9	0.09
TS-920	BG18-3952	3	HWA	Avc	1940.0	50.0	93.0	0.32	20.9	279.1	13.6	17.1	4.9	0.05
TS-921	BG18-3952	3	HWA	Avc	4914.0	19.0	61.0	0.82	80.6	1218.6	8.3	8.2	22.7	0.20
TS-922	BG18-3952	3	HWA	Avc	5252.0	12.0	75.0	0.88	70.0	1063.4	6.8	7.3	15.7	0.18

Table I.2 Continued.

Sample ID	DDH	n	Strat Member	Rock Code	Ti *ppm*	Cr *ppm*	Zr *ppm*	Ti/Zr	TiO_2 %	*Total Measurment Error*				
										Ti *ppm*	Cr *ppm*	Zr *ppm*	Ti/Zr	TiO_2 %
TS-923	BG18-3952	3		Md	5683.0	6.0	50.0	0.95	113.7	734.3	1.6	4.4	17.7	0.12
TS-924	BG18-3952	3	H-W	QFP	1014.0	17.0	105.0	0.17	9.7	102.4	5.4	9.2	1.3	0.02
TS-925	BG18-3952	3	H-W	QFP	1791.0	31.0	187.0	0.30	9.6	271.6	8.8	28.8	2.1	0.05
TS-926	BG18-3952	3	H-W	QFP	1012.0	20.0	105.0	0.17	9.6	111.7	5.2	3.9	1.1	0.02
TS-927	BG18-3952	3	H-W	QFP	741.0	18.0	100.0	0.12	7.4	72.2	4.7	4.6	0.8	0.01
TS-928	BG18-3952	3	H-W	QFP	816.0	26.0	89.0	0.14	9.2	99.9	7.3	5.5	1.3	0.02
TS-929	BG18-3952	3	H-W	QFP	984.0	27.0	107.0	0.16	9.2	99.3	7.3	5.0	1.0	0.02
TS-930	BG18-3952	3	H-W	QFP	1317.0	30.0	115.0	0.22	11.5	153.0	8.0	9.0	1.6	0.03
TS-931	BG18-3952	3	H-W	QFP	1036.0	28.0	97.0	0.17	10.7	100.9	7.4	5.2	1.2	0.02
TS-932	BG18-3952	3	H-W	QFP	1171.0	22.0	117.0	0.20	10.0	177.6	6.2	13.5	1.9	0.03
TS-933	BG18-3952	3	H-W	QFP	1213.0	28.0	101.0	0.20	12.0	183.9	7.4	3.7	1.9	0.03
TS-934	BG18-3952	3	H-W	QFP	1019.0	25.0	109.0	0.17	9.3	171.1	7.2	5.8	1.6	0.03
TS-935	BG18-3952	3	H-W	QFP	1367.0	32.0	118.0	0.23	11.6	196.6	8.4	6.3	1.8	0.03
TS-936	BG18-3952	3	H-W	QFP	4022.0	65.0	262.0	0.67	15.4	375.0	17.0	9.7	1.5	0.06
TS-937	BG18-3952	3	H-W	Fvc	4193.0	122.0	248.0	0.70	16.9	390.9	31.9	8.8	1.7	0.07
TS-938	BG18-3952	3	H-W	Fvc	1331.0	42.0	113.0	0.22	11.8	140.2	11.2	4.6	1.3	0.02
TS-939	BG18-3952	3	H-W	C	652.0	24.0	78.0	0.11	8.4	109.5	6.8	7.5	1.6	0.02
TS-940	BG18-3952	3	H-W	Fvc	1445.0	29.0	88.0	0.24	16.4	167.9	8.6	11.9	2.9	0.03
TS-941	BG18-3952	3	H-W	Fvc	1339.0	32.0	89.0	0.22	15.0	124.8	8.5	3.3	1.5	0.02
TS-942	BG18-3952	3	H-W	Fvc	741.0	19.0	74.0	0.12	10.0	90.7	5.0	5.2	1.4	0.02
TS-943	BG18-3952	3	H-W	Fvc	755.0	22.0	62.0	0.13	12.2	120.5	6.5	2.5	2.0	0.02
TS-944	BG18-3952	3	H-W	Fvc	1995.0	30.0	186.0	0.33	10.7	189.2	8.3	14.6	1.3	0.03
TS-945	BG18-3952	3	H-W	C	134.0	18.0	8.0	0.02	16.8	24.8	4.9	1.0	3.7	0.00
TS-946	BG18-3952	3	H-W	C	83.0	14.0	3.0	0.01	27.7	7.7	3.8	0.3	3.7	0.00
TS-947	BG18-3952	3	H-W	C	900.0	44.0	28.0	0.15	32.1	83.9	11.7	1.0	3.2	0.01
TS-948	BG18-3952	3	H-W	Bvc	1968.0	25.0	57.0	0.33	34.5	183.5	6.7	2.3	3.5	0.03
TS-949	BG18-3952	3	H-W	Bvc	2834.0	45.0	88.0	0.47	32.2	573.8	14.8	24.0	10.9	0.10
TS-950	BG18-3952	3	H-W	Bvc	3211.0	22.0	113.0	0.54	28.4	593.8	6.2	13.1	6.2	0.10
TS-951	BG18-3952	3	H-W	Bvc	4719.0	100.0	69.0	0.79	68.4	476.4	27.6	3.2	7.6	0.08
TS-952	BG18-3952	3	Price Fm	PA	5211.0	31.0	137.0	0.87	38.0	1101.6	11.6	22.5	10.2	0.18
TS-953	BG18-3952	3	H-W	Bvc	2393.0	38.0	104.0	0.40	23.0	252.0	10.7	11.0	3.4	0.04
TS-954	BG18-3952	2	H-W	Bvc	2540.0	29.0	67.0	0.42	37.9	385.2	8.9	4.7	6.3	0.06
TS-955	BG18-3952	3	H-W	Bvc	3825.0	27.0	121.0	0.64	31.6	878.0	7.0	15.1	8.3	0.15
TS-956	BG18-3952	3	Price Fm	PA	7187.0	33.0	202.0	1.20	35.6	1147.5	8.6	8.2	5.9	0.19
TS-957	BG18-3952	3	H-W	C	498.0	13.0	27.0	0.08	18.4	46.2	3.4	1.0	1.8	0.01
TS-958	BG18-3952	3	Price Fm	PA	3613.0	31.0	97.0	0.60	37.2	466.8	8.1	3.6	5.0	0.08
TS-959	BG18-3952	3		Md	1490.0	24.0	72.0	0.25	20.7	141.3	6.3	2.9	2.1	0.02
TS-960	BG18-3952	3		Md	1550.0	14.0	74.0	0.26	20.9	260.3	3.6	2.7	3.6	0.04
TS-961	BG18-3952	3	Price Fm	PA	4261.0	34.0	105.0	0.71	40.6	715.5	8.9	4.3	7.0	0.12
TS-962	BG18-3952	3	Price Fm	PA	4518.0	30.0	107.0	0.75	42.2	524.8	7.8	5.0	5.3	0.09
TS-963	BG18-3952	4	Price Fm	PA	3378.0	22.0	118.0	0.56	28.6	315.0	5.9	4.2	2.9	0.05
TS-964	BG18-3952	3	Price Fm	PA	6623.0	28.0	98.0	1.10	67.6	617.5	7.4	3.6	6.8	0.10
TS-965	BG18-3952	3	Price Fm	PA	5428.0	30.0	88.0	0.91	61.7	506.1	8.4	4.1	6.4	0.08
TS-966	BG18-3952	3	Price Fm	PA	5692.0	26.0	80.0	0.95	71.2	628.5	7.2	4.9	9.0	0.10
TS-967	BG18-3952	3	Price Fm	PA	4785.0	12.0	75.0	0.80	63.8	764.0	6.8	6.6	11.6	0.13
TS-968	BG18-3952	3	Price Fm	PA	5906.0	16.0	79.0	0.99	74.8	547.5	10.9	2.9	7.5	0.09
TS-969	BG18-3952	3	Price Fm	PA	3217.0	21.0	57.0	0.54	56.4	313.4	5.9	2.1	5.9	0.05
TS-970	BG18-3952	3	Price Fm	PA	5475.0	32.0	77.0	0.91	71.1	552.8	8.4	3.6	7.9	0.09
TS-971	BG18-3952	3	Price Fm	PA	5458.0	35.0	84.0	0.91	65.0	531.8	11.3	3.4	6.9	0.09
TS-972	BG18-3952	3	Price Fm	PA	5170.0	35.0	78.0	0.86	66.3	743.7	11.7	4.8	10.4	0.12
TS-973	BG18-3952	3	Price Fm	PA	5813.0	33.0	86.0	0.97	67.6	542.0	8.8	3.2	6.8	0.09
TS-974	BG18-3952	3	Price Fm	PA	4005.0	12.0	68.0	0.67	58.9	846.7	4.5	10.5	15.4	0.14

Table I.2 Continued.

Sample ID	DDH	n	Strat Member	Rock Code	Ti *ppm*	Cr *ppm*	Zr *ppm*	Ti/Zr	TiO_2 %	*Total Measurment Error*				
										Ti *ppm*	Cr *ppm*	Zr *ppm*	Ti/Zr	TiO_2 %
TS-975	BG18-3952	3	Price Fm	PA	4939.0	36.0	76.0	0.82	65.0	748.9	14.0	9.5	12.8	0.12
TS-976	BG18-3952	3		Md	4482.0	267.0	39.0	0.75	114.9	415.5	71.4	1.4	11.5	0.07
TS-977	BG18-3952	3		Md	5270.0	359.0	46.0	0.88	114.6	532.1	95.2	2.1	12.7	0.09
TS-978	BG18-3952	3	Price Fm	PA	5200.0	30.0	90.0	0.87	57.8	484.8	8.1	4.8	6.2	0.08
TS-979	BG18-3952	3	Price Fm	PA	4266.0	18.0	76.0	0.71	56.1	471.1	12.9	4.1	6.9	0.08
TS-980	BG18-3952	3	Price Fm	PA	4033.0	27.0	70.0	0.67	57.6	424.8	9.9	7.4	8.6	0.07
TS-981	BG18-3952	3	Price Fm	PA	4180.0	17.0	76.0	0.70	55.0	633.8	11.9	3.5	8.7	0.11
TS-982	BG18-3952	3	Price Fm	PA	5083.0	19.0	85.0	0.85	59.8	495.3	5.3	7.4	7.8	0.08
TS-983	BG18-3952	3	Price Fm	PA	4561.0	6.0	68.0	0.76	67.1	589.3	1.6	5.3	10.1	0.10
TS-984	BG18-3952	3	Price Fm	PA	3050.0	6.0	48.0	0.51	63.5	321.2	1.6	3.3	8.0	0.05
W2		3		STD	6097.0	64.0	93.0	1.02	65.6	524.9	17.0	3.4	6.1	0.09
W2		5		STD	6128.0	84.0	96.0	1.02	63.8	557.0	21.4	3.2	6.2	0.09
W2		3		STD	6106.0	78.0	96.0	1.02	63.6	513.8	20.8	4.1	6.0	0.09
W2		4		STD	6105.0	77.0	95.0	1.02	64.3	560.7	20.6	3.6	6.4	0.09
W2		3		STD	6116.0	75.0	96.0	1.02	63.7	576.5	20.2	3.1	6.4	0.10
W2		5		STD	6104.0	79.0	94.0	1.02	64.9	552.6	21.7	3.0	6.2	0.09
W2		4		STD	6105.0	77.0	95.0	1.02	64.3	560.7	20.6	3.6	6.4	0.09
W2		3		STD	5941.0	73.1	96.1	0.99	61.8	582.8	20.1	3.6	6.5	0.10
W2		3		STD	6116.0	75.0	96.0	1.02	63.7	576.5	20.2	3.1	6.4	0.10
W2		5		STD	6104.0	79.0	94.0	1.02	64.9	552.6	21.7	3.0	6.2	0.09
W2		6		STD	6169.0	73.0	92.0	1.03	67.1	505.2	21.3	2.3	5.7	0.08
W2		6		STD	6050.0	75.0	96.0	1.01	63.0	563.5	19.6	3.5	6.3	0.09
W2		4		STD	6084.0	77.0	95.0	1.01	64.0	546.8	20.9	3.6	6.2	0.09
W2		4		STD	6060.0	81.0	95.0	1.01	63.8	537.9	19.7	3.0	6.0	0.09
W2		3		STD	5982.0	71.0	94.0	1.00	63.6	559.6	20.8	4.0	6.5	0.09
TasBas		4		STD	14133.0	179.0	264.0	2.36	53.5	1300.2	48.1	9.5	5.3	0.22
TasBas		3		STD	14148.0	182.0	263.0	2.36	53.8	1330.6	47.8	8.6	5.4	0.22
TasBas		5		STD	14158.0	177.0	263.0	2.36	53.8	1280.6	48.4	8.1	5.1	0.21
TasBas		3		STD	14202.0	188.0	264.0	2.37	53.8	1159.6	54.4	6.3	4.6	0.19
TasBas		6		STD	14205.0	180.0	266.0	2.37	53.4	1317.5	46.9	9.5	5.3	0.22
TasBas		4		STD	14162.0	180.0	266.0	2.36	53.2	1261.4	47.8	10.0	5.1	0.21
TasBas		4		STD	14192.0	179.0	264.0	2.37	53.8	1256.0	43.5	8.4	5.1	0.21
TasBas		3		STD	14199.0	181.0	264.0	2.37	53.8	1330.3	53.0	11.0	5.5	0.22
TasBas		3		STD	14158.0	148.0	265.0	2.36	53.4	1219.6	38.7	8.8	4.9	0.20
TasBas		5		STD	14153.0	175.0	264.0	2.36	53.6	1286.3	44.5	8.7	5.2	0.21
TasBas		3		STD	14156.0	179.0	266.0	2.36	53.2	1194.6	47.7	11.4	5.0	0.20
TasBas		4		STD	14133.0	179.0	264.0	2.36	53.5	1300.2	48.1	9.5	5.3	0.22
TasBas		3		STD	14148.0	182.0	263.0	2.36	53.8	1330.6	47.8	8.6	5.4	0.22
TasBas		5		STD	14158.0	177.0	263.0	2.36	53.8	1280.6	48.4	8.1	5.1	0.21
TasBas		3		STD	14223.0	182.7	264.6	2.37	53.7	1395.8	49.6	10.1	5.7	0.23
TasGran		5		STD	1519.0	37.0	149.0	0.25	10.2	140.1	9.9	5.5	1.0	0.02
TasGran		3		STD	1487.0	33.0	150.0	0.25	9.9	139.9	8.7	4.8	1.0	0.02
TasGran		5		STD	1531.0	39.0	149.0	0.26	10.3	138.7	10.8	4.6	1.0	0.02
TasGran		3		STD	1564.0	34.0	150.0	0.26	10.4	127.6	9.8	4.4	0.9	0.02
TasGran		8		STD	1537.0	32.0	149.0	0.26	10.3	142.8	8.4	5.4	1.0	0.02
TasGran		4		STD	1540.0	35.0	148.0	0.26	10.4	138.9	9.4	5.8	1.0	0.02
TasGran		4		STD	1534.0	32.0	149.0	0.26	10.3	136.0	8.0	4.7	1.0	0.02
TasGran		3		STD	1527.0	35.0	146.0	0.25	10.5	143.2	10.5	6.1	1.1	0.02
TasGran		3		STD	1558.0	28.0	147.0	0.26	10.6	134.1	7.7	5.0	1.0	0.02
TasGran		6		STD	1528.0	35.0	151.0	0.25	10.1	139.3	9.0	4.9	1.0	0.02
TasGran		3		STD	1574.0	39.0	147.0	0.26	10.7	132.7	10.8	6.3	1.0	0.02
TasGran		5		STD	1519.0	37.0	149.0	0.25	10.2	140.1	9.9	5.5	1.0	0.02

Table I.2 Continued.

Sample ID	DDH	n	Strat Member	Rock Code	Ti *ppm*	Cr *ppm*	Zr *ppm*	Ti/Zr	TiO_2 %	*Total Measurment Error*				
										Ti *ppm*	Cr *ppm*	Zr *ppm*	Ti/Zr	TiO_2 %
TasGran		3		STD	1487.0	33.0	150.0	0.25	9.9	139.9	8.7	4.8	1.0	0.02
TasGran		5		STD	1531.0	39.0	149.0	0.26	10.3	138.7	10.8	4.6	1.0	0.02
TasGran		3		STD	1547.1	30.6	148.7	0.26	10.4	152.9	8.5	6.3	1.1	0.03
TasMonz		3		STD	3189.0	67.0	158.0	0.53	20.2	293.4	17.9	6.4	2.0	0.05
TasMonz		3		STD	3231.0	65.0	153.0	0.54	21.1	304.6	17.1	5.1	2.1	0.05
TasMonz		5		STD	3185.0	70.0	155.0	0.53	20.5	290.0	19.3	5.4	2.0	0.05
TasMonz		3		STD	3196.0	68.0	155.0	0.53	20.6	260.8	19.8	5.5	1.8	0.04
TasMonz		7		STD	3181.0	66.0	155.0	0.53	20.5	295.2	17.2	5.8	2.1	0.05
TasMonz		4		STD	3194.0	68.0	152.0	0.53	21.0	284.3	18.2	6.5	2.1	0.05
TasMonz		5		STD	3230.0	67.0	154.0	0.54	21.0	286.1	16.4	5.4	2.0	0.05
TasMonz		3		STD	3226.0	69.0	157.0	0.54	20.5	302.1	20.4	6.5	2.1	0.05
TasMonz		3		STD	3183.0	56.0	156.0	0.53	20.4	276.0	14.6	5.9	1.9	0.05
TasMonz		5		STD	3174.0	70.0	154.0	0.53	20.6	288.6	17.8	6.0	2.0	0.05
TasMonz		3		STD	3168.0	67.0	151.0	0.53	21.0	267.6	17.9	6.8	2.0	0.04
TasMonz		3		STD	3189.0	67.0	158.0	0.53	20.2	293.4	17.9	6.4	2.0	0.05
TasMonz		3		STD	3231.0	65.0	153.0	0.54	21.1	304.6	17.1	5.1	2.1	0.05
TasMonz		5		STD	3185.0	70.0	155.0	0.53	20.5	290.0	19.3	5.4	2.0	0.05
TasMonz		3		STD	3161.2	67.7	152.3	0.53	20.8	309.6	18.4	6.8	2.2	0.05

n – number of pXRF analyses averaged per sample
Rock Code – Af, andesite flow; Avc, andesitic volcaniclastics; Bvc, Basal Volcaniclastics; Fvc, felsic volcaniclastics; Md, mafic dyke; PA, Price andesite; QFP, quartz and feldspar-phyric rhyolite; STD, standard reference material